HANDBOOK OF GEOPHYSICAL EXPLORATION
SEISMIC EXPLORATION

Klaus Helbig *and* Sven Treitel, Editors

VOLUME 37

Seismic Stratigraphy, Basin Analysis and Reservoir Characterisation

by P.C.H.VEEKEN

HANDBOOK OF GEOPHYSICAL EXPLORATION

SEISMIC EXPLORATION

VOLUME 37

SEISMIC STRATIGRAPHY, BASIN ANALYSIS AND
RESERVOIR CHARACTERISATION

HANDBOOK OF GEOPHYSICAL EXPLORATION

SEISMIC EXPLORATION

Editors: Klaus Helbig and Sven Treitel

Volume

1. Basic Theory in Reflection Seismology
2. Seismic Instrumentation, 2nd Edition
3. Seismic Field Techniques
4A. Seismic Inversion and Deconvolution: Classical Methods
4B. Seismic Inversion and Deconvolution: Dual-Sensor Technology
5. Seismic Migration (Theory and Practice)
6. Seismic Velocity Analysis
7. Seismic Noise Attenuation
8. Structural Interpretation
9. Seismic Stratigraphy
10. Production Seismology
11. 3-D Seismic Exploration
12. Seismic Resolution
13. Refraction Seismics
14. Vertical Seismic Profiling: Principles
    3rd Updated and Revised Edition
15A. Seismic Shear Waves: Theory
15B. Seismic Shear Waves: Applications
16A. Seismic Coal Exploration: Surface Methods
16B. Seismic Coal Exploration: In-Seam Seismics
17. Mathematical Aspects of Seismology
18. Physical Properties of Rocks
19. Shallow High-Resolution Reflection Seismics
20. Pattern Recognition and Image Processing
21. Supercomputers in Seismic Exploration
22. Foundations of Anisotropy for Exploration Seismics
23. Seismic Tomography
24. Borehole Acoustics
25. High Frequency Crosswell Seismic Profiling
26. Applications of Anisotropy in Vertical Seismic Profiling
27. Seismic Multiple Elimination Techniques
28. Wavelet Transforms and Their Applications to Seismic Data
    Acquisition, Compression, Processing and Interpretation
29. Seismic Signatures and Analysis of Reflection Data in Anisotropic Media
30. Computational Neural Networks for Geophysical Data Processing
31. Wave Fields in Real Media: Wave Propagation in Anitsotropic, Anelastic and
    Porous Media
32. Nuclear Magnetic Resonance Petrophysical and Logging Applications
33. Seismic Amplitude Inversion in Reflection Tomography
34. Seismic Waves and Rays in Elastic Wave Media
35. Seismic While Drilling: Fundamentals of Drill-Bit Seismic for Exploration
36. Information-based Inversion and Processing with Applications
37. Seismic Stratigraphy, Basin Analysis and Reservoir Characterisation

SEISMIC EXPLORATION

Volume 37

SEISMIC STRATIGRAPHY, BASIN ANALYSIS AND RESERVOIR CHARACTERISATION

by

Paul C.H. VEEKEN
22 Rue Colonel Fabien
92160 Antony
France
pveeken@hotmail.fr

ELSEVIER

Amsterdam • Boston • Heidelberg • London • New York • Oxford
Paris • San Diego • San Francisco • Singapore • Sydney • Tokyo

Elsevier
The Boulevard, Langford Lane, Kidlington, Oxford OX5 1GB, UK
Radarweg 29, PO Box 211, 1000 AE Amsterdam, The Netherlands

First edition 2007

British Library Cataloguing in Publication Data
A catalogue record for this book is available from the British Library

Library of Congress Cataloging-in-Publication Data
A catalog record for this book is available from the Library of Congress

ISBN-13: 978-0-08-045311-8
ISBN-10: 0-08-045311-2
ISSN (Series): 0950-1401

Printed and bound in The Netherlands

07 08 09 10 11 10 9 8 7 6 5 4 3 2 1

Sponsorship

The following sponsors have provided financial support to make the full colour print of this seismic stratigraphy handbook possible:

1. **AMEC SPIE Oil & Gas Services**, 10 Avenue de l'Entreprise, Pôle Edison, 95861 Cergy-Pontoise Cedex, France.
2. **Georex**, Les Algorithmes, Bâtiment Platon, 145 Rue Michel Carré, B.P. 73, 95101 Argenteuil Cedex, France.
3. **Shell** International Exploration and Production, External Affairs, Ca 207a, Kesslerpark 1, 2288 GS Rijswijk, Netherlands

The companies are all sincerely thanked for their cooperation in the project. Without their help the visual aspect of the textbook would not have been the same.

About the Author

Paul Veeken has obtained his 'doctoraal' degree in sedimentology and stratigraphy at the University of Amsterdam in the Netherlands.
He joined Shell Research in 1981 as a member of their seismic stratigraphy team and actively advocated the new study techniques within the Shell Group. He specialised in the seismic expression of ancient submarine fans. Subsequently he was transferred by SIPM to an operational working environment in Exploration with postings in the UK and Tanzania. Main tasks were seismic interpretation, 2D/3D mapping, preparation of well proposals, databook compilation, evaluation of hydrocarbon prospectivity for various licensing rounds and farm-ins. Salt tectonic deformation proved a challenging mechanism for HC trap formation. He familiarized himself with more advanced petroleum science technologies (a.o. map migration, depth conversion sensitivities, 3D workstation, geostatistical modelling, attribute analysis) during his stay in Production teams in Brunei and Holland.

In 1994 Veeken changed his professional career and took up a position in academia as associate professor in Applied Geophysics at the Ecole Nationale Superieure de Geologie in Nancy (France). Here he was co-responsible for the LSTS lab and the Option Petrole. He acquainted himself with coalbed methane techniques and georadar applications. The research covered topics like: submarine fan sedimentology, gravity modelling, georadar acquisition and interpretation, high resolution sequence stratigraphy, basin analysis and seismic interpretation.

In 1997 he returned to the petroleum industry by accepting a job in the French seismic contracting company CGG, where he joined the depth-imaging department. As member of the CGG's Pole de Geoscience he was seconded to Total Research for a joint project in colaboration with the IFP on seismic reservoir characterisation and petrophysical modelling. He was moved to PDO in Oman and became member of the Geosolutions team carrying out neural network trace classifications, seismic inversion, attribute analysis, 3D visualisation and geobody sculpting projects. Subsequently he was transferred to CMG in Mexico as project leader for inversion and AVO seismic reservoir characterisation projects conducted for Pemex. Data pre-conditioning was a crucial step for quantitive interpretation of the results. The studies concerned silici-clastic as well as carbonate reservoirs.

Currently Veeken is an independent geoscience consultant based in Antony, France.

Preface

"... created from dust, returned to dust, transported and ultimately deposited..."

Dedicated to the students who enthusiastically took part in the training courses and all those who gave encouragement to pursue this textbook project till its final stage.

The first initial draft on seismic stratigraphy was compiled at the ENSG in Nancy and it formed the starting point for this publication. The students appreciated the hand-out written from a work experience perspective. They enjoyed the practical exercises that formed integral part of the course. One memorable post-doc training session was given on board of the MS "Atalante" of Ifremer, where Prof Dr. J.P. Rehault and his team conducted his oceanographic research. French seamen superstition stipulates that the word "*lapin*" should never be pronounced on board of a ship and the awkward expression "*animal with the long ears*" is conscientiously used instead. During our voyage the weather conditions were excellent till the day there was "rabbit" on the menu. The same morning our cook asked me whether I was superstitious and added immediately that the captain certainly was. I answered "No, of course not", but I must admit that my reply was a bit hasty. That day, close to the Azores archipelago, the wind force suddenly increased and high seas were attacking our Ifremer research vessel. At the same time the magnetometer failed and it was decided to haul the measuring device in, to submit it to a detailed inspection. The tool was carefully examined and found nothing wrong, it was put over-board again the next day. Surprisingly it functioned superbly until the end of our journey and nobody really knew what had been wrong with it in the first place. It shows that sometimes the mysteries of the sea are indeed impenetrable...

Since then the draft got updated and extended with research topics from my CGG days. Cooperation with Dr D. Mougenot, A. Zuidema, C. Pinson, J.-M. Michel, S. Zimine and J.P. Diet was great. In Mexico I met Martine Da Silva, who proved complementary in knowledge and work experience. Our "hot" discussions on reservoir characterisation and seismic processing resulted in the go-ahead for writing this volume.

Geophysics is not difficult, but sometimes it is a rather tough study subject. It may be a classic remark, but "*for interpreting geophysical data it is desirable to know the answer before-hand*". Such statement says something about the complexity of the parameters involved. Experience and adequate working models are called upon. A sound understanding of the restrictions and pitfalls is clearly required. The main interest of geophysics lies of course in the application of the theoretical issues. Mathematics only represents a means to reach the ultimate goal. It is tried to keep the amount of formula's in this textbook to a minimum, in order to avoid swamping the novice with information that is difficult to digest. But some formulas are essential for the proper understanding of the principles. The interested reader is referred to the list of handbooks/articles at the back of the book for more details on various study topics.

This textbook intends to give a practical introduction to the vast domain of integrated reservoir studies. It brings together data from different earth science disciplines: geology, geophysics, petrophysics and reservoir engineering. Selections had to be made on the subjects presented here, with some sacrifices concerning the completeness of the document that are difficult to avoid. The end product should however appeal to a fairly wide audience. The main focus is oriented towards hydrocarbon exploration, as it is currently the main domain where geophysics are applied.

The text is supported by an abundance of figures, because in a certain way a good picture tells more then words can say. For confidentiality reasons not all figures are of the highest scientific standards, e.g. the exact location and scales

are not always quoted. This is not too embarrassing as in many cases the information will not be important to the majority of the readers. The example function is the main goal and not the precise geological setting. The horizontal scale can be assumed 25 metres for the average CMP distance in a 3D survey, unless mentioned otherwise. The figures and captions should speak for themselves and this facilitates a quick-glance overview of the book contents.

I sincerely thank all persons, who made this publication possible. It is hoped that reading this textbook will be as much fun as the joy I had when discussing, teaching and applying the study techniques. So, let's now get on with the more serious business...

Paul Veeken
Le Ban St Martin, April 2006

Disclaimer:

Although the author has done his best to check the contents of the manuscript, no legal responsibility is accepted for application of the work presented in this text book. Suggestions from the reader to improve the text or figures are highly appreciated.

Contents

This page intentionally left blank

Chapter 1

Introduction

The interest in seismic stratigraphic techniques to interpret seismic datasets is expanding continuously. The advent of sophisticated subsurface reservoir studies and 4D monitoring, for optimising the hydrocarbon production in existing fields, do demonstrate the importance of the 3D seismic methodology. The added value of reflection seismics has clearly been proven in the last decades and it was especially beneficial on the petroleum development side. Seismic reflection profiles form a vast and solid data source of information on the structure of the subsurface. The seismic dataset gets nowadays explored in ever greater detail. These kind of investigations provide a vital tool for delineation of subtle hydrocarbon traps and are essential in regional basin analysis. The big advantage of seismic stratigraphy in basin studies lies in the fact that the methodology combines two very different scales of observation: the seismic and well-control approach. This explains why many workers are using seismic stratigraphic principles to evaluate their seismic observations (e.g. Payton et al. 1977, Brown and Fisher 1976 and 1980, Rochow 1981, Halbouty 1982, Berg and Woolverton 1985, Bally 1987, Wilgus et al. 1988, Ziegler 1990, Armentrout and Perkins 1991, Cramez et al. 1993, Den Hartog Jager et al. 1993, Henri 1994, Brown 1999, Cosentino 2001, Biju-Duval 2002, Davies et al. 2004).

Conventional stratigraphy deals with data obtained from studies of outcrops, rock samples and petrophysical measurements from boreholes (Rawson et al. 2001). It allows determination of lithofacies, environment of deposition and assignment of ages to these discrete observation points. The data between these calibration points is normally interpolated, which is often done in a rather crude way (Figure 1.1). The information, stemming from various study techniques, are not always straightforwardly in line with each other and this may lead to erroneous conclusions on the nature of the changes in the subsurface geology (Veeken 1997).

In seismic stratigraphy, however, reflection seismics provides an elegant way to carry out interpolation procedures. It equally allows extrapolation into less well-explored areas. An important aspect of seismic interpretation is the analogy or example function formed by calibrated datasets. It provides a means to make predictions on the geological development in unknown basins, where well control is lacking or very scarce. This analogy approach enables extrapolation of the geological data/working models into virgin areas in a more sound manner than was previously possible.

The reflection seismic method creates a geophysically sampled picture of the subsurface, which has to be interpreted in a geologically meaningful manner. The basics of the sound reflection method are rather old. An early application has been illustrated by Lawyer (2004) who recently published an interesting extract from 'The History Book 4' written by Herodotus around 450 BC (Figure 1.2). It shows that human beings did apply unconventional techniques to prolong their survival if necessary and they were clever enough to realise the potential of the echoed return signal of sound waves.

Seismic information is unique and it is fundamental for assessing the amount of geological change between well calibration points (Figure 1.3). Moreover, the reflection seismic method represents a convenient remote sensing technique, whereby the object under investigation is examined without being destroyed.

The scope of seismic stratigraphic studies is ranging from large-scale basin analysis to detailed reservoir mapping, with as ultimate goal the '**Lateral Prediction**' of the reservoir porefill (**reservoir characterisation**). A multi-disciplinary solution to the given problems necessitates good communication whereby the jargon needs to be adapted to the audience (cf Berkhout 2005). It can be easily appreciated that seismic analysis is extremely beneficial for the exploitation of energy resources like hydrocarbons, but also other domains are of potential interest (e.g. mining industry, archaeology, environmental management, etc.).

The focus in this textbook will be on the regional aspects of seismic stratigraphic interpretation. 'Lateral Prediction' topics are presented in a more general way. The main objectives from a petroleum explorer's point of view are:

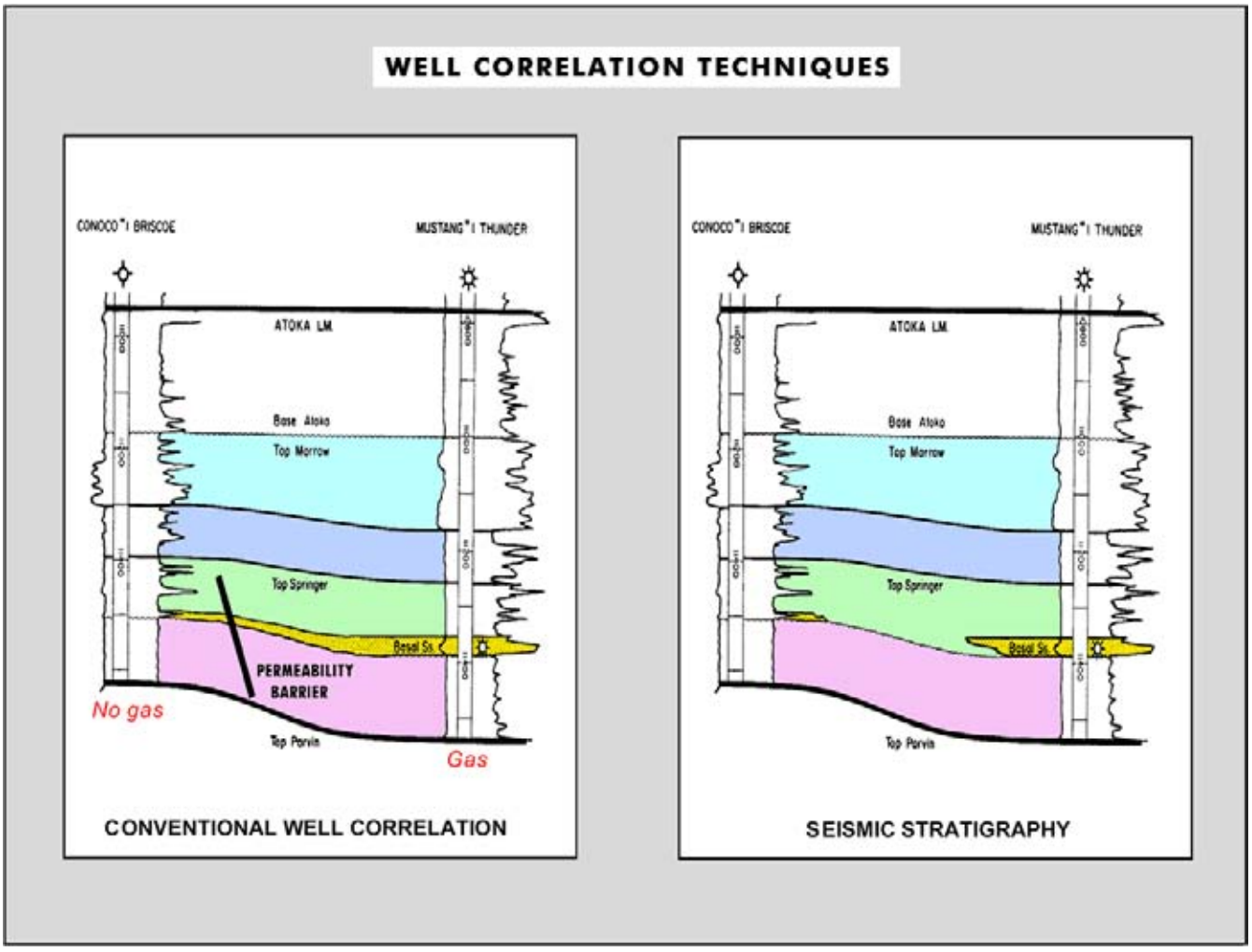

Figure 1.1: Two scenarios for interpolation between well calibration points. The gas sand is only present in the well at the right. Seismic stratigraphic interpretation techniques are needed to document the pinch-out of sands, instead of introducing a hypothetical permeability barrier in he model (modified after Clement 1977, reprint from AAPG whose permission is required for further use).

- To gain an understanding of the geological evolution of sedimentary basins and establish their litho- and chronostratigraphic framework; this is even achieved when only limited amount of calibration data is available.
- To pinpoint source rock and reservoir/seal pairs and define possible hydrocarbon plays. This includes the delineation of structural/stratigraphic traps and analysis of possible **DHI's** (Direct Hydrocarbon Indicators).

When all these goals are achieved and the results of the seismic stratigraphic analysis are properly documented, then the geoscientist is in a position to further evaluate the hydrocarbon potential of the area under investigation. For this purpose several issues need to be addressed (Figure 1.4). The mapped structures/traps are assessed in terms of volumetrics and recoverable reserves. Reservoir modelling improves the understanding of the seismic response. Geostatistics and simulations give a better comprehension of the risk and amount of uncertainty related to the expected fluid flow behaviour in a reservoir. Thereafter a ranking of the various prospects is usually prepared, taking fully into account the economics of the projects. Finally a detailed field development plan (FDP) is devised. This document contains basic systematic guidelines on how to recuperate the hydrocarbons. New technologies increase the reliability of the subsurface predictions made by the geoscientists. Advanced 3D visualisation, neural network classification, multi-attribute analysis and 4D/4C monitoring constitute powerful routine evaluation tools, that will play an even more prominent role in the near future.

The first thing to do, in order to meet the above outlined targets of seismic stratigraphic studies, is to ex-

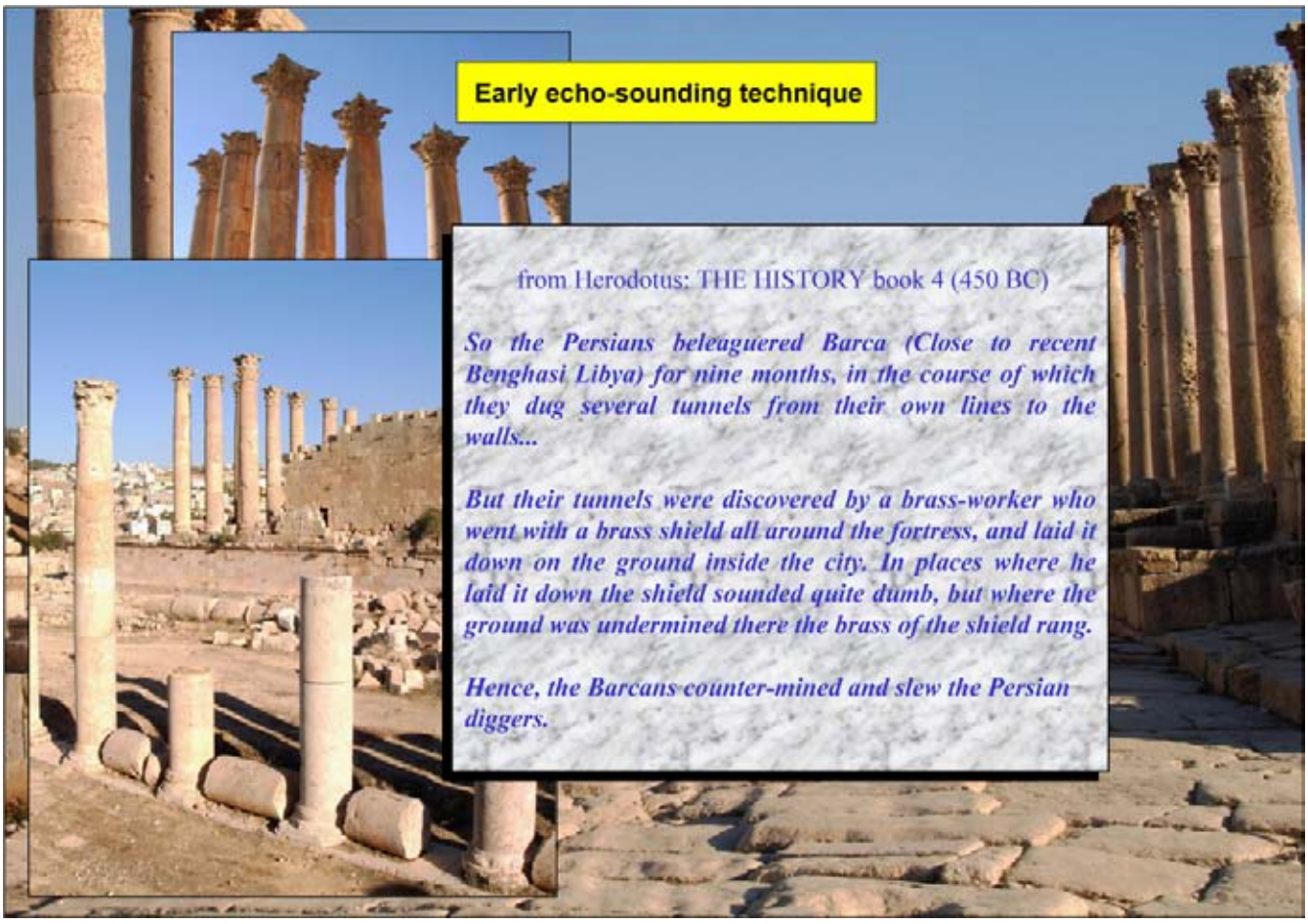

Figure 1.2: Extract from the book 'Histories' written by Herodotus of Halicarnassus around 450 BC, illustrating an early application of the principles behind the acoustic echo-sounding investigation technique (modified after Lawyer 2004).

tract all relevant information from the available outcrop/borehole/geophysical data. The full dataset needs to be incorporated in the geological interpretation. It speaks for itself that it is best to do the data integration in an early phase of each study. Obviously it is crucial to discriminate between genuine seismic events and artefacts introduced by the applied acquisition/processing parameters. Quality control is a hot issue that should never be neglected during the processing and interpretation phases of a project (Da Silva et al. 2004).

Below, first the physical restrictions imposed by the seismic method are examined. Afterwards the basic seismic stratigraphic principles, with the reflection termination mapping and proper well calibration, are presented. Subsequently the various depositional environments and their models are described. Basin analysis gives a means to reconstruct the basin evolution. Synthetic modelling of a basin fill geometry (e.g. Basmod^{TM}, Heresim^{TM}) is however outside the scope of the textbook. The dynamics of depositional systems and sealevel changes are discussed. Thereafter, the hydrocarbon habitat topic will be addressed. Various lateral prediction and reservoir characterisation methods are described. Relatively new techniques – like sequence stratigraphy, seismic inversion, AVO, attribute analysis, reservoir modelling, anisotropic and multi-component processing – open new ways for evaluating the basin fill. Finally, the attention is focussed on different elements of petroleum systems, hydrocarbon plays, ranking of prospects and some financial aspects of the petroleum business are presented.

Mathematics is helpful to summarise geophysical observations. It provides a sort of 'shorthand' to clarify and condense some of the concepts. It is not difficult, although some of the formulas may look somewhat scary at first glance. This certainly goes for the reservoir characterisation section. Do not hesitate to skip them in an initial phase, as the main ideas are anyhow laid down

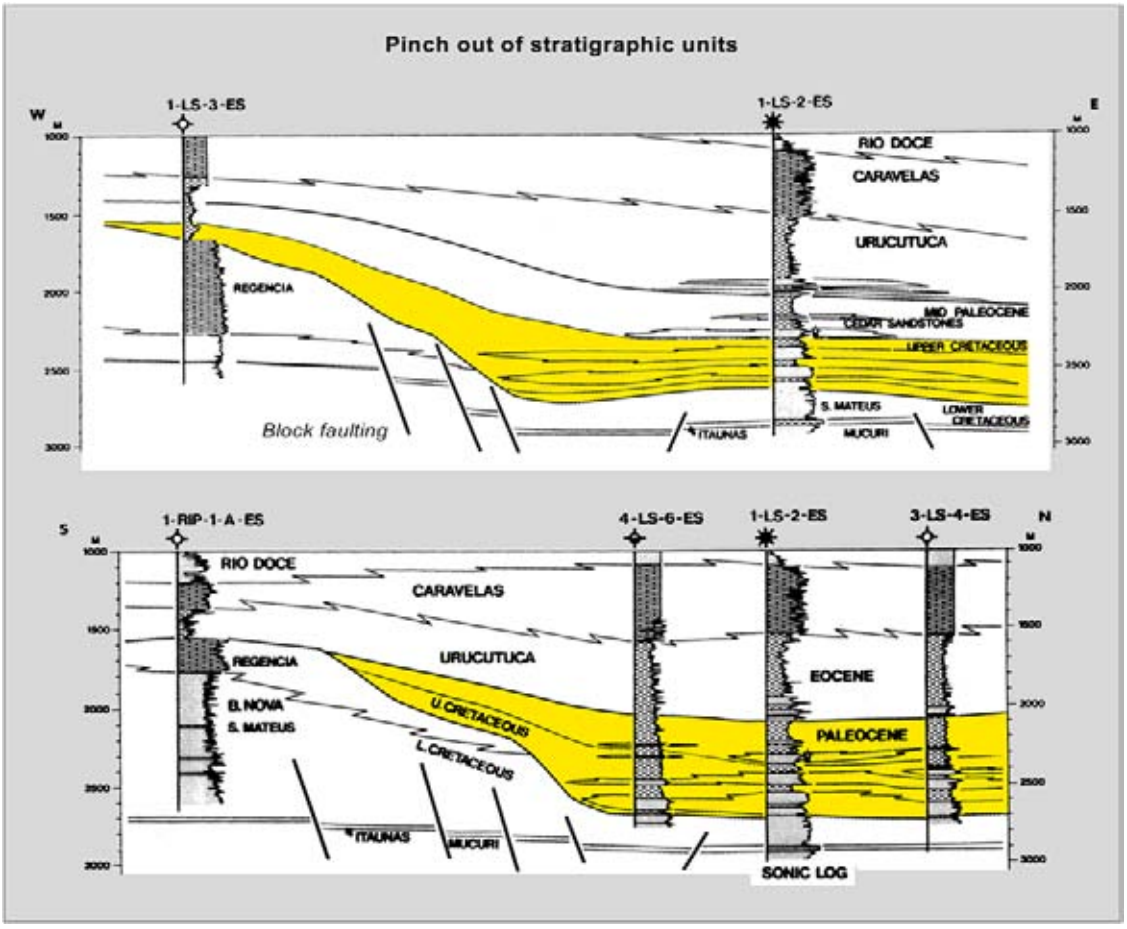

Figure 1.3: Stratigraphic pinch-out of complete stratigraphic time units. Seismic observations are crucial to establish a basin wide frame and a reliable well correlation (modified after Lindseth and Beraldo 1985, reprint from AAPG whose permission is required for further use).

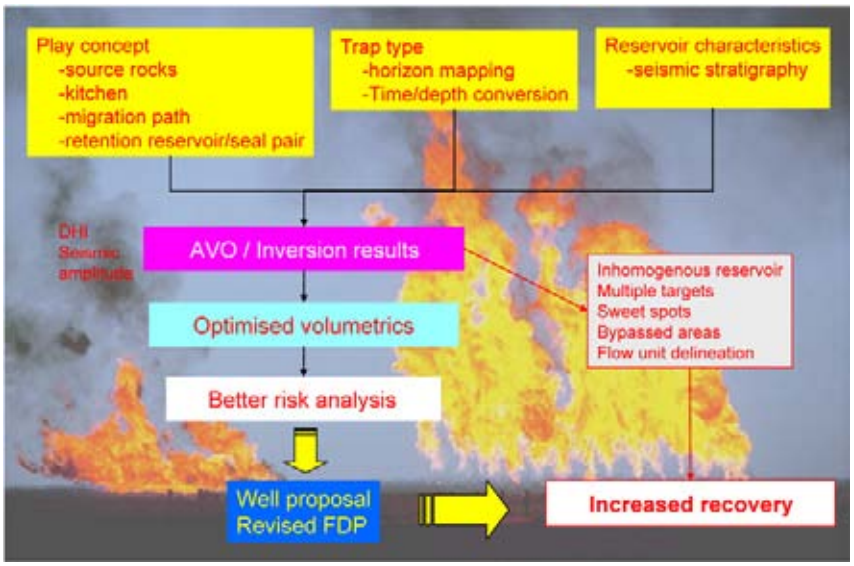

Figure 1.4: Delineation of possible hydrocarbon traps is often supported by seismic attribute analysis. The AVO and inversion processing give access to additional seismic information, that leads to improved volumetrics and better risk analysis. Ultimately it will result in more optimised development plans (FDP) and the HC recovery rate is in many cases augmented considerably, as will be shown in the chapters below.

in the text and accompanying figures. They can always be revisited in a later stage.

The textbook is based on various introductory seismic stratigraphic manuals and articles written by a range of authors (e.g. internal Shell reports, Vail et al. 1977, Brown 1978, Brown and Fisher 1980, Bally 1983, Bally 1987, Berg and Woolverton 1985, Brown 1988, Posamentier et al. 1993, Brown 1999). A break-through publication was the AAPG Memoir No. 26 edited by Payton (1977), who advocated already in an early stage the seismic stratigraphic principles among a wider audience. It still forms a very readable and solid work of reference. In the current volume most of the subjects are covered in an introductory manner; for more in-depth details the interested reader is referred to the studies quoted in the list of publications at the back of the textbook.

This page intentionally left blank

Chapter 2

The Seismic Reflection Method and Some of Its Constraints

An overview is given of the basic principles in seismic reflection acquisition and processing. It is realised that geophysics is sometimes a rather tough subject, but it also represents an essential tool to get access to more interesting study topics. Most people would agree that the benefits of the geophysics lie in the application of its principles, not in the nitty-gritty theory behind it. Nevertheless, the novice interpreter needs a basic understanding of geophysical principles.

The presentation of the seismic processing techniques is deliberately kept simple and restricted to a bare minimum. This approach takes into account that not all readers have the same educational background. A more detailed description of the principles can be found in standard reference textbooks like: Berkhout 1980, Waters 1981, Anstey 1982, Kleyn 1983, Claerbout 1985, Yilmaz 1987, Dobrin and Savit 1988, Cara 1989, Telford et al. 1990, Kearey and Brooks 1991, Henri 1994, Sheriff and Geldart 1995, Brouwer and Helbig 1998, Brown 1999, Yilmaz 2001, Sheriff 2002, Lines and Newrick 2004, Ikelle and Amundsen 2005.

2.1 Basic Processing Concepts

Seismic reflections originate from interfaces that show sufficient density–velocity (Rho–Vee) contrasts. Each seismic layer in the subsurface has it its own acoustic impedance. The acoustic impedance is defined as:

$$\text{A.I.} = \text{density} \times \text{velocity}.$$

The interface between layers is usually related to sedimentary bedding planes, unconformities and/or pore-fill characteristics. The basic raypath geometry at an acoustic impedance interface is illustrated in Figure 2.1. Snell's Law is applicable to the transmitted energy in medium 2.

$$\sin\theta_i/V_1 = \sin\theta_t/V_2 \tag{2.1}$$

θ_i = the angle of the incident wavefront.

θ_t = the angle of the transmitted wave energy in the second isotropic medium.

It is a basic rule that follows from fundamental geometric relationships for the various light ray paths, whereby the Pythagoras principle (537 BC) is applied in the orthogonal triangle. This fundamental property of rectangular triangles was already well known to the old Egyptians (2500 BC), deduced from the specific size of the king's chamber in the Great Pyramid of Khufu (Robinson and Enders 2005). The incidence angle is always defined in respect with the normal to the interface. If $\sin\theta_t = 1$ then a headwave is generated and hence sin $\theta_c = V_1/V_2$. Refraction of the ray energy happens at the **critical angle of incidence**. When the acoustic impedance in the upper layer is smaller than that of the second layer, the transmitted ray will show a larger angle with the normal to the interface, if it travels at angles smaller than the critical angle.

In anisotropic media, where wavefronts are not necessarily perpendicular to raypaths, Snell's Law holds for the angles measured between an interface and the wavefronts, using phase velocities (Sheriff 2002). The phase velocity is a directional velocity. The seismic response of a reflected wavefront is dependent on the amount of Rho–Vee changes over the interface. It is expressed in terms of density and velocity of the media located on opposed sides of the interface. It is normally defined in terms of **reflection coefficient** (2D sense) and **reflectivity R** (full 3D sense for the wavefront). It is expressed by the following formula:

$$R = \frac{\rho_2 V_2 - \rho_1 V_1}{\rho_2 V_2 + \rho_1 V_1}. \tag{2.2}$$

Not all energy is reflected back to the surface; a certain amount is transmitted to deeper levels, proportional to the expression:

$$R_{\text{trans}} = 1 - R. \tag{2.3}$$

This transmitted energy is important as it allows detection at the surface of deeper interfaces with the same

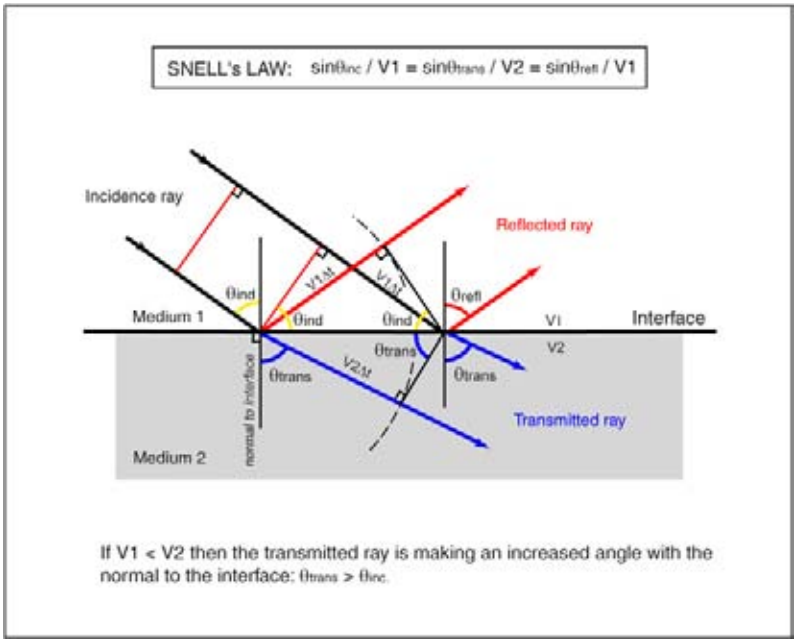

Figure 2.1: Acoustic sound waves are affected by a velocity–density interface between two layers that have sufficient acoustic impedance contrast. The reflected and transmitted plane wavefronts are here only shown. Snell's Law is applied at the interface. Also wave splitting into P-wave and S-wave energy occurs, but is ignored in this representation.

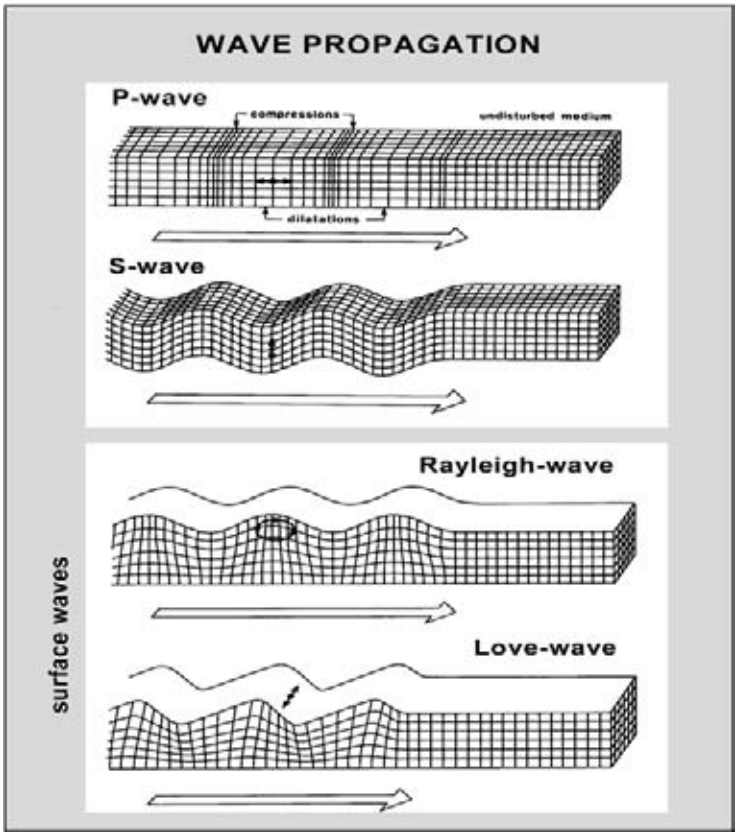

Figure 2.2: P-waves have a particle motion parallel with the propagation direction of the wavefront and it is therefore a compressional wave. The S-wave has a motion that is perpendicular to the direction of propagation, it is a transverse waveform. The Love and Raleigh waves have rather complex particle motions. The latter two are surface-related movements that do not show a great penetration depth and a rapid vertical decrease in amplitude away from the interface (modified after Kearey and Brooks 1991).

shot. The traveltime of the reflected raypath is a measure for the velocity of sound waves travelling through the medium.

Energy from a seismic shot is travelling in radially directions away from the seismic source. The raypath is a mathematical aid to visualise the propagation of a wavefront through a medium. It is always supposed perpendicular to the wavefront. In most of representations only the raypaths detected in the receivers at the surface are shown for convenience sake.

In the seismic experiment the elastic energy is travelling in two distinct modes: P or primary waves (faster) and S or secondary waves (slower). Other wave forms do exist, but these are surface related (Rayleigh and body waves) and not of interest for conventional reflection seismics. The reflected energy is sampled at the surface by geophones or receivers, where the **P-wave** energy is measured. The P-wave is a waveform whereby the propagation direction of the wavefront is coinciding with the sense of deformation (Figure 2.2). **S-waves** travel more slowly (typically V_p is twice as large as the V_s) and their particle motion is perpendicular to the propagation direction. The S-waves show two possible polarisation directions, a slow and a faster S wave propagation direction. Some P-wave energy is also converted in S-wave energy at the reflection point (Figure 2.3). This fact is often ignored in conventional seismic processing, just to keep things simple. It has however some consequences for the amplitude behaviour of the reflectors as will be shown later on. It is nowadays quite common in American geophysical literature that V_p is represented by a Greek α symbol and V_s by a β (e.g. Hilterman 2001, Yilmaz 2001), although the French already used this connotation before (e.g. Cara 1989). In this textbook the less confusing V_p and V_s subscription will be adhered to.

A simple periodic waveform is not only characterised by its amplitude but also by its phase. The **amplitude** is proportional to the reflection strength and plotted perpendicular to the time axis. The **phase** is defined as the difference in degrees for the start of the periodic movement in respect to a standard periodic wave description, where at the T_0 the amplitude is zero (Figure 2.4).

2.1.1 Common Mid Point domain

The basic acquisition set-up for seismic data is formed by several geophones, aligned along a certain trajectory, recording data stemming from the same shot. The geophones and shots are moved over the survey area to create a regular coverage of data points. The geometry of the geophone lay-out can be helpful to suppress certain type of acquisition noise. The recording time is usually below 6 seconds. The first step in processing of the measured reflected signals, is to sort the recorded data from the **Shot** (Figure 2.5) into a **Common Mid Point** domain (abbreviated CMP). This CMP is the midpoint of the shot – geophone array used to measure the seismic energy on the surface. If the reflector is sub-horizontal and the medium is isotropic, than the CMP will be situated directly perpendicular above the Common Depth Point (CDP) on the reflector.

The data is usually displayed in individual **CMP gathers** (Figure 2.6). The vertical traces (wiggle line) correspond to the recorded data at different offset positions. The **offset** is defined by the distance between CMP and geophone position. By moving the configuration (shot and geophones) at the surface along the line trajectory, discrete Common Depth Points are sampled and an image of the reflector in a lateral sense is obtained. A seismic section is thus created.

2.1.2 Normal Move Out and stacking procedure

Lets assume a situation with only one horizontal reflector in an isotropic medium and concentrate on the data belonging to one Common Depth Point on this reflector (Figure 2.7). It can be seen that the raypath belonging to the farest point of the CMP gather, showing the lowest incidence angle, is much longer than the raypath shown in the central part of the picture. This raypath has a much higher incidence angle. The incidence angle is the angle between the down going ray and the normal to the reflector at the impact point. This geometric difference in depth translates in different traveltimes for these raypaths, while they sample the same **reflector point**. The shape of the corresponding reflection time curve in a T–X plot is a hyperbola. If one wants to use the combined energy of all the different time recordings that describe the same CDP, than a correction should be made for these traveltime differences. This is exactly what is done by the so-called **Normal Moveout Correction** (abbreviated: NMO-correction). When the NMO-correction is applied to the CMP data, it allows to sum the energy of the various raypaths (or traces) as they all will line-up in a horizontal sense at the given time T_0. The T_0 is the theoretical traveltime to the reflector at a zero offset position, whereby the shot and receiver are assumed in the same position (physically impossible). This summing of the NMO-corrected traces is done in the so-called seismic "**stacking**" procedure (Figure 2.8). The total amplitude is subdivided by the number of traces utilised in the stacking procedure.

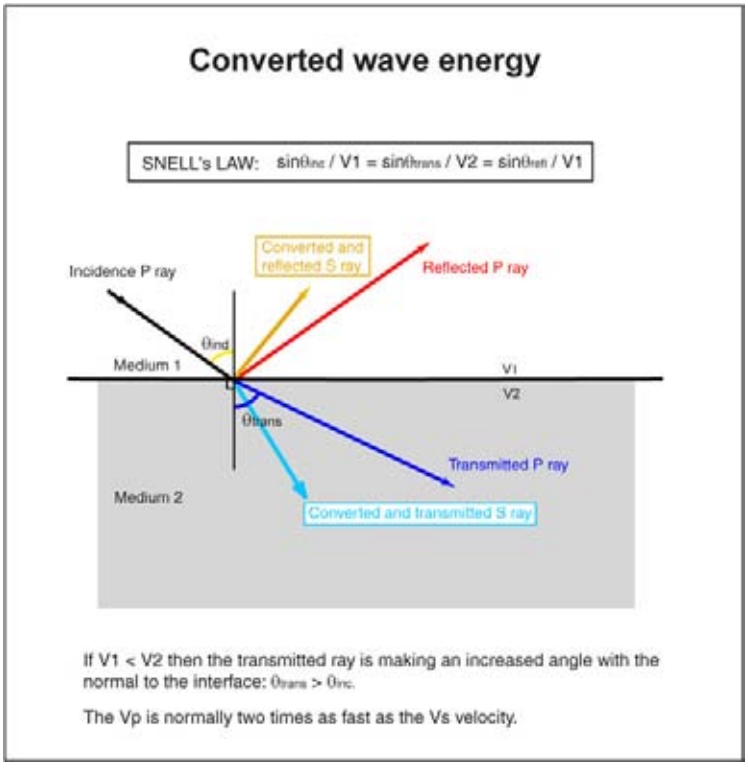

Figure 2.3: Converted wave energy is generated at a reflection point on an acoustic impedance interface. Some energy is reflected back to the surface as S-wave energy that travels typically with a speed two times slower than P-wave energy (P = primary, S = secondary). Also some of the transmitted energy into the second layer is travelling as S-energy. Converted wave energy is of interest for reservoir characterisation purposes, but it requires special acquisition, processing to enhance the data.

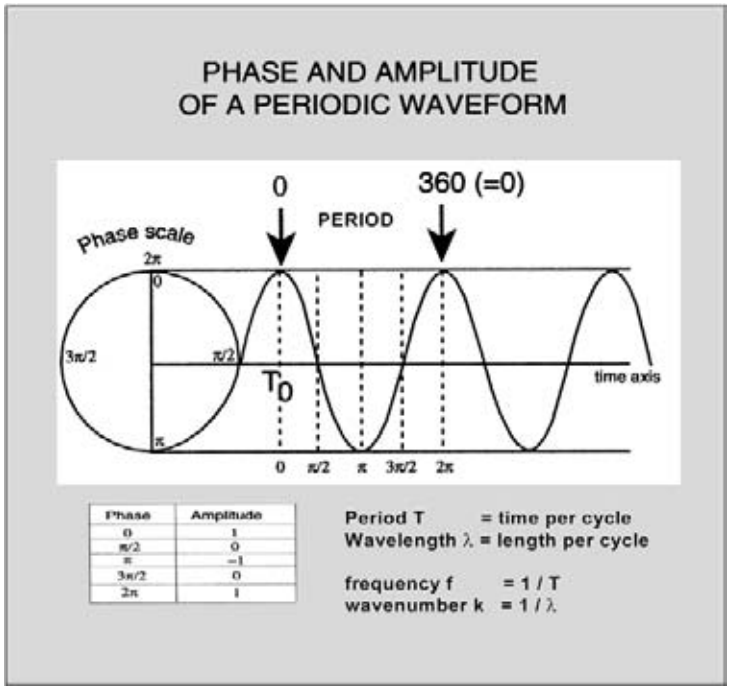

Figure 2.4: Some basic concepts in the description of periodic waveforms. The amplitude response is a measure for the amount of energy contained in the waveform. The amplitude is plotted perpendicular to the time axis. The phase is expressed in degrees. It marks the difference in the waveform cycle for the first time sample T_0 and a standard waveform description for which the amplitude at T_0 is zero.

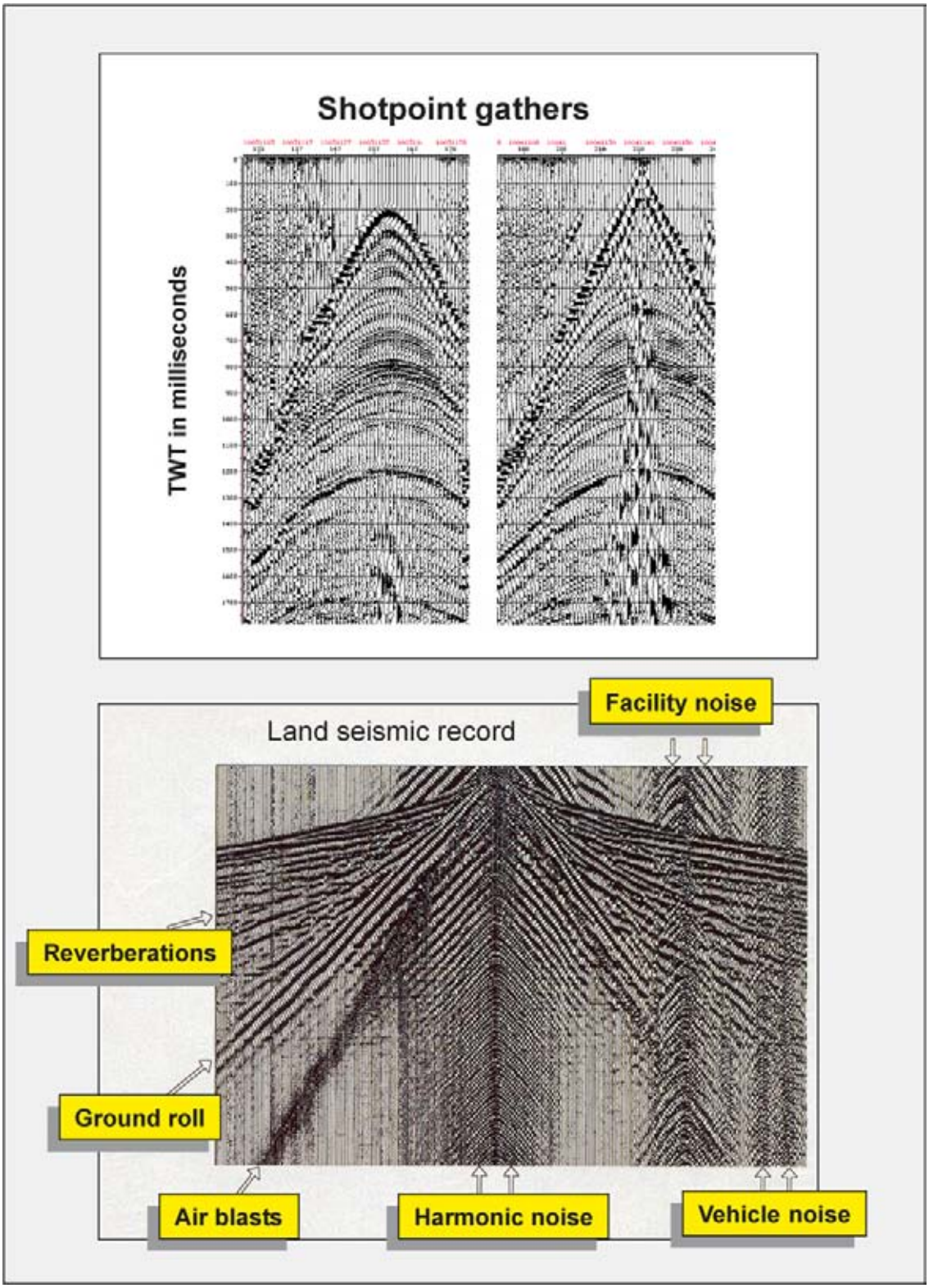

Figure 2.5: (a) Example of a shot-point gather. It is the first visual control to verify the quality of the recorded seismic data. Note the steep noise in the central part of the gather. In fact only the hyperbolic curved-down energy is of interest in reflection seismics. The shot data is subsequently sorted to CMP gathers in the Commom Mid Point domain, where most of the data conditioning and seismic processing is performed. (b) Several types of seismic noise are demonstrated on a land record shown in the lower figure. Environmental noise (wind and traffic) is present independently of the seismic experiment. Intrinsic noise are deformations caused by things electronic measurements and swell in a seismic streamer. Shot generated noise refers to multiple reverberations and groundroll (Dragoset 2005).

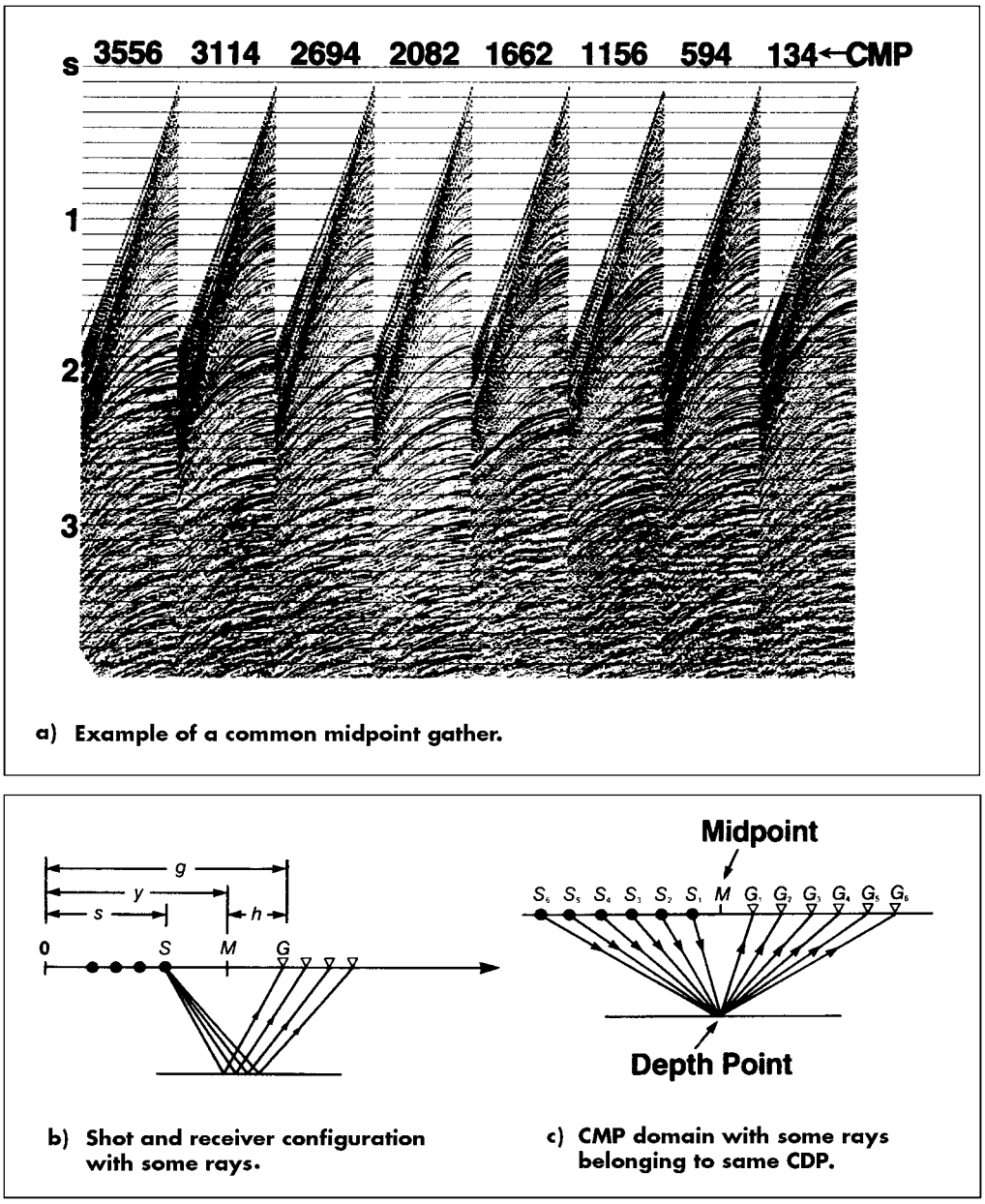

Figure 2.6: An example of a Common Mid Point gather (CMP) with the two-way travel time in seconds as vertical axis (a). In case of a horizontal reflector, this common mid point on the surface coincides with the Common Depth Point (CDP) on the reflector in the subsurface. The shot gathers, recorded in the field, are always resampled to the CMP domain, where the energy is brought together belonging to the same CMP point (b and c). Note the curved hyperbolic reflection on the CMP panels (only half and downward shape due to marine acquisition layout) due to change in length of the various raypaths addressing the same CDP point. The curvature decreases in time because the interval velocity is augmenting for deeper depth (modified after Yilmaz 1987).

The number of traces contributing to the stack is also known as the coverage (or fold) of the stacked CDP. The coverage may vary laterally and vertically in a survey. It is often expressed in a percentage representation. The stacking procedure results in a significantly better signal-to-noise ratio. This is particularly true as background noise normally shows a more random distribution than the genuine signal. The random noise therefore tends to cancel each other in the "addition and divide" stacking procedure.

As said already before, in the stacking procedure the energy of different raypaths belonging to a specific CDP is added, divided by the number of rays and assigned to the **T_0-value** on the trace located straight below the Common Mid Point. It represents the time image

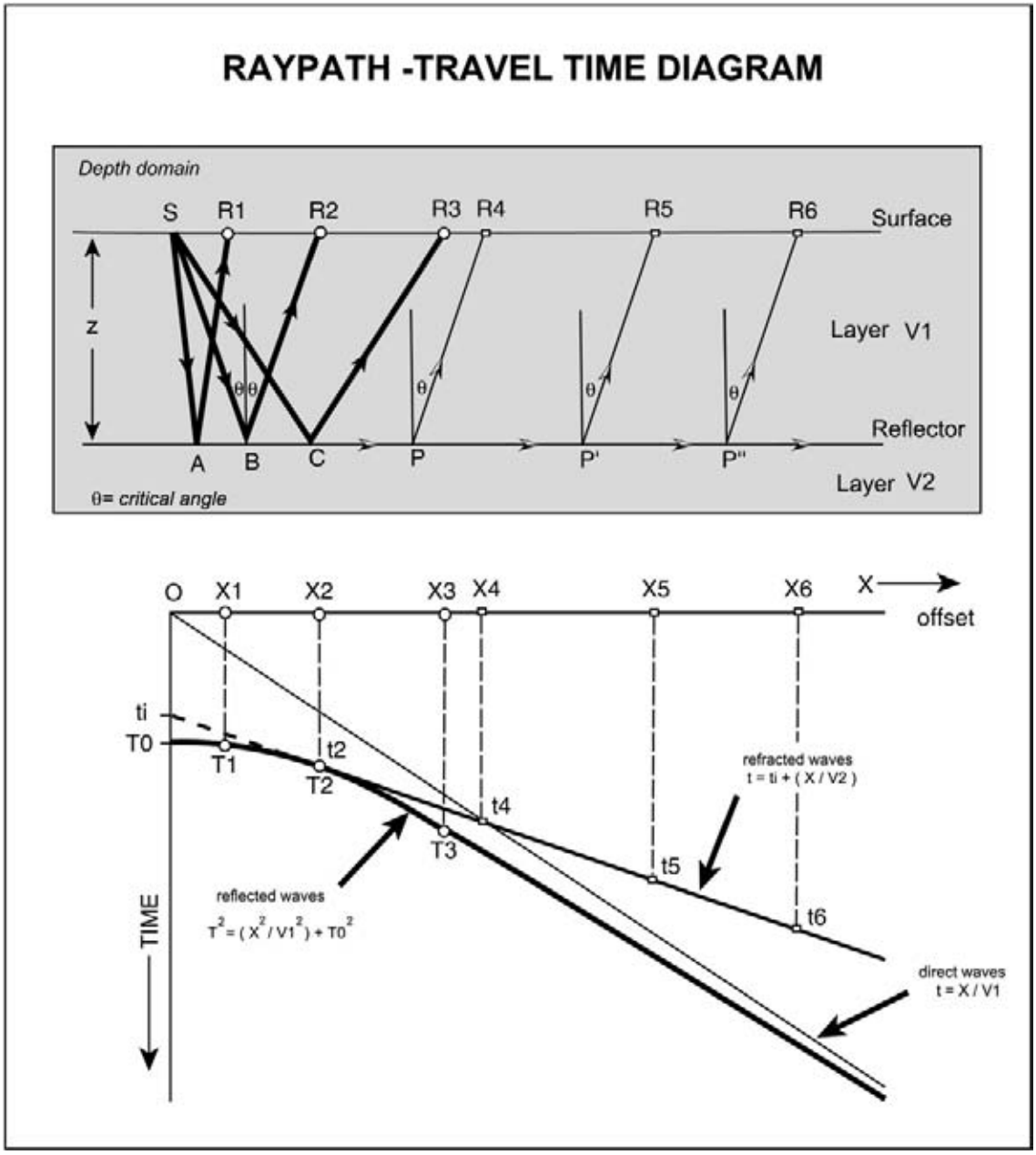

Figure 2.7: Diagram illustrating different P-wave raypath in seismic acquisition set-up for a horizontal interface. Various rays are shown in the depth model at the top and their recording in the time domain TX-graph at the bottom. The reflected waveform is represented by a hyperbolic curve.

of the CDP on the reflector. The result is normally plotted in a X–T diagram and a first seismic trace is thus obtained. This trace displays the amplitude behaviour of the processed seismic recording at a particular X-location along a two-way reflection time axis. The display of the amplitude range is set at such values that it prevents overlap with next trace for the next CMP location. By plotting the various T_0 values of individual CDP points of the reflectors straight under their corresponding Common Mid Point at the surface, and by carrying out a summation procedure on the energy of all raypaths present in that CMP gather, a **Zero Offset Stack** seismic section is obtained.

The stacking procedure allows plotting the energy recorded in various geophone channels addressing the same CDP points. This technique is routinely applied as it provides a convenient way to boost the signal-to-noise ratio without suppressing the primary energy. The method also has some drawbacks especially when it is applied in a semi-2D mode to three dimensional data. It can be compared to a spatial velocity filtering tech-

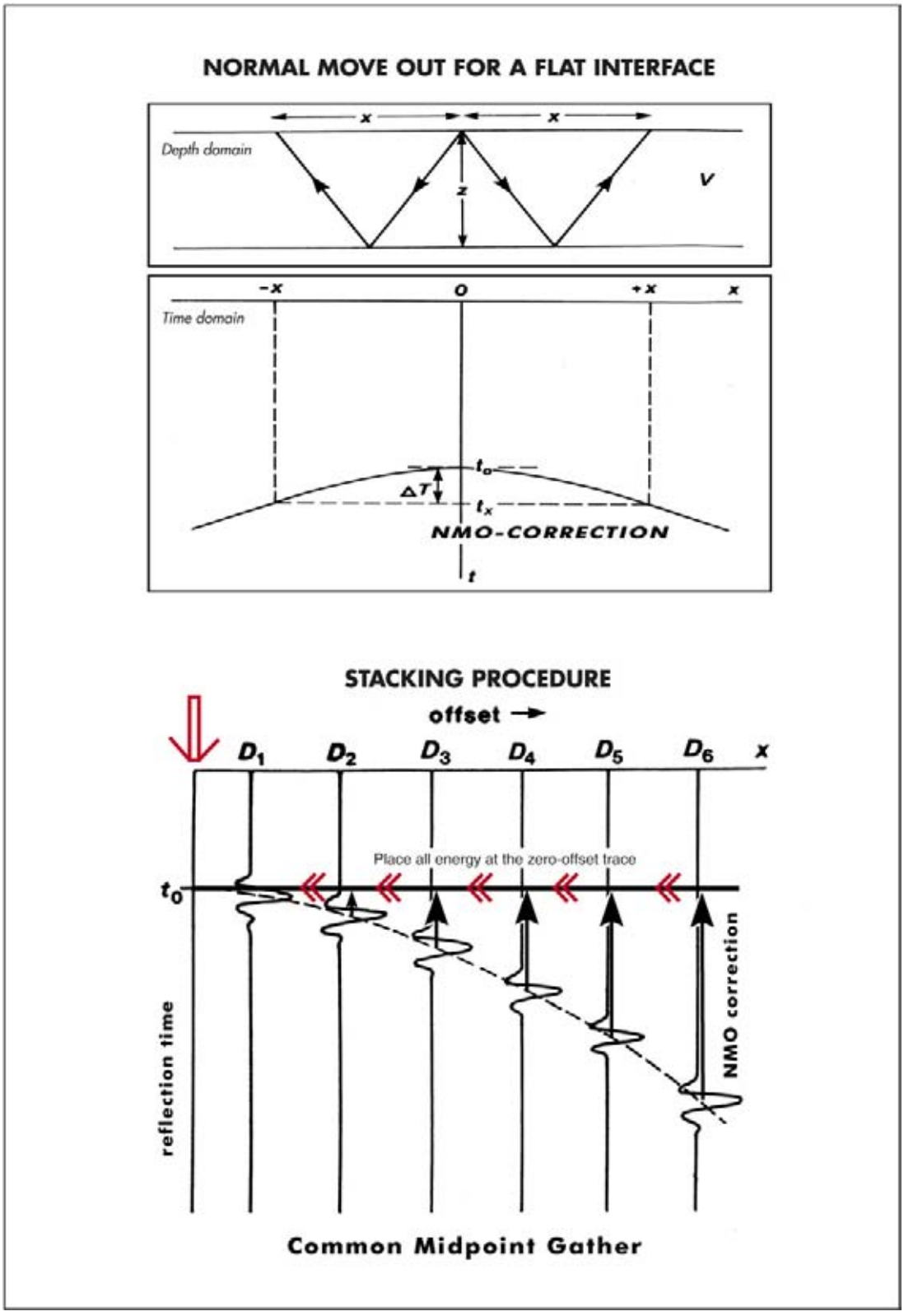

Figure 2.8: Normal Move Out or NMO-correction for a non-dipping interface in an isotropic medium. The correction is the same for positive and negative offsets ($+x$, $-x$). The stacking procedure allows to bring together the energy from different raypaths in the CMP gather addressing the same CDP point and plot their total contribution in the corresponding T_0 position. This correction procedure is known as the stacking of the recorded traces. It is a summation divided by the number of traces. It is a powerful method to reduce the influence of random noise in the seismic data (modified after Kearey and Brooks 1991).

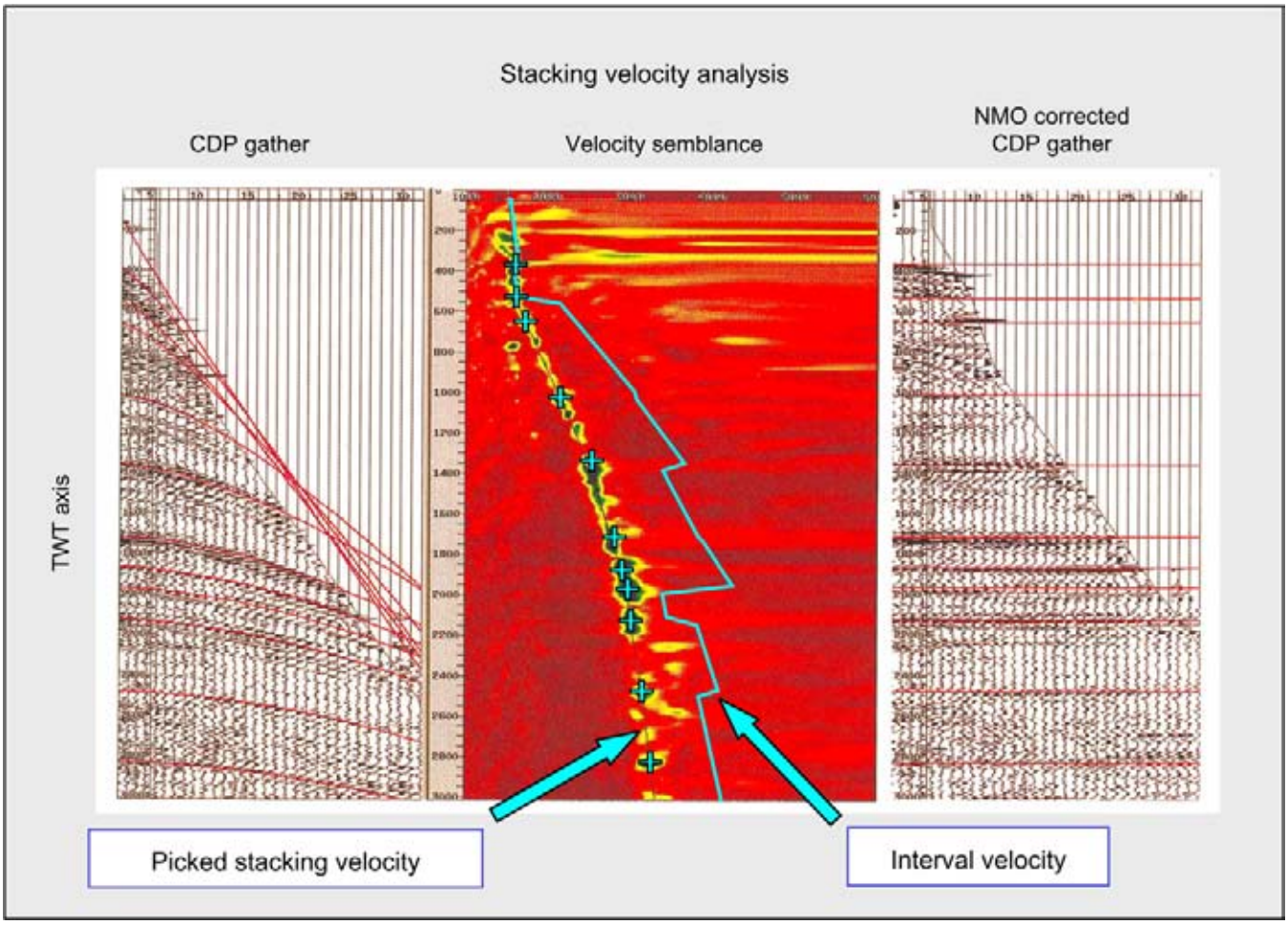

Figure 2.9: Stacking velocity analysis is conducted on CDP gathers. The velocity semblance plot in the middle shows the amount of seismic energy (colour coded) present on the summed CDP traces for different NMO velocities at the time sampling points. Each velocity translates in a different vertical NMO-correction of the traces and hence a different summation is the result. The yellow to bluish colours on the semblance plot are corresponding to the areas with higher seismic energy. The blue crosses are the individual selected velocity determination picks. The interpolated stacking velocity function is assumed to give the best stack. The solid blue line on the right represents the corresponding interval velocity trend. The velocity function is used to correct each time sample in the left CDP gather for the amount of Normal Moveout. The result is shown in the right column. The curved red events are transformed in horizontal lines, which show that the proper stacking velocity has been applied (modified after Yilmaz 2001).

nique that is working in a preferential direction (Gausland 2004). The method is applied for a multi-layered situation and the resulting seismic section is an acoustic representation of the subsurface structure, which only needs to be interpreted in geologically meaningful manner. In case of dipping reflectors additional corrections are required to adjust the geometrical difference. This adjustment is achieved in the seismic **migration** process, which will be discussed later.

2.1.3 Seismic velocity analysis

The NMO-correction is a vertical time-shift for the reflected energy recorded at a certain offset from the source. It is directly related to the velocity of the rocks encountered along the seismic raypath and this is why it is at the heart of seismic velocity analysis. Several events are seen on an uncorrected CDP gather:

- Linear dipping first arrival.
- Refracted energy.
- Reflection hyperbolas with decreasing curvature with increasing time.
- Noise.

A steep dip on the CDP gather means that the event has a rather slow velocity while a weaker dipping event, with less time difference between the near and far offset trace, has a high velocity. In Figure 2.9, several events are

traced in red. The dip and curvature decrease with time and it means that the velocity increases with depth. This is a quite natural condition because sediments get compacted and cemented when they are buried deeper in the earth. Older rocks have typically a higher interval velocity.

The velocity spectrum in the middle column of the figure has a horizontal velocity scale. The total amount of stacked energy on the CDP traces is computed at each time sample and for each velocity. It is colour coded after the NMO-correction is applied. The results are shown in the **semblance plot** in the central part of the figure. The semblance plot is used to facilitate the velocity picking. Semblance represents a specific method of cross correlation, with a summation step instead of multiplication of samples of the two compared waveforms. The traces in a CDP gather are compared with the zero offset trace and this is done for different stacking velocities. Each velocity will generate a cross correlated trace and the energy of the traces in the semblance plot are studied. A good velocity means that the reflection is well horizontalised and the cross correlation procedure will generate a high number. For picking the right velocity profile it is necessary to connect the correct energy patches on the semblance plot. This can sometime be a tricky affair, especially when velocity inversions occur or coherent noise is present (multiple energy). The light and bluish colours in the plot indicate more seismic energy and this usually corresponds to better stacking of the energy on the NMO-corrected seismic offset traces. The crosses represent the velocity picks that have been selected in order to determine the NMO-correction. The velocity is interpolated for the time samples between the crosses. The blue line to the right is the interval velocity based on the picked velocity function. The NMO-corrected CDP gather is plotted on the extreme right. The red lines are now straight horizontal lines and it means that the chosen velocity field for the NMO-correction is pretty good and it will result in the best stacked seismic trace.

2.1.4 Seismic absorption and anisotropy

The **absorption** of seismic energy by the rocks forms a natural constraint for the vertical resolution of the seismic method. Higher frequency acoustic vibrations get more and more absorbed with increasing depth and are negatively affected by the longer travel distance. The absorption is related to the non-elastic behaviour of the rocks and is often expressed in the **Q factor** (Figure 2.10). The Q or quality factor is equal to the ratio of 2π and the energy loss per cycle (Chopra and Alexeev 2004). For rocks it ranges between 20 and 300. Sedimentary rocks normally show values between 20 and 200. The attenuation is related to **absorption factor** α:

$$\frac{1}{Q} = \frac{\alpha V}{\pi f} = \frac{\alpha \lambda}{\pi} = \frac{hT}{\pi} = \frac{2\Delta f}{f_\mathrm{r}} \tag{2.4}$$

$V =$ velocity,

$f =$ frequency,

$h =$ dampening factor,

$T =$ period,

$\lambda =$ wavelength,

$f_\mathrm{r} =$ resonance frequency,

$\Delta f =$ change in frequency that reduces the amplitude by a factor $1/\sqrt{2}$.

Attenuation provides an additional perspective on the lithology and reservoir characteristics (Taner and Treitel 2004). The **spherical divergence** represents the effect that seismic energy is spread over an expanding wavefront as the seismic disturbance propagates in the earth. The amplitude decreases proportionally with the increasing radius of the propagating wavefront sphere (Kearey and Brooks 1991). The decrease in amplitude is proportional to the distance travelled. **Dispersion** is the phenomenon that each frequency has its own distinct propagation velocity and gets absorbed differently (Helbig 1984).

The High Frequency Restoration processing method (HFR) uses well data (VSP) to calculate an attenuation correction (Chopra and Alexeev 2004). It incorporates spherical divergence and Q effects at the same time. The change in seismic amplitude is measured taking into account the shape of the first arrival wavelet on the VSP for successive depth levels to estimate the variation in the frequency components. This is then applied to the surface seismic data.

The fact that the propagation velocity of a waveform is direction-dependent is called **anisotropy**. The most simple case is polar anisotropy or **transverse isotropy** (one axis is different whilst the property behaves the same on the other two axis). Polar anisotropy thus stands for uni-axial anisotropy and the axis can be either vertical, tilted or horizontal (Jones et al. 2003). VTI or vertical transverse isotropy is mainly the result of variations in the geological layering. The HTI (Horizontal Transverse Isotropy) is quantifying vertical fracturing for instance (cf Hilterman 2001, Todorovic-Marinic et al. 2004). It is causing azimuthal anisotropy (Lynn 2004). The direction of the recorded raypath is considered for its quantification and true 3D processing is applied with azimuthal velocity analysis (Angerer et al.

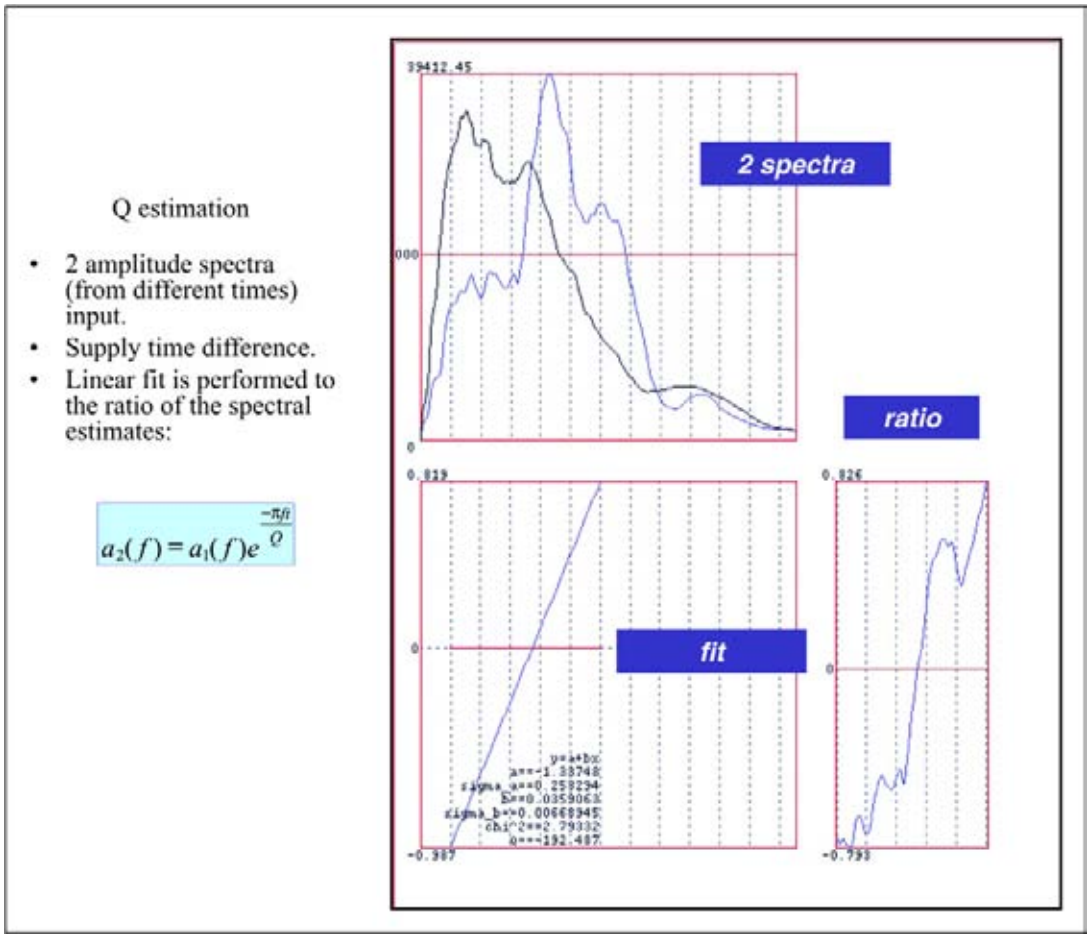

Figure 2.10: Example of a Q factor calculation procedure. The seismic Q or quality factor is equal 2π times the ratio between the energy in the peak of an event to the energy contained in the whole cycle. There are various ways to compute this factor; e.g. via spectral ratios, matching filters, central frequency shift, instantaneous frequency. In seismics the Q normally ranges between 20 and 300. Negative Q factor has no physical meaning and is an artefact introduced by the calculation method based on small computation windows.

2003, Tabti et al. 2004). The velocity variation usually can be described by a cosine function with varying azimuth (cf Parney et al. 2004). Important observation is that the P-waves are slowed down across open fractures; the azimuthal variation is in fact anisotropic and elliptical (empirically proven, Tabti pers. com.) but VTI an-ellipticity also does exist (e.g. Fomel 2004). Ellipse fitting, with a least square optimisation, results in the following parameters:

- The average (isotropic) azimuthal NMO velocity.
- The amount of azimuthal velocity variation.
- The azimuth of the principal axis of the ellipse.

The amount of azimuthal velocity variations, together with the orientation of the principal axis of the velocity ellipse, is related to fracture density and orientation.

The velocity along a bedding plane is typically 10 to 15% higher than the perpendicular velocity in the same bed (Sheriff 1991). The anisotropy effect is becoming increasingly important for longer offset ranges and can no longer be ignored (Figures 2.11 and 2.12). The observed normal moveout deviates from the conventional hyperbolic function. The hyperbolic function is only an approximation that is valid for the smaller offset range. A fourth order expansion of the approximation takes into account the longer offsets and describes much better the observed reflection curve, compared to the standard two term formula. Alkhalifa and Tsankin (1995) proposed a moveout equation that takes care of the **non-hyperbolic moveout** with an extra term that incorporates the **effective anisotropy parameter** η:

$$T^2(x) = T_0^2 + \frac{x^2}{V_{\mathrm{NMO}}^2} - \frac{2\eta x^4}{V_{\mathrm{NMO}}^2(T_0^2 V_{\mathrm{NMO}}^2 + (1+2\eta)x^2)}, \quad (2.5)$$

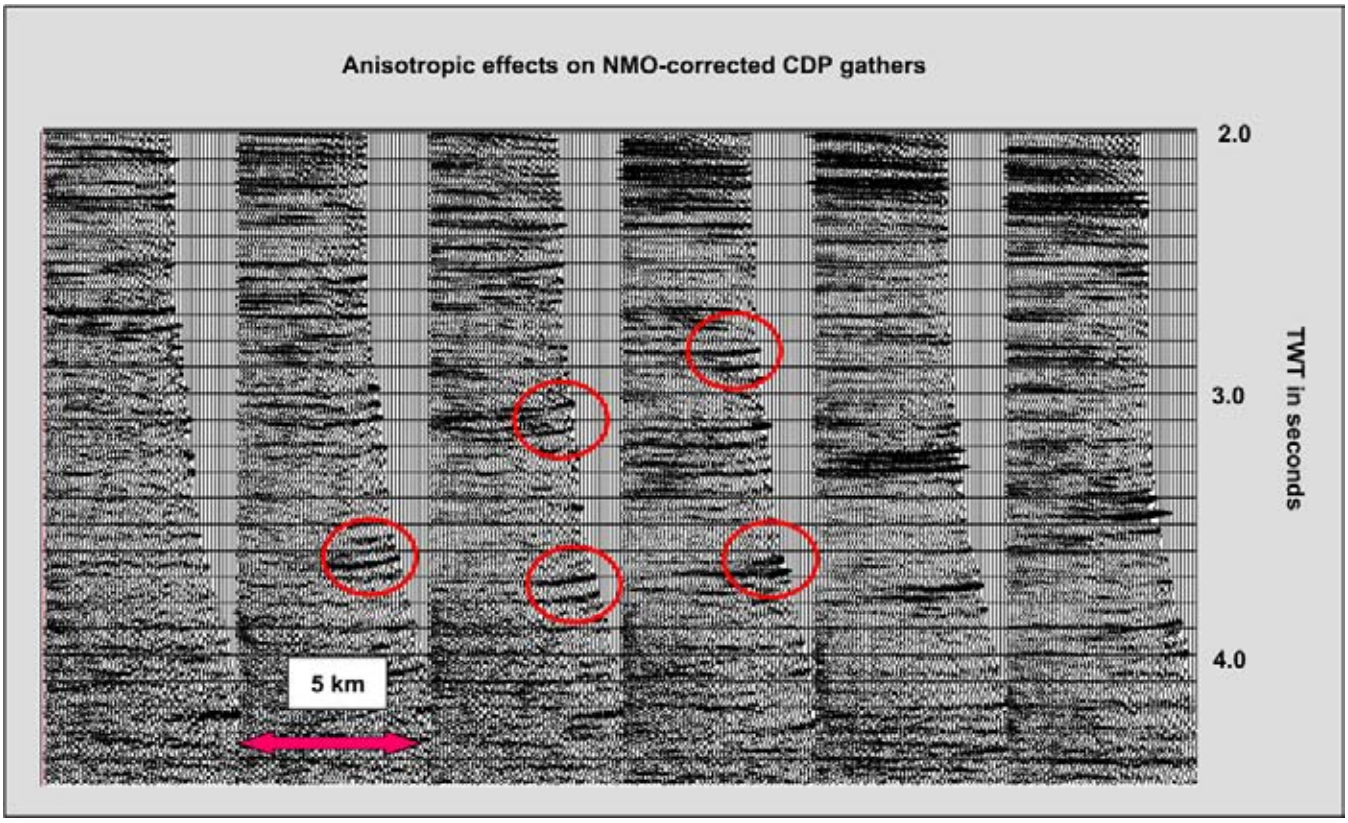

Figure 2.11: Anisotropy is expressed by under-correction of the observed NMO for the long offsets in a CDP gather. It is characterised by the curved upward trends on the reflections for the far offsets on the flattened CDP-gather. It means the moveout is not hyperbolic and a residual correction is needed.

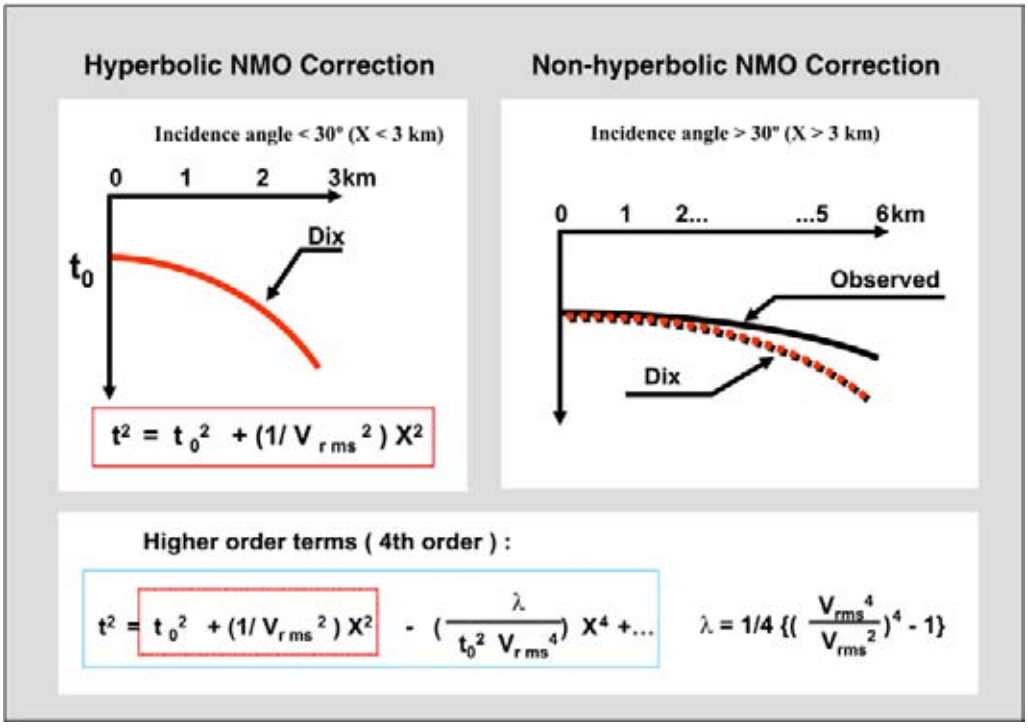

Figure 2.12: Non-hyperbolic move-out as a result of anisotropic behaviour of the layers. The use of large offsets in the stacking procedure amplifies the effect of anisotropy and the residual moveout needs to be compensated by a higher order term NMO moveout correction.

$$\eta = \frac{\varepsilon - \delta}{1 + 2\delta}, \tag{2.6}$$

$$V_{\mathrm{NMO}}^2 = V_{\mathrm{v}}^2(1 + 2\delta), \tag{2.7}$$

$$V_{\mathrm{h}}^2 = V_{\mathrm{v}}^2(1 + 2\varepsilon). \tag{2.8}$$

V_{v} is the vertical P-wave velocity in the well and V_{h} is the horizontal velocity. Epsilon and delta are the **Thomsen anisotropy parameters** (Thomsen 1976, 2002). The effects of changing delta and epsilon on the prograding wavefront is shown in Figure 2.13. The delta is easily obtained from the depth mismatch between the well and the depth-migrated seismics. The epsilon is determined either from the far offset **residual moveout analysis** or via **tomographic inversion** (Figure 2.14).

Tomographic inversion involves estimation of an error criterion on the initial model, perturb the model and to minimise this error (Jones et al. 2003). The '**Deregowski loop**' is often utilised for a simple post migration update of the model, whereby the migrated gathers are subjected to a residual move-out analysis. The new RMS velocity is translated in a different interval velocity via a vertical Dix's conversion. Problem is that the input data to the Deregowski loop is not properly migrated, because the velocity field was not fully correct in the first place and hence the seismic energy is not positioned in the right location. It is better to update the velocity field before migration and establish the velocity model in 3D along the normal incidence raypath. The update of the model is here done in a progressive manner from layer to layer.

The epsilon is also used as a other method to estimate the crack density from the seismic response:

$$\varepsilon = Na^3 \tag{2.9}$$

N = number of cracks per unit volume.

a = crack radius.

Unfortunately the crack density ε does not give unique information on the fluid flow behaviour. A lot of mini cracks or a few major cracks result in a similar crack density. The Thomsen equant porosity model assumes that the fluid pressure in the rock and the crack are the same (Thomsen 1995).

Fracture density, orientation and fracture size can be estimated from the compressional and shear wave behaviour. In each medium only two orthogonal polarisation directions for the S-wave energy exist, S1 and S2. If micro-fractures exist, then the S1 will be polarised parallel to the fracture system and it will be faster than the S2 (also known as quasi-shear). The shear wave splitting is also frequency dependent and it is sensitive to the fracture length (Maultzsch et al. 2003). Fracturing and its relation to the in-situ stress pattern

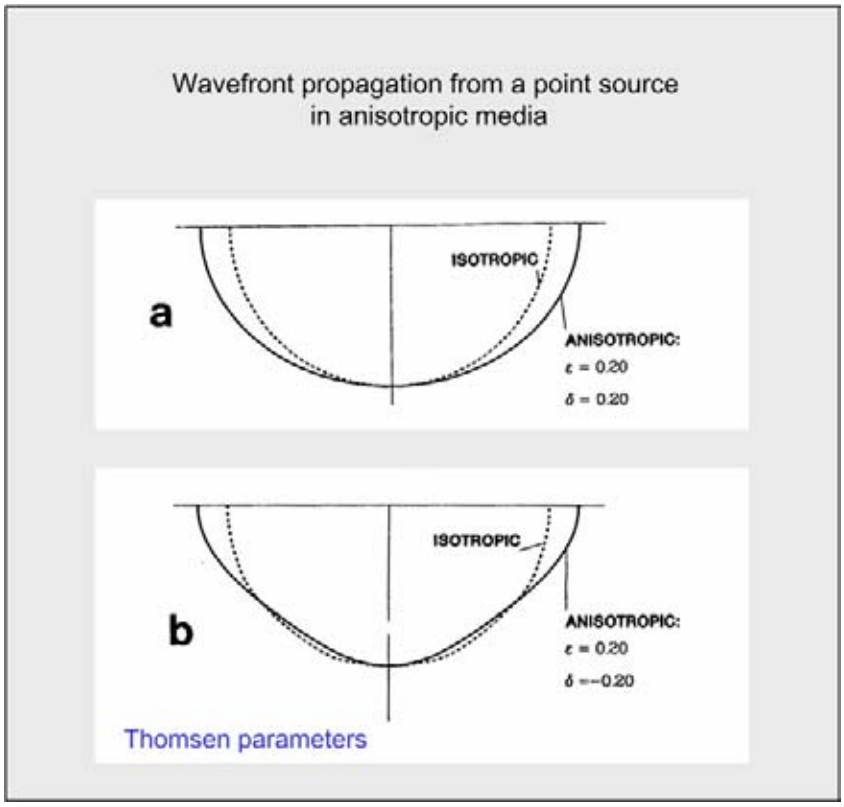

Figure 2.13: Wavefront propagation is shown in two anisotropic media. The Thomsen parameters delta and epsilon are changed; in the first case $\delta = \varepsilon$ and in the second $\varepsilon > \delta$ (modified after Yilmaz 2001).

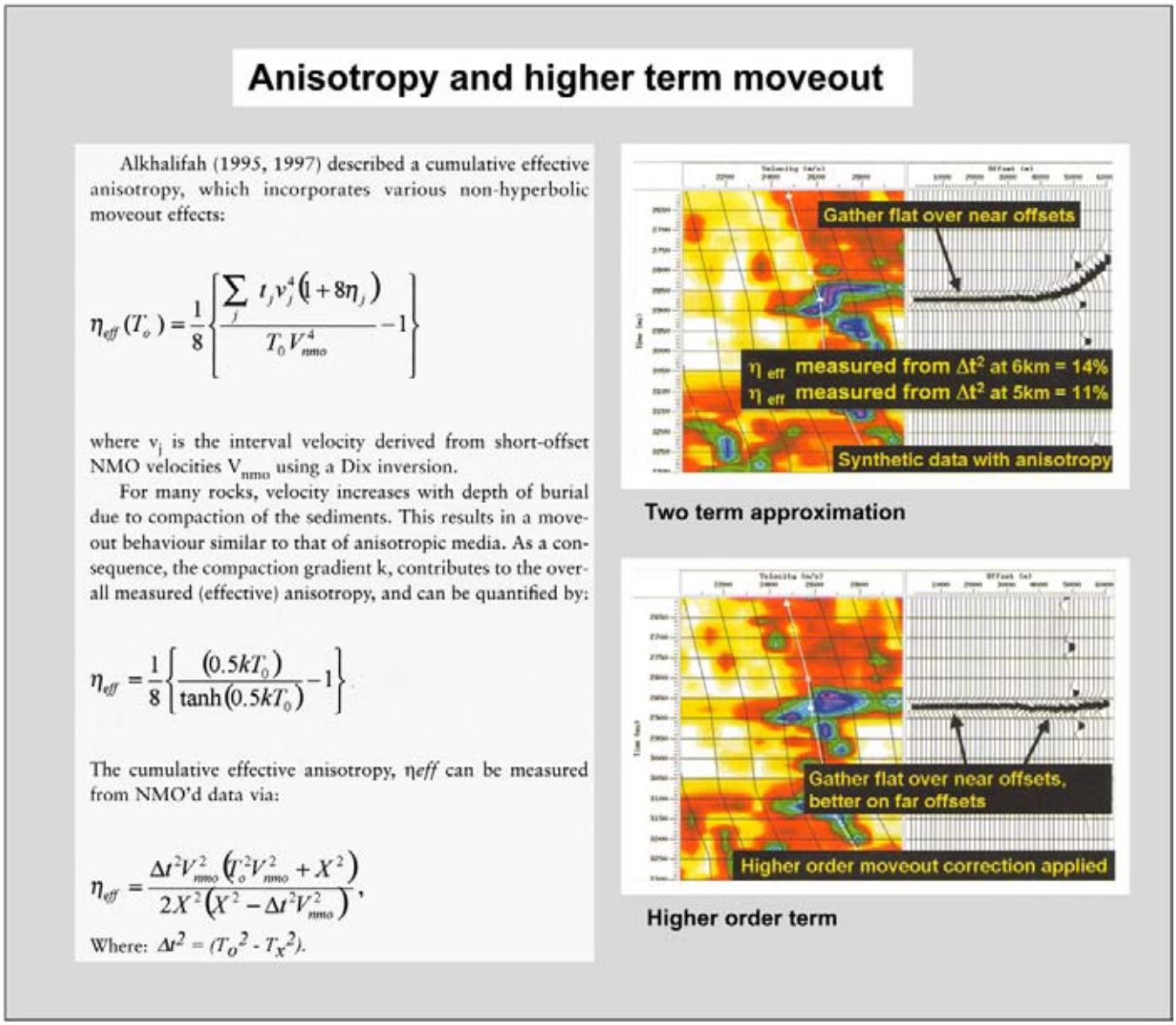

Figure 2.14: The higher order term approximation of the normal moveout gives a better flattening of the reflection hyperbola's in the CDP gather. Anisotropy effects are seen best on the long offsets where the two term approximation does not work properly; this is expressed by the upturning of the reflection. The forth order correction of the anisotropic panel results in a good line-up of the reflection over the full offset range (modified after Jones et al. 2003).

is a subject that attracts vivid interest by researchers worldwide, in order to better assess the fluid flow behaviour (e.g. Goulty 2003, Ameen 2003, Wong and Boerner 2004).

Many detailed studies on anisotropy show the keen attention of the petroleum industry to the subject. Incorporating anisotropy effects in the processing is necessary when long offsets are utilised (Figure 2.15). A more accurate velocity determination will automatically lead to better seismic focusing of the subsurface structuration. This better image is better suited for reliable amplitude measurements. The anisotropy subject is unfortunately beyond the scope of this book, for more details the reader is referred to: Thomsen (1986), Tvsankin and Thomsen (1994), Tvsankin (2001), Thomsen (2002), Jenner (2002), Tabti et al. (2004).

2.1.5 Migration of seismic data

The stacking procedure, to create a seismic section, is using some basic assumptions. It is assumed that the CMP point is located directly below the CDP point. This is obviously not correct, when dealing with dipping reflectors and/or when strong irregular velocity

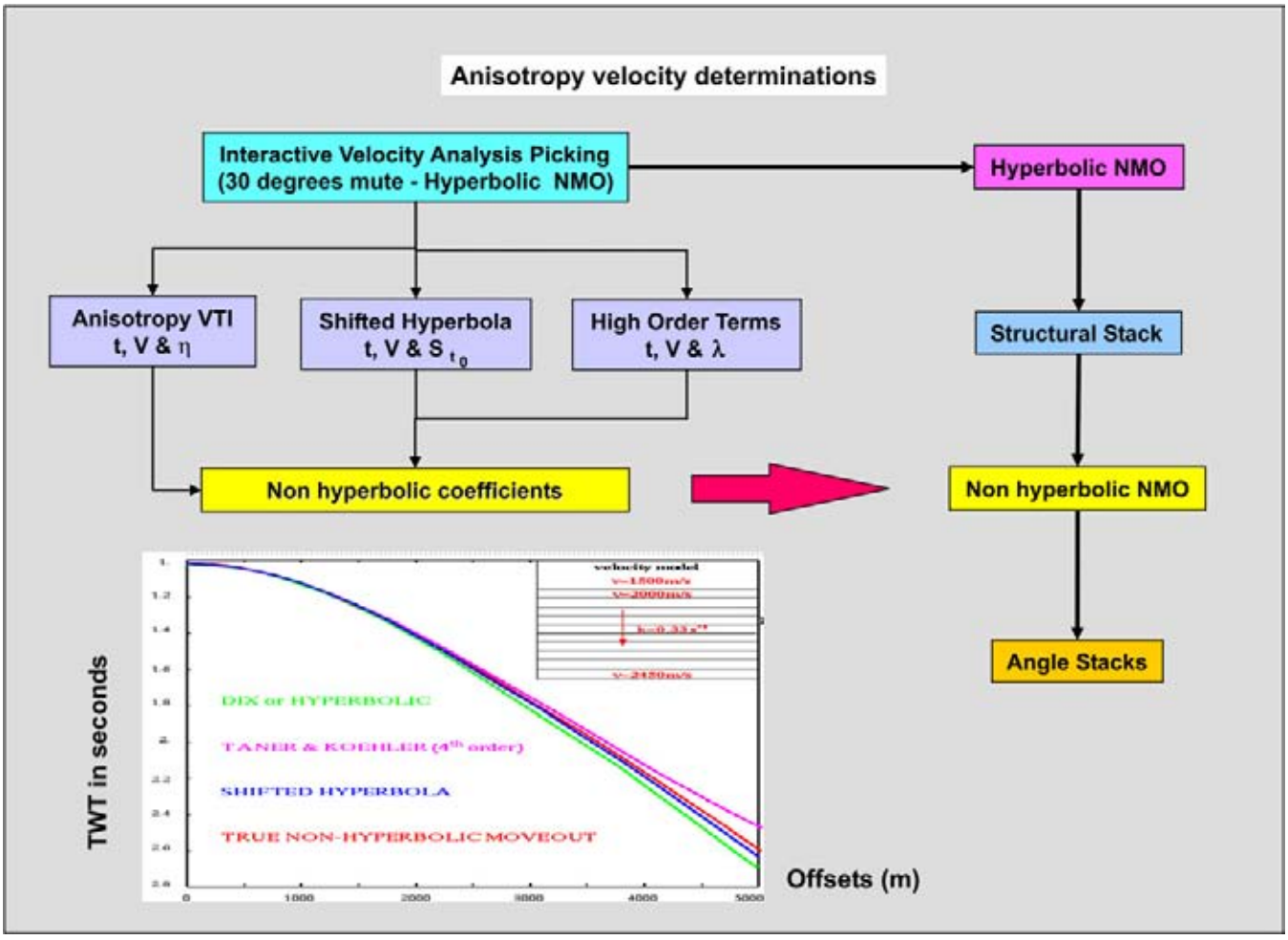

Figure 2.15: Various ways to determine the non-hyperbolic moveout. It will result in a better stack suitable for reservoir characterisation studies, inversion and AVO analysis (modified after Jones et al. 2003).

changes occur in the overburden. Therefore, an additional correction is required and this is exactly what is done in the **migration** processing step. Kearey and Brooks (1991) give an excellent introductory description of the different migration techniques, algorithms and operator characteristics, while Yilmaz (1987 and 2001) is more of interest for the hard-core geophysicist in the audience (2550 pages is a bit much for a lonesome Saturday evening bed-time reading).

Migration removes or reduces the effects of:

- Mis-positioning in case of dipping and strongly deformed reflectors.
- Diffraction energy caused by point sources.
- Diffraction energy from tectonic disturbances.

The migration step itself will result in the following geometrical characteristics of the newly positioned reflections:

- Steeper dips.
- Narrowing of anticlines.
- Broadening of synclines.

Synclines with a reflector curvature exceeding the curvature of the incident wavefront are represented on non-migrated CMP stack sections as so-called '**bow-ties**'. This is caused by the existence of three discrete reflection points for each CMP over the structure (Figure 2.16). Let us have a look on how migration of seismic data can be achieved.

2.1.5.1 Simple wave front migration

A zero-offset geometry (T_0-stack) is first analysed, whereby the reflected ray path is equal to the incident raypath in inverse direction. The wavefront in the corresponding depth model with a constant-velocity medium will be circular (Figure 2.17). Further it is assumed that

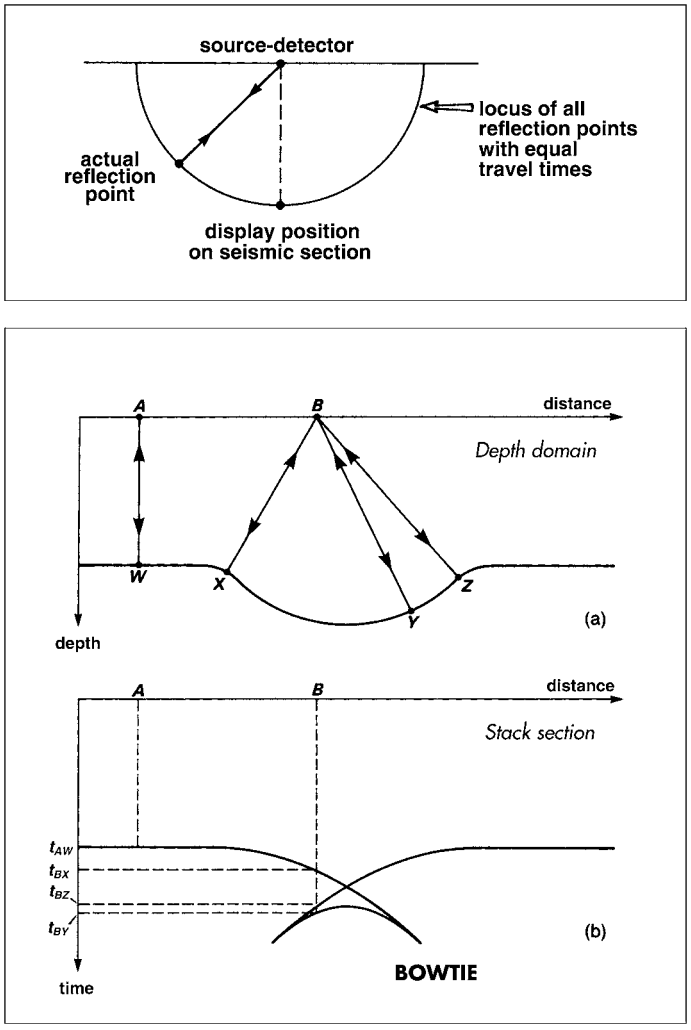

Figure 2.16: Stack sections display sometimes three reflections for the same subsurface reflector point. This is the case when the curvature on the interface is high (synclines or anticlines). The geometric features resulting from this condition are known as 'bowties'. Migration is needed to collapse these bowties and put the energy in its correct time position (after Kearey and Brooks 1991).

the section represents the real dip direction and the down-going raypath has the same length as the upcoming ray have. All these assumptions are hardly the case in real life. In the stacking procedure it is taken for granted that the CDP and the CMP point are located orthogonally above each other. The NMO-corrected T_0 energy is mapped straight under the CMP point. The zero-offset reflection corresponds to a theoretical situation where the shot and detector are positioned in the same place (zero offset) with a straight down and up raypath to the reflector. In reality the recorded energy is located on a semi-circle with a radius of T_0 and with the CMP location as centre point. Shot and receiver in the same place is not a feasable physical experiment.

If the reflector is:

- Horizontal, than the vertical raypath is correct.
- Dipping, than the reflection point is offset with respect to shot position and it is moved in an up-dip direction.

The wavefront in a constant velocity medium is represented by segments of circles. It is possible to construct the circles (wavefront segments) corresponding to individual reflection points on the reflector. Energy recorded at the surface geophone can be stemming from any point on these circles. The true position of the reflection is now determined by the tangent line to all these circles, drawn on the stack time section. This tangent forms the only straight line, honouring all points on the various circle segments at the same time. This procedure represents a very simple form of migration, whereby the wavefront is reconstructed back in time at about half the travel distance from the CMP location. Important to note is that the dip of an inclined reflection on the stack section is increased on the migrated output.

If α_s is the dip on the zero-offset stack section and α_m is the migrated dip than:

$$\sin \alpha_m = \tan \alpha_s. \tag{2.10}$$

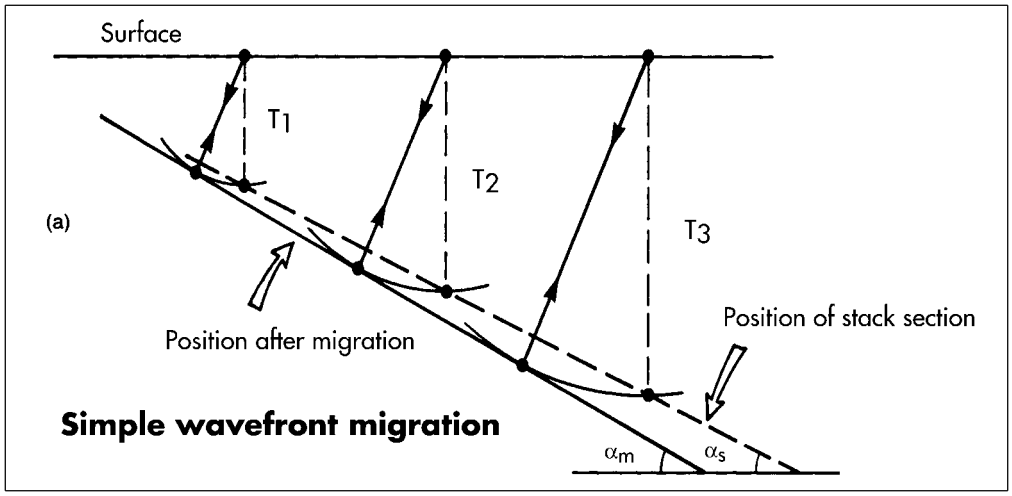

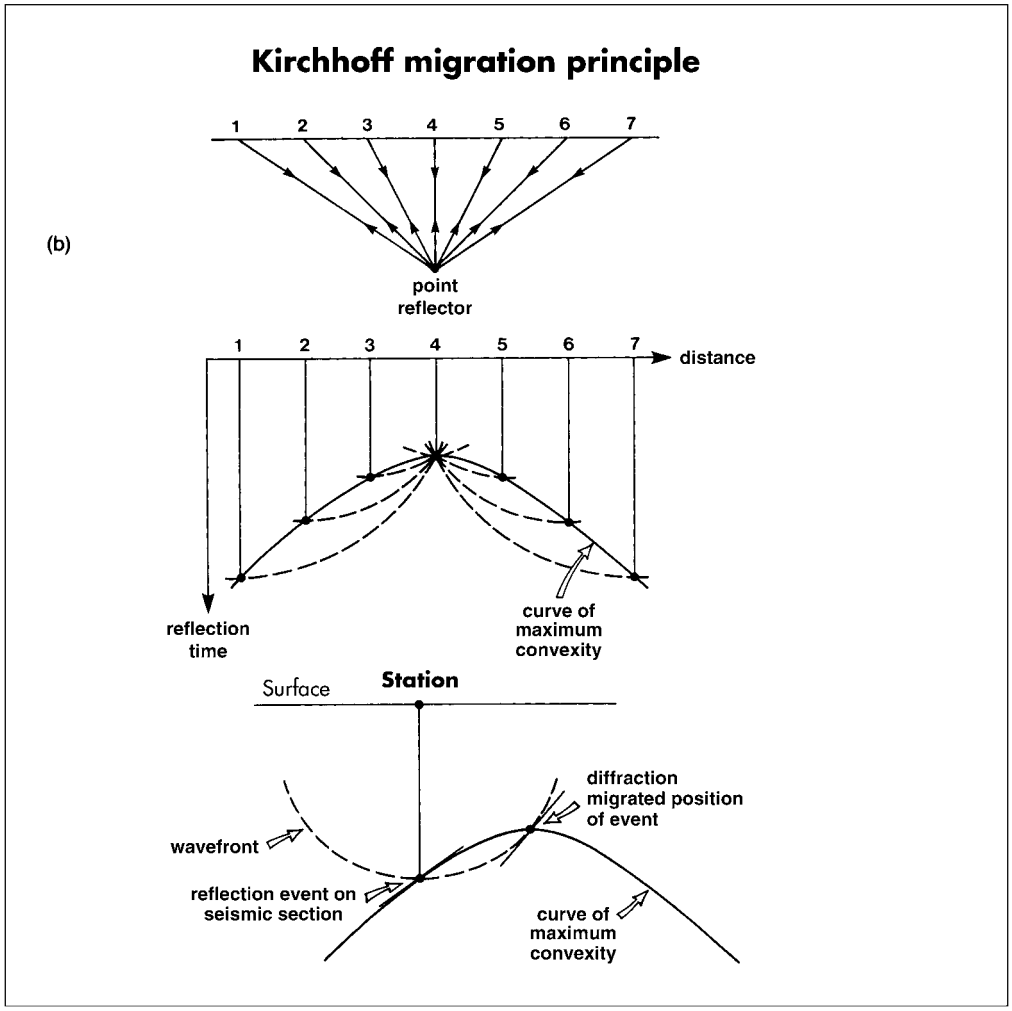

Figure 2.17: (a) Simple wavefront migration for an isotropic medium. Seismic energy is located on circles drawn from the surface with the CMP as centre. The common wavefront is now constructed by using the constraints given by information from several CMP's. (b) The Kirchhoff migration uses the Huygen's Principle for a diffraction point. A reflection constitutes the inference of numerous aligned diffraction points. Migration is achieved by drawing circles through the energy below the CMP points on the stack section and migrating it along circles to the apex of the diffraction curve as shown in this figure (modified after Kearey and Brooks 1991).

This **simple wavefront migration** method can be used even to resolve irregular surfaces by incorporating an integration step.

If variable velocities are present above the reflector, then the raypath is no longer linear and the wavefronts are no longer circular. In such cases adjusted wavefront charts are designed for the prevailing velocity-depth relationship and these can be fitted through the reflection points to migrate the data.

2.1.5.2 Diffraction migration (Kirchhoff)

An other time migration method exploits the **Huygen's Principle**, that states: '*A point taking part in a waveform acts as a secondary point source for the propagating wavefront*'. The wavefront from a point source in an isotropic medium, measured some distance from the point source, is recorded in the time-offset domain as a hyperbola. The diffraction migration assumes that each individual reflection point on a reflector is the source of a diffraction curve. The constructive and destructive interference of infinite diffraction curves results in the continuity of the reflection. The diffraction arrivals of a point source, embedded in a constant velocity layer, is a hyperboloid in a 3D sense. This translates in a 2D vertical intersection into a hyperbola. This hyperbola describes the relationship between X (horizontal distance or offset) and the arrival time T_x recorded at the surface.

If circles (= wavefront) are drawn through the T_x values of the curve, with the centre located in the corresponding vertical X-position at the surface, than these circles will intersect each other in the actual point of diffraction. In fact this point coincides with the apex of the

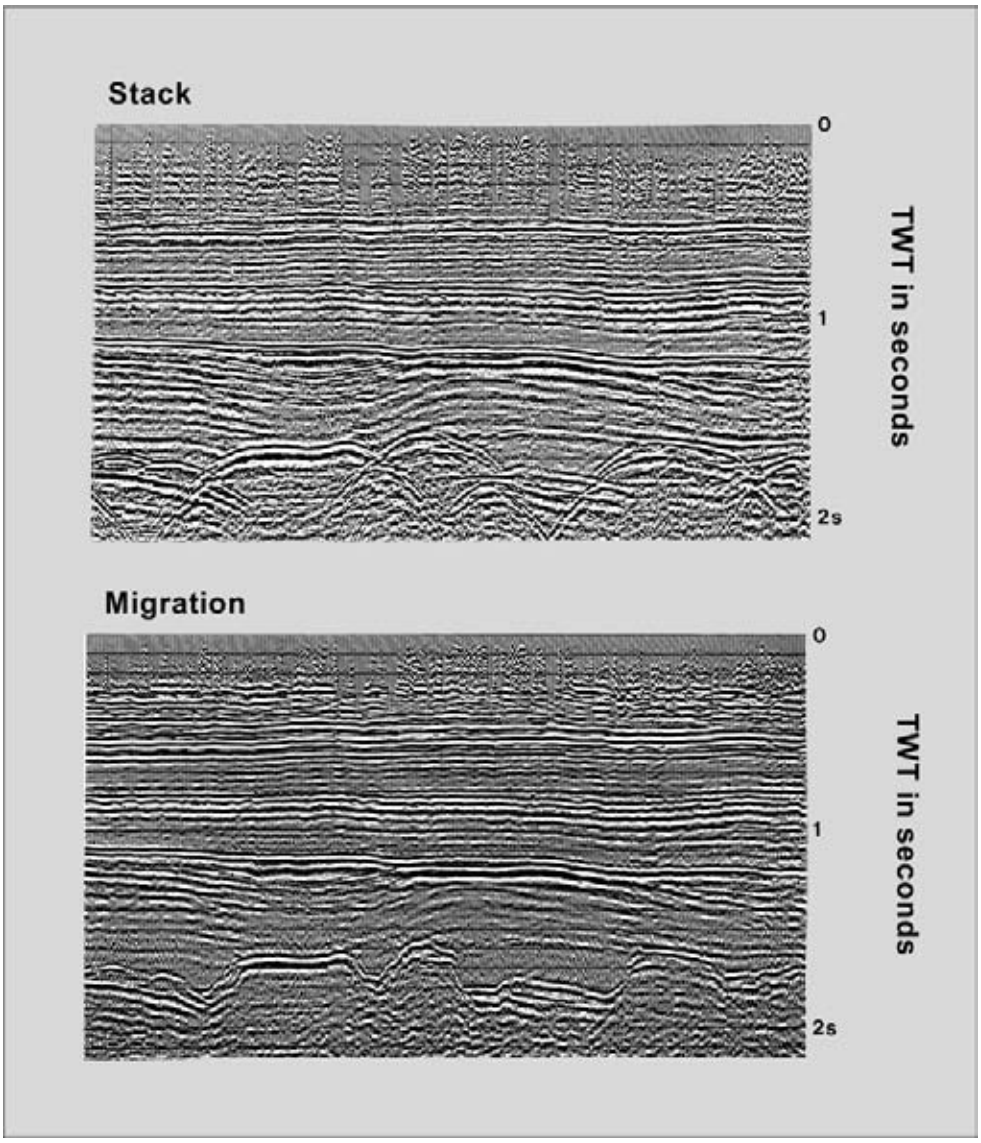

Figure 2.18: Diffraction energy on the stack is removed by the repositioning process of seismic migration. The migration moves the energy up-dip, it tends to shorten the anticlines and broaden the synclines. If the migration velocity model is not correct and over-migration occurs, than it will give rise to 'migration smiles' on the sections. Here the velocity field is correct (after Kearey and Brooks 1991).

diffraction curve (Figure 2.17b).

$$\text{Point of diffraction} = \text{point source}$$

$$\Rightarrow \text{APEX of diffraction curve.}$$

When dealing with variable velocities above the diffraction source, then the diffraction hyperbola is deformed. However, it still shows a close resemblance to an hyperbola, it is called a curve of similar convexity. No reflection event on a seismic section can show a greater convexity then the diffraction event itself and hence the diffraction curve is also referred to as the '**curve of maximum convexity**' (Kearey and Brooks 1991).

In diffraction migration it is assumed that all reflections are tangential to some diffraction curve. A **wavefront chart** – honouring the prevailing velocity/depth relationship – allows to construct the appropriate wavefront segment through the reflection point. Intersection of the segment with the diffraction curve will automatically indicate the 'true' position of the reflection. This point is located on the apex of the corresponding diffraction curve.

The Kirchhoff migration procedure can be thought to represent the summation of all energy distributed along the diffraction curve and collapsing the energy in one point located at the apex of the diffraction curve. The Kirchhoff migration procedure is a special type of diffraction migration that implements the following corrections:

- Obliquity is taken into account.
- Spherical divergence is compensated.
- Wavelet shaping is done correctly.
- The reflection energy is properly redistributed.

The difference between a stack and a migrated section is shown in Figure 2.18 and it can be seen that:

- Energy is moved in up-dip direction.
- Reflection dips get steeper.
- Diffraction energy is collapsed.
- Bowties are resolved by placing its energy in a proper position.
- Anticlines tend to become smaller and synclines broader.

2.1.5.3 Wave equation migration

A modern approach to migration uses the wave-equation (Figure 2.19). The **wave equation** is a partial differential equation describing wave motion generated by a wave source within a medium. The wave equation migration problem can be summarised as reconstructing the wave propagation through a complex medium like the Earth's crust. The technique is currently more and more often applied (Robein 2003). It may give very satisfactory results compared to the conventional Kirchhoff migration (e.g. Glogovsky et al. 2002).

To solve the migration problem, a **recursive method** is usually chosen and the position of the wavefront is evaluated going back in time. Recursive means that a feed-

WAVE EQUATION

An equation that relates the spatial and time dependence of a disturbance which can propagate as a wave. In rectangular coordinates x, y, z, it is:

$$\nabla^2\psi = \frac{\partial^2\psi}{\partial x^2} + \frac{\partial^2\psi}{\partial y^2} + \frac{\partial^2\psi}{\partial z^2} = \left(\frac{1}{V^2}\right)\frac{\partial^2\psi}{\partial t^2},$$

where ψ represents wave displacement (pressure, rotation, dilatation, etc.) and V the velocity of the wave. Functions $f(\ell x + my + nz \pm Vt)$ are solutions to this equation. In spherical coordinates where r is the radius, θ the colatitude, and ϕ the longitude, the wave equation becomes:

$$\left(\frac{1}{V^2}\right)\frac{\partial^2\Psi}{\partial t^2} = \left(\frac{1}{r^2}\right)\left[\left(\frac{\partial}{\partial r}\right)\left(r^2\frac{\partial\Psi}{\partial r}\right) + \left(\frac{1}{\sin\theta}\right)\left(\frac{\partial}{\partial\theta}\right)\left(\sin\theta\frac{\partial\Psi}{\partial\theta}\right) + \left(\frac{1}{\sin^2\theta}\right)\frac{\partial^2\Psi}{\partial\phi^2}\right].$$

The foregoing are forms of the **scalar wave equation**. These forms do not provide for the conversion of P-waves to S-waves nor vice-versa. The **vector wave equation** is more general; it is:

$$(2\mu+\lambda)\nabla(\nabla\cdot\psi) - \mu\nabla\times(\nabla\times\psi) = \rho\partial^2\psi/\partial t^2,$$

which can be written in component form as:

$$\mu\nabla^2\psi_x + (\mu+\lambda)\left(\frac{\partial}{\partial \boldsymbol{x}}\right)\left(\frac{\partial\psi_x}{\partial x} + \frac{\partial\psi_y}{\partial y} + \frac{\partial\psi_z}{\partial z}\right) = \frac{\rho\partial^2\psi}{\partial t^2}.$$

If div $\psi = 0$, this gives an S-wave; if curl $\psi = 0$, a P-wave.

Figure 2.19: Mathematical definition of the wave equation (Sheriff 2002). It describes the wave propagation in the subsurface. It is nowadays more and more used for migration purposes, because the computation costs have come down with the Linux PC clustering configuration, allowing parallel computing.

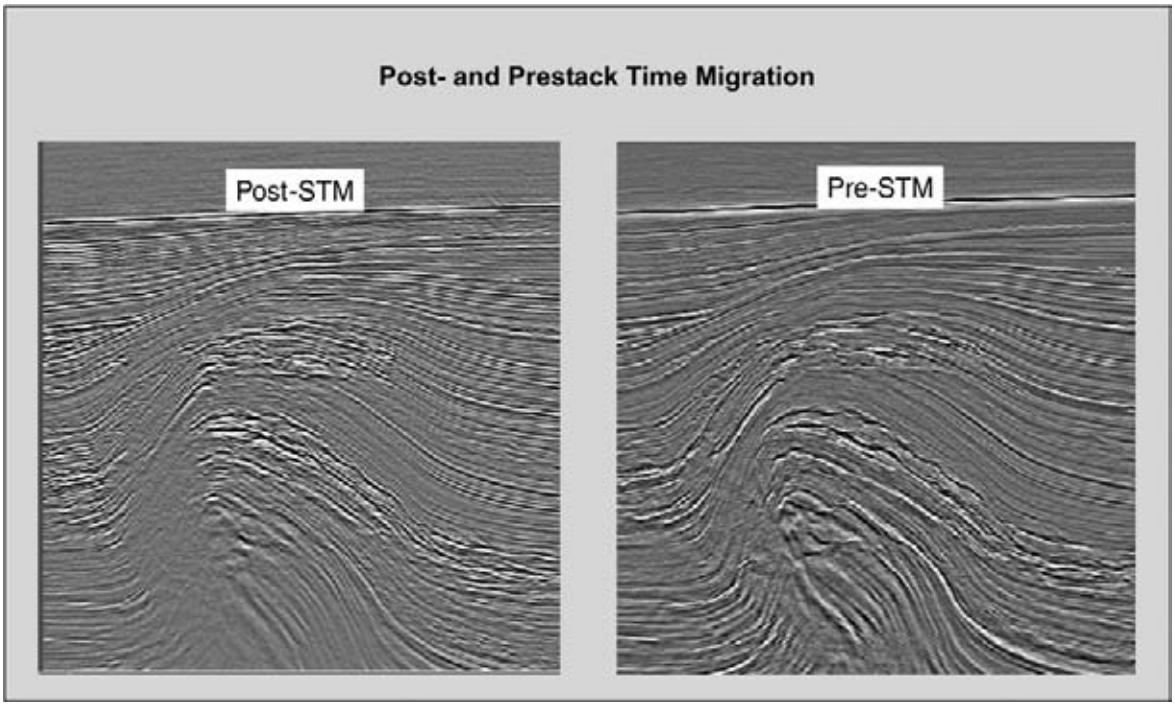

Figure 2.20: A comparison between the conventional Post- and Prestack Time Migration. Migration before the stacking procedure (PSTM) leads to a substantially better seismic image with a better determined velocity field. Note the remarkable better definition of the deeper fault blocks and the overhang.

back step is incorporated in the procedure. The form of the wave field for any reflection event at the surface is reconstructed from the measured travel times at various shot/receiver positions. For proper migration of the reflections it is necessary to reconstruct the exact form of the wave field in close proximity of the reflector. It is possible to reconstruct the wave field by solving the wave equation for each time sample and the wavefront is effectively moved backwards in time. Moving the wavefield back to its half-time position (= one-way time value) places the wavefield exactly at the reflector position. The form of that half-time wavefield determines the actual shape of the reflector.

Migration using the wave equation solution is known as 'Wave Equation' migration. There are several ways to achieve this goal:

- '**FINITE DIFFERENCE**' migration.
  This method is using a finite difference approximation to solve the wave equation by applying a downward continuation algorithm.
- '**FREQUENCY–WAVENUMBER**' migration.
  In this F–K migration approach a Fourier transform is utilised and all spatial steps to perform the migration are done in the frequency domain. Afterwards the result is being transformed back into the T–X domain by an inverse Fourier transformation
  It are the Stolt (named after its original inventor B. Stolt from Conoco) and phase shift methods.
- '**FREQUENCY–SPACE**' migration.
  This F–X migration is based on a continuous fraction expansion technique to allow wider angles in the approximations.

The above described migration techniques all have their own limitations. They use certain assumptions on the overburden, which are not necessarily valid. If the velocity distribution in the overburden is very complex (e.g. in case of a salt diapir overlying a possible hydrocarbon trap), then these conditions are not fulfilled and hence other more robust methods are needed. These methods involve prestack time migration (Figure 2.20), 2D or 3D ray-tracing and depth migration. The behaviour of the image ray should be examined to evaluate whether sophisticated migration techniques have to be employed. The **image ray** is the raypath that arrives at an vertical angle in the geophone. If no velocity irregularity exists, than this image ray is located straight above the apex of the reflection 'hyperbola' in the CMP gather. If the X position is different for these two points, an alternative migration method is highly advisable if high accuracy is needed for resolving the structuration and adequate well proposals. These alternative migration techniques are more costly and therefore a good justification of the extra expenses is always required.

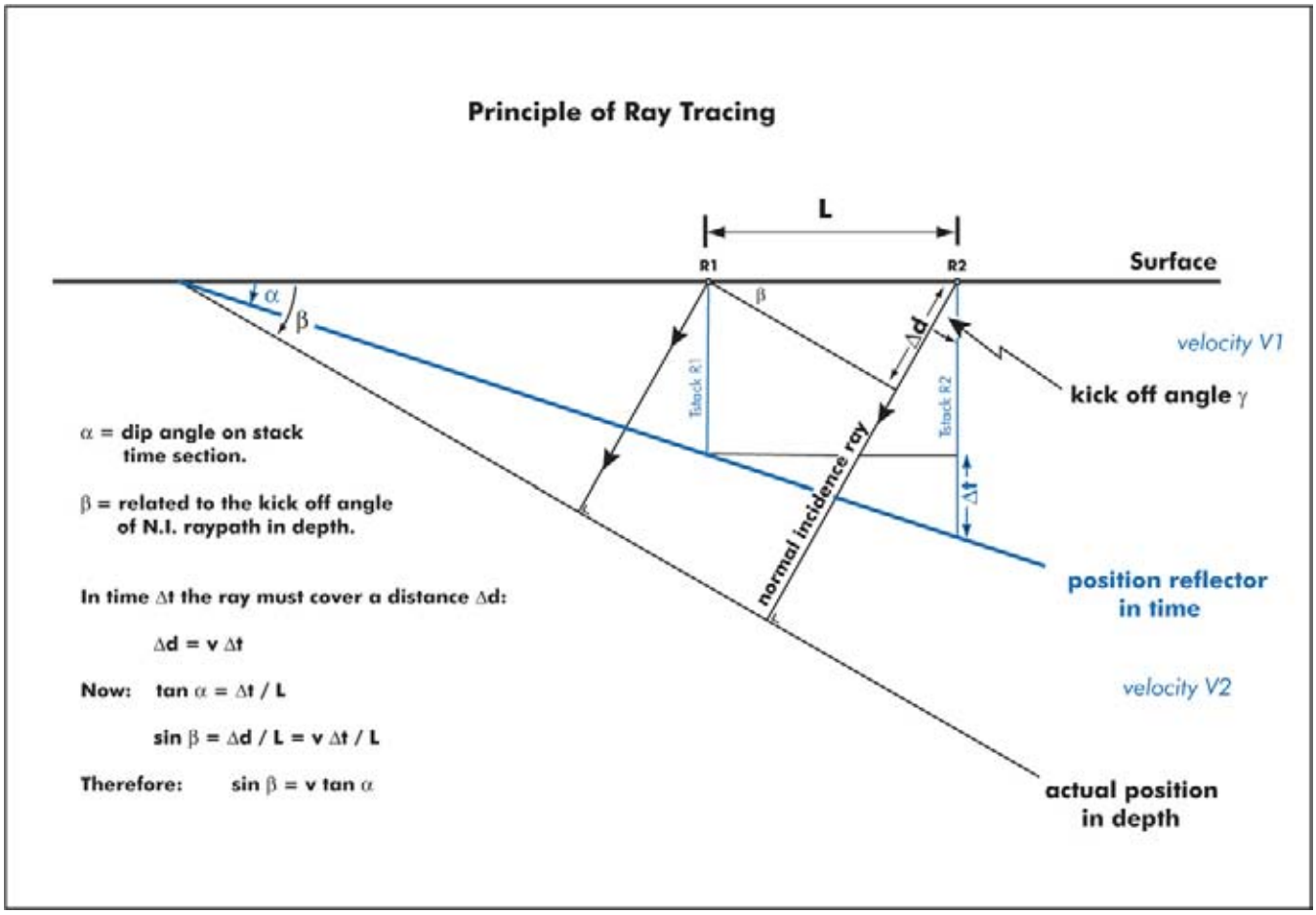

Figure 2.21: Principle of ray tracing illustrated for a single dipping interface. The travel time of the normal incidence ray is determined on the stack section. The length of the image ray is thus given and only the kick-off angle γ at the geophone position needs to be established. It is equal to $90° - \beta$ and simple geometry relates β to α in the time domain: $\sin\beta = v\tan\alpha$, whereby α is measured on the time section. Reducing ΔL to zero gives the instantaneous dip on the reflection.

2.1.5.4 Ray tracing or map migration

Ray tracing migration uses a model of the sub-surface to carry out the ray tracing exercise. The results are iteratively updated to reduce the discrepancies between the observed and calculated reflection times. This ray tracing method is the only migration technique to give satisfactory results in complex areas. It is however necessary to know the full velocity field in the subsurface to obtain the best results in the migration. In practice only a rough estimation is given by the velocity analysis in the stacking procedure. The calibrated velocities are used in the ray tracing algorithms. Iterative updating of the model is needed to refine the velocity distribution. In spite of this drawback the ray tracing migration processing does improve the quality and interpretability of the seismic data considerably. If all ray tracing steps are done fully in a 3D sense, then a very reliable velocity model is obtained. Ray trace modelling can also optimise the acquisition parameters of 3D surveys (e.g. shooting direction, Ray et al. 2004).

The input of the ray-tracing algorithm is a stack section. As seismic interpretation is usually carried out on migrated data, it means that the marker horizons have to be transferred to stack sections. This is done in a so-called **de-migration** step.

Lets first consider a simple two layer situation with one dipping interface at a given time angle α (Figure 2.21). The model is recorded in time (migrated and stack) and the velocity is known. From the stack the T_0 is read off for a given CMP position. This TWT corresponds to the 'normal incidence ray' to the first horizon. This **normal incidence** ray is the ray that shows a perpendicular angle at the reflector impact point in depth. It is assumed to be the shortest and fastest raypath to the reflector, if the velocity distribution is not changing drastically in the layer. From the local dip α of the reflector on the

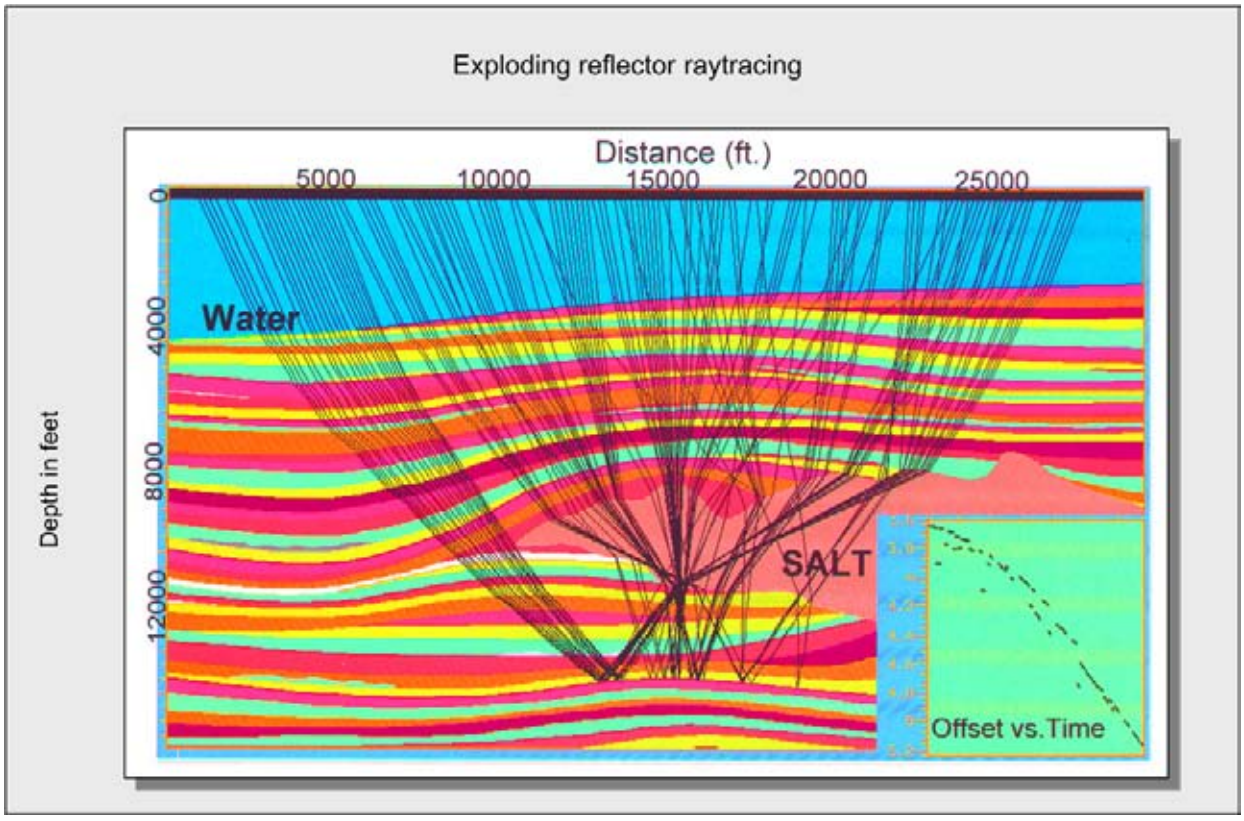

Figure 2.22: The exploding reflector ray-tracing applied on a complex depth model. At the various interfaces Snell's Law is applied. Illumination problems on the target reflector can be easily visualised in this way; i.e. problems in raypath coverage are identified where undershooting will be advisable (after Abriel et al. 1999, reprint from AAPG whose permission is required for further use).

migrated data and the normal incidence requirement, the **kick-off angle** γ of the normal incidence ray in the geophone position at the surface is calculated. A problem hereby is how to establish this dip in depth.

In the 2D starting model the dip component angle α in the two-way time domain is known. There exist a relation between α and β, whereby β is the dip of the reflector in depth measured along the section:

$$\tan\alpha = \frac{\Delta T}{l}. \tag{2.11}$$

$l =$ distance between two given X positions in between which the dip is constant.

The interval velocity is v_1, than:

$$\sin\beta = \frac{\Delta d}{l} = \frac{v_1 \cdot \Delta T}{l}, \tag{2.12}$$

$$\sin\beta = v_1 \cdot \tan\alpha. \tag{2.13}$$

Once this angle β is established, then the kick-off angle γ at the surface is easily calculated ($\gamma = 90° - \beta$). Remember that the ray-tracing is done in the depth domain and therefore the migrated position of the reflector is reconstructed. For this purpose '**image ray**' tracing has to be done on the depth section. The image ray is the raypath that has a 90 degree kick-off angle in the geophone position at the surface. The distance, travelled by this image ray in the first medium, is calculated from the measured TWT at the X location on the stack section.

$$\Delta d = \frac{v_1 \cdot \Delta TWT}{2}. \tag{2.14}$$

The **instantaneous dip** of the reflector is calculated by reducing the interval l to zero. The reflector points are reconstructed by ray-tracing in the depth domain, with launching the 90 degree ray from the CMP at the surface with length of Δd.

Let us now assume a situation with two differently dipping reflectors in their migrated position. For the second horizon the perpendicular normal incidence raypath is traced back to the surface using the exploding reflector principle (Figures 2.22 and 2.23). The ray will cross the layer 1 interface, where Snell's Law is applied to find the direction of the ray in the first medium. The ray is extended to the CMP at the surface. The stacked time section gives the traveltime for the normal incidence ray

Ray Tracing Procedure

Given: A time interpretation up to the target horizon H_n and a depth model up to layer H_{n-1}.

Objective: To find depth position of the target horizon H_n.

1) Exploding reflector *Normal Incidence* ray tracing back to surface from the H_{n-1} depth position. T_{stack} computation of all segments to H_{n-1}. Velocity gradients result in a curved trajectory and Snell's Law is applied at the encountered interfaces.
2) Determination of CMP and T_{stack} to target horizon from stack seismic section. De-migration if necessary (Geomig).
3) Computation of ΔT_{stack} in target layer between H_{n-1} and H_n.
4) Launching of *Image* ray through depth model. Snell's Law is applied at velocity/density interfaces. This is the ray path for properly migrated seismic data up to the H_{n-1} reflector.
5) The ray path in the H_{n-1} layer is established and therefore the kickoff angle of the transmitted ray into the next layer is known. Snell's Law is applied at the interface and the distance travelled in the new layer is: $d = V_{\text{int}} \cdot \Delta T_{\text{S}}/2$.
6) At the end point of the new ray segment a point of the target horizon is located in depth.

Figure 2.23: Procedure for exploding reflector ray-tracing. It illustrates how the reflector is illuminated in the seismic method and how the raypath is reconstructed.

to the second reflector at the CMP determined before. The new kick-off angle of this n.i.-raypath to the second reflector is deduced from the time dip on the migrated section. The raypath consist basically of two segments: one in layer 1 and one in layer 2. As shown in the foregoing paragraph, the time (stack and migration) and depth position for the layer 1 interface are known for each CMP or X-location.

The distance travelled in medium 2 is given by: *the total time measured for the reflection 2* minus *the time spent in the first layer*. The OWT in layer 1 depends on the reconstructed trajectory taken by the ray under consideration. The traveltime to the second layer impact point is known for the corresponding CMP on the stack. Once the amount of traveltime for the ray in the second layer is known, it is converted in a distance with the given velocity v_2. This is the distance that the ray travels in layer 2. The ray-tracing consists now of launching a image ray in the depth model under a 90 degree kick-off angle at the surface. The distance travelled in layer 1 is given by the OWT to the interface 1 at the CMP position on the stack. Snell's Law is applied and the ray is continued in medium 2. The traveltime difference and therefore the time spent in layer 2 is known. It is translated in a distance by using a velocity v_2 and the reflector point on interface 2 is located in depth. The trick is to read off the times in the stack section (normal incidence ray) and do the ray-tracing in the depth domain for the migrated position (image ray).

Visualisation of the new reflector position is a convenient way to evaluate the correctness of the procedure. Overlap of reflector segments should be avoided. Iterative updating of the input model allows fine-tuning of the results. Because the approach is 2D, only components of the dips are resolved and this will lead to discrepancies. In complex areas a proper map or data grid should be used instead to establish real dips. The lateral shift of imaging points is normally represented in tadpole plots with an annotated colour scale. These shifts can be considerable and in the order of 100's of metres depending on the geological overburden structuration. The map migration based on ray-tracing techniques gives very good results on the structure of the subsurface (cf Kleyn 1977, Ray et al. 2004). However, the number of velocity layers, that are considered, should be sufficient. The output is depth maps, so the seismic cube itself is not converted to depth. The latter is only done in the depth migration procedure described below.

2.1.5.5 Depth migration

Depth migration (or depth imaging) uses a velocity model for the layered earth, which is iteratively updated by conversion back into time of the depth migration results and comparing the two seismic sections. One of the techniques is **PSDM** or prestack depth migration. In the prestack approach the velocities are updated in **CRP gathers**, which are CMP gathers in depth (Figure 2.24); these gathers are also known as **image gathers** (e.g. Schulz 1999). CRP stands for Common Reflection Point. Migration scanning techniques are applied on the CRP gathers (Jones et al. 1998, Jones 2003). This means that the velocity model is perturbed with a certain percentage and the gather with the best imaging and event flattening is retained (focusing technique, Robein 2003). This is done in a layer-per-layer manner,

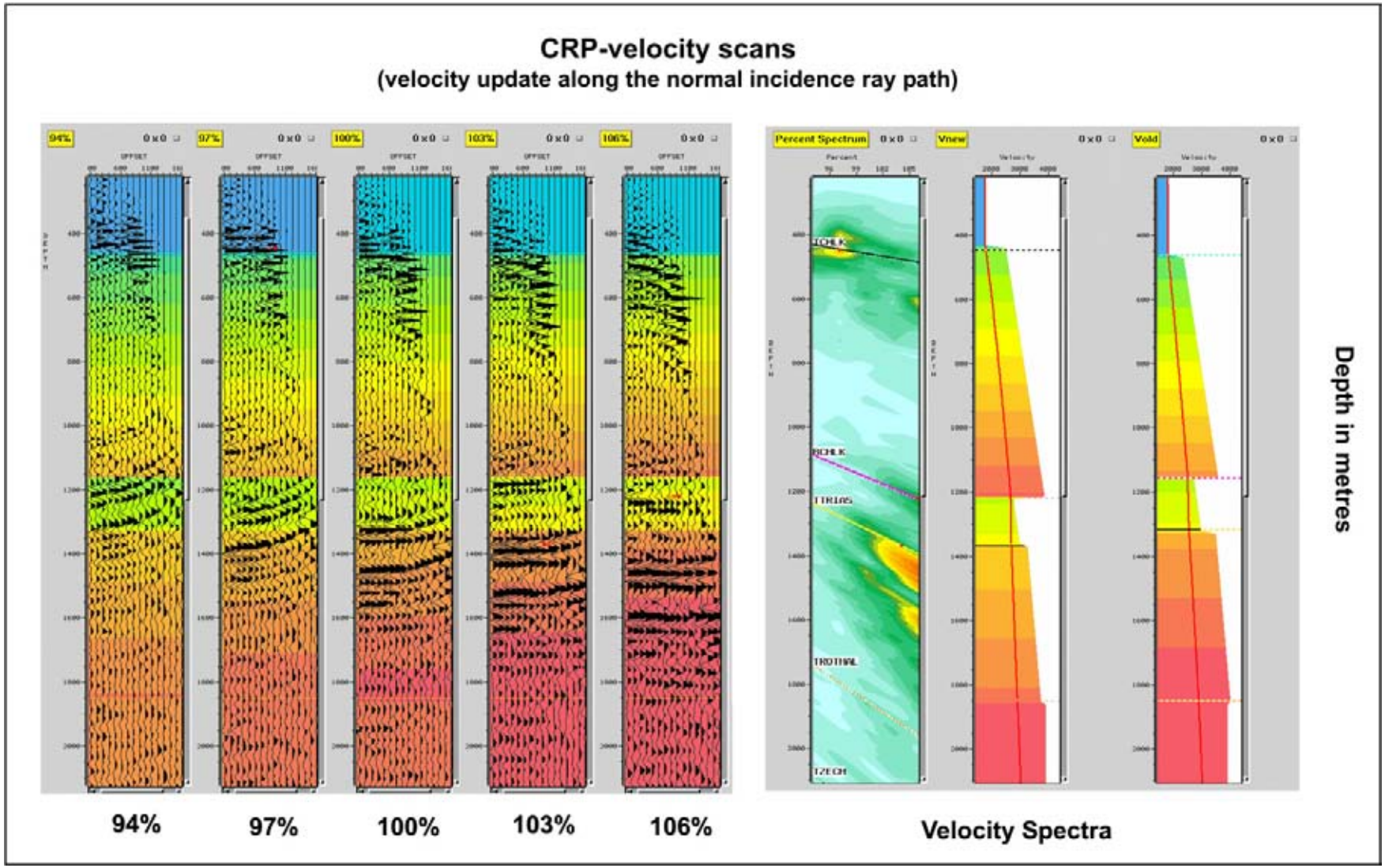

Figure 2.24: Example of a CRP gather (or image gather) which represents basically a CMP gather in the depth domain. The iterative flattening of the reflections in the CRP gather allows to compute a more accurate velocity model, suitable for subsequent ray tracing and depth conversion. A velocity scanning method is used to update the velocity field (courtesy CGG).

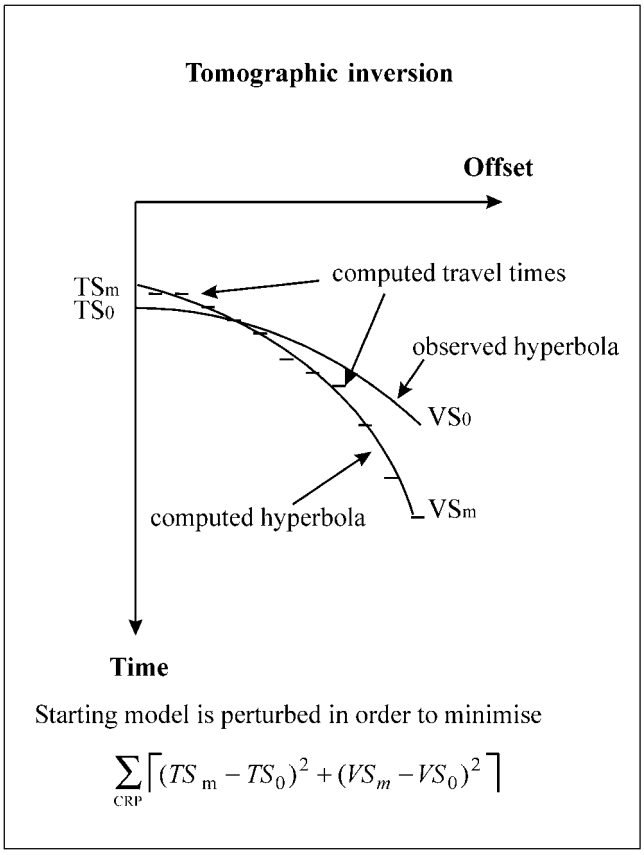

Figure 2.25: Tomographic inversion techniques are used to determine an accurate velocity model in an iterative way. The ray tracing allows to find a velocity depth model that best fits the observed time data. Here it is done on a gather, but it is equally applied on time sections or a migrated stack seismic cube (courtesy CGG).

applying an iterative approach. The velocity model is then smoothed. This velocity smoothing has as consequence that individual NMO-corrected CRP gathers do not always show 100% flat reflections. Ray tracing is used in the overburden layers to determine the traveltime of the rays. Ray bending is properly taken into account. **Ray bending** depends on the velocity changes and is linked to acoustic impedance changes (Sheriff 2002). Important is to select the correct number of layers to start with. Mostly this can be derived from the various units seen on the velocity logs in the wells. Tomographic inversion, with normal incidence ray tracing, is utilised to build an accurate velocity model in an iterative way for the layer-by-layer approach (Figure 2.25).

Kirchhoff depth migration handles much better the lateral velocity changes related to steeply dipping reflectors and a complex geological overburden (Figure 2.26). For better comparison between the PSTM and PSDM results, the PSDM output should be converted back into the time domain. The cost involved for this type of PSDM depth imaging is the main reason why it is not yet run on a routine basis. Parallel computing and cluster technology of PC's is however a cost effective solution nowadays. It even puts wave equation depth migration within reach of the interpreter. Most Kirchhoff migration algorithms consider the first arrival or a high energetic event and the migration will not image correctly energy stemming from an alternative travel path. It might result in less reliable migration below high velocity layers, especially when the interface shape is rugose. Wave-equation migration is capable to provide a solution for the wavefield in depth taking into account all travel paths (Pharez et al. 2005). Wave-equation migration is applied in the shot domain. It can be based on either the shot gather (shot profile migration) or shot-receiver data (common azimuth and narrow azimuth migration; Bevc and Biondi 2005). It considers both the down- and upcoming wave-fields. It is possible to extract the local angle information from the wavefield and compute artefact-free angle gathers for velocity depth evaluation and residual moveout determination. The amplitudes are better respected by applying innovative weighting schemes (e.g. Voronoy or Beylkin). High dips should be properly captured by a sufficiently wide aperture of the migration operator (Yilmaz 2001). An other advantage of the wave-equation migration is the simultaneous handling of multi-valued arrivals, amplitude and anti aliasing issues in one pass, without the necessity of a high frequency assumption (Pharez et al. 2005).

Anisotropic wave-equation migration is also feasible. A stable anisotropy parameter estimation is obtained when intergrating seismic and well data, or as shortcut general geological constraints help to make a better estimation (Bear et al. 2005). V_0 is determined by comparing the checkshot and the sonic velocities with the seismic velocity. Then the delta, which represents the short spread deviation from the V_0, is estimated by flattening the gather on the well location for the near to mid offset range traces after applying the appropriate V_0 trend. Then the epsilon is determined from the remaining residual moveout at the far offsets. Tomography can be used to build a more accurate velocity model, with Cost function analysis (extreme determination method) and proper weighting.

A great advantage of depth migration is that the interpreter has immediately depth sections or a depth cube at his disposal. Time distortion artefacts are removed in the depth representation, if everything is done correctly. The interpreter should realise that there are still some uncertainties related to this type of depth conversion. The degree of smoothing of the velocity field is particularly a matter of concern. With a good velocity field the focusing of the depth migration operation is superb

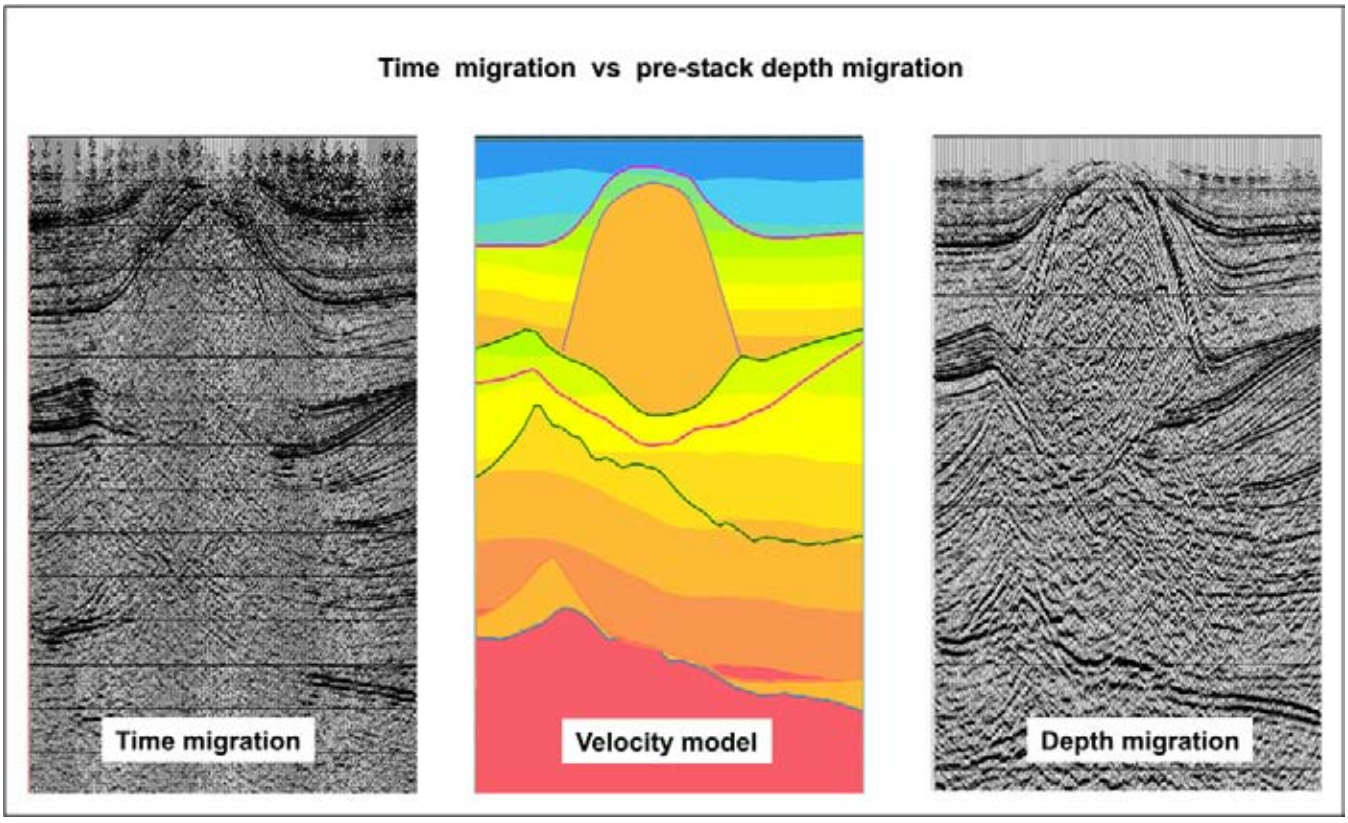

Figure 2.26: Comparison between time migration and Pre-stack Depth Migration (PSDM). The PSDM depth section shows an increased resolution, because the velocity model is more accurate and the processing procedures are more efficient. The flanks and base of the salt is much better imaged (courtesy CGG/BEB).

(e.g. CGG's PSDM of the Elsflet 3D survey, BEB). It really can improve dramatically the interpretability of the seismic data. 3D prestack depth migration processing with preserved amplitude is of course the best solution (Baina et al. 2002).

When is depth migration needed? Only if the dips are steep and/or strong velocity variations exist. The reflection hyperbolas are under such conditions no longer symmetrical around the T-axis, but they are skewed due to ray bending effects. Again, the image ray is used to evaluate the necessity to do depth migration. Remember that the image ray is the raypath that arrives at a vertical angle in the geophone. If no velocity irregularity exists, this image ray is located straight above the apex of the reflection 'hyperbola' in the CMP gather. If the X-position is different for these two points, then depth migration is advisable. When the amount of shift of the apex is small, it can safely be ignored. This is the case for low to moderate dips. Non-hyperbolic move out points to lateral velocity changes and/or anisotropic behaviour in the overburden that should be resolved, if longer offsets are to be utilised in the imaging.

PSDM was cited as critical success factor in the discovery and appraisal of many deep-marine reservoirs, because the imaging of the reservoir architecture is superior and resolving some of the problems in the delineation of the field extent for multi storied channels that form stratigraphic traps (Weimer and Slatt 2004). In fact this goes for other settings as well. PSDM will move from special processing towards a more standard routine in the near future as the advantages and added value are gradually better realised by geoscientists.

2.1.6 Common Reflection Surface processing

An alternative to prestack depth migration is the CRS (common reflection surface) processing technique proposed by Bergler et al. (2002). Opposed to the CMP stack, the traces are not restricted to one gather, but data can come from areas in the vicinity of the zero offset X_0 location (Jaeger et al. 2001). In this way **supergathers** are created. This special processing increases the signal-to-noise ratio and produces high resolution time sections (Gierse et al. 2003; Figure 2.27). The data

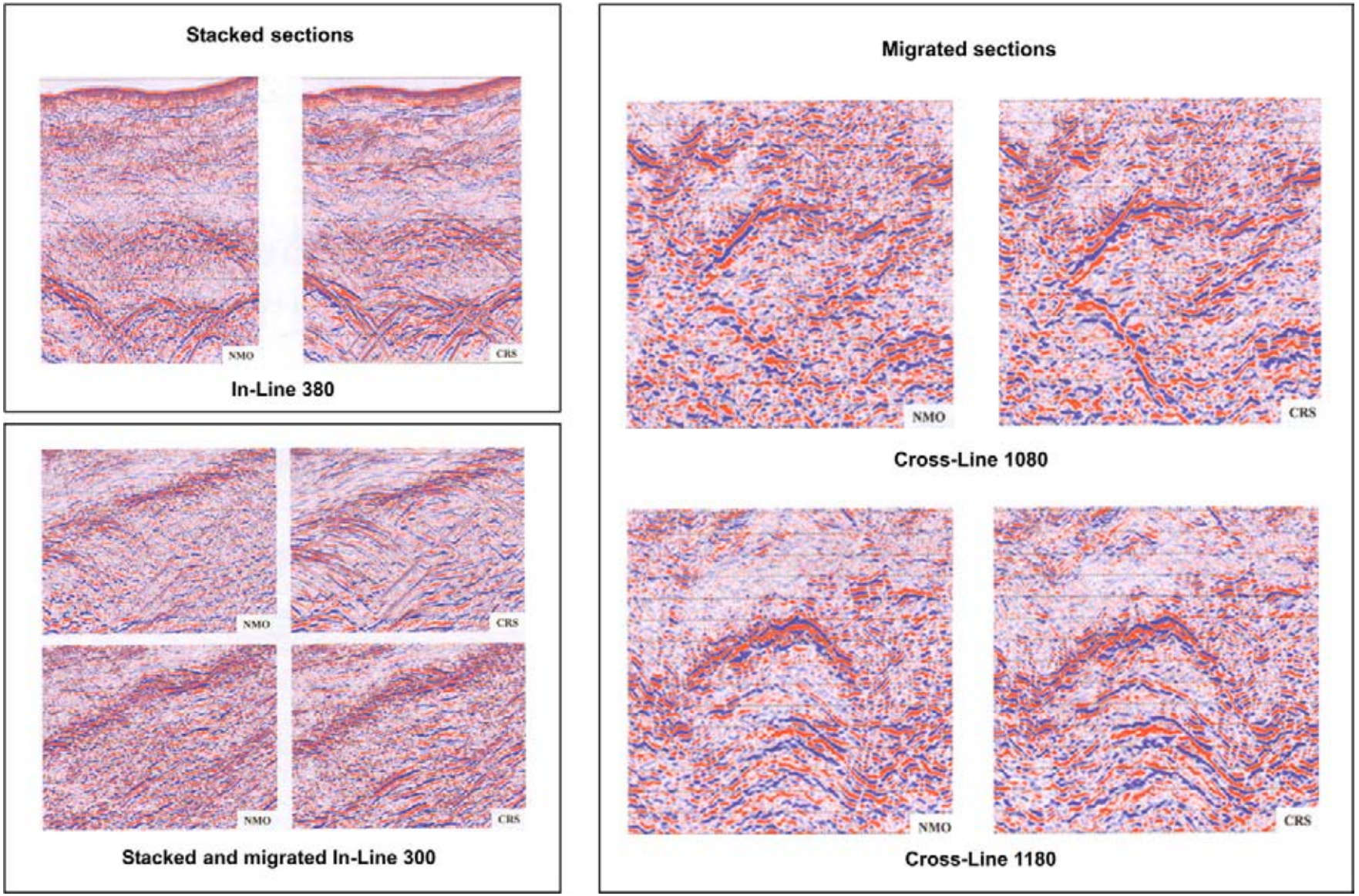

Figure 2.27: CMP and CRS processing comparison for data from offshore Costa Rica. The Common Reflection Surface technique uses a super gather and does not need a macro-model as input. The lack of such a requirement can improve the S/N-ratio considerably (modified after Giese et al. 2003).

in the gather is not assumed to stem from individual reflection points in depth, but comes from local reflector elements. These elements constitute a common reflection surface that has a dip and curvature. The stacking procedure needs three parameters as input (Preussmann et al. 2004):

- α, the emergence angle at the surface for the normal incidence ray to the subsurface reflector.
- R_{NIP}, the radius of curvature of a wave from a point source at the normal incidence point on the reflector.
- R_{N}, the radius of curvature of a wave from an exploding reflector at the subsurface reflector.

A simple guiding model is used for the ray tracing that is optimised in semblance representation for each time sample in the stack zero offset section, while the conventional NMO stacking procedure requires a detailed velocity model that is often tricky to calculate.

The CRS method yields eight different seismic attributes, that can be looked at by the interpreter. Subsequent post-stack depth migration is claimed to give comparable results to the PSDM method at considerably lower costs. In addition, the AVO analysis is improved in this kind of processing (Preussmann et al. 2004). The practical usefulness of the CRS processing has still to be proven, but it looks a promising working domain in the near future.

2.1.7 Tau–P domain processing

For a ray travelling at a certain constant angle θ_1 it is known that:

$$\frac{\sin\theta_1}{v} = \text{constant} = p. \tag{2.15}$$

This constant 'p' is also known as the **ray parameter**. Instead of sorting all seismic data to shot and CMP domains, it is possible to sort the energy in a **Tau–P domain**. Tau is standing for the corresponding traveltime. In the Tau–P domain also processing can be done and this has certain advantages (Figures 2.28 and 2.29). Sometimes localised energy patches are related to noise and these can be filtered out quite conveniently. A $p = 0$ corresponds to a horizontally downward moving wavefield.

In the Tau–P domain the seismic energy is decomposed in individual plane wave components. In case of a horizontally layered subsurface, a '**slant stack**' is obtained by applying a linear move out and summing the amplitudes over the offset axis. Migration can also be done in this domain.

2.1.8 3D seismic surveys

The basic tools for the seismic stratigrapher are seismic sections, surface geological information and well data. The seismics are either stemming from 2D or 3D seismic surveys loaded on a workstation. The basic difference is that the 2D seismic lines are often spaced 2.5 km apart and will follow individual directions (crooked if need be), while the 3D is processed with a well organised line spacing that is normally 25 or 12.5 metres apart, depending on the bin size. Marine streamer 3D acquisition is basically 2D and therefore it samples data with one azimuth (Cambois, TLE, Vol. 24, No. 5, p. 474).

The **bin** is a rectangular area used in processing and it brings the data to a regular grid, defined by the bin centres. The size of the bin is dictated by the sampling theory which states that at least two samples per wavelength of the highest frequency need to be recorded. Normally the line spacing is taken as a dimension and the receiver point or common depth point is assigned as centre of the bin. Usually the data within the bin is simply projected to the bin centre. This approach introduces extra jitter in the stacked data. It would be better to interpolate the value to the bin centre (Gausland 2004). This type of processing noise can be even worse when using the flexi-binning method, whereby the bin centre can be filled with data from adjacent bin areas. Such simplistic binning technique has a detrimental effect on the anisotropy analysis of a seismic dataset. If detailed reservoir characterisation is required then a more delicate procedure should be implemented, that better respects the azimuthal information of the data.

2D lines are often interpreted on paper sections. The intersections in a 2D survey are often not tying very neatly and small corrections are necessary. Between surveys the problems can be even worse. These discrepancies are mainly introduced by differences in the migration operator. Severe structural aliasing problems are caused by irregular line layout and wide spacing between 2D lines. Amplitude regularisation may prove necessary (cf Delaughter et al. 2005).

The huge amount of data in a 3D survey requires a different interpretation approach and usually a seismic workstation is used. Large 3D exploration surveys are acquired on a routine basis in more mature areas (e.g. Gulf of Mexico, NW Europe, Middle East, SE Asia), illustrating the cost effectiveness of such operations. Harmonising individual 3D surveys and merging them together in a larger regional 3D dataset is a substantial effort, but very much worthwhile (Brown 1999, Bacon et al. 2003, Veeken et al. in press). The 3D working environment is preferred nowadays because it has certain advantages:

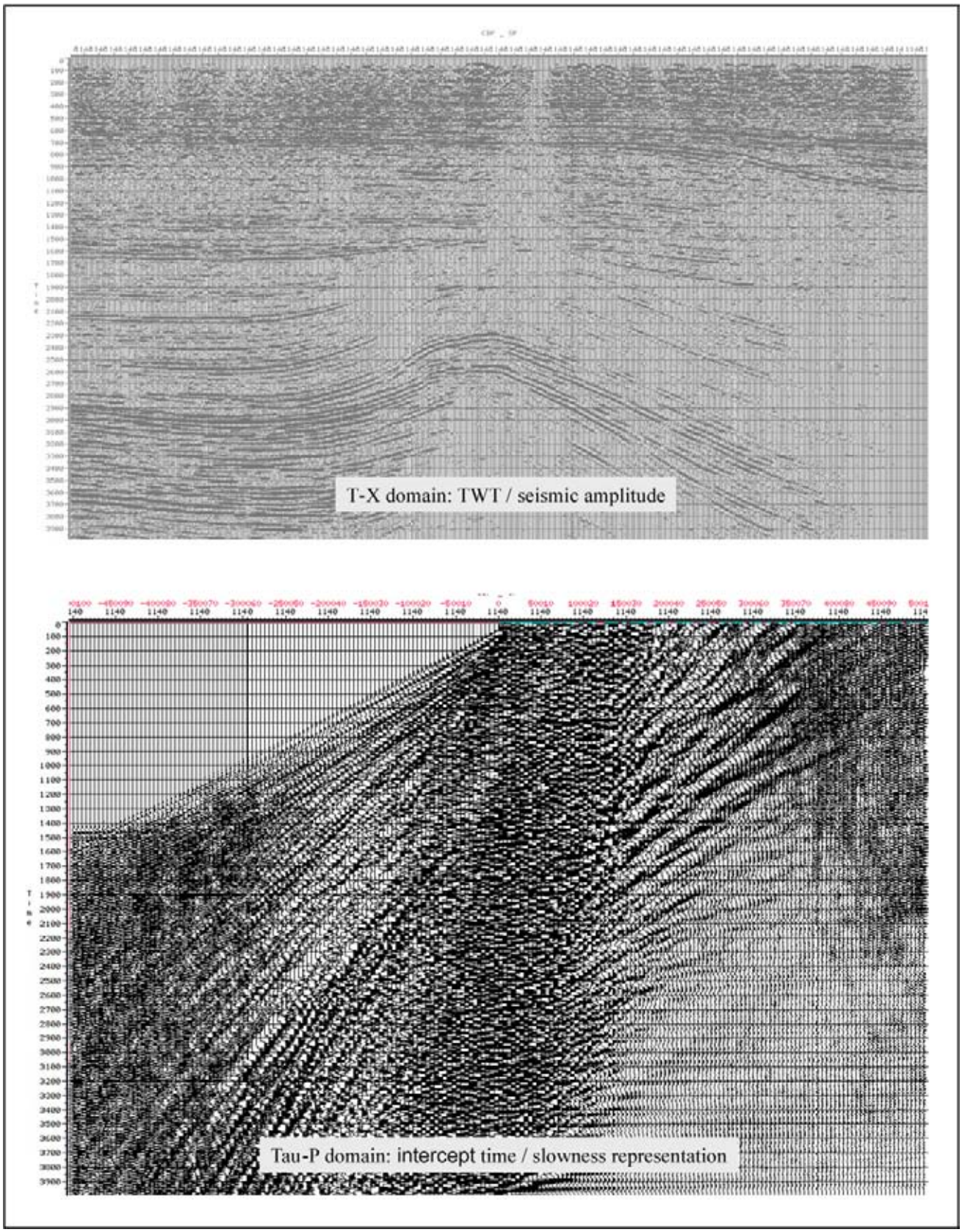

Figure 2.28: The time section is transformed into a Tau–P domain representation by means of the Radon transform. A difficulty with this type of processing is the later re-transformation back into the time domain, but the algorithms are improving (courtesy Pemex).

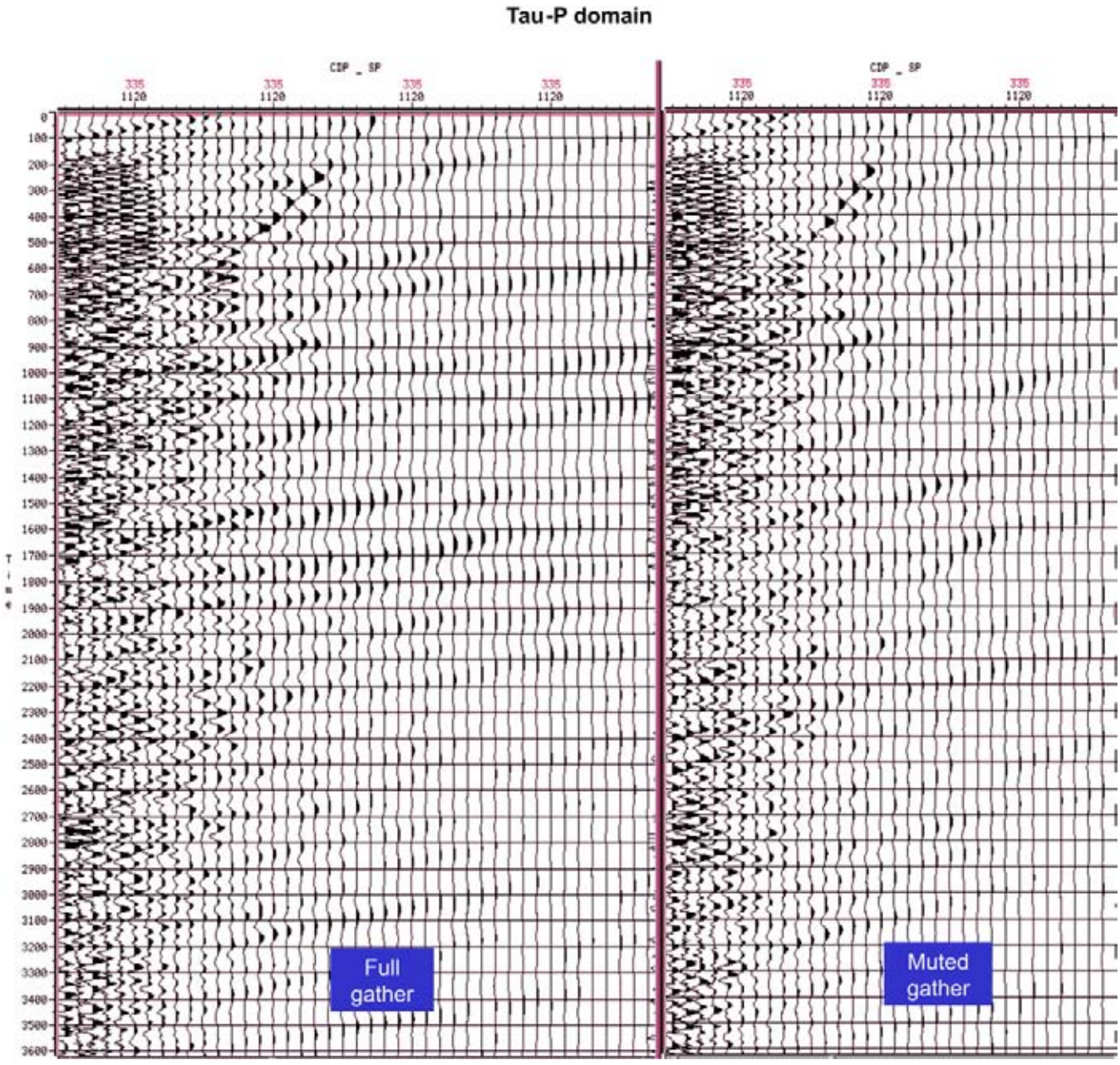

Figure 2.29: Tau–P domain: intercept time/slowness representation of CMP gathers (courtesy Pemex).

– Better structural definition of the subsurface, with less structural aliasing effects. Aliasing means here the false line-up of the faults due to limited seismic sampling. Lines every 25 metres apart is better than a line spacing of 1 kilometre.
– Direct connection with well data base for calibration purposes. Identification of markers along deviated well trajectories and convenient well-to-seismic tie options.
– The possibility to create time slices and arbitrary seismic lines through the large seismic data volume.
– Visualisation of 3D seismic data cubes.
– Easy flattening on time horizons to study the depositional geometries.
– Automated and easy extraction of seismic attributes (e.g. time thickness, amplitude) to assist in the evaluation of the data set.
– Voxel displays (3D pixel defined volumetric unit) and volume rendering.

3D seismic surveys play an essential role in integrated field studies (Vazquez et al. 1997). The 3D seismic

data has clearly proven its benefits by augmenting the drilling success ratio substantially. The number of dry wells has been reduced considerably over the last two decades (Brown 1999). This trend was mainly driven by the improved reservoir mapping (cf Ruijtenberg et al. 1990). Basin wide 3D surveying is in many cases a viable option (Davies et al. 2004). However, in frontier areas and virgin territory the 2D surveying mode is still preferred, as is illustrated by the 2D data shot in 2005 by the Shell/Total/Aramco consortium searching for gas in the Rub Al Khali desert in southern Arabia. It is considered cost effective for the initial inventory of the prospectivity of a region and when only large HC traps are of interest.

The above described developments are very exiting, but let us first come back and have a closer look at the seismic dataset, to what kind of information it actually represents. Once the limitations of the seismic reflection method are known, then the seismologist is in a much better position to proceed with the other relevant interpretation tasks.

2.2 Seismic Resolution

Seismic reflections are generated by interfaces between rock units which show sufficient velocity–density contrasts. The multiplication of density and velocity is known as the **acoustic impedance** value of a layer. The number of reflecting interfaces is not only related to the amount of Rho–Vee contrast, but also depends on other factors like for example:

- Original shape of the seismic input wavelet.
- Frequency and bandwidth of the recorded data.
- Filtering/automatic gain level applied.
- Interference effect caused by the presence of closely spaced bedding planes of different lithologies.
- Interval velocity of the rocks.

The geologist relies in the field and laboratory on a virtually unlimited resolution of the bed thickness. In the borehole, however, the geoscientist is limited by:

- The sensor arrangements in the measuring devices.
- Frequency of the input signal.
- Recording speed.

A resolution of 30 cm is generally achieved by the standard well logging methods and sometimes it is even better (e.g. Boyer and Mari 1994). The resolution power of the conventional reflection seismic method is more poor and only under favourable circumstances individual beds of 10 metres are resolved.

2.2.1 Vertical seismic resolution

The vertical resolution of seismic data is determined by:

- The frequency of the seismic signal.
- Its bandwidth.
- The interval velocity of the investigated rocks.
- The acoustic impedance contrast.

Special high resolution surveys (100 MHz input signals with boomers and pingers as a sound source) have an increased vertical resolution of up to 10 cm, but here the penetration depth of the signal is much reduced (10 metres). The Ground Penetrating Radar technique, using an electromagnetic signal as input, has a resolution up to 5 cm (Laitinen et al. 1996, Veeken et al. 1999). The display of GPR sections resembles that of reflection seismic data (Figure 2.30). Similar interpretation techniques can be applied (Dagallier et al. 2000). There is a difference between resolution and **detection capability**. Resolution deals with clearly separate events, while detection exploits subtle interference effects to distinguish individual layers.

The seismic resolution is depending in a multi-layered case on the vertical spacing between the layers. It can be demonstrated that, if the layers are too closely spaced together, the reflected seismic energy from both interfaces give rise to interference patterns (cf Sheriff 1977). In such situations the two-way time interval between two interfaces becomes too narrow, the reflected wavelets will overlap in time and a complex composite waveform is registered. It also implies that boosting of the signal's amplitude is to be expected, if the interference is positive (constructive interference). It decreases when the interference is negative (destructive interference, Figure 2.31). As a consequence the bed thickness distribution plays an important role in determining the vertical resolution power of seismic sections.

The **bed-thickness resolution power** normally decreases with increasing depth (e.g. Widess 1973, Sheriff 1977, Hilterman 2001). This phenomenon is caused by the fact that higher frequencies get absorbed progressively when seismic energy is travelling at an increased depth (or distance) within the Earth's crust. This means that the wavefront is travelling a larger distance before it is captured by the geophone and hence more **frictional losses** occur. Additionally, interval velocities at deeper levels are higher in response to ongoing compaction and diagenesis. **Diagenesis** is the cementation process taking place in the pores between grains, that leads to lithification of unconsolidated sediments. Compaction can be mechanical or chemically driven (cf Storvoll et al. 2005). The chemical compaction is the result of dissolution and precipitation. It is mainly a temperature controlled process.

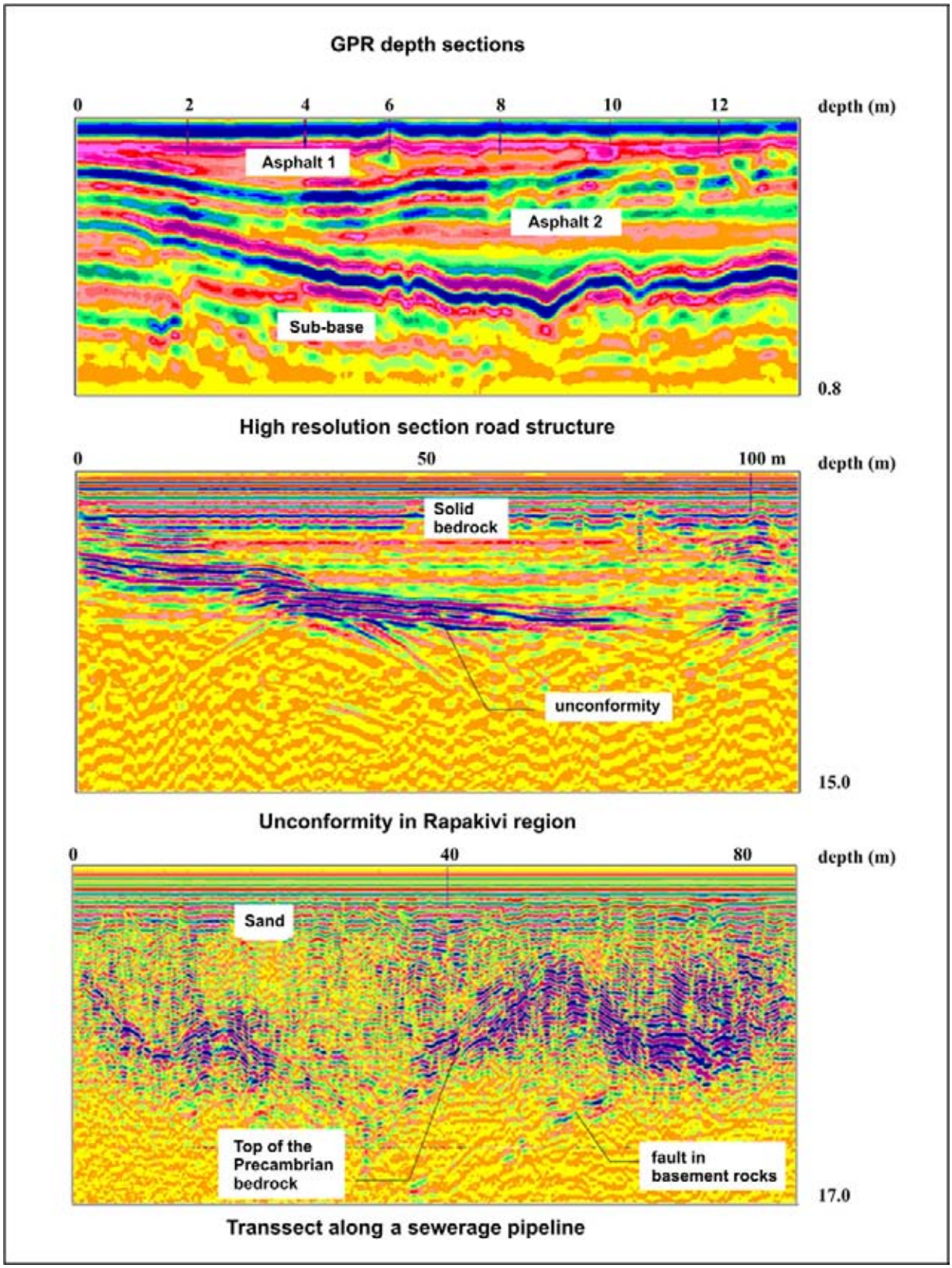

Figure 2.30: Ground Penetrating Radar sections, using an electromagnetic input signal, are quite similar in display to reflection seismic sections. Note the high resolution aspect of the profiles and the small penetration depth. A high clay content of the rocks has a negative effect on the propagation of the electromagnetic signal (courtesy Viatek/Geofox).

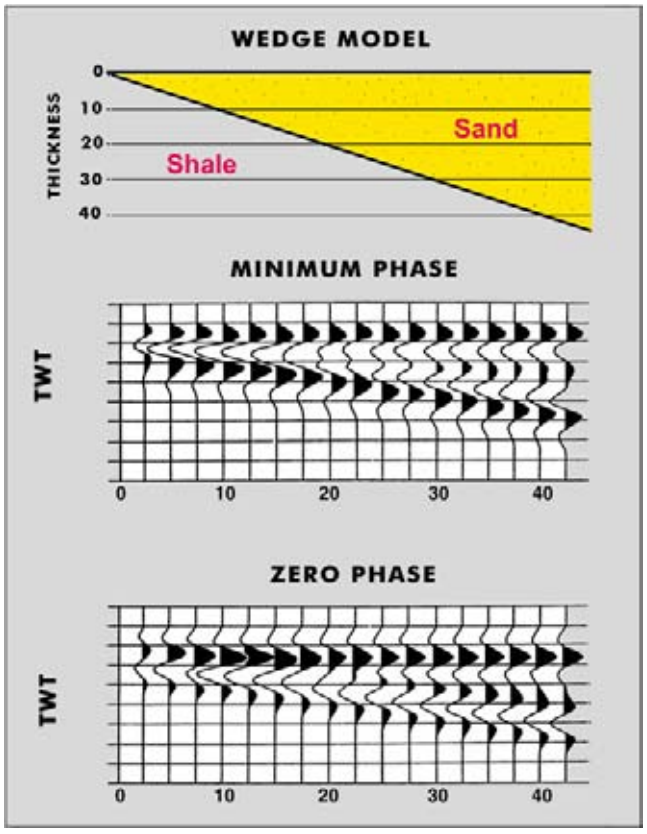

Figure 2.31: Seismic interference pattern of reflections from interfaces belonging to a wedge-shaped body. Note the lateral change in amplitude of the individual reflections. The overlying and underlying sediments are the same. The wedge has a 2500 m/s interval velocity. A 50 Hz wavelet is equivalent to 50 cycles per second and results in a 20 milliseconds basic waveform with a wavelength of 50 metres. The time lines are 10 ms apart (after Sheriff 1977, reprint from AAPG whose permission is required for further use).

Precipitation of quartz usually starts around 70 to 80 degrees Celsius, illitisation of the smectite clay mineral also occurs in this temperature range.

The amount of noise on seismic traces does also limit the seismic resolution. The S/N ratio is typically defined as being simply the logarithmic ratio of the maximum amplitude on the signal and the noise spectra (Long 2003). For a S/N of two the signal clearly dominates the visual aspect of the data (Junger 1964). The stacking procedure improves the S/N ratio by a factor square root of n, whereby n is the fold or coverage of the CDP point (Kearey and Brooks, 1991). Other factors contribute to the clarity of seismic images: geophone lay-out, shooting template, illumination discontinuities (Figures 2.32 and 2.33). High-quality illumination and high quality spatial sampling is paramount to obtain better sections (Long 2003). Ray tracing can be used to illustrate the subsurface coverage along a reflector (e.g. De Beukelaar et al. 1998). Overburden related problems can have an effect on the amplitude behaviour seen on the deeper target levels (Ibrahim 2005).

The vertical resolution can be artificially reduced (or attenuated) by applying **high-cut frequency** filters. This filtering is usually done as a quick way to reduce the amount of background noise in the data. **Anti-aliasing** filters (suppressing artificial line-ups due to sampling interval) are renowned for their negative effect on the resolution. Filtering also affects some of the genuine data and decreases therefore the theoretical resolution power. Care should be taken, when applying the filters, not to destroy the interpretability of the seismic data. **Hands-off acquisition** techniques assure that the filtering in the field is kept at a minimum, so that all cleaning efforts can be efficiently done in the lab afterwards (Ongkiehong and Askin 1988).

2.2.2 Horizontal seismic resolution

Not only vertical resolution limitations exist, but also in a horizontal direction there are restrictions. The lateral resolution is controlled by the **trace spacing** and therefore by the distance between the subsurface sampling points. The CMP spacing normally ranges between 50 and 12.5 metres. For analysing the lateral resolution, it is necessary to take into account the difference between stacked (i.e. un-migrated) and migrated seismic data. As stated already before, the stacking process is only correct when dealing with non-dipping reflectors and in the case that no strong lateral velocity changes exist in the subsurface. If these assumptions are not valid, then it is incorrect to plot the summed energy straight under the Common Mid Point. An additional correction is needed to compensate for this positioning error.

2.2.2.1 Fresnel zone

Reflected energy, detected by the geophones at the surface, travels in the earth via the so-called '**Fermat path**'. The Fermat path is '*the path for which the traveltime between two points in the medium is at a minimum*'. If there exist velocity changes in the subsurface, this path will not be straight. It is curved in such a way that the overall traveltime is minimised. The recorded signal on stacked seismic sections is not only composed of the reflected signal, travelling along the Fermat path between the 'shot location / reflector impact point / receiver position at the surface', but – as a 3D wavefront with a certain wavelength is emitted at the shot – also neighbouring interception points on the reflector will contribute to the received signal in the geophone (Hubral et al. 1993).

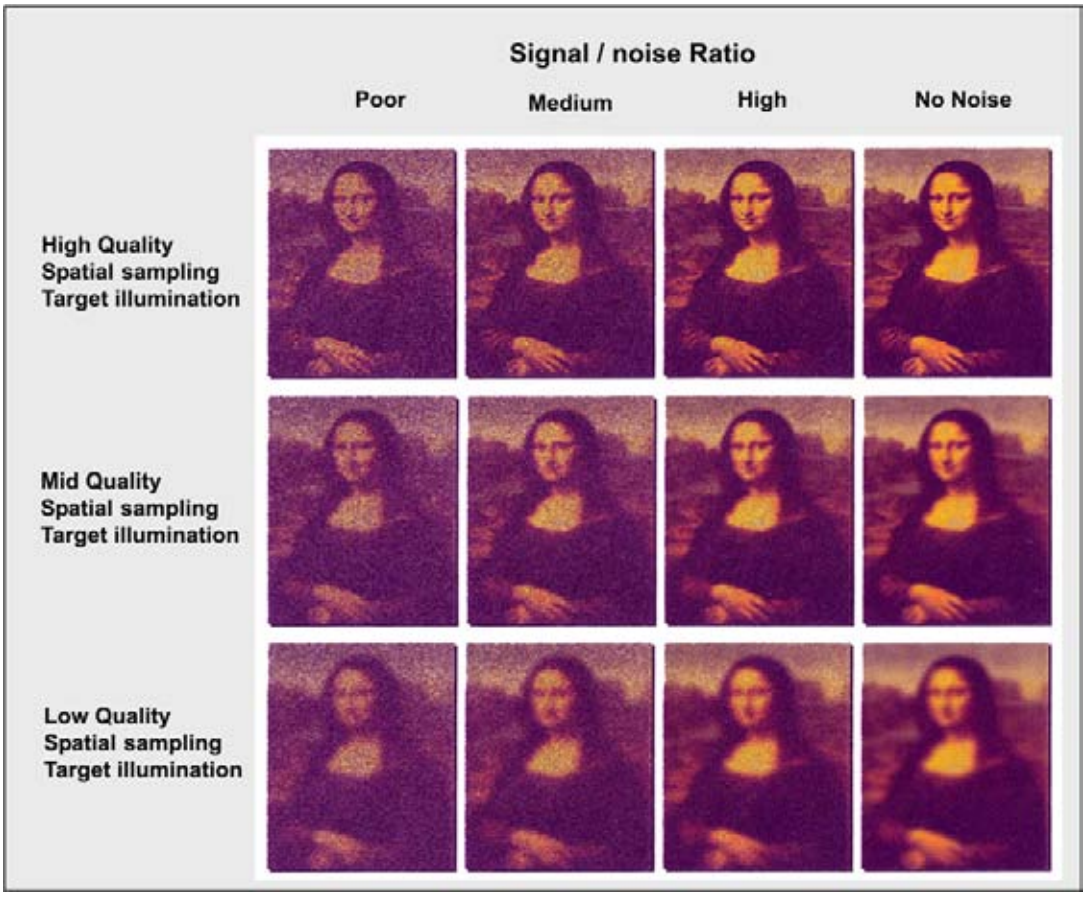

Figure 2.32: The influence of noise, spatial sampling and target illumination in the stacking procedure is illustrated on an image of the Mona Lisa (modified after Long 2003).

This area, contributing to the energy of the reflected wavefront, is known as the **Fresnel zone** (Figure 2.34). The radius of the Fresnel zone depends on the wavelength of the acoustic signal and also on the depth of the reflector as the wavefront gets wider with increasing depth. The Fermat path belonging to an individual image point is also known as the **specular ray** (Tabti et al. 2004). The Fresnel zone in the time domain gets translated in the equivalent **Fresnel aperture** in the depth domain. A Fresnel Aperture Kirchhoff Depth Migration is proposed, whereby the diffraction curve is used over a limited areal extent, that corresponds to the Fresnel aperture. This technique gives very encouraging results in bad data zones (Tabti et al. 2004).

The lateral resolution of the seismics is depending on:

- Bandwidth or frequency content of the pulse.
- Interval velocities.
- Two-way travel time to the top of the reflecting unit.

Figure 2.35 illustrates the effect of these parameters on the seismic response of a 200-metre gap in a reflector at various depths. The gap in the modelled reflector cannot be detected on the seismic section below a two-way time (abbreviated TWT) of two seconds. As stated earlier, the frequency of the input signal influences the lateral and vertical resolution of the seismic data. In Figure 2.36, the difference in resolution power of a 20 and 50 Hz wavelet is shown. The separation of individual sandstone layers is much better for the higher frequency signal. High frequencies get much faster absorbed in the earth and their penetration depth is less. Therefore a 8–60 Hz bandwidth is typical in conventional seismic processing. Efforts are made to boost the frequency contents to its upper limit, but the success for each survey depends on the overall conditions of the dataset. Claims of reliable seismic reflection data with frequencies up to 120 Hz at 3 km depth should be taken with some scepticism.

2.2.2.2 Raleigh radius and Hubral shift

The migration step generally improves the lateral resolution of the seismic data, as all in-line scattered energy

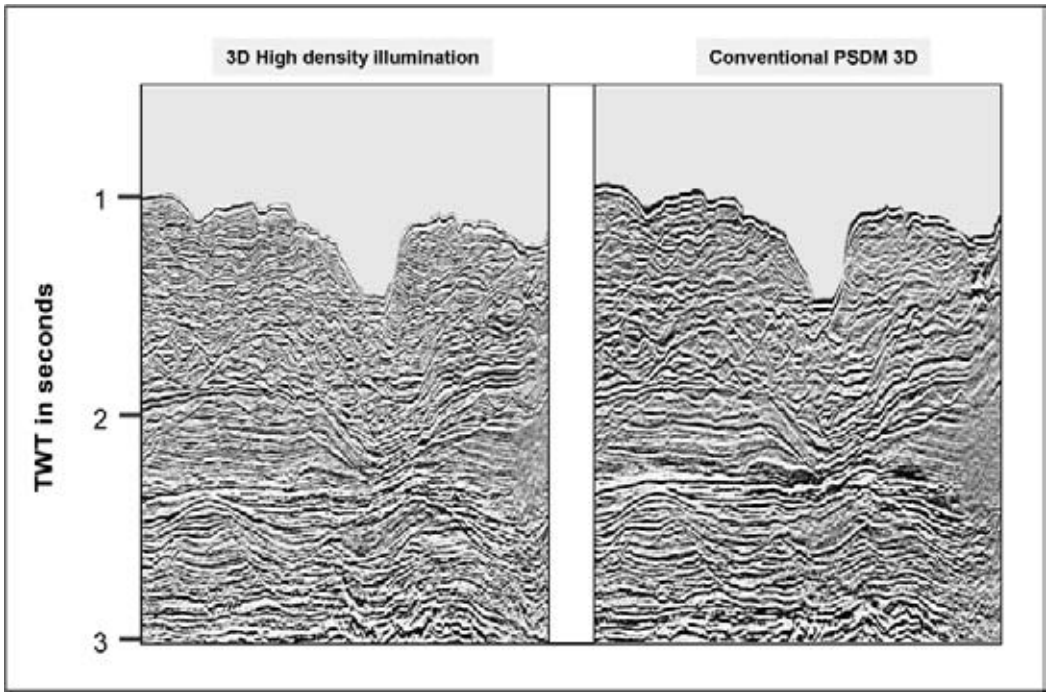

Figure 2.33: A high density illumination line across the Malampaya structure in the Philippines by applying better 3D acquisition techniques. The conventional section on the right has a bin of 13.33 m by 26.66 m and 95,000 traces per km^2, while the HD3D bin size is 6.25 m by 12.5 m resulting in 691,000 traces/km^2. The conventional PSDM section has been converted to a time scale for this comparison (modified after Long 2004).

is positioned more correctly. The migration processing uses velocity information to re-position the reflected data. Inaccuracies in these migration velocities – together with the limited width of the migration operator, the influence of noise and the bandwidth of the seismic data – does put constraints on the horizontal resolution. In analogy with the Fresnel zone radius on stack sections, the lateral resolution of migrated data is dependent on the **Raleigh radius**. This radius is determined by the:

- Length of the migration operator.
- Wavelength of the signal.
- Depth of the reflector.

Migration tries to compensate the amount of obliqueness (skewness) and asymmetry of the reflection hyperbolas along the time-axis in a CDP gather, due to dipping reflectors and velocity anisotropies (cf Dautenhahn et al. 1994, Tsankin and Thomsen 1994). It usually does this in an in-line direction and hence only under special circumstances the true 3D nature of the geology is correctly compensated. The residual discrepancy in reflector position after migration is known as the '**Hubral shift**'. The Hubral shift is directly related to ray-bending of seismic sound waves within the 3D rock volume. This is caused by internal changes in interval velocity and the geometry of the subsurface reflectors overlying the target horizon (Hubral 1977, Yilmaz 1987).

2.3 Amplitude and Frequency

The amplitude behaviour of a reflection gives valuable information on the lithologies at both sides of the acoustic interface. The amplitude is proportional to the velocity–density contrast and depends on the lithologies inclusive their porefill.

Maps, displaying attributes of individual horizons, are compiled to examine the behaviour of a reflector over the studied zone. For example the amplitude of a specific reflection is investigated in this way (Figure 2.37). If lucky, anomalies are observed on the amplitude map that are related to the outline of hydrocarbon accumulations.

A remark of caution has to be made here: 5% hydrocarbon saturation in a reservoir can already trigger considerable amplitude and velocity anomalies, but these occurrences are not commercial.

2.3.1 Wave propagation and elastic attributes

The seismic amplitude is directly related to the square root of the energy contained in the waveform and depends on the **elasticity moduli** of the media. These moduli govern the rock behaviour to deformation, when

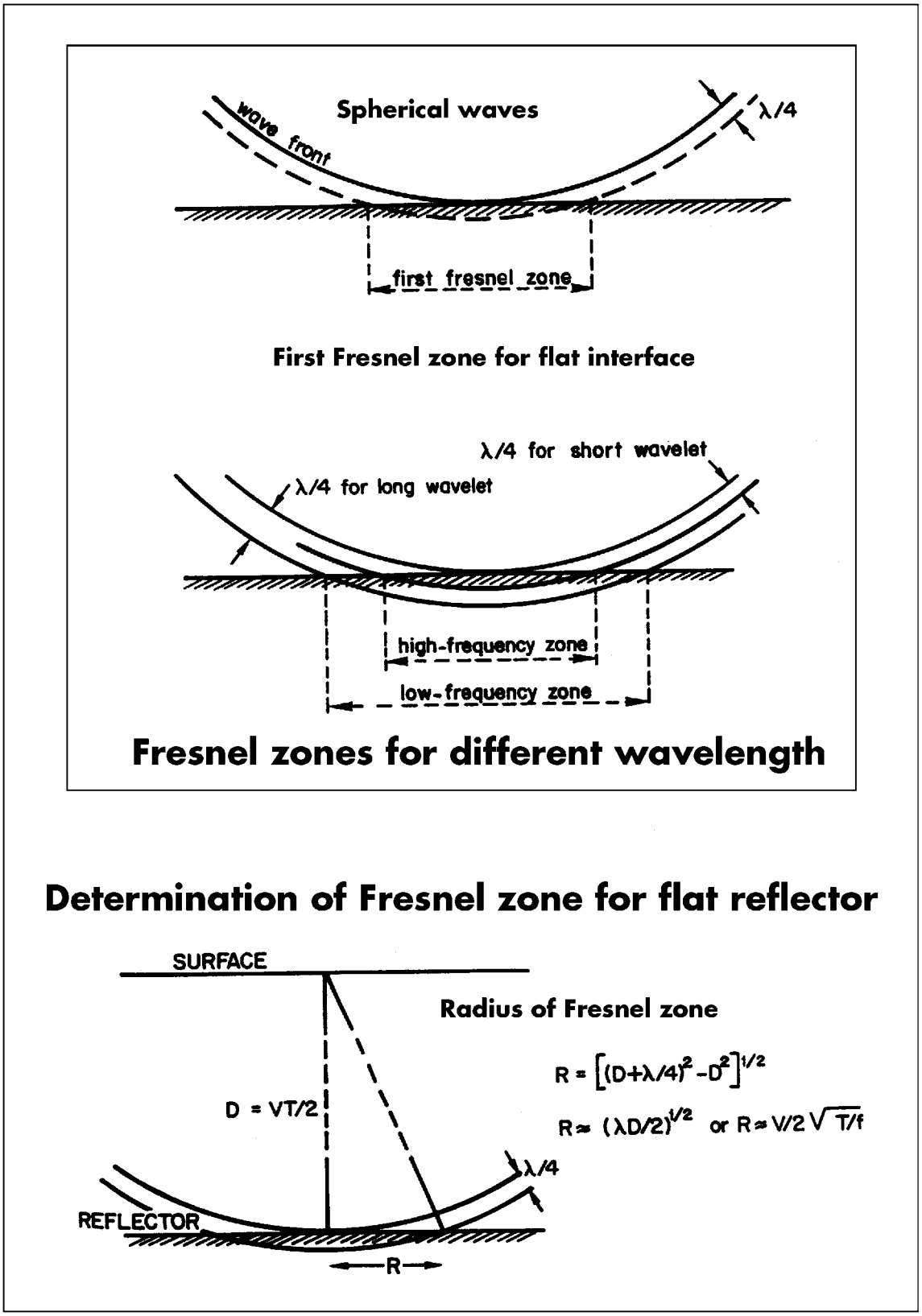

Figure 2.34: Schematic representation of some physical aspects of the Fresnel Zone. The seismic wavelet has a certain wavelength with energy spread over a discrete time interval. It means that neighbouring points on the reflector close to the reflection point are contributing to the seismic response. In this figure the effect of the first Fresnel zone (lambda/4) is shown (modified after Sheriff 1977, reprint from AAPG whose permission is required for further use).

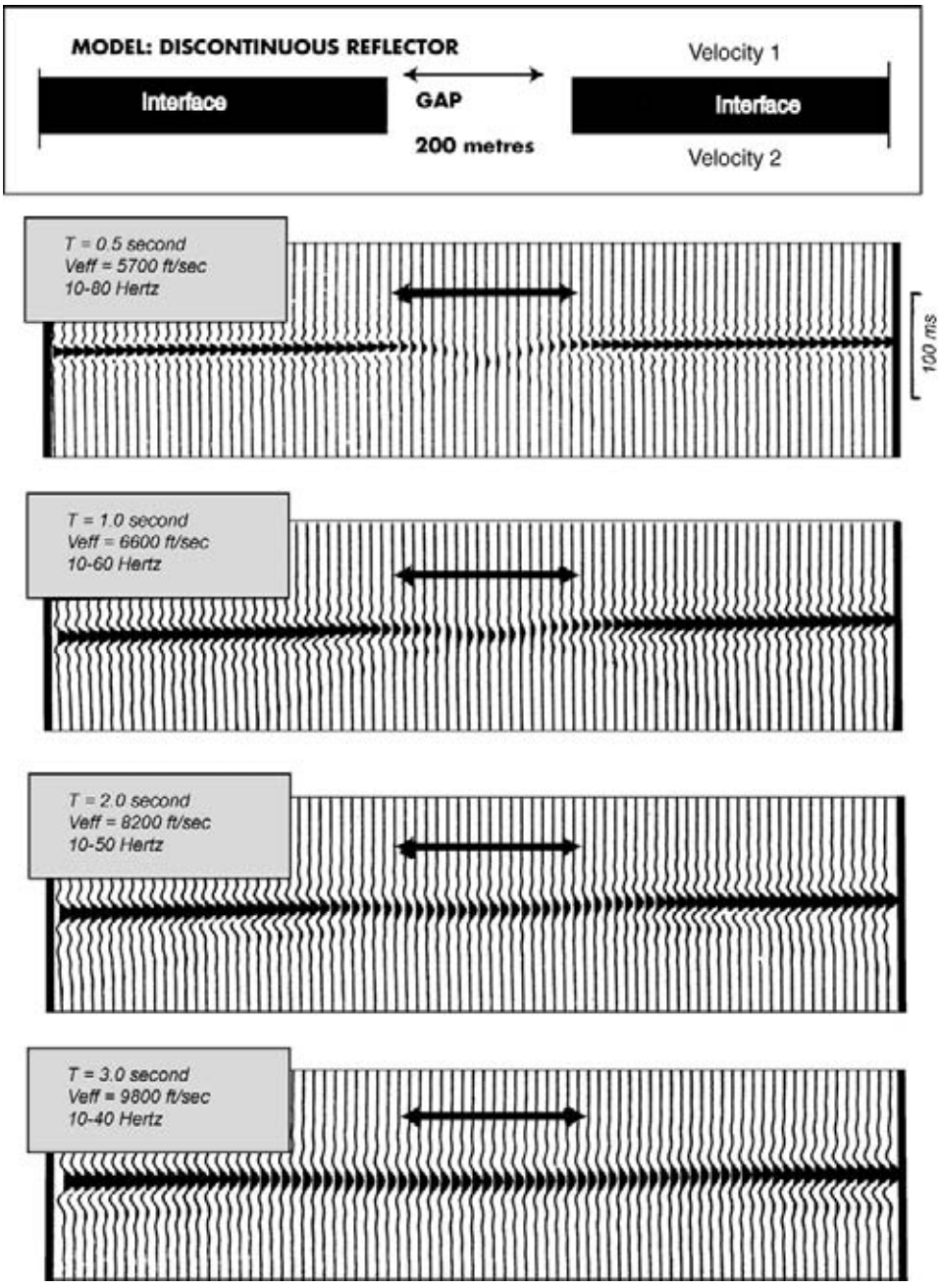

Figure 2.35: 200-metre gap in reflector, which is not resolved at depths greater than 2 seconds TWT. The frequency contents is altered due to frictional losses, absorbtion effect and dispersion.

a seismic wavefront is travelling through a rock sequence. The **strain** is equal to the amount of deformation. Stress represents the force that induces the deformation. Some definitions and fundamental formulas for a simple isotropic case are recalled:

Young's modulus:

$E =$ stress/strain (small deformations, else fracture),

Lame's constants:

$\mu =$ stress/strain (under simple shear),

$\lambda = K - 2\mu/3,$

Bulk modulus:

$K =$ stress/strain (under hydrostatic pressure, 3D volume),

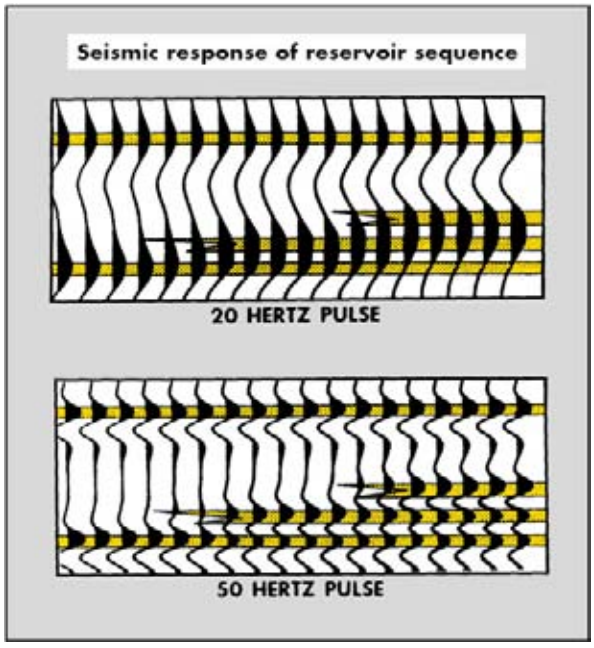

Figure 2.36: Multi-velocity/density interfaces and the resolving power of two seismic wavelets containing 50 and 20 Hertz signal. The higher frequency 50 Hz wavelet resolves the individual sand intercalations much better (after Vail et al. 1977, reprint from AAPG whose permission is required for further use).

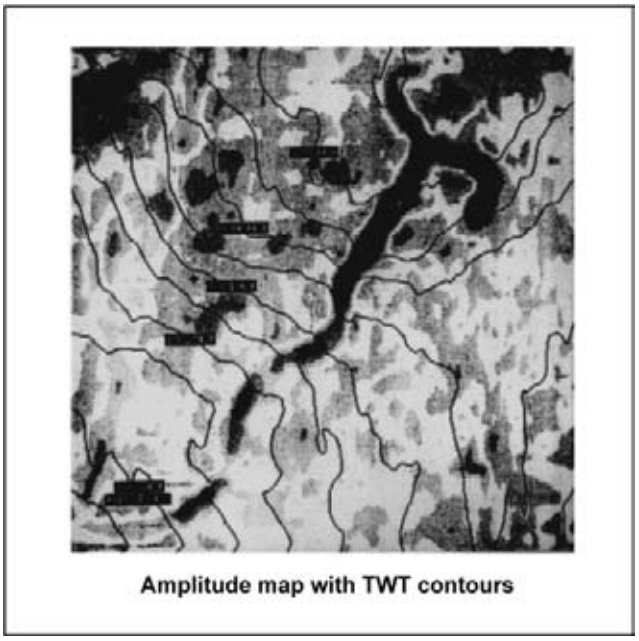

Figure 2.37: Amplitude map extracted along a seismic horizon, with time contours. Paleo-geomorphologic features like sedimentary channels show up as a distinct dark anomaly in the central part of the map (after Brown 1985 data courtesy Chevron).

Poisson's ratio:

$\sigma =$ transverse strain/longitudinal strain (uni-axial stress),

$$K = \lambda + 2\mu/3, \tag{2.16}$$

$$\sigma = \frac{\lambda}{2\lambda + \mu}, \tag{2.17}$$

$$V_{\mathrm{p}} = \sqrt{\frac{K + 4\mu/3}{\rho}}, \tag{2.18}$$

$$V_{\mathrm{s}} = \sqrt{\frac{\mu}{\rho}}. \tag{2.19}$$

The V_{p} and V_{s} are influenced by the following factors (Angerer and Richgels 1990):

- Mineralogical composition of the rock.
- Porosity.
- Depth of burial.
- Pressure.
- Temperature.

The Poisson's ratio $\boldsymbol{\sigma}$ depends on the V_{p} and V_{s} and the relation is usually described by the following formula's:

$$\boldsymbol{\sigma} = \frac{V_{\mathrm{p}}^2 - 2V_{\mathrm{s}}^2}{2(V_{\mathrm{p}}^2 - V_{\mathrm{s}}^2)} = \frac{(V_{\mathrm{p}}/V_{\mathrm{s}})^2 - 2}{2[(V_{\mathrm{p}}/V_{\mathrm{s}})^2 - 1]}. \tag{2.20}$$

This formula is true for **linear elastic** materials. Rocks are however characterised by **poro-elastic deformation**. Under such conditions the pores are either dry or saturated and behave drained or undrained during the passage of an elastic movement. The draining of the pores depends on the energy, speed and time that the particles are submitted to the wavefront (Gretener and Thomson 2003). These constraints make the direct $V_{\mathrm{p}}/V_{\mathrm{s}}$ estimation from the above formula less reliable. In many AVO studies this difference from the reality has been conveniently ignored.

The **Poisson's ratio** is the ratio between the amount of compressional deformation in one direction over the amount of extension in the other direction (transverse strain/longitudinal strain). It is related to the reflection coefficients (Koefoed 1955). The Poisson's ratio is smaller in the gas invaded zones than in the water filled reservoir sands. This distinction is utilised to get a better separation between water wet and gas filled reservoir. Water bearing sand has a Poisson's ratio of around 0.3, gas sand around 0.1 and shales have approximately a value of 0.4 (Robein 2003). When making a crossplot between Poisson's ratio and P-wave velocity, it is obvious that the various lithologies no longer overlap. There exists a clear separation for the rock samples having different pore fill contents (Figure 2.38). This is the main reason why many geophysicists are interested in an elastic approach, that goes back to the pre-stack domain (e.g. Castagna et al. 1985, Castagna and Backus 1990,

Connolly 1999, Krief et al. 1990, Garotta 1999). These kind of reservoir characterisation studies call upon a close cooperation between the petrophysicist and geophysicist to obtain optimal results.

When V_s is not measured in clastic sequences, than an estimate can be made. The following information is needed:

- V_p from the sonic log.
- Density.
- Lithology with clay, quartz, calcite, dolomite and/or other minerals.
- Total and effective porosity.
- Water saturation.

Linear regressions are for instance computed over the shaley intervals using Castagna's formula:

$$V_s = aV_p^2 + bV_p + c \qquad (2.21)$$

$a = 0,$

$b = 0.77,$

$c = -867.4.$

In the sandy interval Gassmann's formula can be applied to estimate the V_s (see Chapter 6).

If gas is in the system, than the rock physical and seismic attributes change in the following way:

Attribute		**Change in gas zone**
Density	ρ	Decrease.
Bulk density	K	Decrease.
Rigidity or shear modulus	μ	Very small increase.
P-wave velocity	V_p	Decrease.
S-wave velocity	V_s	No change (small increase?).
Acoustic impedance	I_p	Decrease.
Shear wave impedance ($= I_p/(V_p/V_s)$)	I_s	Small decrease (rho).
Poisson's ratio	σ	Decrease.
Rigidity of the matrix ($= I_S^2$)	$\rho\mu$	Small decrease (rho).
Pore fluid discriminator ($= I_P^2 - 2I_S^2$)	$\rho\lambda$	Decrease.
Compressibility/Rigidity modulus ($\lambda/\mu = \rho\cdot\lambda/\rho\cdot\mu = (V_p/V_s)^2 - 2$)	λ/μ	Decrease.
V_p/V_s, low values in gas zone		Decrease.

Fluids do not affect the shear velocity, because S-waves are not propagating in fluids. So within the same matrix the V_s will be the same in brine or in gas filled reservoir.

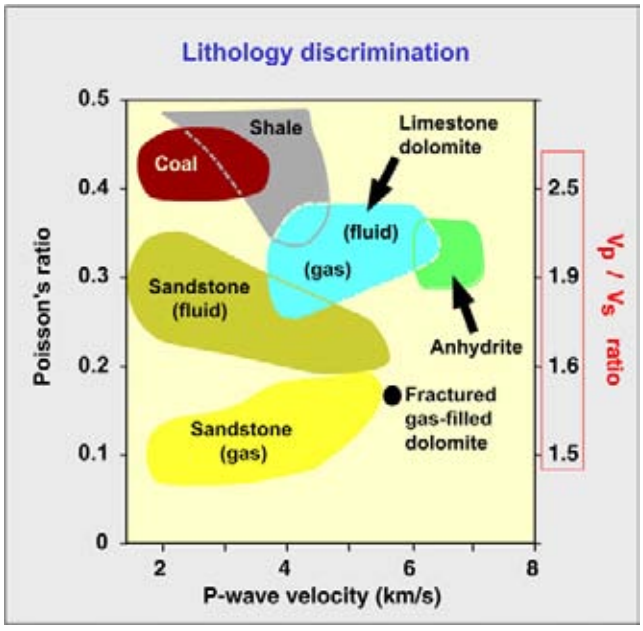

Figure 2.38: Crossplot between the Poisson's Ratio and the P-wave velocity. The crossplot illustrates a good separation between the lithologies and even the various pore fills are resolved.

The V_s depends on the characteristics of the rigid rock framework (mineral particles and the cement).

The Poisson's ratio ranges from 0 for solids to 0.5 for fluids and drops in a gas reservoir. Poisson's ratio is one of the most reliable fluid indicators.

Lambda represents the incompressibility of the matrix. A gas reservoir has a high compressibility, which translates into a low Lambda. Mu is the rigidity modulus and fluids do not affect it, hence it is insensitive to the fluid type in the rock.

Tuning effects, due to a **thin-bed configuration** between two closely spaced reflecting interfaces, causes interference of the generated seismic response by the wavelet. It can show up as variations in the reflector's amplitude. Exact picking of the time horizon on the interface is crucial to establish the amplitude behaviour correctly. Seismic inversion is needed to get a better definition of the earth layering and to reduce the side effects stemming from the thin bed configuration. Preserved amplitude data is a must, when quantitative analysis is required.

2.3.2 Preserved amplitude

It is important that, where possible, the seismic interpretation is done on so-called '**preserved amplitude**' sections (Figure 2.39). At first glance these type of displays might not look very attractive, but the relative reflection strength differences are still preserved and these

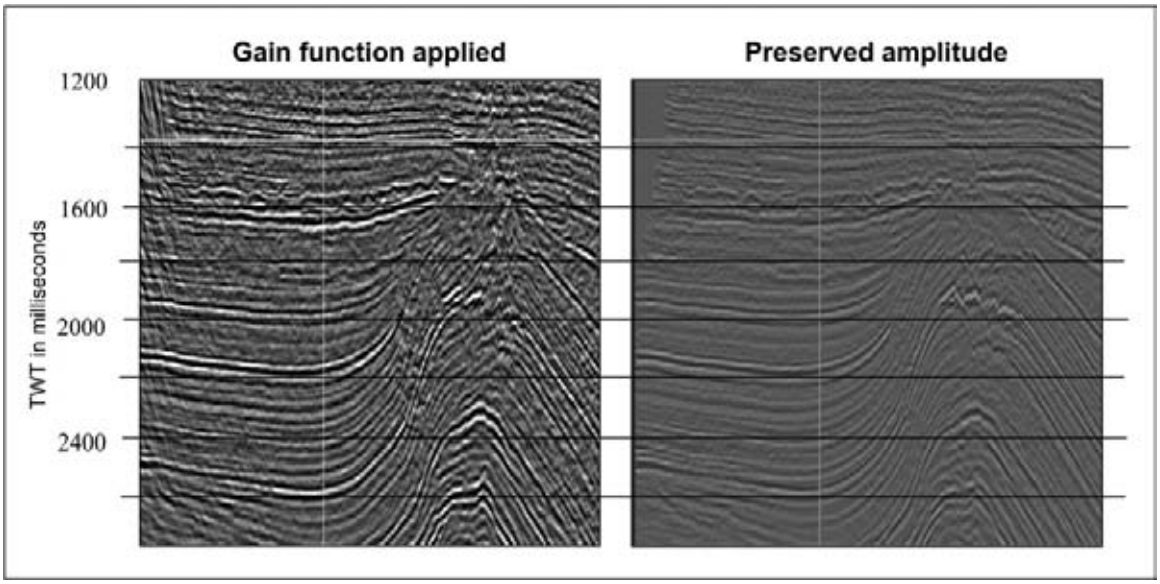

Figure 2.39: 'True amplitude' stack compared with a normalised stack section. 'True amplitude' processing preserves better the gross lithology character of the individual seismic units and facilitates their interpretation (courtesy Pemex).

changes tell something about the gross lithology of the various units in the subsurface. The amplitude differences are important if quantitative predictions are to be made from a seismic dataset. Special attention during the various processing steps ensures that the relative amplitude behaviour of the reflectors is preserved. Serious distortion effects, caused for instance by the **Automatic Gain Control** (AGC), are avoided in this way. A certain amount of AGC is necessary in order to compensate for the fact that the signal gets weaker and weaker. This is due to absorption effects as the signal reaches greater depths and it travels a longer distance inside the earth's crust. The initial seismic energy is spread over the expanding sphere of the prograding wavefront (**spherical divergence correction**). Dispersion and frictional losses are to be addressed.

The preserved or 'true (?!!)' amplitude display enhances the expression of gross lithological units. It gives a better chance to extract this information during the interpretation efforts. The question is now: how true is 'true'?! Acquisition and processing of data implies that the signal is influenced by the filtering and convolution process. Convolution is the change in wave-shape when a signal is passing through a filter. It is the task of the geophysicist to make sure that the signal is not unnecessarily deformed in the consecutive processing steps. It is his responsibility to counterbalance the negative effects of the **acquisition footprint** (e.g. dynamite versus vibroseis source signal) in a satisfactory manner. Even in a preserved amplitude processing sequence some amplitudes can be altered, as long as the changes are improving the quality of the data and corrections are made in the right sense. Preserved amplitude processing does not mean '*Preserve the amplitude distortion*'. This kind of approach does put some responsibility on the shoulders of the geophysicist, because he has to decide what is good and what is bad. There are examples in the past where the geophysicist has shown a rather laid-back attitude and preferred to live with obvious artefacts in order to preserve the 'original' amplitude behaviour, although the response was clearly artificially influenced. Nowadays it is realised that there is a price tag attached to a slack attitude in processing. Anisotropic effects of the overburden also influence the amplitude at the target level (Maultzsch et al. 2003). Proper processing and data conditioning is of utmost importance when quantitative interpretation is the ultimate goal (Da Silva et al. 2004).

In case of working with multiple surveys the issue becomes even more pressing. The 'true amplitude' can vary from survey to survey. When they cover the same area of interest, the delicate problem is posed: which survey has the best true amplitude. Some data normalisation is then required. This can be achieved by re-scaling the surveys using the Z-score method (Delaughter et al. 2005). The Z-score represents the difference of the value from the mean of a population, expressed in number of standard deviations and it is thus a relative measure. It is a well known statistical parameter that has proven its value already in other science disciplines. The Z-score method allows for complete rescaling with preservation of the original data character. The method works because the distribution of the amplitudes in a sufficient large survey area is basically bell

shaped or in other words it has a normal distribution. Alternative methods are the High-Low approach to the scaling, using the 95% and 5% value to avoid extreme outlier values. It gives results that are comparable to the Z-score method but offset with a constant value. This High-Low method exaggerates extreme values and flattens the character of the dataset (Delaughter et al. 2005). The root mean square method transforms the data distribution towards a more log normal trend when the mean of the dataset is not equal to zero. And this is clearly a less desirable property of the RMS method. If the mean is zero the results are approximately conform the Z-score method.

2.3.2.1 Q-acquisition and processing

WesternGeco's **Q-processing** looks very promising in quantitative reservoir characterisation studies. During the acquisition phase the response of each geophone is recorded individually. Later in the lab special filtering can be done to suppress specific types of noise. This single sensor technique is more efficient than the traditional approach, whereby the geophones were grouped in the field and the array geometry took care of some noise suppression (A. Curtis, pers. com.). The Q stands here for quality seismic (or quantum leap?) and not for absorption or signal attenuation behaviour. The geophone array has as disadvantage that it smears the data on the CDP gather and aliasing of several types of noise can occur; e.g. ground roll, Love and Raleigh energy, linear air blast, harmonic energy. This mixing makes it difficult to remove the noise later on (Shabrawi et al. 2005). The Q approach has proven already its benefits in reservoir characterisation and 4D time lapse studies, but of course the advantages come at a certain cost. The capability to control the feathering of the streamers in 3D acquisition is helpful for the repeatability of the surveys. Full wave processing is another domain that looks promising for improving the 3D time imaging of the subsurface (Criss et al. 2005). It takes into account the P-wave and converted PS-wave energy. It gives access to:

- Broader bandwidth.
- More accurate amplitudes and AVO effects.
- V_p and V_s.
- Some data that was previously considered noise can now be used in the interpretation.

2.3.2.2 Automatic gain control

The automatic gain function (= multiplication factor at each time sample in a seismic trace) is usually defined

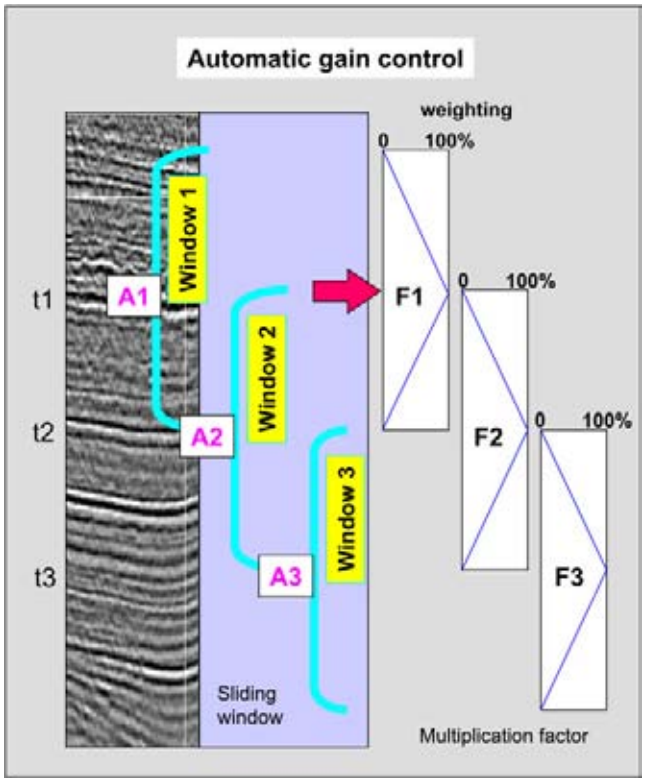

Figure 2.40: Gain function applied in sliding window. Tapering of the correction function (blue line) in the overlap areas results in a correction factor for each time sample.

in a sliding window. The amplitude is computed for the time samples in the first window. The value is compared to the desired output level and a multiplication factor is determined. This factor F1 is assigned to the window's midpoint M1. The window is slided down to its new time position with an overlap of half the window size. An other calculation is done with the multiplication factor F2 assigned to the new midpoint M2. In between the midpoints the multiplication values for each time sample are interpolated in the following manner (Figure 2.40). At M1 100% of gain value F1 is applied and reduced to 0% at M2, where the F2 value attains its full 100% weighting. In this way all time samples have a multiplication factor assigned to correct its amplitude. The method works on a trace per trace basis and this can distort the amplitude behaviour in a 3D sense. A larger window size of one second TWT is giving usually quite acceptable results. Smaller values tend to influence the balance between the individual reflections.

There is an advantage to establish the amplitude correction factors in a small 3D volume and average them. This approach results in a more balanced 'preserved amplitude' aspect for the seismic data. Again the window size should not be too small. In the processing modules often AGC is needed to boost some of the reflections

and to clean up the data. Some of the processing procedures are not very effective when the amplitude is too low. If the AGC function is recorded during processing, than an undo step can be performed later on. It allows to reconstitute the original 'preserved amplitude' character of the data.

A down-to-earth interpreter looks at several sections and makes up his mind which type of processing is preferred. When the data contains a lot of noise and the foregoing processing steps cannot be re-done, a certain degree of amplitude distortion has to be accepted and should be lived with. The processor should realise that nowadays the quality demands are much more stringent. New study techniques try to extract the maximum information from the seismic dataset, pushing the processing efforts to its limits. Sophisticated processing is much more unforgiving, whilst in the past it was possible to get away with many things without further worries. The recent demands for more accuracy by the reservoir engineers does not make the processor's task any easier.

2.3.3 Reflection frequency and composite seismic loops

The frequency of a reflection is determined by:

- Natural frequency absorption profile of the earth.
- Signature of the reflected wavelet.
- Actual sharpness in the velocity-density contrast.

Under the same given circumstances a sharp acoustic impedance boundary is generating a higher frequent event than a more gradual transition. In case of a very gradual transition no reflection may be generated at all.

Interference of the closely spaced seismic events gives rise to **composite seismic loops** (Figure 2.41). Under those conditions it becomes difficult to discriminate between the effects stemming from the individual interfaces (Todd and Sangree 1977). Consequently the apparent amplitude and frequency should be treated with care in the interpretational procedures. A **seismic loop** is defined by a consecutive sequence of time samples and the corresponding amplitude wiggle trace segment between two subsequent zero crossings (zero amplitude values).

Stratigraphic deconvolution is performed to undo some of the signal interference effects. This technique is also known as **seismic inversion**. The seismic signature is replaced by a spiky response, that corresponds better with the acoustic impedance layering. Inversion facilitates the interpretation of meaningful geological and

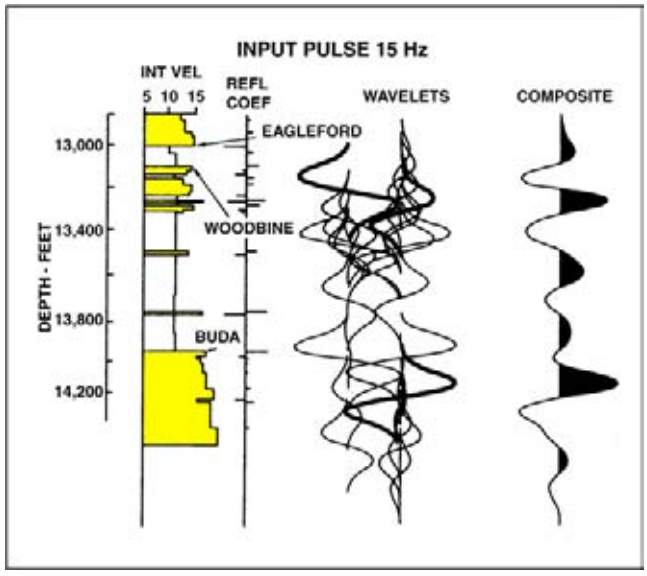

Figure 2.41: Seismic response of multi-layered sequence resulting in a complex composite trace. The interval velocity is expressed in thousands of feet per second. Next to the lithological column the position is shown of the reflection coefficient spikes, then the individual response of these spikes and the resulting seismic trace, incorporating interference effects (after Vail et al. 1977, reprint from AAPG whose permission is required for further use).

petrophysical boundaries in the subsurface (see also Section 2.7). The acoustic impedance cube allows studying the reservoir parameters in greater detail. Often this is done in conjunction with AVO analysis (e.g. Veeken et al. 2002a, Da Silva et al. 2004). The ultimate goal is better a ranking of prospects, delineation of unswept areas and the definition of 'sweet spots' in reservoir development studies. Some upfront financial investment in these kind of study techniques will save a lot of money in the development phase, even moreso when bad holes are avoided and the hydrocarbon evacuation is optimised.

2.4 Seismic Wavelet

There are two basic shapes of seismic wavelets in data processing:

- The **minimum-phase** wavelet, whereby the start of the wavelet is coinciding with the exact position of the subsurface interface.
- The **zero-phase** wavelet, whereby the maximum amplitude of the wavelet is coinciding with the lithological interface.

The difference in wavelet shape is illustrated in Figure 2.42. The reason, why zero-phase processing is preferred above minimum-phase, is because it reduces the

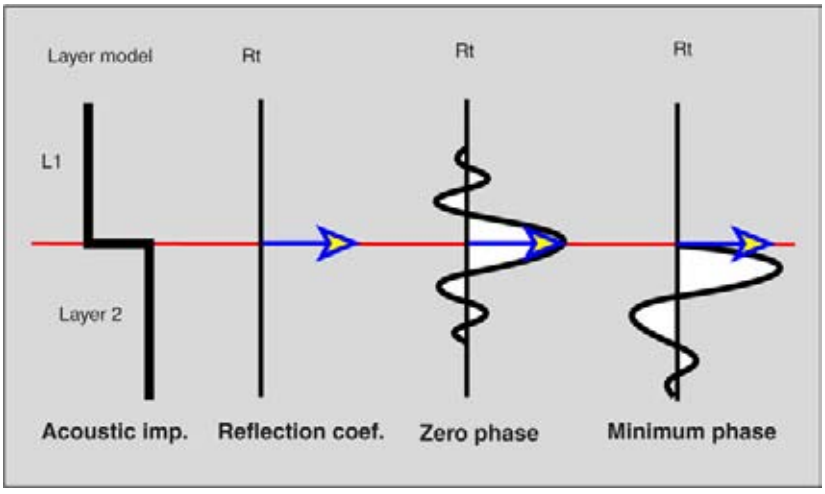

Figure 2.42: Typical minimum-phase and zero-phase wavelets. The minimum phase wavelet has the seismic energy located directly below the reflecting interface. In the zero-phase representation the same interface is corresponding with the peak in the central lobe energy. The zero-phase wavelet has symmetrical pre- and postcursor side lobes. Typical size of the wavelet is 40 to 150 ms. The central lobe is usually 18–30 ms wide.

length of the wavelet and increases the vertical resolution of the seismic data. The size of the side lobes (pre-cursor/post-runner) in the zero-phase wavelet can create sometimes artefacts on the seismic section. In general it can be assumed that the total length of a typical seismic wavelet of 10–60 Hz ranges between 40 and 100 milliseconds TWT. The identification of the position of the AI interface is facilitated by the zero-phase processing. Mixed waveforms do exist, but digital processing with these kind of wavelets is much more difficult and hence constitutes an additional source of error.

The zero-phasing of the seismic is usually achieved only over a small time window. It is very difficult to obtain a correct zero-phasing for a complete seismic cube. For checking the zero-phase condition of the dataset, it is necessary to go into the frequency domain. This done by applying a Fourier transform (cf Mari et al. 1999) and by studying the phase spectrum. The zero-phasing is a special topic, which is covered in more detail in Section 3.4.2 below.

Seismic data is sampled usually with a 2 or 4 millisecond TWT time interval. This is done because smaller datasets are a lot easier to handle. It reduces acquisition and processing costs. A proper data reduction ensures that the original signals can be restored from the stored data. This time sampling implies that the description of the seismic loop is not continuous along the time scale, but that amplitude values only vary along the time axis in 2 or 4 milliseconds long intervals (blocky appearance). In this 2 millisecond time window only one discrete amplitude number is assigned. The restrictions imposed by this time sampling technique can cause artefacts (interference patterns) on the maps derived from the seismics, but normally it does not hamper the interpretation. When doing detailed reservoir characterisation studies it should realised that the shape of seismic wavelets is always somewhat approximated. Often a **curve fitting** procedure is performed for reconstructing the seismic trace. This partly explains differences in autotracking results when using software of various contractors.

2.5 Seismic Display

Display parameters may influence the interpretability of a seismic section considerably. The mode of display is an important visual aspect. There are several different black-and-white modes available:

- **Wiggle** display (Figure 2.43), which depicts the positive and negative loop trace as a continuous sinusoid line.
- **Varwiggle** display (Figure 2.44) which show both the positive and the negative seismic loops, one of which is coloured in. This mode is the mostly used as it gives the interpreter better information on the amplitude behaviour. The processor can decided on the amount of infill on the black loop, a parameter sometimes useful to change in order to bring out certain features.
- **Var** display, whereby the information contained in the white positive loop is suppressed. An equivalent colour display is also known as the variable density display. Many times the zero-crossing is given a white annotation whilst the negative and positive loops are differently coloured in.
- **Dual polarity display** (Figure 2.45) which means that one polarity is shown for all loops regardless

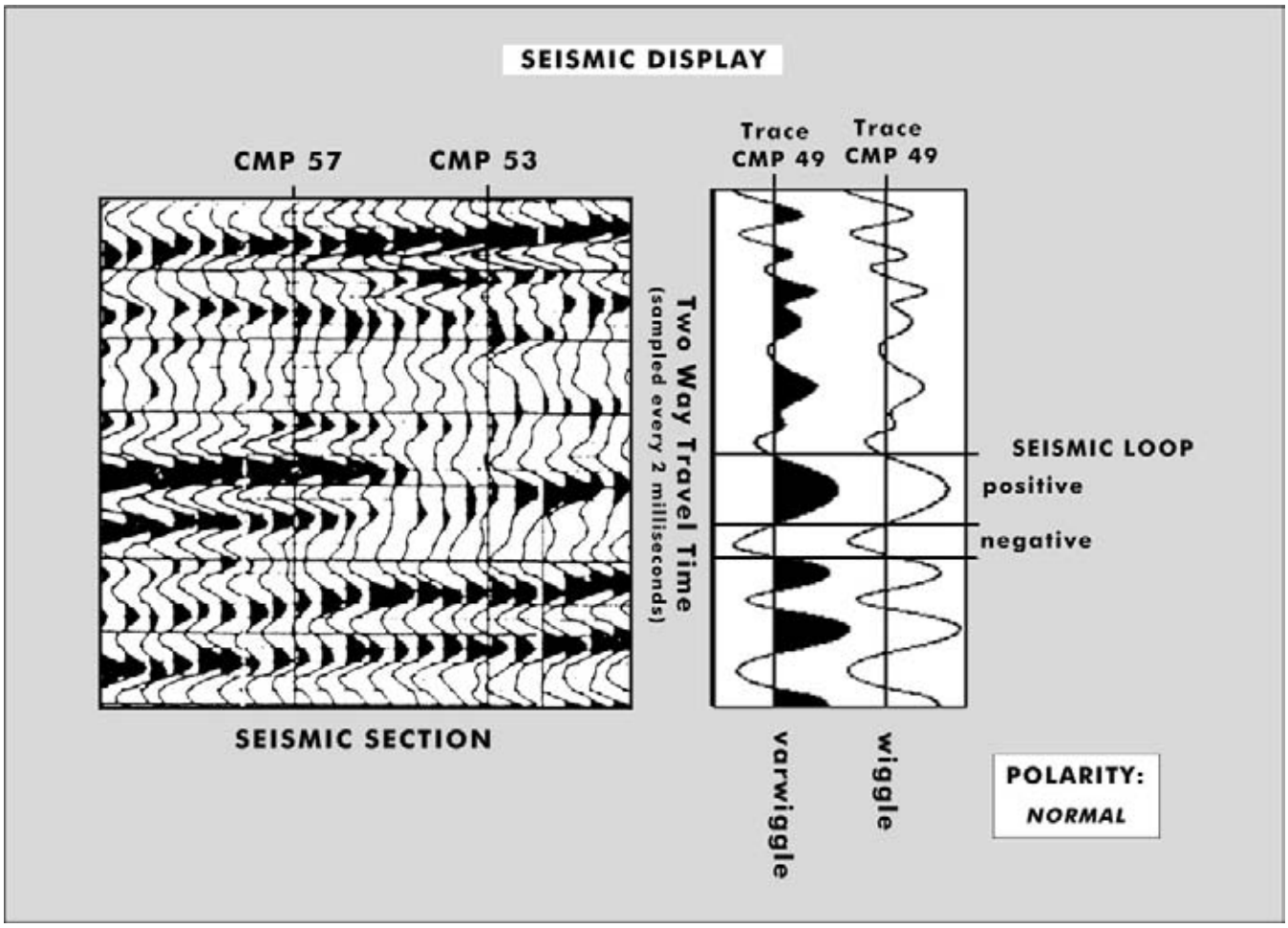

Figure 2.43: Seismic representation of a seismic section with varwiggle and wiggle display of some traces. The normal polarity nowadays means that an increase in acoustic impedance (AI) with depth (or time) is also represented by a positive increase in AI. Reversed polarity means the opposite: an increase in AI is corresponding with a negative response.

of the positive or negative character of the loop excursions; they are all displayed in the same sense. Sometimes this display can have some advantages.

The use of coloured sections with a varwiggle overlay is more and more popular with the current advent of 3D seismic workstations. The colours are shown in a **density display**. This colour display brings out certain details on the reflections which are lost in the normal black-and-white displays. High amplitudes above a user-defined level can be given an outstanding colour to put emphasis on the contrasting properties (Figure 2.46). Also boosted pixel displays are produced, conveniently illustrating the behaviour of various attributes (Brown 1988). Our colour perception is not linear and this is often ignored by the interpreter (Welland et al. 2006). Careful colour coding can augment the discrimination power of the representations.

In 3D seismics the interpreter has the possibility to generate **time slices** which are horizontally oriented sections (Figure 2.47), that can be interpreted. It represents an extremely efficient method to quickly check the internal consistency of a vertical time section interpretation.

Normalisation procedures like Automatic Volume Control (AVC, also known as automatic gain control), trace equalisation and time-variant scaling enhance the visual aspect of the reflection geometries. But on the other hand they hamper the extraction of reliable reflection strength estimations, needed for the gross lithological interpretations as discussed earlier on.

Occasionally it may be handy to change the **trace spacing** of a seismic section. It permits to bring out the dynamic range of the seismic response and prevents the loops from **clipping** or overlapping in a lateral sense (Figure 2.48, Neidell and Poggiagliolmi 1977). The amplitudes of the time samples on the trace can be so high that the wiggle will overlap with the adjacent trace,

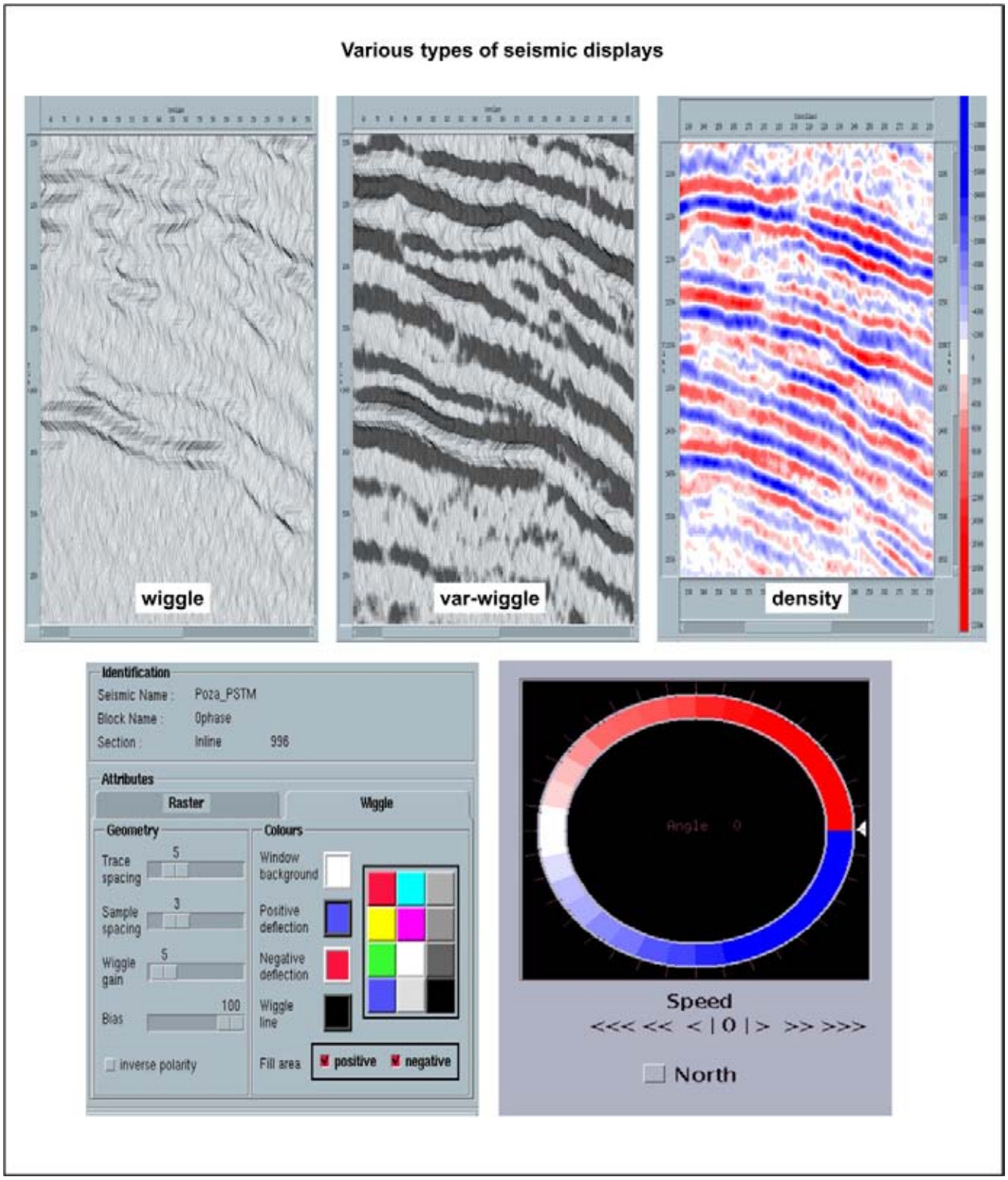

Figure 2.44: Various seismic representations: Wiggle, Varwiggle and colour Density display.

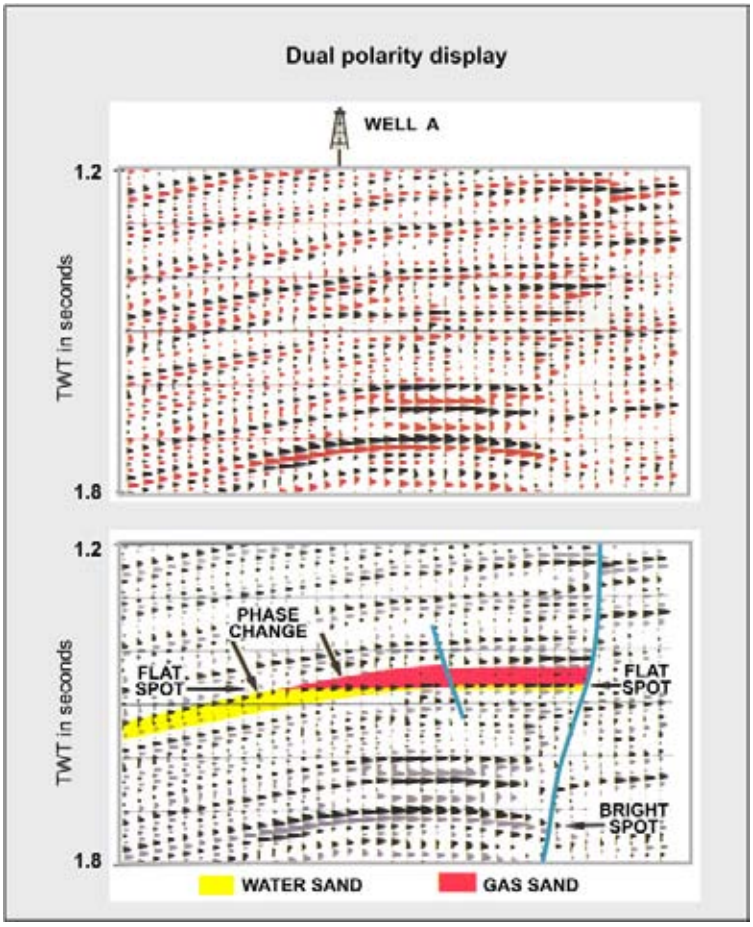

Figure 2.45: Dual polarity display whereby both negative and positive loops are plotted in the same direction. Sometimes this visual display helps to discern subtle changes in the reflection characteristics (after Brown 1999, data courtesy Geophysical Services Inc).

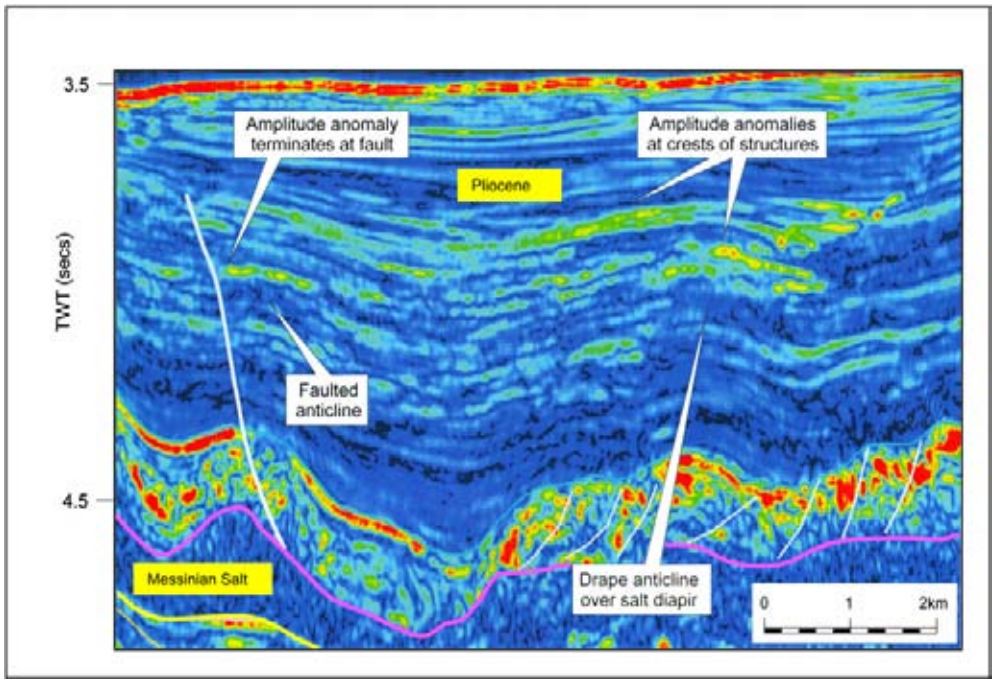

Figure 2.46: Colour density display of an amplitude section offshore Algeria. The chosen colour bar brings out the gross lithological units. The Messinian salt layer below 4.5 seconds TWT is acting as a decollement surface for the overburden tectonics. This Upper Miocene salt layer is related to the Messinian salinity crisis in the Mediterranean Basin. Amplitude anomalies are corresponding with possible closures (HC leads) and structural highs (Cope 2003).

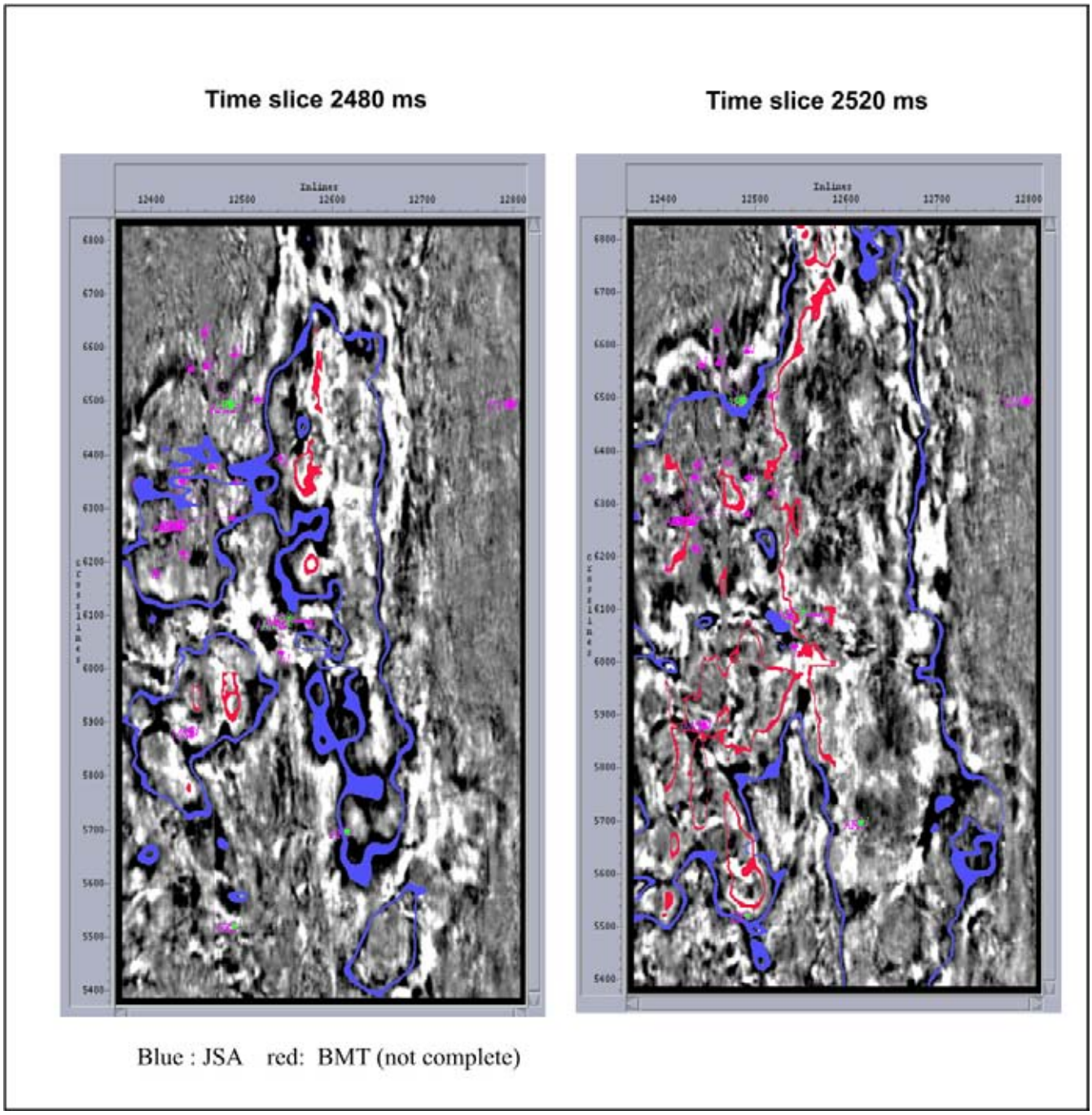

Figure 2.47: Time slice through a 3D seismic survey is extremely helpful to check the consistency of the interpretation. Faults show up as reflection discontinuities. Here an irregular anticlinal structure is shown (courtesy Pemex).

which causes the optical clipping. Its exact value cannot be appreciated and unnecessary loss in resolution occurs. Usually the amplitude data is displayed up to a digital value of 127 (8 bit). Multiplication of the amplitude values, as recorded in the field, by a certain AVC factor can bring the amplitudes beyond this 127 value. It falls then outside the **dynamic range** of the display system and is automatically set at the 127 maximum value, whereby the original variability of the amplitude data is being lost. Such data can be however crucial in detailed reservoir modelling studies. The level of digital clipping is controlled by the applied AVC factor. The right scaling factor is essential for the correct display of 8 bit, 16 bit and 32 bit data on the screen. The value range of the time samples plays a role for the colour scale that can be used. The colour palette has a lim-

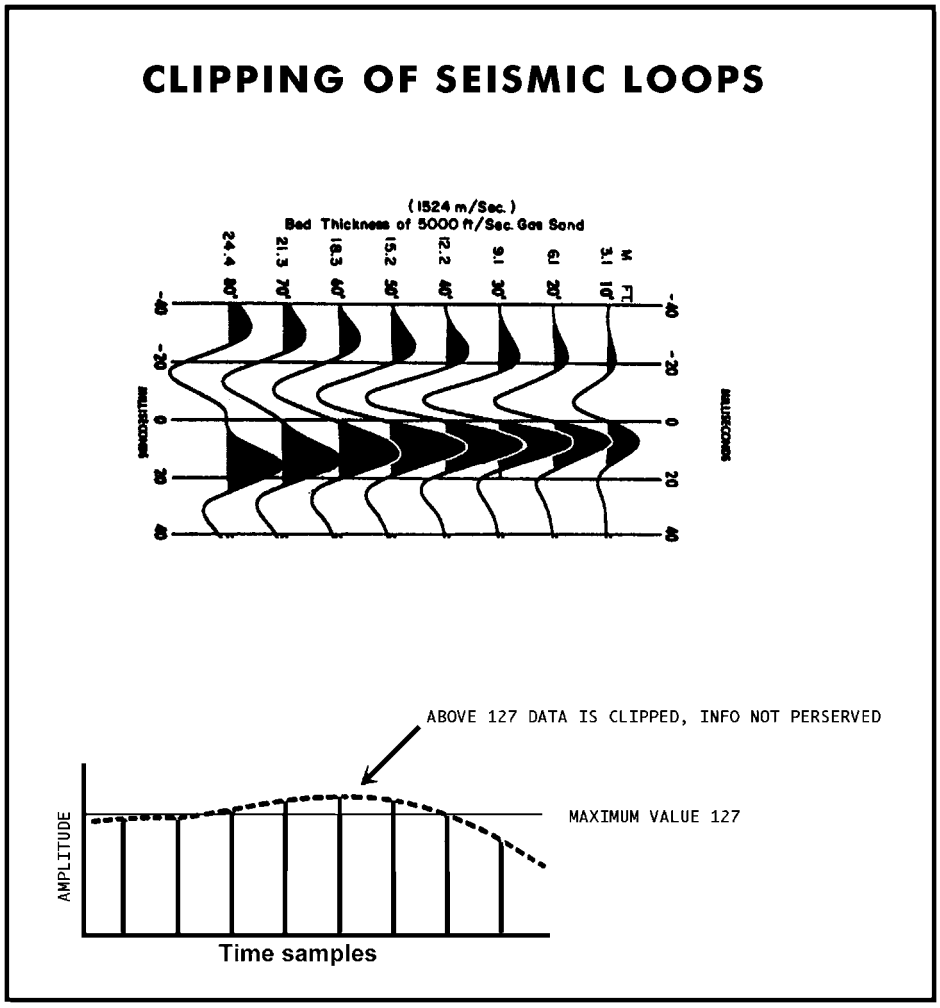

Figure 2.48: Clipping of seismic traces reduces the dynamic range of the displayed amplitudes. All values beyond the thresholds of 127 and −128 are set at the maximum or minimum value. (modified after Neidell and Poggiagliolmi 1977, reprint from AAPG whose permission is required for further use).

ited amount of colours available. 16 bit displays are the standard nowadays, but often the colour scale on workstations are poorly adapted for this seismic data (e.g. Landmark^{TM} and Charisma^{TM}). Sometimes the seismic values have to be scaled differently to adjust them to the display capabilities of the interpretation system.

The horizontal and vertical scales of seismic sections are of importance to the seismic stratigraphic interpretation. A normal format is 1 : 25000 and a 10 cm : 1 sec TWT scale. For regional work a 1 : 50000 and 5 cm : 1 sec TWT is more suitable. **Squeezed sections** are helpful boosting subtle sedimentary dips and give better overview of the dominant fault pattern. One of the axis is exaggerated with respect to the other.

2.5.1 Seismic polarity

Polarity is defined as the sense in which the seismic wiggle is drawn on the seismic sections. Negative reflection amplitude numbers on the field tape are either displayed by an excursion to the left or the right of the wiggle line in respect to the vertical time axis. It can be either a black or a white seismic loop. The SEG polarity convention specifies *that the* **normal polarity display** *corresponds to an increase in acoustic impedance with depth, that is registered on the field tapes as a negative number and displayed on the seismic section by a white loop, being a trough to the left of the wiggle line.*

The reason for this display convention is that in the seventies the hard kick (= increase of AI for deeper layer) was considered the most important event to follow. In those days only paper sections and colour pencils were available to carry out a seismic evaluation study. The pencil sharpener and rubber were very valuable instruments in the office. Traditionally the positive wiggles, with an excursion to the right, were filled with a black colour by the geophysician. Colour pencil on the blackened wiggles was not very visible and also the rubbing out of the interpretation on the black loop was annoying. As all interpreters make mistakes once in a while, the SEG normal polarity display was born. Adhering

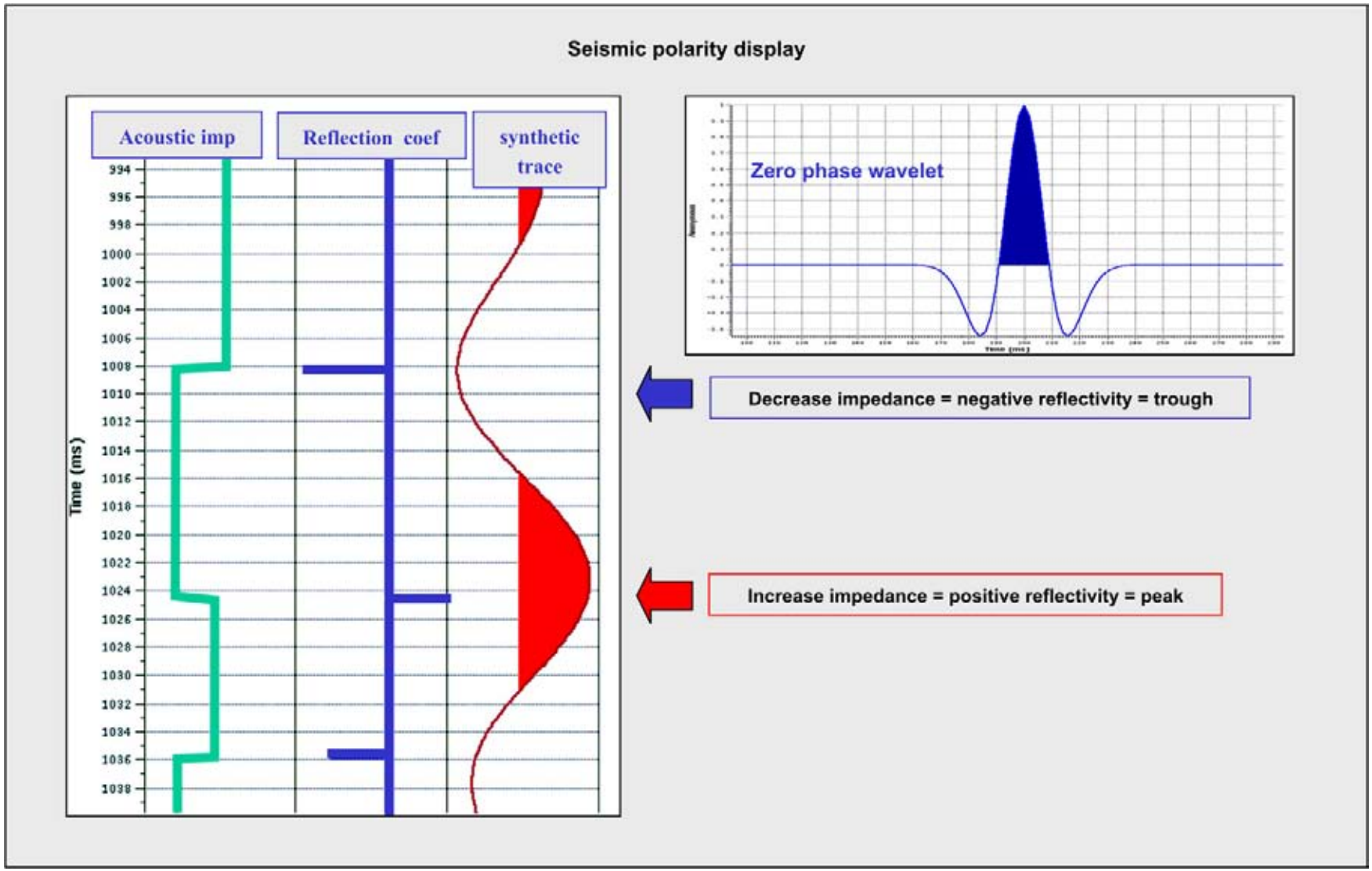

Figure 2.49: Positive polarity display, whereby an increase in acoustic impedance is represented by an excursion to the right of the seismic loop.

to the SEG polarity rule meant that the interpreter could put his colour line in the white loop (top reservoir marker) and generate his prospect maps with some ease. Nowadays the SEG does not seem to support this convention any longer as their Encyclopaedia of Geophysics (Sheriff 1991) gives a confusing and contradictory definition of the concept. It has been corrected in a later edition (Sheriff 2002). Some major oil companies in Europe (e.g. Shell) are conservative and often still adhere to the original SEG standard. Schlumberger is displaying their synthetic and VSP traces on a routine basis in the SEG normal polarity format. For CGG, on the other hand, an increase in AI with depth is always displayed as an excursion to the right of the wiggle line (Figure 2.49). A simplistic dual subdivision between an American and European polarity, as presented by Brown (1999), is somewhat misleading. The best advice is to check always the applied polarity for the seismic dataset. For this a hard water bottom reflection can be used or a characteristic interface identified on a well log.

The interpreter should verify the validity of the display polarity for each survey. The polarity signature may enhance certain subtle features hidden in the seismic data. The polarity is important for inferring lithology changes correctly from the seismic sections. In order to be able to decide whether a reflection is stemming from a hard acoustic impedance interface, whereby $\rho_2 V_2 > \rho_1 V_1$, it is necessary to establish the polarity of the display. As seen above, normal positive polarity means that a white loop represents an increase in acoustic impedance for the deeper unit. The white loop on a varwiggle display can be either an excursion to the right of the seismic wiggle line (positive: CGG) or the left (negative: SEG). This hard AI contrast corresponds for example with a transition from a shale sequence into carbonate rocks with increasing depth. In a negative polarity display the white loop coincides with a soft AI kick and therefore reflects a decrease in velocity-density contrast ($\rho_1 V_1 > \rho_2 V_2$). In general a positive polarity is used in displaying seismic data. The display often depends on the contractor doing the processing. In addition, the term **reversed polarity** has been introduced, adding even more to the amount of confusion on the polarity of the seismic data. It simply means flipping the sense of the wiggle display.

Changing the overall **polarity** of the seismic display gives another view on the data set. The polarity of a zero-phase section may yield valuable information on the nature of the lithological change along the interface and porefill of the units. The same lithological interface (top reservoir) may trigger different velocity-density contrasts, depending on the fluid contents of the pores. These characteristics are varying with depth. Compaction and diagenesis are obviously important factors. In this respect it is noteworthy to remember that a shale and a sand unit can have similar acoustic impedance values, depending on the porosity distribution, fluid contents and degree of compaction (Figures 2.50 and 2.51). Compaction is an irreversible process. In heavily tectonised areas differently compacted lithologies can be juxtaposed, but still give rise to only a weak acoustic impedance contrast. Another important feature is the fact that the change in porefill within reservoirs can produce a sudden lateral flip in polarity of the top reservoir marker when followed from trace to trace. This phenomenon is normally known as a '**Polarity Reversal**' of the reflection (e.g. Brown 1988). This should not be confounded with the reversed polarity display presented earlier on.

2.5.2 Hilbert transform

Instead of plotting the amplitude behaviour along the time scale for each seismic trace, sometimes the **instantaneous phase** or the **instantaneous frequency** is plotted. These attributes are obtained when a **Hilbert Transform** is performed on the data (Figures 2.52 and 2.53). The Hilbert Transform gives access to the imaginary part of a seismic trace. A complex trace can be computed from the seismic trace. The measured or real seismic trace is in one plain (reflection amplitude) and the imaginary trace in a plain perpendicular to this (cf Taner 1978). The amplitude is now a vector composed from the two components: the real and imaginary part of the full seismic trace. This is also known as the envelope or reflection strength (cf Brown 1999). The complex seismic trace forms a corkscrew trace that rotates around the time axis. These kind of seismic attributes represent an other view of the info contained in the seismic dataset. It gives a better handle on the lateral continuity of the reflections. It is extremely useful when studying anomalies related to presence of hydrocarbons.

Taner gives a wide definition of seismic attributes: all the information obtained from the seismic data, either by direct measurement or by logic or experience based reasoning. He introduced numerous seismic attributes based on the Hilbert transform. Five categories can be distinguished (D'Agosta et al. 2005): complex trace, Fourier, travel time, windowed, geometric attributes. The latter are multi-trace attributes that include coherence, dip, azimuth and amplitude gradients. All seismic attributes show a slightly different aspect of the same seismic cube. It is difficult to assess their added value to the seismic interpretation and they often leave the interpreter stunned with the amount of information generated by a physician. The help of the computer is called upon to make the best choice from the wide range in attributes. Automated analysis of cross-plots

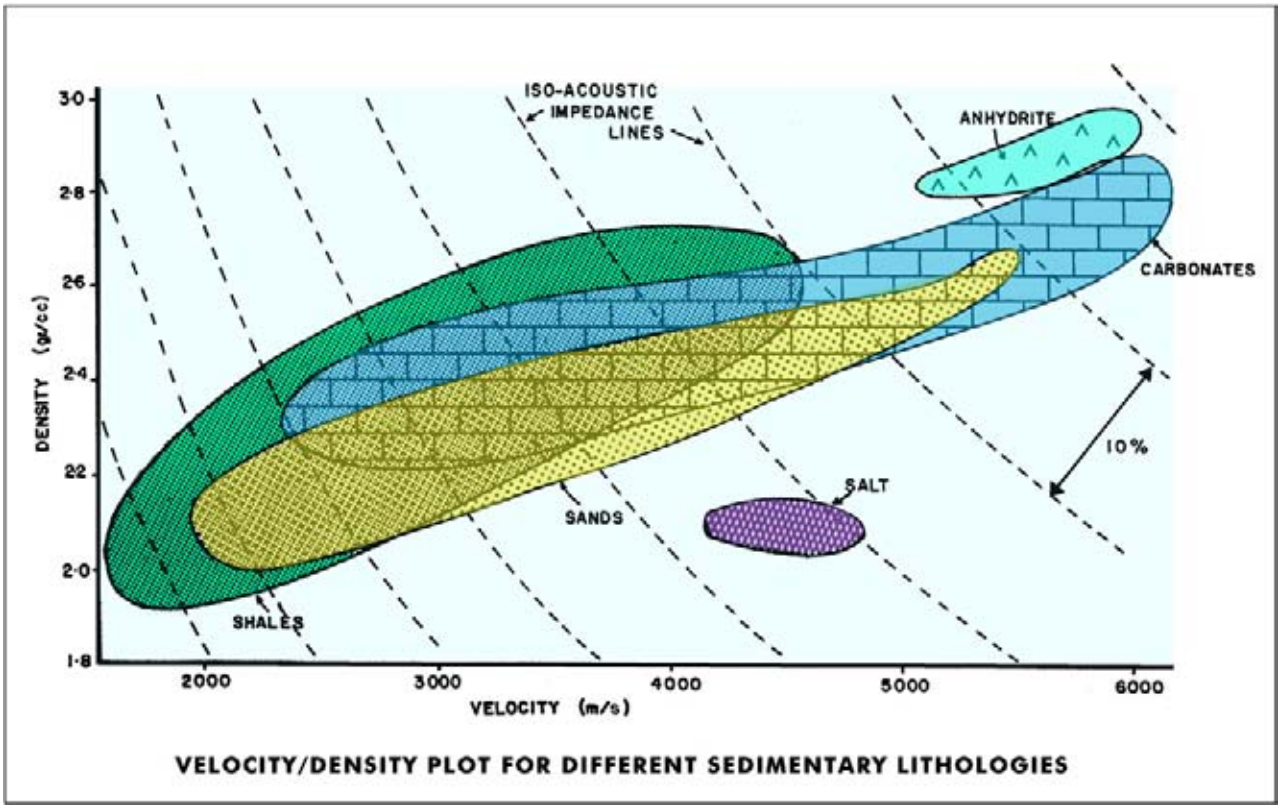

Figure 2.50: Interval velocity/lithology cross plot. The lithologies are overlapping, making their direct identification from the P-wave velocities more difficult. An additional discriminator is often needed.

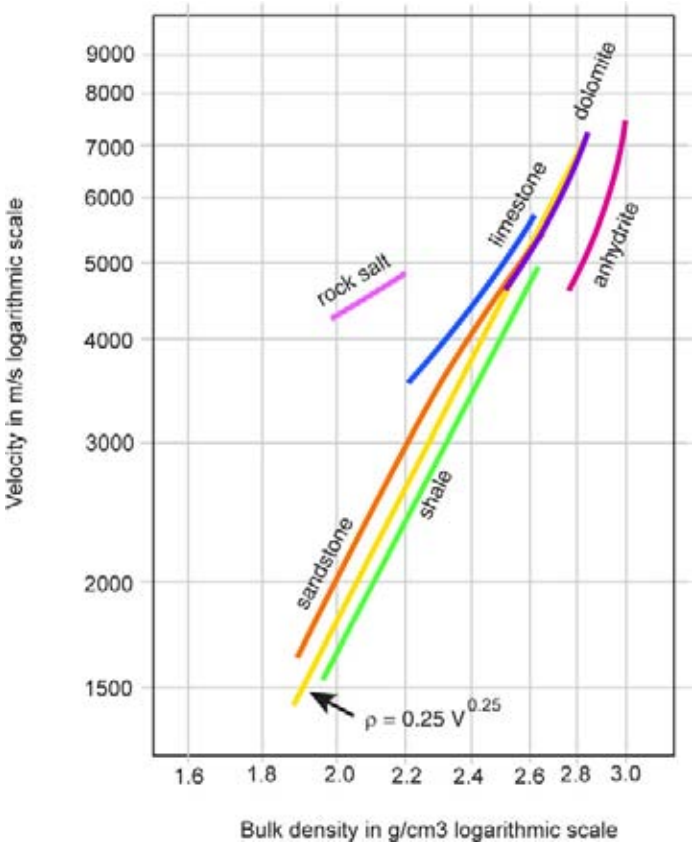

Figure 2.51: Velocity/density logarithmic cross plot for different lithologies. A linear trend approximates the increase in velocity with increasing density. This systematic variation is mostly due to burial, diagenisis and compaction effects (after Gardner et al. 1974 and Gregory 1977, reprint from AAPG whose permission is required for further use).

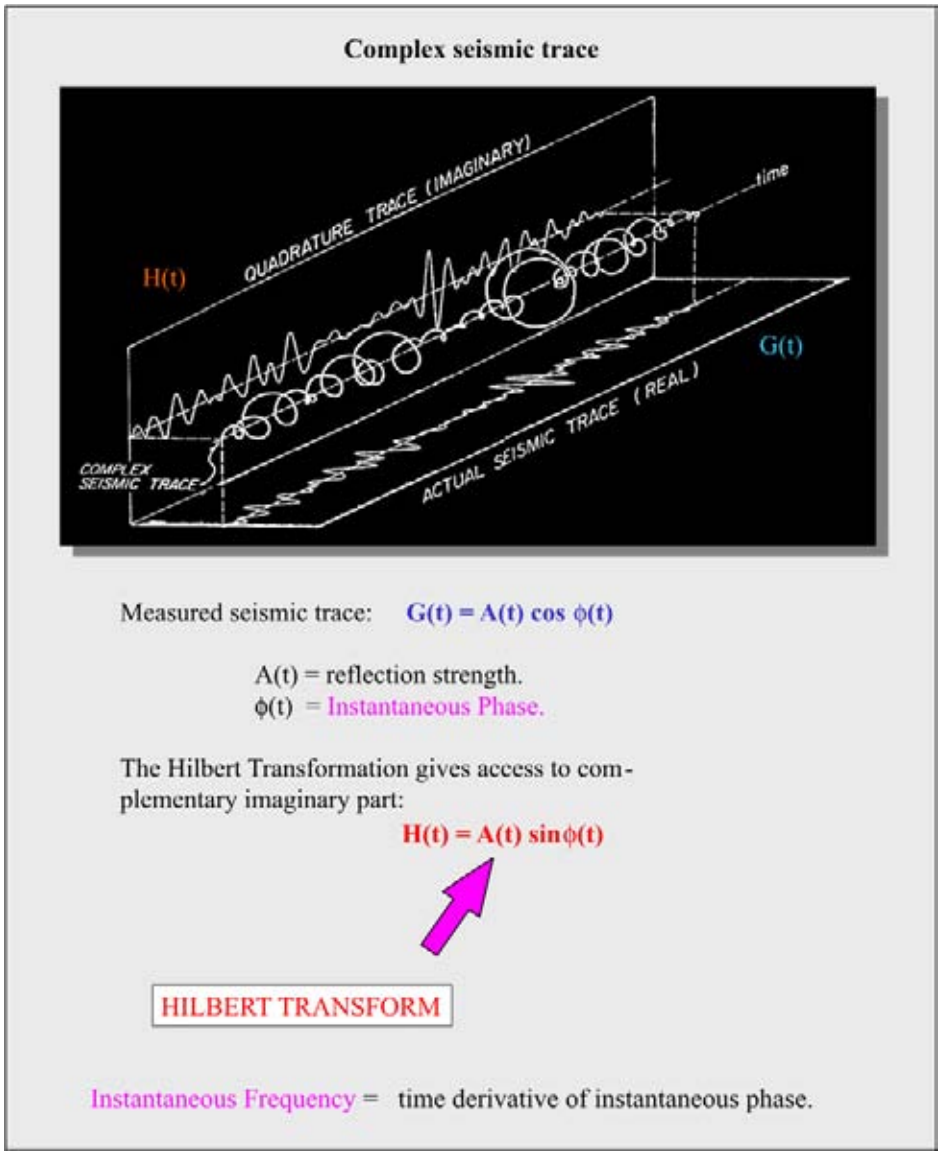

Figure 2.52: The measured seismic trace has an imaginary counter part that is accessed by the Hilbert Transform. The 'Instantaneous Phase' and 'Instantaneous Frequency' attributes are computed by applying the Hilbert Transform to the seismic trace representation. The envelope is usually referring to the reflection strength or amplitude of the total complex trace. The complex trace is obtained by adding the imaginary and real components together. It can be imagined as a corkscrew trace with the amplitude envelope vector rotating around the time axis.

is hereby very helpful indeed. The '**Principle Component Analysis**' technique establishes a basic function, whereby all data points are generated from a basic function by applying certain weighting coefficients (Figure 2.54). These coefficients are inter- and extra-polated over the totality of the study area. It allows a prediction for each point in the survey using this PCA method. New synthetic PCA-based attributes are computed in such a way that they give a better separation between reservoir characteristics of interest (Figure 2.55). The PCA technique is best described as a means to find the cross correlation in a multi-dimensional dataset. It represents a rotation of the multi-dimensional point cloud so that the maximum variability is projected on the pair-wise combination of axis (Prasad et al. 2005). Classification or facies maps are computed and a lithological/fluid contents prediction is made. The use of these type of multi-attribute classifications make the forecasting more reliable and easier to interpret (Linari 2003).

2.6 Interval Velocities

The velocity of the recorded seismic signal (P-wave) is dependent on the gross lithology, porosity and porefill.

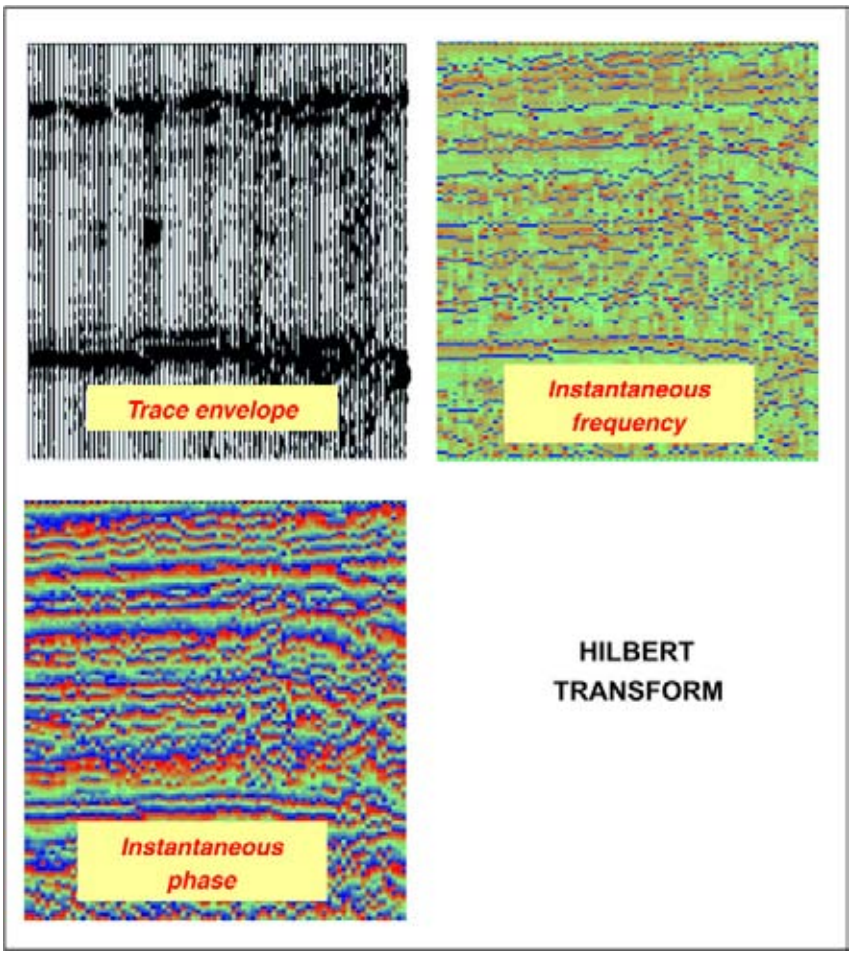

Figure 2.53: Amplitude Envelope, Instantaneous Phase and Instantaneous Frequency display after Hilbert Transform of the seismic data.

Also the amount of compaction has a major influence on the velocity behaviour. These compaction effects are empirically proven to be irreversible after unloading (uplift and erosion). The range in P-wave velocities for sedimentary rocks is shown in Figure 2.56. It can be seen that the interval velocities for different lithologies overlap and therefore it is not a straightforward discriminating factor. Nevertheless it is often assumed that, for a certain depth, the lateral velocity changes are related to lithological/porosity/porefill parameters; especially when these sediments all underwent the same burial history.

Interval velocities can be calculated from the stacking velocities, that are used in seismic processing to determine the Normal Moveout Correction (e.g. Hubral and Krey 1980). The stacking velocities are processing velocities to permit the best stack of energy on the NMO-corrected CDP gather (a.o. Al Chalabi 1994). The so-called **Dix's Formula** is normally used to calculate these interval velocities (Dix 1955):

$$V_{\text{int}}^2 = \frac{T_2 \cdot V_{\text{stack2}}^2 - T_1 \cdot V_{\text{stack1}}^2}{T_2 - T_1}. \qquad (2.22)$$

Dix's formula has some restrictions attached to it and it is assumed:

- No strong dips are present.
- Some degree of parallelism between the layer boundaries.
- No drastic lateral velocity changes, which give rise to non-hyperbolic Normal Move Out.

The reason for the last restriction is that in those cases the stacking velocities do no longer represent a legitimate approximation of the effective velocity field. The effective velocity or root mean square velocity is defined as:

$$V_{\text{effect}}^2 = V_{\text{RMS}}^2 = V_{\text{average}} \cdot V_{\text{mean}}. \qquad (2.23)$$

The **average velocity** takes into account only one layer for the velocity calculation, whilst the **mean velocity** is using an infinite number of sub-layers (Figure 2.57). It is the value whereby 50% of the population is below this velocity value. The use of average velocities gives a deviation from the **Fermat path** (shortest travel distance between two points) in case of non-isotropic velocity conditions, because a simple straight line travel path in

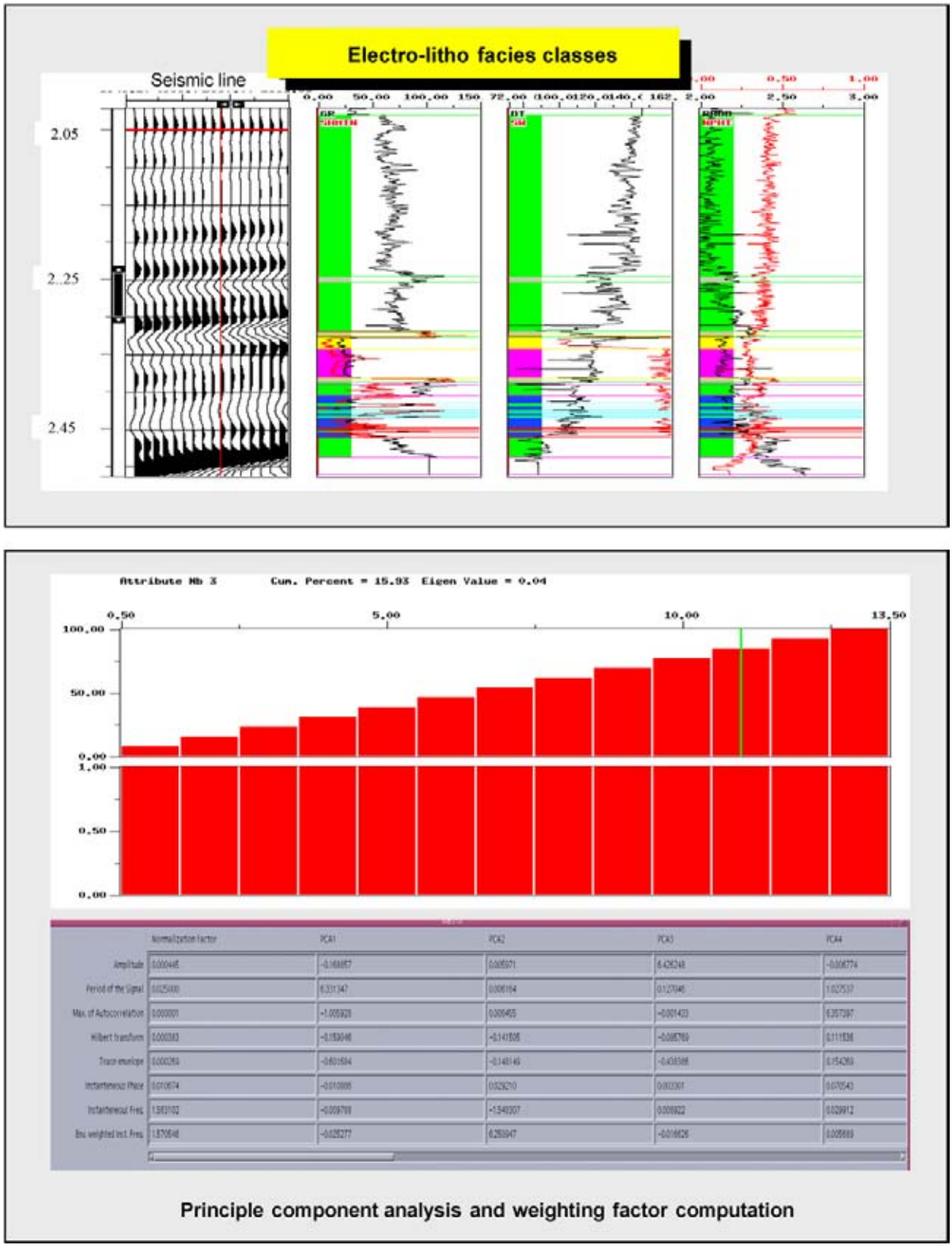

Figure 2.54: Lithofacies determinations on logs are helpful to distinguish the main petrophysical units. A link is made with the seismic trace in the well. Principle Component Analysis exploits the characteristics of the seismic and well data. New PCA attributes are computed by applying weighting functions on the initial attributes. These PCA attributes show a better separation of the lithofacies clusters on the crossplots and are hence better for doing later predictions from the seismics.

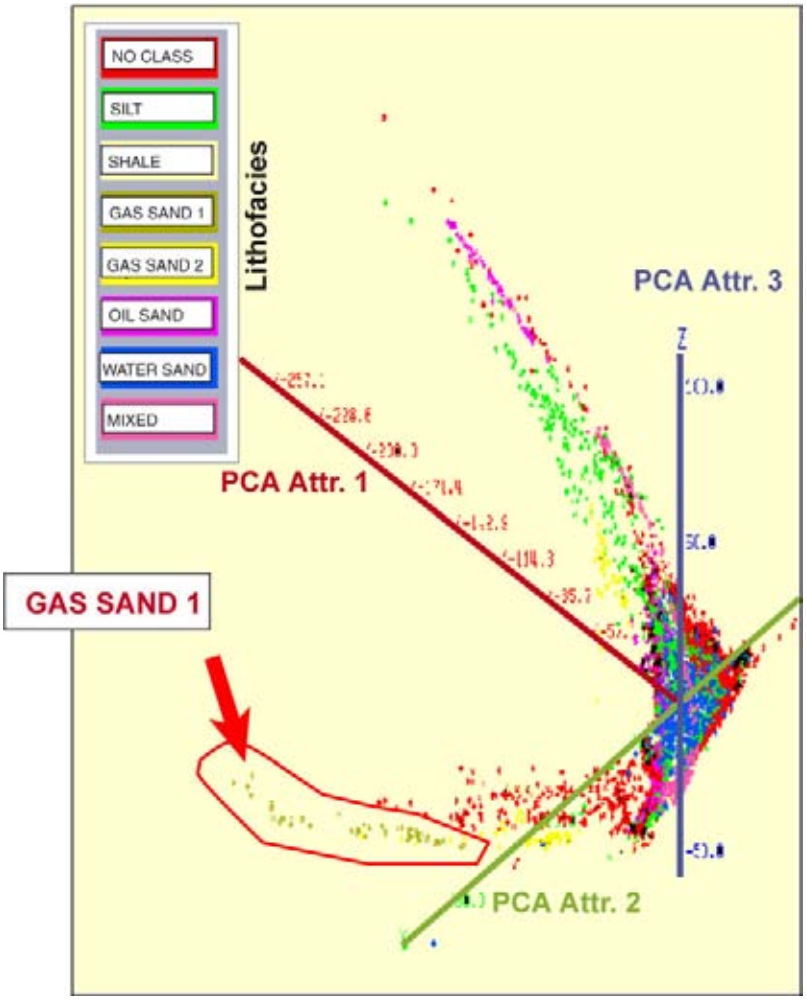

Figure 2.55: Three-dimensional crossplot between three Principal Component Attributes. The gas sands are separated in the crossplot. Each seismic sample has a discrete value for each PCA attribute assigned and therefore the gas sand cut-offs can be used to highlight their distribution in the seismic data cube.

the one layer model is assumed. In the mean velocity model the Fermat path is better approximated.

The accuracy of the interval velocity calculations depends on the thickness of the interval over which they are computed. When the interval is too small, the error in time pick may become so important that non-realistic velocities are derived. Spurious extreme excursions in velocity determinations have a great influence on the final result, especially if the interval is small there is a severe danger to make mistakes. In thicker intervals these extreme values will tend to be cancelled and are lost in the background. As a rule of thumb a bottom margin of 200 milliseconds for the time thickness is normally thought adequate to generate trustworthy results. Moreover, the top and bottom reflections should be well defined, so that a valid NMO-correction is established in the CMP or CRP gathers. **Horizon consistent velocity picking** on CMP gathers is needed to obtain reliable interval velocities suitable for depth conversion of the stratigraphic units. The best results are obtained when the data is DMO-corrected before the seismic velocity determination is done. Prestack time migration is recommendable and at the same time taking care of anisotropic effects is even better. An other source for estimating rock velocities from seismic is tomographic inversion, but the non-uniqueness of its solution can sometimes be a problem.

It is known that the stacking-velocity-derived interval velocities are always in error with the real rock measured values in the wells. This is related to the fact that:

- Seismic velocities incorporate a larger lateral component (anisotropic effect).
- Seismic acquisition uses a source signal that is lower frequent (8–100 Hz) and slower than the sonic log signal (5–10 kHz).

Hence it is always necessary to calibrated these Dix's calculated interval velocities with the well observations. This correction is needed to obtain the vertical velocity suitable to for time–depth conversion. The stacking-velocity-derived interval velocity field can be used to

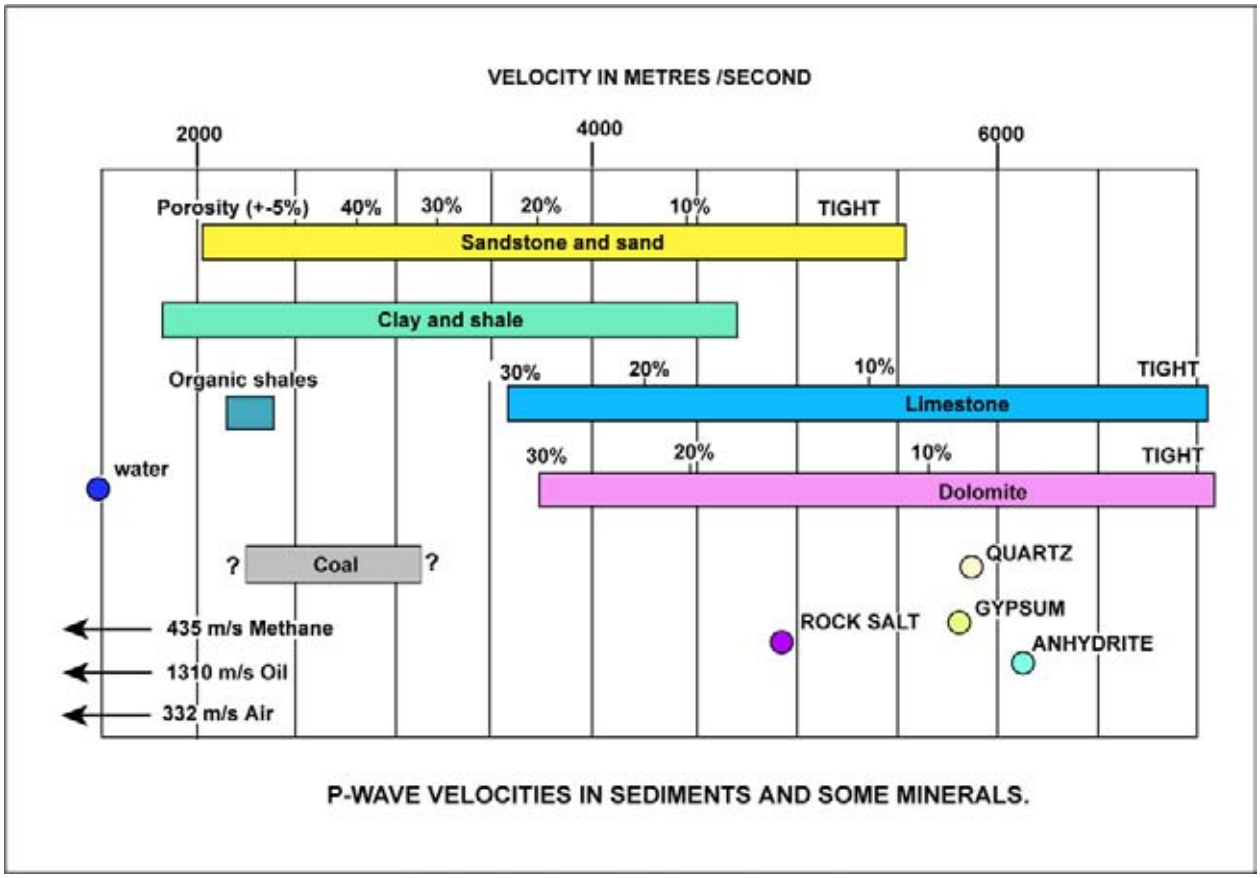

Figure 2.56: The P-wave velocity plotted against the various types of sedimentary rocks.

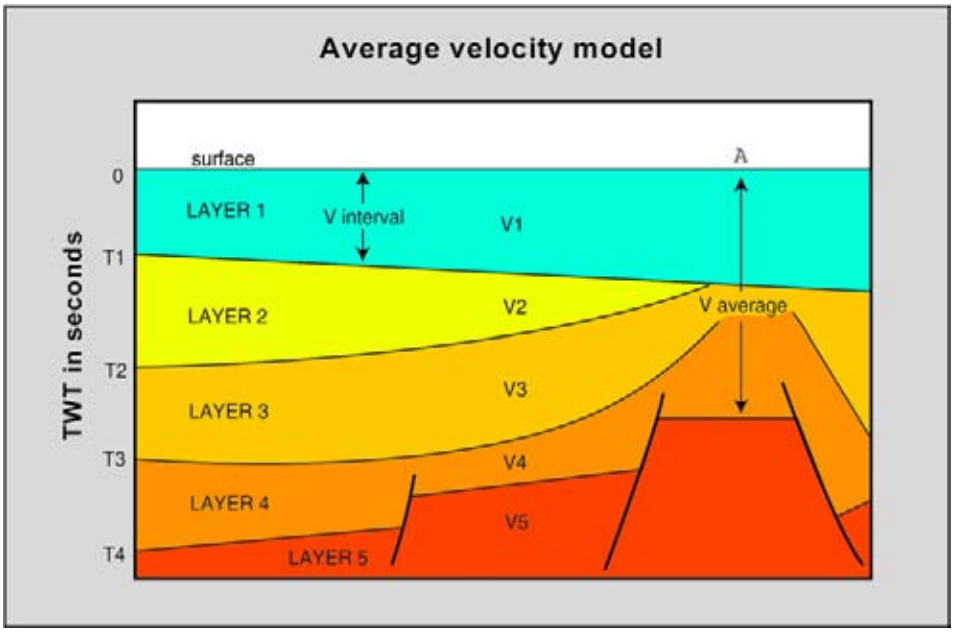

Figure 2.57: Diagram showing the interval velocity and average velocity concepts.

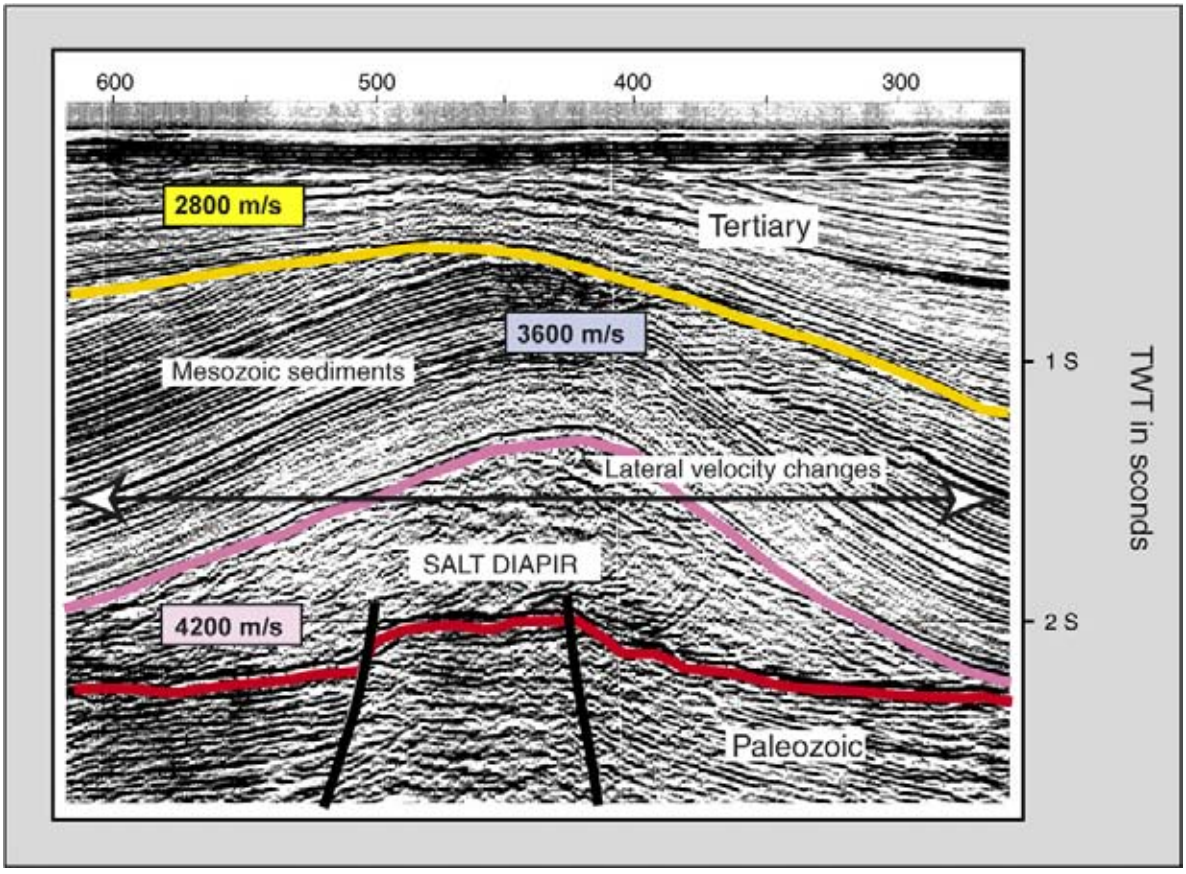

Figure 2.58: Lateral velocity changes due to the presence of a high-velocity (4500 m/s) salt diapir transecting overlying younger sedimentary sequences (modified after Owen and Taylor 1983, reprint from AAPG whose permission is required for further use).

inter- and extrapolate the velocity values seen by the wells in a more sophisticated way (collocated kriging). These stacking velocity data may serve as input for a quick and dirty depth conversion of the time sections (e.g. Time Depth Quick and TD Express of Landmark). The vertical depth conversion allows the interpreter to appreciate depositional/structural dips in a more realistic way and gives valuable feedback on the overall interpretation. The procedure removes some artefacts and distortions inherently hidden within the geometries of TWT time sections (pull-up and pull-down effects). These distortions are related to strong lateral velocity contrasts along the section trajectory, as for example salt diapirs cross-cutting the overburden geology (Figure 2.58).

The calibrated velocity field can be displayed on the seismic sections as a coloured attribute, with the amplitude behaviour plotted as an varwiggle overlay. It facilitates delineation of gross velocity units that may, or may not, correspond to discrete reflection packages correlatable to gross lithofacies units. It is customary that a velocity determination is made only every 250 or 500 metres and the velocity field is interpolated between these computing points. New visualisation techniques and powerful workstations of today allow a velocity analysis at each CDP if necessary (PGS 2003). More accurate velocity picking leads to better focusing and more reliable seismic imaging.

2.7 Data Conditioning and Reprocessing

Sometimes it is necessary to consider reprocessing of the seismic dataset in order to improve the signal-to-noise ratio. To decide for such a costly operation, the interpreter must make sure that the previous processing sequence did comprise a non-appropriate sequence of processing steps. These should be improved upon by

applying more modern techniques. The new sequence should get rid of artefacts and it should utilise an improved velocity model. Sometimes a complete new reshoot of a whole 3D survey can be a valid option (e.g. Onderwaater et al. 1996, Figure 2.59; Shabrawi et al. 2005).

Processing parameters should be chosen in such a way that they optimise the end results. For this purpose first the raw and processed CDP gathers are compared. When a lot of noise is present on the panels, then there is clear scope for improvement (Figure 2.60). The **mute function** can be changed, which means that the CDP gather is only used between a certain offset and time range. The data beyond these ranges is simply blanked (Figures 2.61 and 2.62). Often a very simple mute function is taken as an initial starting point. A more sophisticated function can be designed, better adapted to the data needs. Simple bandpass filtering can be applied (Figure 2.63). The effectiveness of the applied gain function should be investigated. Spurious energy burst in some panels are clearly to be avoided and filtered. If the noise is persistent, than the benefits of other suppression methods are examined; for instance **F–K** or velocity filtering and Radon transforms might prove a viable option. Special **spatial filters** respect the 3D nature of the seismic dataset (Da Silva et al. 2004).

Also **vector filtering** is an option when multi-component data is involved in full wave acquisition and processing. This is a trace by trace filtering technique. It uses vertical and radial trace pairs. The vertical trace is assumed to contain the desired signal and noise. The radial trace is an independent estimate of the noise (groundroll for instance) without the desired vertical signal. Vector filtering exploits cross correlation and inversion filtering to remove signal and keep the noise and this is then subtracted from the vertical trace estimate to arrive at the wanted signal. Advantage are:

- Trace by trace methodology and no data is required from adjacent traces.
- There is no spatial mixing.
- No geometric requirements needed.
- It works for aliased as well as non-aliased noise.

It can remove groundroll, Love and Rayleigh waves, and semi coherent noise like backscatter from discontinuities and point sources (Criss et al. 2005).

2.7.1 Fourier and Radon transforms

Shot-generated noise and multiples are often drastically suppressed by **F–K filtering**. **F** stands for the frequency (cycles per unit time) and K is the wavenumber (cycles per unit distance). This technique does incorporate a Fourier Transform that brings the data with the normal T–X reference axis into the F–K domain. Amplitude and phase spectra describe the data characteristics in the F–K domain.

The Fourier Transform breaks the transient seismic traces down in a continuous series of periodic sine functions. The sine waveform for a frequency f_x is described by:

$$\text{Sine function} = A_x \cos(2\pi f_x t - \phi_x) \tag{2.24}$$

A_x = maximum amplitude of f_x function,

ϕ_x = phase.

Each frequency has its discrete amplitude and phase. The phase of each individual sine wave is computed at the $T = 0$ sample. The results are visualised in a spectral analysis where the corresponding amplitude and phase spectra are plotted (cf Mari et al. 1999).

F–K plots are made for the data in this F–K domain. Often it is found that inconsistent noise in the T–X domain suddenly forms a coherent energy patch in the F–K plot (Figure 2.64). This coherent noise is easily removed by the design of linear filters. These linear filters are also known as velocity filters as their slope corresponds to a specific velocity. Care should be taken not to cut out primary energy (Figure 2.65). The F–K filter affects the amplitude of the reflections and therefore some processors are hesitant in applying such a crude filtering algorithm. When the F–K filter only cuts out the noise and leaves the primary energy untouched, then the change in amplitude is in fact beneficial as it restores the energy belonging to the real acoustic impedance contrast. It takes out the interference effect of the noise and changes the amplitude as a consequence.

Sometimes it is handy to apply a Radon transform to bring the data to the Tau–P domain (see Figures 2.28 and 2.29). The Tau stands for intercept time and P for the slowness parameter of the ray. In the Tau–P domain sometimes the noise can be removed more easily (Haneveld and Herman 1990). The transform back to the T–X domain has to be done very carefully as the operator is not orthogonal (Trad et al. 2003). Furthermore, the Radon Transform suffers from loss of resolution and aliasing, that arises from incompleteness of information due to limited operator aperture and the discretization of the digital data. Special care is therefore required.

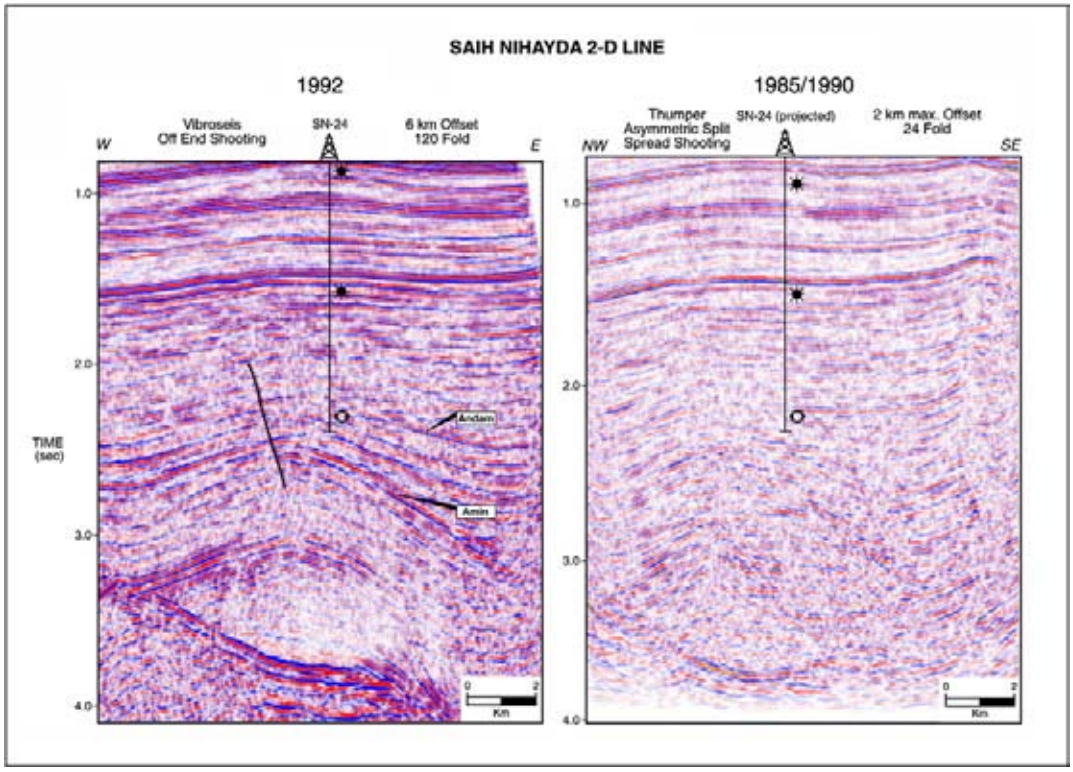

Figure 2.59: Comparison of two seismic surveys at same location. The 1992 survey with 120-fold acquisition and a 6 km maximum offset is shown on the left, while on the right the section is shown for 24-fold data with a 2 km maximum offset that has been reprocessed in 1990 (Onderwaater et al. 1996). For large offsets the anisotropy effect on the gathers can be substantial and should be addressed during the processing.

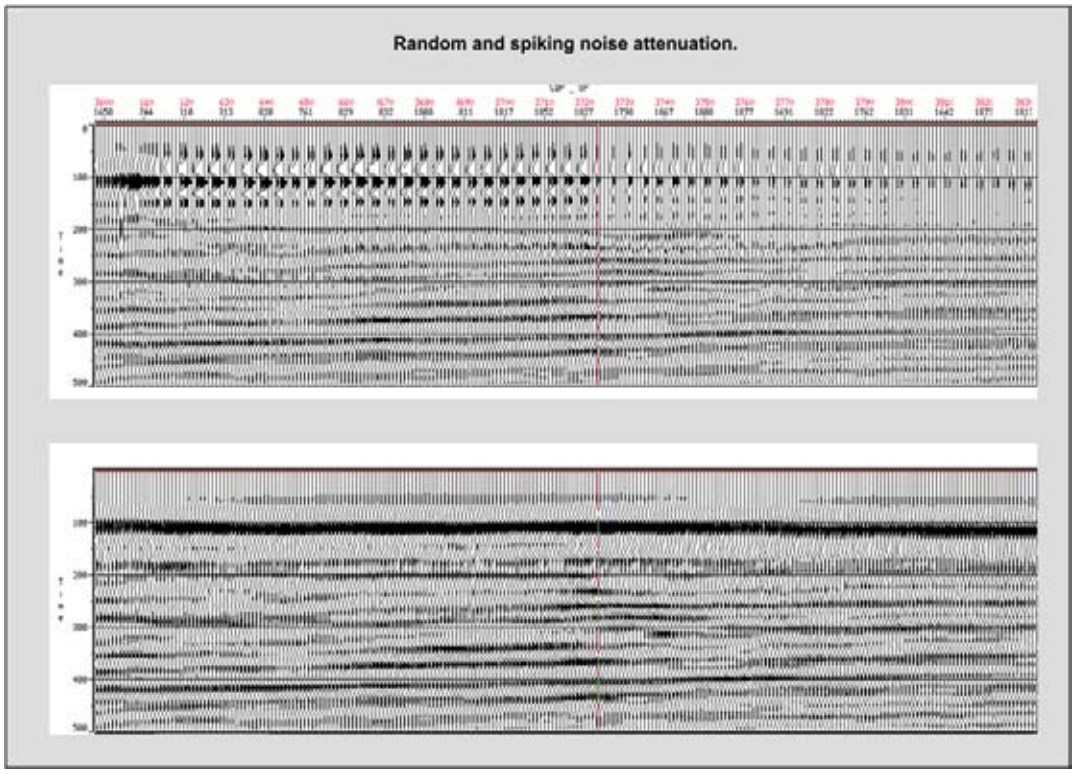

Figure 2.60: Random noise attenuation improves the quality of the seismic display and facilitates the interpretation (courtesy Pemex).

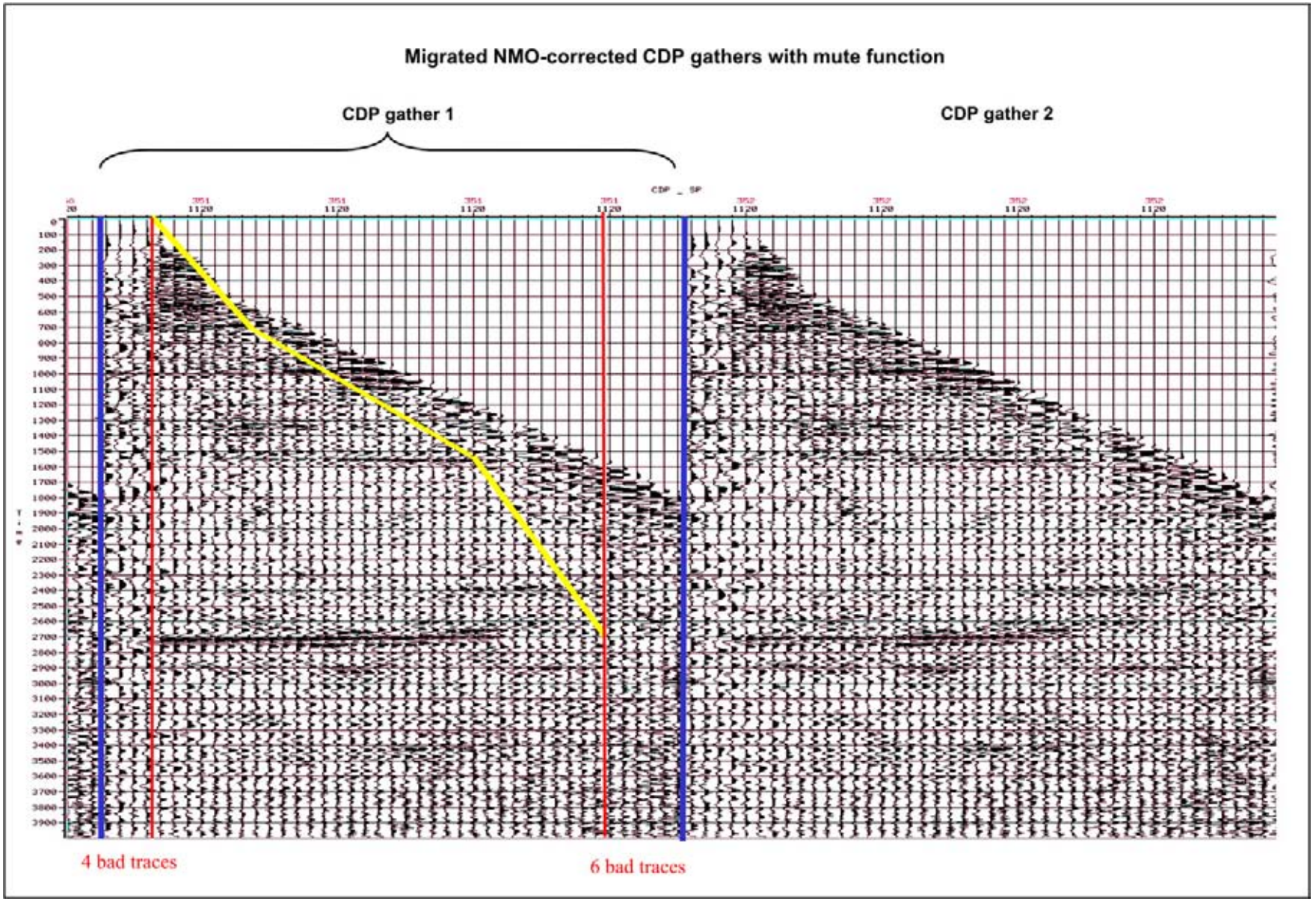

Figure 2.61: Mute function applied on CDP gather. For each trace a specific time sample range is selected. Outside this window the data is blanked. In this way the amount of noise on the traces is drastically reduced.

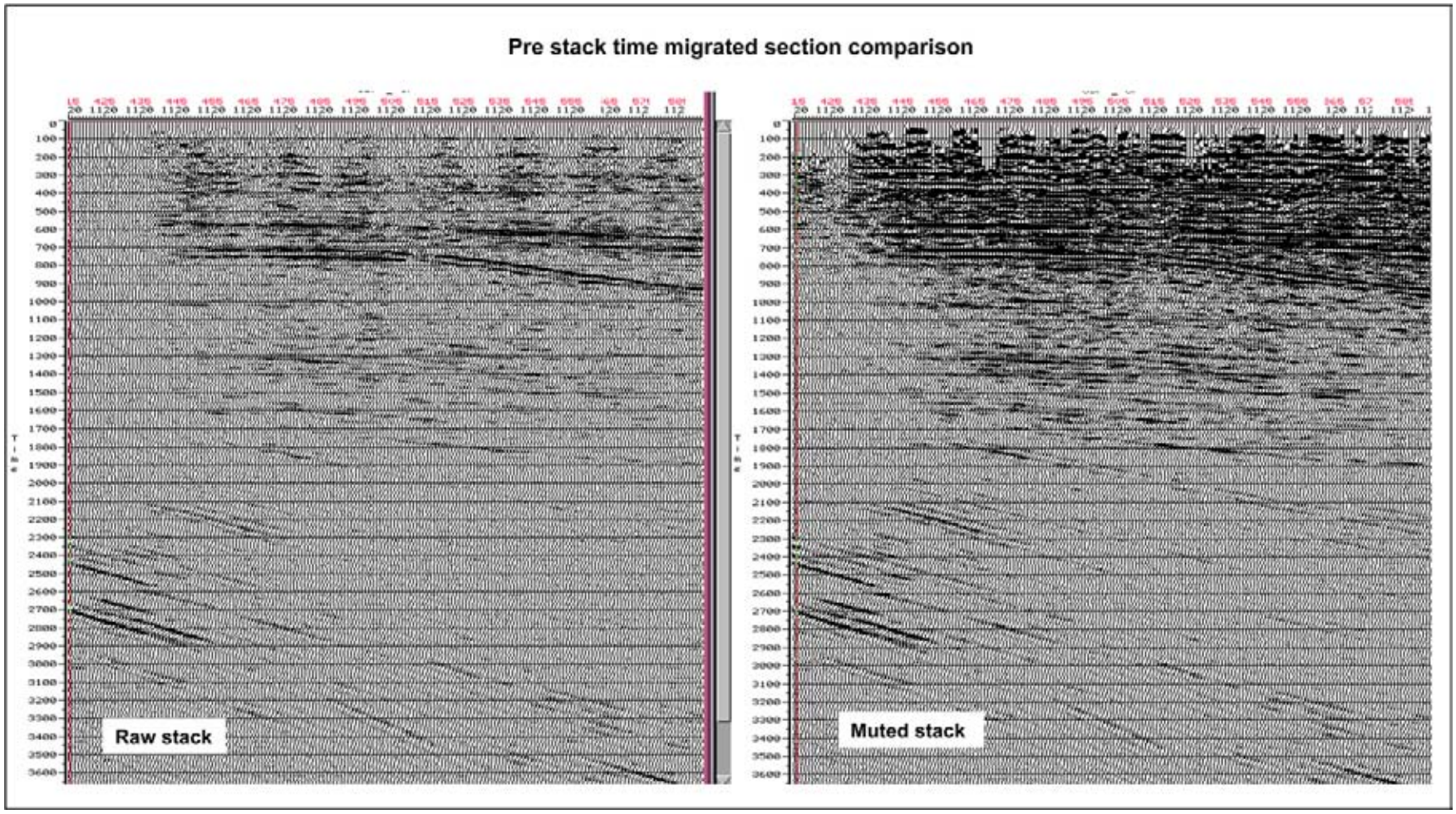

Figure 2.62: Comparison of raw stacked seismic line and the same line whereby the mute function is applied on the CDP gathers before stack.

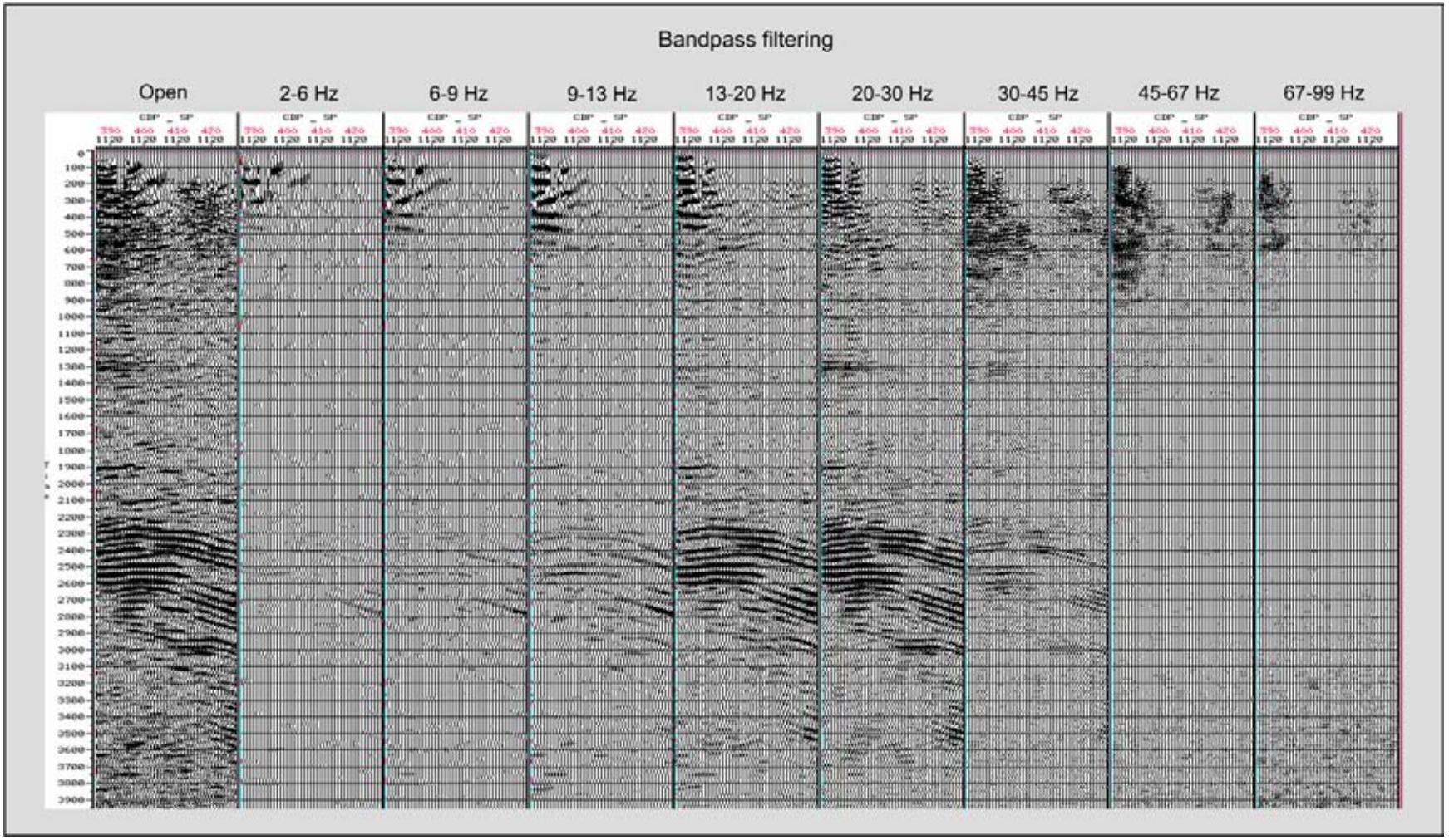

Figure 2.63: Simple bandpass filtering can be effective to remove noise. It often also cut outs primary energy, so more sophisticated ways are needed to improve the data quality. The data shows that most of the real seismic energy is present between 9 and 45 Hz. The high frequencies are restricted to the shallow part of the dataset due to progressive energy absorption with increasing depth.

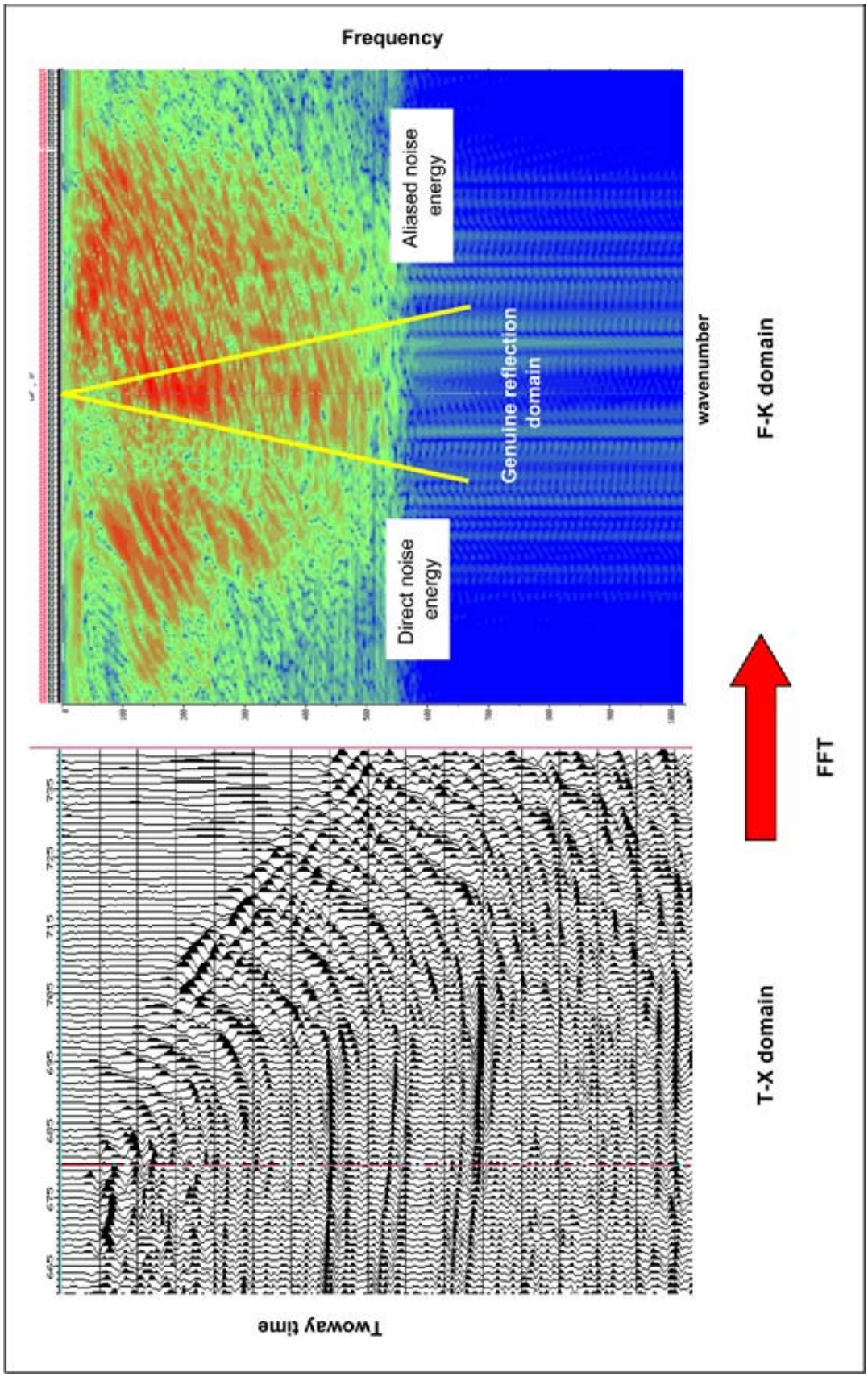

Figure 2.64: Velocity filtering in the F–K domain. Energy areas can be identified in the F–K plot, that correspond to certain types of noise. A discrete velocity is represented by a specific slope of the lines in the plot.

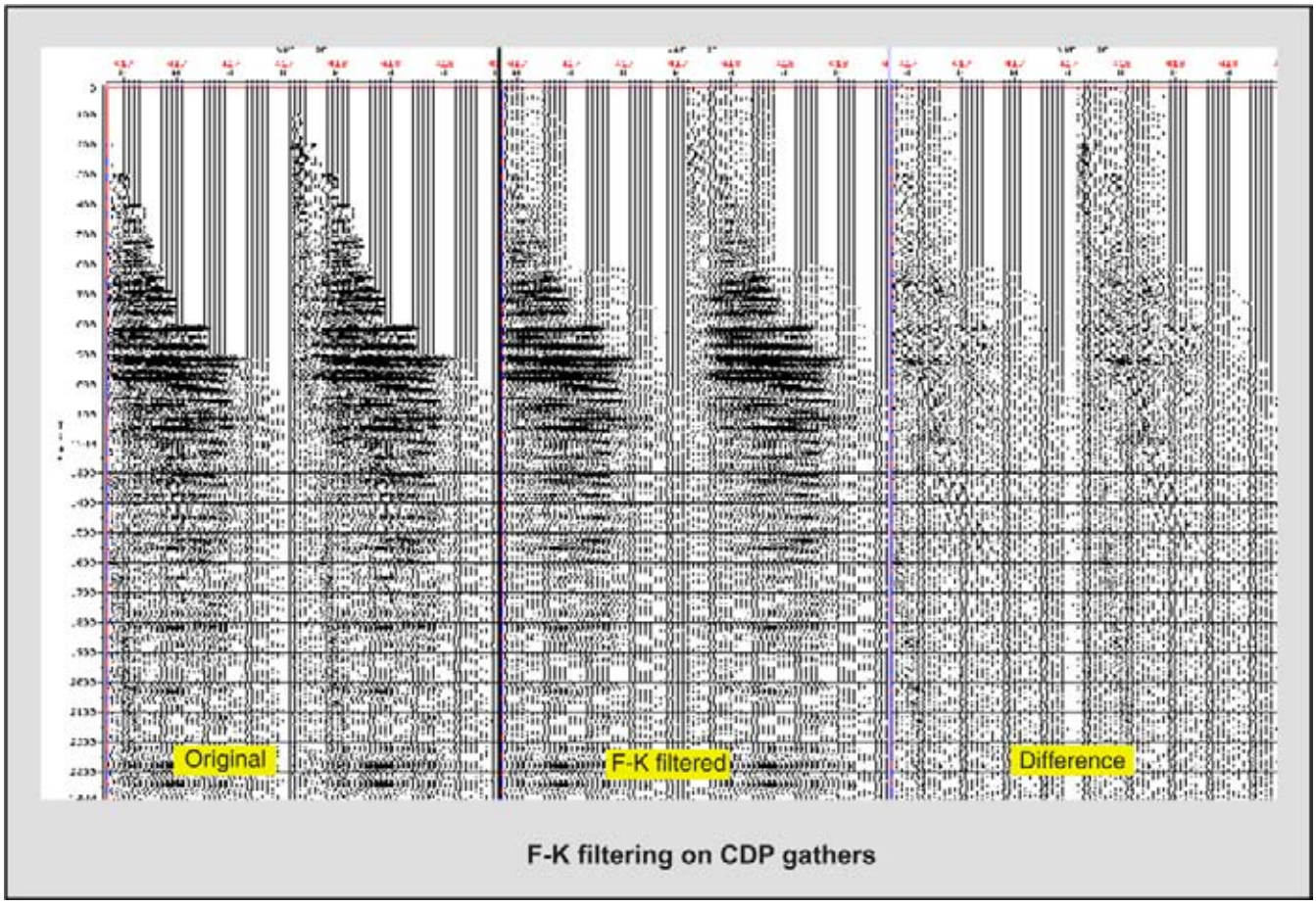

Figure 2.65: Effect of F–K domain filtering on some CDP gathers.

2.7.2 Dip Move Out (DMO)

A Dip-corrected Move Out **or DMO** step is useful in areas with rather steep dips. DMO corrects the skewness of the reflection hyperbola due to dipping reflectors (Figure 2.66). It is also known as a partial migration operation (Yilmaz 1987). The DMO correction leads to a better velocity spectrum with a better defined stacking trend (Figure 2.67). The velocity spectrum computed from the DMO-corrected CDP gather yields a much more satisfactory velocity function that is easily delineated. It ensures that automatic velocity pickers have less problems to work accurately. The partial migration character of the DMO operation suggests it is best applied before doing the velocity analysis and the stack.

An even better solution to the positioning problem is to perform a complete depth-migration exercise. The depth migration is based on ray-tracing techniques and takes into account the best velocity model for the subsurface (see Section 2.2.2). This improves the positioning of the seismic energy and focuses the subsurface imaging (Jones et al. 1995, 1996). More adequate removal of shot-generated noise and multiples is one of its benefits, because better velocities and the proper raypath are taken into account.

2.7.3 Deconvolution or inverse filtering

In order to establish the polarity of an interface unambiguously, it may prove necessary to reprocess the lines. In minimum phase processing there might exist a degree of ambiguity on the polarity of an interface. This is for example the case when the onset of the loop is overshadowed by the high-amplitude tail of the previous reflection. As stated already before, **wavelet deconvolution** is often done to focus (or sharpen) the seismic data and it changes minimum-phase data into a zero-phase response. This deconvolution step tends to shorten seismic response from a reflector and tries to re-position the maximum energy of the wavelet on the velocity/density interface. In fact it is attempted to replace the registered seismic signal by a spike at

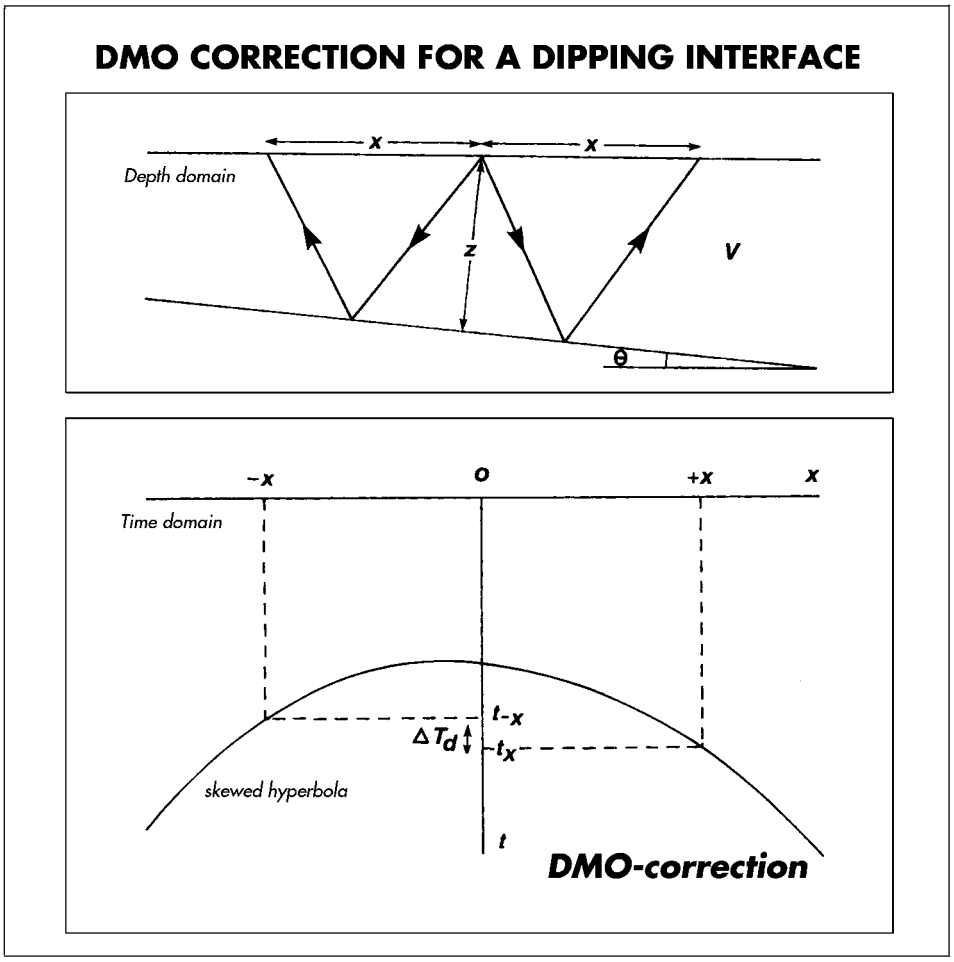

Figure 2.66: Dip Move Out or DMO correction for a dipping interface. The reflection hyperbola is skewed and the T_X is not equal T_{-X} travel time. The correction is equivalent to a prestack partial migration and the amount of vertical time shift is equal to $T_X - T_{-X}$ (modified after Kearey and Brooks 1991).

the acoustic impedance interfaces. A spike is never obtained as the filter would have to be of infinite length and this is physically not feasible. Deconvolution is a delicate process and it should be done with some care. Otherwise the inferred polarity and phase of the seismic response may be incorrect and the reservoir characterisation will become a rather tricky affair.

Many components of seismic response cannot be removed by simple frequency filtering as it contains the same frequency bandwidth as the primary data. Suppression of consistent noise is achieved by inverse filtering or deconvolution.

The decon procedure compensate for the filters that are formed by the earth along the transmission path of the input pulse and the recording system. When the earth and recording filters are convolved with the seismic signal, it tends to lengthen the original input signal. Lengthening implies more overlap and interference of reflector response and therefore the end section is more difficult to interpret. Often the seismic trace is viewed as a **Green's function** convolved by a source wavelet. The Green's function is the solution of a differential equation with an impulse response as exciting force (Sheriff 2002).

Several types of deconvolution exist:

- **System deconvolution**, taking care of the distortion (or filtering effect) caused by the recording equipment.
- **Gapped decon**, whereby multiples are expected at a certain time distance from the primary and the auto correlation values in the gap are not used in the deconvolution operator (Telfort et al. 1990).
  * **De-reverberation**, which is removing ringing of multiple energy.
  * **De-ghosting** removing short-path multiples.

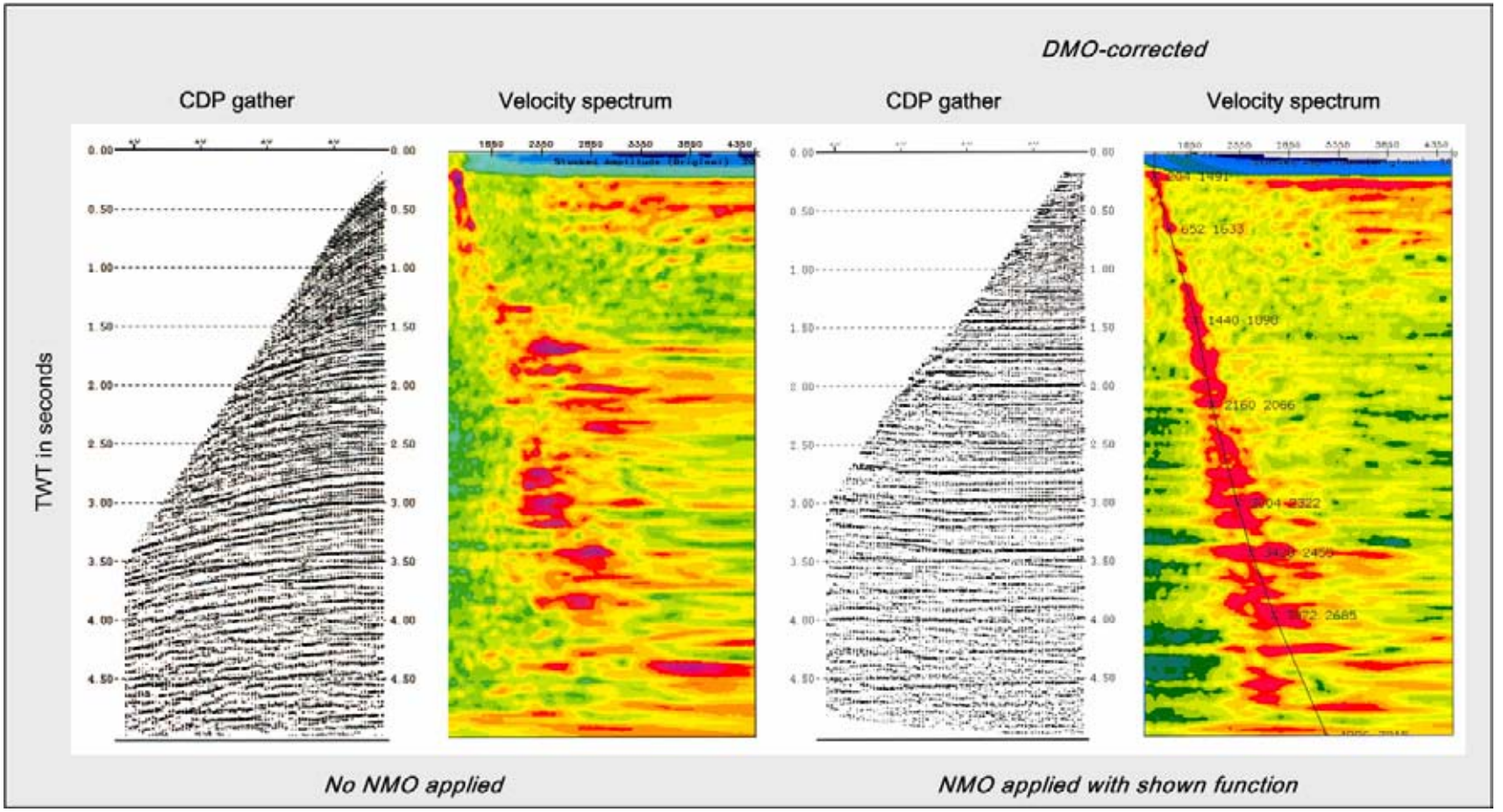

Figure 2.67: CDP gathers and velocity spectra for initial seismic input and data that has been DMO corrected. This partial migration procedure does a very good job in cleaning up the data as shown by the semblance plots. The automatic picking of velocity functions is facilitated by an earlier DMO correction (modified after Yilmaz 2001).

- **Spiking decon**, which tries to restore the position of the acoustic interfaces by spiked events (Dirac type of signal = spike).
- **Whitening decon**, which takes all frequencies to the same amplitude level, assuming anomalous absorption, and will result in a better spiked result.

To illustrate the deconvolution process let us assume the following:

- A composite waveform W_K composed of a spiked input extended by waterlayer reverberations.
- R_K is a reflectivity function.

The seismic response trace S_K is given by the simple convolution of W_K and R_K:

$$W_K * R_K = S_K. \tag{2.25}$$

The convolution process is mathematically represented by an asterix. Nowadays also a simple multiplication is often shown with an asterix. Convolution is equal to the change in wave shape when passing through a filter. When dealing with closely spaced reflectors the result S_K will be a complex trace because of interference of the various signal responses due to overlap in time.

Multiple energy may conceal important primary reflections and should therefore be adequately removed. Note that the short-path multiples are not removed by the CDP-stack procedure as they have very similar stacking velocities to the primary data!! Multiple attenuation does not mean that the resulting sections are completely multiple free (cf Reshef et al. 2003).

Deconvolution is the process to compress composite waveform response and represent them by a more spikey output instead. For this purpose let us assume a decon operator that is represented by the inverse filter I_K. The spike out is represented by δ_K. The decon process is now described by the following convolution:

$$I_K * W_K = \delta_K \ (= \text{spike}) \tag{2.26}$$

and also

$$I_K * S_K = R_K \ (= \text{reflectivity}). \tag{2.27}$$

If W_K is known, then the deconvolution is achieved by a matching filter utilising cross-correlation on the output of an known input signal (comparable to the Vibroseis technique). When the input signal is known, '**Wiener filters**' can be applied.

2.7.3.1 Wiener or least squares filters

A **Wiener filter** converts a known input signal into an output that is the best estimate, in a least-square sense, to a desired output. The filter optimises the output by making sure that the sum of the square differences between the actual output and desired output is at a minimum.

A digital Wiener filter has five desired kinds of output:

- A zero-lag spike.
- A spike with a certain time-lag.
- A time advanced form of the input signal.
- A zero-phase waveform.
- Any desired arbitrary wave shape.

The digital Wiener filter is conveniently represented by a matrix format.

2.7.3.2 Predictive deconvolution

In most cases S_K, the seismic response trace, is the only function known as it has been recorded at the surface. In marine surveys the input signal is measured by putting a hydrophone along the shot position, however R_K (reflectivity) and W_K (waveform with multiple energy) are the great unknowns.

To carry out deconvolution it is necessary to adopt a special approach using statistical techniques in order to design suitable inverse filters. Two basic assumptions are made:

- Reflectivity W_K is random, implying that the auto-correlation function of the recorded seismic signal S_K is equal to the auto-correlation function of the composite waveform W_K.
- The composite waveform W_K is minimum phase, which means that all energy is contained in the frontal part of the wavelet. This implies that the auto-correlation function is providing all data on the shape, with phase info derived from the minimum delay assumption.

Using these basic assumptions, the approach allows the **stochastic prediction** of the composite waveforms shape, which can then be used in a Wiener filter.

If the desired output of the Wiener filter is a spike function, than this kind of deconvolution is known as '**spiking decon**'. As a spike is composed of all frequencies with the same amplitude (white noise) it is logic to apply some whitening to the data as this will result in a better spike. This is exactly what is done in

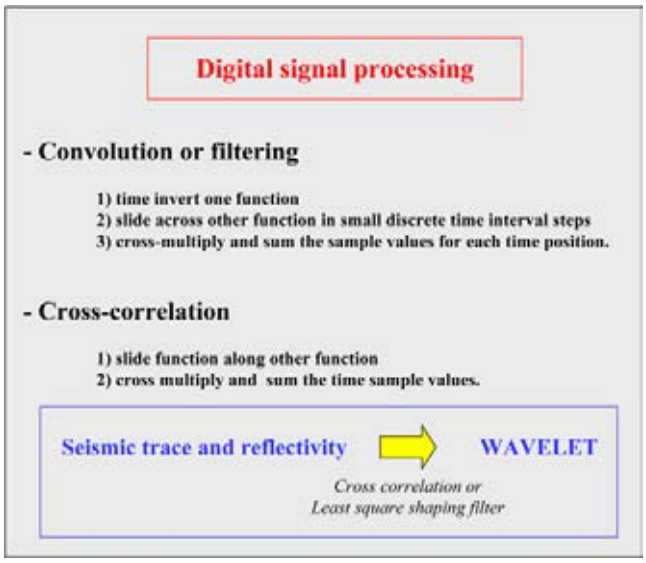

Figure 2.68: Cross correlation technique performed on waveforms provides a measure for their similarity. Cross correlation is a digital operation that is quite similar to convolution. The difference is that the time inversion step for one of the waveforms is here not included.

the '**whitening decon**' procedure. This whitening of the frequency spectrum should only be done in the context of deconvolution. There is a danger that uncontrolled whitening of the frequency spectrum can enhance artefacts (e.g. boost unwanted multiples in the Magpie 3D, Brunei offshore) or degrade the accuracy of seismic thickness prediction (Hill 2005). Testing can prevent such processing errors.

Auto-correlation functions are important in designing **predictive deconvolution** filters. They are a special case of cross-correlation (Figure 2.68). In practice only approximations of the spiked response are obtained because:

- The ideal filter should have an infinite filter length, which is clearly not feasible.
- The statistical assumption about the random subsurface geology is not true.

The deconvolution is applied before or after the stacking operation:

- DBS = Decon Before Stack.
- DAS = Decon After Stack.

Decon before stack is usually preferred as it augments the efficiency of the stacking procedure. Deconvolution usually gives dramatic improvements on the interpretability of seismic sections, despite all the assumptions made. Apart from the above described procedures, deconvolution can be taken a step further when reservoir characterisation is the aim and stratigraphic deconvolution is done, as shown later in this textbook.

2.8 Enhancements in the Seismic Reflection Techniques

Seismic interpretation has improved a lot during the last decade. It is illustrated by the shapes of the contours on various depth maps from the same investigation area in time (Figure 2.69). Acquisition and processing of **3D surveys** has stimulated better interpretation techniques (Figure 2.70). The design of special source configuration may help to reduce artefacts and improve the resolution as well as the penetration depth (e.g. Maresh and White 2005). The use of micro-electronic mechanical system sensors (MEMS) help to improve the sensitivity, the dynamic range and reduce the noise (Mougenot and Thorburn 2004) of the seismic captors. The **pseudo-3D migration** (based on in- and cross-line information) resolves much better complex subsurface structures. Real 3D migration algorithms are giving even more precise results, but on the other hand it is also more costly. **Structural aliasing** (wrong line-up of faults), due to an erroneous pattern recognition, are considerably reduced by the denser seismic coverage (Figure 2.71). The 3D cube provides the interpreter with more reliable and better sampled fault pattern. The line spacing is typically 25 by 25 metres. The availability of horizontal **time slices** gives improved control on the internal consistency of the seismic interpretation (Figure 2.72). Interpretation of time-slices can prove pretty time-consuming, but the reward is a great feedback on the geometry of the mapped seismic marker. The dip information is directly read from the time slice. Flat horizons are represented by very broad loop intersections on the time-slice, while steeply dipping events will result in many closely spaced loop crossings. Sometimes the fault intersections are very subtle discontinuities, difficult to discern. Sedimentary features are enhanced by the slices, but should

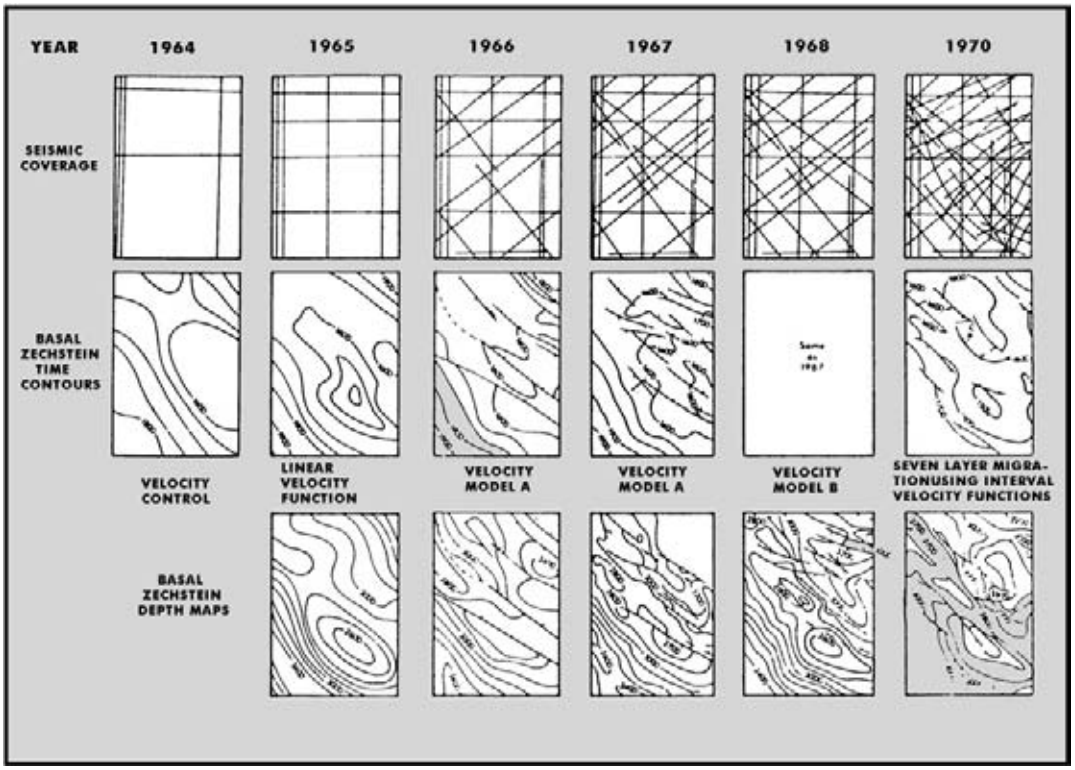

Figure 2.69: Advances in seismic interpretation are illustrated by successive depth maps over the same study area. The fault pattern gets more complicated and becomes more realistic by incorporating additional data (modified after Yilmaz 1987).

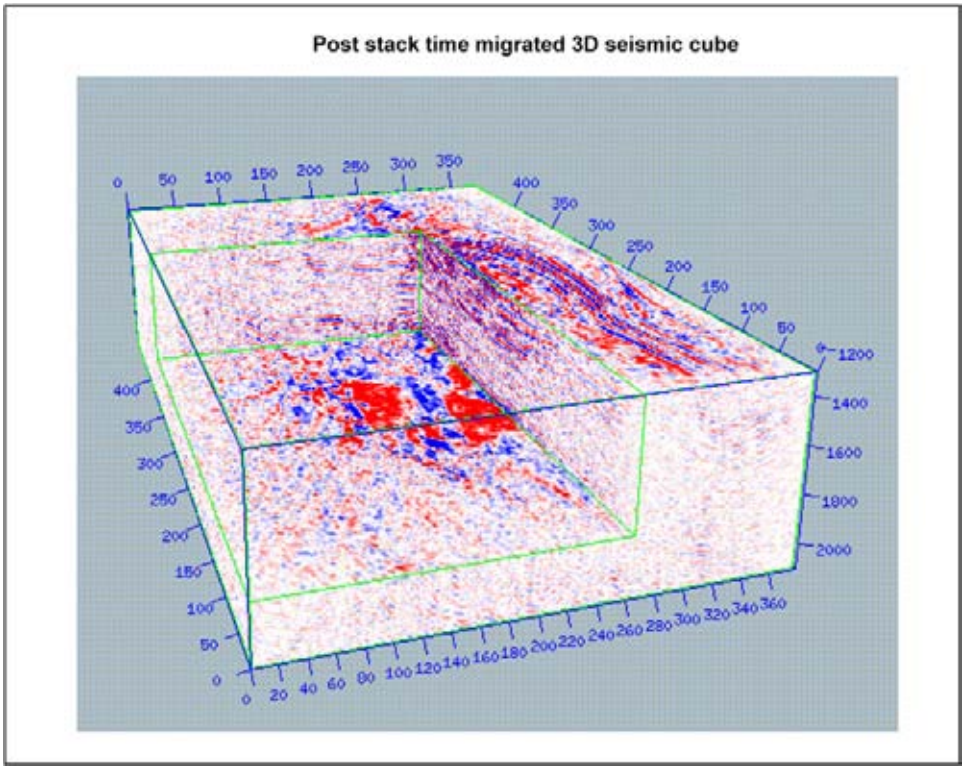

Figure 2.70: 3D visualisation of a 3D seismic survey. The data time cube is shown with inlines, crosslines and horizontal timeslices.

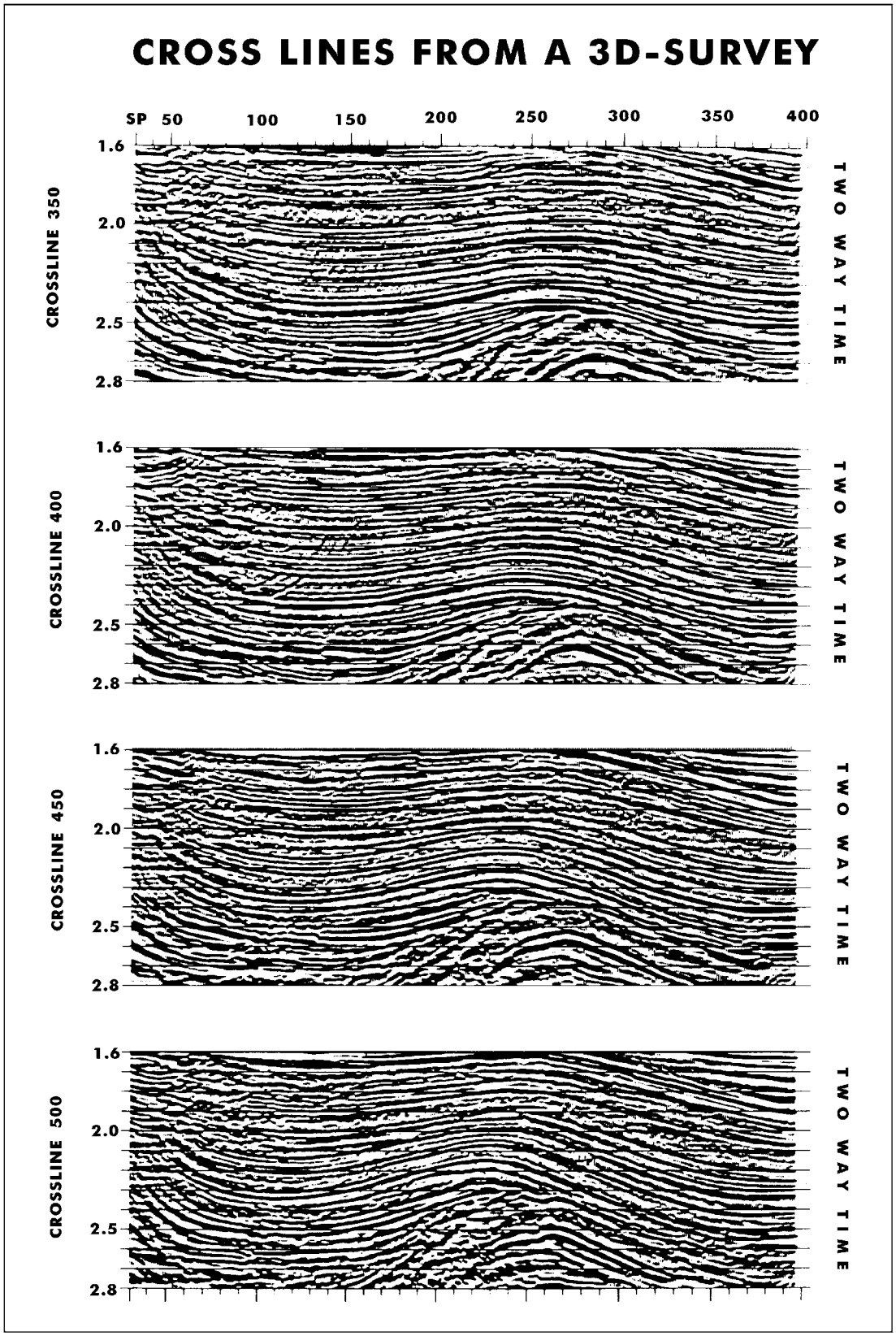

Figure 2.71: Panel of 3D seismic lines giving a convenient overview of the lateral change of sub-surface structures (after Yilmaz 1987).

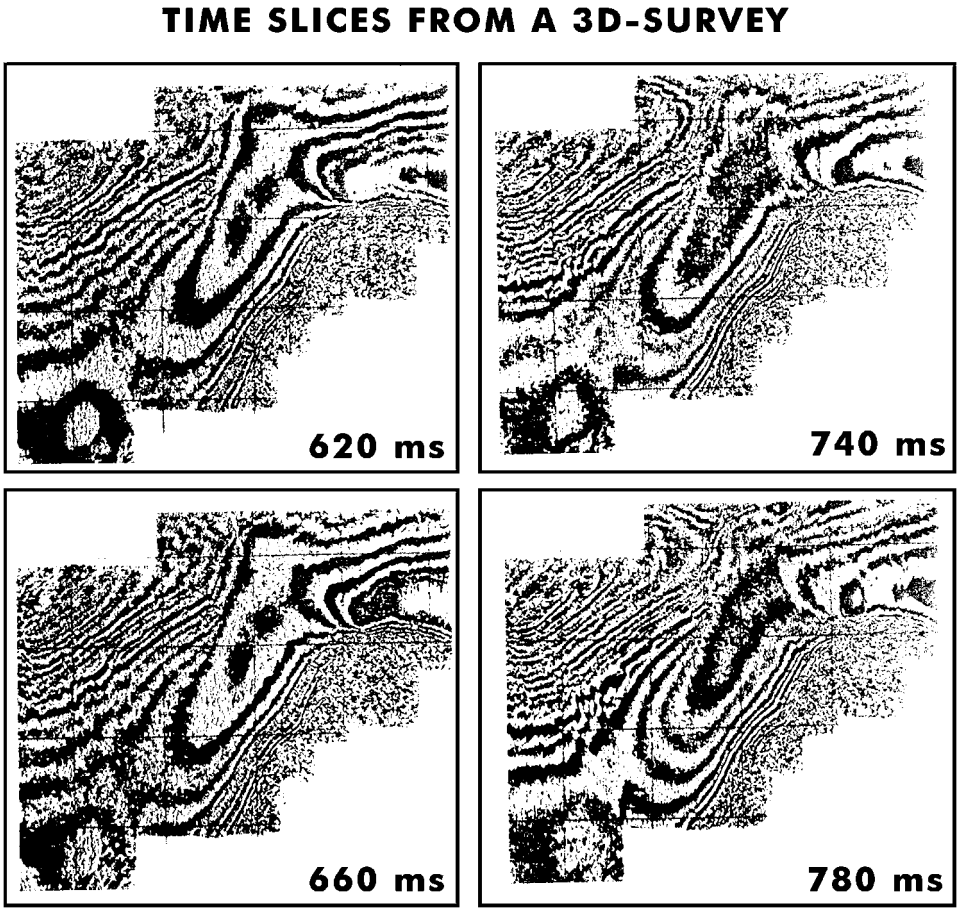

Figure 2.72: Horizontal time slices from a 3D seismic survey (modified after Yilmaz 1987).

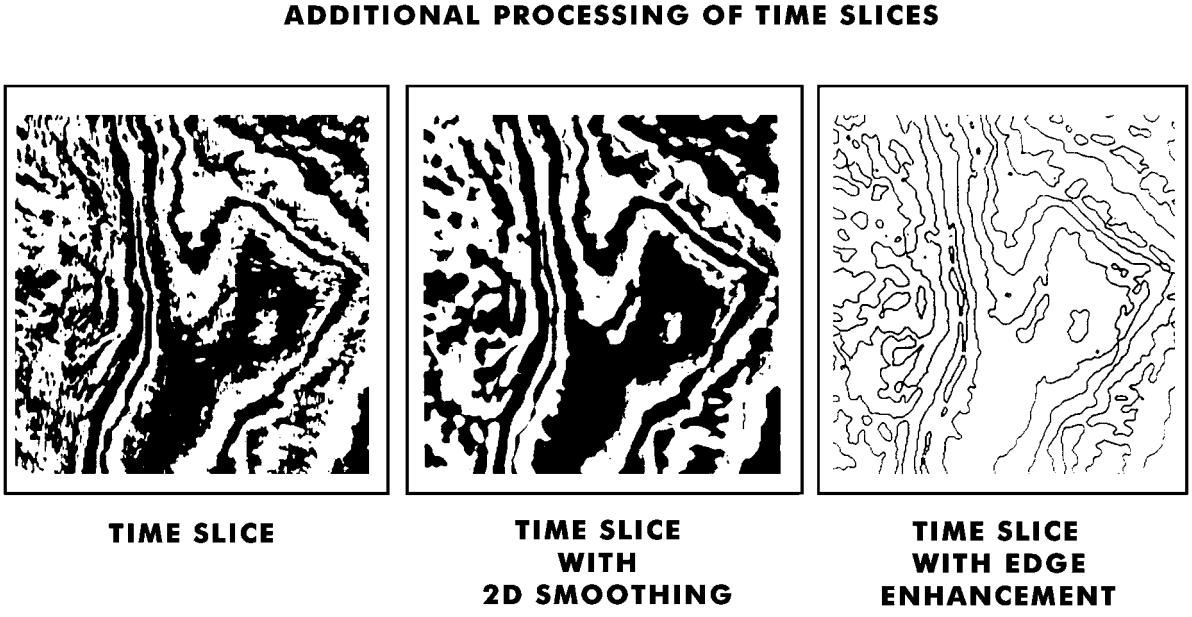

Figure 2.73: Special processing effects on horizons and maps. A short median filter helps to smooth the interpretation without destroying the geometry of the fault planes (modified after Yilmaz 1987).

not be confounded with tectonic disturbances and/or processing artefacts.

Additional map and horizon processing, like for example smoothing with edge enhancement (median filter), help to maximise the resolution of the subsurface data (Figure 2.73). Subtracting the smoothed horizon map from the unsmoothed version (residual maps, Brown 1999) brings out structural lineations that might be of interest. **Flattened horizon** displays often illustrate sedimentary features quite nicely (Figure 2.74). **Horizon slices** can be made as opposed to the earlier mentioned time slices. These slices can be useful to determine the presence of depositional features. Even **strata slices** can be made, that are slices with a constant relative geological time age (Stark 2004).

Imaging software and **3D visualisation** (e.g. GoCad™ and Voxelgeo™) provides a better feel for the mapped surfaces (Figure 2.75). Co-visualisation of multiple datasets is extremely useful and the possibility to browse at will through these datasets is essential (cf Hardy 2004). **Voxels** are 3D unit cells (inline, crossline, time sample) that have attribute values stored in them. These characteristics are then used to make selective displays. **Opacity** or **transparency** of voxels are essential features in the 3D visualisation. Cut-off values permit to select voxels corresponding with certain reservoir characteristics. Sedimentary patterns are thus highlighted. Opacity controlled horizon slice is a powerful option (Srivastava et al. 2005). **Gated amplitude** measurements and detailed **geobody checking** is of interest in this respect (e.g. Massafero et al. 2003). It is well suited to illustrate the continuity of sedimentary units in a 3D sense, via a volume rendering technique.

Ray tracing and map migration (e.g. Petrocaem™ and Geomig™) results in more reliable depth contour maps. Depth migration (e.g. Geovista™) puts depth maps directly at the interpreter's disposal. It uses a better defined velocity model of the subsurface and also allows the processing algorithms to work more efficiently.

Geostatistical methods (e.g. Sigmaview™) allow to quantify uncertainties in the interpretational method (Figure 2.76). It also provides a convenient means to model or simulate the subsurface structures and compute volumetrics for the different scenarios (Haas and Dubrule 1994, Haas et al. 1994, Jensen et al. 2000). However, sufficient well control is needed as input to make reliable predictions later on.

Different **seismic attributes** can be displayed and examined in detail (Figures 2.77 and 2.78). Acoustic impedance gives an improved link between seismics and the well data (Figures 2.79 and 2.80). AVO effects on CDP gathers need to be examined (Figure 2.81).

Artificial illumination of maps re-enforce fault plane edges and highlight interesting anomalies (Figure 2.82). It may enhance sedimentary features, like channel systems. Three types of light sources are in general available (James and Kostrova 2005):

- Diffuse light, attenuated by the cosine of the angle between the light direction and the normal to the incidence plane.
- Specular light, attenuated by the cosine of the angle between the normal to the plane and the bisect of the angle between the light source direction and the viewer direction.
- Emissive light, with radiation from the object itself.

The material and texture of objects are conveyed by the size, the intensity, colour of the specular reflections, added to some real world knowledge. These aspects are often used to bring out the 3D structuration of surfaces in cube displays.

It is possible to carry out seismic attribute analysis not only on a particular horizon, but apply the techniques to a certain time interval or window. The **energy** contained in seismic loops, which is the square of the seismic amplitude, is for instance computed. The number of zero-crossings in the zone of interest can be determined. Also the characteristics of the loop at the top or base of the reservoir are examined. The area below the wiggle line can be determined and the wiggle (or arc) length extracted. The **composite amplitude** is given by the combined amplitude response at the top and base of a mapped reservoir sequence (Brown 1999).

A processing window is applied to compute a representative attribute value. This methodology implies some sort of averaging technique and makes it possible to visualise the spatial distribution of various reservoir characteristic features. It is for instance rather easy to calculate the average amplitude contents of the seismic reflections within a salt diapir interval on time sections. The info of a geo-body is often displayed in a normalised way. For instance a '**RMS amplitude**' attribute map (Root Mean Square; measure for energy in a loop or time window) is compiled. It is calibrated with the amount of hard rock layers (or floaters that consist of carbonate and dolomite) found within the salt deposits in the wells. This gives the interpreter a possibility to extrapolate these observations all over the survey area. It equips him with a prediction tool on the distribution of these hardrock bodies. The delineation of these high-velocity

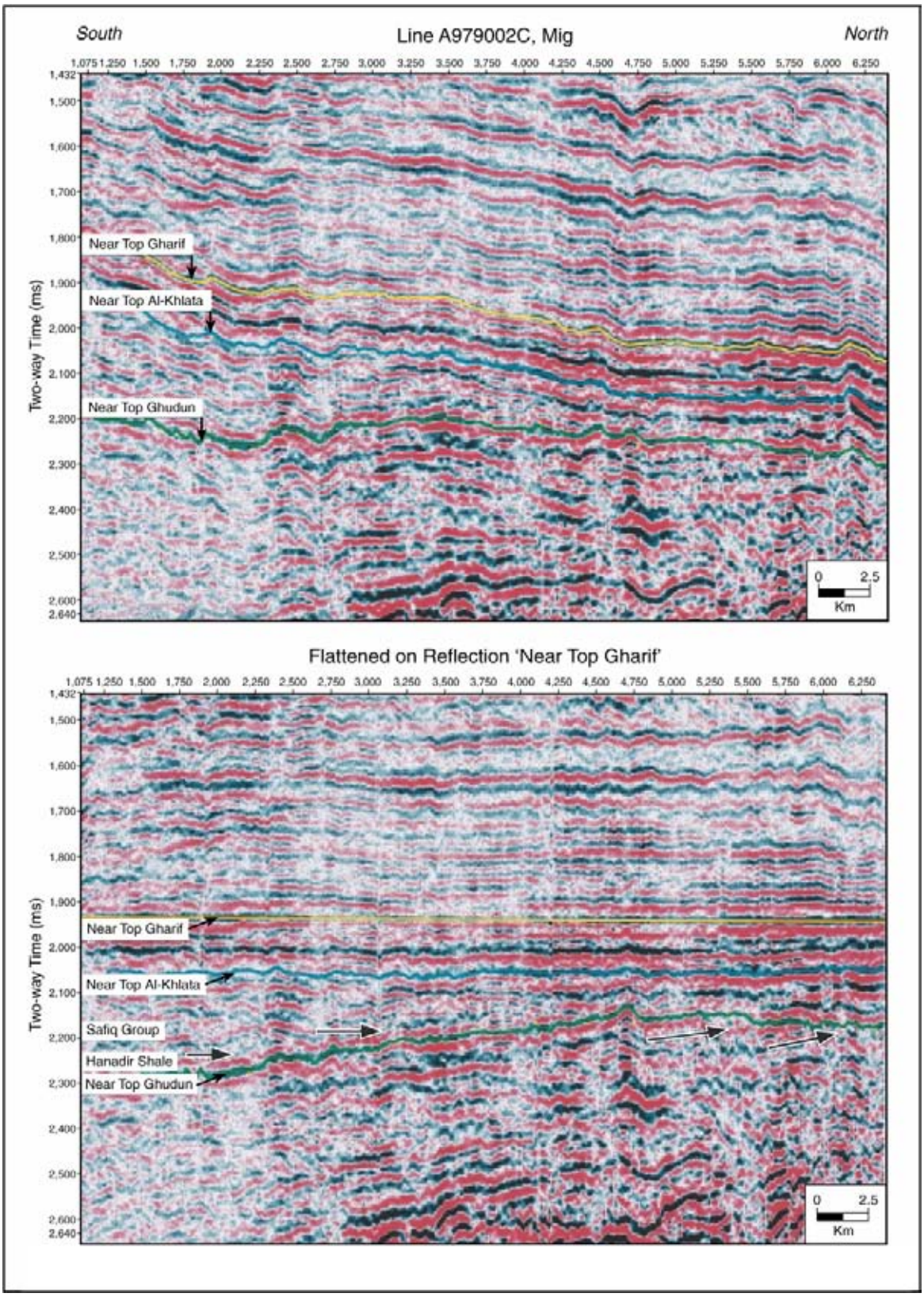

Figure 2.74: Horizon flattening helps to appreciate the original depositional geometries. An apparent 'downlap' on the section above, becomes an onlap on the section below when the later tectonic deformation is compensated (Oterdoom et al. 1999).

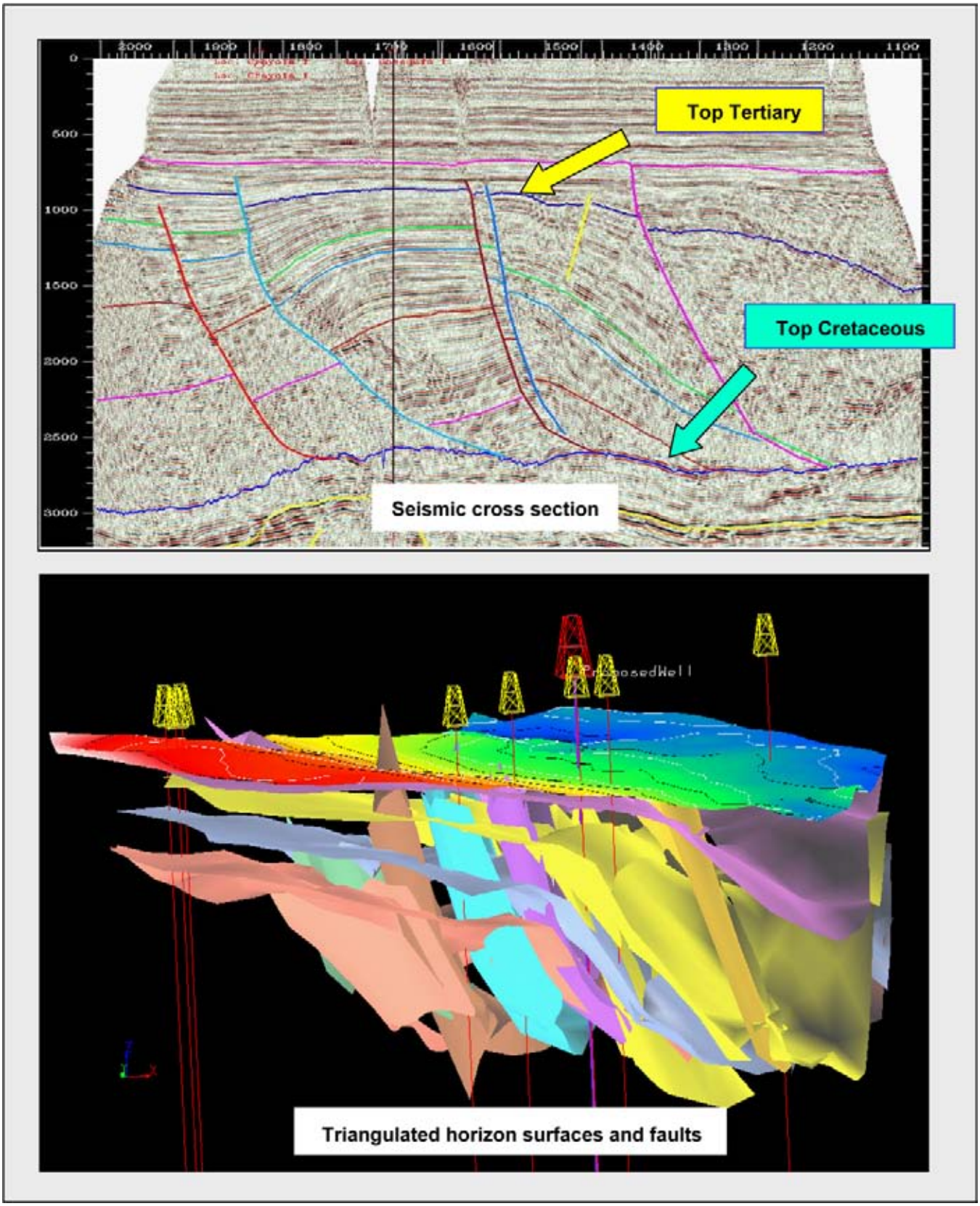

Figure 2.75: GOCAD surface modelling visualises the 3D structuration of the subsurface. Not only mapping, but also volumetrics and modelling facilities are provided by this integrated software package. The geometry of horizons and fault planes are here shown, which are input for property modelling in a subsequently constructed 'shared earth' model (courtesy Pemex).

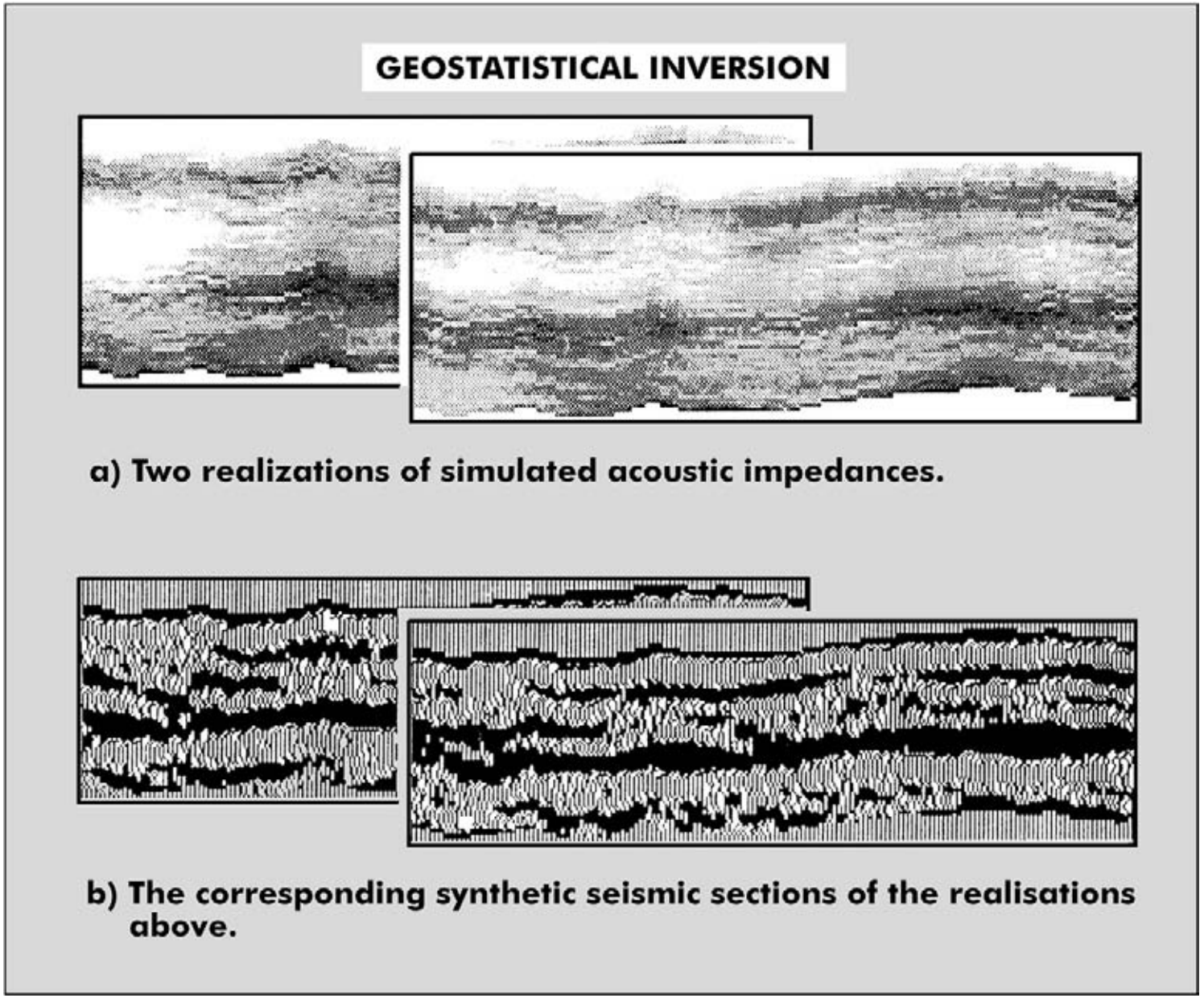

Figure 2.76: Geostatistical techniques help to assess the structural configuration of the subsurface by taking uncertainties into account (modified after Haas and Dubrule 1994).

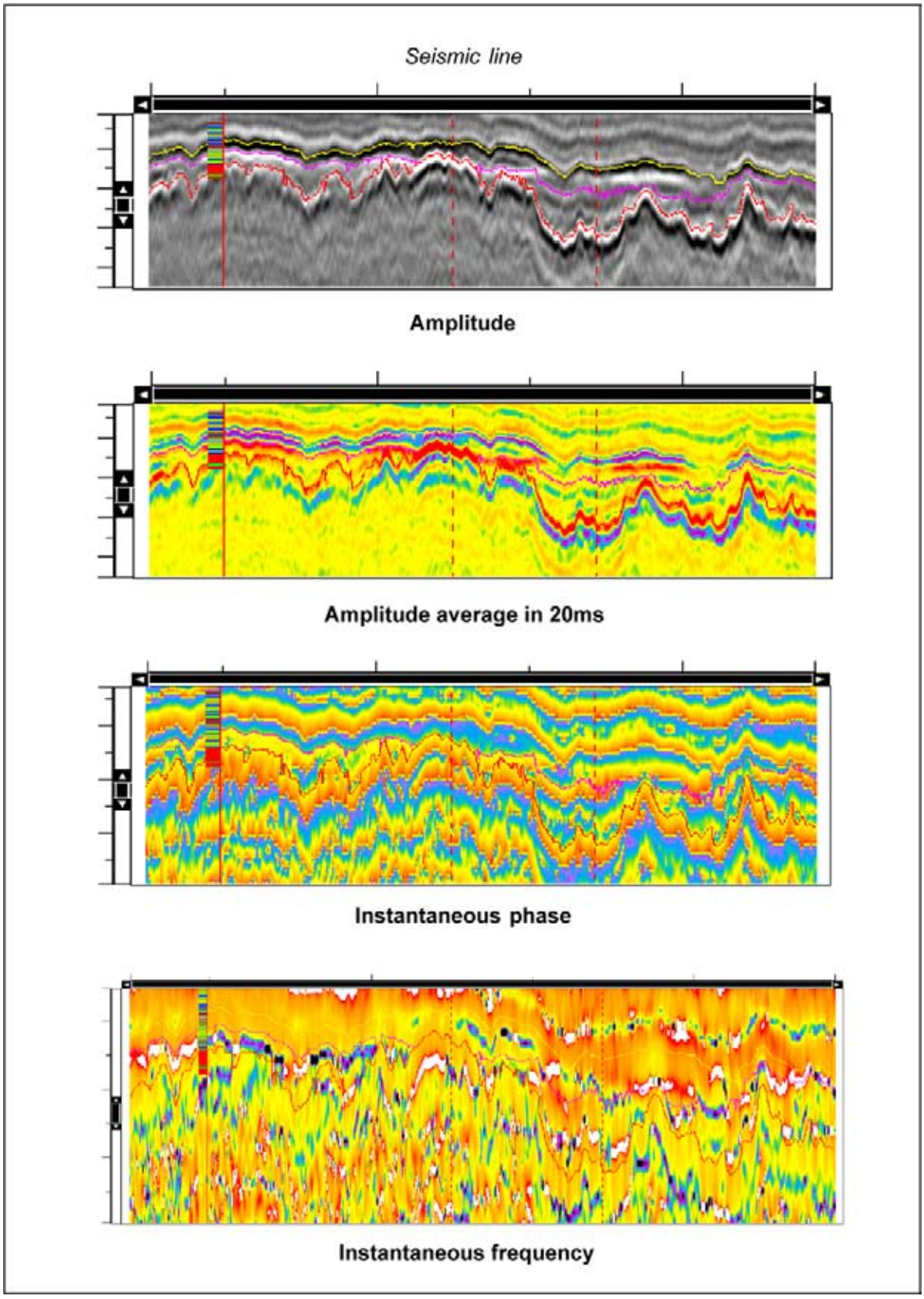

Figure 2.77: Seismic attribute displays help to check the consistency of the interpretation and to verify in detail the subsurface earth model. Instantaneous phase and frequency is computed via the Hilbert transform.

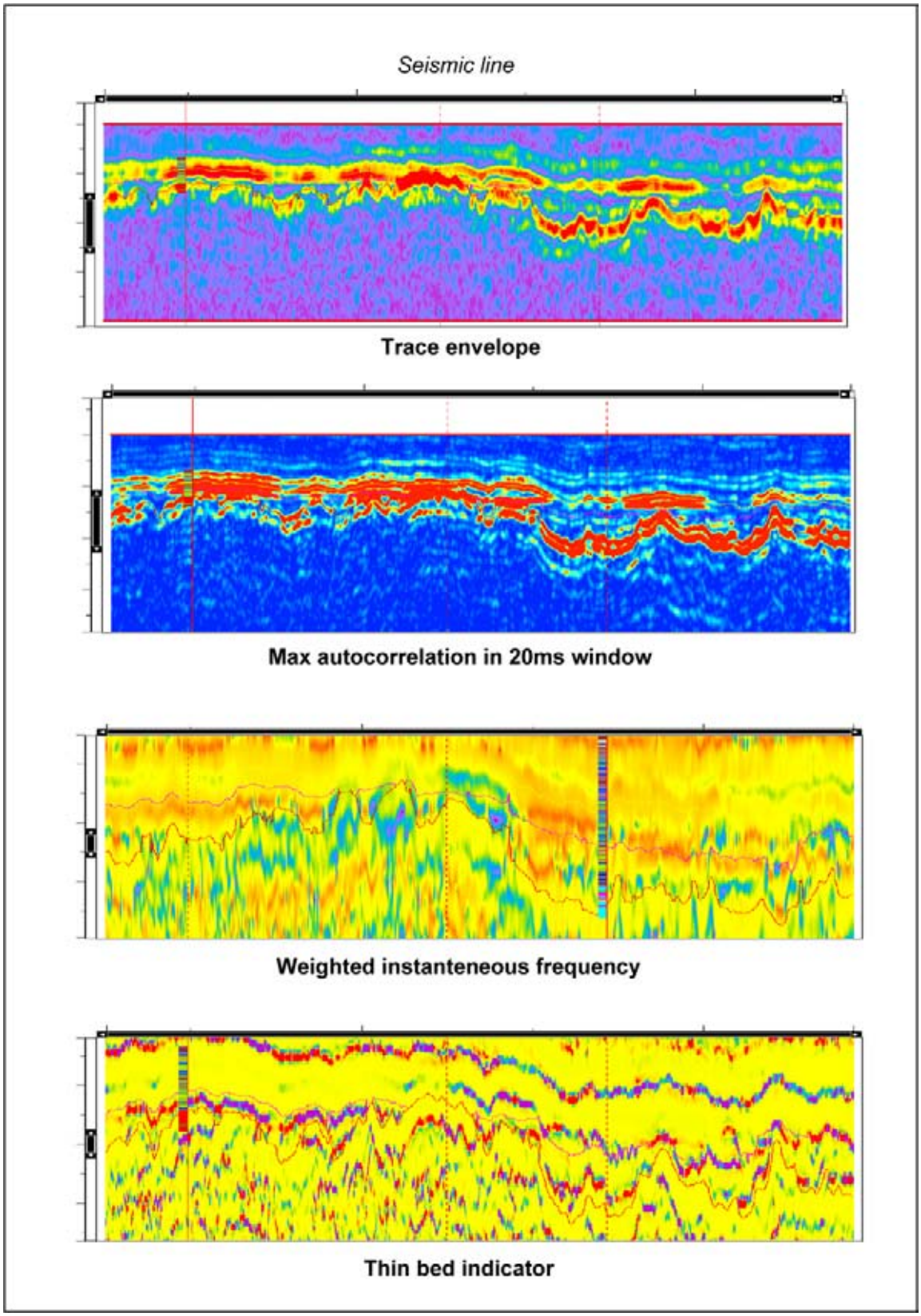

Figure 2.78: Various seismic attributes: (a) The trace envelope = the amplitude component from the real and imaginary part of the seismic trace. (b) The maximum autocorrelation over a 20 ms window. (c) The weighted instantaneous frequency = instantaneous frequency × envelope. (d) The thin bed indicator = instantaneous frequency − weighted instantaneous frequency.

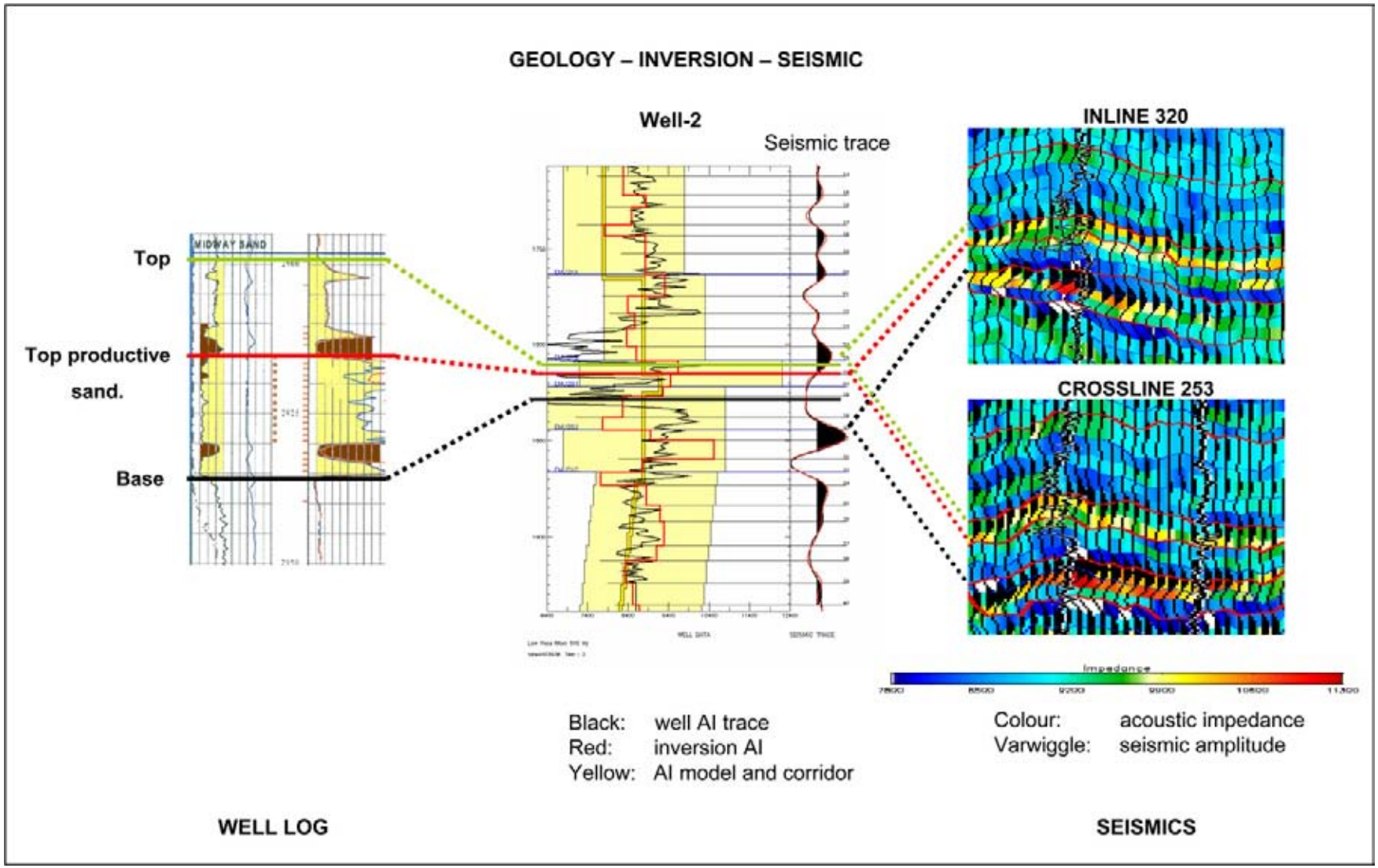

Figure 2.79: Acoustic impedance attribute gives an improved link between seismic and well data. Special seismic inversion processing generates this attribute, by taking out the effect of the wavelet shape. It tries to compensate the tuning effects caused by a thin bed configuration and hence reservoir parameters are more easily inter- and extrapolated over the survey area (courtesy M. Da Silva).

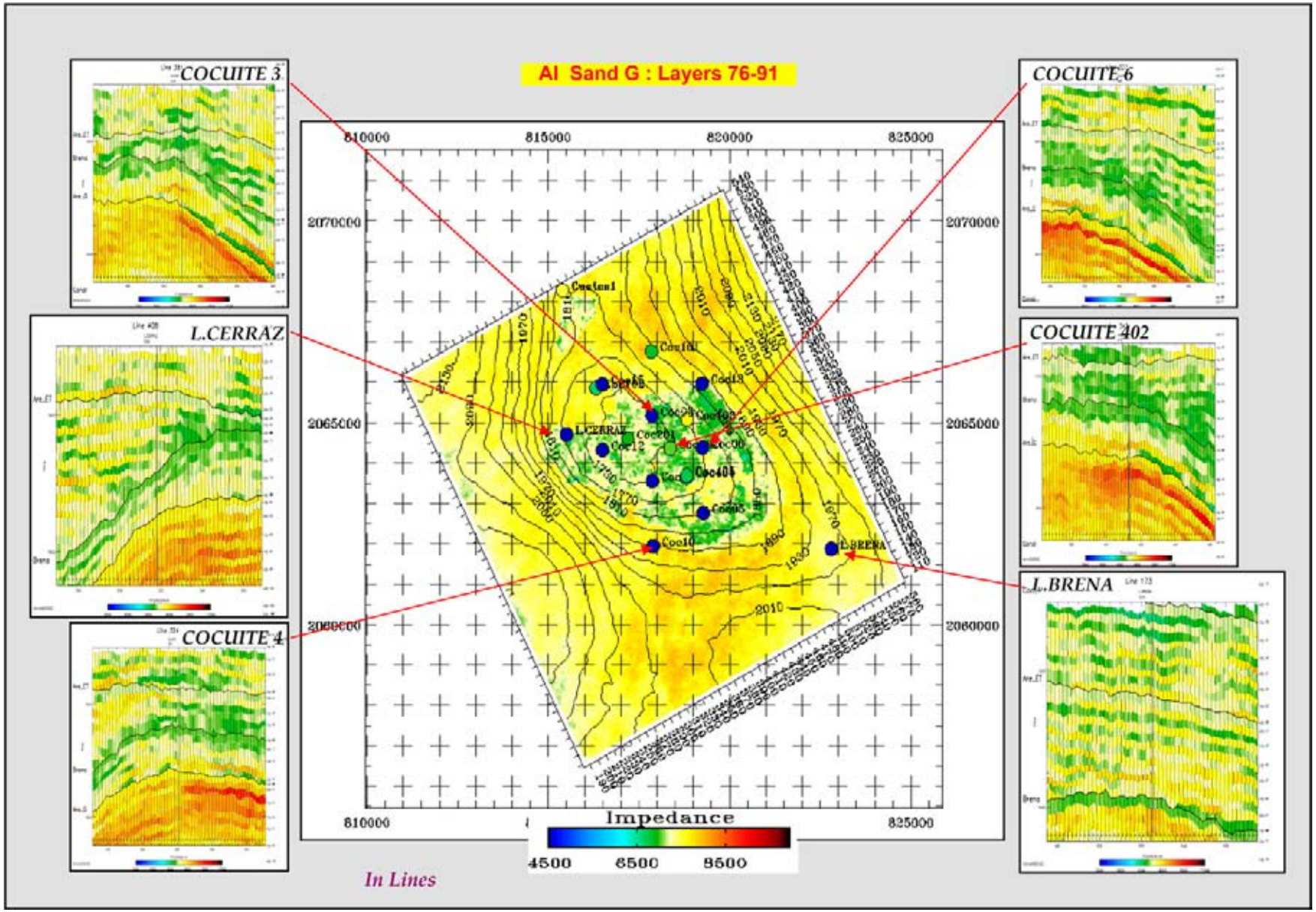

Figure 2.80: Layer map showing Acoustic Impedance behaviour at a gas reservoir level. The AI layer map of the G sands clearly demonstrates a central anomaly. The time contours are also plotted and they show a closure. The green anomaly is limited to the north by a fault, while the time contour is closing the structure to the south. Some degree of reservoir inhomogeneity is also observed. The AI inlines further illustrate the changes in the AI cube (data courtesy PFMEX).

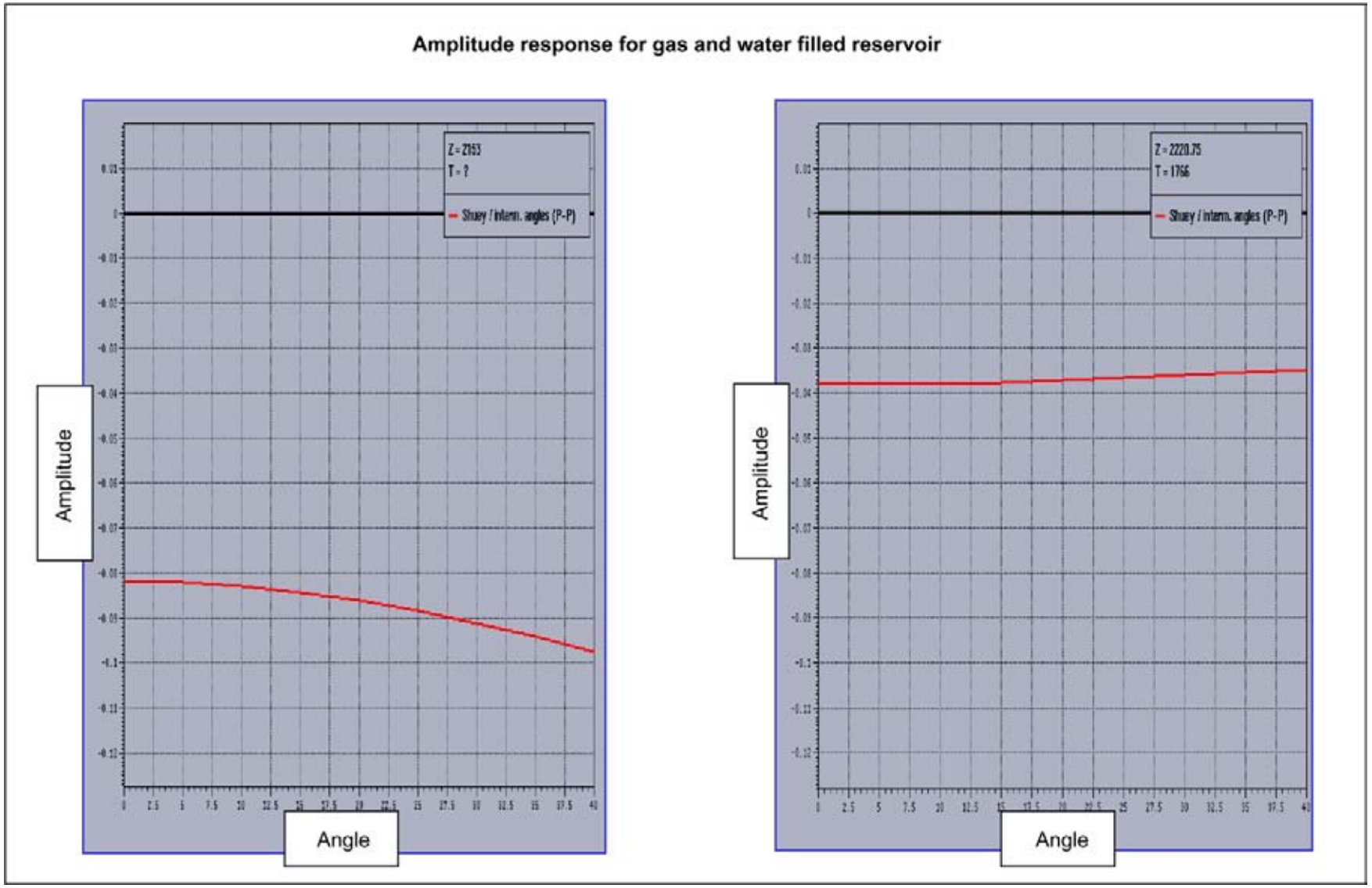

Figure 2.81: Amplitude versus incidence angle crossplot for a CDP gather. The curved red lines demonstrate the clear AVO effect for the gas filled reservoir.

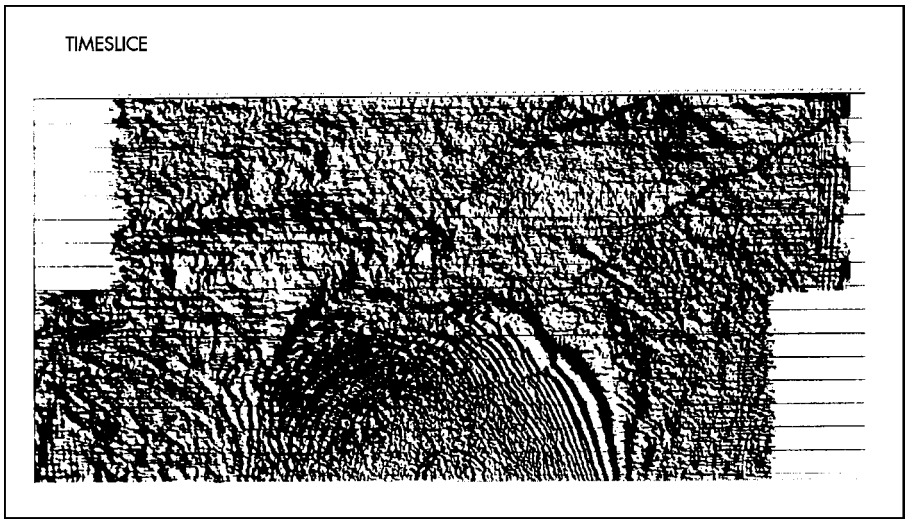

Figure 2.82: Artificial illumination allows to improve the edge detection horizon dip maps and time slices (modified after Yilmaz 1987).

rocks is important, because they often form drilling hazards. These hard carbonate stringers are in a lot of occasions overpressured and thus constitute a risk for a well blow-out. In order to prevent a violent blow-out the mud weight should be controlled adequately. The stringers may also form interesting HC exploration targets (e.g. Athel silicilyte play in Oman, Hartstra et al. 1996; Figure 2.83). The high pressure in such reservoirs increases the volumetric contents of the pore space. An example of a RMS amplitude map is given in Figure 2.84, where the higher amplitudes correspond with areas of better HC production.

An other possibility is to study the shape of seismic trace over the reservoir sequence to get a feel for the relation with the thickness of the reservoir (Figure 2.85, Swanenberg and Fuehrer 1999). If a statistically relevant trend is demonstrated at the wells, then it can be applied in the further evaluation of the survey area.

Interval velocity changes can be visualised by plotting the results of velocity analysis along a seismic line. Horizon-specific time picks on the CDP gathers are crucial to get useful results (Al Marooqi et al. 1999, Veeken et al. in press). This procedure stimulates a closer cooperation between the processor and interpreter, which guarantees more optimal velocity data.

Studying the sealing potential of fractures and faults in great detail is another technique (e.g. Koestler and Hunsdale 2002, Wong and Boerner 2004). Faults are showing up on sections, but there is a limit to their resolution (Figure 2.86). A fault throw of three metres can be already sufficient to create an effective seal, but these faults are well beyond the seismic resolution and detection capabilities. The well production data can help to prove their existence, as for instance is the case in the Cougar field in the Gulf of Mexico (McCarthy and Bilinsky 1999). The '**fault/seal potential**' analysis involves the construction of time slices parallel to the fault plane. The fault slice on the downthrown side is overlain by those through the upthrown faultblock. Sand prone and shale prone loops are identified and in this way sand overlap areas are traced. The degree of juxtaposition of reservoir against non-reservoir section is examined and assists in the definition of possible spill points. It can be quantified in an attribute called **juxtaposition index** (cf Brechet et al. 2004). Moreover, the estimation of the **clay smear potential** along fault and fracture planes is important. Injection of impermeable clays into the fault plane provides a very good lateral seal. Injection of fluidised sands on the other hand will increase the permeability and creates vertical migration path way for fluids (Veeken and Van Moerkerken, 2005). Automated fault plane recognition is a tool. Key elements characterizing a fault are analysed for each individual fault plane:

- Orientation.
- Dip and azimuth.
- Size and length.
- Position.
- Statistics on displacement values such as minimum (90th percentile), median (50th percentile) and maximum (10th percentile) displacement.

A visual representation of the fault displacement values on the fault plane helps understanding the orientation of paleo-stress and allows checking that it has a kinematic meaning (Carrilat et al. 2004).

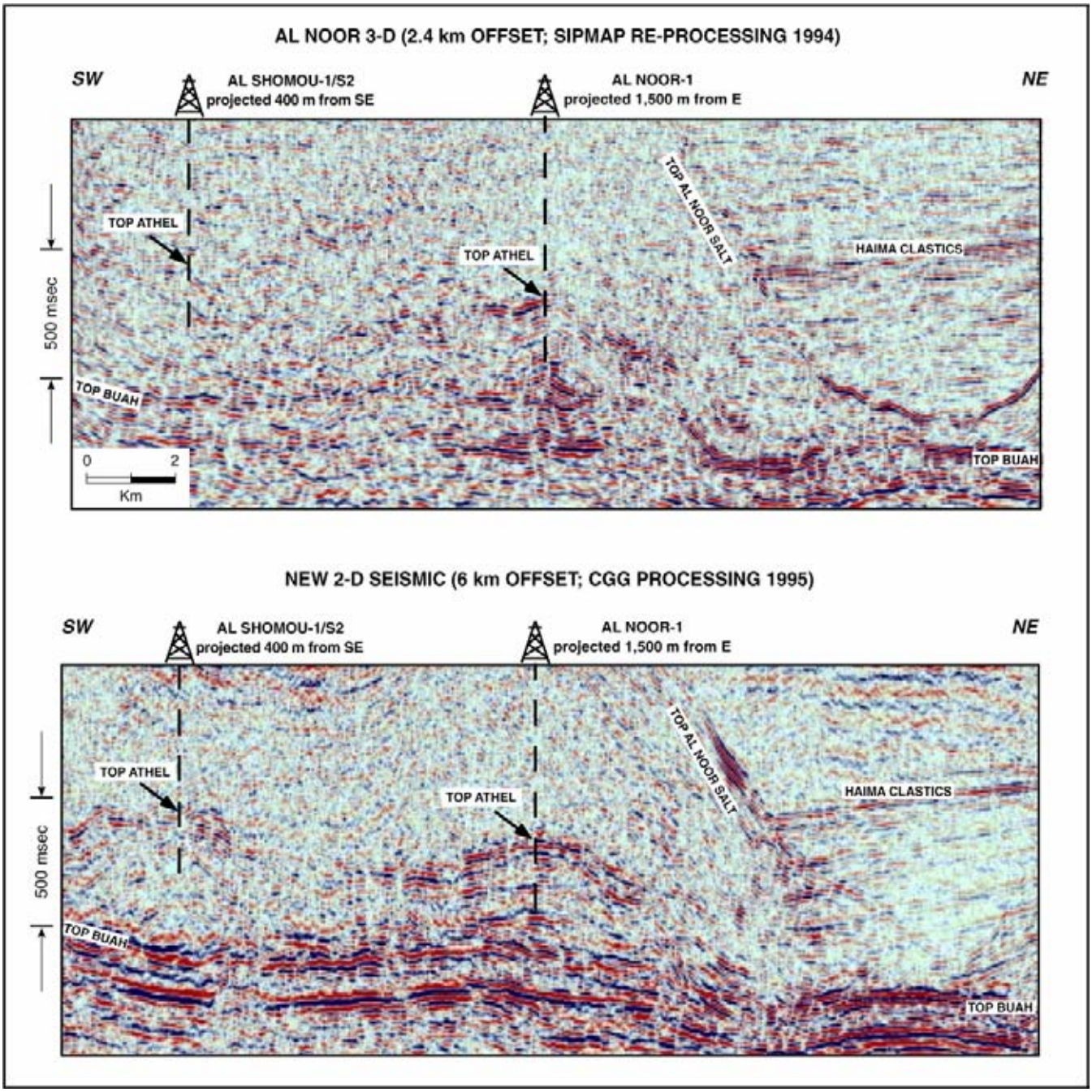

Figure 2.83: Seismic line showing the Athel carbonates at the base of the Al Noor Salt in central Oman. A specially designed processing sequence brings out the structuration and makes more precise mapping possible (Onderwaater et al. 1996).

Also **decompaction** and **backstripping** studies improve the knowledge of depositional geometries displayed by the different seismic stratigraphic units and give a better handle on their internal organisation (Figure 2.87, Steckler et al. 1993).

The construction of **balanced cross sections** is useful in this respect (Gibbs 1983). It puts constraints on the seismic interpretation by considering the listric/undulating nature of the shape of faults (prevention of overlap during palinspastic reconstructions) and depositional geometries, whilst applying certain decompaction algorithms.

Important new techniques are 3D visualisation and classification of seismic attributes. Voxelgeo^{TM} and ER

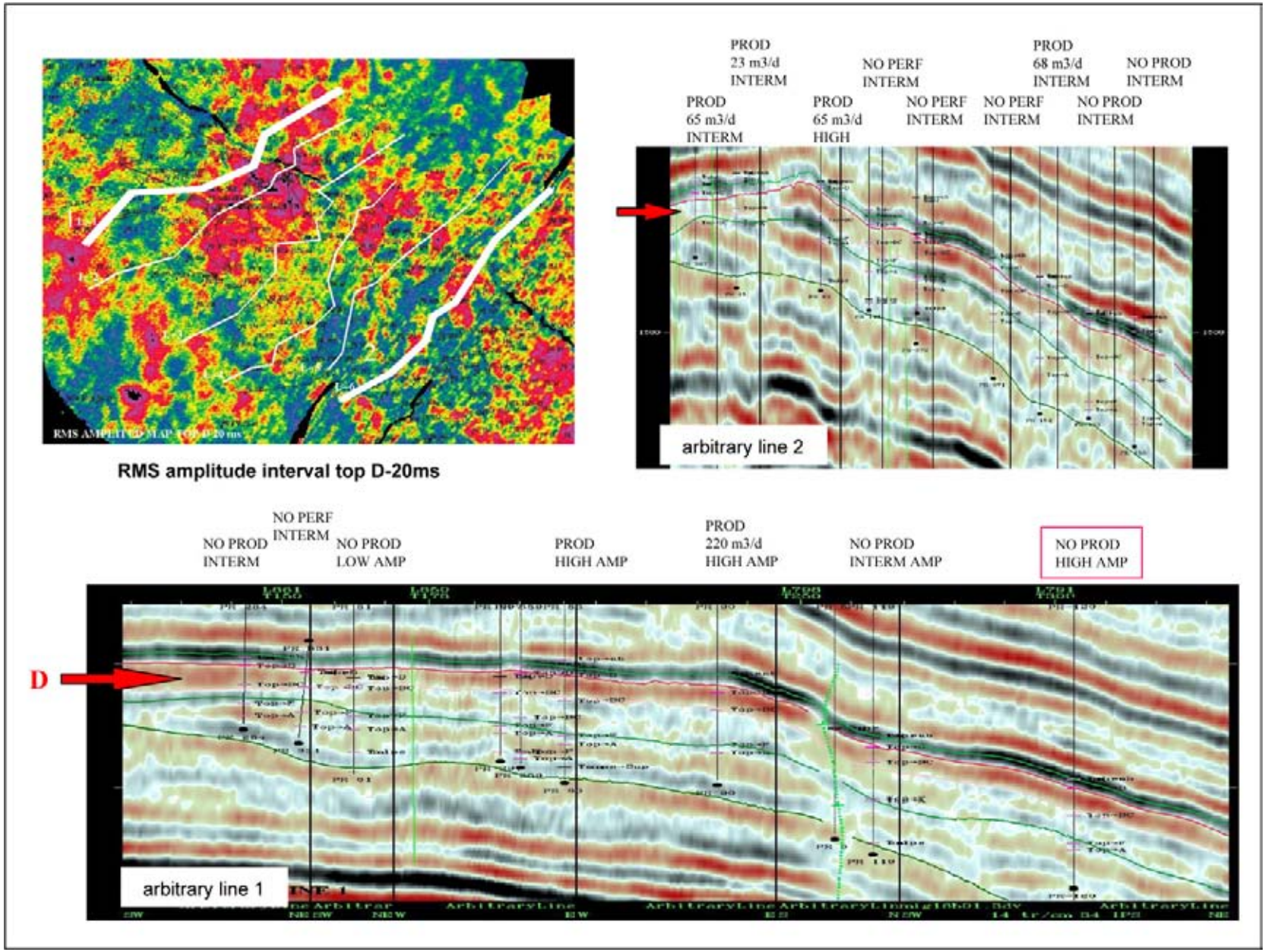

Figure 2.84: RMS amplitude map for the Poza Rica Field in Mexico. The two arbitrary lines illustrate that the carbonate reservoir shows a correlation between the higher production figures (= better porosity and permeability) and the higher amplitude in the *D* interval. Such relationship is used to optimise well locations for future development (red colours; courtesy Pemex).

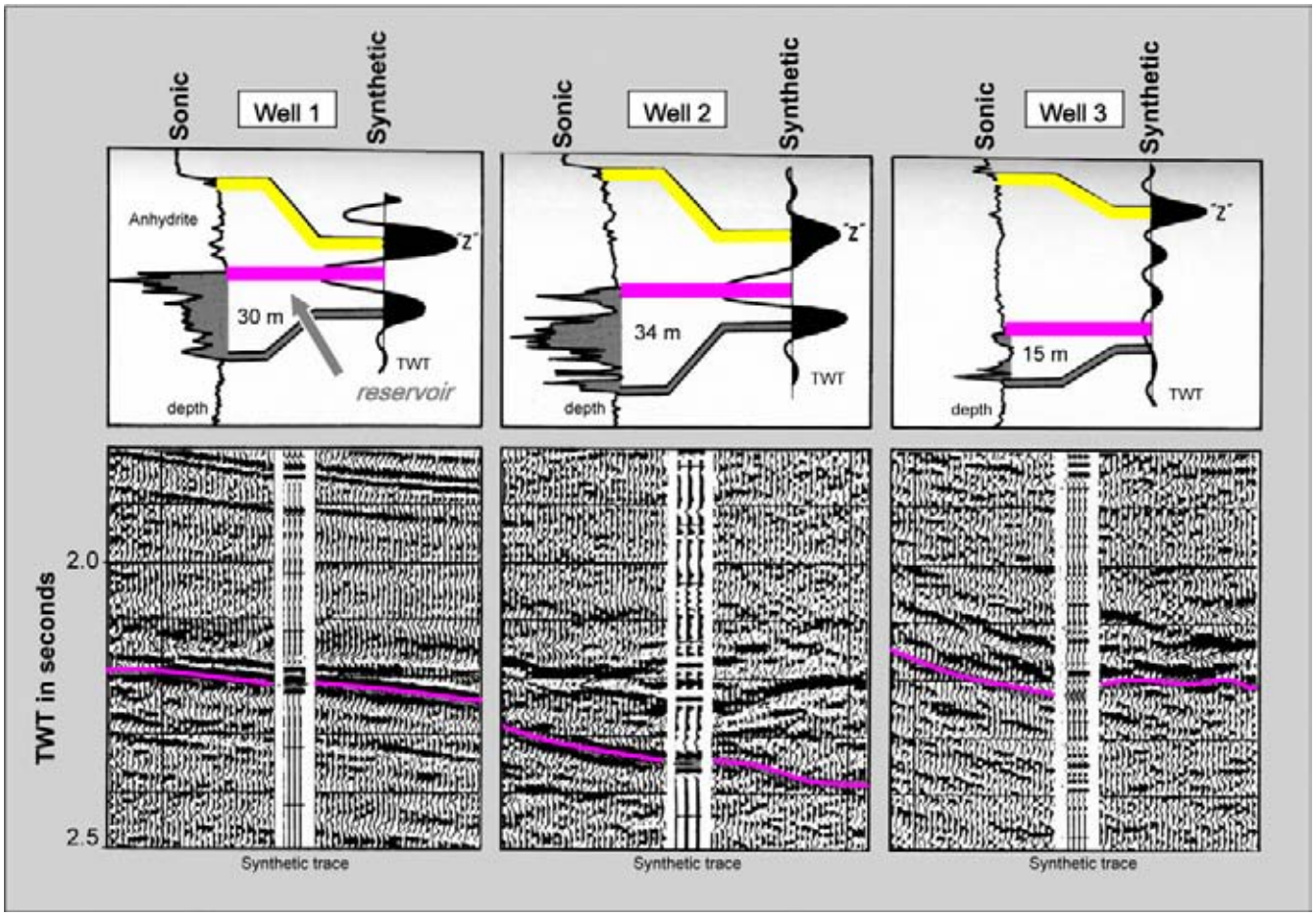

Figure 2.85: Sonic log and the zero-phase synthetic trace for three wells penetrating a Permian reservoir sequence. Note that the difference in trace shape is also depending on the reservoir thickness. The change in seismic trace shape is used in the lateral prediction study. The Z-marker is generated by a layer of anhydrite overlying the Zechstein carbonate reservoir (modified after Swanenberg and Fuehrer 1999).

Mapper^{TM} provides sophisticated methods to do 3D pixel displays of seismic data. SRCattribute^{TM} lets the interpreter calculate loads of seismic attributes. Many of these attributes are not very complementary to the conventional ones; but they provide a new view on the same data. They are sometimes difficult to interpret and their additional value to the prospect evaluation efforts is rather subjective.

Computation of a **coherency cube**, or semblance, is certainly useful. Coherency is originally defined in the frequency domain, but it is basically equivalent to cross correlation in the time domain. This cross-correlation consist of taking the product at each time sample of the two waveforms and then summing the values together. Subsequently the investigation window is lowered one time sample and a new calculation is obtained. Simple cross correlation has a disadvantage because it does not recognise timeshifts of time traces in respect to each other. This disadvantage is circumvented by considering several timeshifts in the input trace, computing the corresponding cross correlation values and then taking only the largest observed value (Hill et al. 2006). Cross correlation is done between two traces to investigate their similarity. It can be achieved in a 3D sense by considering 9 adjacent traces as input and do some sort of averaging. Each time sample on a trace or in a seismic cube has therefore a correlation value assigned. The coherency attribute allows fast detection of 3D zones with similar characteristics (Figures 2.88–2.92). Local coherency is measured in an analysis window with the same number of time samples on the target trace and the surrounding traces defined by the user. High-coherency values are encountered where there is a lot of similarity and low values when the input trace is less resembling the neighbouring traces. Fault zones are easily traced within the coherency cube. It is of great help when establishing a consistent fault pattern in an area. **Automatic Fault Extraction** (AFE) techniques are very

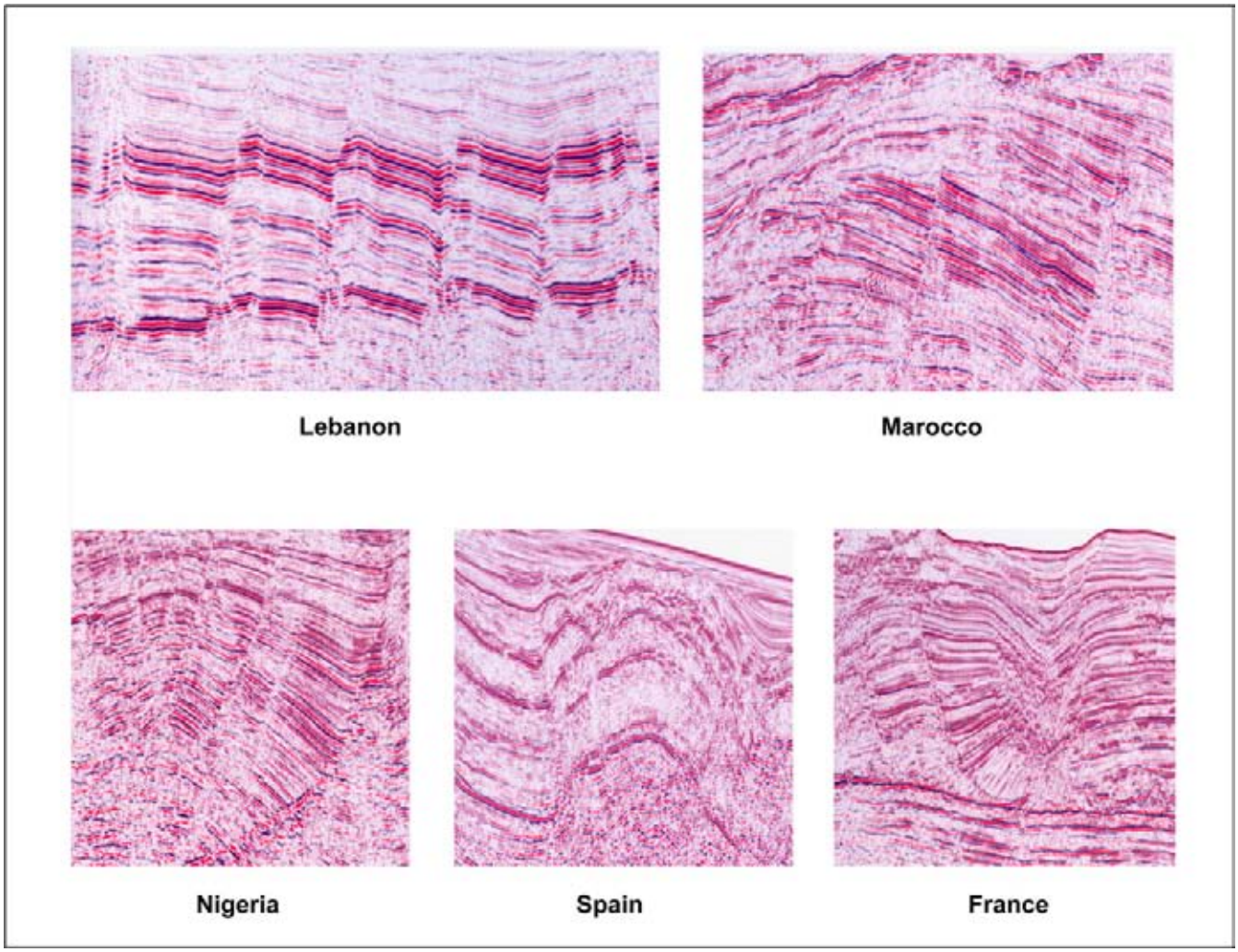

Figure 2.86: Faults are visible on seismic sections, but with a certain resolution. Determination of the fault seal capacity is important to evaluate the behaviour of fluid flow units. Sub seismic faulting can be important from a reservoir management point of view. Clear breaks in the reflections help in the delineation of faults. Reliable processing of the dataset is essential for this purpose (courtesy of TGS/Nopec 2004).

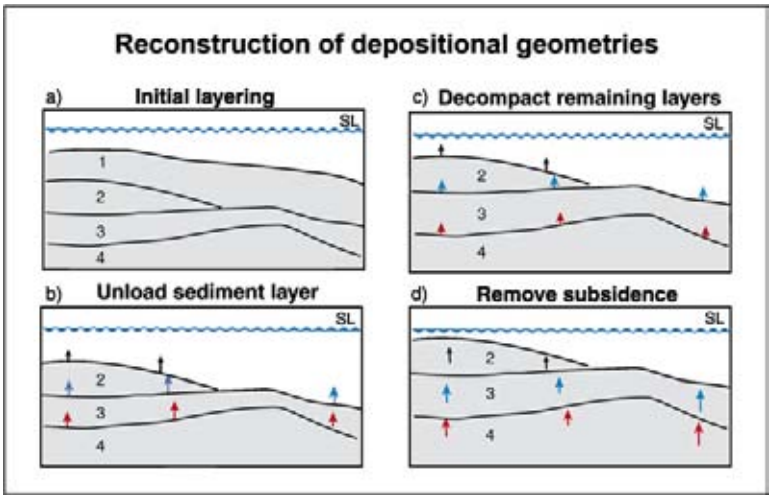

Figure 2.87: Backstripping and decompaction gives a better grip on the original depositional geometry of the geologic sequences. It is done in a layer by layer approach (modified after Steckler et al. 1993).

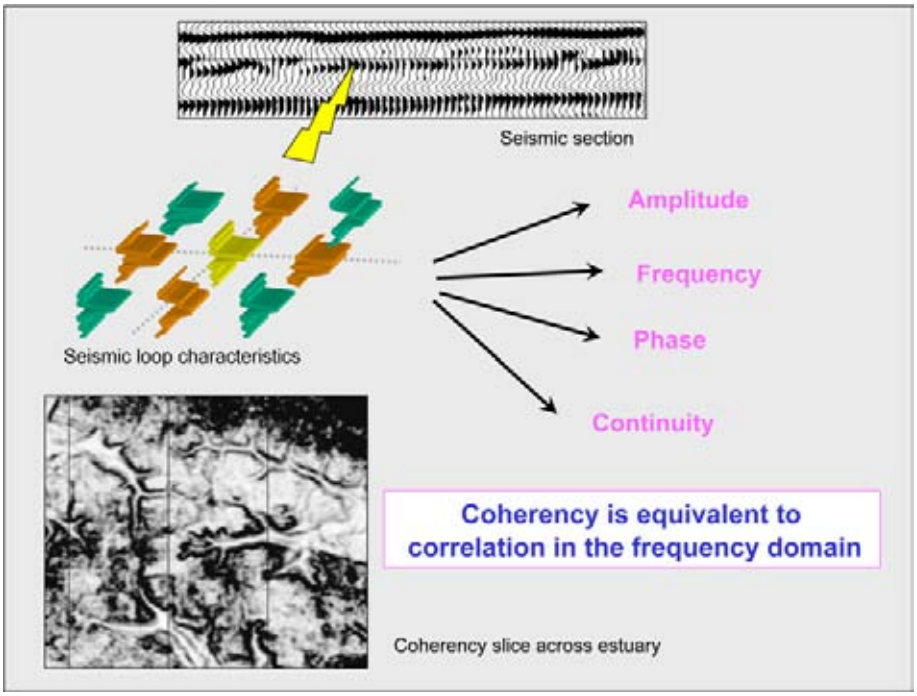

Figure 2.88: An example of visualisation of a coherency cube. Coherency is the equivalent of cross-correlation, but the operation is carried out in the frequency domain. Discontinuity in seismic reflections are highlighted by this technique. It is to outline faults, pinch-out or gas effects. Processing parameters should be carefully chosen in order to bring subtle changes in the dataset (R. Guzman Javier, courtesy Pemex and Paradigm).

powerful to quickly provide a look on the structural development of an area (Marsh et al. 2005). But also sedimentary features are highlighted by this type of display (e.g. James and Kodstrova 2005). Various similar techniques exist to bring out the discontinuity in the seismic data volume like: semblance, continuity, and covariance. The cross-correlation techniques are also used to determine the local **dip** and **azimuth** attributes. Coherency processing requires certain parameters to be specified (e.g. time window, amount of dip, etc.) and this should be carefully checked to control the quality of the output (cf Marsh et al. 2005). Reflection discontinuities can be caused by:

- Structural events like faults, uplift, subsidence and erosion.
- Stratigraphic and sedimentary events like channels, onlap, offlap, etc.
- Seismic acquisition/processing and poor imaging.

Links are possible between the inversion results and lithologic crossplots. These crossplots summarise the relationship between various petrophysical and seismic parameters. Subsequent **3D clustering** provides a means to do prediction of reservoir characteristics in the studied data set (Guilbot et al. 1996). Seismic attributes may be utilised to classify the seismic response in a certain interval (Figure 2.93).

Neural network analysis can be done (e.g. GDI^{TM}, Emerge^{TM}, Stratimagic^{TM}) to perform both non-supervised and supervised prediction of reservoir characteristics (cf Balz et al. 1999, Walls et al. 2002; Figure 2.94). The neural network establishes a non-linear relationship between the datasets (Aminzadeh and De Groot 2004). Often a full seismic trace waveform forms input for the classification procedure. This info combines the variation in time, amplitude, frequency and attenuation of the seismic data. Automated seismic facies maps are easily produced (Guilbot et al. 1996).

There are essentially two approaches: an unsupervised and supervised classification. The results of the latter are more easy to interpret, but the exercise is more time consuming and hence more costly. Partial stacks and interval maps illustrate AVO effects in a seismic dataset (Figures 2.95–2.98). The **supervised classification** procedure starts from numerous reservoir scenarios and computes first an unsupervised trace classification. The reservoir models have known parameters and their distribution is known within each class. The synthetic traces are classified and the master traces are retained (Figure 2.99). These synthetic master traces are then used to do a classification of the real seismic data and classification maps are produced with a certain **probability distribution** attached to each facies unit (Figure 2.100). This supervised classification procedure

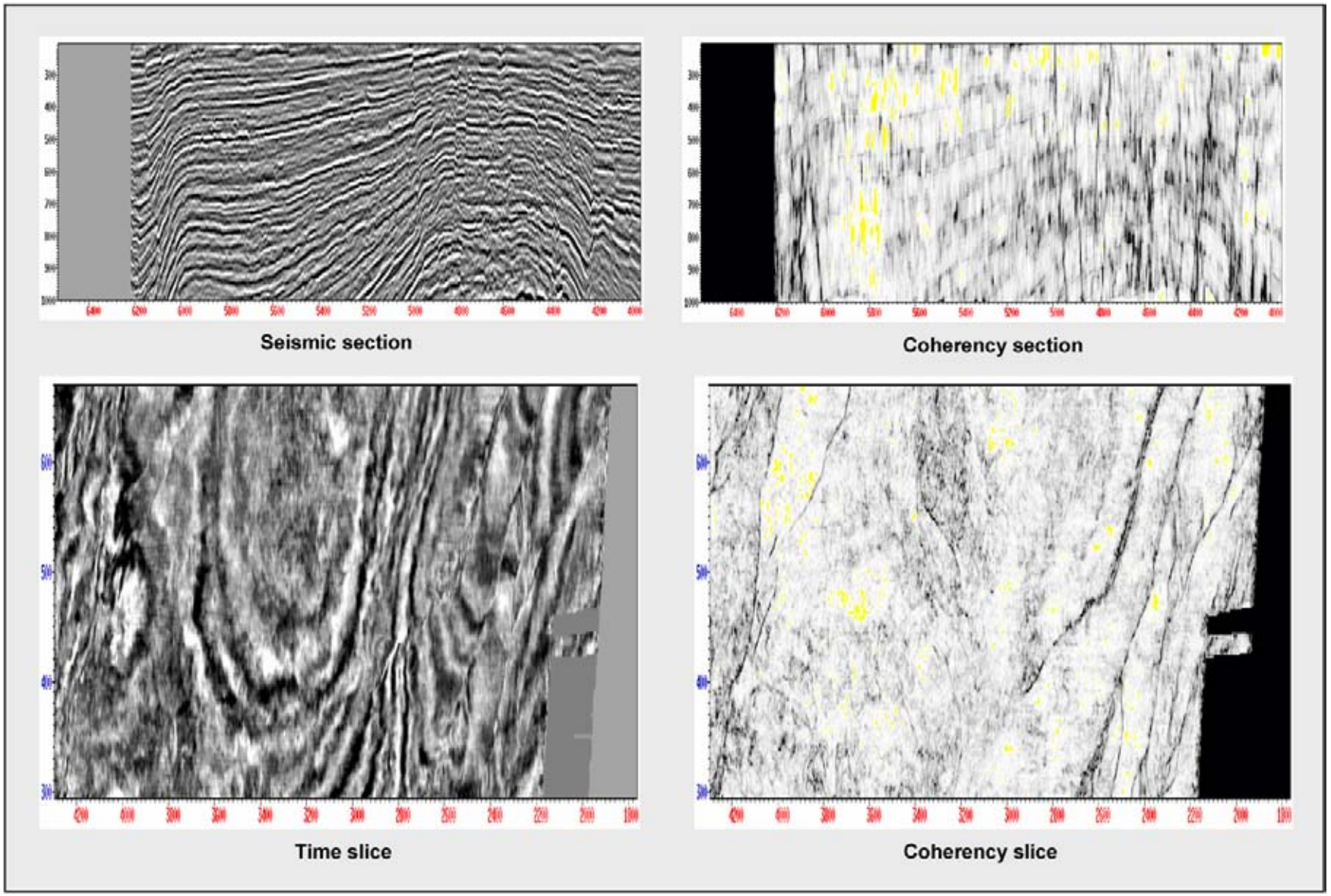

Figure 2.89: Reflection seismic section, time slice and the coherency response. Coherency emphasises the discontinuities in the seismic dataset and tectonic trends are more easily appreciated (R. Guzman Javier, courtesy Pemex and Paradigm).

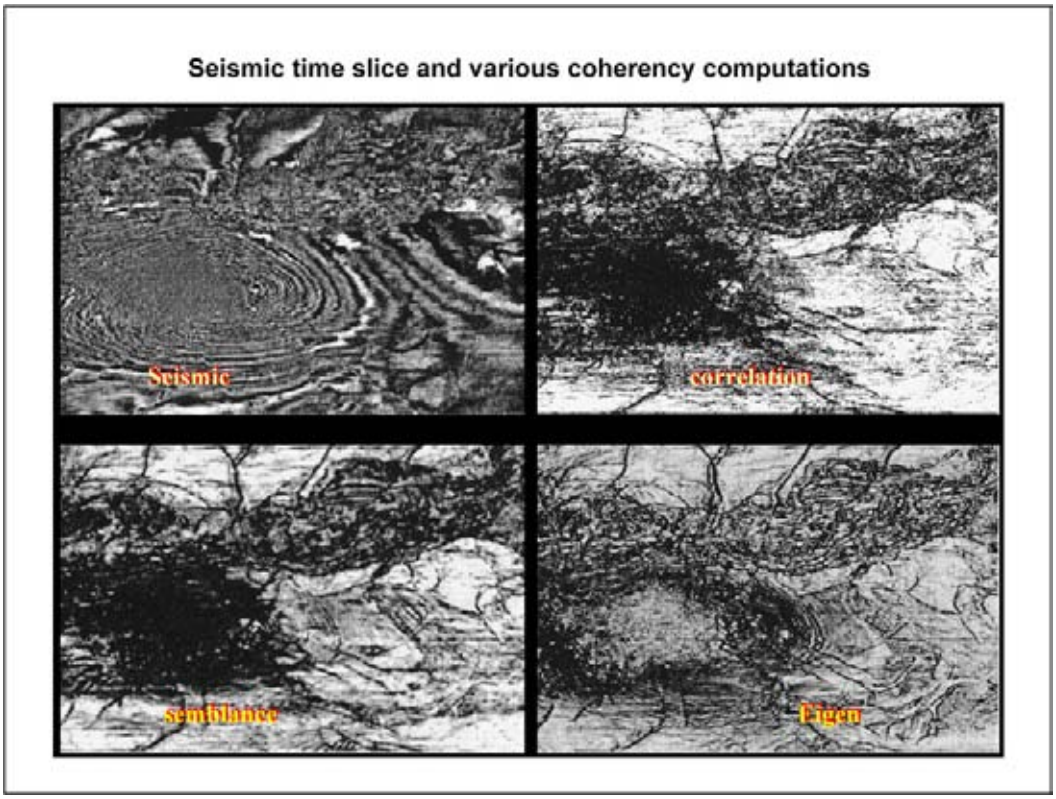

Figure 2.90: Time slice and coherency slice (R. Guzman Javier, courtesy Pemex and Paradigm).

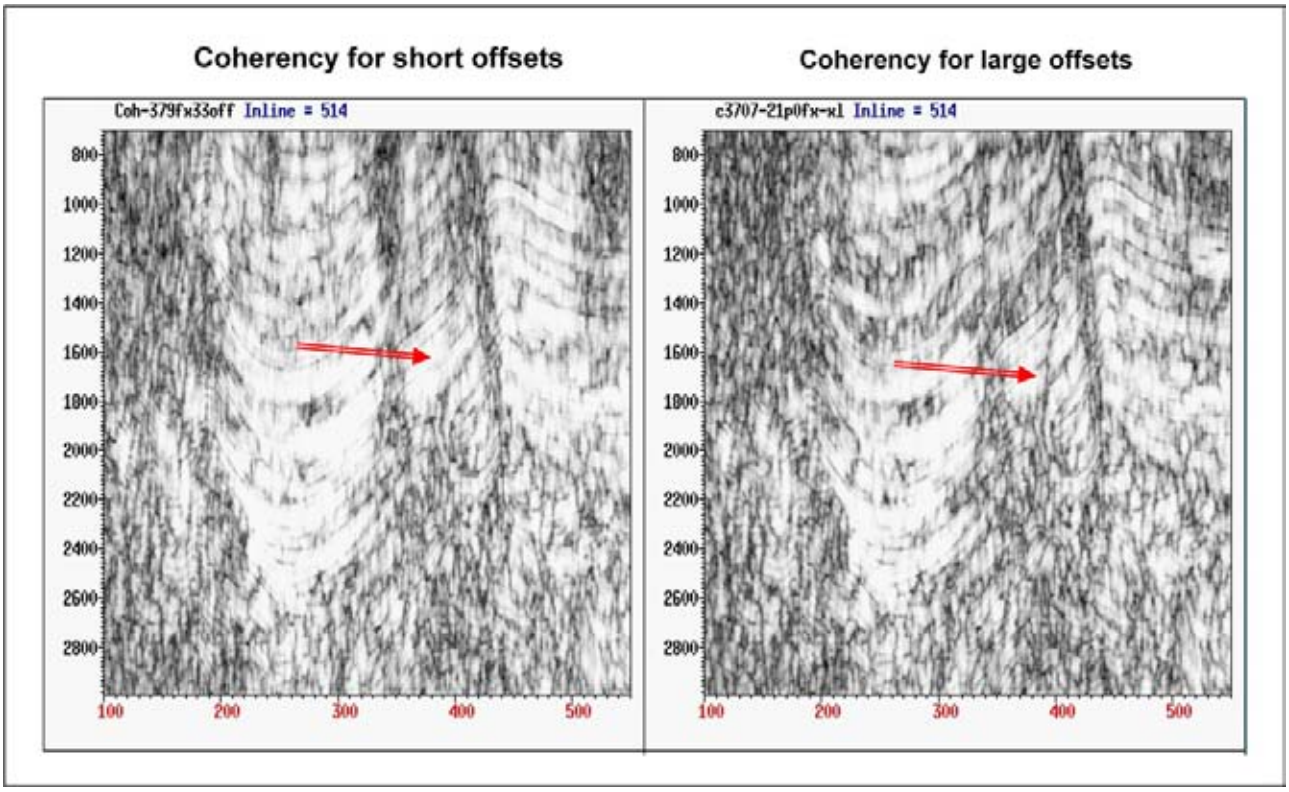

Figure 2.91: Coherency behaviour examined along offset ranges to assess subtle changes in reflection continuity. Near and far coherency cubes show a distinct signature (R. Guzman Javier, courtesy Pemex and Paradigm).

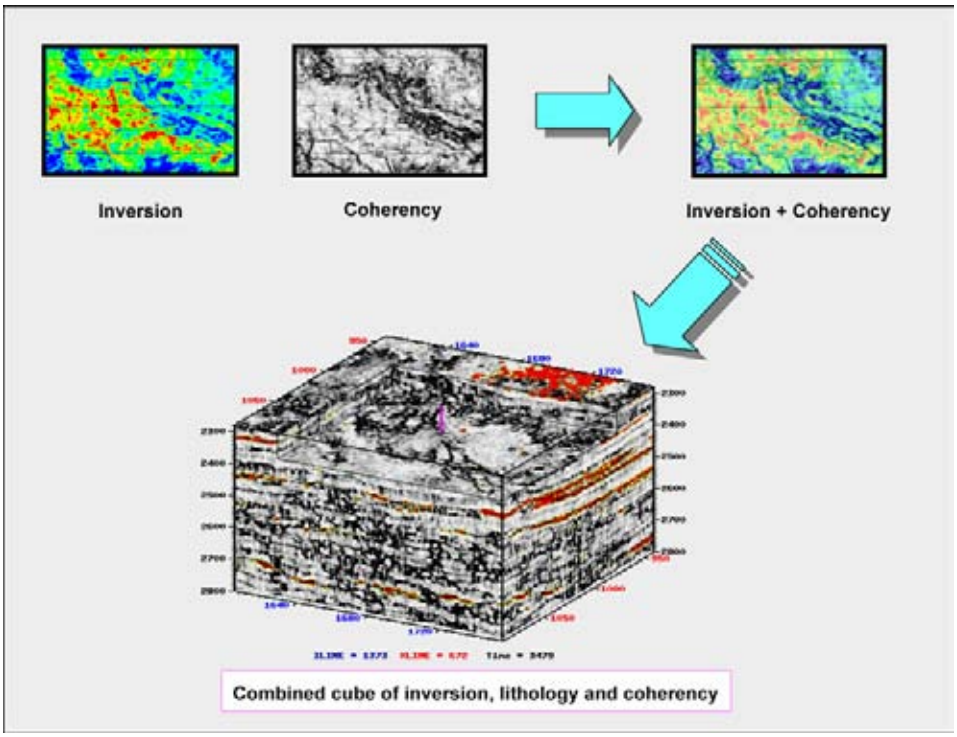

Figure 2.92: 3D cube whereby inversion is combined with the coherency behaviour. Crossplot cut-offs are here used to visualise lithology effects (R. Guzman Javier, courtesy Pemex and Paradigm).

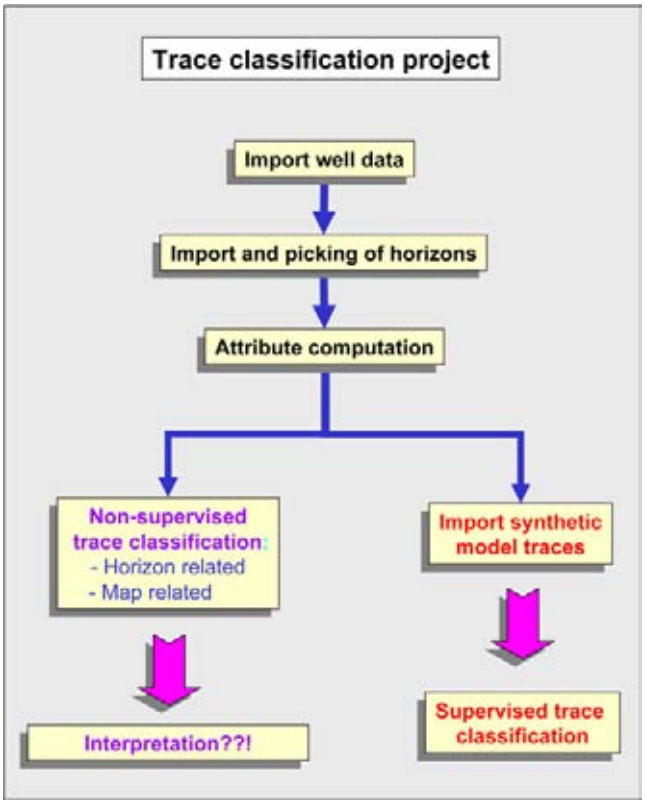

Figure 2.93: Flow diagram for supervised and non-supervised trace classifications. The supervised method allows direct interpretation of reservoir characteristics for the classified traces. In the non-supervised method an experienced eye is needed to extrapolate the well calibration in a sensible way.

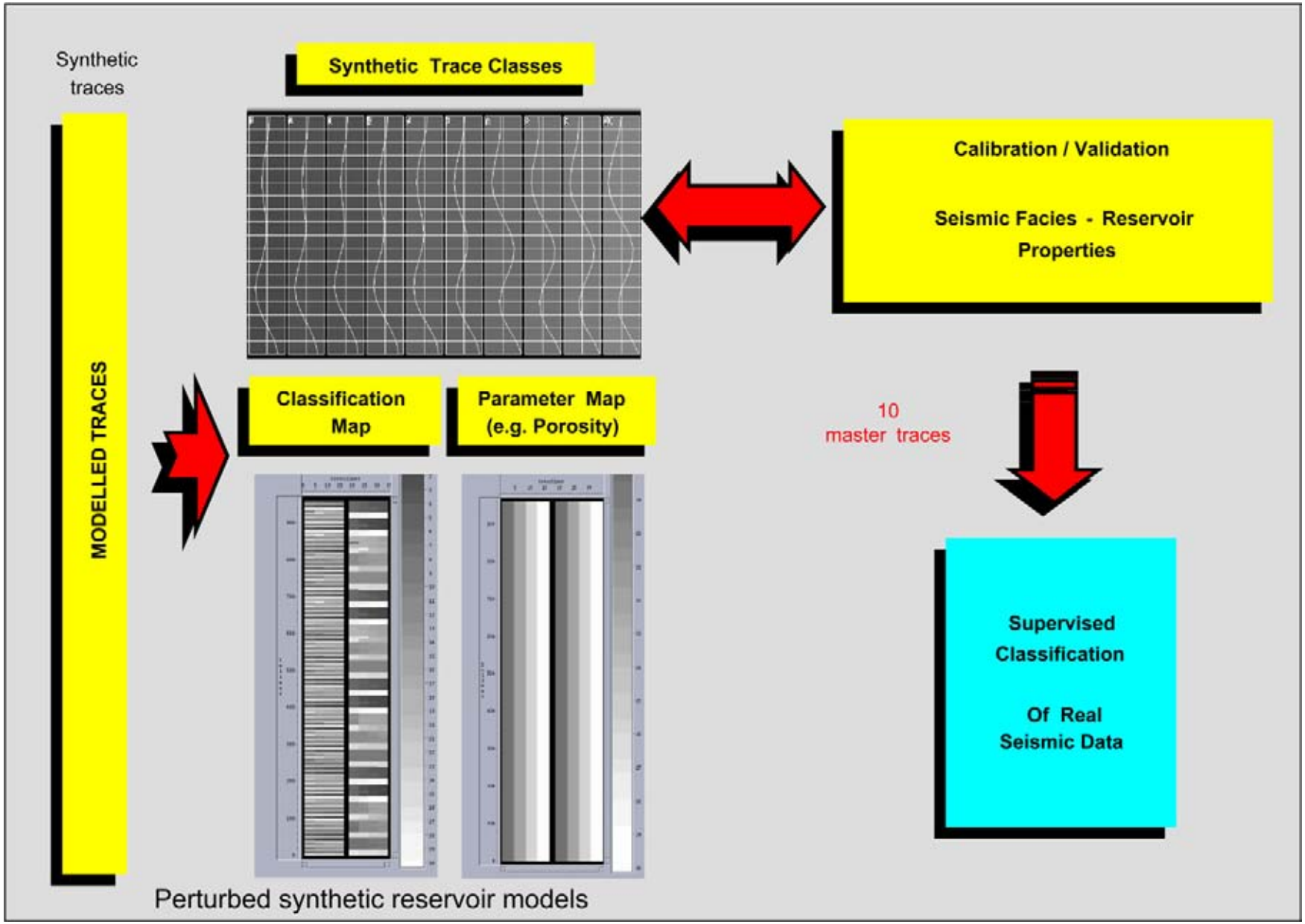

Figure 2.94: The supervised classification workflow facilitates the interpretation of the facies units, because the master traces have known distributions in reservoir characteristics.

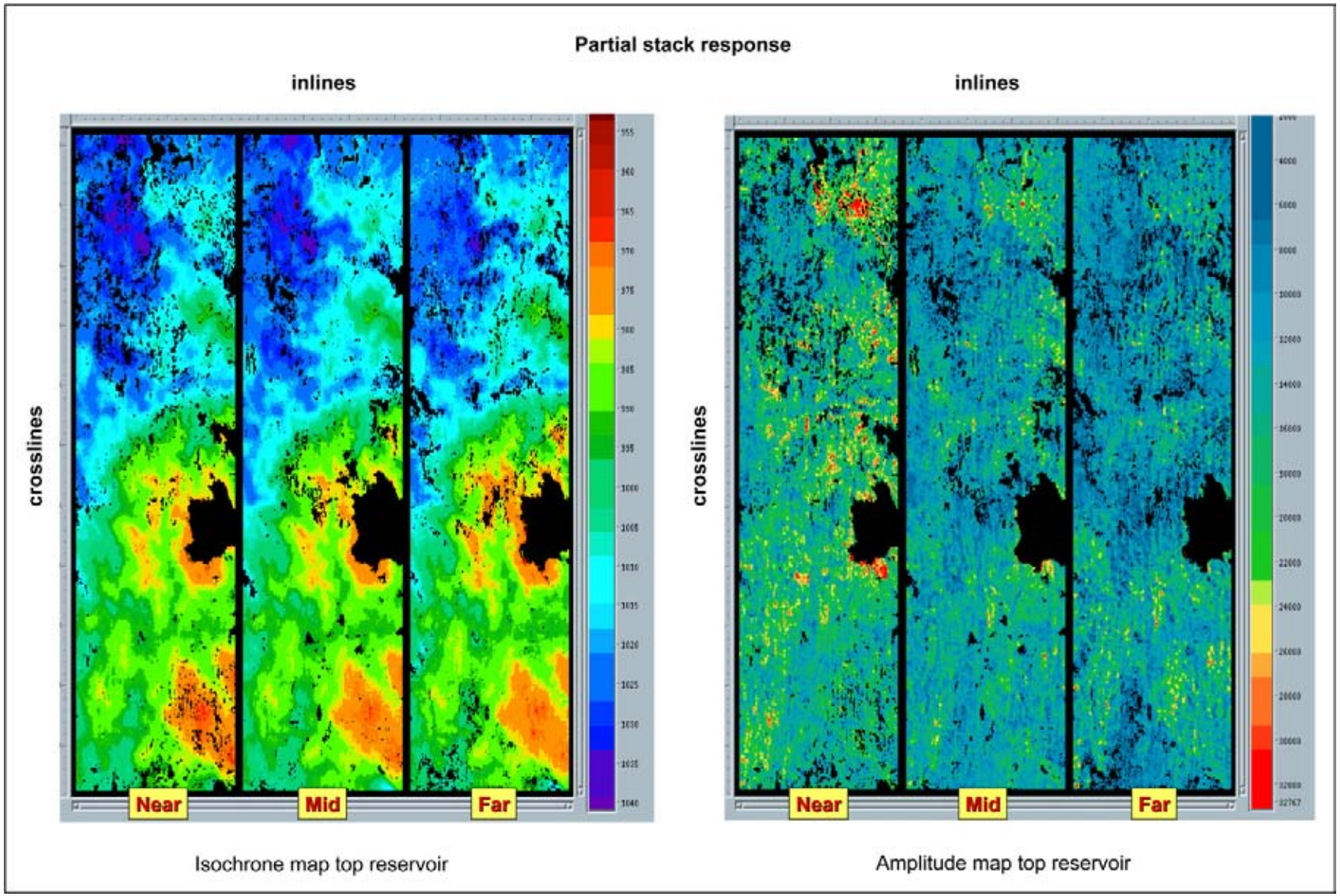

Figure 2.95: Map view of partial stack response with isochrone and amplitude values of the top reservoir reflection. Differences between the partial stacks show that there are AVO effects. It is important to determine whether this feature is caused by porefill changes (data courtesy TFE).

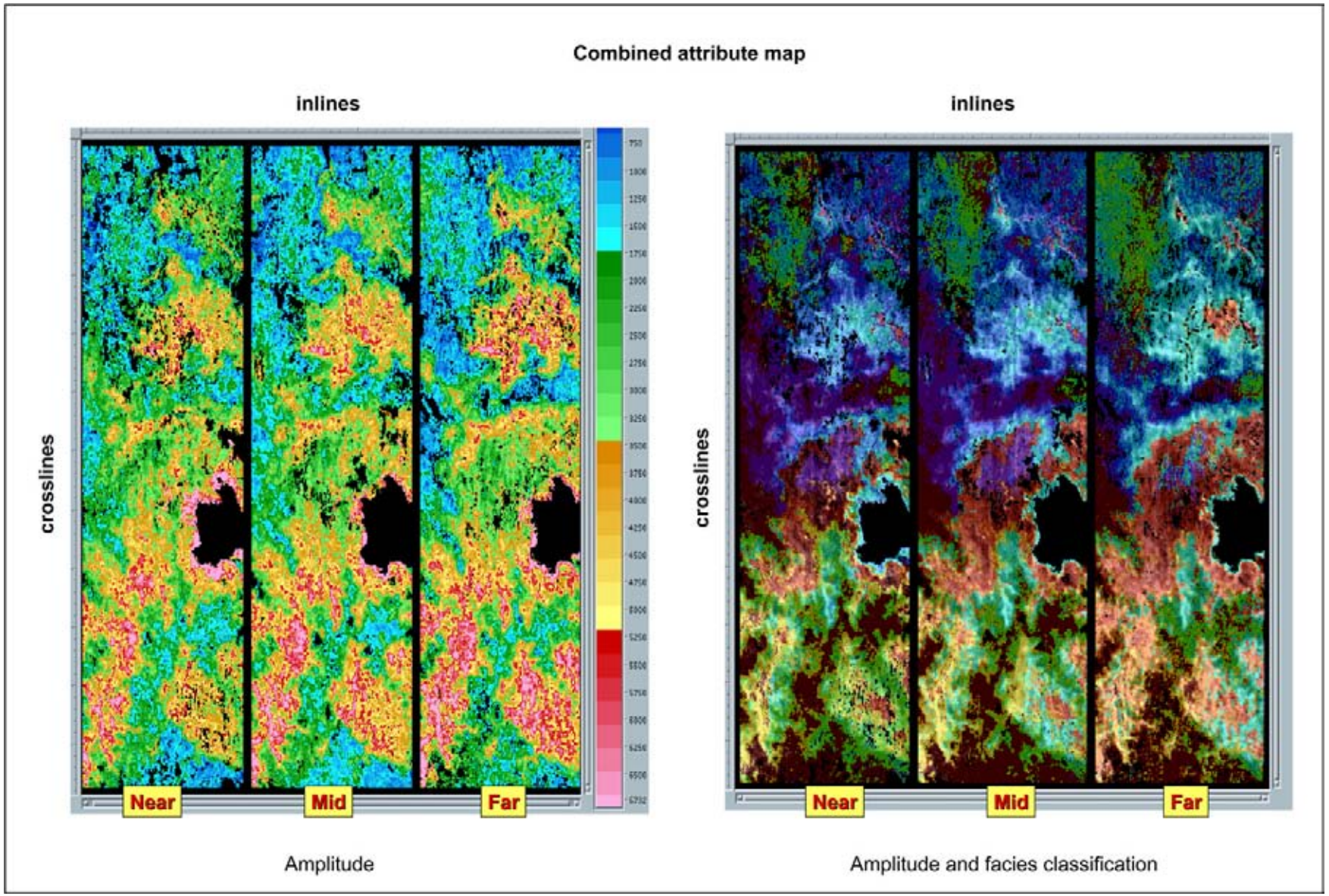

Figure 2.96: Combined seismic attribute maps for migrated partial stacks. The black colour is a basement high (data courtesy TFE).

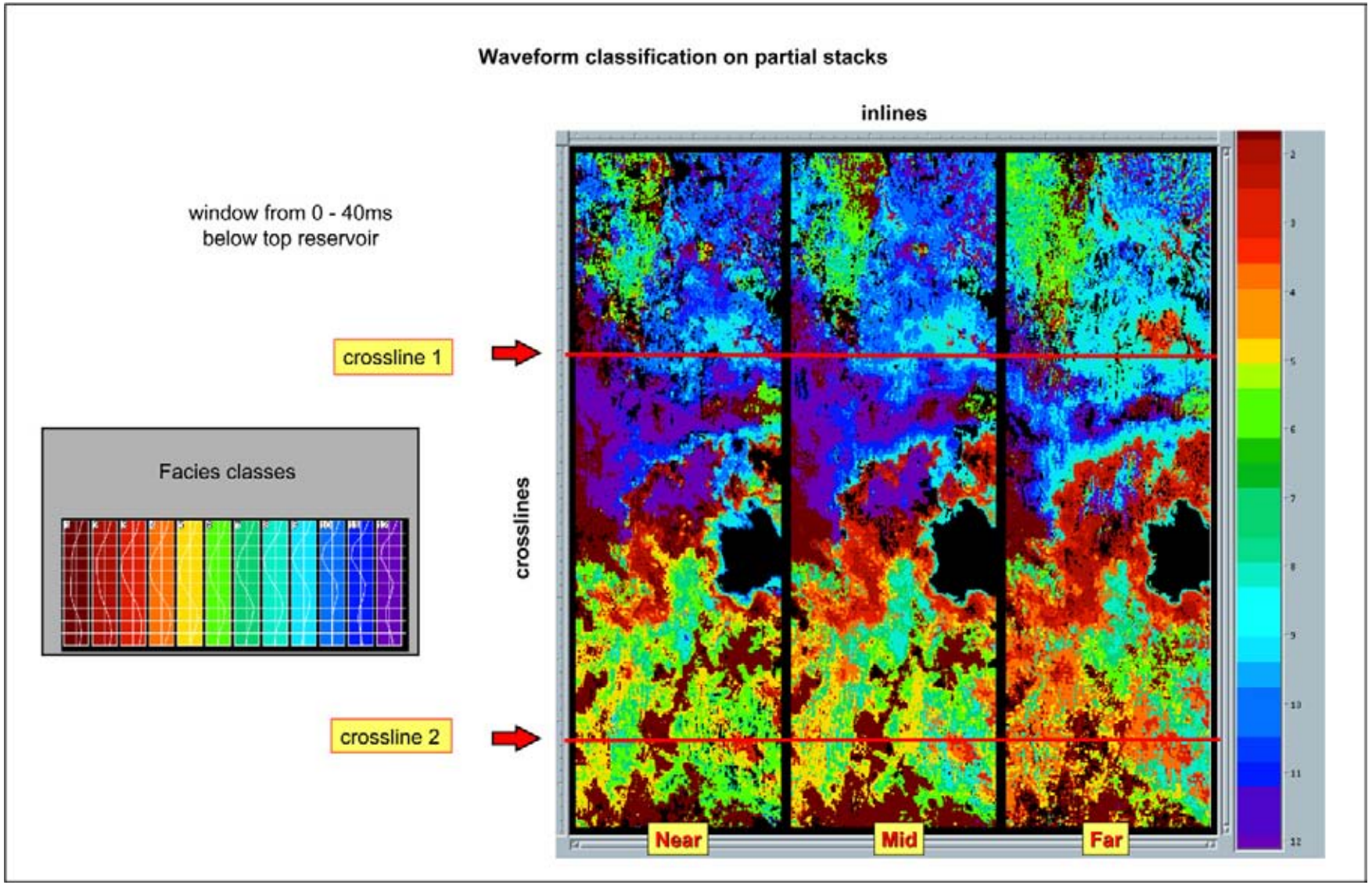

Figure 2.97: Unsupervised neural network trace classification for migrated partial stacks. The traces in the interval of interest are grouped by the non-linear algorithm. The interpretation of reservoir characteristics of the classes is always open for discussion among specialists. A supervised classification scheme assigns probabilities to the reservoir characteristics of the classes as is shown later on. It will give less rise to ambiguities in the interpretation of the classification results (data courtesy TFE).

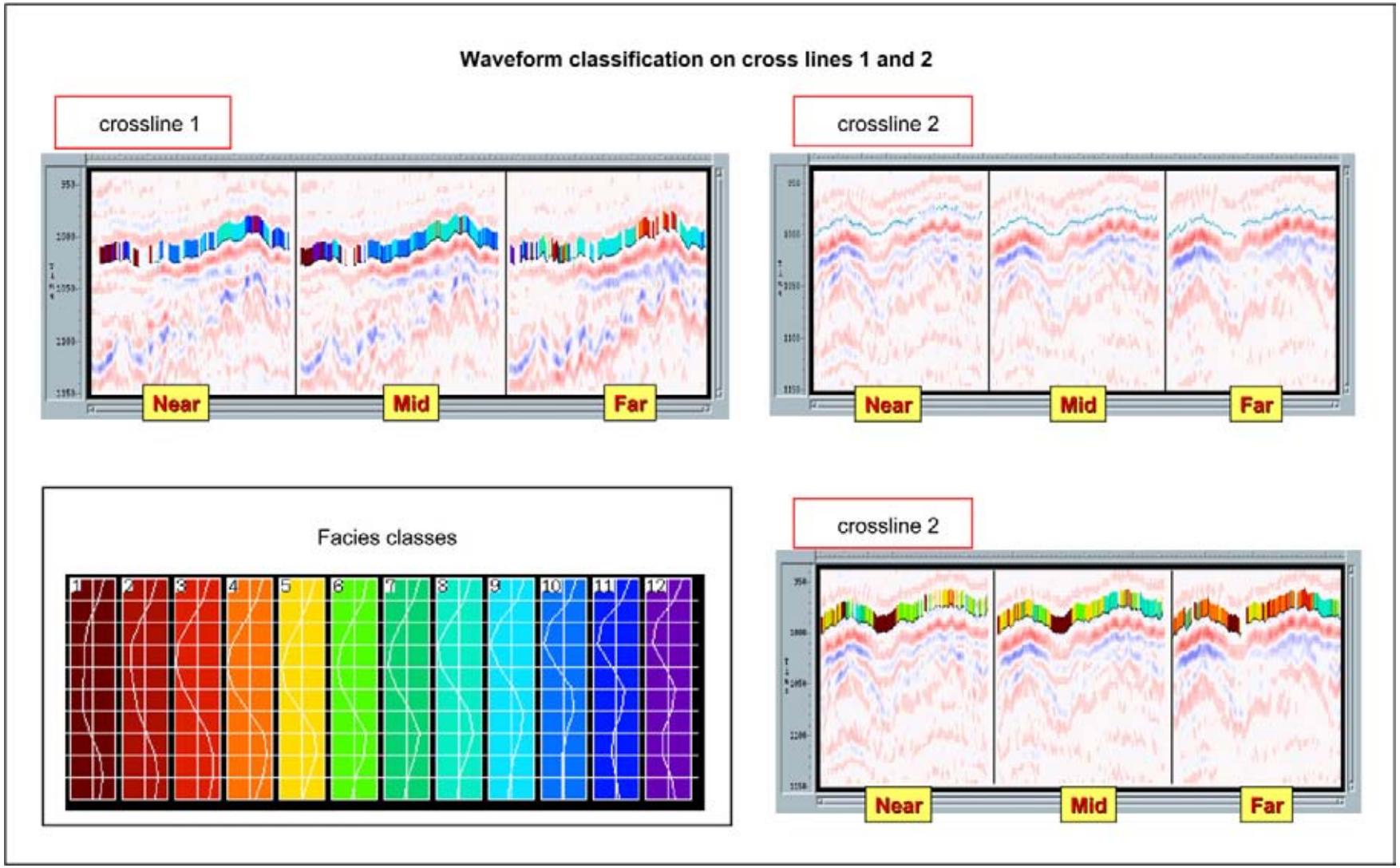

Figure 2.98: Simple trace form classification on Line 1 and 2. The facies units are shown in a band, plotted above the time window that has been analysed (data courtesy TFE).

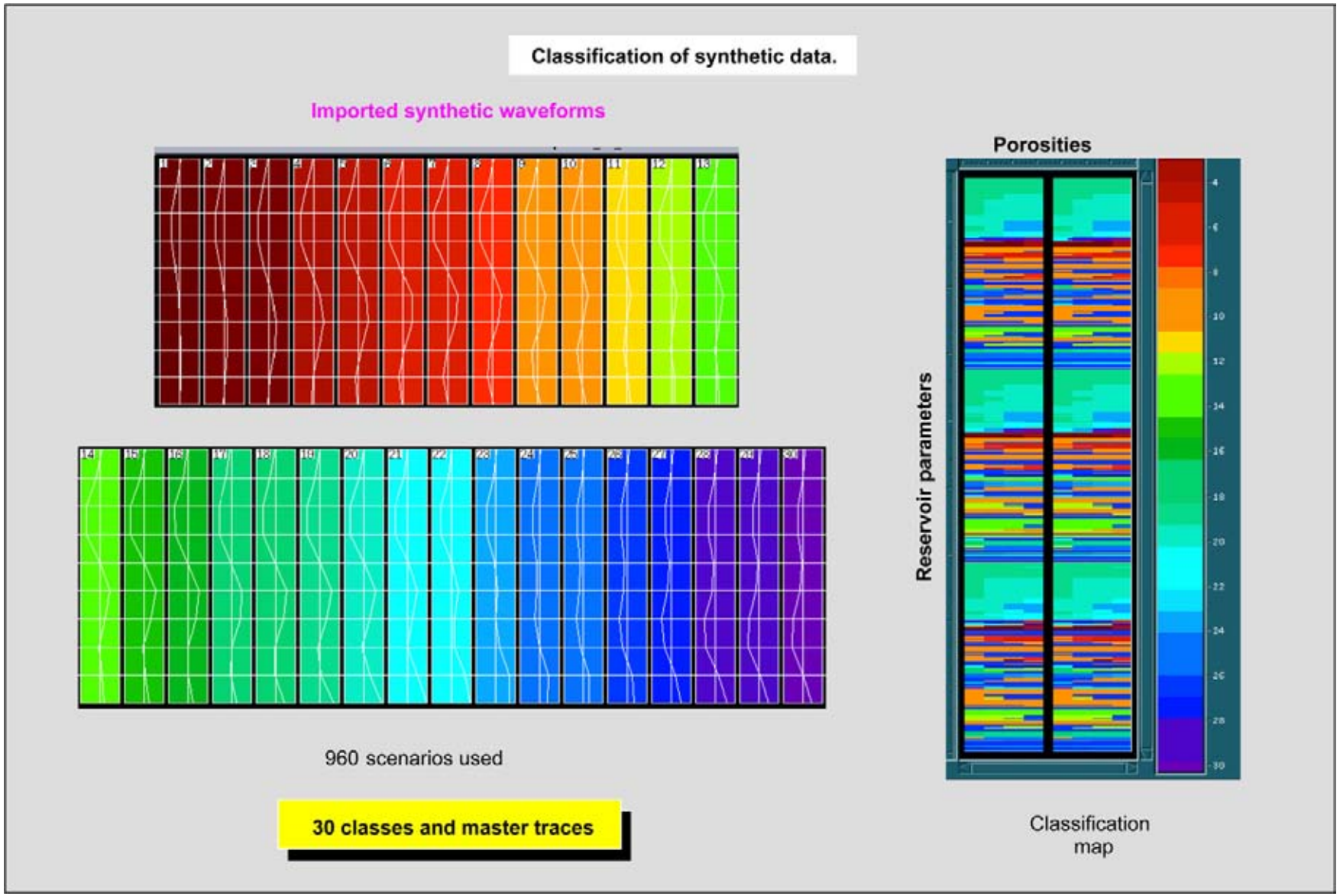

Figure 2.99: Classification of the control traces from the perturbed reservoir scenarios and the determination of the master traces. All reservoir parameters are known for these synthetic perturbed models. As a consequence the range in parameters for the master trace per class is also known. These master traces are subsequently used for a supervised classification of the real seismic traces. The probabilistic distribution of the reservoir characteristics within each class facilitates tremendously the later interpretation of the classification results. Here 960 different scenarios have been computed and serve as input traces to the supervised classification exercise (data courtesy TFE).

facilitates the interpretation of the neural network results and resolving the reservoir configuration and doing **pattern recognition** (Aug et al., in prep.). The overlying and underlying sequence of the reservoir are also modelled in the shown exercise, which are important to understand the changes in the reservoir boundary reflections. The prediction error can be assessed by hiding some wells from the classification scheme and checking the outcome in these control points. This blind well testing can be done in a sequential order to evaluate their influence on the analysis (e.g. Srivastava et al. 2004).

Even the Fuzzy Logic technique – a system of concepts for exploring modes of investigation that are approximate rather than exact – tries to get its place within the geologic discipline (e.g. Demicco and Klir 2002, Aminzadeh and De Groot 2004). Unlike in the crisp logic, the data in fuzzy logic can belong to several groups at the same time (Aminzadeh and Wilkinson 2004). The data adhere to classes that show a certain overlap in order to avoid too rigid boundaries that do not exist in the real world. The membership function is complex. Bois (1984) suggest that fuzzy logic is in particular of interest to seismic interpretation, which are notoriously imprecise, uncertain and even include an human error factor. The importance of '**soft computing**' has been demonstrated by Nikravesh et al. (2003). It comprises several methodologies like Fuzzy Logic, Neuro Computing, Genetic Computing, Probabilistic Reasoning. The latter consists of several techniques like: Genetic Algorithms, Chaotic Systems, Belief Networks, Learning Theory that provide a basis for conception, design and deployment of intelligent systems. These techniques avoid the tedious approximations (often non-realistic in nature) that have to be made in conventional crisp systems in order to handle the analysis of an imprecise dataset.

Conventional **multi-attribute mapping**, like density, acoustic and elastic impedance, Poisson's ratio, is certainly useful for lithology and fluid content identification (Walker et al. 2005). Complex multi-attributes or **meta-attributes** customised per study can be computed to discriminate better certain reservoir characteristics in a N-dimensional space. The PCA technique is hereby of great help. The automated detection of relationships hidden in the seismics is a non-biased prediction tool, even more so because the computer is a very robust observer of details.

Multi-attribute autotracking will gradually become more mature (cf Sternbach 2002). The amplitude coherency display shows the resolution power of such displays (Figure 2.101). The delineation of voxsets is then done on a routine basis. These **voxsets** are assemblies of voxels within a 3D volume, having specific multi-attribute characteristics. Their careful selection will ensure a better description and reveal more details in individual or composite **geobodies** (i.e. flow units).

Time-lapse seismic data is useful to document the change in seismic response due to production and injection in the wells (cf Oldenziel 2003). The differences are due to change in pressure and water saturation for the reservoir rocks. Swept areas are conveniently visualised and bypassed zones are easily recognised (Figure 2.102). The flow pattern in the reservoir is better resolved (Figure 2.103). The prediction of water breakthrough is feasible and a better estimation of the well production figures are obtained. The main problem for time-lapse interpretation is to assure similar acquisition and processing conditions from survey to survey. Special acquisition and processing are recommended for this purpose, because other wise the comparison between the base case survey and the later survey is meaningless (cf Calvert 2005). Positioning and coupling of the geophones is an important issue to address. The installation of a fixed geophone array over the field can be a solution. This also allows micro-seismicity to be monitored in a passive way. Time-lapse acquisition makes it possible to monitor the production behaviour within reservoirs and this is very important from a reservoir management point of view. The technique is also known as **4D seismics** (Jack 1998). Even micro-changes in the gravity field, induced by the new hydrocarbon water contact, has been monitored in a 4D sense for the Izaute gas storage project in southern France. A variation of 24 metres gives measurable differences in gravity at a reservoir depth of 500 metres, a thickness of 80 metres with an average porosity of 30% and a permeability of 6–20 Darcy (Bate 2005). **Q acquisition** and processing might be a viable option as proven in the recent seismic imaging of the Minagish field in Kuwait, with increased resolution and a better preserved signal fidelity (Shabrawi et al. 2005). The cost saving of such studies is potentially tremendous. The initial expenses for the Valhall field OBC for instance were 45 million US dollars and the additional production gains are estimated as 15 million a month (= 10,000 barrels/day). OBC is a special acquisition technique that stands for ocean bottom cable, whereby the receivers are placed directly on the seabed. The Gullfaks project experienced an added value of 200 million and the Draugen field shows a 20 percent increase in recovery rate (Calvert 2005). This makes 4D seismics certainly a very interesting option in the near future.

The fracture density can be assessed by anisotropic behaviour of the seismic velocities (Thomsen parameters).

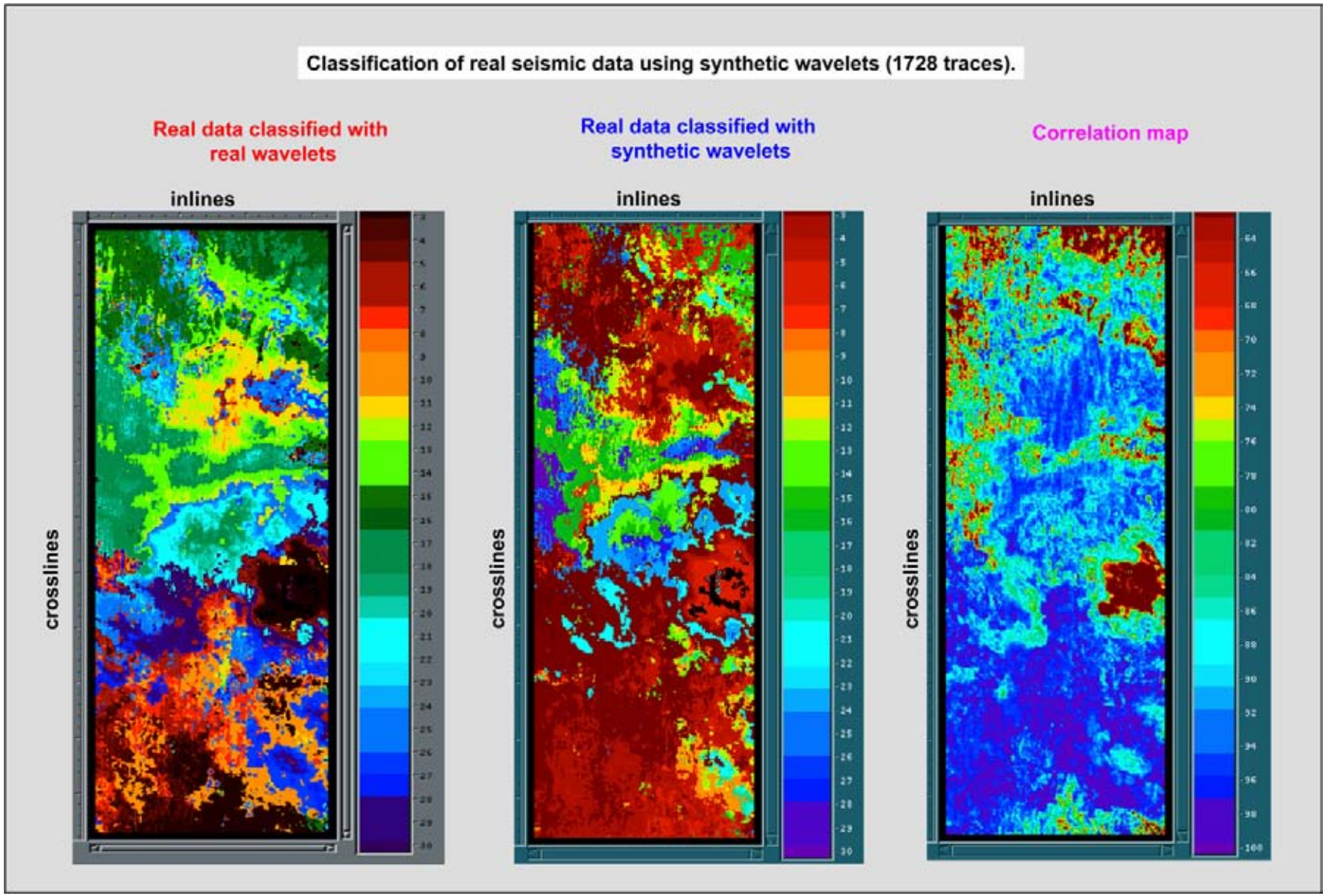

Figure 2.100: Supervised classification of the seismic traces based on imported master traces from the perturbed reservoir scenarios. The number of perturbed reservoir models has been increased to 1728 traces. The probabilistic distribution of reservoir characteristics within each class is a powerful prediction tool for the interpretation of the results (data courtesy TFE).

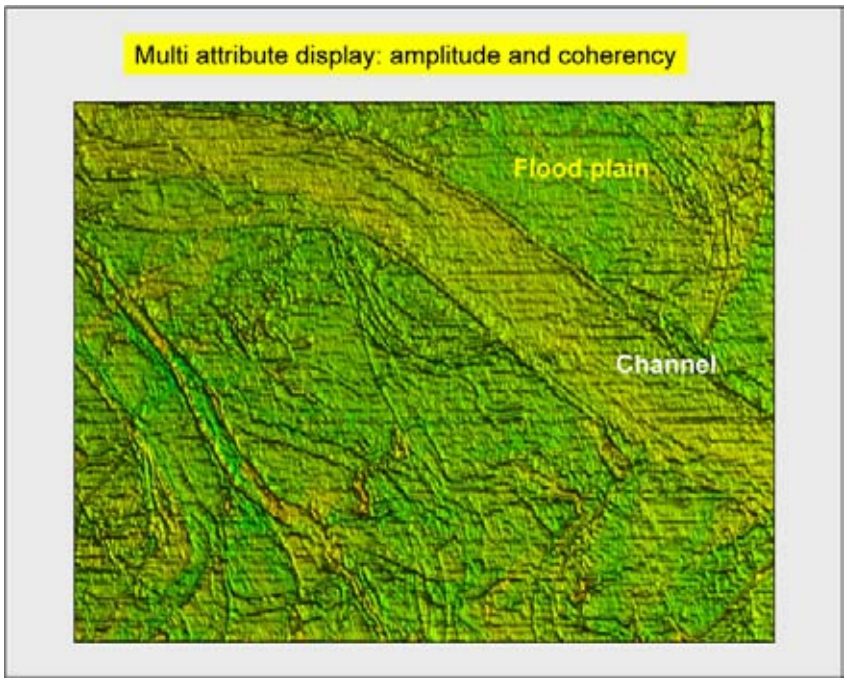

Figure 2.101: Multi-attribute display with the coherency and seismic amplitude combined. The offshore region shows a meandering channel system in a time slice mode. The nearly EW linear line-ups are artefacts related to the acquisition footprint (data courtesy Dr H. James from ParadigmGeo).

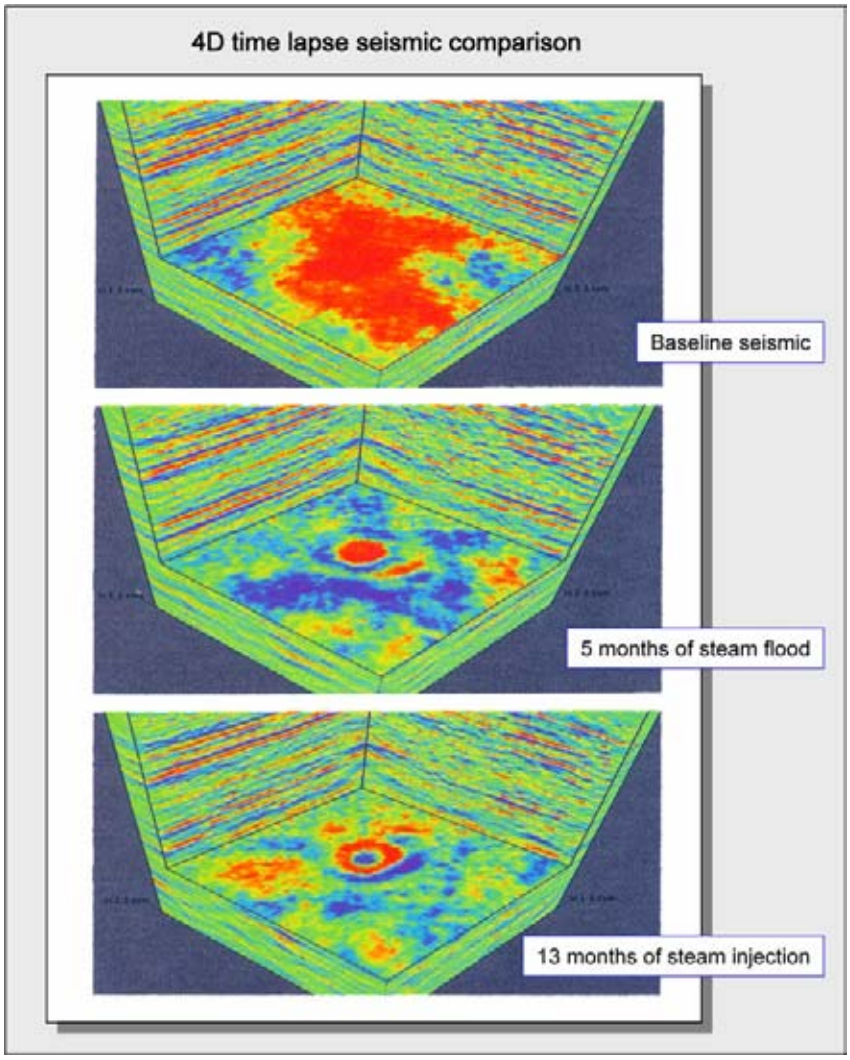

Figure 2.102: Time lapse reservoir monitoring in a steam flood program for the development of the Duri Field (Indonesia). The reservoir is made up of Miocene deltaic sands. Steam injection in this heavy oil field is assumed to increase the recovery factor from 8 to 60 percent. The injection causes local traveltime push-up and pull-downs on vertical sections, which translate in concentric circles on the time slices (modified after Brown 1999, data courtesy Chevron Standard Caltex Pacific Indonesia).

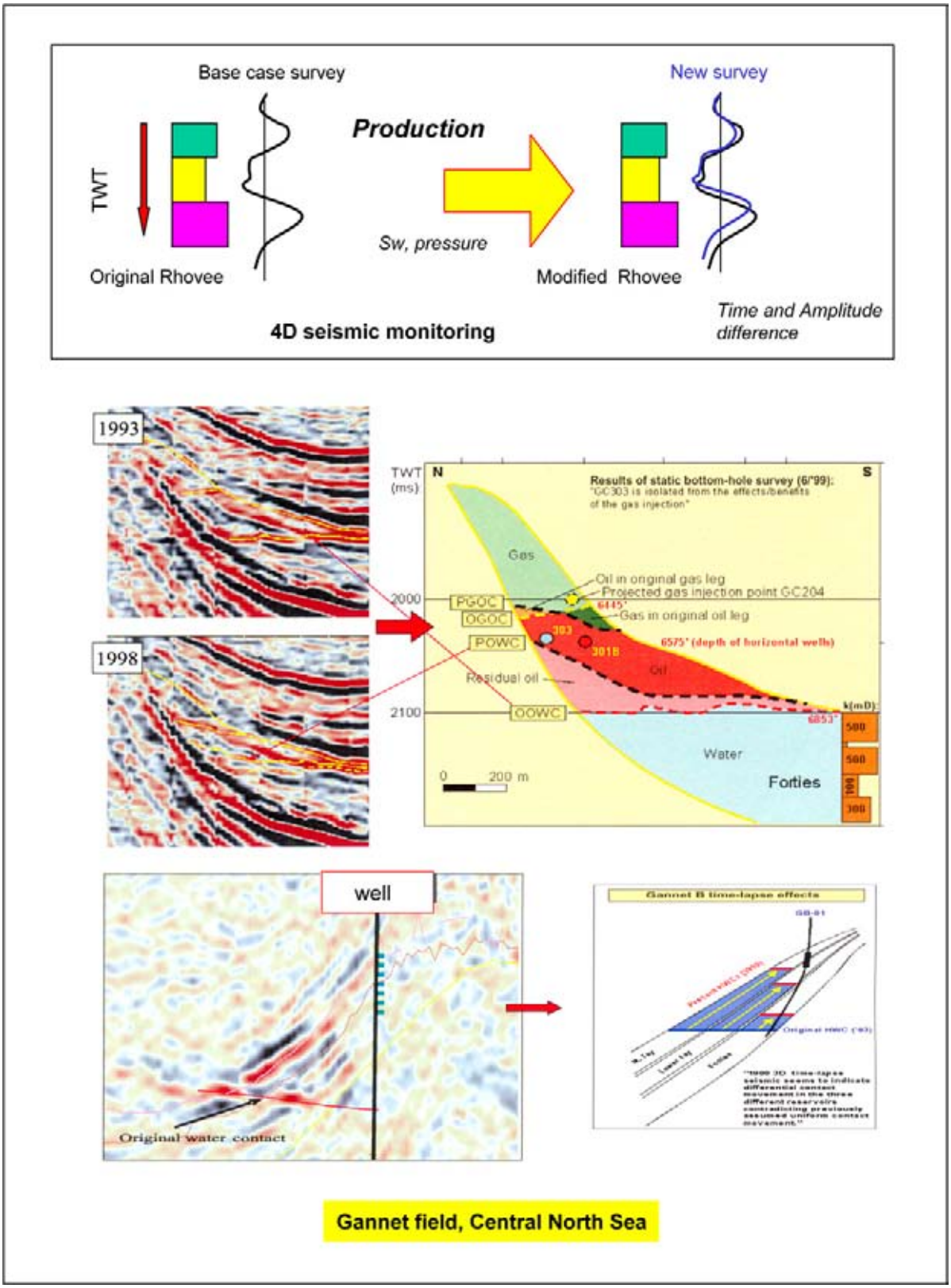

Figure 2.103: 4D seismic time lapse monitoring. The production of hydrocarbons changes the acoustic impedance contrast. It results in a time and amplitude difference in and below the reservoir sequence. Here the seismic across the Tertiary Gannet field is shown. In Gannet D the risk of early water break-through along the Middle Tay sands was detected and curative measures were taken (modified after Calvert 2005).

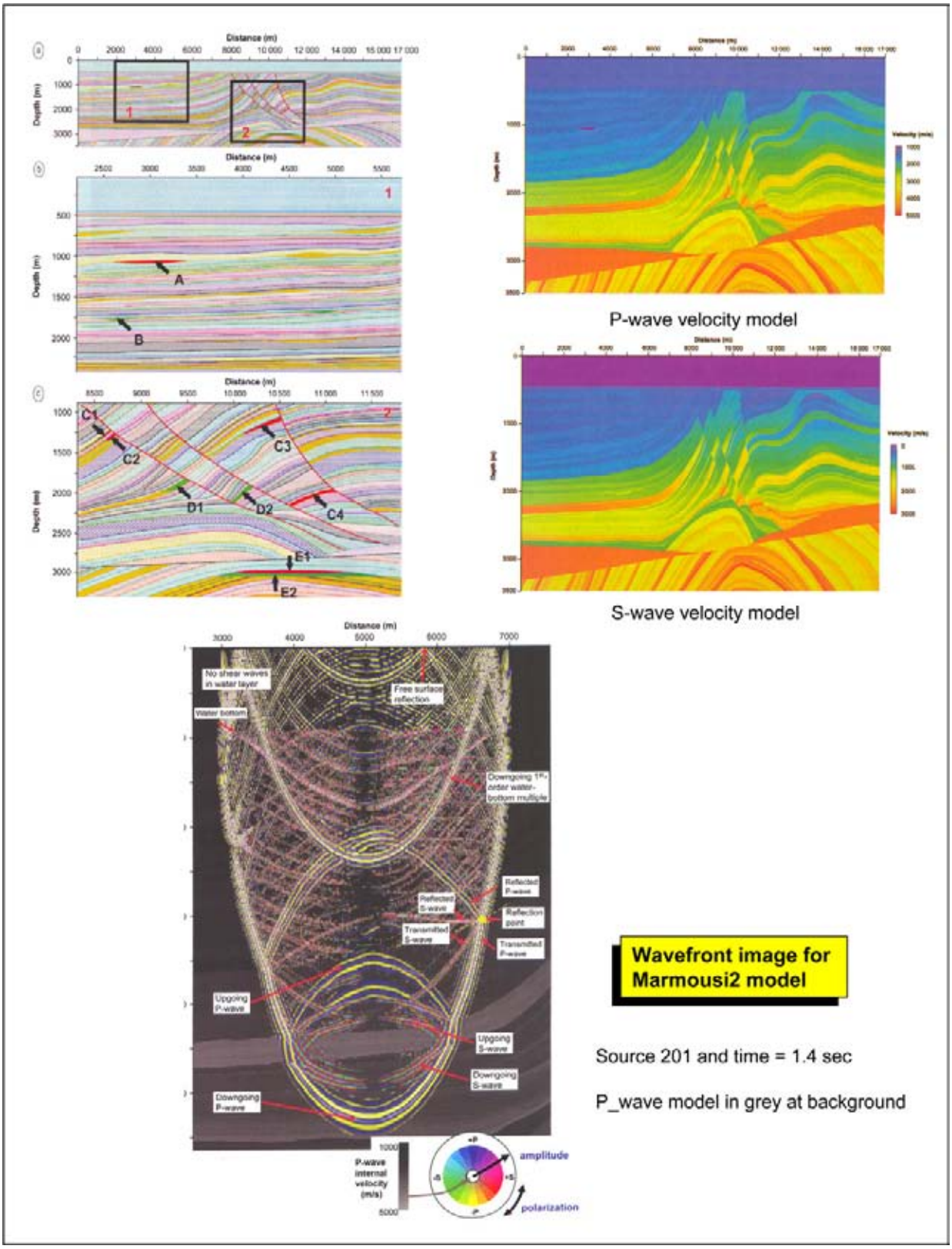

Figure 2.104: The Marmousi2 synthetic earth model represents a complex geologic configuration that is often used to test the efficiency of processing algorithms. Here the wavefront snapshot is shown at $T = 1.4$ seconds. Wave conversion occurs art the subsurface reflector and some upgoing P-waves (blue yellow) as well as S-waves (red green) are labelled (modified after Martin et al. 2006).

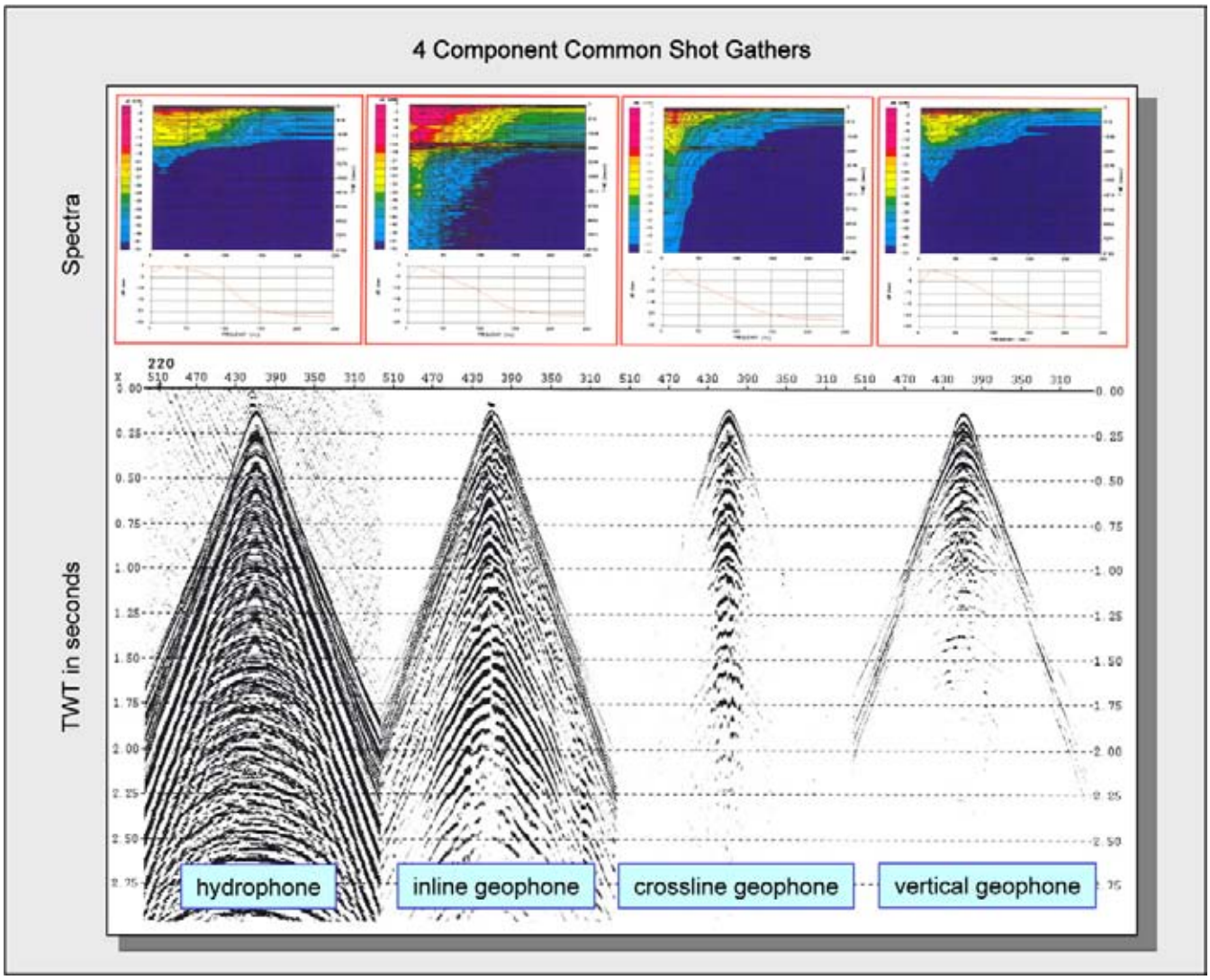

Figure 2.105: 4C common shot gathers for the hydrophone and 3 oriented geophones. The hydrophone has clearly the best coupling. The frequency spectra are shown in time and an average amplitude spectrum is depicted directly above (modified after Yilmaz 2001).

For this purpose the degree of non-hyperbolic Move Out (residual move out) is determined. Geostatistical decomposition can be useful to quantify the anisotropy effect in the data gathers with separation of a common part in all azimuth gathers, the anisotropic signal and the noise (Coleou et al. 2002). The fracture intensity map forms input for **Discrete Fracture Network** modelling to derive various flow properties like fracture permeability tensors, matrix–fracture interaction parameters, which can be used as input for flow simulators (Wong and Boerner 2004). Production history matching provides constraints for the static reservoir model and the dynamic flow simulations (Casciano et al. 2004).

Multi component acquisition and processing is also of interest. It exploits the wave conversion that occurs when P-wave seismic energy hits a seismic interface. The wavefront snapshot through the Marmousi synthetic model illustrates the conversion (Martin et al. 2006; Figure 2.104). Some of the energy is converted in S-mode and it is reflected back. This S-wave is detected by geophones at the surface. Multi component means utilising 3C geophones and a hydrophone ($3 + 1 = 4$C; Figure 2.105). The hydrophone and the vertical geophone or Z data is sometimes summed to attenuate receiver side water layer reverberations and a PZ volume is obtained (Duffaut et al. 2000). **Ocean Bottom Cable** (OBC) is deployed for this purpose in the offshore, because shear waves are not transmitted in a fluid. Also independent seismometers (OBS) are utilised that are gimballed to the horizontal (Flueh et al. 2002). It allows detection of converted shear wave energy. The CDP concept gets now translated into a CCP (Common Conversion Point). It results in PS sections and gathers.

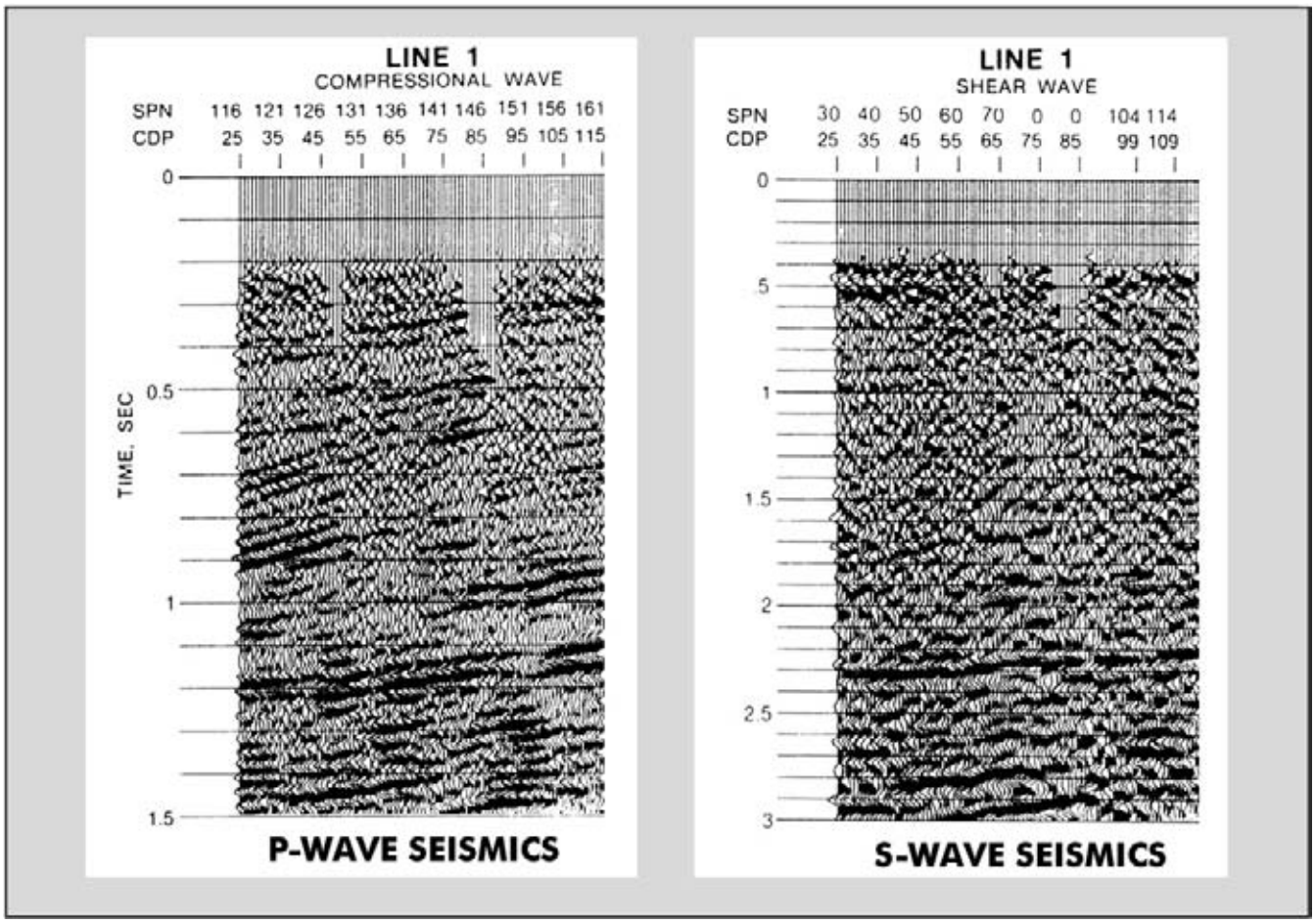

Figure 2.106: Comparison between a P-wave and S-wave seismic section. The comparison should be made in the depth domain, because the P and S-wave travel with different velocities. Here a simple factor two has been applied to the time scale of the S data, implying that V_p/V_s is constant and equal to two (Mc Cormack et al. 1985, reprint from AAPG whose permission is required for further use).

Determination of the direction of the natural coordinates, with axis parallel to the orientation of slow and fast directions, in each processed layer and the measured traveltime differences yields a significantly better stack (Granger and Bonnot 2001). Shear wave energy is less influenced by the fluid contents of the porefill. In most cases the multi component dataset allows easy identification of flat spots generated from gas, that have no equivalent on the PS-section. The difference with the P-wave response is interesting in this respect (Figure 2.106). It is a useful criterion for discriminating between brine and hydrocarbon filled reservoir. Ideally the P–S comparison should be made in the depth domain. A gas related fluid contact is not visible on the PS-sections because the S-waves are not propagating and transmitted in a liquid or gas, as there is no shear stress. Even the fracture network can be established with wide azimuth OBC seismic data (Luo et al. 2005).

The **converted wave** energy is able to resolve reflections in gas-chimneys (Stewart et al. 2003). It helps in defining the structure in these poor data zones, e.g. Plio-Pleistocene lacustro-deltaic reservoirs in the Gunashli Field in Azerbaijan (Manley et al. 2005). The ray path in a complex situation like a salt dome might be better resolved (Garotta 1999). The P-to-Sv converted energy is also known as **C-wave** energy (De Angelo et al. 2003), with an approximated velocity $V_c = \sqrt{V_p/V_s}$. The PS data is expected to have a slightly better vertical resolution than the PP data. This is caused by the slower propagation velocity and the larger bandwidth of the PS frequency spectrum (D'Agosto et al. 2005).

Multi-component or 4C acquisition is gradually becoming useful to outline hydrocarbon occurrences more precisely (cf McCormack et al. 1985, Lucet and Fournier 2001). The combination of 4D and 4C techniques is currently applied on the Valhall field operated by BP. A 4C seabed cable, with geophones and hydrophones, is permanently installed over the field to allow repetitive shooting of seismic datasets. The Life of Field Seismics

(LFS) is expected to boost the very low initial recovery factor of 14 to 40 percent and an additional 60×10^6 barrels will be produced. In the first 18 months six surveys will be shot and processed to evaluate the changes in saturation and pressure induced by the hydrocarbon production (First Break 2003, Vol. 21, pp. 26–27). The **smart field** concept (multi-sensored or instrumented oil field), with many sensors permanently installed in and around the wells, allows monitoring of the field production behaviour with great care (Eenhorst 2003). The high initial capital investment is easily offset by the long term gains generated by this advanced new **e-field** technology. The IT method is also labelled as the digital oil field (Holland 2004). Passive 4D seismic monitoring is certainly helpful in the efficient management of reservoirs by visualising the distribution of the microseismicity events related to small changes in the subsurface stress state due to ongoing hydrocarbon production (cf Wilson et al. 2004). It equally allows for detailed fracture mapping (Maison et al. 2005). Permanent or passive borehole seismic monitoring has already demonstrated its merits on several occasions and will certainly play a more prominent role in the near future (Th. Bovier-Lapierre, pers. com.).

This page intentionally left blank

Chapter 3

Seismic Stratigraphic Techniques

The first phase in seismic stratigraphic studies of a basin fill is to delineate genetically related units, which are called **Depositional Sequences** (Mitchum et al. 1977). These sequences are of regional importance and are further subdivided into individual **system tracts** (Van Wagoner et al. 1987). The system tracts are delineated based on the presence of local unconformities and their laterally equivalent conformities. They contain a grouping of deposits from time-equivalent depositional systems (Armentrout and Perkins 1991). The depositional sequence is composed of a stack of system tracts. A distinction can be made between lowstand and highstand system tracts, referring to changes in relative sealevel as will be shown later on. The basic method for the delineation of Depositional Sequence boundaries, is called the '**reflection termination mapping**' technique (Vail et al. 1977).

In the chapters below the nature of the observations on a seismic dataset will be further examined. Subsequently the breakdown of seismic sections into depositional sequences and the delineation of various internal seismic facies units will be discussed. After this the geological/depositional implications of these observations are evaluated.

3.1 Basic Seismic Observations

Four major groups of systematic reflections are distinguished on seismic sections (Figure 3.1):

- **Sedimentary reflections** representing bedding planes.
- **Unconformities** or discontinuities in the geological record.
- **Artefacts**; like diffractions, multiples, etc.
- **Non-sedimentary reflections**; like fault planes, fluid contacts etc.

In the sections below the different types of reflections are described in more detail. Thereafter the attention is focused on various groups of reflections that are generally distinguished. Their internal organisation and seismic facies character are presented. Finally the interpretation of all these features in terms of their geological meaning is discussed. The major emphasis on sedimentary seismic reflections is related to the fact that seismic data analysis is an essential tool for hydrocarbon exploitation. Most of the known HC occurrences are of **organic origin** and the sedimentary beds are their host rocks.

3.1.1 Sedimentary reflections

One of the basic concepts behind seismic stratigraphy is the observation that individual sedimentary reflections can be considered **timelines**. More precisely: they are representing a rather short time interval of continuous sedimentation conditions. This observation was made by several workers (e.g. R. Leblanc, P. Kruyt) before Peter Vail and his coworkers (Exxon) finally published the same idea in 1977. Each reflector coincides with a short time period of similar depositional conditions in a geological sense. This timeline concept equally signifies that seismic reflections tend to cross laterally through different depositional environments and therefore they can incorporate various lithofacies units.

In Figure 3.2 (Hinz 1983), it is seen that, if a specific seismic loop is followed from the left to the right, it goes from a sub-parallel topset into a gently dipping foreset and finally it is transitioned into a sub-parallel bottomset. This TWT time geometrical relationship can be translated in terms of depositional environments: it goes from a sand-prone shelf (proximal = closer to source area of sediments), into a shale-prone slope (further from the source and thus finer-grained) and ending up in the distal shale-prone deeper basinal environment (distal = far from sediment source). The word 'prone' means here that the dominant (or gross) lithology is likely to be of a certain type. It is mainly related to the average grainsize and energy of the environment of deposition. The expression **shelf** is usually restricted to deposits up to a waterdepth of 200 metres. There is a distinction between inner and outer shelf. The inner shelf comprises the coastal, transitional to marine environments, while the outer shelf is purely marine with a waterdepth of 50 to 200 metres. Beyond 200 metres the

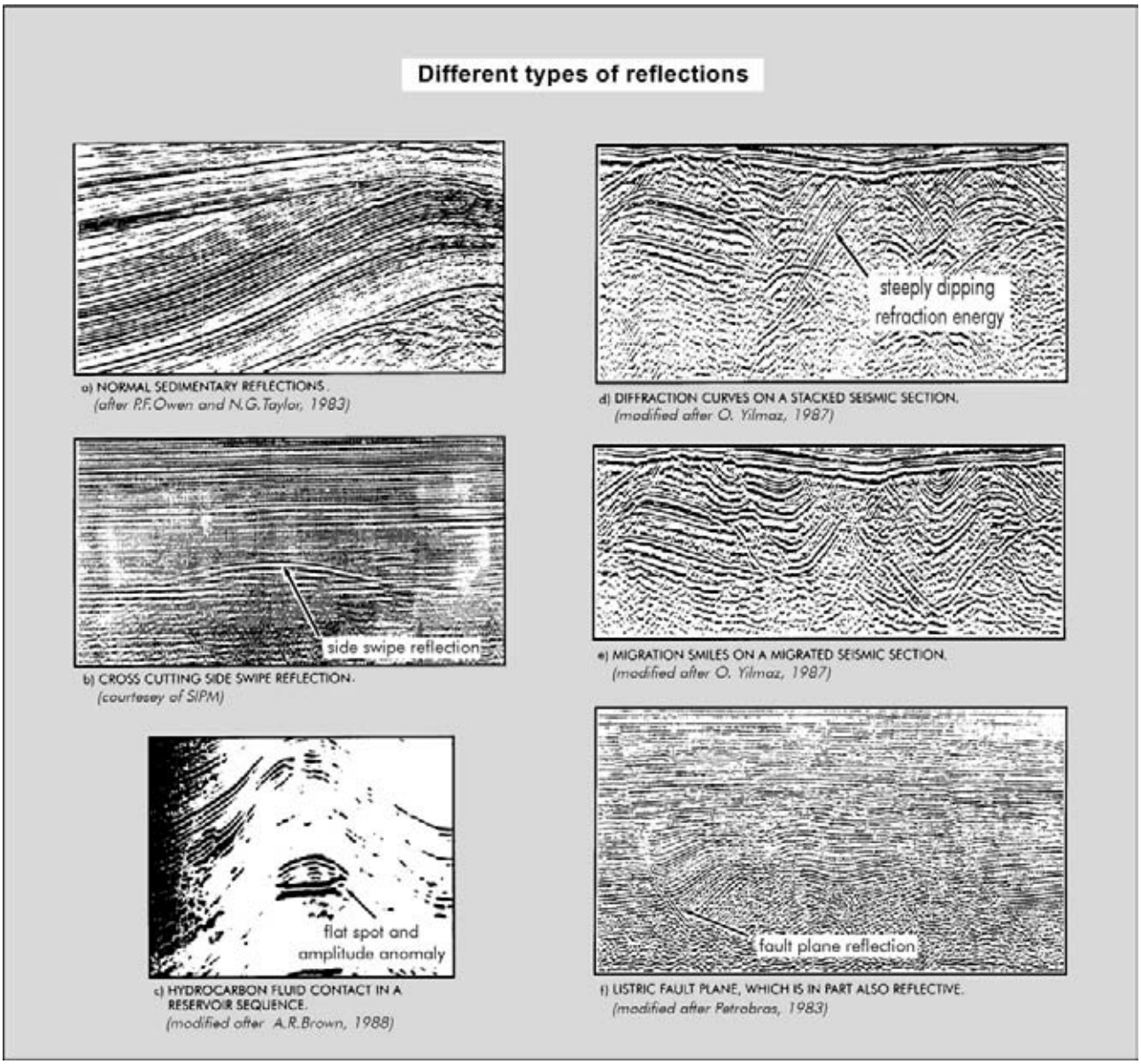

Figure 3.1: Examples of different types of seismic reflections. Not only rock interfaces but also fluid contacts can have a sufficient acoustic impedance contrast to generate a seismic reflection.

waterdepth is bathyal; it constitutes the domain of the continental slope and abyssal plain.

The sedimentary reflections represent bedding planes that correspond to conformable changes in depositional regime, i.e.:

- Energy level.
- Sedimentation rates.
- Environment of deposition.
- Input source.
- Degree in diagenesis.
- Pore contents.

As reflections tend to cross depositional environments, it is assumed that the pore contents (fluid fill and cement) plays a role in creating the acoustic impedance contrast. Also the fact that reflections are seen in nearly homogeneous shale deposits does suggest the validity of such a hypothesis. Even changes in seawater temperature can cause reflections (Yilmaz 2001) or density contrast between stratified waterlayers in response to distinct salinity changes.

As seen earlier on, reflections are generated by interfaces that show sufficient velocity–density contrast. This can be a single lithological boundary or the combined response of several closely spaced interfaces. There are

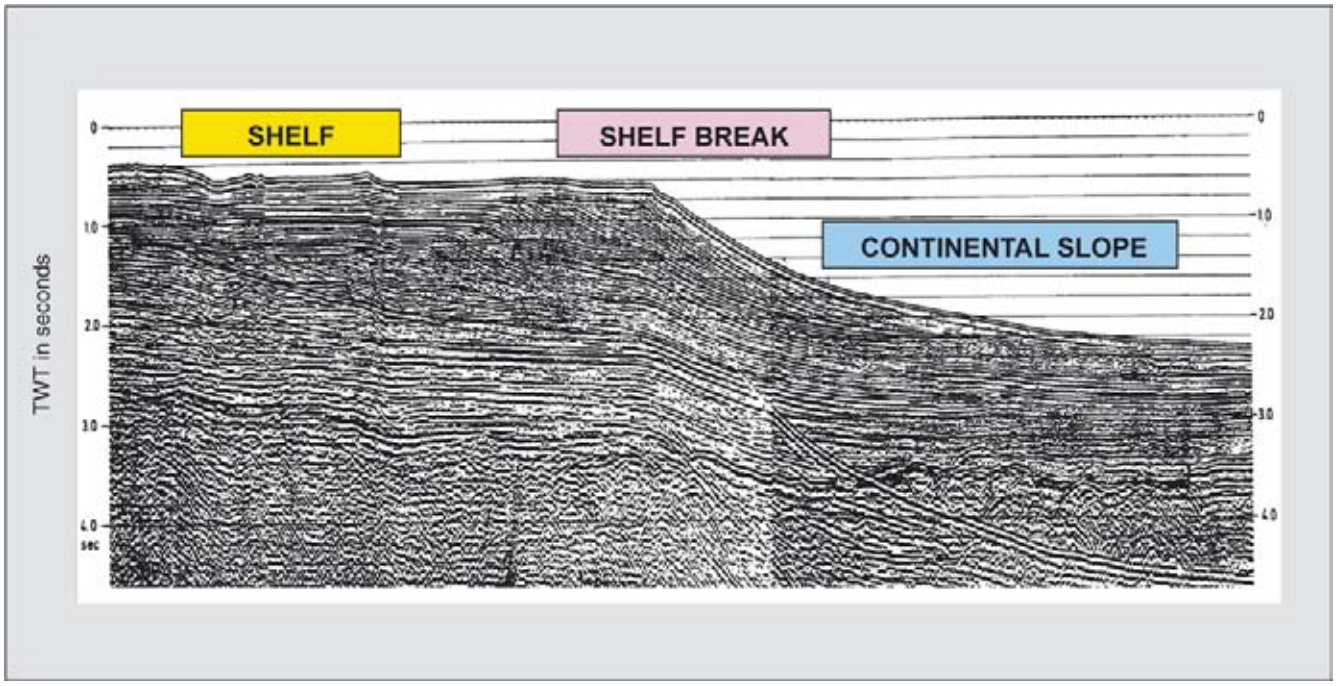

Figure 3.2: Seismic reflections passing continuously from a top-, fore- to a bottomset configuration. In a geological sense it means going from a sand-prone shelf (proximal = closer to source area of sediments), into a shale-prone slope (further from the source and thus finer-grained) and finally ending up in the distal shale-prone deeper basinal environment (distal = far from sediment source; modified after Hinz 1983, reprint from AAPG whose permission is required for further use).

several features that help to describe the reflection character of a seismic loop:

- Reflection **configuration**, which is related to the geometry of the bedding pattern resulting from specific depositional processes, the original paleotopography and fluid contacts.
- Reflection **continuity**, which describes continuity of the layers. It is directly related to sedimentary processes and therefore also to the environment of deposition.
- Reflection **amplitude,** providing a measure for the reflection strength, lithological contrast, bedding spacing and fluid contents.
- Reflection **frequency**, which gives an estimation of the bed thickness and possibly also the fluid contents.

The interval velocities give additional information on the gross lithologies, the porosity distribution and the fluid contents. In a wider context the external and internal form of a group of seismic reflections – i.e. **seismic facies** – together with the spatial association is important to assess the depositional environment, the position of the input source and the overall geological setting of the unit under study.

3.1.2 Unconformities

Unconformities are surfaces of erosion and/or non-deposition which constitute time-gaps in the geological record (Dunbar and Rodgers 1957). Unconformities generate reflections because they separate beds with different physical properties, cq lithologies, and therefore different acoustic impedance characteristics. Strata below the unconformity are older and the beds overlying the surface are younger than the time-gap (e.g. Pomerol et al. 2005). Consequently the strata between two unconformities form a **time stratigraphic** unit. Reflections generated by unconformities are representing a hiatus in the sedimentation record and are normally **diachronous**. The latter indicates that the time captured in the time gap is not everywhere the same. Hence the time gap varies in importance along the unconformable surface.

Often an unconformity coincides with a change in structural dip of the units above and below the interface. If this is the case, than there exists an angular contact between the two different time units on both sides of the unconformity. This angular relationship indicates a certain amount of tectonic deformation before the younger sediments were deposited. Erosion leads to truncation of the underlying strata or time units. If the beds in both units are parallel, then other techniques like biostratigraphy, isotopic analysis may help to establish the

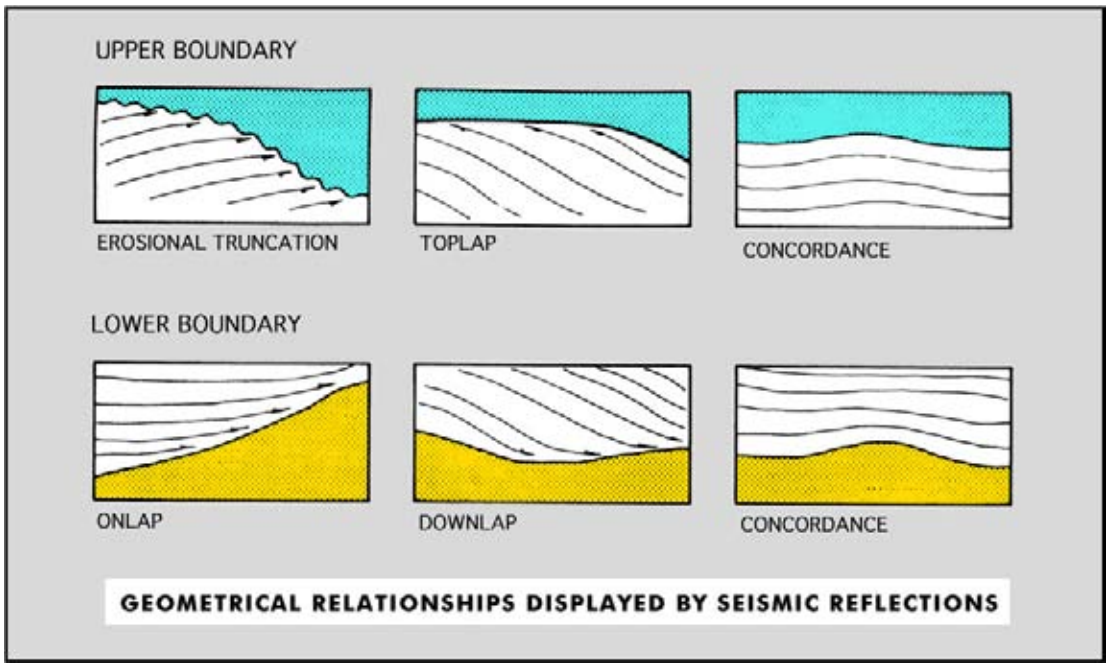

Figure 3.3: Various unconformable relationships displayed by the reflection geometries on seismic sections (modified after Vail et al. 1977, reprint from AAPG whose permission is required for further use).

amount of time captured in the layer boundary. There are situations where the time involved for a hiatus can only be defined in a relative way.

Many unconformities are non-reflective and these are more difficult to trace on the seismic sections. In a lot of cases the reflectivity of an unconformity varies laterally. This is due to lithological changes of the sediments subcropping and overlying the interface. Therefore an erosional surface is described more precisely on the basis of geometric relationships. Several types of reflection relationships are distinguished at these unconformable interfaces (Vail et al. 1977). If the substratum is considered, the following relations are seen (Figure 3.3):

- '**Erosional truncation**', whereby older sediments are eroded and removed over larger areas (Figures 3.4 and 3.5). The substratum can be deformed tectonically.
- '**Toplap**' if the erosion is affecting a prograding shelfedge geometry. The underlying unit must show a depositionally inclined layering or foresetting.
- '**Concordance**' in case the interface and the substratum are deformed in same manner. This geometry does not necessarily say that there is no important time gap between the layers.

If the configuration displayed by the upper sequence is considered, the following reflection relations are distinguished:

- '**Onlap**' whereby the younger sediments are progressively overstepping each other (Figures 3.6 and 3.7).
- '**Downlap**' in case of foresetting abutting on an unconformity. The younger strata are depositionally inclined. The inclined foresetting gives an indication for the direction of the sediment supply. Starved sedimentation conditions prevail in the distal area.
- '**Concordance**' if the overlying sediments show the same deformation as the separating interface and the underlying unit.

The structural configuration of the beds on both sides of the unconformity, and also the internal reflection patterns displayed by the under- and overlying units, gives information on the tectonic and environmental significance of the boundary surface. Several characteristics are deduced from the unconformity type:

- Subaerial, submarine, fluvial or glacial in origin (Figures 3.8 and 3.9).
- The time gap is either erosional or non-depositional; the latter is indicating sediment bypass.
- The topographic relief is planar, irregular or with a certain inclination.
- The significance is either regional or local.
- The degree of tectonic deformation gives an idea about the rate of instability of the region.
- In special cases information is deduced on the relative sealevel behaviour, sediment supply and rates of subsidence changes.

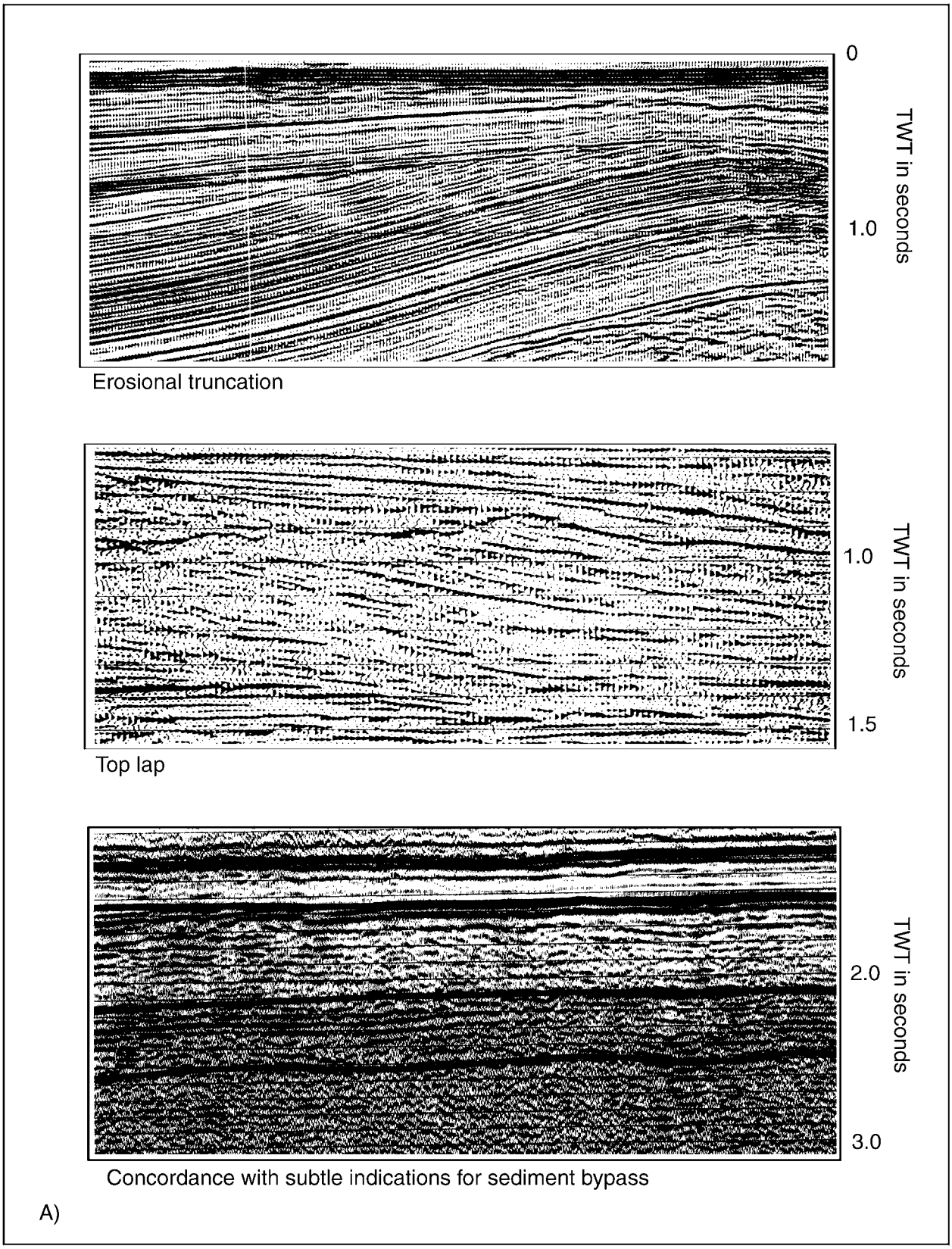

Figure 3.4: An example of erosional truncation, toplap whereby foresetted sediments are truncated by an overlying unconformity whilst concordance is shown for the lower and more distal part of the unit. A time hiatus can be present between parallel layers without evidence for tectonic differential deformation.

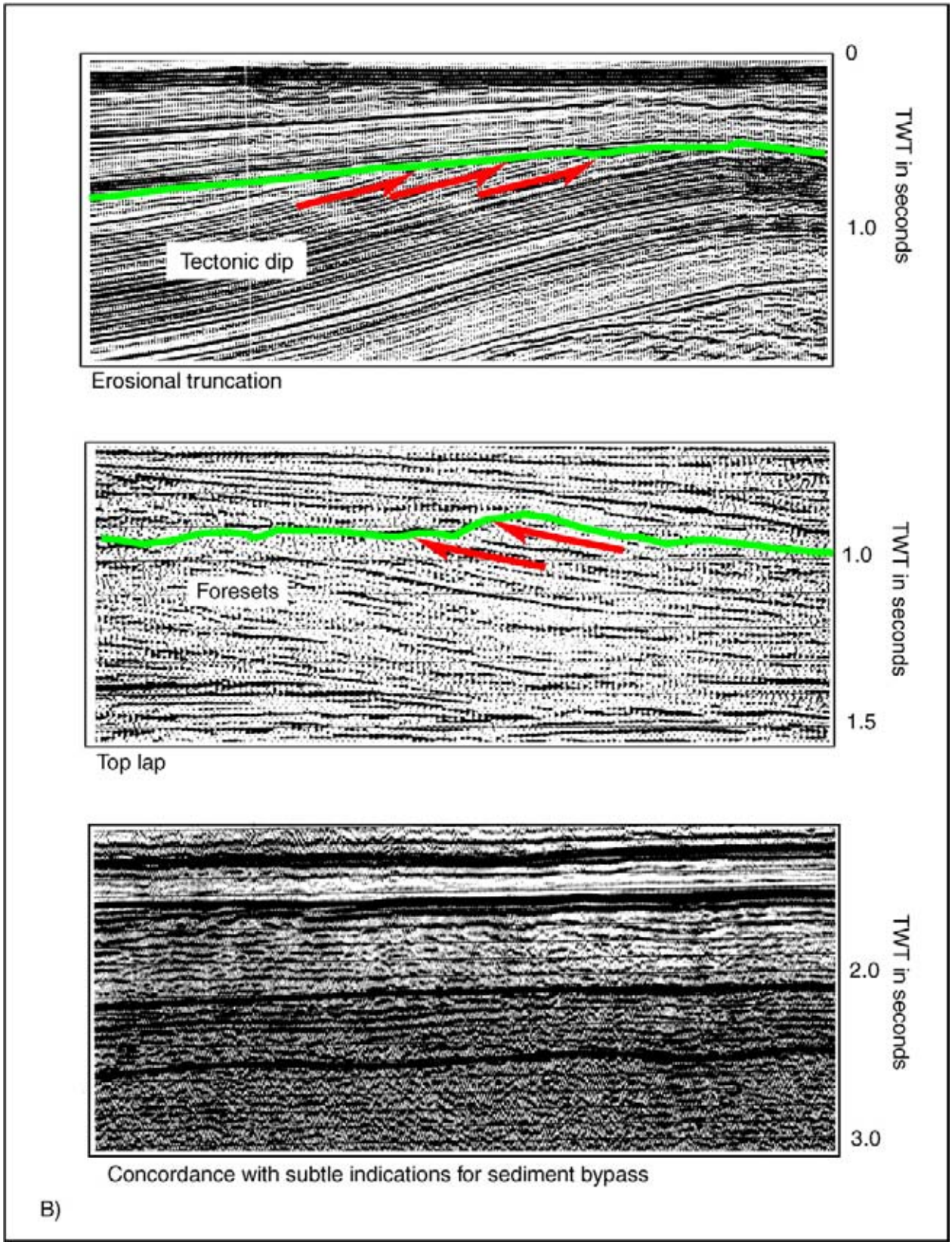

Figure 3.5: Interpretation of the reflection terminations (red arrows) in order to define the position of unconformities (green line). The unconformity represents a depositional gap in the geologic record. If it has a regional significance it is considered a depositional sequence boundary.

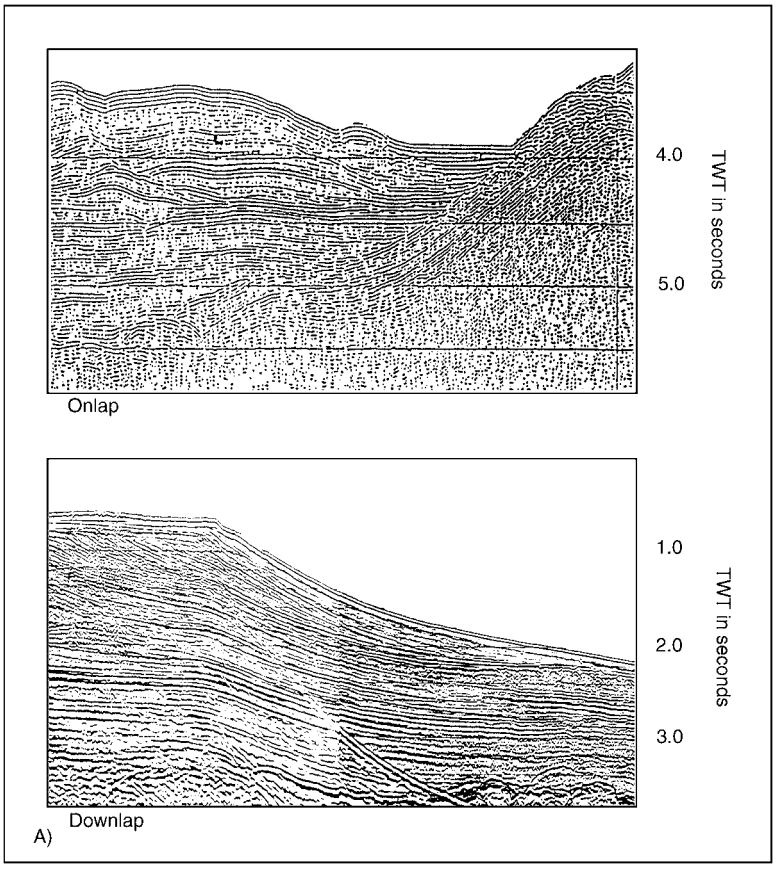

Figure 3.6: An example of onlap and downlap reflection configurations. The inclined foresetting gives an indication for the direction of the sediment supply. In the distal area (furthest away from the source) starved sedimentation conditions prevail.

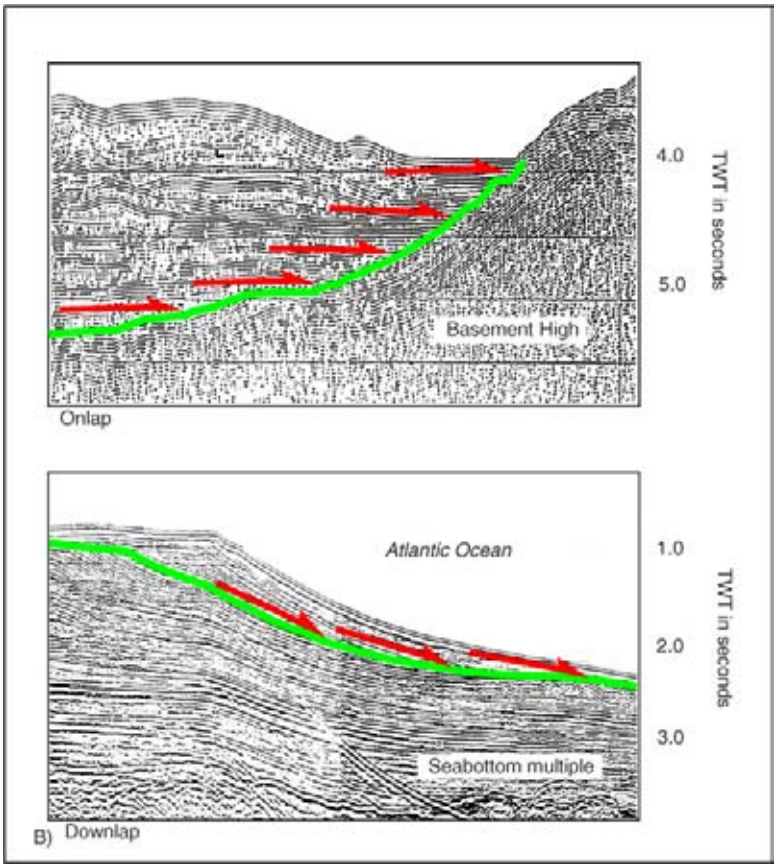

Figure 3.7: Interpretation of the reflection terminations as indicated by red arrows and defining unconformities (green lines) which are basically sedimentation gaps.

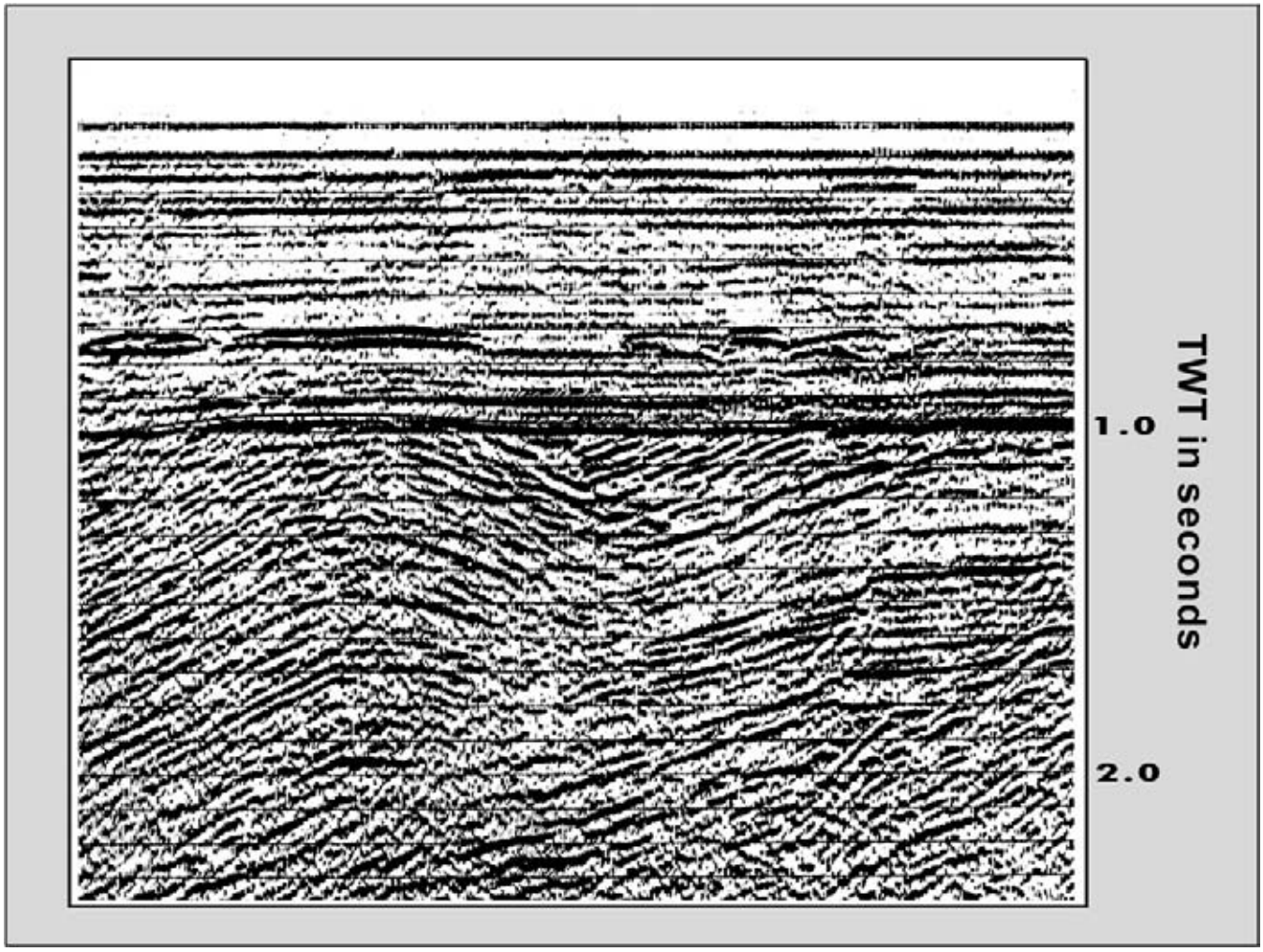

Figure 3.8: Evidence for subaerial erosion with an important time hiatus. Peneplanisation (erosional flattening of the paleo-topographic relief) occurred before the younger sediments were deposited.

3.1.3 Non-sedimentary reflections

There are several types of coherent non-sedimentary reflections on seismic data. Fault planes may show up as prominent seismic reflections. This is specially so when a high acoustic impedance contrast is present between the two juxtaposed lithologies on either side of the fault plane (Figures 3.10 and 3.11). Coherent fault plane energy is normally attenuated in the seismic processing because of its high dip. The processing operations usually tend to suppress highly inclined line-ups and hence the fault plane reflections are not well imaged. Fine-tuning of migration parameters may bring out the fault plane geometry and improve the focusing.

Fluid contacts within porous bodies – like the gas–water contact in a hydrocarbon bearing reservoir – also generate individual reflections (Figure 3.12; Brown 1988). The porefill influences the reflectivity of a lithological unit. The presence of gas (reduced density and velocity) is often detectable on seismic sections as amplitude anomalies. There is a distinct decrease in acoustic impedance over the reservoir unit (e.g. Veeken et al. 2002b). Gas has a slower P-wave velocity and lower density than a brine porefill. Slower velocity translates in longer traveltimes and hence a pull-down effect below the gas zone on the seismic twoway time sections is often noticeable.

Mineral phase changes are responsible for some of the deep-seated reflections. The Moho discontinuity, separating the crust from the mantle and which forms a mineralogical interface within the lithosphere, can sometimes be seen clearly (e.g. Malod et al. 2004). It coincides with an increase in P-wave velocity from 6.5–7.2 to 7.8–8.5 km/sec and a density increase from 2.9 to 3.2 gr/cm^3 (Sheriff 1991). Other deep-seated reflections don't seem to coincide with a measurable density/velocity contrast and have to be attributed to

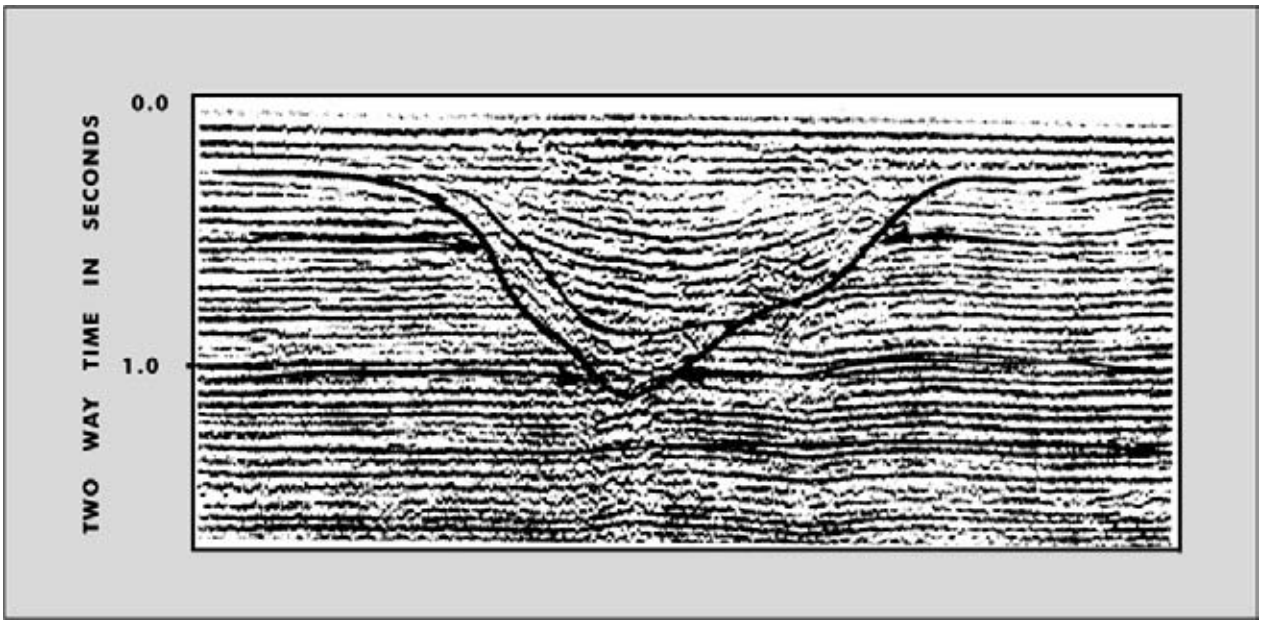

Figure 3.9: Submarine currents can cause considerable local erosion. Note the concordant contact lateral away from the submarine canyon fill (Mitchum 1985, reprint from AAPG whose permission is required for further use).

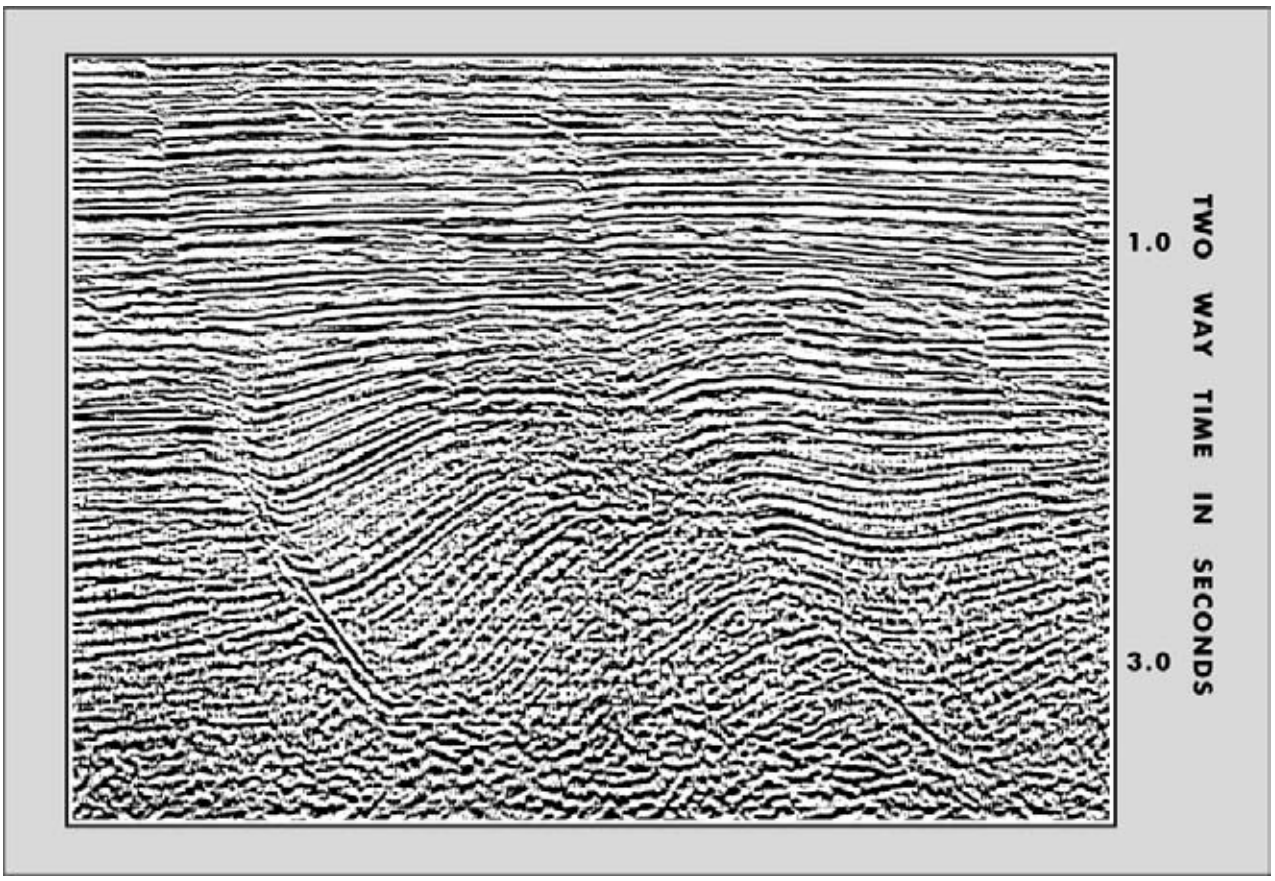

Figure 3.10: Non-reflective fault plane with clear fault-related reflection terminations. There is a regular spacing to the faulting, indicating a uniform stress pattern and lateral continuity of the layers. The deeper part of the section is rather chaotic and characterised by discontinuous reflections. The curved fault planes sole out in this plastically deforming layer (decollement surface; modified after Petrobras 1983, reprint from AAPG whose permission is required for further use).

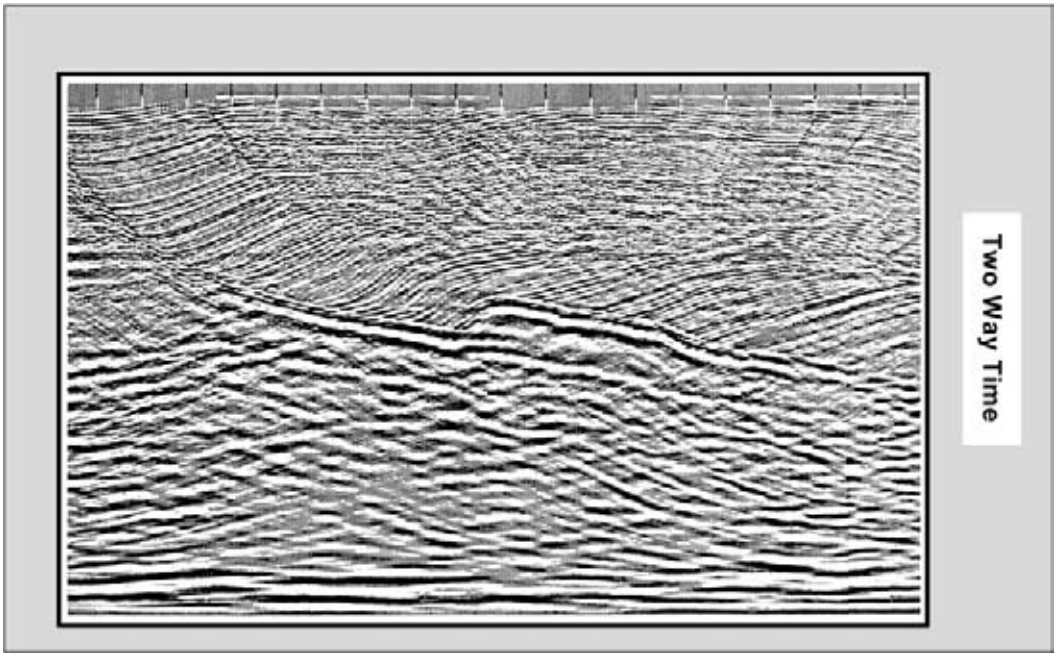

Figure 3.11: Partly reflective listric fault plane, with strong rotation and tilting of the hanging wall sediments in respect to the sub-parallel foot wall deposits. Note that the oblique dip of the reflections are here tectonically induced and should not be confused with sedimentary dips. Criteria to discriminate between the two distinct origins is the rather uniform and regular character of the lateral thickness variation of the layers and the presence of the curved fault plane.

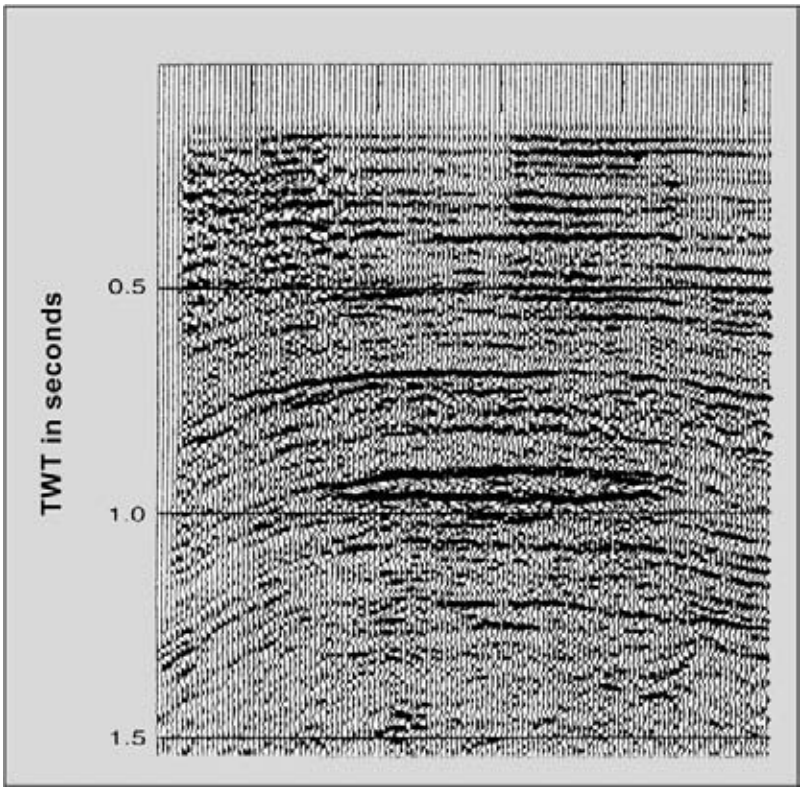

Figure 3.12: Fluid contact in a reservoir coinciding with a velocity/density contrast that is sufficient to generate a seismic reflection. The gas has a lower density and lower P-wave velocity than the brine porefill. The amplitude anomaly corresponds to a bright spot. It is caused by the presence of a 'class 3' AVO reservoir. The flat spot is the result of the change in porefill, it corresponds to the gas/water interface (after Brown 1988, reprint from AAPG whose permission is required for further use).

minute differences in pore content and/or chemical compositions of the rock building compounds (minerals and cement). A constructive interference element can not be ruled out. The Moho is seen affected by faulting on some deep regional seismic lines and brittle deformation occurs again at such depth for the Olivine-rich rocks. This is caused by the high temperature – high pressure conditions of 700–800 degree Celsius (Pomerol et al. 2005). Deeper in the mantle and at a temperature of around 1200 degrees the peridotites become very ductile and a low velocity seismic zone is found (LVZ) that assures the decoupling of the litho- and astenosphere. Also ancient paleo-Moho contacts can be traced onland if tectonic movements have been very drastic in the recent past. The ophiolite belt in Oman (SE Arabian peninsula) contains an excellent example of a paleo-Moho contact with outcrops of layered gabbros (base of magna chamber) on top of truncated Harzburgite (olivine-rich peridotites). The lithosphere transition zone of the oceanic crust is upthrusted upon the Arabian shield. The geological exposure of the Moho in the Omani mountains is almost 700 km wide. It is easily accessible along the Muscat-Emirates tarmac road (Figure 3.13; see also Section 3.5.5) and also in the Wadi Abyad there is a sensational outcrop exposed at the surface (Hanna 1995).

3.1.4 Artefacts and artificial reflections

Seismic artefacts can have several causes. Some are formed by diffraction curves. These diffraction curves are generated by scatter of seismic energy around a point source in the subsurface. The diffraction energy is represented on a stack section by a typical convex curve. For instance, a faultblock edge represents such a diffraction-generating reflection point. Migration will collapse the scatter energy and repositions it on the apex of the curve, where the diffractor point is located.

Multiples are artificial reflections created by acoustic waves that are travelling several times between two strong reflectors before being intercepted by a geophone (Figure 3.14). Two basic types exist:

- Short path multiples. These multiples are difficult to remove because they have similar velocities as the primary energy. Deconvolution can reduce the length of the long wavelet and take out some of the interference effects.
- Long path multiples. Velocity difference with **primary energy** (genuine seismic reflections) is substantial and gives a decent possibility to remove this energy in the stacking procedure.

Very often the water bottom is a strong first order multiple generator. '**Peg legs**' are formed by signals bouncing several times between certain subsurface layers before being recorded at the surface. This bouncing effect of the wavefront is also known as '**reverberation**'. If it occurs between closely spaced interfaces, the effect is known as '**ringing**'. If the reflected signal is internally reflected in the waterlayer, just before interception by the geophone, the multiple is called a '**ghost**'. Multiples can be attenuated by special processing (e.g. Pettersson 2003), but it is sometimes difficult to remove this kind of consistent energy completely from the seismic section.

The migration process can create artefacts known as '**migration smiles**' in the deeper part of the section. The expression 'Keep smiling' has a rather negative connotation in this context. The presence of the upward curving smiles means that the migration velocity is not correct and it has been set too high. It results in serious overmigration of the data. The wrong migration velocity will also give rise to artificial deformation of the reflection (Yilmaz 1987, Versteeg 1993). If only one side of a diffraction curve is present on the stacked data, then the migration process will not be able to collapse the diffraction properly and will not place the right amount of energy at the apex of the hyperbola. This creates asymmetric smiles on the time section. Migration of the seismic data results generally in a better focusing of the reflections, it broadens the anticlines and reduces the areal extend of the synclines. It moves the energy in an updip direction. Diffraction curves are collapsed to their apex (Figure 3.15).

If the subsurface structure is dipping strongly and the seismic line is running more or less parallel to the strike of a 3D structure, then it is possible that seismic energy is coming from outside the vertical plane of the section. The flank of the structure has a higher and shallower position outside the line trajectory. The raypath perpendicular (normal incidence) to the flank of dipping horizon is the fastest and will reach the geophone first. This energy is stemming from CDP points outside the vertical plane of the seismic line in case of a steep cross-dip. The resulting reflection can be quite consistent and is known as a '**sideswipe**' (Figure 3.16). Often the side swipe shows up as a crossing event. The presence of crossing or conflicting events also may indicate that the migration operation has not achieved its objective. A real 3D approach to the migration procedure should resolve these imaging problems. Seabottom artefacts, like for instance shipping junk, have often an important side-effect on seismic sections, laterally away from the object.

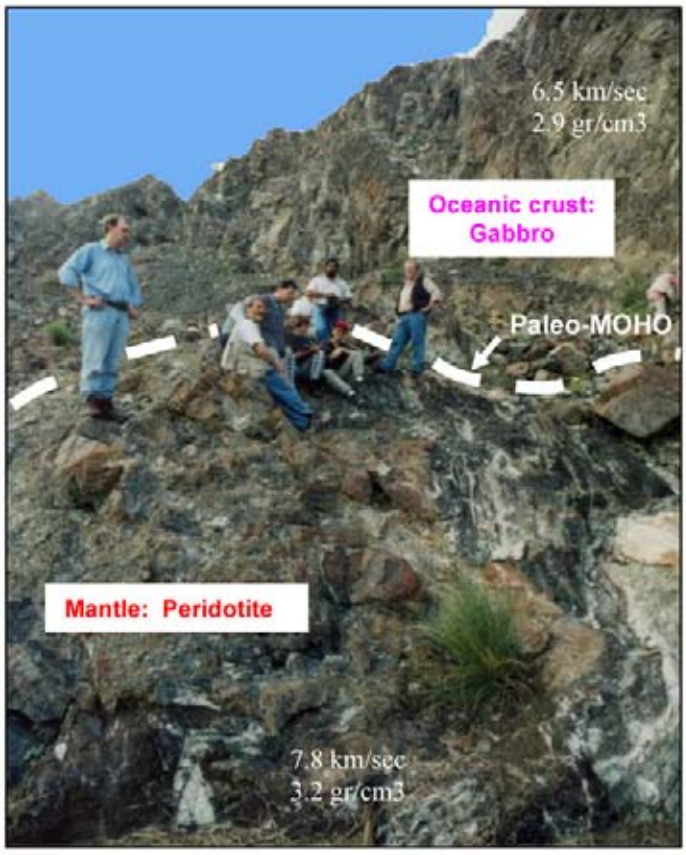

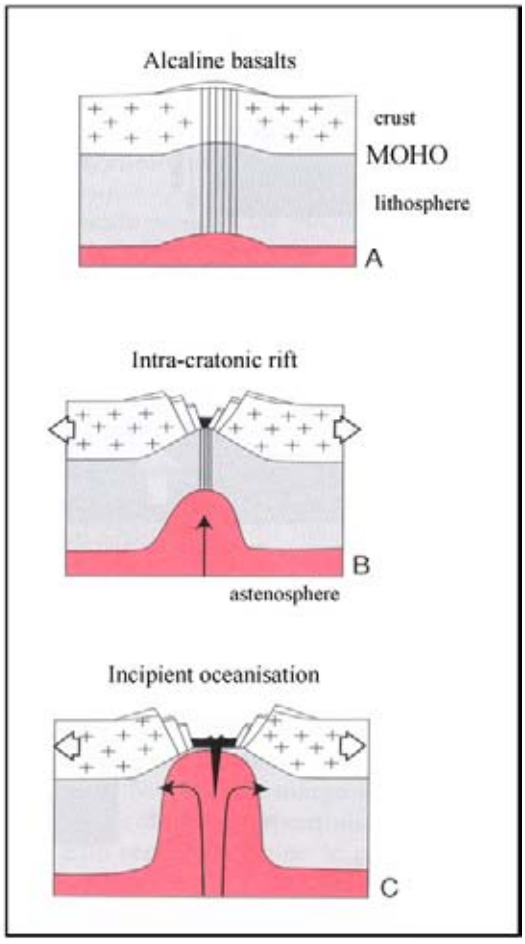

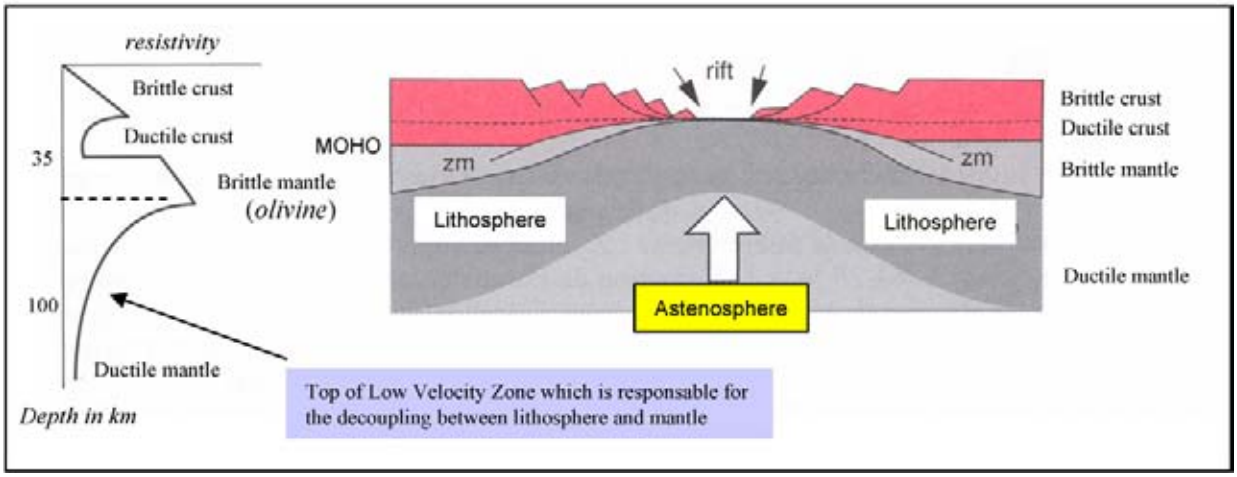

Figure 3.13: A paleo-Moho contact between the crustal gabbros ($V_p = 6.5$–7.2 km/s, $V_s = 3.7$–3.8 km/s, density 2.9 g/cm^3) and peridotites from the mantle (Harzburgite; $V_p = 7.8$–8.5 km/s, $V_s = 4.8$ km/s and density 3.3 g/cm^3). The contact zone is rather chaotic, but easily accessible along the Muscat-Dubai tarmac road in the Omani Mountains. Various PGK members serve here as a scale of reference. Model for rift formation and rheologic behaviour of the crust and mantle. The lithosphere is the crust and the upper part of the mantle (100–125 km thickness). The astenosphere is the part of the upper mantle that has a ductile behaviour (modified after Pomerol et al. 2005).

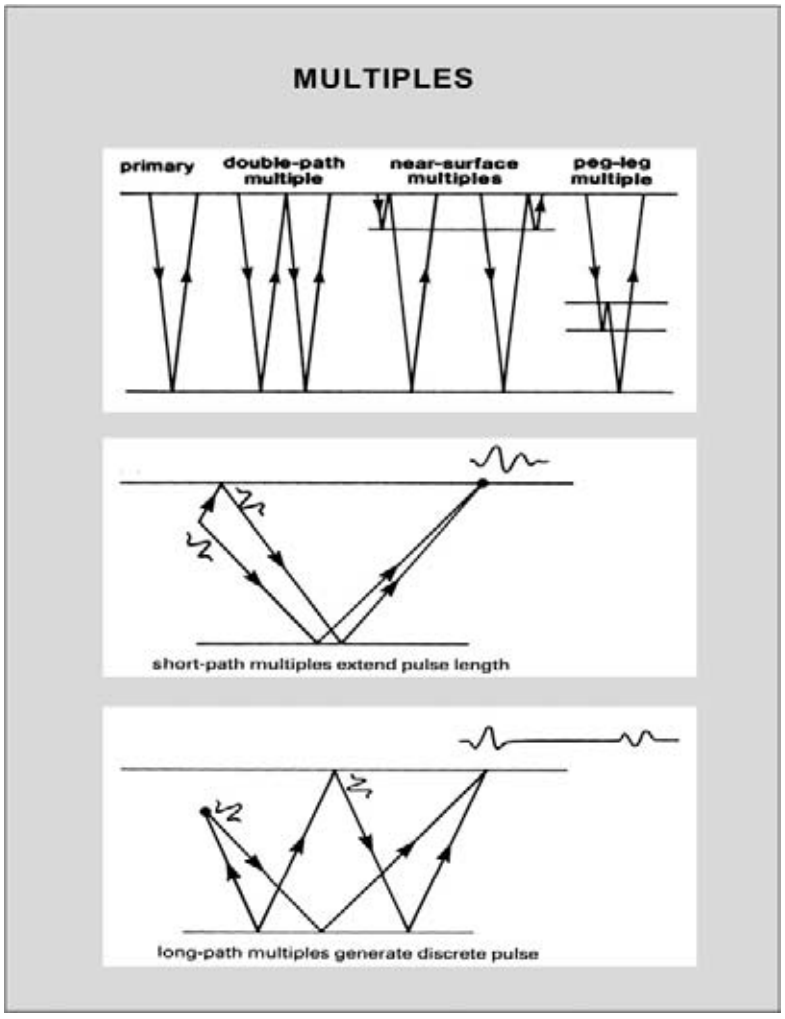

Figure 3.14: Multiple reflections corresponds to seismic energy reflected back and forth in a seismic layer before being intercepted by the receiver. Several types of multiples can be distinguished. The short path multiples are difficult to separated from the primary energy because their velocity is quite similar (after Kearey and Brook 1991).

3.2 Reflection Termination Mapping

The fill of sedimentary basins is normally subdivided into discrete depositional cycles. Likewise the seismic sections are subdivided into genetically related units or depositional sequences, based on the presence of unconformities.

Mitchum et al. (1977) define such a **Depositional Sequence** as:

> '*A stratigraphic unit composed of a relatively conformable succession of genetically related strata that is bounded at its top and bottom by unconformities or their correlative conformities.*'

The technique to delineate these bounding unconformities on seismic sections is called '**Reflection Termination Mapping**'.

In the application of this mapping technique it is important to make a distinction between fault-related terminations and depositional terminations. The fault-related terminations are recognised by the fact that the terminations are affecting series of overlying reflections with a consistent obliquely dipping line-up. This guideline is valid on dip sections. The fault intersections on strike lines are much more difficult to interpret. The depositional terminations show a more pronounced arrangement in a lateral sense. It is the easiest, when the fault pattern is first established and subsequently the seismic section is scanned in a systematic way for reflection terminations which are of depositional origin, starting from top to the bottom of the section. The outline of the

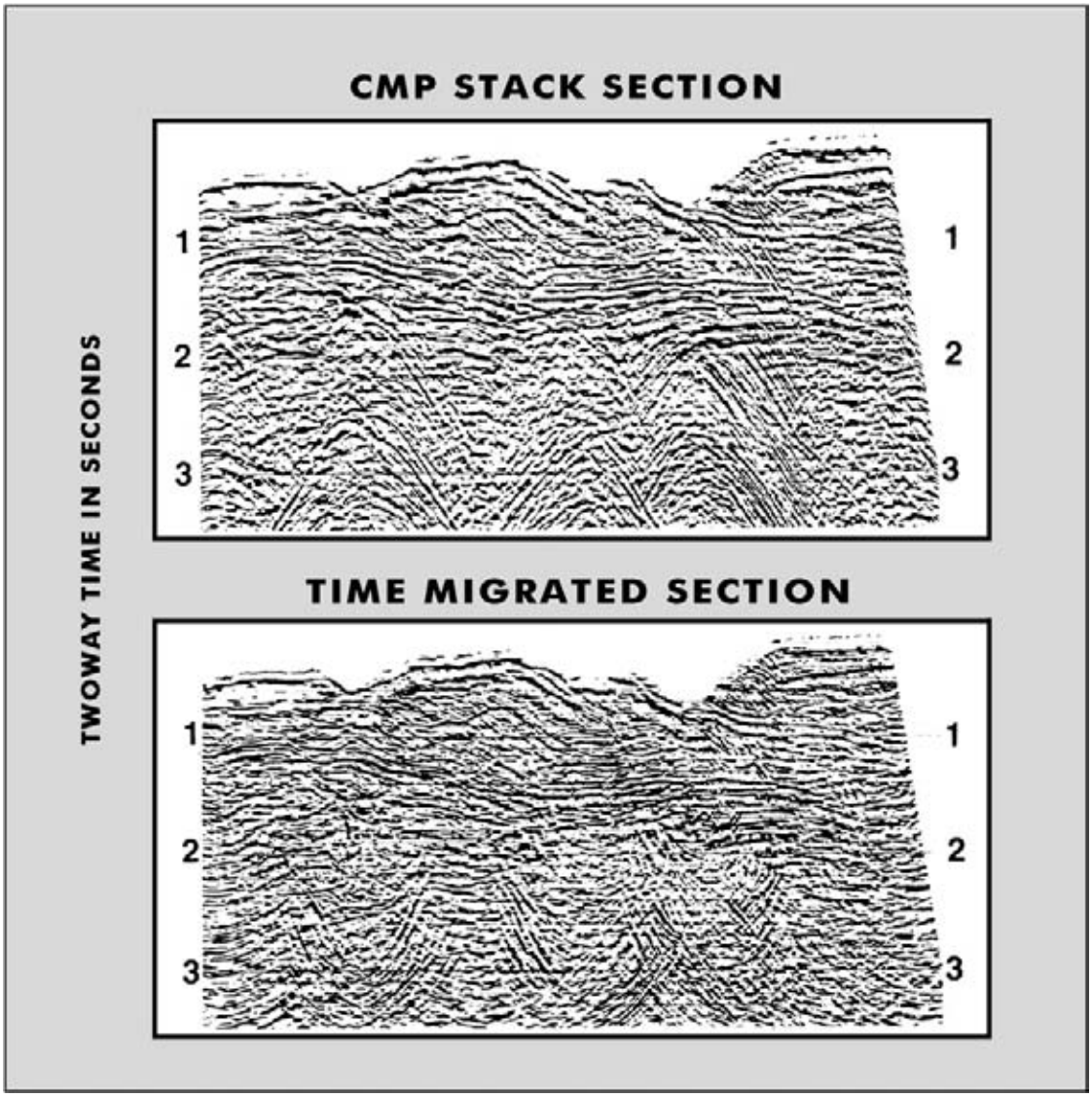

Figure 3.15: Comparison between a stack and migrated time section. Migration repositions the seismic data to a more reliable location in the subsurface and that is important when dealing with dipping reflectors. Over-migration and diffraction energy at deeper levels of a seismic section gives rise to migration smiles. These smiles are artefacts stemming from the migration operator. The migration moves the energy in an updip direction. It tends to shorten the synclines and broadens the anticlines (after Yilmaz 1987).

deformation in the overburden will facilitate to deduce the fault throws for the deeper layers. Consider first the deformation shown by the most obvious seismic markers as this will help in outlining the complexly faulted layers.

Once all relevant reflection terminations are properly indicated, then it is possible to outline the unconformities. These boundaries separate genetically related depositional units and thus subdivide the seismic section into various '**Depositional Sequences**'. The unconformities are reflective or non-reflective, depending on the acoustic impedance contrast. This observation implies that not all unconformities can be mapped by following one discrete seismic loop; their position is defined by the discordant reflection terminations. The polarity of the unconformity interface is likely to change in a lateral sense.

The following convention is adhered to: reflection terminations, stemming from bedding planes against an unconformity, are highlighted by red arrows. The unconformable surfaces, defined by these red termination arrows, are usually given a green colour. If clear multiple energy is present on the section, it is indicated by a blue tint.

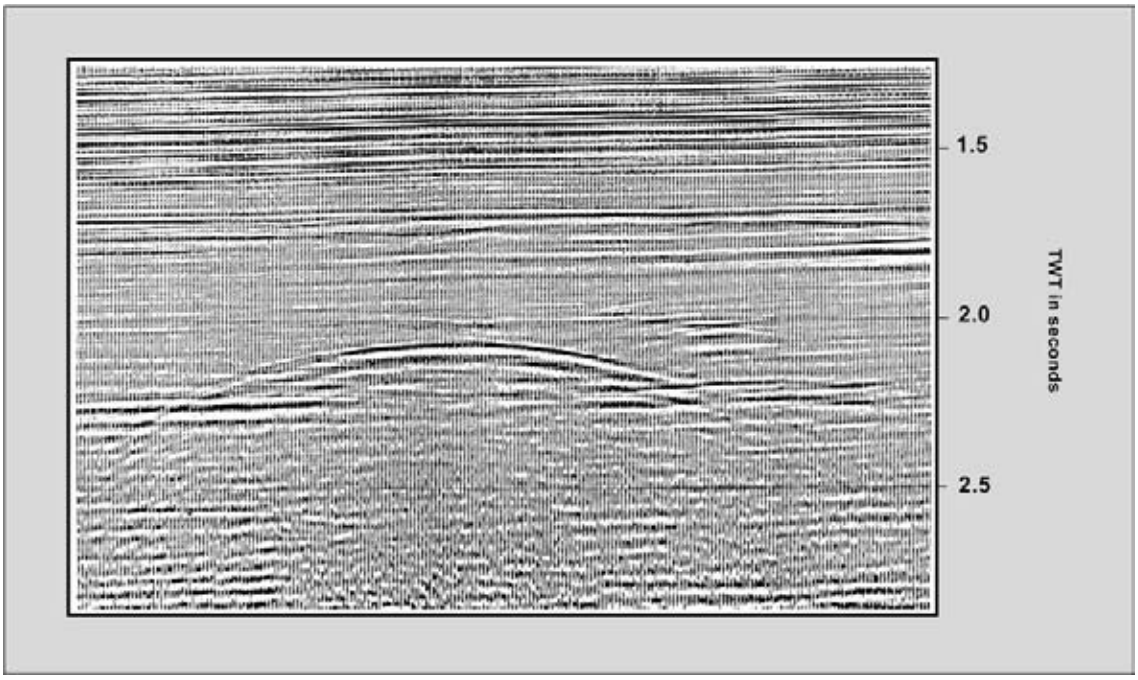

Figure 3.16: 'Sideswipe' on a structural strike section, indicating presence of a high block in the direct vicinity and more or less parallel to the seismic line. It represents laterally derived, out-of-the-plane seismic energy with a shorter ray path. The criteria to distinguish this kind of reflections from genuine data are: crossing events and anomalous dip. Some structural knowledge is certainly very helpful.

The identification of depositional sequence boundaries by reflection termination mapping is repeated on all the other intersecting lines of the seismic survey. This procedure permits to build a three dimensional picture of the units, that needs to be interpreted in a geological sense. This 3D approach will allow the interpreter to discriminate between local and regional events.

The depositional sequence is bounded by unconformities (and their lateral equivalents in the deeper domain where the sedimentary sequence is generally more continuous) and constitutes a time-stratigraphic unit. It is for this reason that they are important in basin analysis and for the reconstruction of the depositional history. Internally the strata are belonging to the same depositional episode. A variety of facies units can be present within a single depositional sequence and the reflections may encompass several lithofacies units. On the shelf various depositional environments exist laterally next to each other. For example alluvial fans, floodplains, levees and overbanks, channels, swamps, lakes and deltas are found bordering each other. These environments all have their own typical geological expression and seismic character as will be shown below. It are these kind of variations that need to be pinpointed on the seismic data if a good and detailed interpretation is required.

3.3 Seismic Facies Units

The next step in the seismic stratigraphic analysis is the delineation of individual seismic facies units. These units are three dimensionally traced and they consist of areas where specific reflection characteristics are detected (cf Sangree and Widmier 1977). These seismic facies units are based on:

- Reflection configuration.
- Continuity.
- Amplitude (horizontal excursion from time axis).
- Frequency contents (vertical separation between zero crossings on the same seismic trace).

Examples of different seismic units are given in Figure 3.17. Interval velocities are another discriminatory element. Geomorphological characteristics are features that may be quite useful in the interpretation of seismic facies units (cf Zeng 2004). These characteristics are traced in a 3D sense along a depositional surface (horizon slices).

Seismic facies units can cross depositional sequence boundaries. The aim of seismic stratigraphic studies is to interpret the elements of the seismic facies units in terms of environment of deposition and lithofacies distribution. The following features are therefore important to consider:

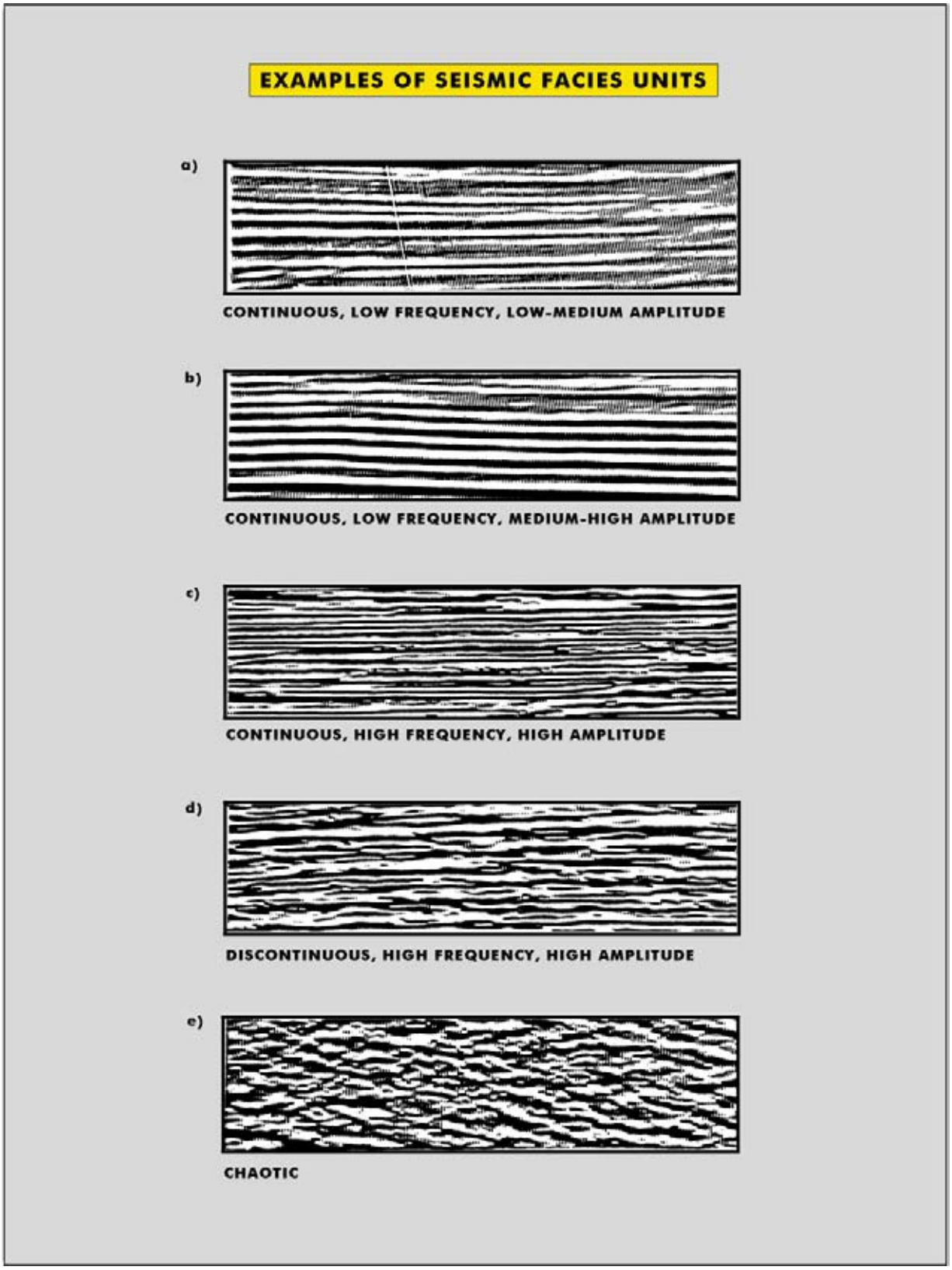

Figure 3.17: The expression of some seismic facies units based on amplitude, frequency, continuity and reflection geometry.

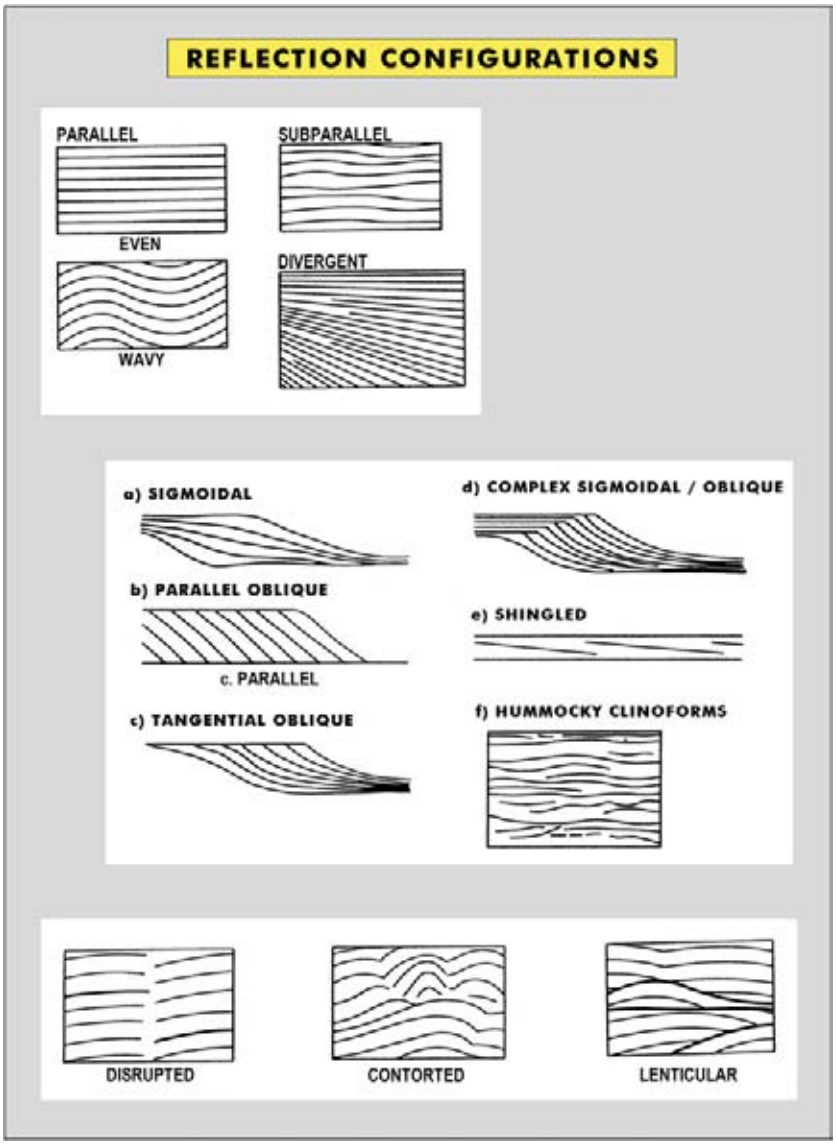

Figure 3.18: Various reflection configurations and their interpretation (Mitchum et al. 1977, reprint from AAPG whose permission is required for further use).

- Internal reflection organisation.
- Boundary relationships.
- External geometry.
- Lateral facies relationships.

Let's now have a closer look at these reflection characteristics.

3.3.1 Internal reflection configuration

Several principal reflection configurations are recognised. Each of them are interpreted in terms of depositional environment and lithofacies distribution (Figures 3.18 and 3.19; Mitchum et al. 1977). The following geometries are distinguished:

- Parallel or sub-parallel.
- Wavy.
- Divergent.
- Clinoforms or foresetted.
- Shingled (low-angle foresetted with low foreset height).
- Hummocky (some degree of internal organisation).
- Chaotic.
- Reflection free or transparent.

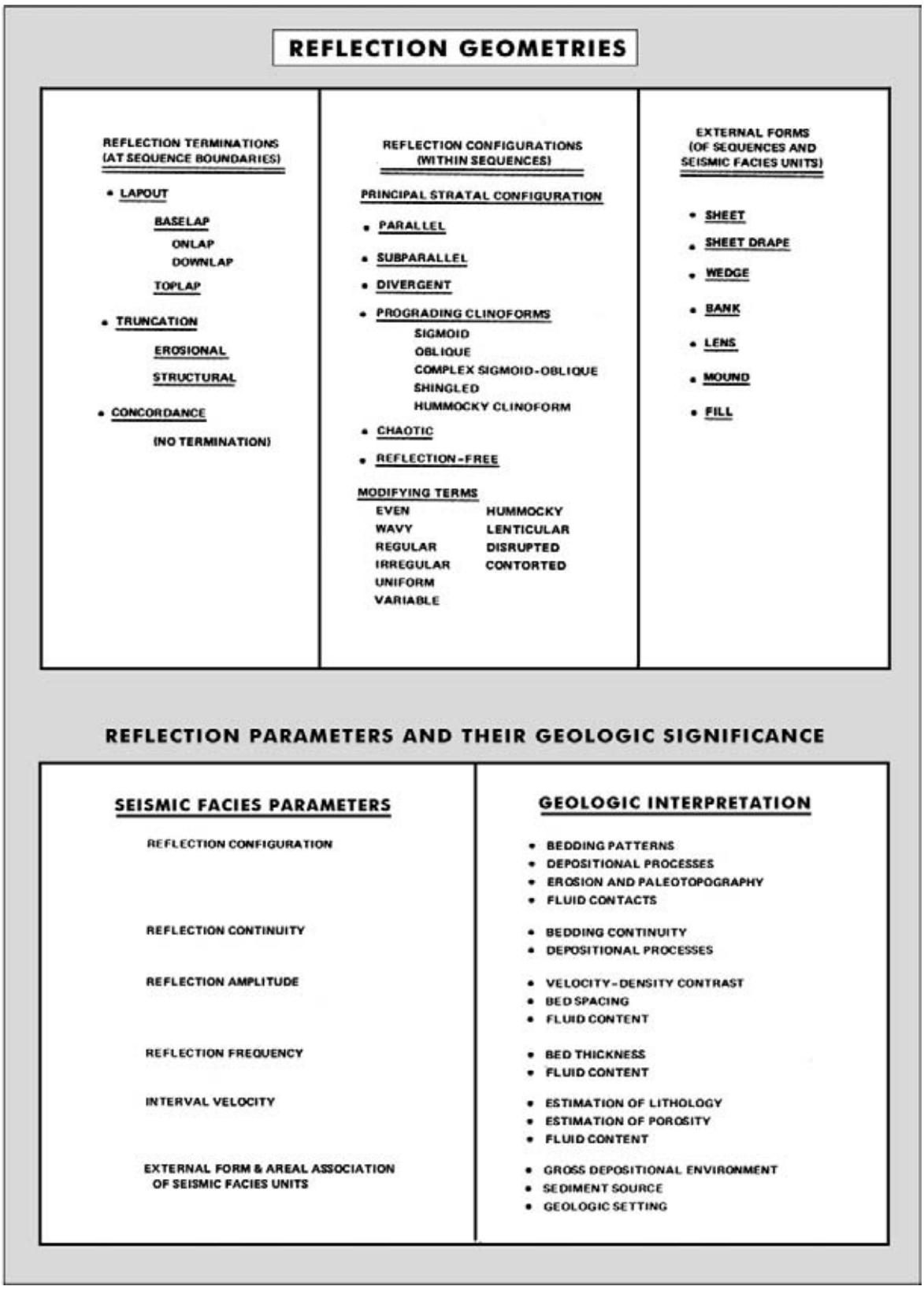

Figure 3.19: Reflection geometries and their interpretation. The greater continuity of the reflections is usually found in the distal offshore domain where quiet water conditions prevail. The sedimentation is here mainly dominated by fall-out from suspension (Mitchum et al. 1977, reprint from AAPG whose permission is required for further use).

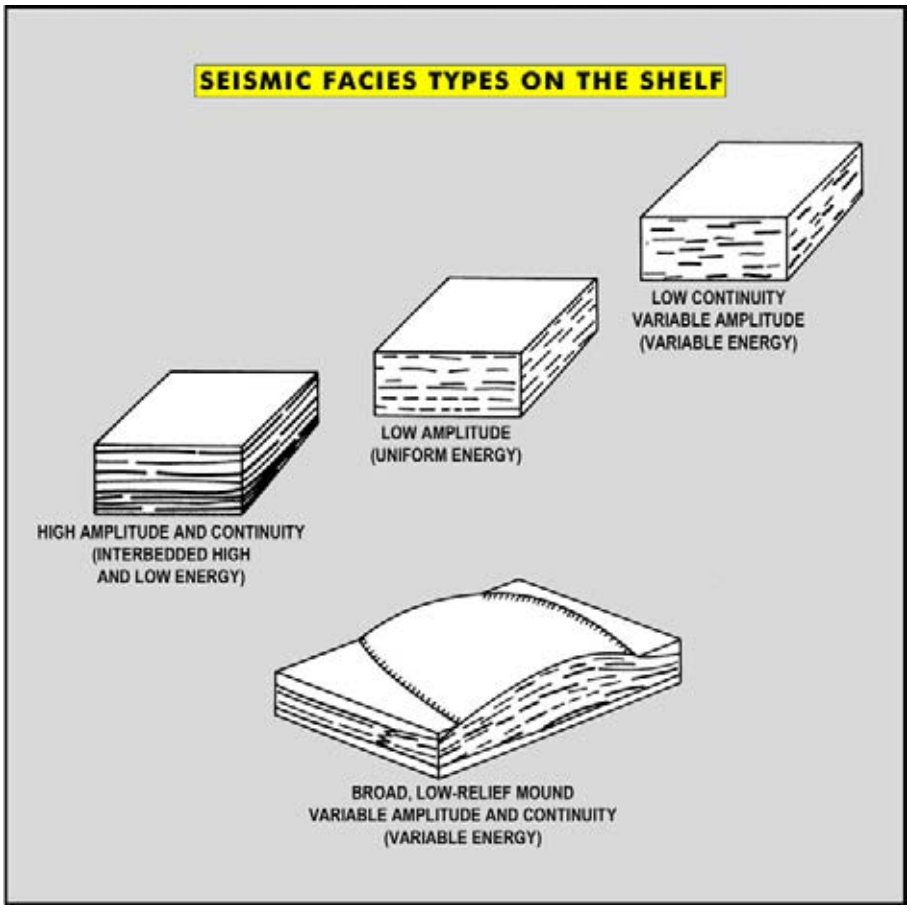

Figure 3.20: Seismic facies units on the shelf, which corresponds to a topset position on the seismic data. Continuity is related to energy level of environment of deposition, while amplitude reflects interbedding of lithologies (modified after Sangree and Widmier 1977, reprint from AAPG whose permission is required for further use).

The foresetted reflections give some idea about the paleo-waterdepth in which they were deposited. Differential compaction and other burial effects overprint the original depositional geometries. This should be taken into account when drawing any conclusions on the TWT observations.

3.3.1.1 Parallel to wavy reflection configuration

The parallel to wavy reflection character indicates uniform sedimentation conditions for an infill or a sequence on top of a subsiding substratum. Subdivisions within this configuration are made based on continuity, amplitude and frequency of the reflections.

The parallel geometry occurs in both shallow and deep-water, reflecting a topset or a bottomset situation. These latter terms are purely descriptive for the geometry and they do not tell anything about the scale of observation. It is used for describing ripple marks, crossbedding, prograding bars and dunes, separate delta complexes and prograding shelf/slope systems. It covers either a clastic or carbonate depositional environment. In seismic stratigraphy the term topset is often used for deposits laid down in a coastal plain or a shallow marine shelf (basin margin, Figure 3.20), while bottomset is equivalent for a deeper water environment beyond the shelf break (basinfloor).

A high amplitude (horizontal excursion of seismic wiggle from the time axis) reflection character generally points to vertical alternation of contrasting lithologies (e.g. sand/shale; carbonate layers in a shaley sequence). A low amplitude indicates more similar lithologies on both sides of the interface (e.g. sand/silty shale).

The frequency of a reflection (vertical separation on a seismic trace of a seismic loop between two consecutive zero crossings) can give some idea concerning the thickness of the beds. There are pitfalls when dealing with thin bed interference effects (Widess 1973, Niedell and Poggiagliolmi 1977).

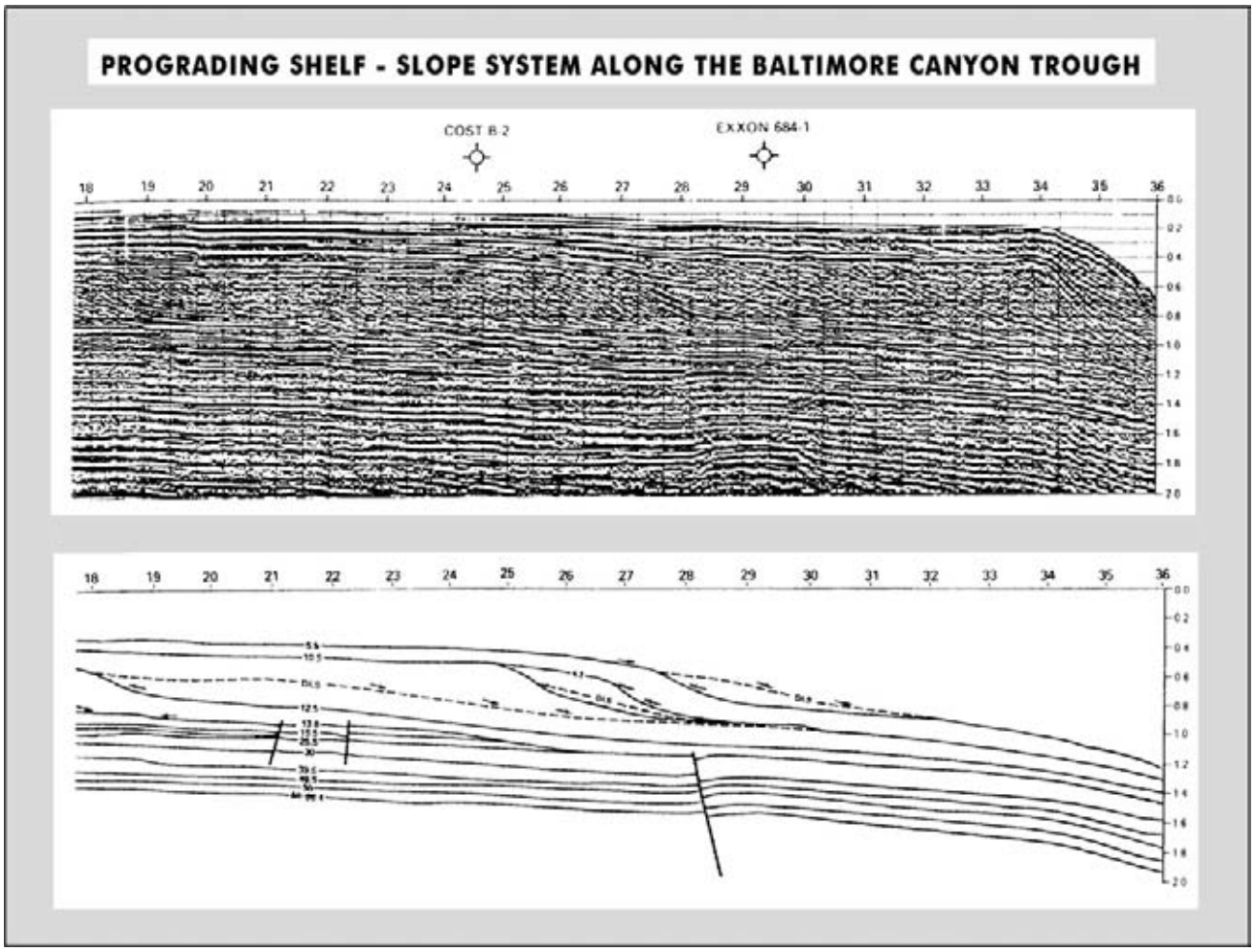

Figure 3.21: Top-, fore- and bottom set relationships. Generally seismic reflections do cross several depositional environments. In the subsurface the coarser shelf sediments are gradually replaced by more shale-prone slope sediments without generating a distinct seismic response. Constraints in the horizontal resolution don't always favour the detection of individual lateral sand pinch outs (Berg and Woolverton 1985).

The continuity gives information on the energy level of the deposits. A high continuity suggests a great lateral extent of the same sedimentation conditions, while discontinuous reflections indicate rapid changes in energy level (e.g. braided and meandering stream deposits on a floodplain).

3.3.1.2 Divergent reflection configuration

Divergent reflection geometries are found in wedge-shaped sediment bodies, where the sediment thickness distribution is asymmetric. Obviously important lateral thickness variations do exist. These geometries can be due to variations in sedimentation rates, subsidence and/or burial effects (differential compaction). The internal reflection terminations occur randomly and do not coincide with a distinct unconformable surface. The divergent geometry indicates syn-depositional differential tectonic movements.

3.3.1.3 Clinoforms or foresets

Clinoforms or foresetted reflection configurations originate from prograding slope systems in standing bodies of water. The shape and angle of repose of sediment on these slope systems is influenced by:

- Composition of the deposited material.
- Sedimentation rate and quantity of sediment input.
- Salinity of the water.
- Water depth.
- Energy level of the environment of deposition.
- Position of the sealevel, which is closely related to the baselevel profile.

– Subsidence rate.

The **baselevel profile** is an ideal profile line, that runs from a mountain range down slope to the sea. It determines the areas of erosion, that are located above the profile line, and areas with active sedimentation that are below the profile line. The overall position of the baselevel is dynamically controlled by the sealevel.

Under ideal conditions the clinoforms display a topset, foreset, bottomset relationship (Figure 3.21). In such cases the geometry allows for a rough estimate of the waterdepth of the basin in which the foresets prograded. The difference in milliseconds between the top set and bottomset level can be measured. If the appropriate interval velocities for the sediments are known, it can be converted into depth. Decompaction effects should be incorporated in the calculation to obtain a more reliable waterdepth. From the shear size of the foresets, observed on seismic sections, it is evident that they very often represent shelfedge progradation along basin margins.

Topsets are better developed under conditions of rising relative sealevel. Such conditions allow the shelf sediments to be stacked on top of each other and these are thus preserved in the geological record. The concept of a **relative sealevel** has been introduced because it is difficult to make a distinction between contributions of various factors like:

– Change in tectonically induced subsidence rate.
– Decrease in sedimentation rate.
– Amount of sediment supply.
– Eustatic sealevel rise.

Stable relative sealevel conditions lead to very thin topset deposits. If the sealevel is suddenly dropped, the inner shelf will be exposed to erosion and the formerly accumulated sediments will be removed, giving rise to important erosional truncation. If the erosion cuts deeper, it affects also the top part of the foresets and this results in a toplap geometry.

The foresets have quite different shapes (Figure 3.22; Sangree and Widmier 1977):

– **Oblique**, whereby the topsets are not preserved. This area is mainly an area of sediment bypass. This type of foresetting represents a somewhat high-energy slope system and coarser deposits may be incorporated in these foresets. The little developed bottomsets do suggest that the fall-out of debris was rather drastic and limited in areal extension. Starved sediment conditions reign on the distal part of the basinfloor. Occasionally it may also point to the presence of contour currents (density/temperature driven) that rework the material at bottom of the slope and transport them further away. The toplap geometry indicates a rapid fall of relative sealevel at the onset of the next depositional sequence. The sedimentation mechanism is most probably traction (bedload transport) and suspension related (gradual fall-out or hemi-pelagic).
– **Parallel oblique**, which points to little change in direction of the prograding slope. It also means a rather uniform filling-in of the basin, as a lot of switching of depocenters would result in different progradation directions. This geometry normally also reflects a high-energy slope system (Figure 3.23).
– **Tangential oblique**, whereby the bottomsets are well developed. This type of foresets points to a very efficient transport mechanism for the sediments over the shelf area and the spreading out of material over vast basinal areas. Most likely the sediments are deposited from suspension, but also turbidity currents

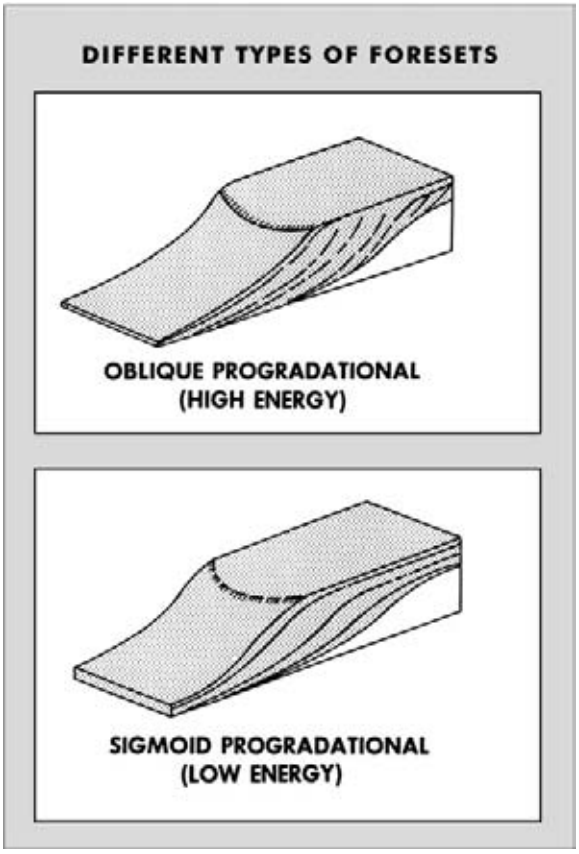

Figure 3.22: Different types of foresets are shown. Above the high-energy oblique tangential geometry is illustrated, whilst below the low-energy sigmoidal draping pattern is depicted, characterised by more uniform sedimentation conditions (modified after Sangree and Widmier 1977, reprint from AAPG whose permission is required for further use).

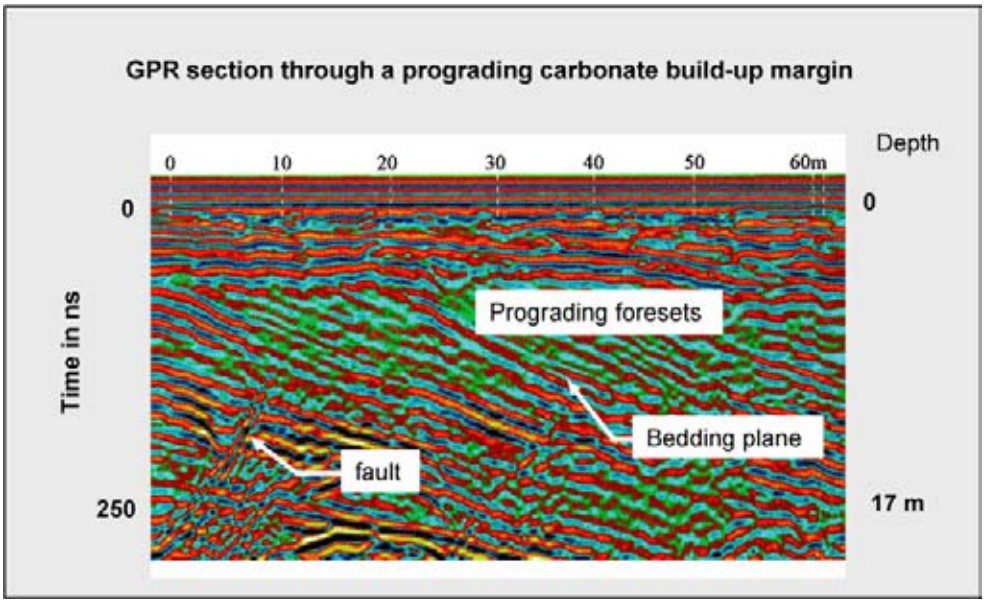

Figure 3.23: Oblique foresetting in carbonates on the eastern margin of the Paris Basin, exposed in the Euville quarry. The height of the foresetting is rather small (approximately 10 metres). The section is a Ground Penetrating Radar traverse (GPR) and its depth scale is given at the right hand side. The bioclastic sediments are laid down in a high energy tidal bar complex.

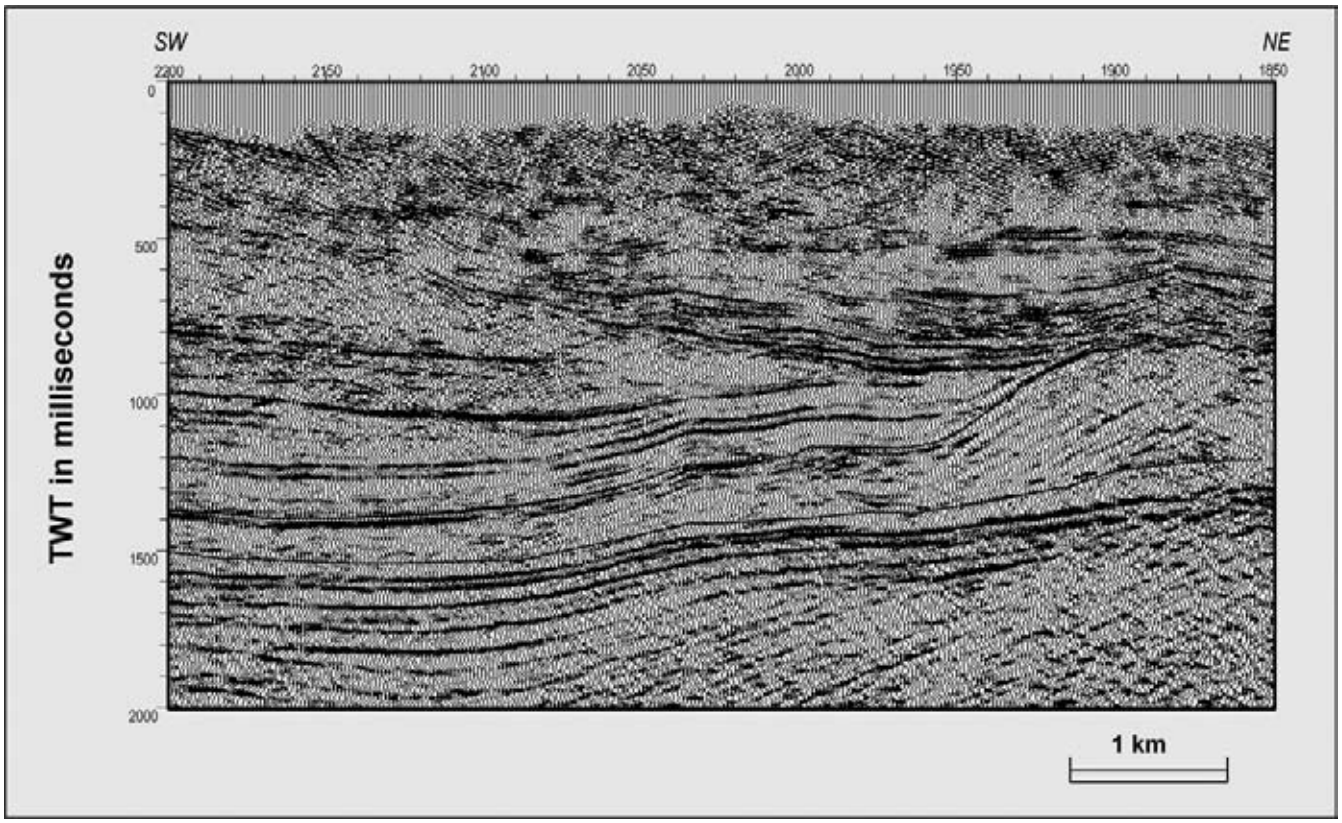

Figure 3.24: Progradational reflection geometry in Cretaceous carbonates from the Gulf of Mexico at 1.0 and 1.5 seconds TWT. The progradation is oriented from right to the left and it represents the outbuilding of a basin margin (>2 km paleo waterdepth). Note the drastic scale difference with the previous GPR figure. A major unconformity is present in the Tertiary overburden, an expression of the occurrence of major mountain building movements in the hinterland (courtesy Pemex).

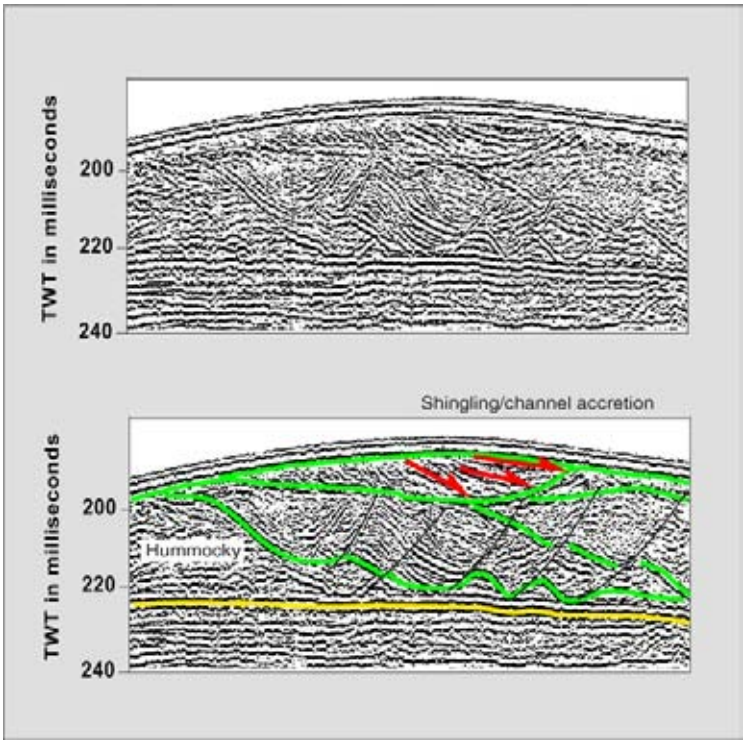

Figure 3.25: Hummocky seismic facies characterised by short, curved and discontinuous reflections. Often it can be interpreted as the result of a cut-and-fill sedimentation pattern (data courtesy Ifremer).

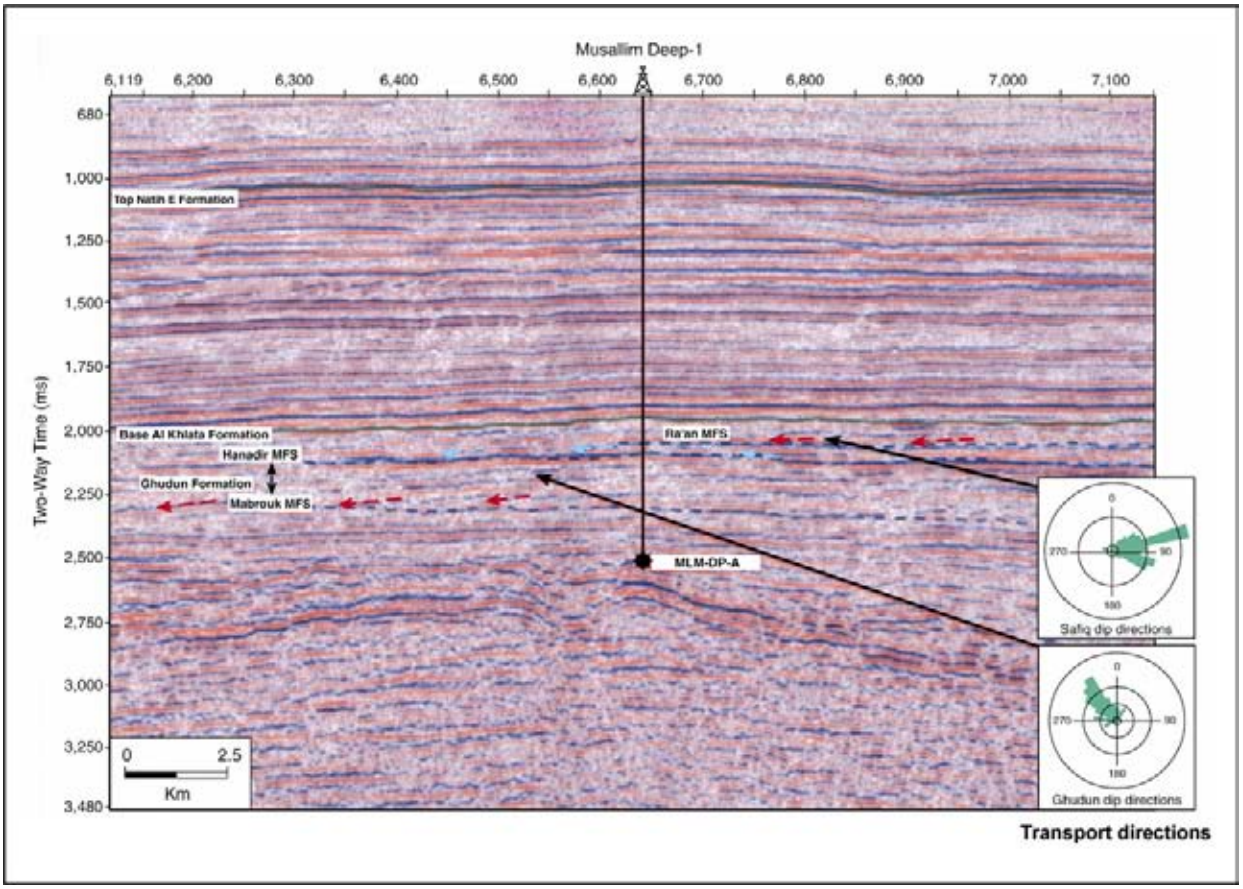

Figure 3.26: Subtle low-angle progradation or shingling, that can be difficult to outline. Transport directions are quite different in the Ordovician Ghudun and Safiq formations. Sometimes sections are flattened on a specific horizon. It may help to compensate for the effects of the later tectonic deformation and facilitates the interpretation of paleo geomorphologic features (Oterdoom et al. 1999).

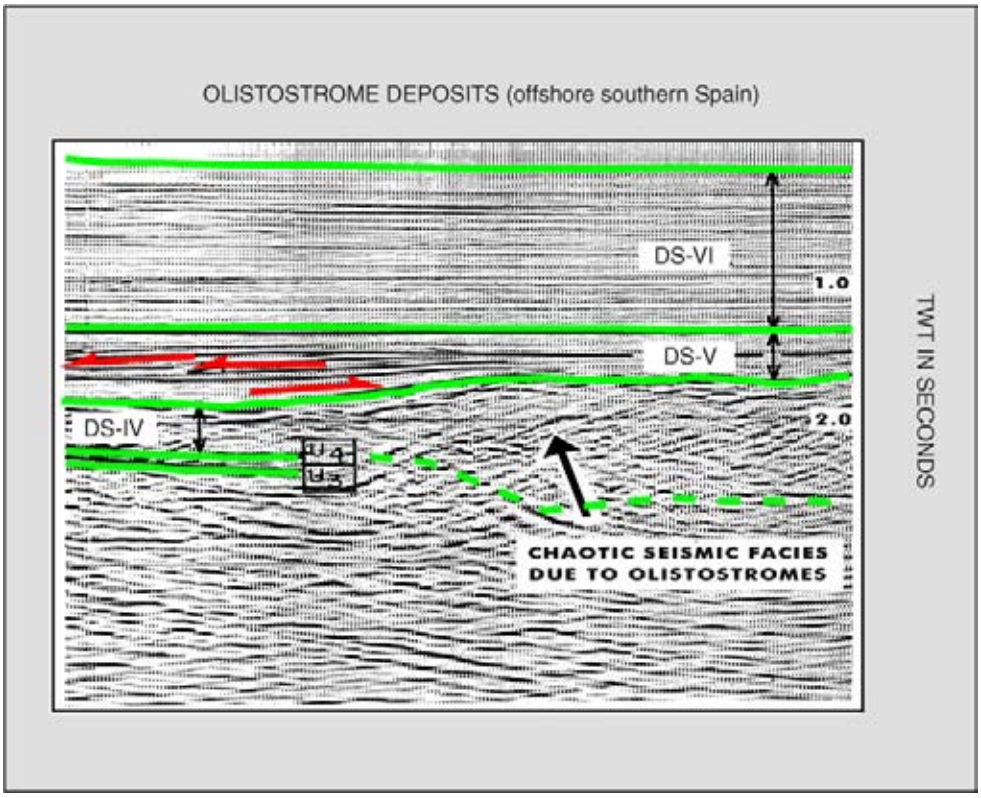

Figure 3.27: Chaotic seismic facies unit, interpreted as olistostrome deposits in the Guadalquivir Basin (Gulf of Cadiz), which is foreland basin created in response to progressive nappe emplacement in the Betic Cordilleras located to the south. Low-angle foresetted turbidites of Depositional Sequence V are downlapping on the chaotic mega-slumps. These sand-prone turbidites are gas bearing.

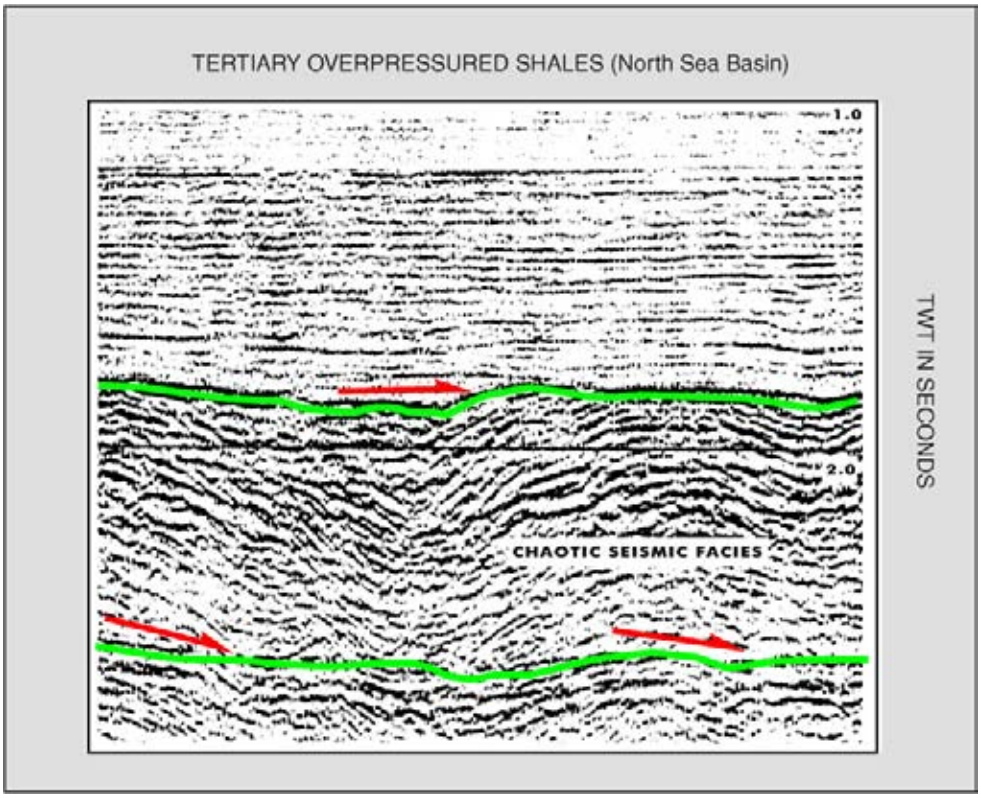

Figure 3.28: Chaotic discontinuous seismic facies unit due to presence of deformed overpressured shales resulting from improper dewatering during rapid burial of the sediments.

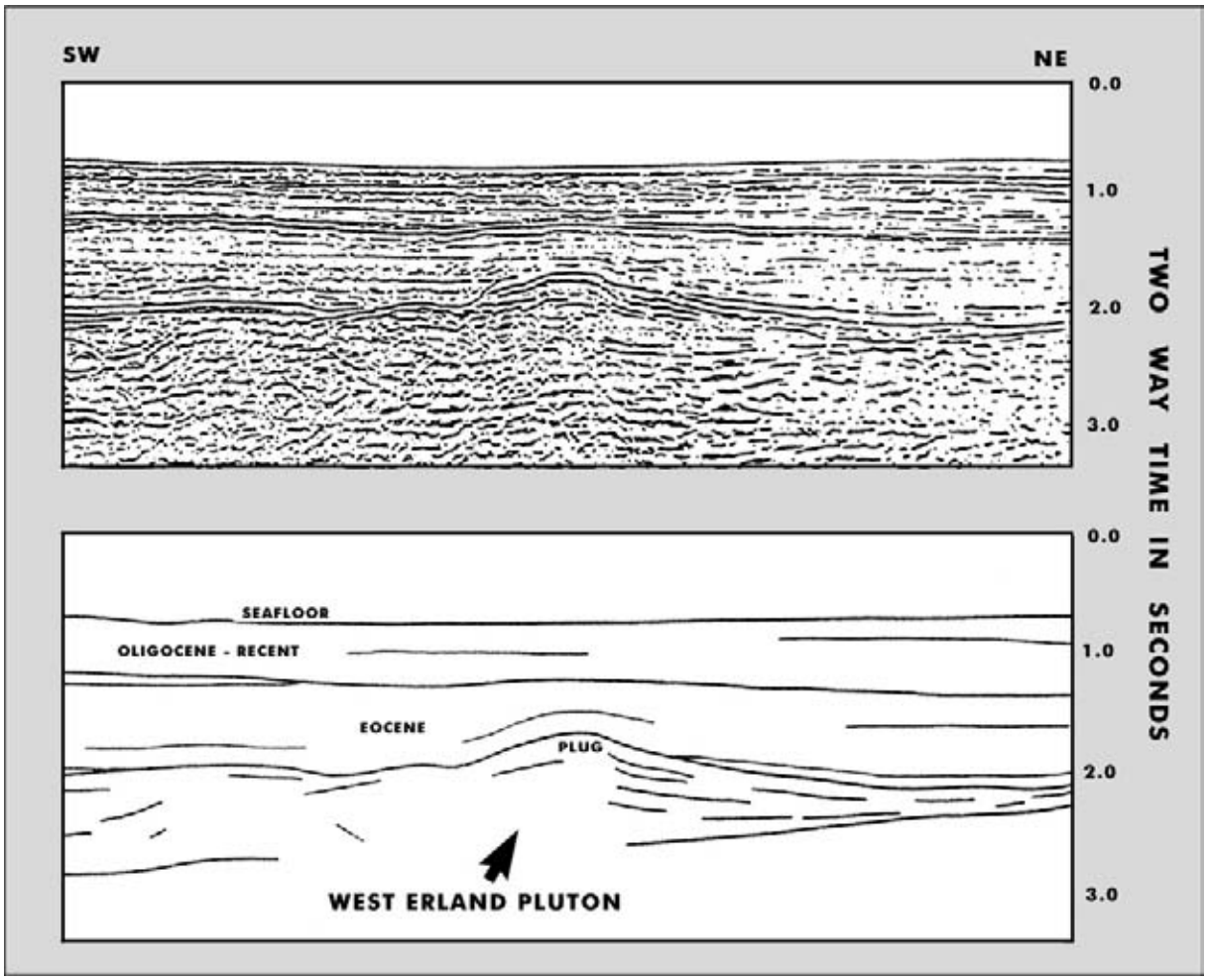

Figure 3.29: Chaotic facies displayed by volcanic rocks from the Erland dome area (Gatliff et al. 1984). Note the typical mounded shape and high-amplitude top boundary. Gravimetrics and magnetics support the volcanic origin. The Erland dome is a volcanic centre, active on the Paleocene–Eocene time boundary. Contemporaneous volcanic activity and rifting has been reported from Eastern Greenland (Jolley and Whitham 2004). From here volcanic ashes were wind-blown and deposited over large parts of the North Sea basin. These ashes form an important regional seismic event, known as the Thulean Tuff marker. Reworking by other agents (turbidites) is often observed in the Central North Sea area (Veeken 1983).

can bring material directly to deeper parts of the basin (Figure 3.24).

– **Sigmoidal**, whereby the topset and bottom sets are preserved. Its geometry does suggest a relative rise in sealevel, with a reasonable sediment supply. This geometry also might point to deposition from suspension (partial sediment drape). It represents therefore a lower-energy slope system.
– **Shingled**, which is characterised by a much smaller foreset height (Figure 3.25). This type of low-angle foresetting is found in both a topset as well as in a bottomset position. It is interpreted either as shallow marine progradation in a high energy environment or as deep marine progradation on the basin-floor (Figure 3.26). In the deeper marine basin this shingling may point to the importance of massflow sedimentation. It may indicate accretion in submarine fans or contour current mounds (contourites). No straightforward waterdepth connotation is assigned to this kind of low-angle foresets. The depositional mechanism is traction, massflow and suspension.

3.3.1.4 Hummocky reflection configuration

This hummocky reflection configuration consists of irregular, discontinuous reflections with variable amplitudes. It is characterised by little systematic reflection terminations. It can occur both in top- and foreset positions. It indicates the presence of cut-and-fill geometries and/or contorted bedding. The contorted bedding is the result from water escape during early burial and

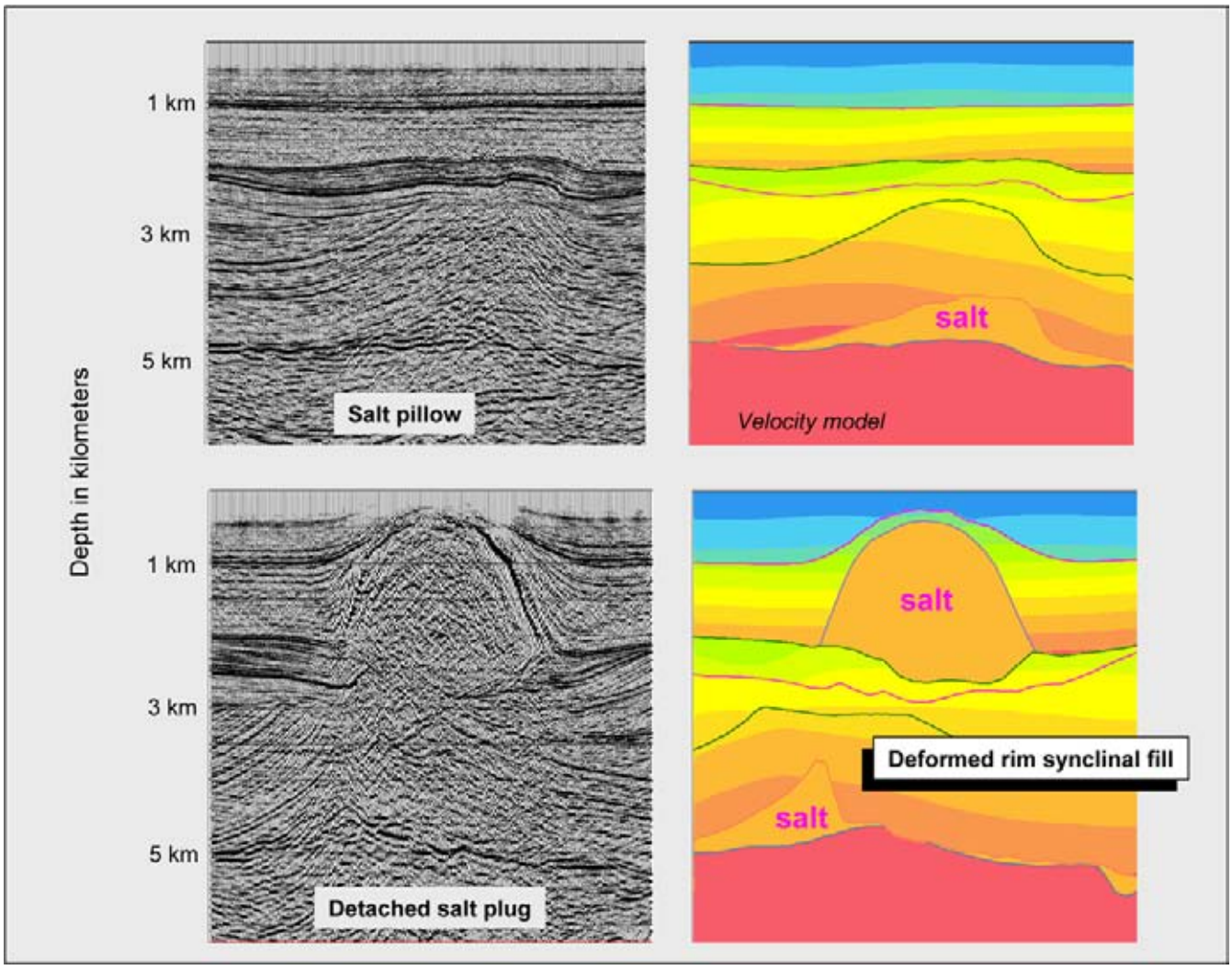

Figure 3.30: Halokinesis of Permian Zechstein Salt. (a) Grounded salt pillow with internally a chaotic seismic facies. Note that the overburden tectonics is detached from the deeper structures and the salt layer acts as a decollement unit. (b) Zechstein salt diapir that shows an internal chaotic seismic facies and associated with severe deformation of the overlying beds. The overburden shows some degree of extensional faulting over the crest and flank of the structure (courtesy of BEB and CGG).

compaction. It is characterised by oversteeping of the sedimentary laminations. Other water escape features are dish and pillar structures (e.g. Hirono 2005). Most of the time the cut-and-fill is interpreted as channelised deposits (Figure 3.25).

3.3.1.5 Chaotic reflection configuration

Chaotic reflection configurations are composed of discontinuous discordant reflections of variable amplitude and frequency. The discontinuous character suggest a highly disordered internal organisation of the deposits. It occurs in all kind of depositional environments and may represent:

- Channel fills in a proximal fan.
- Slumped deposits on a slope.
- Olistostromes (Figure 3.27).
- Overpressured shales (Figure 3.28).
- Volcanic rocks (Figure 3.29; Gatliff et al. 1984).
- Mobile salt deposits (Figure 3.30).

Basalts can be layered, e.g. flows alternating with tuff or breccia layers in the northern Rockall Trough, or display a chaotic organisation. The high impedance contrast and the rugosity of the basalt surface together with the internal flow structure may lead to severe scattering of the seismic energy and generation of interbed multiples (Maresh and White 2005).

The typical dome geometry usually indicates the presence of salt in the system. But also overpressured shales

are deforming plastically and this may result in diapiric bodies on the seismics (e.g. Mexico and Brunei). Gas in the porefill leads to anomalous low stacking velocities in local zones, giving rise to gas chimneys on seismics. These chimneys are also characterised by discontinuous chaotic reflections in a semi-vertical column.

3.3.1.6 Reflection free zones

The reflection free areas coincide with zones where acoustic impedance contrasts are weak or lacking. This implies a rather homogene gross lithology; it can be thick shales, limestones, sands, etc. Massive reefal build ups (Figure 3.31) and even igneous bodies (Figure 3.32) sometimes appear reflection free. Intensely tectonised deposits like salt diapirs and volcanic intrusives may also show a reflection free facies.

Sometimes the AVC parameters are causing artificial reflection free zones. This is the case when the signal at the top of a unit is so strong, that it dominates in the amplitude normalisation process and all other reflections are hence not boosted to maintain the average target value. This is one of the reasons why it is always advisable to ensure that also 'preserved amplitude' sections are put at the disposal of the interpreter.

3.3.2 External geometry of seismic facies units

After delineating the seismic facies on the seismic sections, the shape of these units in a three dimensional sense is mapped. The morphological external shape of the units are described in terms of (Figure 3.33; Mitchum et al. 1977):

- **Sheets or sheet drapes**, which point to uniform sedimentation conditions in the basin and vary little differentiation of environment of deposition. The associated seismic facies is sub-parallel to wavy and undulating. Generally these drapes are composed of fine-grained deposits with sedimentation out of suspension.
- **Wedges**, which indicate a sudden break in the sedimentation pattern. Internally it represents a gradual differentiation in environment of deposition and a lateral change in sedimentation rate.
- **Banks or monoclines**, which point to substantial differentiation in the sedimentation pattern. They have an elongated shape. Locally higher energy conditions exist. Often foresetted internal geometries are detected.
- **Mounds**, which represent 3D depositional build-ups. They indicate higher energy environments in the basin. Mounds are interpreted as:
  - Carbonate build-ups together with their talus deposits.
  - Submarine fan complexes.
  - Contourite deposits resulting from thermohaline density currents.
  - Volcanic eruption cones.

  Mounds show a wide range of internal reflection configurations (Figure 3.34).
- **Slope front fills**, located in front of foresetted units and showing clear onlap relationships. These kind of units are either fan or lens shaped. The internal reflection character varies a lot and is also depending on the lithological content of the unit. They can show both onlap onto the lower boundary as well as basinward downlap for the more distal part. The beds may be depositionally inclined. The onlap does indicate a change in sediment supply compared to the underlying sequence and coincides with a break in the deposition. Generally these slope front fills are more coarser grained than the real slope deposits. They are the locus of deep marine sand deposition.
- **Erosive fills**, which do suggest a drastic lateral change in energy level. These fills represent canyon systems, river valleys and distributary channels in fan systems (Figures 3.35 and 3.36). The channels (or stringers) can be straight, meandering (sinuous) or anastomising (braided).
- **Non-erosive fills**, indicative of a basinfloor topography with areas of starved sedimentation. These areas with low initial sedimentation rates are sequentially flattened out by the further infill.

Regularly the interpreters employ the term mound for any convex upward, lenticular body seen on a seismic line without verifying the 3D pinch-out in all directions. The overall shape of seismic facies units is important for the correct interpretation of the lithofacies contents.

3.4 Geological Calibration and Well Control

It is advisable to calibrate the seismic observations with all available geological information in an early phase of the study. Sometimes reflectors are outcropping in the field and hence a direct tie with some seismic reflections is available (e.g. Veeken and Titov 1996a). The surface

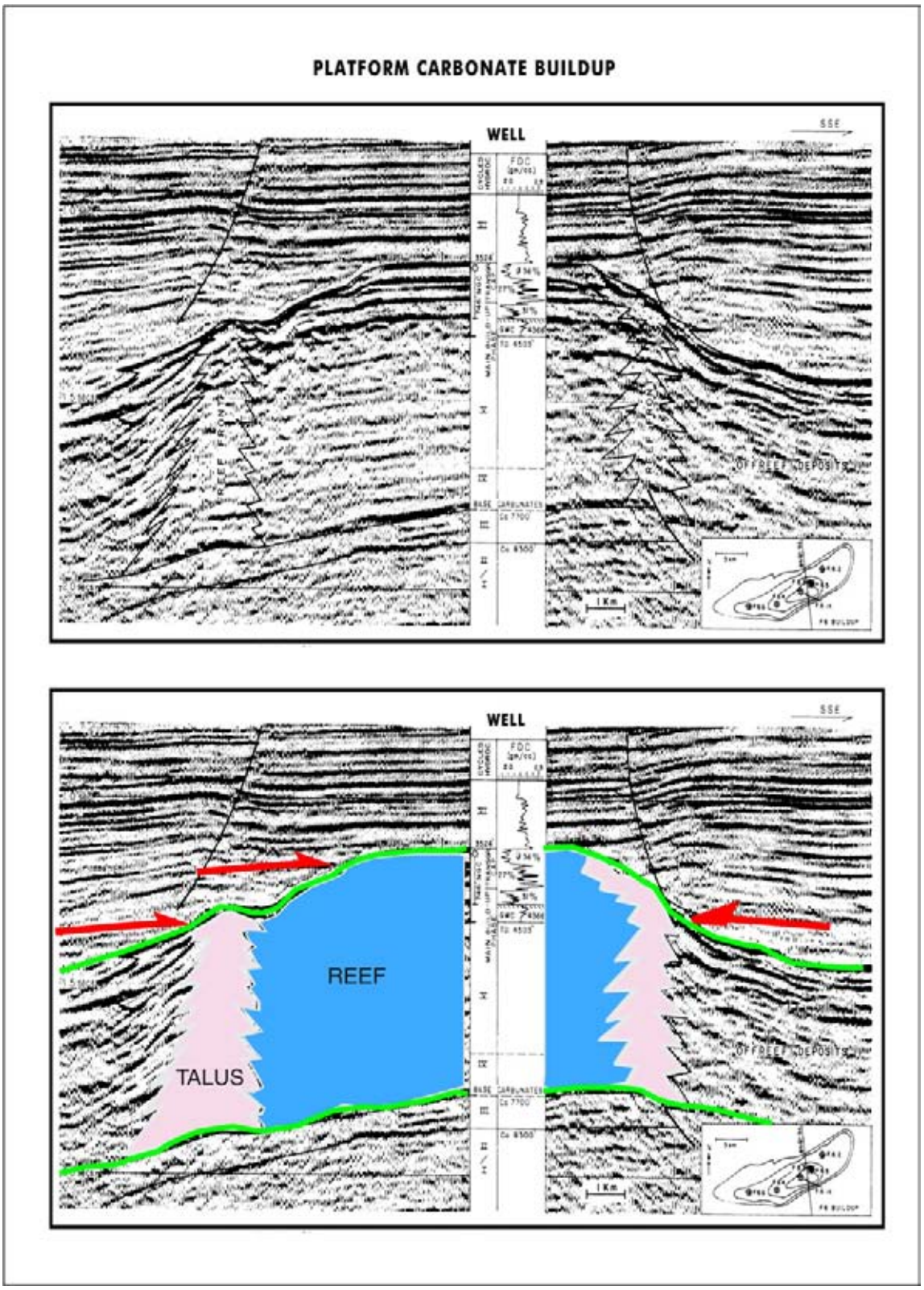

Figure 3.31: Carbonate build-up with several seismic facies units. The high-energy reef front is characterised by lower amplitude chaotic reflections. Note that the gas containing reservoir section is represented by a high amplitude seismic facies unit (bright spot; after Wagner 1982).

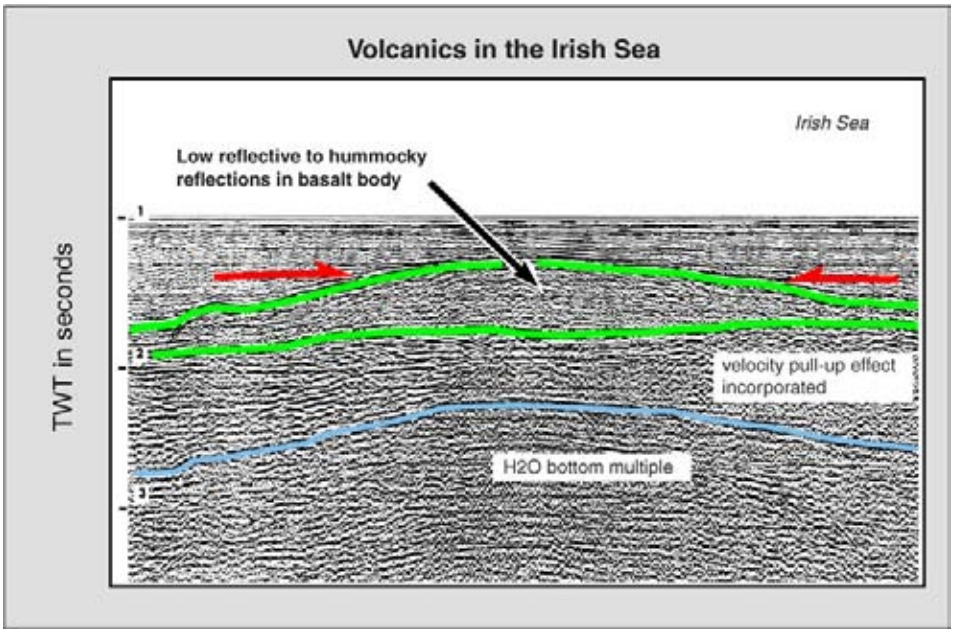

Figure 3.32: Low reflective to hummocky seismic facies unit originating from a lenticular igneous body. Its presence is confirmed by the measured gravity data. The deeper seated time structure are partly caused by a pull-up effect, due to the velocity contrast between the basalt and the Tertiary sediments (6000 m/s versus 2800 m/s). This effect will disappear when a proper time-depth conversion is done.

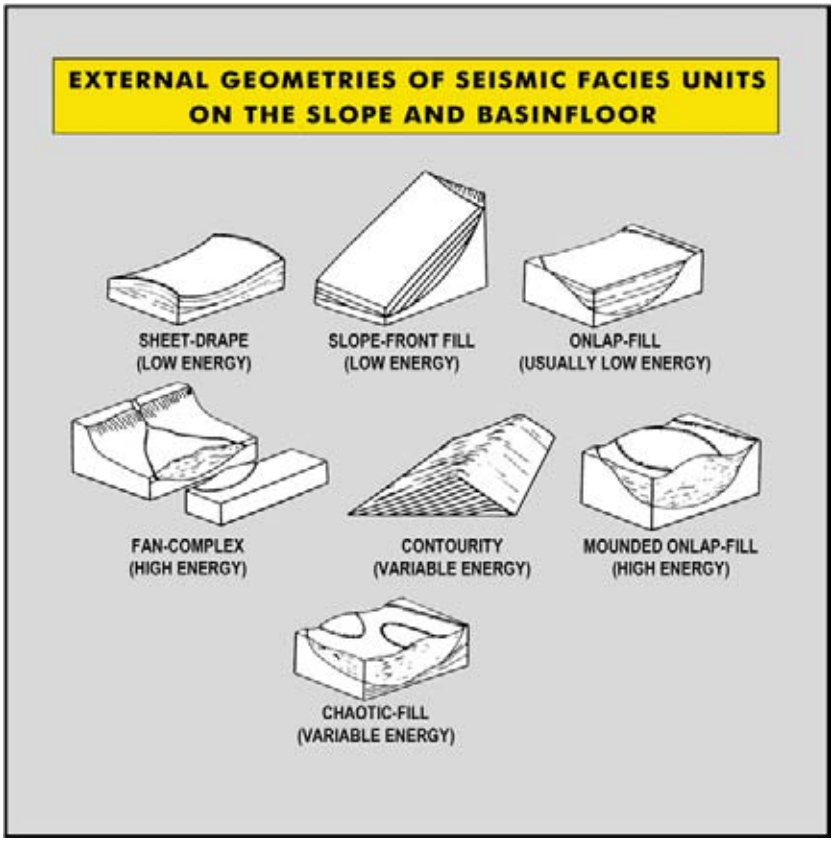

Figure 3.33: Various external geometries of seismic facies units in slope and basinal areas (after Sangree and Widmier 1977, reprint from AAPG whose permission is required for further use).

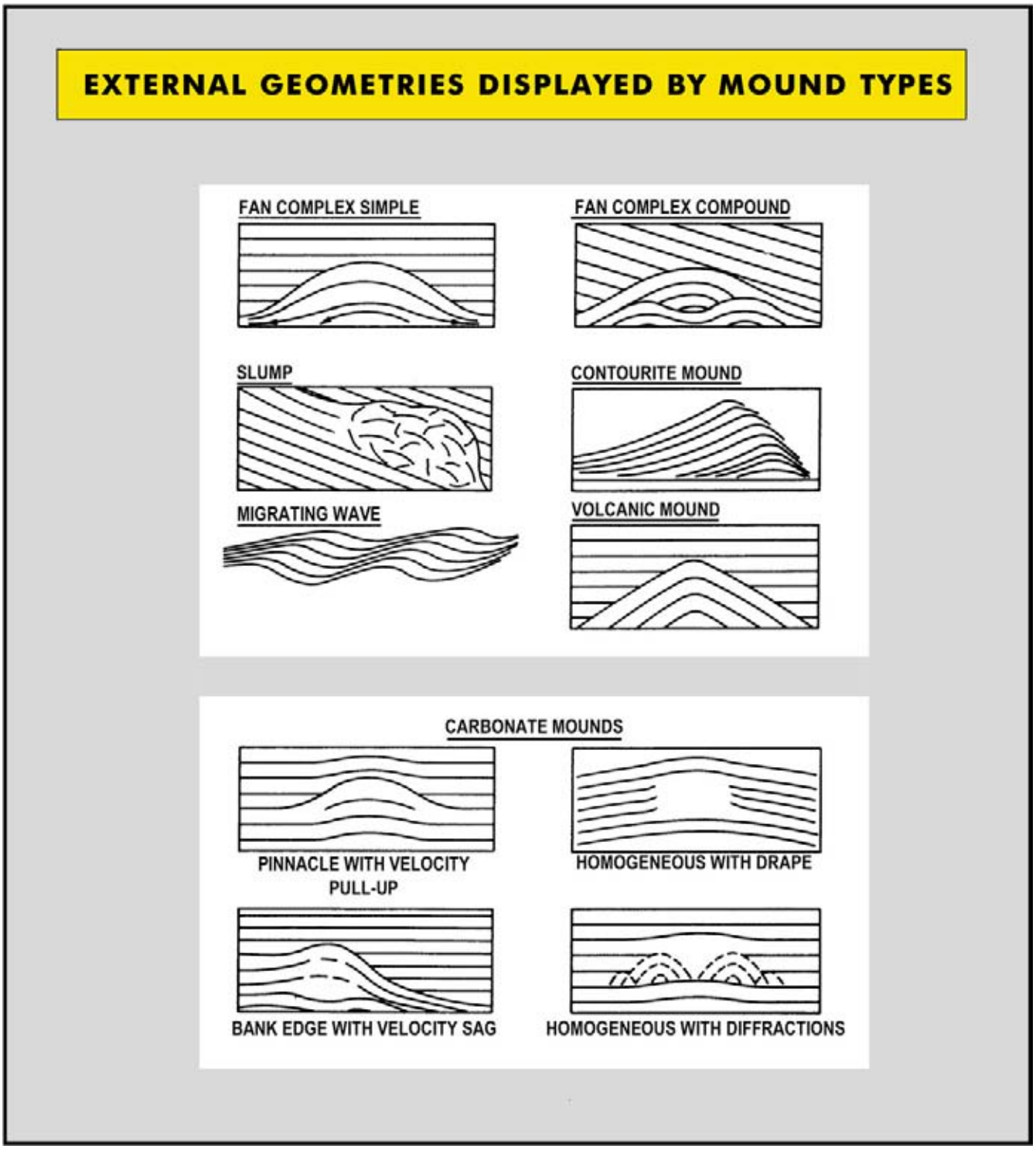

Figure 3.34: External geometries displayed by various mound types. Mounding is a 3D phenomenon and should be verified on at least two perpendicular seismic sections (after Mitchum et al. 1977, reprint from AAPG whose permission is required for further use).

fault pattern from landsat images is often a handy guide for the delineation of the shallow faults on widely spaced 2D data. Structural mapping at the surface may reveal the presence of anticlines and synclines. However, it has also been shown that recent surface depressions may coincide with major structural highs at greater depths.

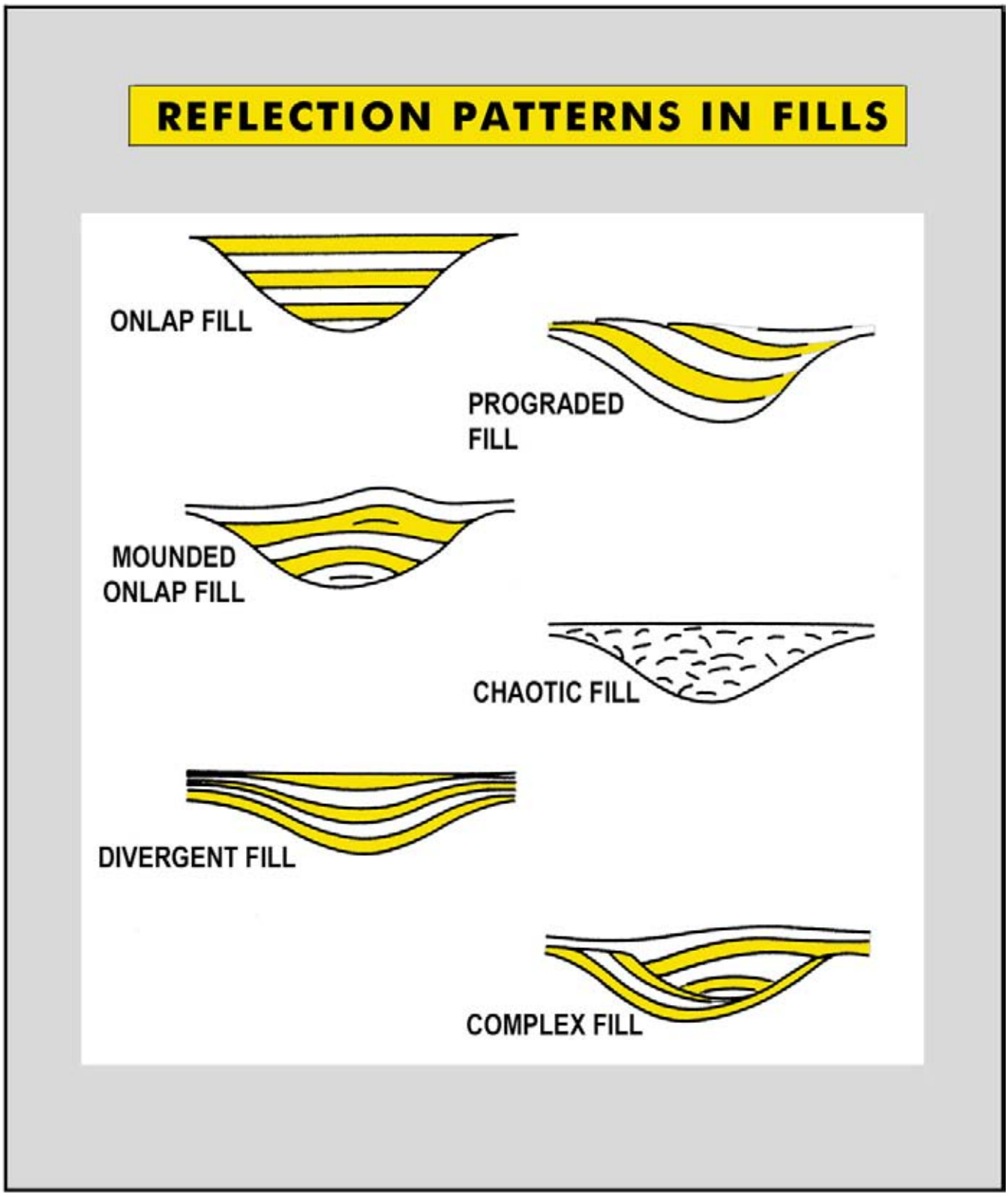

Figure 3.35: Reflection patterns in various sedimentary fills. Differential compaction effects can give a clue on the contents of channel fills. The shaleprone levees are compacted much more than the sands. A convex upward bulge is therefore probably indicative for sand prone sediments (modified after Mitchum et al. 1977, reprint from AAPG whose permission is required for further use).

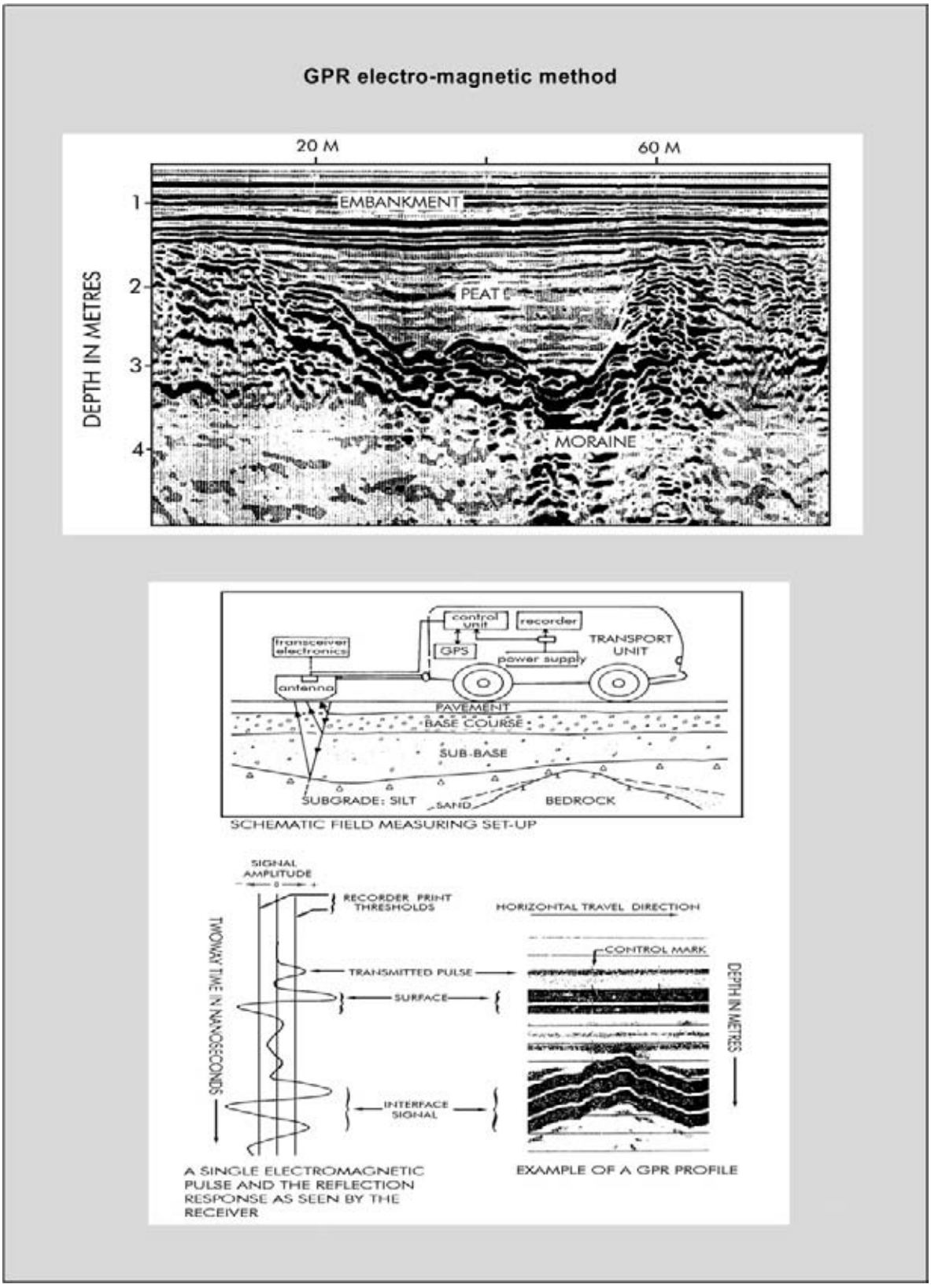

Figure 3.36: Erosive channel fill on a GPR section. The unconformity is outlined by reflection termination mapping, just like on normal reflection seismic data. Ground penetrating radar uses electro-magnetic waves that are reflected at 'permitivity' interfaces. It is a high-resolution method with a maximum penetration depth of about 50 metres under favourable conditions (dry rocks, no shales).

On the Arabian shield several of the major hydrocarbon accumulations are characterised in this way.

In the offshore, samples can be taken of the seabottom by means of box and piston cores. These seabottom samples give additional information on the shallow subsurface structuration; age-dating and composition are of particular interest. Of course these field observations are only calibrating the uppermost part of a seismic section and it reveals little on the nature of deep-seated structures.

Well information is essential for the calibration of the deeper part of the subsurface. Commercial wells may have a reach of 4000 to 5000 meters in depth. Their geographical spread of information is however restricted and basically 1D. Therefore other geophysical techniques like **magnetics** and **gravity** are called upon. These geophysical investigations provide additional constraints for the interpretation of the seismic dataset. Gravity is useful to establish the overall shape of a basin and to pinpoint high/low blocks. It is extremely valuable in poor seismic data zones (Veeken and Titov 1996). The distribution of salt structures is for instance better resolved when incorporating this type of geophysical data. The outline of salt diapirs can be difficult to trace on the conventional seismic data as they usually coincide with poor data zones. Sometimes the top of the salt dome is characterised by the presence of a caprock sequence (e.g. Duin 2001). The caprock is created by severe weathering of the salt diapir. It is composed of less soluble parts of the salt deposits. Insoluble constituents are enriched in the zone where active dissolution of the salt occurred and are typically composed of anhydrite (mixed with limestone or dolomite) in the subsurface. Caprock exposed near the surface is altered, because the anhydrite is not stable under such conditions, into gypsum by incorporating crystal-bound lattice water (Mandawa Basin, Tanzania). The carbonate and anhydrite lithologies have very high interval velocities and therefore easily show-up on seismic data. The gravity force between two bodies is given by the Newton Law and amounts to the gravity acceleration g times the multiplication of the masses, divided by their distance squared.

The proper interpretation of the gravity data is not always straightforward. A drawback of the gravity method is its non-uniqueness, i.e. there is not one solution to the inversion problem and several earth models may equally well explain the measured gravimetric values. Gravity modelling is often done to simulate various subsurface scenarios and to evaluate the shape of their theoretical gravity response. Its results are compared with the measured field data (Veeken and Titov 1996b). For the modelling some basic assumptions are made on the geometry and density of the rocks. An amount of uncertainty is therefore inherent to the outcome of gravity studies. It is possible to use 2D Fourier analysis to separate the effects caused by the deeper-seated background from the more shallow local influences (Leaman 1994). The results of the gravity modelling is compared with both the measured and corrected gravity data. Iterative changes are made to the earth model to get a better fit between the two datasets. It is helpful when the geologist communicates with the interpreter and the processing geophysicist in order to establish the most plausible solution.

Different sort of gravity anomalies are studied, each having its specific application (Figure 3.37). The gravity of the earth is corrected for the centrifugal force that is greater at the equator. Also the equatorial radius is greater (apple shaped globe). This is compensated by the **latitude correction**. The presence (mountains) and absence (valleys) of mass near the recording station is compensated in the **terrain correction**. A correction is needed for the position of the station with respect to the sealevel datum, this the so-called **free air correction**. The **Bouguer correction** replaces the air by the mass between the station and the sealevel datum. The isostatic correction corrects the presence of density roots below the mountains or oceans. The **residual anomalies** are useful for interpreting the variation of the subsurface geology in a sedimentary basin. 2D modelling can prove here extremely helpfull (Figures 3.38 and 3.39). It is important that all other corrections have been implemented before modelling of the gravity response is undertaken (Veeken and Titov 1996), otherwise the interpretation of the results will be misleading.

Magnetic measurements give additional information on the outline of a sedimentary basin and/or the presence of volcanics/ore deposits. Gravity and magnetics are two complementary techniques. These potential data are very helpful in the first outlining of structural elements in a zone under investigation (Figure 3.40a). They can be used to reconstruct the plate tectonic evolution, dynamic basin modelling and the identification of new play concepts (Jacques et al. 2004). Also magneto-tellurics and electro-magnetic methods are useful to determine anomalies that are of interest to mineral and petroleum exploration (Henke et al. 2005). In the electro-magnetic method the periodic pulses in the primary field are exiting currents in the subsurface in conductive bodies and the decay of the current is measured. A slow decay indicates a conductive body (Fountain et al. 2005). In the offshore the problems are somewhat different, but there is less noise from the telluric or earth electrical current origin. Important is the quality of the source and the receivers. The

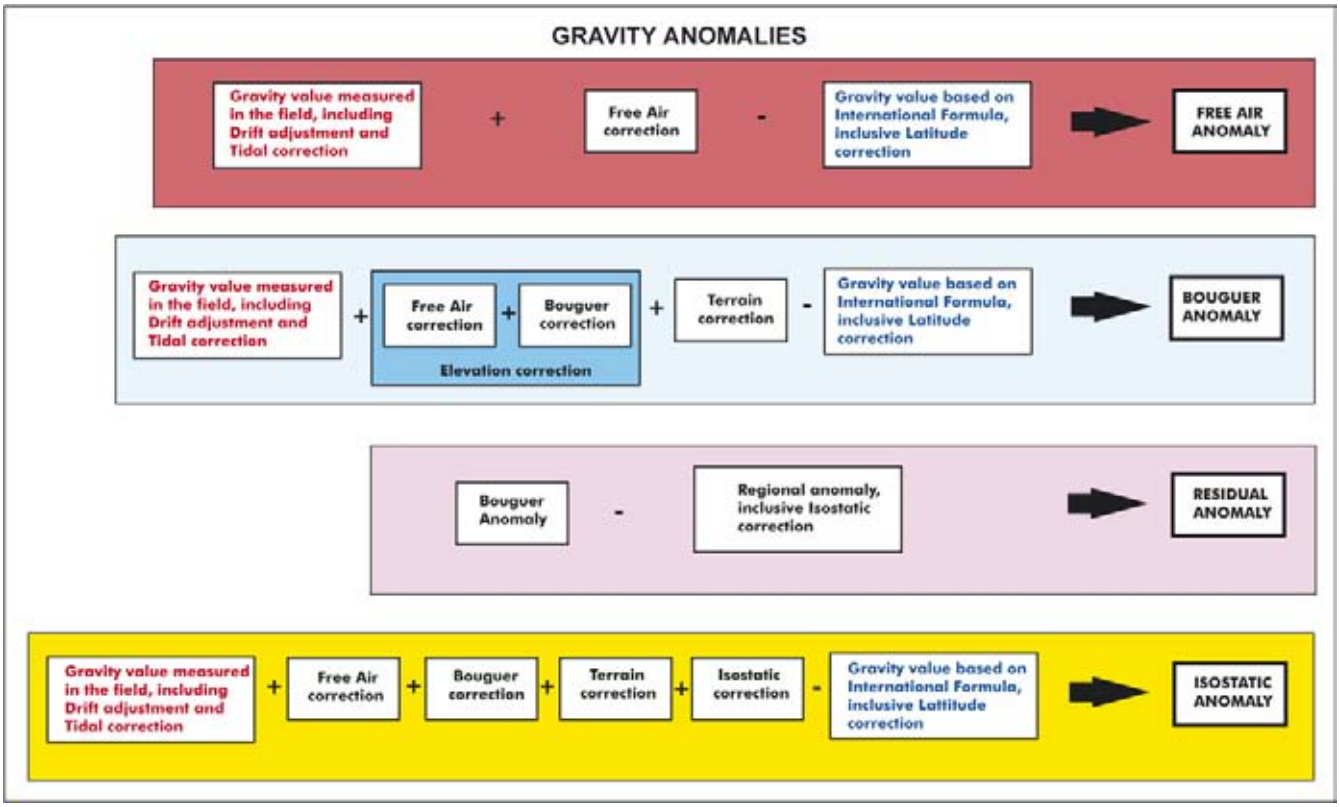

Figure 3.37: Corrections have to be implemented on gravity measurements to make their interpretation easier. Various gravity anomalies are usually calculated for this purpose; each anomaly has its own application for the distinction of local and deep-seated influences on the overall gravity response. International Gravity Formula for the theoretical gravity, as of 1987, at latitude ϕ is: $978\,032.68\ (1 + 0.001\,931\,851\,386\,39 \sin^2\phi)(1 - 0.006\,694\,379\,990\,13 \sin^2\phi)$ mGal.

penetration depth depends also on the oscillation period and the resistivity. Fixed detectors at the seabed are often deployed and the offset should be far enough to get sufficient penetration depth; up to 2000 metres of investigation depth is possible at a frequency range of 0.1 and 5 Hz (Hesthammer and Boualenko 2005). The value of the controlled source electro-magnetic method for hydrocarbon detection seems proven and it provides a new tool for the explorationists. Hydrocarbon filled sediments are resistive inclusions that scatter the EM field and the response propagates back to the surface receivers. This new marine EM investigation technique is also known as seabed logging (Figure 3.40b).

Well results constitute hard data for the calibration of seismic data. The observations in the wells should therefore be honoured in an early phase of the interpretational process. The scale difference between the well control and seismics is tremendous. Well data vary from microscopic to the macroscopic kilometre domain in a vertical sense (Figure 3.41). It is a 1D point calibration in that the hole diameter rarely exceeds a width of 1 metre. The borehole can be vertical with little deviation between the surface location and the TD (total depth) coordinates. Or it is deviated with an oblique irregular well path. Horizontal wells have a curved well trajectory and are drilled horizontally at the target interval. Their reach can be quite long (5 km or more). The horizontal well geometry increases the drainage efficiency and production from the reservoir.

3.4.1 Petrophysical measurements and well logging

The petrophysical measurements on the wall of the borehole reveal the nature of the penetrated rocks (cf Serra and Serra 2004). The contractor lowers an emitting and measuring device along a cable into the borehole and the data is recorded at the cabin on the drilling location. The well logging program nearly always includes the gamma-ray, calliper, P-wave sonic, density, neutron, dipmeter and resistivity logs (Figure 3.42):

– The **gamma ray** tool measures the natural radiation from the formation. In shales a lot of radioactive elements are incorporated in the clay mineral structure and a high gamma ray reading is the result.

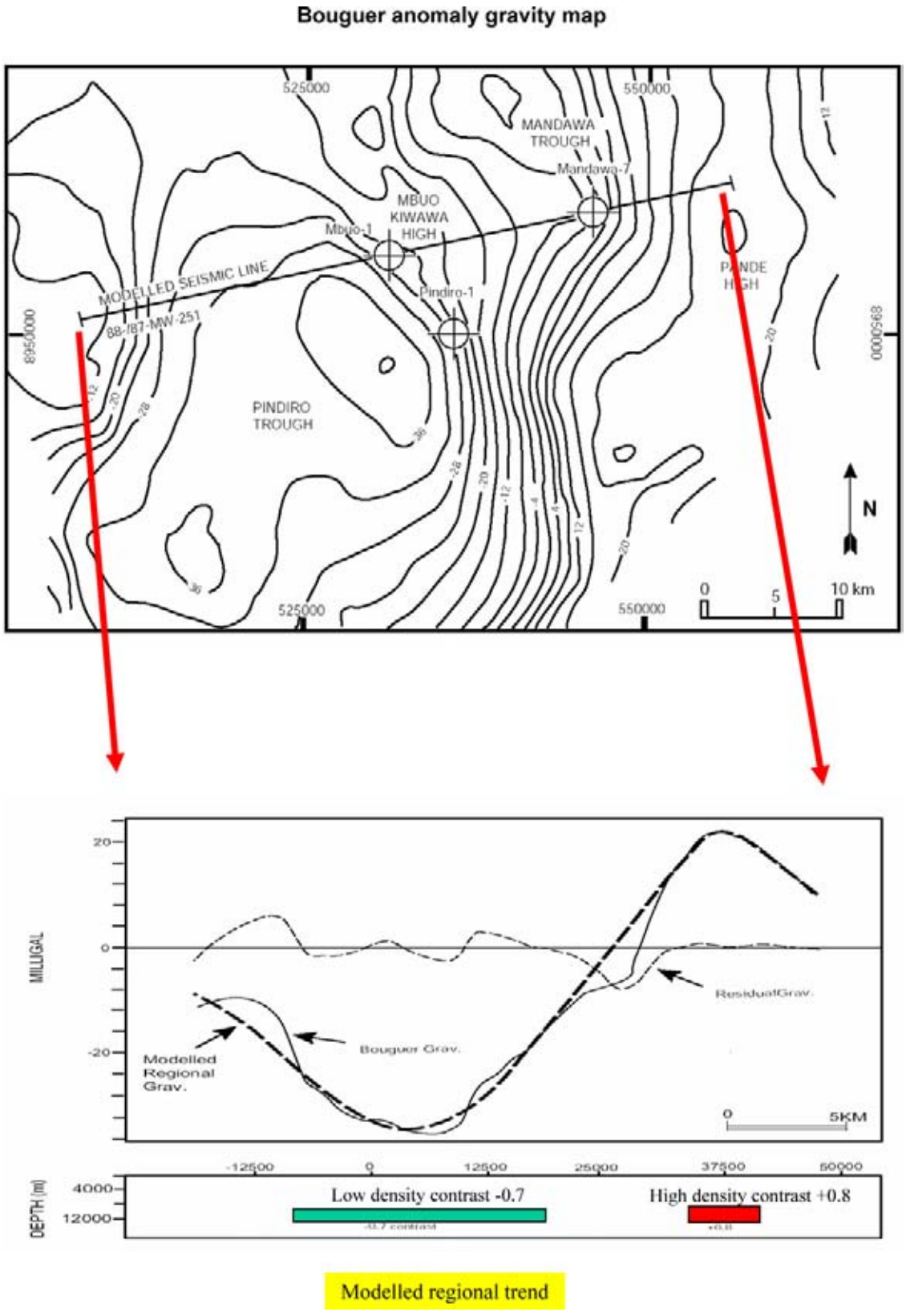

Figure 3.38: Bouguer anomaly map in the Mandawa basin (onshore Tanzania). The regional trend is modelled by two different density bodies as shown in lower figure. The causes for the residual gravity behaviour are thought to reflect changes in the overburden geology.

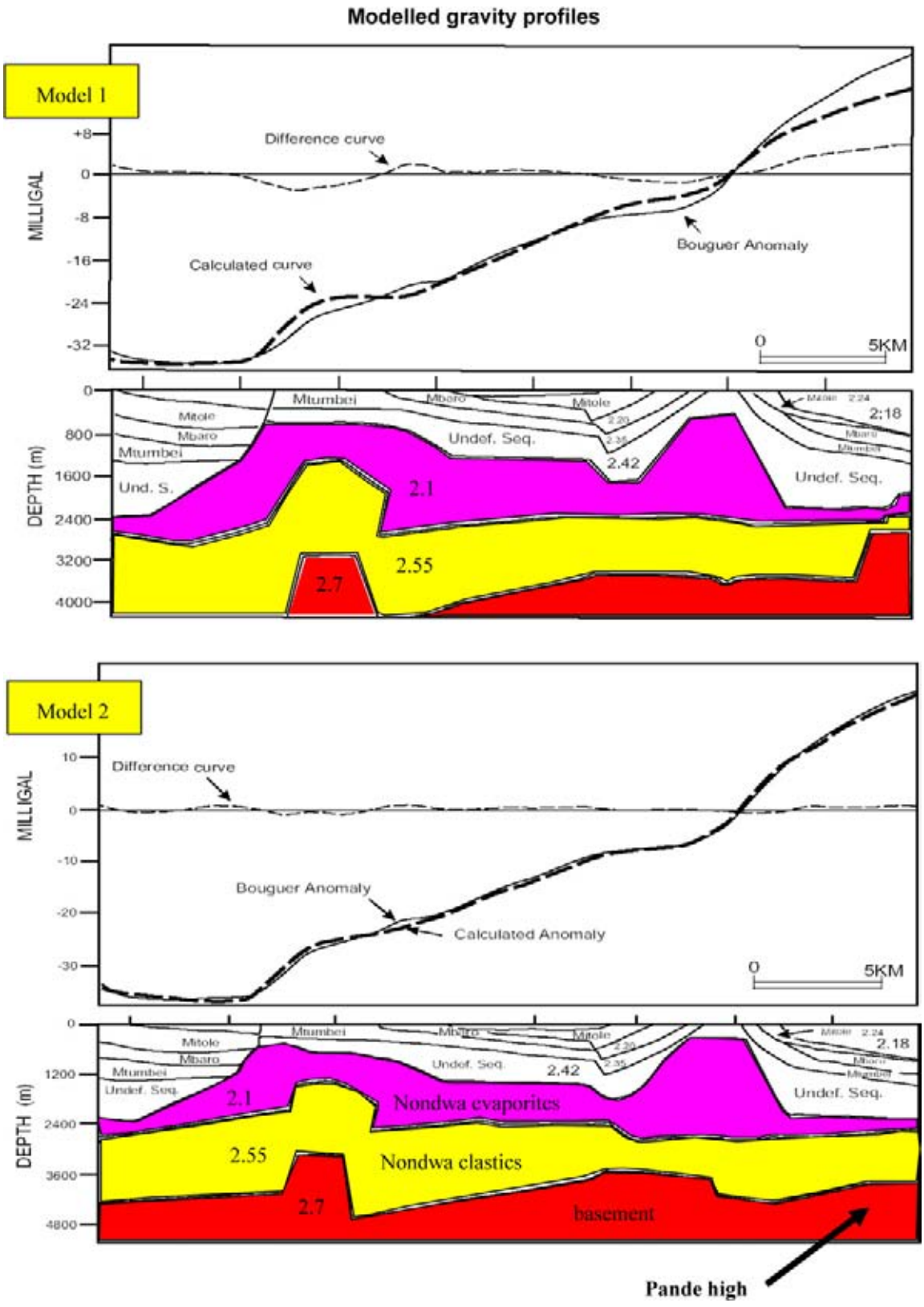

Figure 3.39: Two different subsurface models for which the gravity response was computed and compared with the observed response. The second model gives a better fit and it indicates that the Pande high area is having a substantial section of sediments. These can contain also reservoirs and therefore the prospectivity of the closure is augmented.

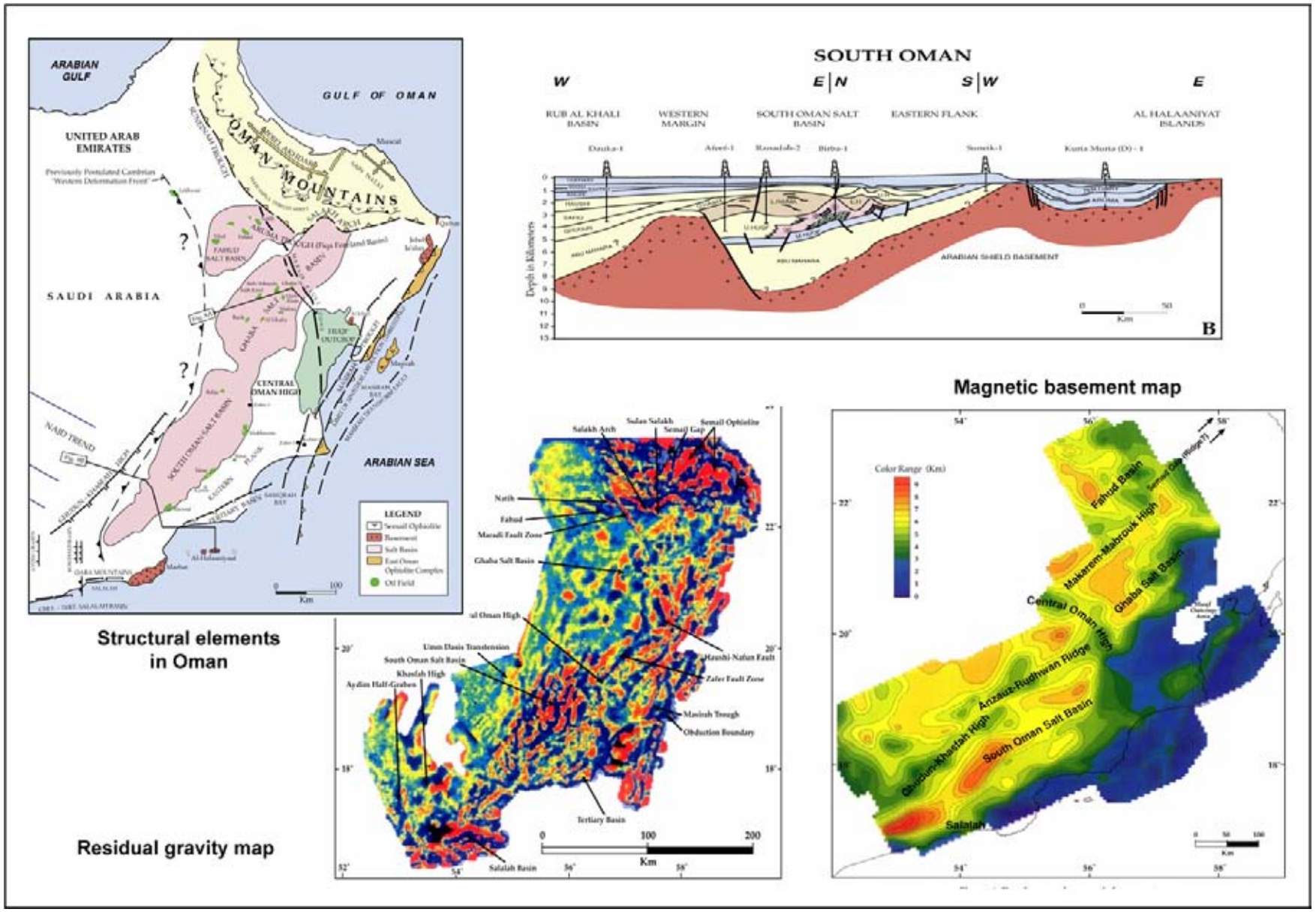

Figure 3.40a: Gravity and magnetic maps from Oman. The broad outline of basins and fault blocks is possible with this kind of data. There is a reasonable correspondence with the known structural elements (modified after Loosveld et al. 1996).

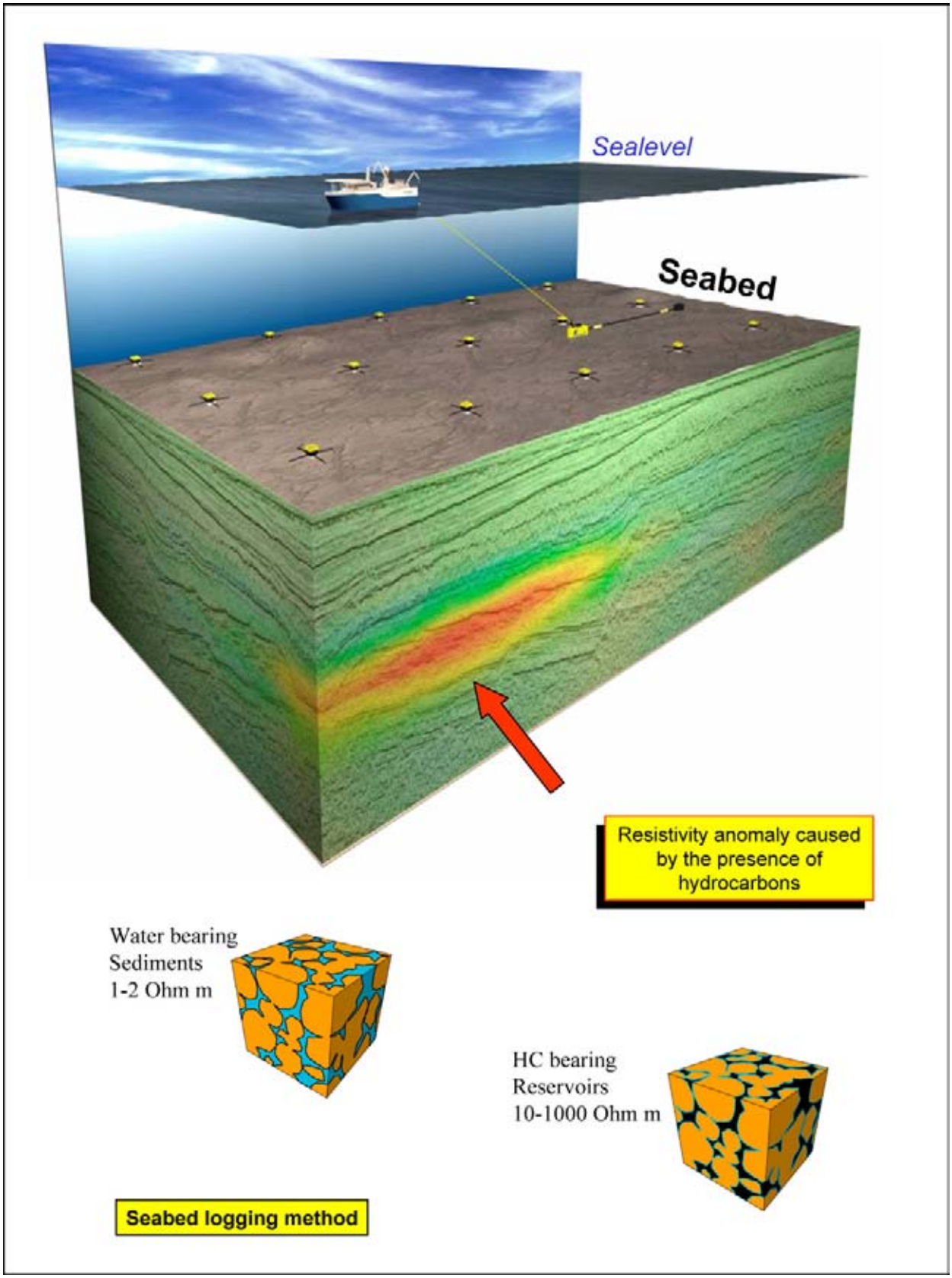

Figure 3.40b: Seabed logging method uses electromagnetic signals and records the behaviour of resistive bodies in the subsurface. Under favourable condition a penetration depth upto 2.5 km is feasible.

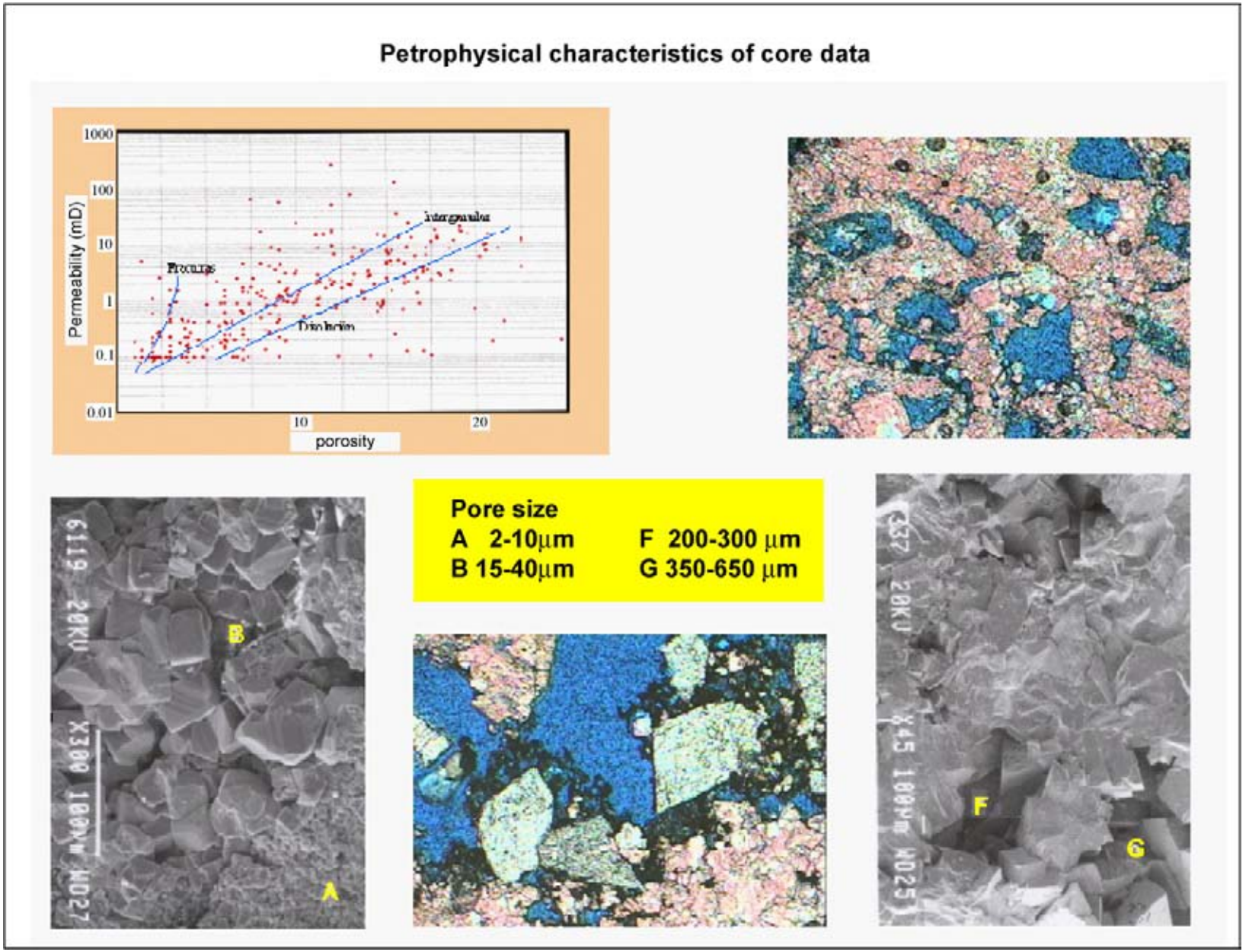

Figure 3.41: The pore size distribution in carbonate reservoirs determined on core data, illustrated with micrographs for appreciation of the internal rock fabric (courtesy Pemex).

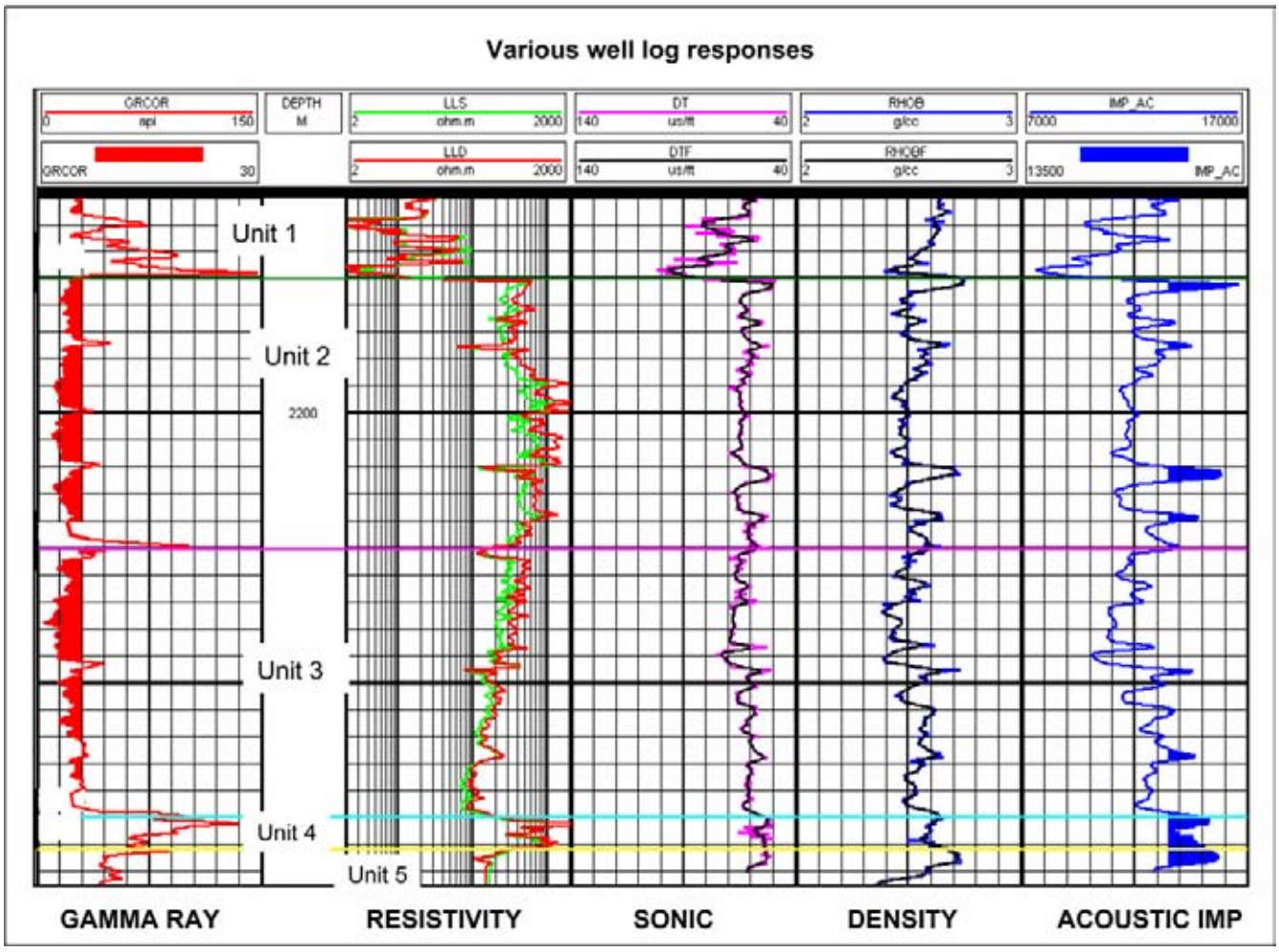

Figure 3.42: Well logs measured in a borehole permit to distinguish various petrophysical units. These observations (depth scale) are subsequently tied to the seismics (time scale) in special manner, as will be shown later on. Well data cover a wide variety in scale of observation: from microscopic to the macroscopic kilometre scale. It is however a 1D point calibration as the penetrated column is very limited in width (normally <1 metre; courtesy Pemex).

The radiation level in carbonates and sands is normally much less. The gamma ray is convenient for discrimination of the shaley intervals. Several types of radiation can be analysed, which help to subdivide the sedimentary succession. These are: potassium (^{40}K), uranium (^{230}U) and thorium (^{232}Th). The gamma ray log is measured in API units that have been defined by the American Petroleum Institute and are calibrated in a quarry pit owned by the University of Houston.

– The **calliper** records the width and shape of the borehole by lowering a simple sonde with retractable arms. The circulating drilling mud will wash out a bigger hole in soft rocks. These holes give rise to erroneous readings for the other logging tools. It is important to determine these zones of reduced reliability of the petrophysical measurements. In plastically deforming formations, the shape of the hole can tell also something about the in-situ stress pattern. The break-out pattern of the borehole wall in the shaley deposits is investigated for this.

– The **sonic** logging tool measures the transit time of an acoustic waveform between an emitter and receiver, spaced several feet apart. The recorded transit time (ΔT) is a slowness measured in μsec/feet. It is easily converted in a velocity log. The penetration depth of the sonic log depends on the wavelength is in the order of a few inches (one wavelength, Vasquez et al. 2004). The full waveform tool (dipole sonic imager or DSI^{TM} of Schlumberger) measures the P- as well as the S-wave velocities. This information is needed in more sophisticated reservoir modelling and gives an accurate view of the rock physical parameters directly around the borehole (De Beukelaar et al. in press). Stoneley wave

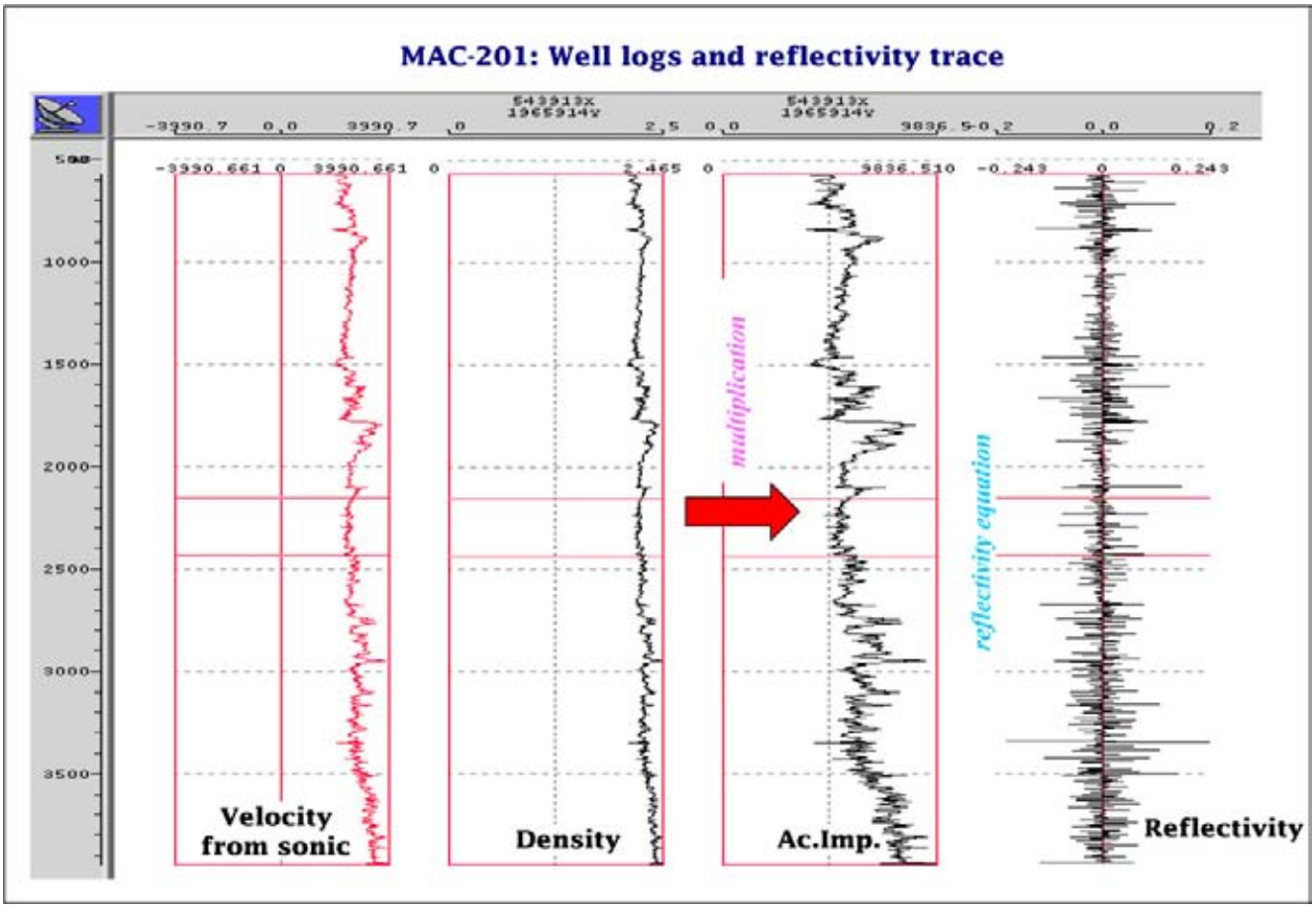

Figure 3.43: Well log example with calculated Acoustic Impedance response. The sonic transit times are converted for this purpose in a velocity log and multiplied by the density.

energy is used in soft formations and gives a better grip on permeability and open fractures. Dipoles are directional and sensitive to anisotropy and azimuthal dispersion (Sheriff 2002).

– The density of the rocks is registered by lowering a radioactive source in the borehole. The emitted radiation encounters electrons and is backscattered by the Compton effect. The amount of back scatter is counted by the specially shielded detector. The number of electrons is proportional to the bulk density. The measurements are usually done with a compensated density tool, correcting automatically for mudcake and bore irregularities. Together with the velocity response from the sonic log, the acoustic impedance curve can be calculated and hence the reflectivity behaviour is analysed (Figure 3.43).

– The **neutron log** emits neutrons and gives a measure for the hydrogen density. Fast neutrons form the input and are slowed down at the collision with hydrogen that brings them back to thermal speed. These thermal neutrons are then captured by the nuclei of surrounding material (mostly chlorines) and gamma ray radiation is emitted, which is detected. It is expressed in API units, whereby the Indiana limestone with 19% porosity and fresh water in the calibration pit is set at 1000 API. It is also possible detect directly the slowed-down thermal neutrons (Sheriff 2002).

– Electrical logs illustrate the **resistivity** and the **spontaneous potential** (SP) of the rock sequence. The shallow resistivity reads 10 inches into the formation (invaded zone plus virgin formation, Figure 3.44), while the micro resistivity reads basically the mud cake (Vasquez et al. 2004). The **dipmeter tool** is a micro-resistivity logging device with azimuth dependent sensors. The dip is inferred from the cross correlation of the recordings from the various pads and is often visualised in a **tadpole plot**. The heavy point corresponds to the dip value and the line segment gives the direction of the dip (azimuth). Nowadays a formation imaging device (like the FMI^{TM} of Schlumberger) is often run, it

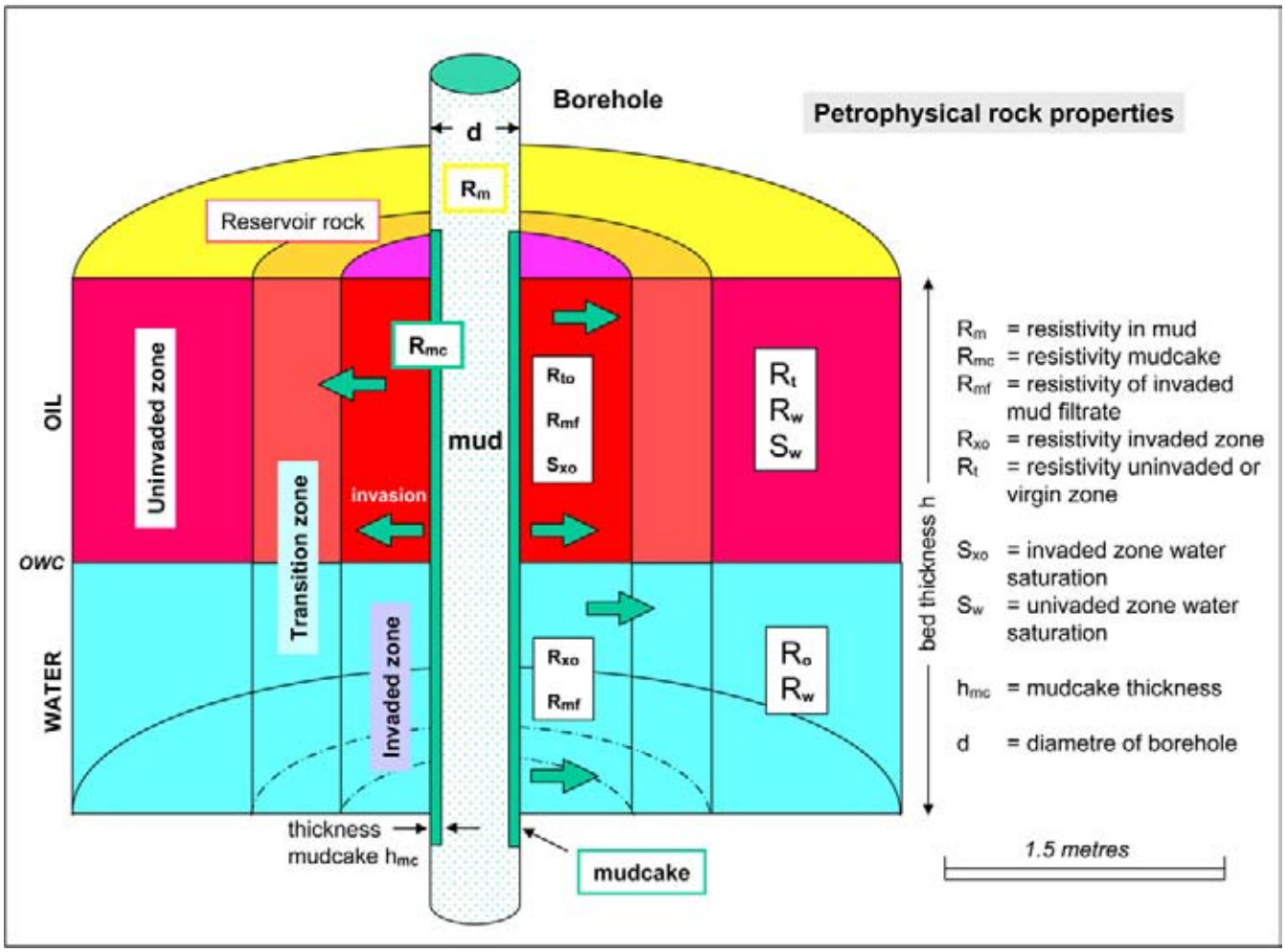

Figure 3.44: The drilling mud invades porous zones around the well borehole. Mud particles are filtered and retained against the borehole wall and forms a mudcake that has little permeability. The finest part of the mud suspension invades the host rock and changes its characteristics. The logging tools are partly reading the invaded zone as well as the uninvaded (or virgin) zone. Heavy density mudfluid prevents an eventual blow-out of the well, but it also damages the formation by clogging the pore throats in the rocks directly surrounding the bore hole wall (with permission of copyright holder Shell/Schlumberger).

provides a view on the borehole and allows to detect dips, faults, fractures and sedimentary features (Figure 3.45).

– **Mud logging** is done and samples of the rock cuttings are taken at regular time intervals. These cuttings are small rock fragments in the drilling mud, that are circulated along the drill string to the well head. The samples are collected on the shale shakers on the bore platform. Gas detection and isotopic analysis can be useful (MGIL, Ellis et al. 2003). Drilling mud serves several purposes: it lubricates the rotating drill string, it transports the debris from the bit and it allows to control the pressure in the borehole. Additives like barite increase the mud density and the total weight of the fluid column prevents the pressurised reservoir fluids to enter the well. The lubrication capacity is altered by oil based mud (pollution, logging problems) and it prevents that the drill string gets stuck in swelling overpressured clays (Oligo-Miocene sticky shales in the North Sea) or big holes are washed-out in a salt section for example.

– **Nuclear Magnetic Resonance** log is using initially unoriented hydrogen dipole spins to be oriented along a certain axis B_0 by applying a magnetic field. Now a pulse is applied B_1 perpendicular to this B_0 direction and the nuclei are forced to align to the new field. After the pulse is passed the nuclei re-orient themselves to the previous magnetic direction and they emit a signal (resonance). This energy is captured and represented in a relaxation time T_2 plot that can be interpreted.

– The **Photo Electric Factor** of a formation is recorded in a log. A chemical gamma ray source emits gamma

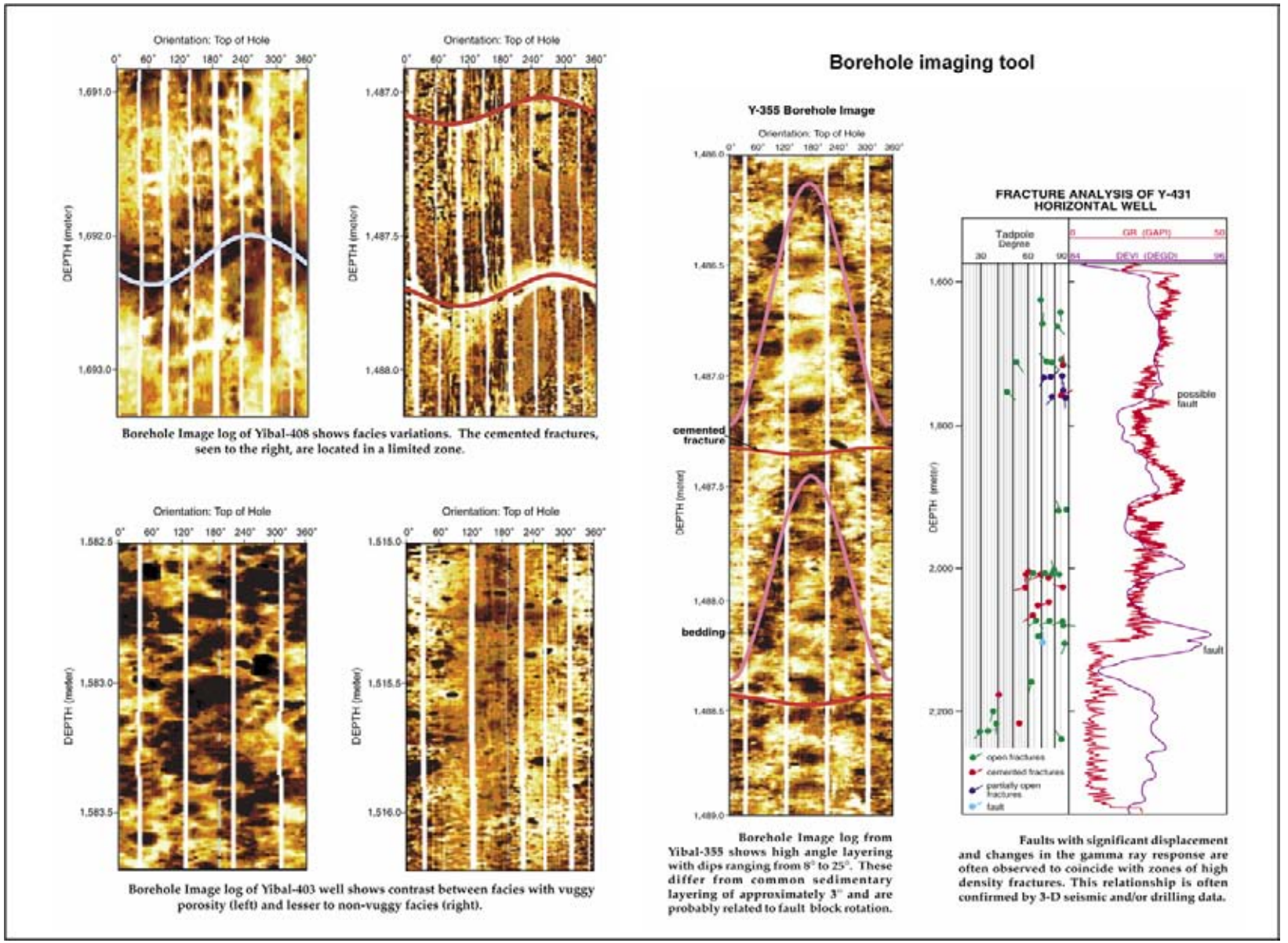

Figure 3.45: Borehole imaging tool provides detailed information on the borehole. Eight tracks are recorded and give together a 360 degree picture of the borehole wall. Dipping events are represented by sinoidal curves. The fracture analysis is given at the right hand column. The direction and degree in dip are shown in a tadpole plot. The dot indicates the dip value and the attached straight segment shows the azimuth direction (modified after Al Busaidi 1997).

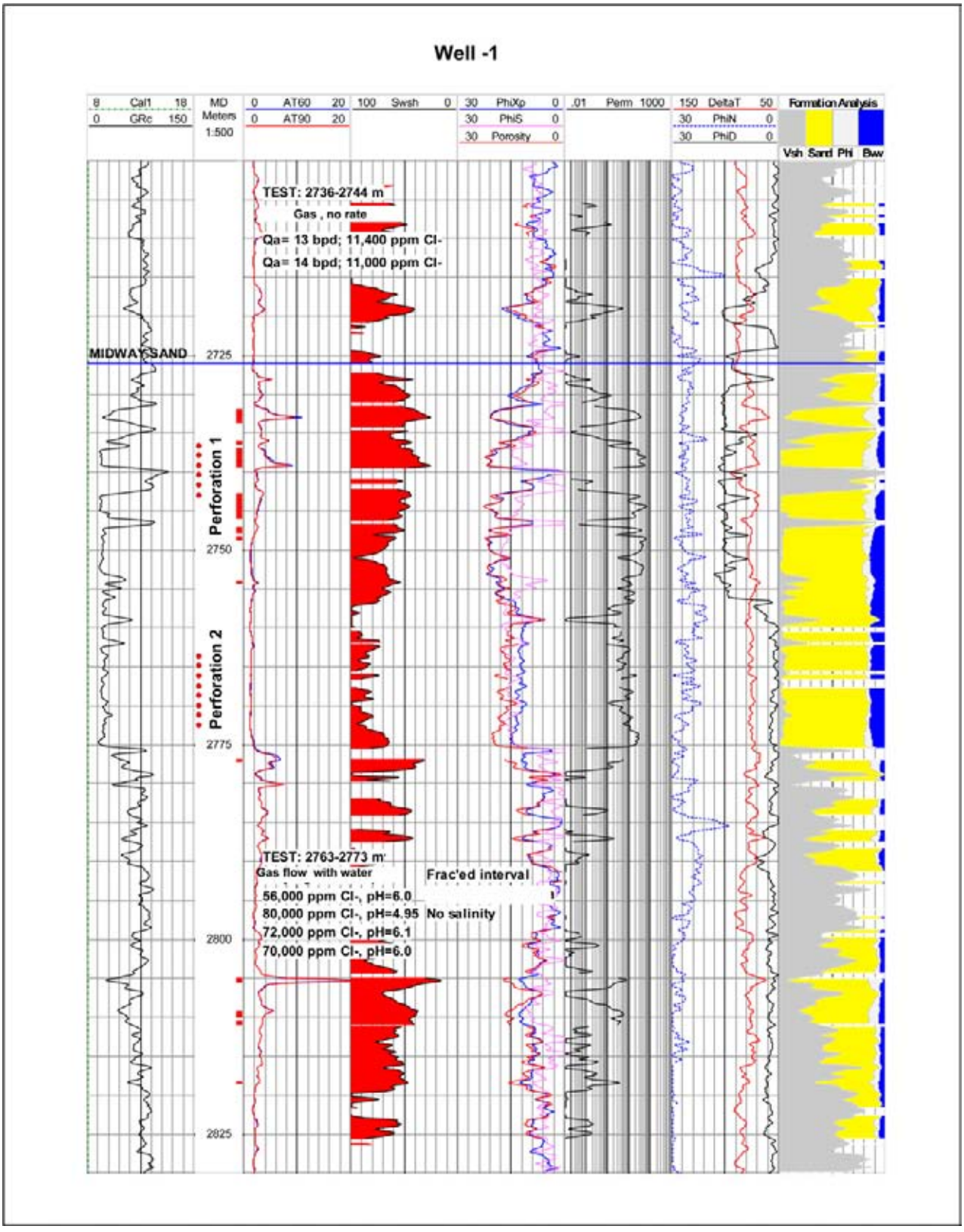

Figure 3.46: Well summary sheet with main petrophysical flow units, position of perforations and production figures (courtesy Pemex).

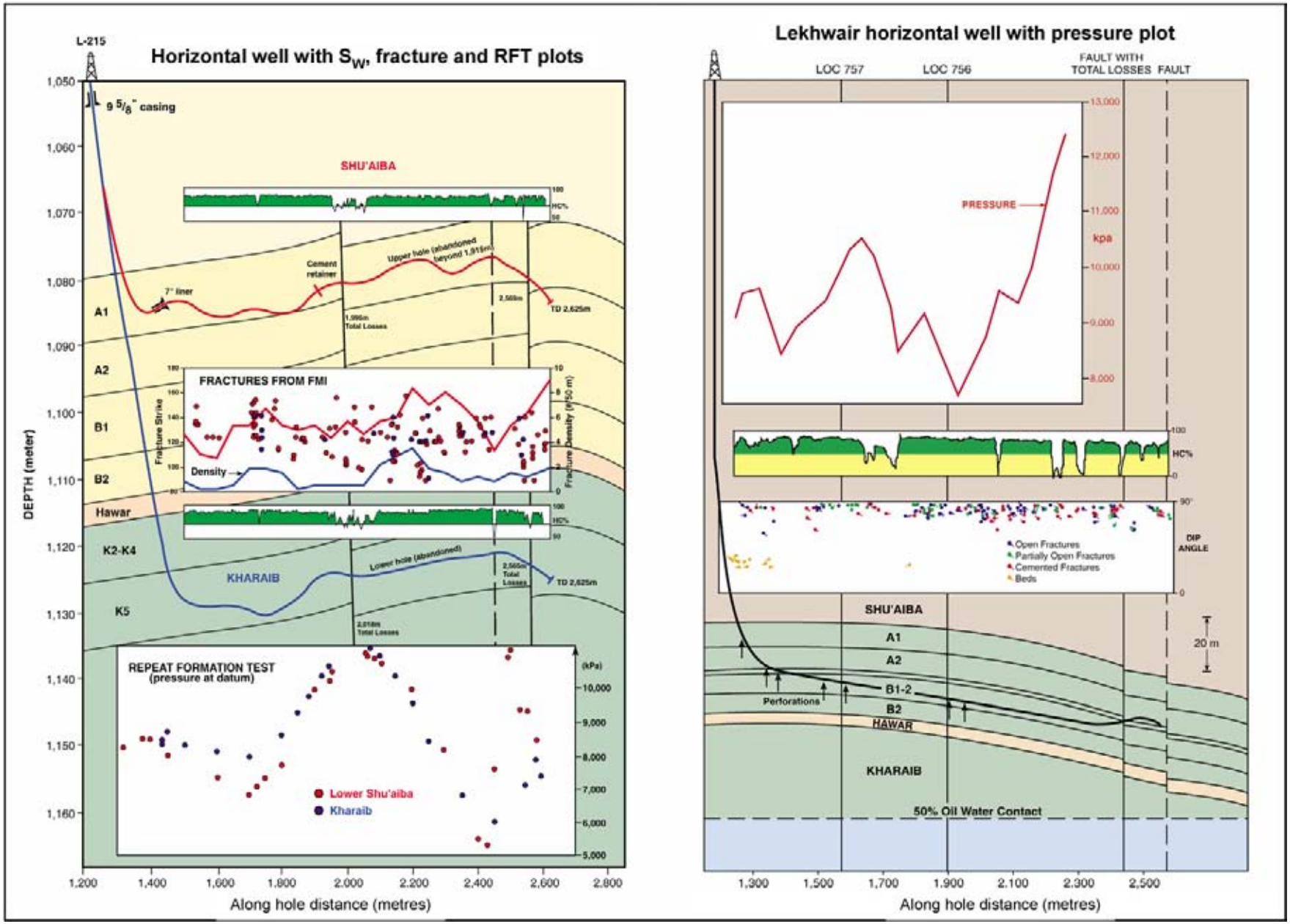

Figure 3.47: Horizontal well trajectory plotted on geological cross section. The fracture and fault analysis is done with the high resolution Formation Micro Imager (FMI^{TM}) tool. The Repeat Formation Tester (RFT^{TM}) tool gives information on the pressure distribution within the reservoir (modified after Al Busaidi 1997).

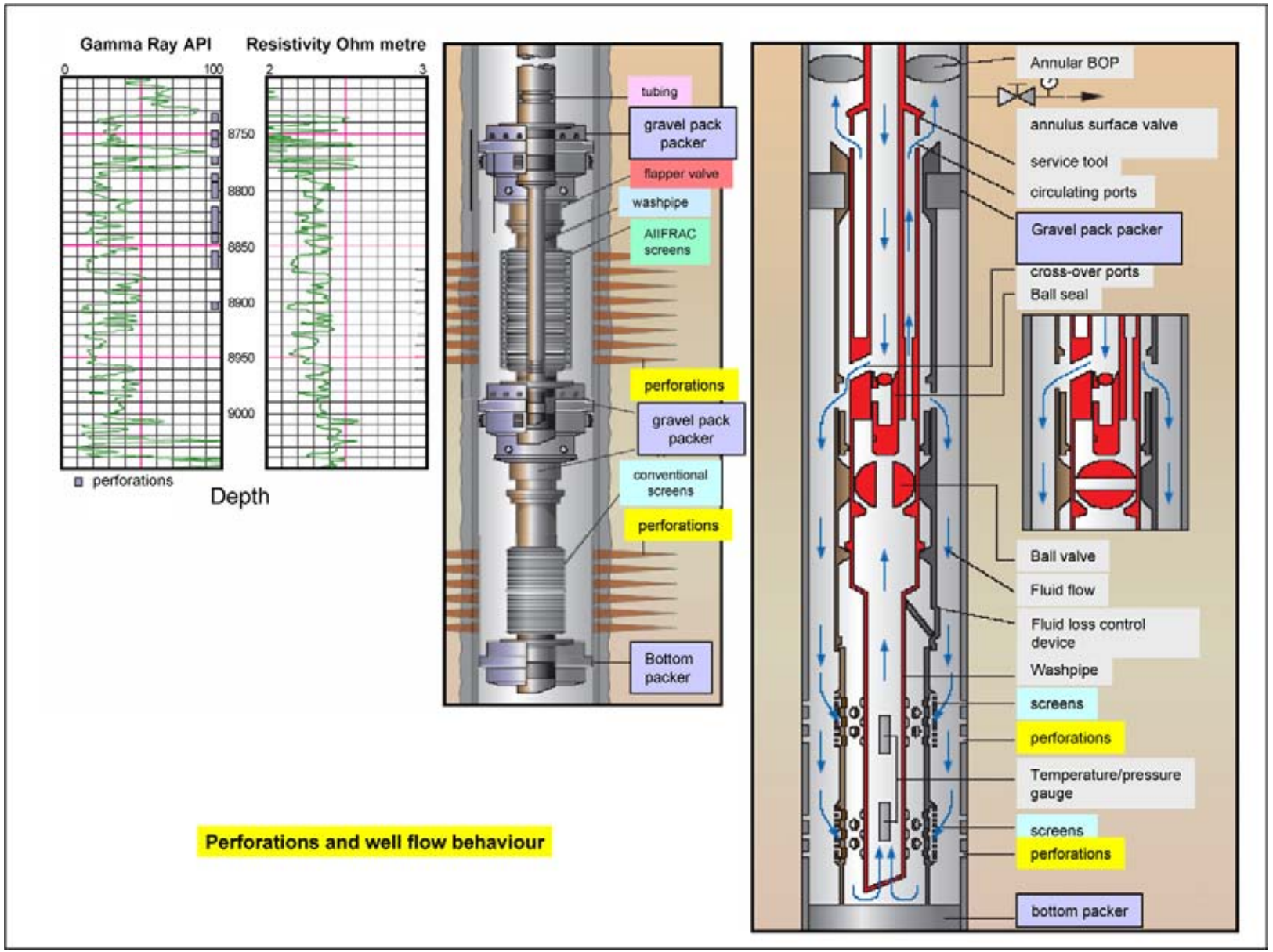

Figure 3.48: Bottomhole assembly for testing the production from specific formation interval. The casing is perforated and the well is divided in compartments with its own circulation separated by packers. The fluid flow is shown on the right-hand side. The position of the perforations are indicated on the completion well log. The Drill Stem Test (DST) is often performed to monitor the pressure/flow behaviour of the perforated interval (modified after Ali et al. 2002 with permission of copyright holder Schlumberger Ltd).

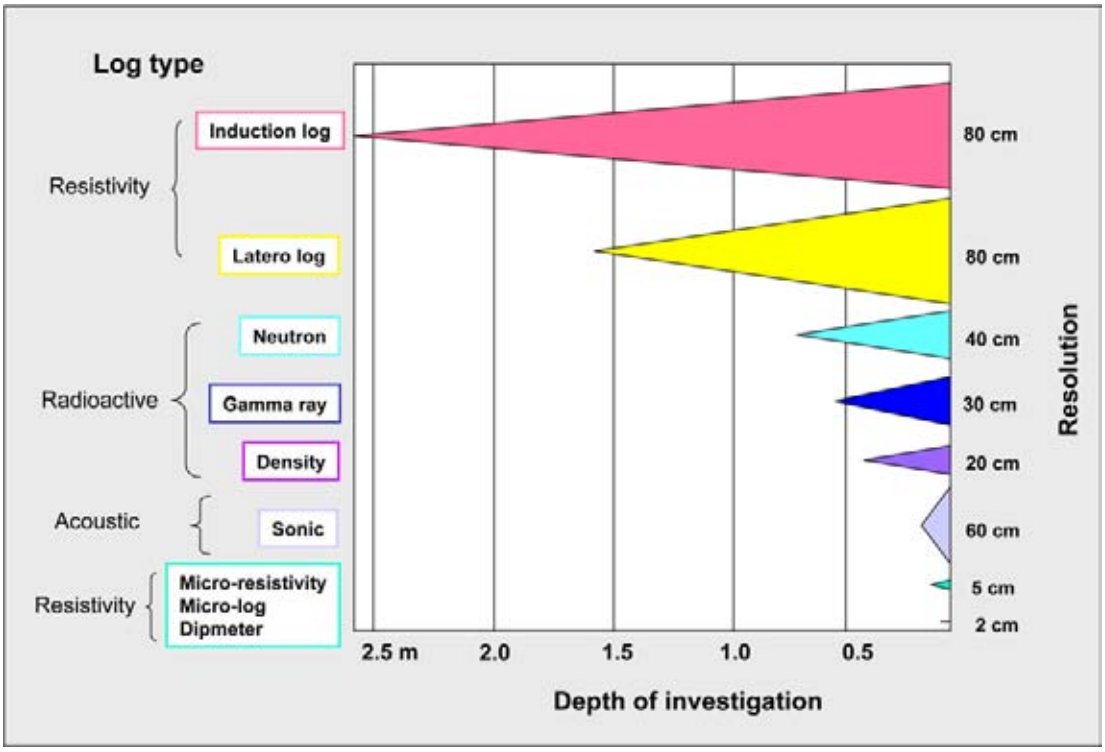

Figure 3.49: The vertical resolution of various logging tool and their depth of investigation (with permission of copyright holder Shell/Schlumberger).

rays that are backscattered to the detector, but on their way they interact with the formation. One way of interaction is absorption of the low energy part of the gamma rays. This is caused by collision of the gamma ray particle with the atom and ejection of an electron from its stable orbit. A parameter links the amount of absorbed gamma rays to the surrounding lithology and this is expressed in the photo-electric absorption index, also known as the **PEF**.

- The **drill bit penetration rate** is monitored. Sudden breaks may point to an important changes in lithology.
- **Sidewall samples** are taken from the walls along the well track. This is done by lowering a special gun barrel into the hole, mounted with retrievable hollow bullets that are ballistically shot into formation. In extremely hard formations also plugs are drilled hydraulically. This sampling technique alters somewhat the petrophysical characteristics of the rock fragment. These plugs are not fully representative for the in-situ formation.
- **Cores** are cut over a prospective interval. A special drill bit with a central hole is used, which leaves the middle of part of the penetrated rock column in tact. This column is cut at regular intervals and recuperated for careful study in the lab. The core barrel can be sleeved, so that also unconsolidated sediments are retrieved for closer examination at the surface. The pressure can be maintained during the recovery to give a better impression on the real rock in-situ conditions.
- Fluid flow measurements and pressure data are acquired during production or special **Drill Stem Tests** in hydrocarbon containing intervals (Figures 3.46 and 3.47). Intervals can be isolated by so-called 'packers', which are inflatable plugs preventing open circulation in the annulus of the well (Figure 3.48). The **annulus** is the space between the drill string and the bore hole wall. These selected intervals are perforated and the production from these zones is tested. Several perforations can be operated simultaneously and the co-mingled flow rate is obtained.

Some of these parameters are also '**measured whilst drilling**' (MWD) or 'logged while drilling' (LWD). The big advantage of MWD or LWD logging is that the info is rapidly available and put on the interpreter's desk at the push of a button (Bonner et al. 1993, 1996). The resolution of the tools depends on the input signal, the size and the distance between the sensors (Figure 3.49). Dynamic and precise **geosteering** of a well certainly belongs to the possibilities (Adigun et al. 2004). The bit is rotated by a downhole mudmotor driven by the circulation of the mud fluid (Figure 3.50). Measuring a

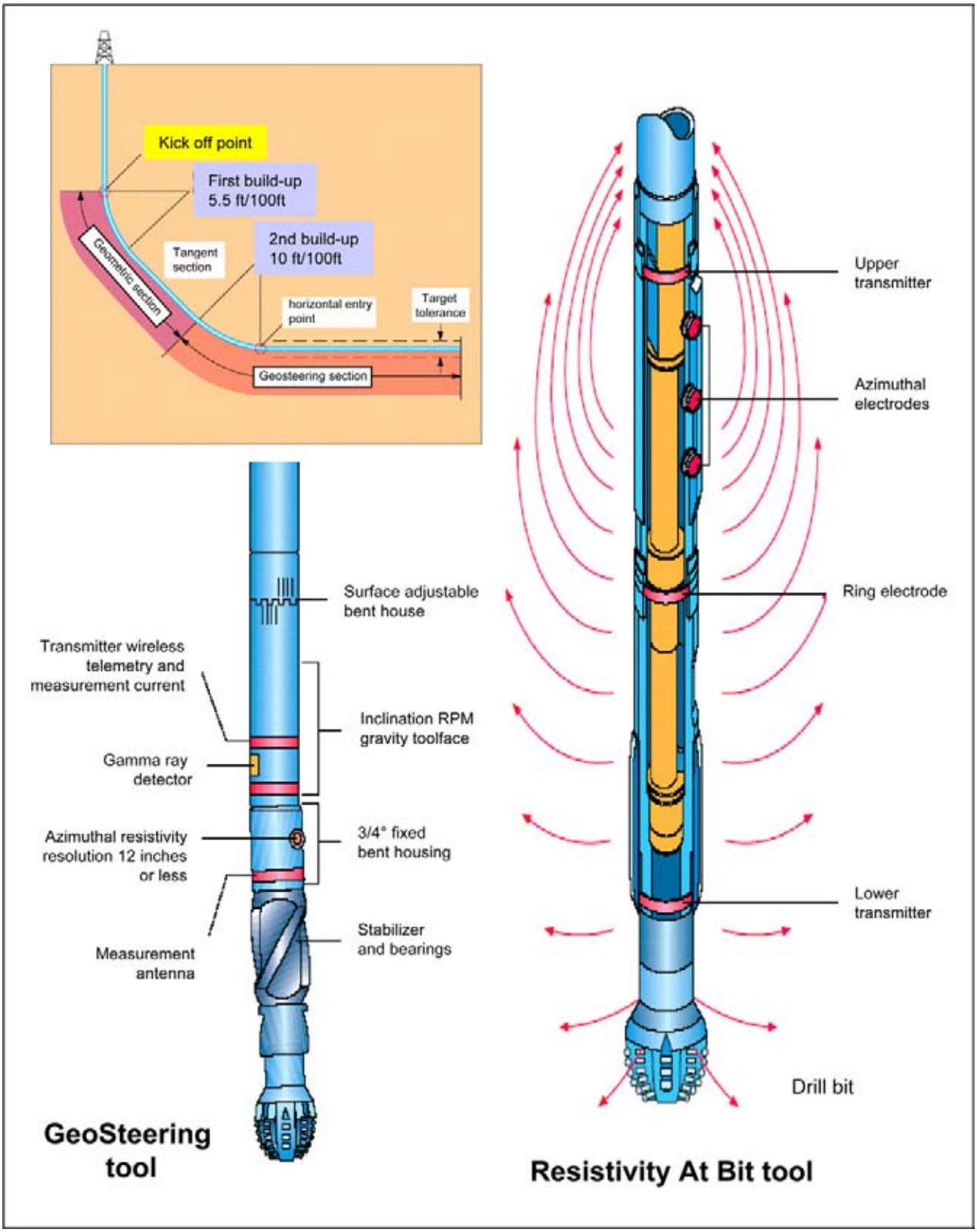

Figure 3.50: Bottomhole assembly for drilling a deviated hole. Geosteering and control over the well trajectory is possible using a bottomhole mud motor, driven by the mud circulation in the well. More reliable measurements whilst drilling are obtained in this way. The layout of the Resistivity-at-the-Bit (RAB tool^{TM}) is shown on the right-hand side (modified after Bonner et al. 1993 with permission of copyright holder Schlumberger Ltd).

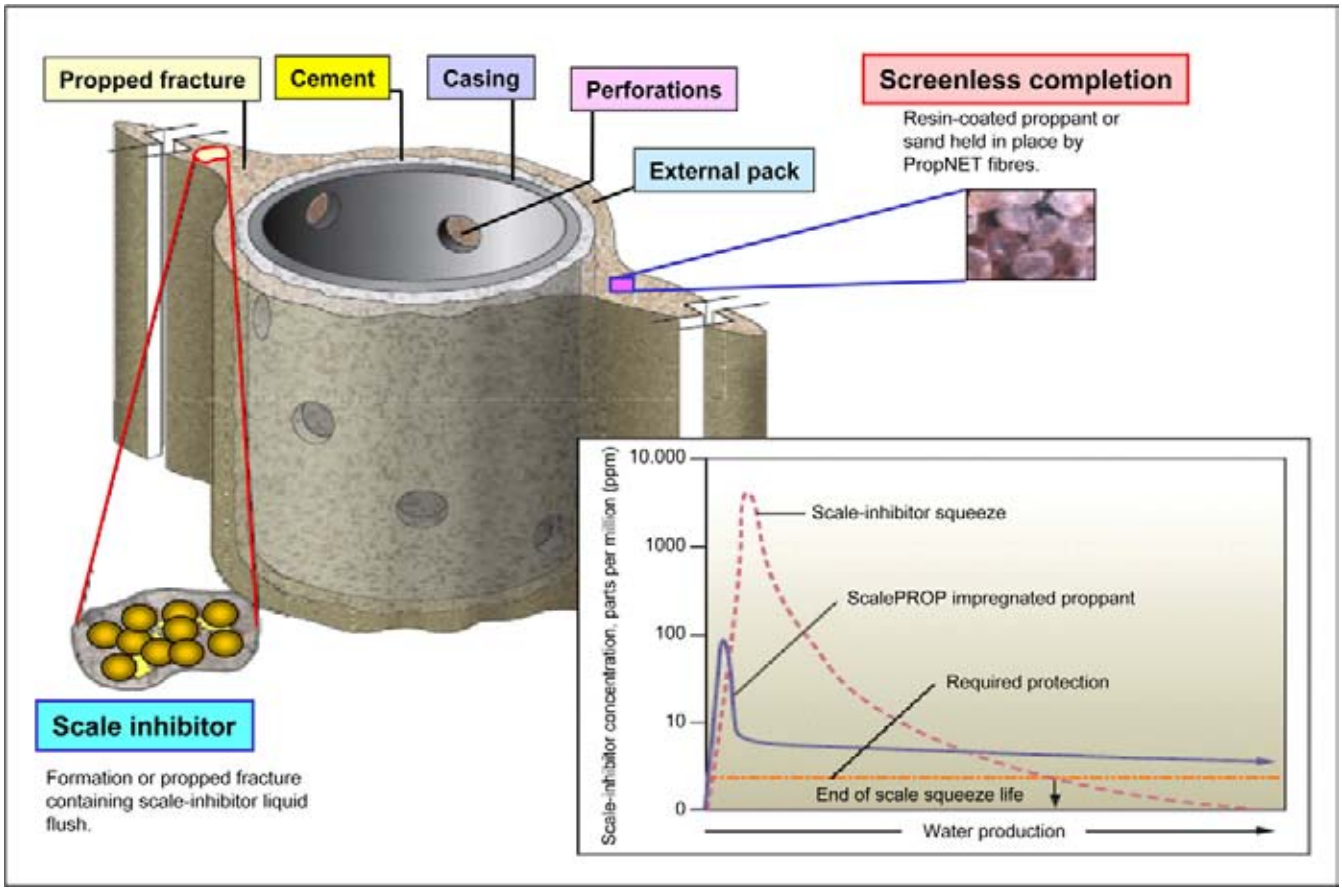

Figure 3.51: Well casing is perforated to test the flow from a porous zone. The casing and the cement are shown. The cement is penetrated in an open fracture that has been propped with proppant to ascertain sustained flow and/or reduce the sand production as the borehole wall is stabilised (modified after Ali et al. 2002 with permission of copyright holder Schlumberger Ltd).

deep resistivity whilst drilling is certainly very helpful in this respect (e.g. Grane field in the Norwegian sector of the North Sea; Seydoux et al. 2004). Some of the logs can also be acquired in cased boreholes and that is good news for well workovers. This is the regular reconditioning of the well to improve the production. **Casing** is the metal protection of the borehole wall. It avoids unnecessary deterioration of the reservoir close to the borehole by wall collapse and thus ensures a better production performance (Figure 3.51). It allows isolation of target flow units during production by setting packers or plugs in the well. The cement bond between the casing pipe (or tubing) and the formation should be of good quality so that unwanted leakage is prevented. Nowadays, well testing can be conducted either while perforating the well with tubing-conveyed perforating (TCP) guns or even through casing using cased-hole formation testing tools (Figure 3.52).

The quality of the measured well logs should always be checked by a trained petrophysicist. His/her professional input is definitely needed to clean-up the raw log data (M. Krief, pers. com.). Omission of this quality control step can prove very costly. Sometimes major editing is required to obtain reliable well log data (cf Boyer and Mari 1994). The mud invasion correction is essential for computation of reliable synthetics (Vasquez et al. 2004). If this is done, then corrections should be applied in a normalised way, whereby all wells in the data base are treated in a similar way and the log results are of comparable quality. Velocity and density curves can be estimated from other logs, but it should be kept in mind that those results are only valid under special assumptions.

Seismic data is measured along a two-way time axis, whilst the well data is recorded with a depth scale. It is important to establish the correct velocity function to time-convert the well results. This will make a direct comparison possible between the two datasets.

If no calibration is available for the seismics, then the gross lithofacies distribution is deduced directly from the general aspects displayed by the seismic units under

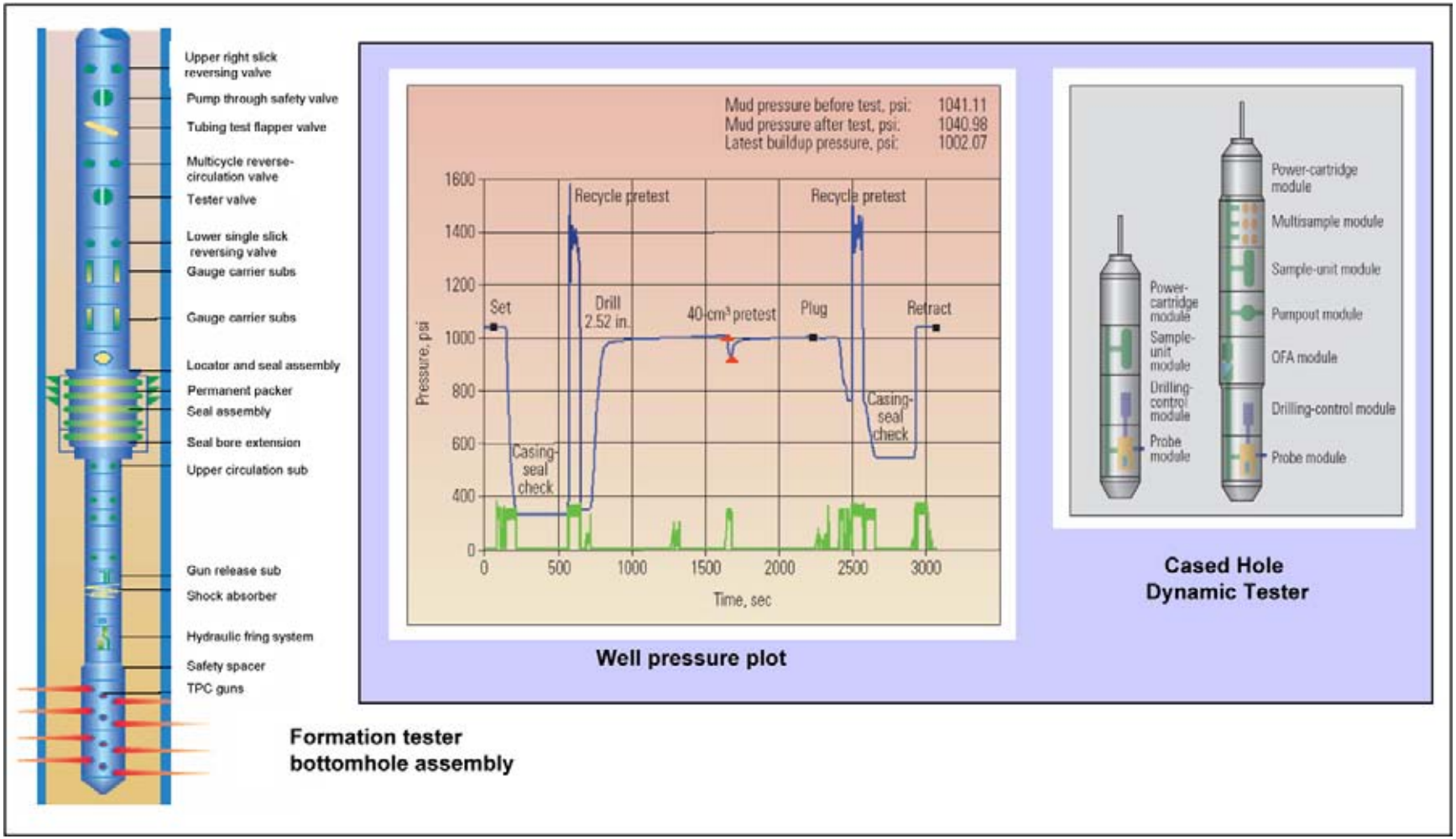

Figure 3.52: Well Testing can be carried out using a TCP gun to perforate the borehole wall and a packer providing the seal. The pressure is monitored in this blocked off compartment and plotted in the pressure plot, where the main events are annotated. Well formation testing can also be conducted using the Cased Hole Dynamics Tester (CHDT tool^{TM}) which allows testing in cased wells without compromising the integrity of the casing for future production. This tool drills a small hole via the casing into the formation. Resistivity is measured for fluid typing and samples can be collected in several small chambers. The drillhole is sealed after the measurement with a Monel corrosion resistant plug (modified after MacAndrew et al. 1993 and Burgess et al. 2002 with permission of copyright holder Schlumberger Ltd).

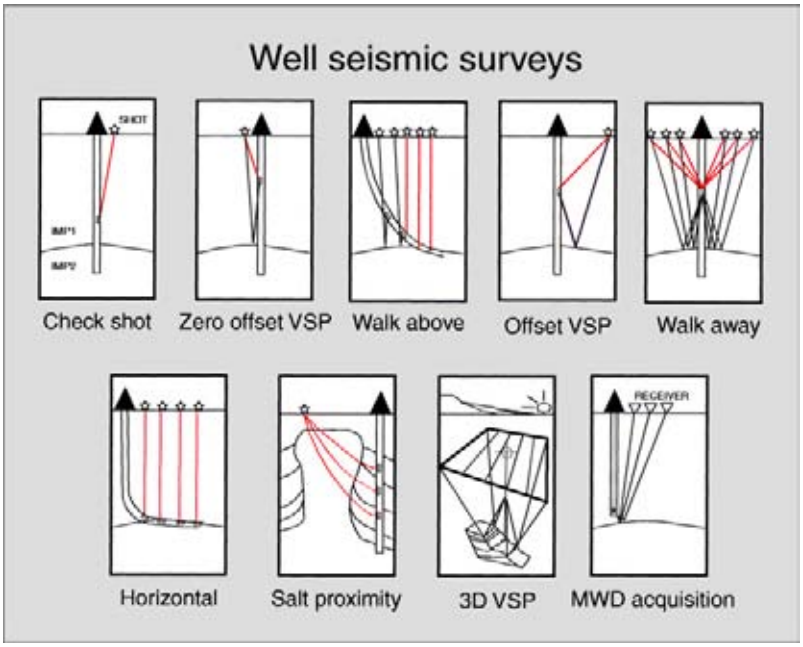

Figure 3.53: Different types of well shoot velocity surveys and their main characteristics (modified after Breton et al. 2002; used with permission of copyright holder Schlumberger Ltd).

investigation. An environment of deposition is assigned with the aid of criteria presented in Section 3.5. References to analogue situations with sufficient well control are very helpful for this purpose.

3.4.2 Well velocity surveys

Well velocity surveys are acquired to increase the reliability of time-depth conversion (Figure 3.53). Nearly always a **checkshot** or **well shoot survey** (Figure 3.54) is run to document the behaviour of seismic velocities around the well (Goetz and Dupal 1979). A geophone is lowered in the well, clamped against the borehole wall and a seismic signal is emitted at the well surface location. Usually a small pit is dug up to the water table and an airgun is lowered in the hole to serve as energy source. The **one way traveltime** to discrete geophone positions in the well is computed from the registered and corrected first arrival time. A data point is recorded for geophone positions at every 25 or 50 metres along hole. In the past only a few shots were recorded, coinciding with the major breaks in stratigraphy. A T–Z curve is constructed from these time–depth measuring points. A continuous interpolation of the T–Z values is obtained by integrating the sonic log data in the plot. The sonic log measures transit times of a high frequent signal within small vertical intervals. The interval velocities around the well bore are calculated from these transit time measurements. These sonic velocities are not identical to the checkshot and seismic velocities. The reasons are:

- The sonic velocities are measured in a nearly vertical position, while the seismic waves also have a horizontal component incorporated. Remember that the interval velocities derived from seismics are calculated via Dix's formula and this is based on stacking velocities determined on the NMO-corrected CDP gathers. The stacking velocities guarantee the best stack with the most energy lined-up horizontally on the CDP gather. This does not mean that it is always the best estimate for the interval velocity.
- The frequency of the signal used in the sonic log measurement is much higher than those used in the seismic method.

The empirical discrepancy between sonic and checkshot velocities is known as the '**drift**' of the sonic curve. The sonic log should be corrected for this drift before doing any well calibration. It is important that the correction of the sonic is done in geologically consistent way. In heavily deviated holes two different source locations are used in the well shoot survey. In fact a real walk-away velocity survey, with several different source positions is preferred as it will give much more detailed information (Figure 3.55).

It is possible to conduct a **VSP** (Vertical Seismic Profiling) **survey**, that theoretically provides an even better seismic-to-well tie (Figures 3.56 and 3.57). Not only the

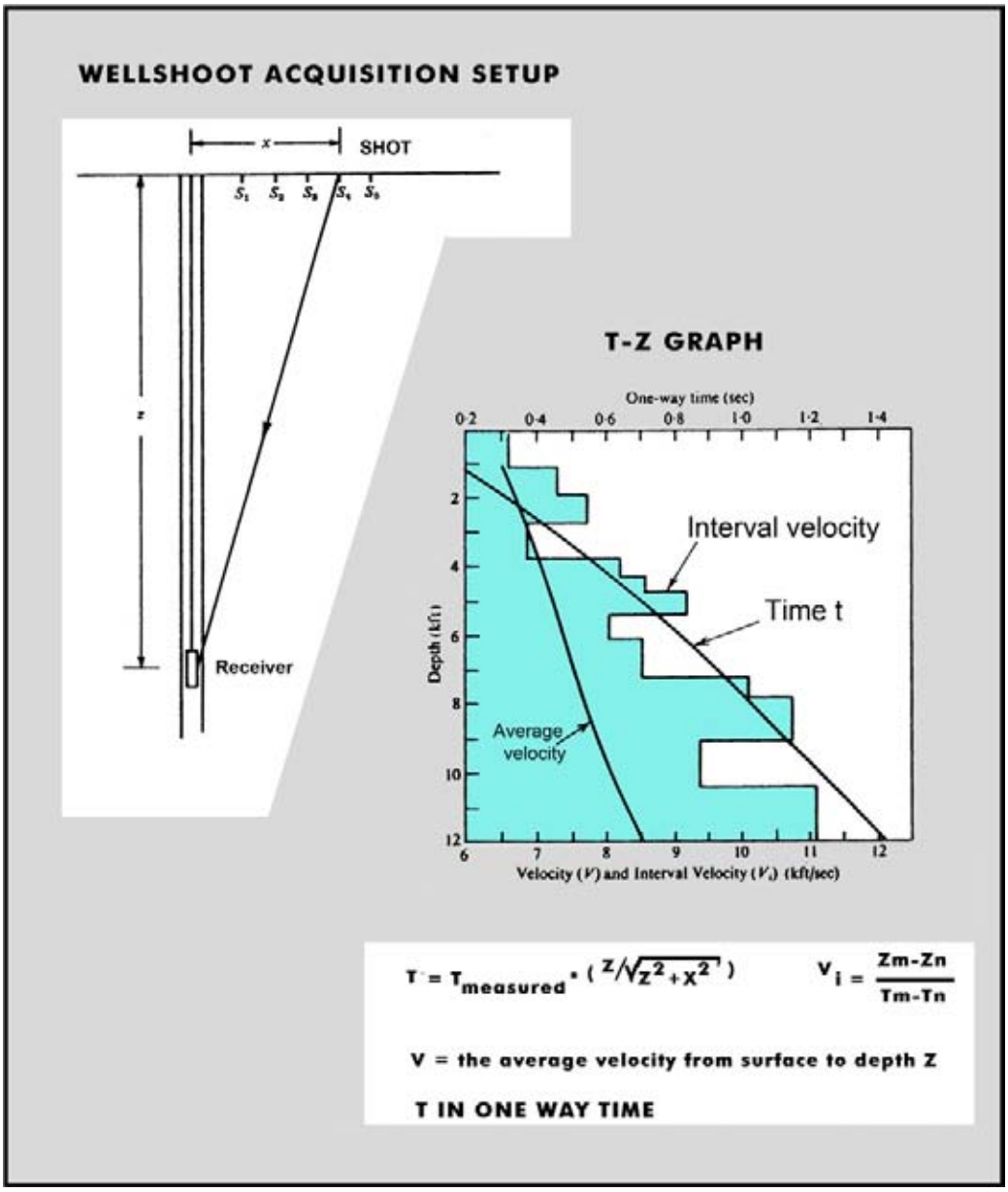

Figure 3.54: Schematic geometry of a wellshoot survey acquisition and the computed TZ-graph (modified after Telford et al. 1976).

first arrival energy is considered, but a trace length up to six second is now examined. The geophone is lowered in the well, locked to the wall of the borehole and a recording is done (Hardage 1983, 1985, 1999, Toksoz and Stewart 1984, Serra and Serra 2004). This clamping of the geophone prevents a whole string of geophones to be used. Several shots are needed to simulate a seismic section with this obligatory one geophone configuration. Some stacking of the data (several shots at the same geophone position) can performed to improve the signal-to-noise ratio. The lateral resolution of the VSP is higher than the normal surface seismics, because the distance from the source is smaller and the first order Fresnel zone is thus reduced. The measurements are made for several geophone positions and processed to obtain interpretable final VSP results. One source position, clearly offset from the well location, or several shotpoint positions (walk-away) on the surface can be used to generate the seismic signal.

The VSP data is not only recorded for determining the first arrival time (like in the checkshot procedure) but a whole trace is analysed and seismically processed (Christie et al. 1995). The **downgoing** as well as **upcoming wavefronts** are considered. The reflected upcoming wavefront contains essential information on the geol-

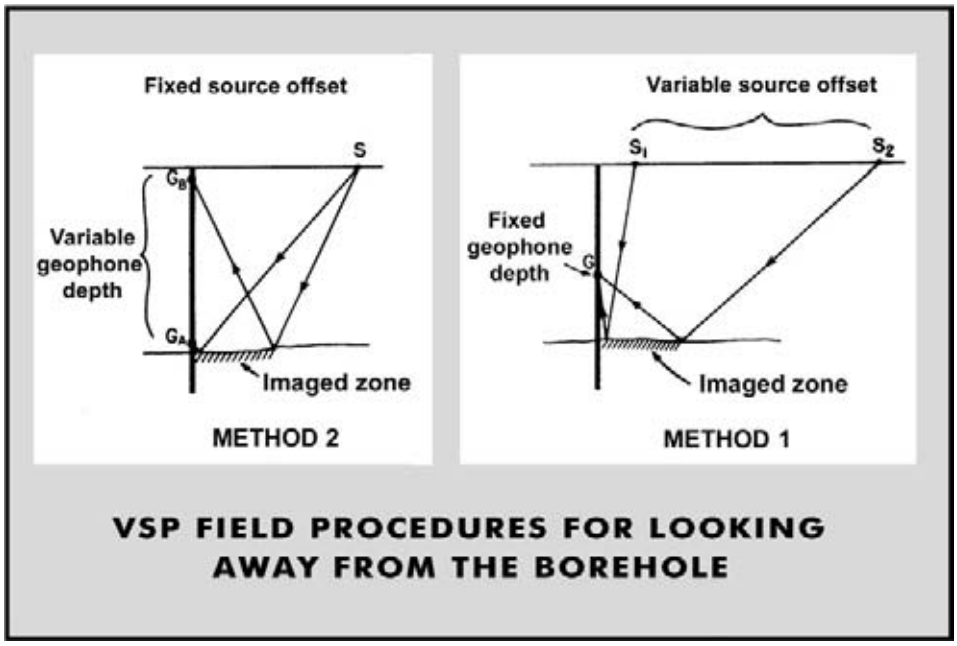

Figure 3.55: Geometrical set-up of a VSP acquisition to look away from the borehole. Contrary to a checkshot survey now the wavefield is considered and not only the first arrival times. Special processing is needed to separate down-going from up-coming energy (after Hardage 1985, reprint from AAPG whose permission is required for further use).

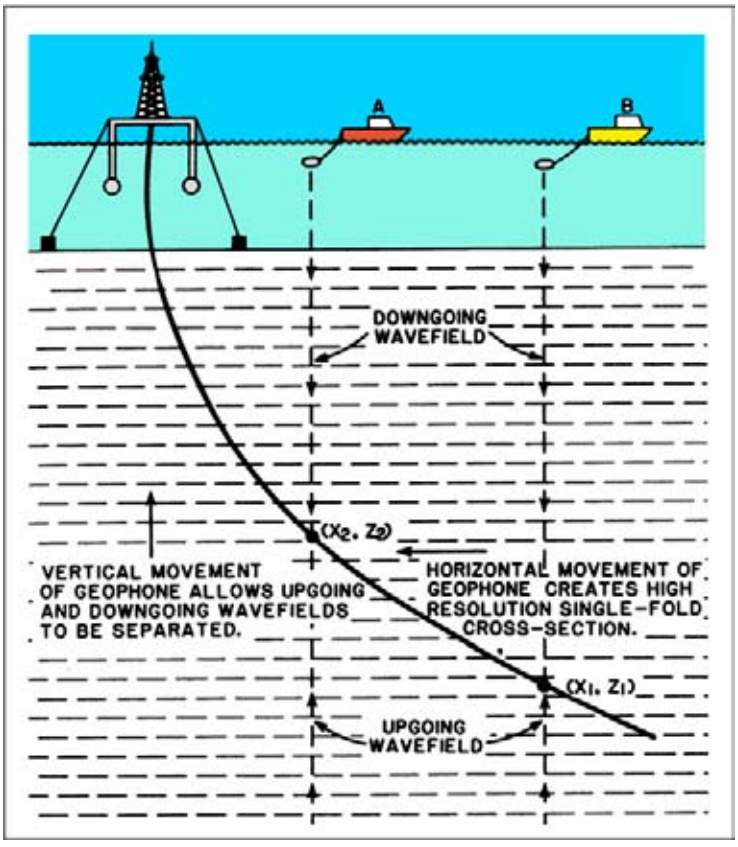

Figure 3.56: VSP acquisition in a deviated offshore well (after Hardage 1985, reprint from AAPG whose permission is required for further use).

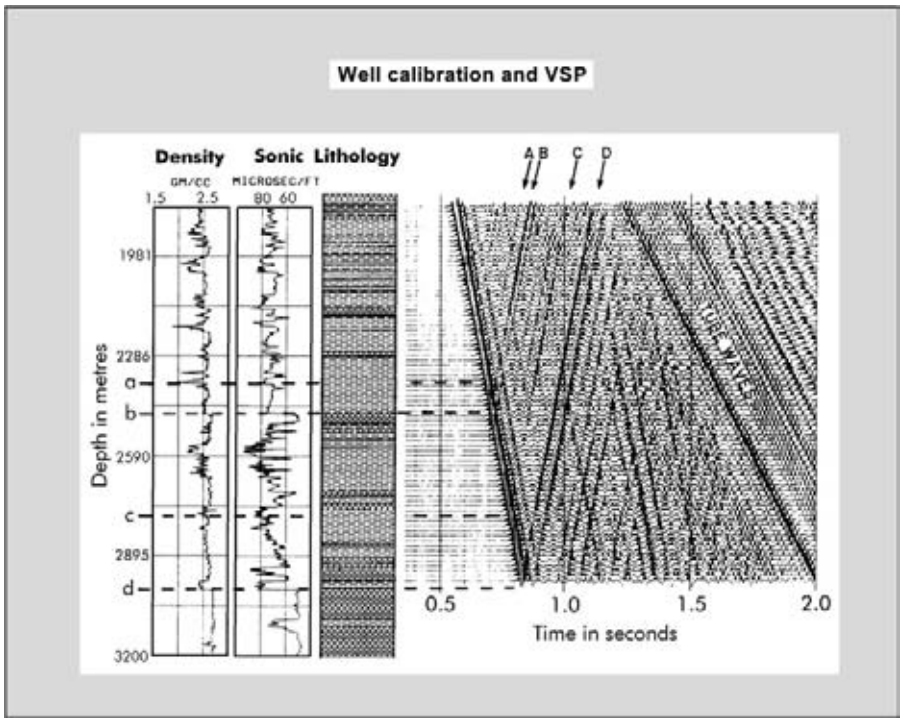

Figure 3.57: Well control and VSP data. The traces are not yet corrected for the uphole time. The downgoing and upcoming energy is clearly seen as data with different dip directions in the time plot. The position of the markers is indicated on the depth and time scales. On the VSP it corresponds with the intersection of the reflection with the first arrival energy (after Hardage 1985, reprint from AAPG whose permission is required for further use).

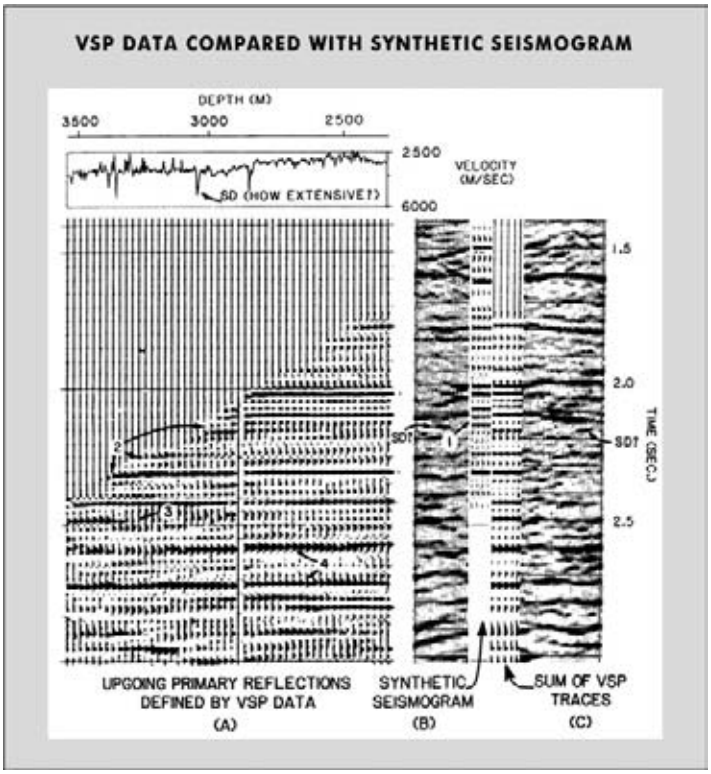

Figure 3.58: VSP and synthetic seismogram display for comparison of their resolution. The upgoing waves are separated from the downgoing waves by FK or velocity filtering. The VSP trace (or corridor stack) has a frequency contents that is better comparable to the surface seismic dataset (after Hardage 1985, reprint from AAPG whose permission is required for further use).

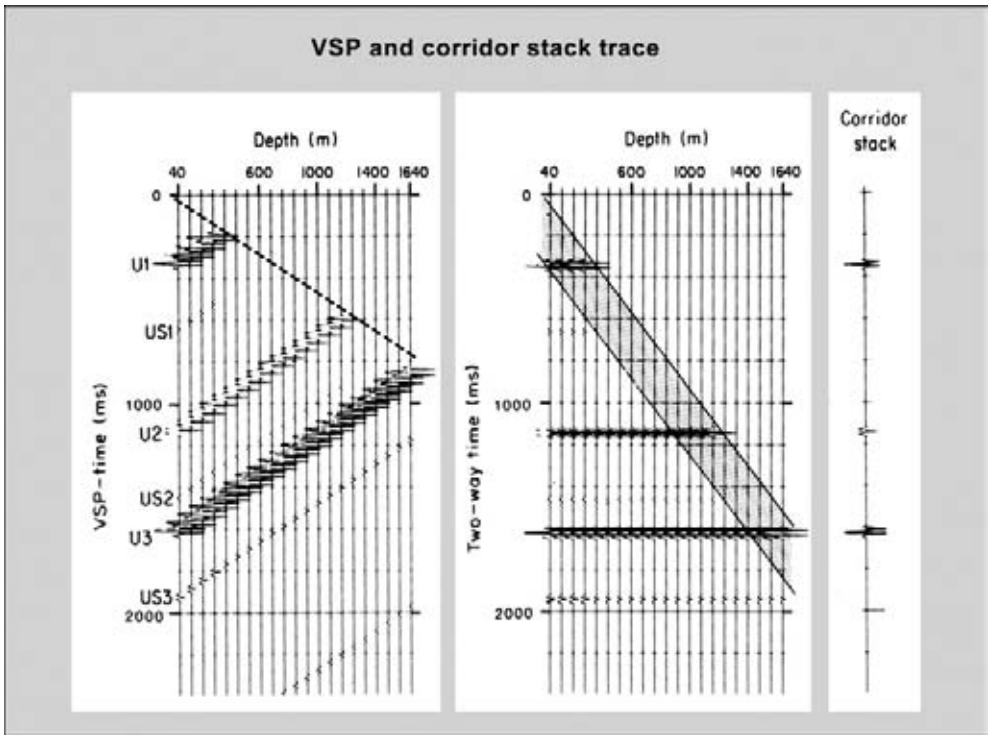

Figure 3.59: Procedure to calculate the corridor stack trace. On the VSP the downgoing energy is removed by F-K filtering. Each trace is shifted by the uphole time to simulate the recording surface and this procedure flattens the primary reflections U1, U2 and U3. A stacked synthetic trace is obtained by stacking of the energy contained in the shaded corridor. The multiple energy US1, US2 and US3 is suppressed and better synthetic trace is obtained. The near offset response if in general less noisy than the further offset traces (after Kearey and Brooks 1991).

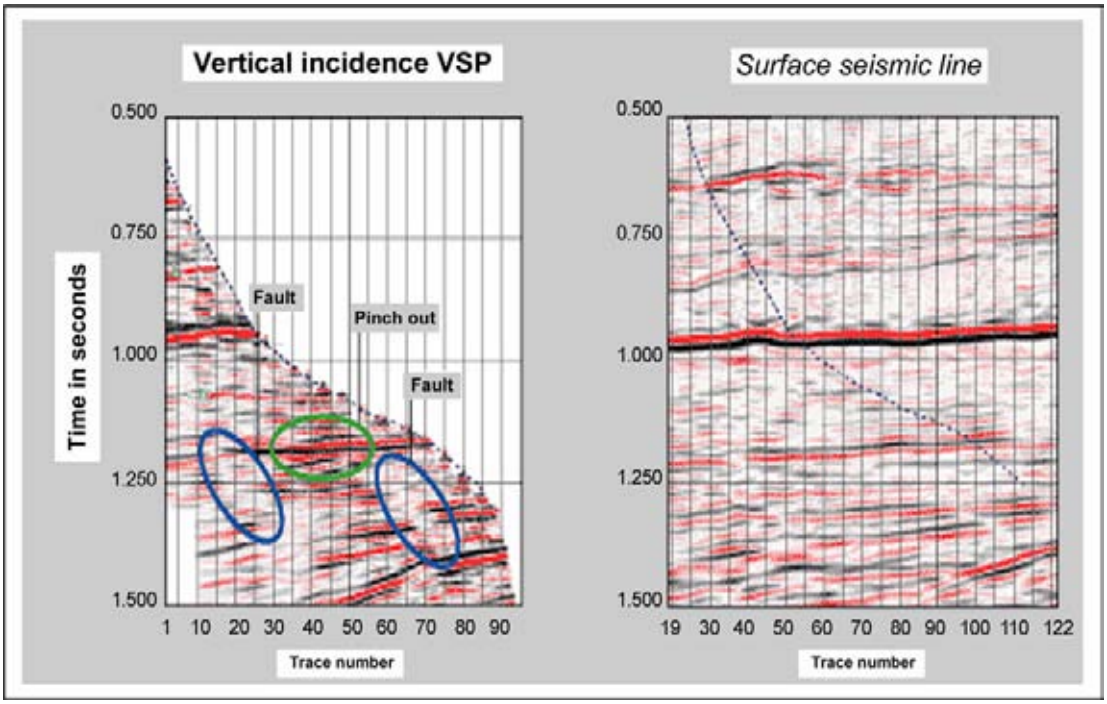

Figure 3.60: A VSP survey for a deviated well. The trajectory is plotted on the conventional seismic section plotted at the right-hand side. The VSP shows details like faults and pinch outs that can be important from a reservoir development point of view (used with permission of copyright holder Schlumberger Ltd).

ogy in the immediate surrounding of the borehole. The processing of the VSP data results in a single trace that can be directly compared with the seismic trace at the well location. The **VSP trace** is better comparable with the actual seismic data than the conventional synthetic seismograms that are described below. It gives a more reliable tie for the well data (Figure 3.58). The data around the first break time is less influenced by multiple energy and is utilised to compiled a **corridor stack** (Figure 3.59). This is a composite trace using segments of the processed VSP data with selected offset ranges for different time intervals. This corridor stack is straightaway comparable with the seismic response, recorded from the surface.

A word of caution on verticalised well trajectories. The exact intersection for the well match is given by the well 3D trajectory. If the 3D trajectory is verticalised (projected to the vertical), then the intersection point is no longer the same and the geology might change considerably. This is particularly true when dealing with structural/depositional dip and lateral changes in lithofacies (e.g. channel sands pinchout). The full use of the 3D well trajectory, with a detailed accurate tie-in for depth and time domains, is nowadays becoming more and more common practice in the integrated seismic workstation environment (Figure 3.60).

3.4.3 Synthetic seismogram

In order to tie-in the well results, it is customary to compile a so-called **synthetic seismogram** or trace (Figure 3.61). The basic input is formed by:

- A sonic log.
- A density log.
- A checkshot survey or VSP.
- A seismic wavelet.

The integrated sonic log, calibrated with the checkshots, allows for time conversion of the well data. A T–Z graph is normally constructed for this purpose. The time axis is usually one way travel time, but also two way travel time can be applied if the right correction is made. A velocity log can be computed from the sonic log, which measures transit times (DT). The sonic velocity is given by:

$$\text{Sonic velocity} = (1/\text{DT})\,304800. \qquad (3.1)$$

The velocity is multiplied by the density to generate an acoustic impedance log. The AI contrast at each sampling point is computed and a spikey reflectivity trace is obtained. The reflectivity trace is subsequently convolved with a seismic wavelet and a synthetic trace is created. This trace is compared to the seismic traces on the seismic sections through the well. For this purpose the same synthetic trace is usually repeated four or five times in the display. It is then overlaid or split-in with the seismic data at the well location. In case of deviated holes the synthetic trace is plotted along the curved well trajectory. Intersection points of the various markers are plotted along this curved trajectory.

Well logs are normally measured along hole from the **Kelly Bushing** (KB). The kelly is the edged drill pipe that rotates the drilling string. The kelly bushing is the box that guides the kelly on its way down the hole. It is set on the rotary table, which is the workfloor where the tool pusher and rough necks manipulate the drill pipes. This is also known as the **derrick floor**. Below the rotary table are located the **Blow-Out Preventers** (BOP), which are big valves controlling the access to the bottom of the well trajectory. This tubing assembly is also known as the **Xmas tree** (Figure 3.62). The well location has a certain topographic elevation with respect to the main sealevel or a local reference datum plane. It has a waterdepth if located offshore. The measured depth is usually referenced:

- Along hole depth below kelly bushing.
- Along hole depth below mean sealevel.
- True vertical depth sub sea.

There is also a difference between driller's depth (the amount of steel piping screwed on top of each other) and the logger's depth (who uses a steel cable to lower his logging tool). Both are measured from the kelly bushing. The logger's depth includes a cable stretch effect of several meters for a 3000 m deep hole. The Total Depth or TD according to the drillers and the loggers depth shows a discrepancy because:

- Cable stretch effect.
- The logging combo's have a certain length.
- The hole conditions at the bottom of the well are frequently bad.

The seismic data has usually the mean sealevel reference as T-zero level. It is necessary to make the right correction for the differences in reference level before comparing the well logs and the seismics (Figure 3.63). If this is not done, it will result in an additional bulk time shift for the synthetic trace.

On the synthetic seismogram the position of various biozones, stratigraphic markers and other relevant well information is precisely known and hence a reliable match is made. It often happens that the match is not perfect.

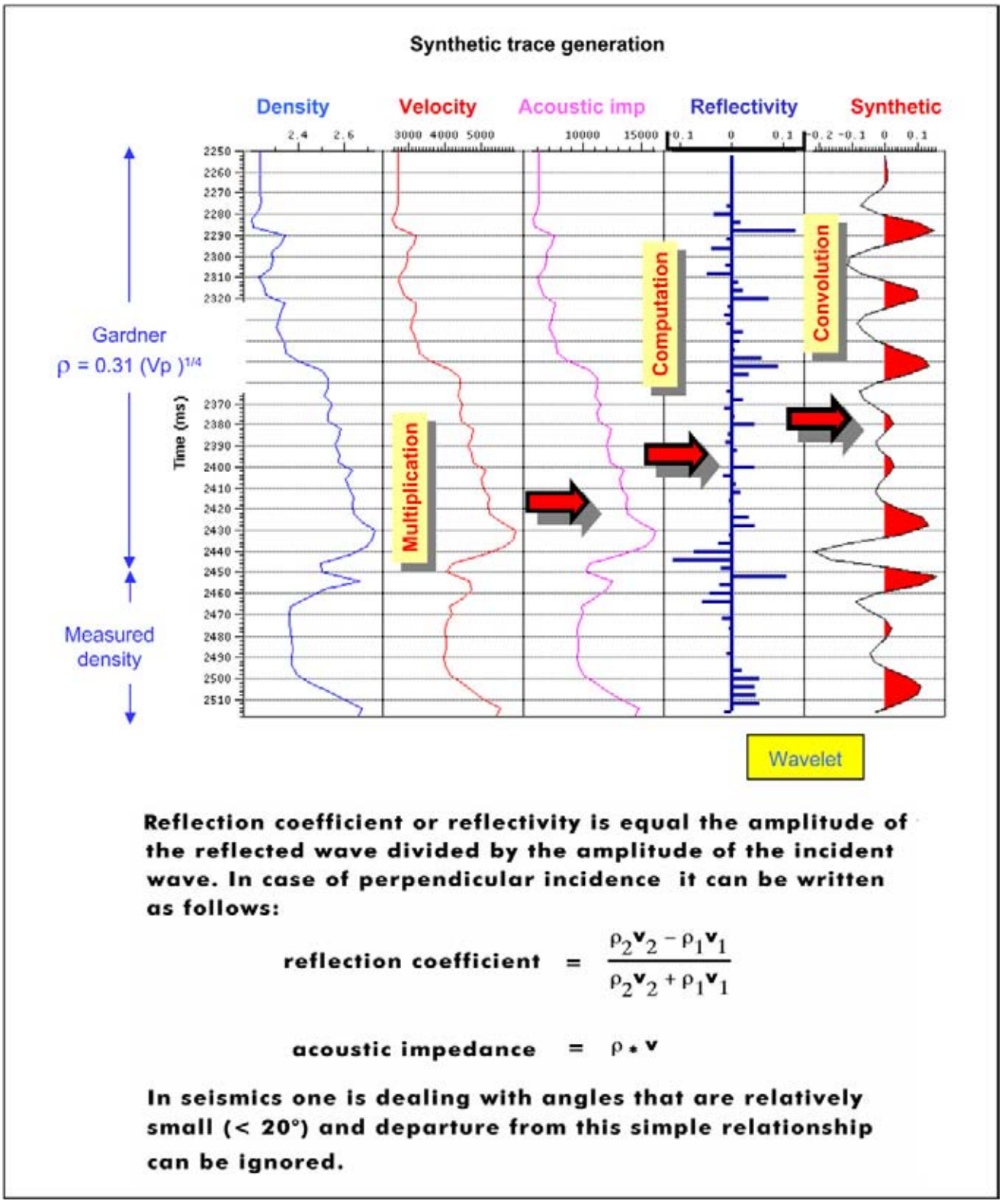

Figure 3.61: Synthetic trace construction method. The acoustic impedance is calculated by simple multiplication of the density and velocity curves. Subsequently the reflection coefficients are computed and convolved with a seismic wavelet to obtain the synthetic trace on the right. Blocking of the sonic log does reduce the frequency contents and creates often a better match with the low frequent seismic response. The Gardner formula RHOB $= 0.31(V_{\mathrm{p}})^{1/4}$ allows to estimate the density value from the P-wave velocity log. The Faust relationship $V_{\mathrm{p}} = 2000(\text{resistivity} \cdot Z)^{1/6}$ can be used to compute the velocity from the resistivity log.

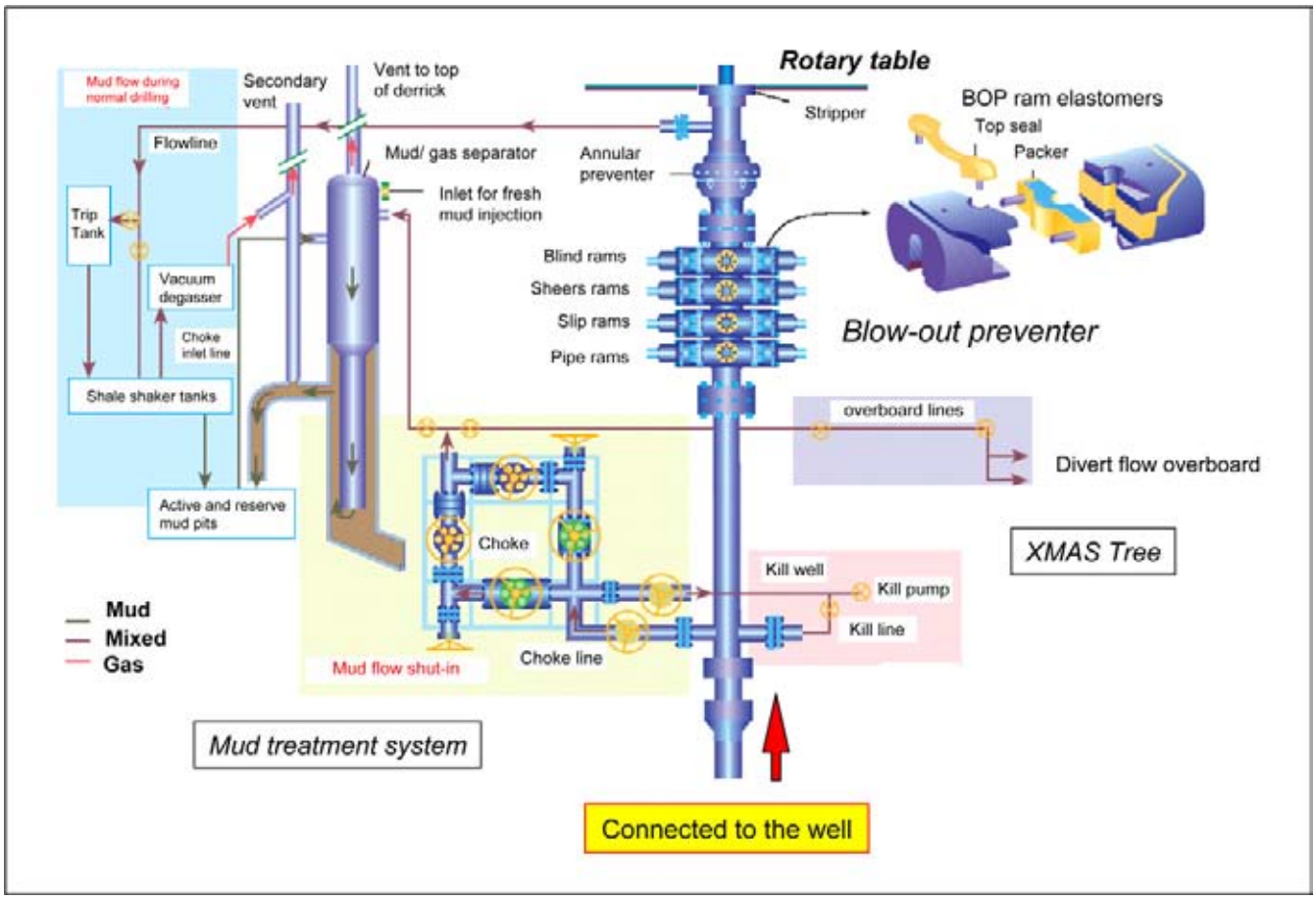

Figure 3.62: The layout of the tubing at the well head (Xmas tree). The drill mud is controlling the pressure in the well and takes care of the transport of the formation debris whilst drilling. Two circulation systems are here shown. The Blow-Out Preventer is a system of safety valves that shut-in automatically when a certain pressure level is reached. The rotary table and more precisely the kelly bushing (physical opening of the well hole on the derrick floor) are often used as depth reference datum planes (modified after MacAndrew et al. 1993).

Discrepancies between the sonic and checkshots have been investigated by Goetz and Dupal (1979). The bad fit is often caused by:

- The well logs are not measuring the same rock volume as the seismics. The well is always a point calibration, while the seismic method tends to average the data stemming from a much wider area.
- No proper editing of the logs before compiling the synthetics.
- The shape of the seismic wavelet can be deformed, if the deconvolution has not been done correctly.
- Multiple energy is present in the real data that has not been modelled in the synthetic trace.
- Wave mode conversion at the reflective interfaces is not taken into account. Elastic modelling might give here a better solution (see below).
- Also the frequency contents of the measurements differ considerably. The sonic log contains a much higher frequent velocity spectrum than the seismic data. It is for this reason that sometimes the sonic log and density logs are smoothed before compiling the synthetic seismogram. The vertical resampling of the logs already represents a sort of a smoothing operation. Of course the subtle differences over the reservoir intervals should not be destroyed by this procedure, else wise other techniques like inversion and AVO will have a hard time to do their job properly.

Blocking of the sonic log, prior to the synthetic computation, gives many times a better match with the real seismic data. Blocking is required for some of reservoir modelling packages in order to be able to perform fluid substitution. Smoothing is very effective to reduce the higher frequent variation of the log response, but it is also a dangerous operation. Care should be taken not to loose the main reservoir features on the logs.

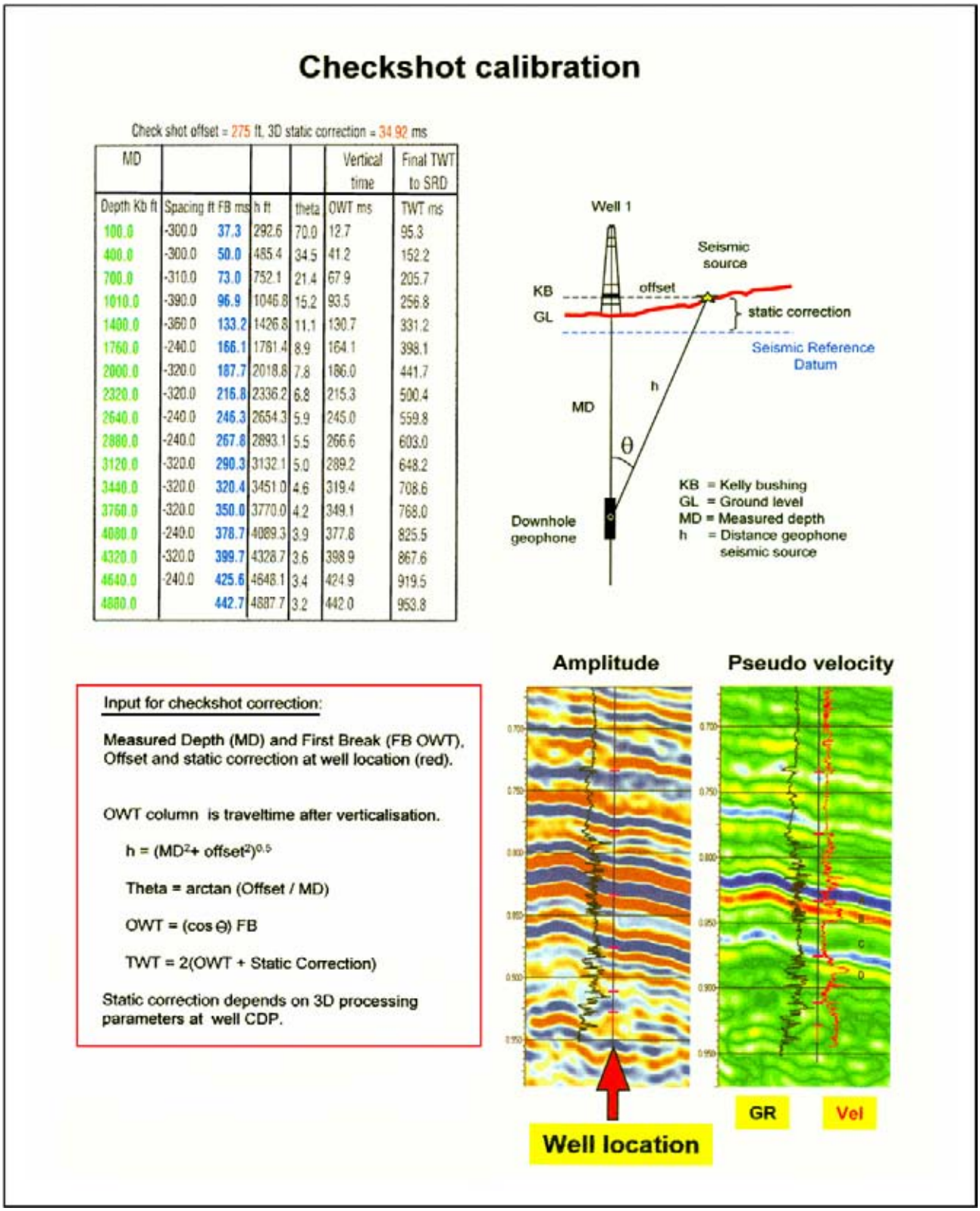

Figure 3.63: A method to correct the checkshot calibration. The static correction is survey dependent. It takes into account the geometry of the shot in respect to the geophone position and the used reference levels. Determination of a bulk time shift for the well logs is here achieved by computation of a pseudo velocity cube (modified after Linari 2004).

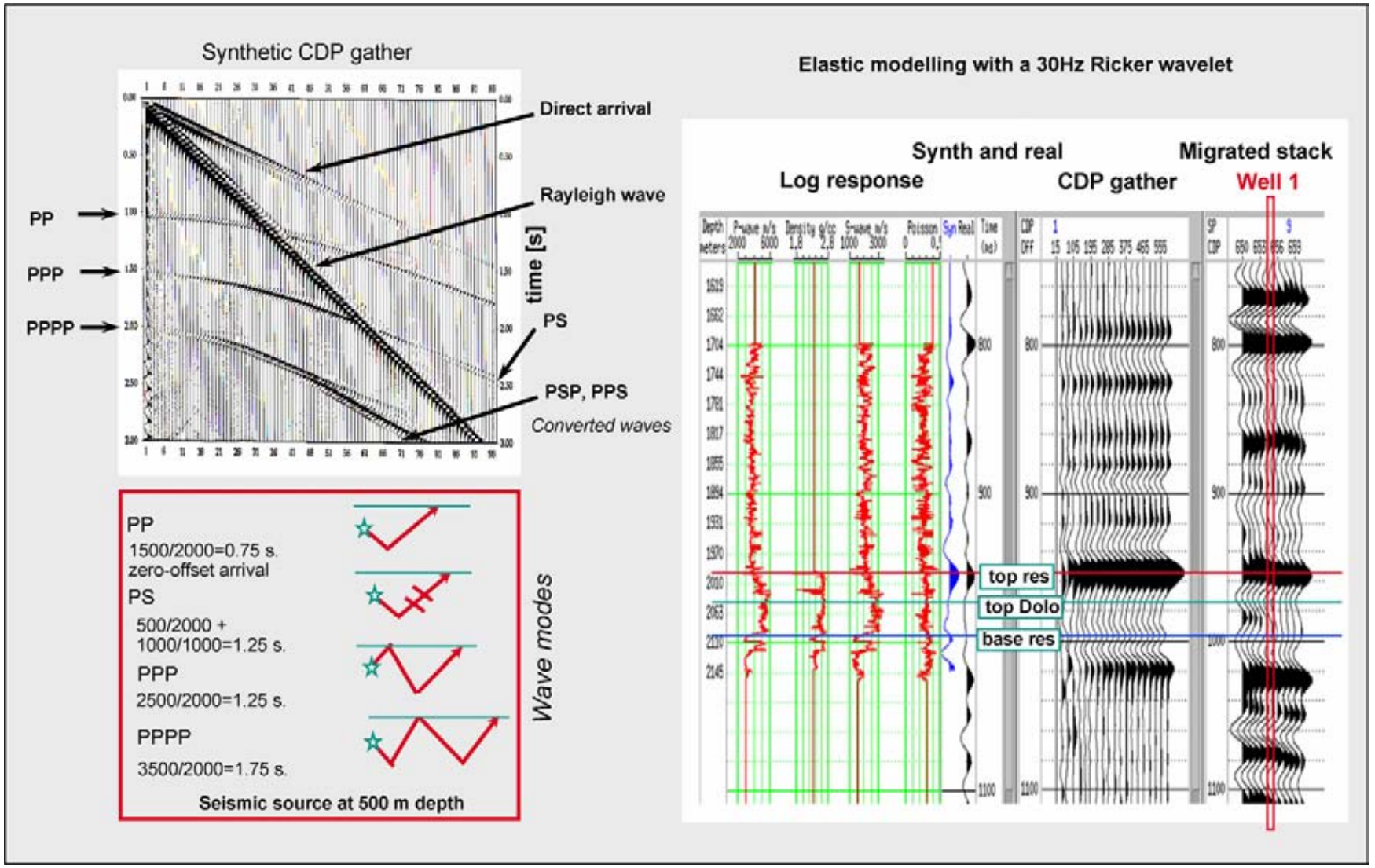

Figure 3.64: Elastic modelling of well logs takes into account the response of P- and S-waves. It uses the full set of Zoeppritz equations to generate the expected seismic response. Converted waves are considered and also multiples are simulated (courtesy TotalElfFina and Solegeo).

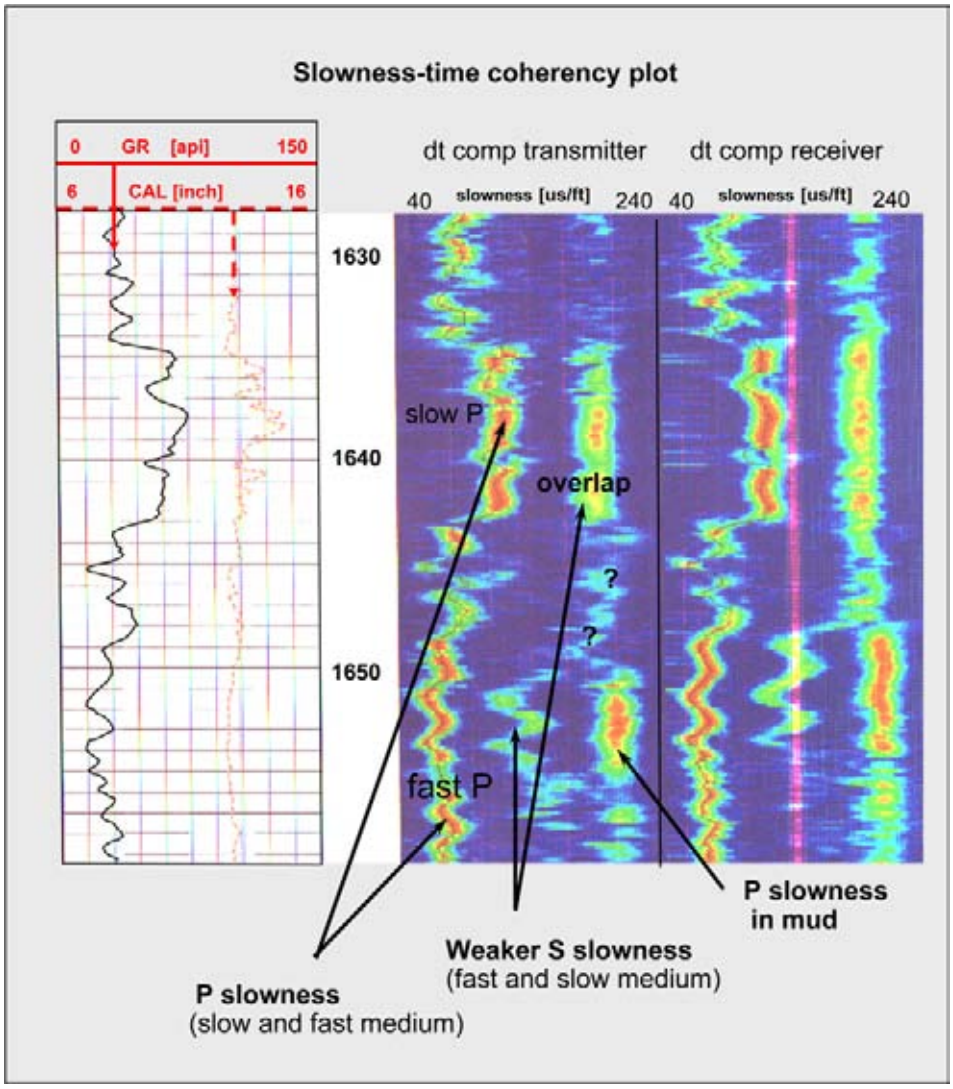

Figure 3.65: The measurements of the shear sonic with the Dipole Sonic Imager (DSI tool^{TM}) are summarised in a slowness-time coherency plot. The velocity determination has an uncertainty attached to it. The S-wave energy is often rather poor in specific zones and the velocity pick is then not so straightforward (courtesy TotalElfFina and Solegeo).

If no satisfactory well-to-seismic match is obtained, than elastic modelling can be considered for generating the synthetic response. Elastic modelling takes into account the effects of wave mode conversions at the reflection interface and does not restrict itself to only P-wave energy (Figure 3.64). The behaviour of the P and S-waves are assessed in such approach. The S-wave information is coming from the shear sonic or DSI tool (dipole shear wave imager), that measures the slowness of the formation and is usually represented in a time coherency plot (Figure 3.65). Even multiple energy is simulated and incorporated in the end results.

When the sonic log is not available, then a velocity curve is estimated from the resistivity log using the **Faust relation** (Faust 1951, 1953):

$$V_{\mathrm{p}} = 2000\,(\mathrm{resistivity}\cdot z)^{0.166666}. \qquad (3.2)$$

A correction should be made when gas is present in the reservoir.

Subsequently the density is estimated from the velocity curve using **Gardner's relation** (Gardner et al. 1974):

$$\mathrm{Density} = 0.31(\mathrm{velocity}_{\mathrm{Pwave}})^{1/4}. \qquad (3.3)$$

The 0.31 value is a general value for all sort of lithologies. This is a rather rough estimate and certainly not very accurate. The trends are in fact lithology dependent. The gamma ray can be used as a shale cut-off. In some cases the interpreter gets away with it, but discrepancies in the well tie may be introduced by this

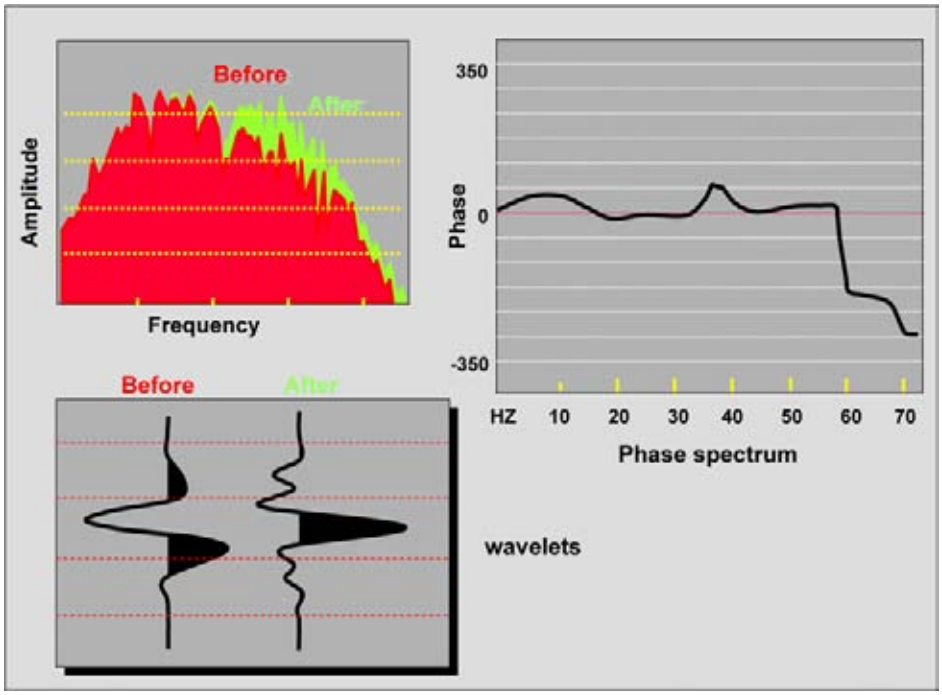

Figure 3.66: Amplitude and phase spectra computed for a seismic survey via the Fourier transform. The difference in amplitude spectra is shown before and after applying a phase rotation. This phase rotation of the seismic ensures a better match in the zone of interest. The zerophase aspect is maintained up to 60 Hz. Two wavelets have been computed; the last one is much better zerophase in character.

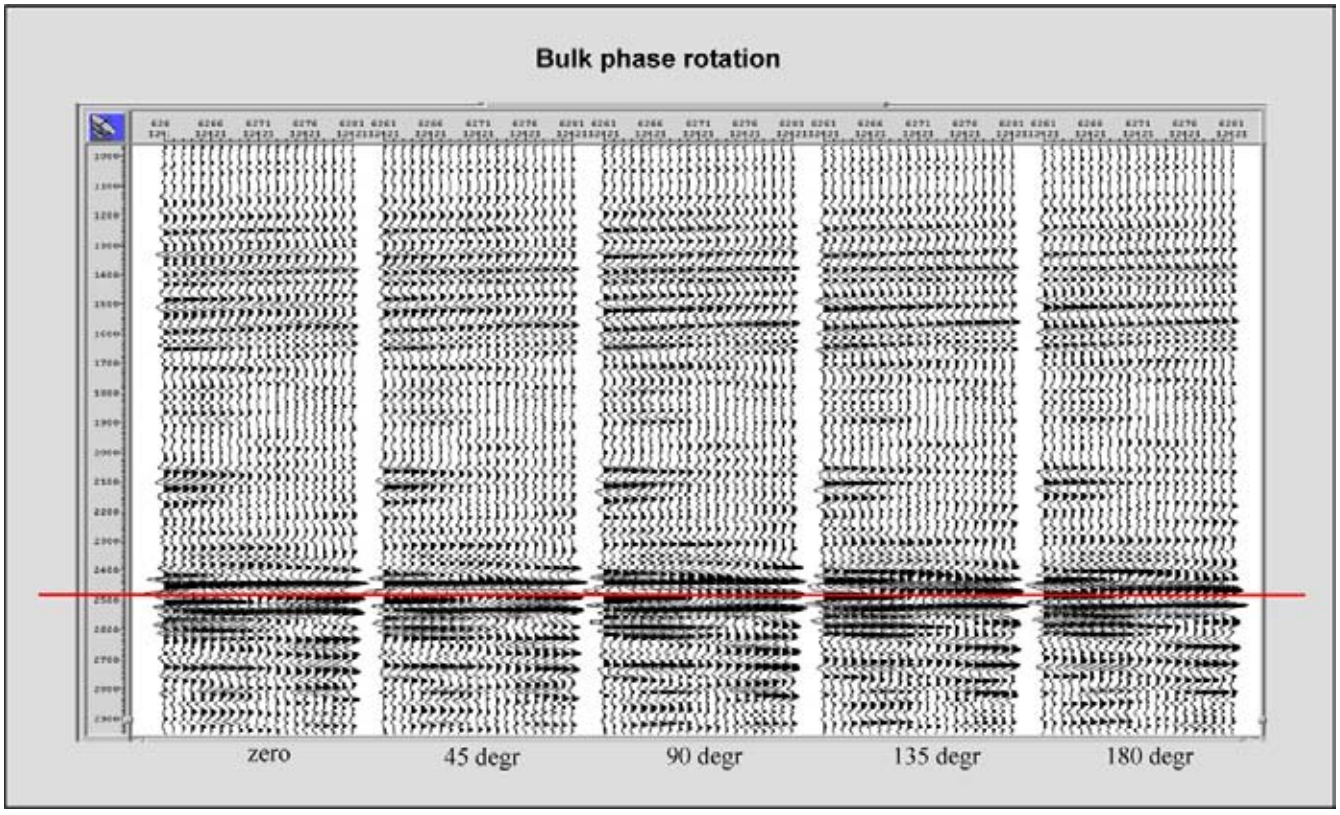

Figure 3.67: Bulk phase rotation of the seismic data does leave geometry of seismic reflections untouched, but changes the amplitude values in a systematic way. A 180 degree phase shift leads to an opposite polarity.

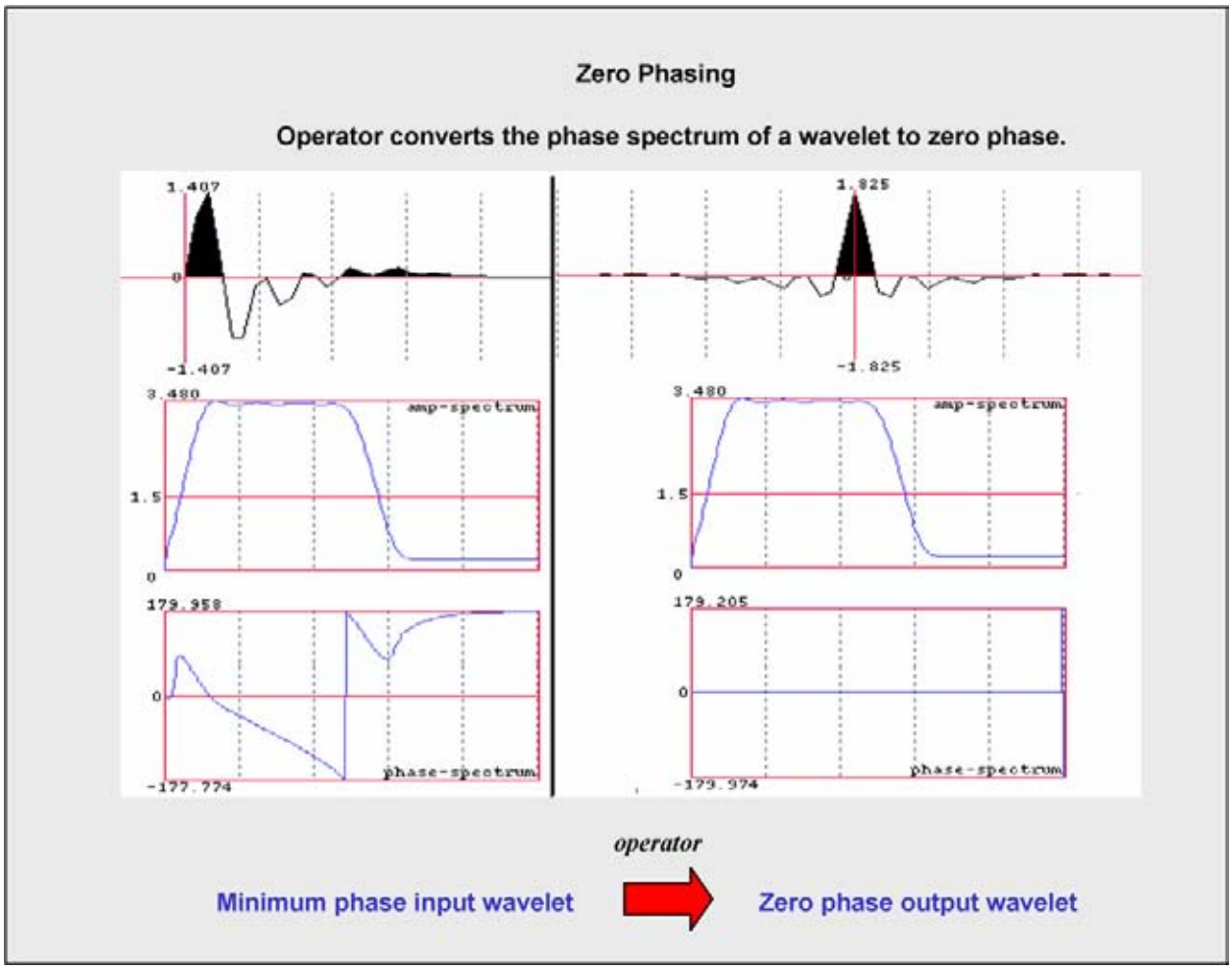

Figure 3.68: Zerophasing operator that converts the seismic cube within a certain time interval to a near zerophase mode.

procedure. If the lithologies are known, than a more adequate function is proposed by Castagna and Bachus (1993).

The acoustic impedance or AI response at the well is calculated by applying a simple multiplication:

$$\mathrm{AI} = \mathrm{density} \cdot \mathrm{velocity}. \tag{3.4}$$

From this the reflectivity is computed for each depth or time sample:

$$\mathrm{Refl} = \frac{\mathrm{AI}_2 - \mathrm{AI}_1}{\mathrm{AI}_2 + \mathrm{AI}_1}. \tag{3.5}$$

This reflectivity is convolved with the seismic wavelet to obtain the synthetic trace.

3.4.4 Seismic phase rotation and zerophasing

In order to make a good seismic-to-well tie, it is also possible to apply a phase rotation to seismic. This is done because the seismic is not always zerophase over the zone of interest. For determining the phase rotation of the seismic trace, it is necessary to perform a Fourier Transform (FT) whereby the data is taken into the frequency domain. The seismic trace is decomposed into its periodic sine wave representation. Each frequency has a certain amplitude and phase assigned. The phase of each individual sine wave is computed at the $T = 0$ sample. The results of the FT is visualised in the amplitude and phase spectra (Figure 3.66).

It is possible to apply a bulk rotation on the phase of these individual frequencies. This bulk phase rotation does not change the shape of the seismic trace, but it optimises the match with the synthetic trace. The time position of the reflections is respected, but their phase is altered (Figure 3.67). The phase rotation is calculated in the matching procedure between the synthetic and seismic trace via cross correlation techniques (e.g. Veeken et al. 2002a; Figures 3.68 and 3.69). The **cross correlation function** is constructed by sliding one of the traces

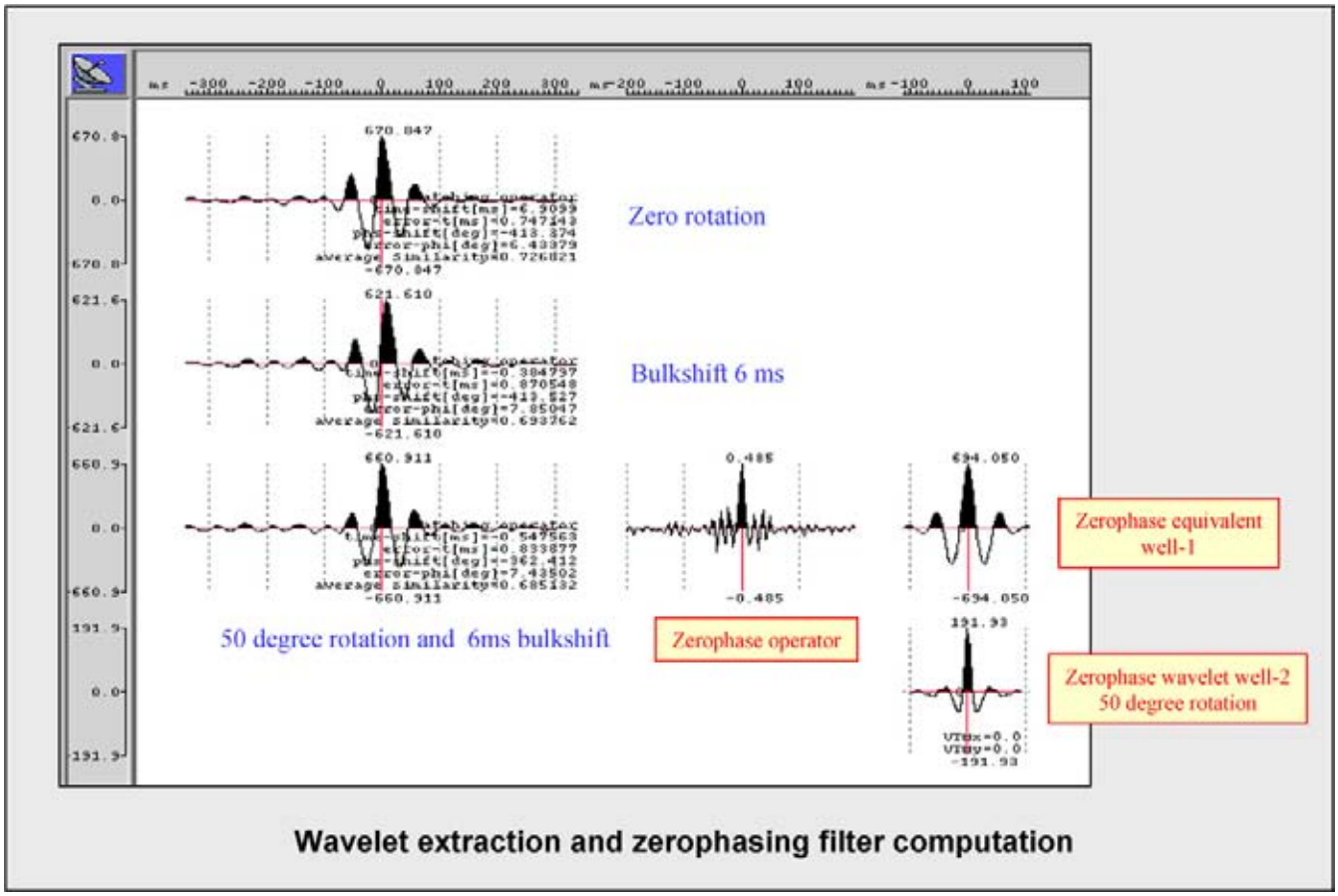

Figure 3.69: Example for wavelet extraction and computation of zerophasing operator. The matching operation permits to exact a wavelet via cross correlation procedures. An other method is to apply the least square filtering technique between the reflectivity trace and the real seismic trace.

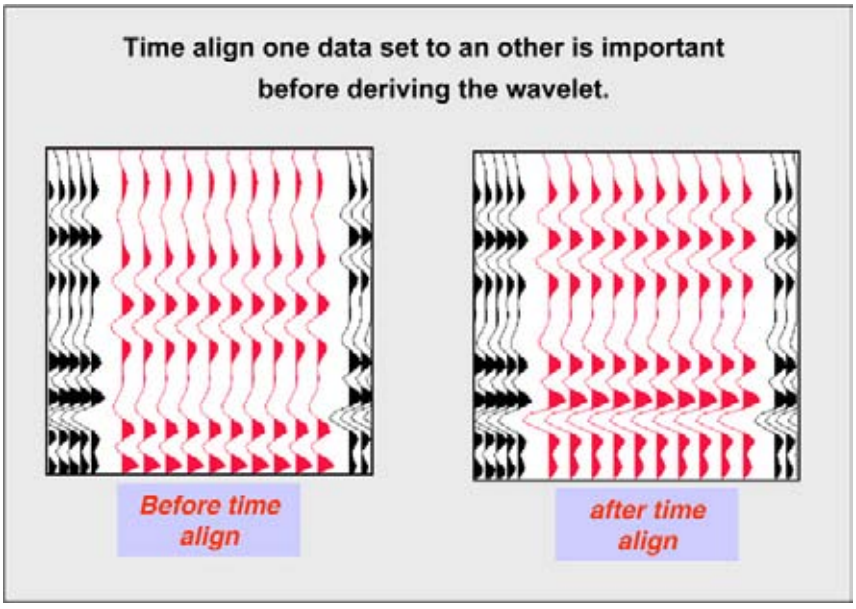

Figure 3.70: Bulk time shift is important to establish the right match between the synthetic and the seismic cube. Errors in this time shift has a major impact on the calculated phase rotation in matching operation and the wavelet extraction.

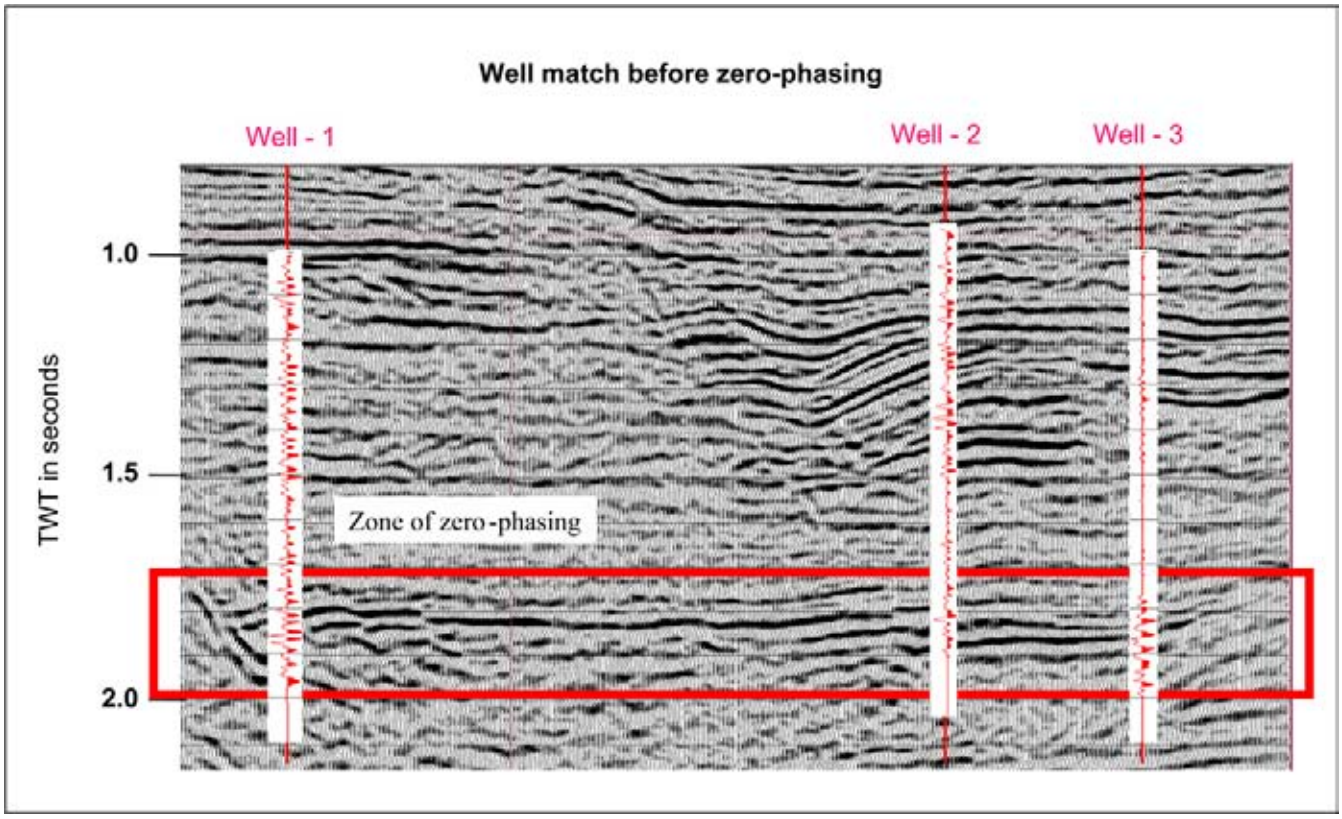

Figure 3.71: Match between synthetic trace and unrotated original seismic cube (M. Da Silva, courtesy Pemex).

along the other in regular vertical steps or lags. At each step the function is computed by cross-multiplication of the aligned time sample values and their subsequent addition. This is quite similar to the digital convolution procedure, whereby one of the traces is time inverted and then slided along the other. The cross correlation technique is to discriminate between random noise and signal (Dash and Obaidullah 1970). It is also possible to design a shaping filter (or Wiener filter) between the reflectivity and the seismic trace to extract a wavelet (cf Pendrel and Van Riel 1997, 2000).

In the matching procedure the best fit is established together with the bulk timeshift; the optimal uniform phase rotation is computed. The bulk phase rotation affects all the frequencies in a similar way. The bulk time shift should be applied before the final phase rotation is determined (Figure 3.70). In practice it means that at least two well match procedures have to be run before the seismic wavelet is extracted. The wavelet estimation is however only valid in the computation window (Figures 3.71, 3.72 and 3.73). The best wavelet determination is normally done in a small time window (<1 sec TWT). Too small a window does not resolve the low frequency spectrum and this introduces unnecessary errors. The optimal phase rotation should give a better cross correlation function output, that is more zerophase in shape. From this output two functions are derived:

- A '**minus phase only**' **operator**, valid for the time interval under investigation, that contains only info on the phase and does not alter the amplitude spectrum of the seismic. This operator is convolved with the seismic data to obtain a zerophase seismic cube over the interval of interest (Figure 3.74).
- A '**zerophase equivalent**' **wavelet**, suitable for the deconvolution of the zerophased seismic cube (see also Section 2.7 above). This wavelet is also input for seismic inversion processing.

A multiwell approach will yield an average wavelet that is less influenced by the presence of local noise and more representative for the target interval (cf Lucet et al. 2002).

The input for seismic inversion should be zerophase over the target interval. This zerophase requirement is hard to achieve with the bulk rotation method described above. Mostly there exist a residual phase rotation for the data. A 30 degree rotation is hardly visible on the seismic trace with the bare eye and therefore a smaller residual phase rotation can be safely ignored.

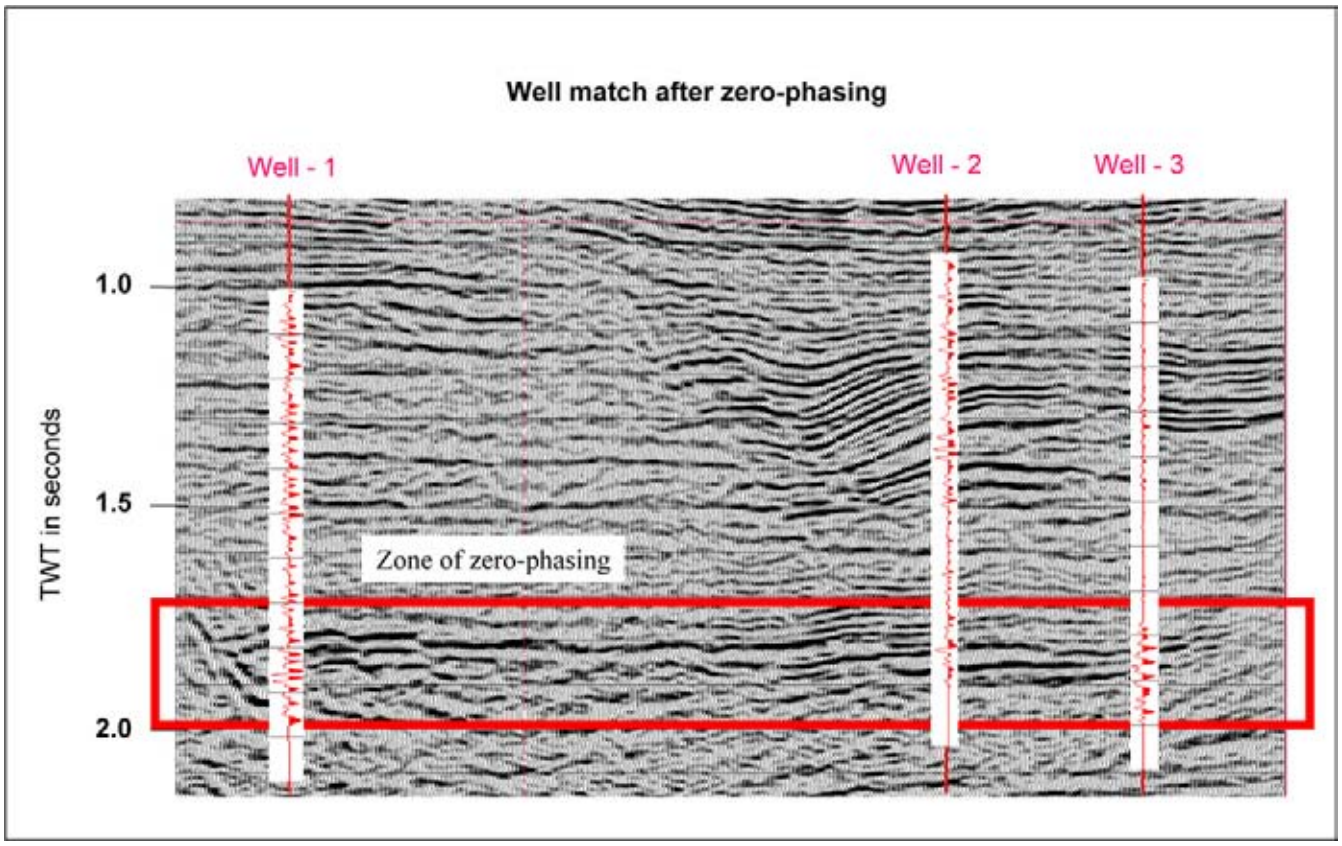

Figure 3.72: Match of synthetic traces shown in previous figure with the now rotated and zerophased seismic cube. The zerophase condition is only valid in the red inset time window (M. Da Silva, courtesy Pemex).

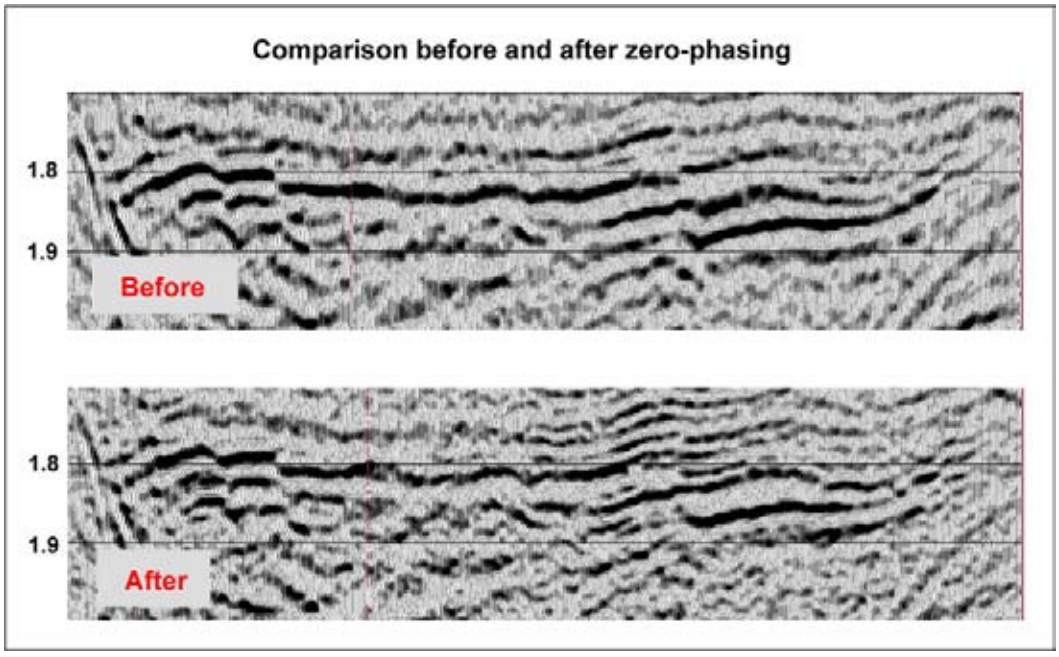

Figure 3.73: Blow-up of seismic section from previous figure, before and after the phase rotation (M. Da Silva, courtesy Pemex).

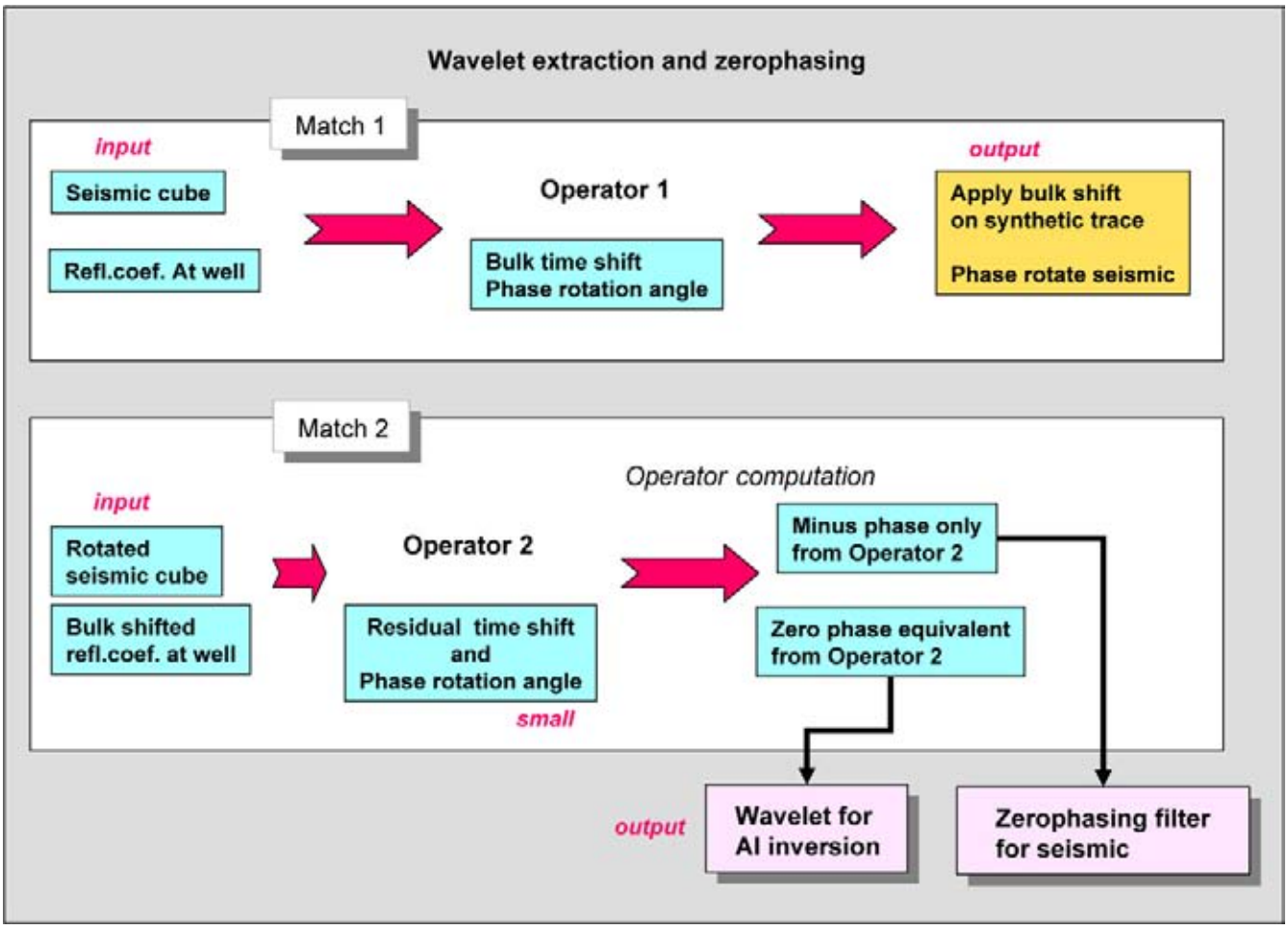

Figure 3.74: Summary of zerophasing and wavelet extraction procedures.

In some PC-based seismic workstations the wavelet is derived by considering the frequency spectrum of the seismic dataset. A wavelet is computed that corresponds directly with this spectrum. Per definition it is zerophase in shape. The synthetic trace looks great, but the reliability is of course limited.

The interpreter should realise that for each new version of a seismic dataset it is necessary to make a new well-to-seismic tie with a new bulkshift and phase rotation. Also a new synthetic trace needs to be calculated because the wavelet is no longer the same. This is an important issue when time-lapse or 4D processing is done. Because the seismic wavelet changes with depth, it does not make much sense to check the zerophasiness of a dataset by investigating only the character of the seabottom reflection as suggested by Brown (1999). It is better to study the character of a known fluid contact or the DHI flat spot in the target reservoir, if there exists any.

Some workers use the instantaneous phase behaviour to estimate the phase rotation of the wavelet (Perz et al. 2004). The simple technique helps in detecting lateral wavelet instabilities. The method uses a regional isolated and stable seismic event to compute the instantaneous phase at the peak of the instantaneous amplitude (envelope) of the associated seismic waveform. Under certain restrictive conditions (constant phase box car/bandpass wavelet), this instantaneous phase is equal to the phase rotation of the wavelet.

It is possible to adopt a statistical approach to zerophase the seismic subcube. The seismic traces themselves are compared with auto correlation techniques to derive a wavelet. In this approach it is feasible to alter the phase of individual frequencies. This type of rotation has however an impact on the shape of the seismic wiggles. There is a danger that reflections are 'created' by this statistical procedure. If these 'artificial' reflections correspond with the response seen on the synthetic trace, then the match will improve; but it also implies

that the amplitudes have been altered in a less desirable way. It is still a hot debate among specialists to what extend this approach can be extrapolated outside the well control. Applying it rigorously over a larger survey area, is a questionable act to say the least. These type of alterations of the character of the original seismic cube have a serious impact on the results of seismic inversions and/or amplitude studies. Chapter 6 on reservoir characterisation deals with these aspects in more detail.

3.4.5 Lithofacies calibration

The calibrated well data are correlated with the depositional boundaries and seismic facies units as outlined already on the sections. Important changes on the logs may or may not correspond to Depositional Sequence boundaries and individual system tracts. It all depends on the resolution of the seismic data and the input signal. Normally there is a reasonable correspondence between the boundaries and the breaks on the logs. If not, then the cause of the discrepancy should be investigated (e.g. wrong well location, wrong TZ curve, wrong well trajectory, wrong logs, etc.).

The seismic subdivision allows to distinguish genetically related deposits in the various wells and provides a means to correlate these over larger areas. The changes in seismic facies often coincide with gross lithological changes. Nevertheless, the opposite is also true: the same seismic facies response may represent different lithofacies units. For instance a low amplitude character can equally be a clean sand package in one place, as well as a shaley interval in an other location. This ambivalent character of the seismic facies concept necessitates the use of other criteria to determine the gross lithological interpretation of the subsurface units. The overall setting of the deposits is often the key for a proper lithological subdivision.

Moreover, the seismic character varies from survey to survey. The same lithofacies unit can have different expressions on seismic lines from different vintages. These surveys are in general processed with other algorithms and the parameters are not the same. The relation between seismic facies and lithofacies is in most situations only relative and it should therefore not be considered as a rigid frame. A more flexible approach, whereby the geometrical relationship is playing an essential role, allows the interpreter to come up with a consistent interpretation, even when dealing with a heterogeneous set of seismic lines (e.g. Veeken 1997).

3.4.6 Age-dating of depositional sequences

The **biostratigraphic datings**, done on the sediments penetrated by the well, calibrate the age of the different depositional sequences (Figure 3.75). The occurrence and duration of a hiatus is thus estimated. The age dating is usually done in a combined bio- and lithostratigraphic way (Figure 3.76). In the hierarchy of layers the notion of a stage is very important. The stage is a chronostratigraphic unit, defined at a certain **type locality** with a section of reference (stratotype) having certain paleontological (fossils and micro-fossils like: foraminfera, nanno-plancton, pollen) and lithological and structural characteristics (Pomerol et al. 2005). The **stratotypes** have to be located in a marine section, in order to best guarantee continuity of sedimentation and a better comparison with other faraway locations. The stratotype of the limits contains the two stages and the interval between is here as short as possible. The resulting stratigraphic subdivision is not perfect and does leave some scope for interpretational adjustments. The majority of the proposed ages result from extrapolation that is more or less justified. Little of the boundaries are solidly calibrated by other agedating techniques (isotope analysis). The boundaries that have been determined are: base of the Cambrian, the limit between the Ordovician and Silurian, the limits of most of the stage in the Silurian and Devonian, the top of the Cretaceous, the top of the Eocene and the limit between the Plio- and Pleistocene. Magnetic polarity reversal are also incorporated in the scheme.

If the biostratigraphic age determinations are contradicting the depositional sequence subdivision, it might indicate that the biostratigraphy is hampered by severe reworking and/or caving, making the results less reliable. **Reworking** is a sedimentation mechanism whereby originally deposited biostratigraphic markers are again transported and laid down in completely different settings within the basinfill. The result is a rather confusing situation for the biostratigrapher: older organisms are incorporated in younger sediments. The transportation itself does however leave its trace (de-colouring, rounded aspect, fracturing) and a good scientist can make out the difference. The biostratigrapher might decide to use other bio-markers, like palynology, to unravel the stratigraphy (Schroeder 1992). **Caving** is the contamination of sampled well data by material stemming from overburden sequences, i.e. material tumbling down the hole. Younger bio-markers are hence found below their real first occurrence in the geological layering.

Different researchers, using various criteria to come up with a stratigraphic subdivision, may have an influence on the obtained age datings. This is clearly not very desirable situation, but it happens.

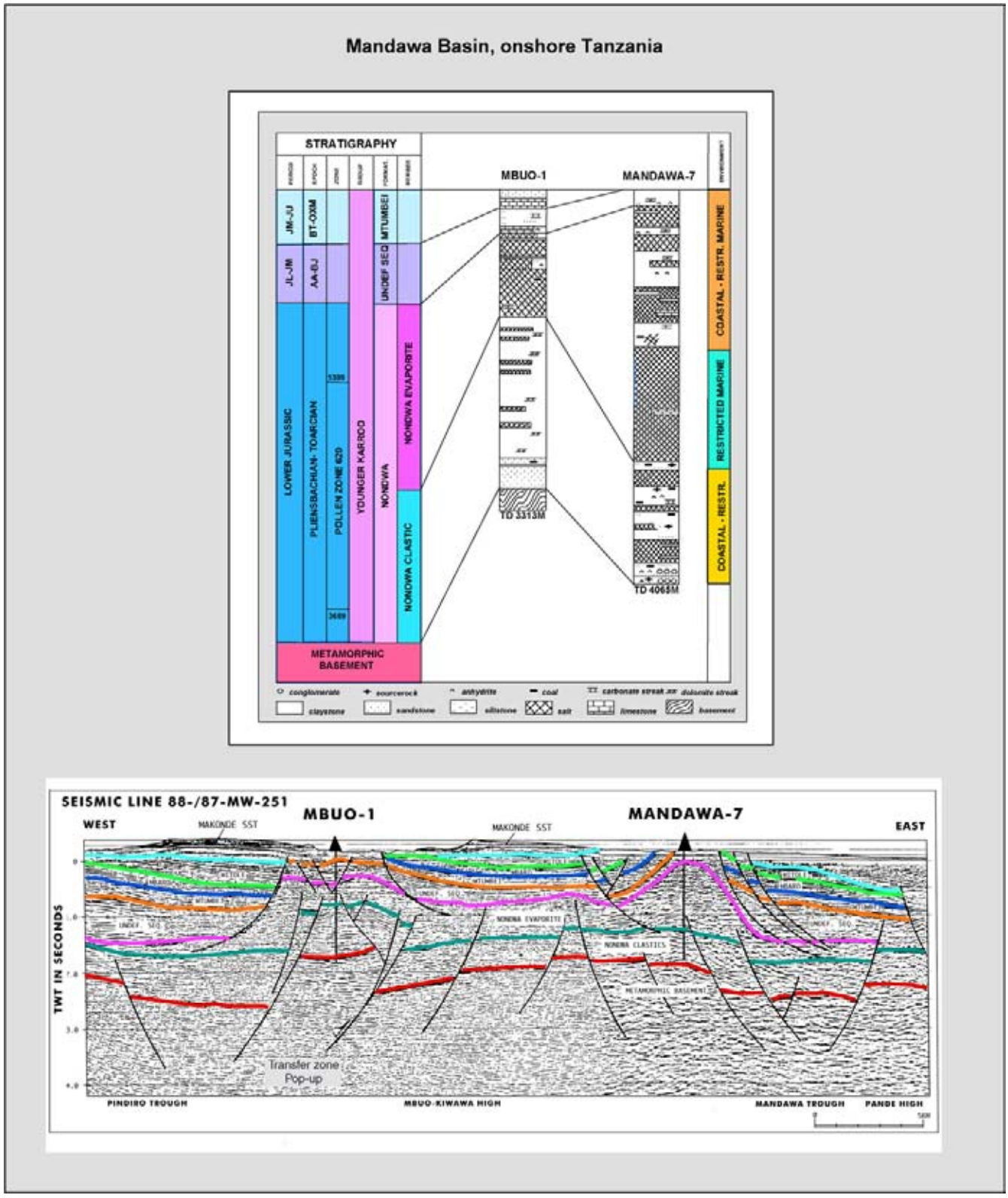

Figure 3.75: Stratigraphic subdivision in two wells from the sedimentary Mandawa Basin (Tanzania) based on biostratigraphic, seismic and lithostratigraphic information. The 2D seismic line below illustrates the structural style of the basin fill. The transfer zone penetrated in the Mbuo-1 well contains sands with hydrocarbon shows directly overlying the basement pop-up block.

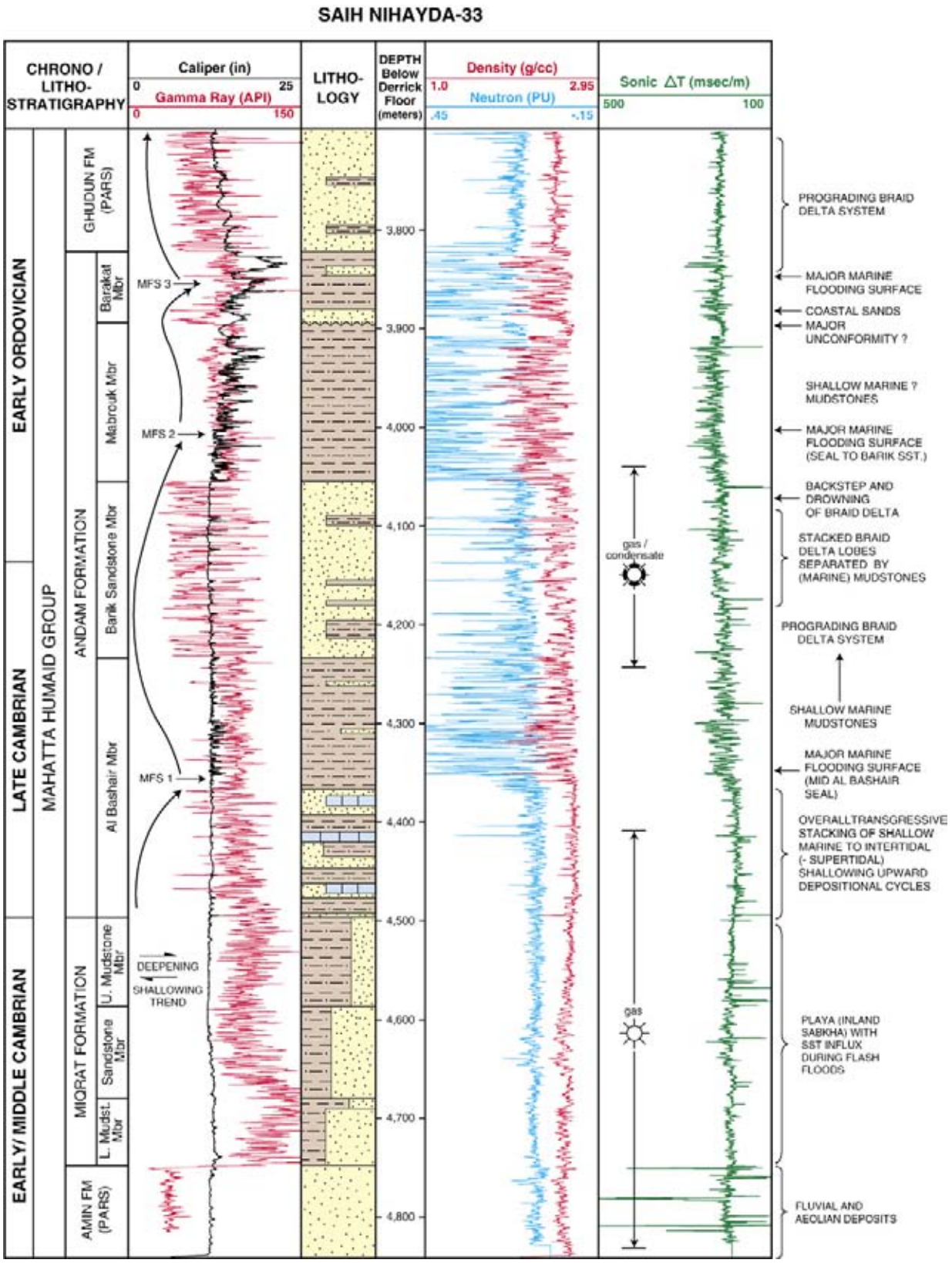

Figure 3.76: Detailed correlations are possible with refined subdivision. Here a well summary sheet is shown with sequence stratigraphic subdivision based on field observations, biozonations, seismic and lithostratigraphic correlations (after Van Buchem et al. 1996). MFS stands for maximum flooding surface, a terminology used in sequence stratigraphic that will be presented later on.

Other dating techniques are helpful to establish a chronological subdivision. **Heavy mineral analysis** for instance is useful to unravel the relative sequence of deposition and changes in provenance (Whitham et al. 2004). Apatite, zircon, tourmaline, rutile are some of the minerals used (Ratcliffe et al. 2004). Various ratios are significant like: K_2O/AL_2O_3, Zr/Al_2O_3, Na_2O/Al_2O_3, TiO_2/Al_2O_3, Rb/Al_2O_3, Nb/Al_2O_3, P_2O_5, Cr/Al_2O_3. The Paleogene submarine deposits in the North Sea Basin show typical heavy mineral assemblies that correspond to drastic changes in the source area with time (Morton 1979 and 1982). It provided basic information to unravel the genetic subdivision of the deposits and the age of various fan lobes. This type of analysis supports the interpretation of geometrical relation as seen on seismic data.

Isotope analysis and age datings from volcanic rocks assist in building a consistent stratigraphic framework (Jacque and Thouvenin 1975, Evans et al. 1973). Radioactive methods have been used to determine the age of igneous rocks and minerals. The amount of radioactive uranium and the quantity of decayed material (lead) is precisely determined in a supposedly closed system and an age is calculated from this ratio. The age of the oldest rocks on earth has been studied by C. Patterson in 1953 and he already proposed a 4550×10^6 year age (plus or minus 70×10^6 y). A number that is nowadays generally accepted by the scientific world, but it was really revolutionary at the time. The radioactive age determination method assumes that no lead is present in the mineral sample from the start. The same scientist has later focused his attention to the effects of toxic lead in our daily environment. He made the banning of lead as an additive to fossil fuels his life quest and finally succeeded (Bryson 2003), which was a great achievement.

Also **paleo-magnetic age determinations** proved useful for stratigraphic purposes. For instance the flip in the earth magnetic polarity is exploited in predicting the age of the oceanic crust.

Fission track analysis gives information on the age of individual minerals in rocks. Exposure to natural radiation of the minerals in the rock sample leads to changes in the crystal structure. It shows up as lineations on the crystal faces of the mineral. Counting the number of tracks on a crystal surface gives an indication for the time interval of the ongoing decay. Resetting of the fission track 'clock', by rocks reaching a certain mineral annealing temperature, must be properly taken into account, else misleading age datings are obtained.

The concept that seismic reflections are corresponding to 'timelines' is often used as a rough guide for the relative age dating of the sedimentary rocks. In some cases it is the only means to do sequence stratigraphy. It is a very powerful working hypothesis in seismic interpretation.

3.5 Depositional Environment and Gross Lithofacies Interpretation

Once the Depositional Sequence boundaries are established and inventorisation of the seismic facies units is done, then an interpretation for the different environments of deposition is given. The three dimensional shape of the unit under investigation is extremely useful for this purpose (Figure 3.77). It is important to realise that the signature of the seismic facies sometimes differs on dip- and strike lines. The seismic facies units are often not isotropic, but there are preferential directions in the sedimentary system. This does not only reflect the normal geometrical anisotropy observed in most sedimentary bodies, but acquisition and processing parameters may even play a role here.

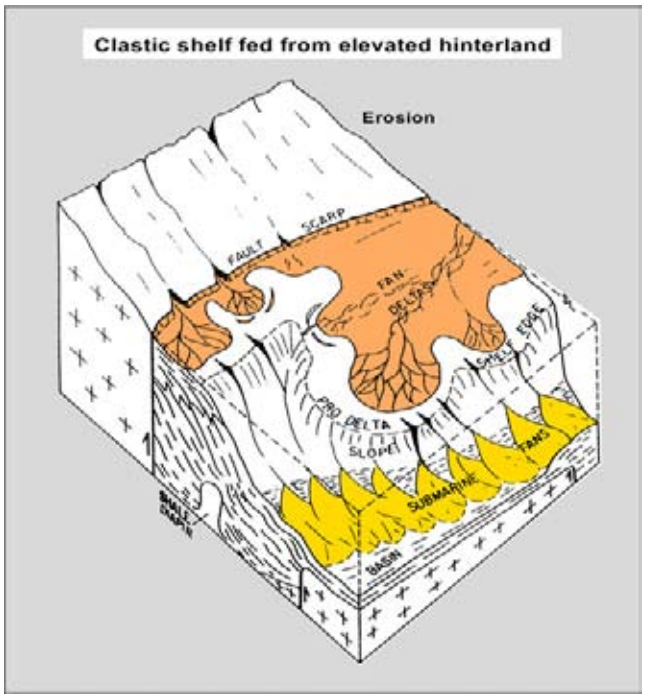

Figure 3.77: Block diagram with clastic depositional environments. The uplifted hinterland provides the debris that is deposited in the basin. Areas of erosion and deposition are determined by the shape of the ideal baselevel profile (after Brown and Fisher 1977, reprint from AAPG whose permission is required for further use).

The facies units within each depositional sequence are genetically related and therefore the interpretation of the environment of deposition should be done in a consistent manner. The basic concept is: proximal continental deposits grade into fluvio marine and transitional sediments which are in turn replaced by more distal marine slope and basinfloor deposits. This simple subdivision gives a helpful frame for the seismic interpretation.

As mentioned earlier, it is often possible to make a distinction on seismic lines between top-, fore- and bottomsets, which stands for shelf, prograding shelfedge and basinfloor deposits (Figure 3.78). Occasionally it is observed that the transition from shallow marine into deeper marine environment is very gradual and no distinct foresetted facies unit is discerned in between. The slope area is in such case extremely wide and sedimentation conditions are very uniform, so that a sort of subhorizontal drape of the basinfloor morphology is produced (e.g. Pearl River Mouth Basin, offshore China). A very subtle low-angle transition exists, that is difficult to appreciate on the size of individual seismic sections. The visibility of the transition is sometimes enhanced by choosing an other horizontal scale display that permits a different overview of the dataset. Squeezed sections might be helpful for the distinction between structural and sedimentary dips.

3.5.1 Terrestrial shelf

A difference with respect to the source area can be made for sequences deposited on the shelf. A distinction between proximal (or close to source area) and distal (for the deposits laid down far from the provenance area) is commonly made (e.g. Reading 1986). Very close to the hinterland mountain belt **alluvial fan** deposits are preserved in local pockets. These alluvial fans are near their apex mainly composed of badly sorted rock fall and massflow sediments, grading downslope into braided stream deposits where the sediment is mainly water transported (cf Veeken 1997). Imbrication of boulders and pebbles is an indication for traction by a water current. In the field these alluvial fan deposits clearly show a high angle of repose. Hence it is logic to expect some foresetting and wedging in these sediments when seen on the seismics. The bad sorting and discontinuous character of the deposits will generate seismic facies units with discontinuous, variable amplitudes. The lithologies are a mixture of conglomerates, sands, silts and clays. Inverse grading of grainsize in individual beds is a characteristic feature, as well as frequent erosional bed contacts. Often the deposits display a typical reddish oxidation colour, indicative for subaerial exposure. Sometimes the alluvial fans are oriented in a transverse direction, while the downslope fluvial system is more longitudinal oriented in respect to the tectonic strike (Ramos et al. 2002). The shape and geometry of the fan body heavily depends on the paleo-geographical lay-out. If the fan is standing with its toes in a body of water, then a **fan delta** is formed (Figure 3.79). A **scree cone** is a fan related to a fault scrap. It has a very steep gradient with rock fall, mass transport and slumping as major mode of deposition (cf Nemec 1990).

Under arctic conditions (high altitude, geographic position, periodic climatic deterioration) also important **glacial** and **peri-glacial deposits** are formed that contain different lithologies. The badly sorted **tillites** or **diamictites** are mainly waste zones for hydrocarbons and the better reservoirs are found in the associated waterlaid peri-glacial sediments (channels and delta's).

If water discharge is locally blocked, than **lakes** are formed. The infill of these lakes are mostly characterised by rather continuous sub-parallel seismic reflections (Figure 3.80; Anadon et al. 1991). The lake deposits are generally fine-grained silts and clays, reflecting a quiet depositional environment. The finely laminated sediments are known as varves. These varves are thought to be related to seasonal changes in the sedimentation pattern. The laminae have been used in stratigraphy to get a feel for the changes in sedimentation rates and their timing. Milankovitch cycles (induced by regular changes in the Earth's orbit as discussed later) have been recognised in recent and ancient lake deposits. At the margins of the lake there probably exist delta complexes, characterised by cut-and-fill geometries (channels) and low-angle foresetting. This foresetting points to either progradation or lateral accretion surfaces. If the waterdepth is large enough, even steeper depositional dips are created.

When the water discharge is low, than deserts may develop with inland **evaporite basins** comprising sabkhas and bordering sand dunes fields (Figure 3.81; Evans 1989). Reactivation surfaces are often well expressed in the eolian deposits. The good grainsize sorting and the impressive size of the foreset bundles are typical. Avalanching and grain saltation are the main transport mechanisms. The stacked dunes can build important piles of sediment, that are interesting from a hydrocarbon reservoir point of view (e.g. Permian Rotliegendes, NW Europe). Numerous reactivation surfaces (Stokes surfaces) are present in the eolian deposits, with complete erosion up to the ground waterlevel as an end member. The eolian sands have very good porosity and permeability because of their excellent sorting. The sabkha deposits are fine grained and typically contain large amounts of organic material. Gypsum and salt

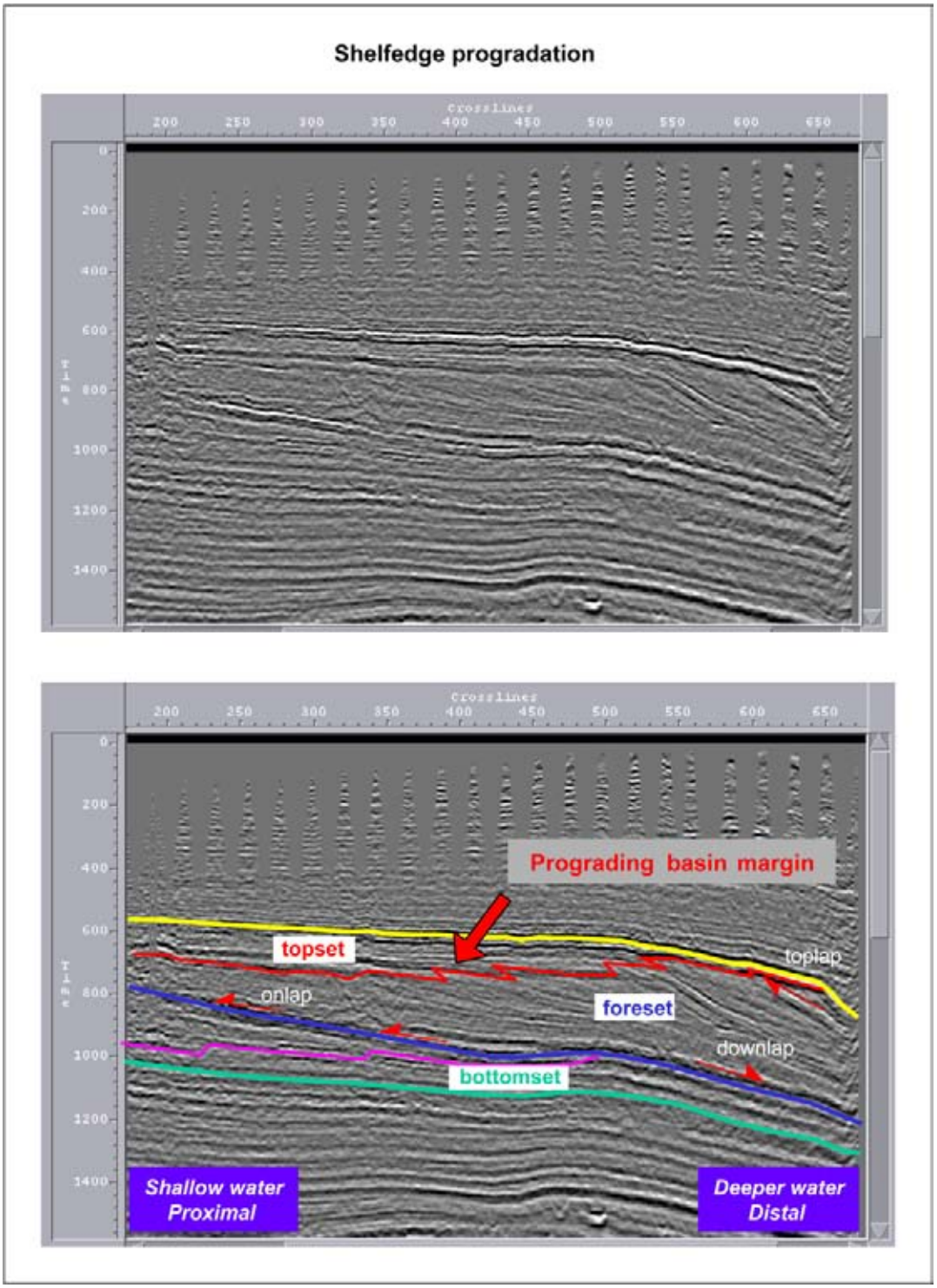

Figure 3.78: Shelfedge progradation is indicated by the foresetting on this seismic section. This geometrical configuration of the reflections is helpful in making a gross lithological interpretation of the basinfill. In a geological sense the topset is a proximal facies and it is more likely to be sand-prone. The foreset is further away from the input source and normally more shale-prone. The slope is sand-prone when no time-equivalent shelf deposits are present and the coarser material is transported further into the basin. The bottomset is a distal facies and therefore even more likely to be shale-prone. The interpreted unit is overlain and underlain by sub-horizontal sediments and therefore a sedimentary origin for the observed dip is inferred (data courtesy Pemex).

Figure 3.79: A fan delta is a fan standing with its toes in the standing body of water. The coastal plain is virtually non-existent. This example is from Buru Island in the Indonesian archipelago (data courtesy NASA).

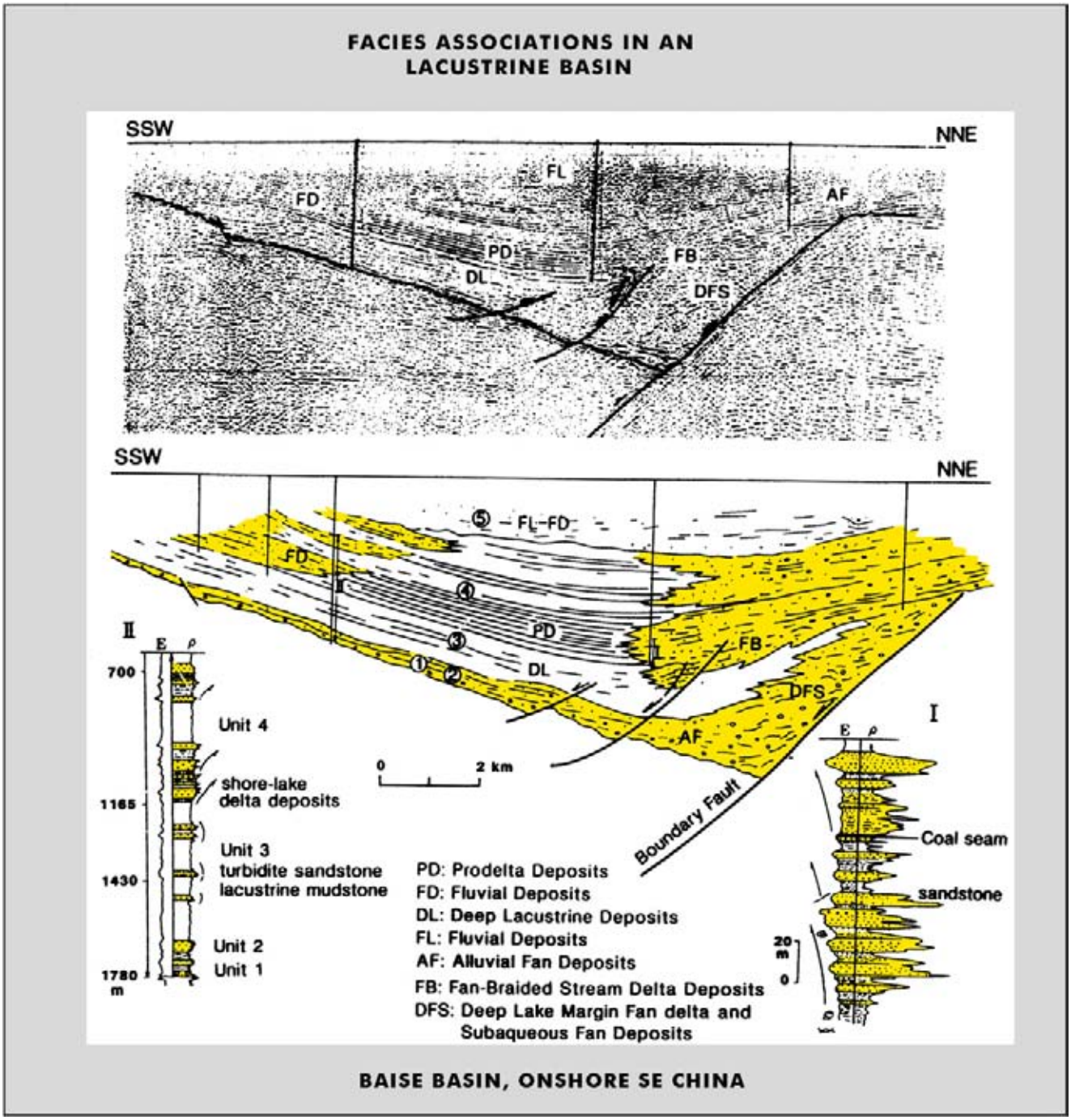

Figure 3.80: Depositional facies associations related to a lacustrine environment in an asymmetric halfgraben setting (modified after Lin Changsong et al. 1991). The lake deposits are often filled by finely laminated monotonous shale deposits as the result of the stagnant water conditions. The fine parallel lamination in the sediments is also known as 'varves'; they are often related to the influence of seasonal changes in the prevailing climate on the sedimentation pattern.

can be deposited in the inland lake, characterised by irregular discharge and high evaporation rate. Wind-blown flaky gypsum sand dunes is an interesting phenomenon in such environment (e.g. Chot El Jerid, Tunesia). It should be realised that the term sand only connotates a grainsize range and it says nothing about the composition of the grains. Most of the geologists assume automatically a quartz composition for a sand, but other lithic fragments should not be excluded beforehand. A **mature sand** is composed of more resistant fragments like quartz and heavy minerals, while an immature sand (arkose or grauwacke) contains a lot softer

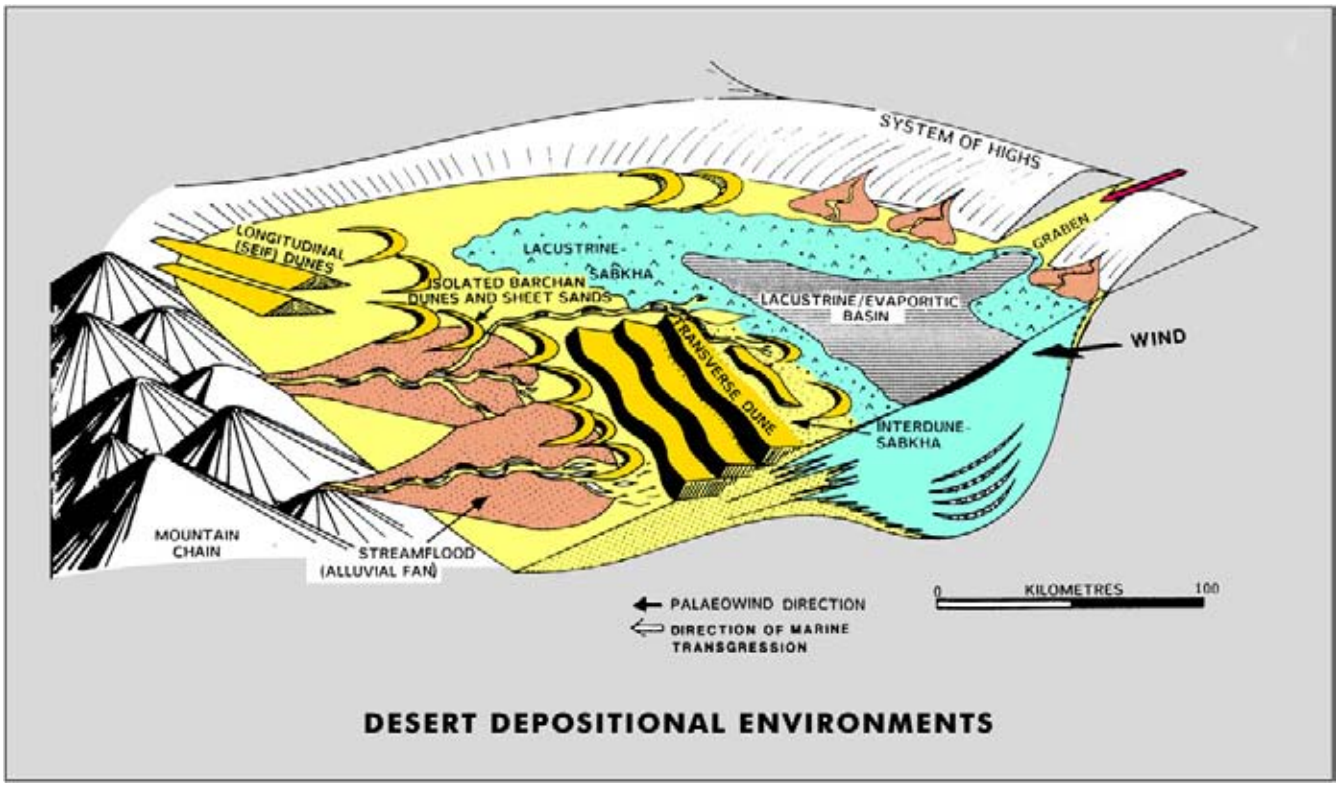

Figure 3.81: Sedimentation patterns in the desert environment. Alluvial fan, braided stream and eolian sediments are usually good reservoirs. Organic matter has a high preservation potential in the sabkha and lake environments (modified after Evans 1989).

mineral assemblies. Feldspar is for instance more easily weathered than quartz (Masson and Berry 1968). The degree of sand maturity is an indication for the transport distance of the clasts (cf Blatt et al. 1972). The grains in mature sands have probably travelled a larger distance and/or the particles are reworked. The roundness and sorting of the grains are other criteria for the transportation mode and distance. Statistics on the morphology and assembly of the grains can be quite revealing for the origin of the mineral components and the environment of deposition (Dr M. Fey, pers. com.).

Under more humid climatic conditions **braided streams** are found in the proximal domain. The water discharge is irregular and bed load transport is important. Conglomerate and sandstones form the coarser grained deposits. Channelling and erosional contacts are frequent. Channels are shifting in position in an irregular way and an anatomising discharge pattern in a wider channel valley is the result. Crossbedding, channel bar progradation, imbrication and paleosols are often observed. **Levees** and overbank deposits are build by lateral overflow of the channel. The levees are normally composed of fine-grained deposits flanking the actual channel and dipping away from the channel axis. The fluvial deposits show up as discontinuous or hummocky seismic facies units on the seismics (cut-and-fill). Downstream these rivers enter a floodplain, which is characterised by much more continuous reflections. The slope gradient on the **coastal floodplain** is reduced and here **meandering** systems develop when the water discharge is regular (Figures 3.82 and 3.83). Pointbar sequences – erosive base, crossbedded (a.o. current ripples) fining upward and thinning upward trends – are typical for this type of environment. The meandering system is often represented by cut-and-fill geometries on seismics or by sheet-like geometries. Various bounding surfaces in these channel deposits are distinguished, as illustrated in Figure 3.84 (De Rooy et al. 2002). Note the increase in scale of observation. Lateral migration of the channel axis produces a typical layered geometry with foresets that are the result of **lateral accretion**. It can be a substantial element in a system of sinuous channels (Abreu et al. 2003) Intensive channel switching and lateral migration leads to rather extensive cut-and-fill facies belts. Several sedimentation environments are present:

– The fine-grained **overbanks**, where the influence of the river is apparent by sandy intercalations (hummocky because of directional changes in thalweg), coarser grained crevasse splay complexes or avulsion indicate areas where the river eroded its own banks.

Figure 3.82: View on the Tabasco coastal plain in Mexico. The gradient and regular discharge results in meandering channels. Channels, overbanks, crevasse splays, coastal swamps and lakes are found on the flood plain, while along the coastline is formed by a delta and a sandprone barrier complex (data courtesy NASA).

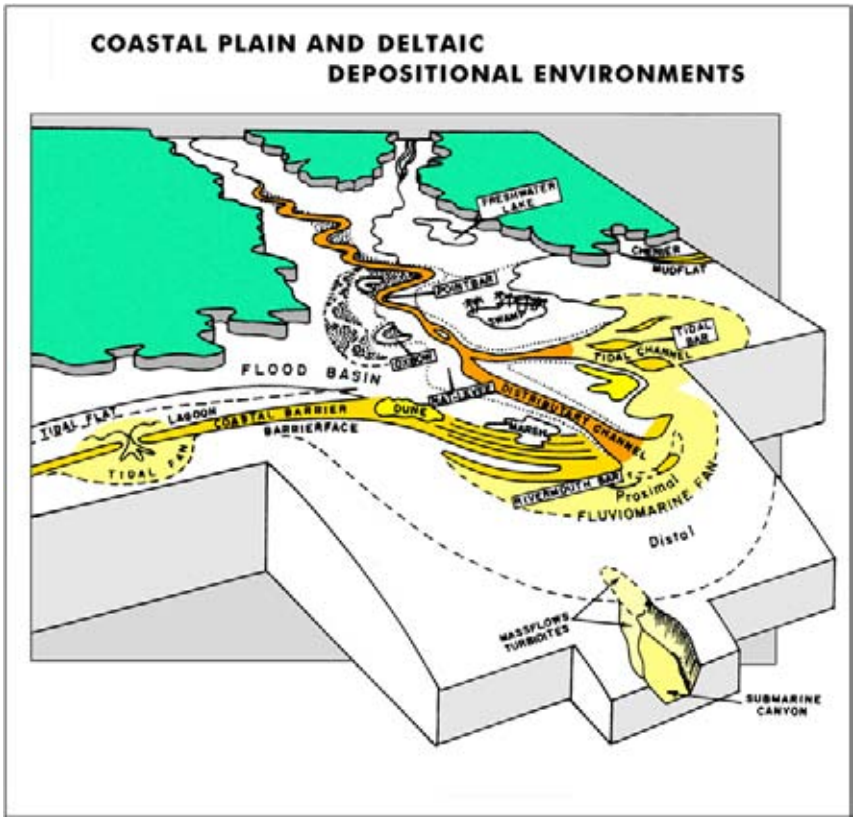

Figure 3.83: Block diagram illustrating the interplay and sedimentation pattern in the coastal, deltaic to shallow marine depositional environments.

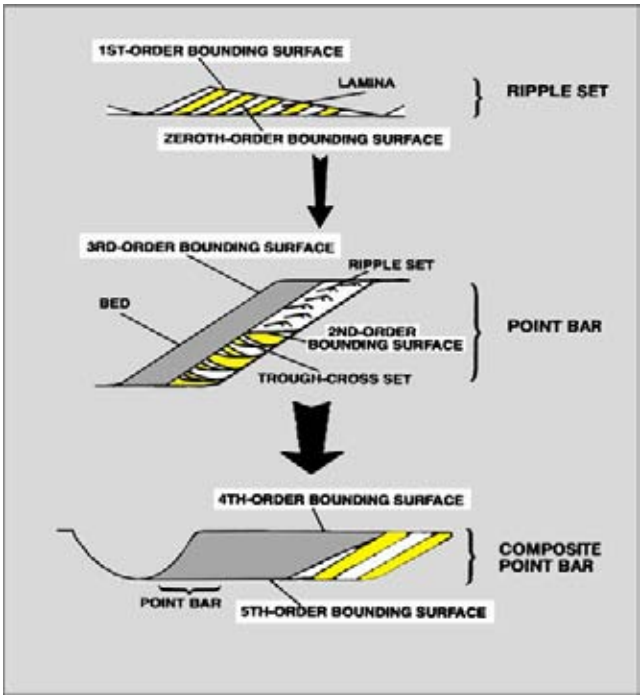

Figure 3.84: Bounding surfaces in a meandering channel complex with point bar deposits (after De Rooy et al. 2002).

The term levee has a distinct geometrical connotation to it, while overbank deposits are a broader general term.

- **Channel fill** sequences with prolific bar progradation that are often sand-prone. Point bar sequences are the result of meandering river channels. These sediments are mostly characterised by discontinuous seismic reflection patterns.
- Oxbow lakes that are filled with fine-grained material due to **channel abandonment** (concave upward top, low amplitude, thinning upward trend).
- Possible bordering windblown **dune** fields consisting of well sorted sands (low-angle shingling).
- The fine-grained distal flood plain itself with coastal **marshes and swamps** (parallel continuous, various amplitudes; high amplitudes may point to coal layers).

At the terminus of the river system a **delta** (wave or river dominated) or **estuary** (tide dominated) system is found (Figure 3.85). There exist three basic types of deltaic systems: fluvial, wave and tidal dominated systems (a.o. Berg 1982). The change in flow dynamics, wherever a fluvial system meets a standing body of water, causes a sudden drop of the river bedload. Some of the coarser material, held before in suspension by the water particle velocity, is settling down. This mechanism is responsible for the massive sand-prone **mouth bar complexes**, where the bulk of the river's coarser grained sediment load is deposited (Figures 3.86 and 3.87). Marine sedimentation processes are from now on acting upon these deposits. The clastic material is further transported into the basin or re-distributed along the coast, where it is submitted to wave action, longshore currents and eolian forces. If wave action is important, then coastal barrier complexes are formed. Wind-driven **longshore currents** transport material along the coastline and redistribute material further away from the delta, resulting in a rather smooth coastline. When the tidal energy is dominant, then an **estuary** is the typical deltaic end result. Several parameters can be considered for subdividing the deltas (Postma 1990):

- Physiography with regular or irregular shoreline.
- Gradient; steep Gilbert type, gentle mouthbar type.
- Toe of delta system below or above wavebase.

Nemec (1990) proposes a separate class for volcanic fan/delta systems.

Massive dumping of material at the terminus of a river system can cause rapid dewatering of the underlying sediment, which ultimately results in contorted bedding (incipient soft sediment deformation). If the pressure is released at the surface, than sand- and mud volcanoes may be created at the seafloor. It is an expression of subsurface sediment mobilisation (cf Van Rensbergen et al. 2003). Slope instability and slumping may also lead to similar sediment remobilisation, the rise of clay diapirs and extrusion of sediment volcanos (e.g. Niger delta continental slope, Adeogba et al. 2005).

The rapid deltaic outbuilding can give rise to slope instability which may lead to the development of **listric faults** affecting the sedimentary pile (e.g. offshore Brazil, Petrobras 1983). These spoon-shaped, curved faults are often active during sedimentation. They normally sole out in a plastically deformable unit at their base (Veeken 1983). The sediments on the downthrown side of the fault (actively moving, also known as hanging wall) are in general thicker than those found on the upthrown block (foot wall). This thickness variation is an indication that the fault was syn-sedimentary active. Because of the lateral thickness variation of the deposits across listric faults, this type of fault is also called '**growth-fault**' (Crans et al. 1980). Growth faults are a typical product of thin-skin tectonics.

The listric shape of the fault plane does induce other characteristic features that helps in their identification. It causes a progressive rotation of the sedimentary pile in the down-faulted block and leads to a so-called '**roll-over**' structure (e.g. Veeken 1983). The Niger delta

Figure 3.85: A delta complex is built at the terminus of a river system where a standing body of water is met. The Amazon delta in Brazil illustrates that the clastic material is reworked by the coastal currents and waves. It results in a characteristic geomorphological shape of the delta (data courtesy NASA).

is quite well known for this type of gravitational induced roll-over anticlines, that are important hydrocarbon traps (e.g. Durand 1996). Over this anticlinal 'roll-over' geometry a crestal collapse is often developed, due to extensional stresses in the upper layers of the affected sequence. Because of space problems in the inner central part of the roll-over, it is possible that some reverse faults are present in the deeper inner part of the sequence. The fault system may develop a so-called compressional **toe-thrust** at the distal end of the structure. This toe-thrust accommodates the gravitational stresses in a basinward direction. The structure of growth faults has been simulated in sandbox and plaster deformation experiments (e.g. Lindanger et al. 2004).

Growth faults tend to sole out into a plastically deformable layer (Figure 3.88). Be aware that, when interpreting faults on TWT time sections, it is still necessary to depth convert the data in order to be able to appreciate the real geometry of the fault planes. When dealing with increasing interval velocities with depth, it will result in an artificial curvature of the fault planes in time (Withjack and Drickman Pollock 1984). Therefore it is good practice to draw the faults on time sections always with a slight curve. The angle of a fault plane transecting a heterogeneous package is also dependent on the lithologies encountered. The fault plane will become more steep in the more brittle behaving rocks. This feature is useful when interpreting the gross lithology of seismic units. The shape of growth faults can be quite complex and their recognition is not always very easy (e.g. thrust versus growth fault model, Hossack 1984).

Good examples of growth faulting on a seismic scale are exposed in the sea-cliffs of County Clare in western Ireland (Rider 1978). Multidirectional extension is typical in a such sedimentary margin setting. Polygonal fault patterns (Goulty 2002) and syn-sedimentary shear zones are sometimes associated with these features (Moretti et al. 2003). In a passive margin setting the latter SSZ are the result of sedimentary discontinuities that change the principle stresses due to multidirectional gravitational deformation. The Carboniferous delta and shelf system is affected by gravitational

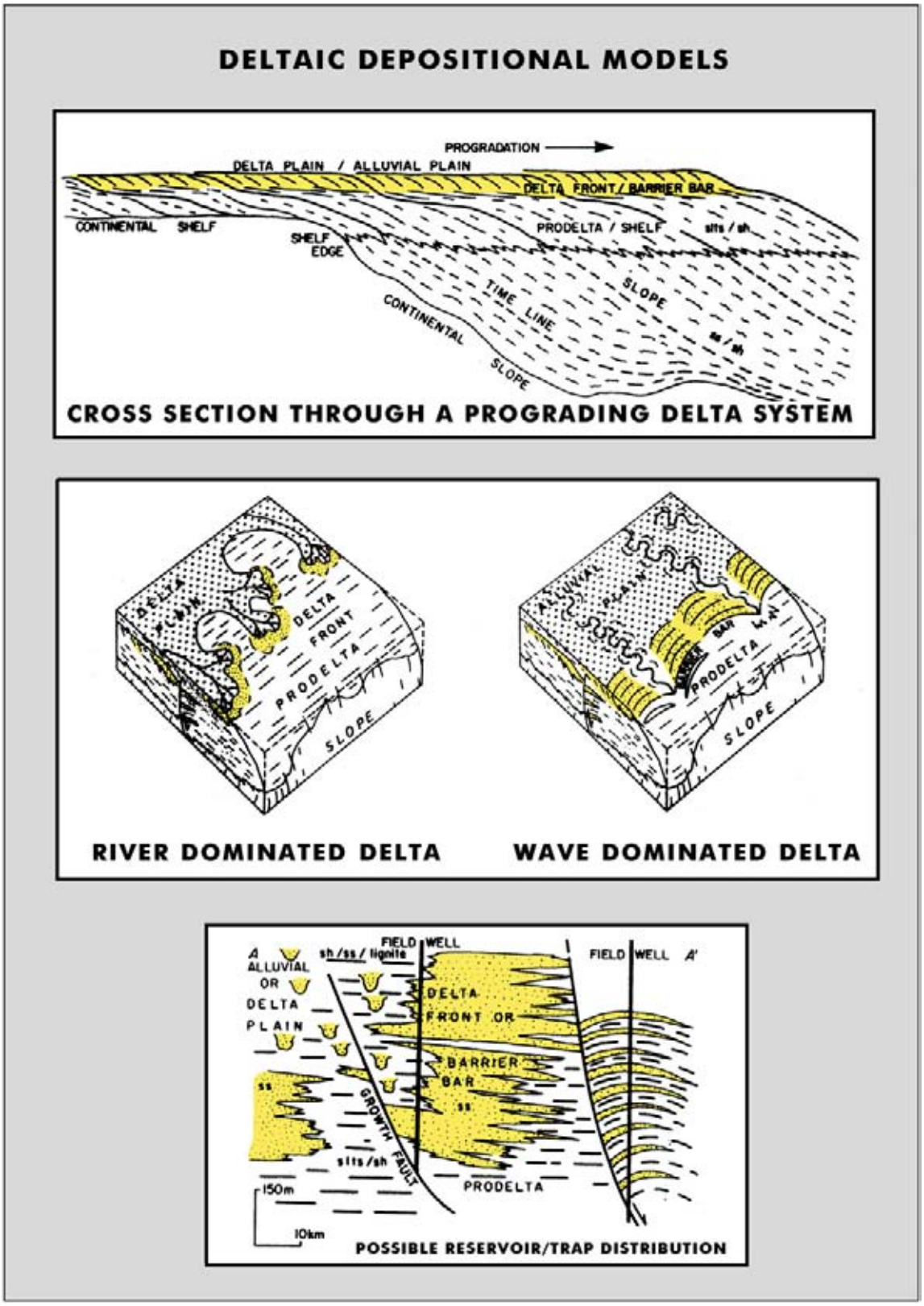

Figure 3.86: Deltaic progradation pattern and its reservoir potential (after Brown and Fisher 1977, reprint from AAPG whose permission is required for further use).

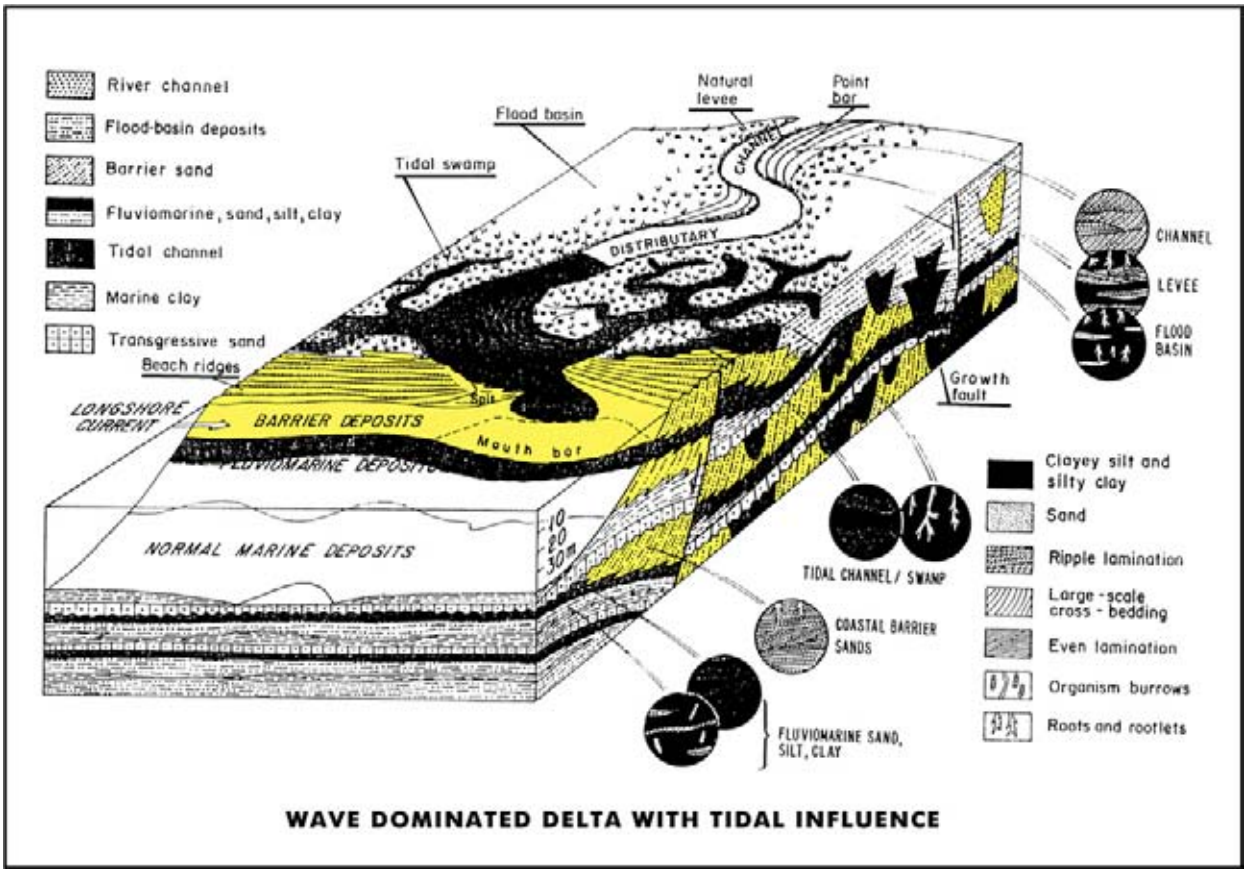

Figure 3.87: Facies associations within a wave-dominated deltaic setting. Important quantities of sands are concentrated in the barrier bar, river mouth bar, channel fill, tidal channel and pointbars.

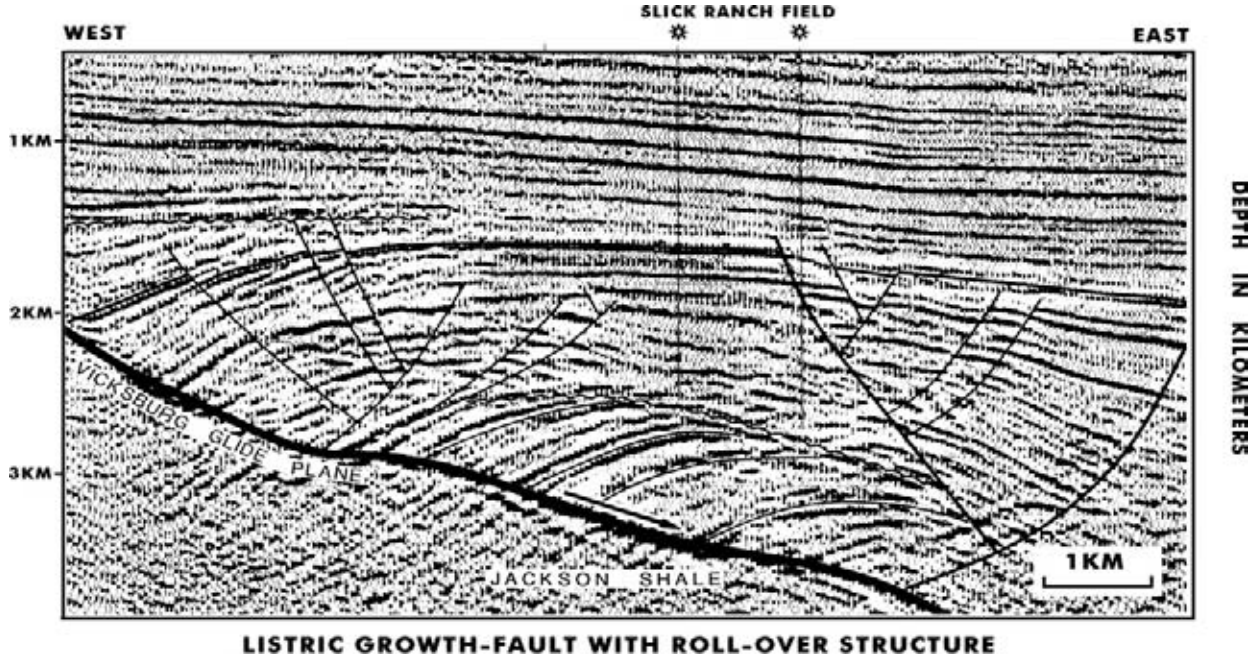

Figure 3.88: Growth faulting in a deltaic setting, showing a roll-over structure and crestal collapse tectonics. This type of deformation gives a good possibility to trap hydrocarbons (modified after Erxleben and Carnahan 1983, reprint from AAPG whose permission is required for further use).

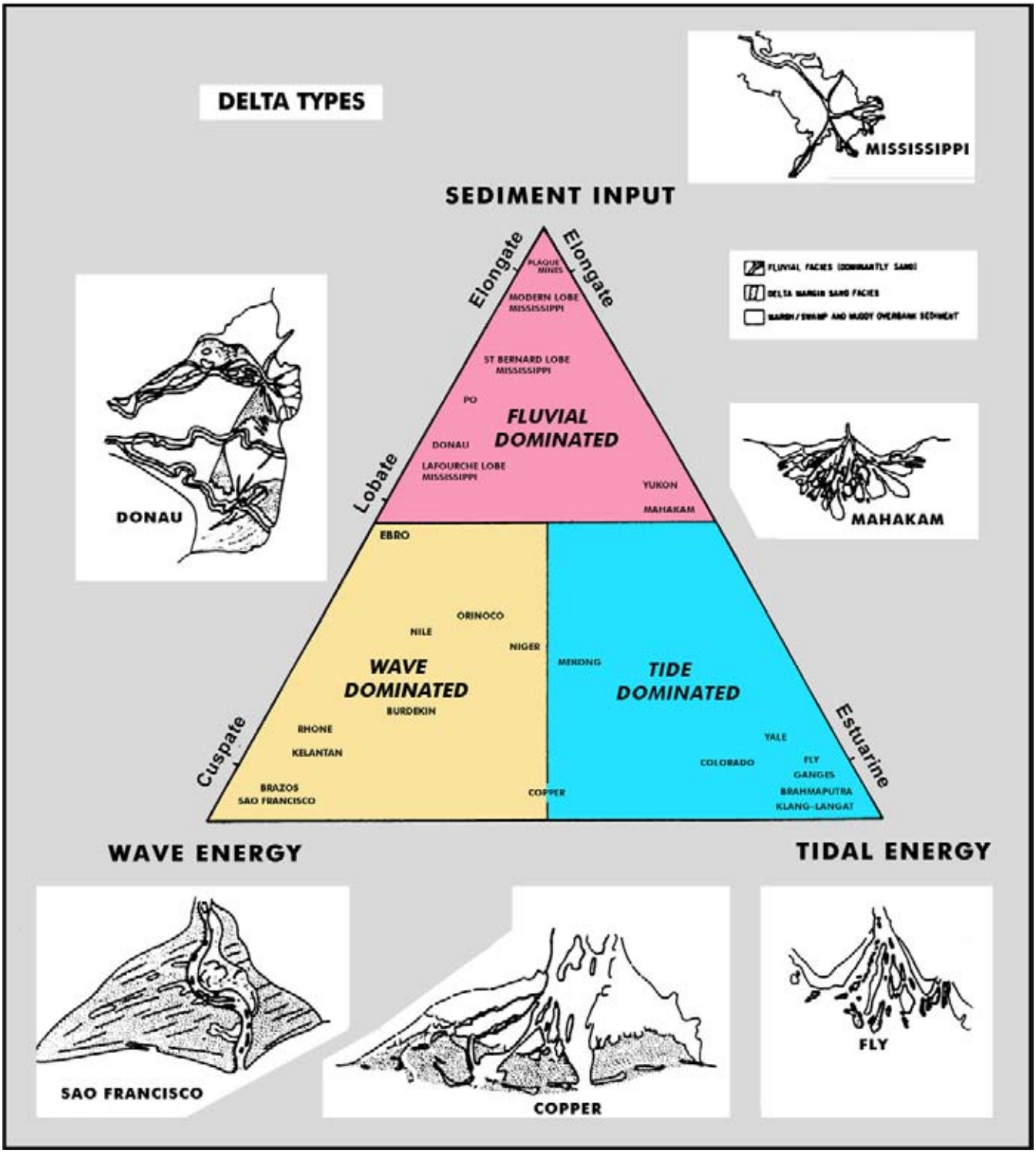

Figure 3.89: Delta morphology and basic delta types. A special type of delta is formed by the Gilbert type of delta, characterised by steep foresets and coarse grained deposits. The Gilbert type of delta forms a transitional high-energy delta, intermediate between an alluvial fan and a fan delta system.

Figure 3.90: Coastal barrier bar complex and tidal inlets with tidal delta complex. These are characterised by a tidal channel and landward oriented wash-over lobes. The lagoon and tidal flats are protected from the open sea by the barrier island (data courtesy NASA).

sliding of the sediments. Also spectacular slumping occurs, indicative for sudden slope instability. Sand volcano's are the result of rapid burial and overpressuring of the original sand body. It stems from the fact that the normal dewatering is prevented by the presence of permeability barriers (cf Veeken and Van Moerkerken, 2005). The role of sandstone intrusion/injection and fluidised flow as geologic phenomena has been underestimated in the past, especially in deep water clastics (Huuse et al. 2003). The sand remobilisation mechanism has an impact on the expected connectivity (compartments, brecciation, thief sands) and the HC production. Some authors propose fluid injection as a mechanism for triggering earth quakes (Segal 1989) but most of the time it is the seismicity that creates the instability causing the sudden seal breach (Veeken and Van Moerkerken in prep.). Jonk et al. (2005) envisage injection of sand at a relatively shallow burial level (400 metres) due to tectonic instability. This causes slumping and sedimentary loading with a sudden increase of the pressure, triggering the subsequent break down of the seal integrity. They even propose an early hydrocarbon migration contemporaneous with the sand injection for the North Sea Paleogene turbidite reservoirs. The diagenesis is characterised by several phases (Jonk et al. 2005):

- Ankerite and early oil formation in Late Eocene.
- Oxidation and sulphate reduction with pyriyte/calcite/siderite in Oligo-Miocene.
- K feldspar during gas migration in Mio-Pliocene.
- Later dissolution of K Feldspar, Quartz growth, Kaolinite and illitisation of smectite in Plio-Quaternary times.

The illitisation of smectite takes place at a temperature range of 70 to 100 degrees Celsius.

A simple geometric tool to visualise the stratigraphic thickness variation is provided by the fault throw versus depth plot. It can also be use to infer lithological changes from seismic data only. Shales are thought constant thickness, while the sand packages correspond to thickening units (Pochat et al. 2004). It is a rather simplistic working hypothesis.

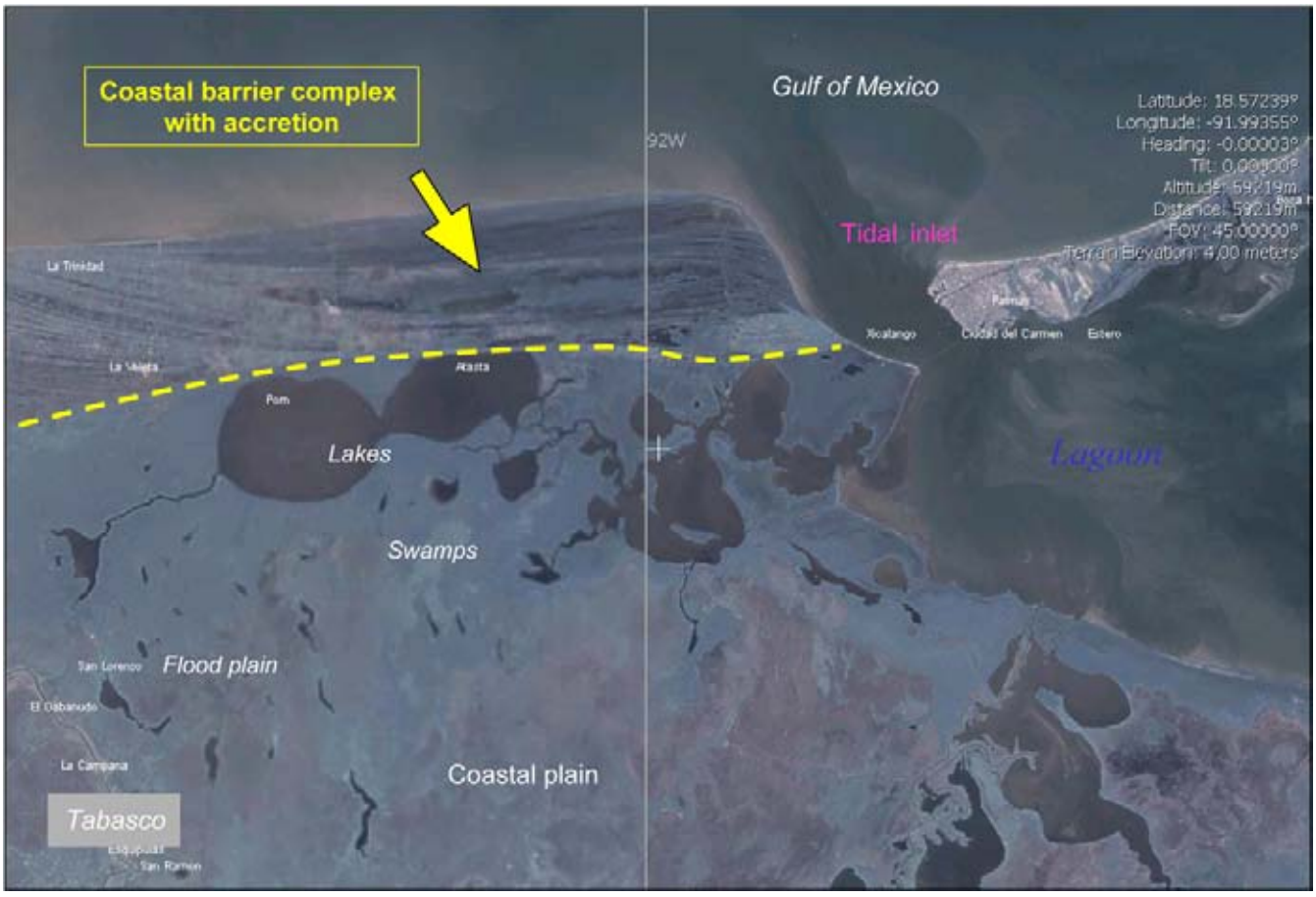

Figure 3.91: Barrier complex bordering the Gulf of Mexico and clearly the accretion lines are visible. Note the abrupt change with coastal flood plain behind the barrier system (data courtesy NASA).

3.5.2 Coastal or transitional domain

At the rivermouth the transitional domain between terrestrial and marine sedimentation is entered (cf Broussard 1995). The fluvio-marine and marine deposits are typically yellowish white in colour. Marine transport conditions affect the flux of input material to the marine basin. The delta will show up on seismics as a low-angle shingled facies unit, putting in evidence several stages in delta lobe progradation. The seismic amplitude of the foresetted reflections is either high or low, depending on the amount of heterolithic deposits (package of alternating lithologies, usually mud- and siltstones intercalated with sands of various extends). The height of the foresets is proportional to the waterdepth of the basin into which the delta system is prograding. The actual thalweg, i.e. active part of channel for funnelling clastics to the marine shelf, is mostly represented by a chaotic seismic facies. This facies is in general confined to the river valleys, forming preferential sediment transportation areas where frequent channel axis switching occurs. Several different types of deltas are recognised, each with their own specific sedimentological characteristics (Figure 3.89). The **Gilbert type** is a special steeply foresetted delta complex, composed of very coarse grained material. It is the result from an episodic mode of bedload transportation with avalanching down slope where the deeper standing body of water is reached. In the **prodelta** environment large amounts of silts and clays are deposited. It is the offshore part of a delta complex, often characterised by foresetting on the seismics and typical for outbuilding of a sedimentary system.

If the wave energy and the wind-driven longshore currents in the marine domain are strong enough, then the debris dumped at the rivermouth will be reworked. It is laid down as a **barrier complex** bordering the coast line (Figures 3.90 and 3.91). These barriers protect the coastal plain, lagoon and/or tidal flat. The barrier bars are composed of sand-prone crossbedded and parallel laminated deposits. The overall geometry of a barrier system is elongated in nature. The deposits in such barrier complex can be in part water-laid as well as be wind-blown (sand dunes).

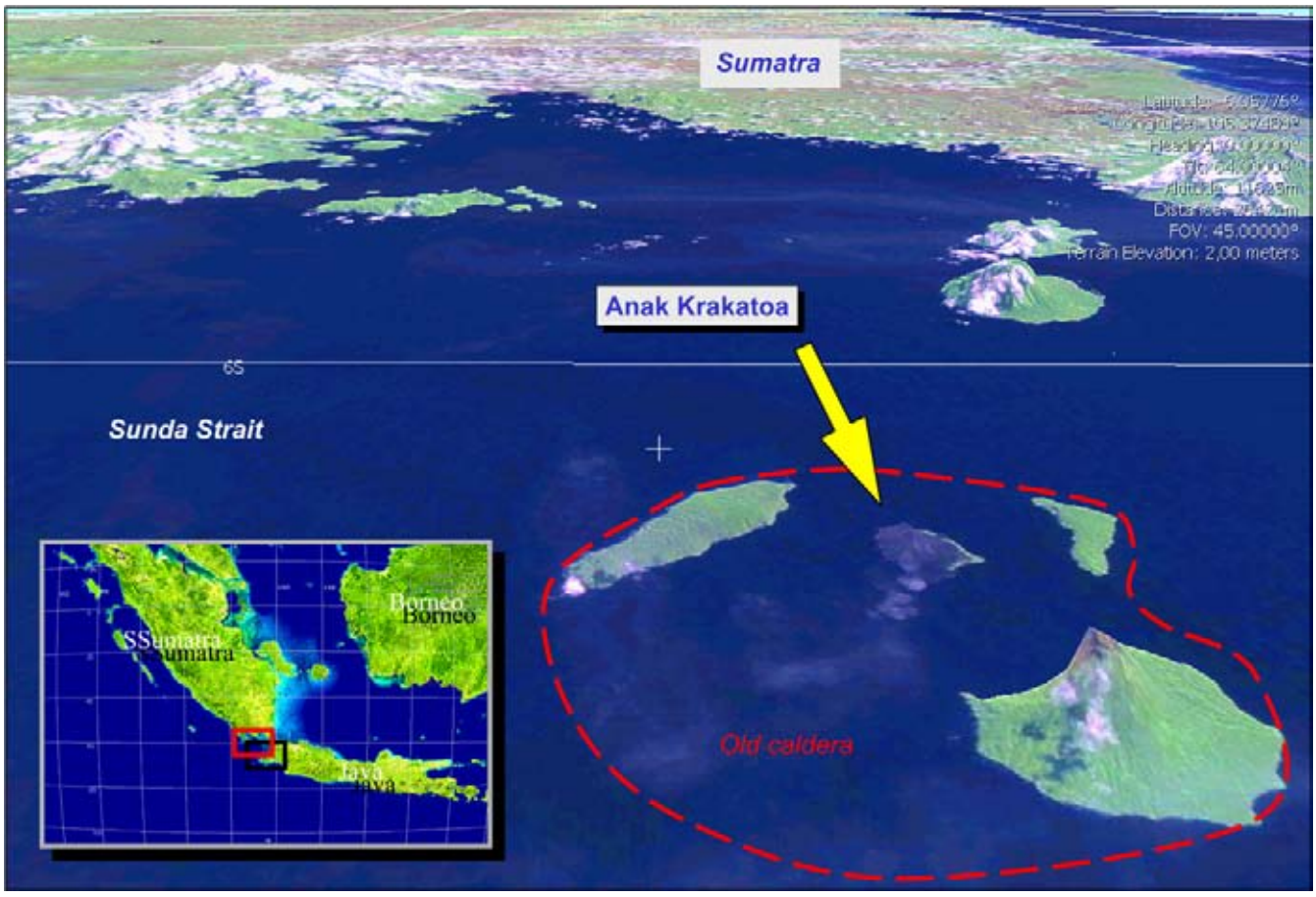

Figure 3.92: The explosion of the Krakatoa Caldera in 1883 resulted in a 40 metres high tsunami hitting the coasts of the surrounding Indonesian islands. The disaster left three little islands as the remainder of the huge volcano. Since then a new island has appeared at the surface in the Strait of Sunda on the location of the ancient crater pipe, called Anak Krakatoa, i.e. child of the Krakatoa volcano, which is more or less constantly in activity.

Wave ripples are frequent in the sediments laid down in the shallow offshore domain. Hummocky cross stratification is often observed, which is indicative for wave action. The **wave base** is normally above 50 metres. This is related to wind driven movements affecting the zone just below the water surface. Only exceptional storm surges might have a deeper reach. The tsunami (exceptionally high waterwave) is for instance a natural phenomenon that is mostly generated by submarine earthquakes related to plate tectonic adjustments (cf Berman 2005). This type of water particle movement involves the totality of the oceanic water mass and the wave train has a tremendous destructive power when the shoreline is reached. The 15 metres high sea waves that hit SE Asia on 26th of December 2004, caused the death of more than 200 000 people in a single moment. The Krakatoa volcano explosion in 1883 was even worse as it was accompanied by a 40 metres high sea wave. Three remnants of the old caldera outline are still preserved and a new volcano (Anak Krakatoa) has come to the surface where the old crater was located (Figure 3.92). To illustrate its destructive power: a military battle ship was picked up and dropped 4 kilometres inland, where it was left as a prey to rust till recent days (Winchester 2003). The tsunami, induced by the meteor impact at the Cretaceous Tertiary boundary on the Yucatan platform, represented even a bigger seawave of 400 metres, with as a result the deposition of an important conglomeratic layer and several sand intervals. The latter are interpreted as repeated wave arrival (Stewart 2003). The repeated arrival of the anomalous seawave disturbance, caused by the bouncing back mechanism in the Gulf of Mexico, would have led to tremendous havoc in the surrounding coastal region, onshore as well as offshore. The event was also accompanied by the intrusion of sedimentary dikes and sills.

The swash and backwash of the wavebreak at the beach is represented by parallel laminated layers. Fossil rich sediments are an other typical product in such a setting, with many broken fragments. Gravel beds might be preserved, indicating proximity of exposed cliff faces.

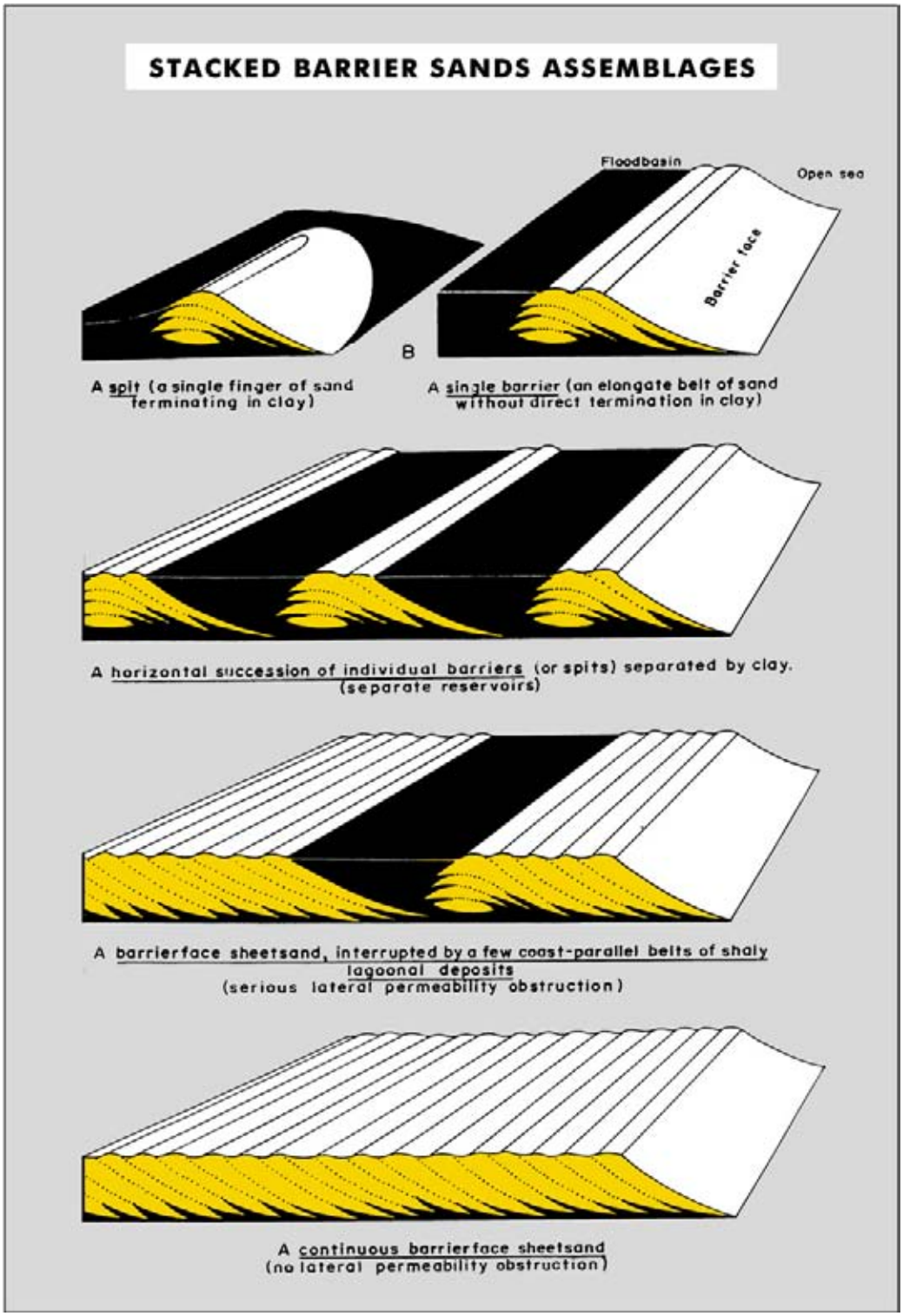

Figure 3.93: Coastal barrier systems and the distribution of stacked sands. These sands are often well sorted and form excellent hydrocarbon reservoirs with good porosity and permeability.

Figure 3.94: Tidal flat in the northern part of Holland with several tidal inlets and typically curved tidal channels. Part of the Groningen gas fields are located beneath these tidal flats, which are a national nature reserve. Gas production is causing a regional compaction subsidence that is thought compensated by the amount of sediment supply arriving from the Rhine delta. The sand is transported by longshore currents along the Dutch coast. Small scale seismen are accompanying the gas production. These are monitored to obtain information on the active fault zones (data courtesy NASA).

Eolian sand dunes may develop along the landward side of the coastline. These dunes can show foreset orientations that are opposite to the regional structural trend as they depend largely on the prevailing wind direction. Wash-over fans, only active during heavy storm surges, may produce landward oriented foreset directions.

The sand-prone **barrier complexes** do contain stacked beach bars and offshore bars (Figure 3.93). These foresetted units show up on seismic as low-angle shingled units of reasonable continuity. Muds are deposited in the low-energy lagoons behind the barrier complex and on the adjacent **tidal mudflats**. The coastal barriers are interrupted by tidal inlets, giving connection to the protected lagoon and tidal flats. The latter are represented on seismics by hummocky/chaotic erosional features and even as shingled units. The shape of these sand-prone tidal inlets, is somewhat elongated and the corresponding tidal deltas have a cone shape. **Tidal deltas** have a land and seaward part with opposite transport directions. Important diagnostic features for tidal inlets are the overall setting and the orientation perpendicular to the general trend of the paleo-coastline. The mudflat is cut by tidal channels that regulate the daily difference in amounts of seawater due to high and low tide (Figure 3.94). Herring bone cross stratification is very typical. The bi-directional sedimentary bundles in the foresets are the product of the daily lunar induced high and low tides in sealevel. The heterolithic beds are often characterised by current ripple cross lamination with flaser (discontinuous mud), wavy and lenticular (discontinuous sand) geometries depending on the mud drape distribution (Reineck and Singh 1975).

A **fandelta** develops easily in areas where the coastal plain is extremely short, i.e. tectonically active regions. Debris from the hinterland is directly dumped into the

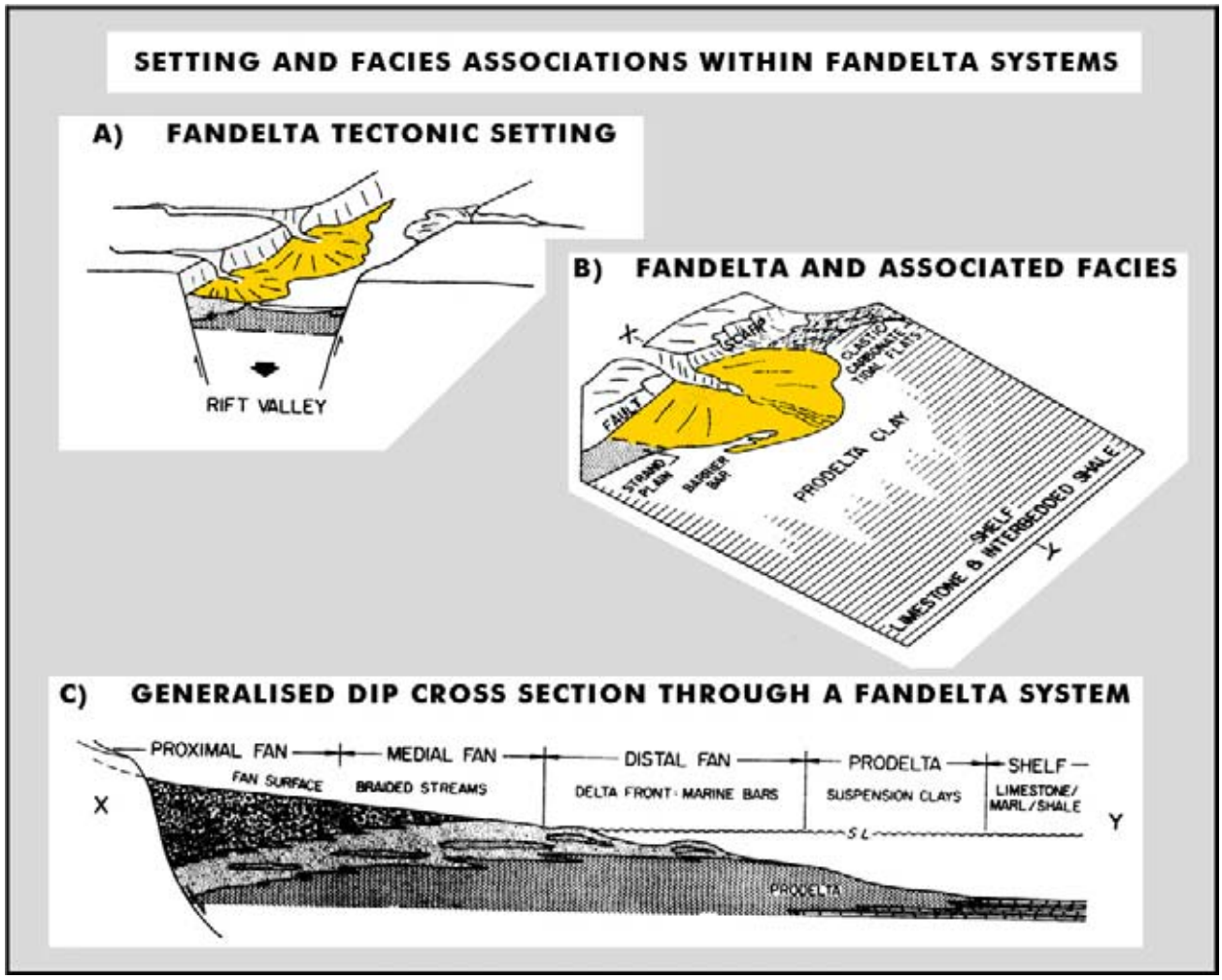

Figure 3.95: Setting and facies associations in a fandelta complex. The distance between the hinterland and the marine domain is extremely short (after Brown and Fisher 1977).

marine environment without a proper floodplain system (Figure 3.95). But also rifts and pull-apart basins are favourable (e.g. southern Spain, Dabrio 1990 and Van der Straaten 1990). The seismic expression of a fandelta can be quite complex and varies considerably. The proximal part is usually characterised by chaotic, discontinuous channelised seismic facies, while the distal section shows a better continuity of the reflections. Geometry and position within the basinfill is important to identify these deposits correctly. Often they are associated with active boundary fault zones (e.g. Halibut Horst fandelta, Veeken 1997; Suphan Buri Basin, Ronghe and Surarat 2002).

3.5.3 Shallow marine shelf

The marine shelf is a rather continuous and laterally extensive sedimentary environment. This is expressed by the continuity of the seismic reflections found in this domain. Only locally there are indications for erosion by bottom currents. These currents usually occur in the vicinity of the discharge of a delta system. Otherwise the reflections are more or less sub-parallel and form part of a distinct topset configuration.

Further away from the shoreline these topsets become increasingly shale-prone, because the distance from the sediment source is getting larger. In general homogeneous offshore shale deposits are typified by low amplitude seismic facies units. As said already, also other homogene lithologies will produce low amplitude facies units. It is therefore the general setting which provides essential clues on the gross lithological interpretation for this type of seismic facies.

If clastic sediment supply to the shelf is limited and the water temperature is favourable, than an **organic carbonate shelf** develops with high-energy build-ups along

the edges fringing the deeper basin (Figure 3.96). Carbonate rocks are subdivided in several types based on the presence of lime-mud and their mode of deposition (Dunham's classification, Figure 3.97). The packstone, grainstone, rudstone and boundstone lithologies form the higher energy members, while the mudstone and wackestone are deposited in less agitated water. Rud- and boundstone are made up by colony-making organisms like corals, that provide a solid skeleton for the rocks. Corals are also found in the Norwegian waters, so the temperature conditions for carbonate deposition can vary a lot. On the eastern margin of the Rockall Trough (offshore NW Ireland) the **cold water carbonate mounds** are fed by strong nutrient rich upwelling of bottom currents and/or faultzone related escape of thermogenic or hydrate gasses (O'Reilly et al. 2005). Higher moderate temperatures in a basin will usually favour the biological activity and productivity. Lime-mud is also known as micrite, while crystalline carbonate is called sparrite (Folk's classification). Mud is usually deposited in a quiet sedimentary environment. Carbonate platforms are offshore zones where the biologic productivity is high. Contrary to silici-clastics shelves, the carbonate environment generates its own sediment supply. The waste material is dumped on the reefal talus mainly under the influence of stormy events. Many times a progradational geometry is the result (Figures 3.98, 3.99 and 3.100). Bioclastic offshore bars in Oxfordian carbonates on the eastern flank of the Paris Basin at Euville (France) show this very well (Dagallier 2000; Figure 3.23). Oolites are typical limestone deposits, created in a high energy environment. An oolite is a well-rounded grain particle, formed by the concentric precipitation of calcite around a nucleus. It is the wave action that rolls the nucleus particles back and forward creating the symmetrical aspect of the oolite. The oolite deposits can build massive shoals and offshore bars with foresetting on the shelf. Oncolites are the product of algal coating around a grain. Their shape is much more irregular and it reflects a lower energy environment. They are normally a bit bigger in size (1–2 cm) as the oolites. The high energy oolite deposits show excellent reservoir characteristics because of their sorting and the rounded nature of the grains. Bi-modal sorting may be the result of biologic activity. Fine grained sediment accumulate in the protected lagoon. They are characterised by parallel to wavy bedding and layers with a fine internal lamination. These laminations or stromatolites are mostly stemming from algal mats. Local small scale undulations are quite frequent and underline a wavy aspect.

If the evaporitisation level is high, water salinity is increased and salt deposits may accumulate in the restricted marine basin. Hypersaline waters tend to sink to the bottom and run downslope to deeper levels due to their increased density, compared to normal seawater. Deposition and crystal growth (gypsum and halite) does take place not only at the surface, where highest salinity is reached due to intense evaporation, but also at the bottom of the basin under quiet water conditions. Upper Miocene Messinian salt deposits in parts of the Mediterranean are a good example of this type of sedimentation, with spectacular in-situ growth of gypsum crystals (Sorbas-Nijar basins, SE Spain). Time equivalent reefs demonstrate the submarine setting for these deposits (cf Van de Poel 1991, Pomerol et al. 2005) which also is seen in other areas (e.g. Niagaran reef; Wylie and Wood 2005). Wave ripple lamination in the intercalated mudstones are indicative for a 50 metres deep water level (H. Pagnier, pers. com.). The Upper Miocene salt is quite widespread in the eastern Mediterranean. It was most likely deposited in isolated sub-basins. This interpretation is supported by seismic lines in the Algerian waters, where there are indications for strong diapiric salt movements giving rise to severe structuration of the overburden (see Figure 2.46). Such tectonism is good news for the hydrocarbon prospectivity and exploration efforts, because trapping is stimulated by the degree of structural deformation.

Reefal build-ups (mounded, foresetted) protect the inner shelf, where lagoonal/inner shelf carbonates and shales are deposited (sub-parallel, high amplitudes, high continuity). These reefal build-ups may show up on the seismics as reflection free zones with on their seaward side indications of foresetting, pointing to larger water-depths. The shape of the build-ups is prograding, aggradating or retrograding depending on the degree of relative sealevel rise. The detailed 3D structure of reefal complexes are even revealed on high resolution GPR data acquired on the eastern flank of the Paris Basin in NE France (Dagallier et al. 2000). The georadar sections are directly calibrated by the geologic units recognised in outcrop in the field. The GPR method is gradually becoming more popular in academia because of its cost effectiveness and the good results obtained. It is very efficient and a helpful tool to define high resolution 3D reservoir working models, suitable for detailed fluid flow characterisation. Models, based on combined 2D outcrop data alone, are most of the time not sufficient. Calibration of the spatial relationships is of course a very important matter (cf Zeng et al. 2004, Pringle et al. 2004).

Similar sedimentation mechanisms operate on siliciclastic as well as on carbonate particles. For instance tidal ridge complexes, seen in field outcrops in eastern France, are very comparable to those described in siliciclastics (Figure 3.101). The recognition of fan geometries in carbonates further demonstrates that the separation between clastic and carbonate geology is quite

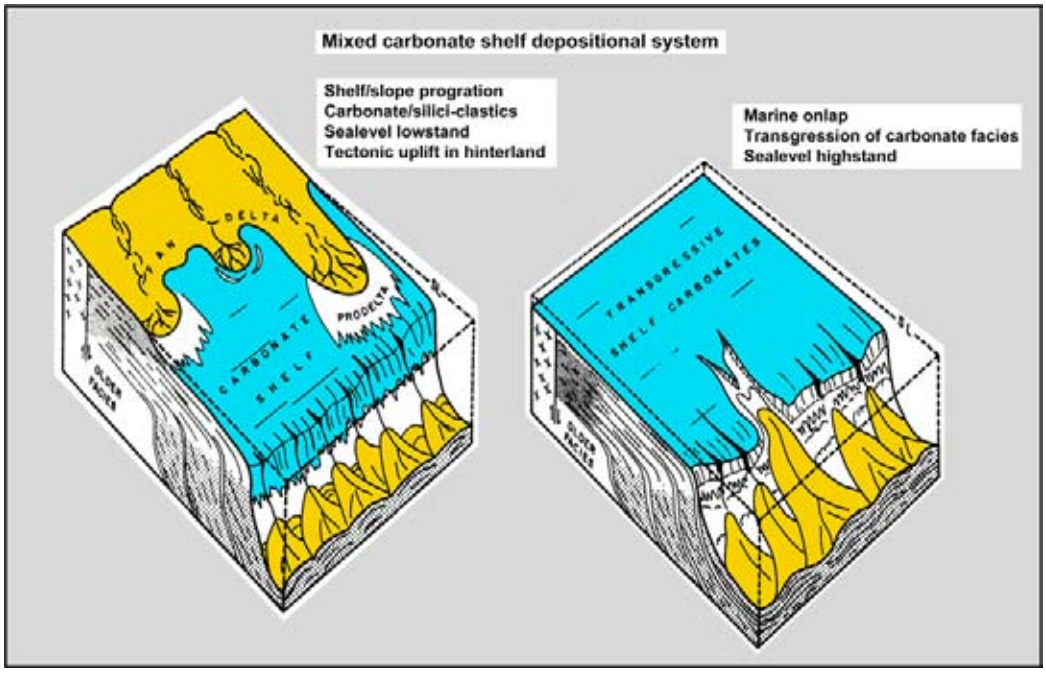

Figure 3.96: Depositional environments on a carbonate shelf. The inner shelf is characterised by more discontinuous reflections (cut and fill) while the outer shelf shows more continuous seismic facies units, indicative for more uniform sedimentation conditions. The sealevel rise reduces the topographical relief in the hinterland and results in less erosion products reaching the marine shelf (modified after Brown and Fisher 1977, reprint from AAPG whose permission is required for further use).

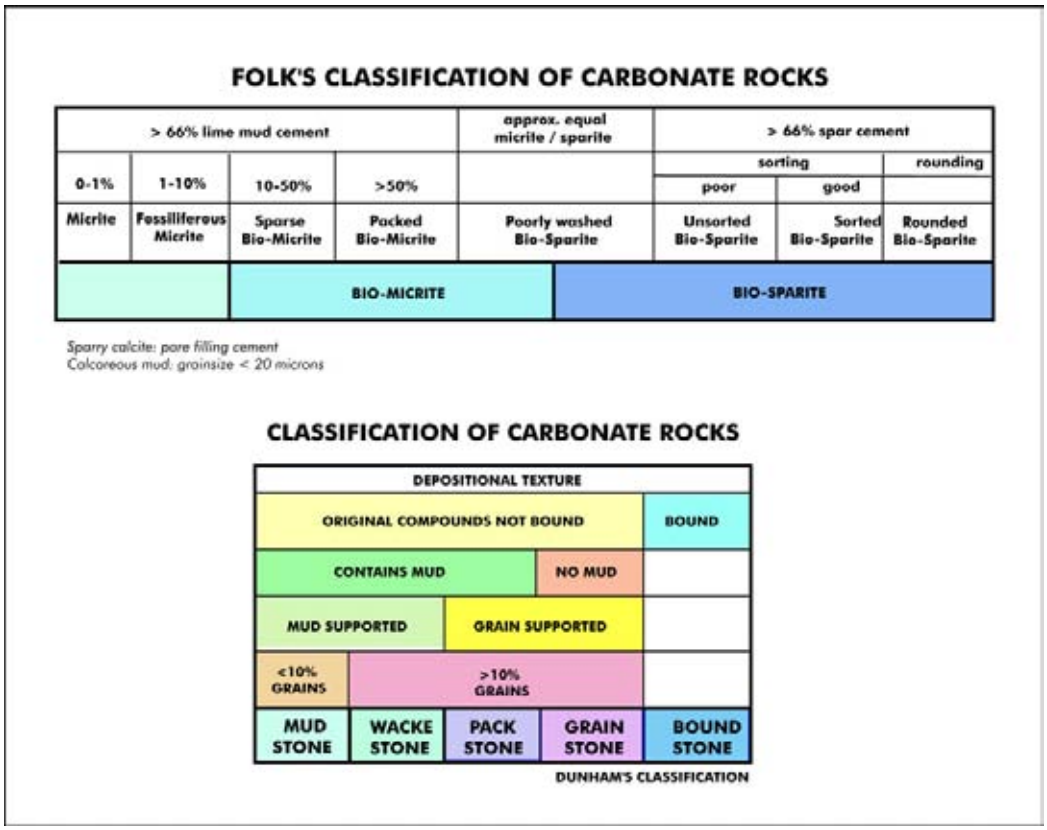

Figure 3.97: Folk's and Dunham subdivision of carbonate rocks. The presence of lime-mud is an important criterion to distinguish the energy level of the various environments of deposition.

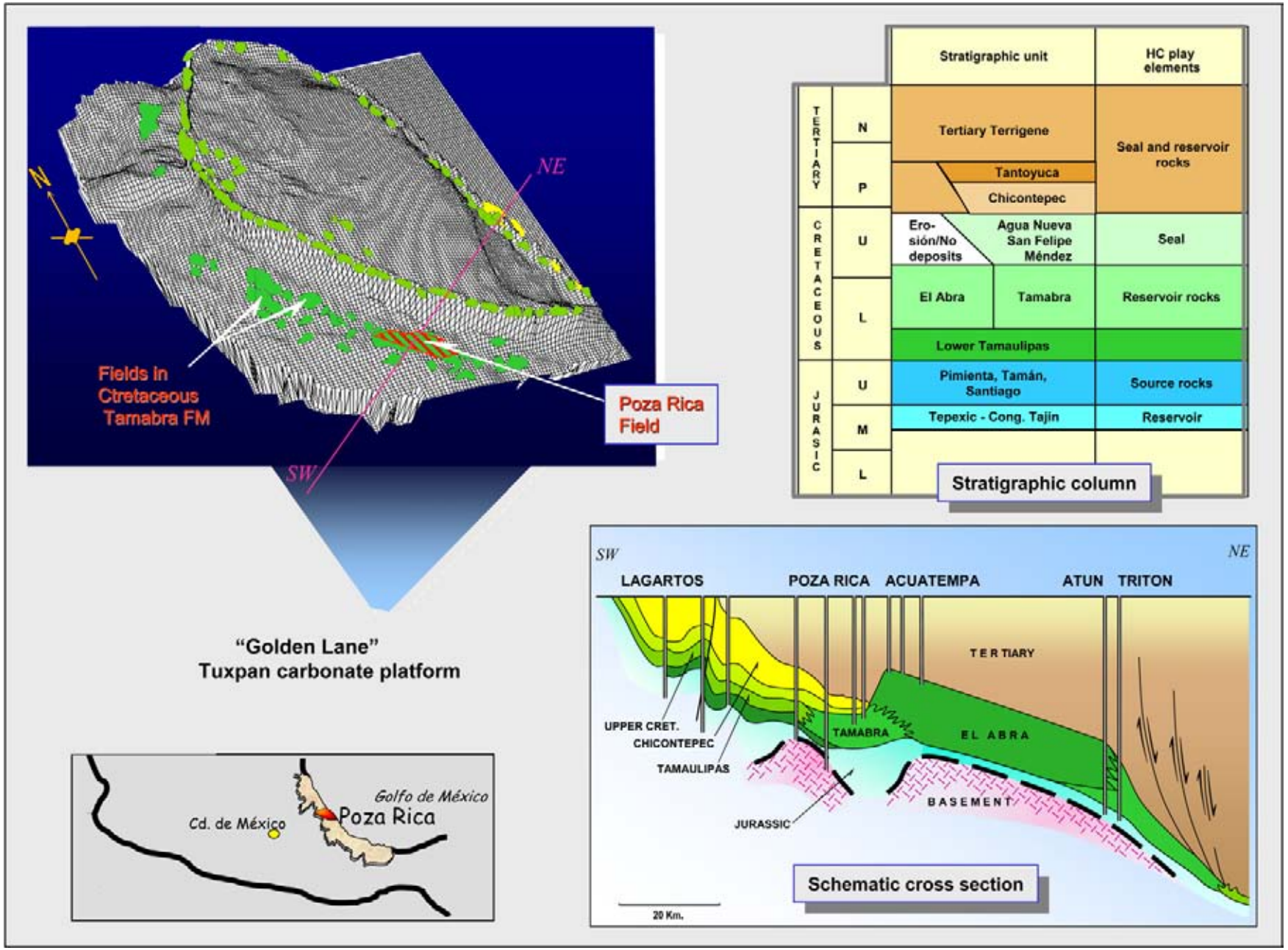

Figure 3.98: The stratigraphic setting of the Tuxpan carbonate platform in the Gulf of Mexico. The presence of hydrocarbons in build-ups along the fringe of the carbonate platform gave rise to the name 'Golden Lane'. The high-energy reefs and the hydrocarbon accumulations follow this outline of the platform margin (courtesy of A. Marhx, Pemex).

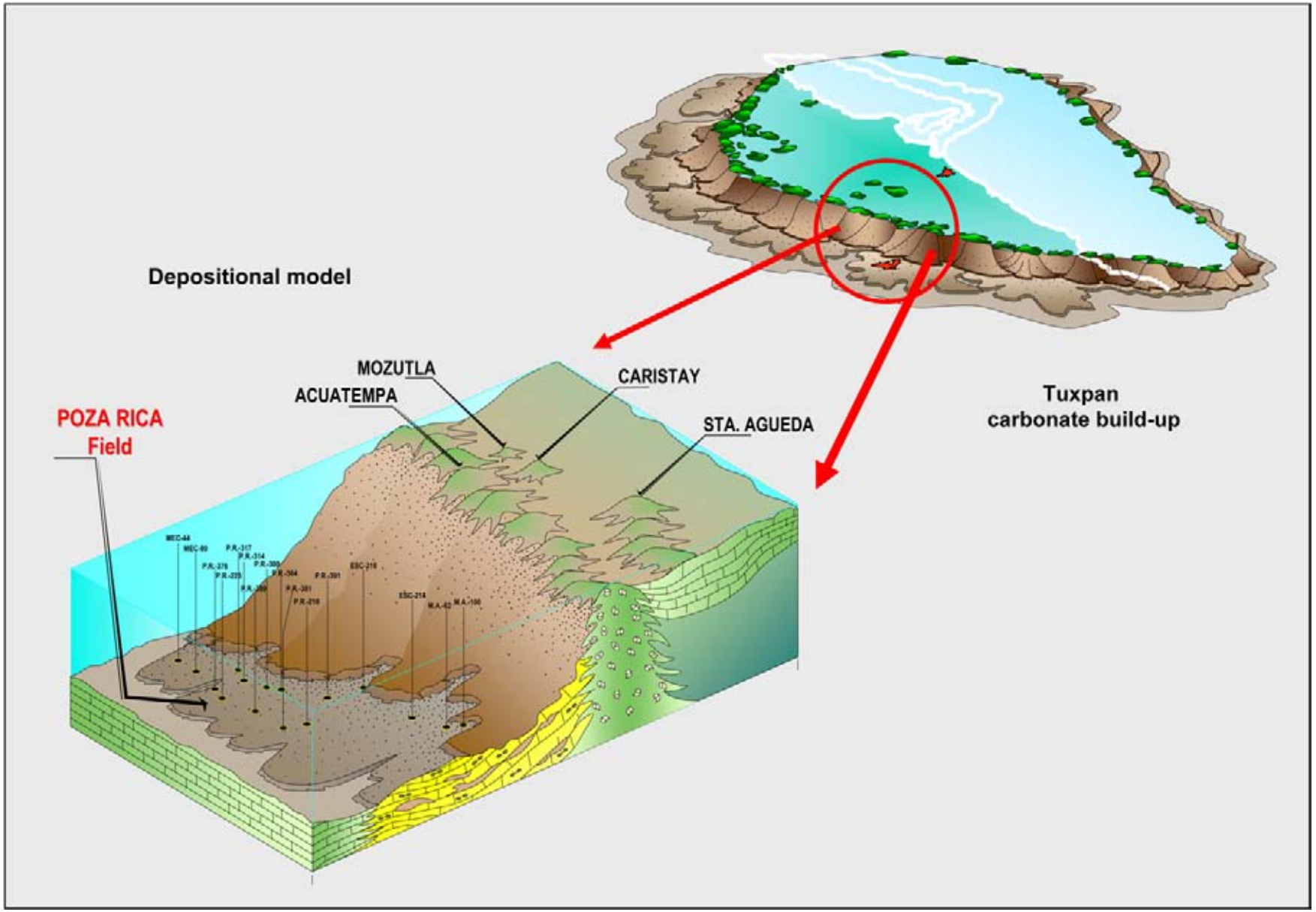

Figure 3.99: Reefal carbonate platform surrounded by a fringing talus. When organic production is high, than a the platform margin is prograding and the talus is characterised by important foresetting. In a carbonate environment this can even occur under conditions of rising sealevel (courtesy of A. Marhx, Pemex).

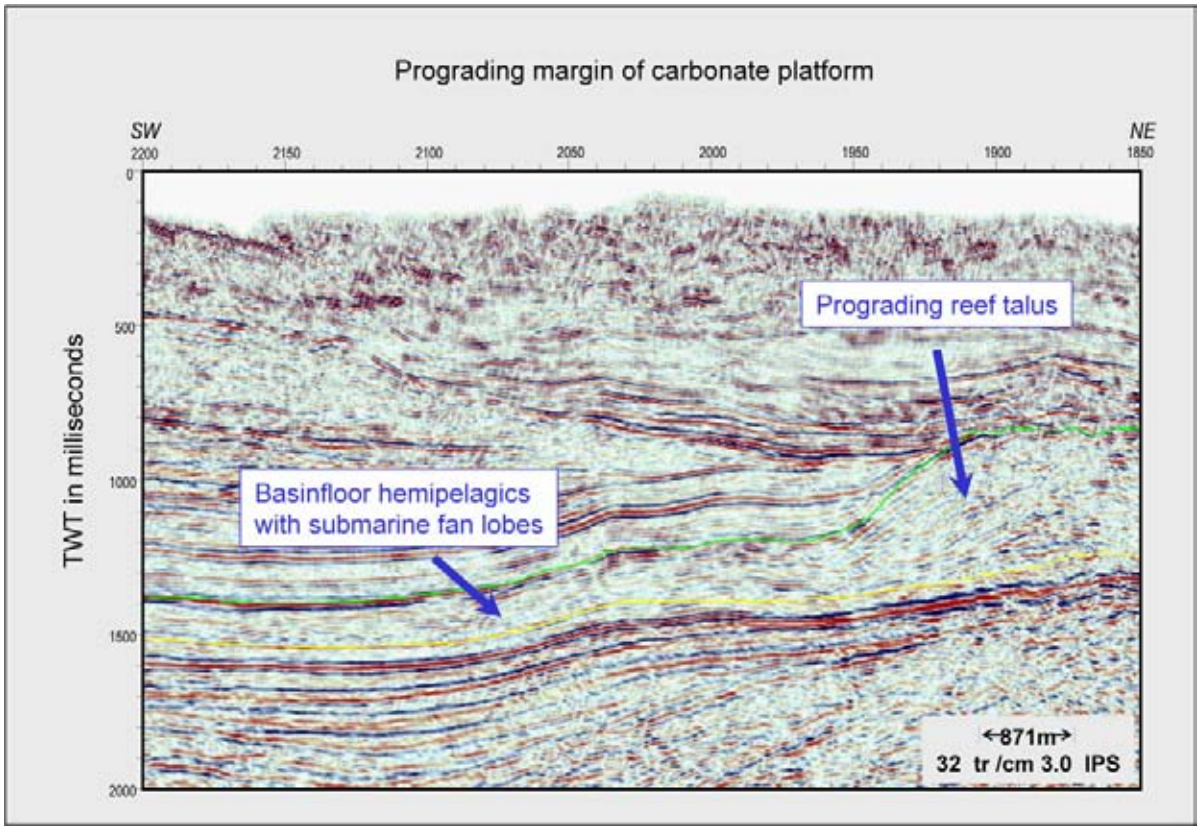

Figure 3.100: Seismic section illustrating the progradation of the platform talus of the Golden Lane carbonate platform in the Gulf of Mexico (courtesy of A. Marhx, Pemex).

arbitrary. It is only recently realised that carbonate particles are submitted to the same depositional mechanism as silici-clastics. The seismic data provides good support for the interpretation of the depositional environment within carbonates. Criteria are wedging, mounding, slope progradation and drastic thinning of the sediments.

Bottom currents may exist on the marine carbonate shelf and massflow transport mechanisms are documented (e.g. San Andres Formation, offshore Mexico). The currents are driven by tectonic instability, storm energy, and/or density and temperature differences (thermohaline). These currents transport coarser material from the coastal delta systems and funnel them further out onto the open marine shelf or abyssal plain. A certain basinfloor morphology is created by the lobes of the fans, with locally some shingling and mounding. Storm-energy brings out larger amounts of the coarser sediments into the more distal parts of the shelf and basinfloor. This seasonal transport mechanism is active at regular time intervals and is to a high degree responsible for the cyclicity seen in the marine sedimentary record.

3.5.4 Deeper marine slope and basinfloor

At the shelfbreak the waterdepth is suddenly drastically increased and it reaches depths of more than 200 metres. At such a location the substratum is either downfaulted or a regional tilt is responsible for creating the greater waterdepth. The deepening of the basinfloor, together with the larger distance from the hinterland, results in a reduced sediment supply. In fact it is no longer sufficient to sustain parallel deposition of the beds and consequently a tapered and inclined sedimentary slope is created. Often the sediment supply is reduced even more towards the deep marine basin centre and on the distal sub-parallel basinfloor starved (or condensed) sedimentation conditions prevail.

On the slope there are some preferential areas where important erosion occurs. Traction currents along the bottom produce **submarine canyon** systems. These canyons are eroded by high-density currents and form feeder channels to submarine fan systems that are located at the base of the slope (Figure 3.102). These submarine fans can be sand-rich, like the Crati submarine fan offshore Italy (Figure 3.103), or shale-rich. Examples of the

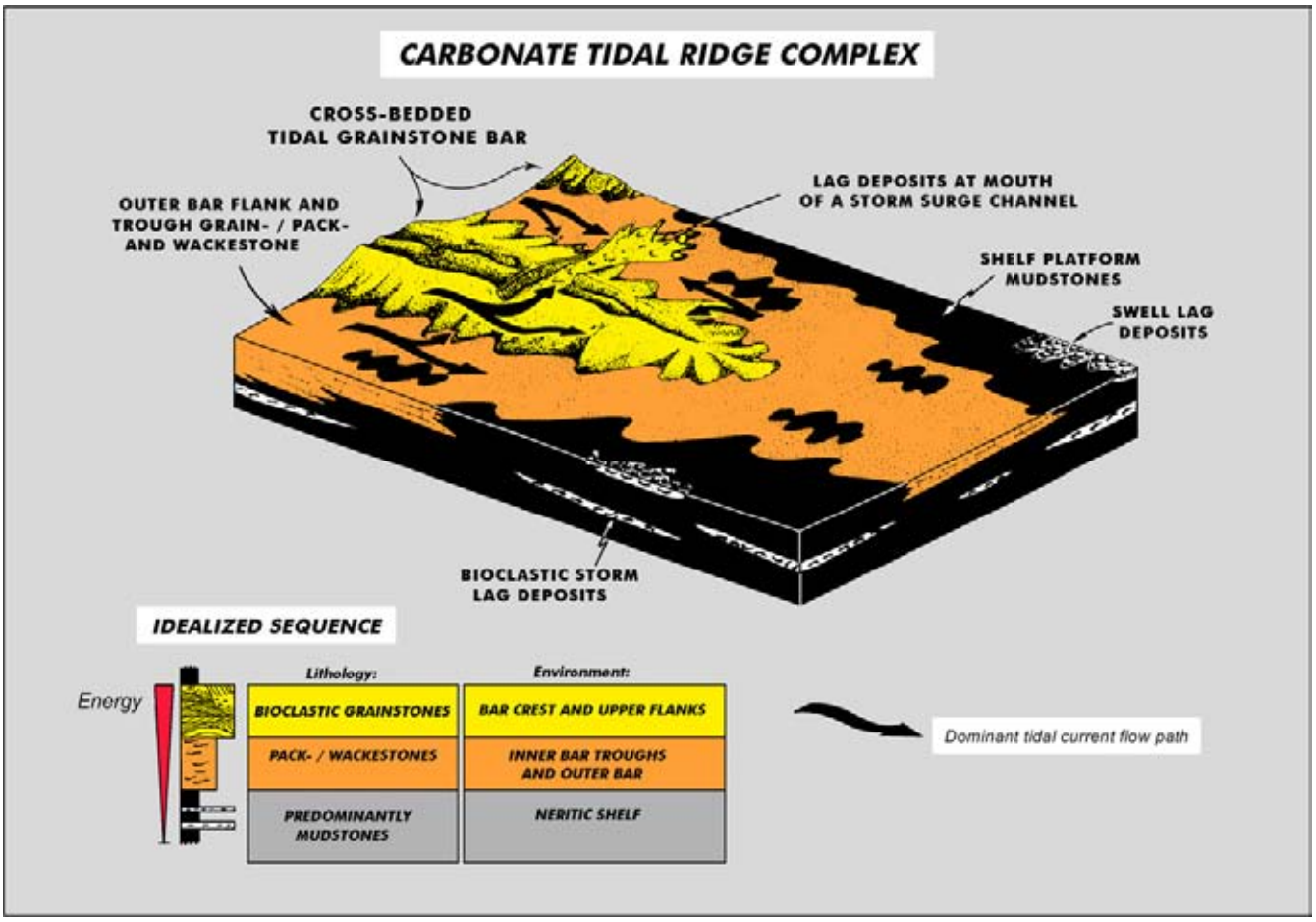

Figure 3.101: Tidal ridge complex as recognised in the Oxfordian carbonates exposed on the eastern flank of the Paris basin. A comparable depositional model exists for silici-clastics. It proves that carbonate and silici-clastic particles behave in a similar way during transportation and subsequent deposition.

latter are the large Amazon cone, offshore South America (Figure 3.104), Zaire Fan, the Indus fan (Kolla and Coumes 1987) and the Bengal Fan (Weber et al. 2003). The side scan sonar images of the Amazon fan system were one of the first to show that even in deeper water meandering channel systems exist (Damuth et al. 1988). Sinuous channels are in fact rather common, also in the submarine domain (e.g. Kolla et al. 2001). But also braided systems have been reported upon (e.g. Belderson et al. 1984). Apparently the geometry depends on the traction forces in the channel, related to discharge and local gradient. Meandering means regular discharge and low gradient. These fan systems are present in really deep water (>4 km). The sand-rich fans are in general much smaller in size than the mud dominated ones. The shape of a submarine fan complex varies a lot and is dependent on:

- Sediment supply.
- Basinfloor morphology and mobility of substratum.
- Number and shape of the input sources.
- Degree of tectonic instability.
- Presence of bottom currents which can rework the sediments.
- Position of relative sealevel.

The sedimentation modes vary from traction by bottom currents to **massflow** processes and **hemipelagic** deposition (Figure 3.105; Nelson and Kulm 1973). If the deposit is water laid, then the general term **density current** is also used (Bruhn and Surlyk 2004). One special form of massflow deposition is the **turbidity current** (Mutti and Ricci Lucchi 1978). These currents are often generated on the upper part of the slope and even on the shelf by tectonic instability and/or storm events. The current starts as a density flow that picks up speed and transforms into a turbulent flow with many vortexes/eddies. It results in mixing of the lithologies and larger components are more easily supported by the heavy fluidised matrix (Blatt et al. 1972).

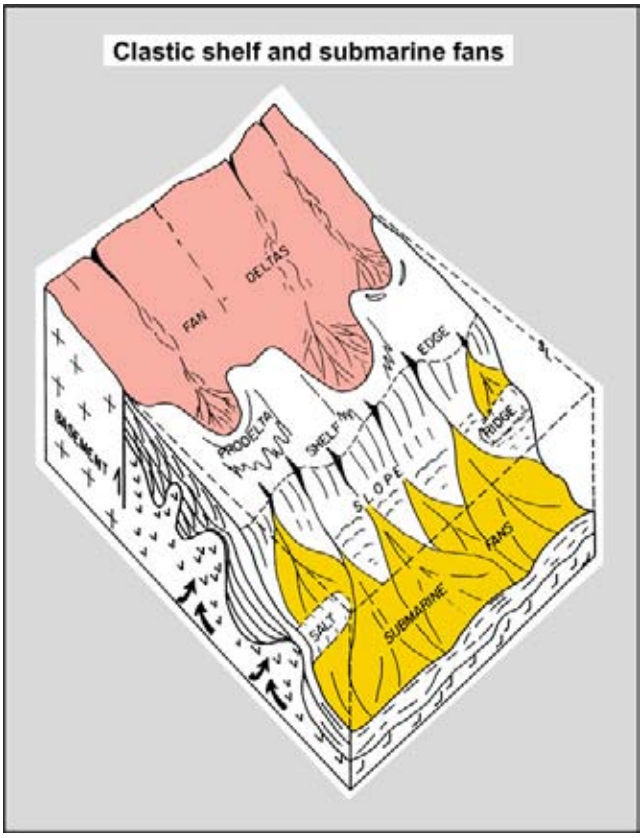

Figure 3.102: Block diagram illustrating submarine fan deposition and underlying salt movement (modified after Brown and Fisher 1977).

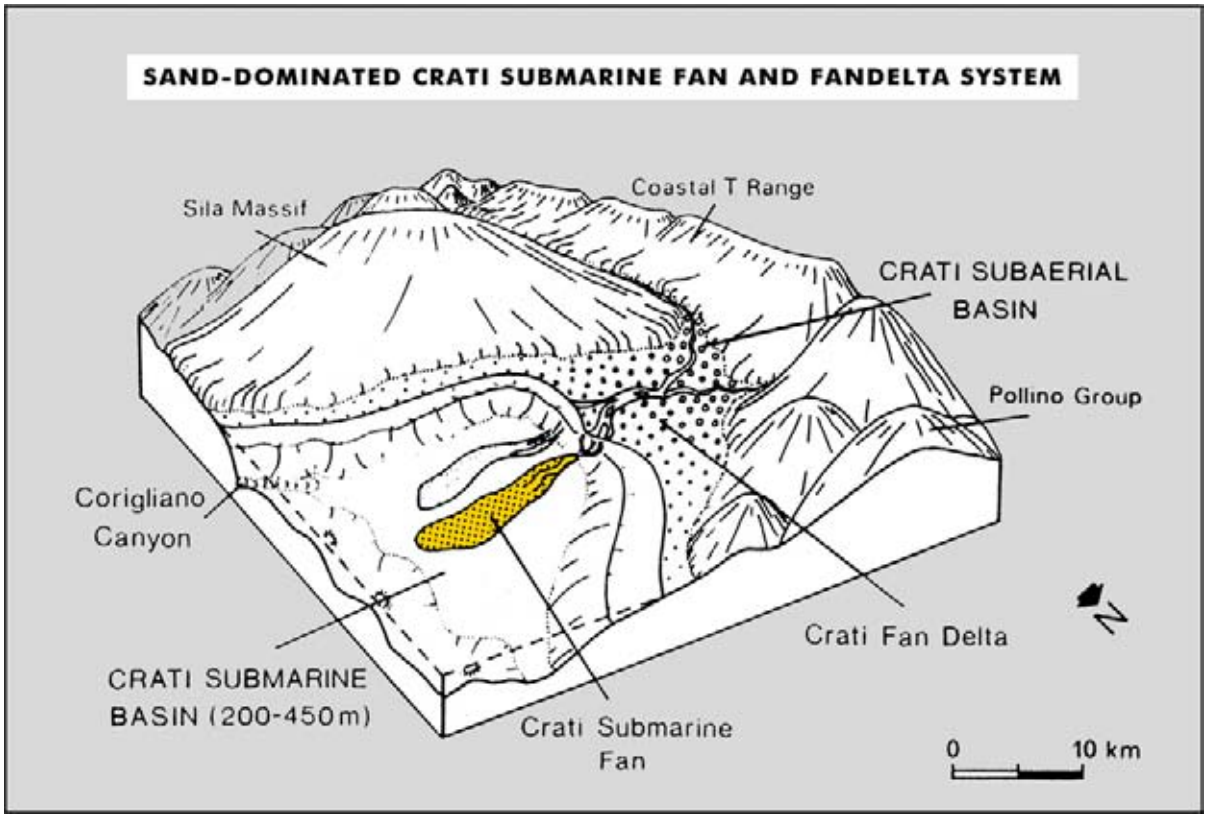

Figure 3.103: Sand-dominated submarine fan system of the Crati fan in southern Italy. Note the rather short transportation distance compared to mud-dominated systems (after Colella and Di Geronimo 1987).

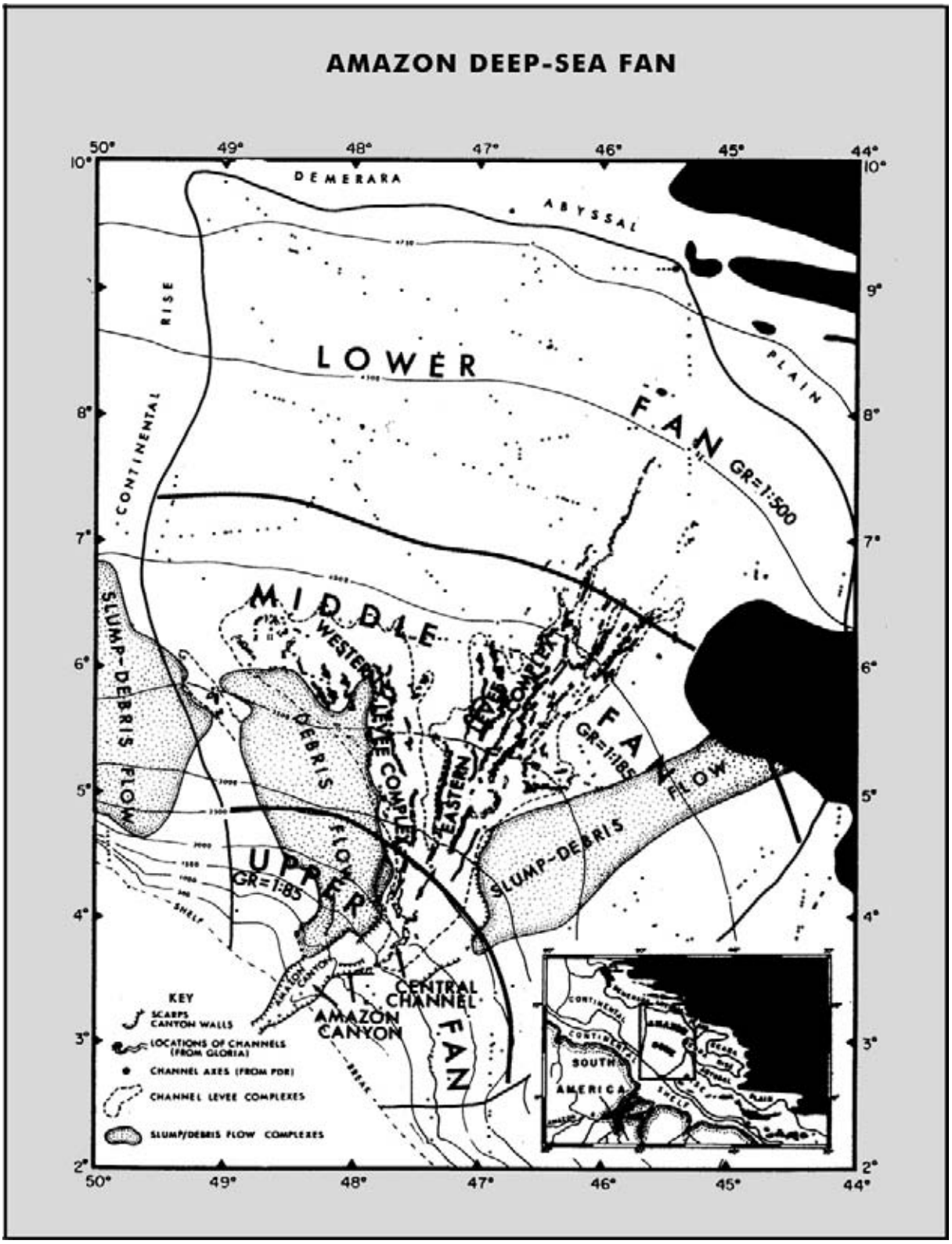

Figure 3.104: Mud-dominated submarine fan system of the Amazon cone, located offshore South America. Note the size of the fan complex and the vast hinterland supporting the clastic system. Just like in fluvial channel systems, a low structural and depositional dip on the fan favours meandering of the submarine channels (after Damuth et al. 1988).

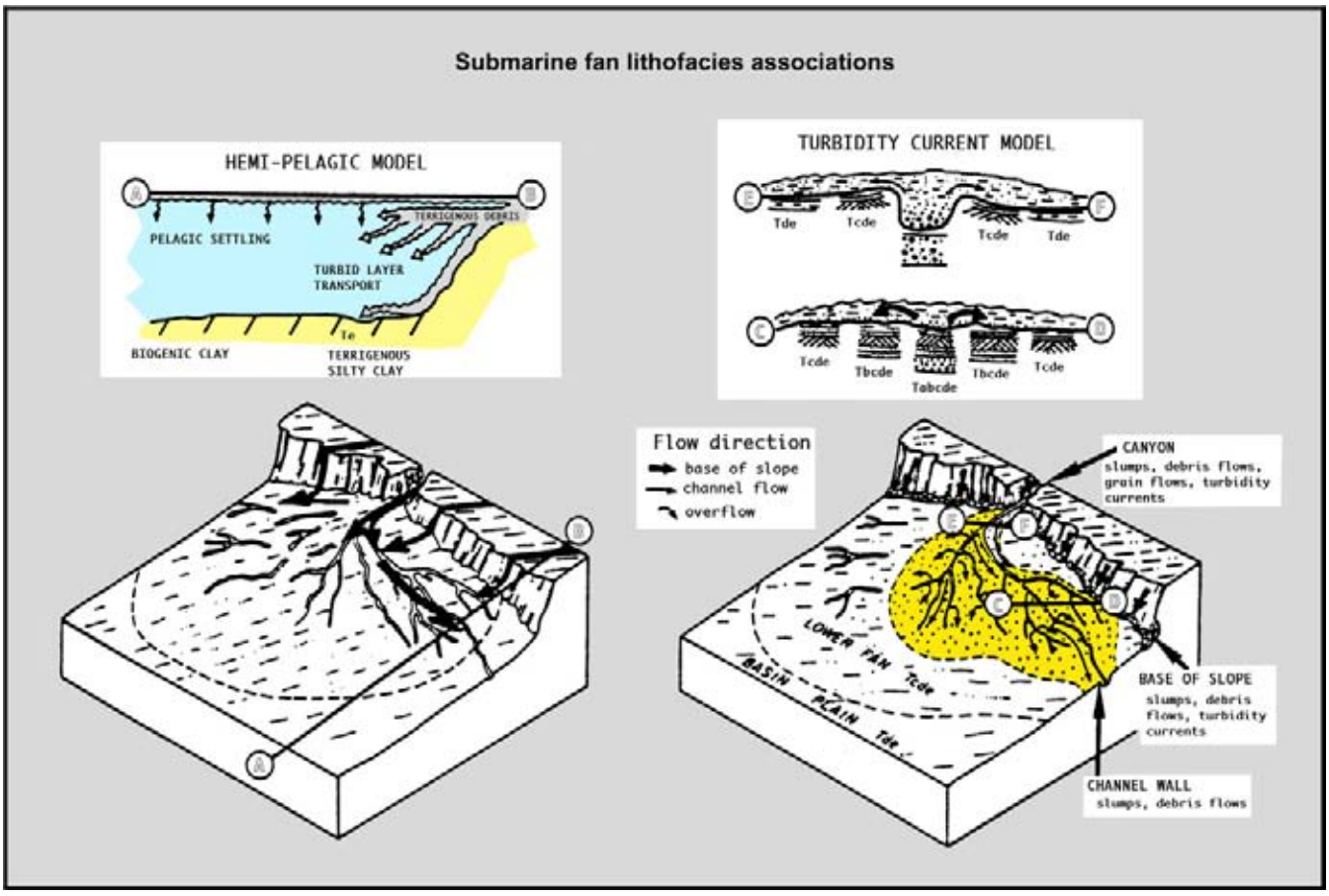

Figure 3.105: Sedimentation patterns on submarine fans and associated lithofacies distribution with Bouma sequences as a result of waning flow behaviour of a turbidity current. Two models are here shown: the hemi-pelagic where the influx of coarser sediment is reduced (sealevel rise condition) and the turbidity current model with increased amounts of silici-clastics reaching the basin (after Nelson and Kulm 1973).

The turbidity event starts suddenly, picks up speed and runs down slope where it gradually will loose its energy. The typical product will be a **waning flow** succession that reflects vertically the different energy stages of the turbidity current. The turbidity flows are characterised by turbulence of their internal flow when the energy is still high enough. This type of flow is in part detached from the basinfloor and keeps in suspension badly-sorted coarse material (Figure 3.106). If the energy is really high, then huge exotic blocks (several metres in diameter) are transported by these flows. It shows the dramatic force of such a massflow event. The resulting deposits are also known as proximal **fluxo-turbidites** (cf Veeken 1983; Kleverlaan 1987, 1989).

A typical succession of related lithologies is produced during the gradual decrease in energy of a fluidised massflow current: the so-called **Bouma sequence.** These Bouma sequences illustrate the waning flow dynamics of the turbidity current. It starts with a coarse grained massive bed T_A with occasional inverse grading, followed by parallel lamination T_B (upper flow regime), cross laminated unit T_C and parallel fine grained deposits T_D (lower flow regime). The inverse grading results from partial freezing of the fluidised flow by sudden water escape.

It is useful to describe here in some more detail the depositional model for massflow systems. Density currents are largely responsible for redistributing clastic material on the slope and basinfloor (cf Weimer and Slatt 2004). They are at the origin of slope fan systems and these deposits contain major hydrocarbon accumulations, which explains their particular interest to the geoscience community. The geometry and internal structure of submarine fans are influenced by factors like: source area, climatic conditions, sealevel and tectonic movements (cf Prins and Postma 2000). They can be incorporated on the shelf, the prograding slope or deposited on the basinfloor. It depends on the relative sealevel position as will be shown later on. The ideal

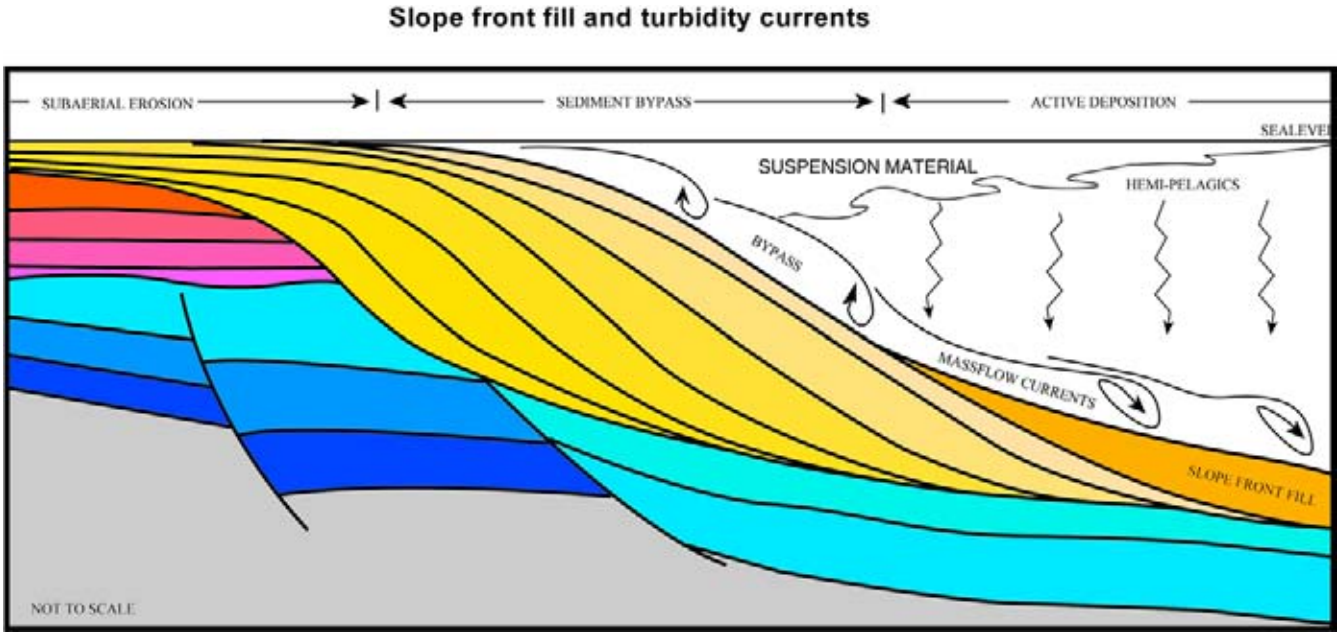

Figure 3.106: Turbidity and massflow deposition at the base of the slope. Turbidity currents start at the top of the slope or on the shelf. They pick up speed as they run down the slope. Finally the flow looses its velocity and its fluids whereby the sediment particles are deprived of their energy. The result of this succession of events is a typical waning flow deposit, characterised by Bouma sequences. A typical slope front fill is often created (brown) that can be tracked down on seismic sections.

form of a fan is a radially outbuilding sediment body (Figure 3.107; Normark 1978, Walker 1978). The geometry and internal architecture of submarine fans is illustrated in Figure 3.108. Three morphological units are normally distinguished on these fans (Normark 1970, 1978; Normark et al. 1979):

* *Large leveed fan-valley(s) of the Upper Fan (also known as inner fan)*, producing wide (1–5 km) valley-floor deposits which are coarsest on the whole fan. These sediments are laid down in meandering and/or braided shallow channels within the confines of the fan-valley itself (e.g. Amazon deepsea fan). The channelised deposits show a chaotic discontinuous seismic response and have clear erosional contacts at its base. The coarser deposits grade laterally into finer-grained, more regular bedded shales and silts with the occasional sand, that build the levees of the fan-valley. These levees are characterised by a low-angle prograding (away from the channel axis), low amplitude seismic expression. Slump scars can be present due to slope instability and eroding activity of the adjacent channel.

** *Suprafan/depositional lobes of the Mid Fan region*, located at the termination of the leveed fan-valley. On a radial profile this suprafan unit shows up as a convex-upward bulge. In the upper part of the suprafan numerous non-leveed channels and also isolated depressions can be found. They gradually disappear down-fan. The width of the suprafan channels is usually less then 1 km and they are filled with thinning- and fining-upward sequences. Because of the cut-and-fill nature of the channels, the seismic response will show a chaotic to hummocky reflection geometry. Erosional contacts are quite frequent.
At the mouth of these distributary channels most of the sediment load of the massflow currents is deposited. This is due to the sudden change in hydraulic conditions of the flow as it is no longer confined by levees. The radially spread-out of sheet-like sediments at the terminus of the channel-system normally show a high sand/shale ratio. These sand-prone sediments will be represented on seismic by low-angle progradation (Rochow 1981) or multi-directional shingles. Coarsening and thickening upwards sequences are the result of the progradation (Figure 3.109). On a cross-section it will be a typical bi-directional low-angle foresetting (Figure 3.110; Veeken 1997).
A distinction can be made in sand- and shale-prone channel abandonment fills. This is based on differential compaction effects: a convex upward top boundary of a channel is most probably filled by sand-prone sediments.

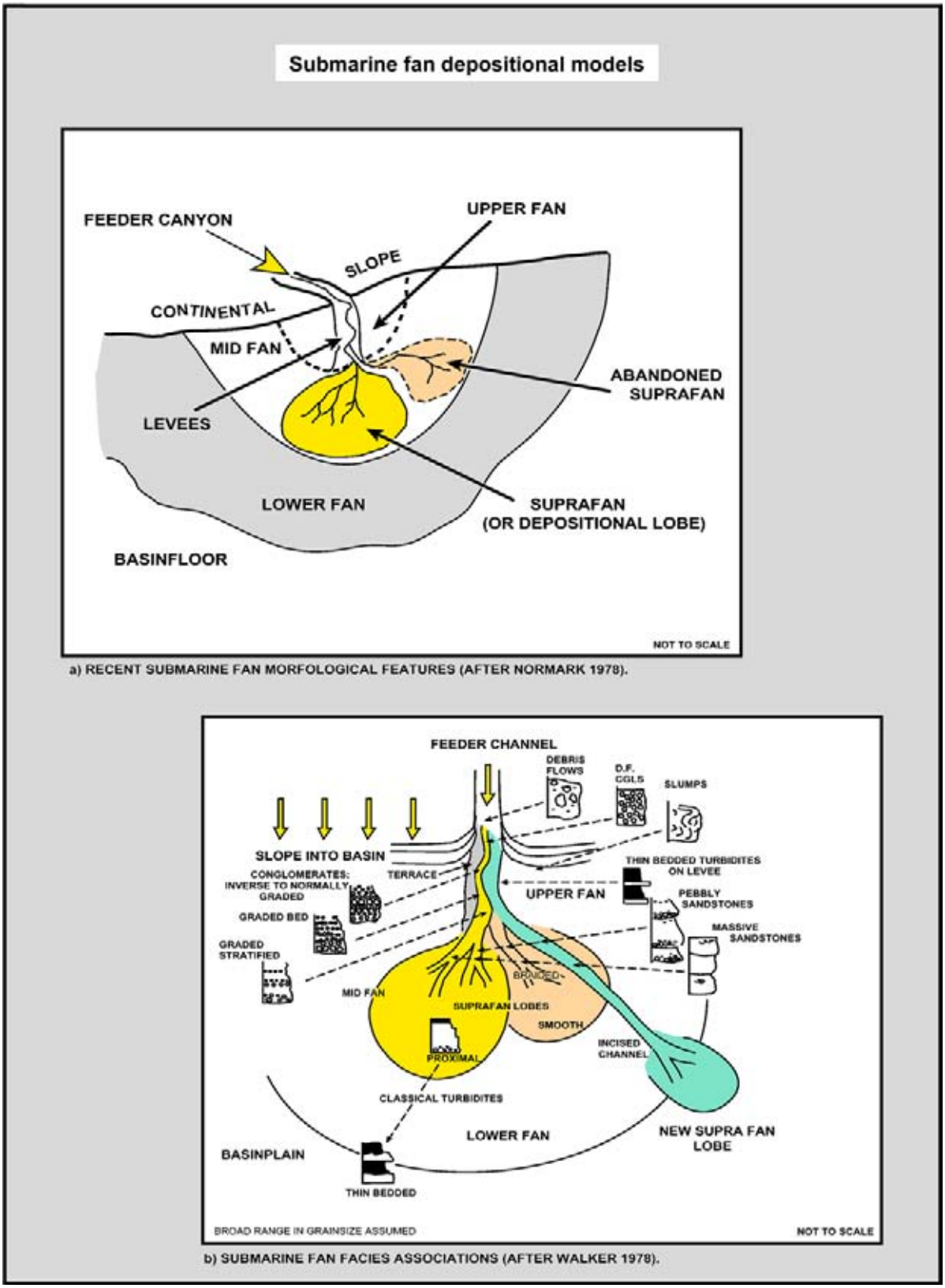

Figure 3.107: Morphology and depositional lithofacies facies associations within submarine fan systems. The Normark model describes the morphological features on recent submarine fan systems, while the Walker model presents the lithofacies associations from ancient submarine deposits (modified after Normark 1978 and Walker 1978).

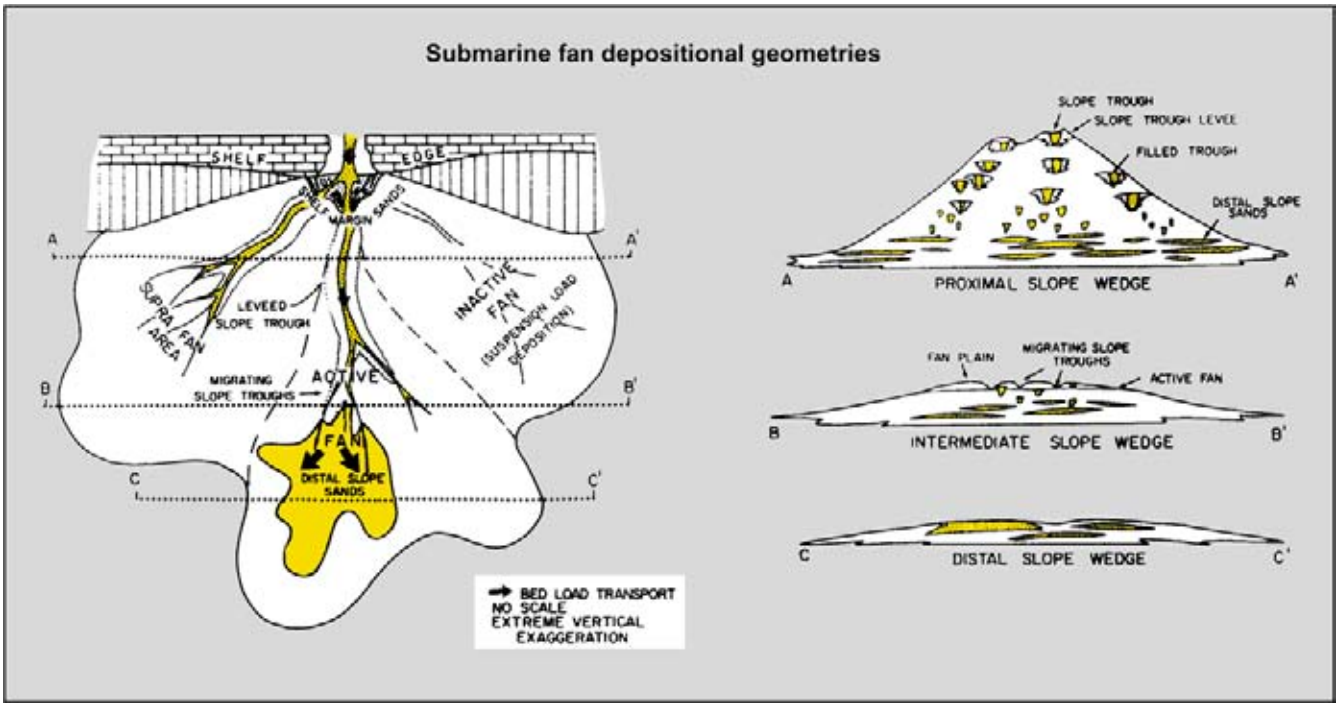

Figure 3.108: Submarine fan geometry and its internal architecture. The leveed channels are restricted to the more proximal domain. Downslope the channels are becoming wider, no longer confined by levees and less deeply cutting. It is transitioned into an irregular groove system as a result of erratic channel overflow (after Brown and Fisher 1977, reprint from AAPG whose permission is required for further use).

*** *Flat and smooth topography of the Lower Fan (also known as outer fan)* which in most cases lacks channel features and is gradually merging into the basinfloor plane. It is characterised by continuous sheet-like deposits with a lower sand-shale ratio. If the fan is outbuilding coarsening- and thickening-upward sequences are most common.

The upper fan essentially forms an area of sediment bypass, while the middle fan represents a zone of active sand deposition (Figure 3.111). The levees dip away from the channel axis. The sheet sands are tabular, erosional base or mounded in geometry. Superposition of several flow events may produce a single massive sandstone layer with an amalgamated nature. Criteria for channel sands are:

- Erosive base and coarser lag deposit.
- Presence of shale clasts.
- Interbedding of debrites and shale clast conglomerates with turbidites.
- Lower lateral continuity.
- Channel abandonment is characterised by a vertical thinning and fining upwards trend, with shale deposition in the final stage.

The width-to-thickness or **aspect ratio** varies considerably. For channel sands it mostly amounts to 10 : 1 (updip) and 50 : 1 (downdip), while sheet sands have a ratio of 1000 : 1 (Weimer and Slatt 2004). Overflow of the channels is a rather common phenomenon when turbiditic currents are coming down the slope, leading to non-confined flow and causing local erosional features or grooves (e.g. Khripounoff et al. 2003). **Flow stripping**, whereby the finer part is separated from the coarser part of the flow by overshooting the channel wall, can lead to anomalous grain size distribution of the turbidites.

The most important transport mechanism is gravity driven massflow transportation. The massflow can be dense or less dense, laminar or turbulent, with a behaviour that is plastic cohesive or fluidised non-cohesive (Postma 1986). Several basic classes of gravity flows are distinguished based on these characteristics: turbidity currents, cohesive turbidity current, liquefied flow, fluidised flow, grain flow, cohesive debris flow, slumps and pure rock fall is an extreme end member, where water is no longer the carrying agent.

Another typical characteristic of freely out- and upbuilding submarine fan systems is the regular shift of the depocentre position in space and time. The deposits can be incised by a younger feeder channel fan system

Figure 3.109: Prograding depostitional lobe sediments in a submarine fan complex with coarsening and thickening upwards sequences. The layers are organised in typical Bouma sequences, products from waning flow conditions.

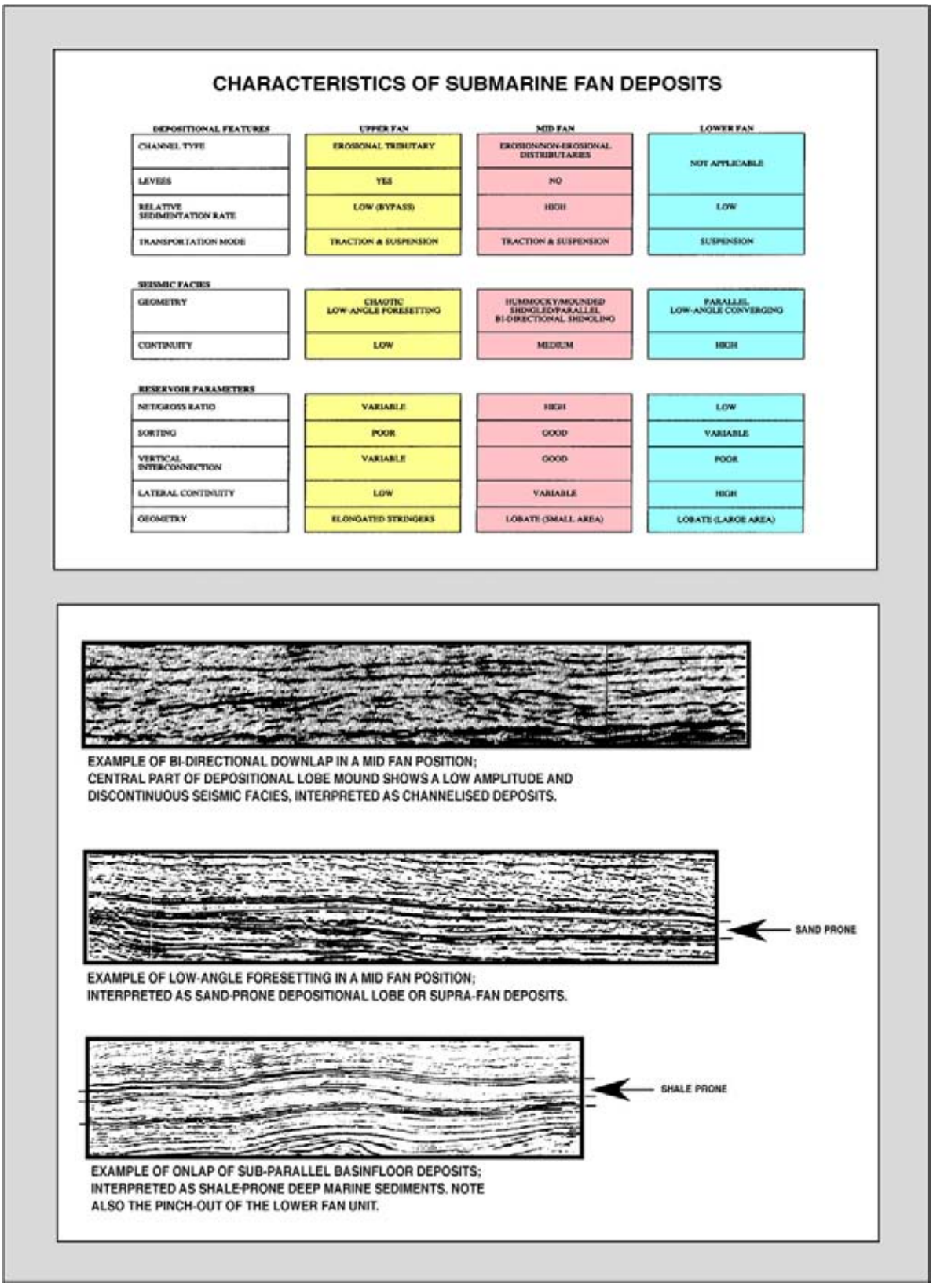

Figure 3.110: Expression of submarine fan deposits on seismics from the Central North Sea area. The upper fan is characterised by leveed channel deposits, while the mid fan is characterised by depositional lobes with typical bi-directional downlaps and mounded cross-sections (Veeken 1997).

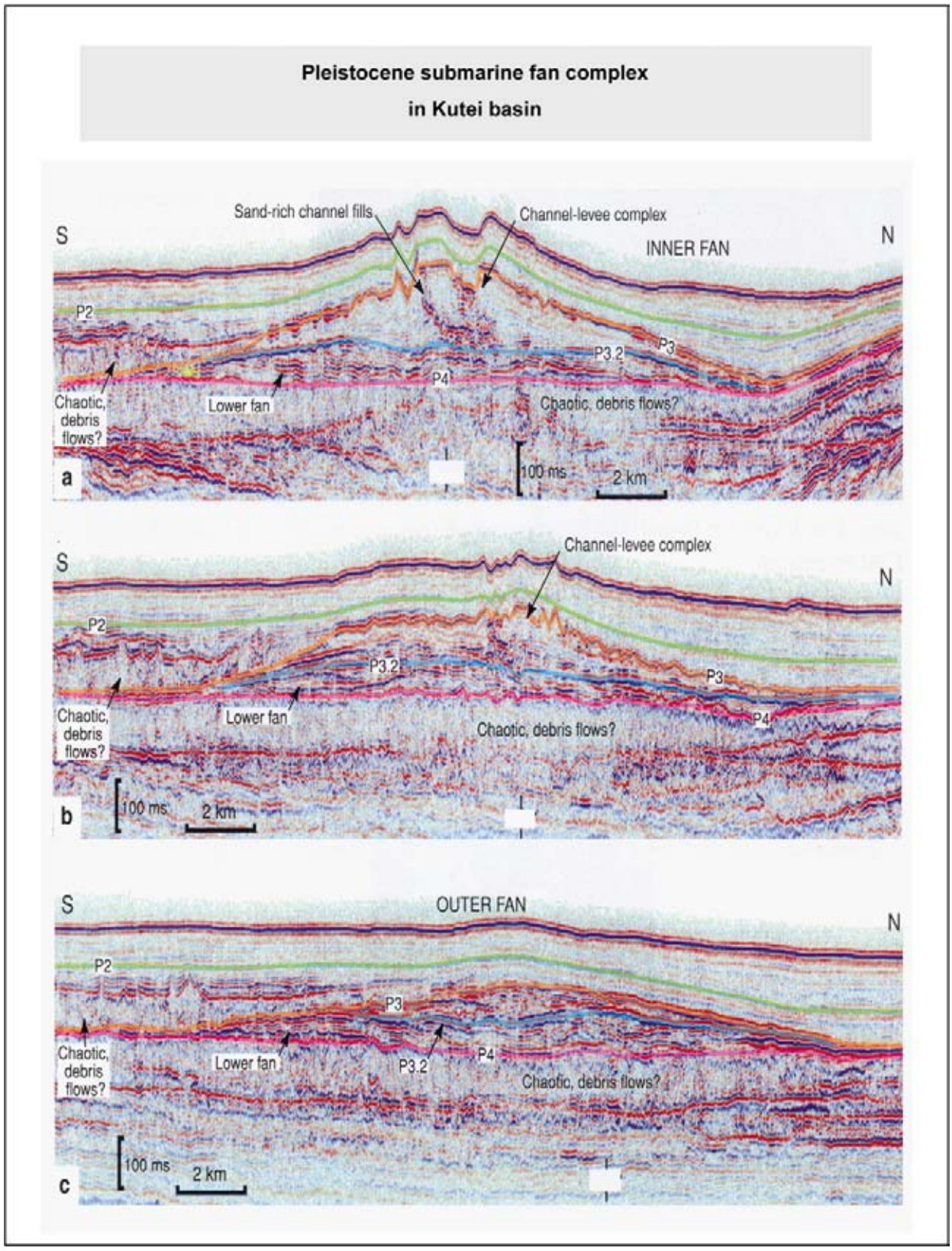

Figure 3.111: Pleistocene submarine fan complex in the Kutei Basin. The inner fan and upper part of the mid fan regions have levees flanking the distributary channel system. These are built by regular lateral overflow of the channels. The levees are dipping away from the channel axis. The outer fan is formed by the distal part of the depositional lobe deposits, with more continuous sheet geometries and bi-directional pinch-outs on the seismic sections (modified after Weimer and Slatt 2004).

(transient fans, Adeogba et al. 2005). Channel avulsions are often seen to be guided by weak external forces, like the **Coriolis effect** (e.g. Popescu et al. 2001) that also cause asymmetric development of the channel levees. **Levees** are build where substantial lateral overflow of the channels occurs. Instability on the slope and the flank of the levees may lead to **slump scars**. The slump masses can be substantial in size (e.g. Gordo turbidite sequence in SE Spain, Klevelaan 1987). Deposition in the channel and on the levee is not necessarily synchronous (Weimer and Slatt 2004).

Often the fans deviate from the ideal radial geometry because of confinement and strong topographical constraints (Lomas and Joseph, 2004). An example of a sand-rich fan system fed by a fan delta complex is provided by the Gres d'Annot outcrops in the Alpes Maritimes and de Haute Provence of southern France (Joseph and Lomas 2004). In fact the fan complex is deposited in a foreland basin, influenced by the emplacement of the Alpine nappes (cf Ford et al. 1999). Tectonics have played a dominant role and led to the elongated geometry of individual fan bodies (Figure 3.112). The sedimentation rate in this Eocene-Oligocene fan complex is rather high and estimated approximately 12 cm/1000 years. The clastics are derived from the Maures–Esterel and Corsica–Sardinia massif in the south. Syn-sedimentary tectonic activity is suggested by soft sediment deformation structures due to restricted water escape (Figure 3.113).

There is a distinction between channelised and non-channelised submarine fan systems (cf ponded and perched fans of Beaubouef and Abreu 2004). The non-channelised system are composed of distal fan deposits with good lateral continuity. No channels are present and the depocentre of the deposits coincides with the maximum deep of the saucer shaped basal horizon. The flow is probably detached from the basinfloor and thus unconfined with a wide open distribution of the sediments. It results in basinfills where time contours and isopach resemble in shape. The channelised type of submarine fans has channelling and a fan shaped outline. Its depocentre is located asymmetrically in respect to the total fan shape (Figure 3.114). It contains a higher energy assembly. Most submarine fans are directly connected to a river delta system but some are disconnected whereby the feeder channel is fed by longshore currents (Posamentier et al. 1991).

For the interpretation of ancient submarine fan deposits it should be kept in mind that the original depositional geometries, for example the relation between levees and channel-axis, are overprinted by burial effects. As a result of differential compaction, the stacked sand-rich channel-fills of the upper/middle fan region often coincide in the subsurface with a convex-upward bulge in respect to their finer-grained associated overbank deposits. These overbanks originally build the elevated levees of these channels. The differential compaction thus may lead to **inversion** of the original depositional morphology. An excellent overview and rigorous subdivision of submarine fans is given by Reading and Richards (1994). Some characteristic features are input source (single, multiple or linear source), grain-size (mud, mud/sand, sand and gravel), slope gradient, feeder area (size, gradient, distance, material), shape (radius, length), supply mechanism (regular, episodic), size of sediment flows. The interplay of tectonics, clastic supply, climate and sealevel has a decisive role on the end result.

Contourites are deepsea deposits generated by basin-floor currents. They are commonly found along continental margins. The sediments often form conspicuous mounds or drifts. The bottom currents are thermo-density driven. The flow is mostly non-confined and influenced by the weak Coriolis force, oriented to the right on the northern hemisphere. The contourite deposits are usually believed shale-prone, but occasional sands are not excluded beforehand. With the move of exploration into deeper waters these sediments may be of interest for the petroleum industry in the years to come (Stow et al. 2003).

Along carbonate shelves similar sedimentary bodies are encountered. The debris, eroded on the high-energy side of carbonate build-ups, is deposited in the inclined talus area as an coarse-grained apron. The talus is forming the foresetted part of the build-up, where massflow deposits (rockfall, slumps, debris flows, turbidity currents) are alternating with hemipelagic shales (suspension). These sediments are mostly badly sorted, but this depends also on the source material. In some cases the carbonate shelf is severely eroded and cut by canyons just like on silici-clastic shelves. These channels funnel shelf material towards the deeper parts of the basin and submarine fans may develop, mainly consisting of reworked carbonates. The Tamabra formation in the Misantla Basin (Mexico) represents for instance a slope apron system composed of stacked depositional lobes (see Figures 3.98–3.100). The sediments are derived from the nearby Golden Lane Tuxpan platform (cf Magoon et al. 2001).

Triassic sequences of Ladinian and Carnian age in the Italian Dolomites display excellent examples of progradation of the carbonate platform margin, with outcrops on a seismic scale (e.g. Bosellini 1984). The thickness of the package varies from 500–1000 metres. Progradation and foresetting is an episodic process. Moments of

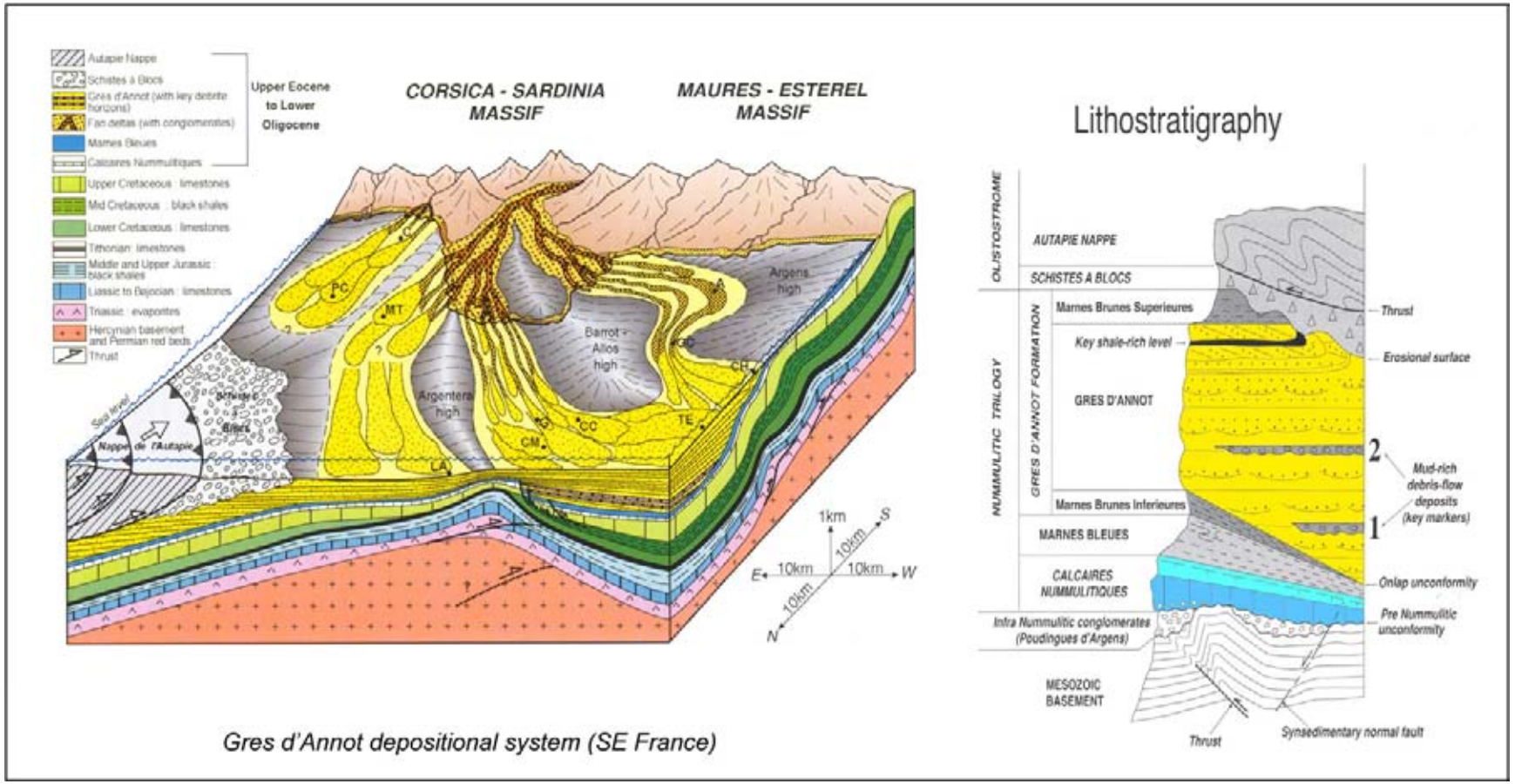

Figure 3.112: The paleogeographic situation for the sand-rich submarine complex of the Gres d'Annot in southern France during the Early Oligocene. The fandelta in front of the Corsica–Sardinia Massif is feeding the submarine fan lobes down-slope. The submarine fans are confined by the shape of the basinfloor topography and this is expressed in their elongated external geometry (modified after Joseph and Lomas 2004).

Figure 3.113: Soft sediment deformation seen in Gres d'Annot submarine fan deposits in southeastern France. Tectonic instability and problematic water escape in these sediments have resulted in a certain degree of overpressure and subsequent plastic deformation of the sands in the heterolithic package. Differential loading at the base of the sandy layer and contorted bedding give rise to incipient flame structures.

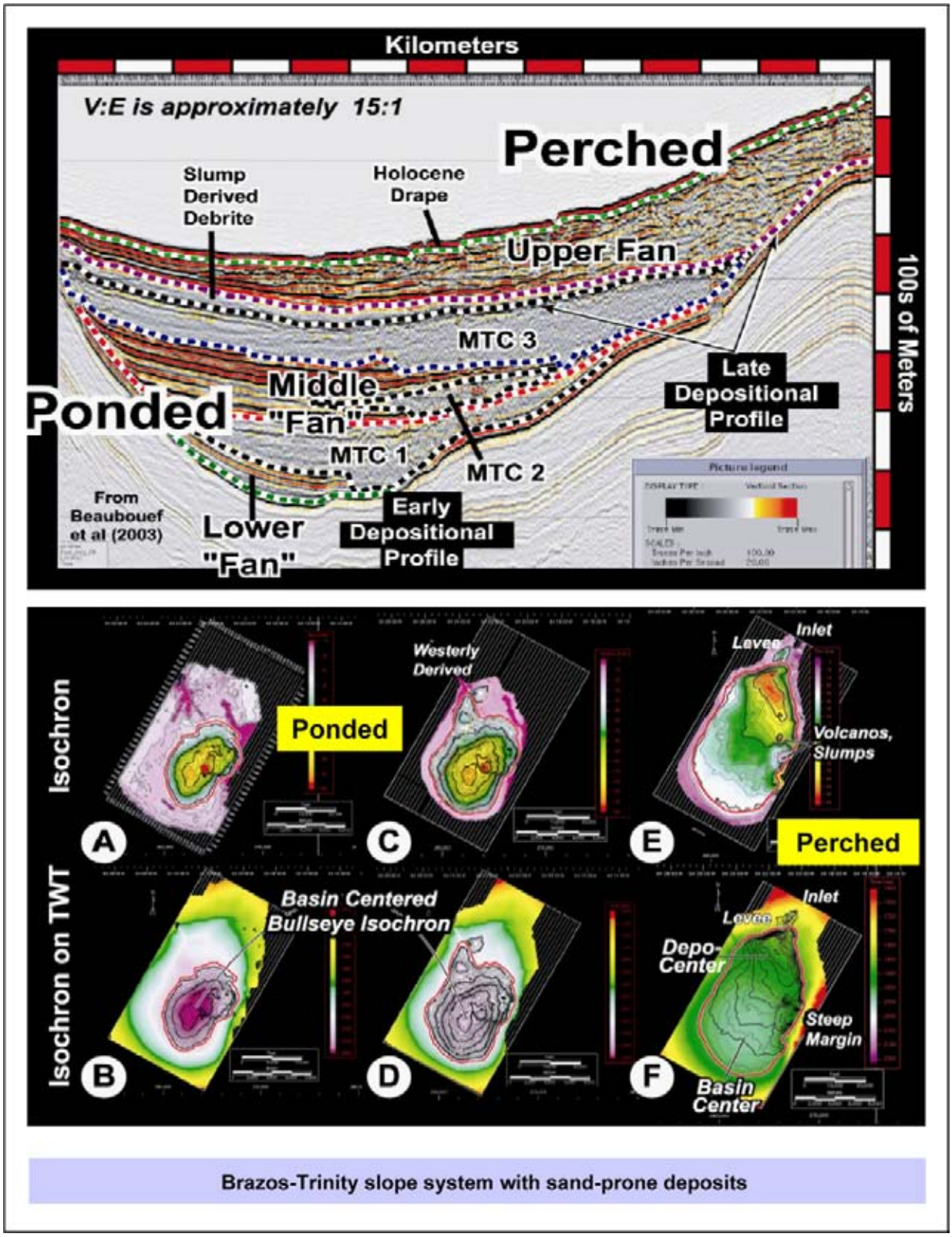

Figure 3.114: The difference between the ponded and perched submarine fan deposits is illustrated. The ponded fan deposits are composed of distal turbidites with great continuity and no channelling. They fill in a low in the paleotopography. The currents are weaker and probably also partly detached from the basinfloor (high salinity seawater?). The time contour of the base and the isopach resemble in shape. The perched or channelised type is a fan system with a clear channelised proximal part. It is a higher energy system and the depocentre is located asymmetrically within the overall fan system (Beaubouef and Abreu 2004).

massive debris input alternate with longer periods of negligible shelfedge progradation, during which basinal sediments are accreted and onlap the toe of the slope. A normal average horizontal progradation rate quoted in the literature is in the order of 1 metre per year, based on silici-clastic and carbonate studies. But for these Triassic dolomites it must have been considerably slower (1–10 cm per year?). Moreover, there are important variations between various platforms: Catinaccio 9–10 km, while Pale di San Lucano prograded only 1–2 km. These Middle to Upper Triassic carbonates underwent severe subsidence and show a growth potential that exceeds 400 metres per million years (Bosellini 1984).

A distinction with clastic systems is that:

- The carbonate platform constitutes its own source, producing debris material dumped around it.
- The isolate nature of the sediment source.
- The flat topography of the hinterland.

During sealevel rise conditions the biologic activity increases and more debris material is hence available for re-deposition. The apron is active during the relative sea level lowstand and early transgressive cycle, while the submarine fans are mainly build in the highstand periods. On the clastic shelf the highstand is the moment when the sediment supply get blocked in the hinterland and basinfloor fan progradation is therefore assumed to coincide with the relative sealevel fall interval.

3.5.5 Carbonate platform margin

As seen earlier on, material deposited on a carbonate shelf is often further transported and laid down in submarine fans at the base of the slope. Tectonic instability, induced by external forces are sometimes at the origin of this reworking. This was for instance the case when a gigantic meteorite, caused a gigantic impact crater on the edge of the Yucatan carbonate platform in the Chicxulub location in Mexico. This astronomic event occurred at the Cretaceous/Tertiary time boundary some 65 million years ago (e.g. Hildebrand 1991, Smit et al. 1992, Alvarez et al. 1995, Smit 1997). It did not only caused the mass extinction of species (cf Smit 1991), whereby 70 percent of the land animals disappeared, but also resulted in the creation of sedimentary breccias in the Upper Cretaceous carbonates at the impact site. The carbonates have nowadays an exceptionally good porosity. The breccias experienced only limited transportation and are not exactly in-situ created but were affected by some slumping on the instable depositional slope. Coarse grained brecciated slope apron carbonate rocks form the main HC reservoir in the Cantarell field. Major tectonic deformation, expressed by the presence of a complex overthrust, plays an additional role in the structuration of this giant oil field (35 billion barrels and a 905 m HC column, Pemex 2000). It is estimated the eighth largest field in the world and has reached a cumulative production of 10 billion barrels of oil already, with a current daily production of 2 million barrels. The structural style and tectonic deformation of the Cantarell field is still somewhat controversial. A certain degree of wrench tectonics seems difficult to circumvent, although the recent 2003 re-interpretation of the 1997 OBC data by Garcia Hernandez et al. (2005) suggests differently. The quality of the data leaves scope for various interpretations. Well data has to confirm the validation of the proposed structural working model. Strike slip and wrenching has played an important role in the structuration elsewhere in the region (e.g. Macuspana Basin, Veracruz Basin).

The tectonic instability, caused by the localised meteoric impact, could have been the by-product of an other dramatic astrological event: the catching of an external celestial body into our planetary system. It is well known that Venus has an opposite spin to all other planets in our solar system (Moore and Hunt 1983). It must therefore have a different origin compared to the other planets. The catching of an celestial body within our planet system has of course a gigantic impact on the overall stability. It will fundamentally change the forces influencing the earth and may thus alter the internal organisation within the globe. The timing of this catching-in event is difficult to reconstruct, but it has to be positioned somewhere on the geological time scale. The end of the Cretaceous is one of the options, but also other major breaks the stratigraphic record are potential candidates.

Six major mass extinctions are known to have occurred during the earth history, whereby more than 60 percent of the life forms disappeared over a short time period: Early Cambrian, Late Ordovician (440×10^6 years ago), Late Devonian (365×10^6 years), Late Permian (245×10^6 years), Triassic (210×10^6 years) and Late Cretaceous (65×10^6 years). Those are all dramatic events in the Earth's history that have left their clear traces in the geologic record (a.o. Kummel 1970). Some of these worldwide stratigraphic breaks may correspond with major planetary changes. These catastrophic events have an influence on the plate tectonic stresses and volcanic activity on the earth. Re-distribution of internal forces leads to long term changes such as:

- A different number and shape of convection cells.
- The speed of mantle material circulation.

- Break-up of continents.
- Creation of new subduction zones and suture lines, etc.

It will have an instantaneous consequence for the living conditions for the organisms present on the blue planet. Changes in water circulation have for instance a severe impact on the climatic conditions. The massive dying-out of the Dinosaurs (*terrible lizard*, a term introduced by Owen in 1841) occurred at the end of the Maastrichtian. The world wide iridium enrichment (rare earth element) found at the K/T boundary could be an argument to place the planetary catching-in event at the end of the Mesozoic period. Alvarez reported a three hundred times increase in iridium at this boundary compared to the normal background levels. This anomaly is believed to be present world wide. Iridium contents in space is a thousand times more abundant than in the earth crust. As a consequence it has been inferred that the Late Cretaceous crisis was accompanied by a catastrophic impact of a large meteoric body coming from outer space and the Chicxulub crater in Yucatan is generally considered the most probable candidate for being the relict of this cosmic catastrophy (Smit 1991). Such impact craters are not unique and others exist in the Late Devonian (Siljan crater, Sweden) and Late Triassic rocks (Manicouagar crater, Canada). It shows that there is some sort of repetition in the occurrence of such dramatic cosmic events. The recent impact of the Shoemaker–Levy 9 comet on Jupiter (16th of July 1994) demonstrates that even in our time-frame large extra-terrestrial collisions are happening in our planetary system. The destructive power of that impact is estimated equivalent to 75 times the total world nuclear weapon capacity (Bryson 2003).

The Permian mass extinction was particularly severe, whereby 95 percent of marine organisms were affected. Three quarters of the land based plant and animal life were extinct. If it is the result of an asteroid collision, than the body must have been super huge in diameter. Shocked quarts grains have been reported from Antarctica, but no iridium anomaly has been demonstrated on this time boundary. Such gigantic impact does not only affect the crust, but also the mantle is influenced. Rebound after the meteoric impact is then expected to generate large quantities of rising magma directly under the crushed weak zone (maybe somewhere in Siberia?). Therefore the impact crater will be soon covered by basalts and this makes it fairly difficult to detect the crater later on. Volcanism, gas and dust release will affect the existing life forms immediately. The extinction is however not necessarily perceived as an instantaneous event. The duration of the Permian extinction is estimated by Dr P. Wignal (Leeds University) lasting some 80 000 years. He deduced this observation from his study of the exposed Permian/Triassic boundary in Greenland, where it coincides with a five to ten meters thick sediment layer. An other conclusion is that the impact and rebound scenario led to a global 5 degrees change in seawater temperature. And this increase had a tremendous effect on the stability of huge gashydrate accumulations (G. Dickens, pers. com.). Release of vast quantities of methane into the atmosphere has of course a devastating effect on the overall living conditions of the planet Earth (see also Section 5.3). The Permian mass killer was most probably a combination of a meteorite impact, dust fall out, increased volcanism, augmenting temperatures and the release of toxic methane into the atmosphere. Drastic atmospheric warming (greenhouse effect) is seen by other researchers as the main culprit (Science Express Jan 2005) with the oxygen level reduced from 21 to 16 percent. Its cause might have been the continuous volcanic eruption in the Siberian Traps.

The Late Cretaceous mass extinction of species is interesting from another point of view. It not only affected the world of the dinosaurs, but even the oceanic life was severely disturbed. The Foraminifera micro-organisms have seen at least three such major evolutionary events (P. Geerlings pers. com.). Each time a new evolution trend is observed, it is characterised by a similar change in shape of the skeleton of the Foraminifera. The tendency is from a simple rounded shell to a more complex form with an intricate rim, double rim and then a sudden return back to the earlier simple geometry. The organism with the uncomplicated skeleton survives the catastrophe and evolutionary branching starts again. It follows a similar direction, using 'new' niches and creating organisms that are better adapted to living under special conditions. It is all based on the '*natural selection and survival of the fittest*' principles as defined by A. Wallace and C. Darwin (1859). The result of this specialisation is an organism with a more complex geometry (i.e. with rims). The equilibrium between niche and micro-organism is fragile and its survival is easily interrupted by external forces. The observation that '*evolution is somehow repeatable*', is quite intriguing and leaves some food for thought.

The resemblance in shape and adaptation of various life forms to different habitats is an other striking phenomenon. Sharks, Mosasaures and dolphins show a completely different internal body organisation and yet have a good resemblance in external appearance. They adapted themselves to the same living habitat. Whales and whale sharks also show an amazing resemblance. This aspect of outer resemblance is not the result of

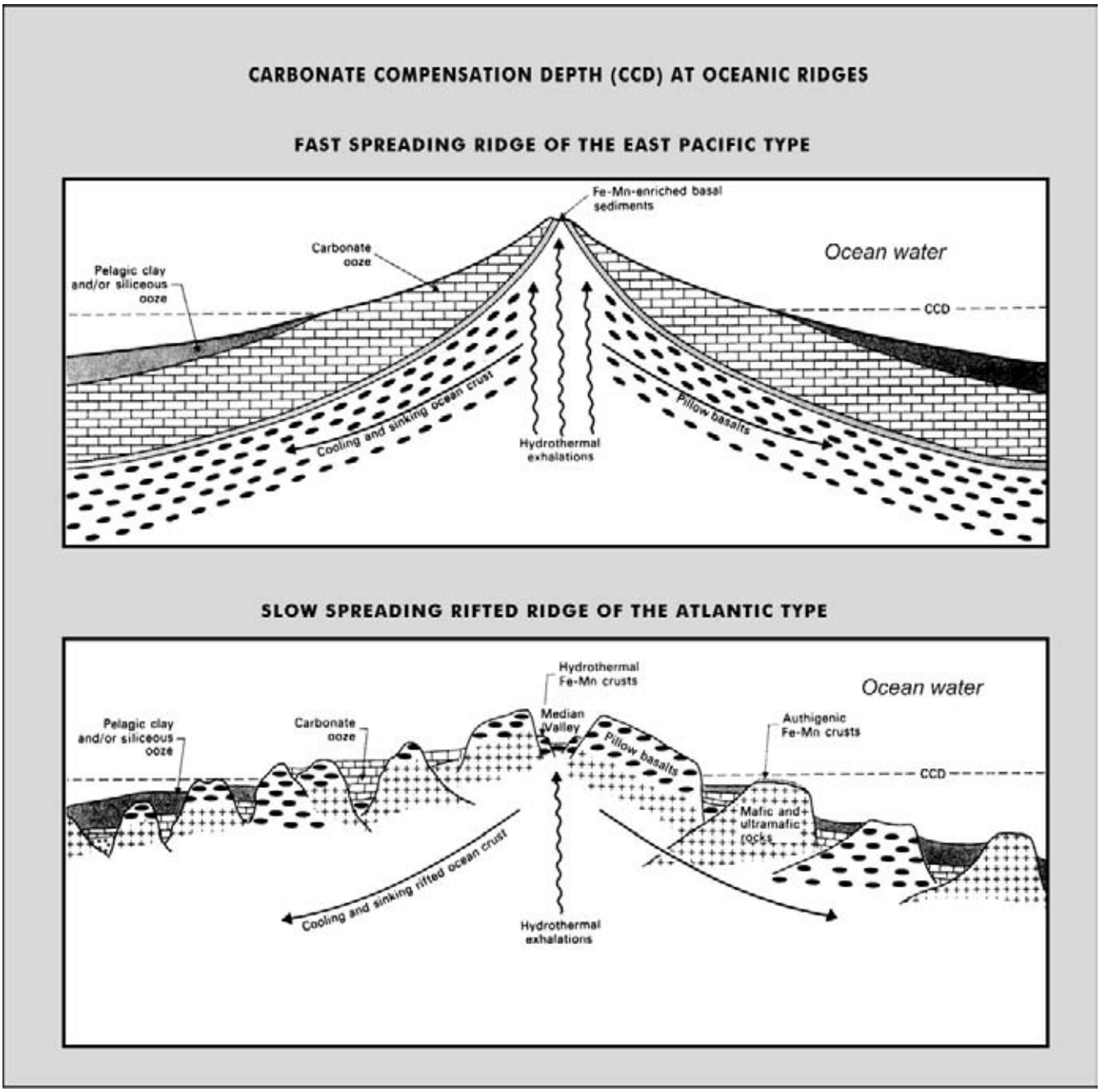

Figure 3.115: Carbonate Compensation Depth (CCD) in the deep marine oceanic environment. Below a critical water depth the CO_2 pressure is increased so that all carbonate material is instable and will get dissolve. The CCD level is located in recent oceans at a depth of approximately 4500 metres. Beyond this depth only Globigerina oozes are deposited. Carbonate deposition below this level is only possible when large quantities of carbonate material are dumped rapidly by turbidity currents. The sedimentation rate should hereby outrun the dissolution power of the ocean waters (modified after Scholle et al. 1978 and Jenkyns 1978).

shear coincidence, but is dictated by the general living conditions. An other example is the Tasmanian tiger, a marsupial extinct around 1936. It was an animal that was the complete counterpart of the mammalian wolf family. Its hunting and living habitats were surprisingly similar. This kind of convergence again indicates that the evolution is not completely random. It proves that external appearances of a life form is in part determined by the environmental niche and the living style of the organism. The niche favours a certain behaviour and stimulates a certain morphology for the organism that can survive under such conditions. A similar convergence

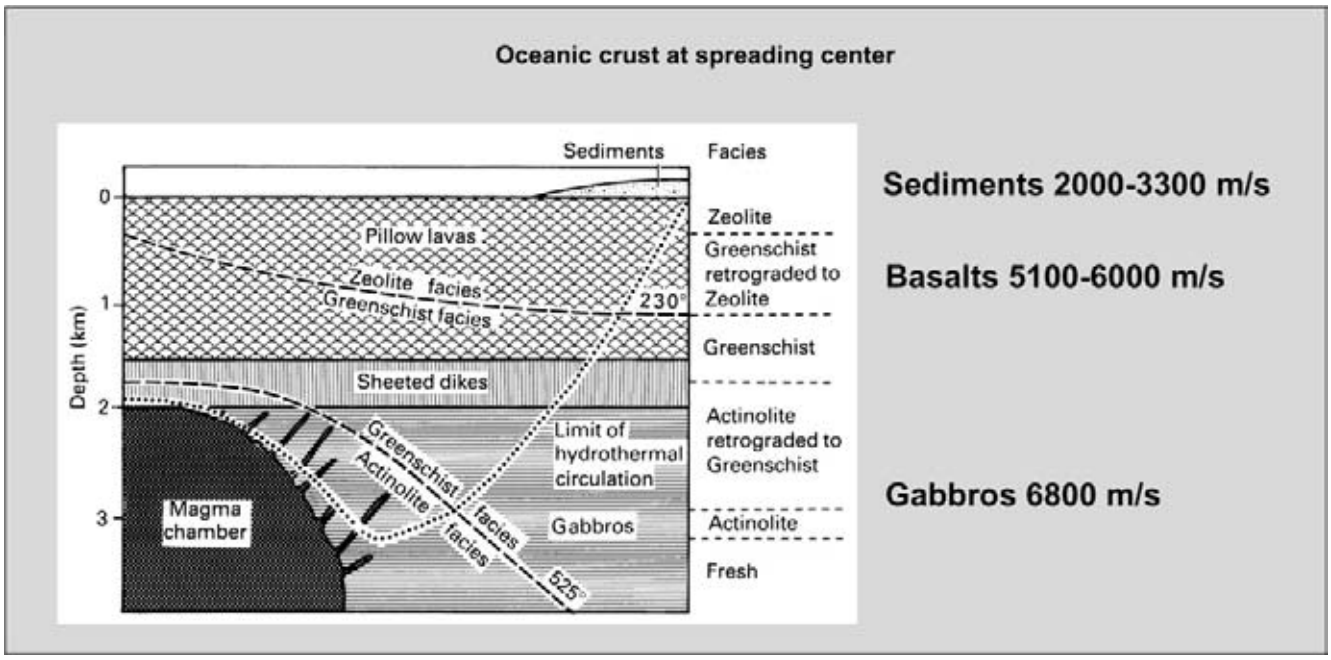

Figure 3.116: Oceanic crust has a distinct composition and is mainly made up of basalt extrusives and gabbros with underlying ultramafic rocks. The Moho discontinuity coincides with the transition zone where crustal gabbros are underlain by mantle peridodites (Harzburgite). The Harzburgite rocks are rich in olivine and generally believed to be the residual product of partial melting of the upper mantle, due to decompression under extensional conditions. The associated magma chamber is characterised by layered gabbro in the base with preferentially oriented crystals. Dyke intrusions rise from this magma chamber into the overlying host rock. Eventually they even reach the ocean floor to create important extrusions of pillow lavas. Ongoing extension results in a new phase of intrusive dyke formation and this pushes the older dykes and surrounding hostrock away to the side. Basaltic oceanic crust is formed at the mid oceanic spreading ridge, building a conspicuous topographical element on the ocean floor. An active ridge is usually a zone with increased hydrothermal activity, nowadays often believed to be the potential locus for the origin of life (modified after Kearey and Vine 1990).

phenomenon is observed in the floral world. For instance desert plants from SE America and Africa do resemble in shape and functionality, but have a completely different internal organisation. Nature apparently does not have an unlimited amount of solutions to solve the existential problems.

As stated before, six mass extinctions of organisms have been reported upon. Each extinction coincides with a major break in the geological record. Every species has an expectation of survival for at least four million years. After that period, statistically speaking, it will be replaced by an other species that takes over the place in the evolutionary chain. This mechanism has left us with the magnificent biostratigraphic dating tool. It also gives an idea of how long Homo Sapiens can be expected to survive. Man-made extinctions of many bird species in the last few centuries (Steadman and Martin 2003) shows our responsibility to manage our planet in a sensible way and the need to protect the current bio-diversity as best as we can. On the other hand, extinction is of course an un-escapable natural phenomenon that is integral part of the evolution process on the earth.

3.5.6 Carbonate compensation depth and oceanic basins

Beyond a certain depth (approx. 4000 m) the ocean water is undersaturated in carbonate. As a consequence all carbonate material is not stable beyond this waterdepth and will get dissolved (Van Andel 1975). The result is the presence of Globigerina oozes (clays) in the deeper part of the oceans. This instability level is generally known as the '**Carbonate Compensation Depth**' (CCD; Figure 3.115). The depth of this level is depending on the seawater composition/temperature and changes in time. In the Pacific Ocean it is around 4.5 km and in the Atlantic it is situated around 5.5 km (Scholle et al. 1978). The depth of the CCD level also fluctuates in geologic time. At depths greater than the CCD boundary, only fine-grained deepsea muds are encountered, but exceptionally some carbonate material can be preserved. The deepsea muds are either chemically precipitated, derived from massflow transport and/or laid down by thermohaline contour currents on the ocean bottom.

Oceanic basins are underlain by oceanic crust (sima = silica and magnesium), made up of basalts, gabbros and

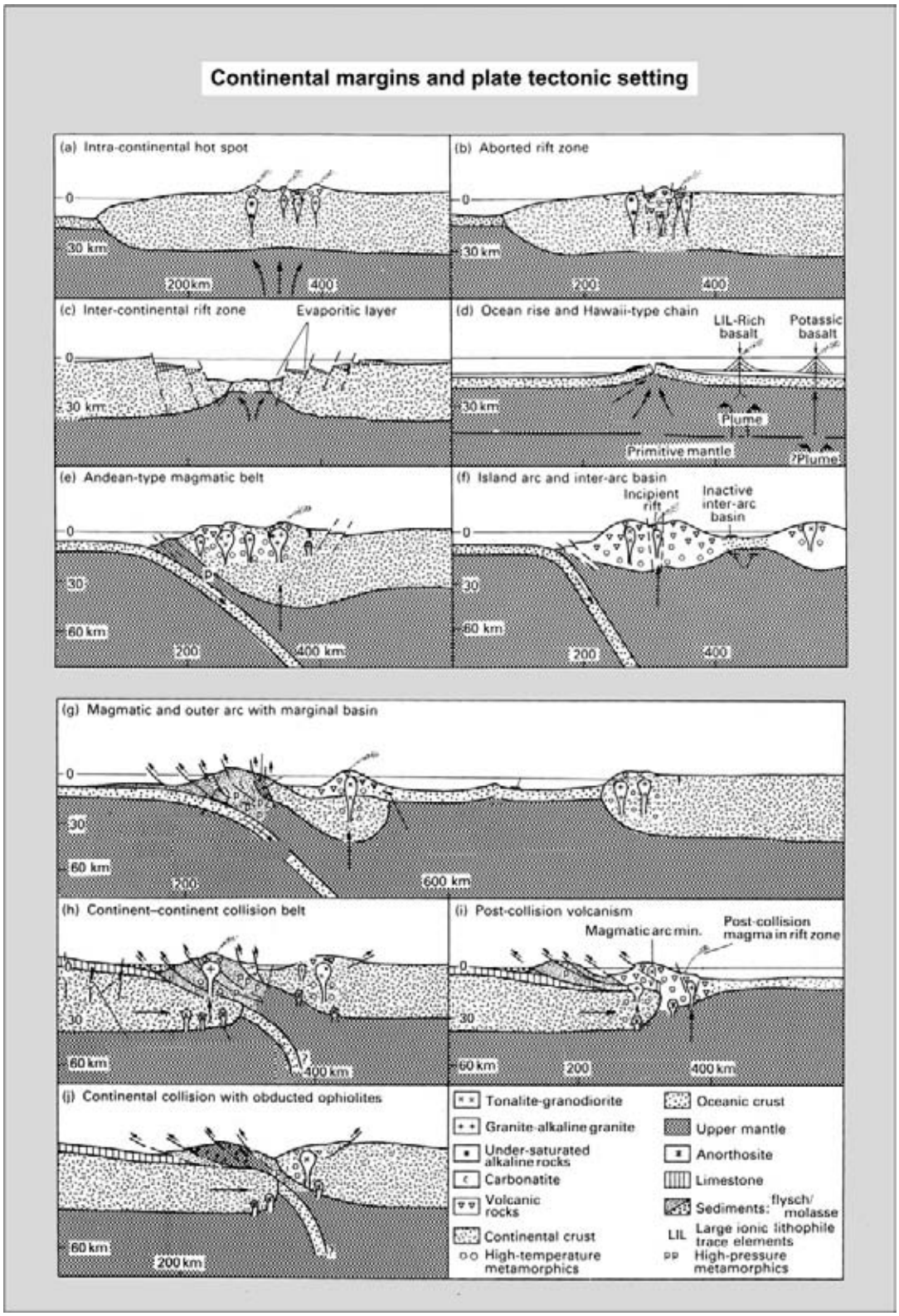

Figure 3.117: Continental margin types and their plate tectonic setting. Upwelling of mantle material causes an initial dome on the continent. Stretching over its crest leads to the creation of a rift valley or graben system in the continental block. This area stays an important weak zone in the crust as this rift develops further. Subsequently the mantle plume cools and the rift subsides leading to a marine transgression. The continental break-up marks the onset of the drifting phase and a proto-ocean is created. Finally a full-blown spreading centre develops, underlain by mantle convection cells, where new oceanic crust is constantly generated (modified after Kearey and Vine 1990).

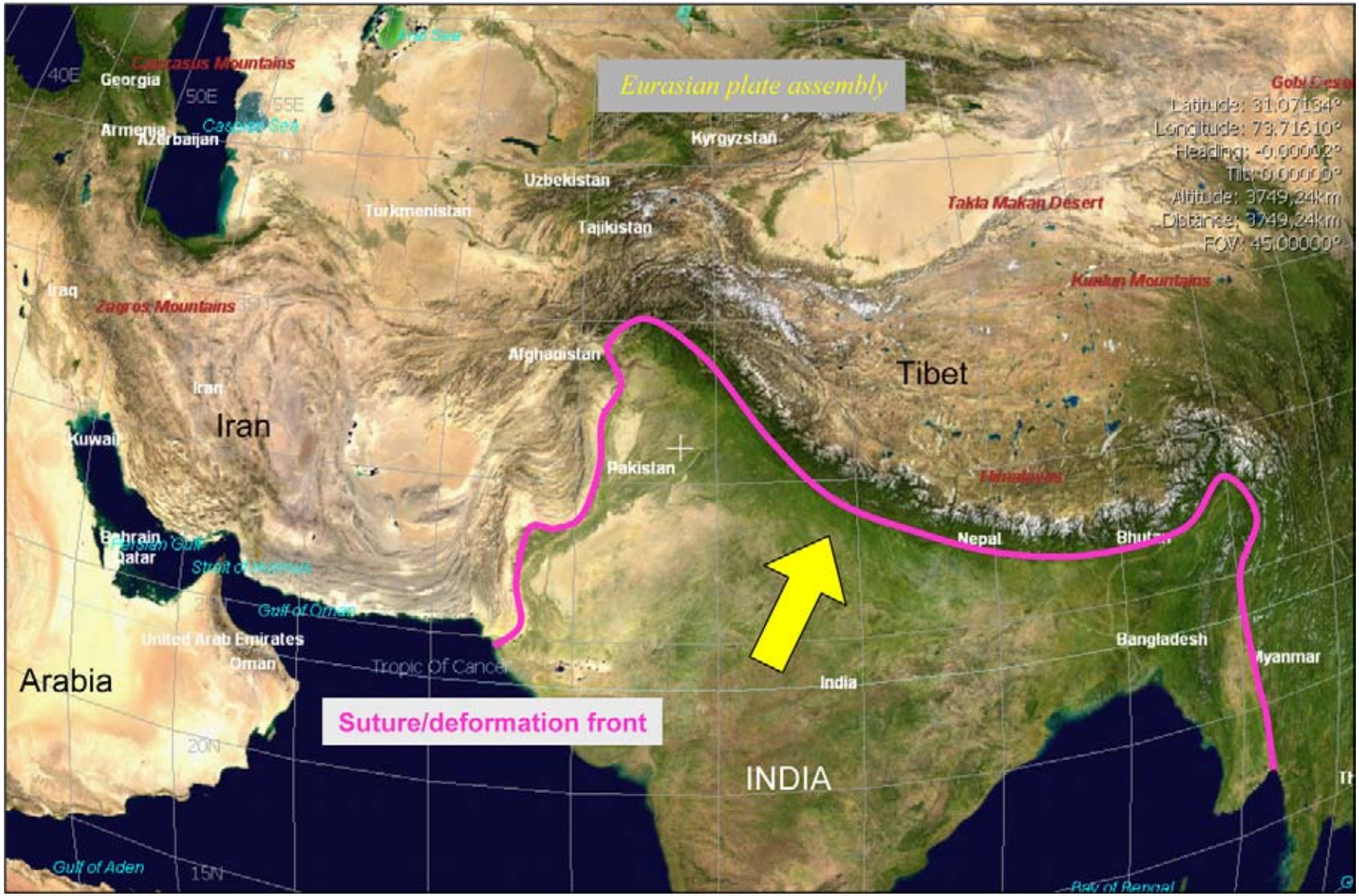

Figure 3.118: Plate tectonic re-arrangements are quite common in the geologic history. Here is shown how the Indian plate has drifted north and underplated the Eurasian continent, thus creating the Himalaya mountain chain and the uplifted Tibetan plateau (data courtesy NASA).

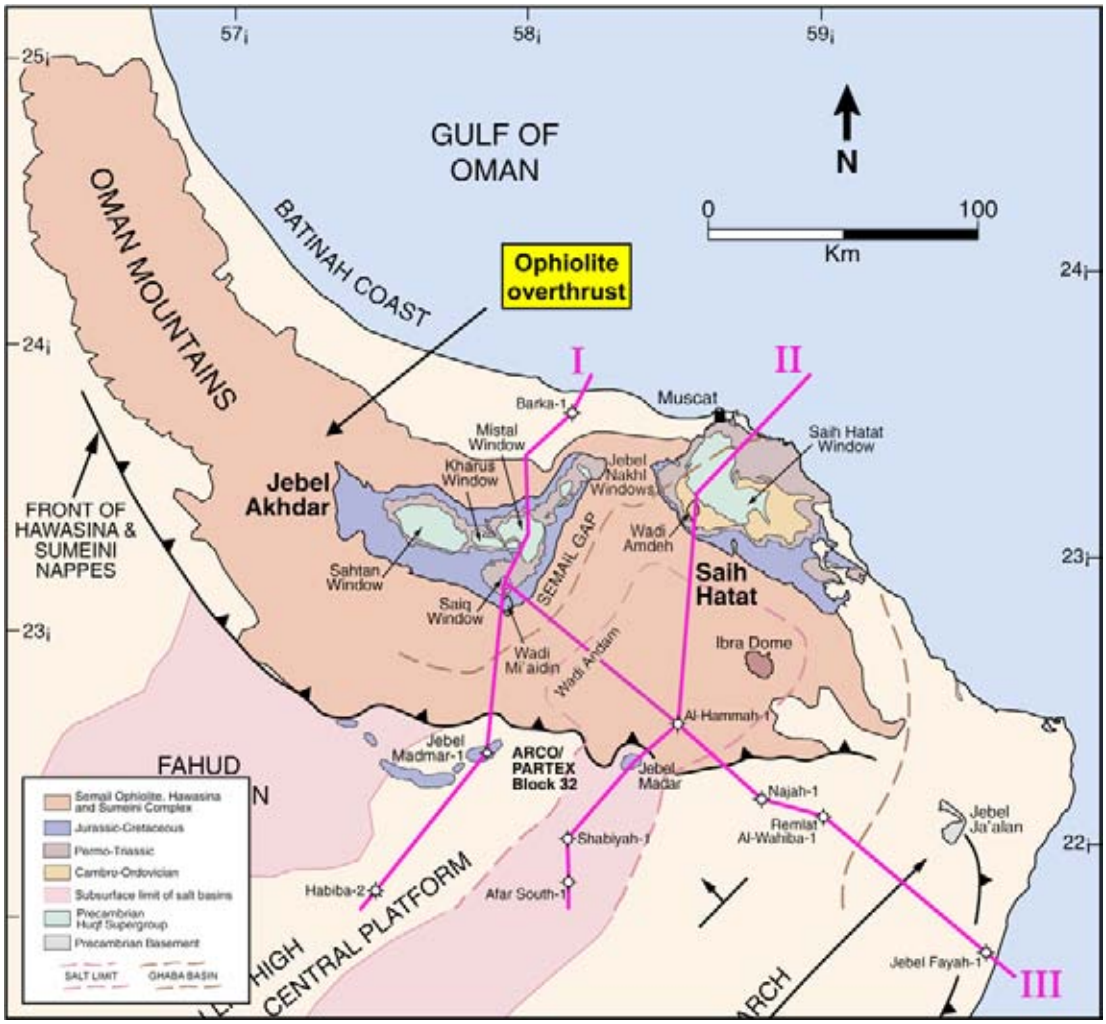

Figure 3.119: Structural elements of Northern Oman. The Oman Mountains are dominated by a stack of ophiolite thrust sheets (oceanic crust), deformed in Tertiary time. Older rocks are exposed in the centre of the Jebel Akhdar and Said Hatat anticlinoria. The position is shown for the two transect I and II in the next figure (modified after Mount et al. 1998).

ultra-mafic rocks (Figure 3.116). Ultra-mafic rocks are dark igneous rocks with abundant Olivine crystals. Typical rocks are Peridotite and Harzburgite, products of partial melting of the upper mantle. The density of these rocks is very different from normal continental crust (sial = silica and alumna) and therefore the oceanic lithosphere sinks deeper into the mantle. This density difference results in the greater waterdepth of over 4000 metres for oceanic basins. Sediment supply is coming from the surrounding continental blocks or deformed oceanic crust that is obducted (Figure 3.117). Global tectonic re-assembly of the continental plates is quite common. The Alpine orogeny is a well documented deformation phase worldwide, whereby the Tethys ocean was subducted and closed between the African and Euro-Asiatic blocks. India has underplated to a large extent the Euro-Asian continent and this resulted in the uplift of the Tibetian Plateau (Figure 3.118). Oceanic crust has a special reflection character on the seismics. The seismic expression is dominated by diffraction energy and otherwise a low amplitude, rather dull character is apparent.

Good examples of obducted oceanic crust outcrops are the ophiolite belt in northern Oman (Figures 3.119 and 3.120). A pile of ophiolite thrust sheets are exposed in the Omani mountains. The Semail and Sumeini complex represent deformed oceanic crust with the Upper Cretaceous Hawasina turbidites as original sedimentary cover. Large geological windows in the Jebel Akhdar and Saih Hatat areas show the autochthonous rocks below these overthrusts (Veeken and Van Moerkerken, in prep.). In the Acaba region in Jordan (Red Sea Gulf of Acaba-Jordan rift valley system) the gradual transition from continental to oceanic rocks is illustrated by the presence of granitic basement rocks infested by nu-

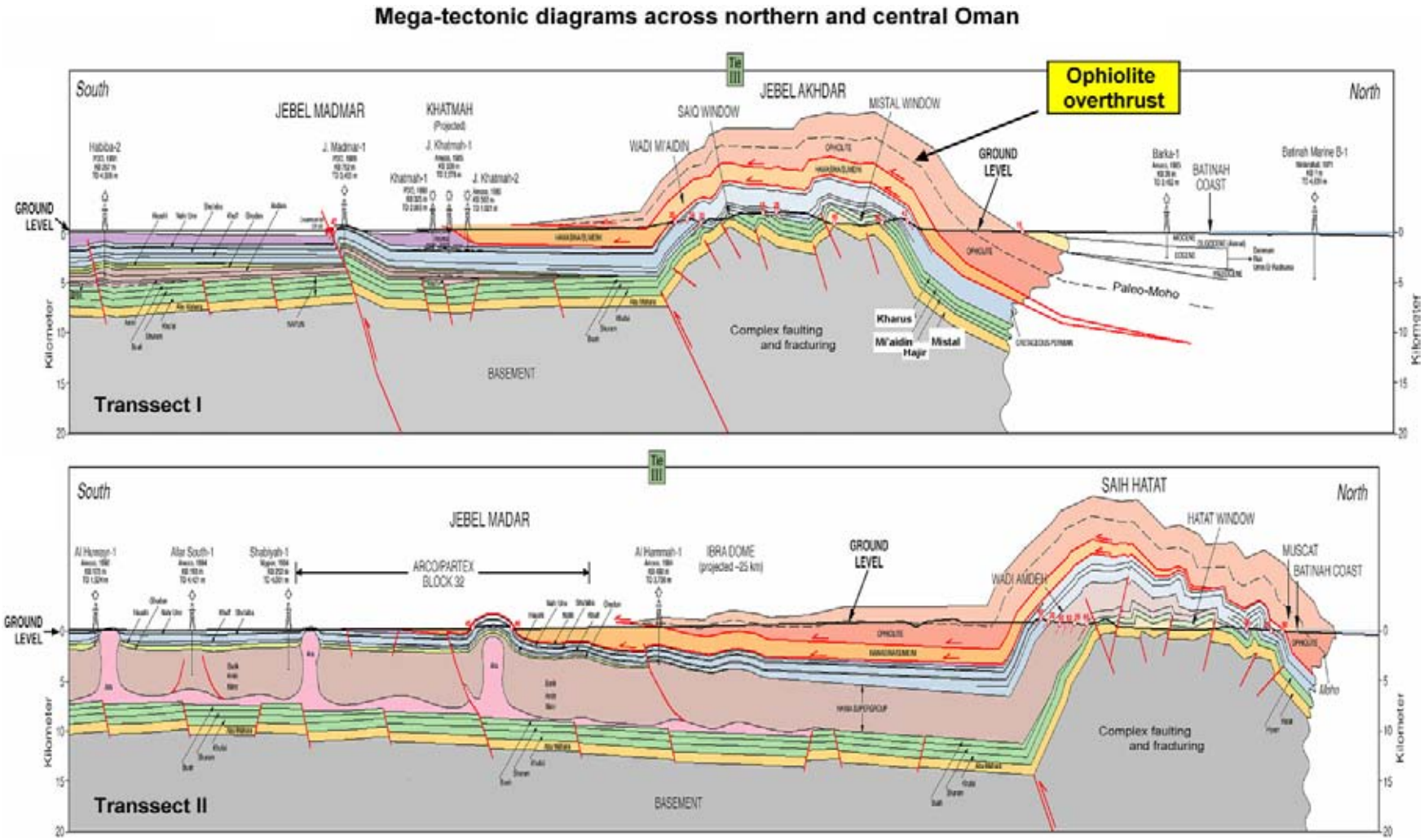

Figure 3.120: Transsects through northern Oman, illustrating the deformed ophiolites thrust sheets coming from the north. The position of the paleo-Moho is indicated to better highlight the structuration. The deformation of the thrust belt is Tertiary in age. A major uplift of the Jebel Akhdar occurred in the Oligocene and more than 10 km of sediments have been removed since. The later erosion has created the tectonic windows, where older sediments are now outcropping (modified after Mount et al. 1998).

merous dikes and intrusion (Figure 3.121). The dikes have penetrated the host rock via zones of weakness in an overall extensional stress regime. They are of different chemical composition and heavier than the surrounding rock. It favours foundering of the fault blocks and downwarping of the basement toward the centre of the graben system. The real oceanic crust is formed in the centre of the marine rift, that later is to become the mid-oceanic ridges. These ridges are the places where hot material from the astenosphere (layer without strength) is upwelling. This upwelling gives rise to magmatic activity at the ocean floor, where submarine volcanoes are erupting basaltic lavas and new crust material is actively formed. The upwelling, caused by an underlying mantle convection cell, is the motor behind seafloor spreading and plate tectonic deformation (cf Ziegler 1992). Several types of plate configurations are distinguished:

- Spreading with divergence of the two oceanic plates pushing away the continents on the side in opposite directions which results in a passive margin (or Atlantic) type of setting.
- Spreading with convergence of the oceanic plate and neighbouring continental block (Andean type of setting) and creation of a subduction zone (Benioff zone). The subduction zone is the area where the heavier plate is forced to go down into the mantle. The existence of the Benioff zone has been demonstrated by the typical distribution of earthquakes along the descending slab trajectory into the mantle. The geometry of the Benioff zone depends on several factors: hot or cold ocean slab (young or old), fast moving plate, obliquity of movement. The melting of the 'wet' oceanic slab starts at a depth of about 100 km into the mantle (vd Werff 1996). Important volcanic activity is observed at the surface (active volcanic zone and/or island arc; calco-alcaline magmatism) perpendicular above this spot in the mantle. Back arc spreading is possible when the Benioff zone is steep and an additional convection cell is created in the mantle (Mariana type of setting; basalt-rhyolite). Oceanic–oceanic plate trench is relatively devoid of sediment, but the oceanic–continental subduction trench has an accretionary wedge developed by scraping the sediments off the down going lithosphere and cannibalism of the forearc basin sediments. The accretionary wedge is basically a pile of trusted sediments that form an important morphological bulge on the ocean floor. The orientation of the trust fault plane is flattening out and dipping in a landward direction.
- Convergence of the plates with subduction and the final collision between two continental blocks. The buoyancy of the lighter continental crust prevents the subduction process to continue and a mountain range is formed (Alps), sometimes with substantial underplating (Himalayas).

Hydrothermal activity associated with mid oceanic ridges is often believed to be the possible locus for the origin of life, although others prefer an extra-terrestrial source, transported to the earth by meteorites (products of large cosmic impacts).

The last option seems to be now supported by the reported SOM (Structureless Organic Matter) in meteorites and rock samples from our planetary system. In the Murchinson meteorite (Australia 1984) there were for instance eighty different amino acids found. The meteorite ALH84001 (Allan Hills locality), collected on Antarctica in 1984, stems from Mars as is proven by the typical mineralogical assembly and isotope determinations done on gas inclusions (Figure 3.122). Its age is estimated around 4.0 billion years, while the 11 other known Martian meteorites are only 1.3 billion years old. The peculiar mineralogical composition and the age discrepancy of the meteorite ALH84001 led to intensive re-examination and the discovery of tubular, bacteria-like relics that are interpreted as evidence for primitive biological activity. Only in 1994 scientists from NASA's Johnson Space Center and Stanford University had the courage to announce probable microfossils in this meteorite from Antarctica. Much of the debate concerns carbonate globules with concentric growth zonations, examined in extensive SEM studies. The high resolution analysis revealed an intricate morphology of the rounded particles. The presence of very small and pure magnetite crystals in its direct vicinity strongly supports the bacterial activity hypothesis proposed by McKay et al. (1996). The co-occurrence of Pyrhotite in the same sample requires a rather complicated chemical explanation, whilst a biologic cause can accommodate this observation rather easily (Frankel 1999).

Signs of organic activity on the planet Mars has been documented by Levin and Straat (1977) in a controversial Mars lander experiment. They fed a solution of radioactive nutrients to a soil sample and studied the release of gas in the compartment. A similar soil sample was first heated to 160 degrees in an control experiment before adding the nutrients and surprisingly it yielded no reaction. A simple mineralogical reaction could therefore be ruled out. Many people stay sceptical in front of all these circumstantial evidence, but the option of extra-terrestrial life can no longer be ignored beforehand. Other experiments (pyrolitic release of Horowitz and gas exchange of Oyama) did not give any positive results, but these tests were also negative when carried out on samples from the Antarctic. The

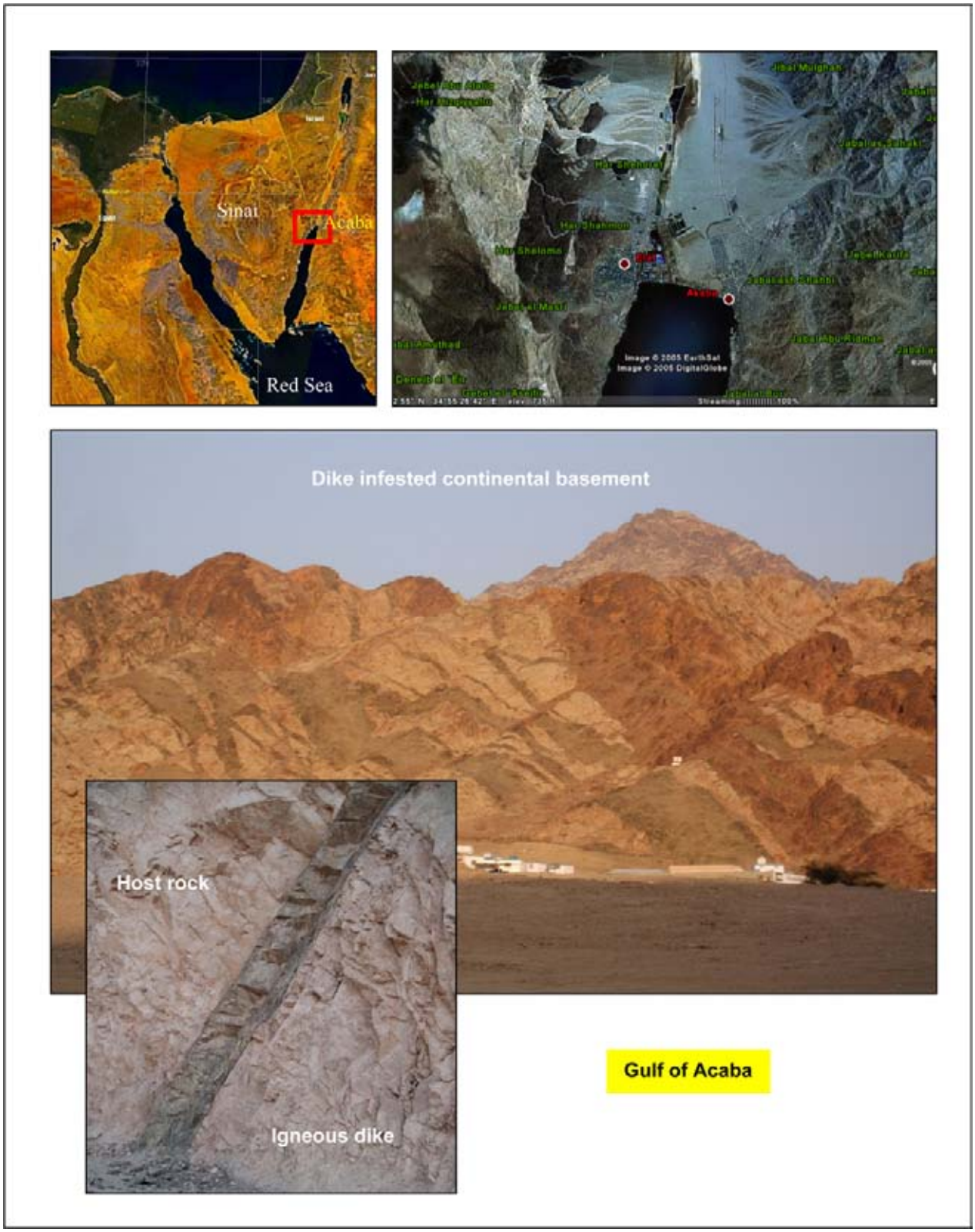

Figure 3.121: The flanks of the Gulf of Acaba-Dead Sea-Jordan Valley rift is characterised by block faulting and intense dike intrusion. Alluvial fans are fed from the uplifted hinterland (top right image). The irregular greenish and brownish units are intrusions in the granulitic hostrock (centre) fed by dikes (lowermost). The overall extensional setting makes it possible for fluidised magmas to penetrate the overlying host rock sequence. It illustrates the gradual oceanisation of the continental crust with the formation of an incipient spreading centre in the middle of a graben system and/or pull-apart strike slip movements.

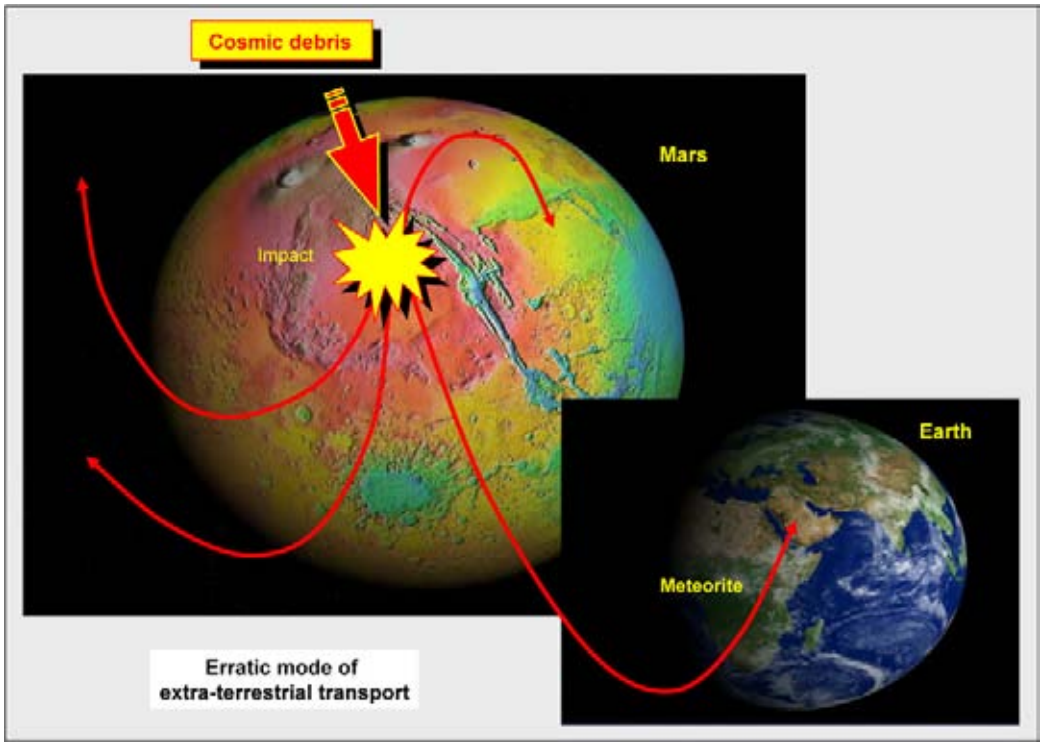

Figure 3.122: Aerial photographs of the planet Mars and the Earth. The polar cap and the Valle Marineris (a 8000 m deep rift with a length of 4000 km length and 600 km wide) is clearly visible on the Mars surface. Impacts of large pieces of cosmic debris can dislocate rocks on the Martian surface, throw them into the sky with an escape velocity larger than 6 km/s and send them on a voyage to the Earth (escape velocity 15 km/s), where they may land as meteorites. In this way organic molecules can be transported from one planet to another in our solar system. Large cosmic impacts also occurred during the history of the Earth; e.g. the Chicxulub impact crater offshore Yucatan coinciding with the Cretaceous/Tertiary geological boundary is well documented (photo courtesy of Geofusion).

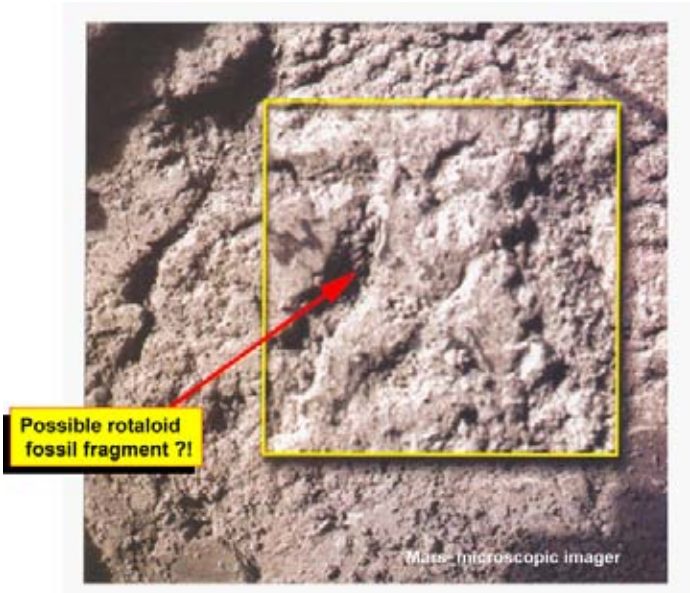

Figure 3.123: Microscopic Imager photograph of the surface of planet Mars as made by the Opportunity robot vehicle of the Mars Rover Exploration team. The arrow indicates a small scale rotaloid structure that could be a micro-fossil of biologic origin (courtesy NASA/JPL; after Schuster 2004). The photo area is about 10 cm wide. Structureless organic matter or SOM (polycyclic aromatic hydrocarbon) has been discovered in a meteorite ALH84001 found on Antarctica that stems from Mars. Waterlaid sedimentation patterns with ripple marks have been documented on pictures taken by the Opportunity. The presence of methane on Mars has been demonstrated by spectrometry (organic or inorganic in origin?).

temperatures on Mars varied from minus 60 to minus 10 degrees Celsius, so the conditions are very similar to those on Antarctica.

The recent discovery of large quantities of free water on Mars is further support for the extra-terrestrial **pan-spermia** theory, first proposed by the chemist J. Berzelius in the 19th century (Frankel 1999), which assumes the natural insemination of life throughout the entire solar system. Canyons, channels and erosional features caused by water agents on Mars have been already described earlier (cf Croswell 2003). Not only freshwater but also salty waters existed in the past on Mars (NASA, 23.03.2004). The peculiar rotaloid features seen by the Microscopic Imager of the NASA is possibly evidence for microfossils (Schuster 2004) and hence ancient life on the red planet (Figure 3.123). A composite Mars photo taken by the Opportunity vehicle clearly shows ripple marks with a topset preserved. This geometry is indicative for a water laid sedimentation mechanism. Evaporitic deposits have been encountered on Mars according to Dr Frankel (pers. comm.). Surprises in the exploration of our solar system are not new. The recent discovery of the Sedna planet, an object 3/4 the size of Pluto and located in the inner Van Oort cloud, halfway between Pluto and Quaoar at 13 billion kilometres distance from the Earth, is an other sensational example (NASA press release 04-091, Savage and Platt 2004). Its name is derived from the Inuit Goddess of the Ocean.

The magnetic minerals in the newly created oceanic crust are polarised by the Earth magnetic field. This geo-magnetic field has regularly changed its polarity during the history of the earth. These polarity changes are preserved in the basaltic rocks as they cool and move away from the spreading centre. The polarity flips are symmetric in rocks of the same age on both sides of the oceanic ridge. A global geo-magnetic polarity chart has been established, that is related to the biostratigraphic time zonations. The paleo-magnetism allows to age-date the oceanic crust in a relative way and to reconstruct the plate tectonic wandering of the magnetic poles (Kearey and Vine 1990).

3.6 Chronostratigraphy

The chronostratigraphic evolution of a basin can be reconstructed, once the following steps have been done:

- All the Depositional Sequence boundaries and the internal system tracts are established.
- The various seismic facies units are outlined.
- The depositional environment interpretation with the distribution of gross lithological units is done, incorporating all available geological control.

Ages are assigned to the various seismic units by using the biostratigraphic datings in the wells and other geological relevant information.

3.6.1 Arbitrary stratigraphic chart

For visualising the depositional history displayed on a specific seismic line, it is convenient to construct an arbitrary stratigraphic chart (Vail et al. 1977). The construction technique is rather simple and the following procedure is applied (Figure 3.124).

It is possible to trace reflections within the system tracts. The sedimentary reflections are considered individual '**timelines**', although they in fact represent small time intervals. These timelines will join or stop at the unconformities and separate certain episodes in deposition. The younger sediments are found at the top. The abutting of reflections against an unconformity implies that a particular sequence (or time interval) is not present everywhere along the seismic section. In case of weak reflections, than the horizon can be **phantomed**. This is a technique whereby the seismic marker is being pushed through bad data zones in order to obtain an estimate for later geological reconstructions. The structuration of the over- and underlying sediments is forming the guide. There are some pitfalls that are attached with phantom horizons (Pennington et al. 2004). Seismic point attributes are meaningless in these zones, but window measurements might be useful.

The geometry of these timelines is used to further illustrate the depositional characteristics of the basin fill. The timelines define distinct arbitrary time intervals which are plotted sequentially in an arbitrary stratigraphic chart. Along the Y-axis of this chart the various arbitrary time units are indicated, while along the X-axis the presence or absence of the time interval units is plotted. This is done for all traced timelines. The end points of these timelines (and/or timeline segments) form the connection points for the various unconformities. The connecting line are now illustrates the shape of the various unconformities on the chronostratigraphic chart. Similarly the different system tracts and facies boundaries are plotted on the same chart. Also the gross lithology of the units can be indicated.

If deposits are absent over a certain time interval – due to onlap, downlap or erosional truncation – it is indicated by a hatched nature, representing active erosion and/or a hiatus/non-deposition. In this way a quick

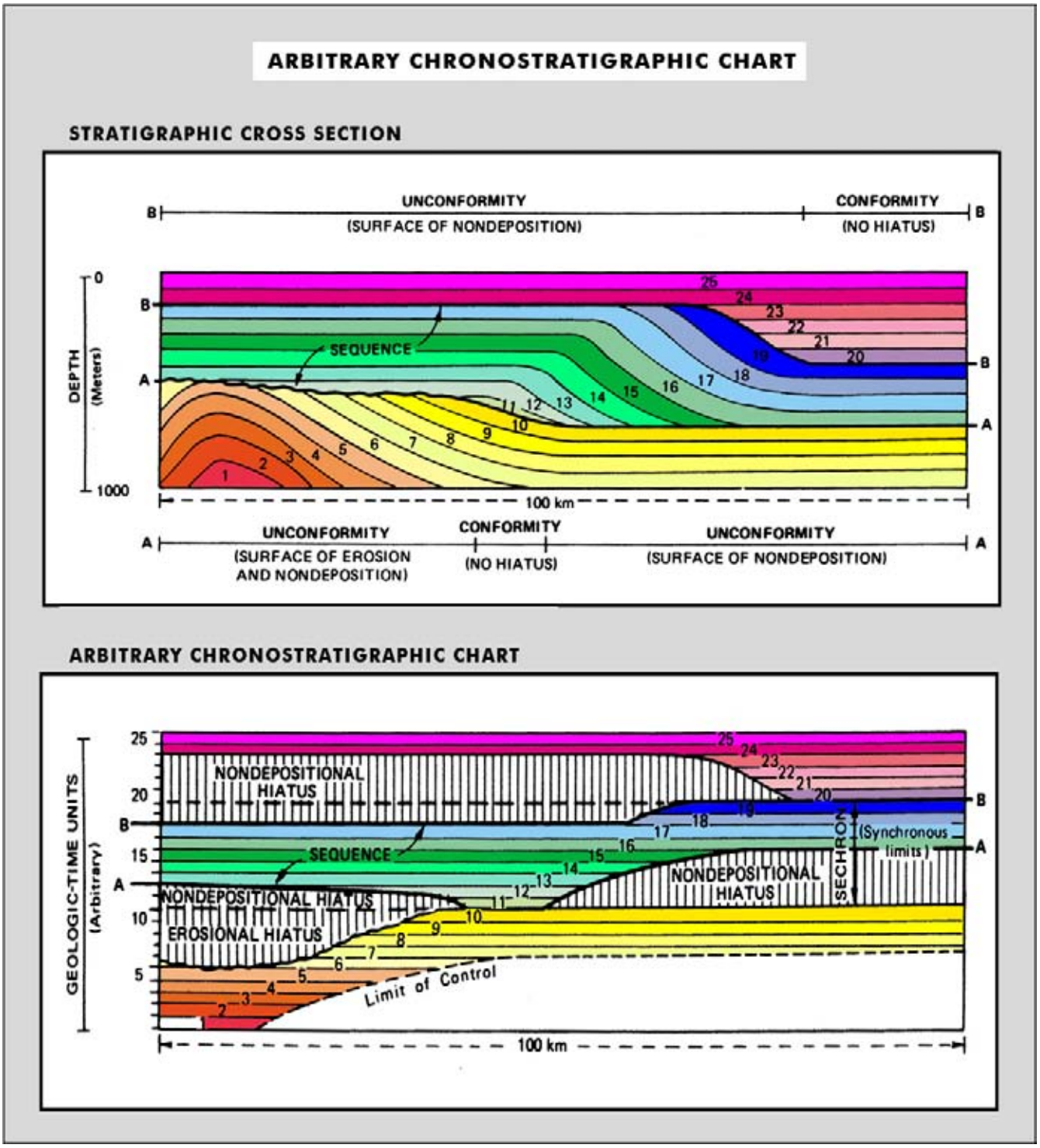

Figure 3.124: Genetic breakdown of depositional sequences along a seismic section and the construction of a chronostratigraphic chart with an arbitrary time scale (after Mitchum et al. 1977, reprint from AAPG whose permission is required for further use).

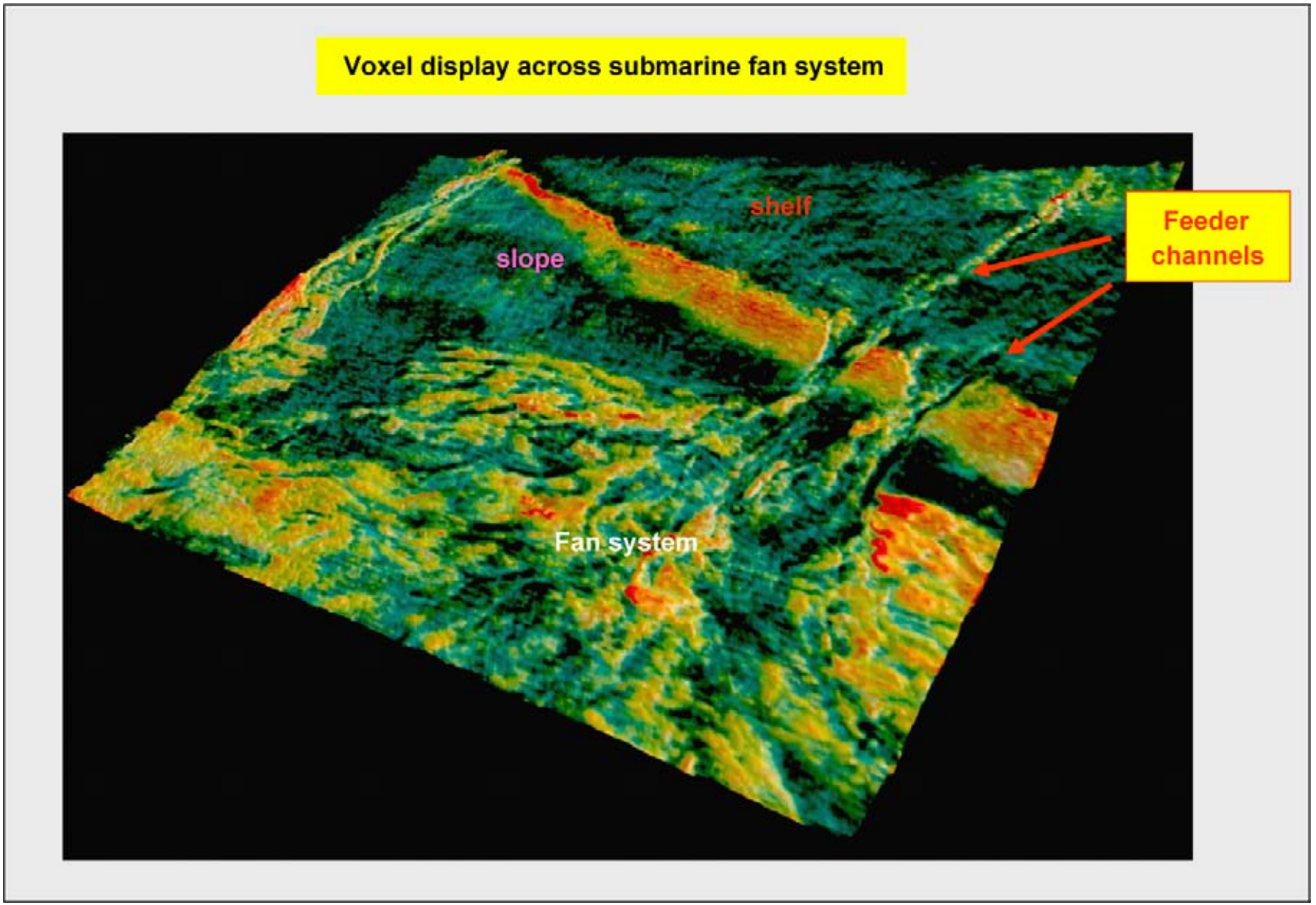

Figure 3.125: A voxel rendering display of a submarine fan system located offshore the West Shetlands. The technique uses a specific seismic attribute parameter or combination of parameters to determine the opacity of the voxel cell (data courtesy Dr H. James of ParadigmGeo).

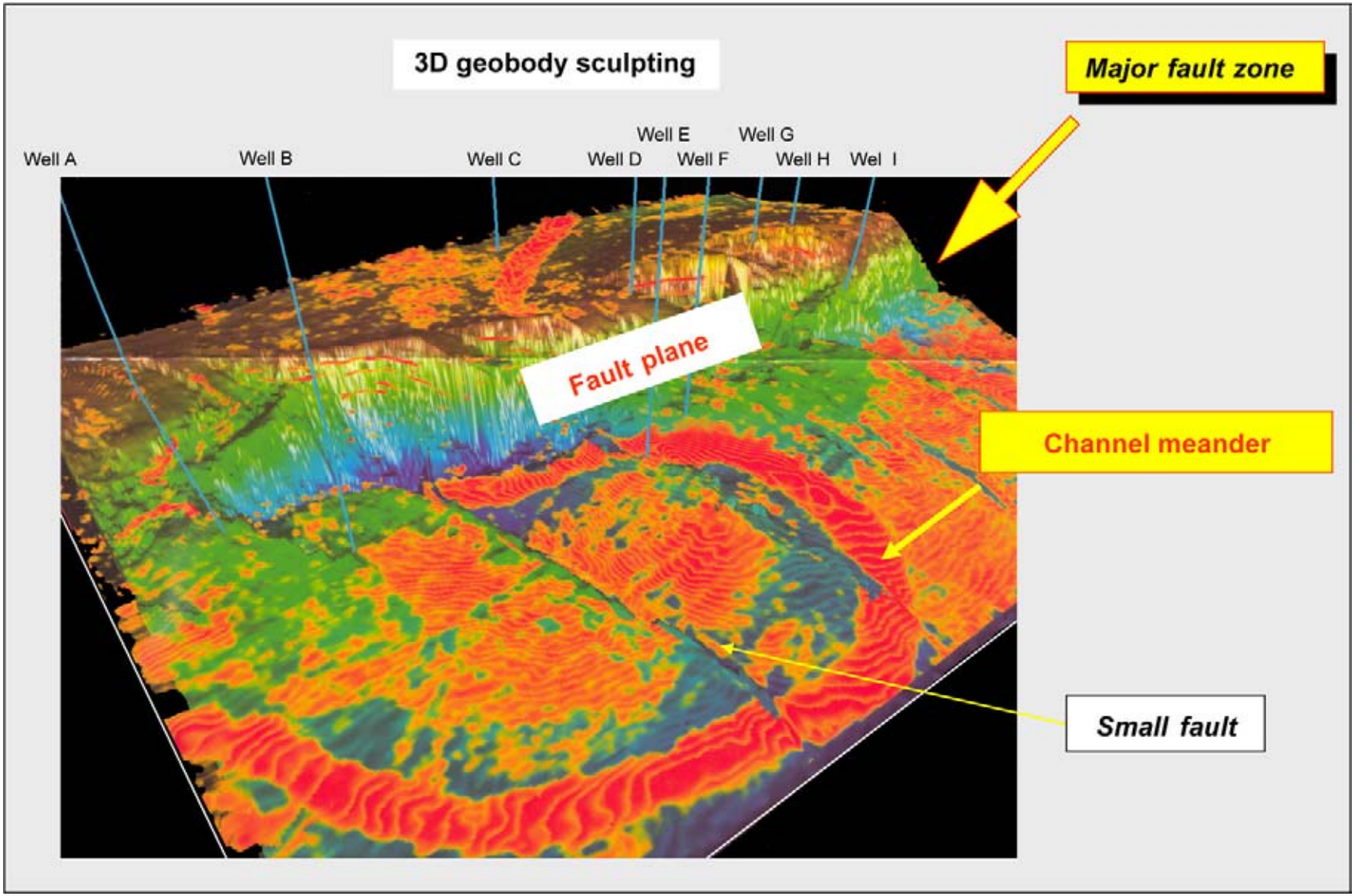

Figure 3.126: The 3D visualisation is done by using geobody-sculpting techniques in Voxelgeo^{TM}. The opacity of voxels is set at certain threshold values and this may bring out the expression of various depositional units. The red facies unit is interpreted as a large meander that is offset by a large extensional fault. The seismic data is from Clyde Petroleum and comes from offshore Indonesia (modified after Davies et al. 2004 and data courtesy Dr H. James of ParadigmGeo).

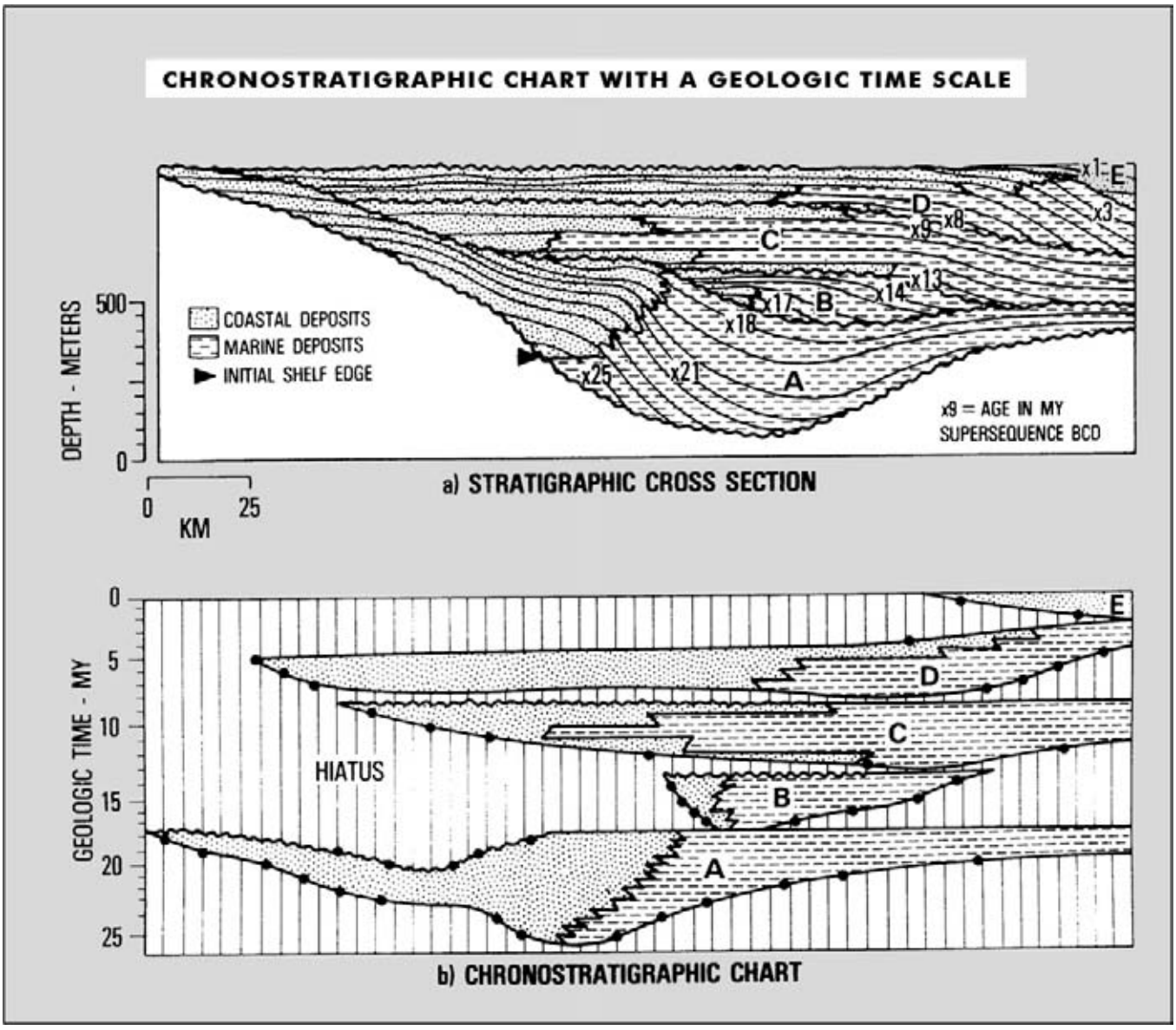

Figure 3.127: Construction of a chronostratigraphic chart with a geologic time scale, enhancing the relative time importance captured in the different unconformities (after Vail et al. 1977, reprint from AAPG whose permission is required for further use).

graphical overview of the stratigraphy is obtained and it is displayed along a seismic section. It allows to see in a one glance where time equivalent deposits are present and to appreciate the relative importance of the various unconformities.

The concept of **Relative Geologic Time** volumes for 3D seismic datasets has been introduced recently. The time samples are all assigned to a relative geologic age by considering their relation with calibrated geologic and seismic horizons. This is done by linear interpolation. An other method uses unwrapping of the instantaneous phase representation of the seismic trace (Stark 2004). This RGT is an attribute to the seismic cube, just like seismic amplitude. The advantage of constructing such a RGT volume lies in the possibility to sculpt the data along a certain horizon and visualise depositional changes as a function of geologic time. Data sculpting is a voxel rendering visualisation technique with specific opacity for multi-attribute ranges as display criterion (Figures 3.125 and 3.126). High gradients in such a RGT volume are indicative for unconformities, faults, fluid contacts and/or interpretational errors. A constant RGT value is corresponding to an equi-time surface. A slice through an attribute cube following a constant relative geological age surface is known as a **strata-slice**.

These type of slices can be scrutinized for the presence of stratigraphic/depositional features (Stark 2004). The time sampling of 2 ms for seismic surveys is beyond the seismic resolution and several slices are captured within a single seismic loop. Subtle variations in loop shape are hence resolved by this strata slicing technique, just like in the neural network trace classification systems described by Balz et al. (1999). Mallet et al. (2004) proposes to use a similar relative time concept in their effort to get rid of stratigraphic grids in the shared earth modelling, that will be discussed elsewhere in this textbook.

Sometimes this type of time representation is also known as the Wheeler transform. The Wheeler domain is a seismic cube that has been transformed in the equivalent "stratigraphic chart" dataset.

3.6.2 Chronostratigraphic chart

After the arbitrary stratigraphic chart is established, then the distinguished time units are calibrated by the biostratigraphic observations. This will allow a more precise representation of the time involved for the deposition of a specific interval. A chronostratigraphic geologic time scale is now taken as Y-axis. The arbitrary time units are stretched-and-squeezed to fit this new time scale (Figure 3.127). Some of the arbitrary time units will have to be reduced in vertical size, while others are increased, because they represent a longer time interval. In the X-axis direction nothing is changed, as for example the position of the onlap point stays the same. In the chronostratigraphic chart the displayed geometries are more proportional to the actual time elapsed. Especially the hiatuses show more accurately their specific time importance. The time calibration is better for the shallow part of the section and lot of uncertainty in the interpretation is present in the deeper units on the section, because they were never penetrated by wells.

Chapter 4

Dynamics of Basinwide Sedimentation Patterns and Sealevel Changes

In this chapter basinwide sedimentation patterns are discussed and their significance is illustrated in respect to the change in relative sealevel. The shape and character of a basinfill depends on various factors like:

- Morphology of the substratum.
- Tectonic subsidence.
- Input sediment supply and composition of the available clastics.
- Baselevel profile and eustatic sealevel changes.
- Climatic conditions.

Climatic conditions on the earth are governed by the amount of radiation received from the sun. The global climate shows latitudinal zones arising from the thermal gradient between the equator and the poles. The precipitation and evaporation variations are related to the so-called Hadley circulation cells (Figure 4.1; Matthews and Perlmutter 1994). Seasonal temperature changes influence the size and position of these cells. But greater variation is induced by the amount of sun radiation reaching the earth surface. This leads to a different climatic distribution pattern with changes in humidity and runoff. All these factors have their impact on the stratigraphy (Figure 4.2).

Several types of basins can be distinguished. It includes criteria like sedimentary history and tectonic setting. It depends on (Cojan and Renard 2003):

- The nature of the lithosphere
- Position of the basin with respect to the plate boundaries
- Interaction of plates during the sedimentation.

The overall plate tectonic setting separates three major basin families according to Bally and Snelson (1980):

- Basins on a rigid lithosphere (rifts, Atlantic type of passive margin and cratonic basins).
- Peri-sutural basins on rigid lithosphere associated with mega-sutures (deepsea trenches associated with Benioff subduction zones, foredeeps).
- Epi-sutural basins within a mega-suture zone and influenced by mega-shear systems (fore arc basins, back arc basins, pull apart basins).

A suture zone is here the rock pile associated with a dynamic boundary zone of an plate tectonic assembly, showing a record of subsequent phase of folding, trust faulting, igneous activity and possibly some evidence for subordinate extensional tectonics.

A concise description of the classification of various types of basins is given by Kingston et al. (1983).

Sedimentary basins all undergo similar histories with a basic three fold subdivision:

- Basin forming phase caused by geodynamics and tectonics.
- Depositional infilling phase.
- A phase of basin modifying tectonics.

Basin fills are often complex entities with stacked poly-history sequences and a number of standard tectonic/sedimentary cycles superimposed on each other (Figure 4.3). Each cycle passes through a number of stages separated by regional unconformities. The principle basin or cycle types in a continental divergence setting under extensional tectonic conditions are:

- Interior continental sag (Figure 4.4).
- Interior continental fracture system, regional upwarping and graben formation.
- Marginal continental sag or differentially subsiding continental margin.
- Wrench related basin or sheared margin.

In a convergent plate tectonic setting:

- Wrench related or sheared pull-apart basin (Neogene basins SE Spain).
- Trenches.
- Foredeeps (foreland, forearc).

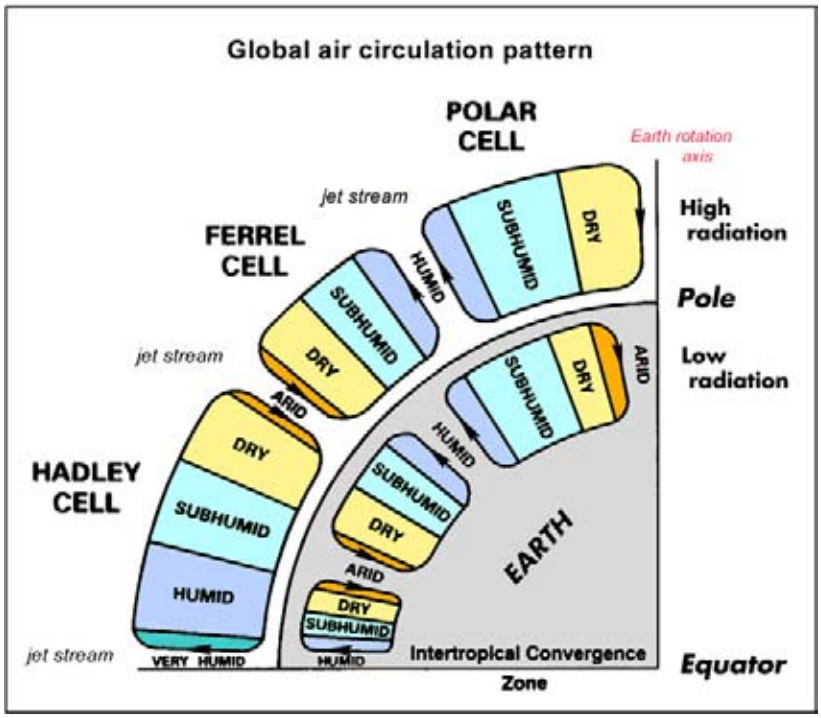

Figure 4.1: Hadley air circulation cells have an impact on the climatic conditions on the earth. The size of the cells depends on the amount of solar radiation reaching the earth surface (modified after Matthews and Perlmutter 1994).

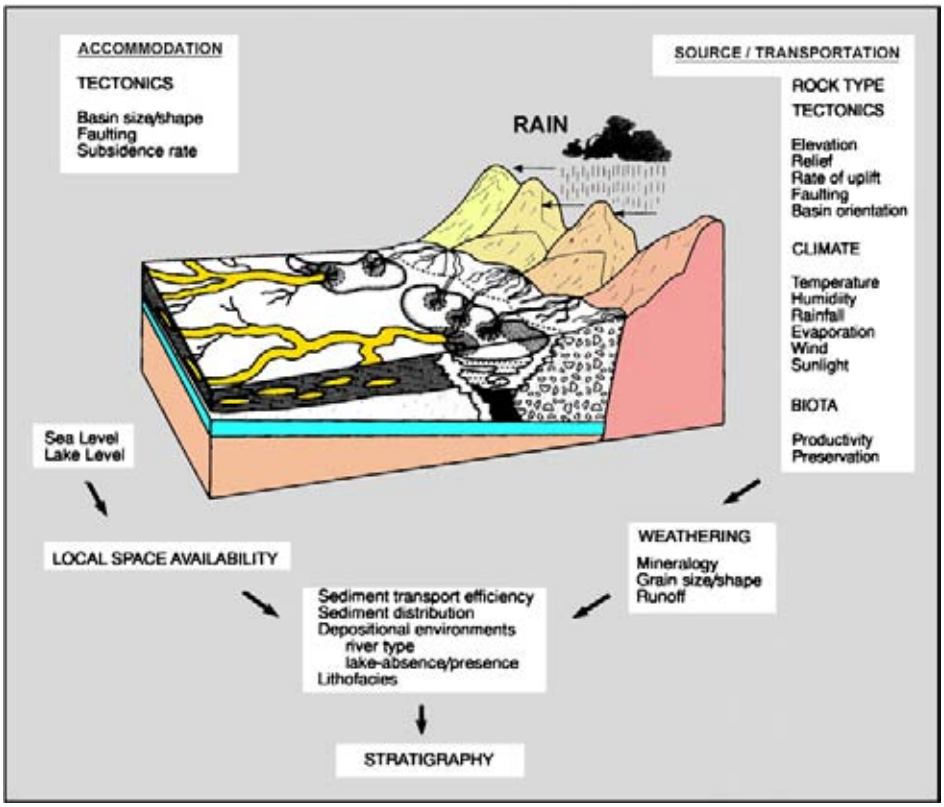

Figure 4.2: Factors controlling the stratigraphic record. The interplay of tectonics and sealevel changes directly influence the accommodation space. Weathering and denudation has an impact on the sediment supply and is depending on water run-off conditions in the hinterland. Biologic activity depends on climatic and topographic conditions (modified after Matthews and Perlmutter 1994).

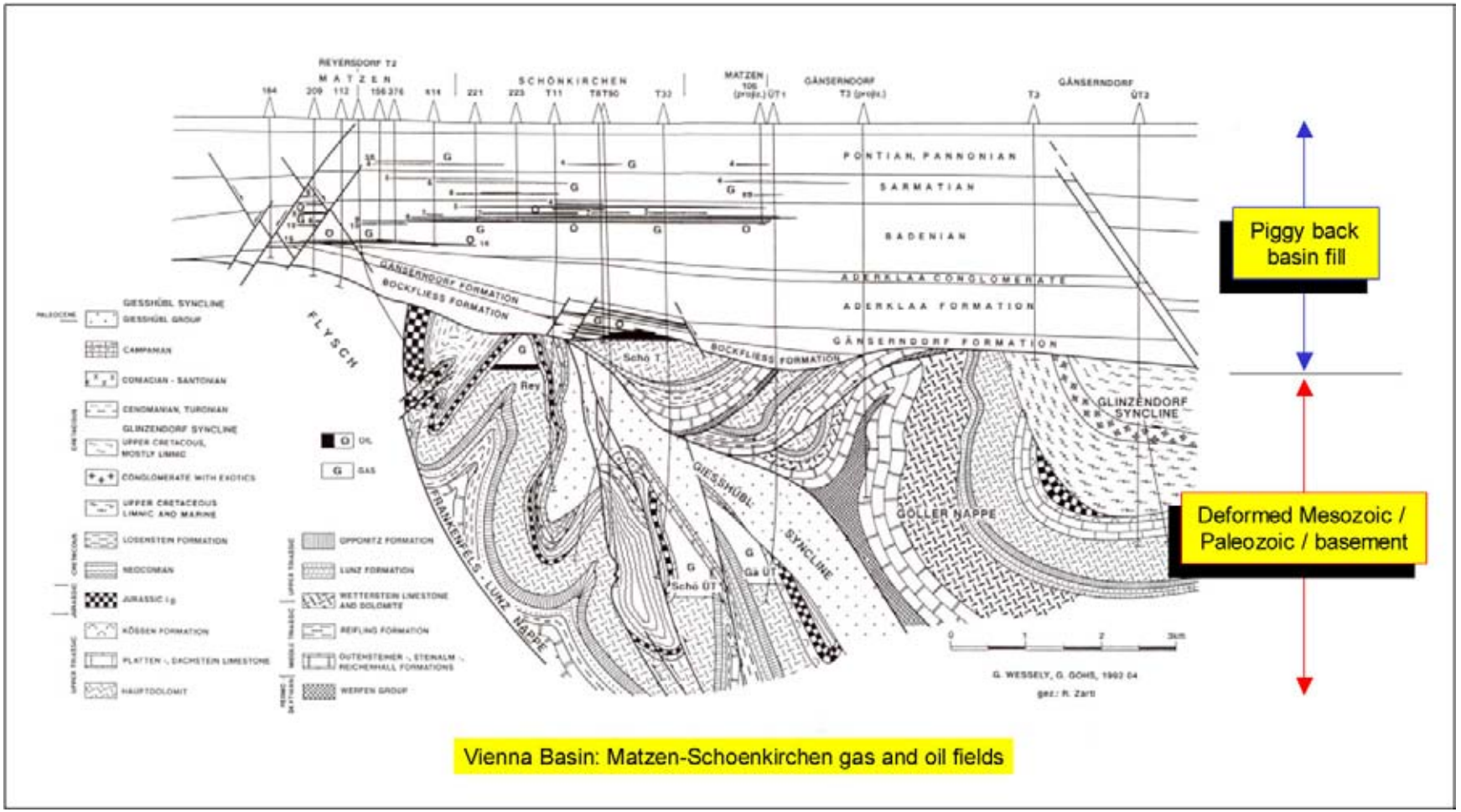

Figure 4.3: Basin fills give often evidence of polyphasing in the sedimentation history. Here severe tectonic deformation is shown for sediments below the Vienna piggy back basin sitting on top of the Alpine–Carpatian nappe structure. Oil and gas have been found at several levels (modified after Sauer et al. 1994).

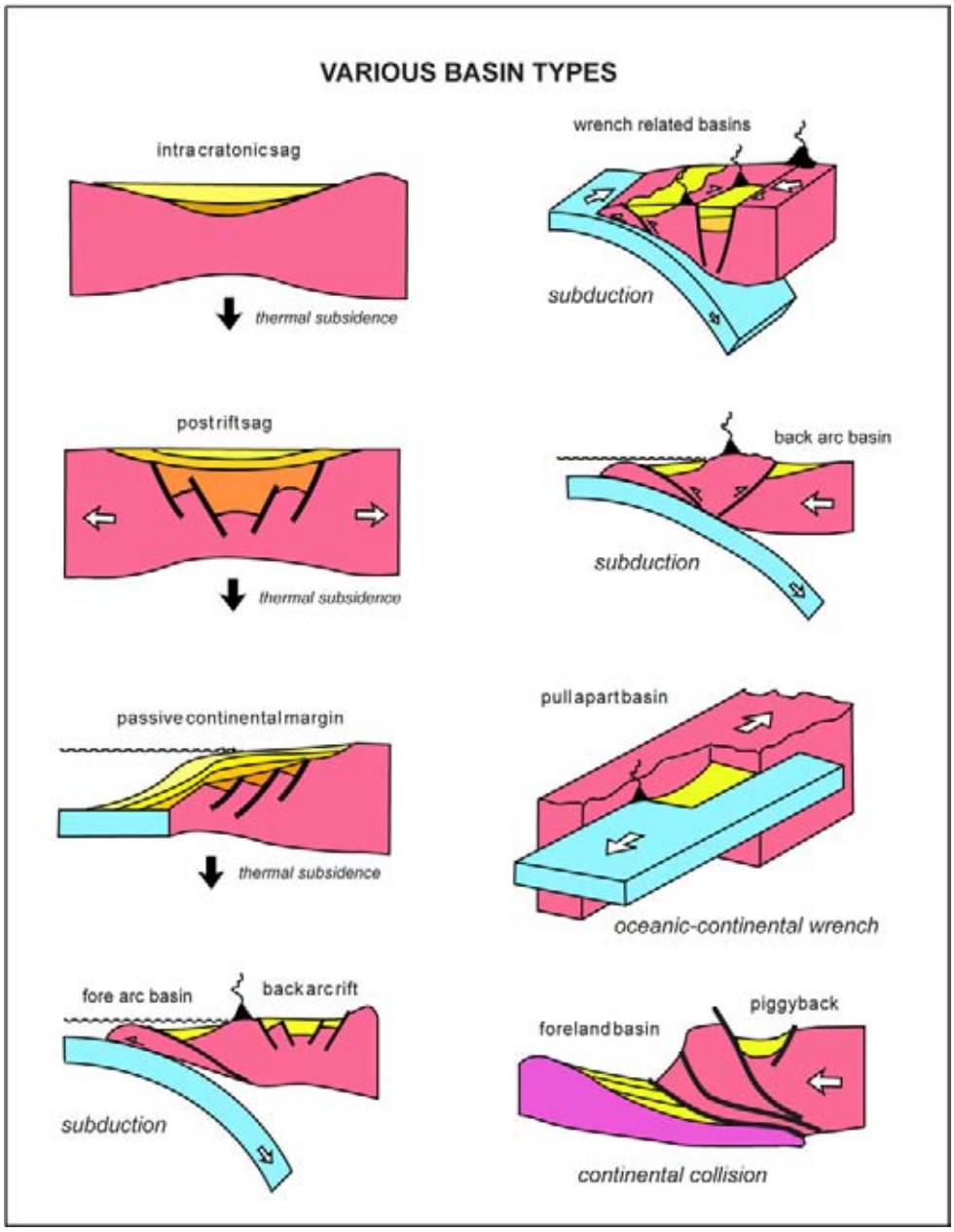

Figure 4.4: Various types of sedimentary basins in different tectonic settings (modified after Jacques 2004).

- Volcanic back-arc basins.
- Piggy back basins, riding at the back of a trust belt (Vienna basin).

Such cycles in the tectono-stratigraphic evolution provide a convenient frame for assessing the nature of petroleum systems (Kingston 1983, Doust 2003). Analogue situations are a helpful support for the proper interpretation of the seismic data.

In a basinfill the terrestrial fluvial, coastal and marine environments are not separate entities, but they are closely inter-related. For example a change in distributary channel configuration has an influence on the position of the prodelta depocentre in the marine domain. It has been observed that throughout the Phanerozoic era many regional sedimentary cycles on different continental margins occur more or less simultaneous. In addition, the magnitudes of the change are comparable. These observations led to the concept of **eustatic sealevel change** (worldwide stable). The variability in local subsidence rate and the change in eustatic sealevel control together the amount of relative sealevel change, for which local charts have been compiled. From these schemes worldwide applicable charts are deduced,

which provide an interesting tool to establish a time-stratigraphic frame between various sedimentary basins (Vail et al. 1977, Pitman 1978, Vail and Todd 1981, Watts 1982, Haq et al. 1988, Cramez et al. 1993).

4.1 Dynamics of Depositional Environments

Sedimentation in a coastal area is usually dominated by regression and transgression of the sea. This inter-play depends on:

- The sediment supply.
- The amount of marine erosion.
- On the changes in the **baselevel profile**.

The baselevel is a hypothetical equilibrium line describing the gradient of the depositional slope. It runs from the mountains towards the sea. It determines the areas where erosion and sedimentation are to occur. Areas topographically above the baselevel profile are submitted to erosion, while areas below it correspond to active depocentres. The position of the baselevel is related to the sealevel (Wilgus et al. 1988). In fact it controls the **accommodation space** that is available for sediment accumulation. Tectonic movements have in their turn an influence on the relative sealevel position (Williams and Dobb 1993). Excessive supply of clastic material – due to the presence of a rising mountain belt – results in coastal progradation. This is expressed by rapid outbuilding of delta systems and/or barrier complexes fed by longshore currents. Sediment supply by longshore currents leads to important accretion of barrier shoreface sands and offshore sand bars.

As a result of coastline progradation in time, more landward depositional facies like coastal plain deposits are overlying older shoreface sediments. When the coastline retrogrades, due to transgression of the sea, it will result in a configuration whereby coastal paralic deposits are overlain by shoreface and shallow marine deposits (Figure 4.5). A delta lobe can be abandoned during transgression because of upstream diversion of a branch in the river system.

The already deposited sediments are often reworked by the sea, redistributed and winnowed (i.e. removal of the finer grained fraction of the sediments). They are laid down and preserved as a **marine lag deposit** (basal conglomerate). As normal marine sedimentation takes over, then finer-grained sediments are deposited. A renewed regression of the sea may lead to the re-activation of the earlier delta lobe system in a similar position. This alternation of trans- and regression cycles results in a vertically stacked nature of different delta lobe deposits in time. Normally the regressive part of the cycle is represented by large-scale coarsening upward sequences, while the transgression is coinciding with fining upwards trends. The subdivision often also corresponds to thickening upward cycles and thinning upward trends of the beds. It should be mentioned that the vertical stacking of marine muds and coarser grained deltaic sediments also may result from natural delta lobe avulsion (e.g. Stouthamer 2001). This phenomenon is characteristic for the lateral switching of the deltaic depocentre. Consequently, the change in gross lithology in an isolated outcrop is not necessarily a sole indicator for changes in relative sealevel. This switch mechanism is also known as the **autocyclic** character of the deltaic deposits.

4.1.1 Passive continental margins

When a flat substratum is considered, dipping in an oceanward direction, most sediments will be stored in the coastal plain, marine shelf and slope prism. This situation is more or less representative for a **passive continental margin** setting. This area is underlain by the continental to oceanic plate transition. At the oceanic ridge new plate material is created by the rising of mantle plumes. The newly formed material is hot and is accreted to the plate edge at the spreading centre. In doing so it pushes material away and the width of the ocean is increased. When the plate moves away from the spreading centre the material gets cooler. The relatively old and cold plate edge of the oceanic plate at the continental rise is therefore denser and sinks deeper into the mantle (Burk and Drake 1974, Pitman 1978, Ziegler 1982, 1990). The continental plate at the edge of the continent is infested with dykes that have been created during the initial continental break-up. Hence the continental plate edge is here somewhat denser and sinks deeper into the mantle than the normal crust. It creates the general dip and accommodation space for sediments coming from the continent.

Subsidence due to the cooling effect of the crust is also observed on the continental plate itself. A rising mantle convection cell is the locus of regional upwarping, followed by the initial hot rifting and its crestal collapse results from extensional tectonics (Figure 4.6). It leads to the formation of major grabens and half grabens (e.g. Kearey and Vine 1990, Ziegler 1982, 1978, 1983). For many grabens this rifting phase, in consequence of the thinning of the crust, was not followed by a drifting phase. The drift means that oceanic crust is actively formed at a new spreading centre. This abortion of the rift is probably caused by fundamental changes in the

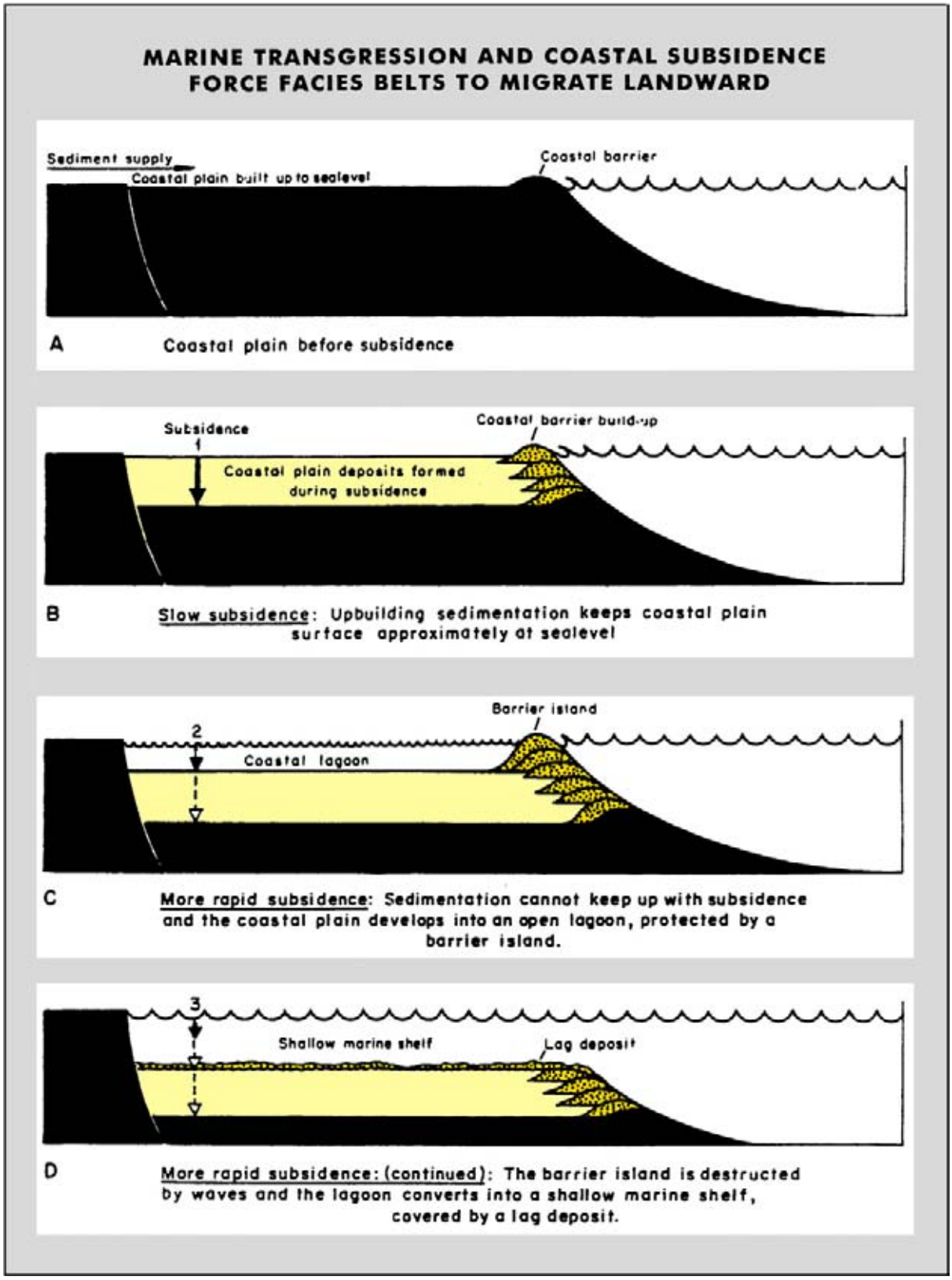

Figure 4.5: Transgression of the sea and retrogradation of the coastline. When the transgression is fairly rapid and sediment supply is not in equilibrium, then a coarse grained lag deposit (basal conglomerate) is created.

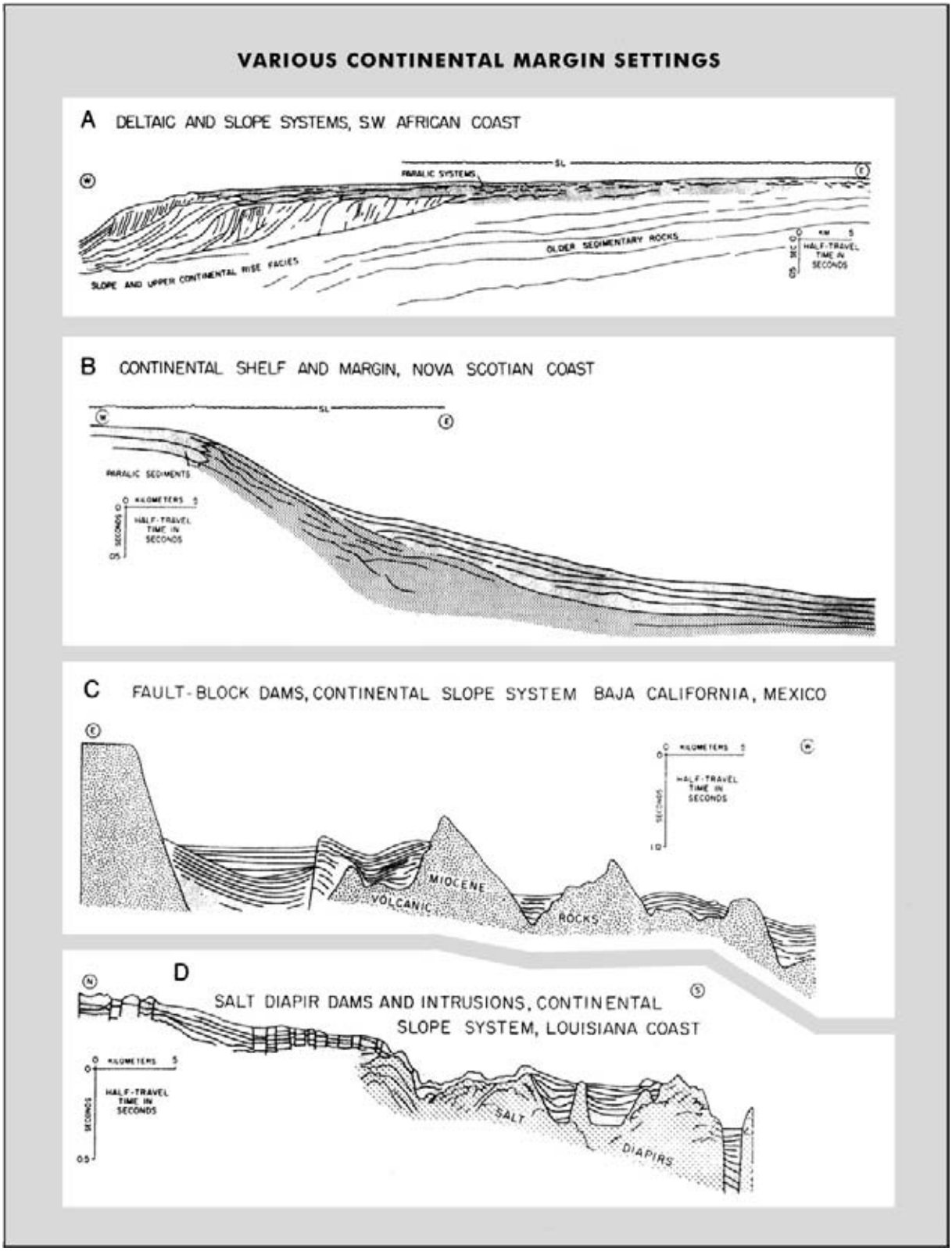

Figure 4.6: Various continental margin settings. The passive continental margins are characterised by regional downwarping of the substratum under influence of lithospheric cooling. This subsidence mechanism and creation of accommodation space is further assisted by sedimentary loading at the margin of the continental plate. The onset of the lithospheric cooling corresponds to the actual break-up phase of the initial continental rift and subsequent moving away of the continental plate from the mid-oceanic ridge (after Vail et al. 1977, reprint from AAPG whose permission is required for further use).

stress regime. Intra-plate stresses can locally also lead to compressional deformation in an overall graben setting (e.g. North Sea Basin, Kooi and Cloetingh 1989).

The coastal area forms an effective trap for the more coarser part of the supplied clastics. The heavier fraction of the debris, under transportation from the hinterland to the basin centre, is dumped at the coastal plain margin due to a drastic change in energy conditions. The bulk of the suspended finer-grained material is, however, transported further over the shelf and settles gradually in the slope region. The fundamental decrease in sedimentation rate in a basinward direction does translate in a typical inclined pile of sediments. The sediment supply gradually peters out. This effect is amplified by the dampening effect on the energy of the currents when a large water mass is encountered. The combination results in the creation of a shelf/slope geometry, while in the same time condensed sedimentation takes place on the distal basinfloor (Figure 4.7; Mitchum et al. 1977, Loutit et al. 1978, Mougeneot et al. 1983).

Under **rising relative sealevel** conditions the sedimentation in the deeper parts of the basin is reduced and mainly (hemi-) pelagic in nature, that is to say from suspension. The bulk of the material is locked into the coastal domain. On the shelfedge minor amounts of the sediments are reworked by massflow transport mechanisms. These sediments are likely to be shale-prone, as the coarser fraction is already stored in the inner parts of the shelf. Contour currents are triggered on the slope and along the basin floor by thermohaline density differences. These currents further redistribute the available sediments (fine grained contourite mounds). A view is shown in Figure 4.8 on how an idealized beach model profile is behaving under sealevel rise conditions (Nummedal et al. 1993). Note that erosion takes place at the shallow water depth and at the same time resedimentation occurs in the deeper waters.

The coastal plain and adjacent marine shelf form areas of non-deposition and/or erosion during conditions of **relative sealevel fall** (Figure 4.9, Fisher and Brown 1972, Brown and Fisher 1977). It is possible that an eustatic sealevel rise is overprinted by a major regional uplift and the accommodation space in the proximal domain is effectively reduced. These zones constitute now areas of sediment bypass. The sediments derived from the hinterland are transported over the shelf and dumped at the shelfedge, where the standing body of water is encountered. Under drastic sealevel fall conditions the entire shelf is exposed and submitted to active subaerial erosion. Such a dramatic event is known as a **forced regression**. The coarser grained sediments are transported further in direction of the deeper basin centre than usual. A toplap geometry may be the result, indicating that topset material is carried further down slope.

Sediments on the bordering shelfedge and slope are frequently submitted to reworking. Slope instability may lead to continental margin failure. Slumping of shelfedge sediments (deformation with some degree of internal consistency) and the formation of olistostromes (chaotic mixture incorporating huge exotic blocks) is favoured. The material is transported downslope and dumped into adjacent basinal areas. Sedimentation in the Gulf of Cadiz (a.o. Malod and Mougenot 1979) is a good example that this can occur on a seismic scale (see Figure 3.27). Sediments accumulate at the base of the slope and tend to form **slope front fills**. These fills can be internally quite complex. They are composed of amalgamated sediment prisms at the foot of the slope and form a **slope apron**. Under such lowstand circumstances submarine fan systems become very important depocenters and fan lobes are prograding on the basinfloor. Lobe switching is a characteristic feature in these systems, when there are no basinfloor constraints. Rivers on the shelf tend to be meandering as the topography is rather flat. These river systems are cutting major river valleys also known as **incised river valleys**.

The lowering of the sealevel and the increased gradient on the slope encountered by the river runoff causes important erosion in the slope regions. **Canyons** are cut at the shelfedge which form feeder channels for fan systems further down slope (Figure 4.10). As said already above, the sealevel lowstand coincides with important sediment accumulation on the slope and also in basinal areas. It usually corresponds with erosion and/or a hiatus in the sedimentary record on the shelf.

4.1.2 Carbonate platforms

When the supply of sediment from the hinterland is blocked and the basin is starved of clastic input, shallow marine carbonates are deposited on the shelf (Figures 4.11 and 4.12). Restricted marine conditions may prevail along the landward border of the marine basin. High-energy **reefal barriers** and **build-ups** develop along the shelfedge margin, protecting the inner shelf area. Isolated build-ups on the shelf are formed when conditions are favorable:

- Right water temperature range.
- Salinity.
- Amount of nutrients.
- Quantity of sunlight.

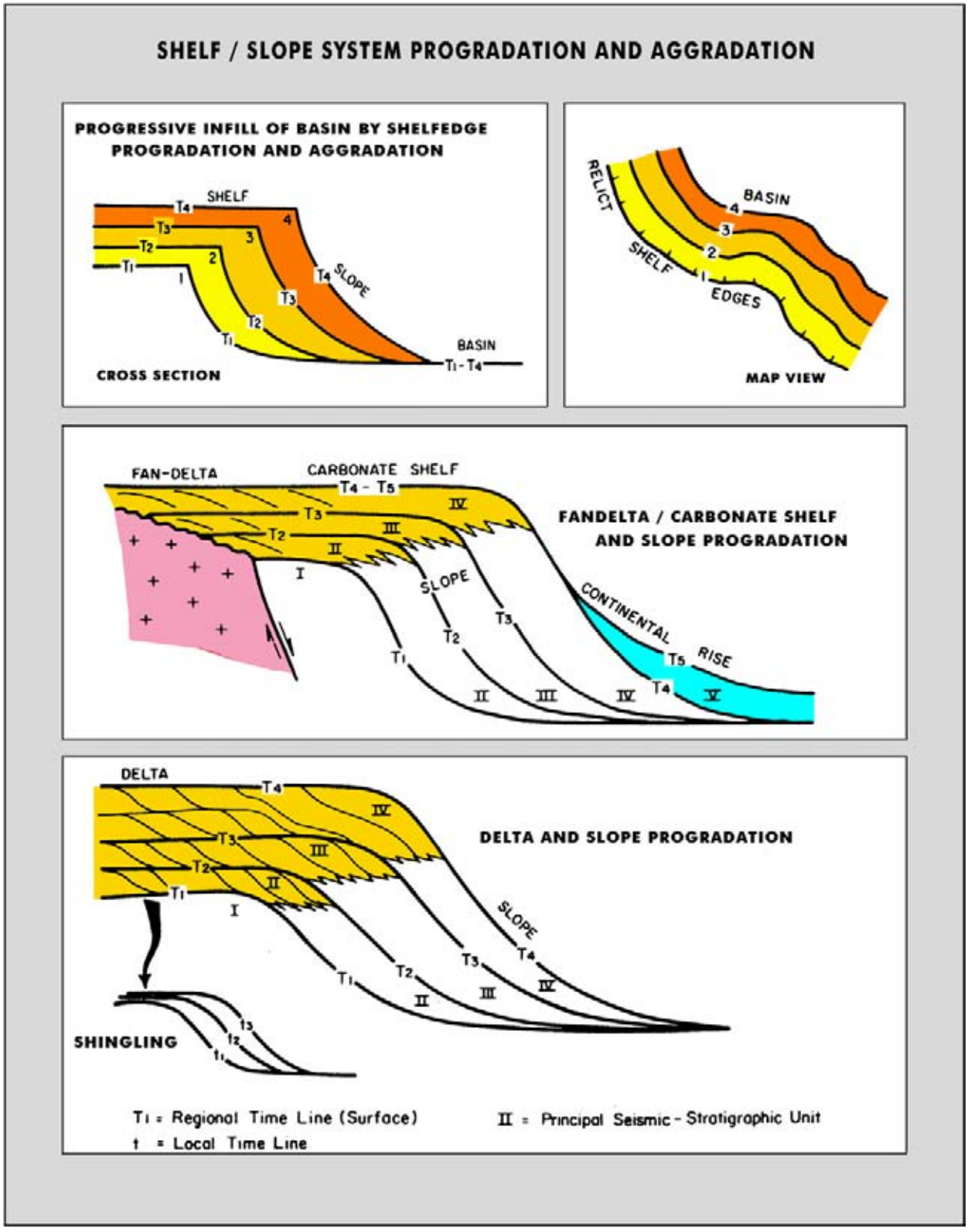

Figure 4.7: Some different hypothetical slope forms are shown. The shelfedge is prograding and its intersection line plots at different locations on the map. The sandprone topsets are time-equivalent to shale deposits on the slope. The foreset geometry implies condensed sedimentation on the basinfloor. Shingling is foresetting with small height difference between top- and bottomset. On seismics the shingling is often indicative for high energy, sand-prone deposits (modified after Mitchum et al. 1977, reprint from AAPG whose permission is required for further use).

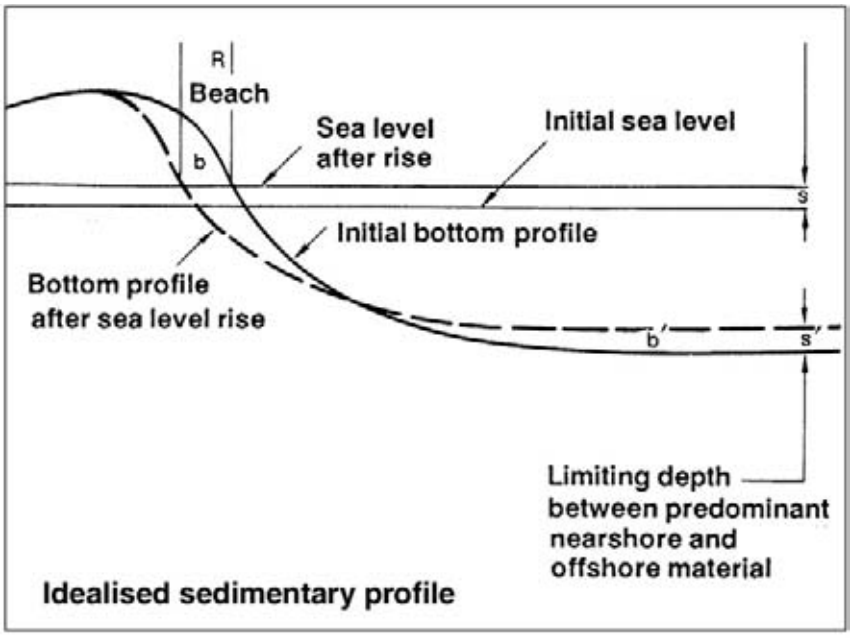

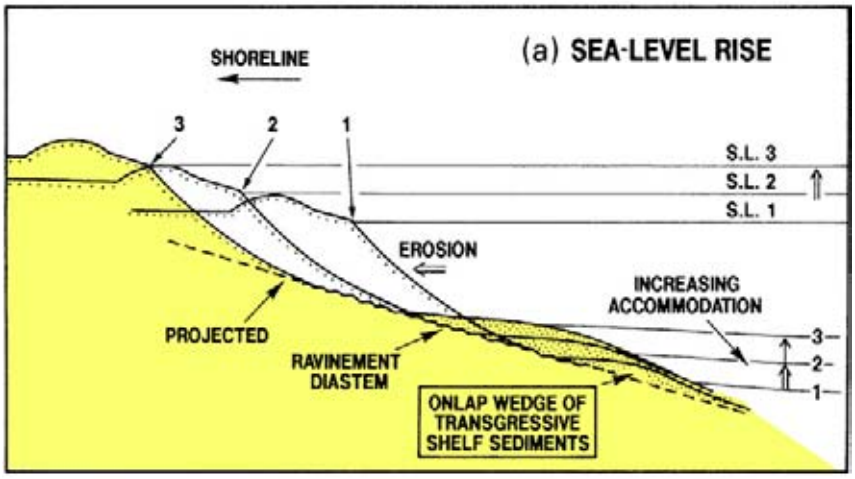

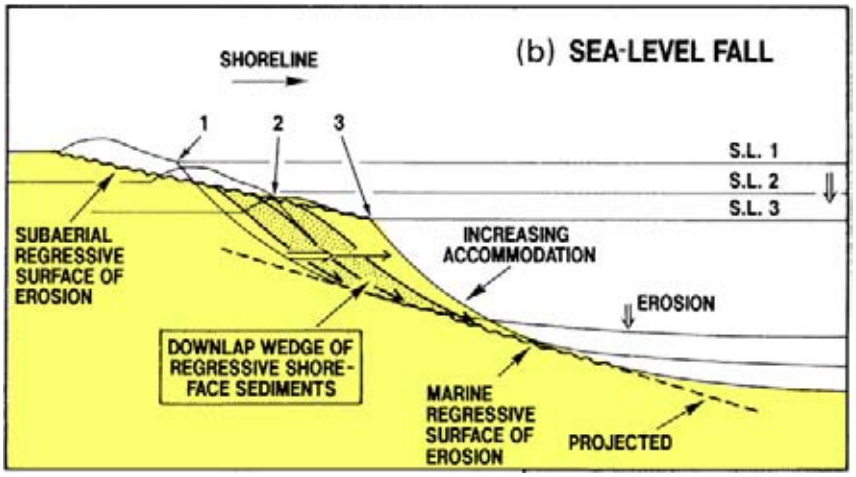

Figure 4.8: Relation between the change in sealevel and the shape of the stable sedimentation profile in a beach environment (modified after Nummedal et al. 1993).

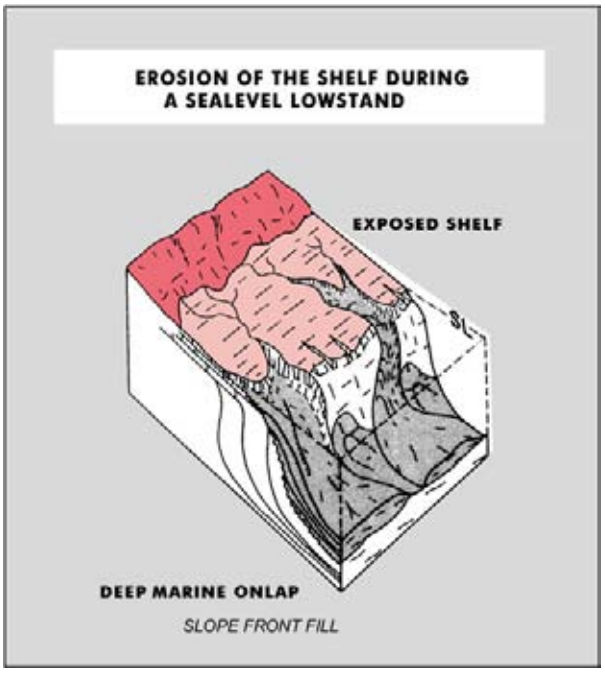

Figure 4.9: Subaerial erosion of the shelf area during a period of sealevel fall. Deep fluvial channels are cut at the shelf, connected to slope canyon systems feeding coalescent submarine fans at the base of the slope. Slope drape deposition is less important. Onlap of submarine fan deposits, laid down as slope front fill prisms, is quite common under these circumstances. These fans do form the main depocenters and are potentially sand-rich with good reservoir characteristics (modified after Fisher and Brown 1977, reprint from AAPG whose permission is required for further use).

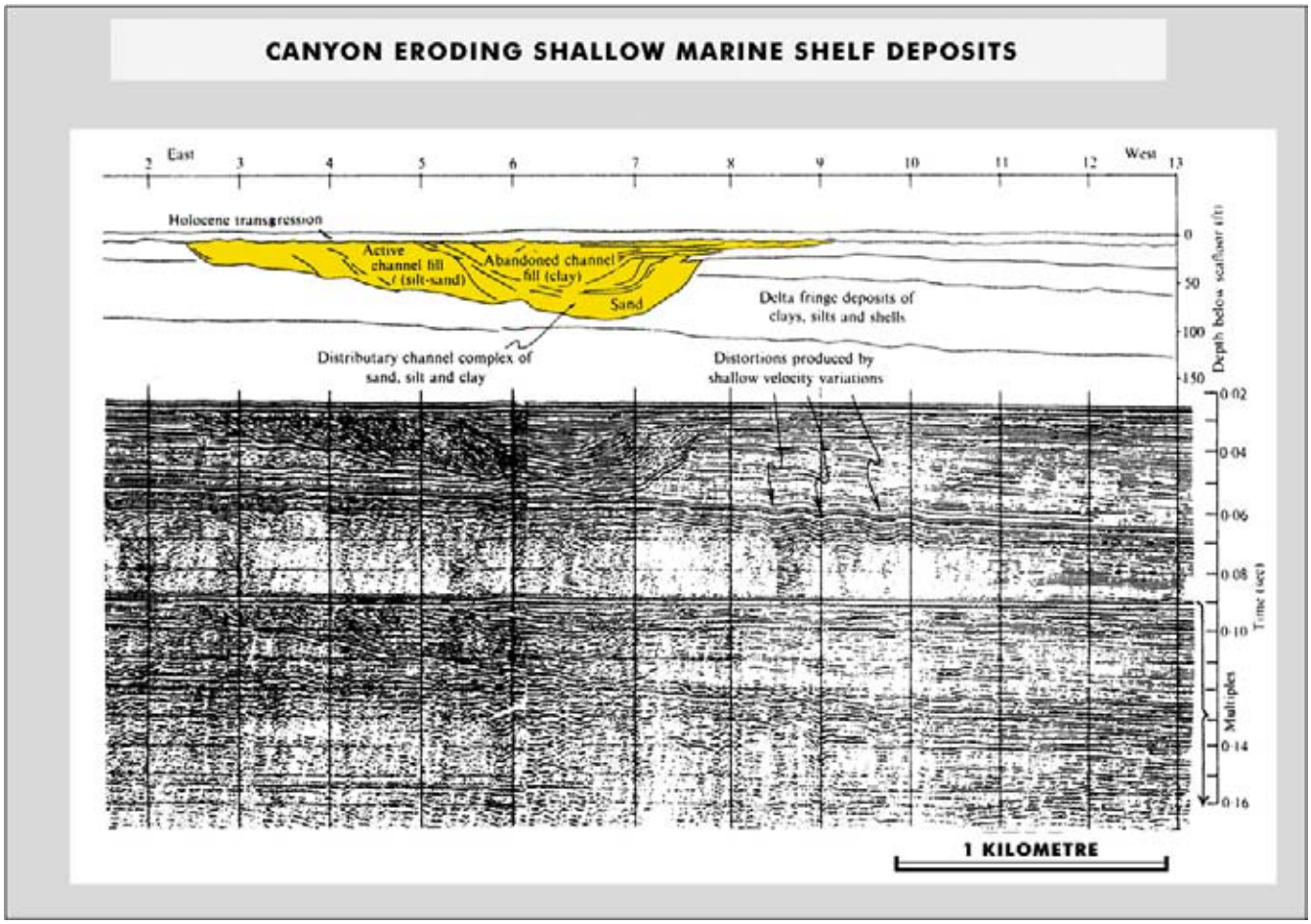

Figure 4.10: Erosive submarine canyon complex with an intricate infill. Various stages of infill can be recognised and these are characterised by different seismic facies units. Lateral change in interval velocity over such canyon fills can be a notorious source of error for the depth conversion of deeper levels, when these variations are ignored by the interpreter (modified after King 1973).

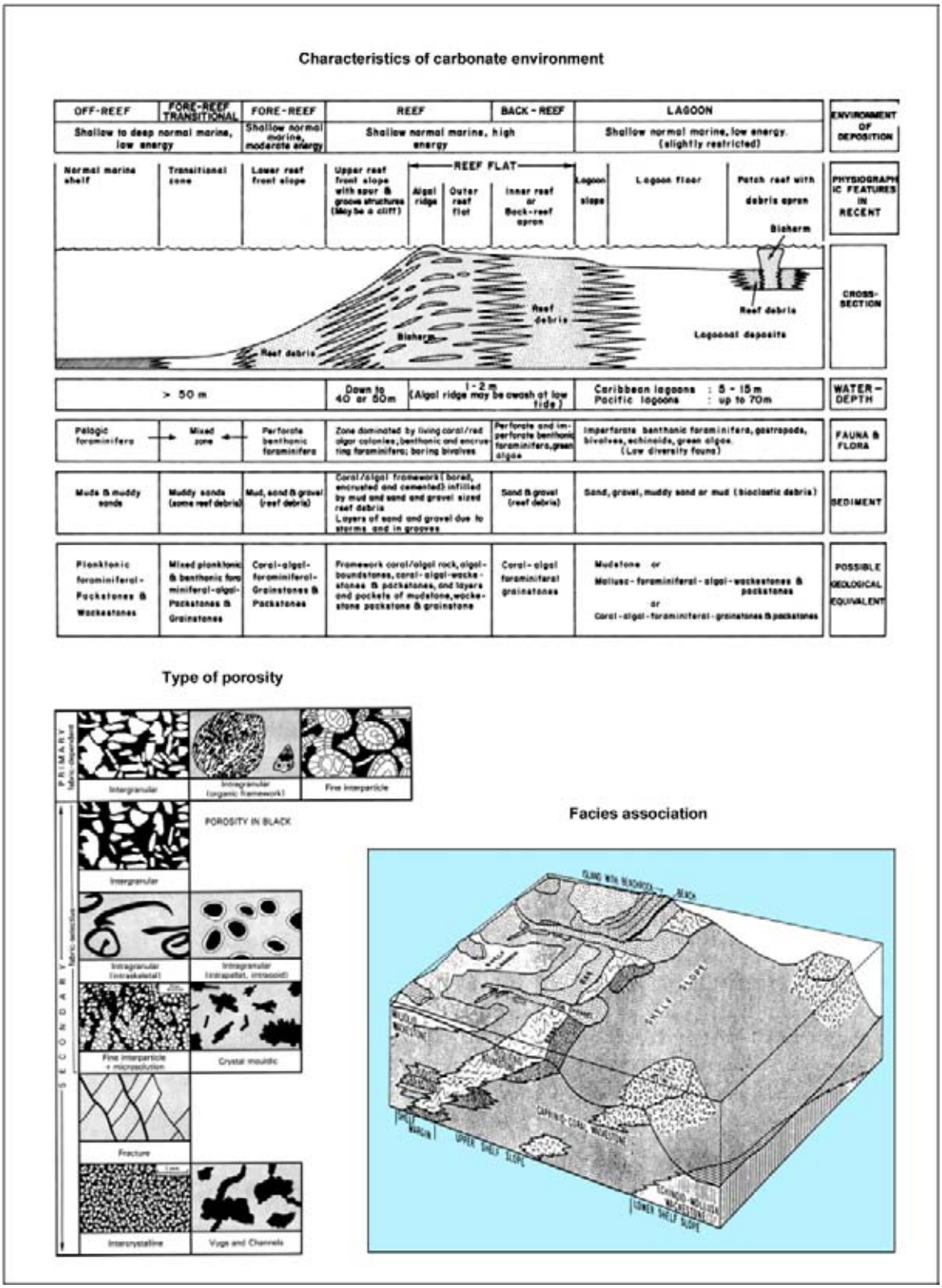

Figure 4.11: Characteristics of the carbonate depositional environment (modified after Wagner 1983). Various types of porosity are seen in carbonate rocks. Also the schematic facies distribution for a carbonate environment is shown. Note the interplay with clastic depositional systems (after Bebout and Louks 1974, Scholle et al. 1978).

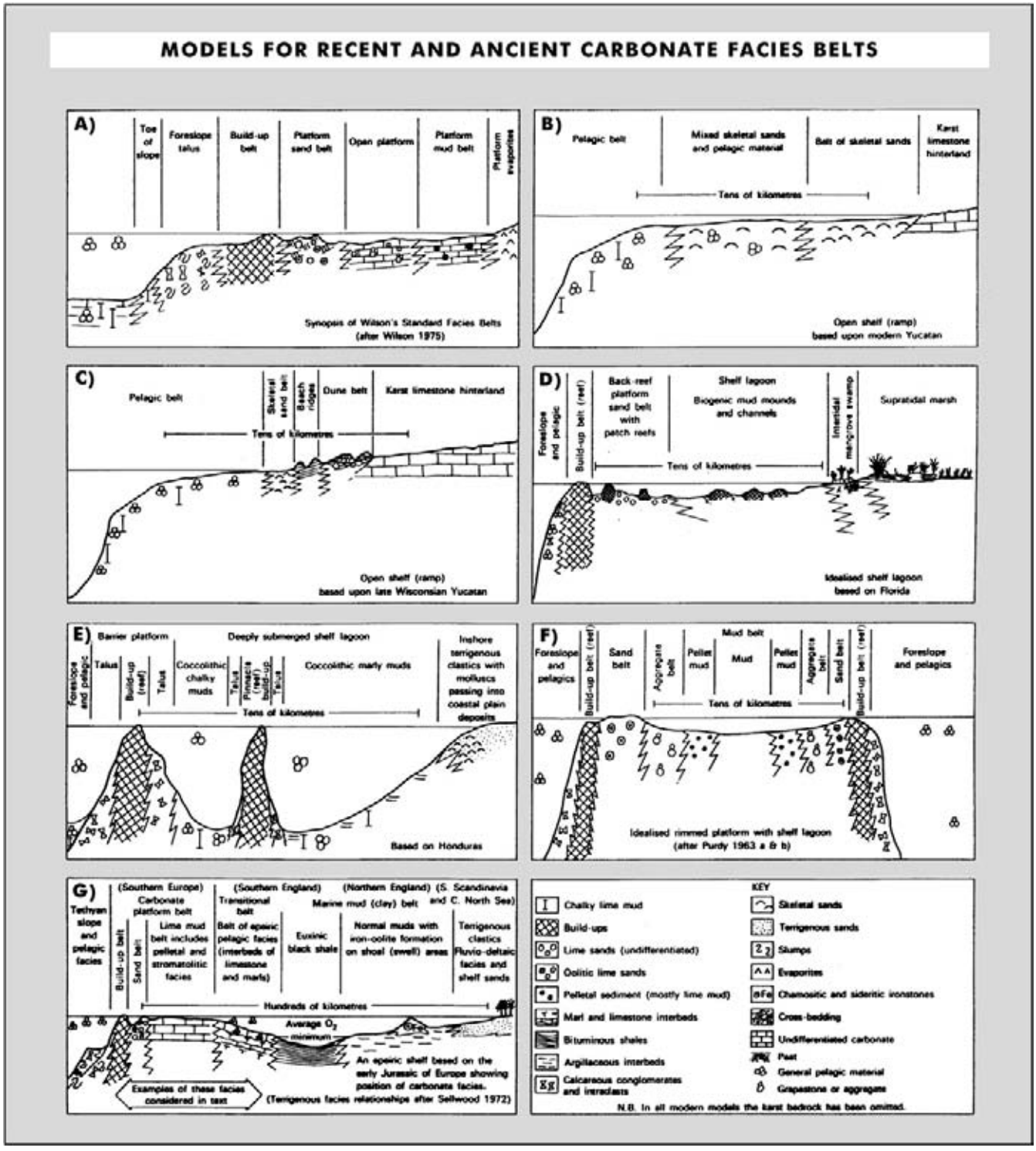

Figure 4.12: Comparative depositional models for modern and ancient carbonate facies belts (after Sellwood in Reading 1978).

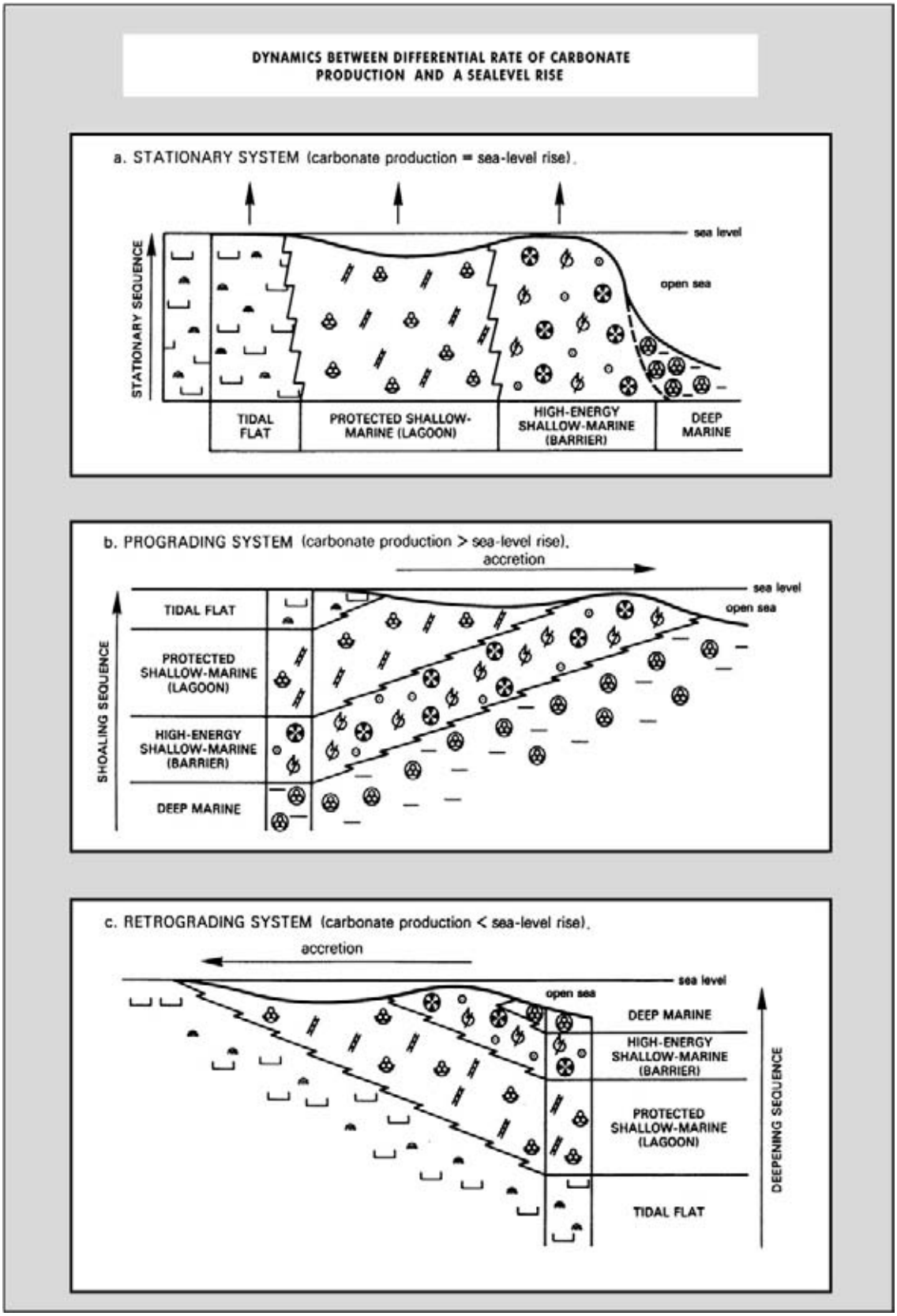

Figure 4.13: Geometry of carbonate shelves under changing relative sealevel (modified after Wagner 1983).

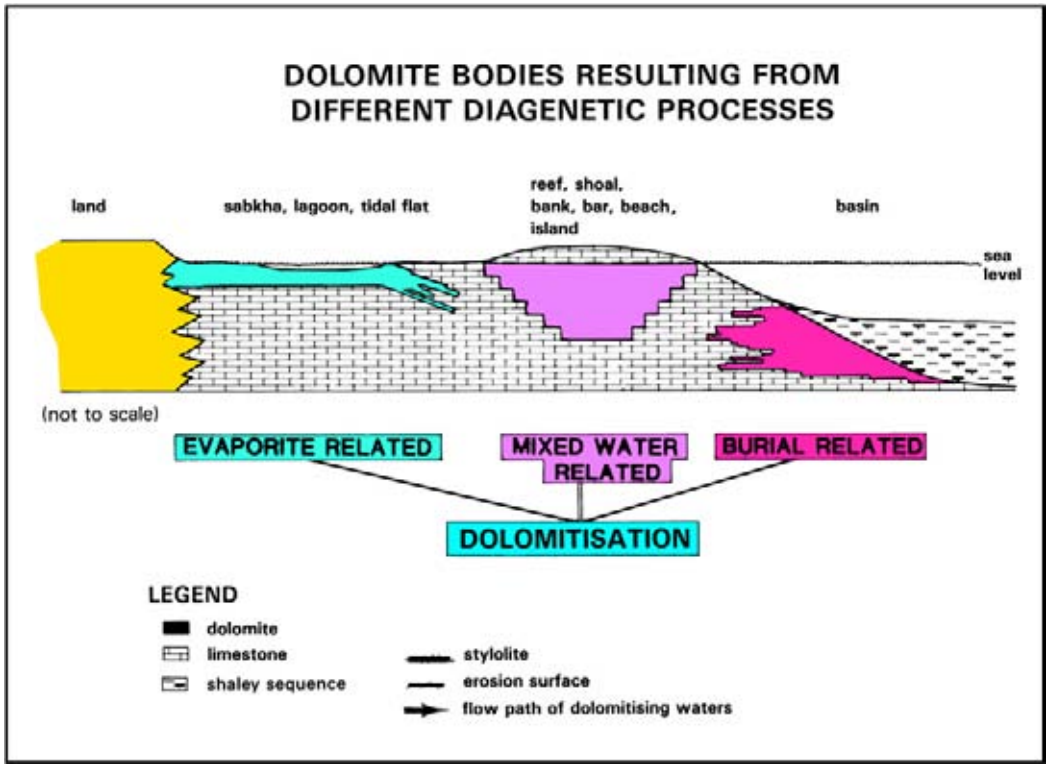

Figure 4.14: Dolomitisation of a carbonate build-up, whereby magnesium is added to the calcium in the calcite crystal structure. The alteration often occurs in the subsurface when a brine porefill is in contact with fresh water and an exchange in cations is possible in the transition zone.

– Restricted amounts of clastic input.

Under relative sealevel rise conditions the carbonate shelf edge can be rather steep. This geometry is maintained due to little erosion on the platform and hence relatively low sedimentation rates on the basinfloor (Figure 4.13). The shape of the slope depends a lot on the amount of material available for re-deposition at the slope and base-of-slope regions. **Storm-generated wave energy** is important as an eroding agent and for the transportation of shelf sediments (cf Veeken et al. 1999). In addition, tectonic slope instability triggers large quantities of massflow currents. Prograding slope systems with submarine fan complexes at their base are recognised within carbonate rocks. Cretaceous limestones in the southern Pyrenees are good examples of this (Drzewiecki and Simo 2002).

If the relative sealevel fall is large enough, then the reefs and bordering shelf area are submitted to subaerial erosion. Under such circumstances the carbonates are leached and the porosity of the rocks is increased (e.g. Jurassic Casablanca field, offshore Spain; Watson 1982). **Karst** is an extreme weathering type found in exposed carbonate regions. It is characterised by extensive subterraneous cavern systems. High losses of drilling mud, resulting in severe problems in pressure control for the well, are some of the dangers associated with those anomalously porous zones.

Dolomitisation, resulting in a change in porosity/permeability, takes place when the carbonates are invaded by pore fluids rich in magnesium (Figure 4.14). There exist three basic mechanisms for producing dolomite in carbonate rocks:

– Evaporation related dolomitisation, interlayered with carbonates, parallel to bedding.

– Mixed water related dolomitisation, cross-cutting original layering. It is fact an early diagenetic process.

– Burial related dolomitisation, also cross-cutting the layering. Updip migration of expelled Mg-rich brines from compacting shales.

Dolomitisation often increases the permeability of the rocks and therefore improves the overall reservoir quality (e.g. Mancini et al. 2004). Anhydrite cement is formed as the initial transformation product in virgin limestones invaded by the reflux groundwater in dolomitisation process. The magnesium in the groundwater is enriched by evaporation.

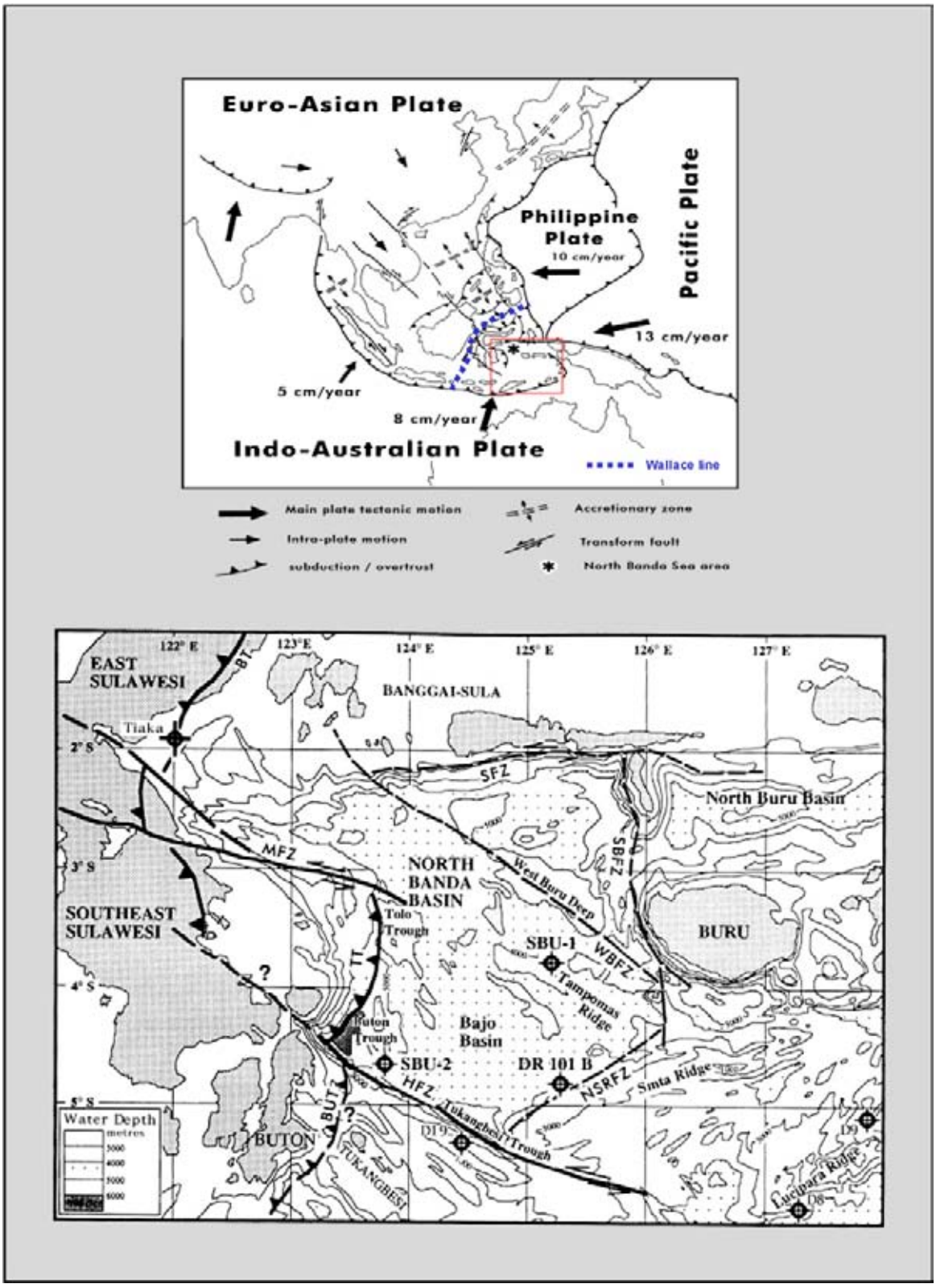

Figure 4.15: Setting of the Banda Sea area in SE Asia with relative tectonic plate movements indicated. The area is underlain by oceanic crust. It is affected by spectacular strike slip and overthrust faulting (modified after Taponnier 1986 and Burhanuddin 1994).

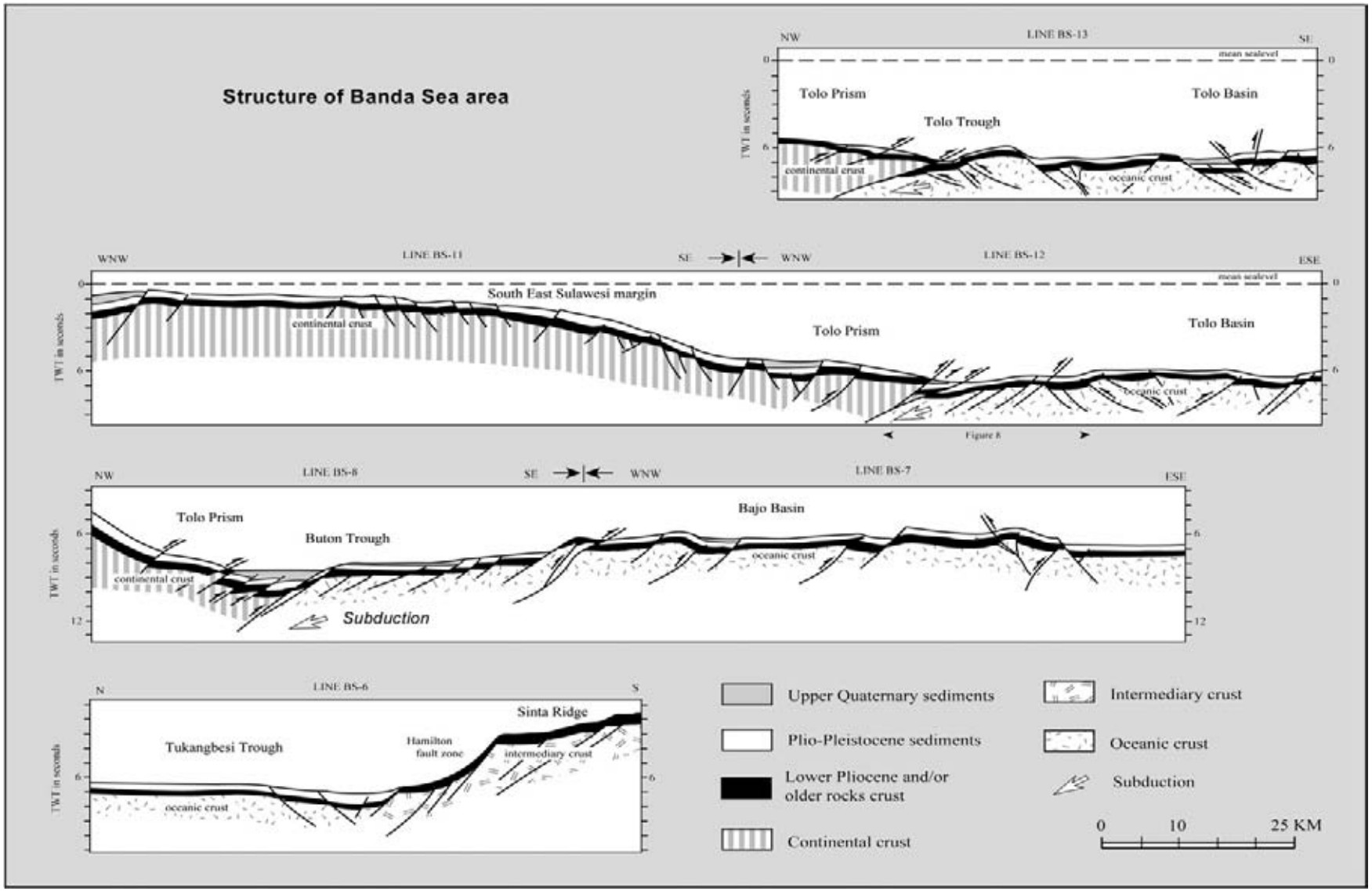

Figure 4.16: Collision between oceanic and continental plates in the Banda Sea area with important lateral movement along major fault zones. Note that the Plio–Pleistocene sequence is involved in the deformation. The Tolo accretionary wedge in the west is the result of subduction of the oceanic plate (more heavy and basaltic in composition) below the island arc block.

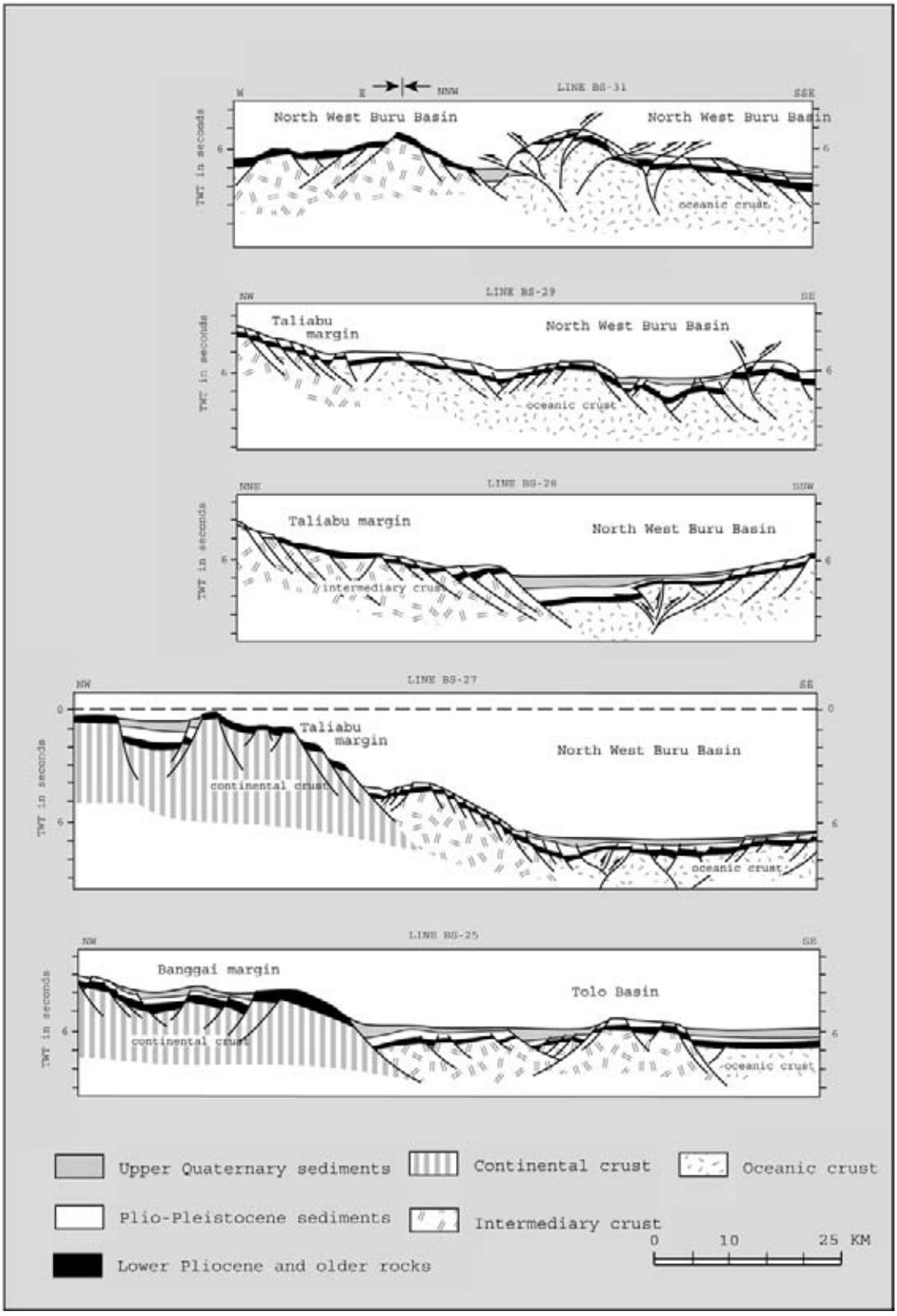

Figure 4.17: Accretionary wedge in the Banda Sea as a result of the collision of an oceanic plate. This event induced severe tectonic deformation with spectacular push-up structures. The pop-up and flower structures are the result of important lateral movements between plate fragments. This wrenching deformation mechanism explains the typical elongated geometry of some islands (e.g. Sulabesi) in the Banda Sea archipelago.

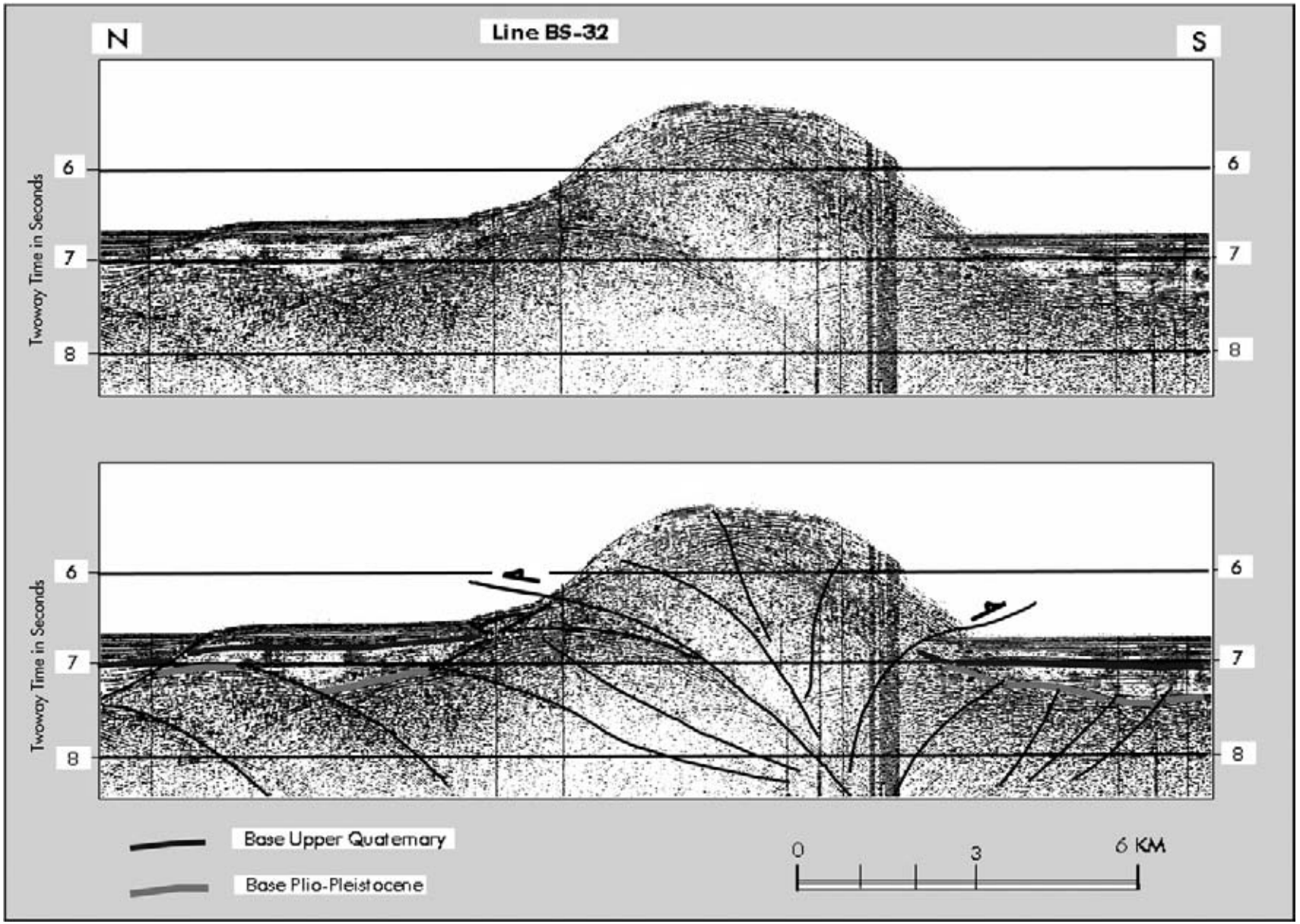

Figure 4.18: Blow-up of the Buru Faultzone pop-up or flower structure. Pliocene–Pleistocene sediments are actively involved in the movements (data courtesy Prof Rehault, University Bretagne Occidentale, Ifremer).

4.1.3 Syn-sedimentary tectonic deformation

Syn-sedimentary tectonics do complicate the described models. Faulting and basement deformation dictate the position of local depocenters, areas where sediments are trapped and preserved. Tectonics puts an important constraint on the behavior of freely outbuilding systems. It may be the dominant factor in controlling the position of the shelfedge and the shape of the basinfloor topography. Differential subsidence is governing the position and distribution of high and low blocks. It makes it possible to have a relative sealevel rise in a particular fault compartment or region, while in another area the sealevel is dropping due to differential tectonic uplift.

When basins are bordering areas in an active orogenic belt, as for example offshore Brunei in SE Asia or around the Gulf of Mexico, the differential subsidence is considerable (4–10 km for the Tertiary sequence alone). The **accretionary wedge** of the uplifted mountain belt and its associated deformation front influence the sedimentation conditions (Banda Sea, Figures 4.15 and 4.16). The sedimentary pile in the accretionary wedge at the margins of the basin is involved in the deformation. These sediments are eroded and the clastic material is re-deposited further away, towards the centre of the basin.

The presence of **pop-up structures** are evidence for important lateral movement along underlying fault zones. Tectonic **flower structures** are expressions of these fault movements (Figures 4.17 and 4.18). This kind of structural style is usually the result of deep-seated deformation affecting basement blocks (a.o. Storti et al. 2003, Nieuwland 2003). Also 'en echelon' **Riedel shears** (a suite of S-shape faults in map view) are indicative for lateral movements, but here the lateral displacement is probably less. These thin skin tectonic faults tend to join themselves up with ongoing lateral movements along the underlying faultzone and thus create a major through-going faultzone. The wrench faults can be left hand or sinistral in nature, whereby in map view the left hand block is moving towards the observer. Or they can be dextral. **Transfer zones** in the fault pattern of a graben system also point to horizontal adjustments (Rosendahl 1987). Laboratory modeling experiments have demonstrated that the transfer zones comprise a series of en echelon normal faults that connect to the basement fault responsible for the lateral offset in rift basins (Figure 4.19, Gartrell et al. 2004).

The substratum, underlying the foredeep basin, is usually tilted and asymmetrically rotated. This is caused by loading effects on the lithospheric plate due to the proximity of the accretionary wedge. The distal shoulder of the opposite flank of the basin is often over-compensated and uplifted. It may form an additional source area. Under these circumstances a normal shelf/slope-system is not always developed. The ongoing tilting and uplift, together with the tectonic instability, does favor massflow transport and **cannibalism** of earlier deposited sediments.

Very narrow depositional systems are encountered in many rift and **pull-apart** basins (e.g. Brown and Fisher 1976, Veeken 1983). Here the graben boundary faults are an important controlling factor for the distribution of sedimentary environments. Under these circumstances the alluvial fans border directly the marine basin and no coastal plain, with an extensive draining river/floodplain system, is developed. Badly sorted, coarse grained **fandelta** complexes are a typical product under such conditions (Veeken 1997).

4.2 Coastal Onlap Curves

The monitoring of the sealevel behavior during the geologic time is important from a correlational point of view. When age-dating a certain unconformity in a basin and correlating the event to a sealevel change, it can be inferred that a similar event is probably also present in a bordering basin. Although it might be overprinted by severe local tectonics. On the other hand, major geologic events have their effect on a worldwide scale (e.g. the Alpine movements). It is difficult to separate the influence of local tectonics from sealevel behavior, but still it has been attempted by a lot of researchers. The sealevel controls the position of the baselevel and the accommodation space in the marine domain. This has a decisive impact on the coastal onlap trends and unconformable contacts. A sealevel curve can be deduced from the shift in coastal onlap. Credibility of the correlational tool is even better, when the unconformities can be traced back in several places of the globe at the same time. Delineation of such sealevel change in time provides a powerful means to establish more firmly the chronostratigraphic frame between various unknown sedimentary basins (Vail et al. 1977, 1987).

4.2.1 Relative changes in sealevel

The sealevel does control the position of the baselevel profile (a.o. Holmes 1970). Ultimately it governs the position of localities with active deposition and erosion (Figures 4.20, 4.21, 4.22 and 4.23). The cyclicity

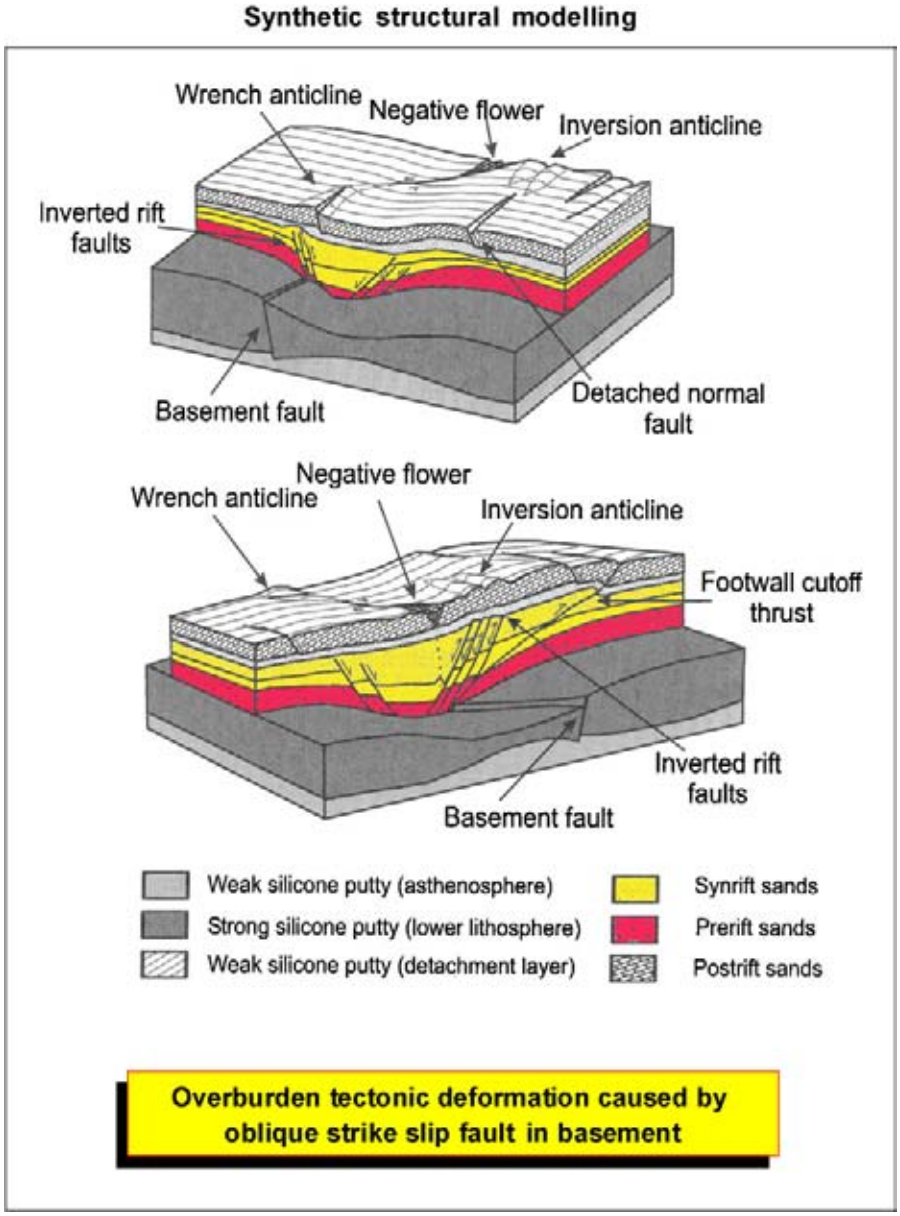

Figure 4.19: Laboratory structural modeling of a basement strike slip fault and the overburden deformation. The detached overburden is affected by normal faults and relay structures over the rift segment transferzones. There is a progression from broad buckling and folding to rift fault reactivation and inversion anticline formation, to the development of footwall cutoff thrust faults, finally followed by cross-trending wrench faults (modified after Gartrell et al. 2004).

of transgression and regression in the geological record is well known and similar cycles are recognised in the behavior of sealevel curves. An estimation of the duration and magnitude of the sealevel fluctuations is needed and for this the amount of coastal onlap aggradation (upbuilding trend) can be used. Vail et al. (1977) demonstrated that the relative change in sealevel can be determined by the different amounts of onlap of coastal deposits. This is directly read off from depth-converted seismic sections. They proposed a worldwide applicable coastal onlap chart (Figure 4.24). Well control gives vital information on the distinction between coastal and shallow marine onlap. Biostratigraphic datings and additional methods, like for instance fission track analysis and paleo-magnetic reversal correlations, provide also constraints on the time involved for the deposition of a package of sediments.

The vertical amount of onlap is determined from the seismic sections and of course compaction effects should be properly discounted for (Figure 4.25). The measuring of the vertical component in coastal onlap is carried

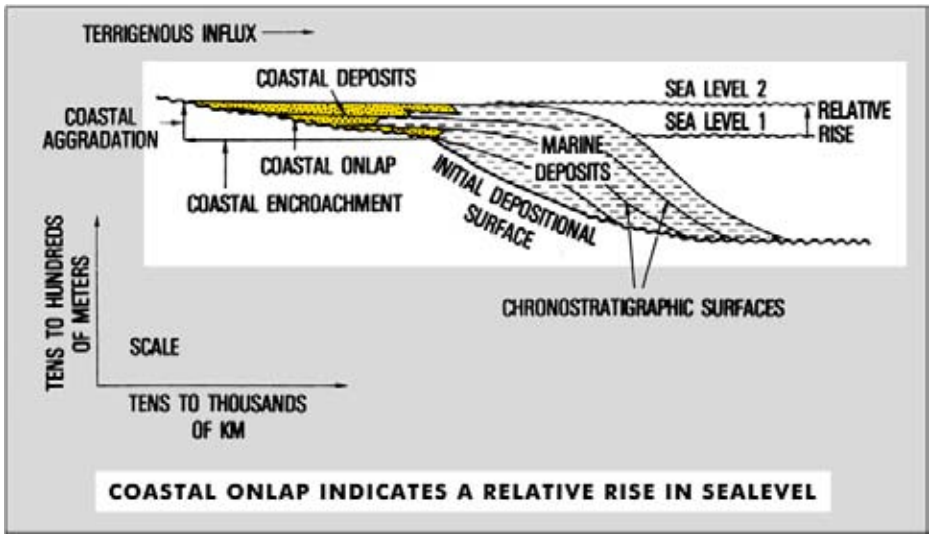

Figure 4.20: Coastal onlap relationship pointing to a relative rise in sealevel and aggradation of topset sediments (after Vail et al. 1977, reprint from AAPG whose permission is required for further use).

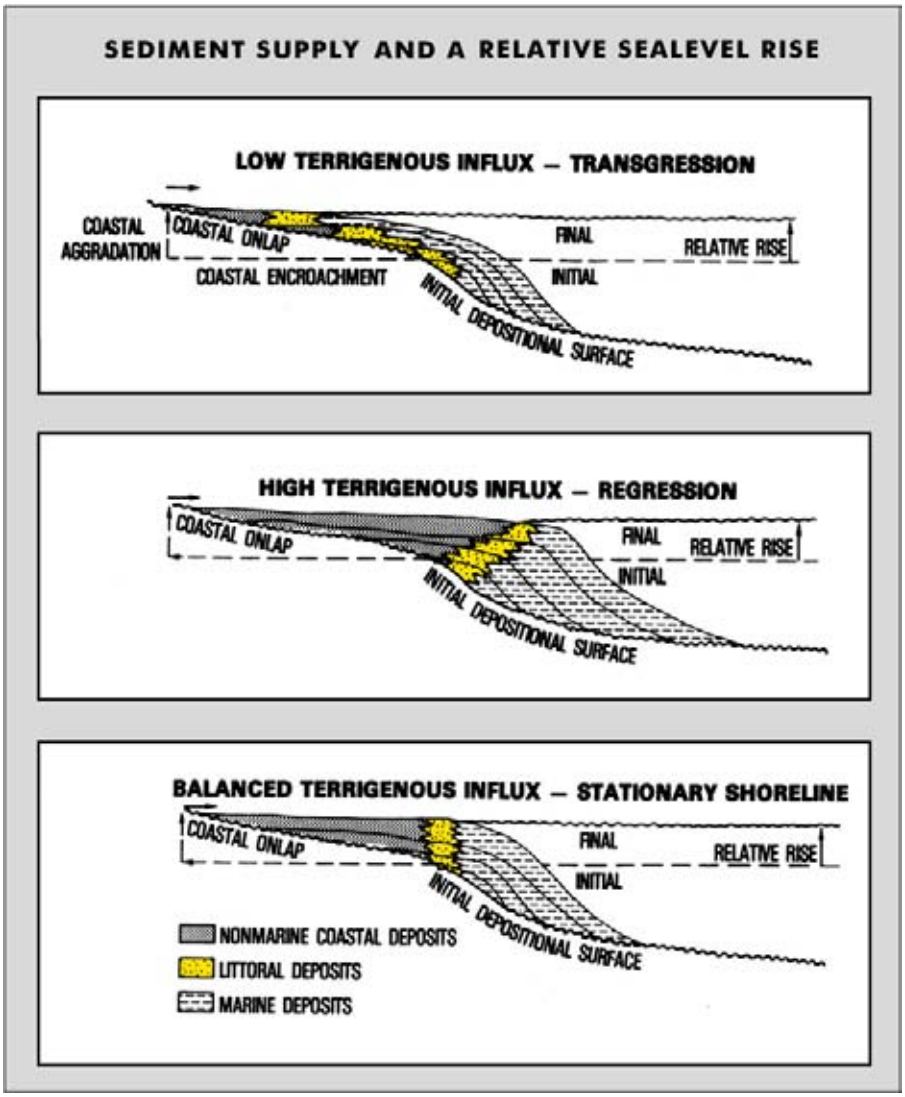

Figure 4.21: Variations in sediment input and their interplay with coastal onlap and the change in relative sealevel position (after Vail et al. 1977, reprint from AAPG whose permission is required for further use).

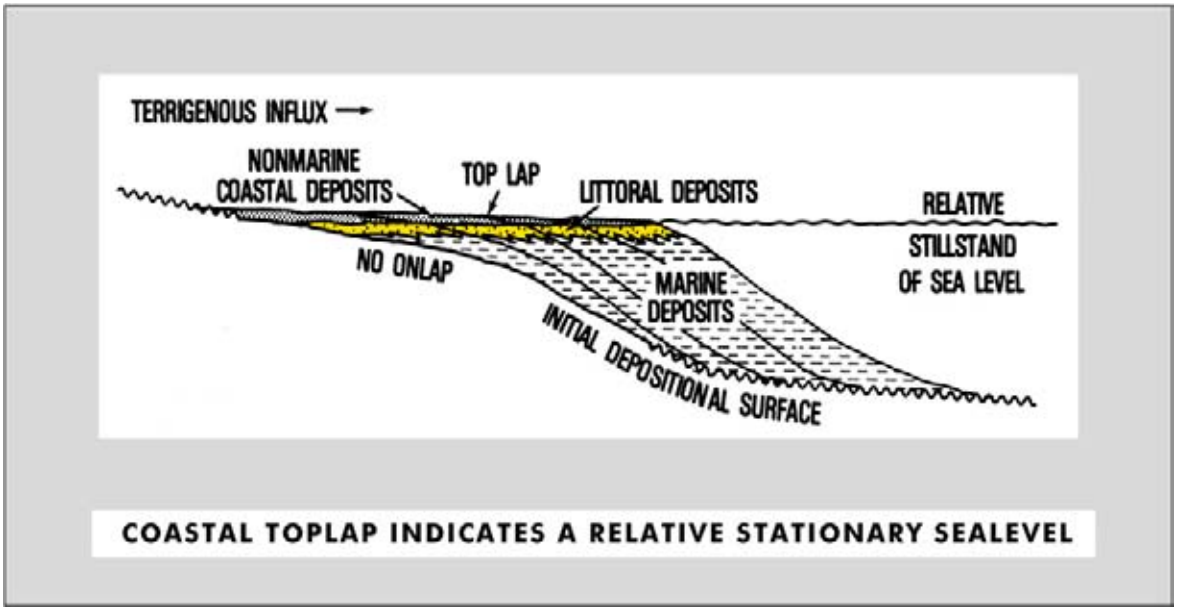

Figure 4.22: Coastal toplap combined with rapid progradation can be considered indicative for a relative stationary sealevel position (after Vail et al. 1977, reprint from AAPG whose permission is required for further use).

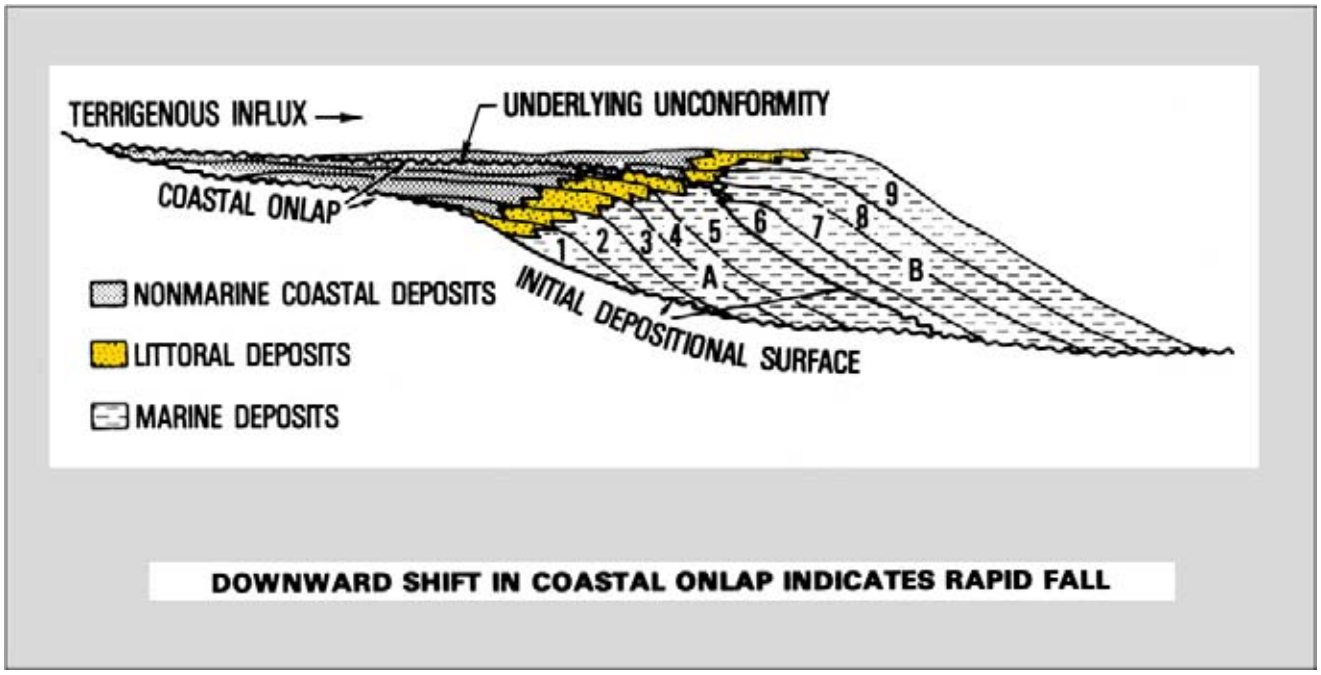

Figure 4.23: Downward shift of the coastal onlap reflecting a fall in relative sealevel (after Vail et al. 1977, reprint from AAPG whose permission is required for further use).

out in a stepwise manner. It is tried to stay as close as possible to the initial starting position of the onlap. This is done to avoid unnecessary errors due to the always observed **differential subsidence** pattern of continental margins. In many situations a landward **hinge zone** exists beyond which no subsidence is observed. For the measurements it is best to be restricted to areas that are little affected by tectonic deformation, so only rather stable sedimentary basins are selected. The time duration of the overlying sequence is determined and an estimate for the timegap between the two packages is obtained.

It is observed that the periods of rise in sealevel are on the overall much larger than the periods of relative sealevel fall. The falls are rather rapid events and the subsequent rise in sealevel is rather gradual and longer in duration. On the Vail curve this is expressed by the extreme short and instantaneous character of the sealevel falls (horizontal breaks in curve). It is however more realistic to assume that these changes are somewhat more gradual and diachronous in time.

Criticism on the curve has been expressed by several authors:

- Imprecision of the age dating methods (Miall 1991).
- Inadequate documentation of the curve construction (Hubbard 1988).
- Local tectonics can vary at the same frequency as the 3rd order variations (Cloetingh 1986, Cloetingh et al. 1989).

Despite the scepticism the Vail curve has been widely accepted as a valuable correlation tool.

4.2.2 Eustatic sealevel changes

Eustatic or global changes in sealevel can be produced by a change in seawater volume and/or the shape of the oceanic basins. Change in volume of seawater depends on climatic factors like glaciation, air circulation patterns and additions of juvenile waters from magmatic sources. If all ice caps would melt instantaneously, a 60 metre difference in sealevel is the expected consequence. The change in shape of the oceanic basin depends on sedimentary infilling and other geotectonic mechanisms (rate of seafloor spreading, shift in geoid shape, lithospheric loading). The rate in seafloor spreading controls the amount of material upwelling along the mid-oceanic ridges and the increase in temperature of the surrounding lithosphere, which will cause uplift. These features are considered the most suitable to produce gradual long term effects (cf Donovan and Jones 1979).

The coastal onlap curve shows first, second and third order cycles. The **first order cycles** are based on structurally important tectonic movements which have a worldwide influence, like plate tectonic re-arrangements and rate of seafloor spreading. For the Upper Cretaceous for instance a sealevel curve was calculated by Hays and Pitman (1973) and Pitman (1978) taking into account the varying rates in seafloor spreading and the volumes of rock contained within the mid-oceanic ridges. **Thermal expansion**, expressed by doming, and later subsidence effects during the cooling phase are important factors. The exponential subsidence on passive continental margins over the last 50 million years is a well known effect related to geodynamic processes and heatflow variation (e.g. Royden et al. 1980). The Pitman curve can be compared to Vail's coastal onlap curve and it is noted that the basic shape is corresponding rather well (Figure 4.24). Discrepancies are attributed to the fact that Vail et al. (1977) measured their sequences in an overall subsiding setting. Therefore a fall in sealevel still can be represented by a rise with a substantial amount of coastal onlap. Moreover, Pitman did not take into account the effects of glaciations. The **second order cycles** are partly related to glaciations, while the **third order cycle** are thought to result from sealevel fluctuations. A link between tectonic subsidence, flexure and global changes in sealevel has been demonstrated by Watts (1982).

As stated already, the sealevel in a marine basin is dependent on several factors:

- Amount of sediment input.
- Rate of deposition.
- Tectonic deformation resulting in uplift/subsidence and tilt.
- Type of sediment source.
- Climatic conditions and hinterland vegetation.
- Thermal expansion.

Moreover, it also depends on the shape of the **geoid**. It is known that the sealevel is not a perfectly smooth surface but it contains certain undulations: highs and lows depending on gravitational distortions caused by anisotropy in the structure of the earth (Figure 4.26). These distortions are not stable, but do migrate in time at variable speeds (Moerner 1976, 1980). A deep-seated origin for these geoid or sealevel anomalies has to be assumed. As these migrations happen relatively fast, it can be appreciated that – in areas with a high gradients – a shift in geoid pattern has a major impact on the local sealevel behavior. Even if the global sealevel remains the same, it is possible that the geoid migration pattern leads to local transgressions and regressions. It is perfectly feasible that the geoid migration creates situations whereby a transgression in a particular basin coincides at the same time with a **forced regression** at an other location. Forced regression means that the regression is induced by a dynamic relative sealevel fall.

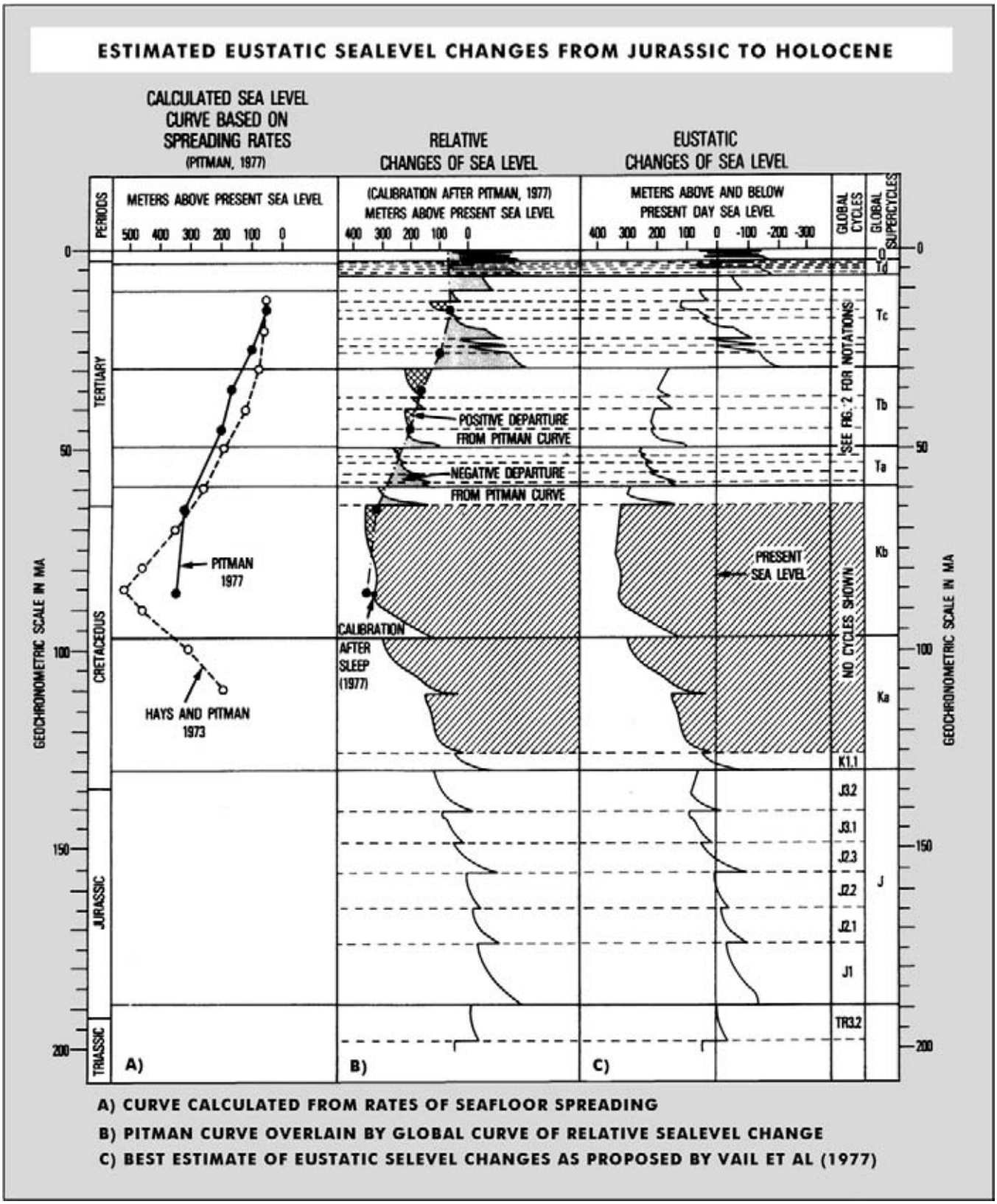

Figure 4.24: Global cycles of relative sealevel change (after Vail et al. 1977, reprint from AAPG whose permission is required for further use).

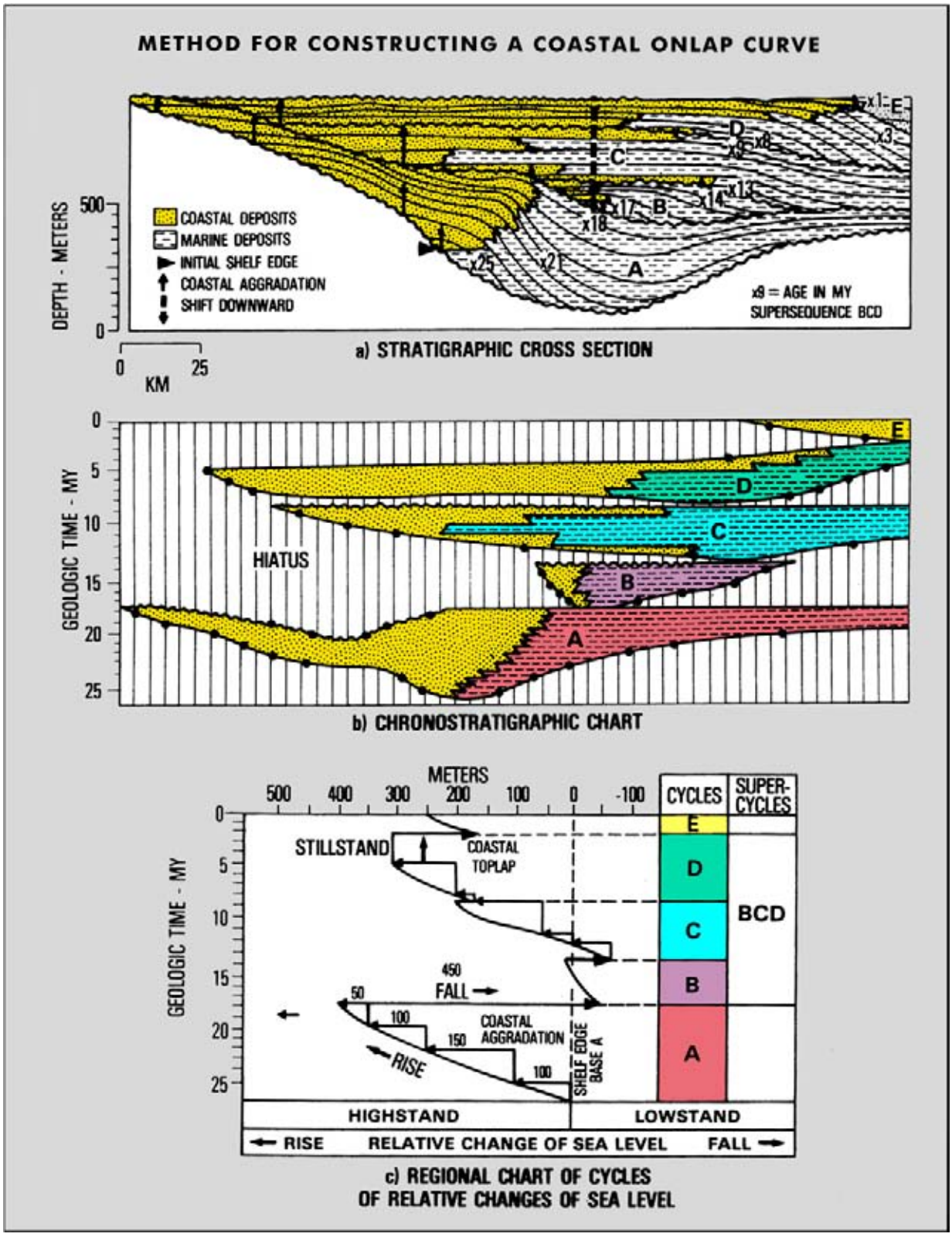

Figure 4.25: Procedure for constructing a coastal onlap curve. The aggradation is measured in a stepwise manner in order to stay close to the point of coastal onlap. (Modified after Vail et al. 1977, reprint from AAPG whose permission is required for further use).

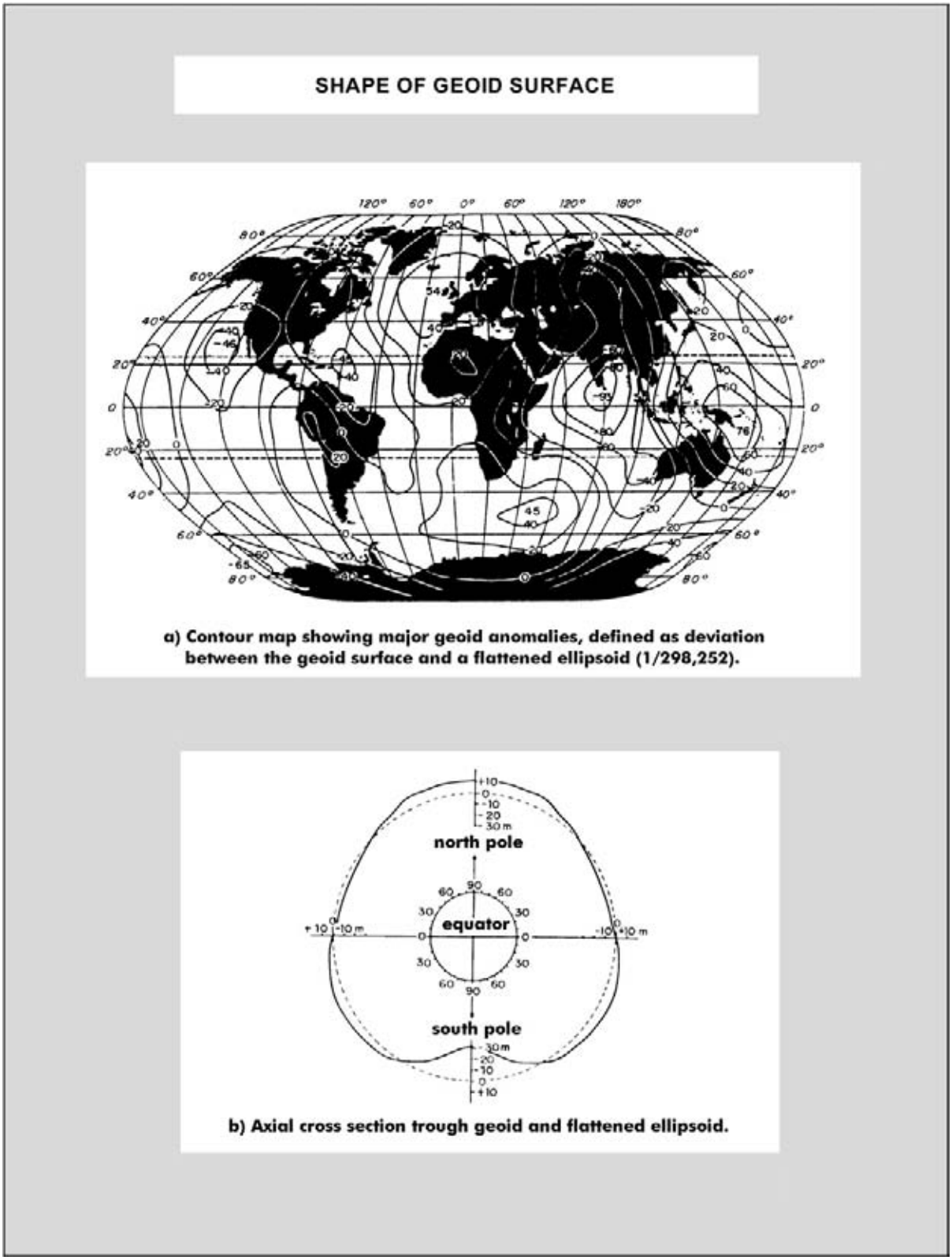

Figure 4.26: Global distribution map of variations in the shape of the geoid. The geoid is the precise description of the earth equiporation surface. It is not circular, but in fact resembles a giant apple with flattening at the poles as is shown in the lower figure. The position of the geoid undulations (deviation from the flattened ellipsoid) is not stationary and it varies with time. Consequently it is perfectly feasible that a sealevel fall in a particular basin on the globe is contemporaneous with a sealevel rise in an other basin. Therefore care should be taken in the interpretation of eustatic (or worldwide) sealevel changes extracted from the geologic record (modified after Pomerol and Renard 1989).

Considering the above, it is difficult and tricky to separate the individual contributions of the various influencing factors by only analyzing the currently found geometries on seismic data. The same thing goes for the geometries observed in the field (e.g. Booler and Tucker 2001). Vail used input from all over the globe (Vail et al. 1977, Vail and Todd 1981) in order to cancel out local tectonics, but of course plate tectonic re-arrangements have their influence on a worldwide scale and are contained within the Vail curve. Miall (1992) has modeled a **synthetic onlap curve** with a random number generator and compared this result with the onlap curves from different basins. He analysed the correlation and detected some regularity in the known non-systematic input data. It shows that one should be very careful to infer trends from random data. An other classic example of erroneous interpretation of data is the processing of random seismic noise, that actually may result in consistent reflections, which are completely artificial (e.g. migration operator; Yilmaz 2001). The relative sealevel curve can be split into several contributions: a linear subsidence and tectonic trend, a low frequency cyclicity part and a high frequency part (Durand 1996). Subsequently the causes of the various cyclicities can be investigated.

After heavy criticism from various colleagues Vail decided to rename the seismically derived global relative sealevel curve as a **coastal onlap curve** in order to avoid unnecessary confusion (Figure 4.27; Haq et al. 1988). Accuracy of the curve is very much dependent on the resolution of the biostratigraphic analysis and correct determination of the depositional environments. Global tectonic events are hidden in the curve as plate tectonic adjustments occur worldwide, and on the other hand important local ones are disregarded.

It is noticed that the steady migration of the geoid shape in time has not been accounted for in the Vail curve. The eustatic sealevel curve presented by Haq (1993) is much more satisfactory, because the sealevel falls are not assumed to occur instantaneously. This sealevel curve is considered more appropriate as a working hypothesis; but obviously it should be handled with care. Overinterpretation of data should be avoided: a good distinction between observations and interpretation in reporting can help to circumvent some of the negative aspects of working with a rigid model.

4.2.3 Influence of regional tectonics

Regional tectonic events can have a dramatic effect on the sedimentation pattern in individual basins. Combined with climatic conditions they may play a substantial role in determining the character of the basin infill (cf Postma et al. 1993). The **Messinian salinity crisis** in the Mediterranean serves here as an illustration. The event caused a drop of several hundred meters below the world wide sealevel in the southern Cyprus Basin (Rouchy et al. 2001). The subsurface of the recent Mediterranean Sea contains several sub-basins, each with its own tectonic and depositional history (e.g. southern Spain pull-apart basins, Veeken 1983; offshore Nile delta, Marten et al. 2004; Algerian offshore, Cope 2003, Kheidri et al. 2005). Local tectonics and plate adjustments have contributed to these differences (cf Geel et al. 1992).

Messinian evaporites were deposited in the centre of some of these basins, while the margins were exposed to erosion (Sorbas Basin, Figure 4.28). In the South Alboran Basin, offshore Morocco and Algeria, the Upper Miocene salt deposits are lacking (Kheidri et al. 2005) and therefore the question is raised whether non-deposition or later erosion is responsible for the patchy distribution of the Messinian salt. A complete drying out of the Mediterranean basin has been suggested by several authors (Figure 4.29). In the Pulpi-Vera Basin (onshore SE Spain) part of the geologic succession has been removed (hiatus) along the basin margin before the Early Pliocene marine sedimentation sets in (Figure 4.30). The erosion is not always easy to demonstrate in the field, but the Asperilla section constitutes in this respect a clear example (Veeken 1983). The sediments just below the Mio-Pliocene unconformity are truncated and eroded. Most probably they were subaerially exposed. The latter is suggested by the presence of Chara microfossils in the top of the Messinian Abad Formation in the adjacent Vera Basin (Geerlings, pers. com.). The subaerial exposure at the basin margin does not necessarily indicate the complete drying out of the whole Mediterranean Sea. An unconformity can have its correlatable conformable time equivalent in the deeper part of a basin. The thick Miocene gypsum layer (100 meters), exposed in the Sorbas Basin (onshore SE Spain) has been deposited in quiet water conditions, evidenced by the presence of gigantic (metre scale) individual gypsum crystals. A complex depositional model is envisaged whereby hot climatic conditions favored evaporation at the water surface and creation of high salinity brines (cf deep water isolated basin with larger water depth, Pomerol et al. 2005). These brines were transported by high density currents towards deeper parts of the basin (Figure 4.31). This sedimentation mechanism also explains the rhythmic alternation between shale and redeposited gypsum crystals in sub-aquatic high density flows as seen in the Sorbas Basin. The open seaway between Africa and Europa at the Strait of Gibraltar was probably closed at that time. An important reduction of the water volume in the Mediterranean by evaporation at the end of the Miocene is evident

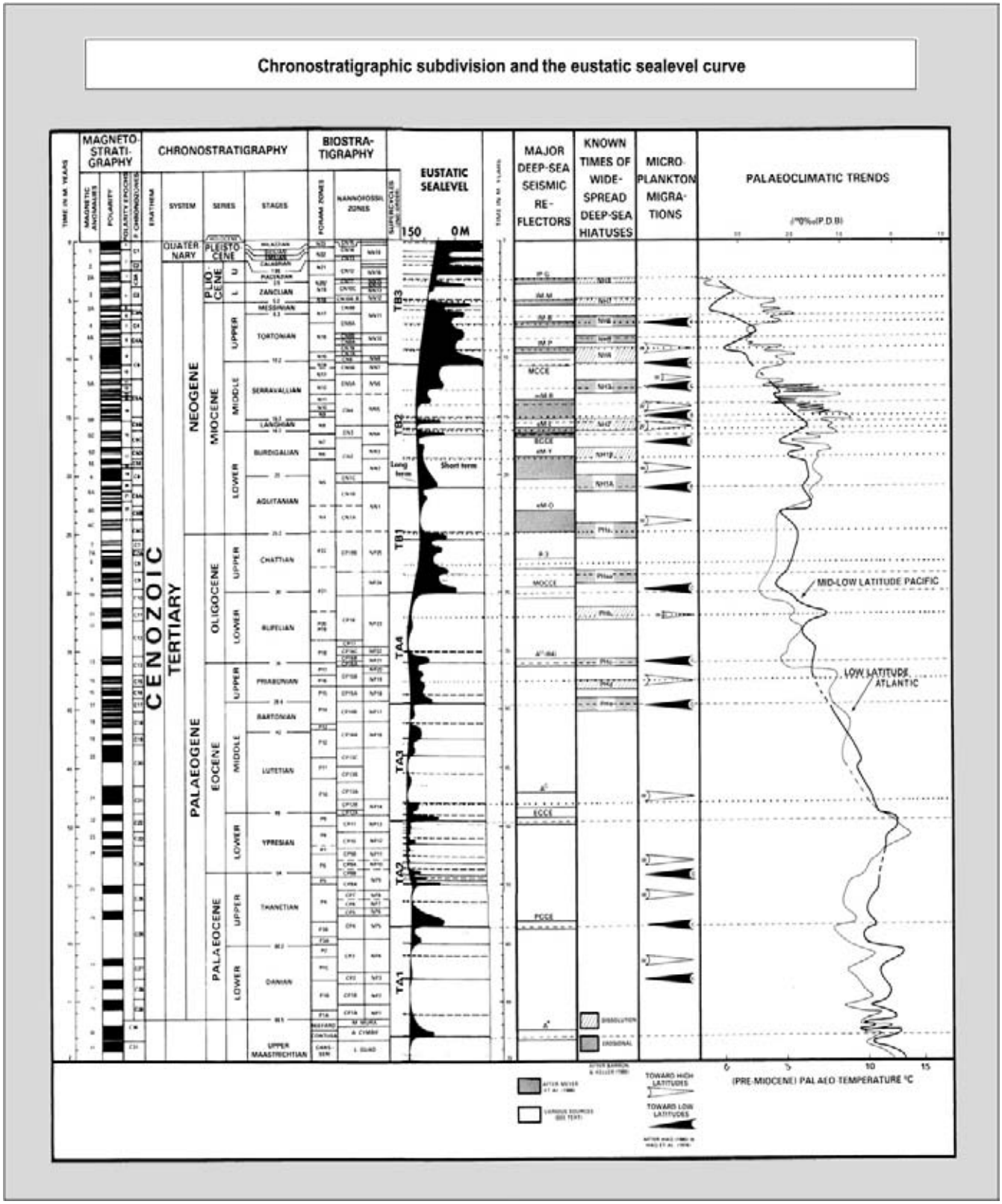

Figure 4.27: Eustatic sealevel chart as presented by Haq (1993). The sealevel drops are less instantaneous and occur over somewhat larger time periods, which seems more realistic than those shown on the 'Vail curve'. Criticism involves imprecision of age datings, inadequate documentation of the construction method (confidentiality reasons?) and degree of influence of local tectonics.

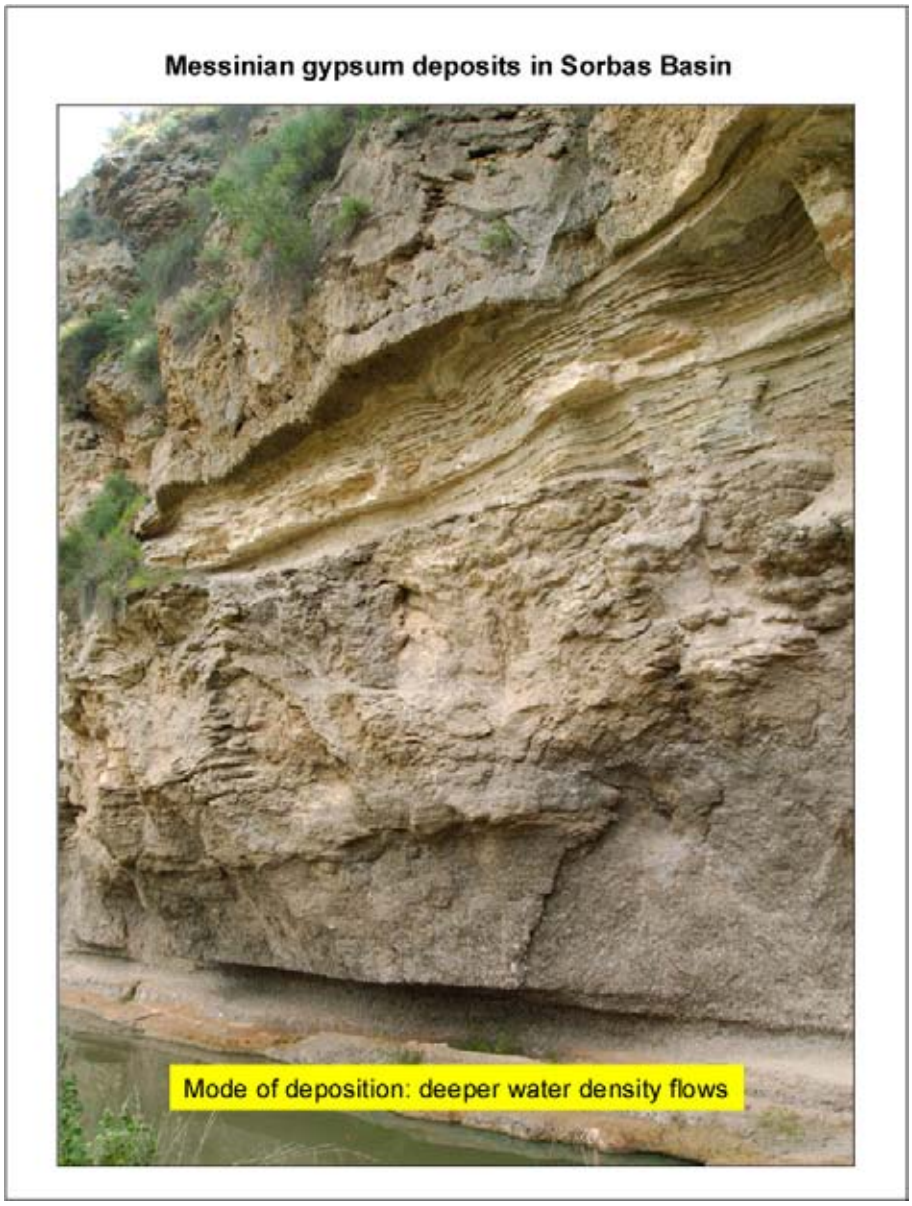

Figure 4.28: Messinian gypsum deposits exposed in the Sorbas Basin (SE Spain). The deposits are transported and probably deposited by high density flows under subaquatic conditions. Contemporaneous carbonate reefs indicate that the basin was not completely dried out in Messinian times and substantial salinity differences existed in the marine basin.

(cf Fortuin et al. 1995). The high rate of evaporation helped to increase the salinity of isolated sub-basins to extreme high levels. Density water layering and stagnation of the water circulation are very probable in such basins.

It illustrates the dramatic influence of sedimentological changes that have occurred in geologic history. Especially the spectacular Early Pliocene waterfall, that must have existed across the Strait of Gibraltar when the eustatic sealevel rose above the Early Pliocene land bridge between Africa and Europe, stimulates the imagination. Major unconformities and various depositional sequences are seen on seismic data from this part of the Alboran Sea and witness a high energy infill. Miocene salt tectonics in the Algerian and Egyptian offshore increase the prospectivity of these areas for important hydrocarbon accumulations (Cope 2003, Marten et al. 2004, Kheidri et al. 2005).

Lately the existence of hyper saline bottom layers in some recent deep basins have been documented (e.g.

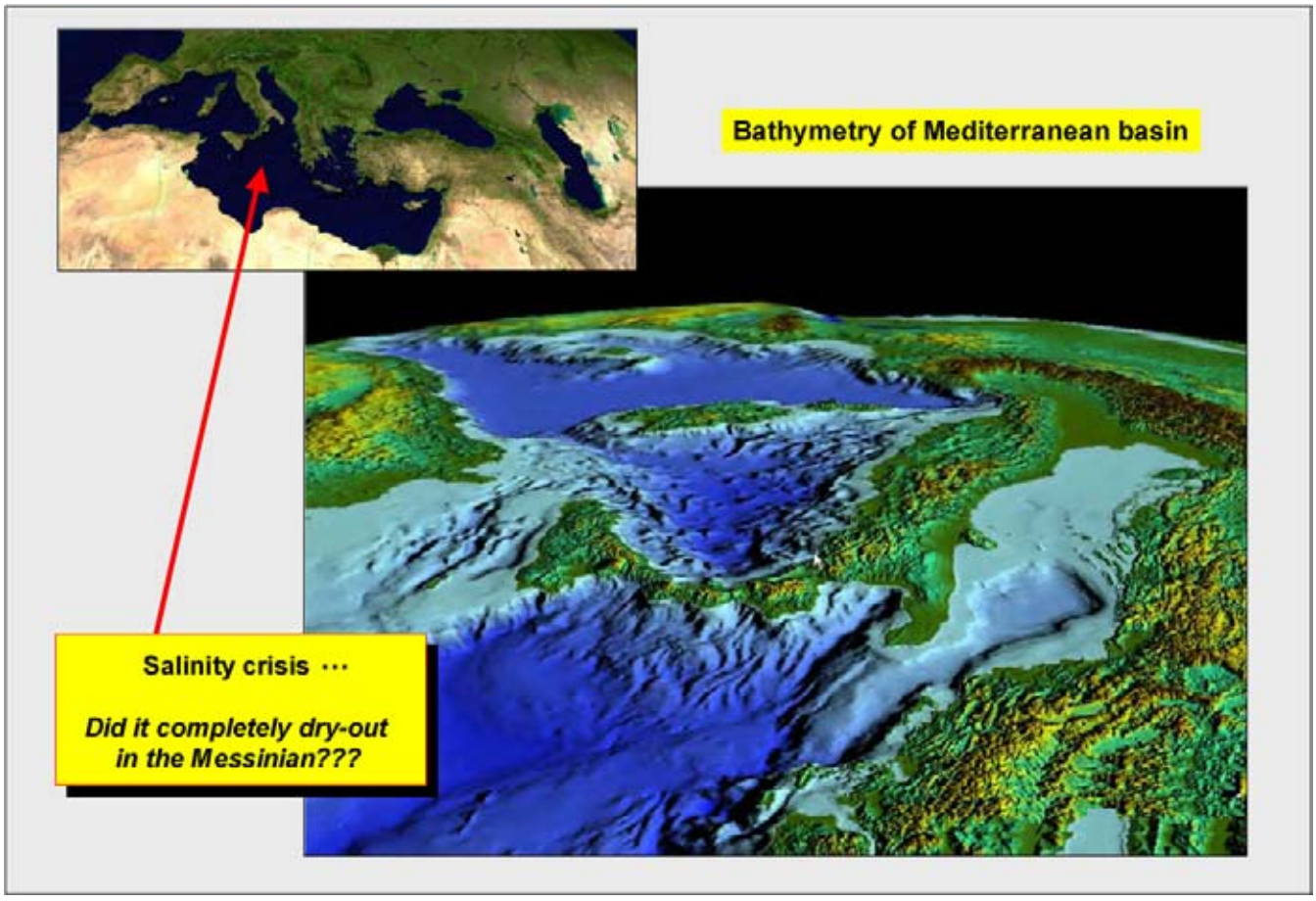

Figure 4.29: The bathymetry of the Mediterranean basin is here shown. In several sub-basins there are indications for a Messinian salinity crisis at the end of the Miocene (photo courtesy Geofusion). Massive evaporite deposits express the termination of the Miocene sedimentation in the Sorbas Basin (southeastern Spain). The subsequent refilling of the Mediterranean in the Early Pliocene is often thought accompanied by the existence of a spectacular waterfall across the Strait of Gibraltar. Giant salt crystals, deposited under quiet water conditions, in the same Sorbas Basin indicate that a partial drying-out of the Mediterranean is a more plausible scenario. High density flows from the shallow edges of the basin gave rise to the hyper-saline water in the centre of the sub-basin. Contemporaneous reefs point to a deeper water setting for a part of the evaporite sequence. Erosion along the shallower margins of the Miocene Mediterranean basin has been documented elsewhere, e.g. in the Neogene pull-apart Pulpi Basin (Veeken 1983).

Discovery trench west of Crete, Pomerol et al. 2005). Special biological communities exploit the interface of the dense and less dense layer above. Deep sea dives with submarine vessels have proven the existence of extensive 'mussel and tubular annelids' banks at this level, that are well shielded off from all sunlight. This new evolutionary niche is called 'cold seeps'. This sensational new discovery is an analogue to the hydrothermal hotspot in the oceanic ridges, where biologic activity has been described in sulfurous water of 80 degree Celsius. Extremely adapted lifeforms have recently even been discovered in these hydrothermal waters with a temperature of over 200 degree celsius and a pressure of 200 atmosphere (Pomerol et al. 2005). The revolutionary energy management of these organisms is based on sulfur and methane conversion. In stead of relying on conventional photo synthesis the energy management depends on a chemnosynthetic process:

$$6O_2 + 24H_2S + 6CO_2 \rightarrow C_6H_{12}O_6 + 24S + 18H_2O$$

(chemnosynthesis),

$$6O_2 + 6H_2O \rightarrow C_6H_{12}O_6 + 6H_2O$$ (photo synthesis).

Lowering of sealevel and plate tectonic adjustments have also astounding effects on the distribution of recent life forms. The Banda Sea area (offshore Indonesia) serves as an example (see Figures 4.15–4.18). It is a region with a rather complex plate tectonic history (Burhanuddin 1994). One theory postulates that various plate slivers collided with each other 15 million years ago and now form part of the Sulewesi island. These slivers stem from different continental blocks: Asia in the northwest and Australia in the southeast. Evidence for

Figure 4.30: The broad outline of the Neogene/Quaternary Vera and Pulpi Basin in the Betic Cordilleras (SE Spain). The display has a five times vertical exaggeration. The rio Almanzora follows a zone of weakness, where the basinfill to the north is somewhat downwarped. The Sorbas Basin is in the background is uplifted in respect to the Vera Basin. Strike slip played an important role in creating the Neogene basins in southern Spain. The Palomares/Aguilon faultzone is characterised by strike slip with a sinistral movement (righthand block moves away from observer). It offsets the Sierra Cabrera and the Sierra de Almagrera with an important deformation phase in the Plio-Pleistocene (data courtesy NASA).

these dramatic events is also provided by the distribution of life forms on the Indonesian islands; in particular the bio-diversity of the Sulawesian fauna is rather unique.

The co-existence of the straight-horned Anoa water-buffalo (Asian plate) and the marsupial Cuscus (*Ailurops ursinus*; Australian plate) on Sulawesi is intriguing and needs a complex explanation. The Cuscus is more primitive than the species currently found on Papua New Guinea. A man-supported transport mode seems highly unlikely, even moreso as evolutionary steps are supposedly rather slow and very gradual in time. The Cuscus live in dense forest and are very little migratory. They are related to the Australian Koala bears. Hence, long swimming escapades of several days or weeks to cross a deep ocean are not very probable. Furthermore, the occurrence of a special type of fresh water fish, well known from Papua New Guinea (Irian Jaya), now found in a lake on Sulawesi has left scientists with yet an other intriguing problem. Only drastic plate tectonic movements seem compatible with all these observations (creation of a landridge or drifting).

The endemic Anoa water-buffalo on Sulawesi represents an other unique local adaptation (1 metre high). Introduction on the island by mankind in sub-recent times is excluded as the species is only found on Sulawesi. It can be seen as a genuine local evolutionary adaptation. Furthermore, the world smallest primate is found on Sulawesi, a squirrel-like monkey called Tarsius Spectrum (20 cm) that is only active at night. Its presence underlines the isolated position of the island in time. Moreover, the occurrences of the Babirousa wild pig and the black Macaque monkey are remarkable. These animals are all stemming from the Asian plate.

Wallace (1876) noted already the striking differences in the faunas on the various Indonesian islands. He

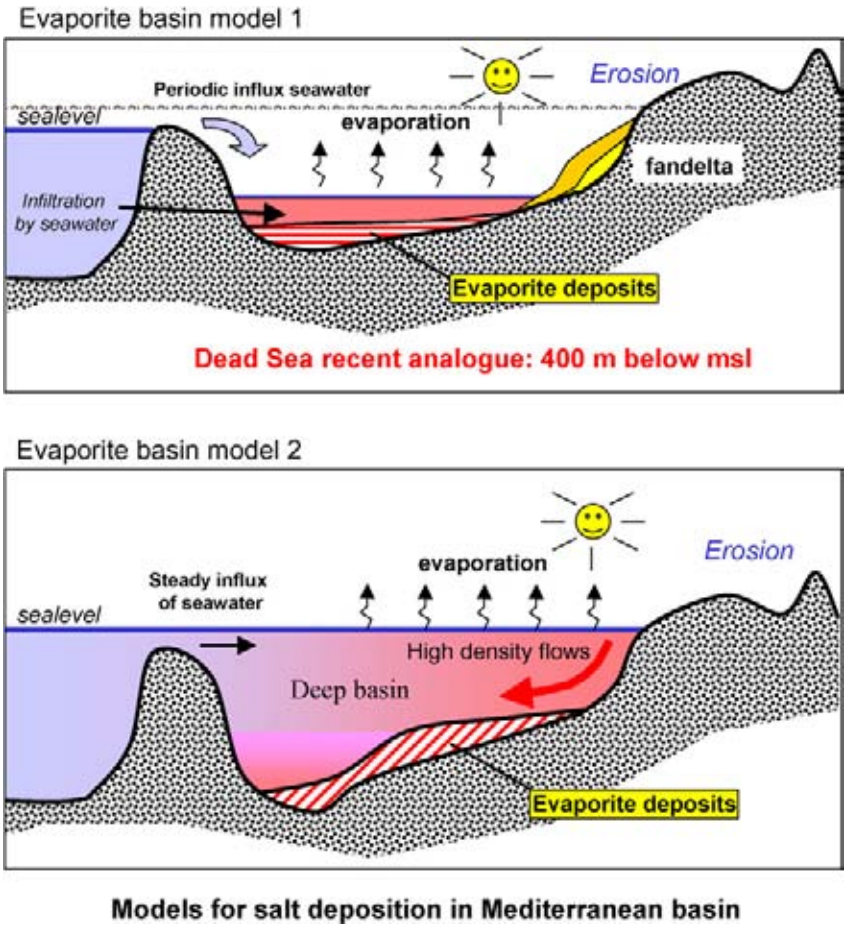

Figure 4.31: Two models for evaporite basins. The first model is a shallow water basin in analogue to the Dead Sea. Typical is the absence of carbonate reef development, while the steep flanks provide a good sediment source for clastic fan deltas. In the second deep-water model the evaporite deposits are transported by density currents into a deeper water environment. Contemporaneous carbonate deposition is possible in the shallower part of the basin. The high rate of surface evaporation creates high density brines that are transported downslope to the deeper part of the basin. The deep water geometry also favors the establishment of a density layering, with stagnant conditions in the deeper basin centre.

studied the distribution of bird families, like parrots. He easily recognised two different groups: an Austro-New Guinea and an Asian population. The SSW–NNE divide line or **Wallace line** runs between Bali and Lombok, across Sulewesi and south of the Philippines (Mindanao). Wallace was the co-inventor of the '*natural selection and survival of the fittest*' evolutionary principle as defined by C. Darwin. Recent English commented reprints of the work of Darwin are Darwin and Cannon (1983) and Darwin and Burrow (1984).

During the Pleistocene eustatic sealevel lowstand there was a land connection between the Australian main land and New Guinea. As a side line: the name Pleistocene means 'Most recent' and was introduced by Lyell in his Principles of Geology in 1833. He also coined the names for other time units: the Pliocene 'Very recent', Miocene 'Moderately recent' and Eocene (dawn of recent; Bryson 2003, Kummel 1970, Pomerol et al. 2005). It was based on the amount of statistical resemblance of mollusks with the recent living forms. The Oligocene epoch (slightly recent) was inserted by the German Beyrich in 1854 (Encyclopedia Britannica 2000). Between Sulawesi and New Guinea there already existed a deep ocean, in the Pleistocene. Hence, the Cuscus must have arrived in Sulawesi well before that time. The docking of an Australian block, with its typical fauna from Papua New Guinea, drifting to the west is supposed to have happened some 15 million years ago. A time period of 18 million years is envisaged for the drifting process across the approximately 900 km forming the initial separation (5 cm/year). The start of the drifting process therefore took place 33 million years ago. That leaves a considerable time period for the evolutionary process to take its effect. An other hypothesis is the existence of extensive land ridges connecting Sula, Buru, Ambon and subsequently strike slip and pop-up structures favour the appearance and disappearance of elongated landmasses leading to New Guinea, making island hopping possible. The isolated character of the bio-diversity on the Sulewesi suggest however that the drifting hypothesis is the most plausible. Biologically speaking the crossing the Wallace Line in the Indonesian archipelago is like traversing from one world into an other. The example underlines the significance of regional tectonics when unraveling the complexity of the geologic evolution of the earth crust.

4.3 The Link with Sequence Stratigraphy

The fill of sedimentary basins is subdivided using seismostratigraphic and high resolution sequence stratigraphic techniques. The ultimate goal is to unravel its internal architecture and deduce the depositional history. A robust subdivision scheme is needed for this purpose, in order to avoid incompatibilities between various geological interpretation techniques. The scale change between the techniques is important (cf Durand 1996). It is illustrated in Figure 4.32, where the outcrop geological stratigraphic column is compared with the size of individual seismic loops.

Sequence stratigraphy is defined as:

> *the study of rock relationships within a chronostratigraphic frame of repetitive genetically related strata, bounded by surfaces of erosion or non-deposition or their correlative conformities* (Van Wagoner et al. 1988).

The basin fill is first subdivided into depositional sequences by the delineation of maximum flooding surfaces, unconformities and their correlatable time-equivalent surfaces (Figure 4.33). In case seismic data is available, than these unconformities should be identified by reflection termination mapping. The unconformities mostly correspond to **first order** (>50 Ma) and **second order** (3–50 Ma) sedimentary **cycles** related to tectono-eustatic processes (Cramez et al. 1993). In some cases also **third order** (0.5–3 Ma) cycles are represented by regional unconformities. The depositional sequences are further subdivided into system tracts based on the presence of genetically related units and local unconformities with their correlative conformities.

The notion, that most of these stratigraphic units are correlated to a specific behavior of the relative sealevel is somehow crucial in sequence stratigraphy (e.g. Posamentier and James 1993). But it also brings in an interpretative element in the description of the subsurface rock succession.

Eustacy is often described as the difference in sealevel measured in respect to a fixed point, for example the centre of the earth. Relative sealevel is a function of the sealevel change in addition to the movement of the seafloor (Posamentier et al. 1988). The latter depends on:

- Tectonics.
- Thermal cooling.
- Lithospheric loading by water and/or sediments.
- Compaction effects due to burial.

The position of the relative sealevel basically controls the accommodation space available for sediment accumulation. Recognition of accommodation cycles helps to subdivide the stratigraphic record. The breakdown in the wells and/or outcrops is correlated over a larger area (Figures 4.34 and 4.35). A fundamental relation between system tracts and relative sealevel behavior is given in Figure 4.36 (Steckler et al. 1993). The **transgressive system tract** is composed of retro-gradational coastal deposits with a clearly retreating shoreline. The **highstand and early fall system tract** correspond to aggradational geometries, while the **lowstand and early rise system tract** are characterised by a progradational sedimentation pattern (Figure 4.37). The highstand is usually assumed to be represented by a widespread shale package, that confirms the blocking of the sedimentary transport system. It is evidence for the fact that no coarser grained material reaches the shelf area. A **maximum flooding surface** (MFS) is located somewhere within these shales.

The systems tracts are related to the behavior of relative sealevel in a basin. A basic fourfold division has been often suggested: lowstand, falling sealevel, rising sealevel and highstand. But in many cases a clear distinction can not be made between lowstand and falling sealevel from a practical point of view (e.g. Ainsworth 2005). The ideal depositional package for one Depositional Sequence would therefore contain lowstand, transgressive, and highstand system tracts formed in response to various stages of the sealevel cycle (Weimer and Slatt 2004).

The cyclic depositional pattern within these system tracts is exploited by the sequence stratigraphic techniques, whereby individual transgressive and regressive packages are outlined (para-sequence). These units are regarded as third to **sixth order** cycles (0.001–3 Ma). The **fourth order** is 100 000 years and **fifth order** about 20 000 to 40 000 years according to Weimer and Slatt (2004). Such detailed subdivision is achieved by tracing several additional surfaces in the genetically related units like:

- Onset of baselevel fall, the maximum flooding stage determining the start of a seaward movement of the shoreline.
- Maximum outbuilding of the shoreline accompanying the initiation or renewal of the landward movement of the shoreline.
- Onset of a baselevel fall which will lead to the subsequent erosion of the earlier deposited underlying strata in the more proximal areas.

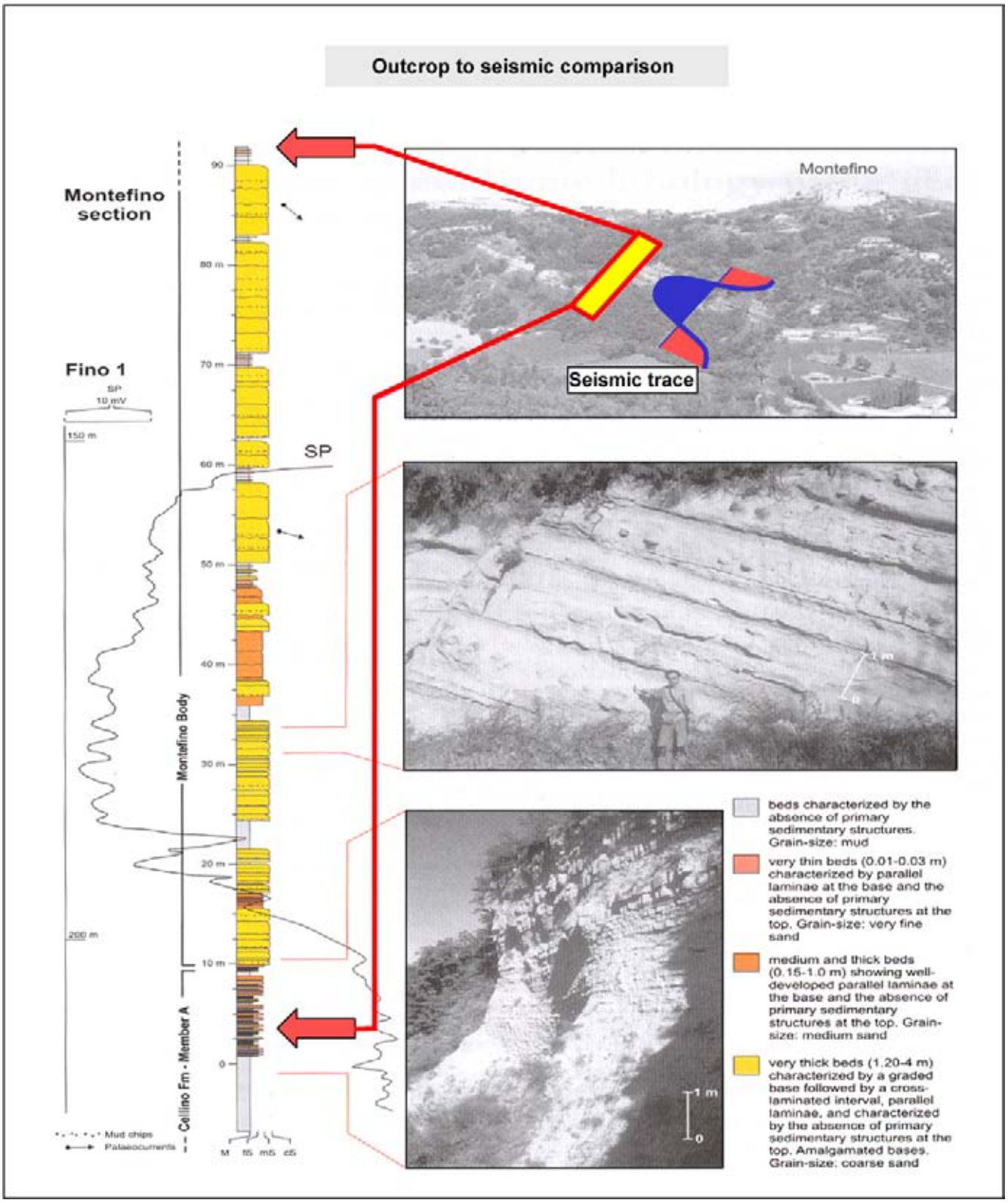

Figure 4.32: The geological column in the field is compared to the size of the seismic loops to illustrate the change in observation scale for the two methods. High frequency lithological changes are lost in the seismic recordings. The sequence stratigraphy and seismic stratigraphy are complementary study techniques. The seismic observations serve as a low frequency correlation frame in basin analysis (modified after Carruba et al. 2004).

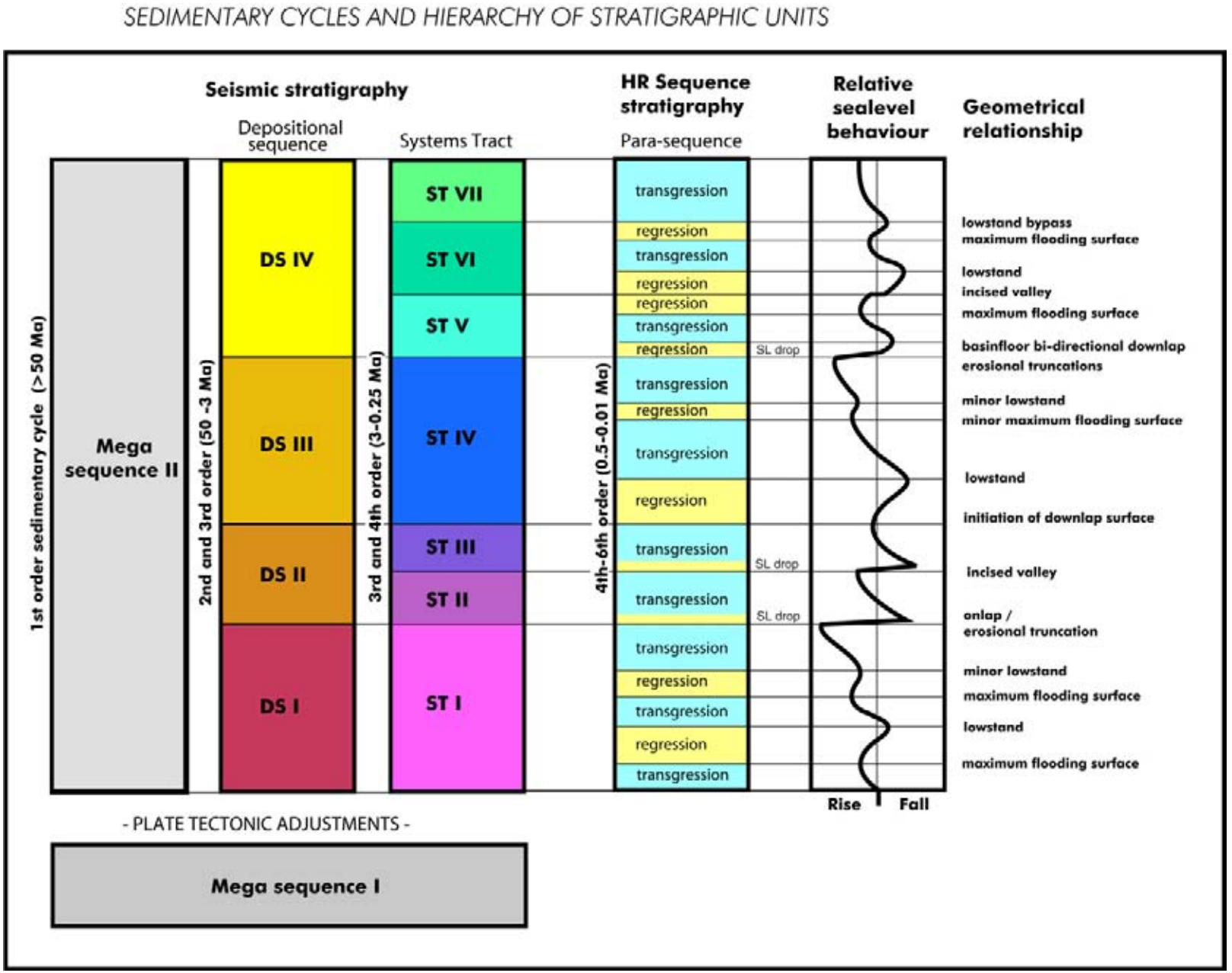

Figure 4.33: Hierarchy of elementary genetic units in sequence stratigraphic and its link to the seismic stratigraphic observation scale.

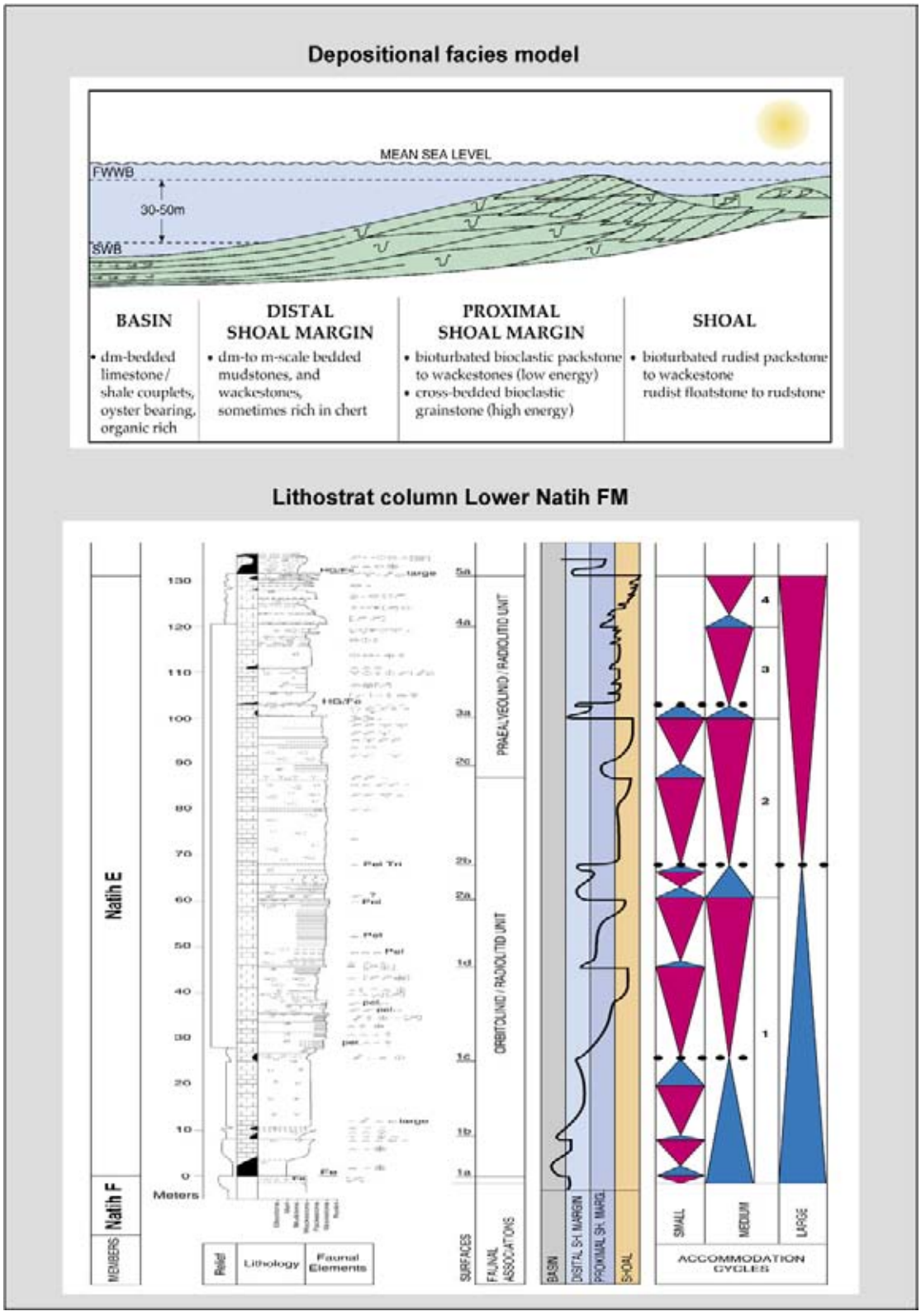

Figure 4.34: The recognition of accommodation cycles helps in subdividing the stratigraphic succession. The vertically stacked sediments cross the facies belts as shown in the depositional model with their typical lithologic characteristics (modified after Van Buchum et al. 1996).

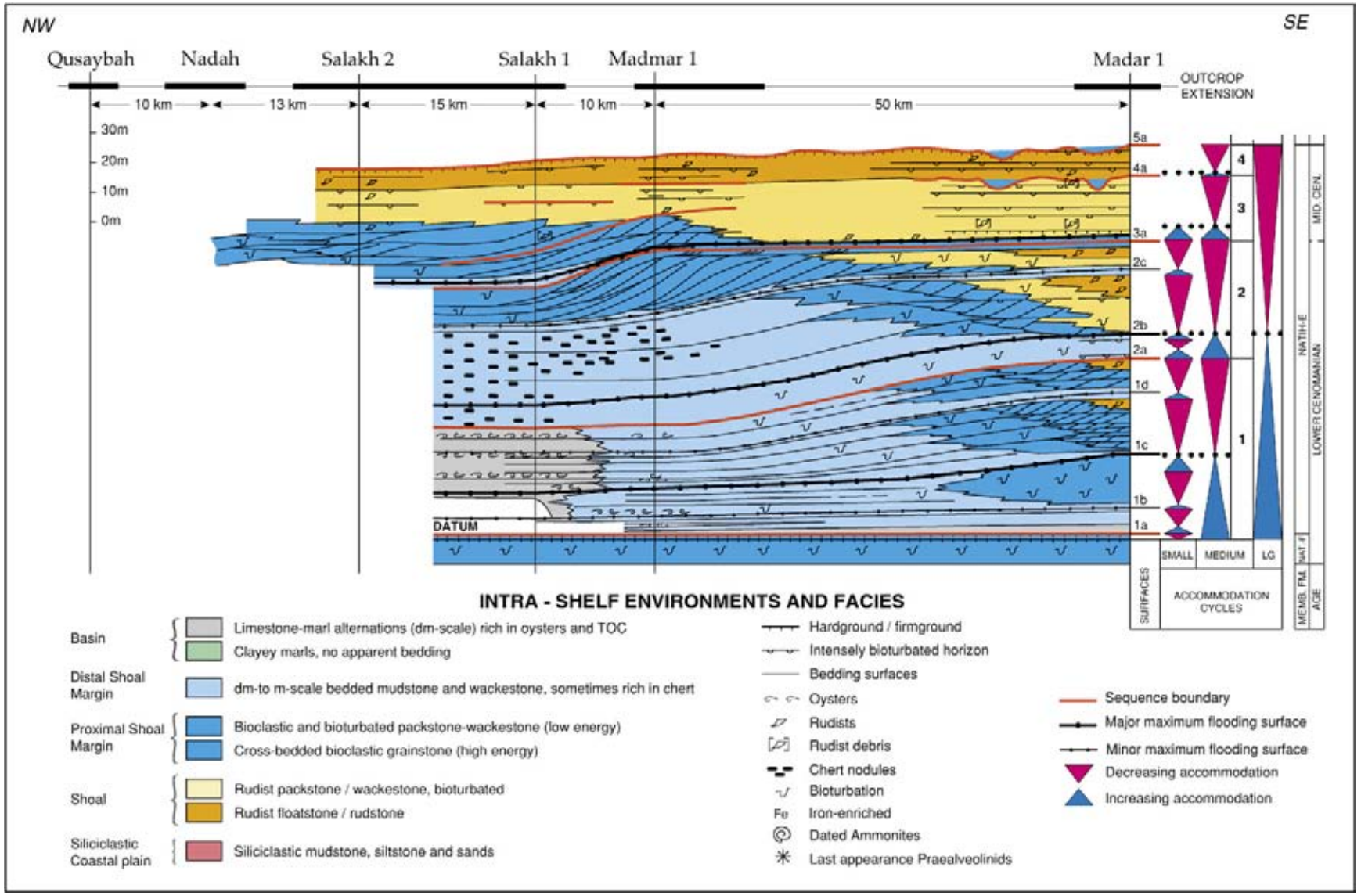

Figure 4.35: High resolution sequence stratigraphic subdivision of the Natih Formation in Oman. The sequence boundaries are based on seismic and lithological breaks in wells. The maximum flooding surfaces correspond with regional shale drapes. The large scale foresetting is essential to correlate the lithogical units correctly in time (modified after Van Buchem et al. 1996).

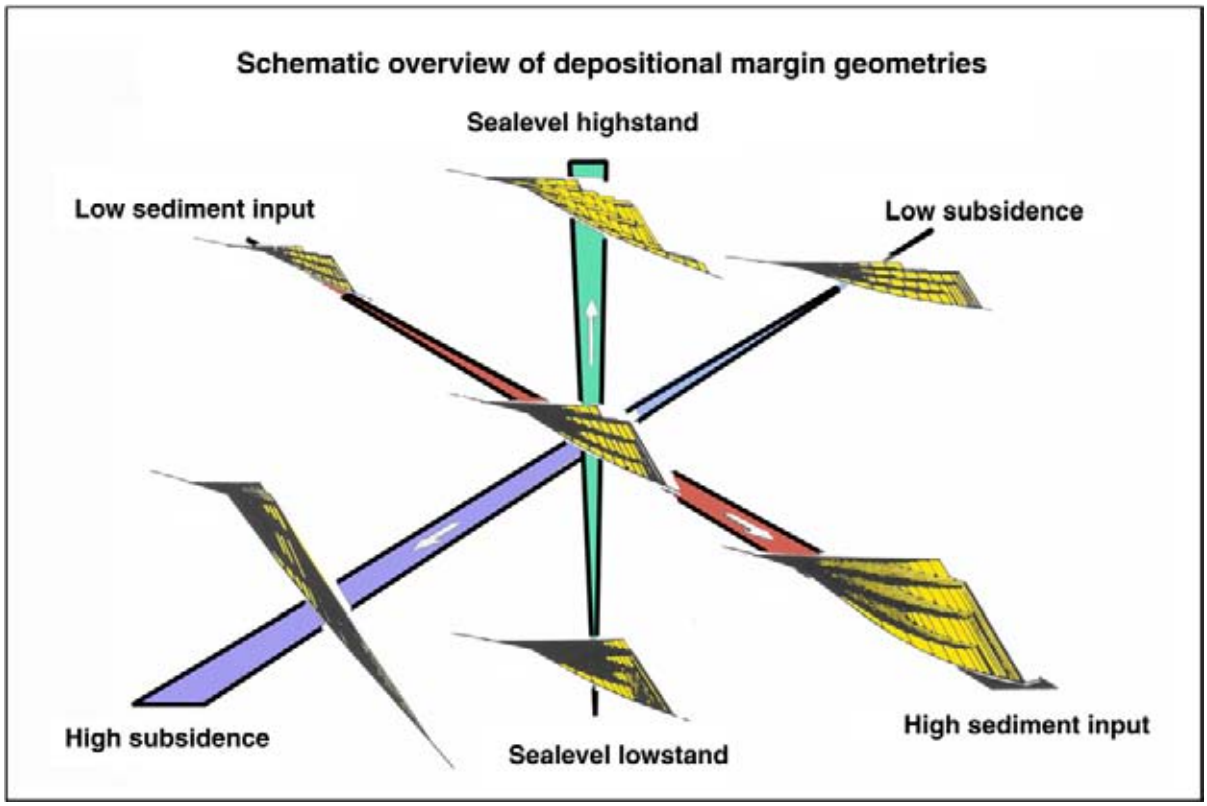

Figure 4.36: Fundamental relation between subsidence, sediment supply, sealevel changes and their influence on continental margin geometries (modified after Steckler et al. 1993).

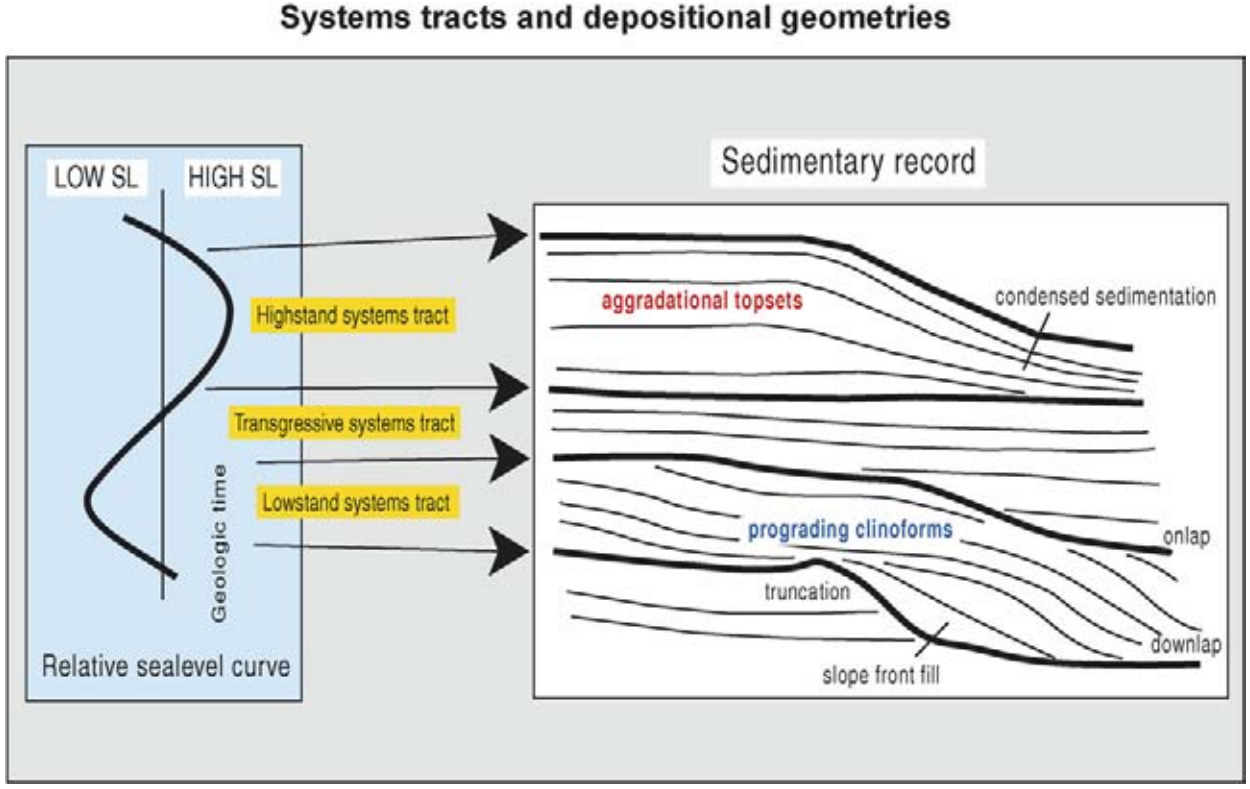

Figure 4.37: System tracts and large scale seismic reflection geometries. The relation with the relative sealevel changes is here shown.

Unambiguous identification of these surfaces is crucial to obtain reliable and meaningful correlation within a basin fill. Even in deepsea turbiditic carbonates it is possible to recognize various sedimentary cycles and place them in an overall hierarchy (Guillocheau et al. 2004, Figure 4.38). On small outcrops it is sometimes difficult to establish events, that are of basinwide significance. Moreover, there are some depositional environments where the autocyclic lateral change in facies and the albrupt breaks in lithology are difficult to distinguish from the real regionally induced ones (e.g. in a dynamically changing deltaic environment). Other surfaces prove very convenient for establishing reliable correlations. **High resolution stratigraphy** tries to explain in great detail the 3D relationships between sedimentary bodies.

Often reservoir units are barren in fossil content and conventional stratigraphic methods do not give proper information for an adequate subdivision. Here new techniques like climate stratigraphy can help out. This relatively new method exploits detailed information contained in wireline logs (cf Nio 2006).

Periodic changes in the earth's orbit around the sun have an impact on the climatic conditions and influence the depositional systems (Figure 4.39, De Boer and Smith 1994). Several parameters are of importance:

- **Eccentricity** reflecting the deviation of the sun position from the focus point of the earth orbital ellipse (100 000 years with superimposed 400 000, 1.3 million and 2 million year cycles).
- Regular change in **obliquity** of the earth rotation axis (41 000 years).
- **Precession** which is the wobbling movement of the rotation axis (19 000–23 000 years).

Their influence on the earth sedimentary record are known as **Milankovitch cycles**. The Serbian mechanical engineer Milankovitch (1941) tried to prove a relation between astronomical parameters and the ice ages. For the Pleistocene and Quaternary periods this cyclicity is nowadays a well accepted concept. Astro-chronology is based on these type of delicate repetition in the geologic record (Coe 2003). The balance between global warming and cooling is quite subtle. It is obvious that Milankovitch cycles of the earth orbital variations, with a rhythmic shift of earth axis angle of orientation, are not only responsible for the change in climatic conditions (e.g. methane release, CO_2). Milankovitch cycles have been demonstrated in deep marine sediments and lake deposits, so they are really affecting the world in its totality. Milankovitch cycles have been recognised on well logs of the continental Permian Rotliegend deposits in the North Sea (Yang and Baumfalk 1994, Yang and Nio 1994) and that came somewhat as an surprise to some geoscience specialists.

The ice ages and growth of ice caps are interesting phenomena. They are believed the consequence of a drop in radiation from the sun reaching the earth surface and this is assisted by a decrease in heat storing capacity of the atmosphere, land and oceans (a.o. Strahler 1971). The latter is related to transformations in global water circulation. Changes in the oceanic circulation pattern have occurred in the past. Relocation of the Gulf Stream axis has been documented in the Miocene (Pinet and Popenoe 1982). Mountain building processes, the rise of the Himalayas and the creation of the land bridge between northern and Latin America (Panama Ithmuth), have an important impact on the global climatic conditions and oceanic water circulation.

The exact reason for the occurrence of ice ages is still part of heated discussions among geoscientists. Some researchers suggest that dust provides a means to block the sun radiation from reaching the earth surface. The Tambora volcanic explosion on Sumatra (Indonesia) in 1815 did put so much ash and dust in the air that it caused a drop in the world average temperature by 1 degree Celsius during a three-year period (Winchester 2003, Berman 2005). This sun light radiation blocking is the main driving force behind the *nuclear winter* concept, a worldwide cold spell generally predicted to follow a large scale atomic explosion disaster. Also a microfilm of oil on polluted oceans would change the albedo of the water surface.

Other researchers postulate a warm period as a possible cause for the ice ages. This warming-up will lead to more evaporation in the hot areas of the earth, thus generating more clouds with increased accumulation of snow on higher latitudes (Bryson 2003). Such mechanism accentuates the extremes in the global climate. It is not the amount of snow that is important, but the fact the snow will last and huge glaciers are built. At the moment we are living in an inter glacial period after the last big glaciation that happened some 12 000 years ago. At the end of the Younger Dryas (a 1000 year cold spell) the temperature was increased by 4 degrees Celsius per twenty years. This is equivalent to changing the Mediterranean climate for a Scandinavian type. Greenland ice cores indicate that even an augmentation of 8 degrees during 10 years has been reached in the past (Bryson 2003). The cores are evidence for the dramatic increase in industrial pollution over the last century, that has its long term consequences. Oxygen isotopes in Neogene to Quaternary fossils yield valuable information on the volume of the polar icesheet and it can be linked to sealevel changes.

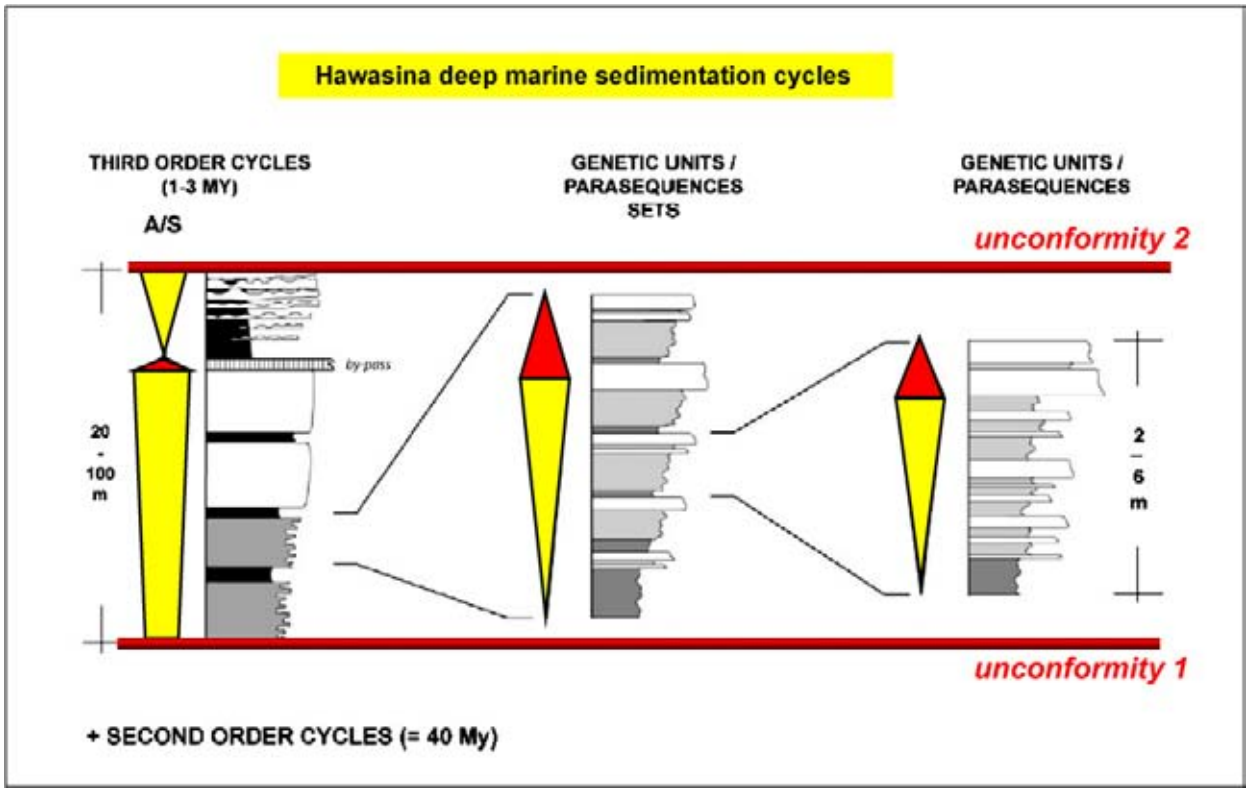

Figure 4.38: The sequence stratigraphic subdivision of deposits belonging to the deep marine Hawasina sub-basin that formed the margin of the mesoloic Tethys ocean. The carbonate submarine fan rocks are exposed in the Hamrat Duru overthrust in Oman. Several generations of sedimentary cycles are distinguished down to the metre level (modified after Guillocheau et al. 2004).

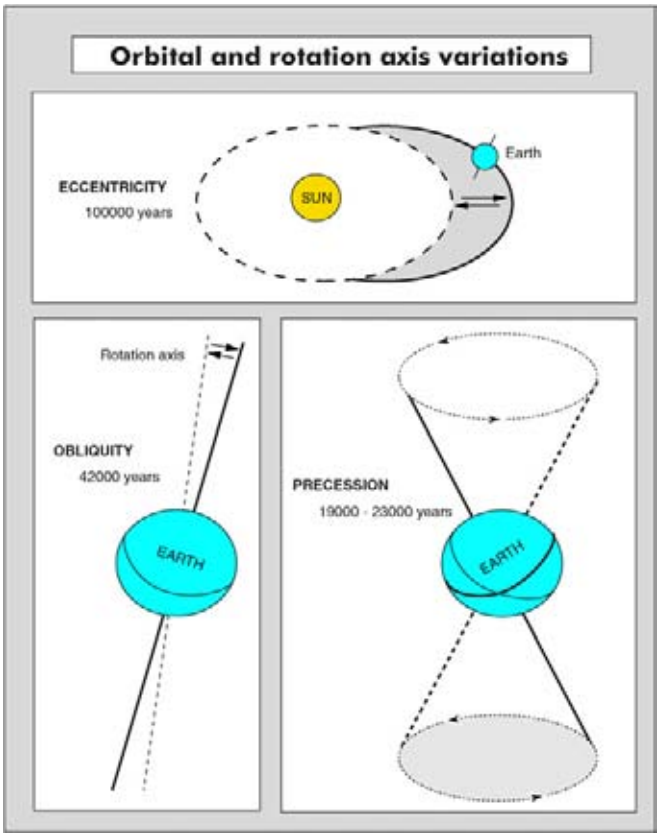

Figure 4.39: Variations in the earth rotation axis have an impact on the cyclicity observed in the sedimentary record (modified after De Boer and Smith 1994).

Orbital forcing is not only restricted to silici-clastics (Van Buchum et al. 1994), but also carbonates adhere to the same kind of repetitive cycles (Reijmer et al. 1994). Some workers suggest a non-linear link between climatic changes and the Milankovitch cycles (Elkibbi and Rial 2001). An estimate for the variations in sealevel depending on different physical factors is given by Moerner (1994):

Factors influencing sealevel variations estimated in metres

Present day tides	
– geoid tides	0.78
– ocean tides	up to max. 18
Present day geoid relief	
– maximum differences	180
Present day dynamic sea surface	
– low harmonics	up to max. 2
– major currents	5
Earth radius differences	
– equator/pole	21 385
Presently stored glacial volume (= metres sea level)	
– Antarctica	60
– Greenland	6
– all mountain glaciers	0.5
Glacial eustasy	
– Ice Age amplitudes	100–200
Geoid deformations	
– on Ma time scale	50–250
– last 150 ka; 20 ka cycles	30–90
– last 20 ka	60
– last 8 ka	5–8
– Holocene oscillations	2
Differential rotation	
– Holocene Gulf Stream pulsations	1.0–0.1
– Holocene Equatorial current E–W pulses	1
– El Ninjo/ENSO events	0.3
– major current topography	5
Rotation rate and sea level	
– meters sea level per 15 ms rotation (LOD)	1.0
Ocean thermal expansion	
– metres sea level per degree C per 1000 m	0.2

Sequence stratigraphy can be applied in situations where seismic correlations are absent. In those cases it means that the geologist is largely depending on biostratigraphic analysis for correlations and age-dating of the sequences and bounding surfaces, that provide the chronostratigraphic frame for the observations. Several different concepts of sedimentary sequences exist in literature dealing with sequence stratigraphic analysis and this leads unnecessarily to a rather confusing situation. The latter is especially true when seismic data is absent and/or when the subdivision is beyond seismic resolution. Many interpretative names have been introduced to describe the separating surfaces of various sequences:

- **Marine flooding (or drowning) surfaces**, which are essentially transgressive surfaces (Van Wagoner et al. 1988, 1990).
- **Maximum flooding surfaces**, which form conformable surfaces that pinpoints in time the extreme landward position of a transgressive trend (Bhattacharya 1993).
- **Transgressive surface of erosion**, showing the activity of wavebase erosion and reworking of the substratum during an ongoing transgression.
- **Transgressive surface** (Vail 1987).
- **Surface of marine erosion** (Nummedal and Swift 1987).
- **Highstand surface of erosion**, pointing to a minor lowering of baselevel during a sealevel highstand.
- **Lowstand surface of erosion** (incised valley), indicative of a drastic lowering in base level associated with a lowstand in sealevel (Weimer 1988).
- **Surface of lowstand onlap**, resulting from renewed rise in relative sealevel.
- **Surface of highstand onlap,** resulting from a sustained rise in relative sealevel.
- **Surface of lowstand downlap**, whereby a condensed sedimentation condition occur in the deeper part of the basin.
- **Surface of maximum starvation** (Baum and Vail 1988).
- **Initial flooding surface**.
- **Ravinement surface** (Thorne and Swift 1991).
- **Interfluve sequence boundary**, reflecting the dynamics of channel avulsion and abandonment and deltalobe switching.
- **Surface of erosion,** without a specific genetic connotation.
- **Forced regression surface** (Posamentier et al. 1992).
- **Surface of bypass**, indicating a conformable contact between two genetic units.
- **Para-sequence boundary**.
- **Re-activation surfaces**.

Problems are numerous in establishing the validity of these surfaces in an unambiguous way (Embry 1994). The interpretational aspects in the names of these bounding surfaces adds to the amount of confusion concerning the uniqueness of their identification on a basinwide scale. Moreover, these surfaces are cross cutting facies belts and this does not make the geoscientist's tasks any easier. Recognition of system tracts on the slope is feasible, while delineation of their equivalent surface in

the basinal areas is hardly ever possible (Scheibner et al. 2002).

Recognition and precise positioning of all these boundaries in the field is an issue of constant debate. The pinpointing of the maximum flooding surface (MFS) is sometimes somewhat subjective as it does not correspond with a clear lithological break. It is believed to coincide with the peak in uranium radioactivity response within a shale package (Davies and Elliott, 1994). Errors of a few meters at individual calibration points (wells and individual outcrops) may result in substantial discrepancies when correlations are done over large distances. Some authors traced the MFS without any difficulty from continental into marine deposits (e.g. Amorosi and Milla 2001), so one should not despair completely in face of all these problems.

Six main types of surfaces are important for correlational purposes from a practical point of view. These regional surfaces are traced without too much difficulty, both in the field and on seismic sections:

- **Sequence Boundaries** (SB) separating the depositional units. It are equivalent to Depositional Sequence boundaries (DS) where seismic data is available.
- **Flooding Surface** (FS) of which the **maximum flooding surface** (MFS) in a correlatable shale layer is of a special type.
- **Transgressive Surface of Erosion and/or Onlap** (TSEO) defined by truncations and onlap.
- **Regressive Surface of Erosion** (RSE), normally coinciding with downlap and progradational geometries in the deeper part of the basin.
- **Reactivation Surface** (RS), non-specified but corresponding to local phenomena like a para sequence boundary.
- **Bypass Surface** (BS), non-deposition without indications of erosion and indicative for concordant sedimentation.

Schulbaum (1996) goes even further and suggests only three surfaces: transgressive surface (TS), maximum flooding surface (MFS) and a surface of regression (SR). This over-simplification is probably a bit too drastic and it is more realistic to adhere to the proposed six-fold subdivision, which is more or less comparable to what Ainsworth (2005) has suggested in his borehole correlation study in a transitional domain (Figure 4.40). He clearly stated that the falling and lowstand system tracts are in many cases impossible to separate, illustrating the disadvantage of a too rigid subdivision scheme. Sequence boundaries are distinguished and in the case where seismic data is available, these sequence boundaries correspond to Depositional Sequence boundaries already outlined on the basis of reflection terminations. A top-down approach in the surface hierarchy from large scale to smaller scale observations is preferred in order to assure a consistent breakdown of the geological record.

The surface of bypass may correspond on seismics with a conformable interface. No direct geometric indications for a major hiatus, erosion or tectonic deformation are present and hence the surface is difficult to pinpoint. In the deeper offshore additional time-equivalent sedimentary layers are seen (e.g. slope front fills). In the field it may be represented by reactivation surfaces like a **paleo-sol** or a so-called '**hard ground**'. The paleo-sol is recognised by a typical **mottling** effect in the clastic sediments (Reineck and Singh 1975). This mottling is a dis-coloration induced by the geochemical activity around plant roots. Severe leaching of the soil by meteoric rain water may result in a complete alteration of the chemical composition of the sediment or rock (e.g. laterite soil rich in alumna). Several types of soils are recognised by the geographers. Reddish-green oxidation colors or mottling effects are frequently seen. The earlier mentioned hard grounds are layers with early cementation containing large amounts of fossil fragments, showing boring activity of organisms (Kummel 1970). The layer represents an episode of condensed sedimentation in the basin. The abundance in fossils indicates that biologic activity was there, but the sediment influx was suddenly reduced and therefore the biologic detritus increases its importance. The hard ground reflects a decrease in sediment input due to a relative rise in sealevel. The hardground layer should not be confounded with storm induced lag deposits or **beach rocks** as their nature is quite different. **Caliche** deposits are also early cementation products, but they are found in a terrestrial setting, while the hard grounds are found in the transitional and marine domain.

As stated before, also the scale of observation has an impact on the delineation of the bounding surfaces. Of course this is a less desirable condition and it only adds to the amount of confusion. A restricted scale of observation does constitute a serious danger, whereby an insignificant conformable contact is not properly related to its correlatable unconformity and an important sedimentary hiatus is thus missed. Isolated 'post stamp size' outcrops used for correlation on a basin wide scale is certainly not very wise and forms an open invitation for later trouble; more info is clearly needed to establish a workable frame (e.g. Weimer et al. 1994, Posamentier and James 1993). The fact that one deals with a

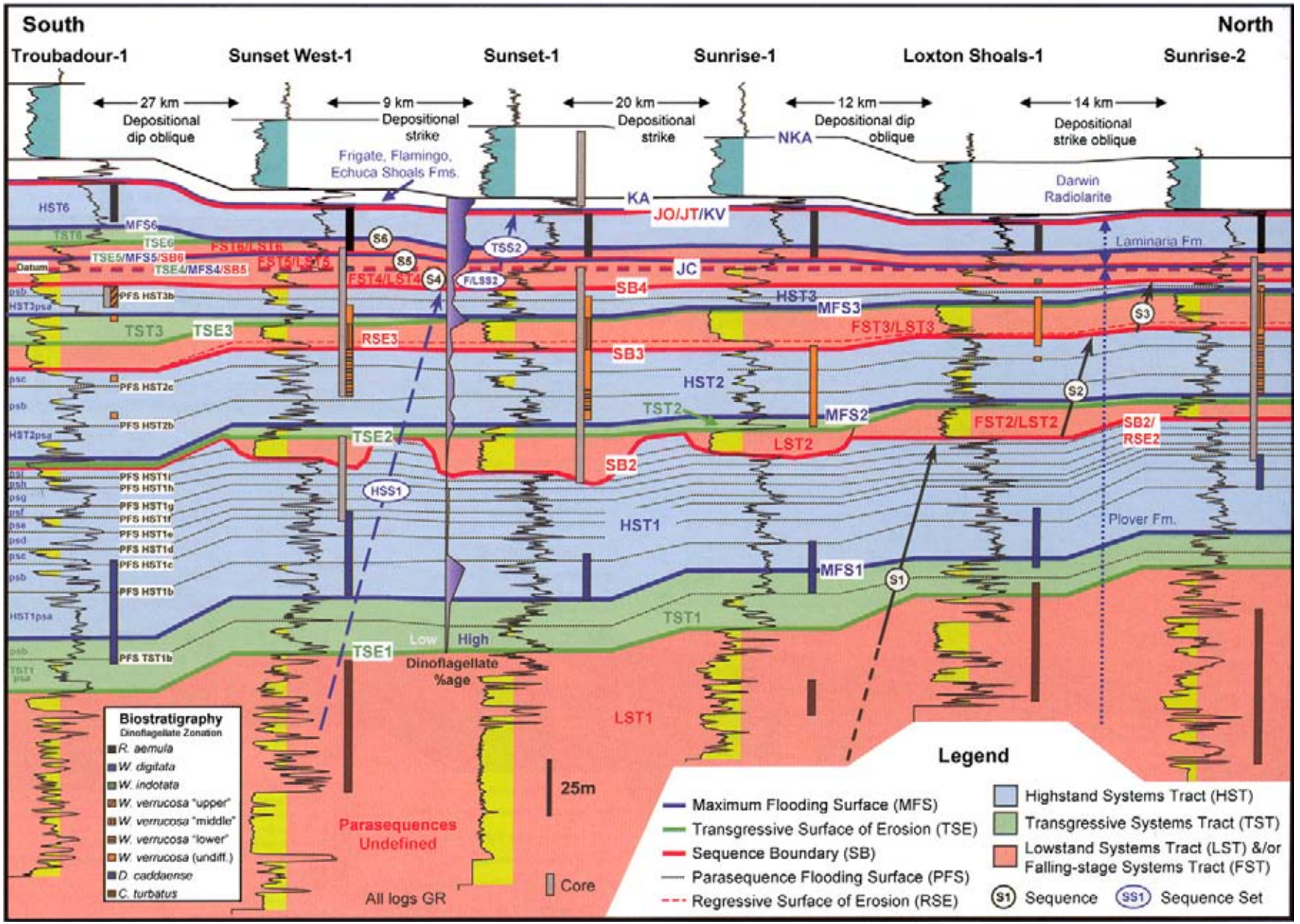

Figure 4.40: High resolution sequence stratigraphic subdivision in wells from the Sunrise and Troubadour fields (offshore northern Australia). Some cores made direct observations possible. Dinoflagellate zones and lithostratigraphic subdivision are also shown (Ainsworth 2005).

laterally non-continuous dataset introduces additional uncertainties in the stratigraphic correlations.

The difficulties, created by the straightforward correlation of lithological units penetrated by individual wells, are a classic example of possible pitfalls due to non-continuous sampling of the subsurface geology. The persistent problems with the stratigraphy and subdivision of the carbonate deposits in the mature Poza Rica field (onshore Mexico) is illustrative in this respect. The field has been producing 1.4 billion barrels of oil from the 1930's onwards, but still there is considerable uncertainty on details of the reservoir working model. The lithostratigraphic subdivision ignored the shingling seen on the seismics (amplitude and acoustic impedance cubes) and moreover it does not correspond to the observed outline of HC flow units. Well production results show that these direct log correlations are much too simplistic to serve as a basis for sound reservoir management decisions. The reality is unfortunately more complex. Seismic inversion supports the existence of a more complex internal structure. The new reservoir model has implications for the proposal of well work-overs and the inventorisation of unswept/bypassed production areas. The revised seismic stratigraphic reservoir model permits significantly better prediction of reservoir characteristics. Early water break-through along permeable reservoir beds can be better anticipated. Correct delineation of timelines is very important for outlining the reservoir flow units.

Seismics constitutes a convenient correlation tool for data interpolation between calibration points in the subsurface. It also gives a guidance when extrapolation is needed. Therefore it is logical to integrate seismic observations as much as possible within the sequence stratigraphic working concepts. The amount of overlap of the two scales of observation is rather large and serves as basis for checking the validity of both methods. For the proper integration of the two methods it should be ensured that incompatibilities within the interpretational procedures are avoided. Hence the need for a simple and standardised approach is more than evident. A high resolution stratigraphic subdivision is required from a reservoir development point of view.

This page intentionally left blank

Chapter 5

Hydrocarbon Habitat

Seismic stratigraphy extracts basic information on the depositional processes, active when a basin is filled. The method works best in areas with relatively rapid subsidence rate like rifts, continental margins and also foredeeps. When there is little subsidence, than the chance to preserve the original depositional geometries is smaller and therefore the number of criteria to interpret the reflections in terms of gross lithology is drastically reduced. In such cases the interval velocities may be an important attribute to distinguish the different lithologies. If the rocks are heavily tectonised, then the seismic data can be of such poor quality that no reliable interpretation of the depositional geometries can be made.

With reasonable-to-good quality data, it is possible for the interpreter to go a step further and analyse the **hydrocarbon potential** of a basin. Potential **reservoir/seal** pairs are identified and examined in more detail as will be shown later on.

It is generally accepted that hydrocarbons are mostly biogenic or organic in origin (e.g. Durand 1980, Tissot and Welte 1984, Biju-Duval 2002, Gluyas and Swarbrick 2004). In the past, Russian scientists have suggested an **inorganic source** for the hydrocarbons. Some researchers still advocate this mechanism, but without too much success. In the planetary system, however, methane is an omni-present substance (Moore and Hunt 1983) and there is no obvious reason to assume that the earth is deviating from the norm. The non-biogenic gas would be formed in the earth interior somewhere in the mantle and is constantly upwelling (Gold 1979). It can get trapped if a proper seal is encountered. Using this scenario it is possible to postulate gas accumulations within basement rocks, if sufficient porosity/permeability has been created. Heavy faulting and open fracturing will result in enough permeability to make any rock a potential reservoir.

The Swedes in Scandinavia have tested the play concept in the nineties for microfractured basement rocks on the Fenno-Scandinavian shield. Their zero nuclear energy policy forced them to explore unconventional prospects. At the chosen drill location, the Siljan Crater ring, the fracturing is induced by a paleo-meteoric impact event. The feature is 52 km wide and of Devonian age (368 million years old). The results of this HC exploration project were rather disappointing (Donofrio 2003). Two wells were drilled to a maximum 6.8 km depth. Some oil was recovered generated from Ordovician sourcerocks. The isotope contents of the encountered back ground gas has proven nevertheless the existence of small quantities of non-organic methane in the deeper part of the crust, with saturations that are very low (background gas). Degassing of the mantle and the crust is inferred from the presence of radiogenic ^{4}He and primordial ^{3}He isotopes (Marty et al. 2003). Fluid inclusions retained in minerals possibly can give some additional clues on the inorganic origin of hydrocarbons (cf Petford and McCaffrey 2003).

Any rock with sufficient porosity and permeability should be considered a reservoir. If the pores are water containing, the rock is called an **aquifer**. This is in contrast to a rock with low permeability that is known as an **aquitard** or waste rock. It can sometimes block the cross formational mass transfer and form a barrier to gas and fluid flow; hence it is an effective seal (Marty et al. 2003). Also fractured basement rocks are potential reservoirs containing commercial hydrocarbons (e.g. Petford and McCaffrey 2003). Some examples are:

- Gas trapped in volcanics offshore of Japan (Weyers et al. 2003).
- Metamorphosed basement rocks in the Beruk field (Indonesia).
- Volcanics and pyroclastic deposits containing hydrocarbons in the Tandung and Suban fields, offshore Indonesia (Koning and Darmono 1984).
- Production from granites in the Mara-Lapaz oil fields in the Maracaibo region in Venezuela (Smith 1955).
- Granites as host rocks for circulating fluids in a geothermal project in the Rhine graben (Le Carlier et al. 1994, Audigane et al. 2002).

Structures at a depth of over 5 km are still prospective to look for commercial accumulations. A recent well

29/5b-F7z drilled by Total in the North Sea reached the objective on the West Franklin prospect at a depth of 5750 metres and at a waterdepth of 89 metres (First Break, Vol. 21, No. 8, p. 14). Special equipment was needed to handle the high pressure of 1150 bars (1 bar is approx 1 kg/cm^3) and a bottom hole temperature of around 200°C. The **economic basement** for exploration has increased steadily in depth over the last century. First 2500 metres was an important cut-off depth to the exploration efforts (before the 1970-ties), after that it was 4000 metres (1970–1990) and now 6000 metres seems the new magic limit for HC development. The Zalzala field in Oman is for instance producing from Cambrian reservoirs (>0.5 milliard years) at a depth of more than 5000 metres. The waterdepth has increased also steadily from 500 metres in Bullwinkle (GOM) to 2320 metres for the latest Na Kika production platform (Shell Venster 2003, No. 2, p. 30), utilising subsea well completions. Since then the Toledo well in Alaminos Canyon 951 strikes yet an other record and was drilled in 3051 metres of water depth (Weimer and Slatt 2004). Explorationists definitely have become more daring over the last couple of years in proposing high risk/high reward wells. And that is good thing because it opens up a whole suite of new hydrocarbon plays.

The deepest well in the world has been drilled on the Kola peninsula in Russia, where a 12 262 metre deep hole was drilled in Archean metamorphics. The main borehole (and several complementary ones) traverses a sedimentary-volcanic sequence of the Lower Proterozoic Pechenga Formation (0–6842 m) and a considerable part (6842–12 261 m) of the Archean granitic-metamorphic complex of the basement (gneisses, amphibolites, migmatites and granitoids). Circulation of rock fluids at deeper levels came as some sort of a surprise. The water, freed from crystal framework by mineralogical changes, apparently could not escape to the surface, due to the presence of an effective impermeable layer or multiple seals. The Russian Kola well penetrated only the upper 1/3 part of the crust.

In the sixties the Americans embraced the ambitious plan to drill through the Moho discontinuity to recover of a piece of the upper mantle. They choose a site offshore Mexico as the well location, in a waterdepth of around 4000 metres. In fact they never succeeded in the operation and only managed to penetrate 180 metres of the Earth's crust. The US Congress cancelled continuation of the project because of the exorbitant costs and withdrew the financial funding. The MoHole project became known as NoHole (Bryson 2003). The rig costs can be estimated nowadays as 425 000 US dollars per day (cf Weimer and Slatt 2004) and that gives some idea about the cost involved in such ambitious scientific projects.

Seals are formed by **permeability barriers to fluid/gas flow**; these are often shales and salt intervals, but also other lithologies can be effective seals (e.g. a dense carbonate layer). **Permeability** K is directly related to the amount of connected porosity, it is expressed in Darcies or milli-Darcy. It is a measure for the flow properties of a fluid through the pore space in the rock. A Darcy is defined as the flow of 1 millilitre per second of a 1 centipoise viscosity fluid through a 1 cm^2 area under a pressure gradient of 1 atmosphere (Sheriff 2002). The permeability depends on packing, sorting and grainsize, because this determines the geometry and the size of throats between the connected pores. The relation between permeability and porosity varies for each area and formation (Nelson 2004). Other influencing factors are: depositional environment, depth of burial, rock age and mineralogy. Statistical analysis on grains and pores can give information on the depositional environment (Dr M. Fey pers. com., Ehrenberg 2004). The heterogeneities in the rocks are related to different scales of observation:

- Pores with diagenetically related factors like mineral overgrowth.
- Lamina of different grainsize/composition.
- Beds resulting from different sedimentary processes. Connectivity and continuity are important parameters (e.g. Jackson et al. 2005).
- Facies associations related to the depositional system.

The vertical permeability is sometimes not the same as the horizontal permeability and this has consequence for the expected hydrocarbon production from the reservoir. The $K_\mathrm{v}/K_\mathrm{h}$ is an important parameter in dynamic fluid flow and reservoir modelling, it has a significant influence on the oil recovery rate (e.g. Nordahl et al. 2005). The cut-off for permeability of a good reservoir depends from area to area, but it can be in the order of 0.01 milliDarcy to 0.1 mD in Lower Jurassic tidal sandstones in the Halten Terrace, offshore Norway at a depth of 4700 metres (Martinius et al. 2005). The effective permeability is a concept used in reservoir modelling. It also depends on the perculation factor that is related the flow in the pore throat system. The effective permeability is given by:

$$\frac{K_\mathrm{effective}}{K_\mathrm{sand}} = A(V_\mathrm{mudstone\ critical} - V_\mathrm{mudstone})^\mathrm{a}. \quad (5.1)$$

Where V_mc is the critical mudstone fraction, A and a are perculation factors. $K_\mathrm{effective}$ is given by:

$$K_\mathrm{effective} = \left(V_\mathrm{mud}K_\mathrm{mud}^\omega + (1 - V_\mathrm{mud})K_\mathrm{sand}^\omega\right)^{1/\omega}. \quad (5.2)$$

V_mud is the mud volume fraction, ω is the averaging power and K_sand and K_mud are the mean permeabilities of sand and mud components (Ringrose et al. 2005).

Porosity is the total open space in the rock that is occupied by fluids and gas. Different packing of equally sized spheres results in the following porosities:

- Cubic 47%
- Orthorhombic 39.5%
- Rhombohedral 32%
- Tetragonal 26%

If the pores are connected, it is known as **effective porosity**. Effective porosity is also a concept used by the petrophysicist, when determining the porosity from the logs. If the pores are non-connected, it is known as **vuggy porosity**. If the porosity is located within the grains, it is said that the porosity is **moldic**. Unconformities are major breaks in the sedimentation and are therefore particularly important as permeability barriers (Schlee 1984, Bouma et al. 1978). The most commonly used porosity-permeability relationship is the **Kozeny–Carman function** that is adapted for the pore shape (Prasad 2003):

$$\text{Permeability} = \left(\frac{1}{F_\text{s}\tau S_\text{vgr}^2}\right)\left(\frac{\phi^3}{(1-\phi)^2}\right) \tag{5.3}$$

$\phi =$ fractional porosity,

$\tau =$ tortuosity,

$S_\text{vgr} =$ specific surface area per unit grain volume,

$F_\text{s} =$ pore shape factor.

This can be simplified to:

$$\log \text{RQI} = \log \text{FZI} + \log \varepsilon. \tag{5.4}$$

Reservoir quality index

$$\text{RQI} = 0.0314\sqrt{\text{permeability}/\phi}, \tag{5.5}$$

Flow zone indicator

$$\text{FZI} = \frac{1}{\sqrt{F_\text{s}\tau S_\text{vgr}^2}}, \tag{5.6}$$

Epsilon is the Void Ratio

$$\varepsilon = \frac{\phi}{1-\phi}. \tag{5.7}$$

A larger FZI means a better connectivity between the pores. There are several types of connectivity (Ainsworth 2005) that are related to:

- Sand/shale ratio and the depositional architecture/facies distribution.
- Faulting and fault transmisibility characteristics.
- Related to permeability of reservoir as discussed earlier (a.o. diagenetic processes).

There is often a good relation between velocities and permeabilities (Prasad 2003). It depends on the initial lithology, compaction and cementation history of the sediment. Addition of clay, diagenetic alteration, leaching of constituents minerals and cementation will lead to deviations from the normal velocity–permeability trend. These relationships are dataset specific and their validity should be investigated on a case-to-case basis.

It is noteworthy to mention that Upper Cretaceous and Danian Chalk oilfields (Ekofisk and Valhal) in the North Sea show exceptional porosities up to 48 percent at an approximate depth of 2900 metres subsea. The permeabilities range between 1 and 100 mDarcy. Salt induced structuration stimulated the natural fracturing and increased the connectivity of the pores. This extraordinary porosity distribution is caused by special circumstances: overpressure as a result of under-compaction and early entry of hydrocarbons in the carrier bed, inhibiting pressure dissolution and calcite precipitation (Goulty 2003). The seismic properties of the Chalk, determined in an AVO inversion exercise, may yield a direct relation with the porosity and pore fluid (Japsen et al. 2004). Early charge of hydrocarbons in a reservoir may block pore fluid flow and minimise the cementation effect (Han and Batzle 2006). It can give rise to very local anomalies in the porosity/permeability distribution.

Porosity is also studied by using X-ray computed tomography. It reveals detailed differences in density and atomic structure (Mees et al. 2003). The perculation factor is important to consider when studying the fluid flow.

The IFP claims to have a reliable method to calculate a permeability log from measurements on well cuttings (First Break, Vol. 22, p. 21). These rock fragments are transported by the drilling mud and recovered at the well head at regular time intervals. Contamination from overlying units seems to be less a problem. There is a good correlation of their Darcylog$^{\text{TM}}$ with other logging tools and a better correspondence with the values as seen by the core samples.

5.1 Source Rocks and Hydrocarbon Migration

Certain specific source rock intervals can be identified, based on the lithological and depositional interpretation. These intervals are often calibrated by well control. If no well data is available, then it depends solely on the interpretational skills of the exploration geophysicist and his knowledge of the regional geology. Regular

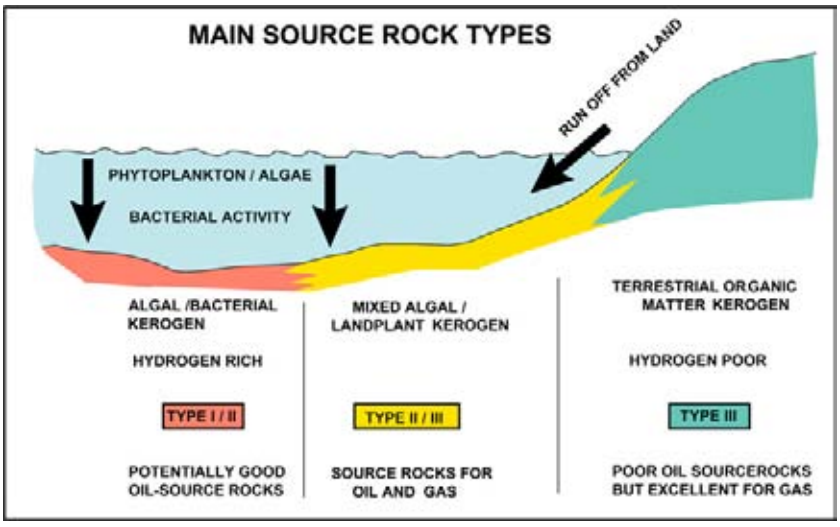

Figure 5.1: Main source rock types and their origin. Each source rock type has its own specific organic contents, that will generate specific hydrocarbon strings when sufficient maturation levels (increased temperature/pressure) are reached during ongoing burial.

geological field excursions are therefore not a waste of money, but good managers appreciate the benefits of these trips to their business. They are also great for teambuilding efforts.

Source rocks are rocks that are capable of producing hydrocarbons when submitted to certain physical conditions. Important factors are temperature, pressure and also time allowed for the chemical reaction to take place. The source rocks have a relatively high concentration in organic matter, which is expressed in the **TOC** (or total organic matter contents) value. Several types of source rocks are distinguished (Figure 5.1). An estimation can be made of the alteration of the organic material as an adaptation to changing temperature conditions. Their degree of **maturity** for further hydrocarbon production is assessed. A Rock Eval^{TM} analysis is usually done to determine the TOC of rock samples (Durand 1980). It is achieved by heating a standard quantity of rock sample with analysing the volatile parts and the residue (Figure 5.2).

5.1.1 Source rock types and maturity

There are three types of source rocks:

- **Type I** or **kerogenous** (mainly algal derived).
- **Type II** or **mixed** (mainly bacterial derived).
- **Type III** or **humic** (mainly landplant derived).

All these source rocks have the potential to generate oil and gas, except for the pure type III which will exclusively produce gas.

Once the organic matter is buried and protected from early breakdown, it is submitted to different temperature levels during further subsidence of the basin and the sedimentary loading. The organic matter is gradually changed under the increased temperature conditions and at a sufficiently high level the first hydrocarbons are produced. The degree of metamorphism of the organic matter is usually expressed by the **vitrinite reflection coefficient** (VR); it is a measure for the amount of alteration of the organic matter (Figure 5.3). Vitrinite itself is a special type of plant-derived organic matter. Sometimes the coefficient is represented as VR/E and this means that the value has been estimated from other material and has not been actually measured from the vitrinite because it is lacking in the sample. The expression SOM stands in this context for other Structureless Organic Matter. SOM has even been recognised in rock samples coming from our neighbouring planet Mars. The alteration of organic material is basically irreversible when the rocks are again submitted to cooler conditions during later uplift. The maximum degree of alteration is therefore always preserved by the rocks.

Lets consider a source rock, progressively buried and submitted to increasing temperatures and pressure (Figure 5.4). **Burial graphs** are constructed to illustrate the subsidence history (Figures 5.5 and 5.6). At a certain level, known as the top of the **oil window**, the first oil is generated but it stays in the source rock. Only under a further increase of the temperature and maintaining it during some period of time, the organic material will be expelled into the surrounding rocks. This is the onset of the migration of the hydrocarbons. The migration path is determined by permeable layers and conduits. The density-driven **migration** of the

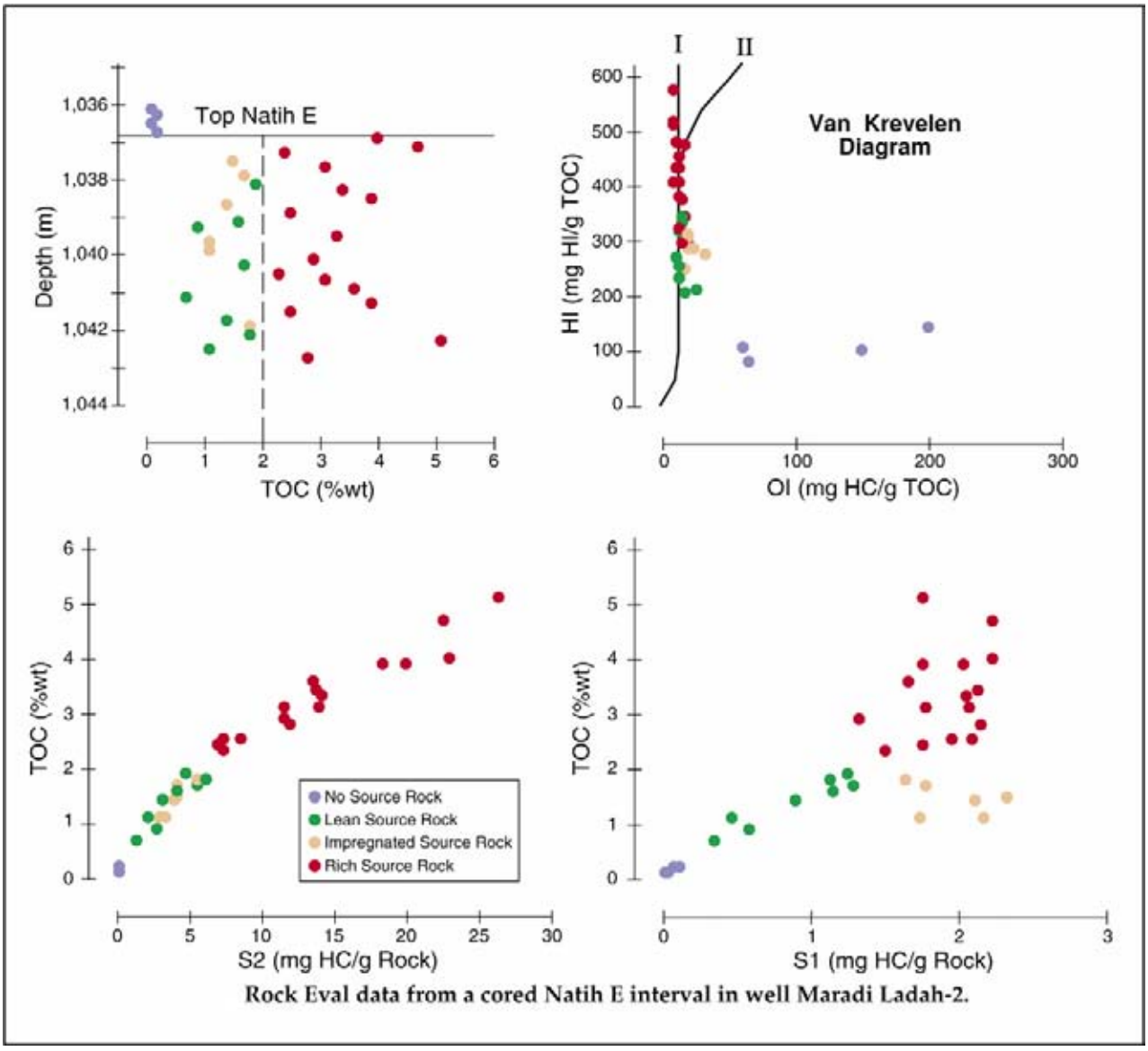

Figure 5.2: Rock Eval plots for a rock sample from the Natih Formation in Oman. The Total Organic Contents (TOC) is determined by heating and analysis of the volatile products within the remaining residue (Terken 1999).

oil will take place until the hydrocarbons are trapped or emerge on the surface, thus doing it will create an **oil seep**. Normally the expulsion takes place at a vitrinite reflectance level of around 0.6. But this depends on the type of source rock. As said already, the vitrinite reflectance is an universal measure for the degree of metamorphism of organic matter. If the source rocks are buried even deeper – and there is still sufficient organic material left – lighter fractions of hydrocarbon (condensate and gas) are generated. At an VR/E of 1.1 only gas is being produced from the remaining organic matter. First this is **wet gas**, which means it contains substantial amounts of **condensate**. A condensate is a gas under subsurface conditions in the reservoir, but at normal P and T it is unstable and becomes a liquid. In fact condensate is a very light oil, that needs little cracking in the refinery downstream. Above a certain VR/E no further hydrocarbons are formed and the yield from the source rock is considered 100%. If the source rock is submitted to still higher temperatures, then the residual organic matter within the source rock interval is said to be "**over-cooked**".

A **sour gas** is a gas that contains relatively large amounts of sulphur. This is in contrast to a **sweet gas,** that contains a small quantity of sulphur. The sour gas has to be processed in a special de-sulfurisation plant in order to make it less corrosive and to meet strin-

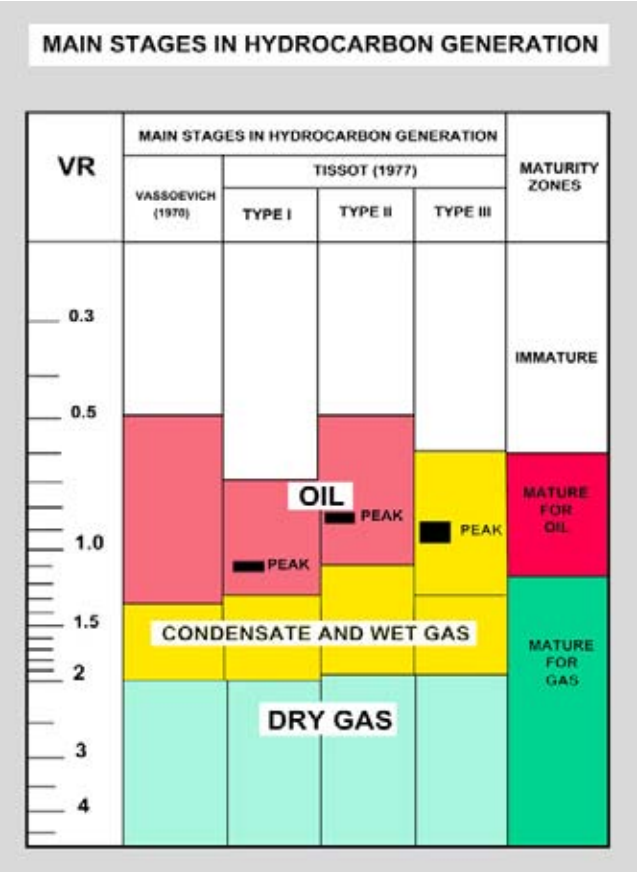

Figure 5.3: Diagram showing the main stages in hydrocarbon generation and the corresponding maturity levels of the different types of source rocks.

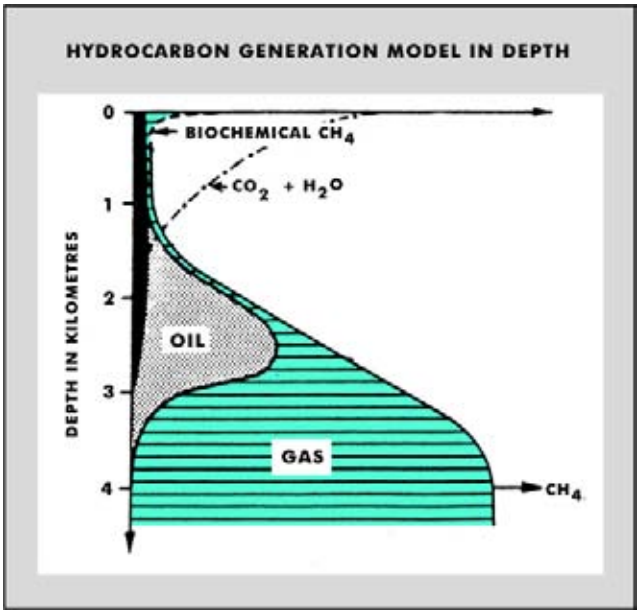

Figure 5.4: Hydrocarbon generation model for source rocks buried to different depths.

gent anti-pollution requirements (anti acid rain) when burning the fossil fuel. Associated gas is **wet gas** that is kept in solution within the oil accumulation and it is separated when the oil is produced. In the last century this gas was often flared in the open biosphere at great environmental costs. Hefty financial investment in large LNG projects were necessary to prevent such energy wastes (e.g. Bonny Island, Nigeria). The quantities of associate gas are considerable; in Nigeria it amounts to 28 cubic metres of gas for each barrel of oil produced. LNG stands for Liquid Natural Gas (methane) and LPG is Liquid Petroleum Gas (butane, propane). LPG is mainly produced from condensate.

LNG projects were pioneered in the Far East, but now globally the interest in LNG projects is steadily mounting. End 2003 there were 17 LNG export terminals with 70 trains functioning, having a total capacity of 135 million ton/year. A large explosion in Algeria recently blew up three of the production trains. Security and safety is a serious issue for this kind of commercial activity. By 2007 the number of trains will be increased by 44 and the production lifted by an other 128 million ton per year. 1 million ton of LNG is approximately equivalent to 1.4 billion cubic metres of gas under standard conditions for the customer. In the coming four years 40 billion US dollars are expected to be invested in the LNG sector (de Wit 2004). The LNG costs have been coming down steadily, but a LNG tanker of 160 million dollars is still three times more expensive than a normal oil tanker. Moreover, the economic life of such vessels is currently set at only 25 years (International Maritime Organisation IMO), which is fairly short.

The thermal history of rock samples can be refined by applying techniques like U–Th–He **thermochronology** (CSIRO, First Break, August 2003, p. 30–31). Determination of timing and magnitude of paleo-thermal events is done on individual apatite and zircon crystals. It can discriminate between slow and multi-episodical cooling. The measurements are based on the accumulation and diffusive loss of helium produced by the alpha decay of Uranium and Thorium impurities within apatite grains. Analogue to fission track analysis an age can be assigned to the sample based on the amount of radiogenic helium and the U–Th contents. The ages are reset by heating at temperatures above 80–90 degrees Celsius. In combination with vitrinite reflectance the U–Th–He thermochronology can give a better resolution on the temperature history of the rock sample between 50 and 80 degrees. In some marine source rocks the vitrinite reflectance estimation is influenced by the compositional variations. Here the fluorescence alteration of multiple macerals (FAMM) can give a better evaluation of the sourcerock maturation level (Ujilie et al. 2004).

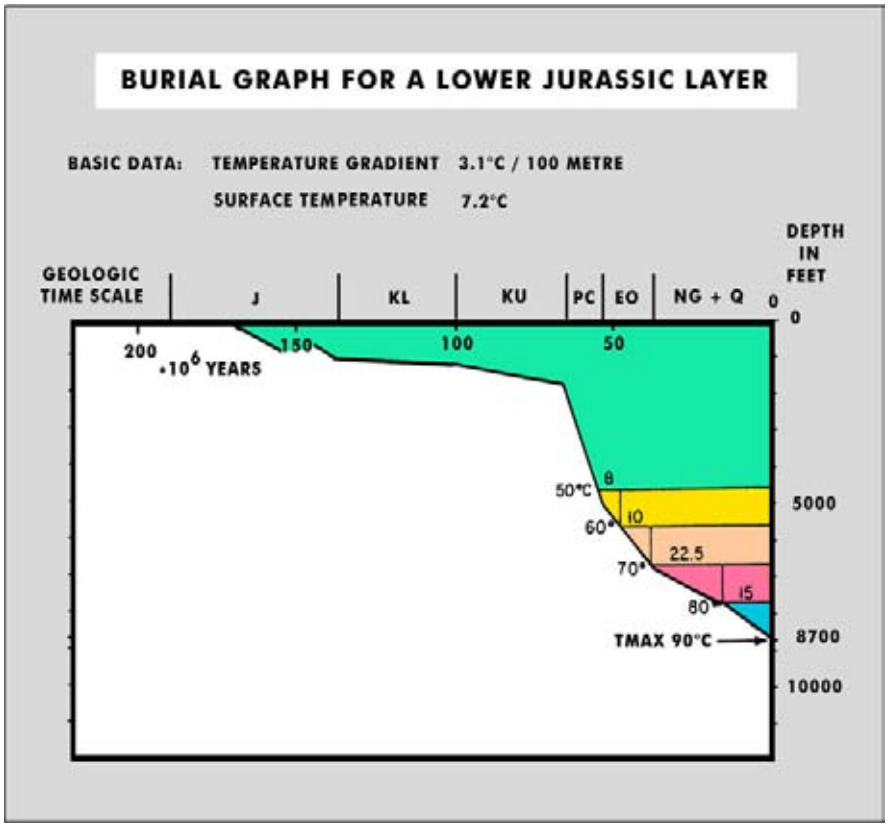

Figure 5.5: A burial graph visualising the maturation profile of a source rock interval; it also displays in a convenient way the amount and timing of the structural deformation. When compensating for compaction effects, it gives access to proper thicknesses and burial history. By assuming a constant heatflow gradient in time, than the depth scale can be translated in a maturity level scale for the sourcerock (courtesy Shell).

The area in the subsurface, where hydrocarbons are actively formed, is called a '**Kitchen**'. In the kitchen area source rocks are sufficiently mature to produce hydrocarbons (Figure 5.7). Often a kitchen area is postulated, i.e.:

- The TWT structuration gives some indications on the pressure/temperature that the rocks are experiencing.
- The type and presence of sourcerocks are assumed based on regional geological considerations.
- An estimate is made for the tectonic/subsidence history.
- Paleo-heatflows are assumed.

All this information is sufficient to get a rough idea where hydrocarbons might have formed or are still forming. Hydrocarbons migrate away from the kitchen area in an updip direction due to its low density (Figure 5.8). It is for this reason that most wells are centred around structural highs and only few calibration points are available to assess the sedimentary fill of the surrounding low areas or synclines. It needs an interpreter with a lot of guts to propose management to drill a well on a speculative stratigraphic trap in a synclinal position. Sometimes it is not possible to identify a specific sourcerock layer. The organic matter is dispersed in a thicker sequence, but still can generate huge amounts of hydrocarbons; e.g. 1 billion barrels of recovered oil for the Tertiary Seria field in Brunei for which no specific sourcerock interval can be assigned. Biogenic gas is an other possibility, generated by biologic activity of micro-organisms. If several source rock intervals can be demonstrated present in certain area, it will increase the prospectivity of the concession blocks. Mixing oils from the various mature intervals frequently occurs, depending on joined migration paths and the effectiveness of the seals.

5.1.2 Depositional settings favouring source rock development

Source rocks are deposited in environments ranging from fresh water lakes to brackish lagoons and even up to deep marine basins (Figure 5.9). Several mechanisms

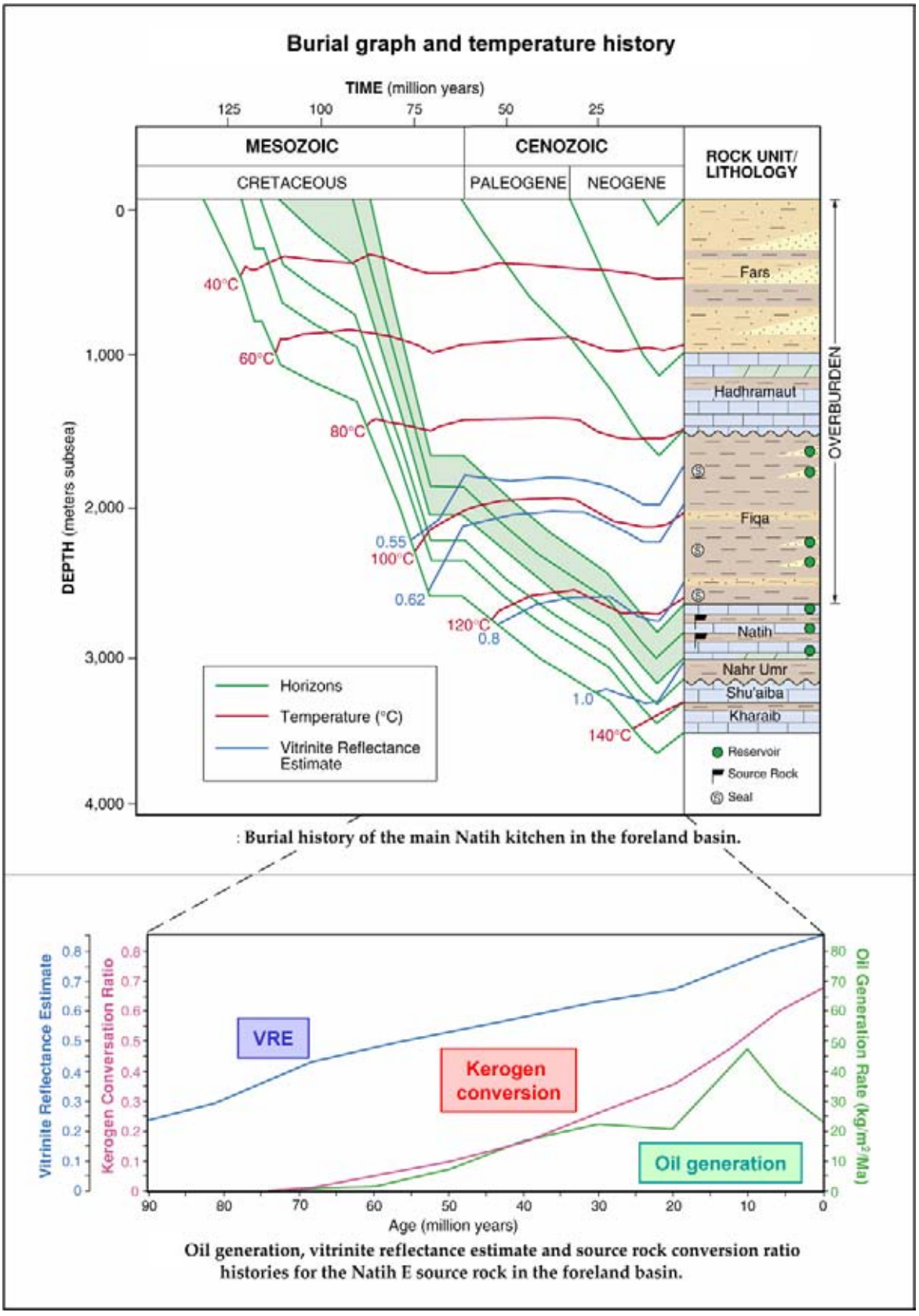

Figure 5.6: Burial graph illustrating the increasing temperature experienced by the sediments during ongoing subsidence and compaction.

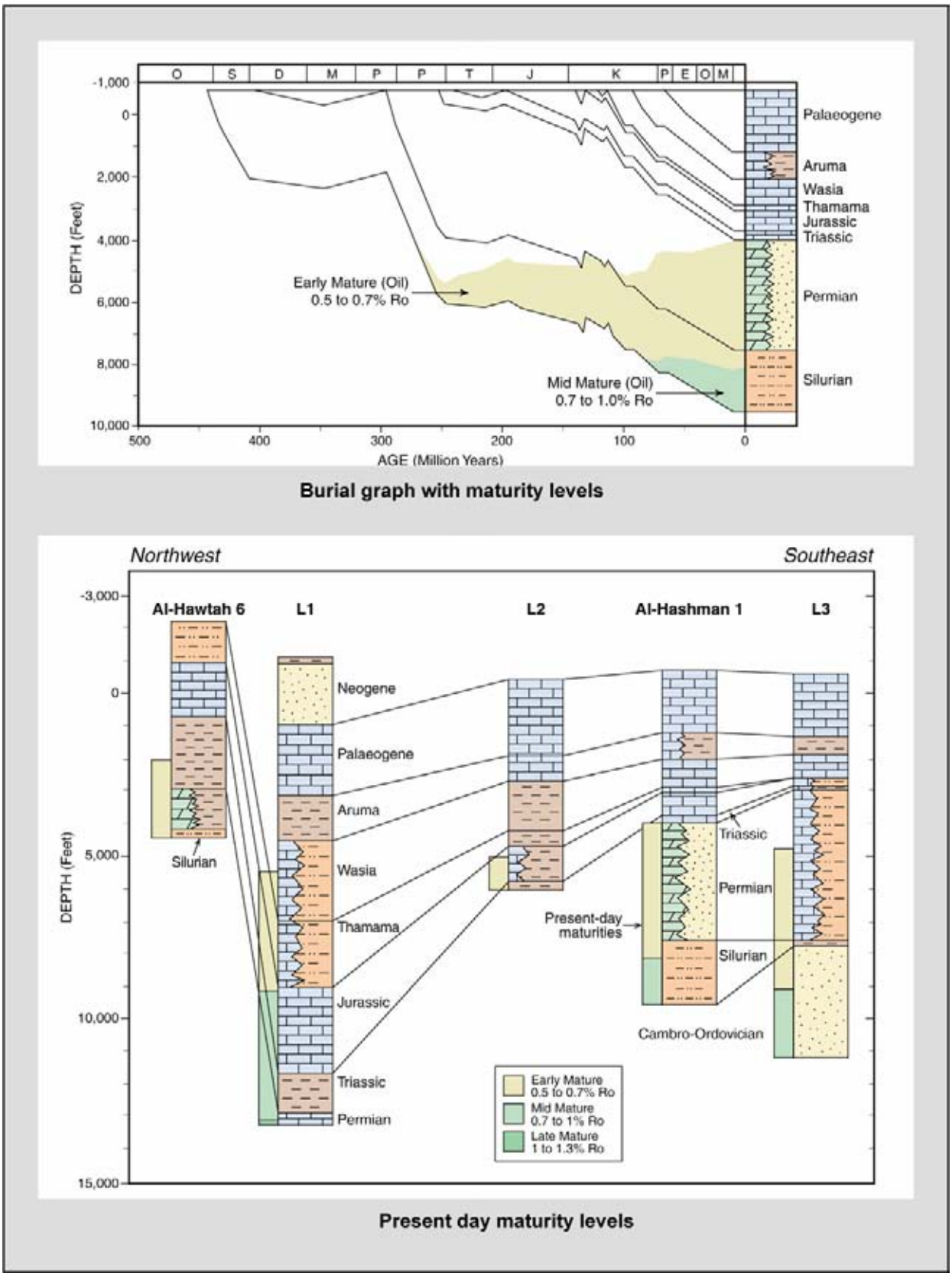

Figure 5.7: Burial graphs and the depth position of the oil maturity window in time. Below the present day situation for some wells in northern Oman is given (modified after Milner 1997).

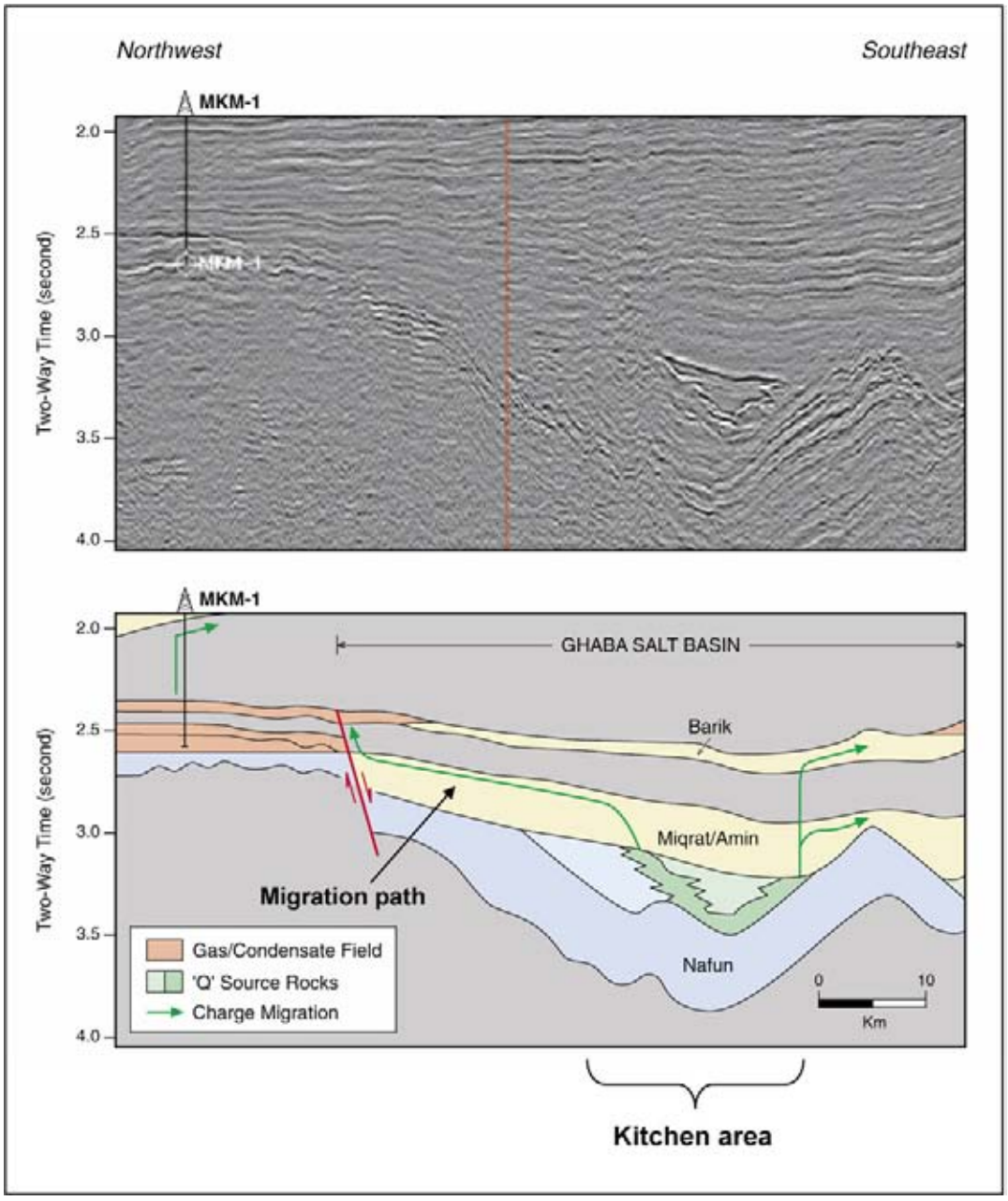

Figure 5.8: The source rocks in the kitchen area are buried deep enough and are sufficiently hot to start alteration of the organic matter in the sediments into oil. By increasing the temperature even further the oil is expelled from the mature source rocks and migrates via permeable layers and/or fractures in an preferential updip direction. The migration is density driven.

are favourable for the deposition of source rocks. There exist various ways to ensure that organic matter is preserved and fossilised:

- **Anoxic** conditions prevent early breakdown of organic material, so it gets buried and preserved.
- High production of organic material tend to increase the organic contents of the sediments if it exceeds the degradation capabilities of the system.
- Slow sedimentation rates in condensed sequences increases the relative percentage of the organic matter as it gets less dispersed.

Good water circulation in a basin has a negative effect on the establishment of an anaerobic environment of deposition. The water circulation is stimulated by the presence of a **lateral water temperature gradient** and this depends on the degree of icecap development. Good oceanic water circulation does imply, however,

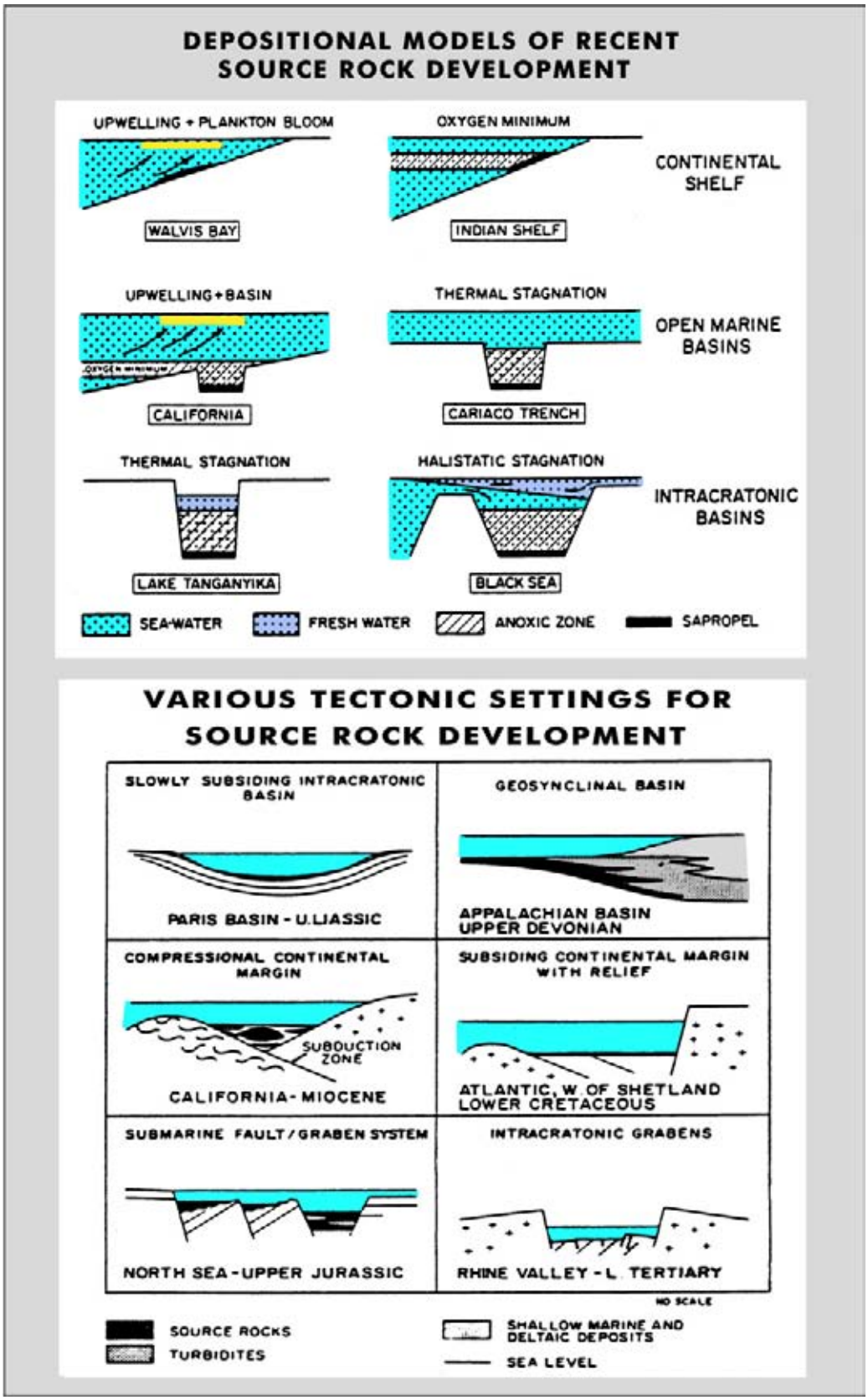

Figure 5.9: Various depositional models for recent source rock environments and their tectonic settings (courtesy Shell).

that there exist zones where nutrient-rich colder water is forced to the surface. This rising water column is generally known as **upwelling**. These upwelling areas in the ocean coincide with zones with increased biological production. It can be so important (algal bloom) that it outnumbers the **degradation capabilities** of the biologic ecosystem and organic-rich sediments are deposited at the basinfloor underneath.

In the continental domain several settings are favourable for source rock development:

- Swamps (coastal and inland) in which mainly land-plant material accumulates as peat and lignite.
- Lakes within an early rift/graben setting and also interior inland basins. In the lake the circulation of the watermass can be blocked by thermal or density driven layering. This stratification enhances the organic material preservation potential. **Oil shales** can be deposited under such conditions.

The deltaic setting in the fluvio-marine domain has a good source rock potential. Stagnant conditions may prevail in oxbow lakes and lagoons (e.g. Lagoon of Abidjan, Ivory Coast). Transportation of organic material from the hinterland can be considerable. The organic matter may be dispersed, but it still can be a major contributor to hydrocarbon generation (e.g. offshore Borneo). The river discharge also stimulates the biological activity by bringing in nutrients. Furthermore, the density difference between saline and fresh water can cause stagnant conditions.

Partially closed-off seas are often excellent settings for the deposition of source rocks. The circulation in such basins is restricted or blocked and **euxinic** conditions are installed on the basinfloor (e.g. Black Sea).

In the marine domain several features are favourable for source rock development:

- Tectonic events result in a drastic deepening of the basin and the basal watermass is cooled to such an extend that thermal stratification sets in. Differential movements lead to localised deeps and the collapse of lateral currents. The deepening and associated transgression results in a decrease in clastic supply onto the basinfloor and the enrichment in organic content is thus favoured. Draping of the basinfloor morphology points to such conditions (e.g. Jurassic of the North Sea Central Graben, Brooks and Glennie 1987; Cretaceous oceanic anoxic events, Arthur and Schlanger 1979).
- In the initial stage of foreland basins, just before the main deformational phase is taking place, source rocks can develop in the distal part of the basin (e.g. Appalachian foredeep). There should be some indication of sediment starvation (downlap) on the basinfloor. Along the margin of the basin there might exist a carbonate shelf and locally submarine fans may reach the proximal part of the basinfloor. Stagnant water circulation possibly occurs due to the presence of a sill blocking the entrance to the basin.
- Also in slowly subsiding basins there are possibilities to accumulate source rocks. The source rocks are found in the centre of the basin due to decrease in clastic supply and the relative enrichment in organic compounds.

As shown above there are quite a number of scenarios that stimulate the preservation of organic material.

5.1.3 Hydrocarbon migration and trapping

As said already before, hydrocarbons are formed in source rocks that are submitted to burial and exposed to changing temperature/pressure conditions, whereby a sufficiently high maturity level is reached (Durand 1980, Tissot and Welte 1984, Hunt 1990). The hydrocarbons are expelled from the hostrock and migrate into the surrounding rocks. They tend to **migrate upwards** due to density contrasts until they meet resistance. This is when they encounter an **effective seal** on their way up. They follow the base of the seal and migrate laterally to the highest point, until they encounter another permeability barrier which blocks the lateral flow and a trap is defined (Figure 5.10). The migrating oil will fill the trap to its **spill point** (last closing depth contour on a map) if no **dynamic flow** in the reservoir is assumed and enough hydrocarbons are produced by the kitchen. If more hydrocarbons are generated, then the trap will be completely filled and the overflow will continue its voyage up the permeable host rock sequence.

With ongoing burial the source rock is moved through the **oil-window** into the **gas-window** and gas is being produced. The gas basically follows the same migration path as the oil and at its arrival at the trap the density contrast will force the gas to replace the oil. The oil is now pushed below the spill point of the trap and will migrate further along the bottom surface of the topseal until it reaches another trap or the earth surface (oil seep).

Vertical migration along inclined beds, fractures and fault planes is normally preferred, although downward migration cannot to be ruled out. Downward migration occurs only when there exists a reversal in the pressure differential along the migration path. Sometimes a complex migration path has to be inferred in order to

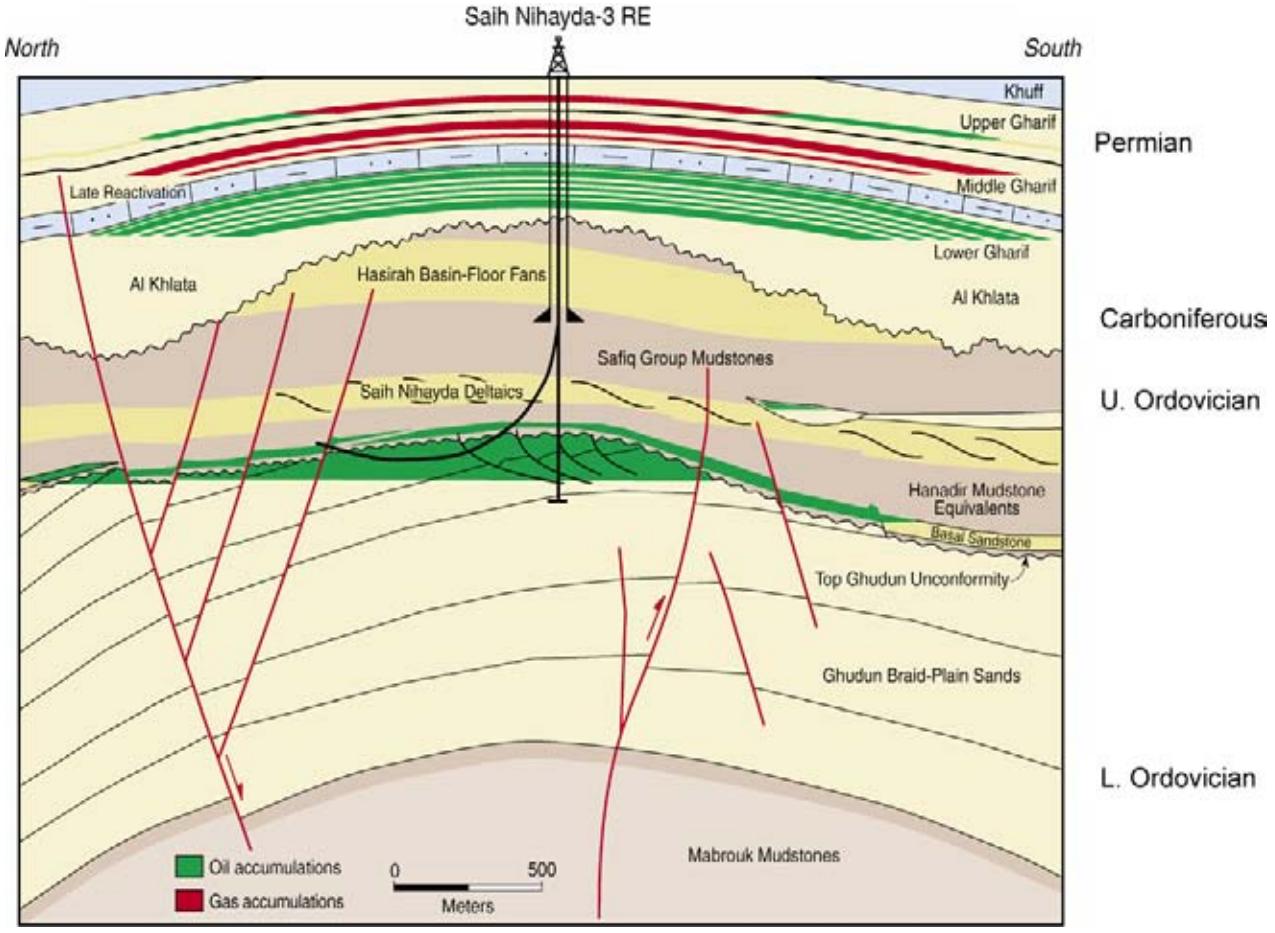

Figure 5.10: An anticlinal structure forms often a potential trap for the retention of migrating hydrocarbons. A convex-upward curved impermeable shale layer is in many cases an effective seal. Multiple reservoir/seal pairs can be present in the structure, as is shown in this section.

provide a connection with the kitchen below, with migration distances up to 100 km or more (Figure 5.11). Complications in long distance migration are more easily overlooked and the risk for charging the prospect is becoming accordingly higher. The migration system is defined by the migration channels (highly HC saturated zone of the carrier bed), their surrounding sediments (carrier bed and seals) and the reservoirs containing the hydrocarbons. When oil migrates it will exchange some parts of it with the surrounding. It interacts with the water and the solid phase (mineral framework and organic matter) encountered on its pathway. This happens by partitioning into the water, absorption onto the surface of the solid phase and diffusion into the water (Yang et al. 2005).

Along a poor migration path also fractioning of the hydrocarbons may take place. If the migration path is badly permeable than only the lighter fraction of the hydrocarbons can move updip, while the heavier molecules are retained by the effective seal. In the Egyptian Nile delta for instance such a fractioning mechanism is put in evidence. The shallow Pliocene sequence is purely dry gas prone, while the deeper Miocene reservoirs contain gas and condensate. The deeper Oligocene traps contain light oil. Some authors have suggested a biogenic cause for the shallow dry gas, with bacterial action responsible for the breaking down of the condensate (Dr Zaki, pers. com.).

The hydrocarbons in an accumulation have a certain density and therefore a varying viscosity. **Viscosity** is a measure for the resistance of a fluid to flow, whereby a high viscosity substance is very slowly moving. The density of hydrocarbons is expressed in API units, whereby a low API value means that the viscosity is high. API stands for the American Petroleum Institute that defined the parameter under standard pressure and temperature conditions. The following formula is applied:

$$\text{API} = \frac{141.5}{\text{specific gravity}} - 131.5. \qquad (5.8)$$

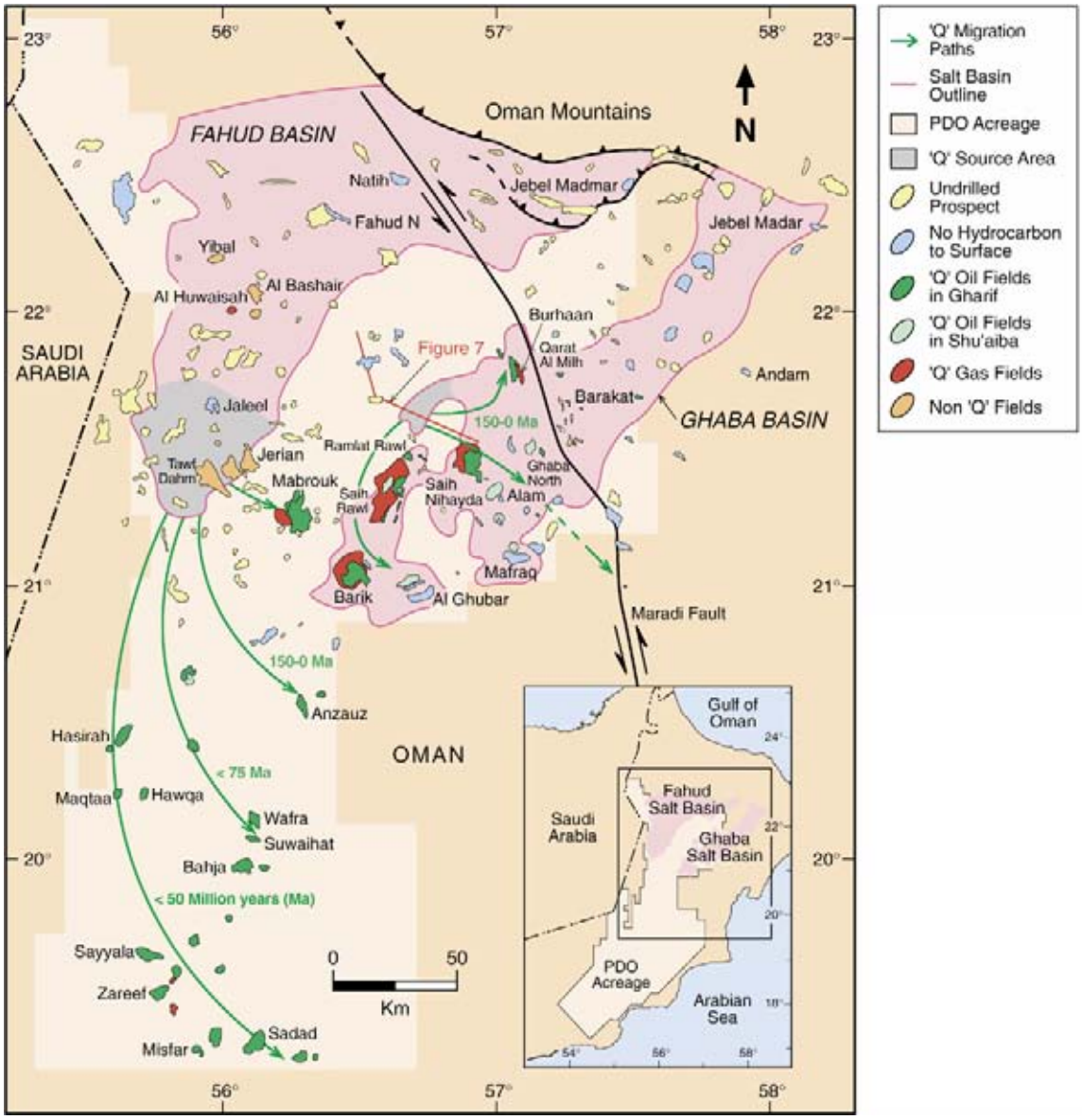

Figure 5.11: The migration distance can be quite large. Here the migration path for the 'Q' oil in Oman is reconstructed and results in migration distances of 150 km or more. Geochemical oil finger printing, with a precise determination of its chemical composition, is at the origin of this reconstruction.

For instance an API of 5–22 corresponds to **heavy oil**, that is rather sticky and difficult to move in the reservoir. An API of 23–30 represents medium oil, and a value above 31 corresponds to **light oil** and condensate (Sheriff 2002). The latter are easily producible because it behaves like a gas in the reservoir and little refinery costs are needed for cracking the hydrocarbon chains in shorter elements.

The composition of the hydrocarbons, accumulated in a reservoir, can also be altered. Gas is produced from oil at very low formation temperatures due to **bacterial degradation**. If the reservoir contains the right nutrients, and is submitted to favourable conditions, bacterial activity within the reservoir is so high that organic components are broken down into ethane and subsequently in methane. The original composition of the oil is drastically altered in this way.

Each sourcerock contains a specific assembly of organic constituents. The hydrocarbons derived from this material have therefore a special composition. Determination of the exact geochemical composition of oil samples can be quite revealing for the origin of the hydrocarbons (Cubitt et al. 2004). This analysis technique is known as **HC fingerprinting** (Figure 5.12). The **chromatogram** reflects the origin of its source rock (Figures 5.13 and 5.14). The presence of various constituants

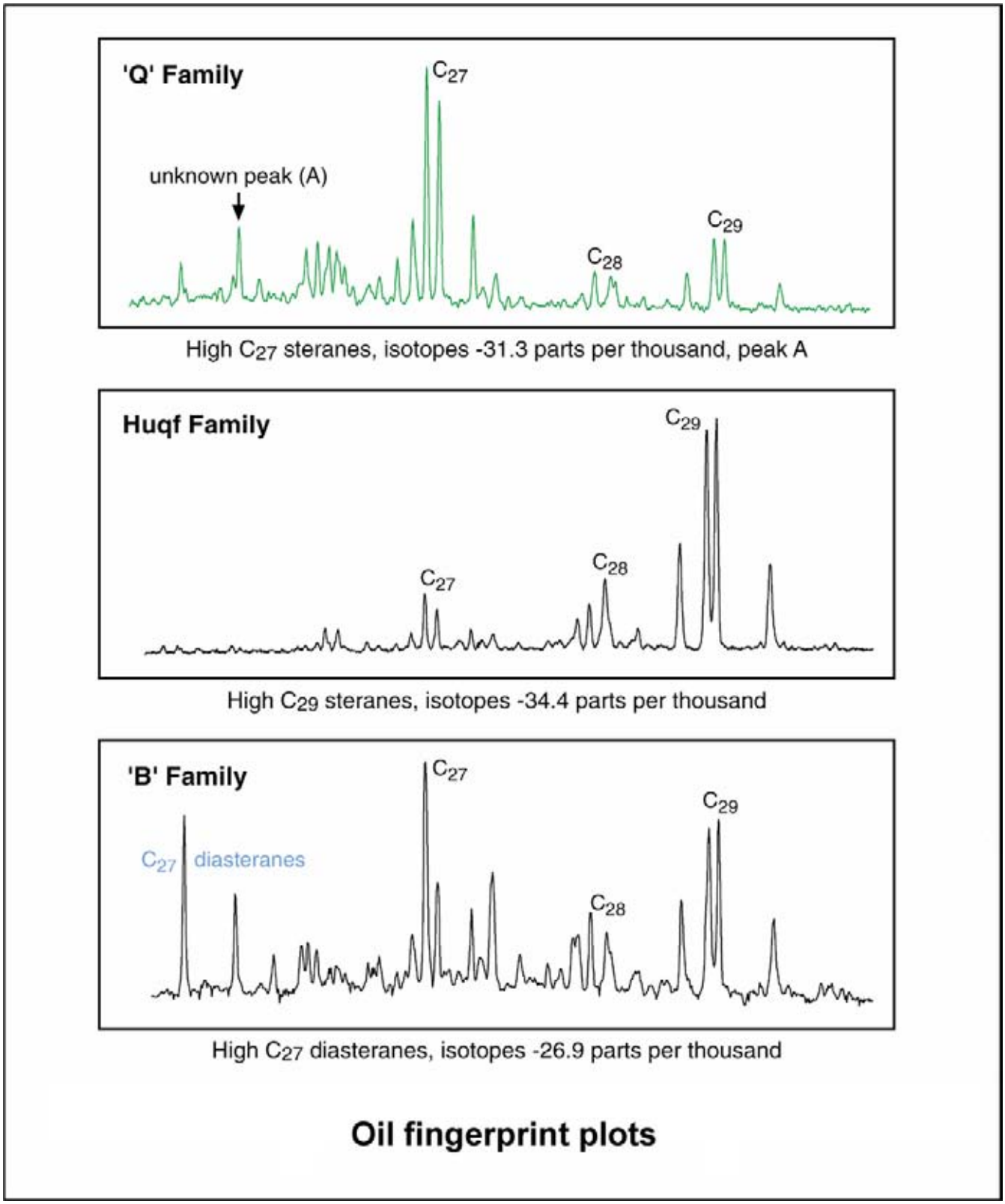

Figure 5.12: The chemical composition of the oil is analysed by using mass spectrometry, gas chromatography and organic carbon isotopes. Each oil has a characteristic composition that is related to the organic compounds in the original sourcerock. The technique to determine the chemical composition is known as oil finger printing. The relation of oils encountered in the various accumulations is established in respect to specific sourcerock intervals (Richard et al. 1999).

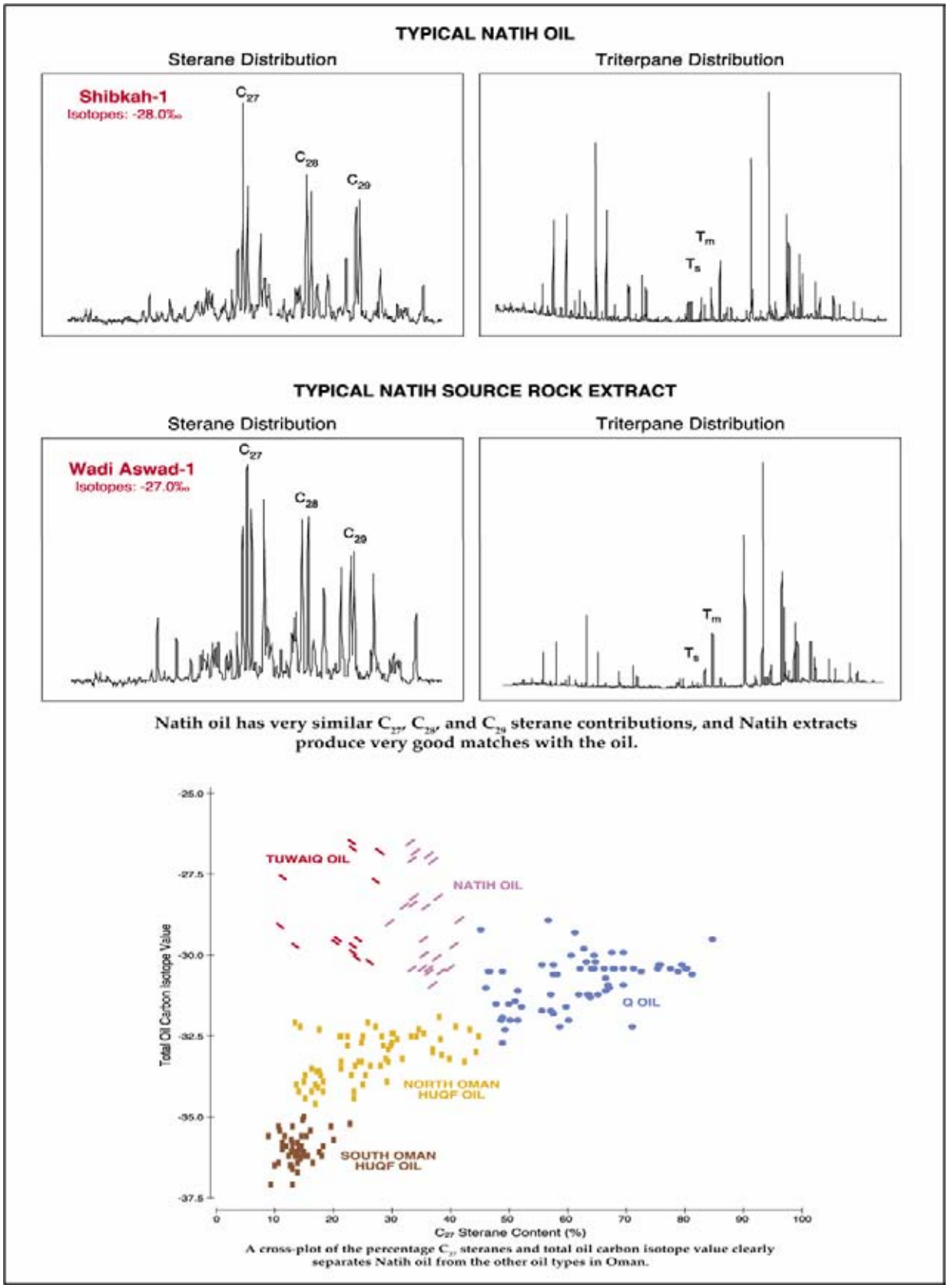

Figure 5.13: The chemical composition of the Natih oil resembles closely the Cenomanian Natih sourcerock in Oman. The composition of other oils is quite different as is shown in the plot below (Terken 1999).

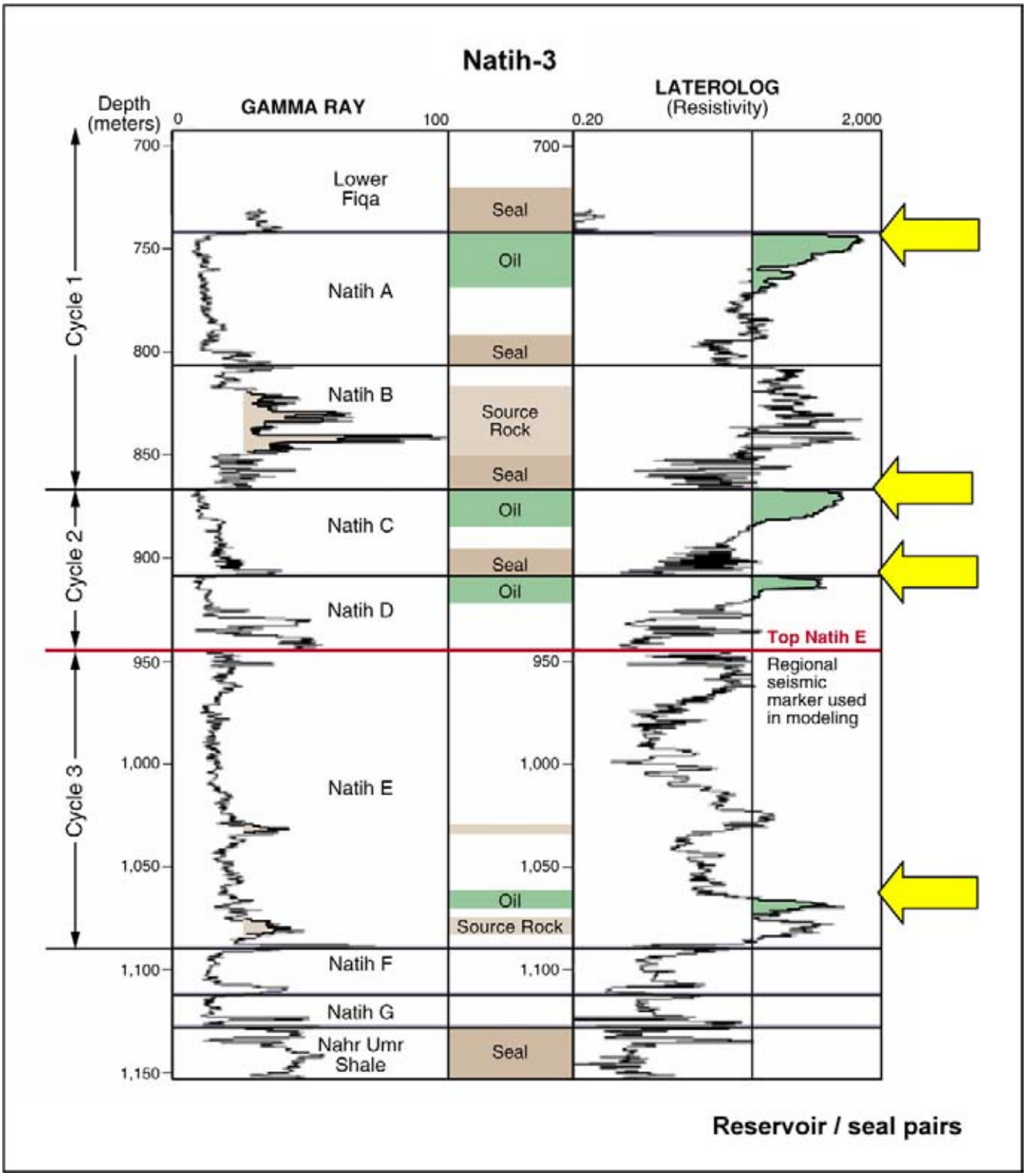

Figure 5.14: High resolution breakdown of the Upper Cretaceous Natih Formation in well Natih-3 in northern Oman. Several source rock intervals are present within the Natih package. Seven lithostratigraphic units are distinguished in the Natih carbonates. The oil bearing reservoirs, seals and source rock intervals are highlighted in the central column. The top Natih E is an important regional seismic marker (Terken 1999).

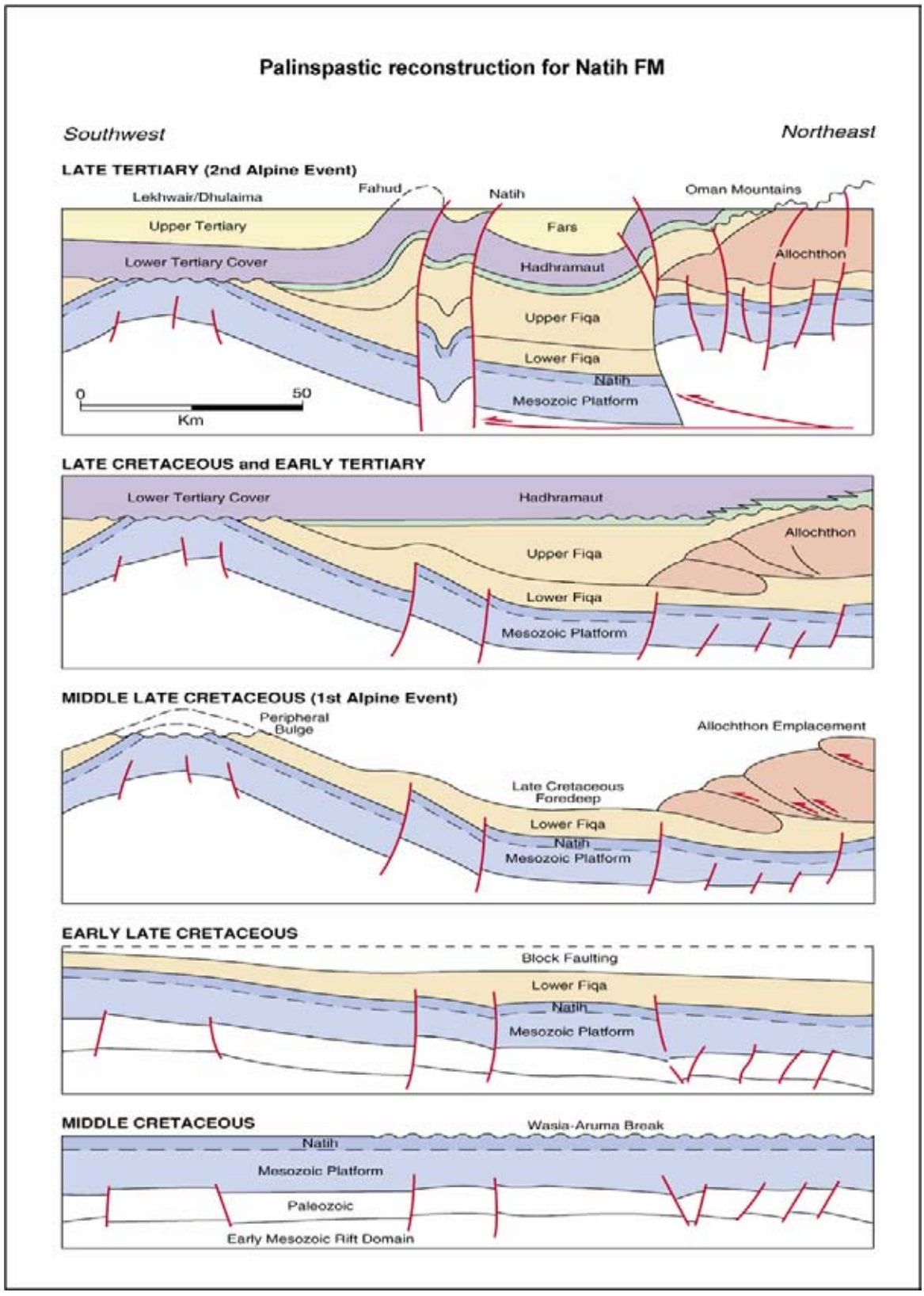

Figure 5.15: Reconstruction of history of the Fahud foreland basin illustrating the deformation of the Natih Formation. Note the topographic relief after the 1st Alpine tectonic event with the creation of a peripheral bulge in response to the ophiolite nappe emplacement in the north. It is unconformably covered by late Cretaceous and early Tertiary sediments (Terken 1999).

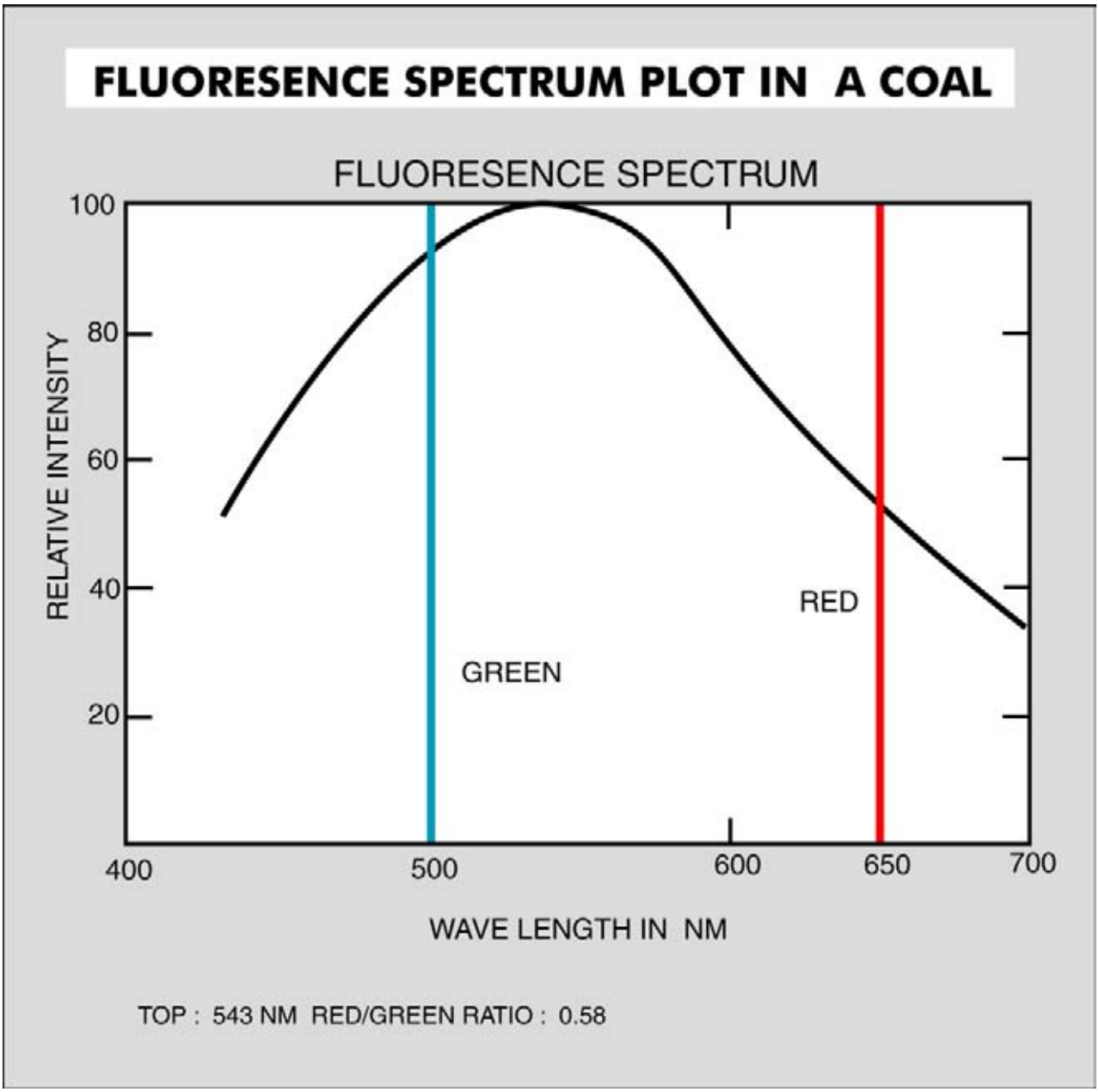

Figure 5.16: Fluorescence spectrum for a coal deposit. Fluorescence is an important tool to detect hydrocarbons while drilling a well. Non-mineral hydrocarbons used in the drilling mud can be differentiated from fossil oil by its fluorescence behaviour. Hydrocarbon shows are important to establish the presence of a nearby kitchen with mature sourcerocks and a migration path. Only a valid trapping mechanism is needed to retain the hydrocarbons.

like steranes, deasteranes and tripertanes are for example useful to study. Oil mixing can be traced in this way. Proper reconstruction of the basin infill history will help in determining the timing of the reached maturity levels and palinspastic reconstructions are handy in this respect (Figure 5.15).

Hydrocarbon impregnated rocks often show characteristic **fluorescence** (Figure 5.16). This fluorescence is found in the source rock interval, along the migration path and in the actual reservoir. This phenomenon enables the geologist and mudlogger to identify more precisely zones of direct interest in and around the well. Oil impregnated rocks normally show up in a yellowish colour. **Dead oil** – traces of oil left behind after migration of hydrocarbons in the pore space and that is irremovable – has a slightly more purplish colour under UV light. It is a very useful feature in tracking down hydrocarbon accu-

mulations. These kind of **HC shows,** prove the presence of a mature kitchen and demonstrate a valid migration path. A special type of HC shows are also known as **geotracers** (phenol and carbazol compounds, Yang et al. 2005). When dealing with high porosity/high permeability reservoir the results of the fluorescence tests should be handled with some care. Testing at the derrick floor is not always representative as flushing of the hostrock by the drilling mud has often removed the hydrocarbons originally present. The drilling mud build-up around the permeable borehole wall is usually known as the **mudcake**. Initially borehole fluids passed through into the formation, but the larger drill mud particles are filtered and clogged together to form the more impermeable mudcake. Some of the mud penetrates into the **virgin formation** and this phenomenon is known as the invaded zone, having particular petrophysical characteristics. The **invasion zone** is important when dealing with good permeability reservoirs and ironically enough these are just about the best targets a geologist can dream off.

Nowadays **under-balanced drilling** (UBD) tries to prevent infiltration of the drilling mud into the pores of the formation and reduces the amount of formation damage around the borehole. Under-balanced means drilling with a borehole pressure gradient that is less than the natural formation gradient. It technically means installing drilling and production facilities at the same time. It requires more efficient planning, but the additional costs are easily offset by the advantages. The extent of the invasion zone around the borehole is reduced and the build-up of mudcake in porous zones is less. Sometimes an inert gas like nitrogen is used to keep the pressure in the drill string extremely low. It is a stable gas and does not react with the formation or the drilling fluid. Nitrogen can be produced by a simple and inexpensive air filtering technique (IHRDC 2004). An advantage is that the invasion by gas particles does not block the pore throats and it preserves the original permeability in the direct vicinity of the well bore, which is much appreciated during the later HC production phase. A certain gas circulation speed in the well bore ensures proper transport of cuttings to the surface. Production testing is on-going whilst drilling and this is new information that was not available to the reservoir engineer before (First Break, Vol. 22, No.1, p. 24). Production improvements up to 500 percent have been reported upon. This N-drilling technique sounds very promising indeed. The initial extra capital investment is easily offset by the gains. The recovery factor is easily increased by this revolutionary drilling method, e.g. Tinker gasfield in Queensland (Australia) operated by Mosaic Oil.

5.1.4 HC plays and the Petroleum System concept

The assembly of the various HC elements like type of source rock, maturation and kitchen area, migration path and trap configuration with reservoir/seal make up a hydrocarbon play (Figure 5.17). In the Mesozoic-Tertiary Macuspana basin (onshore Mexico) several plays have been defined. The stratigraphic column illustrates where sandy reservoirs occur. The seismic section shows the structural deformation and degree of burial of the basinfill (Figures 5.18 and 5.19). Two high areas are seen, which are possible **leads** for hydrocarbon exploration. Leads are subsurface structures that can contain HC's, but further work is needed to mature the mapped closure into a drillable **prospect**. The structure on the right was transformed in a drillable prospect by the interpreter and a well proposal has been written. A **well proposal** is a document that summarises the vital aspects of the geological structure to be drilled and it contains all the proposed drilling/logging procedures. Information from various disciplines is brought together (geology, geophysics, reservoir engineering, petrophysics). The well proposal also presents a prognosis on the rocks expected to be penetrated by the well bore. Extensive volumetric calculations are included on the possible HC reserves. The environmental impact and safety issues form integral part of the report. The proposed well has been drilled successfully and hydrocarbons were encountered in several intervals within the Miocene-Pliocene sequence. The other structure on the left is still untested, but has amplitude anomalies associated with it. It has been matured into a **drillable prospect** with a rather high potential for success. This is especially true because:

- The presence of a mature kitchen with valid source rocks has already been proven by the earlier Macuspana well.
- Presence of multiple reservoir targets further augment its prospectivity. A vertical migration mechanism has to be demonstrated.
- Presence of a local amplitude anomaly (Figure 5.20).
- Associated AI and AVO anomalies.

Drilling of the well has been retarded by its environmental impact and a new deviated trajectory has been devised.

If nothing tangible is known about the prospective structure, it is also called a **green field**. More work is needed to make sure that it is a viable HC project in the later phase of the exploration. A well test in a situation where nothing substantial is known on the geology

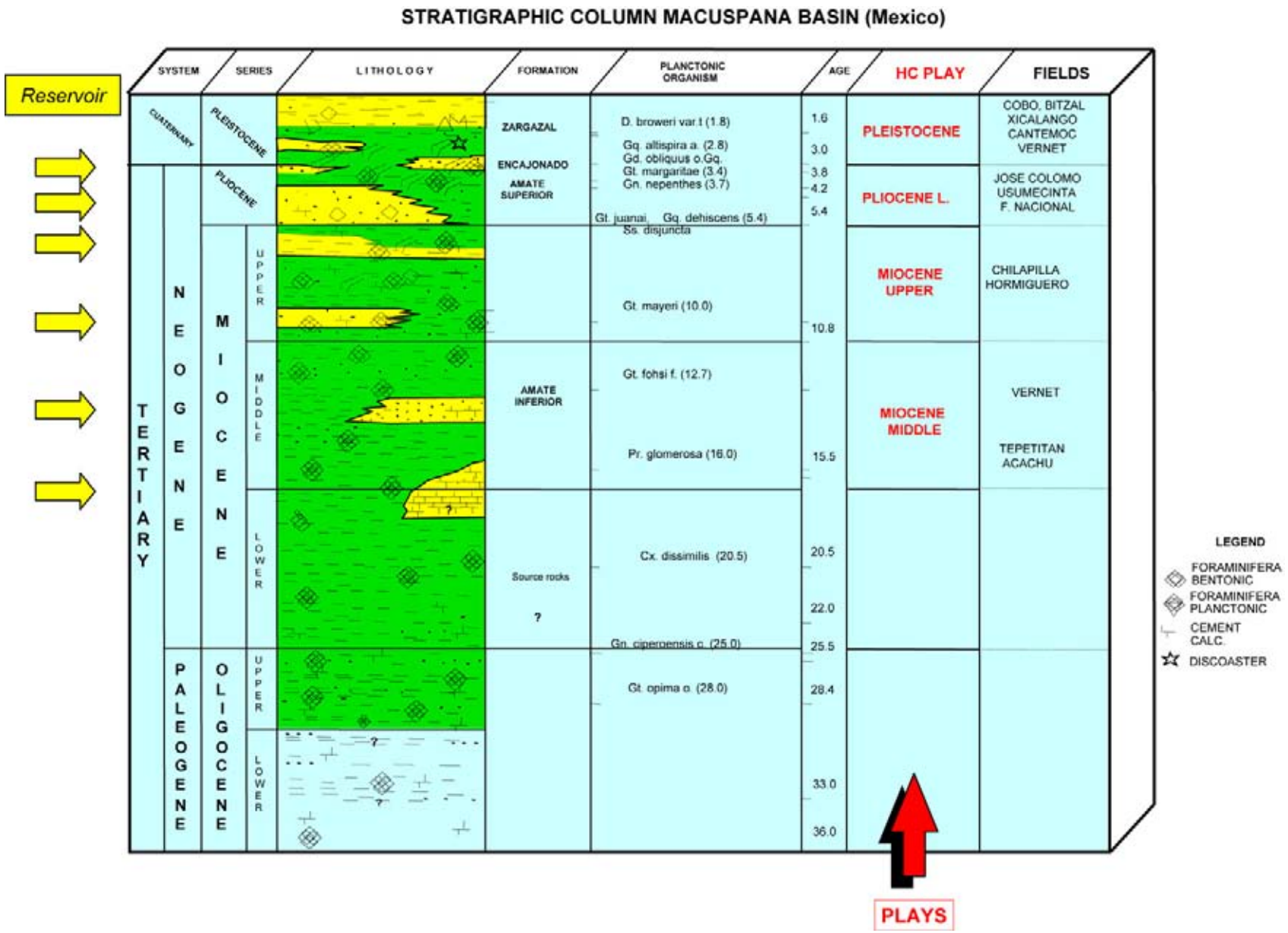

Figure 5.17: Hydrocarbon play concept is made up of several elements: sourcerocks for generating hydrocarbons, kitchen area where the sourcerock is reaching a sufficient maturity level, migration path, reservoir rocks and trap configuration with a seal to retain the expelled hydrocarbons. Here several plays are shown in the stratigraphic column that share the same Mesozoic source rock and kitchen area. Fault zones provide the vertical path way for the charge (courtesy Pemex).

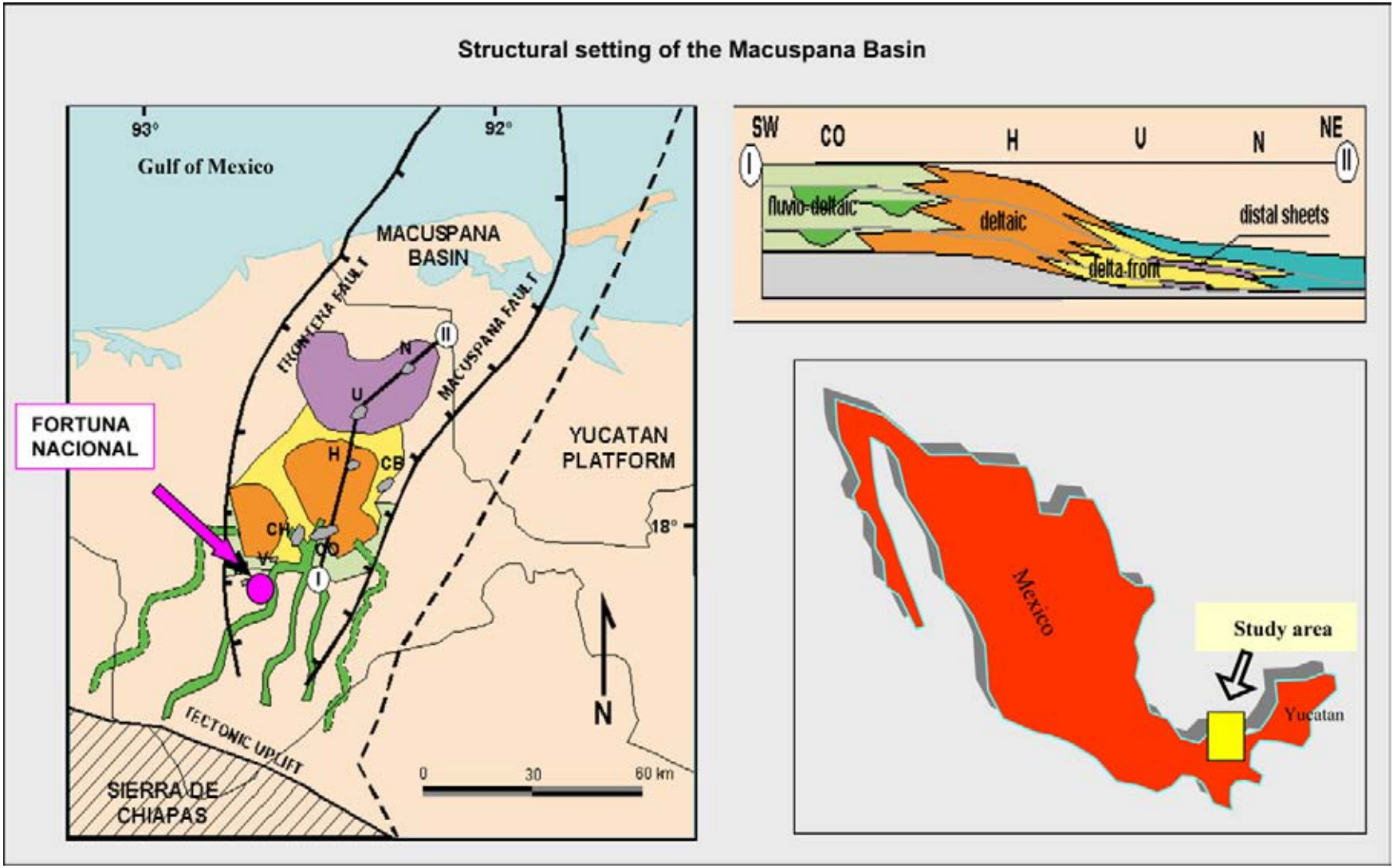

Figure 5.18: The setting of the Mesozoic/Tertiary Macuspana basin (onshore Mexico). The basin is deepening to the north-northeast. Extensional and strike slip movements have shaped the basin, partly in response to the advancing deformational front of the Chiapas trust belt in the south (courtesy Pemex).

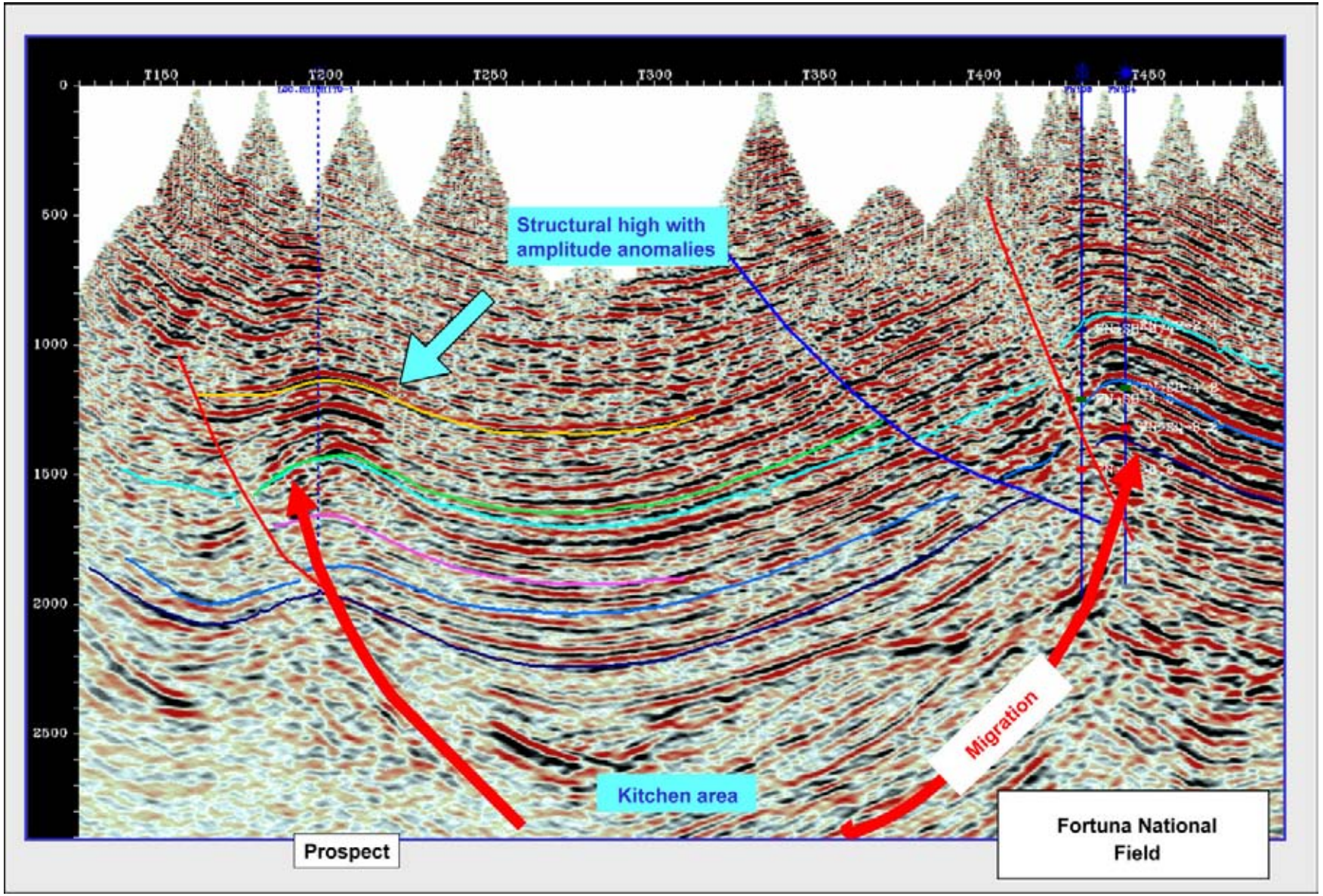

Figure 5.19: Seismic section illustrating the structuration of the Macuspana Basin (onshore Mexico). The two high areas are prospective areas for hydrocarbon exploration. The structure on the right has been tested and contains HC's in the Miocene-Pliocene sequence. The structure on the left is untested, but has amplitude anomalies associated with it. The kitchen is situated in the deeper graben below, in which Jurassic and Cretaceous source rocks are mature (courtesy Pemex).

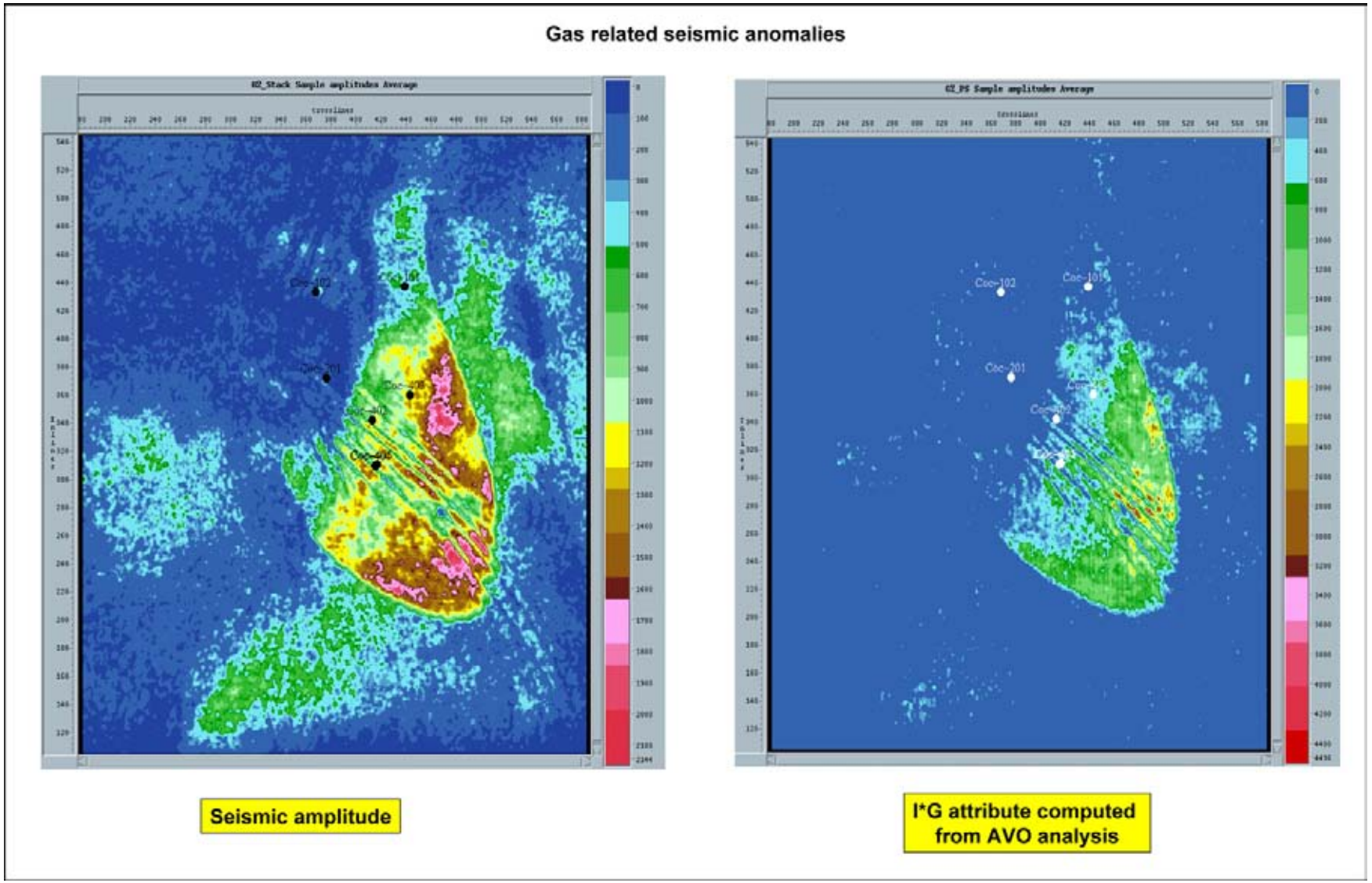

Figure 5.20: The presence of amplitude anomalies help to define the extend of hydrocarbon accumulations and to evaluate the reservoir development. AVO analysis supports here the fluid content model. It reduces the risks in the delineation of outsteps and bypassed zones.

is called a **wild-cat**. This name is chosen because it is difficult to predict the well results beforehand. A cornered cat can make unexpected jumps and the outcome of a wildcat well can be either good or bad. Wild cats are often drilled in **frontier areas**, where little info is available on the prospectivity of the rocks. These frontier areas are new acreage just opened up for HC exploration. In such case the drilling risk is quite high as the HC concepts are still very hypothetical and basically untested (cf Gluyas and Swarbrick 2004). The prospectivity is largely based on analogue situations. The concept of frontier plays also exists; it are HC plays until now not reached by the drill bit (too deep, too high pressure). The frontier exploration stands in contrast to drilling in basins belonging to a proven **hydrocarbon province** (e.g. North Sea, Gulf of Mexico, Caucasus, Middle East).

Surface **gas sniffing** surveys may prove useful to delineate potentially attractive areas. Glasgow University developed with Shell the LightTouch^{TM} ethane sensor (First Break, Vol. 22, No. 1, p. 19). The geochemical technique uses a laser light that emits at the frequency of ethane. The energy gets absorbed by the ethane molecules present in the test-tube and this absorption is detected. Very low concentrations are measurable and subtle anomalies can be detected. Wind speed and direction are recorded simultaneously. It allows the quick identification of zones of increased interest. The presence of hydrocarbons is detected even at several kilometres from the station. Ethane is used because it is not as abundant as the biological end product methane and it has very low background values. Petrobras has used similar techniques successfully in the Amazonas in the early 1990's to obtain a quick inventorisation of prospective structures. Even seabottom sniffing can be performed.

The petroleum system concept (Doust 2003, Kingston et al. 1983, Magoon and Dow 1994) is important for taking advantage of similarities in HC plays in different geographical locations (Figures 5.21 and 5.22). A petroleum system can be defined as all those geologic elements and processes that are essential for HC trapping and an HC accumulation exists (cf Metwalli and Pigott 2005). A petroleum system contains a set of hydrocarbon plays that have some basic elements in common. A HC play is defined by:

- Setting.
- Source rock interval.
- Kitchen area.
- Migration path.
- Reservoir sequence.
- Trap formation and configuration.
- Seal.

The play comprises a grouping of HC accumulations, prospects as well as leads. A good description of petroleum systems and the HC plays will allow better comparison of the characteristics found in different basins. It helps in evaluating their HC prospectivity and to establish the potential of less known areas. The existence of analogue situations is a valuable tool in HC development and prediction.

The various elements of a HC play are organised in the following hierarchical manner (cf Doust 2003):

1) Tectono-stratigraphic context.
   Plate divergence or passive continental margin.
   - Early rift with terrigene sedimentation.
   - Syn rift with major marine transgression.
   - Post rift (aborted or drifting stage).

   Plate convergence or subducted oceanic margin.
   - Tectono-sedimentary loading (foreland basin).
   - Wrenching.
   - Collision stage (back arc basin and accretionary wedge).
2) HC charge.
   - Source rock type.
   - Migration path.
   - Kitchen area.
   - Maturity history.
3) Reservoir/seal.
   - Non-marine clastics.
   - Deltaic, fluvio-marine or transitional clastics.
   - Shallow marine shelf clastics.
   - Deep water clastics.
   - Shallow marine shelf carbonates.
   - Deep marine carbonates.
   - Other.
4) Trap configuration.
   - Dip closure.
   - Fault-dip closure.
   - Stratigraphic pinch-out.
   - Other.

It has been noticed that the fill of sedimentary basins can be subdivided in several phases during its tectono-stratigraphic development. These phases allow to distinguish the various petroleum systems from each other. Four basic categories of petroleum systems have a clear relation to source rock development (Doust 2003):

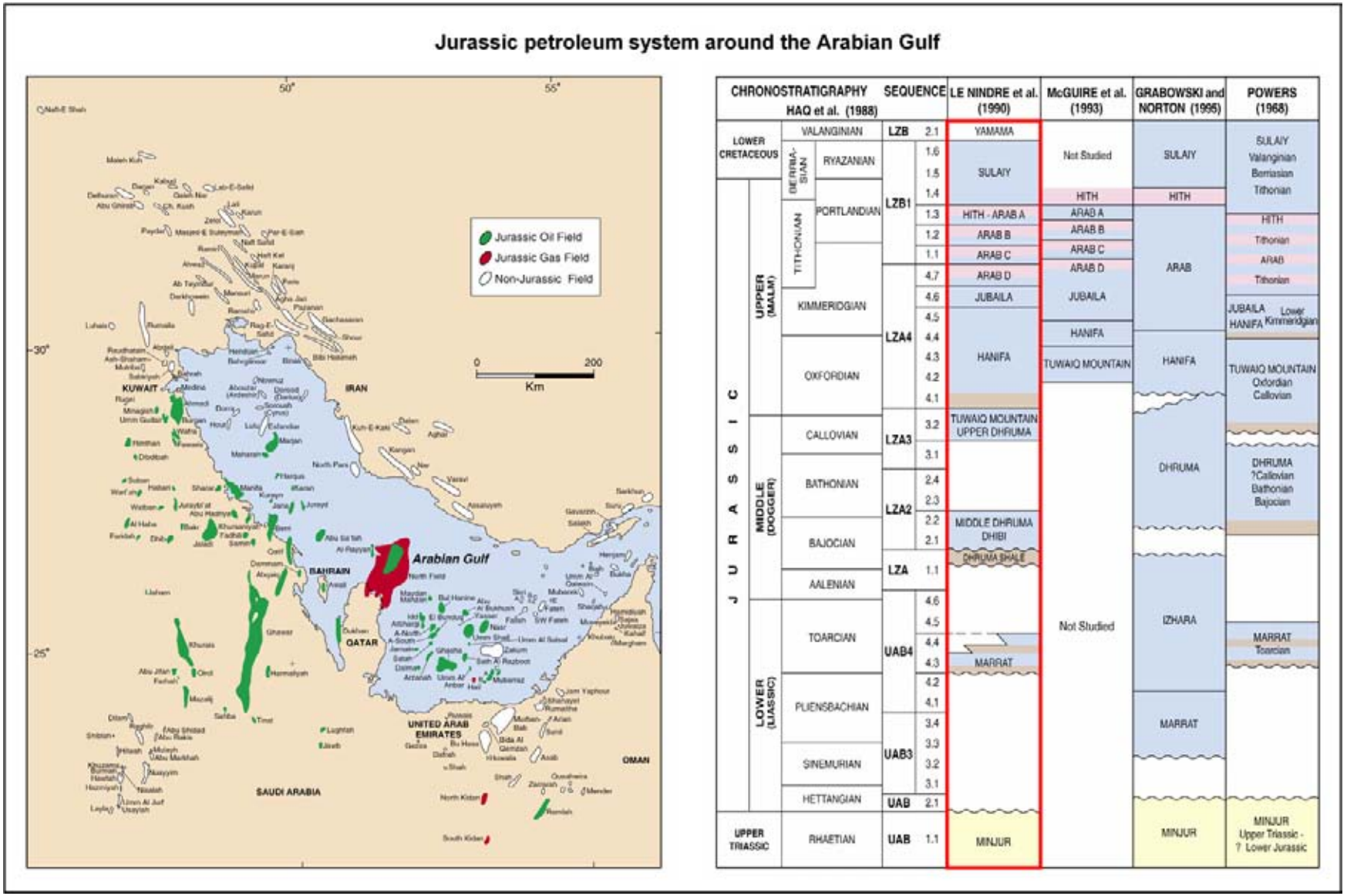

Figure 5.21: The Jurassic petroleum system in the Arabian Gulf. The Jurassic hydrocarbon accumulations are coloured that are charged from Jurassic sourcerocks. Several HC plays are grouped within the petroleum system. The chronostratigraphic succession for Central Saudi Arabia is shown on the righthand side. Yellow: sandstone, brown: shale, blue: carbonates and pink: anhydrite/halite (modified after Al Husseini 1997).

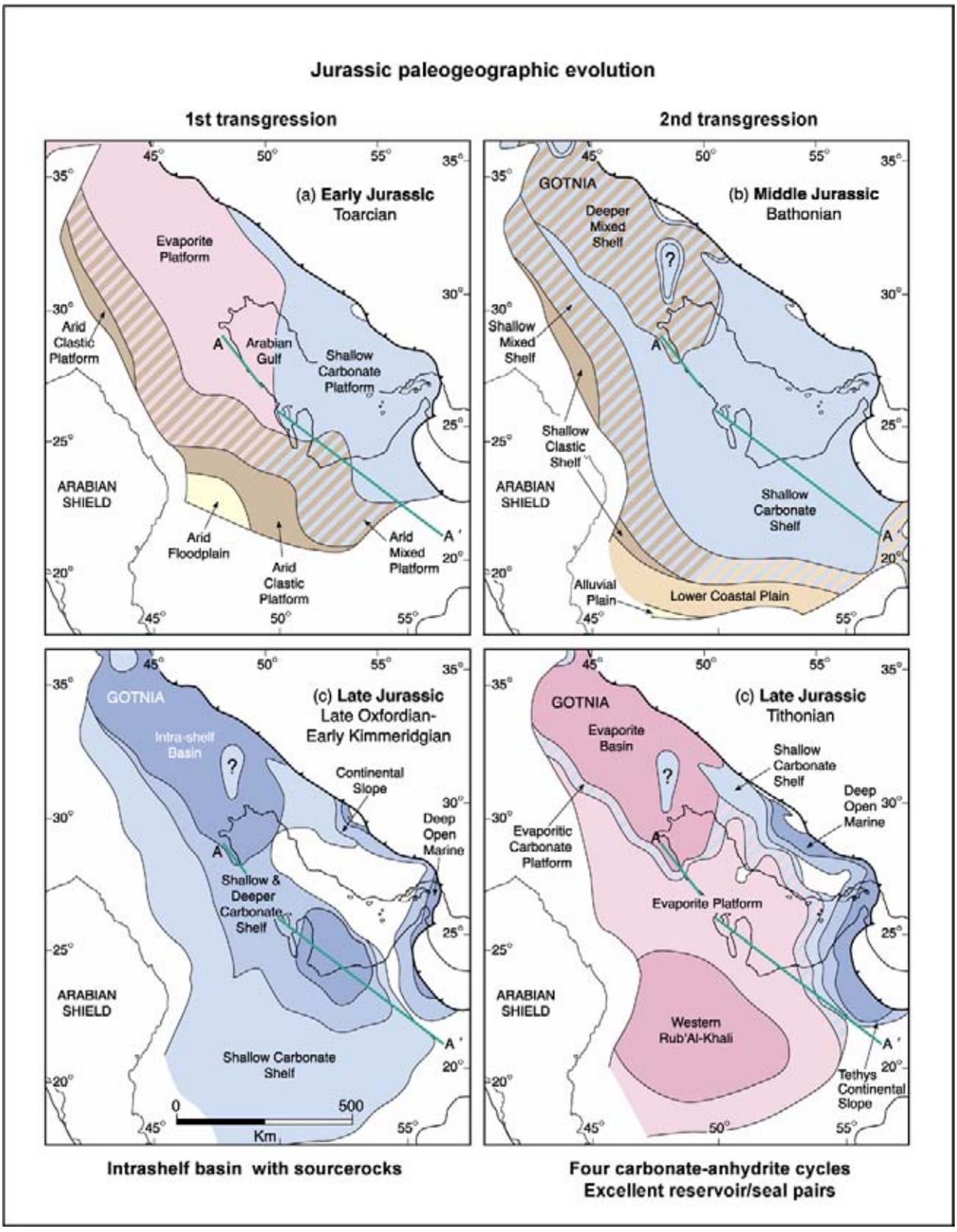

Figure 5.22: Jurassic paleo-geographic evolution in the larger Gulf of Arabia region with post rift sedimentary cycles. Two transgressive cycles are followed by a subsiding intra shelf basin and four carbonate/anhydrite cycles (modified after Al Husseini 1997).

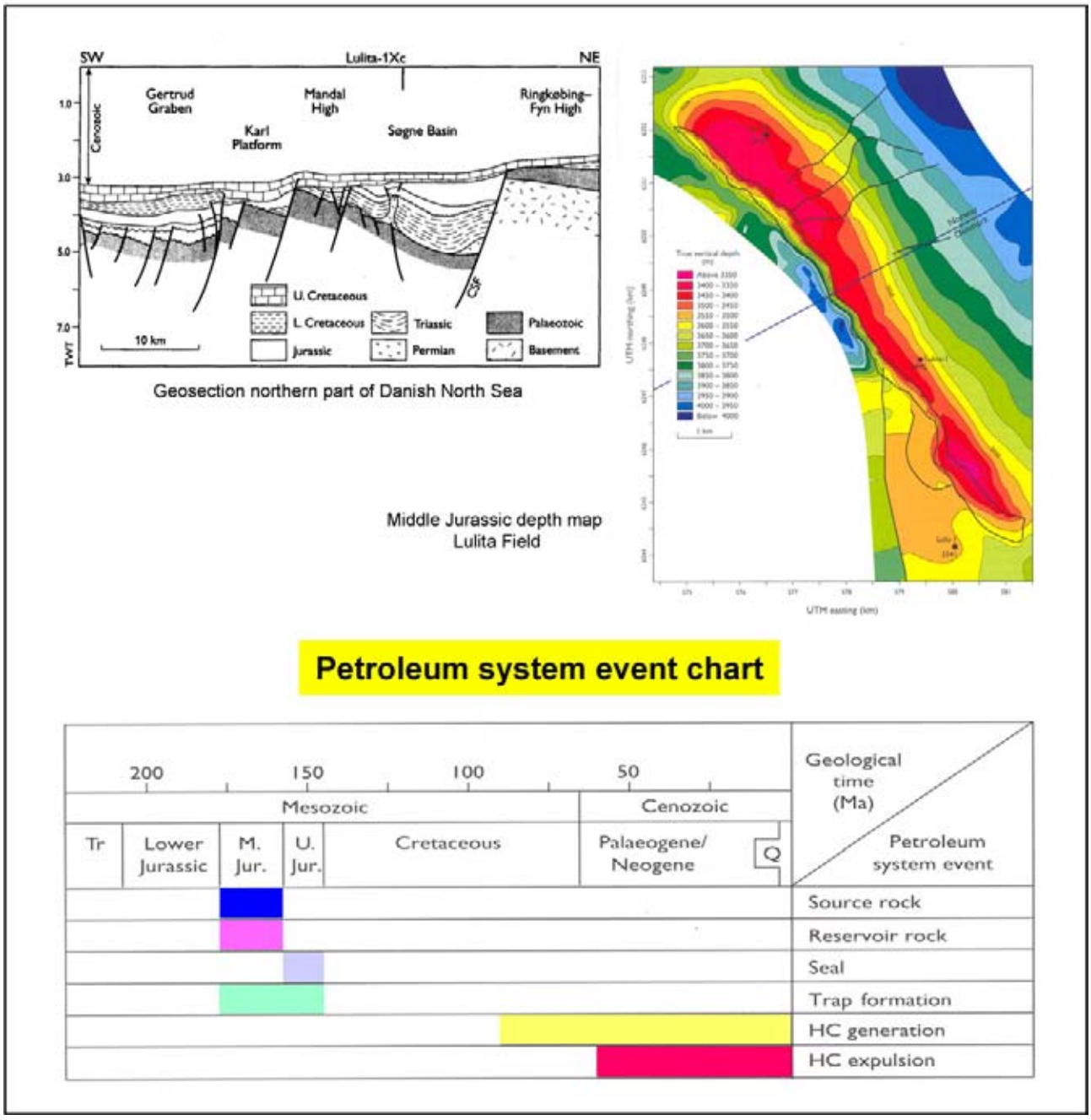

Figure 5.23: The concept of the petroleum system provides a frame for comparison from basin to basin. Systematic evaluation of PS events are very valuable to appreciate various play concepts and will make the identification of prospects more efficient (modified after Car and Petersen 2004).

- Early syn-rift lacustrine system with Type I/II source rocks.
- Late syn-rift with transgressive deltaic systems and Type II/III source rocks.
- Early post-rift marine system with lean Type II/III source rocks.
- Late post-rift regressive deltaic systems with rich Type II/III source rocks.

These basic petroleum system types are easily recognised in the poly history basinfills seen on seismic data. Their systematic delineation and inventorisation will assist in the proper evaluation of the HC prospectivity of basinfills (Figure 5.23). Burial modelling, based on the

reconstruction of the thermal and maturation history, helps to gain an understanding of the hydrocarbon potential of sedimentary basins (Makhous and Galushlin 2004). The following petroleum system criticals are import to consider (Metwalli and Pigott 2005):

- Source generating volume in kitchen, with variables size, distance from reservoir, permeability of its contents (expulsion related).
- Source rock richness.
- Source rock quality and type.
- Source rock maturity.
- Reservoir rock volume.
- Reservoir rock quality permeability, thickness, lateral extent.
- Reservoir rock hydrocarbon type, with richness liquid and/or gas/oil GOR, API, shrinkage factor, HC saturation.
- Reservoir rock seal and closure, with spill point, permeability barriers, multiple migration events.
- Flux of migration pathway, with source expulsion efficiency, migration conduit, effective permeability and viscosity of fluid/gas, pressure differentials, rates of flow.
- Timing of all above mentioned petroleum system criticals.

Evaluation of a petroleum system is an iterative process of model building, examination, updating and validation. In the modelling there are two types of variables to consider: those that depend on spatial dimensions and those depending on processes and rates.

5.2 Structural Mapping and Interpretation

Mapping of time horizons is one of the main goals of seismic interpretation. The time horizons need to be depth converted and possible HC traps are outlined (Figure 5.24). The reservoir volumetrics are calculated and ultimately an estimation of the recoverable reserves is made.

The structural mapping can be done on 2D paper sections, but nowadays 3D seismics is much more common. Data from 3D surveys are loaded on a seismic workstation like Charisma^{TM} or Landmark^{TM}. The picked horizon data are stored in **grids** and contour maps are made to illustrate the structuration (Figure 5.25). The fault pattern on a 3D survey is much better resolved than on 2D data (cf Yilmaz 1987, Ruijtenberg et al. 1990). Erroneous line ups are less frequent, but there is still an interpretational element especially in poorer data zones.

Faults are an important structural element for defining a HC trap configuration. A proper understanding of the mechanism behind the tectonic deformation will help the interpreter substantially. Faults can be normal, with a positive separation between the footwall and hanging wall block, or reversed. Which type of faulting is prevalent, depends on the stress pattern. **Normal faults** are caused by extensional conditions (rifting), while **reversed faults** are the product of compression. **Strike slip** deformation is intermediary; it can be either trans-pressional or trans-tensional. There exist a basic relationship between the displacement and dimensions of the normal faults (Walsh and Watterson 1988) and this can help in establishing a realistic fault pattern. It depends on the maximum fault offset, the length of the fault and the material that is deformed:

$$\text{Maximum fault throw} = C \cdot (\text{Maximum horizontal length})^2.$$

C is a constant depending on the deformed material. Sand box modelling is helpful to understand timing and spatial development (4D) of a fault pattern (Marchal 1997). With ongoing deformation individual faults will tend to connect up with each other and form a long composite fault plane with lateral offset variations. This connection phenomenon partly explains the irregular fault traces seen on 3D seismic surveys. Good natural examples of fault patterns are also provided by crack development in ordinary pavement tarmac.

Information on X, Y points with multi values for the Z is problematic to deal with. It is not straightforward to map reversed faults and overhangs on a conventional workstation. In the past it was customary to follow the high position as far as possible and jump to the low position vertically down, thus ignoring the overlap geometry. Alternatively a segment approach was chosen. The Gocad^{TM} software package handles these kind of geometries rather well. Full integration with geostatistical algorithms, facies recognition capabilities, geological model building and volumetric simulation options, makes it a powerful platform.

The **shared earth model** is a great step forward. It contains a structural model (horizons and faults), that is used to compute a stratigraphic grid cell volume. This grid cell volume is filled with several property models (velocities, permeabilities, net/gross, etc.; De Beukelaar et al. 1997). The DSI technique is therefore deployed (Mallet 2002). The necessity for a stratigraphic grid volume is not strictly needed as the triangulated surfaces

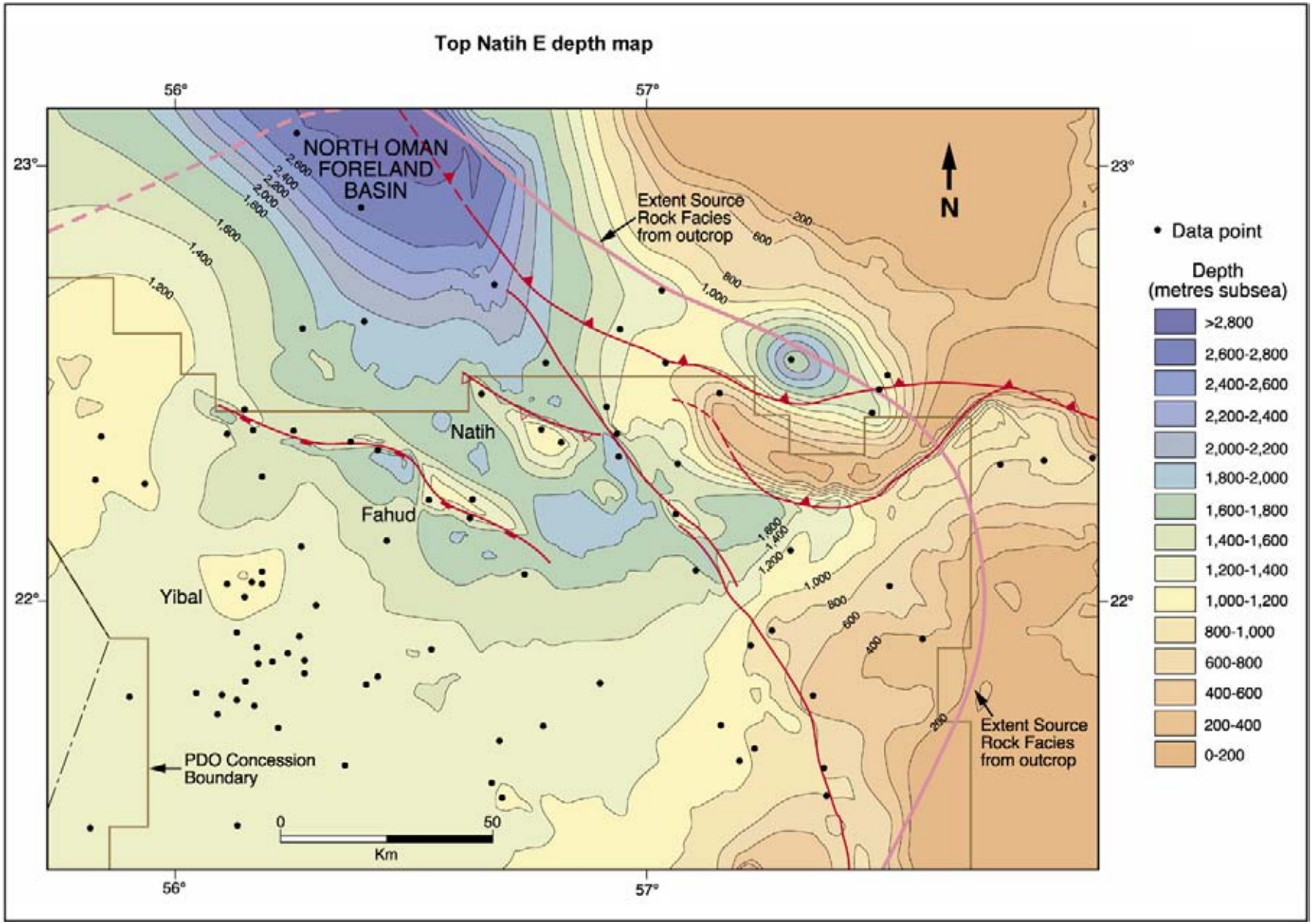

Figure 5.24: Depth map of the Natih E horizon that belongs to the Upper Cretaceous petroleum system in Oman. Sourcerocks and seals are contained in the Natih Formation (Terken 1999).

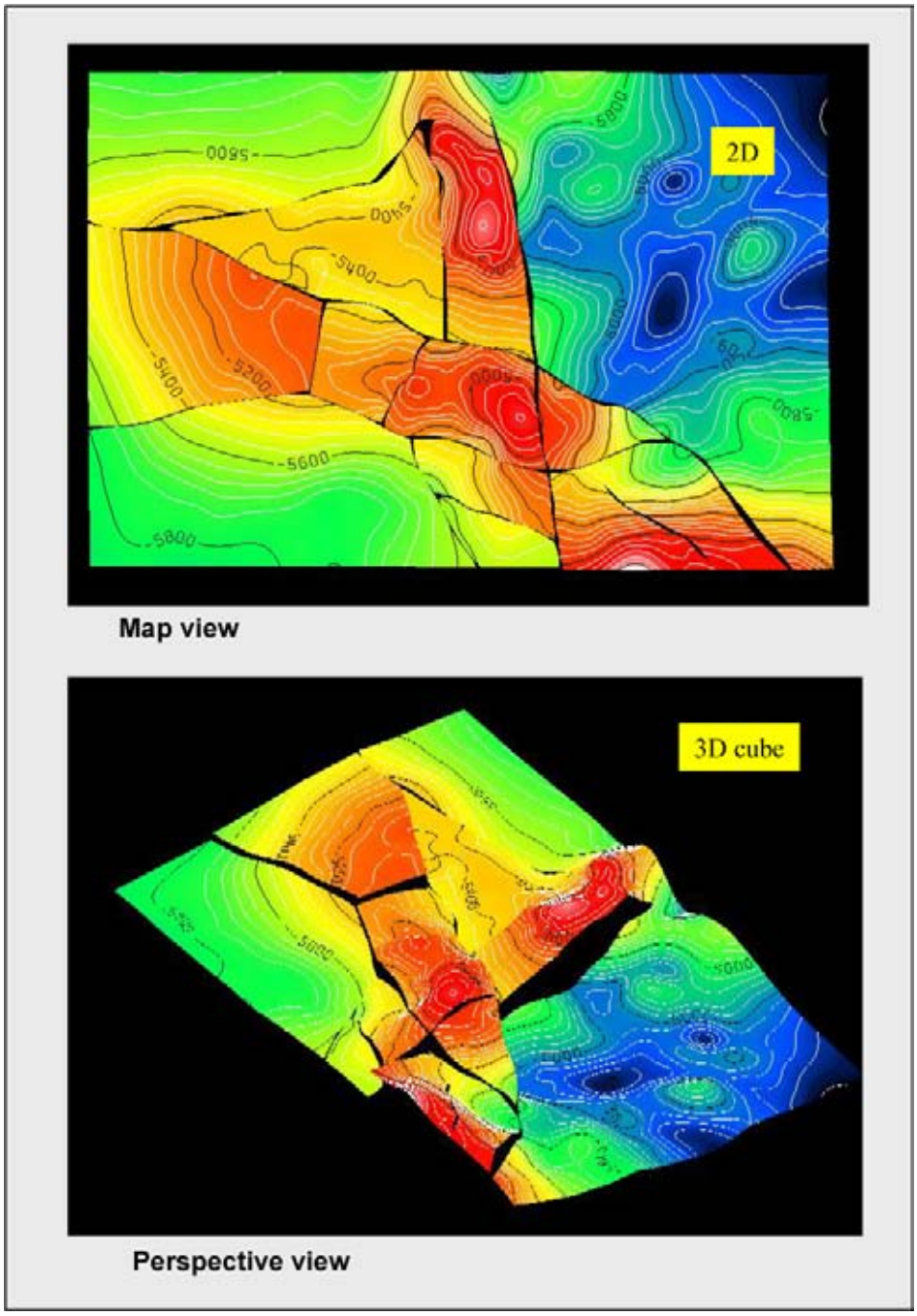

Figure 5.25: Map view of seismic horizon data. The contours follow the two way traveltime values of the traced reflection. It is interesting to study the shape and volumetrics of the high areas (smaller TWT values).

define a tetrahedral mesh that can be used straight away for the property definition (Mallet 2004). All modelling involves some kind of simplification. The tetrahedral approach is however more flexible and more accurate than the stratigraphic grid. This triangulated mesh is transformed in a **geochron** cell volume (Mallet et al. 2004). The shared earth model makes the static reservoir concepts suitable as input for dynamic simulations. It can reduce the risk attached to exploration and production targets (Lopez et al. 2004).

The **atomic mesh** technique is an other example of an interactive volumetric description procedure (Purday and Benefiel 2004). It produces a sealed structural framework, filled by polyhedrals of various shapes, for input into reservoir modelling and simulation packages. Up-

scaling is always a delicate problem that should be addressed carefully.

Lasseter and Jackson (2004) recommend a ***XY*-orthogonal truncated grid**. It uses the seismic bin as the XY starting mesh. The grid cell volume is build by vertical hexahedrals complemented by polyhedrals around faults, that correspond to truncated hexahedrals. This approach allows the use of a consistent model from seismic interpretation in reservoir simulation. It is an extension to the POSC multi-block methodology. However, let's not dwell too far from our subject and have a closer look at the mapping of horizons and horizon computations.

5.2.1 Gridding and contouring

The concept of a grid is important for the contouring of a seismic horizon. The **grid** is an assembly of regularly spaced sampling points arranged in such a way that it allows easy retrieval by the computer. The grid file has a special format and is defined by:

- Its origin.
- The increment.
- A listing of the data values.

In this way it is not necessary to store the X and Y coordinates of each individual datapoint. The grid cells can be square or rectangular (Figures 5.26 and 5.27). Grids with similar origin and increment can be used in horizon computations and this is an option as will be shown later on (cf Davis and Mc Cullagh 1974).

A grid can be rotated with respect to the N-S axis. The azimuth angle is expressed in degrees or radians. The conversion is done with the following formulas from radians into degrees:

$$AZ_{\text{degrees}} = \frac{180}{3.141592654} AZXaxis_{\text{rad}}. \tag{5.9}$$

And from degrees into radians:

$$AZ_{\text{radians}} = \frac{3.141592654}{180} AZXaxis_{\text{degr}}. \tag{5.10}$$

In contrast to grid data there exist also scatter data or point set data (Figure 5.28). Scattered data is non-organised data in the X–Y domain. The ASCII format of the computer file contains for each point: a X-coordinate, Y-coordinate and attribute or Z value. The Z-value can represent any kind of entity: time, depth, velocity, amplitude, etc. The scattered data is normally gridded to enable horizon computations. The pointset data is approximated by a regular grid format. The grid has ZNON (no Z-value) values where a grid value can not be assigned based the criteria of the gridding algorithm. The algorithm is the procedure followed for the filling of grid cells with values. There are various ways to achieve the gridding of scatter data points:

- **Nearest point** takes the value of the point nearest to the **grid cell** centre. Values are never extrapolated beyond the extremes in the data set.
- **Weighted average** takes into account the distance of the data points to the grid point with a certain weighting factor. It does not take into account the curvature between control points. No values are possible beyond minimum and maximum of data control points. The control points are often selected by searches in circles that are divided into segments. A minimum number of data points is specified for the segments in order for the grid point to be filled.
- **Least square** fits a local least square error surface through the control points. This algorithm takes into account local trends in the data and extrapolates the values. The closer control points have more influence in the surface fitting procedure (distance weighting).
- **Kriging**, whereby geostatistics and variograms are used to fill the grid cells. Several options are available (see Section 5.2.2 below).

In some cases it might be handy to perform an automatic refinement of the grid increment whilst doing the grid value calculation. This approach speeds up the gridding process considerably, especially when dealing with large datasets. Fault compartments should be respected by the algorithm in order to get more accurate grids.

There are different types of gridding procedures depending on the geometry of the input data:

- Point gridding.
- Line gridding (semi-organised).
- Contour gridding.

Gridding parameters should be selected carefully as wrong settings in the algorithm will lead to distortion of the surface that is being modelled.

The grid manipulations are very powerful features. The possibility to do back-interpolation is useful in constructing correction maps. **Back-interpolation** gives the interpreter the capability to determine at any given XY coordinate the exact interpolated grid value (Figure 5.29). This allows for instance to generate a scatter point file for the differences at the well control points. A new grid is computed from these difference points and

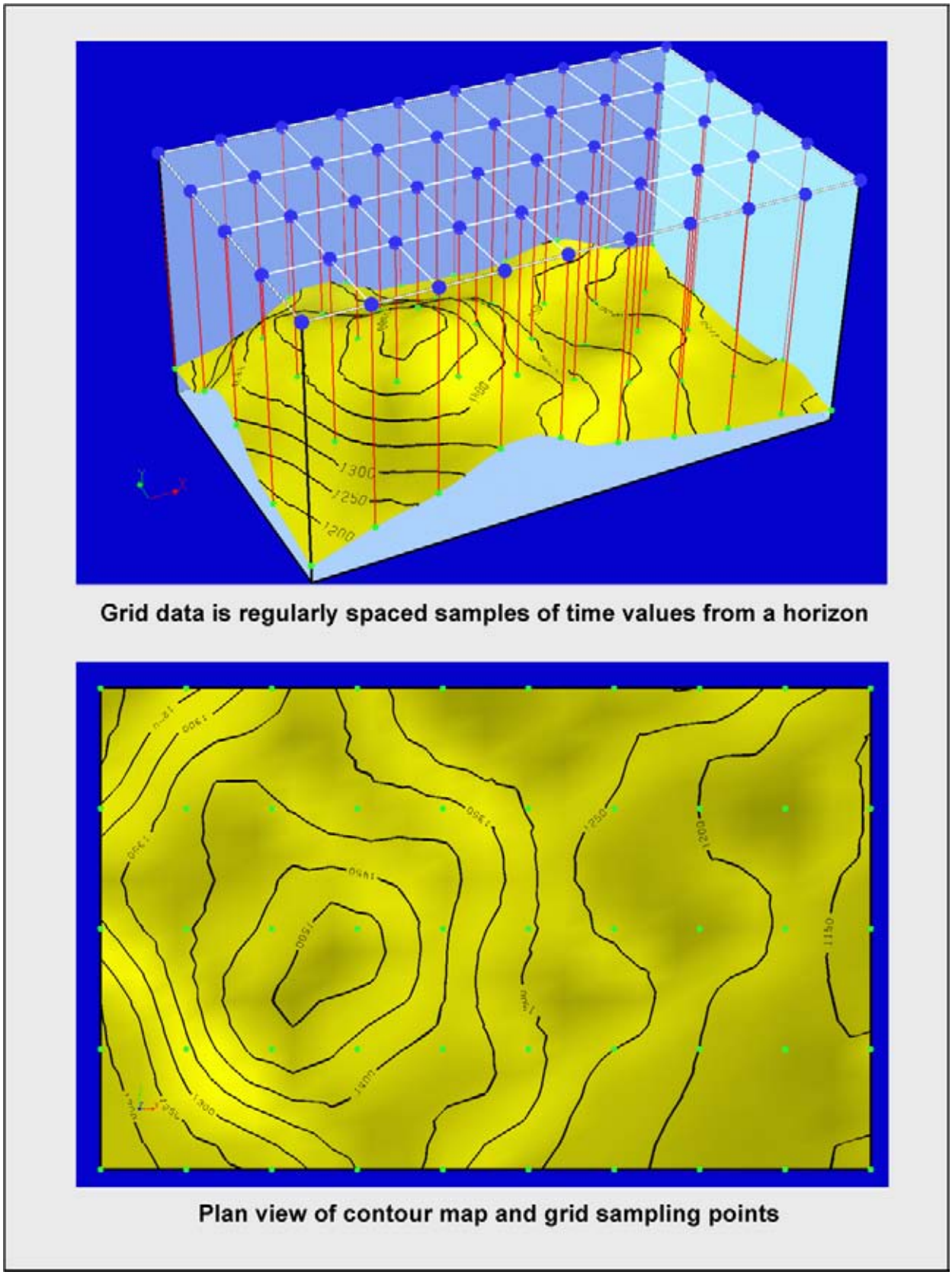

Figure 5.26: A grid is a set of regularly spaced points, defined by an origin with given (X, Y) coordinates and an increment. This file format allows faster computer access than for scatter data or point set data, that is defined by an X, Y and Z-value for each point.

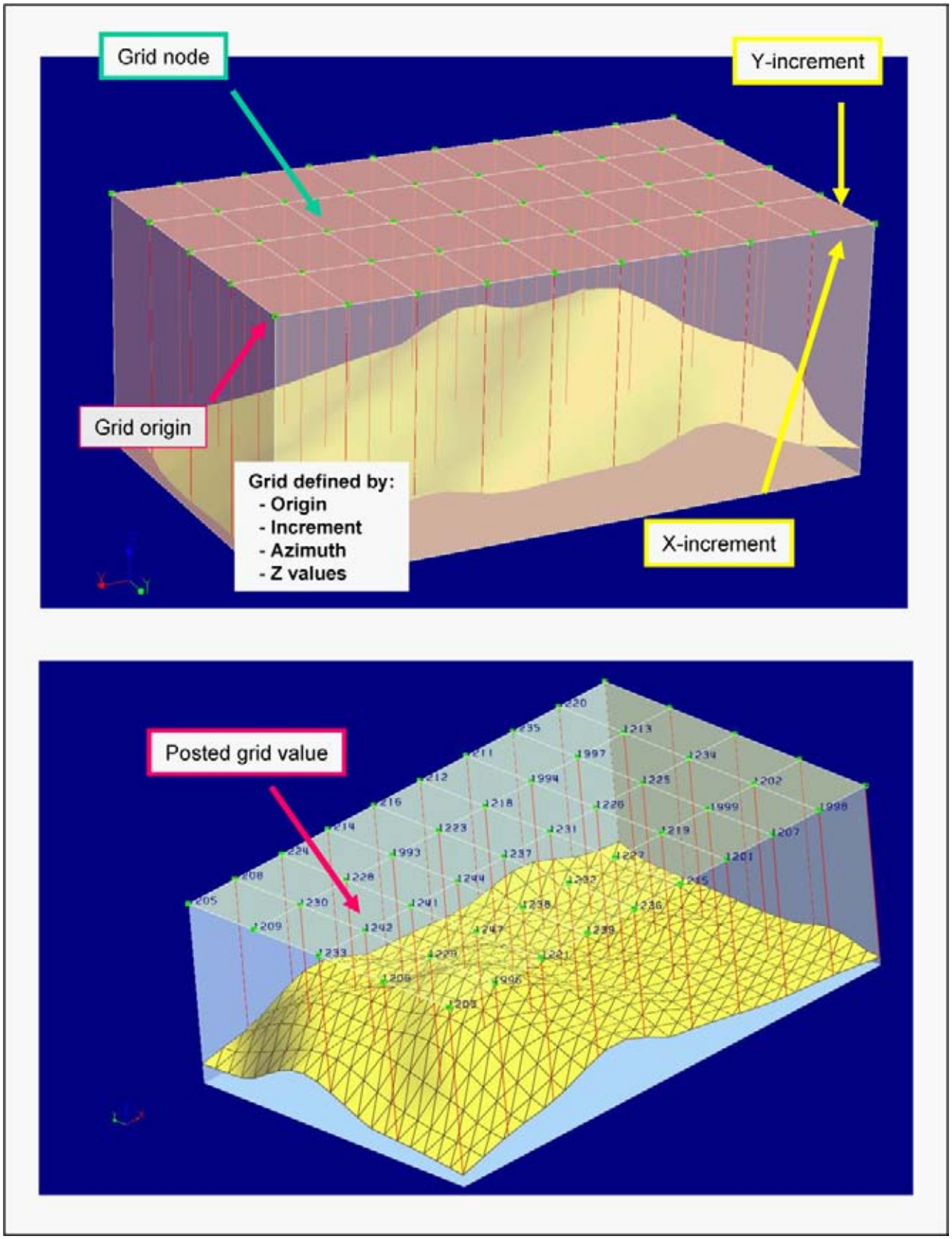

Figure 5.27: A grid is defined by its origin and increment. The grid is made up of regularly spaced grid nodes for which the Z-values are stored. Grid files have a convenient format to facilitate horizon computations (e.g. volumetrics).

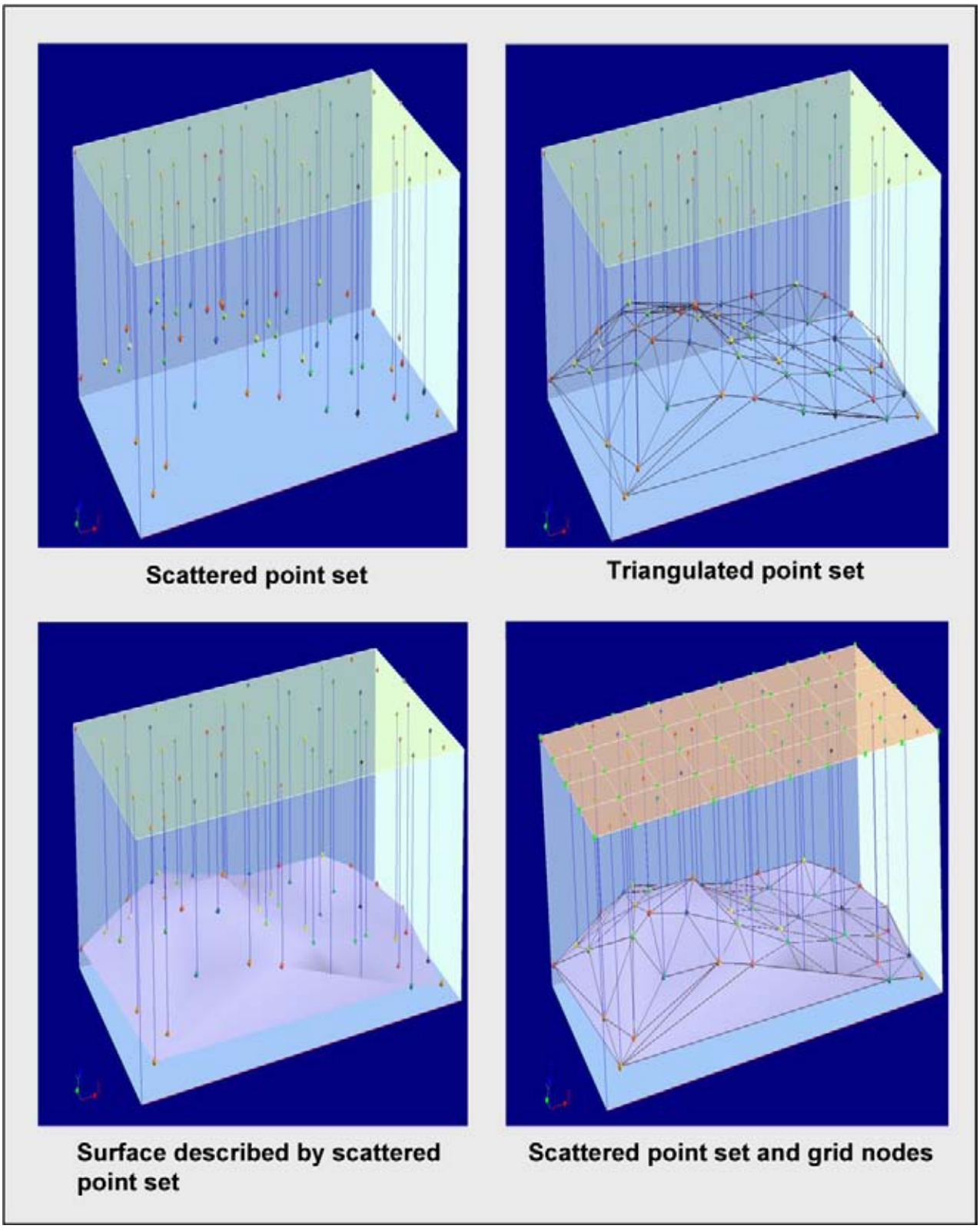

Figure 5.28: Scatter data points are defined by the X, Y and Z-value for each point. Often the data is irregularly spaced in X and Y direction. Triangulation is a method whereby triangles are drawn through the irregular scatter data. The assembly of these triangles describe a complex surface. It is however an approximation of the surface that is being examined. If the triangles are small a good representation is obtained, otherwise large deviations can occur. Gridding transfers the scatter data into a regularly sampled format with an origin and increment (or step). Several procedures are at the hand of the interpreter to perform this gridding operation.

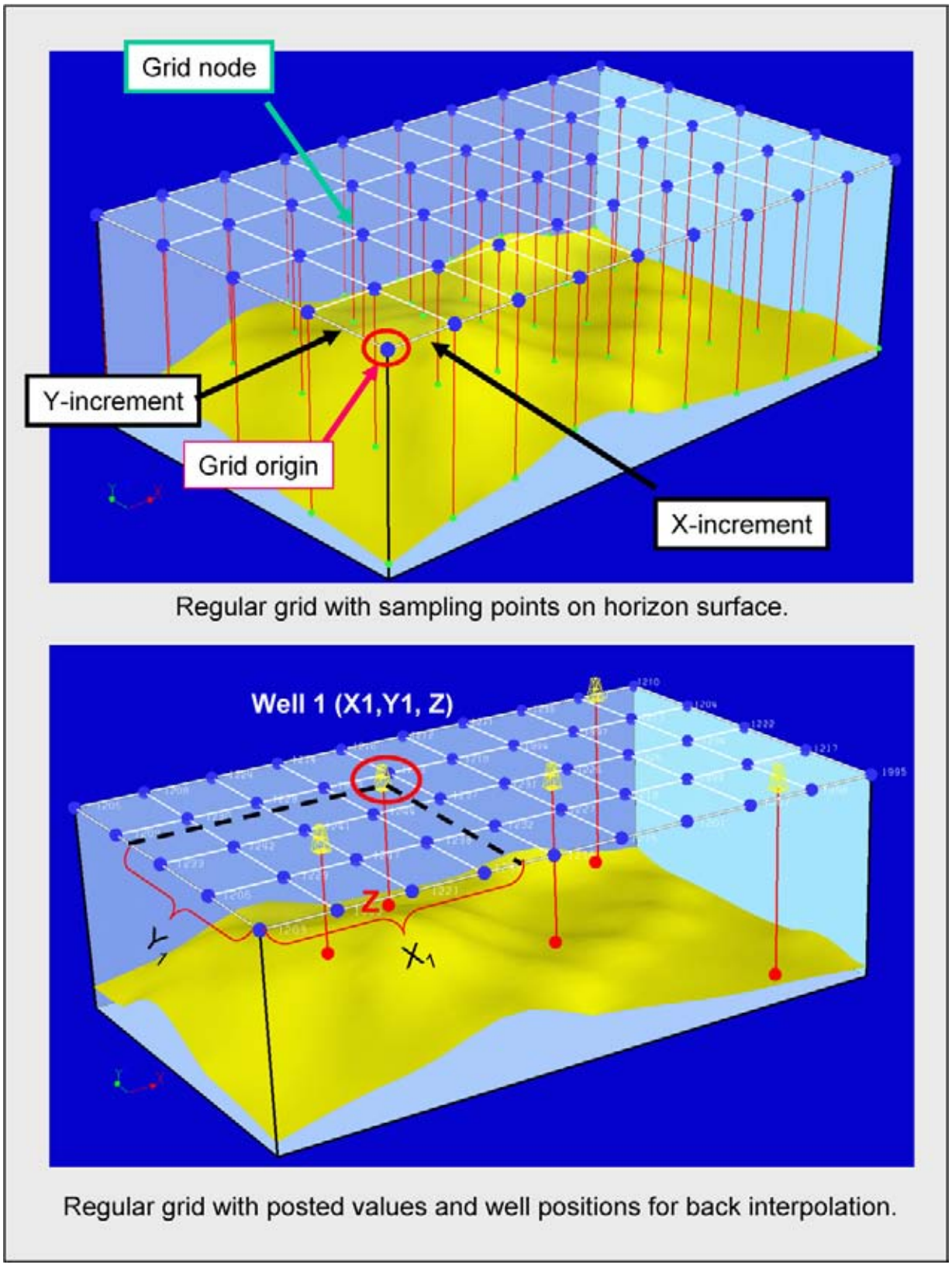

Figure 5.29: Back-interpolation is the procedure that computes the exact Z value of the gridded surface at a specific (X, Y) point. It usually doesn't correspond to a grid node. Here it is shown for a well location. The procedure is extremely useful to establish residual differences and for the computation of correction maps.

applied to the original grid to correct the values. It is an elegant way to ensure that the well values are precisely honoured by the mapping.

Once the contour maps are produced from the grids, it is possible to perform area (2D maps) and volumetric calculations (3D cubes). Graphical displays are made:

- Thickness maps.
- Cross sections and fence diagrams.
- Perspective displays and well correlation panels.
- 3D cube and chair displays.

All this is very helpful in the understanding of the geometry of the data.

5.2.2 Geostatistical techniques

Geostatistics are commonly used in the mining industry to assess the spatial variability of a data set. It exploits the possibilities given by **multi-variable statistics** (Jensen et al. 2000). Unfortunately some basic definitions are necessary to be introduced here; it is not just for the fun of it, but it is useful for the principles discussed later on:

Mean = arithmetic average

$$m = \frac{1}{n} \cdot \sum X_i \tag{5.11}$$

X_i is sample value and n is number of samples.

Median = value of sample so that 50% of population is below this value (Probability 50).

Quantile = value of sample whereby p% of population is below this value. Most commonly divided in 4 groups: $Q1 = 25\%$, $Q3 = 75\%$ probability.

Mode = value that occurs most frequently.

The data is usually visualised in a histogram and a cumulative frequency plot. There are some measures for defining the spread in the population:

Variance = Squared standard deviation

$$\sigma^2 = \frac{1}{n} \cdot \sum (X_i - m)^2. \tag{5.12}$$

Standard deviation

$$\boldsymbol{\sigma} = \sqrt{\frac{1}{n} \cdot \sum (X_i - m)^2} \tag{5.13}$$

Interquartile range $\mathrm{IQR} = Q3 - Q1$.

It is rather unlucky that an other σ unit is introduced here (the sigma is also used for the Poisson's ratio), but the statisticians have chosen this symbol for a long time and their nomenclature should be respected.

There are some parameters to evaluate the shape of the histogram:

Coefficient of skewness

$$\mathrm{CS} = \left(\frac{1}{n} \cdot \sum (X_i - m)^3 \right) \Big/ \sigma^3. \tag{5.14}$$

Usually only the sign of this coefficient is of interest:

positive → high values to the right and median less than mean.
negative → many small values, median bigger than mean.
zero → symmetric histogram.

Coefficient of variation

$$\mathrm{CV} = \frac{\sigma}{m}. \tag{5.15}$$

If the $\mathrm{CV} > 1$ than some erratic values are present in the dataset.

Dealing with bi-variate statistics means that there are two population distributions and hence there are two histograms. A Q–Q plot can be made whereby the quartiles are plotted against each other. Also a simple scatter plot of the data is easily made. The correlation between the two dataset is established:

Correlation coefficient

$$\rho = \left(\frac{1}{n} \cdot \sum (X_i - m_x) \cdot (Y_i - m_y) \right) / (\sigma_x \cdot \sigma_y), \tag{5.16}$$

whereby the term $(1/n \cdot \sum (X_i - m_x) \cdot (Y_i - m_y))$ represents the **Covariance**.

This correlation coefficient is extremely useful in the analysis of the spatial continuity as will be explained below. It is sensitive to the presence of extreme outliers. When the correlation coefficient is:

- Positive, it means large data value in one data set corresponds to large values in the other dataset.
- Negative, it means large value in one dataset corresponds to small values in other dataset.
- Zero means the relation is random.

Linear regression assumes a linear relationship between the datasets in a crossplot. A linear line is fitted through the point cloud, so that the error for all points is minimised in a least square sense. The computed relation is a least square estimate and the individual datapoints should not be situated too far from this regression line. It is dangerous to extrapolate the trend outside the data range.

$$Y = AX + B \tag{5.17}$$

whereby X is known and Y will be predicted.

$$A = \rho \cdot \left(\frac{\sigma_x}{\sigma_y}\right), \tag{5.18}$$

$$B = m_y - A \cdot m_x. \tag{5.19}$$

The **spatial continuity** of the data is now investigated by applying geostatistical techniques (e.g. Haas et al. 1994, Haas and Dubrule 1994). In first instance only one dataset is considered. Sliding dataset statistics are performed by copying the original dataset. In the case when a gridded property is being used, the same sliding vector H is applied to all points, resulting in a directional bulkshift of the dataset. The value v_j at the new position is compared with the value of the original grid point v_i. The degree of variation in the property is examined in a crossplot between the new value v_j and the old v_i. This is a **scatter plot** and it captures the degree of variability of the data in space. If the data is plotting in a straight line, than there is a lot of continuity and the data sets are in fact the same. The shape of the point cloud in the scatter plot is analysed and the moment of inertia around the 45 degree line is measured, as this is a good indicator for the spatial continuity.

The dislocation vector is now being increased in regular steps (or lags) and each time a new scatter plot is made. For each value of H a correlation coefficient ρ_H can be established. The relation between ρ_H and H is called the correlation function or **correlogram.** The correlation coefficient is a measure for the fatness (or spread in values) of the scatter cloud. It is also possible to plot the covariance of H.

A measure for the fatness of the scatter cloud (v_i and v_j) is the so-called "**moment of inertia**" around the line $X = Y$. It is defined by:

$$\text{Moment of inertia} = \gamma_H = \frac{1}{2n} \cdot \sum (X_i - Y_i)^2. \tag{5.20}$$

The crossplot between the gamma and the H is called the **variogram** (Figure 5.30). The H is plotted along the X-axis and has only discrete values. The H is known as the **lag**, i.e. length of the sliding vector for the dislocation in respect to the original dataset. If gamma has a higher value, then the scatter plot gets fatter around the 45 degree line (increased spread).

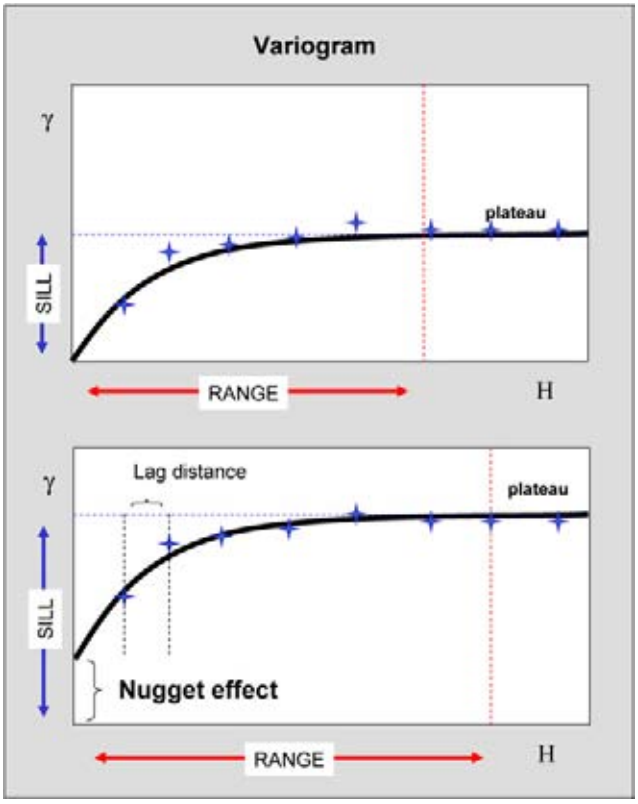

Figure 5.30: A variogram visualises the 3D variation between two datasets. The statistics are calculated on a sliding dataset and the correlation is computed for different offsets or lags (H). A lag is a regular horizontal shift (or step) applied to the dataset with respect to its original position. The spatial correlation is measured by the moment of inertia in the scatter plots for each lag position. The shift is done in a certain direction or several directions can be applied at once. The crossplot between H (offset or lag distance) and the moment of inertia γ is called the variogram. Curve fitting is done to obtain a continuous line that is later used in the prediction procedures. A correlogram is a plot of the difference between the variogram curve and the constant sill value at different lags.

The variogram is a plot of the spatial change of a property as a function of the separation distance. Points close to each other usually have only a minor difference. Further away the difference increases and becomes erratic, more difficult to predict. This behaviour translates in several characteristics of a variogram. The gamma value can start at a cut-off for the zero lag. This is called a **nugget effect**. It means the directly surrounding points are showing already very different values. It then slowly increases with larger H and reaches a **plateau**. The corresponding gamma value is known as the **sill**. The H value for which this plateau is reached is called the **range**. For points, located beyond the range distance, the property values are difficult to predict due to its

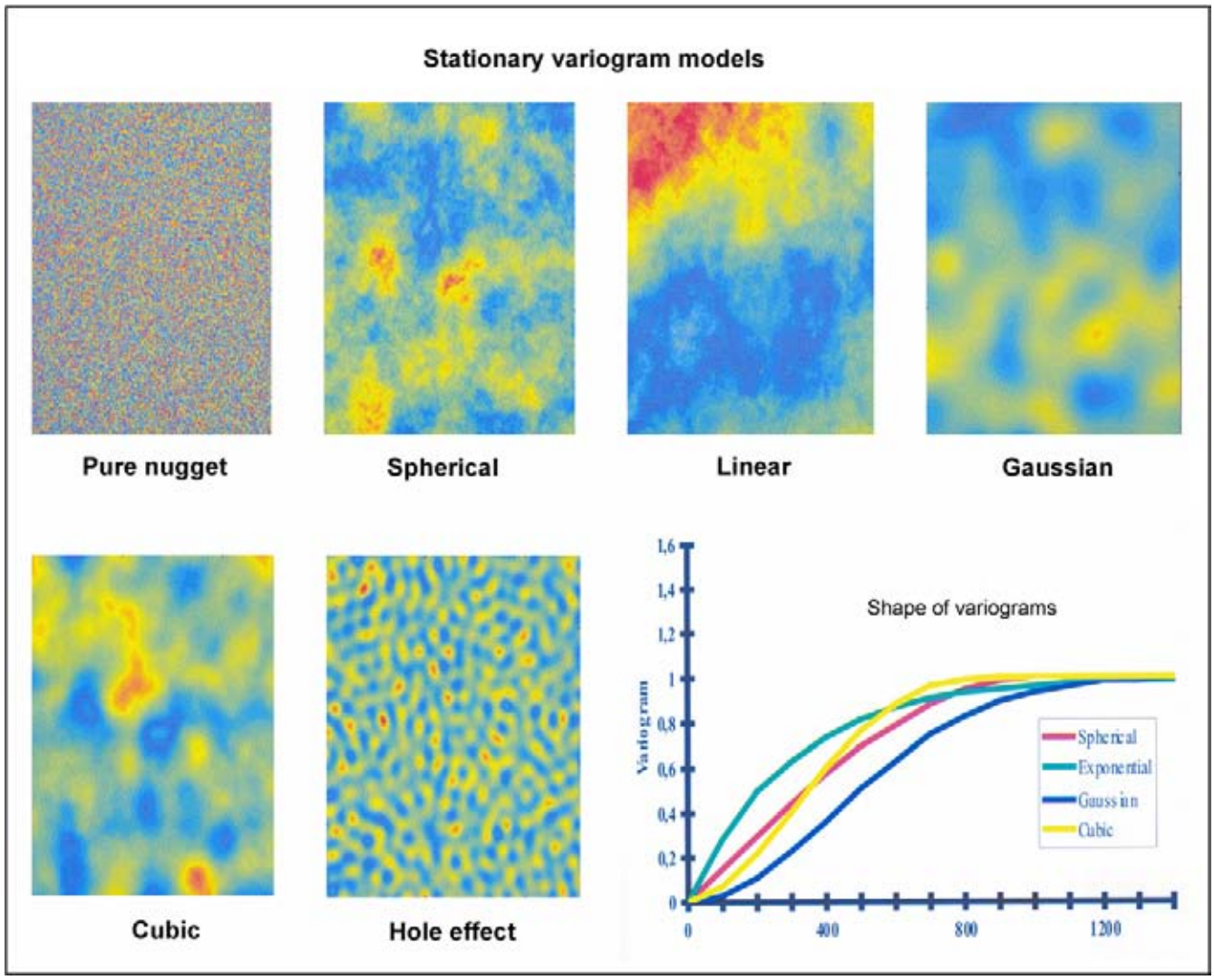

Figure 5.31: Variogram models for stationary data and random noise. The pure nugget effect represents a map with random noise. The scale of observation is important for defining the stationarity of the data (modified after Dubrule 2003).

non-systematic variation. A special type of **correlogram** is a plot between the difference in the variogram value and the constant sill value.

As the variability is computed for discrete lags, curve fitting is needed to get a continuous graph as variogram. The curve, drawn in the γ–H plot, should honour as best as possible the data points at the chosen lag interval. The lag distance is often taken arbitrarily and set quite large. More precision is obtained by taking a smaller lag distance, but it implies more computing time. The curve fitting procedure can be sometimes misleading, in that a small visual error in the variogram plot can translate in a big error in the actual predicted value away from the control point. An experimental variogram is connecting the computation points in the gamma–H crossplot by straight segments.

The variogram is normally direction dependent because H is a dislocation vector. The representation of such direction dependent variogram is called a **semi-variogram**. Often six direction categories are plotted. Or all categories are plotted together in one plot, also known as an omni-directional variogram. The six category plots can reveal anisotropy in the data. The vertical variability can also be captured in a variogram (Dubrule 2003). The various plots have all their own sill (plateau) and range. The increase of the variogram curve from zero can be of different shapes:

- Gaussian or a sigmoidal bell shape.
- Exponential.
- Linear.
- Polynomial.

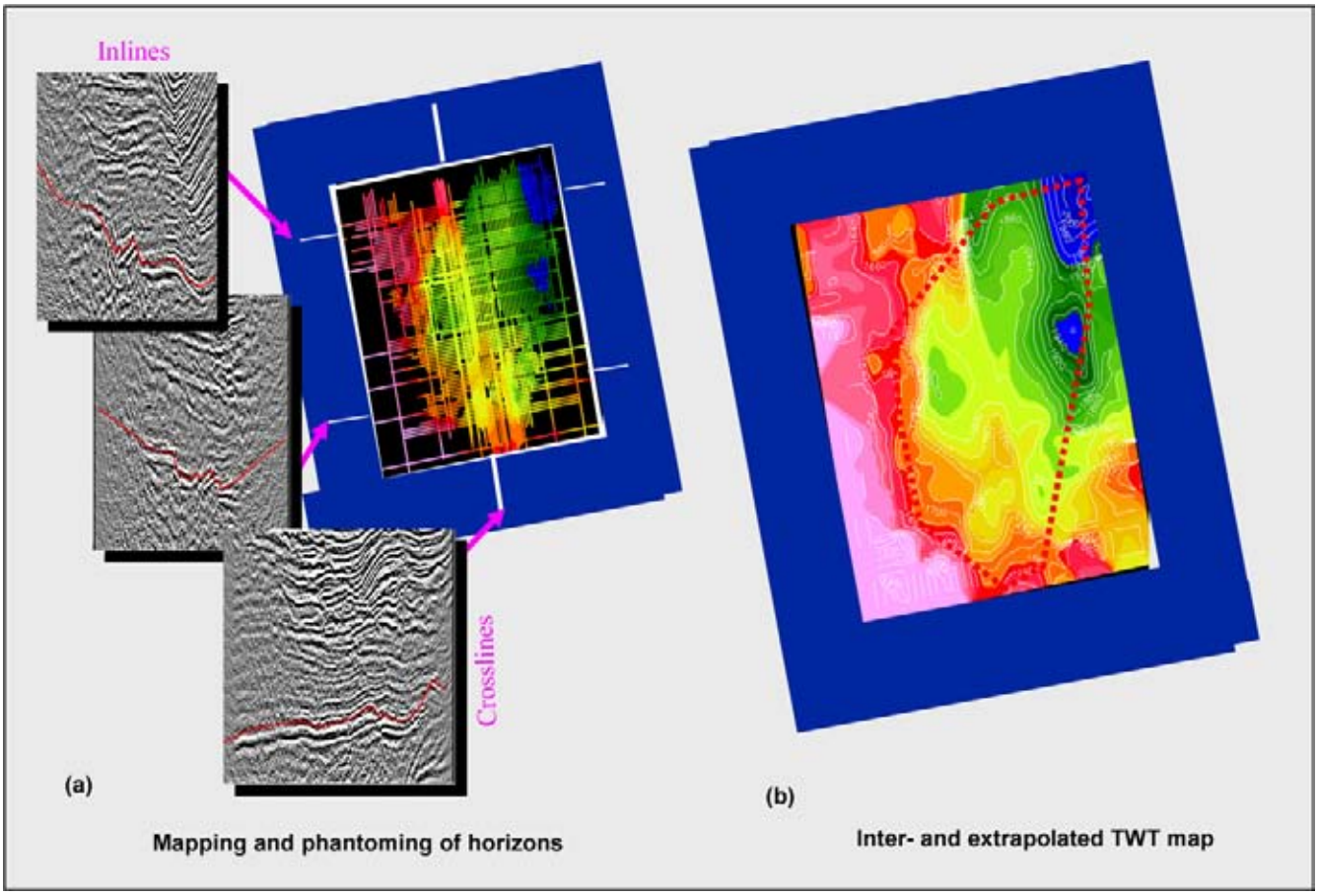

Figure 5.32: Data from a 3D seismic survey with Inline and Crossline directions. Interpretation of the seismic lines allows construction of a TWT time contour map that needs to be depth converted in order to appreciate the real subsurface structuration. The shape of the time high in the centre of the map will certainly change shape in depth, when there exist lateral velocity change in the overburden.

– Spherical.

The shape of the variogram says something about the rate of change in the data at their XY position. The data is stationary (moving within certain limits) or non-stationary. This stationarity property also depends on the scale of observation (Dubrule 2003). The variogram for non-stationary data does not reach a plateau with the given maximum lag distance and a linear trend is used as the approximation. Sometimes a hole is manifest in the plateau. This means that there is repeatability in the data in all directions (Figure 5.31). A nugget effect shows that there is noise in the data. A straight horizontal variogram means that there is only noise in the data (also known as a pure nugget effect). Variograms are very convenient in reservoir simulation procedures. Probabilistic inversion exploits the spatial variation of the geological parameters.

Variograms are essential to the **Kriging** gridding procedure. Kriging is a special way of interpolating and extrapolating control point values based on a multi-varied statistical approach. Kriging is a prediction process, that uses special weighting functions depending on the probability distribution and the spatial variation of the dataset, to ensure the variance of the error in the predicted value is kept at a minimum in a least square sense.

There are several types of kriging:

– **Simple kriging** whereby the global mean is assumed constant.

– **Ordinary kriging** whereby the mean is varying and locally estimated in the moving area.

– **Cokriging** using an imprecise other dataset as a guide for the kriging procedure. Usually the second dataset is much more densely sampled.

– **Collocated cokriging** uses two correlated datasets. The second parameter is often more densely sampled (e.g. seismic grid 25 m $\times$ 25 m). The values for the second dataset are not simulated as in cokriging, but a value is directly interpolated. It reduces the

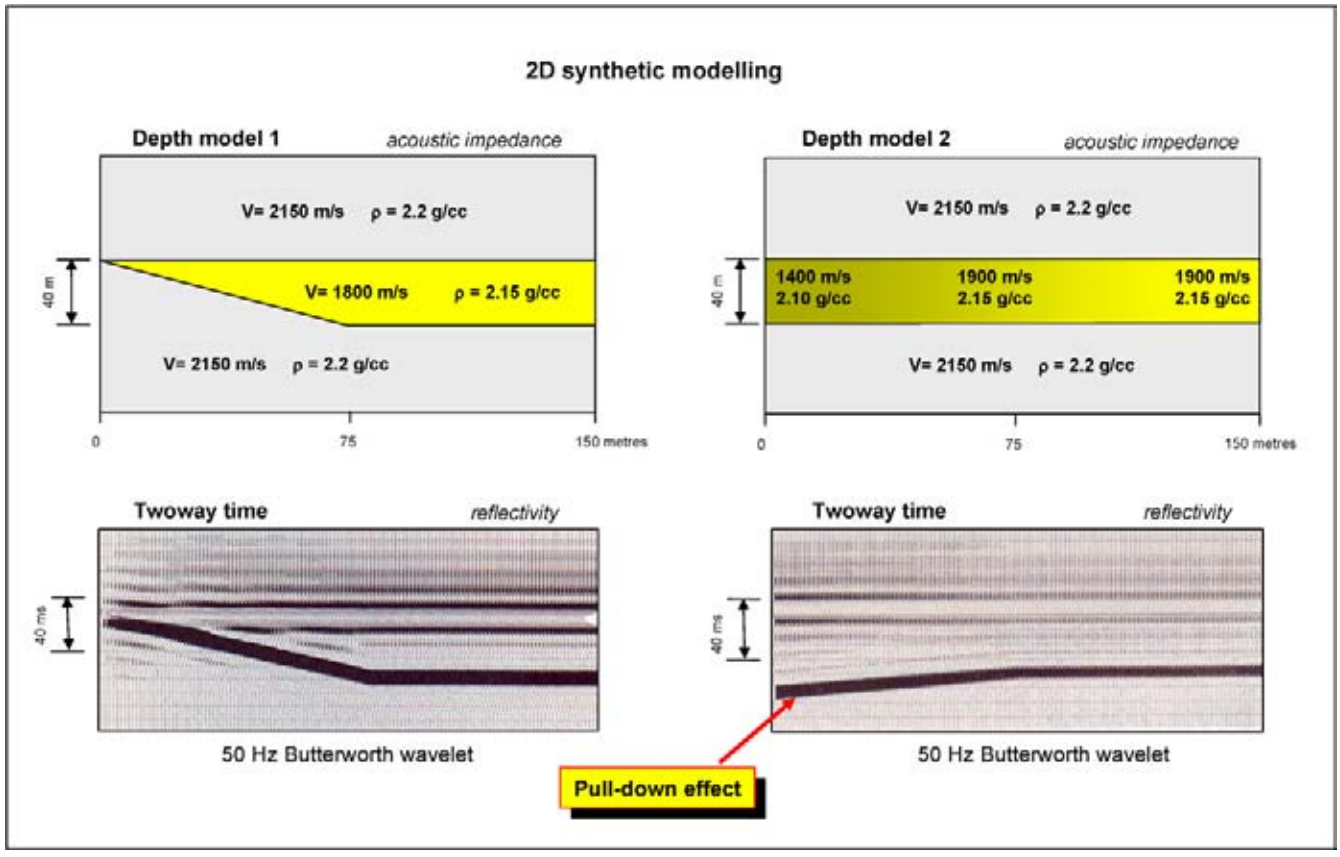

Figure 5.33: Synthetic seismic modelling using a 50 Hz dominant Butterworth wavelet. Note the sag effect when the velocity is decreased in the second depth model, giving rise to a gradual pull-down effect on the time section for the base of the layer (modified after Hart and Chen 2004).

computation time a lot and gives more satisfactory results.

– **Kriging with an external drift**. The results follow the trend of the second parameter beyond the range of the variogram for the data to be predicted and donot go back to the mean as in kriging.

These algorithms are very interesting for gridding and contouring, as a scarce control point data set can be guided by the shape of another property map. It helps to fill in large gaps. Of course there has to be a certain correlation between the two properties, otherwise the exercise is meaningless. Kriging tends to converge to the mean at distances larger than the range away from the control points. It is possible to choose a time horizon map as an external drift parameter to do the collocated cokriging of a velocity field. In this way a compaction trend is automatically introduced in the resulting contour map. Good maps are the key to volumetrics calculations, which are the ultimate aim of the exercise.

5.2.3 Depth conversion and depth contour maps

To examine the possible hydrocarbon trap in detail, a closer look is needed into the structural expression of the top reservoir horizon. The top reservoir is traced on inlines and crosslines of a 3D survey. The marker is pushed or phantomed in areas where the horizon changes character. This phantoming highlights the most probable geometry of the layer under investigation (Figure 5.32). The shape of the markers above and below the target horizon are considered as structural guides. It is important to evaluate the geometry in depth and not in TWT time (Figure 5.33). The easiest way to perform a time-depth conversion is a simple vertical stretch-and-squeeze procedure (Figure 5.34). Velocity anisotropy effects of the overburden can disguise for example the expression of a hydrocarbon filled structure on a map completely or render it so small that it seems at first glance unattractive for further exploration.

It is crucial that the correct velocity field is applied to depth-convert the time data. The velocities are based on:

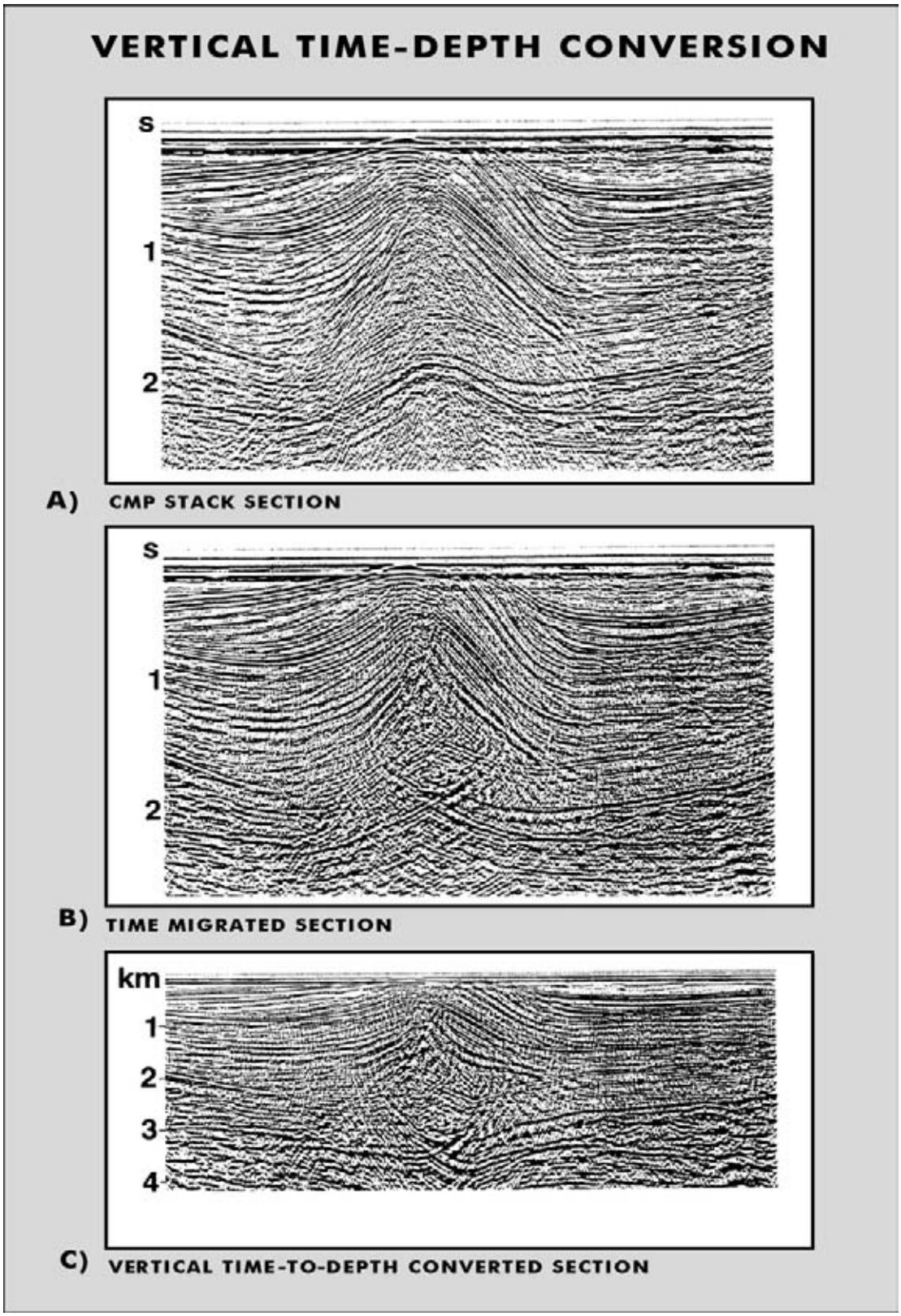

Figure 5.34: Vertical time–depth conversion of migrated seismic data based on an interpolated velocity cube (modified after Yilmaz 1987). Note that the stack section uses a reasonable velocity model because there are not many artefacts (crossing events, diffractions, local irregularities). The migration procedure is less optimal and has introduced a lot of migration smiles. The depth section has the same problem. A more costly depth migration procedure is highly recommended because of the steep dips and lateral velocity changes.

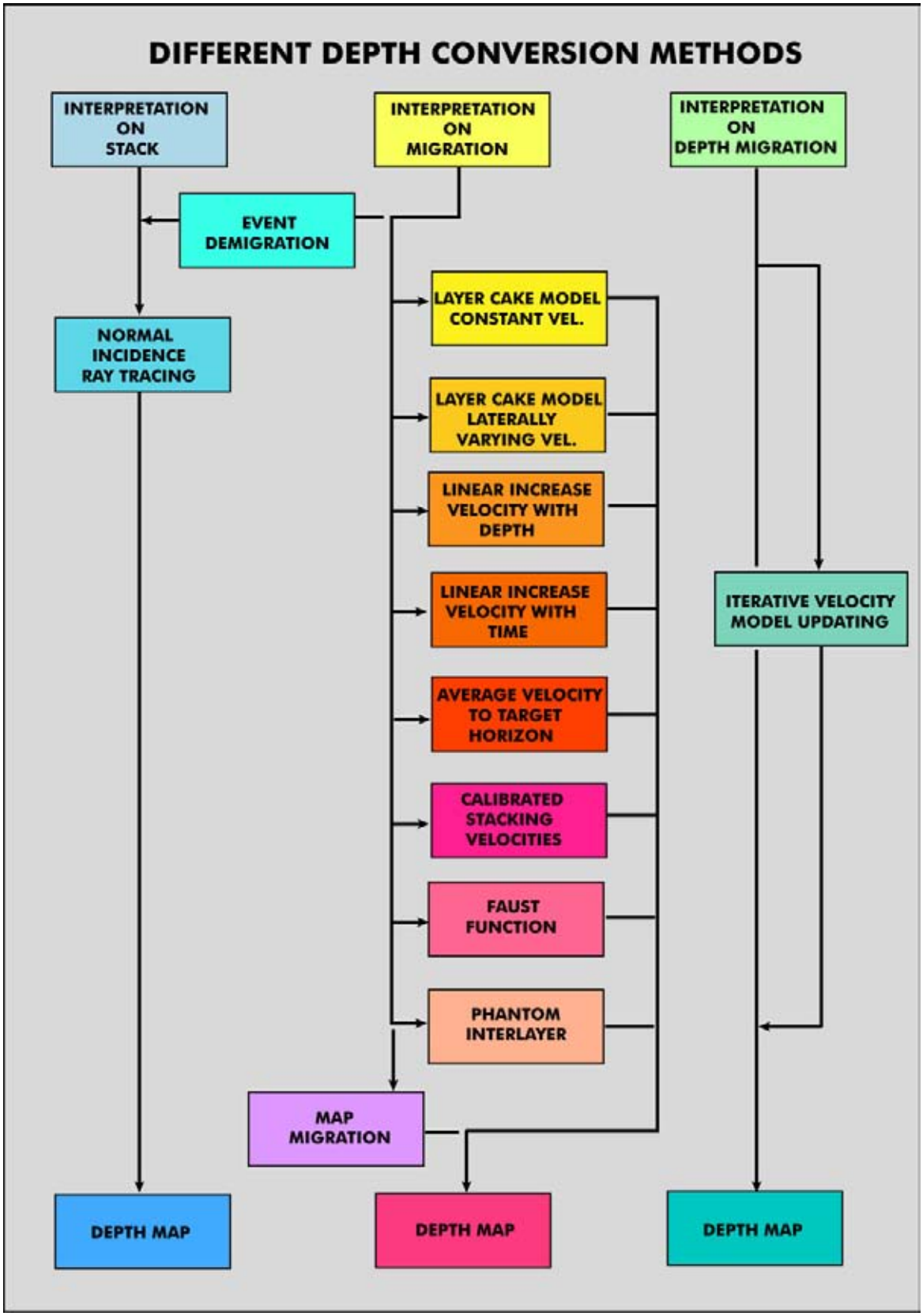

Figure 5.35: Various types of depth conversion methods. For data, interpreted on time-migrated sections, a composite depth conversion scheme can be applied; i.e. applying a combination of the different velocity options for the various layers.

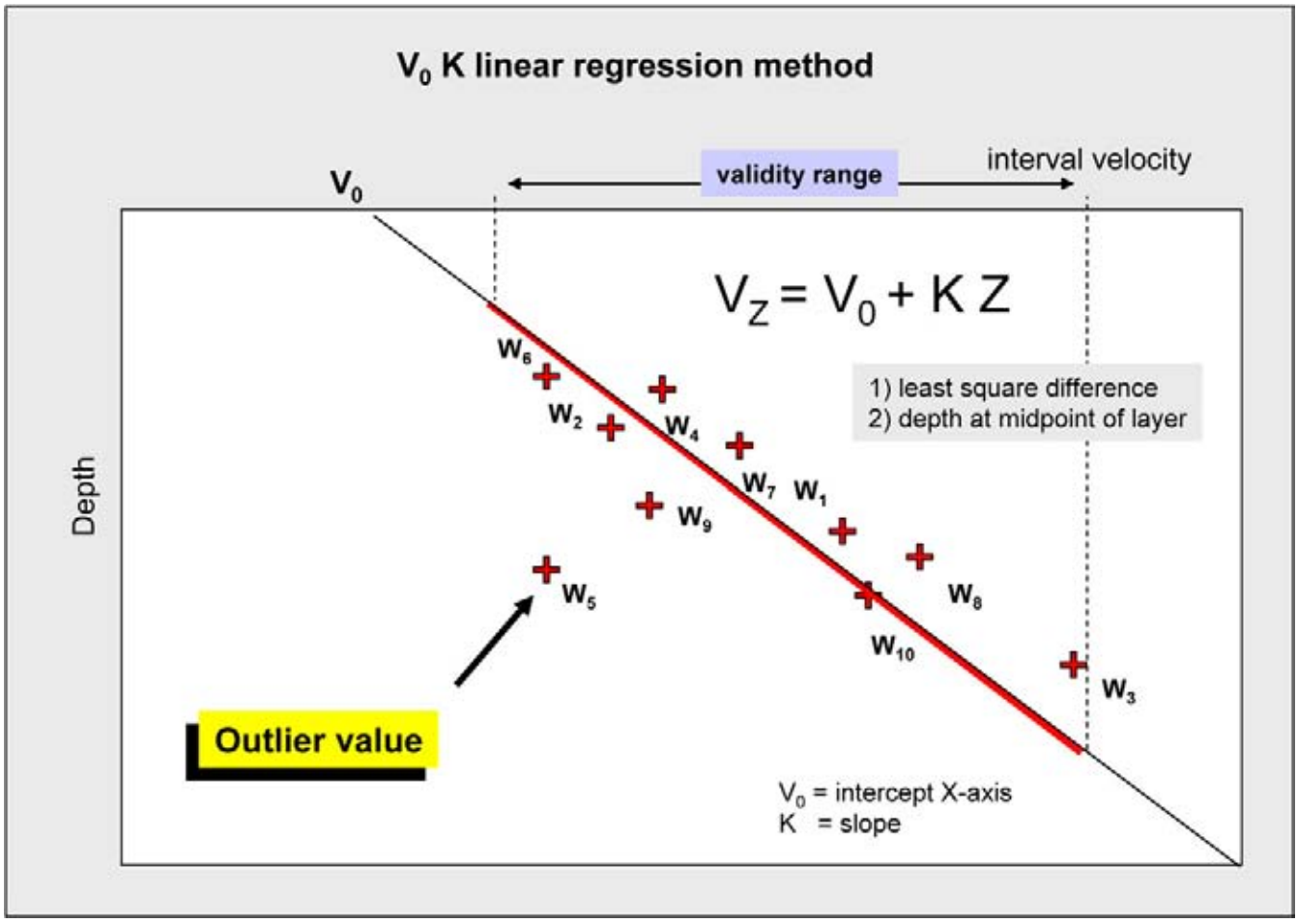

Figure 5.36: The V_0–K method uses a linear regression to compute a interval velocity trend with depth. Usually the interval velocity is plotted at the midpoint depth. Outliers in the plot should be closer investigated and if necessary they are excluded from the computation. The functions are valid over a certain velocity depth range. Extrapolation beyond this range can be dangerous as it may introduce unacceptable large errors.

- Sonic log data,
- Wellshoots and VSP's,
- Stacking velocities,
- Raytracing techniques,
- Pseudo-seismic velocity calculation at the wells.

Seismically derived velocities are usually up to 10 percent in error compared with the well velocities, because a large horizontal component is measured (cf Denham and Agarwal, 1999). The anisotropy behaviour of the layers explains this discrepancy. Shale intervals are renowned for their anisotropic behaviour. It is related to elongated minerals, aligned cracks, periodic thin layering and lamination of the deposits (Yan et al. 2004).

The **pseudo seismic velocity** takes the trustworthy timepicks from the seismic interpretation and combines it with the thicknesses encountered in the wells to calculate a **hybrid interval velocity**. This method ensures that errors in the wells are kept to a bare minimum. Vertical time-depth conversion is achieved in several ways (Figure 5.35):

- A 1-layer average velocity model for target horizon.
- Layer cake model with constant velocities (also known under the 'vertical stretching' method).
- Layer cake model with laterally varying velocities.
- Linear increase in velocity with depth in the form of $V_Z = V_0 + K \cdot Z$, which honours compaction trends (Figure 5.36). V_0 can be constant or laterally varied if necessary (V_0 map). If data from one well are used a local K is the result. If interval velocities from several wells are used in the computation a regional or burial related trend is established (Figure 5.37). The Z_i value of the base of the interval is given by:

$$Z_i = \left(\frac{V_0}{K + Z_{i+1}}\right) e^{(K/2(Ti\text{-}Ti\text{-}1))} - \frac{V_0}{K} \qquad (5.21)$$

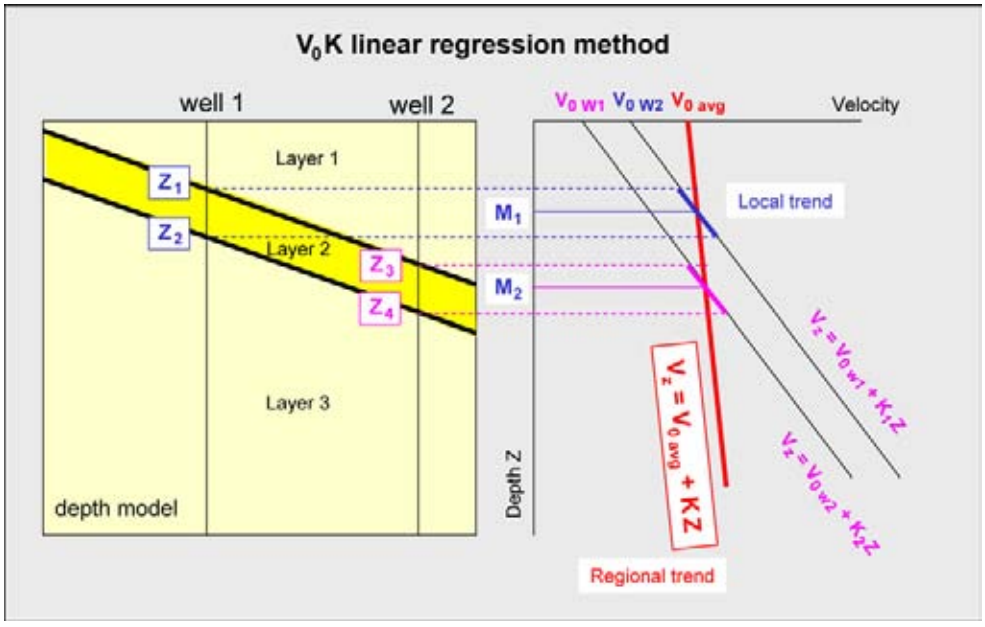

Figure 5.37: The velocity data in the well allows to establish a local V_0–K trend using the instantaneous velocity at the top and bottom of the layer. The regional trend is based on data from several wells. It uses the midpoint depth and the interval velocity to derive a linear velocity trend in a least square difference sense. This regional well trend captures the burial or compaction effect.

- Linear increase in velocity with time. This method does not give realistic results when strong lateral variation are present (e.g. salt diapir).
- Faust function $V = A \cdot Z^{1/N}$, velocity dependant on age of rocks involved (Faust 1951, 1953). N is a constant that depends on the area and the lithology. It is often taken as 6 for silici-clastics and 3 for carbonates. The Faust function breaks down for shallow depth (<200 metres). The A can be made aerially variable so that the wells are honoured correctly.
- Calibrated interval velocities derived from stacking velocity using Dix's formula (Dix 1955).
- A densely sampled 3D cube of average velocity data.
- Wellshoot derived interpolated T–Z curves. For interpolation the stacking velocity trend can be used.

Conventional time-to-depth conversion methods, based on only well data, have their limitations. This is especially true in areas with complex subsidence histories. Most methods are appropriate when enough well control is available. If too large an interpolation or extrapolation distance is given, then these methods tend to become unreliable. In such cases, the seismic velocities may provide the only means to evaluate the subsurface structuration. The velocity data gives information on lithology, depositional facies, pore fluids, overpressure compartments, burial history and temperature. There is a relation between seismic velocity, porosity and clay contents. The seismic velocity is two times more sensitive to porosity than to the volume of shale. Other influencing factors are presence of thin cracks, flat pores, small amounts of cement at grain contact, pore fluid, grain size, sorting, grain to grain contact, pore pressure, anisotropy, contact stiffness and grain contact size (Storvoll et al. 2005).

The **seismic depth conversion** method is quite satisfactory for a quick first look overview of the structuration; it is competitive in terms of effort, timing and costs versus results. It yields a valuable first pass inventory of possible prospects (Veeken et al. 2005). The approach is to compute an average velocity map from the zero level to the target horizon. If the target depth map is constructed in a multi-layer mode, than several error maps are needed, one for each intermediate level. These error maps are of course correct at the well control points, but in the surrounding areas these corrections are in fact unknown and often somehow wrong. Moreover, the correction at individual levels are not necessarily cancelling each other out. This means that fairly large erroneous corrections can be introduced in areas where the position of the markers are unknown. The errors at the wells are usually gridded, contoured and spread out over an larger area in order to avoid artefacts on the depth map (bull's eyes, etc.). It is more easy to introduce as little as possible intervals to depth convert a target horizon. Therefore the one-layer approach is generally preferred. The velocity survey in the wells gives an indication on

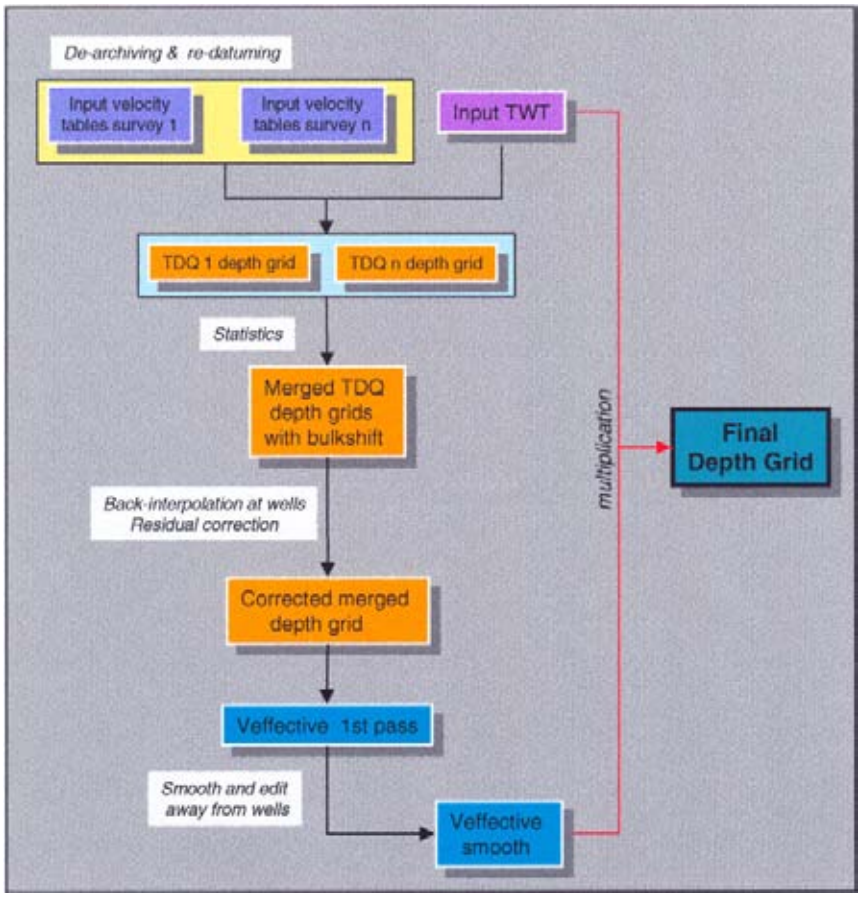

Figure 5.38: Flow diagram for depth conversion of overlapping seismic survey using seismic velocities (Veeken et al. 2005).

how many layers are needed. Clear breaks in the sonic log trend define the units that should be considered.

The compilation of a regional depth map for a target TWT horizon, covering several seismic surveys, involves several steps (Veeken et al. 2005):

1) The regional TWT grid and velocity files are analysed. The stacking velocities are transformed in interval velocities by using the Dix's formula. This function has some assumptions attached to it. A provisional depth conversion is done for individual surveys to assess the depth discrepancies at the wells (Figure 5.38).
2) The survey with the minimum control point discrepancy is selected as reference and is held stationary. In overlap areas the difference between the stationary reference grid and the other surveys are determined. For each survey a bulk correction is computed and applied, in order to bring them more in line with the grid values seen on the reference survey (Figure 5.39).
3) A composite depth map is constructed by applying the bulk correction to each survey in a progres-

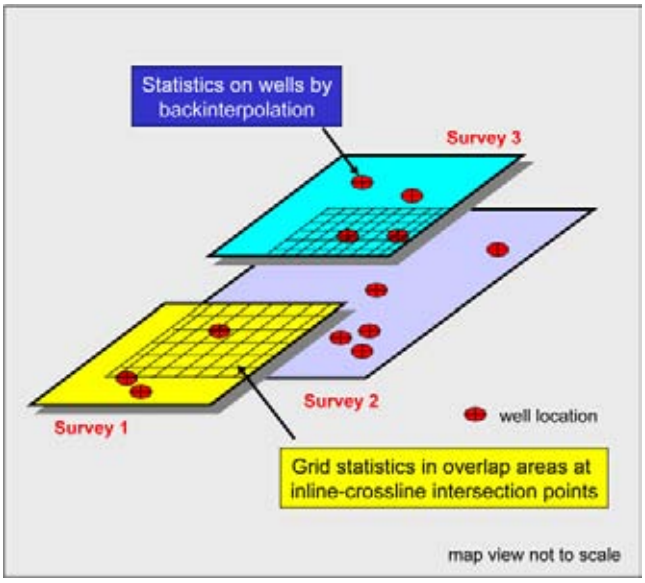

Figure 5.39: Backinterpolation and rigorous geostatistical analysis in the overlap areas is at the basis of the harmonisation step in velocities from the different seismic surveys.

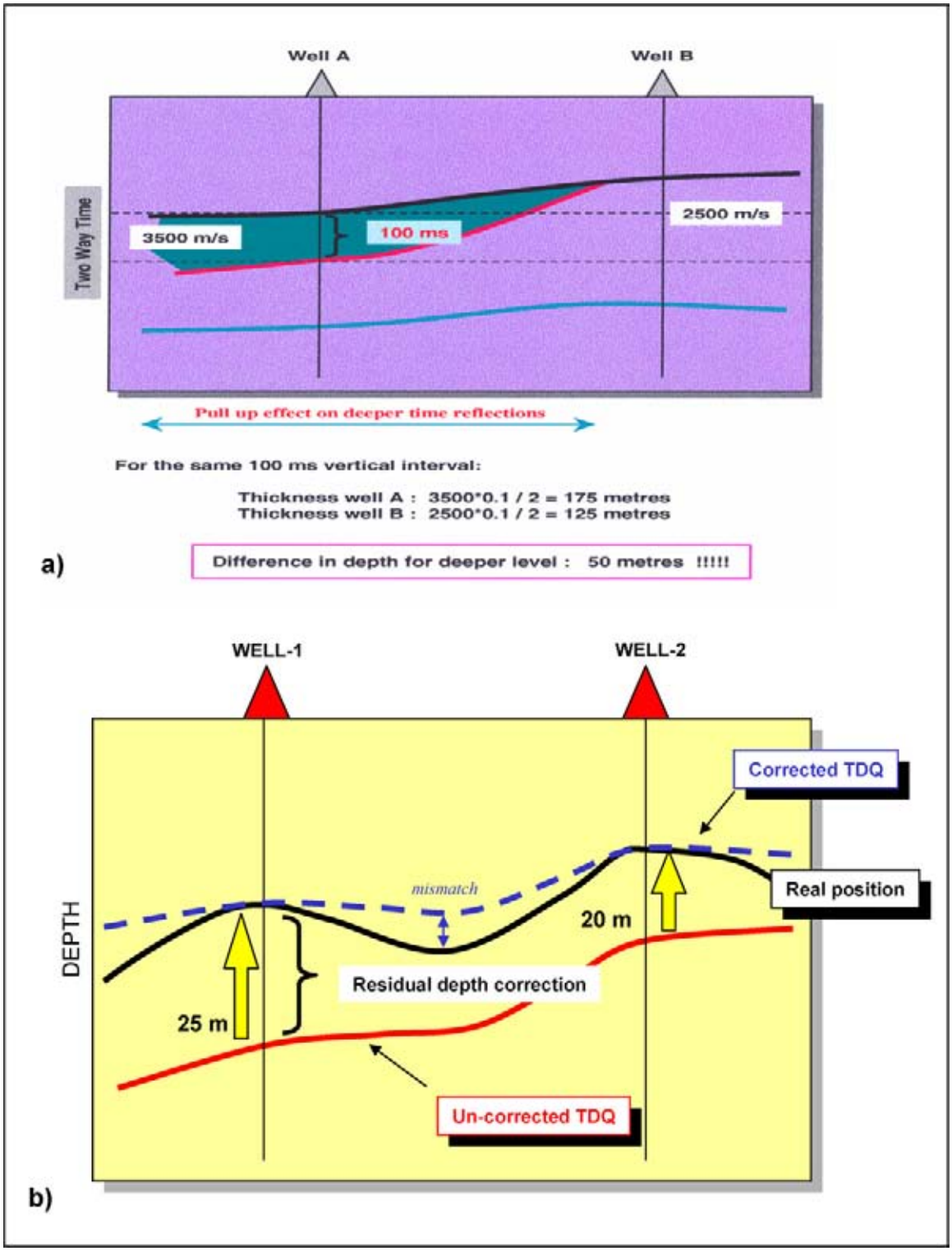

Figure 5.40: a) Time pull up effect on time section. Depth conversion will enhance the mapped time structure at deeper levels. b) The residual correction should improve the depth error in unknown errors, but this not always the case and it also depends on the TD conversion method utilised. If there exists a correlation with a geological feature, this may help to grid the data in a more sophisticated way (e.g. kriging with external drift; Veeken et al. 2005).

sive manner. In the overlap areas an averaging of the values is done to obtain a representative grid point. This depth grid is not yet honouring the well control points.

4) Backinterpolation at the well locations (determination of grid value at arbitrary XY locations) allows construction of a residual correction grid. This grid is applied to the composite depth map.
5) A corresponding $V_{\text{effective}}$ grid is computed from the TWT and depth grids. This $V_{\text{effective}}$ map is corrected, hand-edited, smoothed and flexed to the average hybrid velocity (from surface to target horizon) seen in the wells.
6) This smoothed effective velocity grid is combined with the TWT grid of the target horizon to arrive at the final seismically derived depth map.

The residual depth correction needed in the wells is inter- and extrapolated. It does not mean that the error is reduced in the unknown areas, but hopefully it has been improved (Figure 5.40). It all depends whether the error is systematic or not. It can be difficult to establish a correlation (Al Mahrooqi et al. 1999). If there is a relation with geological features it is useful to consider kriging with external drift (Veeken et al., in press).

The discrepancies between wells and seismically derived depth can be rather large in fault zones, tectonically inverted structures or areas with salt diapirism. Care should be taken when converting the fault zones (Figure 5.41). Fault intersections on shallower levels can have a shadow zone on layers underneath, causing artificial distortions on the computed depth map (e.g. Anstey 1982, Denham and Agarwal 1999; Figure 5.42). The amount of distortion depends on the velocity contrast on the fault plane. The Dix formula for estimating interval velocities is only valid for situations with:

- No strong lateral velocity changes.
- No strongly dipping reflections.
- Parallel reflections.

Many times these criteria are not adhered to and that leads to an additional uncertainty. Proper migration of the seismic data and the correctness of the velocity field is crucial to obtain reliable results. The residual migration error or Hubral shift (Hubral 1977) can be rather considerable with lateral shifts in the data of over 1600 metres and 180 ms vertical TWT (e.g. Hatton et al. 1996).

Non-vertical depth conversion techniques comprise depth migration (post- and pre-stack) and map migration procedures using raytracing methods like tomographic inversion. **Tomographic inversion** is often based on a pre-stack layerstripping Kirchhoff algorithm with geometrical raytracing in heterogeneous media (cf Accaino et al. 2005). The velocity model is iteratively updated by depth focusing the interfaces using the semblance in the image gathers (depth domain). Application of **depth migration** gives the interpreter directly access to depth data and provides a more correct image of the subsurface (Figure 5.43). As said already before, depth migration is a special type of migration that takes into account a detailed velocity model for the subsurface and therefore it images more correctly the subsurface structures (e.g. Versteeg 1993). It takes care of the bending of the raypath in non-isotropic media. The **pre-stack depth migration** (or PSDM) gives much better seismic sections, but the method is more costly. This type of depth conversion is done in a non-vertical way and raytracing techniques or wavefront propagation principles (e.g. Eikonal approximation of the wave equation) are applied. A certain amount of smoothing of the reflections is needed for the raytracing algorithms to work properly. This results in an uncertainty in the computed depth position.

Map migration can be done using the Fermat principle. Snell's Law is applied on interfaces and the velocity distribution is used to compute the length of the curved ray path segments in the various layers. Two types of map migration are available (De Beukelaar et al. 1997, 1998):

- **Normal incidence ray** map migration, whereby the ray path is assumed perpendicular to the target horizon. The input travel-times correspond to picked horizons on a zero-offset stacked seismic section.
- **Image ray** map migration, whereby the ray is assumed orthogonal in the geophone at the surface. The input travel-times are picked on time migrated seismic data.

The 3D ray-tracing method, as presented in Section 2.2.2, uses the velocity distribution to determine the curvature of the ray-path and adheres to Snell's Law at the discrete reflector interfaces. The length of the computed ray segment is related to the recorded travel-time of the ray within the layer. It equals half the two-way time value multiplied with the interval velocity for the normal incidence ray. The travel-time values are vertically measured on a NMO-corrected stack section (zero offset), straight below the CMP coinciding with the kick-off position of the reconstructed ray-path on the ground-level or reference surface.

For accurate ray-tracing the input travel-times are established on stack zero-offset seismic sections. For this two approaches can be adopted:

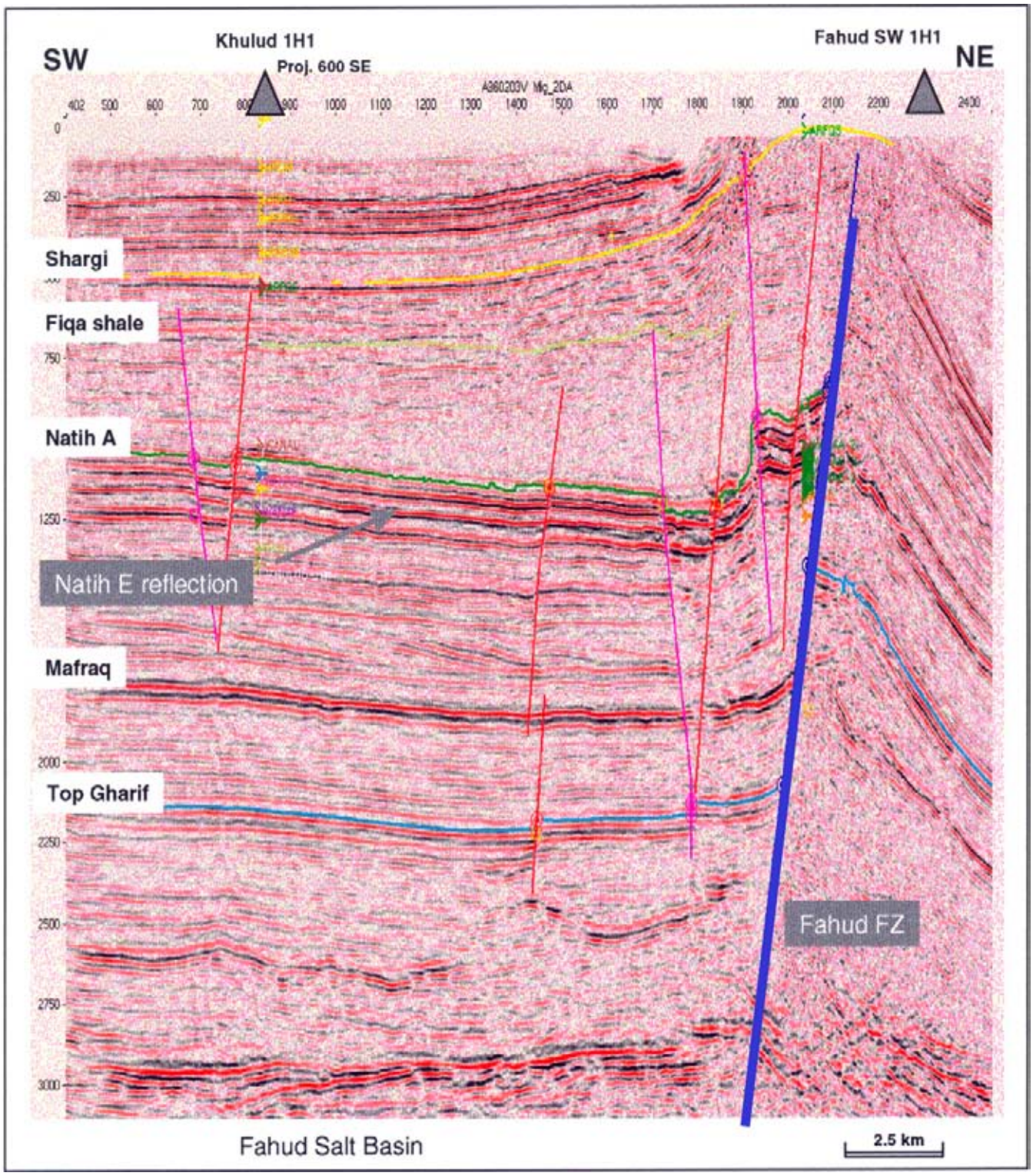

Figure 5.41: Complex tectonic history resulted in tectonic inversion of the sediments across the Fahud fault zone in northern Oman. The velocity distribution is anomalous due to the Tertiary uplift on the right hand side, disturbing the natural increase in velocity due to ongoing burial and compaction is no longer valid. This should be taken into account when doing TD conversion. Local velocity trends are calibrated by wells and should be respected by the conversion procedure (Veeken et al. 2005).

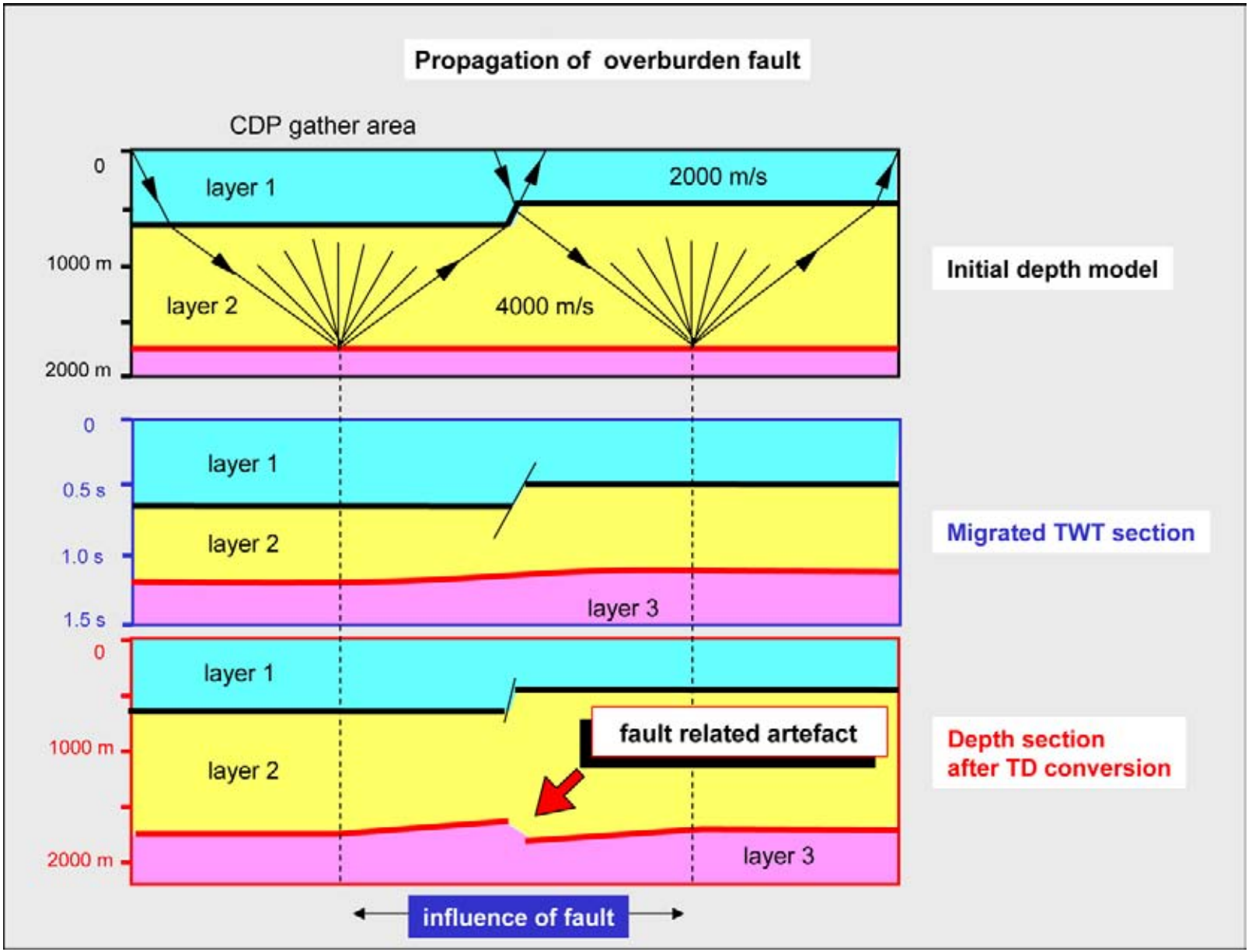

Figure 5.42: Propagation of distortion effects due to a fault in overburden. The vertical TD conversion does not take into account that the raypaths are crossing the different fault blocks. Stacking velocity smoothing smears the energy in the deeper part of the section over a larger area. The flat reflector in the initial depth model is represented by an anomalous dip and discontinuity on the TD converted depth section below.

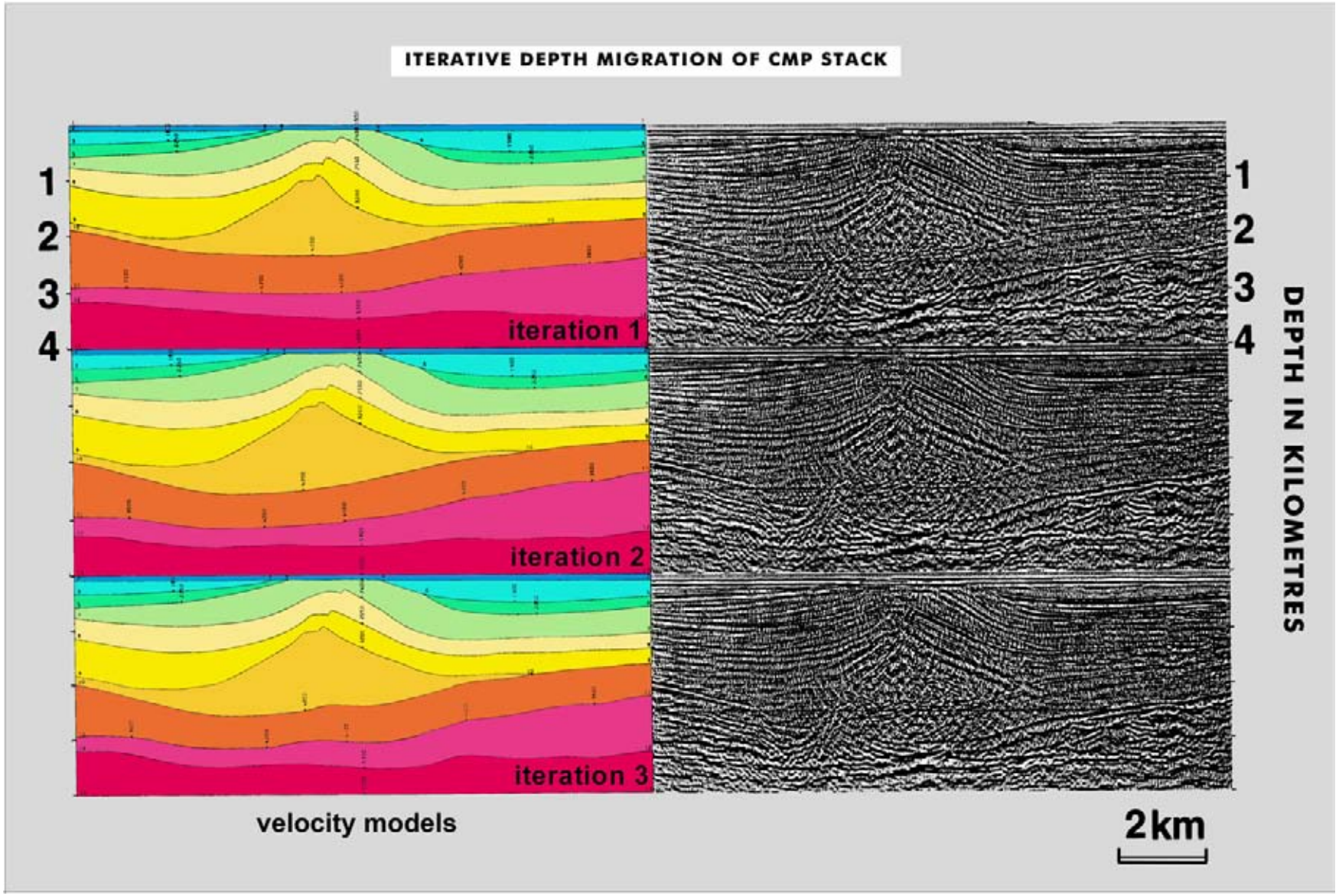

Figure 5.43: Depth-migration processing results in depth sections as output, straightaway ready for interpretation. The reliability of depth-migration depends heavily on the input velocity model. The method takes care of ray bending effects in the overburden. The best results are obtained by applying a pre-stack depth-migration approach (after Yilmaz 1987).

- Interpret the horizons directly on the stacked data set, which is in general a tedious job due to mistic corrections and processing artefacts.
- Take advantage of the interpretation on the migrated data set and de-migrate the picks to obtain interpreted zero-offset sections. This de-migration step is normally done for the horizons only. The seismic cube itself is not altered. Dedicated software is available to perform this de-migration step (e.g. Geomig^{TM}).

There always exists a raypath problem in conventional time migration, when steep dips and laterally varying interval velocities are encountered (Hubral shift). Often these effects are simply ignored and depth contour maps are generated.

The presence of faults, as detected from seismics, is indicated and lined up in a 3D sense. The fault pattern should be taken into account when the gridding and contouring is done. Modern interpretation packages do this properly, but the early workstations had some restrictions in this respect. The geometry of the fault pattern is illustrated on **Dip/Azimuth displays** of the mapped horizon (cf Bose et al. 2004). Also the computation of a **coherency cube** is very helpful (Bahorich and Farmer 1995). The calculation involves the proper selection of the processing parameters and fine tuning is needed to enhance subtle changes in the dataset. Interaction between the geophysicist and geologist is here again advisable.

Closed high areas are highlighted on the depth contour maps because these form possible HC traps. Closure of contours against faults is to be investigated and the **sealing capacity** of the fault plane determined. The sealing capacity is evaluated by considering:

- The amount of fault throw.
- The degree of myolitisation (tectonic crushing of individual minerals and rock fragments).
- The lithologies juxtaposed along the fault plane.
- The pressure differential, which might cause clays to be injected along the fault plane or create pathways for migrating fluids. Faults that are closer to the reactivation pressure within the current stress regime are more likely to fail and become permeable for migrating fluids (Dee et al. 2005). The capillary properties can be modelled.
- Fault slicing, it creates sections parallel to the fault plane in the 3D seismic volume and illustrates the juxtaposition of different lithologies with highlighting possible spill points.

Faults and shear zones can be permeable conduits for fluids or they can form impermeable flow baffles (cf Alsop et al. 2004). Even small faults beyond seismic resolution may act as important flow barriers. These can be detected by analysing the production history of wells in a HC reservoir. **Tracer fluids** can be injected and their propagation in the reservoir can be quite revealing for the reservoir connectivity. **Thief sands** indicate that the fluid flow is different from the anticipated flow and this has consequence for the performance of the field.

5.3 Direct Hydrocarbon Indicators

The seismic data are scanned for DHI's, which stands for **Direct Hydrocarbon Indicators** (Figures 5.44 and 5.45). These DHI's comprise the following types:

- **Flat spots**, which are sub-horizontal events that represent a fluid contact in a reservoir. These can be either gas/oil, gas/water and oil/water contacts (Figure 5.46). The oil/water contact is in many cases not visible due to insufficient acoustic impedance contrast or the limited height of the oil column.
- **Velocity pull-down/pull-up** effects of reflection underlying a hydrocarbon reservoir on a time section; these effects can be very subtle. It is usually caused by the local increase in height of the overlying gas column. The gas has a slower velocity and hence the pull-down. Sometimes the flat spot is somewhat tilted on a TWT section due to velocity effects (Figures 5.47 and 5.48, Brown 1988). It is also possible that each faultblock has its own gas-water contact (Figure 5.49, Brown 1999).
- **Dim spot**, decrease in amplitude of the top reservoir reflection indicative for a change in porefill.
- **Bright spots**, increase in amplitude of the top reservoir pointing to the presence of a different porefluid.
- **Polarity reversal**, flip in polarity of the top reservoir reflection also due to the change in porefill.
- **Chimney effects,** whereby reflections become diffuse in a vertical zone overlying a hydrocarbon containing structure (Figure 5.50). Bad seismic velocity determination may be the result of low background gas saturations.

Eighty percent of the petroleum found in deep water (500–2000 metres) have some sort of DHI associated with them (CSEG interview, Weimer 2005). It shows the importance of the subject. The presence of a **gashydrate** accumulation at shallow depth can be expressed by the presence of an extensive cross-cutting single reflection

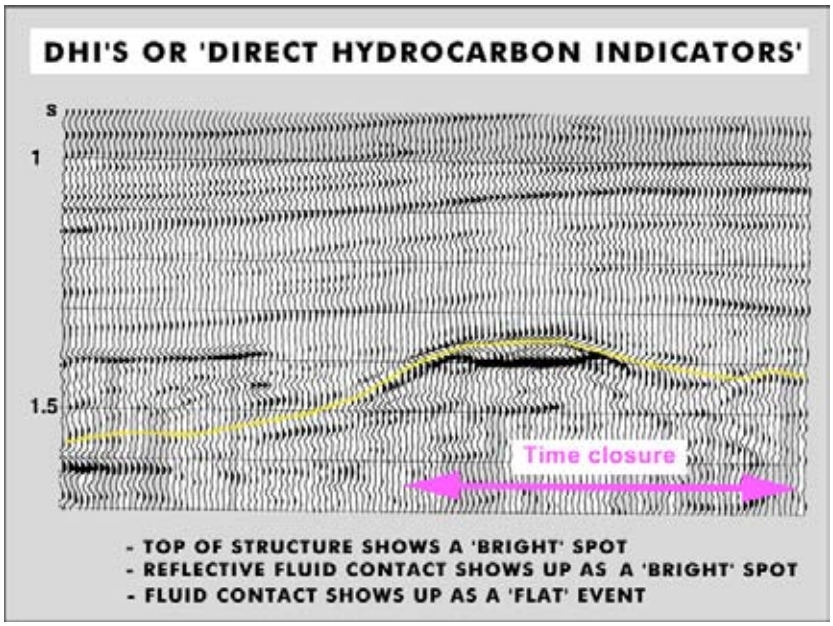

Figure 5.44: Direct Hydrocarbon Indicators help to deduce the presence of a hydrocarbon accumulation on seismic data. They provide support for evaluating the hydrocarbon potential of drillable prospects. DHI's are caused by the porefill contents, fluid contacts and/or height changes in HC column. Notice the small sag effect below the HC reservoir on this time section and curving of the flat spot at its edges, because of the decrease in height of the gas column (slow velocity). The structure is not filled to spill point. This observation needs to be verified on consistency for all seismic lines of the survey. Meticulous 3D mapping of the top reservoir, taking into account possible polarity changes, is essential to draw the right conclusion on the presence of hydrocarbons (modified after Yilmaz 1987).

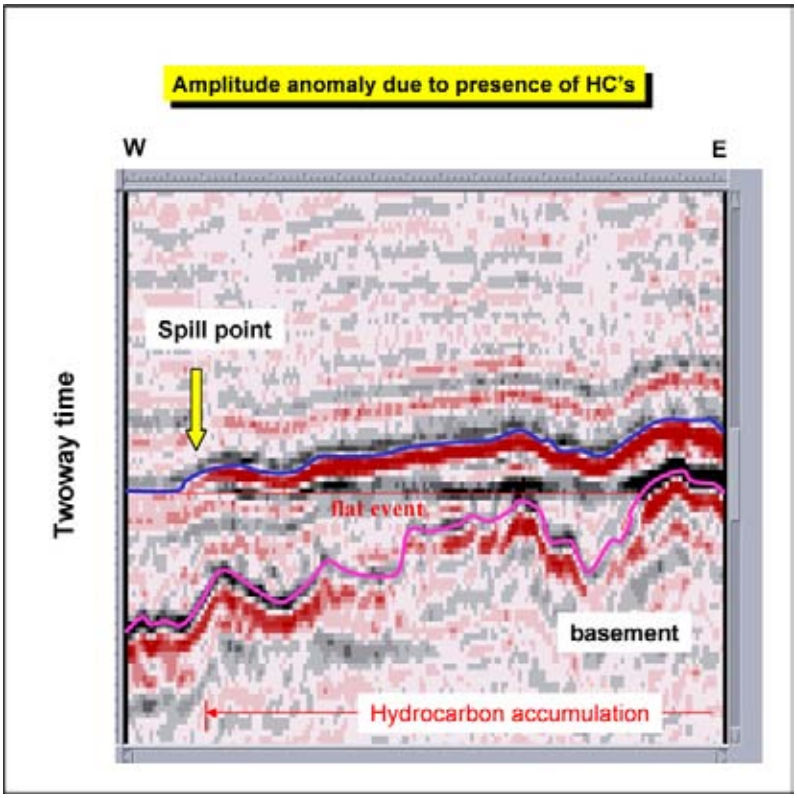

Figure 5.45: Flat event on a seismic section through a hydrocarbon accumulation. The blue top reservoir marker shows brightening (stronger amplitude response) over the zone where the HC's are present. The DHI extents within the closed contour area and the spill point of the structure is seen on the left hand side (data courtesy TFE).

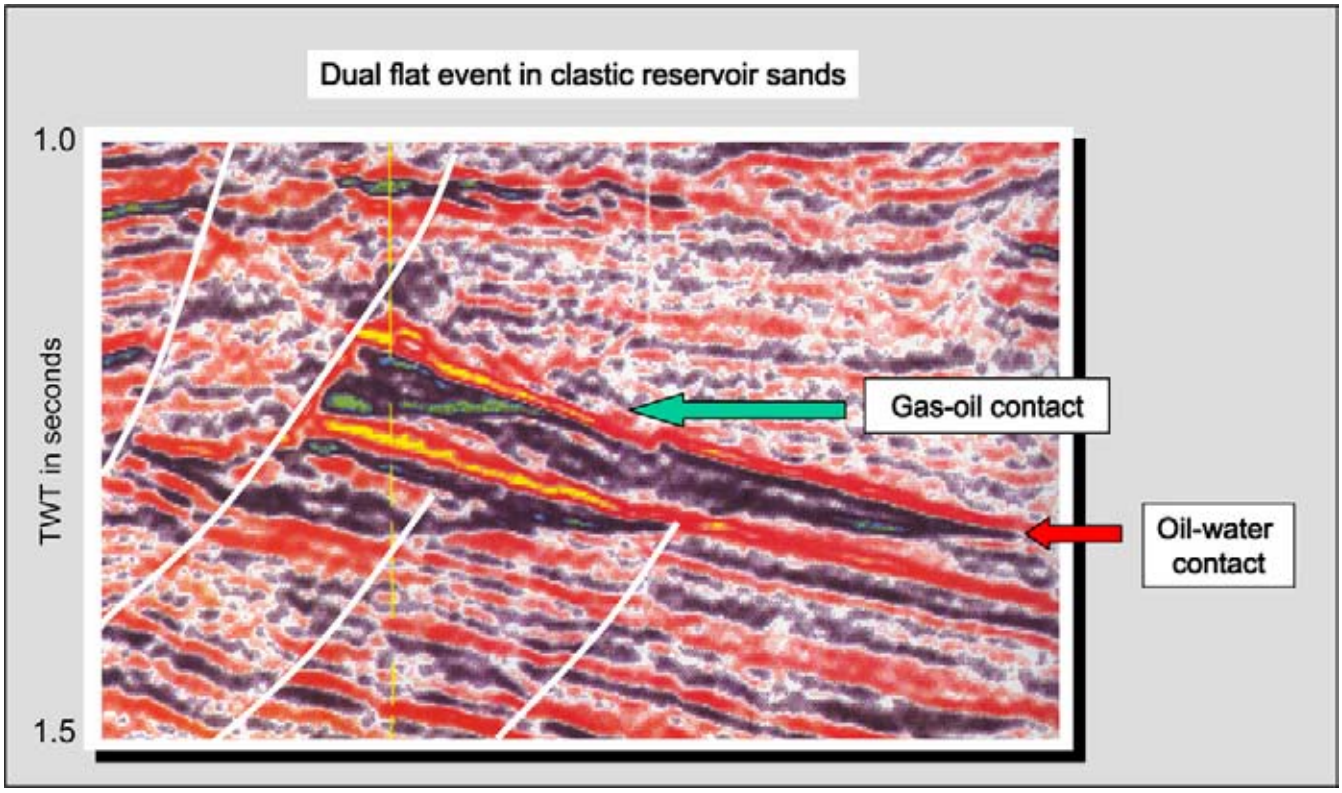

Figure 5.46: Dual flat spot in a clastic reservoir sequence, offshore Nigeria. The gas–oil and the oil–water contacts are both reflective and show up as distinct seismic events. The oil–water contact is more than 2 kilometres wide (modified after Brown 1999, Courtesy Mobil Production Nigeria Inc).

on seismics (Figure 5.51). The reflection is more or less sub-parallel with the seabottom (cf Bottom Simulating Reflectors, Dai et al. 2004). A gashydrate is a solid state of a mixture gas and water, that can only exist under special temperature/pressure conditions: high pressure and low temperature. These conditions exist in fact only very shallow in the subsurface and generally coincide with areas of great waterdepth. Arctic permafrost also contains large gashydrate accumulations. The velocity of the methane hydrate is relatively high and in the order of 3300 m/s (Hornbach et al. 2003). This gives rise to a good reflection on the seismics. Lateral changes in seismic amplitude may reflect changes in hydrate concentration. Detailed velocity analysis help to document these features. The hydrate accumulation may form a viable exploration target (NW Gulf of Mexico, Milkov and Sassen 2001). Care should be taken when production begins, as this will change the pressure regime and hence has an impact on the stability of the trap. Absence of a proper top seal makes the control very difficult. Involuntary liberation of large quantities of gas into the open air will have severe effects on the climatic conditions at the earth's surface (cf Haq 1993).

Care should be taken during the interpretation of these descriptive DHI's terms. There are several issues an interpreter should address when evaluating the validity of the encountered possible DHI's (Figure 5.52). The validity of a DHI is increased when it coincides with a closed contour on the corresponding depth map of the assumed top reservoir level. There are exceptions to this basic rule, when there exists an important **dynamic flow** in the reservoir (waterdrive, Dake 2001). But it is always a good idea to apply the KISS principle (Keep It Simple, Stupid) first, when analysing data. In case of dynamic flow the hydrocarbon fluid contact can be inclined and/or irregular. Flat spots are generated by the acoustic impedance contrast over fluid contacts. They are not only restricted to silici-clastic deposits, but also other lithologies like limestones can be involved. It is perfectly possible to have a flat spot in a homogeneous carbonate reservoir as the difference between gas and water will generate sufficient contrast. In such case the background velocity and density values are of course relatively high.

DHI's are already generated by a slightly higher **hydrocarbon saturation** of the pore-fluid (5% is sufficient, but this is commercially not attractive). Flat spots caused by a fluid contact can be deformed by the slow velocity effect of the overlying gas filled reservoir (relative

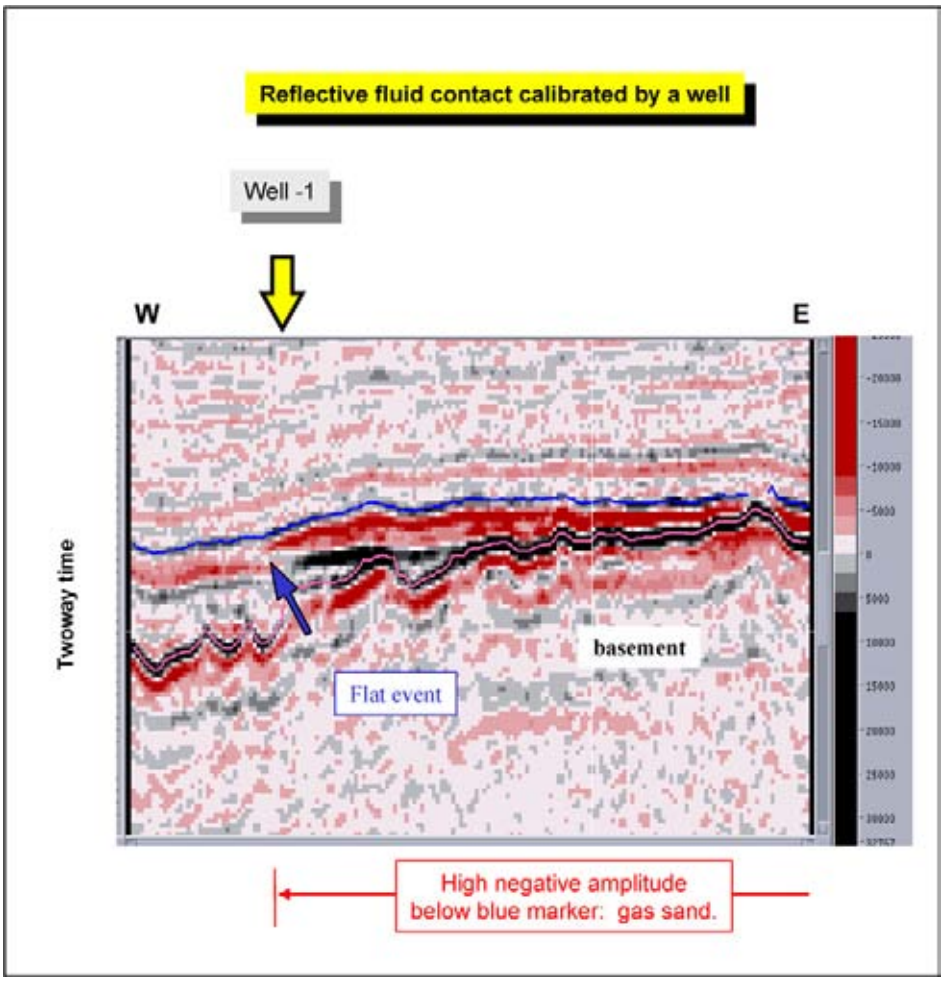

Figure 5.47: Flat event penetrated by a well which corresponds to a fluid contact in the reservoir rocks. The brightening of the top reservoir reflection indicates the presence of a class 3 AVO reservoir (data courtesy TFE).

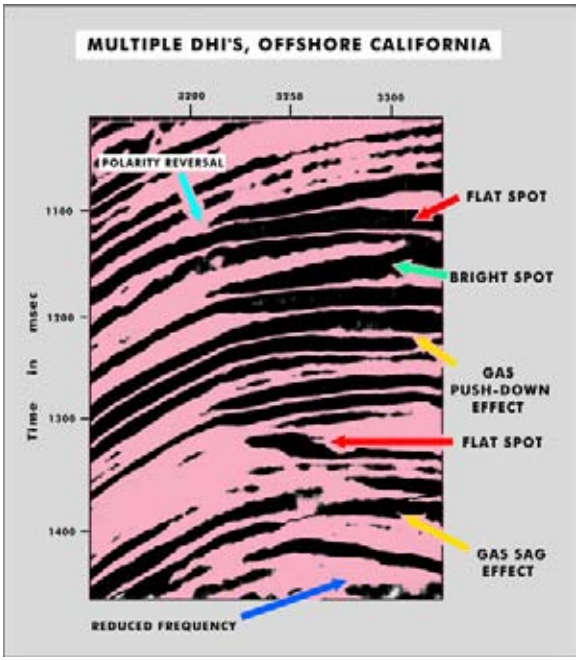

Figure 5.48: A part of a migrated seismic section displaying multiple Direct Hydrocarbon Indicators (DHI's). Slow velocities in gas-filled reservoirs produce a pull-down or sag effect on deeper layers. A marked reduction in seismic frequency contents in the zone underlying the hydrocarbon accumulation is often a powerful discriminating factor for the presence of oil and gas in the subsurface. It lies at the basis of spectral decomposition (modified after Brown 1988, reprint from AAPG whose permission is required for further use).

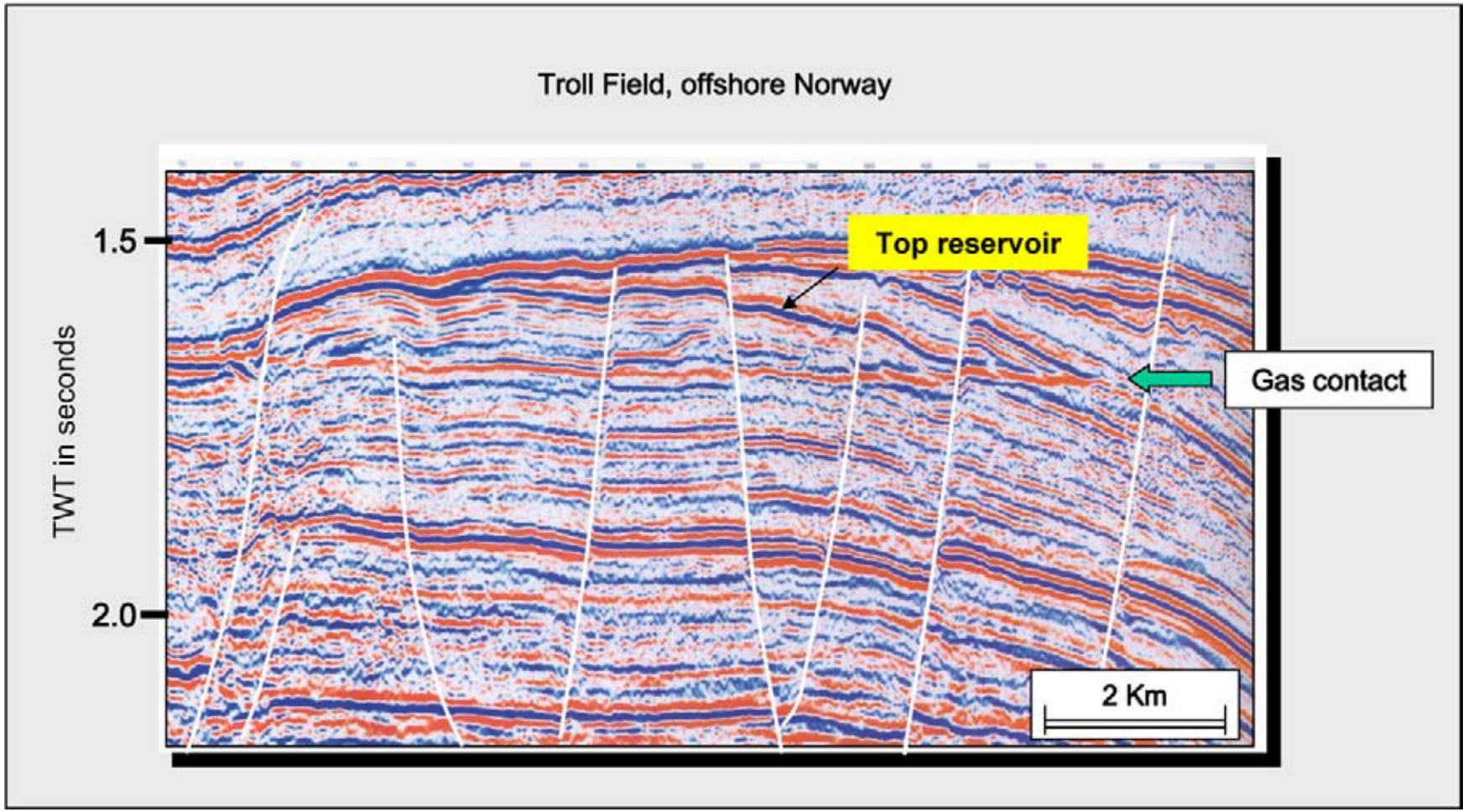

Figure 5.49: Seismic section across the Troll Field, offshore Norway. A flat spot is seen around 1.7 seconds TWT. The gas containing reservoir sands are Jurassic in age and have an average porosity of 28 percent (modified after Brown 1999, data courtesy Norske Hydro).

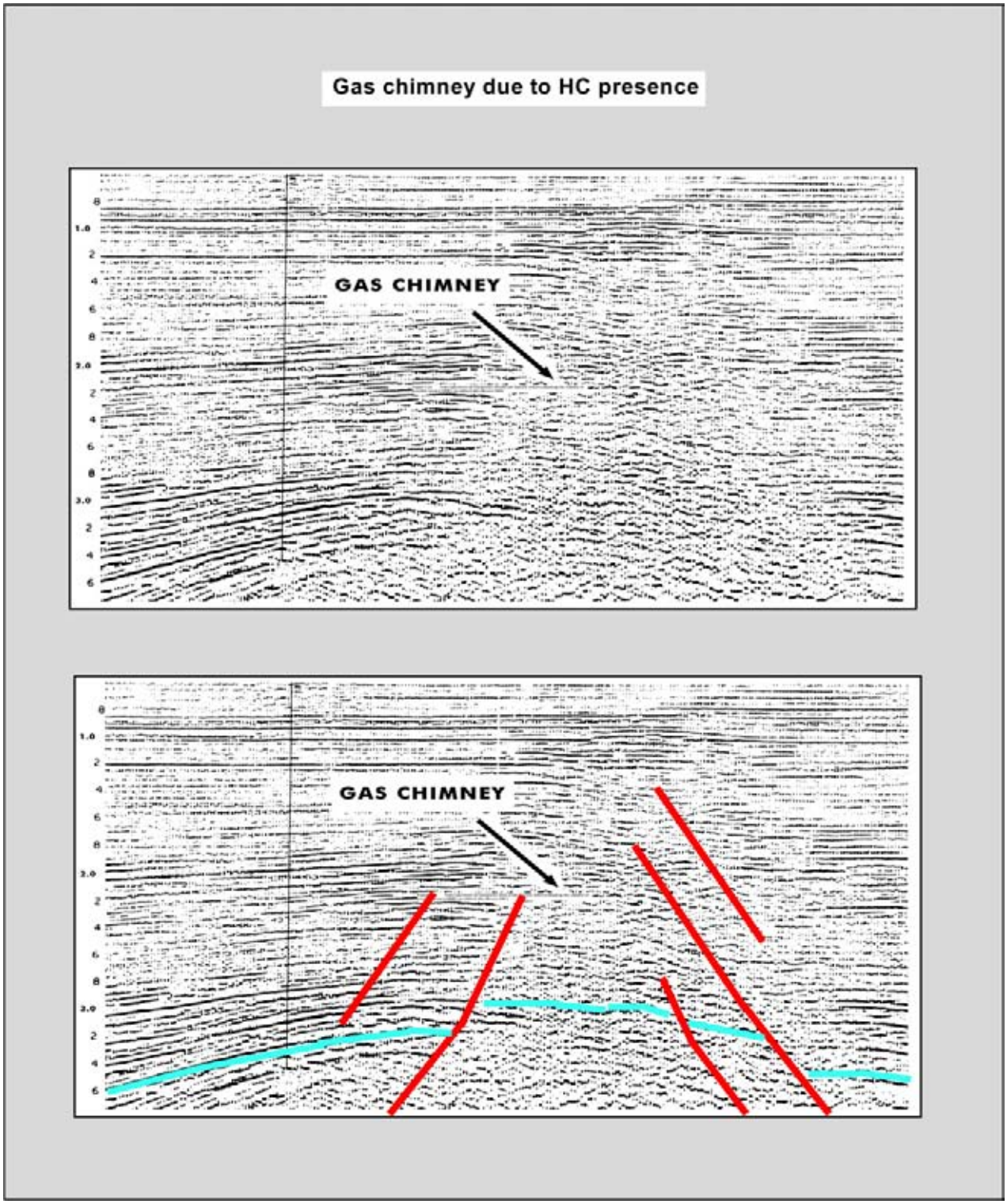

Figure 5.50: Gas chimney effect due to leaking of hydrocarbons from a trap located vertically below. Fracturing of the overlying series stimulates the vertical migration of hydrocarbons. The phenomenon can also reflect episodic partial breaching of the seal. The pressure relief in the reservoir restores the hydrocarbon retention capacity of the seal. The stacking velocities in these chimney zones are normally too high, thus creating artificial discontinuity of the reflections. In nature nearly all seals are imperfect; this gives rise to measurable geochemical anomalies at the surface that are directly related to the HC accumulations beneath (courtesy Shell).

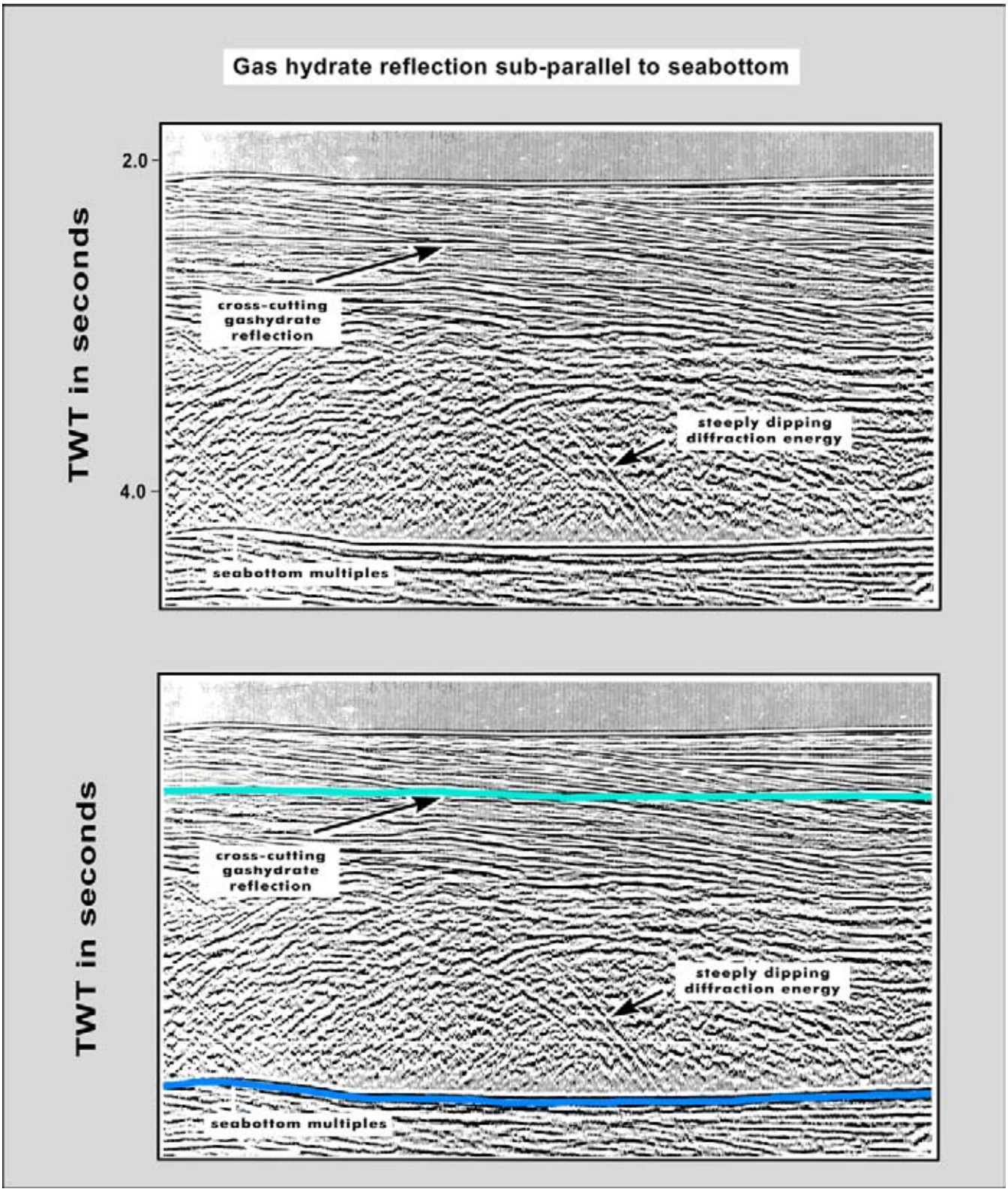

Figure 5.51: Gas hydrate reflection at relatively shallow depth with a geometry that is more or less parallel to the seabottom. The event usually cross-cuts normal sedimentary reflections and is triggered by the presence of biogenic gas. Caution is needed as low gas saturations (5–10 percent) can already produce sufficient acoustic impedance contrast to generate distinct seismic events. Gas hydrate consists of a mixture of gas and water in a solid state. It is only stable at very specific temperature/pressure conditions (courtesy of Shell).

Figure 5.52: Some points of interest when evaluating the validity of possible seismic DHI's (modified after Brown 1988).

pull-up – or less pull-down – at the edge due to a thinner gas column). Also overburden velocity effects and raybending deform its expression. The DHI reflection is sometimes only visible on some of the seismic lines across the structure. Varying noise levels can be responsible for this phenomenon. This observation should not discourage further analysis.

Sometimes it is useful to make an **optical stack** of several crosslines in order to bring out the HC contact reflection (Figure 5.53). This type of stacking is done on the seismic workstation; it is a visualisation technique whereby a suite of parallel lines are added together and a gain function brings out the weaker events. The method works surprisingly well, if the structure is well behaved.

Other investigation methods might give a more accurate answer on the prospectivity. Paleo-flat events have also been reported, whereby the area is tectonised at a later stage after the initial trapping of the hydrocarbons. The seal has been breached and/or the spill point of the structure is changed, which caused the hydrocarbons to migrated further updip. It does point to the presence of hydrocarbons and maturation of source rocks in the vicinity, which is very good for the prospectivity of other structures or traps in the area.

In evaluating **bright** and **dim spots** (exceptional high or low amplitudes on a reflection) the interpreter should realise that the amplitude strength of a reflection is also caused by tuning effects, due to a lateral thickness change of the reservoir section or changes in overburden properties. It can be influenced by differences in the matrix properties, grainsize and composition of the rocks. The AVO effects, present in the CDP gathers, show up in the outcome of the stacked results that are used in the time migration. In case of a Class 2 sand, there exists a polarity flip on the NMO-corrected gather and this may result in opposite amplitude for the top of a gas and water filled sand (dimming). In the Class 3 AVO sand, the stacking results in brightening of the top of the HC containing reservoir (see also next chapter). The amplitude of the full stack trace and the R_0 trace can therefore be quite different.

It should be mentioned that not all gas in the subsurface is hydrocarbon related. There exist for example also substantial accumulations of CO_2, which are however not commercial.

The frequency content of the seismic below a HC reservoir is noticeably different. The higher end of the frequency spectrum is appreciably attenuated (Rapoport et al. 1994). This phenomenon, first noticed by Russian workers, gets more and more attention in the petroleum industry. Abnormal attenuation and velocity dispersion (AVD) of seismic waves in oil and gas fields are frequently observed with a clear deviation from the theoretical elastic wave propagation (Rapoport et al. 2004). Examining the attenuation of specific frequencies can yield anomalies that correspond rather well with the HC accumulation, whilst conventional AVO does not always give good results. Several methods for spectral decomposition exist (Castagna and Sun 2006) to generate a continuous time frequency analysis of a seismic trace, with frequency spectrum for each time sample. It is a non-unique process and the same seismic trace can produce several time–frequency responses, and none are either right or wrong. Several methods exist:

- Discrete Fourier transform, involves a window measurement.
- Maximum entropy method, uses also a window measurement but it is difficult to determine the right parameters.
- Continuous wavelet transform, is equivalent to a temporal narrow-band filtering of the input seismic trace. The window implied by the wavelet description is frequency dependant.

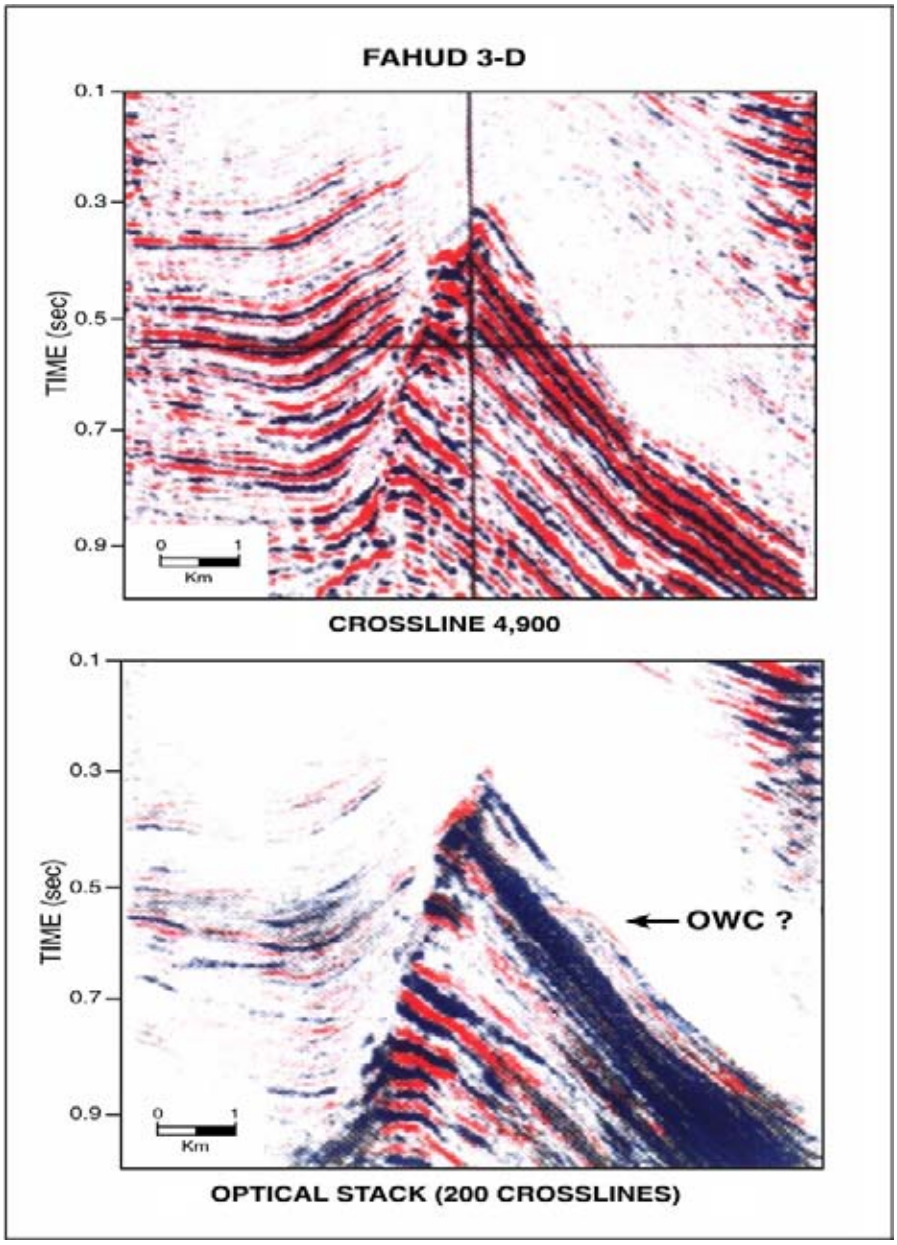

Figure 5.53: Optical stack of 3D crosslines in the Fahud field (northern Oman). Amplitude balancing brings out the HC water contact as a semi flat event (Onderwaater et al. 1996).

– Matching pursuit or wavelet recognition method, involves cross correlation of the wavelet against the seismic trace and its energy is subtracted from the seismic trace. The next wavelet signature is then crosscorrelated with the residual trace and this goes on till a certain small threshold value is reached for the energy on the residual trace. Wavelets are for example described by their centre frequency characteristics. The wavelets are placed on the trace according to the arrival time of the centre frequency. Disadvantage is lateral instability of the solution due to interference of several overlapping signals. Exponential pursuit decomposition can give more satisfactory results, whereby windowing-induced smearing of frequencies is avoided (Castagna and Sun 2006).

Castagna et al. (2003) proposed **Instantaneous Spectral Analysis** (ISA) for the detection of low frequency shadow zones below hydrocarbon accumulations (Figure 5.54). The method comprises several steps:

– Decompose the seismic trace in individual wavelets (spectral decomposition).

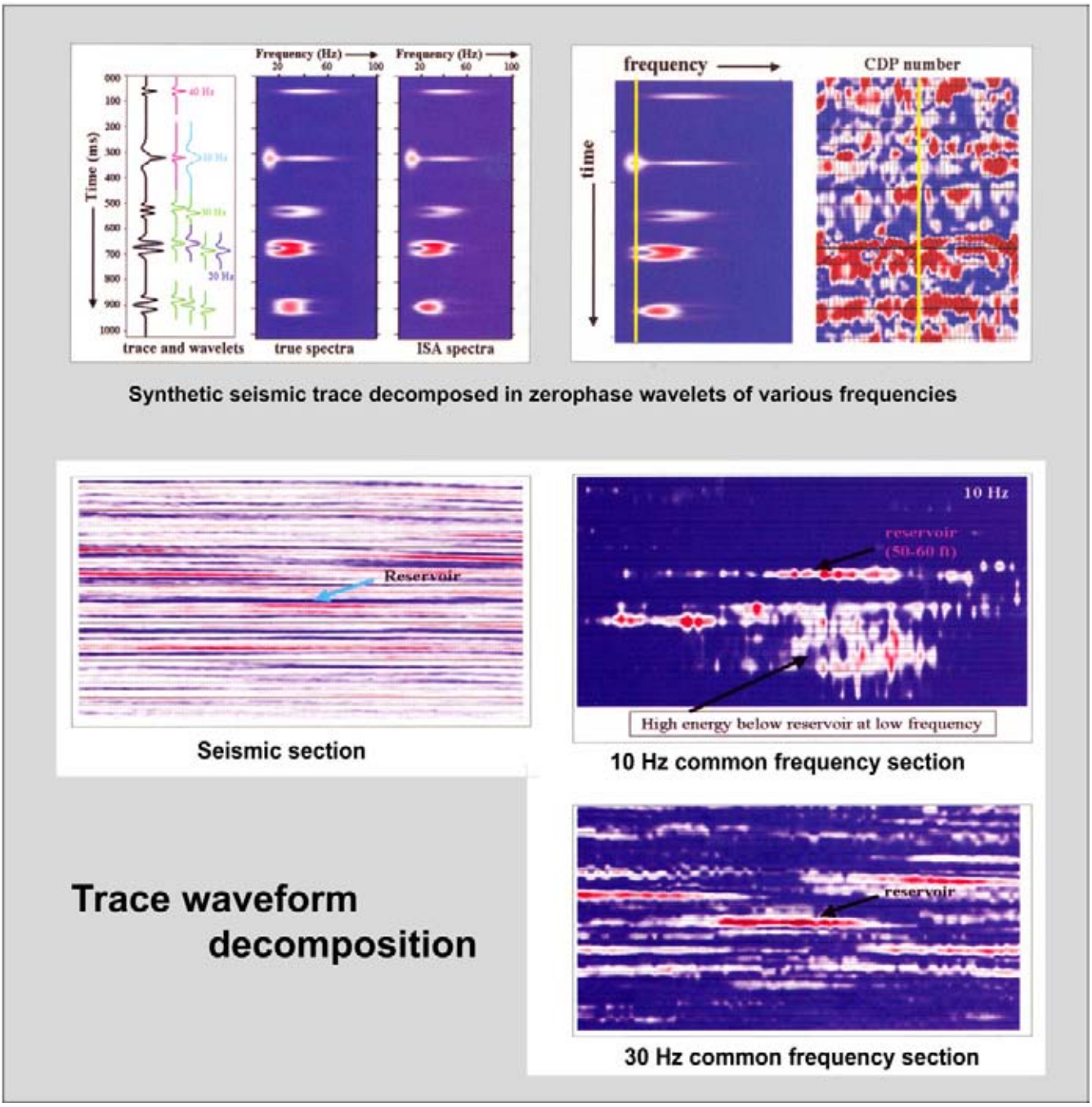

Figure 5.54: The Instantaneous Spectral Analysis (ISA) method allows quick visualisation of the frequency decomposition of a seismic trace. The 10 Hz plot shows here a strong anomaly representing a shadow zone below the base of the gas reservoir (modified after Castagna et al. 2003).

– Sum the Fourier spectra in the time–frequency domain to produce frequency gathers.
– Sort the frequency gather in a 3D time–frequency volume or cube. Section and time slices are subsequently examined on the presence of anomalies.

The wavelet transform decomposition together with singularity analysis resulted recently in a study technique, whereby an alternative seismic attribute SPICE (Spectral Imaging of Correlative Events) is generated (Smythe et al. 2004). It enhances the boundary framework of the subsurface and is rich in structural as well as in stratigraphic detail. It is important to produce time-frequency representations with sufficient spatial and temporal resolution for reliably predicting fluids and

reservoir character (Rauch-Davies and Ralston 2005). Several methods are available:

- Short Term Fourier Transform (STFT).
- Wavelet Transform (WT).
- Wigner-Ville Distribution (WVD) method.

Mathematically, the WVD of a seismic trace $x(t)$ is the Fourier transform of that trace's signal auto-correlation function with respect to a delay variable τ. Algorithmically, this means that for each time sample in the seismic trace, $x(t)$, we form a second series $y(\tau)$ consisting of the products of the signal values at past times, $x(t-\tau)$, with those at future times, $x(t+\tau)$, where time into the past τ is equal to the time τ into the future. A Fourier transform of the series $y(\tau)$ provides the frequency distribution of the signal at the time sample being analysed. Absence of windowing functions, in contrast to the STFT and WT methods, allows the WVD to obtain high-resolution in both time and frequency simultaneously. The method has been demonstrated to successfully differentiate between commercial, non-commercial gas accumulations and high-porosity water sands (Rauch-Davies and Ralston 2005).

Running window spectral decomposition provides a means to investigate seismic features that tune at a given frequency rather than at the dominant frequency of the source wavelet. It will give information beyond the tuning thickness. It can be used for enhancing the delineation of detailed sedimentary features (Giroldi and Alegria 2005).

Trace frequency attributes have a potential to help to resolve high resolution stratigraphic subdivisions as shown by Gengyi et al. (2006), who used it on a Chinese seismic dataset. The well logs are shown to support the subdivision as recognised on the amplitude-frequency spectrum of the seismic trace at the well location (Figure 5.55). The branching supports the hierarchy of the subdivision. It is a potentially powerful new automated subdivision technique of seismic data.

Alternatively a Stockwell or S-transform can be performed on a seismic trace $f(t)$, whereby for each frequency a new trace is obtained corresponding to the specific input frequency. This way a frequency gather can be computed and the data is compared, screened for anomalies (Odebeatu et al. 2006). It should be realised that perfect spectral decomposition is never achieved because of the Heisenberg Uncertainty principle. They suggest there might be a relation between the spectral anomalies observed below a gas reservoir and a velocity dispersion effect, as was suggested by Rapoport et al. (2004). Their conclusion is based on synthetic modelling together with AVO analysis, but the matter is still open to debate. If attenuation and absorption were responsible for the observed anomaly, it is strange that the higher frequencies re-appear in the section at deeper level than the gas accumulation.

Spectral analysis is also applied to log data. Nio et al. 2005 describe the use of an error filter in the linear prediction of the log shape to evaluate the spectral contents. The log attribute is known as the Prediction Error Filter Analysis curve (PEFA). It visualises breaks in continuity of the spectral representation of a log. The PEFA can easily be transformed into an Integrated PEFA curve (INPEFA), that is more stable and easier to interpret geologically. The log attribute is useful in high resolution sequence stratigraphy, where climatic cycles are detected in the sedimentary record.

In the shallow surface also the electro-magnetic response is different in the area with the HC accumulation. There are recent examples where this investigation technique has been successfully applied to distinguish the outline of a field (Strack et al. 1991, Wright et al. 2002). Improvements in the method have led to better interpretable end results and marine controlled source EM (CSEM) is now an additional tool for the explorationist (Tompkins 2004). Multichannel Transient Electro Magnetic surveying (MTEM) is a promising method for detecting hydrocarbons (First Break, 2005, No.1, p. 59). It uses a continuous monochromatic signal. The basic idea is to inject a current in the ground in one place and measuring the response of the earth at an other place, i.e. the gradient of electric potential or the rate of change in the magnetic field. The flow of current is controlled by the resistivity of the rocks and the objective is to determine these resistivities. For this a sudden step in the current can be utilised and the gradient of the electrical potential is examined. The rise from zero to the DC level is related to the resistivity. The DC level corresponds to conventional DC resistivity surveying.

The controlled source EM technique is nowadays applied in the offshore, whereby the receivers are installed on the seabottom (seabed logging or SBL method) and the low frequency source dipole is deep-towed behind a vessel (Johansen et al. 2005). Energy is registered from various pathways: reflection, refraction and guided head waves. The EM signal is rapidly attenuated in the seawater (0.2 Ohm for a 0.25 Hz signal) and brine filled sediments (2 Ohm). These signal pathways dominate the near source to receiver offsets (0 to 3000 metres). The guided headwaves is caused in the HC containing high resistivity (30–500 Ohm) thin bed (20–200 metre thick) layer at the critical angle. It is less attenuated and

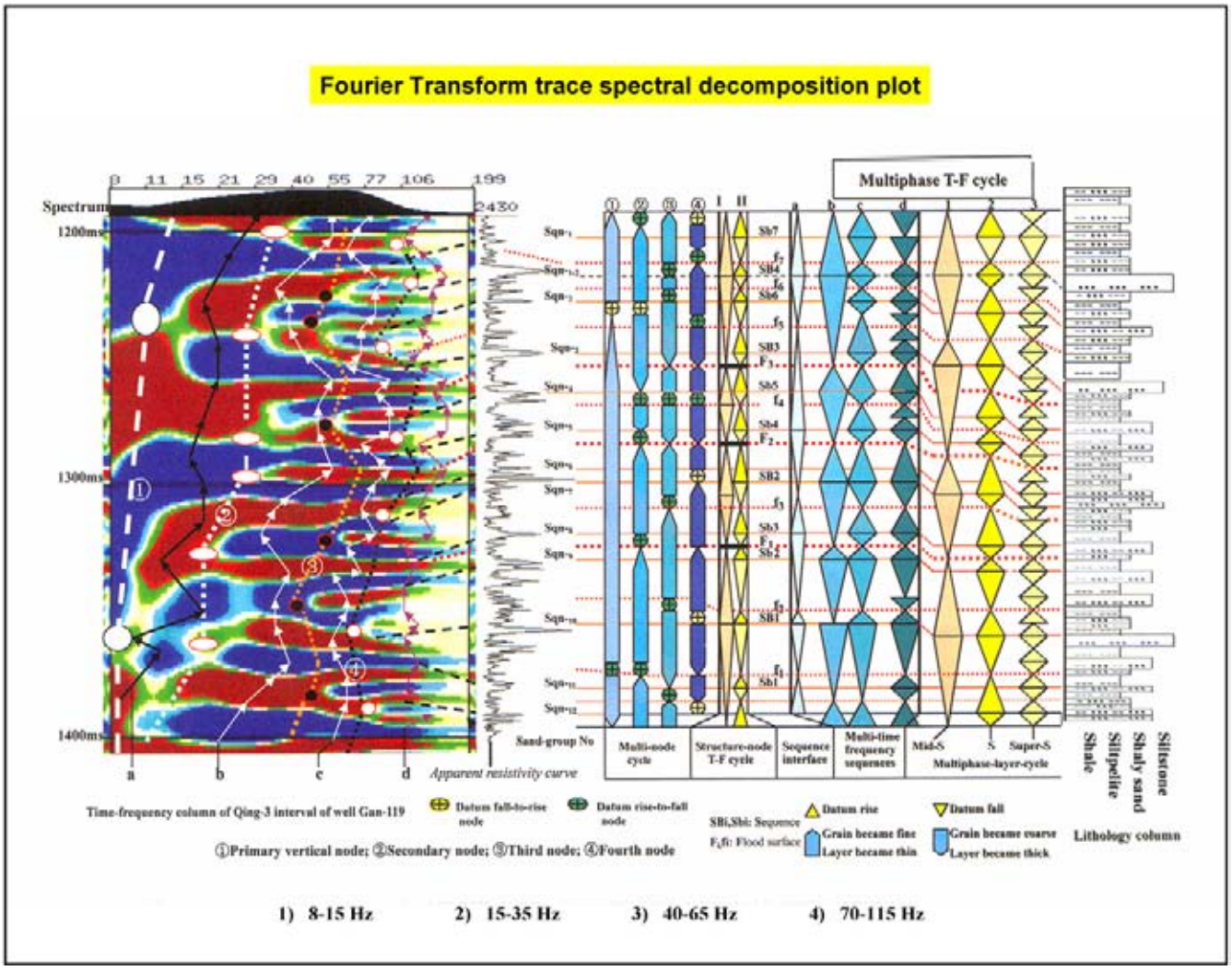

Figure 5.55: Fourier spectral decomposition of a seismic trace in a well location. The amplitude spectrum show a dendritic structure with nodes that correspond to the lithological subdivision as seen by the resistivity well log (after Gengyi et al. 2006).

intercepted by the larger offset receivers (3000 to 6000 metres). At large offsets (>6000 metres) the recording is dominated by the so-called air-wave, generated by the reflected energy and refracted back by the air-water surface (Johansen et al. 2005). Air is very resistive for electrical currents with 10^{10} Ohm. The refracted energy from the highly resistive layer will dominate over the directly transmitted energy when the source receiver distance is comparable to or greater than the depth to this layer. Detection of this refracted and guided headwave energy is the basis of the SBL methodology. In the Troll West gas province, where the method had been tested, a clear anomaly on the 3000 to 6000 metres offset coincides with the high resistivity hydrocarbon accumulation and this is a very encouraging result. An other recent CSEM success story is the detection of gas hydrate on the Cascadia margin offshore Vancouver Island, that corresponds with seismic blank zones (Schwalenberg et al. 2005).

In carbonates, **permeability traps** can be present within the same gross lithological unit (e.g. Moore 2001). These traps are very difficult to map. Their evaluation by conventional methods is hampered by the very irregular outline. Faulting and fracturing are important mechanisms to change the original reservoir properties of rocks. Early structuration and migration of hydrocarbons may prevent the negative effects of late cementation processes (diagenesis) from affecting the rocks in the reservoir; this kind of anomaly is standing in sharp contrast to the properties of the surrounding regional hostrock. Regional crossplots are not indicative for what is there in the field. Early expulsion products (acidic in composition) may cause local leaching along the migra-

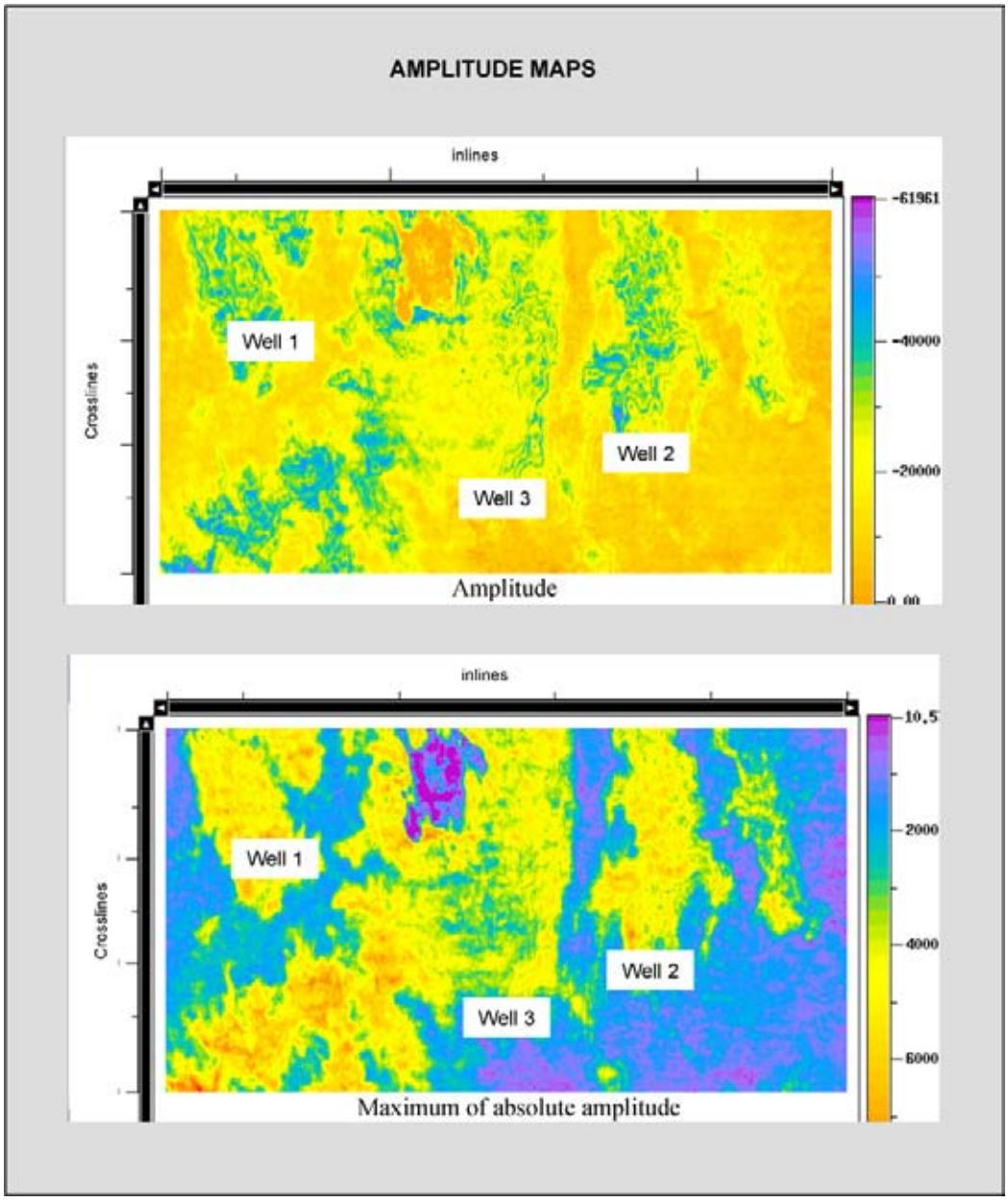

Figure 5.56: Amplitude and maximum absolute amplitude maps. The selection of the right colour scale is important to bring out and enhance visibility of certain features (courtesy TFE).

tion path and lead to an anomalous porosity distribution (Ing A. Marhx, pers. com.).

5.4 Amplitude and Attribute Anomalies

Amplitude maps for individual markers are compiled to evaluate its behaviour along a time horizon. These amplitude maps are very useful in delineating areas of possible hydrocarbon occurrences. If the colour scale is chosen correctly, zones with **amplitude anomalies** are directly visible. These may or may not correspond to the presence of hydrocarbons. There are several types of amplitude maps (Figures 5.56 and 5.57). Seismic data often contains more information than is expected at first glance and it is therefore good practice to assume that the attribute variations have some sort of relation to geological changes unless proven otherwise.

The amplitude map is overlain with the depth contours of the horizon to illustrate the correspondence with a

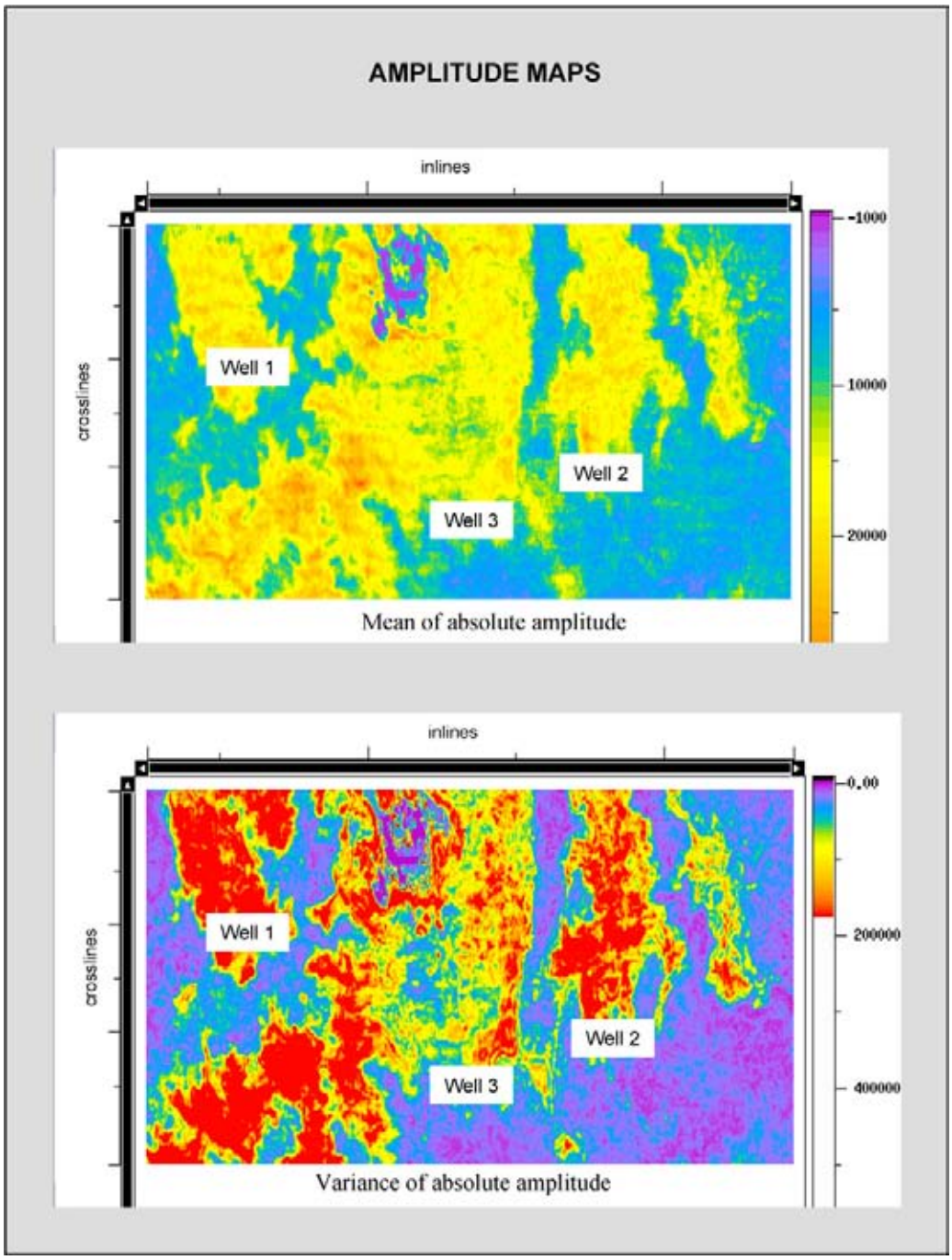

Figure 5.57: Other types of amplitude maps can be generated, for example the "Mean absolute amplitude" and "Variance of absolute amplitude". Each map gives a slightly different view on the same seismic dataset (courtesy TFE).

mapped structure. Before making amplitude maps it is advisable to check the level of clipping applied to the horizon. The amount of AVC (Automatic Volume Control) on the seismic is sometimes so high, that the real dynamic range of the stored amplitudes is too much reduced. The amplitude values can be oversaturated, when they depass a certain upper limit and are all stored at the maximum value of the system (8 bit and 16 bit data clipping). Therefore no reliable amplitudes measurements are obtained later on from this data. **Certainty maps** can be compiled to illustrate the degree of confidence for the attribute. Statistical utilities also help to visualise the amplitude behaviour/distribution. The continuity of a reflection is visualised in order to illustrate the geographical distribution of a picked reflection. This assists in the delineation of potential drilling

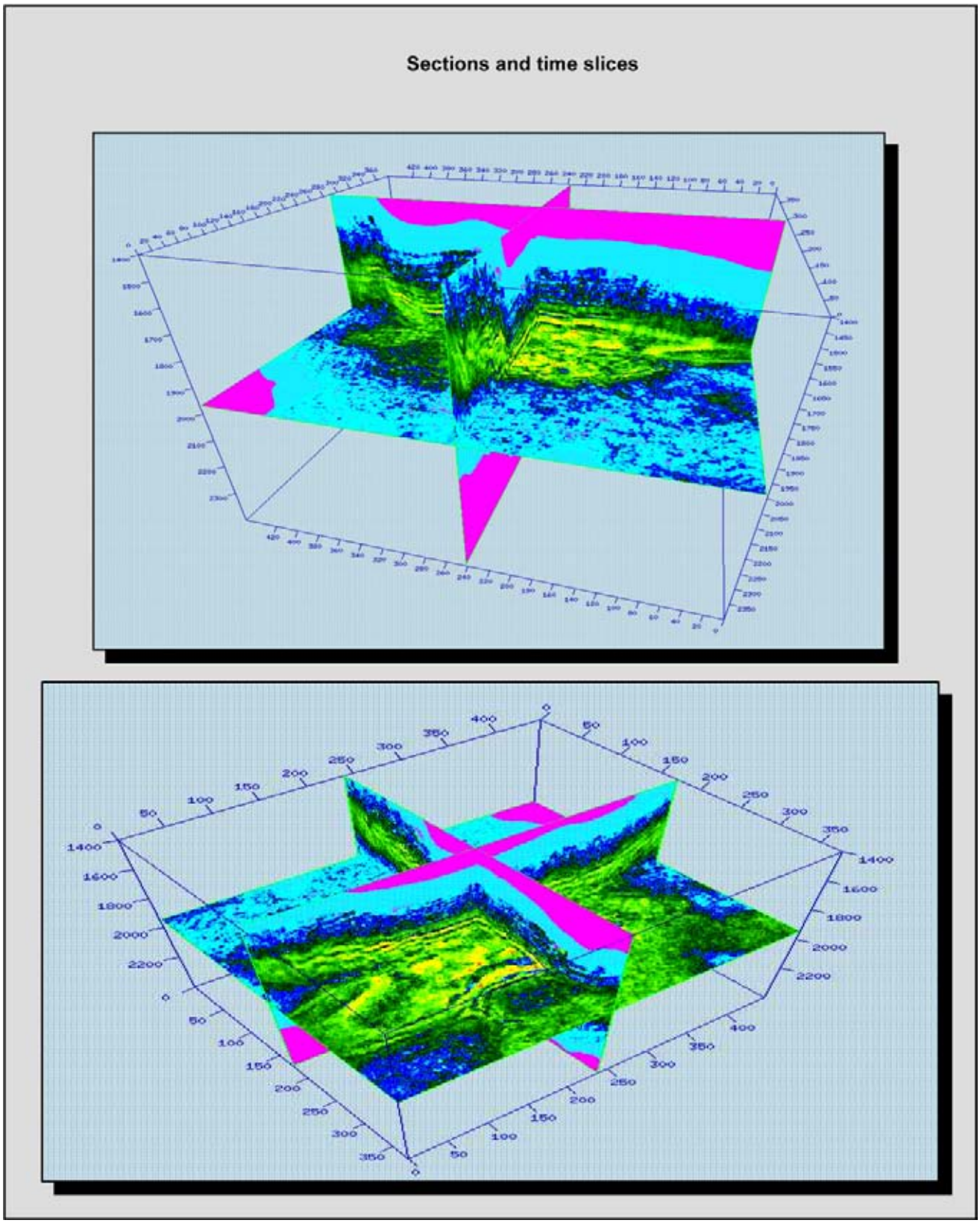

Figure 5.58: Cross sections and slices through a 3D seismic volume is useful to appreciate the structuration of the subsurface (courtesy M. Da Silva).

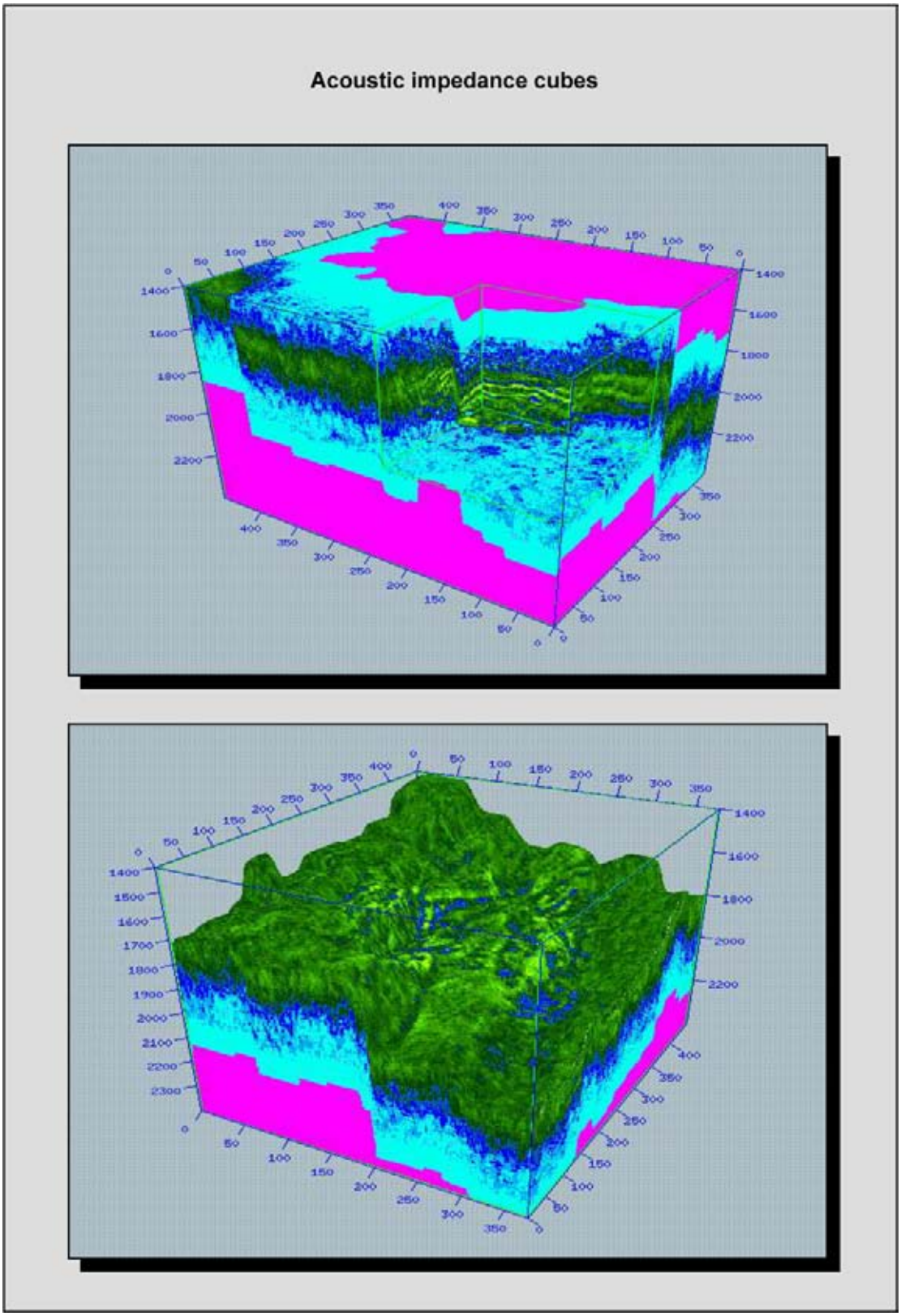

Figure 5.59: The acoustic impedance property is an attribute with an improved seismic resolution. This is due to the fact that wavelet inference effects are removed. Gross lithological units are more easily identified. Also pore fluid changes are better resolved. It is recommendable to carry out pilot studies that prove the usefulness of the exercise before embarking on large projects (courtesy M. Da Silva).

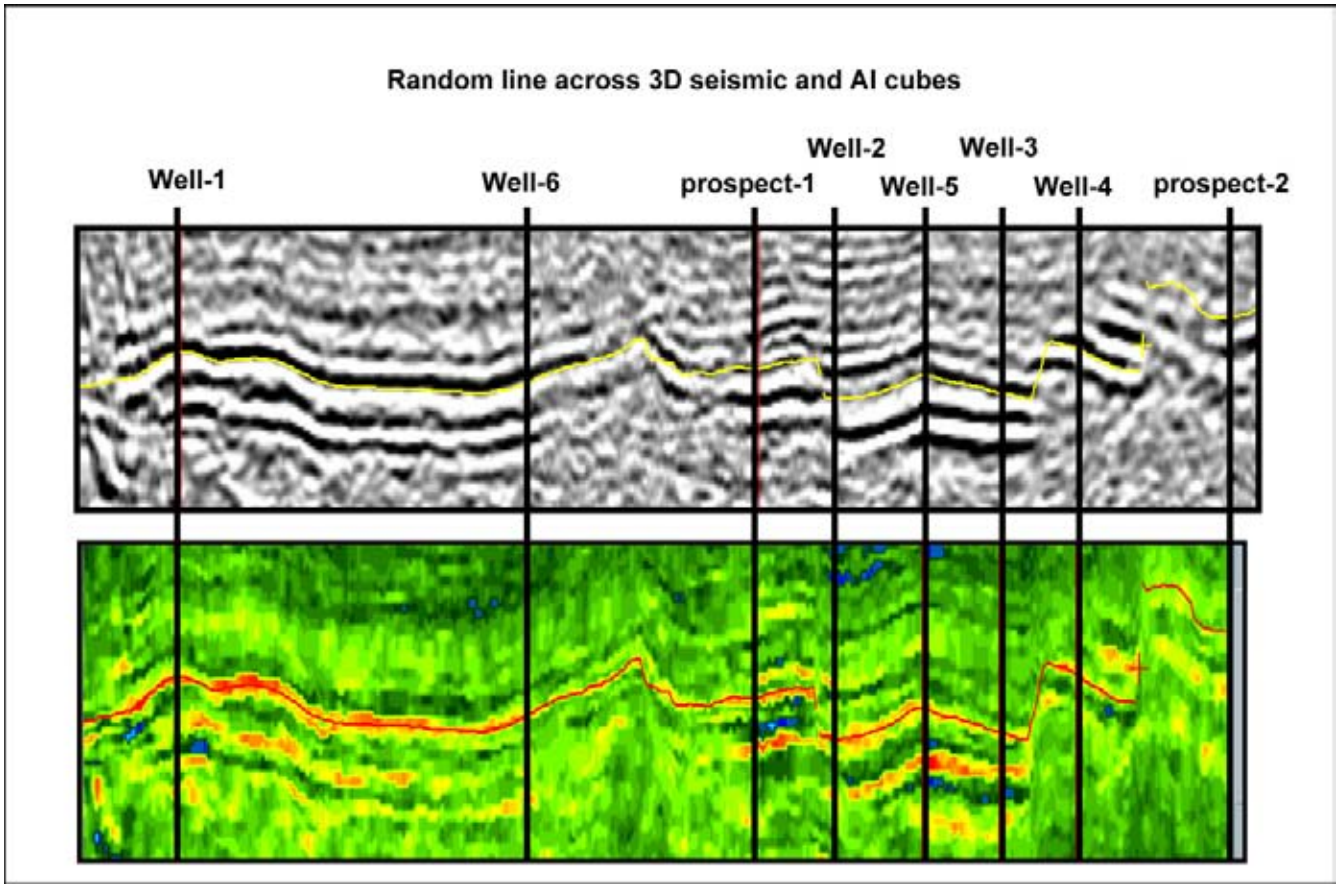

Figure 5.60: Random lines are helpful to give a quick view on certain details of the dataset. Here a comparison between the seismic and the inverted AI cube is made (courtesy M. Da Silva).

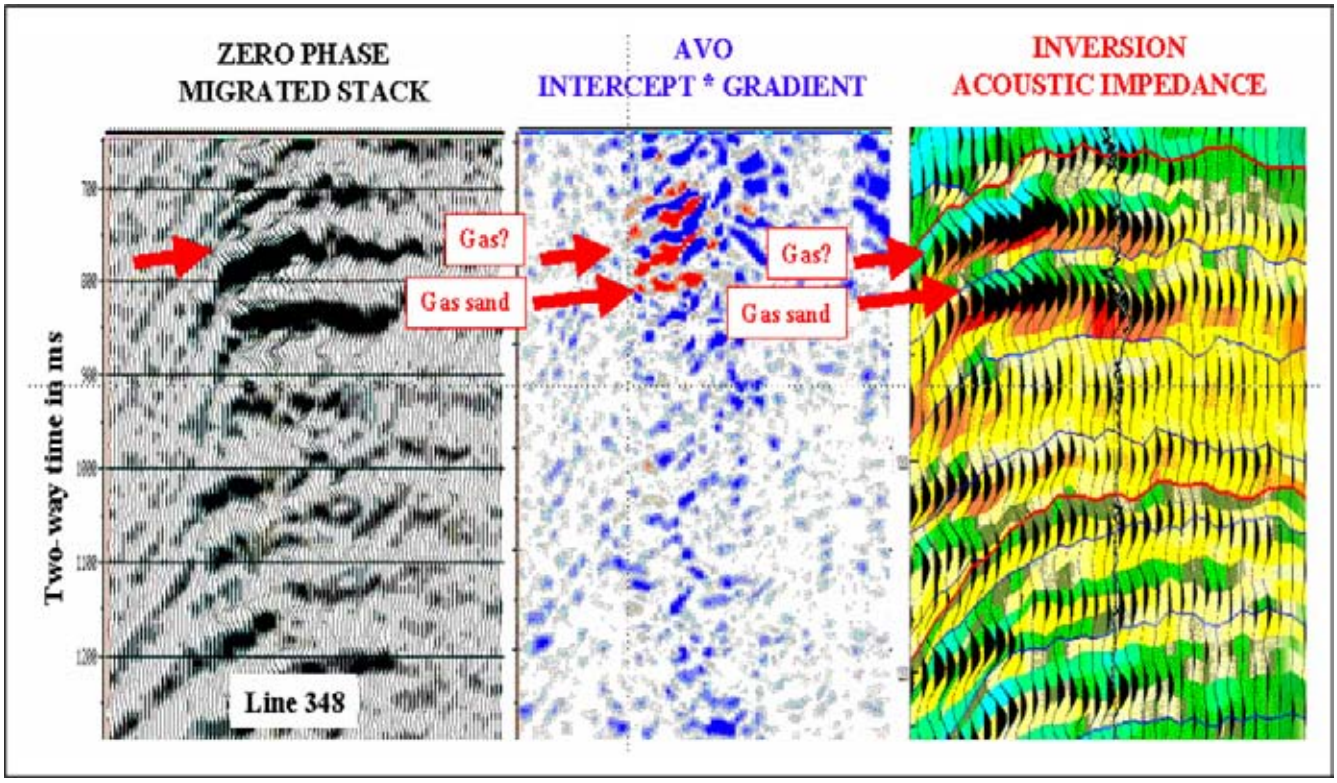

Figure 5.61: The AVO and seismic inversion methods are complementary techniques. Their results increase the confidence attached to the outcome of individual investigation methods. The ultimate aim is prediction of pore fill changes and distribution of reservoir characteristics.

hazards, like 'abnormally' pressured carbonate floaters within a salt sequence.

The **Amplitude-Versus-Offset** (AVO) behaviour of the top reservoir reflection is useful to generate discriminatory evidence for changes in porefill of the reservoir (e.g. Veeken et al. 2002, Rauch-Davies 2003). This evaluation technique means going back to the prestack domain and the CDP gathers.

It is customary to extract an **average-amplitude** map for a certain interval. A constant time window can be utilised, a constant time window hung from a horizon or a window between two horizons. In the last case the attribute measures the amount of seismic energy present between two mapped seismic markers. The amplitude response is calibrated by well control. Such analysis is for instance an useful option for assessing the distribution and amount of hardrock within salt domes. Selecting the proper time window size is an art in itself. It is possible to slice through different seismic cubes (Figure 5.58). The acoustic impedance cube is a very interesting attribute (Figure 5.59). Random (or arbitrary) lines are useful to concentrate on certain details within the dataset (Figure 5.60). Comparison is made between the normal seismic data and the results of the inversion. AVO and acoustic impedance are studied together to verify their correspondence in anomalies. It enhances the confidence carried for the validity of the results of the individual investigation methods (Figure 5.61). These techniques are presented in more detail in Chapter 6 below.

Software package like Stratimagic^{TM} let the interpreter generate very fast a large quantity of interval attribute maps. They permit visual inspection of the data set with sophisticated 3D displays. This brings out subtle trends in the data that might have been ignored otherwise (Addy 1998). Automatic mapping of pinch-outs and channel geometries is possible. Attributes are imported from other software packages (e.g. SRCattrib^{TM}, Matlab^{TM}, Geolog6^{TM}, Emerge^{TM}, Easy Trace^{TM}, Osiris^{TM}). The choice of the right attributes, to evaluate the reservoir characteristics, is essential and this should be established on a case by case basis. The generation of cross plots is hereby of vital importance (e.g. Lithos^{TM} package of Total). If there exist a good correlation between the parameters, then the trend can be used for lateral prediction purposes. For instance the conversion from impedance cube to lithology is often done in this way (e.g. Guilbot et al. 1996).

Figure 5.62: Seismic attributes are easily computed, but it is a hell of job to look at them all. They give a slightly different view on the same dataset. Normally five attributes are selected that are of particular interest: e.g. amplitude, Hilbert Transform, instantaneous phase, instantaneous frequency, acoustic impedance. Crossplots are made to visualise clusters that give a good separation for lithology and/or porefill.

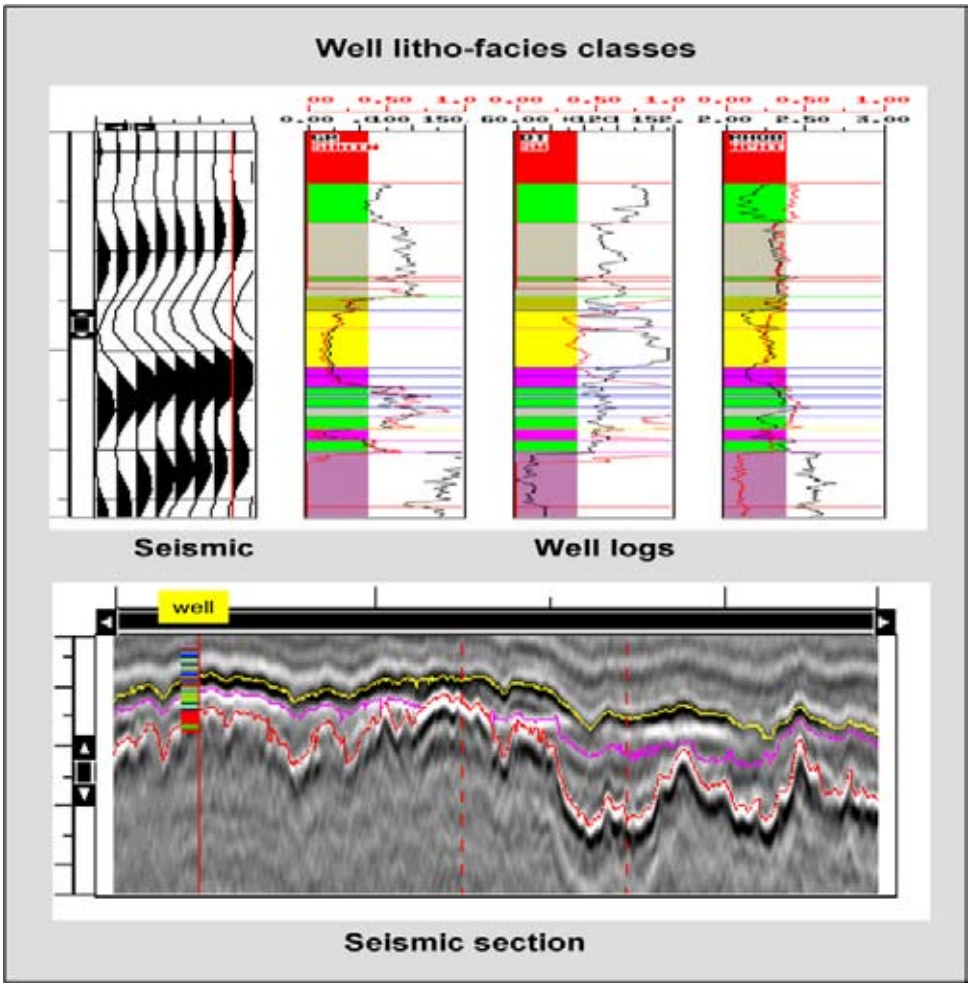

Figure 5.63: Well data with litho-facies units that are distinguished on log value cut-offs. The time samples on the seismic sections are later classified based on cluster analysis of the well data in the crossplot (courtesy TFE).

Numerous attributes are easily produced, but it is a hell of a job to look at them all (Figure 5.62). Sixteen hour working days are not everybody's cup-of-tea. Managers and fellow geoscientists like to see the relevant attributes and are easily bored by long displays of similar data (cf Brown 2005). So, it is more common practice that the interpreter selects four or five attributes and studies those in great detail. It is obvious that the amplitude and frequency are the first attributes to be considered. Cut-off values in well data crossplots are very useful to create groupings and carry out later predictions (Figures 5.63 and 5.64). Structural continuity is conveniently illustrated by the coherency cube.

Neural network classification schemes are helpful to group the seismic response of the various seismic traces in and around the reservoir interval (Stratimagic^{TM}, Emerge^{TM}, DGI^{TM}, DTect^{TM}). The **neural network** approach is a non-linear classification technique (Gurney 1997, Poulton 2001). The algorithm is fed with some learning points to guide the classification. Automatic detection of DHI's is done in this way. Moreover, seismic traces can form input for the Kohonen neural network classification. The trace classification procedure is done in a supervised and non-supervised mode (Balz et al. 1999). The supervised approach is preferred because the interpretation of the results is more straightforward (see Section 2.8). Acoustic modelling and well-to-seismic calibration remains a critical factor to translate the qualitative seismic facies classes into quantified reservoir properties, suitable as input for reservoir modelling (Poupon et al. 2004). One application of a neural network trace classification is the computation of chimney cubes as described by Aminzadeh et al. 2002 (Figure 5.65). It gives instant access to anomalies related to the presence of hydrocarbons (Figure 5.66). If sufficient well control is available, than also a link can be established with specific reservoir parameters, like porosity, permeability, HC saturation, net-to-gross ratio (Aug et al., in prep.).

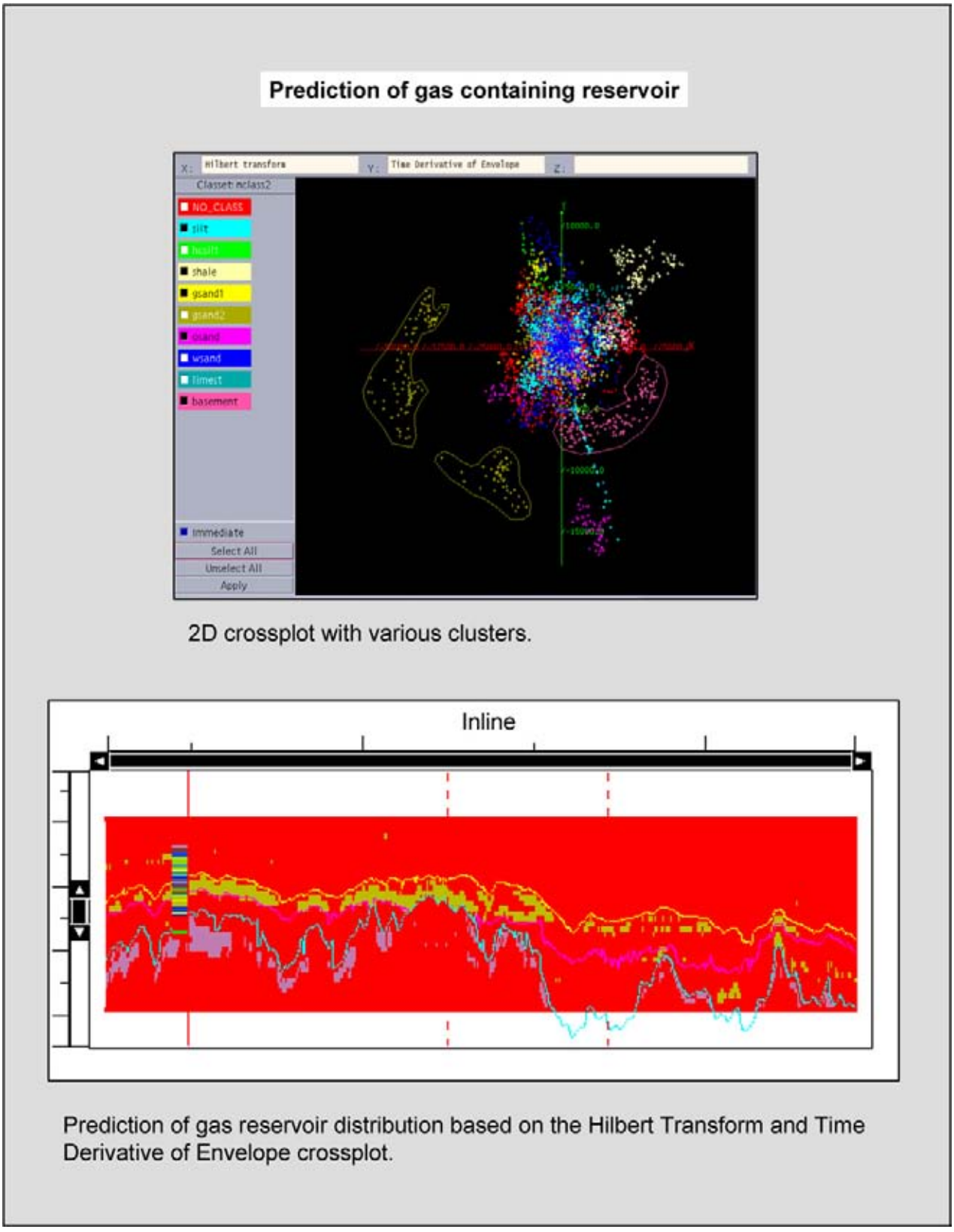

Figure 5.64: Crossplot clustering and prediction of gas reservoir in the seismic cube. The crossplot is made with aid of the vertical samples in the wells. The prediction outside the well control uses the selected attribute cut-off values of the clusters, analysed for each time sample in the seismic cube (courtesy TFE).

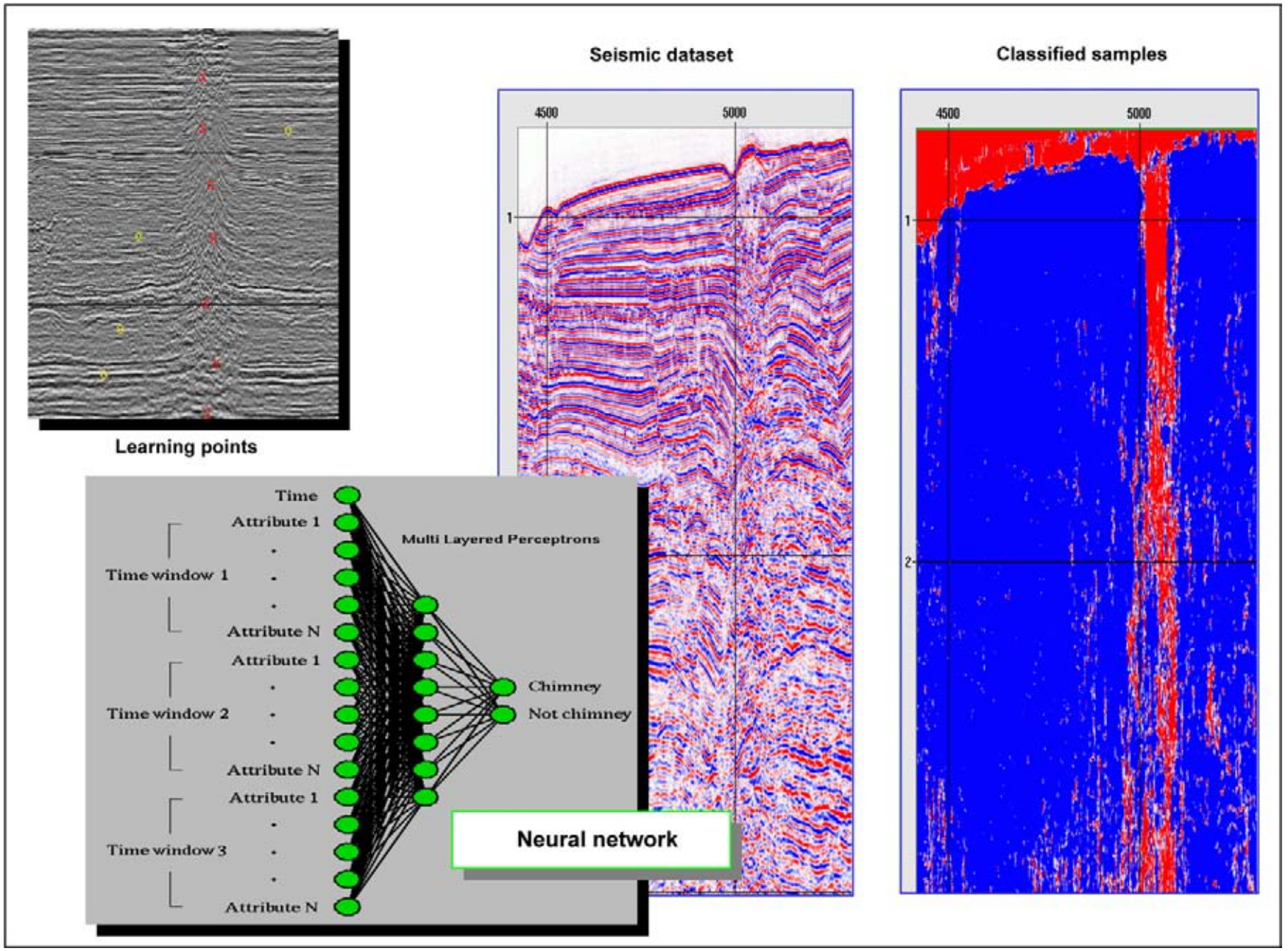

Figure 5.65: The neural network classification makes use of learning points to guide the classification of the time samples. Learning points are provided by the sample values at the well locations where the reservoir parameters are known (modified after Aminzadeh et al. 2002 and courtesy De Groot/Bril).

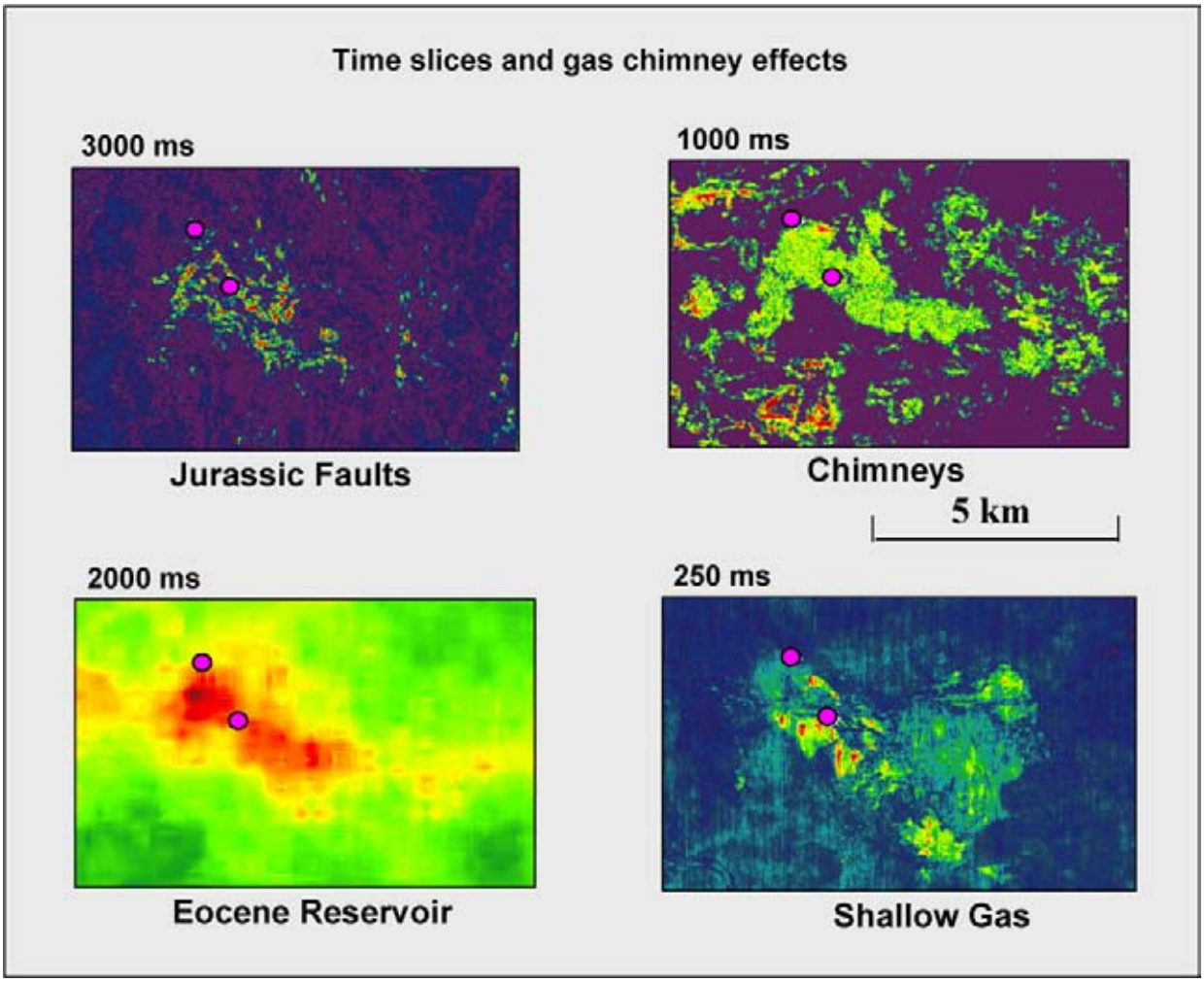

Figure 5.66: Map view of the classified cube at different stratigraphic levels (Meldahl et al. 2001 and courtesy DeGroot/Bril).

The overlying seal may have changing properties and those influence the aspect of the top reservoir reflection. The result is that the presence of HC in a reservoir is possibly disguised within the overall AVO response. Each of the above described methods has its own merits for discriminating reservoir/seal properties.

Chapter 6

Seismic Reservoir Characterisation

6.1 Amplitude-Versus-Offset (AVO)

It can be demonstrated that the amplitude character of seismic reflections varies with offset, due to changes in the angle-of-incidence (Figures 6.1 and 6.2). This feature is evident in the pre-stack CMP gathers, but it has been often ignored by the geophysicist. Zero Offset Stack and migrated time sections are the standard output of seismic processing; the prestack appearance of the data is easily just forgotten. Special studies are conducted to analyse the behaviour of '**Amplitude Versus Offset**' (AVO-studies) and these give detailed information on the porefill of reservoirs (e.g. Ostrander 1984, Castagna and Backus 1993, Chiburis et al. 1993, Hilterman 2001, Veeken et al. 2002b). AVO studies have proven their value in the past and are now rapidly becoming a standard routine in prospect evaluation (e.g. Veeken and Da Silva 2004, Bourque and Stevens 2005, Veeken and Rauch-Davies, 2006).

The reason, why porefill and angle-of-incidence related effects exist, can be better understood by considering the following analogy. It is a well known fact that stones thrown on the air/water interface can bounce three or four times before finally disappearing into the water. Experience teaches that this effect is depending on the angle under which the stone hits the water. It also is related to the actual shape of the object. Thrown perpendicular to the air/water interface the stone enters the water straight away and sinks directly to the bottom. For low incidence angles it is deflected at the interface and stays in the air, where gravity again gets back its grip onto the object. A direct relationship between this bouncing effect and the angle-of-incidence is established, and hence an angular anisotropy exists. To come back to our subsurface velocity/density model, it can now be better understood why it is interesting to investigate the degree of angular anisotropy of the seismic wavefront (velocity and amplitude effects).

It appears that amplitude behaviour of the different raypaths varies according to the porefill of the lithology. Water filled reservoir does show normally a small decrease in amplitude with offset, while hydrocarbon-filled reservoirs exhibit a more rapid decrease. It depends on the geology, the encasing lithologies and the porefill. The near and far offset responses of a gas sand are often quite different. This AVO effect represents a potentially powerful tool to discriminate between water and hydrocarbon saturated reservoirs. It means however that we have to go back to the prestack domain and therefore prestack time migrated data is at least required (Veeken and Rauch-Davies, 2006).

The reflection coefficients at different offset and incidence angles are computed. The correct thing to do, is to use the full set of **Zoeppritz equations** (Zoeppritz 1919), but these are pretty awkward to handle (Figure 6.3). These equations give amplitudes that are correct up to the critical angle, but they do not include the headwave energy (Sheriff 2002). They assume continuity of stress and displacement at the interface. The amplitudes of several rays show an irregular behaviour with increasing offset (Figures 6.4 and 6.5). Also converted P–S rays are here computed, which are currently drawing more and more scientific interest (e.g. Criss et al. 2005).

Aki and Richards (1980) give a more convenient matrix description of the Zoeppritz equations. In a schematic form it is written as:

$$Q = P^{-1}R. \tag{6.1}$$

They came up with the following formula (hold tight and take a deep breath):

$$R_{(\theta)} = 0.5\big(1 - 4p^2V_{\mathrm{s}}^2\big)\left(\frac{\Delta\rho}{\rho_{\mathrm{a}}}\right) + (1/2\cos^2\theta)\left(\frac{\Delta V_{\mathrm{p}}}{V_{\mathrm{pa}}}\right) - 4\big(p^2V_{\mathrm{sa}}^2\big)\left(\frac{\Delta V_{\mathrm{s}}}{V_{\mathrm{sa}}}\right), \tag{6.2}$$

whereby $\rho_a = (\rho_1 + \rho_2)/2$, $\Delta V_{\mathrm{p}} = (V_{\mathrm{p2}} - V_{\mathrm{p1}})$ and $p = \sin\theta_1/V_{\mathrm{p1}} = \sin\theta_2/V_{\mathrm{p2}}$. The a-suffix stands for average.

The p is also known as the ray parameter in Snell's Law as seen already before.

Shuey (1985) proposed a polynomial fit for the reflectivity, that is accurate up to a 35 degrees incidence angle:

$$R_{(\theta)} = R_{(0)} + \left(R_{(0)}V_0 + \frac{\Delta\sigma}{1 - (\sigma_2 - \sigma_1)^2}\right)\sin^2\theta$$

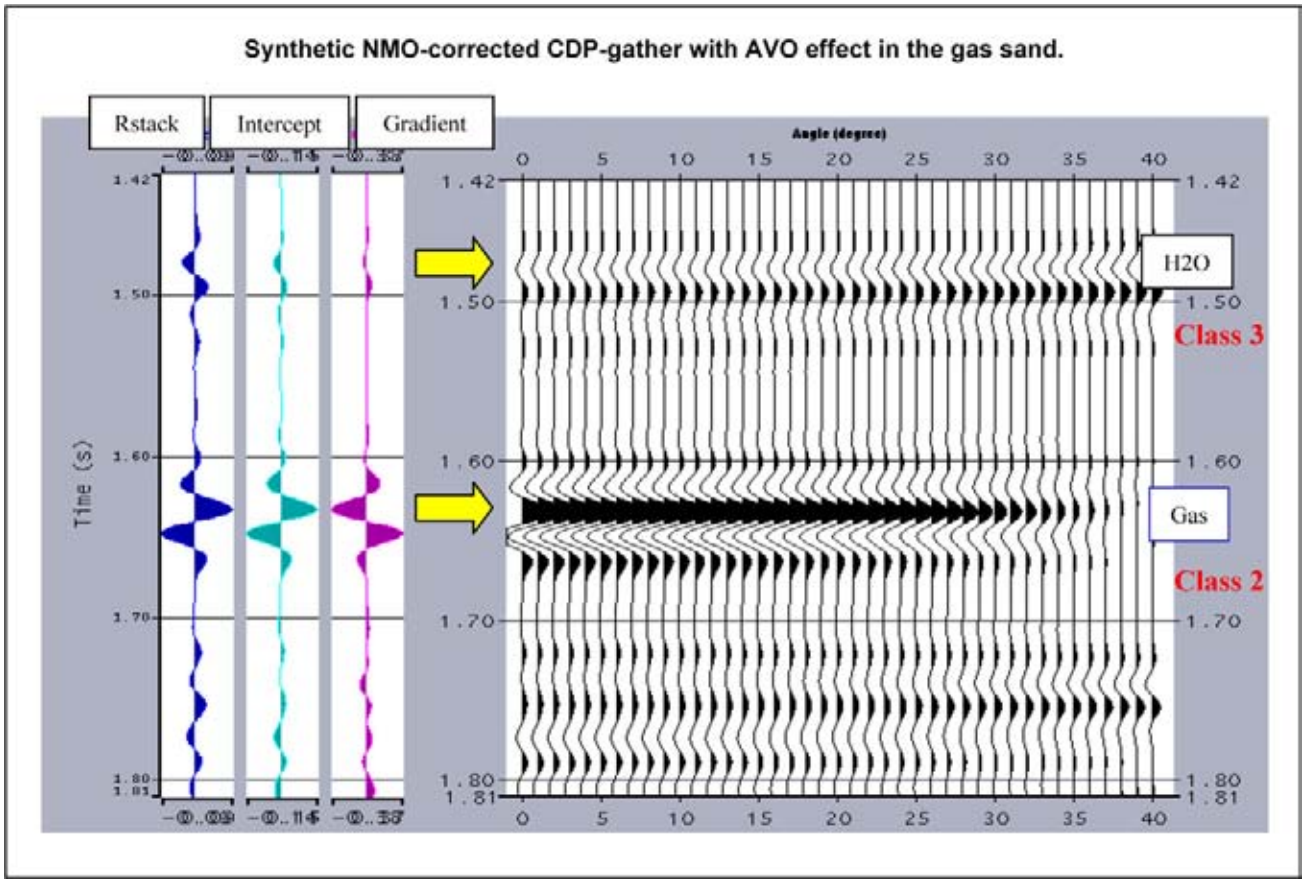

Figure 6.1: AVO effect on a flattened CDP gather caused by the presence of gas in a reservoir sand. The near offset amplitude value is different from the amplitude measured at the far offset trace. Note also the difference with the amplitude of the water-bearing reservoir above. Some causes for the different responses are: petrophysical characteristics of engasing shale with encreasing depth and diagenesis effects.

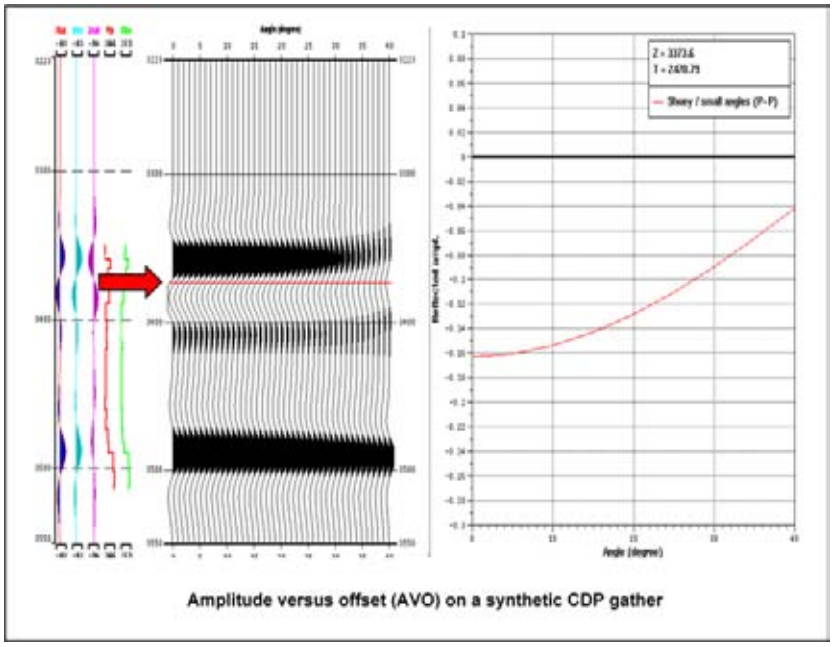

Figure 6.2: AVO effect on flattened gather due to presence of oil in a carbonate reservoir sequence. Arrow indicates level used for data in the AVA plot (Amplitude versus Angle of incidence) on the right.

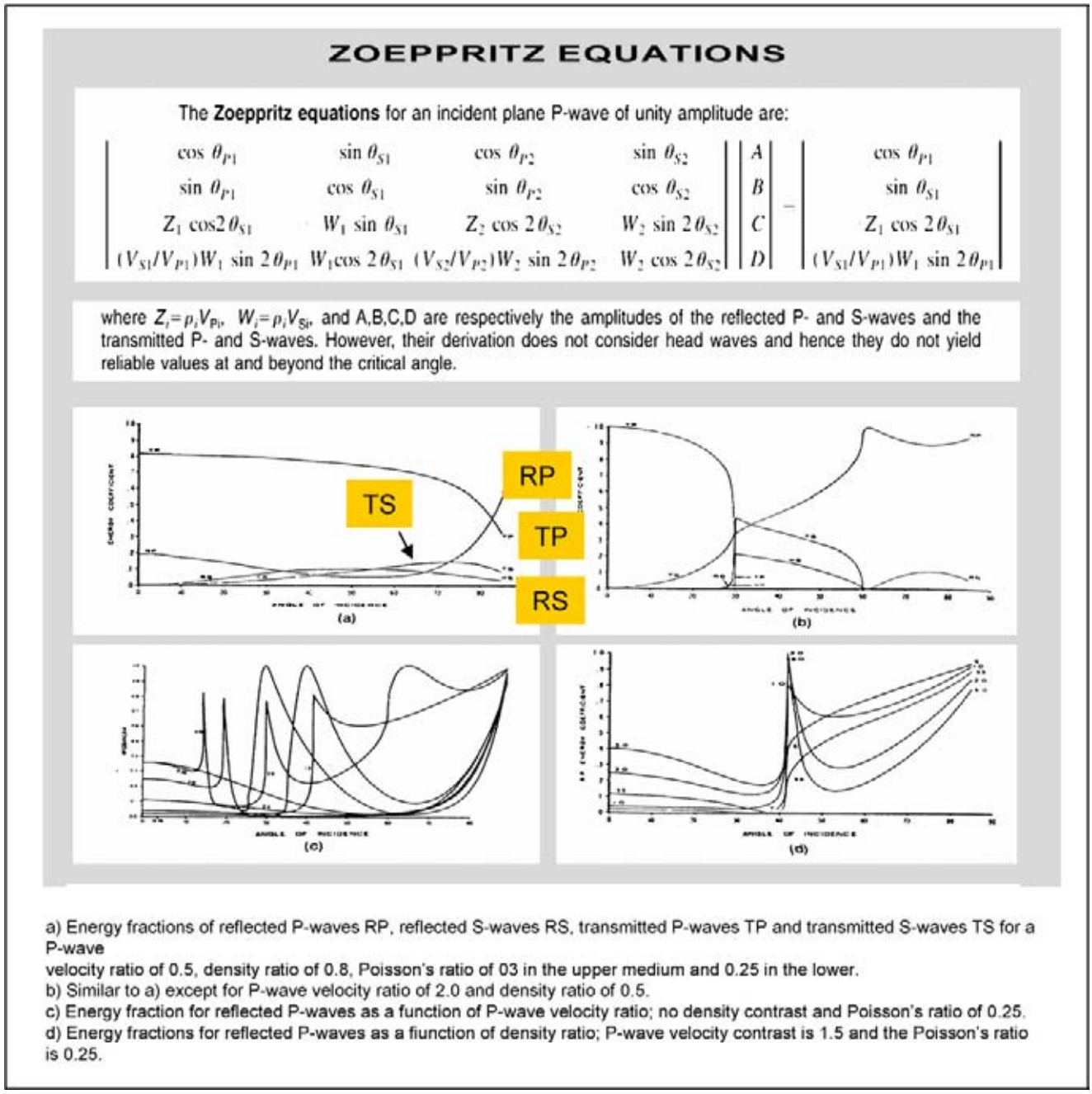

Figure 6.3: Zoeppritz equations for computing the amplitude of the different ray path in a layered medium (after Sheriff 2002).

$$+0.5\left(\left(\frac{\Delta V_\mathrm{p}}{V_\mathrm{p}}\right)\left(\tan^2\theta - \sin^2\theta\right)\right), \qquad (6.3)$$

$$V_0 = A - 2(1+A)\left(\frac{1-2(\sigma_1+\sigma_2)}{1-(\sigma_1+\sigma_2)}\right),$$

$$A = \frac{\Delta V_\mathrm{p}/V_\mathrm{p}}{\Delta V_\mathrm{s}/V_\mathrm{s} + \Delta\rho/\rho}.$$

The Poisson's ratio σ is the ratio of the transverse contraction over the longitudinal extention. Often the formula (6.3) is also written in the following simplified form (Russell et al. 2003):

$$R_{(\theta)} = A + B\sin^2\theta + C\sin^2\theta\tan^2\theta. \qquad (6.4)$$

The formula can be rewritten under the assumption $(\sigma_1+\sigma_2)/2 = 0.33$ $(\rightarrow V_0 = 1)$ and the $V_\mathrm{p}/V_\mathrm{s} = 2$. In this case the higher terms can be dropped and limiting the incidence angle $\theta < 30$ degrees.

$$R_{(\theta)} = R_{(0)} + [2.25(\sigma_2-\sigma_1) - R_{(0)}]\sin^2\theta$$

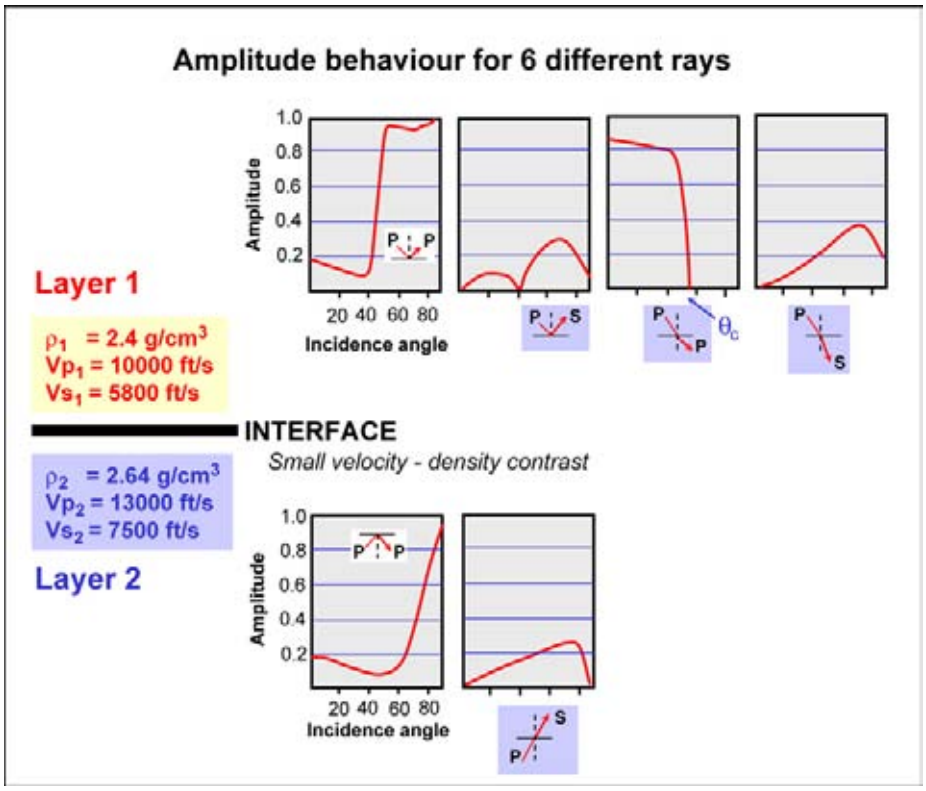

Figure 6.4: Amplitude behaviour for 6 different rays with relatively small velocity–density contrast (modified after Hilterman 2001).

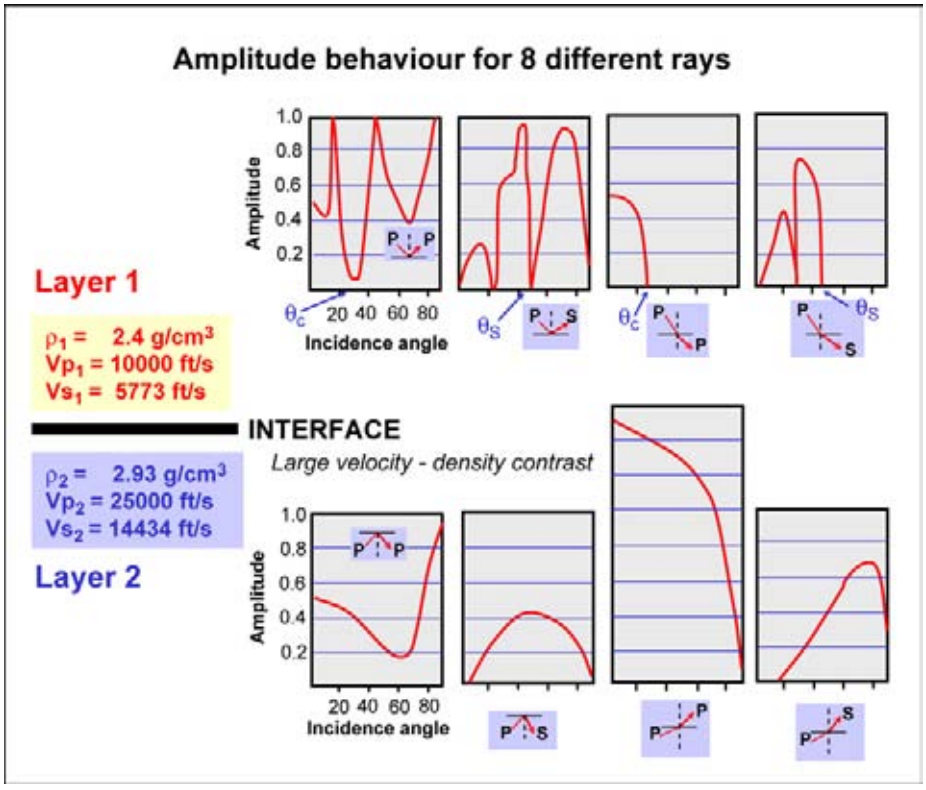

Figure 6.5: Amplitude behaviour for 8 different rays with larger velocity–density contrast (modified after Hilterman 2001).

$$= R_{(0)} + G\sin^2\theta, \tag{6.5}$$

$R_{(\theta)}$ = P-wave amplitude or reflectivity at incidence angle θ.

$R_{(0)}$ = P-wave amplitude at $\theta = 0$ (zero offset), also known as the **intercept I**.

G = the **gradient** (or slope) of line that is approximating the reflectivities at different offsets in a R_p and $\sin^2\theta$ crossplot. Positive gradient means that the amplitude is increased with offset.

According to Hilterman (2001) the Shuey formula can be represented in yet an other simpler formula:

$$R_{(\theta)} = R_{(0)}\cos^2\theta + \mathrm{PR}\sin^2\theta, \tag{6.6}$$

whereby PR is the **Poisson's Reflectivity** and it is defined in the following way:

$$\mathrm{PR} = \frac{\sigma_2 - \sigma_1}{(1 - (\sigma_1 + \sigma_2)/2)^2}. \tag{6.7}$$

The σ_1 is the Poisson's ratio in medium 1 and σ_2 in medium 2. This Poisson's reflectivity is now approximately equal to $4R_{(30)} - 3R_{(0)}$. In a crossplot of $0.5\ln(\mathrm{AI})$ and the Poisson's ratio the lithologies plot along a linear trend defined by the slope of $R_{(0)}/\mathrm{PR}$.

The Shuey two term approximation justifies the linear regression trend in a P-wave amplitude–$\sin^2\theta$ crossplot. It allows to compute the standard AVO attributes I and G:

- **Intercept**, cut-off from the Y-axis or amplitude R_0.
- **Gradient**, slope of regression line with X-axis.

For each time sample on the NMO-corrected CMP gathers a crossplot is made with the offset data to determine the local R_0 and slope. The CMP gather is scanned for variations in the amplitudes with offset. A linear regression analysis is done to compute the I and G values in a 'amplitude–$\sin^2\theta$' crossplot, whereby θ = angle-of-incidence. The physical meaning of the I and G AVO-attributes is shown in Figure 6.6. The AVO analysis means bringing the data from the offset domain into the '**Amplitude versus Angle-of-incidence**' domain (AVA). This is normally done via simple 2D raytracing with applying Snell's Law and using interval velocities from the NMO velocities (Figure 6.7). The synthetic response at the top and bottom of a reservoir unit is shown in Figure 6.8. It is symmetric when the encasing lithologies are the same.

For AVO analysis it is standard practice to calculate a '**Intercept-times-Gradient**' attribute, which is equal to a simple multiplication of the two attributes. It is often represented in *product stack* sections. Also a **Fluid Factor** attribute (FF) is derived (Figure 6.9). This FF attribute is computed in several ways:

a) ***I* and *G* crossplot method**.
The attribute based on a weighted function that brings the Intercept and Gradient in the same value range. These are then crossplotted and in this new I and G plot the difference with the so-called **wet rock line** (also known as **lithology trend**) is determined (Figure 6.10). This difference in distance is the **Fluid Factor**. The wet rock line is the central regression line trough the cloud of points (Foster et al. 1993, Ross 2000, Veeken et al. 2002a). The gas filled reservoir points plot significantly further away from this regression line. The plot has a typical butterfly shape: a lot of points along the central line trend with two clouds of points positioned symmetrically around it.

b) **The V_P–V_S crossplot method**.
In the plot the mudrock line is established and the residual error in a least square sense is a measure of the Fluid Factor (Smith and Gidlow 1987, Smith and Sutherland 1996):

$$\mathrm{FF} = -1.16R_\mathrm{p}(V_\mathrm{s}/V_\mathrm{p})R_\mathrm{s}. \tag{6.8}$$

R_p is the P-wave reflectivity and R_s is the S-wave reflectivity. It is possible to use a local or a fixed slope for the mudrock line, like the one deduced by Castagna et al. (1985):

$$V_\mathrm{p} = 1.16V_\mathrm{s} + 1360\ \mathrm{m/s}. \tag{6.9}$$

The shape of data cloud in an I and G crossplot may tell something about the phase rotation of the data (Roden et al. 2005). They show that the effect in plots with different phase rotation applied to the muted CMP gathers (30 degree increment) results in quite distinct characters. This spread is then used to determine the phase rotation of the data set. The plot with the largest symmetrical spread is chosen as phase rotation for the dataset. It can be used as a check of other phase rotation determination methods. The mute has an influence on the AVO attribute calculation, which is of course a less desirable phenomenon that seriously hampers the quantitative interpretation (cf Cambois 2000). It also might reflect the fact that no residual NMO-correction was applied on the panels. As said already the AVO attributes are calculated for each time sample on the seismic trace and attribute cubes are generated. These cubes are scrutinised for anomalies that may coincide with hydrocarbon bearing reservoirs. Interpretation of the AVO attribute cubes is an art in itself and often data set dependent (M. Rauch, pers. com.). Hence careful analysis by experienced experts is certainly worthwhile.

The top reservoirs are categorised, based on their amplitude behaviour as a function of offset on a CDP gather when filled with hydrocarbons (Castagna 1987, Figure 6.11):

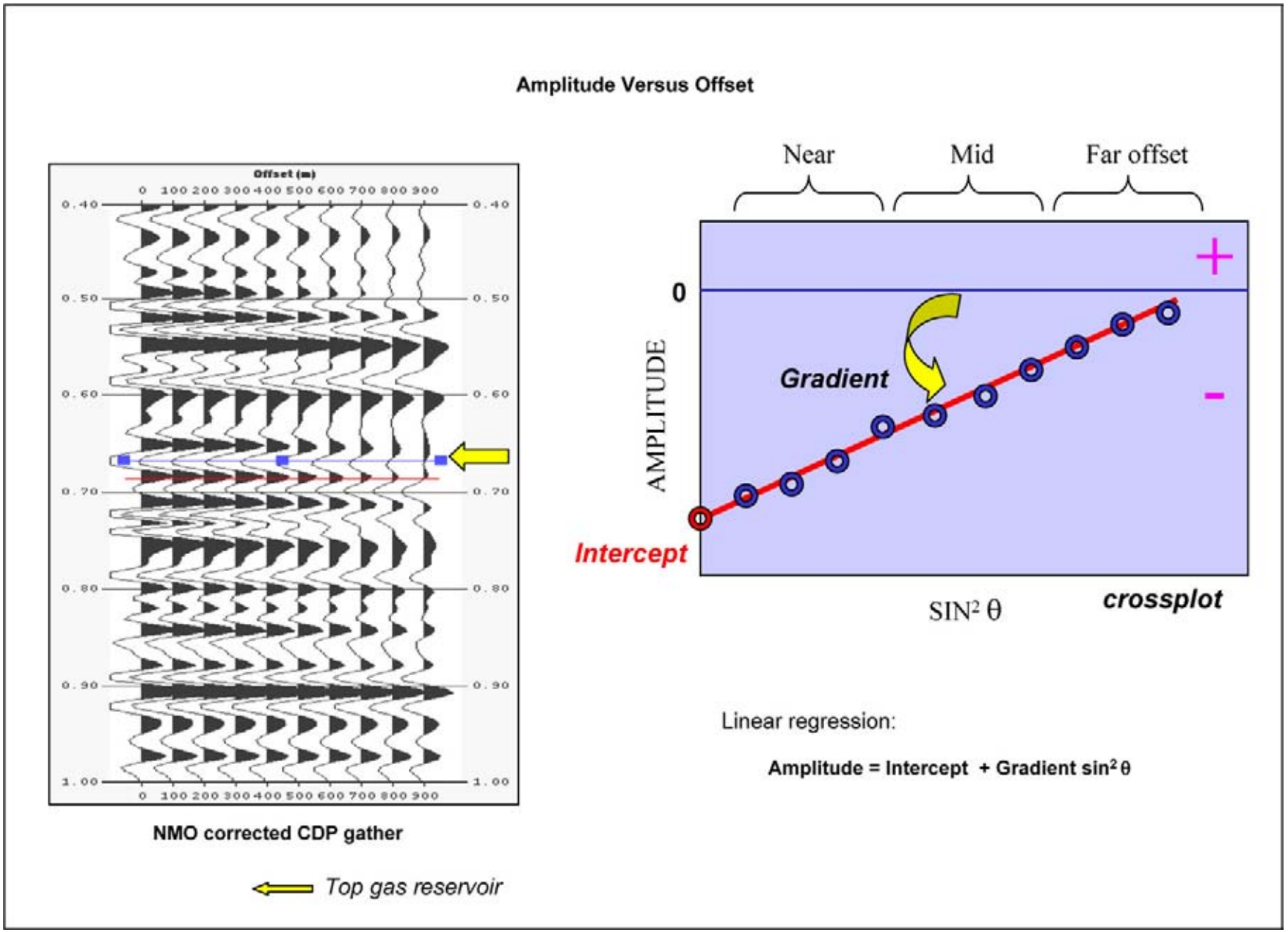

Figure 6.6: NMO-corrected CDP-gather with AVO effects. The amplitude of the near trace is different from the amplitude seen on the far offset trace. The amplitude for a particular reflection can be approximated in an Amplitude–$\sin^2\theta$ plot by a straight line. The line defines the Intercept (cut-off from the Y-axis) and the Gradient (slope of the line with the X-axis). If hydrocarbons are present, special AVO effects are often noticed and the shape of the regression line is studied in more detail.

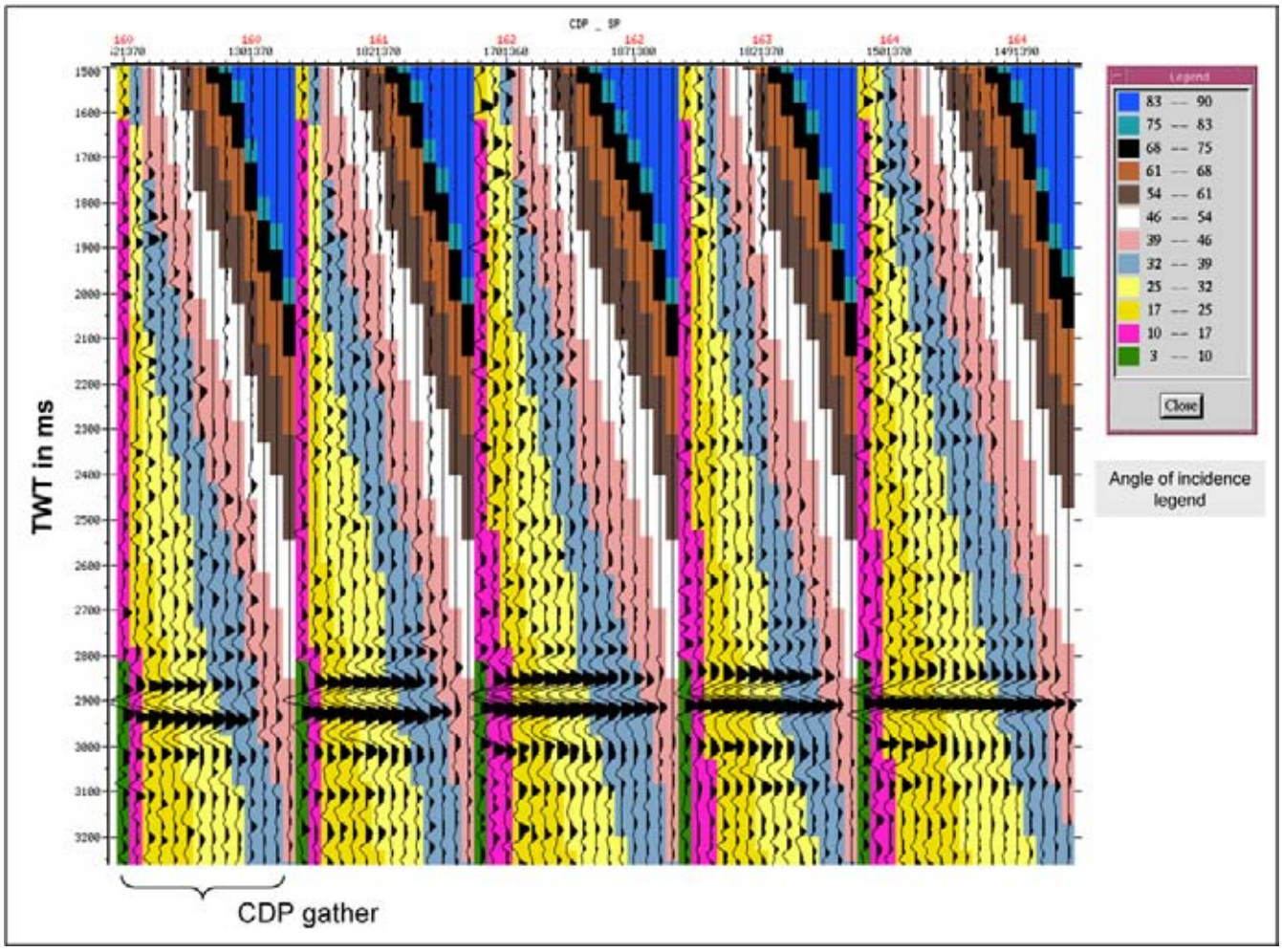

Figure 6.7: CMP gathers with different colours for the various angles of incidence ranges. Simple 2D raytracing is often used for the conversion from offset to angle of incidence.

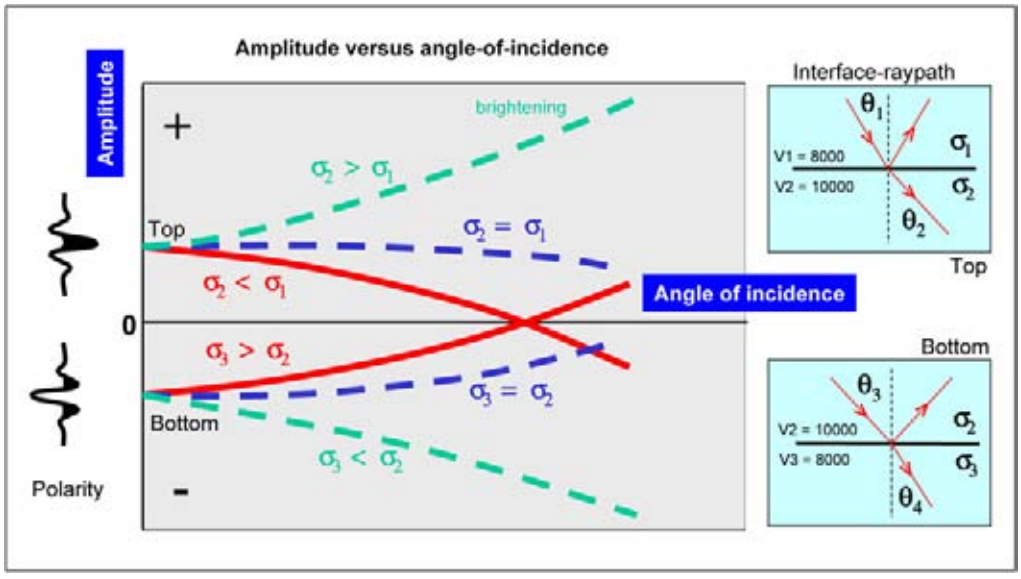

Figure 6.8: AVO response at the top and base of an hypothetical reservoir unit. The Poisson's ratio σ is equal to the amount of transverse over the longitudinal strain, which governs the AVO effect.

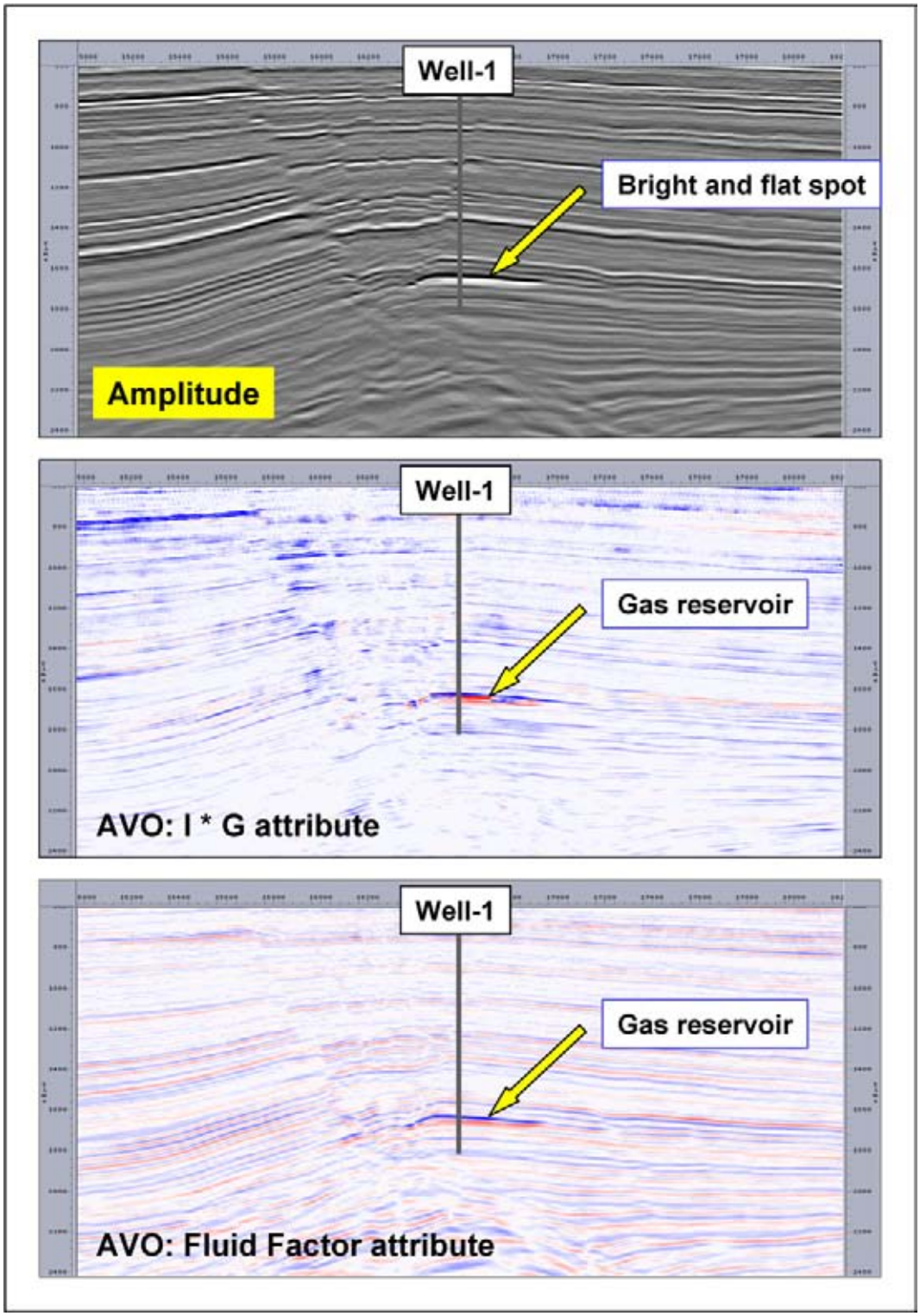

Figure 6.9: (Top) Amplitude section with distinct flat spot, caused by the presence of gas in a reservoir. It also corresponds to anomalies in the Intercept-times-Gradient and the Fluid Factor AVO attributes as shown in the two figures below (courtesy Pemex). (Middle) Intercept-times-Gradient attribute computed from the Amplitude–$\sin^2\theta$ crossplot. The Intercept or R_0 is the cut-off value for the amplitude at a zero incidence angle. The Gradient is the slope of the regression through the amplitude points at the different angles of incidence θ. (Bottom) Fluid Factor attribute is a weighted function between the Intercept and Gradient attributes. The 'wet rock' line is established in a crossplot and the distance from the individual points to this line is a measure for the Fluid Factor (see next figure).

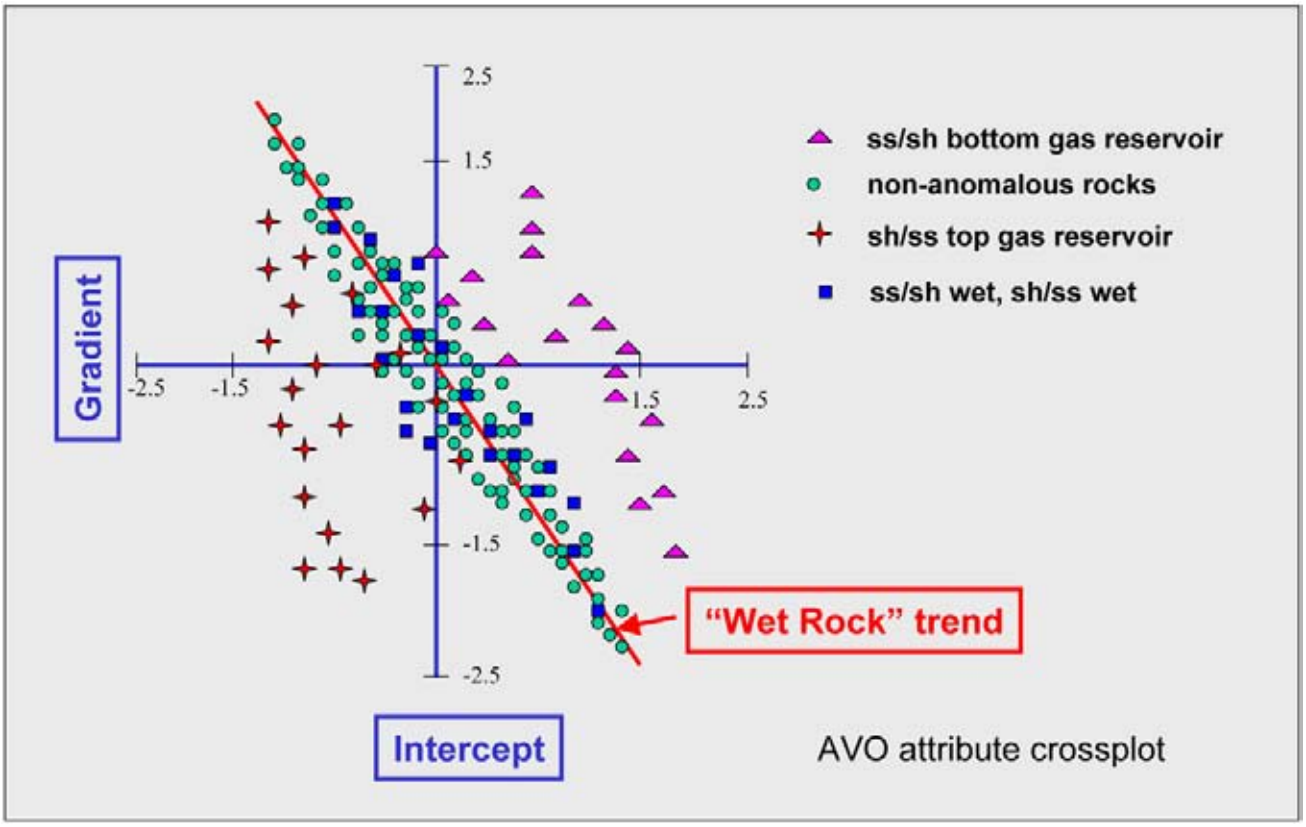

Figure 6.10: Crossplot between Intercept and Gradient. The axis have been weighted by a simple multiplication factor to bring the two attributes closer in line with each other. The regression line is the 'wet rock' line. The distance to this line determines the Fluid Factor value. The shape of the point cloud typically resembles a butterfly outline (positive and negative values outside main trend) when hydrocarbons are present.

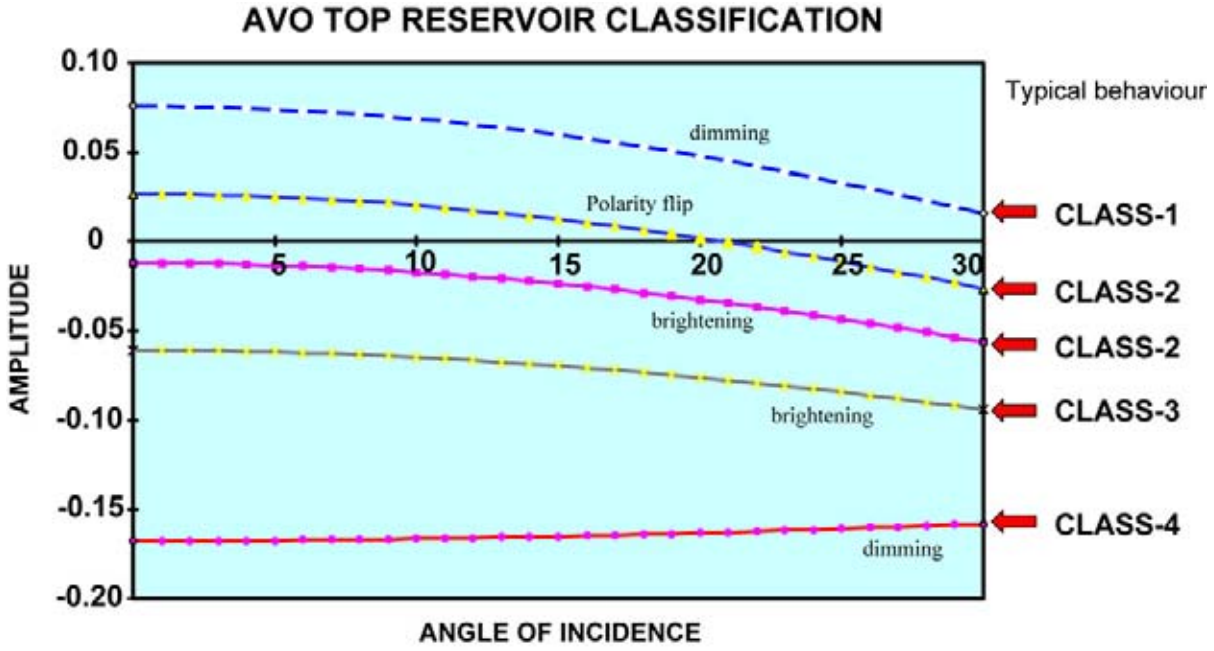

Figure 6.11: Classification of reservoirs based on the AVO response of the top boundary interface. The stacked trace will show brightening, polarity flip or dimming with respect to the zero-offset trace.

- **Class 1** Large positive R_0 amplitude that stays positive with offset (dimming of reflection on stack).
- **Class 2** Small positive R_0 that is transitioned into negative amplitudes with offset (dimming/ brightening of reflection and polarity flip).
- **Class 3** Negative R_0 amplitude that becomes more negative with further offset (brightening of reflection).
- **Class 4** Negative amplitude becomes less negative with offset (dimming of reflection on stack).

The angle of incidence is historically limited to 40 degrees because at larger offsets the approximation of the Zoeppritz equations breaks down. The main discriminator in this classification is the relation of the top reservoir with the overlying lithology. This relation determines the changes in seismic response of the top reservoir (Figure 6.12). The subdivision assumes a normal polarity of the dataset, i.e. a positive peak corresponds to an increase in acoustic impedance with depth.

Let's analyse the behaviour of a Class 3 gas sand in more detail. The top of a gas-filled Class 3 sand has a positive $I \cdot G$ (= negative gradient and negative intercept) and its base is also positive (positive gradient and intercept). The FF (from I and G plot) shows a negative top and a positive value at the base of the same gas reservoir. The sections through the two AVO attribute cubes are examined for the presence of these **dual anomalies**. For quick identification it is useful to display the $I \cdot G$ as a density colour, whilst the FF is overlaid as a wiggle trace. This is done in a Nacho plot (Figure 6.13). It is a very convenient way to visualise the two dataset at the same time.

The following logarithmic attribute (Gas Indicator) is suggested for highlighting gas in Class 2 sands:

$$\mathrm{GI} = \mathrm{Intercept} \cdot (\ln |G|). \tag{6.10}$$

This attribute is specially designed for the Gulf of Mexico region and world wide application requires local adjustment (Figure 6.14; M. Rauch, pers. com.).

Sign of AVO effects and dual attribute anomalies

		I	G	$I \cdot G$	FF	GI
Class 3 reservoir	top	−	−	+	−	
	base	+	+	+	+	
Class 2 reservoir	top	+	−	−		+
	base	+	+	+		+

Verm and Hilterman (1995) proposed for the discrimination of Class 2 gas sands to take the Shuey equation and assume that $V_\mathrm{p}/V_\mathrm{s} = 2$ (higher order terms can be dropped) with $\sigma = 0.33$. This gives:

$$R_{(\theta)} = R_{(0)} + 2.25 \cdot \Delta\sigma - R_{(0)} \sin^2 \theta. \tag{6.11}$$

They use now a crossplot of the Poisson's Reflectivity (or PR) against the normal incidence reflectivity (= R_0) for discriminating anomalies caused by the Class 2 sands.

Class 1 and Class 4 sands are not so commonly reported on. The AVO effect depends on the combination of the petrophysical properties of overlying lithology and the reservoir rock (V_p, V_s and ρ). The impedance contrast over the top reservoir interface is the critical factor. Normal polarity means that an increase in acoustic impedance (or a hard kick) is represented by a positive peak on the seismic data. Class 1 is a response with a relatively high positive intercept and a decrease of the amplitude with offset (negative G). It is often related to tightly compacted reservoirs and/or reservoirs with a high velocity/density cement (cf Odegaard and Avseth 2004, Roden et al. 2005). But it is the impedance contrast that counts. So it can equally reflect the fact that the overlying lithology is very slow and not very dense. Although many authors have suggested a deep-seated compacted reservoir for this type of AVO response and consequently a respectful old geological age for the rocks concerned, Class 1 reservoirs may occur at any depth.

A Class 1 AVO response has been described for Tertiary sediments in the offshore part of the Nile delta in Egypt (Marten et al. 2004). Brightening of gas-filled Class 1 reservoirs in the Pliocene H'apy Field, offshore Egypt, is demonstrated by Wigger et al. (1997). Seal integrity is an aspect that is often ignored when analysing the seismic expression of a gas reservoir. A perfect seal hardly ever exists and therefore some chimney effect due to hydrocarbon leakage will occur. This will change the petrophysical properties of the top seal directly above the reservoir. The phenomenon may lead to an unexpected AVO behaviour and brightening of Class 1 reservoir when gas filled. It is important to check the polarity of the dataset before drawing any conclusions on the AVO reservoir classification. A reliable well-to-seismic tie is in this respect certainly warmly recommended.

Class 4 is characterised by a large negative impedance that shows little difference with offset. It may coincide with the behaviour of shallow burial, unconsolidated sands. Here the decrease in negative amplitude with offset when gas is present in the reservoir can be partly caused by the already mentioned seal integrity problem. The overlying high velocity lithology (shale/siltstone or carbonate) may have a V_s that is higher than that of

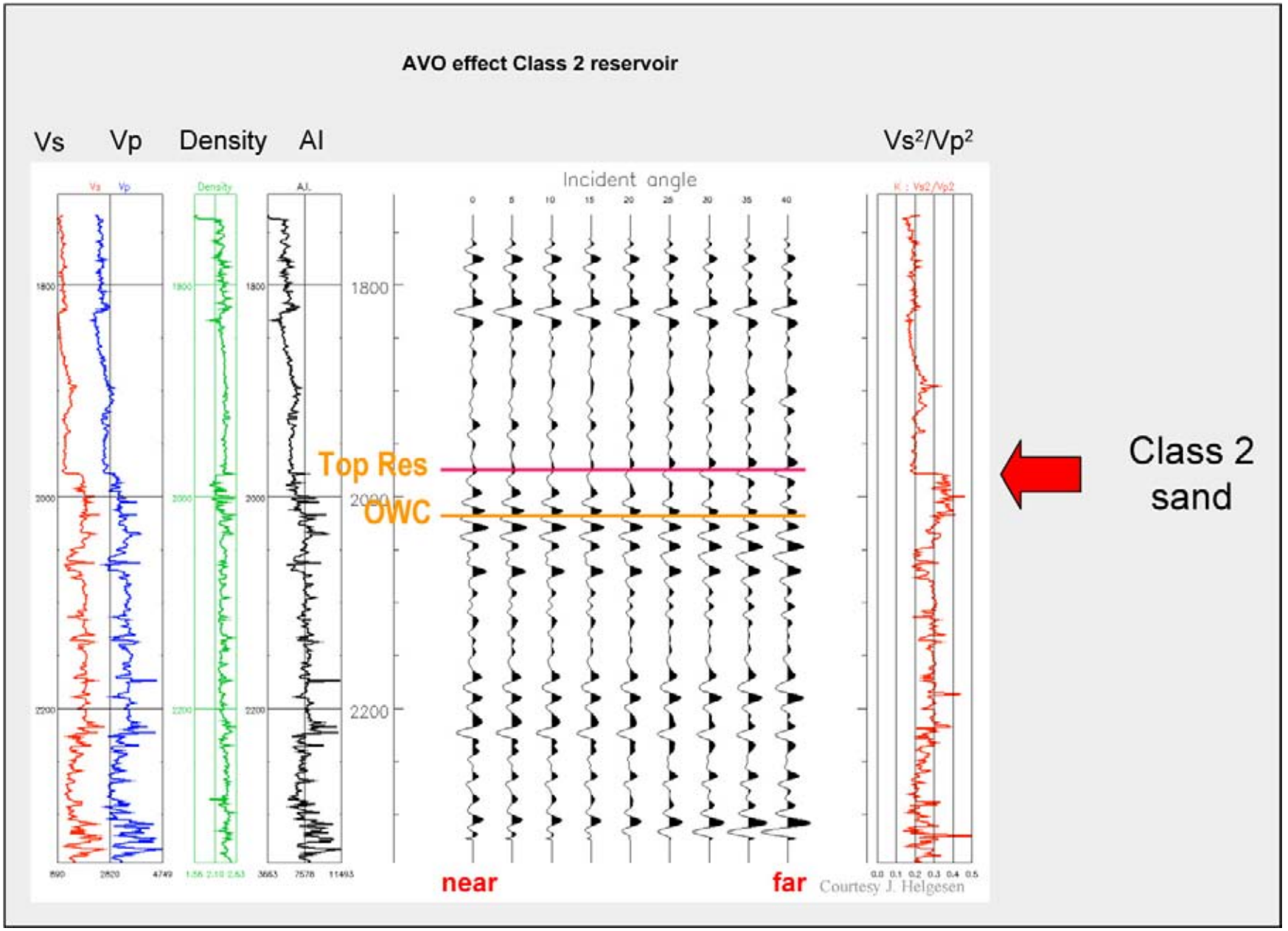

Figure 6.12: AVO effect caused by the presence of hydrocarbons in a class 2 type of reservoir. The curve of $(V_s/V_p)^2$ describes best the HC interval.

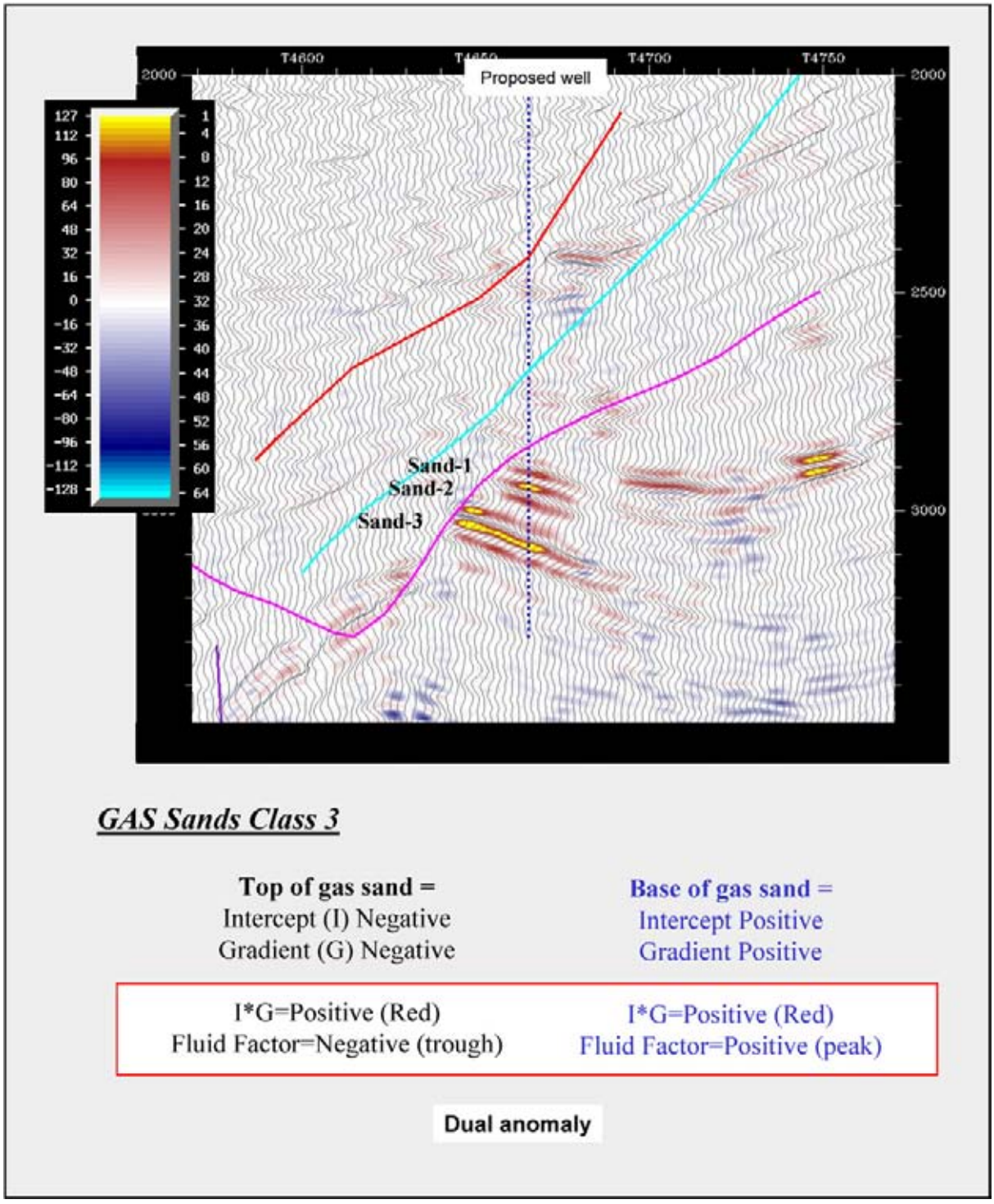

Figure 6.13: A Nacho plot whereby the Intercept-times-Gradient AVO attribute (coloured density is overlain by the Fluid Factor displayed as a wiggle trace). It allows quick identification of dual anomalies of interest with top Class 3 gas sand having a positive I*G and negative FF, while the base shows up as positive I*G and positive FF (courtesy Pemex).

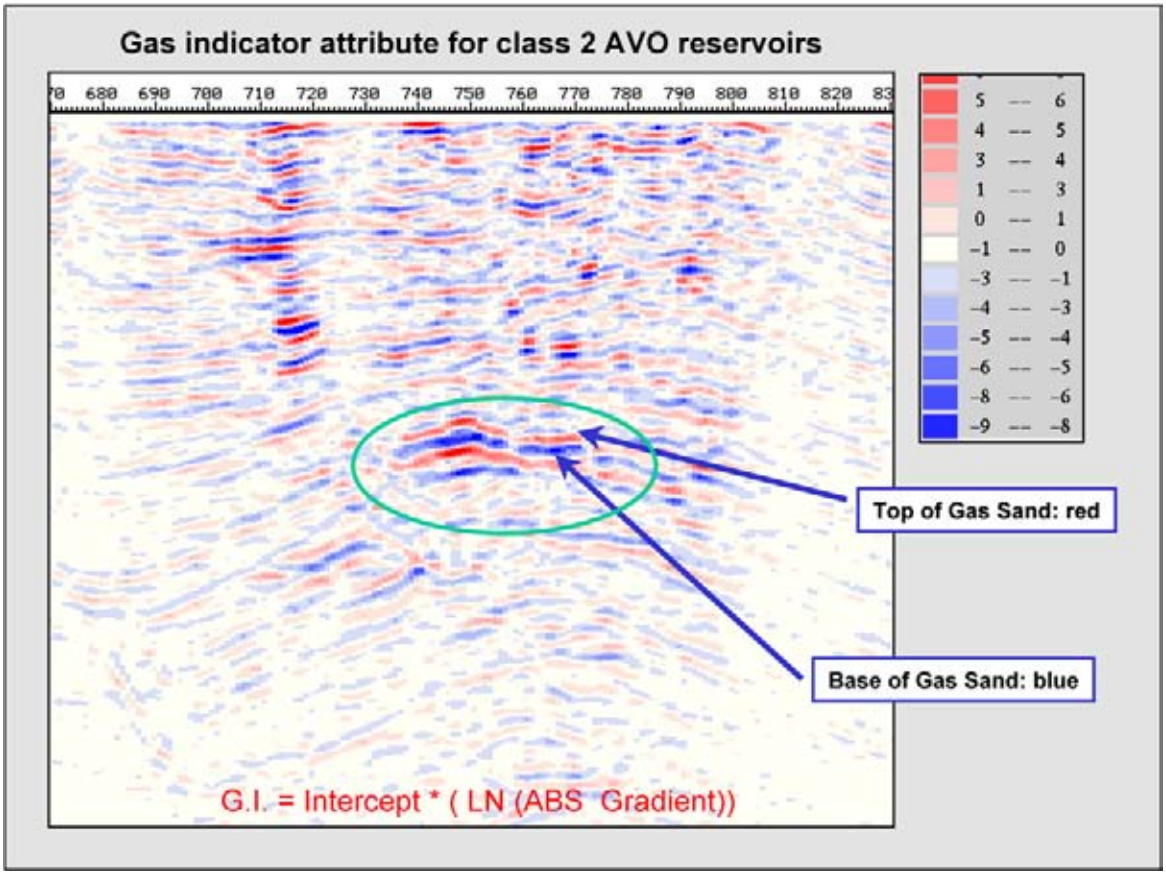

Figure 6.14: Gas Indicator for class 2 AVO reservoirs in the Gulf of Mexico, whereby: GI = Intercept · (ln(ABS Gradient)). This gas indicator attribute is derived for a particular seismic survey and its application to other areas necessitates verification of its validity. Tailor-made local adjustments are probably required to get a useful separation for the HC reservoirs (courtesy M. Rauch and Pemex).

the reservoir (Roden et al. 2005). The P-wave velocity drop at the interface is often in the order of 700 m/sec (Rauch and Craig 1998).

A sedimentological remark in this context: unconsolidated sands are even encountered at great depth below 4700 metres. For example in the Ek Balam discovery well (offshore Campeche) Upper Oxfordian sabkha sands are penetrated that are unconsolidated in the core (Pemex 2000). These sabkha sands were probably prone to very early cementation with gypsum. In the ongoing burial and compaction this cement was not stable and got dissolved at greater depth, thus creating an anomalous porosity/permeability distribution. The unconsolidated nature of these sands at such an extreme depth came as a total surprise to the drillers and the geologist on duty (Ing. G.A. Velasco Vasquez, pers. com.).

Anisotropy effects are of course influencing the AVO response (e.g. Cambois 2001, Jenner 2002, Williams and Jenner 2002). Jenner introduced a linear fit to correct the travel times for azimuthally varying NMO effects (NMOA). Analysis of amplitude varying with offset and azimuth resulted in an other linear fit, that allows calculation of a correction, leading to a more accurate AVOA analysis.

The anisotropy gradient describes the variation in AVO gradient with azimuth and is related to the crack density and the Horizontal Transverse Isotropy behaviour (HTI). Todorovic-Marinic et al. (2004) proposed a new attribute called the **envelope of the anisotropic gradient** to better visualise this behaviour. The azimuth of the anisotropic gradient indicates the fracture orientation. It depends on fracture aperture, fracture density and directional permeability.

As can be seen from the above, it is important to establish in an area under investigation which types of AVO reservoirs are expected. Equipped with this knowledge it is possible to concentrate quickly on special scenarios and do specific analysis (Veeken, in press). There is, however, a danger that several types of AVO reservoirs are present at the same time. Abnormal pressure dis-

tribution may complicate the AVO picture in the reservoir (Hilterman and Dunn 2004). Local diagenesis or unexpected lithologic changes will influence the seismic character. These complications make the interpretation of the AVO response more time consuming. An open mind is always needed to evaluate all possibilities, so that no business opportunities are missed.

Neural network trace classification schemes are an additional means to identify quickly the extend of attribute anomalies. The supervised method has an advantage that the results are more easy to interpret. Multi-attributes can be used (Mercado Herrera et al. 2006). The method has to be developed further in order to reveal its real potential (cf Balz et al. 2000). Verification of the AVO results with the results of a multi-component 4C survey has its merits. For example a HC induced P-wave flat event is not present on the equivalent PS (or C-wave) dataset. False anomalies in the Albacora area in the deep offshore of Brazilian Campos Basin (1850 metres waterdepth) are also better discriminated with the aid of the 4C results. In the nearby Roncador field a Class 3 gas sand has a strong P-wave response, while the C-wave data is dimmed. For a Class 2 AVO gas sand the opposite is true (Cafarelli et al. 2006). In general it can be stated that the AVO analysis method works, but all elements of the reservoir scenario's should be properly incorporated in the evaluation.

6.2 Angle-Dependent Reflectivity

6.2.1 Elastic Impedance Attribute

The Shuey equation gives an approximation of the Zoeppritz reflectivity that is good up to 30–35 degree incidence angle. The assumption is made that V_p is approximately two times the V_s and the higher terms are dropped by the 30 degree angle of incidence condition. When working with prestack data, there is need to do a better estimation that takes into account the difference in V_p and V_s. This is done in the so-called elastic approach to AVO and seismic inversion. Elastic means passing of a seismic waveform without any permanent distortion of the rocks and considering the full wavefield with contribution of the P- as well as the S-waveforms. The acoustic method on the other hand only considers the behaviour of the P-wave energy.

Connolly (1999) introduced the concept of **Elastic Impedance**, a seismic attribute that is angle dependent. He defined a function $F(t)$ that is incidence angle dependent and related to the P-wave reflectivity in the following manner:

$$R_{(\theta)} = \frac{F(t_i) - F(t_{i-1})}{F(t_i) + F(t_{i-1})}. \tag{6.12}$$

This function $F(t)$ is now called the Elastic Impedance or EI, in analogue to the acoustic impedance concept. The angle dependant P-wave reflectivity is also approximated by the simplified description of the Zoeppritz equations by Aki and Richards (1980):

$$R_{(\theta)} = A + B\sin^2\theta + C\sin^2\theta\tan^2\theta, \tag{6.13}$$

$$A = 0.5\left(\frac{\Delta V_\mathrm{p}}{V_\mathrm{p}} + \frac{\Delta\rho}{\rho}\right),$$

$$B = 0.5\left(\frac{\Delta V_\mathrm{p}}{V_\mathrm{p}}\right) - 4\left(\frac{V_\mathrm{s}}{V_\mathrm{p}}\right)^2\left(\frac{\Delta V_\mathrm{s}}{V_\mathrm{s}}\right) - 2\left(\frac{V_\mathrm{s}}{V_\mathrm{p}}\right)^2\left(\frac{\Delta\rho}{\rho}\right),$$

$$C = 0.5\left(\frac{\Delta V_\mathrm{p}}{V_\mathrm{p}}\right),$$

$$\Delta V_\mathrm{p} = V_\mathrm{p2} - V_\mathrm{p1},$$

$$V_\mathrm{p} = \frac{V_\mathrm{p1} + V_\mathrm{p2}}{2}.$$

Combining the two expressions (6.12) and (6.13) gives that the Elastic Impedance is equal to:

$$\mathrm{EI}_{(\theta)} = V_\mathrm{p}^{(1+\tan^2\theta)} \cdot V_\mathrm{s}^{(-8K\sin^2\theta)} \cdot \rho^{(1-4K\sin^2\theta)}. \tag{6.14}$$

Here K is a constant, that is taken equal to the average of $(V_\mathrm{s}/V_\mathrm{p})^2$. This type of EI computation is performed on the pre-stack gathers and takes into account the changes in V_p, V_s and density as well as AVO effects. This approach is accurate for small to moderate impedance changes. If the third term in the Shuey equation is dropped, then the $\tan^2\theta$ is simply replaced by a $\sin^2\theta$ in the Connolly equation.

$$\mathrm{EI}_{(\theta)} = V_\mathrm{p}^{(1+\sin^2\theta)} \cdot V_\mathrm{s}^{(-8K\sin^2\theta)} \cdot \rho^{(1-4K\sin^2\theta)}. \tag{6.15}$$

There are some assumptions that need to be fulfilled:

- Two term NMO approximation is correct.
- Dix's equation is valid.
- Amplitudes are proportional to $\sin^2\theta$.

This translates in dealing with a layer cake geometry, offset is smaller than the depth of the reflector, angle of incidence θ is smaller than 30–35 degrees, transverse isotropic medium and correctly balanced prestack amplitudes. The EI_0 is corresponding to the acoustic impedance AI ($= \rho \cdot V_\mathrm{p}$) and if $K = 0.25$ than the $\mathrm{EI}_{90} = (V_\mathrm{p}/V_\mathrm{s})^2$.

The EI seismic attribute is the basis for performing an elastic inversion, quite similar to an acoustic inversion

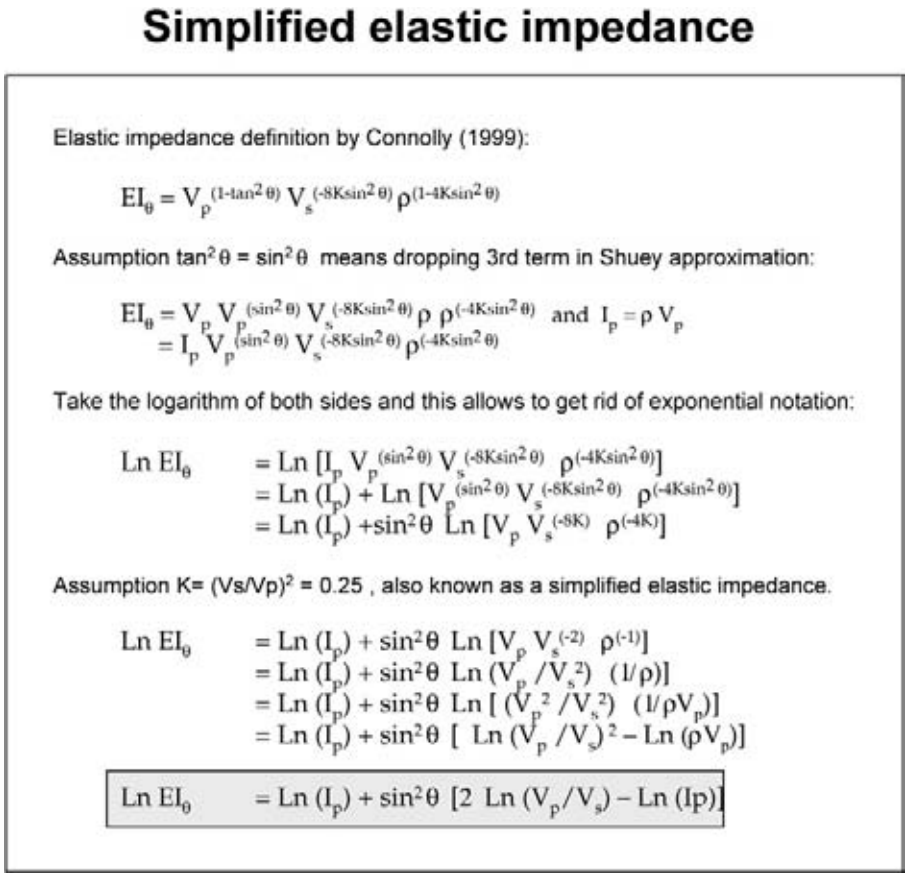

Figure 6.15: Logarithmic approximation of Connolly's Elastic Impedance attribute. K is the average $(V_s/V_p)^2$ and I_p stands for P acoustic impedance.

processing. In acoustic impedance inversion a wavelet (via shaping filter or cross-correlation techniques) is estimated from the AI trace at the well and the seismic trace. In the elastic inversion wavelets are derived for different incidence angle traces of $EI_{(\theta)}$ and the corresponding partial stack trace. The technique is presented in more detail below.

There are other formula's to approximate the elastic impedance, e.g. logarithmic approach or also a less common non-linear function (Tarantola 1984, 1986, Pica et al. 1990). The logarithmic function (Figure 6.15) allows to avoid tedious exponential descriptions and is valid under the condition that $K = 0.25$:

$$\ln(EI_{(\theta)}) = \ln(I_p) + \left(2\ln\left(\frac{V_p}{V_s}\right) - \ln(I_p)\right)\sin^2\theta, \quad (6.16)$$

whereby acoustic impedance $I_p = \rho \cdot V_p$.

All these formulas have their own assumptions and validity range. It means that the elastic inversion results can be used in a qualitative way, but the absolute quantitative value of the inversion is not necessarily correct.

6.2.2 Relationship linearised Zoeppritz approximation with some rock physical parameters

Dong (1996) and Whitcombe et al. (2000) showed when using the linearised Zoeppritz equation from formula (6.13) that:

$$\Delta\text{bulk modulus} = [(3A + B + 2C)V_p^2\rho]/1.5. \quad (6.17)$$

It is difficult to deduce the C from the seismics. Shuey (1985) therefore examined in closer detail the behaviour of the C/A ratio and noticed that it ranges roughly between 0 and 1. The C/A ratio depends on the rock properties of the area under investigation. If it is 0.8 then it follows the Gardner's relationship. If it is assumed that the average values for the bulk modulus and $V_p^2\rho$ are constant, then the formula (6.17) can be rewritten:

$$\Delta\text{bulk modulus} = A + \frac{B}{3 + 2(C/A)}. \quad (6.18)$$

This can be seen as an analogue function of the basic AVO equation:

$$R_\theta = R_0 + G\sin^2\theta, \tag{6.19}$$

where

$$\sin^2\theta = \frac{1}{3 + 2(C/A)}.$$

This analogy translates the behaviour of the C/A ratio in terms of incidence angle.

$$C/A = 0.8 \quad \Rightarrow \quad \sin^2\theta = 0.22 \quad \Rightarrow \quad \theta = 28^\circ.$$

Values of 0.5 and 1.6 have been encountered for C/A and this corresponds to angles of 44 and 23 degrees (Whitcombe et al. 2000).

A similar treatment for Lame's constant lambda can be done and this yields:

$$\Delta\lambda = \frac{1}{2 + C/A}. \tag{6.20}$$

Using Gardner's relationship it results in $\sin^2\theta = 0.36$ and the angle is 37 degrees. The reflectivity at 37 degrees gives an estimate for the change of lambda over the interface.

The shear modulus is related according to Dong (1996) as follows:

$$\Delta\mu = (C - B)\big(V_\mathrm{p}^2\rho/2\big). \tag{6.21}$$

These relations are valid under certain assumptions and when these are not adhered to then the relationship breaks down. Linearisation can only be done for small incidence angles (<35 degrees) and impedance contrasts that are relatively small.

Krail (2004) propose a fifth order polynomial approximation for the Zoeppritz equations with the shearwave velocity ratio as unknown variable. It is possible to solve this fifth order formula and reduce the solution to a first order function with a unique shear wave velocity density combination, when 16 different angle-amplitude measurements are exploited. In this approach the estimation errors will be reduced, but still the headwave energy is not properly taken into account.

6.3 Seismic Inversion Techniques

Seismic inversion or stratigraphic deconvolution tries to put a spiked response at geological boundaries (lithology changes) and the main reservoir characteristic interfaces. This is done by the inversion of the seismic cube into an Acoustic Impedance cube (Figure 6.16). The link between the seismic cube and the AI cube is the seismic wavelet. Seismic inversion is a rather confusing expression. Inversion in itself means to undo a operation, but here in fact it is used for the transformation of a seismic amplitude cube into an acoustic (or elastic) impedance cube. One of the benefits of inversion is that the seismic resolution is increased (e.g. Veeken et al. 2004). Hill (2005) has investigated this phenomenon and found an improvement in thickness prediction that was clearly beyond the seismic tuning thickness.

In the stratigraphic inversion scheme a comparison is made between the synthetic trace at the well and the seismic trace. A wavelet is established by applying cross-correlation techniques. Or the wavelet is derived from the shaping filter that permits transformation of the reflection coefficient trace into the seismic trace.

This wavelet is then used to perform the seismic inversion, whereby the seismic traces are transformed into blocky AI traces. The spiked response is expressed by the limits of these AI units (Veeken et al. 2002a). These spikes are assumed to correspond better to meaningful geological boundaries and reservoir characteristic interfaces. If all works well there is relation between acoustic impedance and reservoir characteristics like porosity, permeability, net-to-gross, HC saturation. Even if the well trends are not exactly honoured, the filtered well average may follow the general picture provided by the inversion and that gives the possibility to delineate 'sweet spots'. A simple relationship often does not exist (Dvorkin and Alkhater 2004), but in individual cases it can be different. For instance in the Kraka field, located offshore Denmark, the Chalk porosity is linear correlated with AI (Klinkby et al. 2005) and this can be used in later prediction.

An overview of various seismic inversion techniques is given by Veeken and Da Silva (2004) who also discuss their main constraints. The presentation below is more or less conform to that publication. The inversion methods are deterministic or probabilistic in approach. The input can be pre- and/or post-stack datasets. Inversion can be done in the time or even in the frequency domain (Sirgue and Pratt 2004). Let us start with a description of the post-stack input methods.

6.3.1 Post-stack inversion methods

The post-stack time-migrated data is input for the inversion algorithm. It is important to have clean seismic data as input and that proper data conditioning is done (Da Silva et al. 2004). This entails CDP

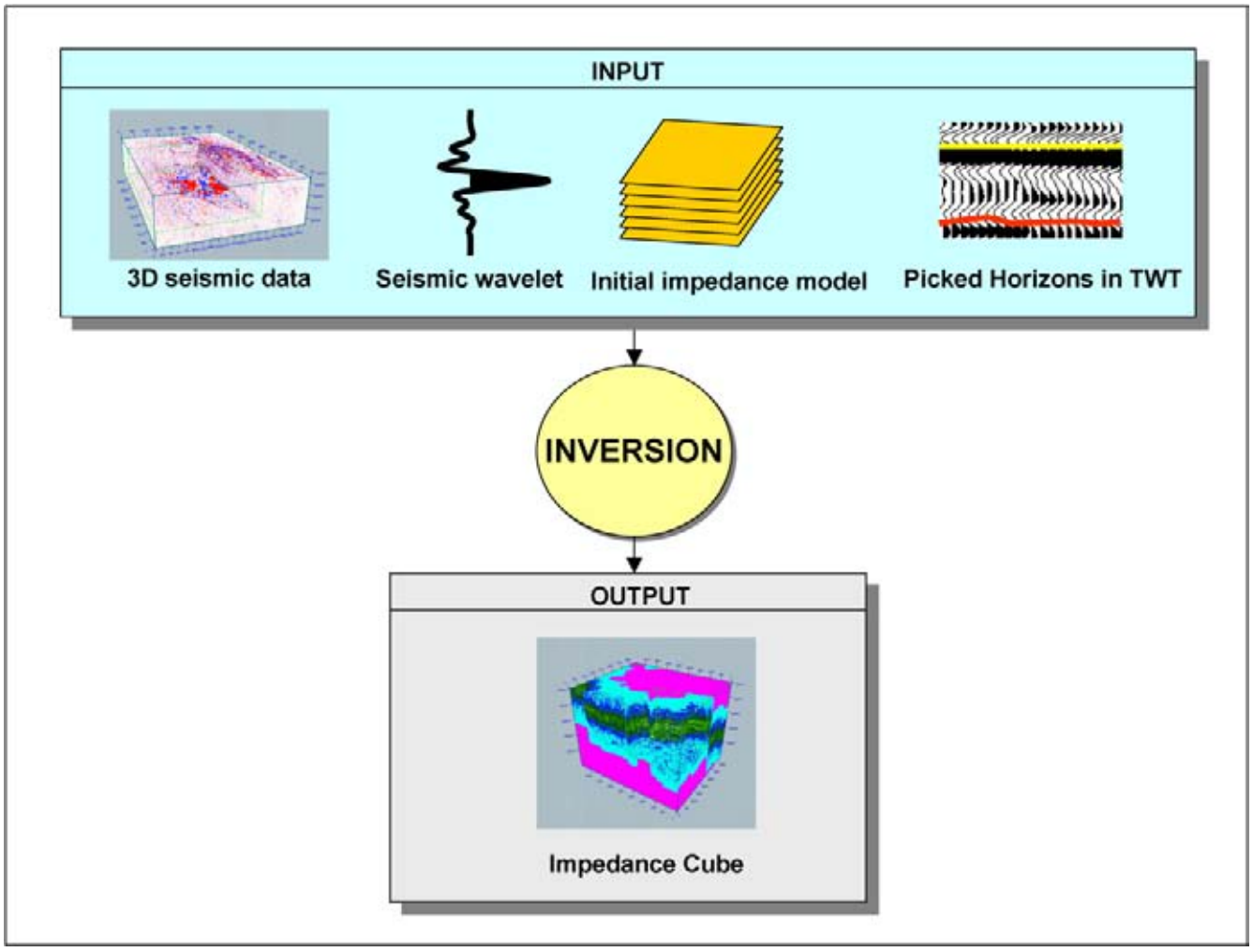

Figure 6.16: Typical input for a seismic inversion exercise. Proper data conditioning is a pre-requisite to obtain reliable results later on. Seismic inversion is never a unique process, i.e. there is not one solution to the given problem. Additional constraints are hence needed in order to determine the most plausible scenario.

gather cleaning, preserved amplitude processing, amplitude balancing with sophisticated gain control, multiple suppression and 3D noise attenuation. Comparative analysis of seismic processing (CASP, Ajlani 2003) is a multi-disciplinary approach to secure the QC of the seismic processing results, whereby quality, turnaround and cost are taken into account. Usually the seismic is processed with a certain target zone in mind. All the processing parameters have been tuned to this objective. The target in the inversion may be somewhat different. Therefore careful examination of all processing steps is needed before embarking on the exercise to transform amplitude into acoustic impedance.

6.3.1.1 Simple integration of seismic trace

Reflection coefficients are obtained under the assumption that the density is constant and equal to two (Figure 6.17; Lindseth 1979, Yilmaz 1987). The seismically derived velocity trends are always limited in their frequency content and to compensate for this it is possible to construct a **synthetic sonic log section**. A high-frequency velocity component is derived from the sonic log data in a well. A basic trend is established between the sonic log and seismic derived velocity field; thus the high-frequency trend is approximated.

No variation in density is assumed and the seismic response is translated in a vertical low-frequency velocity trend for each of the seismic traces. To this latter velocity trend the high-frequency velocity component from the wells is added and it results in a synthetic seismic section partly derived from the sonic log. For this purpose the high-frequency sonic log velocity component is inter/extrapolated between the wells.

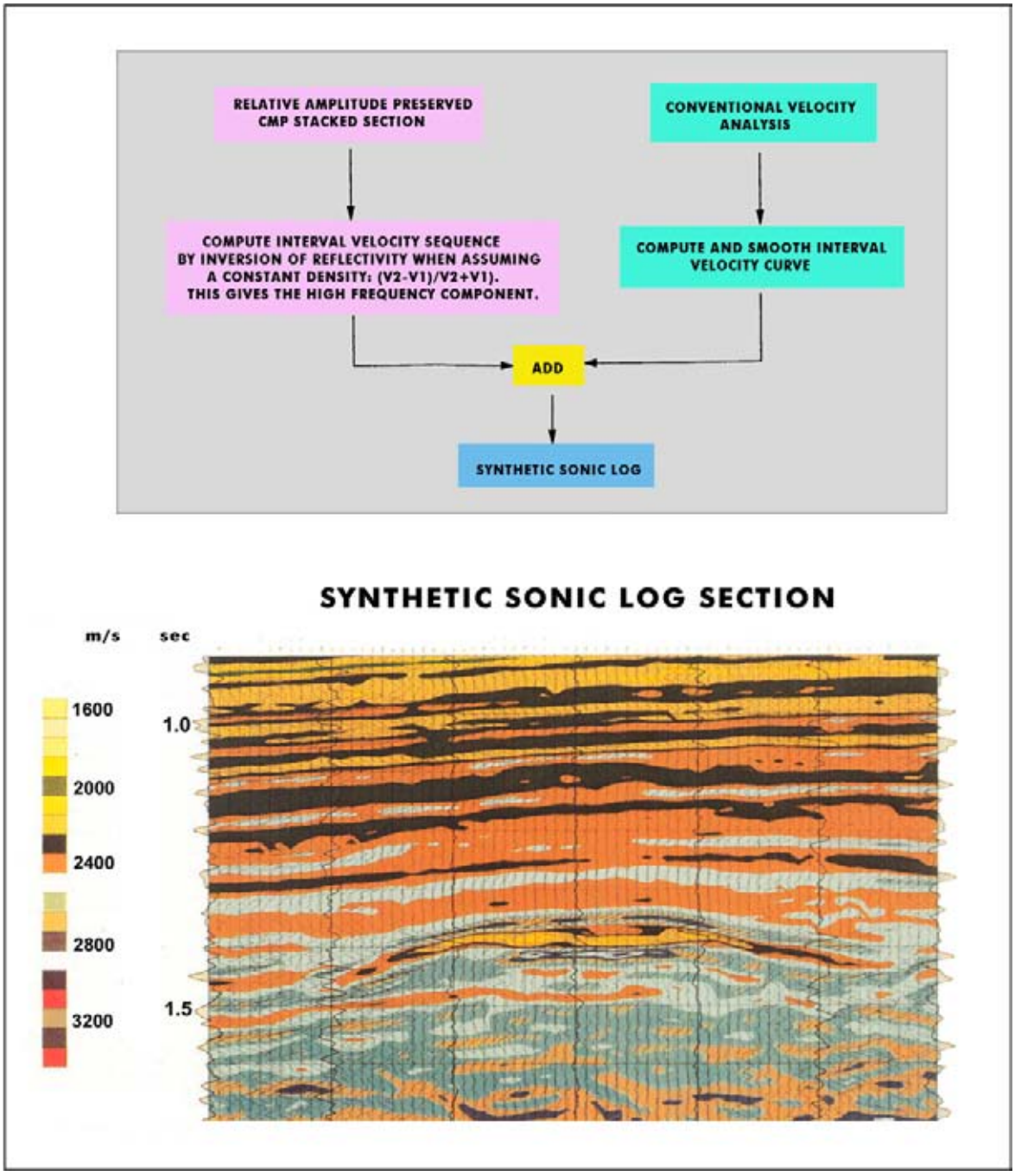

Figure 6.17: Inversion of seismic traces is performed under the assumption that the density is constant and its value is equal to two. Seismic traces are directly converted into a pseudo sonic log traces. The high frequency variations are introduced by using the interpolated well calibration (modified after Yilmaz 1987).

This inversion is however a poor man's job that can be done better.

6.3.1.2 Coloured inversion

The coloured inversion method is basically a trace integration, achieved by applying a special filtering technique in the frequency domain. The amplitude spectrum of the well log is compared with that of the seismic data and that is where the word 'coloured' comes from (Figures 6.18 and 6.19). An inversion operator is designed that brings the seismic amplitudes of the frequencies in correspondence with that seen in the well. This operator is then applied to the whole seismic cube (Lancaster and Whitcombe 2000).

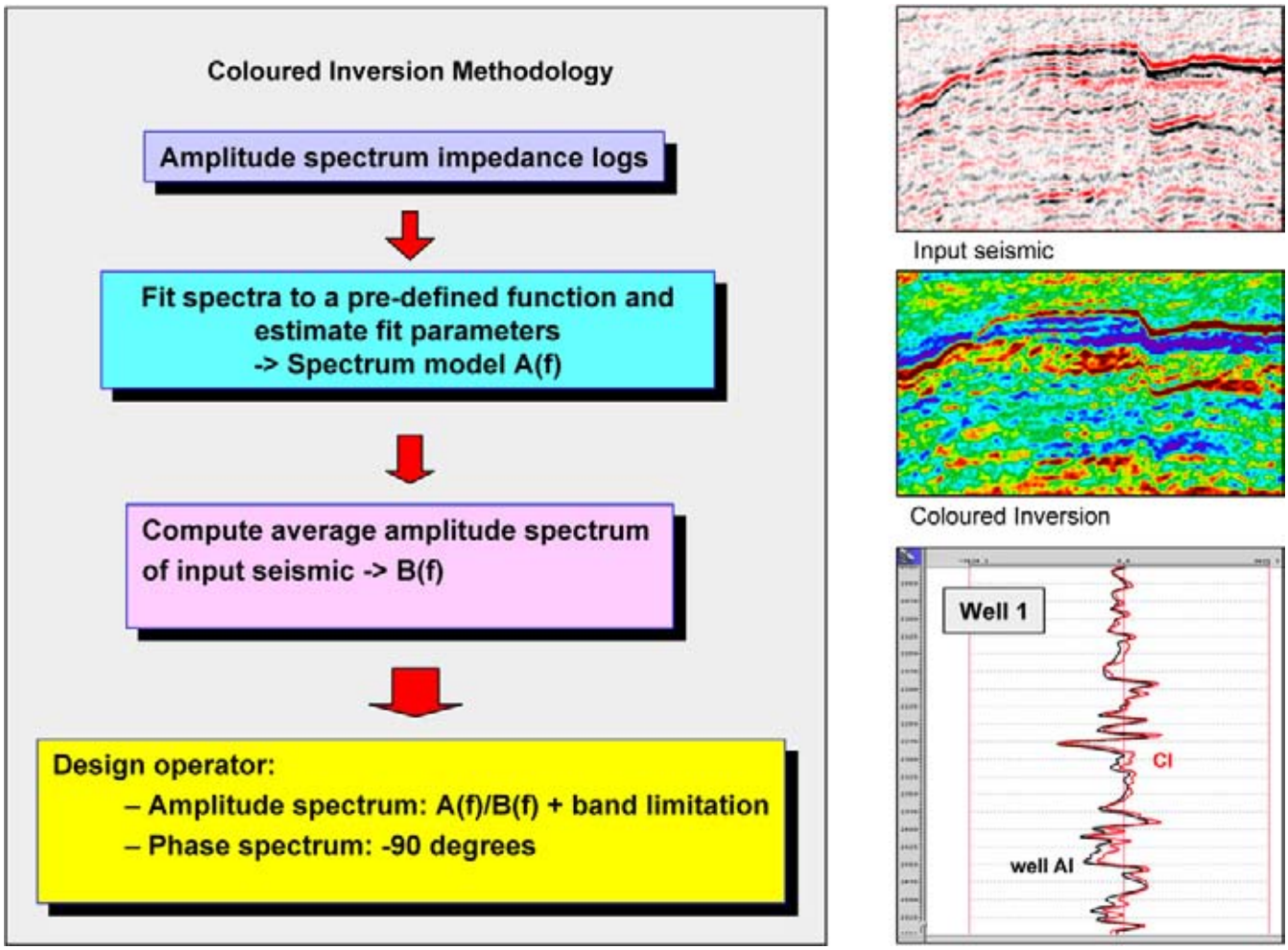

Figure 6.18: Coloured inversion of seismic data exploits the spectra of the logs and computes a average amplitude spectrum of the input seismic to derive an inversion operator. This operator is applied to the seismic cube so that the variation is much better in agreement with the well data.

A crossplot is made between the amplitude and the logarithm of the frequency to compute the operator. A linear fit is performed to calculate an exponential function f^{α} and this serves as a shaping filter (cf Walden and Hosken 1985, Velzeboer 1981). This filter transforms the seismic trace into an assumed acoustic impedance equivalent. The assumption is made that the seismic cube is zerophase, which is hardly the case. In individual cases (Giroldi et al. 2005) the results can be spectacular with a flat spot DHI suddenly appearing in the inverted dataset (Figure 6.20). Again this type of inversion is quick, but it represents a rather dirty method.

6.3.1.3 Sparse spike inversion

The seismic trace is simulated by a minimum amount of AI spikes. The spikes are placed in such a way that they explain best the seismic response. Amplitude, time position and number of the AI spikes is not always realistic, i.e. not conform the geological constraints. To be more specific: if a starting model is not available, the spikes might be placed in unrealistic positions and still the model generates a synthetic that highly resembles the seismic trace. The recursive method uses a feedback mechanism to obtain more satisfactory results.

A low frequency AI variation trend can be imported to generate more appropriate results with a better convergence of the found solution. The inversion algorithm was initially working on a trace by trace basis, but now a multi-trace approach is implemented. The inversion solution may vary considerably from trace to trace, making the reliability of the output weaker. The constrained option uses a low frequency model as a guide (Figure 6.21). The low frequency variation is estimated from blocked well logs and this gives much better results (e.g. Ronghe and Surarat, 2002). QC tests are

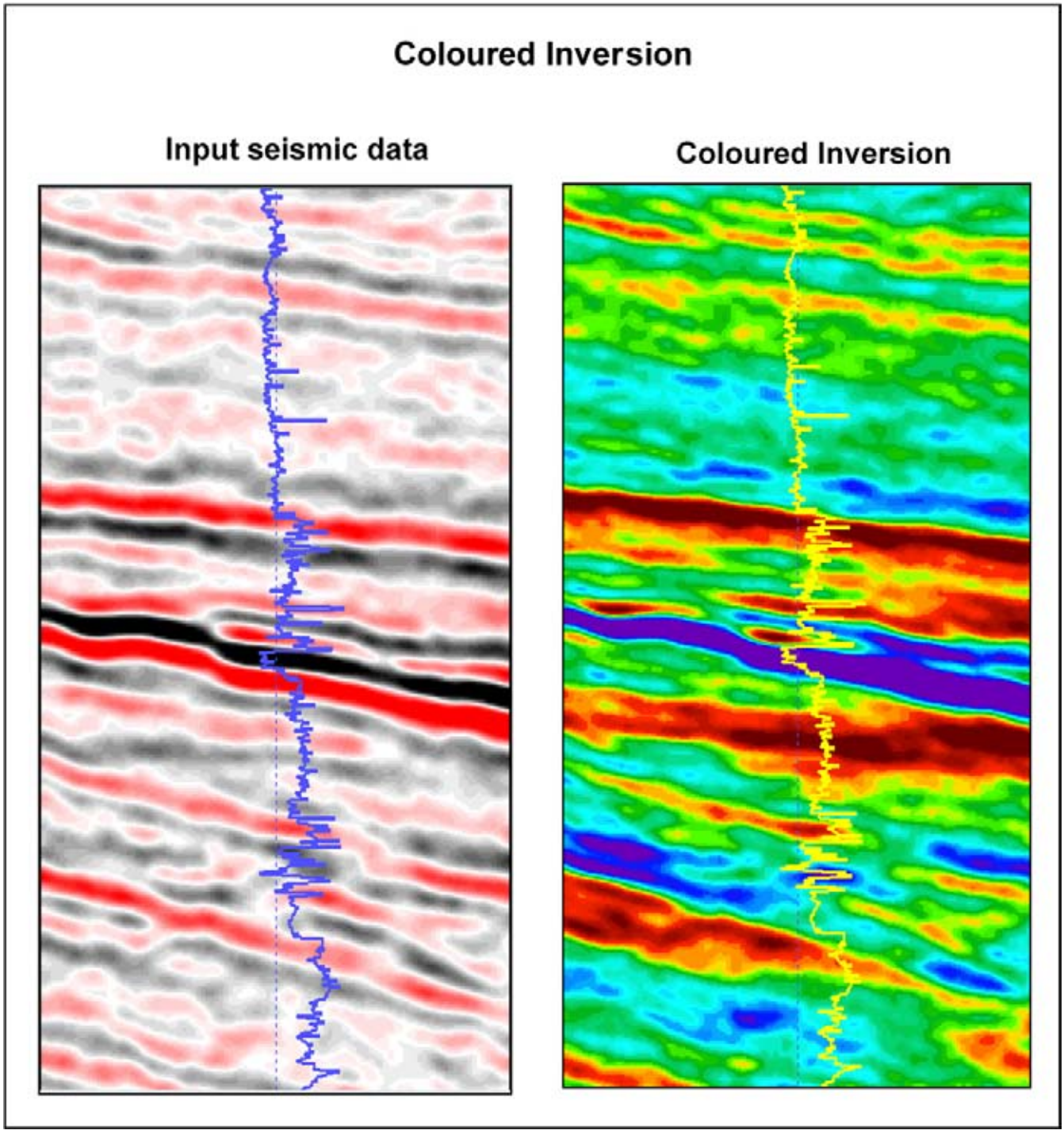

Figure 6.19: Coloured inversion example around a well. Lithological units are much better recognised on the coloured inversion result.

normally necessary, based on the match between the upscaled well log impedance and the inverted traces, because little well info is required in the construction of the a-priori impedance model (Klefstad et al. 2005). It provides a consistency check of the inversion results. The inversion replaces the seismic trace by a pseudo-acoustic impedance trace at each CDP position (Pendrel and Van Riel 2000). The sparse spike hypothesis implies, however, that a thin bed geometry will not always be mimicked in the most optimal way.

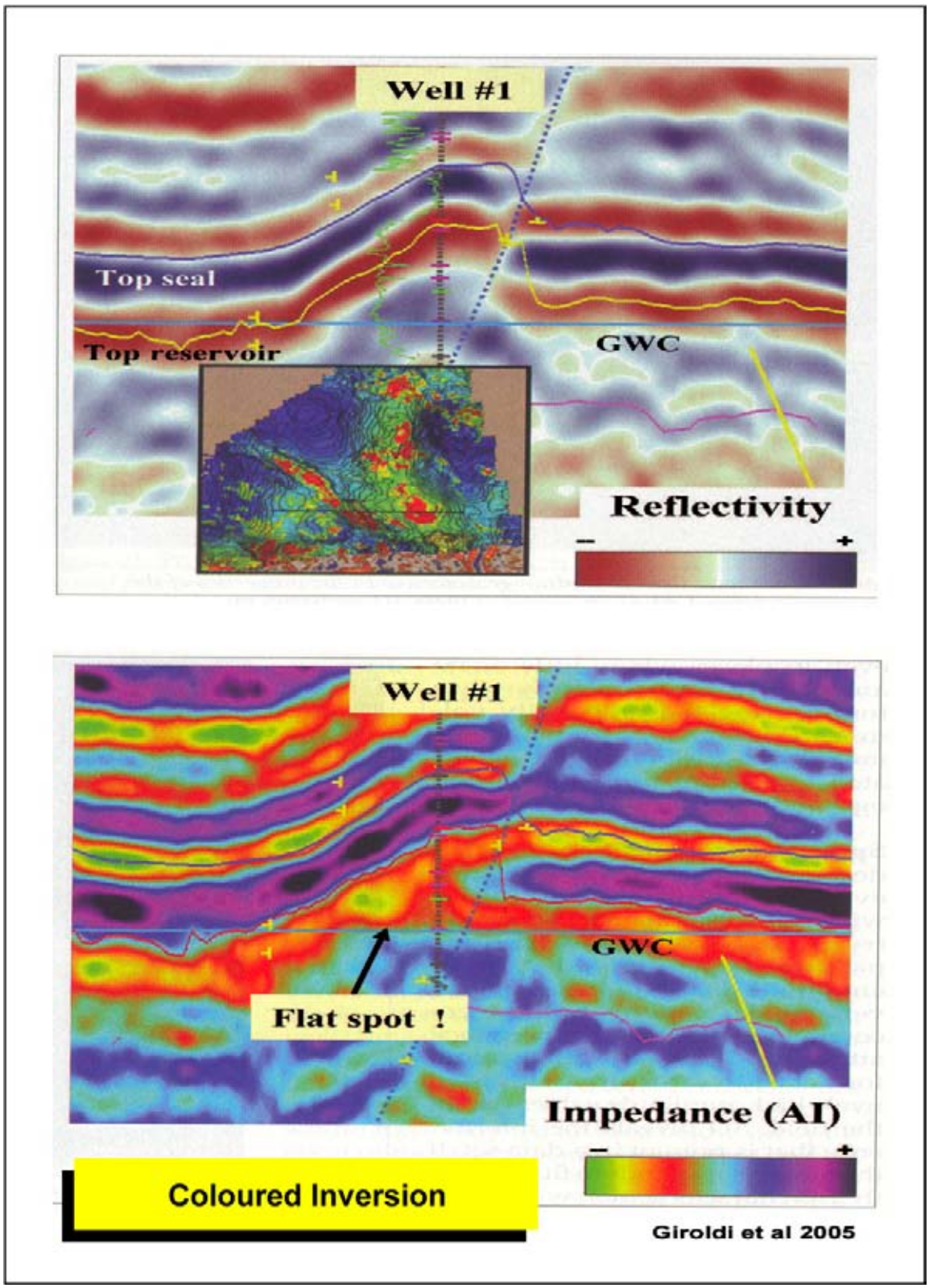

Figure 6.20: Coloured inversion for land data from the Chaco Basin in Bolivia. The reflectivity section on the left does not show the same break at the gas–water contact as seen by the relative AI volume. It illustrates the benefit of extracting the relative AI attribute in these Cretaceous reservoirs.

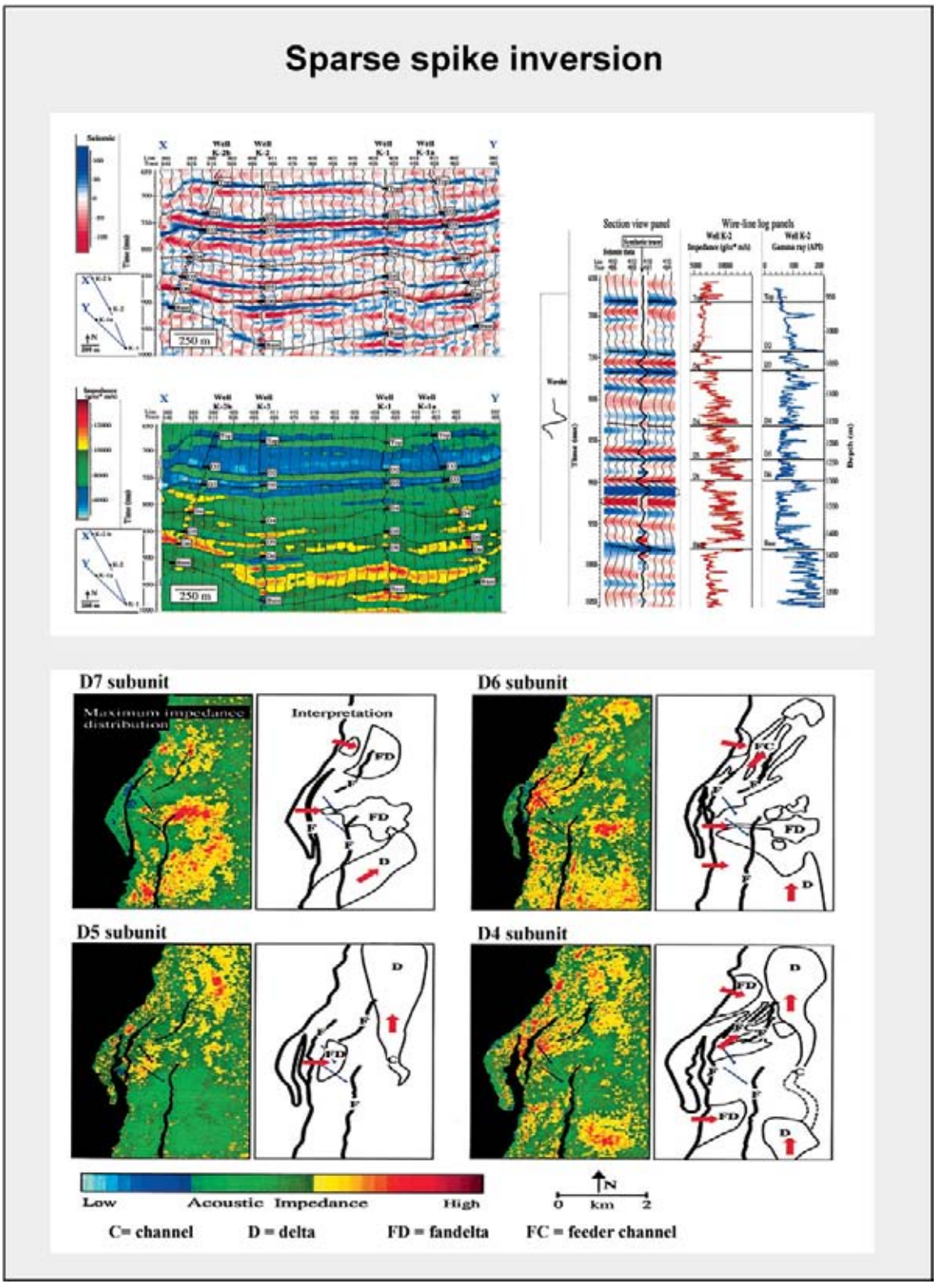

Figure 6.21: Sparse spike inversion uses a minimum number of acoustic impedance interfaces to model the subsurface reflectivity. The algorithm was initially working on a trace-by-trace basis, but this caused instability in the inversion results. A 3D approach is now adopted and further constraints for the solution are provided by the low frequency variations observed by the well control. Note that the wavelet shown here is not zerophase and the mixed nature is directly handled by the inversion algorithm (modified after Ronghe and Surarat 2002).

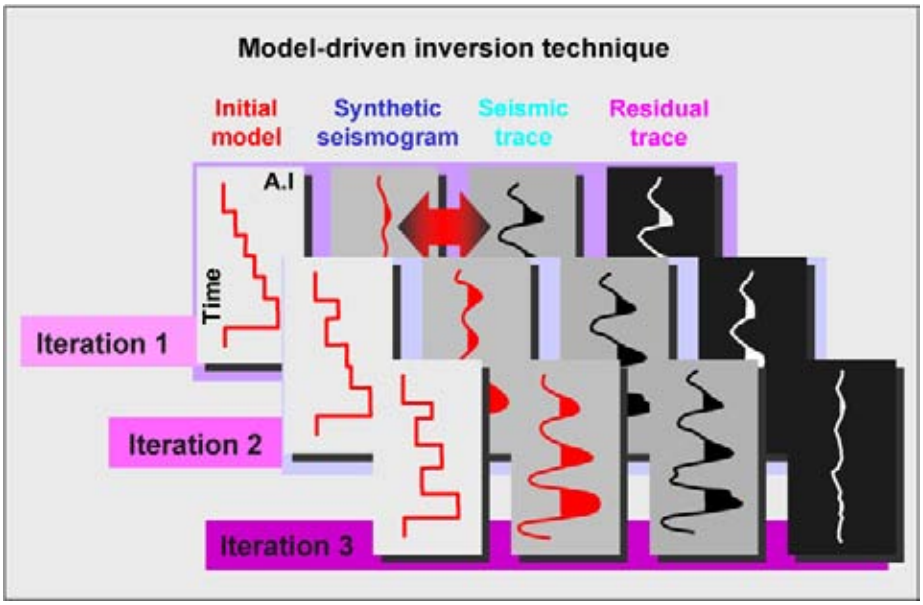

Figure 6.22: Model-driven seismic inversion method. A simplistic initial stratigraphic model is convolved with the seismic wavelet to obtain a synthetic trace, that is compared with the actual seismic trace. The model is then perturbed, whereby the difference between inverted trace and the seismic trace is reduced until a small threshold value is reached. The local 1D AI model is retained and the next trace is inverted. The input is not only one trace, but an average of a small mini-cube (e.g. 8 by 8 traces) around the target trace. This 3D approach ensures a more stable inversion output. The layering in the AI model is partly user defined.

The zerophase requirement can be circumvented by choosing a compound wavelet for the inversion, thus compensating the non-zerophase characteristics of the input data (Figure 6.21). A multi-trace approach results in better stability of the generated inversion solution. Sophisticated model-driven sparse spike inversion gives more realistic output. In some cases the interpreter gets away with the approximation, but in the majority of the cases yet a better job is needed. The latter point has also been illustrated by the study conducted by Sacani Sancevero et al. (2005) for the turbidite play in the Campos Basin in Brazil, where a probabilistic inversion gave more satisfactory results.

6.3.1.4 Model-driven inversion

A simple initial AI model is perturbed, a synthetic computed using the seismic wavelet and the difference with the seismic trace is established (Cook and Sneider 1983, Fabre et al. 1989, Gluck et al. 1997). The AI model with a very small difference is retained as solution (Figure 6.22). A simulated annealing technique using a Monte Carlo procedure is applied (Goffe et al. 1994, Duboz et al. 1998). This technique shows an analogue to the growth of crystals in a cooling volcanic melt (Ma 2003). It starts with a reflectivity model M_0 and computes the difference with the seismic input data after convolution with a wavelet. The model is now perturbed and a new model M_n is simulated, where for the same difference is established. The two differences are compared and if the misfit for $f(M_n)$ is smaller than that for M_0, than the M_n model is unconditionally accepted. If not, than the M_n model is accepted but with a probability:

$$P = e^{(-f(M_n)-f(M_0))/T}, \tag{6.22}$$

whereby T is a control parameter (acceptance temperature). This acceptance rule is known as the **Metropolis criterion** (Metropolis et al. 1953). The process is repeated a large number of times until a very small residual difference is found (threshold value) that is stable. Computation of **Cost functions** permit to determine a real regional minimum for the difference.

The initial AI model is made up of **macro-layers** defined by the shape of the seismic mapped horizons. **Micro-layers** are automatically introduced in this macro model. It provides a **stratigraphic grid cell volume** together with the inline and crossline subdivision for storing constant AI values. The use of micro-layers makes sure that an adequate number of spikes (i.e. vertical change in AI) is utilised in the modelling (Figure 6.23). This model-driven inversion method is much more robust and often a real 3D inversion algorithm is applied to stabilise the solution (Duboz et al. 1998, Coulon

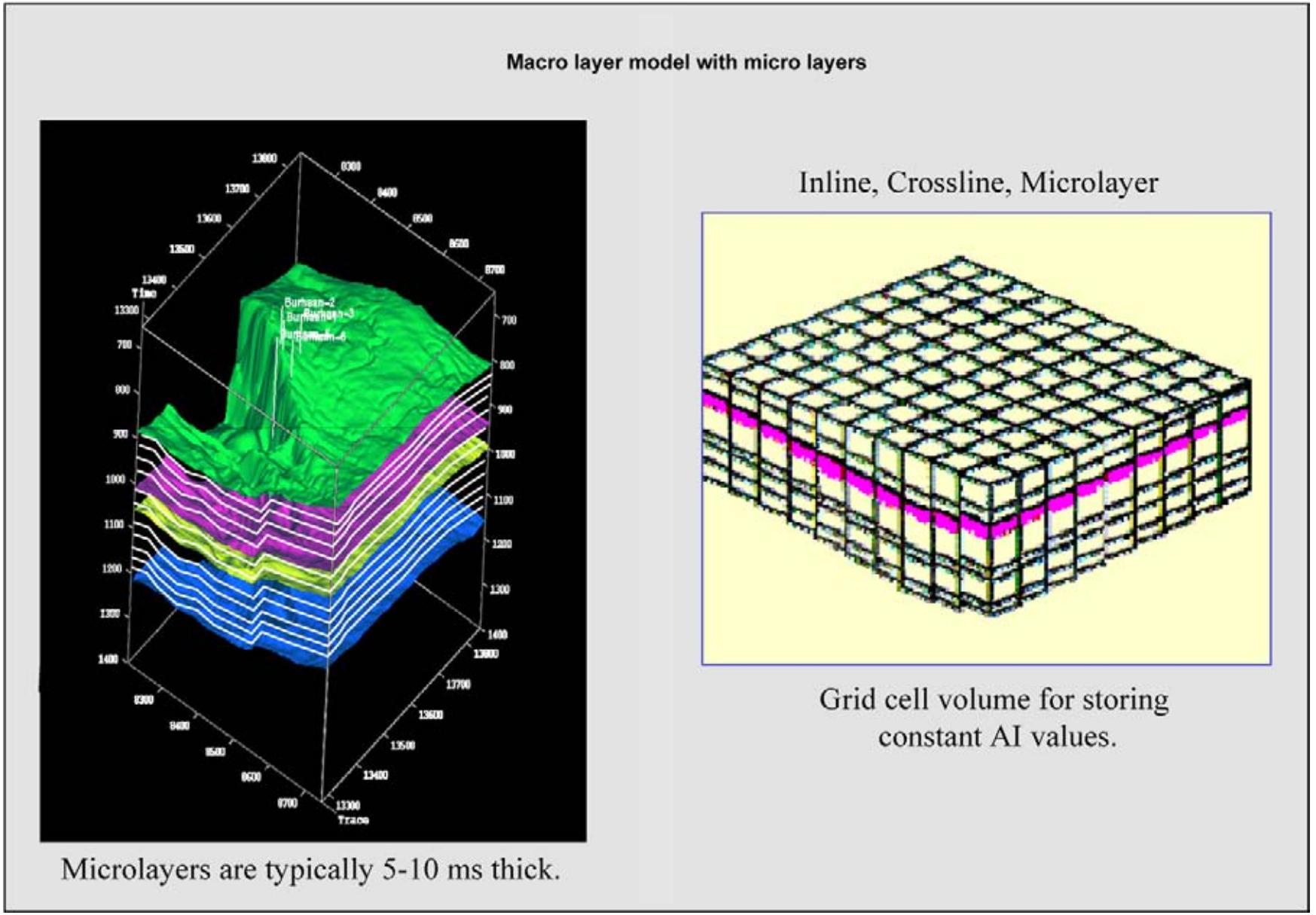

Figure 6.23: A simple initial macro-model is shown with the thinner microlayers. The macrolayers are formed by TWT horizons. The microlayers are introduced automatically into the macro-model and a grid cell volume is built – based on inline, crossline and microlayer thickness – for storing constant AI values. These values are perturbed and vertical synthetics are calculated, that are then compared with the real seismic trace. The geometry of the microlayers are either parallel to the top-, bottom boundary or mixed. If the microlayer follows the seismic reflection geometry, then a microlayer map display facilitates the visualisation of lateral changes. Sometimes it is handy to take several microlayers together in the map visualisation.

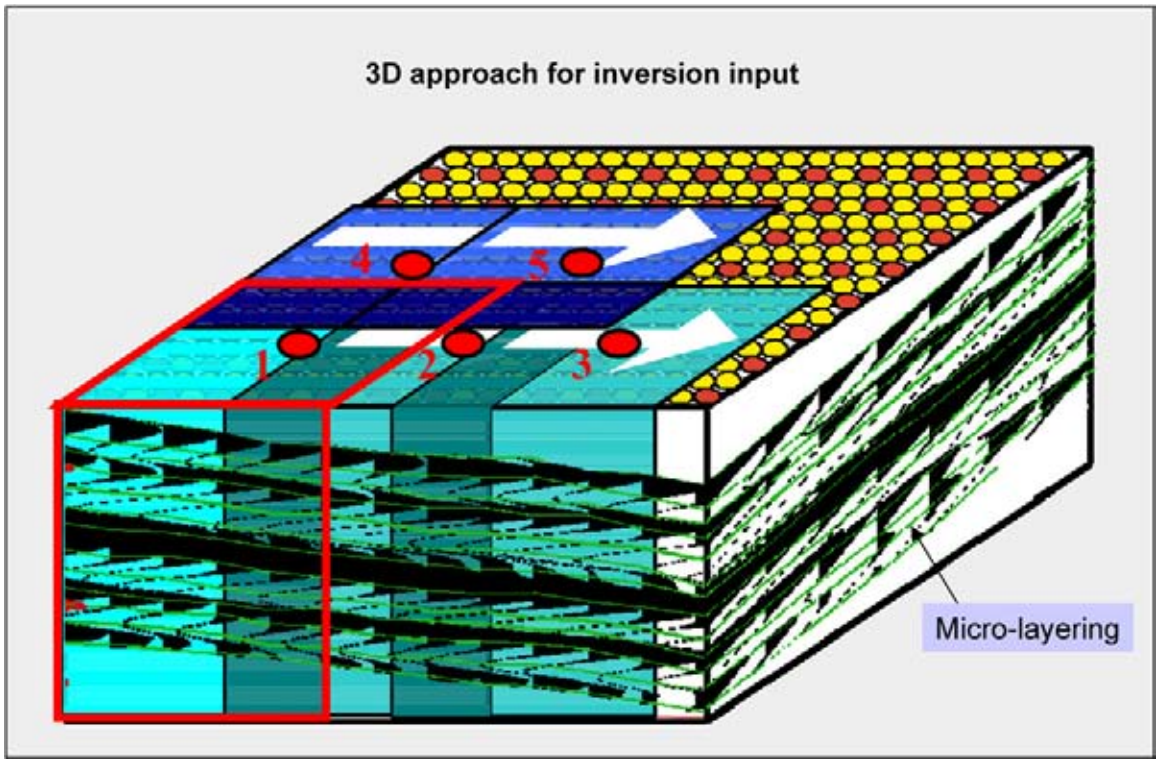

Figure 6.24: A 3D approach to the inversion procedure ensures that the solution is stabilised. A subcube of seismic data around the target trace is used for the AI computation. The subsequent subcube for the next target trace has a certain overlap. This working manner results in a more stable solution from trace to trace. Drawback is that the well results are never 100% honoured by this inversion technique. An advantage is that the inversion is driven by the seismic data and errors, caused by unreliable well data, are not propagated by the inversion algorithm.

et al. 2000, Veeken et al. 2002b; Figure 6.24). A bulk phase rotation can be applied to zerophase a seismic subcube. Normally this procedure is valid for a small time window (<1.5 sec TWT), where a stable wavelet is derived (Figure 6.25). The results are evaluated at the well control points in so-called composite well plots (Figure 6.26). The seismic and the AI cubes are compared (Figure 6.27). Layer maps are quite useful to delineate the extent of AI anomalies (Figure 6.28). The method can give satisfactory results even when well control is limited and the seismic quality is rather poor (Veeken et al. 2002a; Figures 6.29 and 6.30). It is also possible to derive a wavelet straight from the seismic dataset. The model-driven inversion does not always honour the well control completely, but a great advantage is that the seismic data is the guide for the inversion. Errors in the well logs do not propagate in the inversion. This is an advantage when the old well database is unreliable. The averaging effect, introduced by the 3D approach, results in small discrepancies at the well locations that are in fact quite acceptable. Also in carbonates good inversion results are possible. The relative velocity and density changes induced by the porefill are decisive for creating AI anomalies (Figure 6.31).

An other model-driven method (Invermod) is making use of Principle Component Analysis (PCA, Helland-Hansen et al. 1997). The principle component methods computes a standard response from which the input can be generated by applying specific weighting factors. These weighting factors are extrapolated over the study area in order to allow predictions outside the control points. The inversion needs an a-priori model to start with. The structural frame is based on the shape of the mapped time horizons. The initial model with the separate velocity and density distribution is build by PCA applied to the well log data. Weighting factors for the standard log response in the studied area are determined via a linear interpolation technique. The results of the convolution with the seismic wavelet is then compared with the seismic traces and the V_p–rho models are perturbed to reduce the discrepancy. The velocity and density are hereby modelled separately. Detailed low frequency modelling can be very helpful for later acoustic impedance inversion (Guilbot et al. 2003).

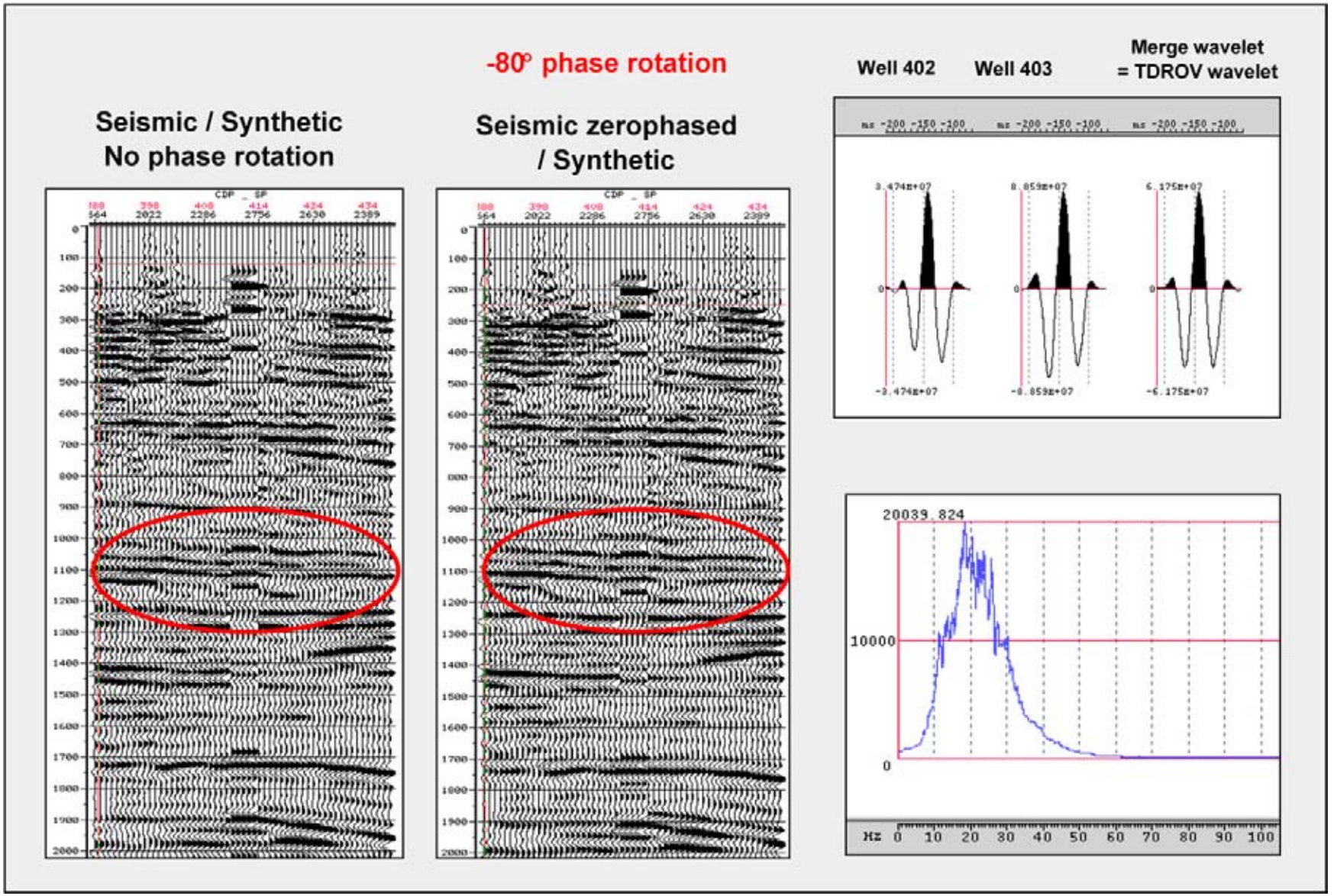

Figure 6.25: Bulk phase rotation of the seismic data is done to better zerophase the data over the target time interval. Usually a stable wavelet can only be derived in a limited time window (<1.5 seconds TWT). The phase rotation improves the synthetic-to-seismic fit.

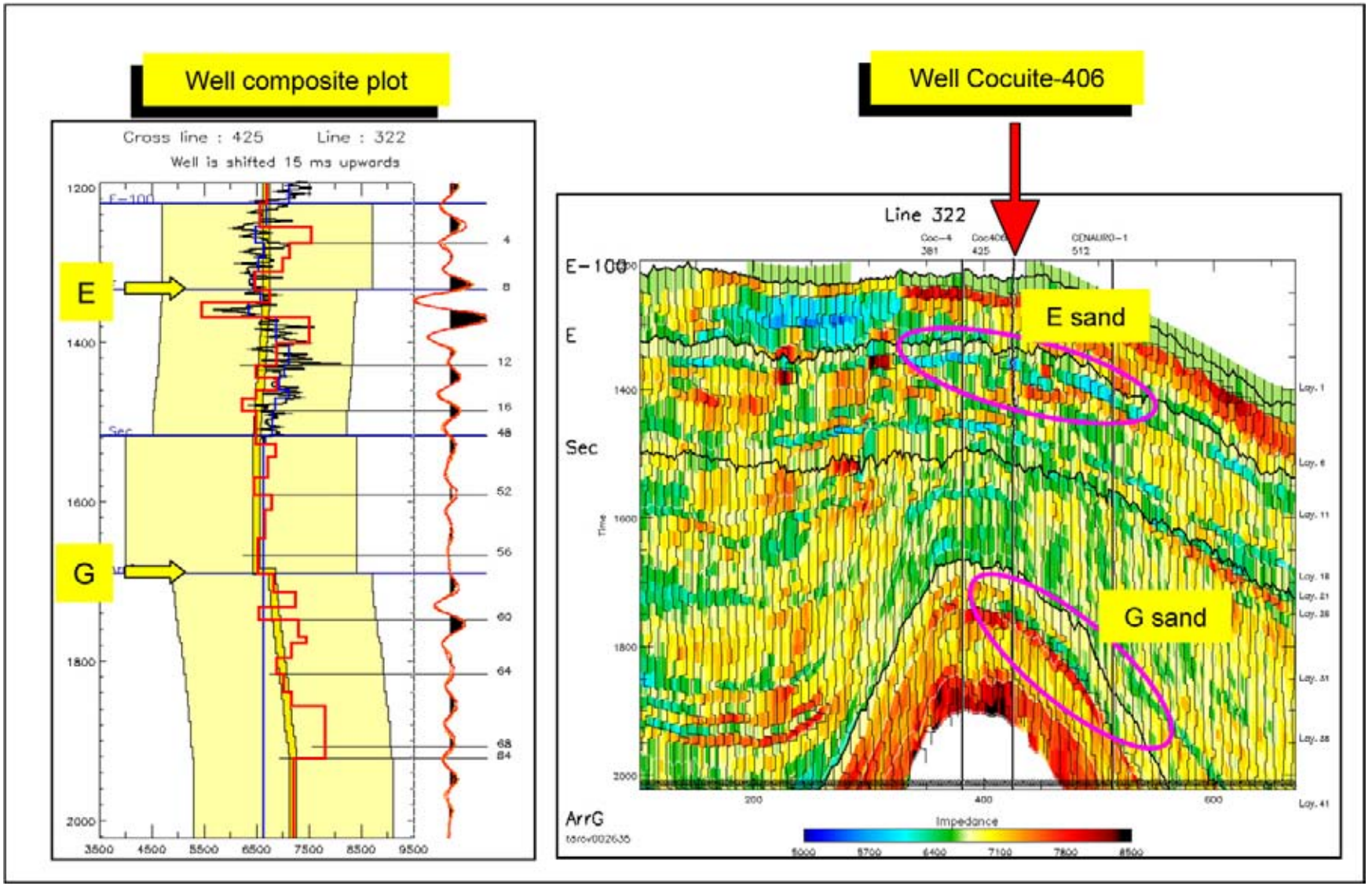

Figure 6.26: Well composite plot summarising the inversion results. The well AI trace is compared with the inversion AI trace at the well location. At the right hand side the AI results are convolved with the seismic wavelet and overlain with the seismic trace. The AI section through the well location is shown. The two HC-bearing intervals E and G are characterised by AI anomalies with low acoustic impedance (green–blue colours). The G sand accumulation is limited updip by a subtle fault (data courtesy Pemex).

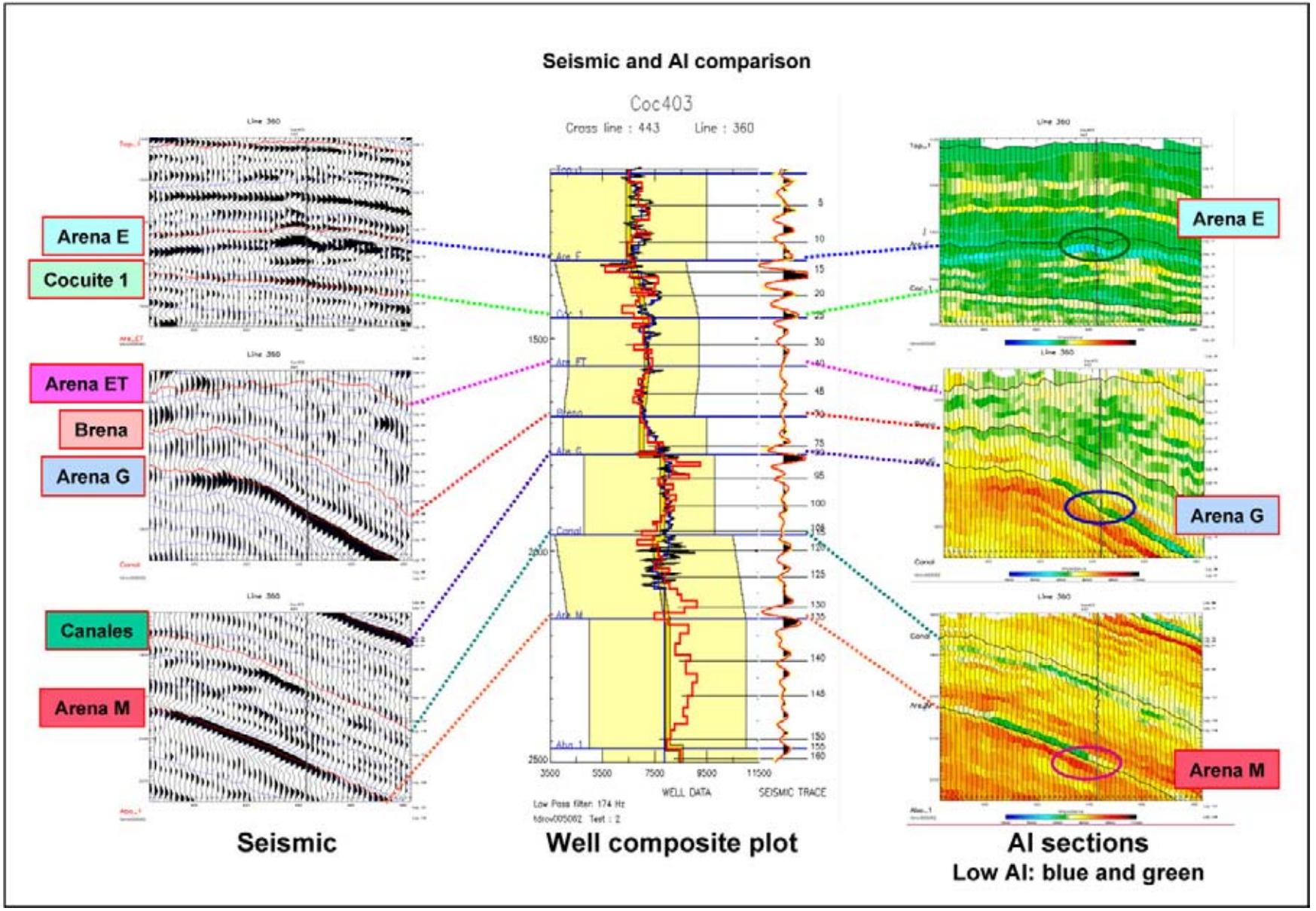

Figure 6.27: Comparison between seismic and AI sections across a well. If the results of the inversion had been available earlier to the reservoir engineer, it would have been easy to move the well location slightly updip. In that case also the AI anomaly seen on the M – sand level would have been tested. Optimisation of well trajectories is an important aspect of the seismic inversion processing. In that way the study will pay by itself and the additional expenses are easily justified in the exploration or production budget (data courtesy Pemex).

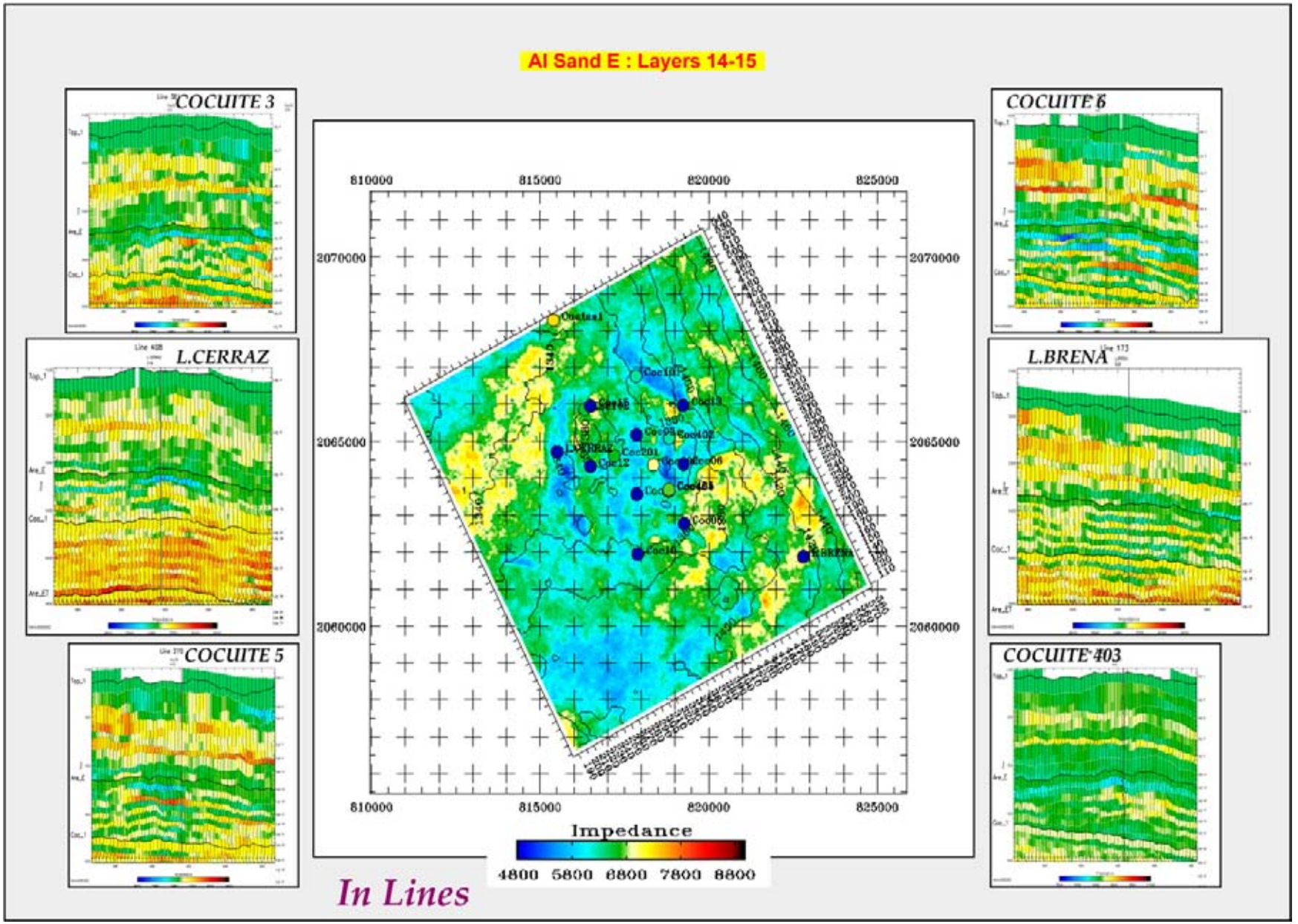

Figure 6.28: The AI layer map of the *E* sands clearly shows low impedance anomalies in dark blue, that correspond to the presence of hydrocarbons. Reservoir inhomogeneities, also seen by the wells, are illustrated by this inversion results (data courtesy Pemex).

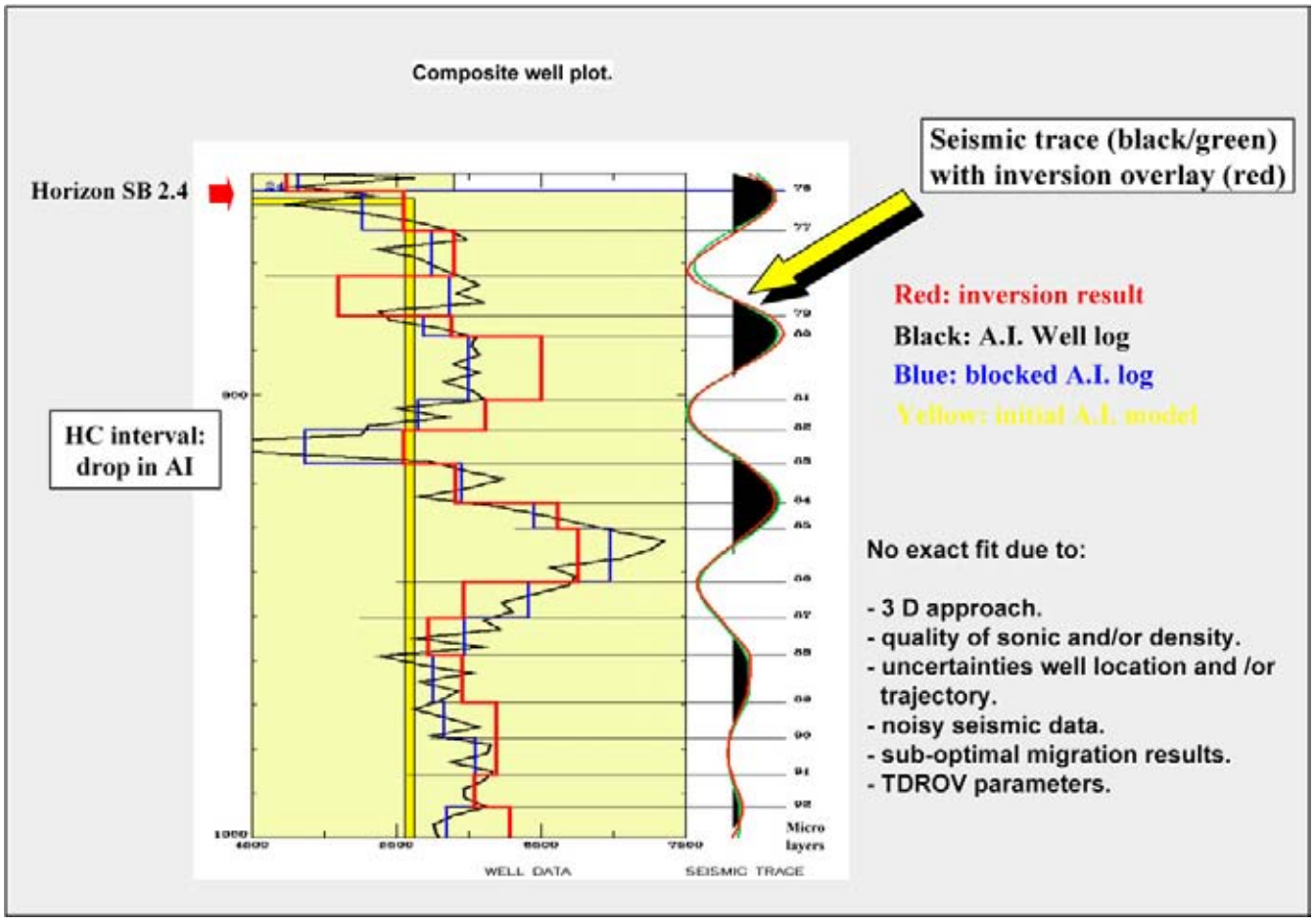

Figure 6.29: Well composite plot summarising the inversion results for the MAC-201 well, onshore Mexico. The well AI trace is compared with the inversion AI trace at the well location. At the right hand side the AI results are convolved with the seismic wavelet and overlaid with the seismic trace. The hydrocarbon reservoir usually has a low acoustic impedance compared to the brine filled host rock. AI microlayer maps are used to visualise the areal extent of the anomaly (data courtesy Pemex).

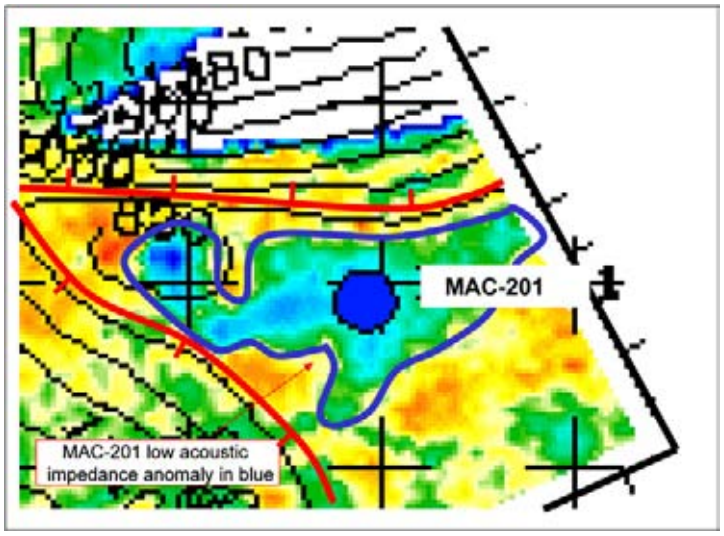

Figure 6.30: Even in poor data zones the model-driven inversion may give reasonable results. The acoustic impedance layer map is showing an anomaly related to the presence of hydrocarbons in the Macuspana-201 well, onshore Mexico. The anomaly is less well defined to the north and west because the presence of important fault zones. Smoothing and interpolation of the mapped time horizon in these areas has introduced an uncertainty (data courtesy Pemex).

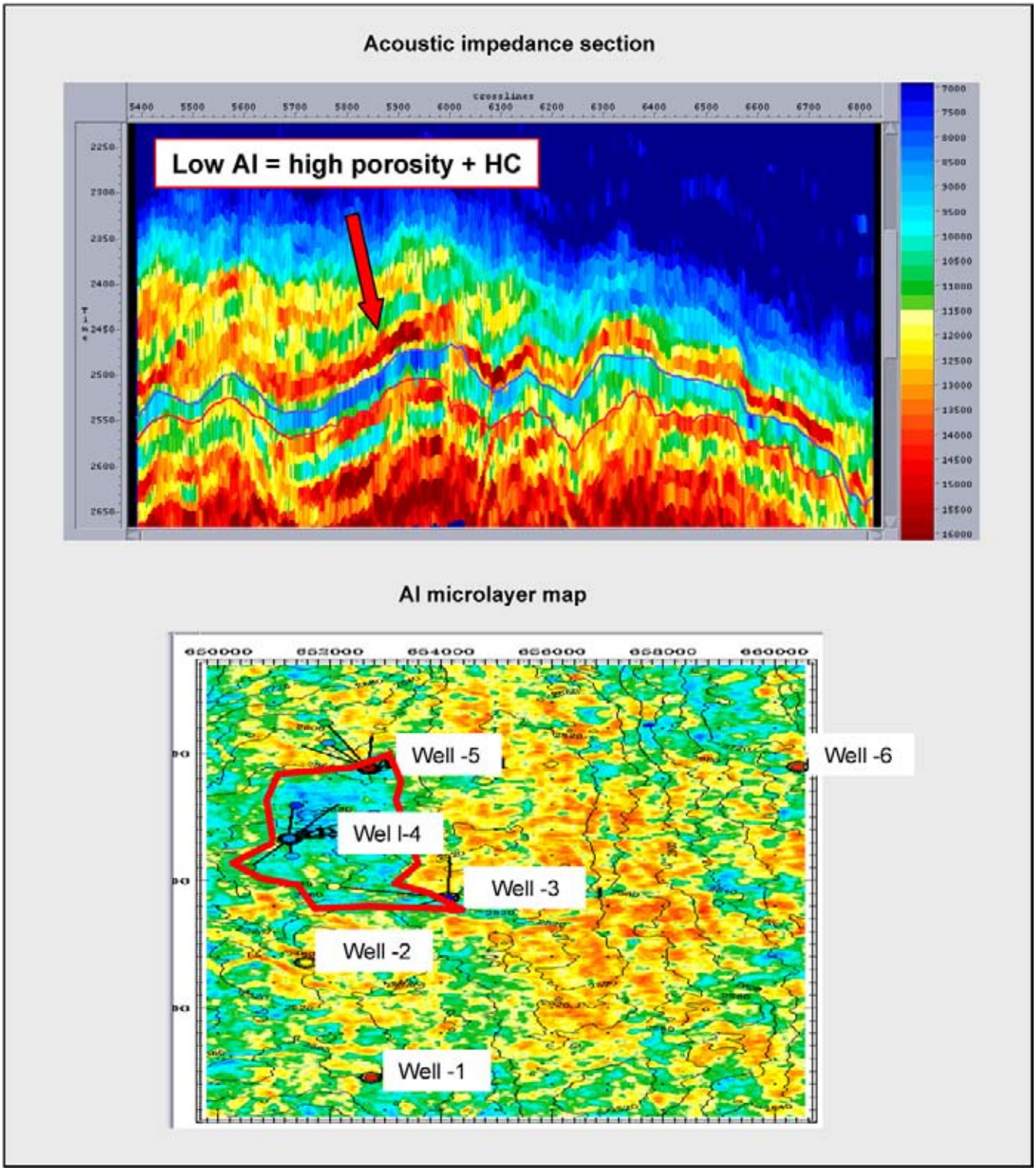

Figure 6.31: Inversion of a seismic line with a clear anomaly due to porosity and pore fill changes in carbonate reservoir rocks. Even in carbonates the inversion gives good results. It is the lateral difference in acoustic impedance variation that is important to outline HC accumulation, not the absolute value. The AI microlayer map shows the areal extend of the anomaly (data courtesy Pemex).

6.3.1.5 Stochastic inversion

Geostatistics are used to build a complete subsurface model and constrain the inversion solutions (Dubrule 2003). Simulation is done on local level as well as globally, on the totality of the generated model (Haas and Dubrule 1994, Dubrule 2003). All models honour the well data, otherwise they are rejected. The architecture of reservoirs is classified in various ways (Weber and Van Geuns 1990) and this helps in selecting the simulation approach. **Probability density functions** (PDF's) are established for each grid point and these are used to perform a random simulation (Van der Laan and Pendrel 2001). The input for the PDF comes from well logs, spatial properties (variograms) and lithological distributions. The stochastic algorithm calculates for each simulation a synthetic trace, compares it with the real seismic trace and accepts or rejects it. A simulated annealing process is utilised. The number of solutions is reduced in this way and probability maps are produced to assess the risk. The retained simulations are examined on their variance (Figure 6.32). If they closely resemble, then the prediction is rather good and the confidence level of the output is increased.

The earth models show a high resolution variability comparable to that found in the wells (cf Helgesen et al. 2000). The proposed variability is clearly beyond seismic resolution (cf Rowbotham et al. 2003). When production data are integrated in the modelling constraints, than the value of the simulated model is increased accordingly. Production history matching and pressure monitoring give an indication for the connected reservoir volume and its effective permeability.

Two stratigraphic factors are important for the recovery efficiency: reservoir connectivity and permeability heterogeneity. Both parameters influence the sweep efficiency of the reservoir. Models that appear visually different, but have the same connectivity, well count and permeability heterogeneity, have similar sweep efficiencies. This observation means that the building a suite of simulations with different reservoir architectures may not help to get a grip on the ultimate recovery efficiency (La Rue and Friedman 2005). Some reservoir architecture parameters that are important to consider in this context:

- Channel width to thickness.
- Sinuosity.
- Stacking pattern.
- Orientation.
- Reservoir element type of facies unit (channel, point bar, etc).
- Porosity distribution.
- Permeability distribution.
- Net to gross ratio.
- Rock types.
- Matrix contribution.
- Hydrocarbon saturation.
- Pressure profile.

Seismic data are indirect measurements of porosity, fluid type, mineralogy and rock compressibility. They serve as guide for extrapolation of pore volume, net-to-gross, fluid contacts and extend of cementation variations. The depositional environment (geological input) controls degree of sorting, shape of particles, and transitions between facies. Its knowledge is useful in delineating flow units within the reservoir and improve the permeability prediction away from the wells (Rowbotham et al. 2003). Geological constraints help to improve the reliability of the simulations and provide more realistic error estimates.

A probability volume is generated for grid points with porosities above 10%, using the simulation histograms. Subsequently bodies are outlined where the probability is above 70% for the porosity to be higher than 10%. As more wells are drilled in the same petroleum system, the best matched simulations are retained to further refine the predictions (Sylta and Krokstad 2003).

Drawback of the probabilistic method is that the interpreter has to quantify the uncertainties in a realistic way. This is a tedious and precarious task (cf Klefstad et al. 2005). Areas without proper well control are still difficult to predict and assumptions have to be made. There is a cumulative increase in prediction error as various reservoir parameters have to be estimated at the same time.

A delicate problem is the presentation of the results. Normally only the P10, P50 and P90 cases are retained and the rest of the realisations are ignored. These P10–P90 expectation maps can be very misleading as the outcome of an individual simulation is sometimes unrealistic, e.g. rapid changes in geological style that are an artefact of the working method. It is better to use maps that are some sort of an average and examine the areas that rather stable in several simulations. Svanes et al. (2004) has adopted an average of 10 simulations to stabilise the modelling and generate one stochastic petrophysical model for further flow simulation. Klefstad et al. (2005) use an average of 30 simulations and conveniently calculate an uncertainty from the standard deviation map. The predictive value of the simulation is strongly reduced in areas with great variability in outcome of the realisations. This averaging procedure has, however, a negative effect on the high resolution aspect of the proposed solution.

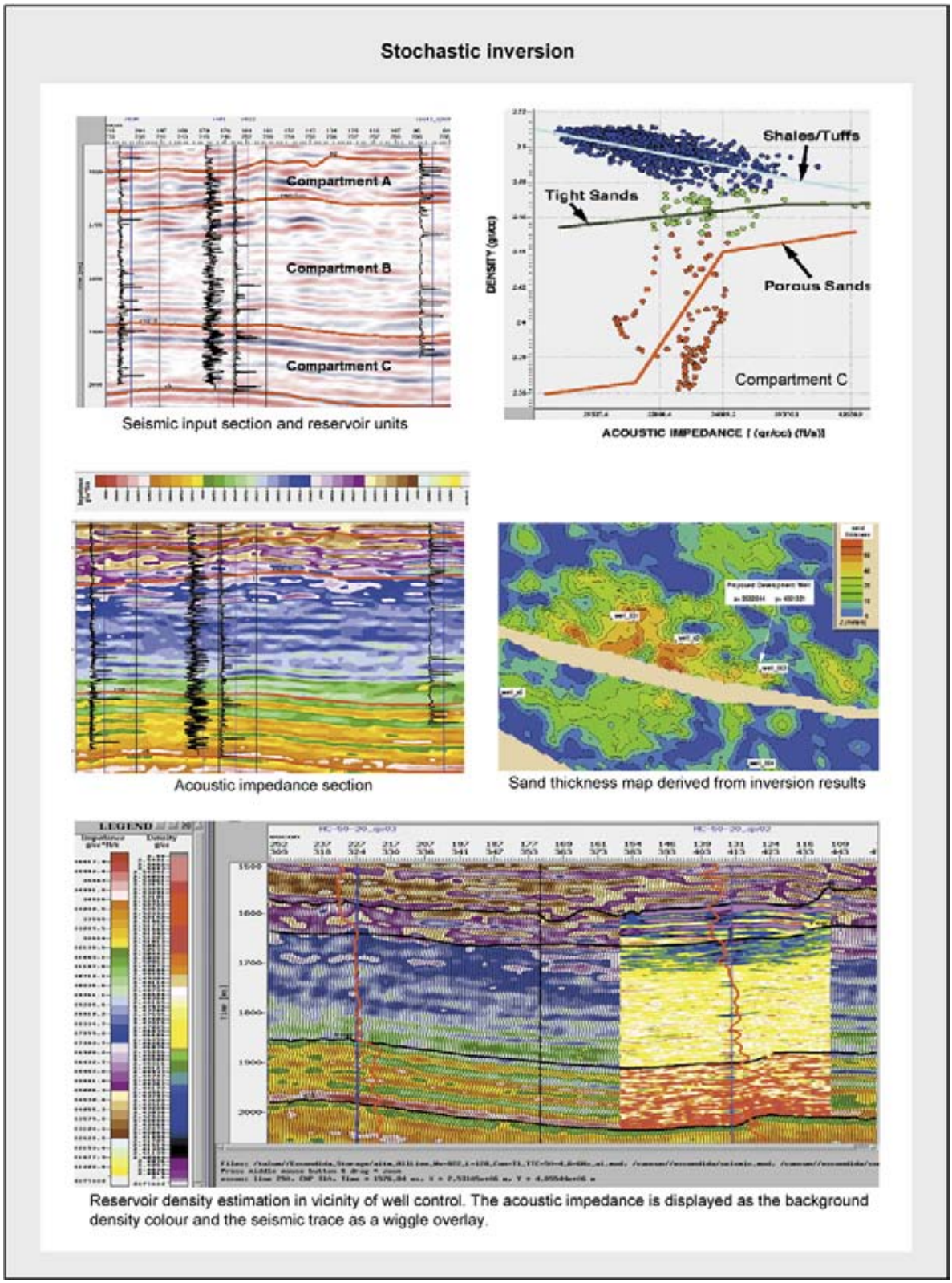

Figure 6.32: The stochastic inversion uses probability density functions to simulate earth models, that are convolved with the seismic wavelet and compared the real seismic trace. Realistic uncertainty quantification play an essential role in this method. The results are presented with a specified probability attached to it (modified after TorresVerdin et al. 1999).

6.3.2 Pre-stack inversion methods

The data pre-conditioning is for this approach even more important. Like in AVO studies, the input should be properly migrated when reflection dips are severe. Therefore pre-stack time migrated CDP gathers are needed. The preserved amplitude processing should be adhered to. Hence the AGC sliding gain window should not be selected smaller than 1 second TWT. This will allow for more reliable quantitative interpretation instead of only qualitative assessment of the inversion results.

6.3.2.1 Elastic inversion

This method exploits AVO effects in the prestack domain and uses V_p and V_s information. In essence it is however a post stack inversion method that works on partial stacks (near, mid and far offset cubes). The shear waves may yield valuable information on the lithological distribution (Pendrel et al. 2000). Several seismic attributes and rock physical parameters can be calculated.

The full Zoeppritz equations give a description of the amplitude behaviour of are reflector with offset (Zoeppritz 1919). These equations are tedious to work with and therefore an approximation is introduced, valid under certain conditions (e.g. Shuey 1985). One of the methods is based on the computation of an **elastic impedance** attribute (EI) as proposed by Connolly (1999). The calculation is first done on the CDP gather at the well position (see Section 6.2 above). The EI value depends on V_p, V_s and theta, which is the angle of incidence. V_p and V_s are known at the well and theta is varied is regular steps. This EI trace is compared with the angle stack traces for the corresponding discrete angle ranges and a wavelet is derived. It is subsequently used to perform a deconvolution to transform the angle stack seismic cube into several EI cubes (Figures 6.33 and 6.34).

The far offsets of these EI cubes give detailed information on the fluid contents. Attributes like R_p, R_s, I_p, I_s, $V_\mathrm{p}/V_\mathrm{s}$, rhomu and rholambda are easily calculated. These parameters can also be obtained from AVO analysis, but the calculation is less robust (Cambois 2000a). Multiple energy, wavelet variations and residual moveout are hampering the quantitative interpretation of the AVO inversion results (Figure 6.35, Cambois 2000b). Cambois even proposes an elastic inversion without shear log information to derive a fluid factor (CGG website).

In a gas reservoir the following changes are expected for the various rock physical parameters:

- V_p decreases in gas reservoir.
- V_s not influenced by liquid/gas porefill. S-wave do not prograte in fluids or gas.
- $V_\mathrm{p}/V_\mathrm{s}$: low values in a gas reservoir.
- P-impedance I_p decreases in a hydrocarbon reservoir.
- S-impedance I_s decreases only a very little amount in a gas reservoir, because density is decreased.
- Poisson's ratio decreases in a gas reservoir, because density is decreased.
- Mu, which represents the rigidity of the matrix, is little influenced by the presence of gas.
- Density Rho decreases in gas filled reservoir.
- The pore-fluid discriminator Lambda decreases in a gas reservoir.
- Lambda/mu has low values in a gas reservoir.

Extended Elastic Impedance (or EEI) is a concept introduced by Whitcombe et al. (2000). By substituting $\tan\varphi$ for $\sin^2\theta$ in the Aki and Richards approximation of the Zoeppritz equations, whereby φ ranging between -90 and $+90$ degrees, EEI is shown to correlate better to the various elastic parameters such as bulk modulus, shear modulus and lambda depending on the angle φ. The EEI attribute is expressed by:

$$\mathrm{EEI}(\varphi) = V_\mathrm{pa}\rho_\mathrm{a}\left[\left(\frac{V_\mathrm{p}}{V_\mathrm{pa}}\right)^a\left(\frac{V_\mathrm{s}}{V_\mathrm{sa}}\right)^b\left(\frac{\rho}{\rho_\mathrm{a}}\right)^c\right], \qquad (6.23)$$

$$a = \cos\varphi + \tan\varphi,$$

$$b = -8K\sin\varphi,$$

$$c = \cos\varphi - 4K\sin\varphi.$$

V_pa, ρ_a, V_sa are average values for the V_p, rho and V_s over the interval of interest. K equals the average value of $(V_\mathrm{s}/V_\mathrm{p})^2$. An angle of $\varphi = 0$ corresponds to the AI value (Whitcombe et al. 2002). The correlation of EEI with different rock physical parameters is investigated. A correlation with the gamma ray log is useful for lithologic discrimination (Neves et al. 2004; Figure 6.36). Computation of a weighted stack has been suggested to make a comparison between EEI and the seismic data possible. The frequency between near and far angle stacks is however different. The far offset panel is usually lower frequent and the cubes can be filtered to a similar amplitude spectrum.

The use of **shear wave elastic impedance** (SEI) is yet an other concept for inversion that claims to generate more robust results (Duffaut et al. 2000). Post stack inversions are applied on the partial stack cubes. For the near offset the AI of the wells can be used as an inversion guide. For the far offset the EI log can be utilised

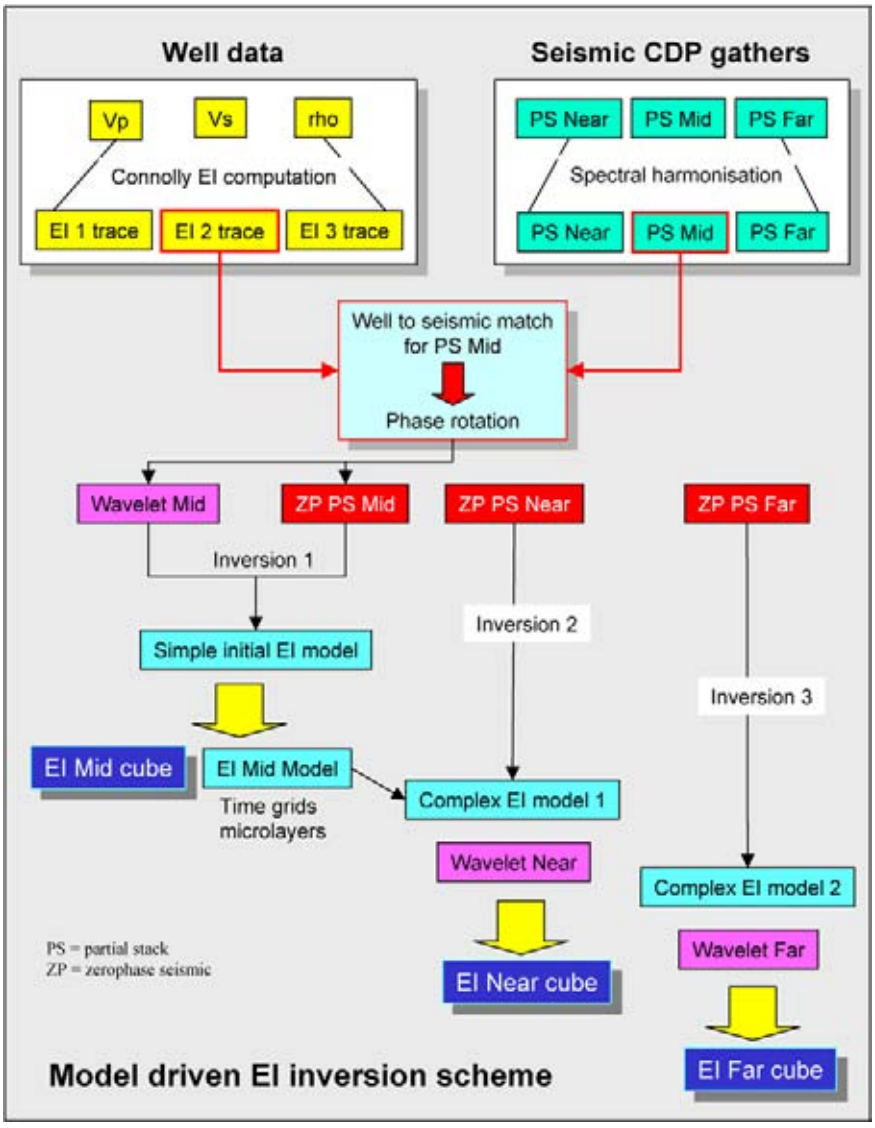

Figure 6.33: Overview of an elastic inversion work flow. There are various ways to determine the wavelet that is used for this kind of inversion. PS stands for partial stack and ZP for zero-phased seismic volume.

as demonstrated by Connolly (1999). The SEI links the converted wave stacks to the wells by linearisation of the Zoeppritz equations. SEI is equivalent to EI but adapted to P–S converted seismic data (Duffaut et al. 2000). 4 component OBS data is the input for this exercise. The hydrophone and the vertical geophone or Z data is summed to attenuate receiver side water layer reverberations and a PZ volume is obtained (Figure 6.37). To relate SEI to P–S reflectivity in the same way that AI relates to P–P reflectivity, the following equation must be fulfilled:

$$R_{\mathrm{ps}(-\theta_\mathrm{p})} = -R_{\mathrm{ps}(\theta_\mathrm{p})} = \frac{\mathrm{SEI}_{2(\theta_\mathrm{p})} - \mathrm{SEI}_{1(\theta_\mathrm{p})}}{\mathrm{SEI}_{2(\theta_\mathrm{p})} + \mathrm{SEI}_{1(\theta_\mathrm{p})}}. \qquad (6.24)$$

Under the conditions that the impedance contrasts are weak and the incidence angles are small, then:

$$\mathrm{SEI}_{\theta_\mathrm{p}} = V_\mathrm{s}^m \, \rho^n. \qquad (6.25)$$

$$m = 4K \sin\theta_\mathrm{p}[1 - 0.5(1+2K)\sin^2\theta_\mathrm{p}],$$

$$n = (1+2K) \times \sin\theta_\mathrm{p}[1 - (K(1+1.5K)/(1+2K))\sin^2\theta_\mathrm{p}].$$

K is here equal to $(V_\mathrm{s}/V_\mathrm{p})^2$. A scaling factor is needed to compare the EI and SEI values. When $V_\mathrm{s}/V_\mathrm{p}$ is close to 0.5 at incidence P-wave angles around 30°, the SEI log is approximately equal to the shear impedance log.

4D or **time lapse elastic inversion** is possible, but as always it demands careful data pre-conditioning (Rutledal

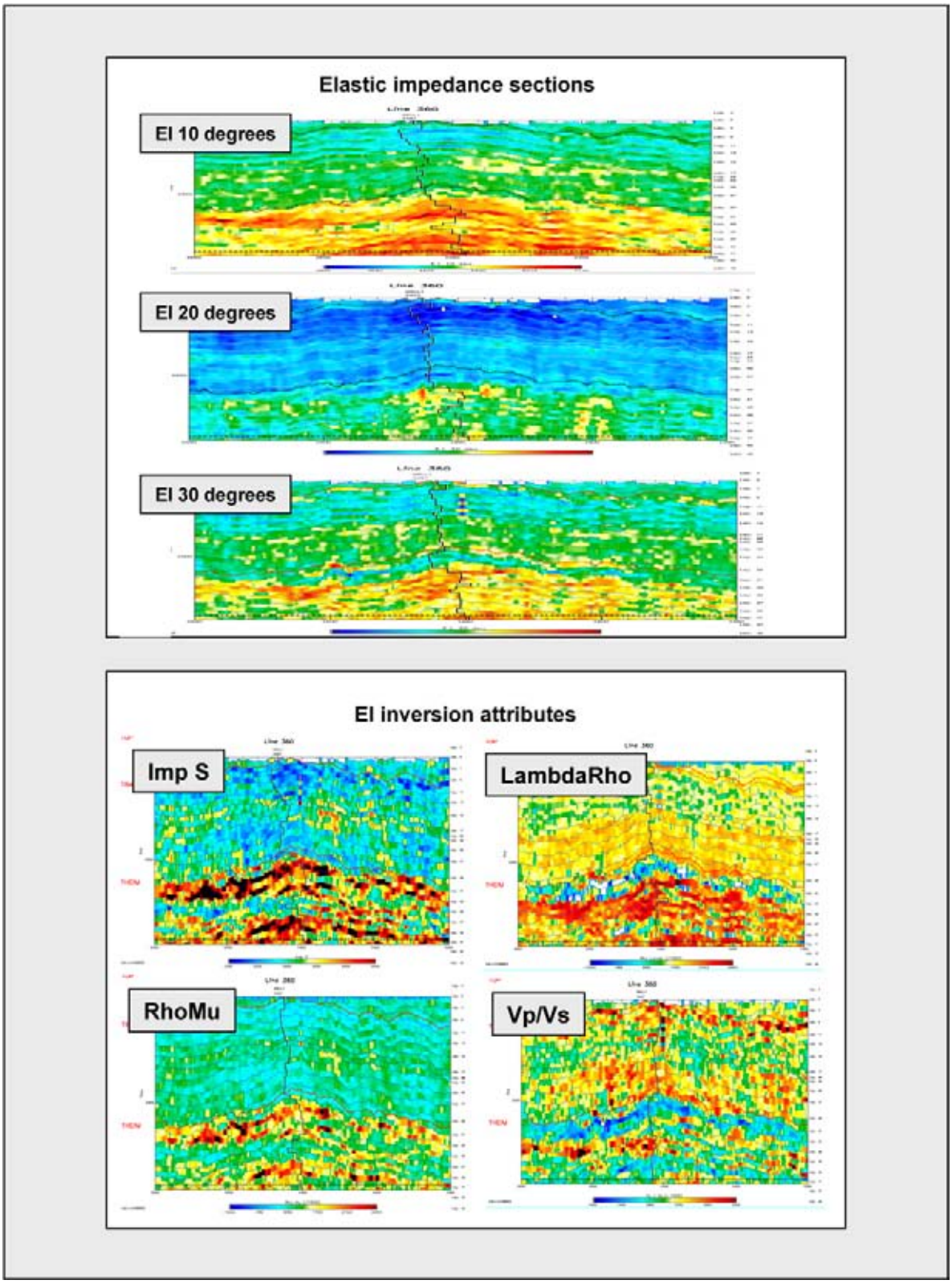

Figure 6.34: The output of an elastic impedance inversion gives access to several EI attributes. The elastic rock parameters are useful because the Poisson's ratio is related to the fluid saturation. The difference between the P-wave (info on fluid and rock framework) and S-wave behaviour (info on rock frame work) is of particular interest for reservoir characterisation purposes.

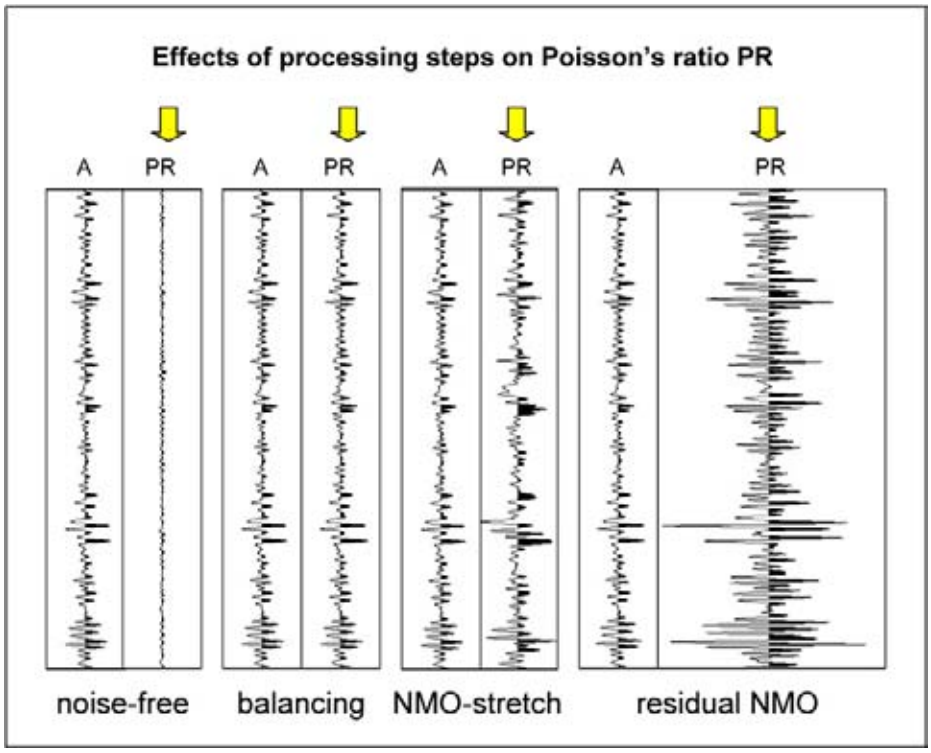

Figure 6.35: Data pre-conditioning is an important step when doing reservoir characterisation studies. Standard processing steps can introduces tremendous changes in the Poisson's ratio as is illustrated by Cambois (2000) and that can not be related to rocks and/or porefill.

et al. 2003). In their Oseberg case study some spectral harmonisation improved the quality of the far offset partial stack. Constrained and coupled inversion is achieved by taking the results of the first inversion as input for the EI inversion of the second survey. The microlayers are kept the same (common layer model) and only the impedance values in the reservoir interval are altered. The time lapse difference cube of the Poisson's Ratio gave the best possibility for discrimination of production effects in the reservoir response.

6.3.2.2 Simultaneous inversion

The simultaneous inversion method uses the Aki and Richards formula (1980) to compute the reflectivity at the various offsets in the prestack domain. It is an AVO inversion technique. The inversion transforms the seismics data into reflectivity cubes at several offset ranges (partial stacks) and computes CDP gathers. In this approach there are no limits on the validity due to constraints in the offset angles. A simple initial V_p model is needed with only the low frequency variation. A density model is constructed applying Gardner's estimation. A simple V_p/V_s model is adopted (as approximation: 2 constant). Advantage is that the same time model can be used for all offset angles. The calculations are done for six discrete offset angles. It gives access to the following attributes: V_p, V_s, rhomu, lambdamu, lambdarho and V_p/V_s. In carbonate rocks the lambdarho-versus-rhomu crossplot can be very useful to isolate discrete shale and porous dolomite populations (cf Pelletier and Gundersen 2005). A higher V_p/V_s ratio is expected in zones with better secondary fracture porosity. Also the shape of the porosity can be reflected in the seismic response. The pore aspect ratio is defined as the length of the short axis divide by the length of the log axis in a 2D pore space and therefore the ratio is always less or equal to one. A lower pore aspect rock would show a greater change in velocity when hydrocarbon is present in the pores (Ng et al. 2005).

Simultaneous inversion is calculating synthetic CDP gathers from perturbed P- and S-reflectivity models. It is simultaneous in the sense that it works on several time samples at the same time. It takes into account the AVO behaviour as well as computation of the seismic impedance. The approach is basically model-driven and the method is well described by Ma (2002). The algorithm uses initial input models to compute synthetic gathers and compares them with the real seismic data. The inversion is achieved by applying a simulated annealing technique (Ma 2002), analogue to the growth

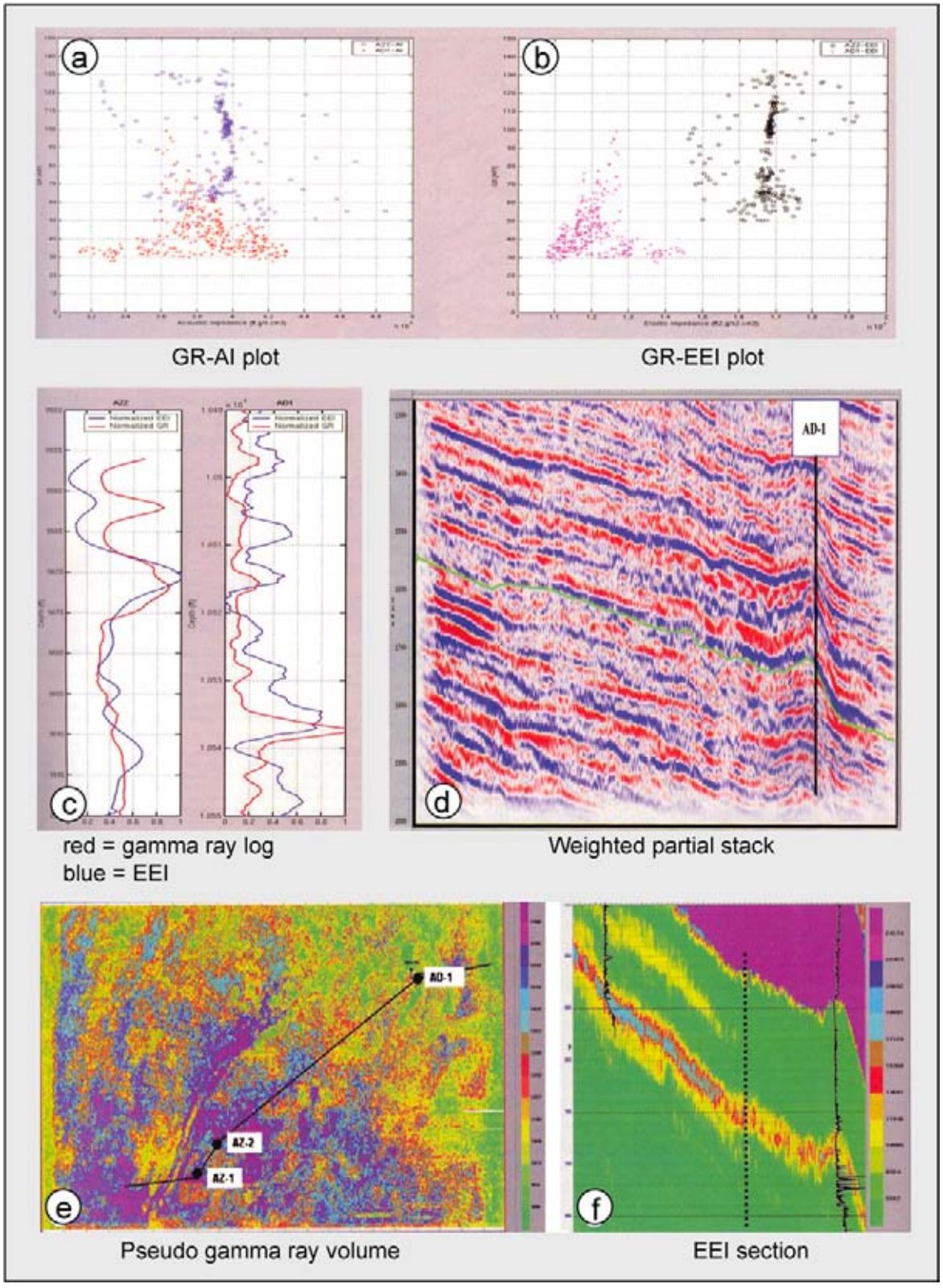

Figure 6.36: EEI attribute is giving a better correlation with the rock physical parameters like bulk modulus, shear modulus, V_p, V_s, rho and lambda. a) and b) The EEI gives a better discrimination between clean sandstone (crosses) and silty sandstones (circles). c) The correlation between gamma ray log and the EEI attribute. d) Weighted partial stacks facilitate the comparison of the EEI attribute and the reflectivity. e) Pseudo-gamma ray volume based on the correlation with the EEI attribute. f) EEI attribute section across well AD-1, with poorer quality reservoirs (modified after Neves et al. 2004).

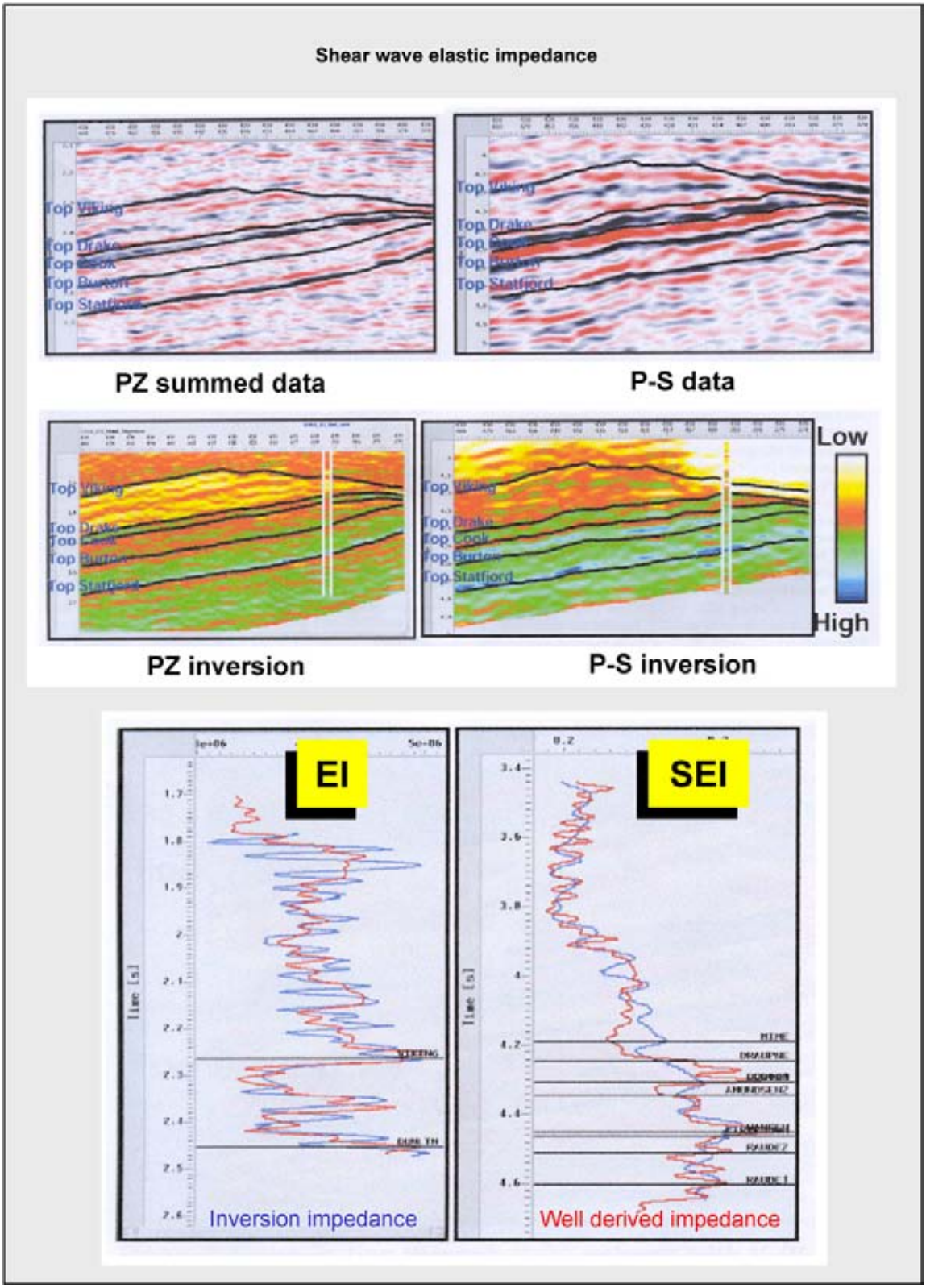

Figure 6.37: The Shear-wave Elastic Impedance (SEI) is used for the inversion of converted P–S seismic data. The SEI inversion for the Statfjord OBS dataset is here shown. The hydrophone P and vertical component Z are summed to reduce the water-layer reverberations and this gives a PZ volume. The blind test below illustrates that the SEI is better following the impedance computed from the well logs. The Statfjord field is subject of an extended production scheme to 2020, two decades longer than expected and a 70 percent recovery rate (modified after Duffaut et al. 2000).

of crystals in a cooling melt, as opposed to a genetic technique that considers the biologic evolution as a basis for the guided Monte Carlo approach (e.g. Mallick et al. 1995).

The Aki and Richards formula (1980) calculates the approximate P-wave reflectivity at the various offsets in the pre-stack domain.

$$R_{(\theta)} = 0.5\left(\frac{\Delta V_\mathrm{p}}{V_\mathrm{p}} + \frac{\Delta\rho}{\rho}\right) - 2\left(\frac{V_\mathrm{s}}{V_\mathrm{p}}\right)^2\left(2\frac{\Delta V_\mathrm{s}}{V_\mathrm{s}} + \frac{\Delta\rho}{\rho}\right)\sin^2\theta + 0.5\frac{\Delta V_\mathrm{p}}{V_\mathrm{p}}\tan^2\theta. \quad (6.26)$$

Whereby V_p is the average P-velocity between two uniform half spaces, V_s is the average S-velocity and ρ is the average density. It can be rewritten in terms of P-wave and S-wave impedances:

$$R_{(\theta)} = (1+\tan^2\theta)\frac{\Delta I_\mathrm{p}}{2I_\mathrm{p}} - 8\left(\frac{V_\mathrm{s}}{V_\mathrm{p}}\right)^2\sin^2\theta\left(\frac{\Delta I_\mathrm{s}}{2I_\mathrm{s}}\right) - \left(\tan^2\theta - 4\left(\frac{V_\mathrm{s}}{V_\mathrm{p}}\right)^2\sin^2\theta\right)\left(\frac{\Delta\rho}{2\rho}\right). \quad (6.27)$$

The assumption is now made that the relative changes in $(\Delta V_\mathrm{p}/V_\mathrm{p})$, $(\Delta V_\mathrm{s}/V_\mathrm{s})$ and $(\Delta\rho/\rho)$ are small and the incidence angle θ is much less than 90 degrees. This makes that second order terms can be ignored (Fatti et al. 1994):

$$R_{(\theta)} = (1+\tan^2\theta)\left(\frac{\Delta I_\mathrm{p}}{2I_\mathrm{p}}\right) - 8\left(\frac{V_\mathrm{s}}{V_\mathrm{p}}\right)^2\sin^2\theta\left(\frac{\Delta I_\mathrm{s}}{2I_\mathrm{s}}\right). \quad (6.28)$$

The background $V_\mathrm{s}/V_\mathrm{p}$ relationship should be known to solve this equation. If the V_p and V_s models are not good approximations of the earth model, than the linear inversion will give incorrect results. Ma (2002) proposes to substitute the average $V_\mathrm{s}/V_\mathrm{p}$ by the average $I_\mathrm{s}/I_\mathrm{p}$ values. This $I_\mathrm{s}/I_\mathrm{p}$ value is not coming from an a-priori model but is derived for each inversion iteration. Inversion is done under the following assumptions:

- The earth has approximately horizontal layers (often not the case!).
- Each layer is described by both acoustic and shear impedances.

The reflection coefficients for the nth layer in the starting model can be calculated:

$$\frac{\Delta I_\mathrm{p}}{2I_\mathrm{p}} = \frac{I_{\mathrm{p}_n} - I_{\mathrm{p}_{n-1}}}{I_{\mathrm{p}_n} + I_{\mathrm{p}_{n-1}}}, \quad (6.29)$$

$$\frac{\Delta I_\mathrm{s}}{2I_\mathrm{s}} = \frac{I_{\mathrm{s}_n} - I_{\mathrm{s}_{n-1}}}{I_{\mathrm{s}_n} + I_{\mathrm{s}_{n-1}}}, \quad (6.30)$$

$$\frac{I_\mathrm{s}}{I_\mathrm{p}} = \frac{I_{\mathrm{s}_n} + I_{\mathrm{s}_{n-1}}}{I_{\mathrm{p}_n} + I_{\mathrm{p}_{n-1}}}. \quad (6.31)$$

The latter is an average $I_\mathrm{s}/I_\mathrm{p}$ ratio. These functions are used to compute the reflectivity at all angles in the formula above. This is convolved with the wavelet to obtain a synthetic CDP gather that is compared with the original seismic (Figure 6.38) and the misfit is computed. The model is subsequently perturbed and a new comparison made. The convolution assumes a plane wave propagation across boundaries of horizontally homogeneous layers and does not take into account geometrical divergence, non-elastic absorption, wavelet dispersion, transmission losses, wave mode conversions and multiple reflections. These issues should be taken care off in the data pre-conditioning.

The inversion transforms the seismic cube into a reflectivity cubes. The advantage is that there are little constraints on the validity of computation due to the offset angles used. A simple initial V_p model is needed as input with only the low frequency variation. A density model is constructed applying Gardner's estimation (Gardner et al. 1975) or a simple $V_\mathrm{p}/V_\mathrm{s}$ model is used (again a constant value of 2). A further advantage is that the same time model is applicable for all offsets. The calculations are usually done for six discrete offset angles. But also three point calculations give a satisfactory result (Rauch-Davies and Portniaguine 2004). The following attributes are computed: V_p, V_s, rhomu, lambdarho and $V_\mathrm{p}/V_\mathrm{s}$. An example of a combined P and S-wave attribute display is shown in Figure 6.38b. The proposed new well discovered gas as predicted. Sometimes overlapping offset/angle ranges are used (Giroldi et al. 2005; Figure 6.39).

As shown earlier, the two term Aki and Richards formula (1980) is often written in a simplified form. It gives access to the R_p and R_s reflectivities for the zero offset in the following way (Figure 6.40):

$$R_\theta = A + B\sin^2\theta + C\sin^2\theta\tan^2\theta, \quad (6.32)$$

$$A = 0.5(\Delta V_\mathrm{p}/V_\mathrm{p} + \Delta\rho/\rho),$$
$$B = 0.5(\Delta V_\mathrm{p}/V_\mathrm{p}) - 4(V_\mathrm{s}/V_\mathrm{p})^2(\Delta V_\mathrm{s}/V_\mathrm{s}) - 2(V_\mathrm{s}/V_\mathrm{p})^2 \times (\Delta\rho/\rho),$$
$$C = 0.5(\Delta V_\mathrm{p}/V_\mathrm{p}),$$
$$\Delta V_\mathrm{p} = (V_{\mathrm{p}2} - V_{\mathrm{p}1}),$$
$$V_\mathrm{p} = (V_{\mathrm{p}1} + V_{\mathrm{p}2})/2.$$

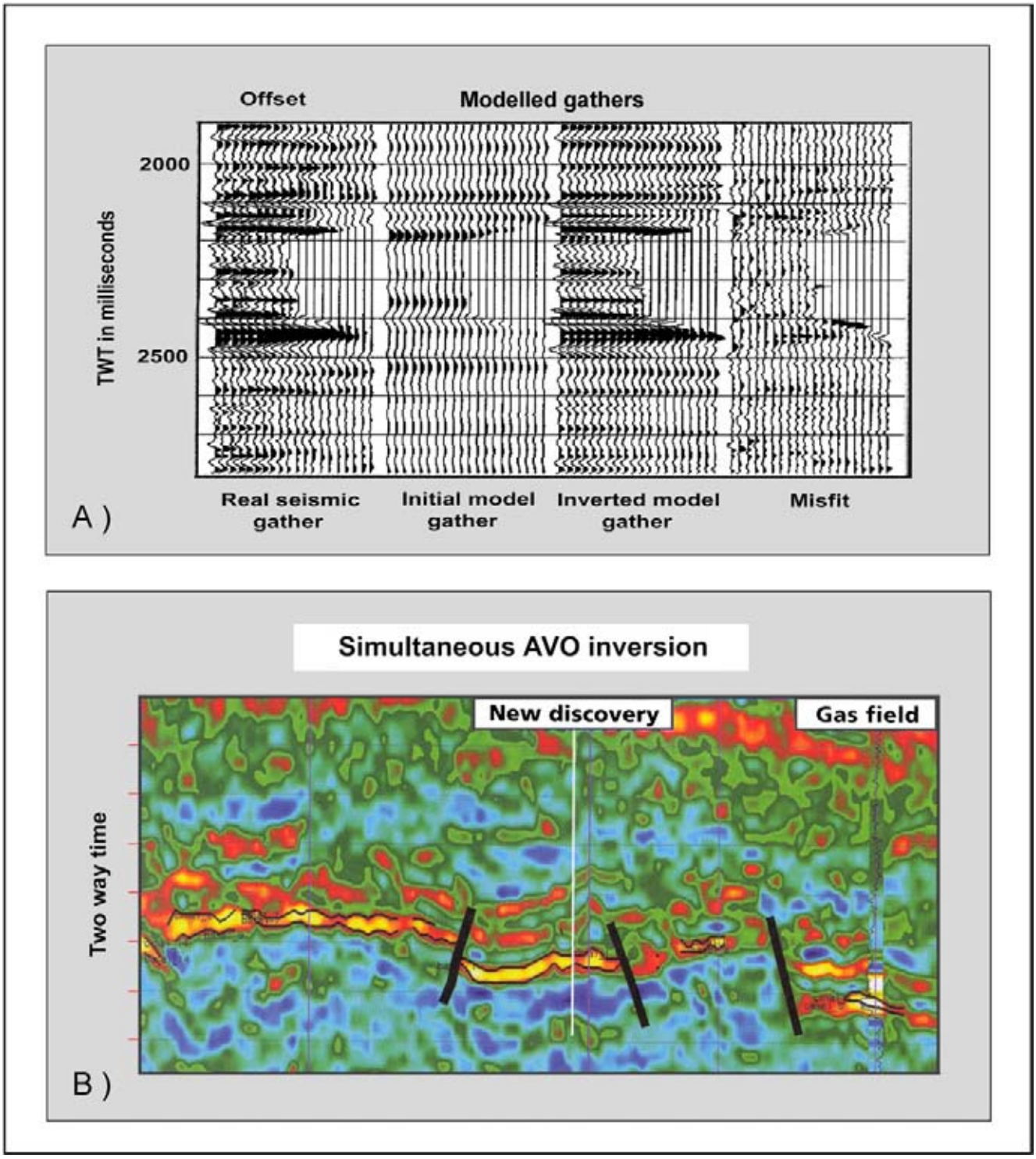

Figure 6.38: A) In the simultaneous inversion a synthetic CDP gather is computed from the initial P and S impedance input model. This gather is compared with the real seismic gather and the impedance models are perturbed. A new difference or misfit curve is computed. The impedance models are retained when reaching a small threshold value for this difference and the next gather is inverted. The output is stabilised by applying an averaging procedure, by putting constraints on the input model and by limiting the variability via parameter corridors (modified after Ma 2002). B) A cross-section view is a convenient way to display the results of a seismic inversion. Here the result of a simultaneous inversion is shown. The anomaly seen on the right has a well on it, while the other anomaly has been tested by a well only later on and proved the presence of good reservoir filled with hydrocarbons (courtesy Jason, website Oct. 2003).

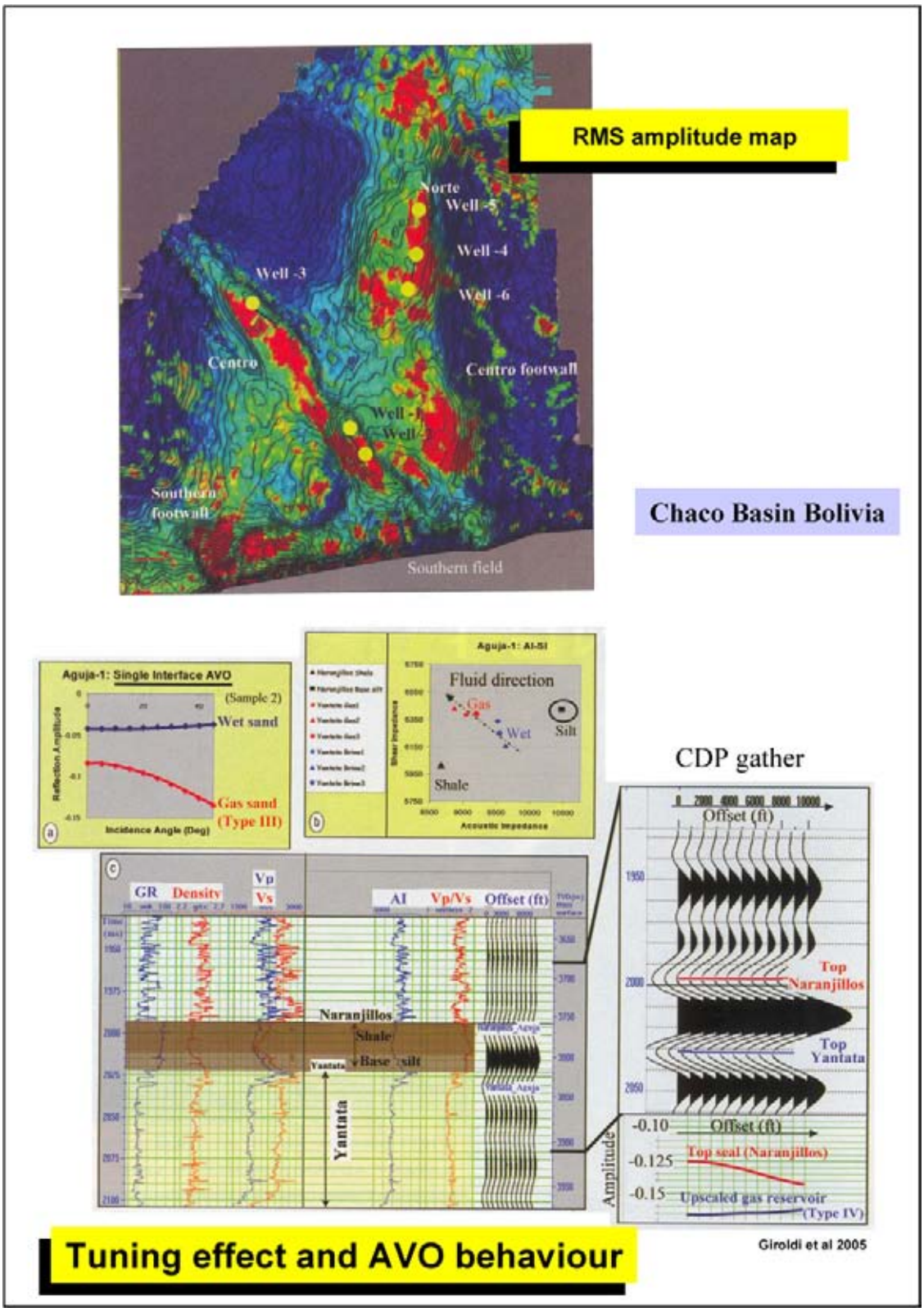

Figure 6.39: Fluid effects are seen in the seismic response of the Cretaceous sand reservoirs in the Chaco Basin, onshore Bolivia. The RMS amplitude, in a 40 msec window below top Yantata, is basically conform the structuration. Individual sands are having a Class 3 behaviour, but when interfaces are closely spaced together, the tuning effect results in an apparant Class 4 response (modified after Giroldi et al. 2005).

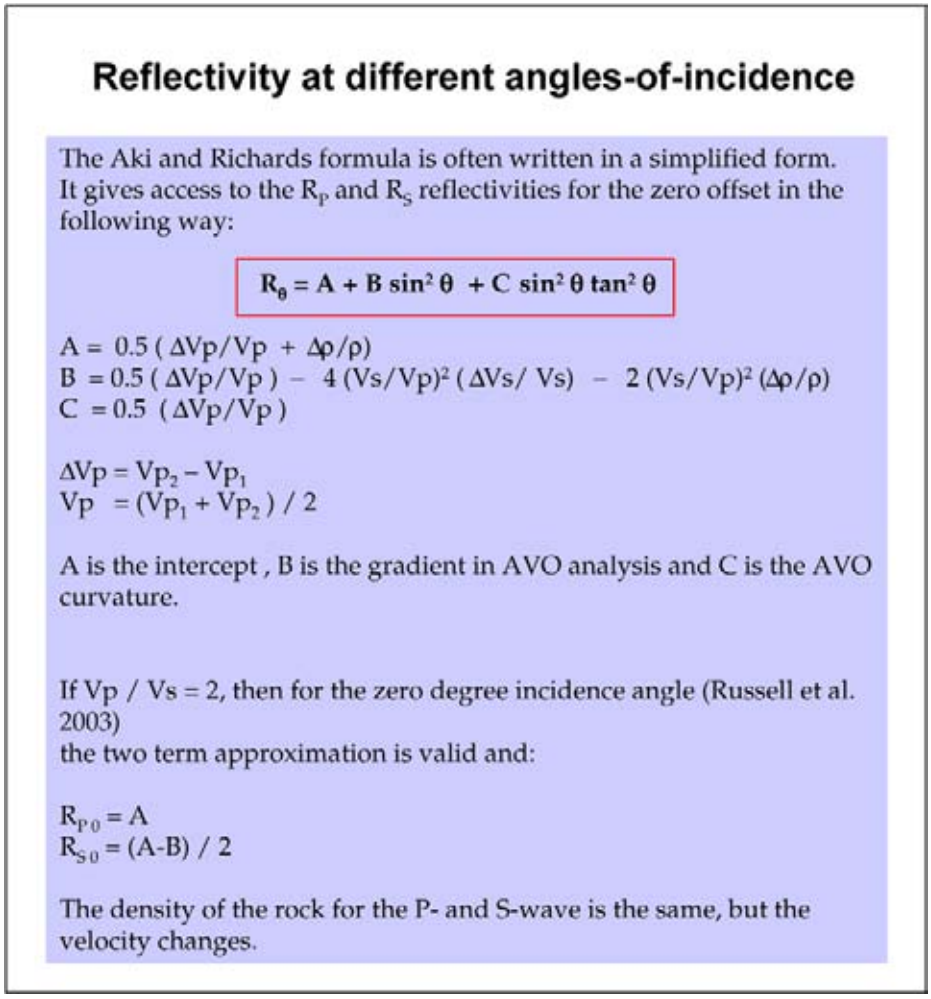

Figure 6.40: The Aki and Richards approximation of the Zoeppritz equations calculates the reflectivity at different offset angles (modified after Ma 2002).

A is the intercept, B is the gradient in AVO analysis and C is the AVO curvature. If $V_\mathrm{p}/V_\mathrm{s} = 2$, then for the zero degree incidence angle the two term approximation is valid and (Yilmaz 2001, Russell et al. 2003):

$$\text{P-wave} \qquad R_0 = A, \tag{6.33}$$

$$\text{S-wave} \qquad R_0 = \frac{A - B}{2}. \tag{6.34}$$

The density of the rock for the P- and S-wave is the same, but the velocity contrasts for the interface change. The P-impedance of the layer is not the same as the S-impedance value.

The simultaneous AVO inversion uses a model driven approach. Independent wavelet estimations are performed for each partial stack. According to Hansen et al. (2004) the simultaneous AVO inversion results are derived through a global optimisation technique, whereby all partial stacks and all samples within each partial stack are used simultaneously through the inversion scheme. Inversion is done directly for the desired rock properties: acoustic impedance, shear impedance/Poisson's ratio/$(V_\mathrm{p}/V_\mathrm{s})$ and density. The angle for each sample and for each partial stack is updated through the seismic inversion using the high frequency velocity model extracted continuously from the intermediate inversion results. Advanced time-varying statistical alignment of the partial stacks is done to optimise their comparison.

For time-lapse seismic data this processing sequence is applied simultaneously for all vintages and all partial stacks (Figure 6.41). Because the wavelet estimations for the different seismic volumes are independent, any variation in amplitude and phase for the various seismic volumes is captured by the computed wavelets. The low frequency models are derived directly for these properties. Recent advances in simultaneous AVO inversion

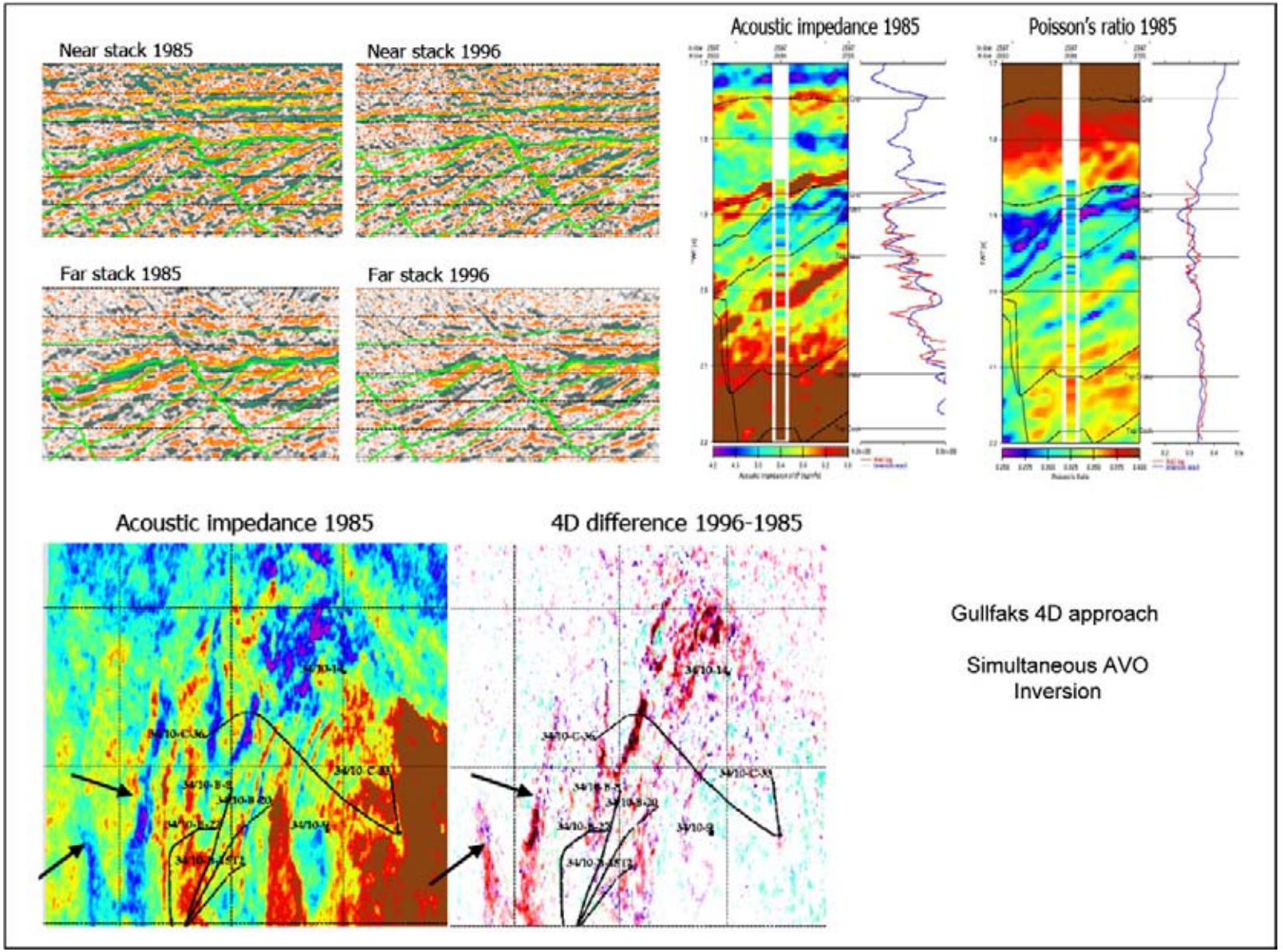

Figure 6.41: The simultaneous AVO inversion, taking care of P and S impedance models at the same time, applied on datasets over the Gullfaks field with Middle to Early Jurassic reservoirs (Block 34/10, offshore Norway). A 4D approach was chosen here, with the baseline seismic shot in 1985. In 1986 the HC production started and 90% of the recoverable oil has been produced so far. More than 100 wells have been drilled on the field. The 4D simultaneous AVO inversion can be used to quantify saturation and pressure effects due to production (modified after Hansen et al. 2004).

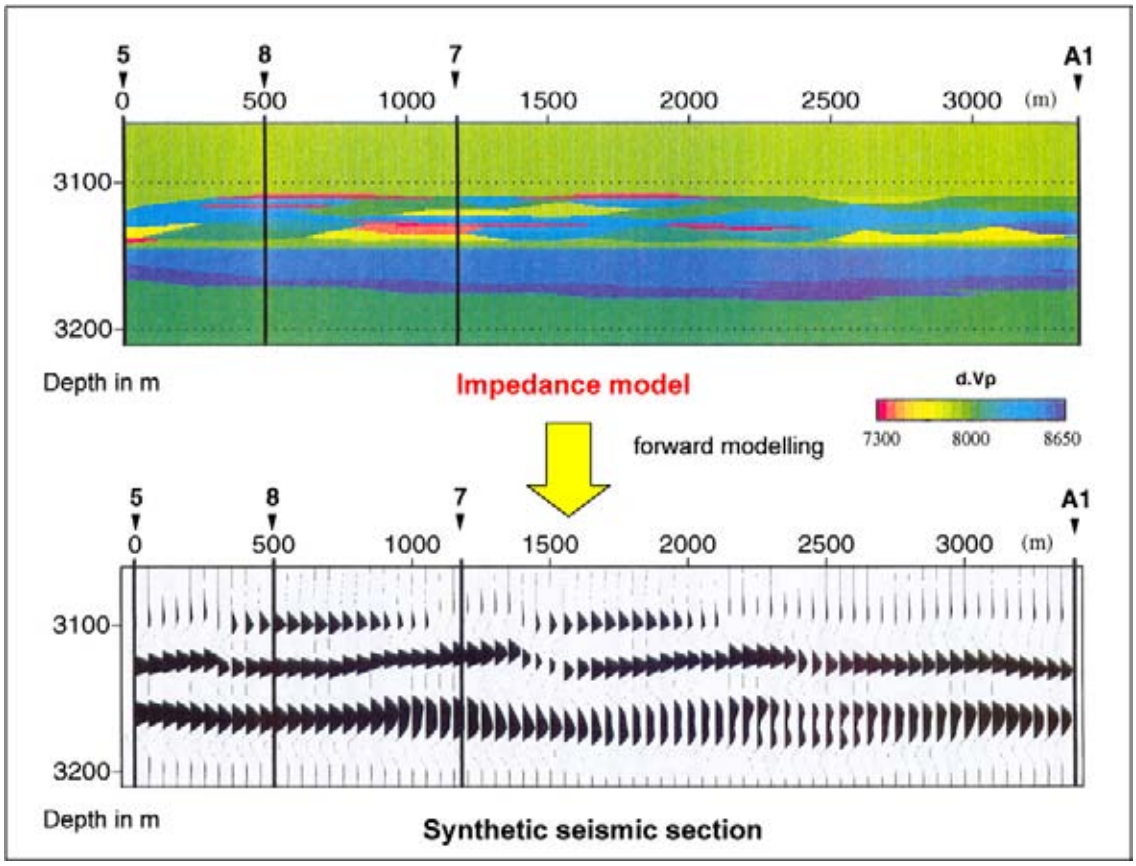

Figure 6.42: The forward modelling technique uses an earth model in depth to compute a synthetic seismic response. This can be compared to the real seismic data after time conversion. The modelling brings out the effect of subtle changes in the earth model (modified after Schulbaum 1996).

have made it possible to extract rock properties (porosity, S_w and lithology) from the seismic data at an accuracy and resolution better than what can be seen just by investigating the seismic data. This applies for both acoustic impedance and Poisson's ratio, even though the Poisson's ratio is mainly related to the far stack, which contains lower frequencies than the near stack. Even in chalk deposits there may exist a relation between the AVO response from oil, the porosity and pore fluid (Japsen et al. 2004).

6.3.2.3 Pre-stack waveform inversion

This technique is based on a wave equation forward modelling algorithm (Figure 6.42). Numerous earth models are fitted to the prestack response of the individual traces. The wave equation is run with converted wave energy, interbed multiples, transmission losses and P-wave reflections (Benabentos et al. 2002, Mallick et al. 2000) and takes into account the full waveform. It is a computing intensive method; therefore it is often combined with other non-linear estimation and correlation schemes. For instance a genetic solving algorithm can be implemented (Chakraborty et al. 2004). Neural network training is an alternative tool to convert seismic data into pseudo well log traces (e.g. Banchs and Michelena 2002). Confidence interval calculation is done as a more statistical approach.

6.3.3 Other techniques

A hybrid inversion can be performed. This technique uses prestack full waveform inversion, geologic interpretation and post stack inversion of AVO attributes (Roden 2004). The P-impedance, Poisson's ratio and density are the most important attributes for interpretation purposes, from which other vital information can be derived like water saturation and net-to-gross (Roberts et al. 2005). A three point approach to the inversion scheme has been proven very adequate (Rauch-Davies and Portniaguine 2004).

A linearised Bayesian approach can be adopted (Buland and Omre 2003) in an AVO inversion. The **Bayes theorem** exploits the conditional probability principle (Figure 6.43). The posterior solution is given by a Gaussian

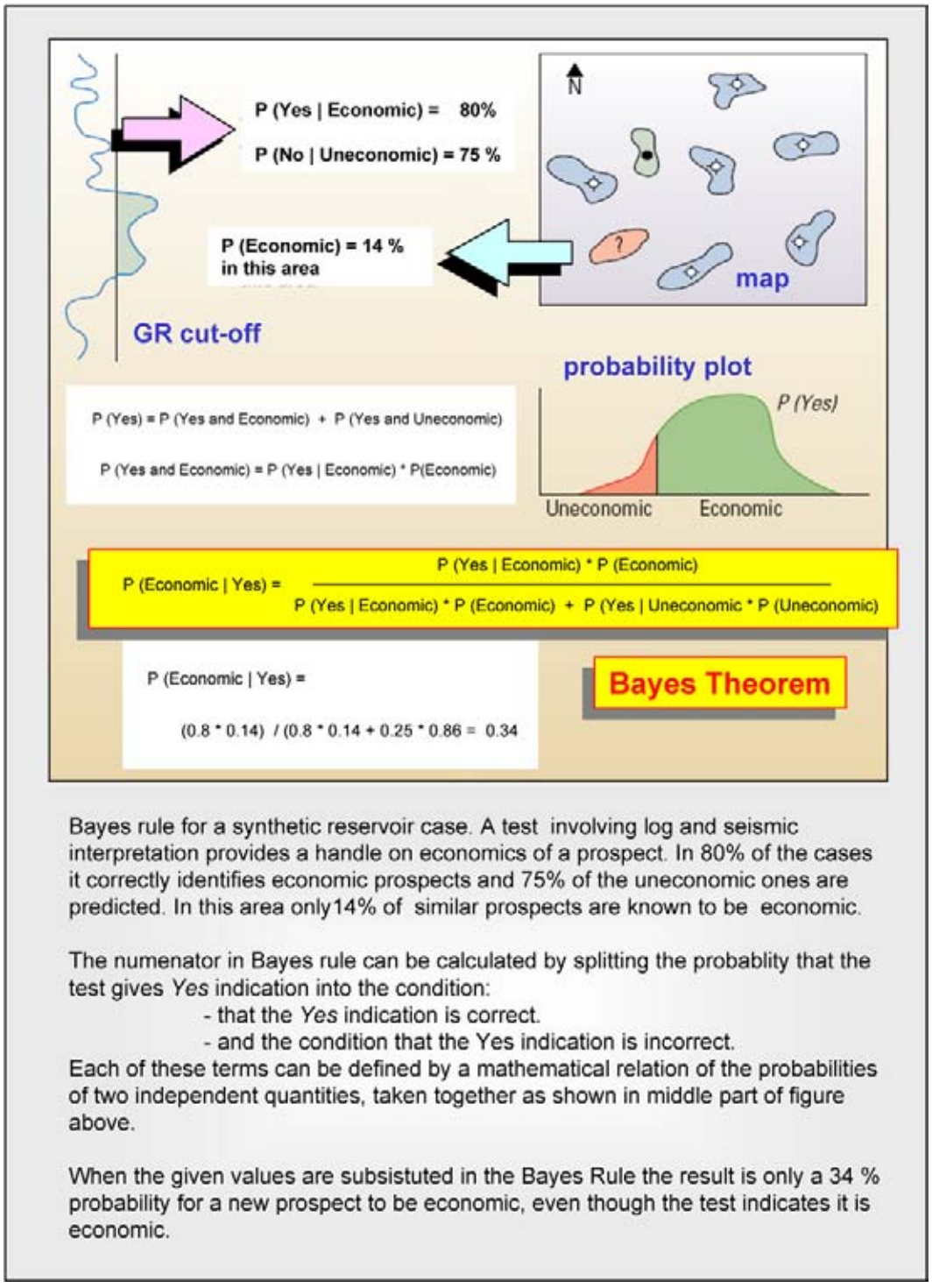

Bayes rule for a synthetic reservoir case. A test involving log and seismic interpretation provides a handle on economics of a prospect. In 80% of the cases it correctly identifies economic prospects and 75% of the uneconomic ones are predicted. In this area only14% of similar prospects are known to be economic.

The numenator in Bayes rule can be calculated by splitting the probablity that the test gives *Yes* indication into the condition:

- that the *Yes* indication is correct.
- and the condition that the Yes indication is incorrect.

Each of these terms can be defined by a mathematical relation of the probabilities of two independent quantities, taken together as shown in middle part of figure above.

When the given values are subsistuted in the Bayes Rule the result is only a 34 % probability for a new prospect to be economic, even though the test indicates it is economic.

Figure 6.43: The principle behind the Bayes rule for conditional probabilities is here explained on a simple prospect evaluation example (modified after Bryant et al. 2002; used with permission of copyright holder Schlumberger).

probability density function, but the calculations are not based on a Monte Carlo simulation. The linearisation is made possible by assuming weak contrasts for the Zoeppritz equations. Bachrach et al. (2004) summarise the principle in the following equation:

$$P(\text{lithology}_n \mid \text{ATR}) = P(\text{lithology}_n)\left[\frac{P(\text{ATR} \mid \text{lithology}_n)}{P(\text{ATR})}\right]$$

ATR = Combination of seismic inversion attributes.

$P(\text{lithology}_n \mid \text{ATR})$ = Posterior probability density function (PDF).

$P(\text{ATR} \mid \text{lithology}_n)$ = The conditional probability of having a set of seismic inversion attributes ATR given a certain lithology and $P(\text{ATR}) = \Sigma P(\text{lithology}) P(ATR \mid \text{lithology})$.

Bayes rule provides a means to combine the probabilistic a-priori knowledge with information contained in the observed data to update the prior model. Noise in the data has a tremendous effect on the uncertainties in the inversion solution (Buland and Omre 2003).

The **cascaded two-step elastic inversion** performs an elastic inversion of the seismic data to obtain P- and S-impedance models (Saltzer et al. 2005). And these impedances are in the second step inverted into lithology (or Volume of Shale) and a porosity component. Information on the expected fill, faults and stratigraphic horizons are taken into account during the modelling. The specific rock physical model is used to transform the impedances into V Shale and porosity estimates. The effect of sand (large aspect ratio) and clay pores (smaller aspect ratio) on the rock elastic moduli are computed based on differential effective media theory. The sand is dry and the clay pores are brine filled. Gassmann fluid substitution serves to calculate the bulk modulus of the saturated sand. Explicit non-linear relationships between clay content, porosity and water saturation are exploited. A Bayesian approach is applied to the constraints, with estimates of the data noise and a-priori model parameters to deduce the most likely model. By incorporating the model and data covariances, it is possible to estimate the combined uncertainty of the data error and a-priori model uncertainty in the inversion solution. Thus it calculates a posterior covariance (Saltzer et al. 2005).

Alternatively a stochastic approach can be chosen. It allows an increase in the resolution compared to the conventional elastic inversion methods (Contreras and Torres-Verdin 2005). On the Marco Polo testcase (Gulf of Mexico) they have found an increase in vertical resolution from 20 to 5 metres. The input consists of:

- Four partial angle stacks with the corresponding wavelets.
- Well logs for V_p, V_s, density, lithotype.
- Geostatistical property variograms and histograms.

The geobodies could be modelled with an increased amount of detail. 3D spatial distribution of porosity, permeability and water saturation are generated via a co-simulation with the AVA derived inversion results (V_p, V_s?, density). It allows to construct with the aid of multi variate statistics, a high resolution 3D distribution of the petrophysical properties.

6.3.4 A word of caution

The first four post-stack methods are also known as **acoustic impedance inversions**. The model-driven inversion is the best suited for poor data quality surveys with limited well control (no sonic, no density, no checkshots?). Elastic inversion is rather labour intensive and should only be undertaken when a feasibility study has demonstrated its benefits. A shear sonic is needed or has to be estimated, but even that is not always necessary according to Cambois (2002). Taking out the anisotropy effect in the dataset before doing the analysis will improve the end result (e.g. Jenner 2002).

As a word of warning: '*The seismic inversion is not a unique process*'; i.e. there maybe several AI models that generate, when convolved with the wavelet, similar synthetic traces. The number of possible solutions is drastically reduced by putting constraints on the modelling and thus a most plausible scenario is retained (Veeken et al. 2002a, Veeken and Da Silva 2004). The confidence is also increased by conducting other reservoir characterisation studies like AVO (Figure 6.44). The usefulness of inversion studies is demonstrated by the optimisation in reservoir prediction studies. The Marmul field project in the southern Oman salt basin has benefited tremendously from the seismic inversion study. It made it possible to distinguish between tillite and the peri-glacial reservoirs and a tailor-made HC evacuation scheme could be devised (De La Grandville 1982). The discovery was considered uncommercial until then (2 billion barrels of STOIP). But even fields on a depth of 4800 metres can be good candidates for such studies as is shown in the Smorbukk Field example (Klefstad et al. 2005).

Seismic inversion depends heavily on the proper integration of the well data. Incorporation of anisotropy effects in the inversion scheme will improve the quality of the output data (Rowbotham et al. 2003). This is especially important when dealing with deviated holes that are difficult to match. Seismic inversion is gradually established as a routine processing step in both field development as well as for exploration studies. The AI attribute is replacing the normal amplitude seismic representation and its analysis is becoming integral part of the reservoir characterisation workflow (cf Latimer et al. 2000, Van Riel 2000). The past track record demonstrates the added value of these type of reservoir studies.

6.4 Reservoir Modelling and Fluid Substitution

In the case when there are possible DHI's present on the seismic data, a forward modelling exercise should

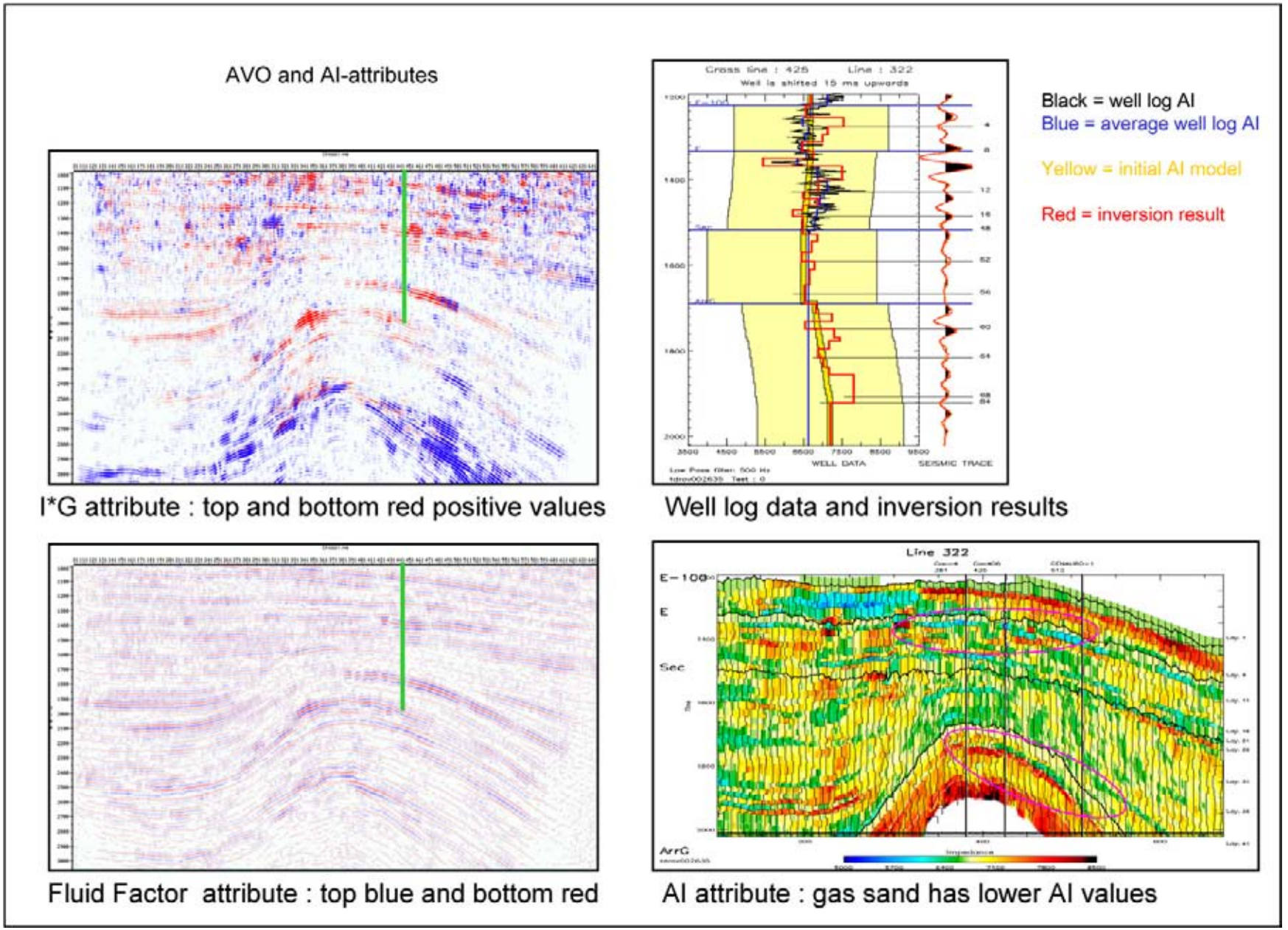

Figure 6.44: AVO and AI inversion are complementary processing methods. Correspondence in the outline of their anomalies increases the confidence for both methods in being able to delineate genuine traps/prospects and 'sweet' spots (data courtesy Pemex).

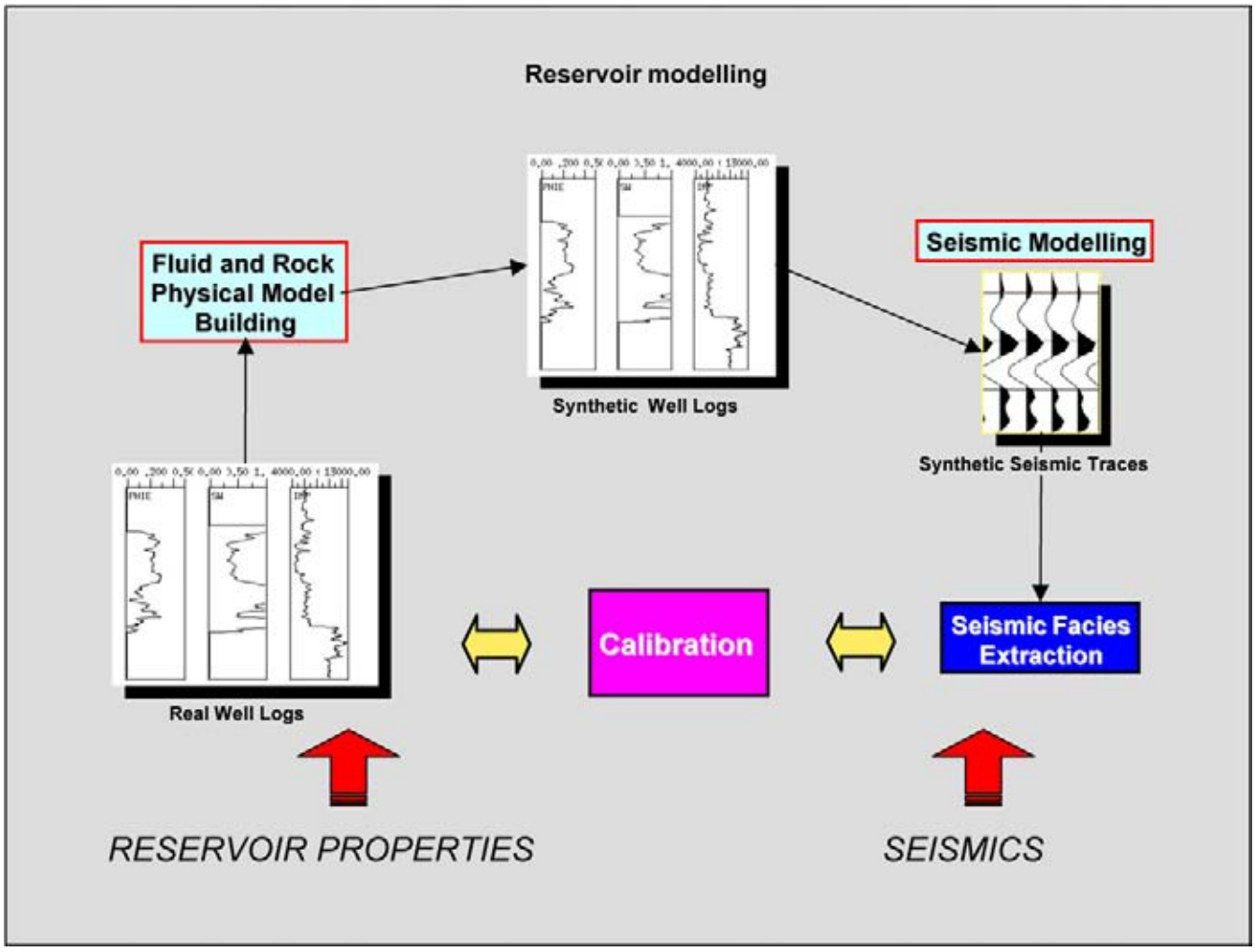

Figure 6.45: Reservoir modelling gives a possibility to compare the well data and the expected seismic response. Changing the reservoir model results in a suite of output, whereby the sensitivity to certain reservoir characteristics is highlighted. It is a convenient way to get familiar with certain aspects of a seismic dataset.

be seriously considered (Figure 6.45). But even in other situations, the modelling helps to get a better understanding of the dataset (e.g. Guilbot et al. 1996, Balz et al. 1999, Veeken and Da Silva 2004, Hart and Chen 2004, Veeken, in press). Certain assumptions are made about reservoir parameters like:

- Porosity.
- Permeability.
- Pore contents.
- Geometry.

The initial reservoir-hostrock model is generally based on well log response (e.g. V_p, V_s, and bulk density RHOB). The model is convolved with a seismic wavelet and a synthetic seismic section is generated. This synthetic section is compared with the original seismic line and similarities and/or discrepancies detected. If there is well control available, then it is possible to estimate the wavelet more correctly and compute a better synthetic and modelled trace. Fluid substitution is done to get a feel of the sensitivity of the seismic response for the presence of gas or brine in the pores of the reservoir rocks (Figures 6.46 and 6.47). The Gassmann method is often chosen but it will give erroneous results when wrong cut-off values for the logs are used (Skelt 2004). The basic difference in response between a brine, gas and oil filled reservoir is shown in Figure 6.48.

For computing petro-acoustic fluid substitution models it is necessary to make reliable estimates for the V_s, V_p and density ρ. The V_p/V_s ratio contains information of the lithology of the rocks (cf Tatham 1982). It also tells something about the fluid contents. It is related to the porosity of the rocks. V_p and V_s decrease with increasing porosity, whereby V_p decreases twice as fast as the V_s

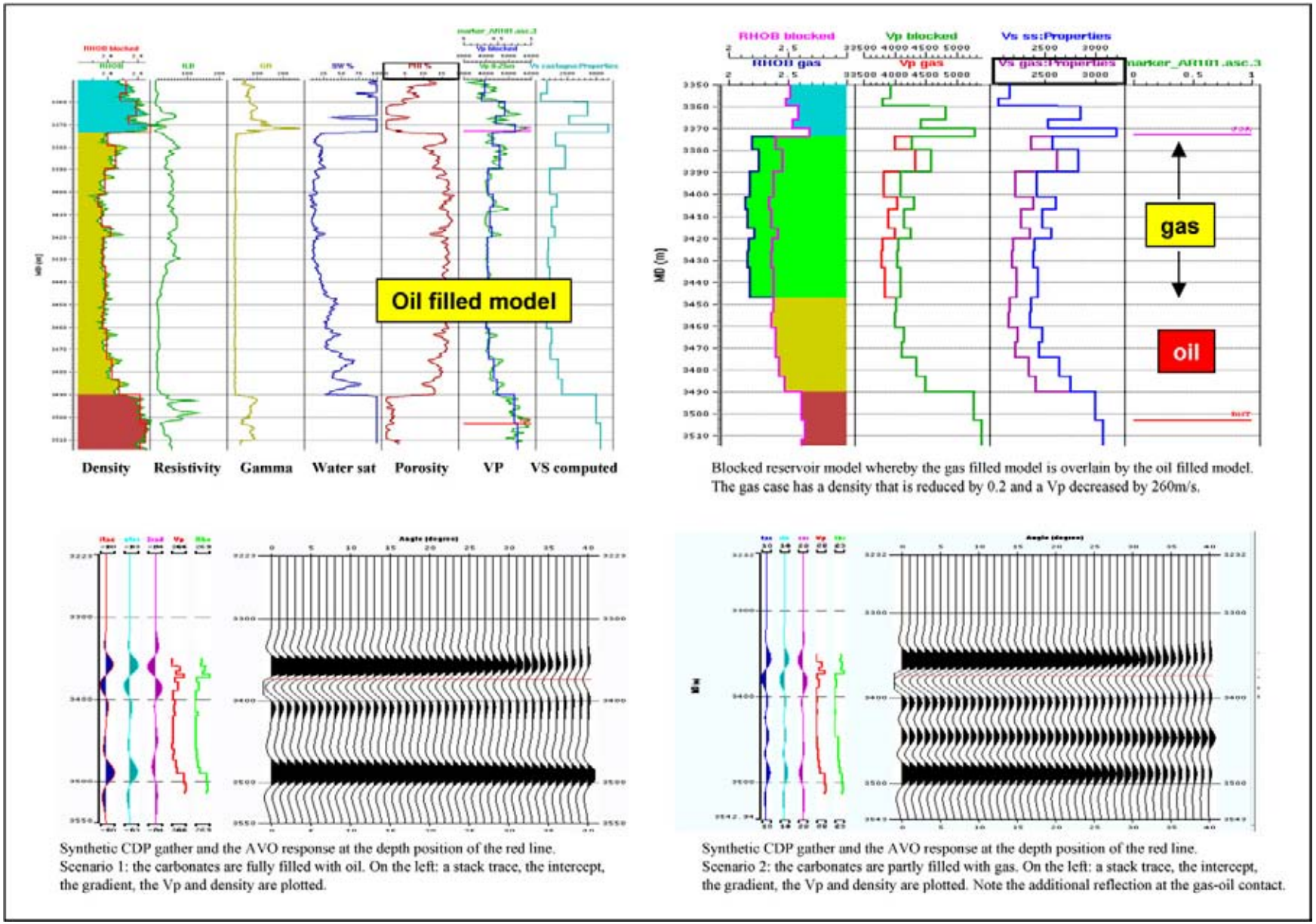

Figure 6.46: Modelling of synthetic response of amplitudes by changing the thickness and fluid contents in a reservoir (fluid substitution). The water case has a smaller R_0 value (amplitude at zero offset). Keep in mind that the R_0 is different from the R_{stack}, especially when AVO effects are present.

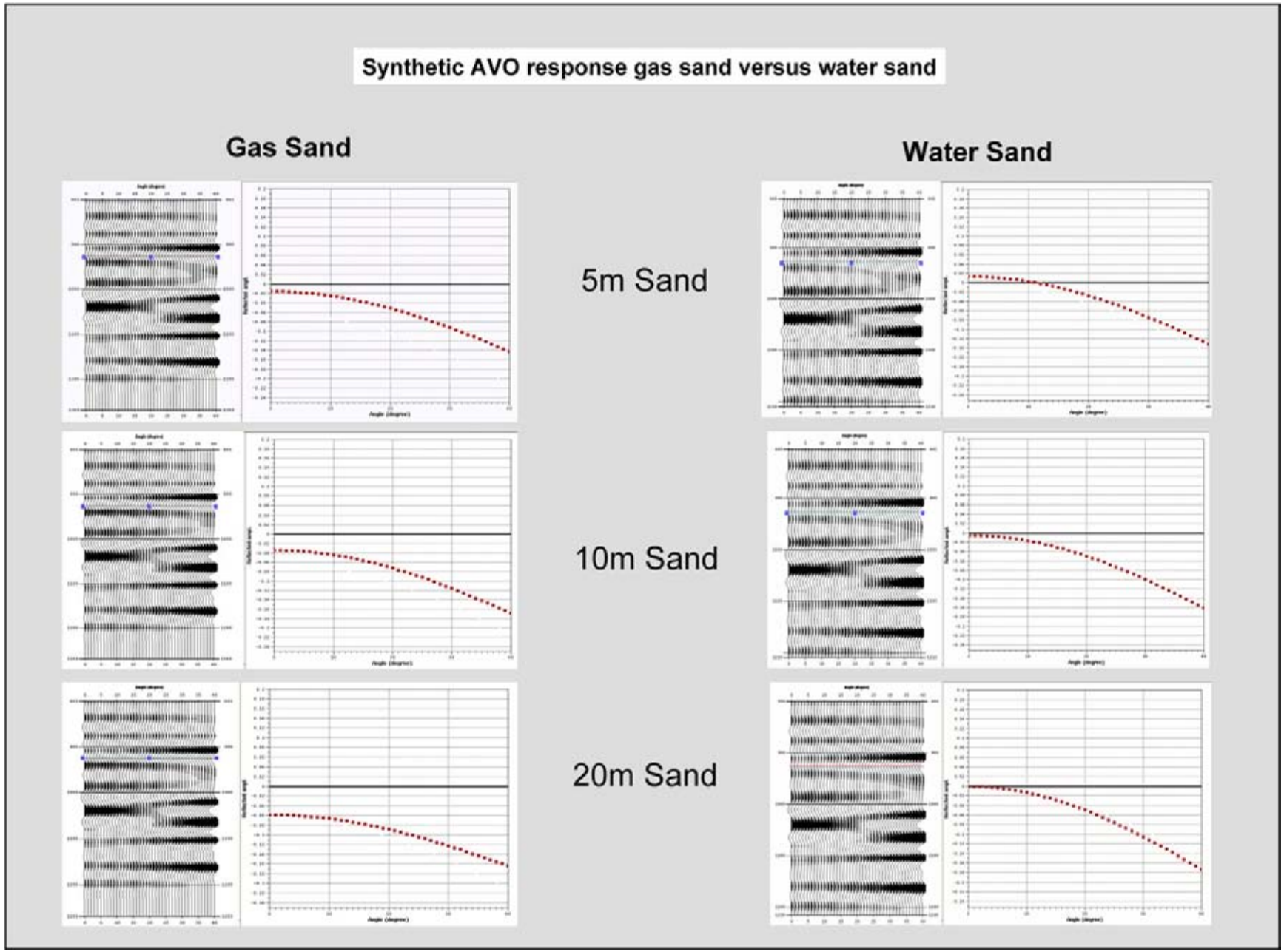

Figure 6.47: Fluid substitution modelling, whereby the oil is partly replaced by gas and the synthetic AVO response is computed. Note that there is an additional reflection for the oil–gas contact. Based on this observation, it is suggested to examine the real seismic data on the presence of a flat spot.

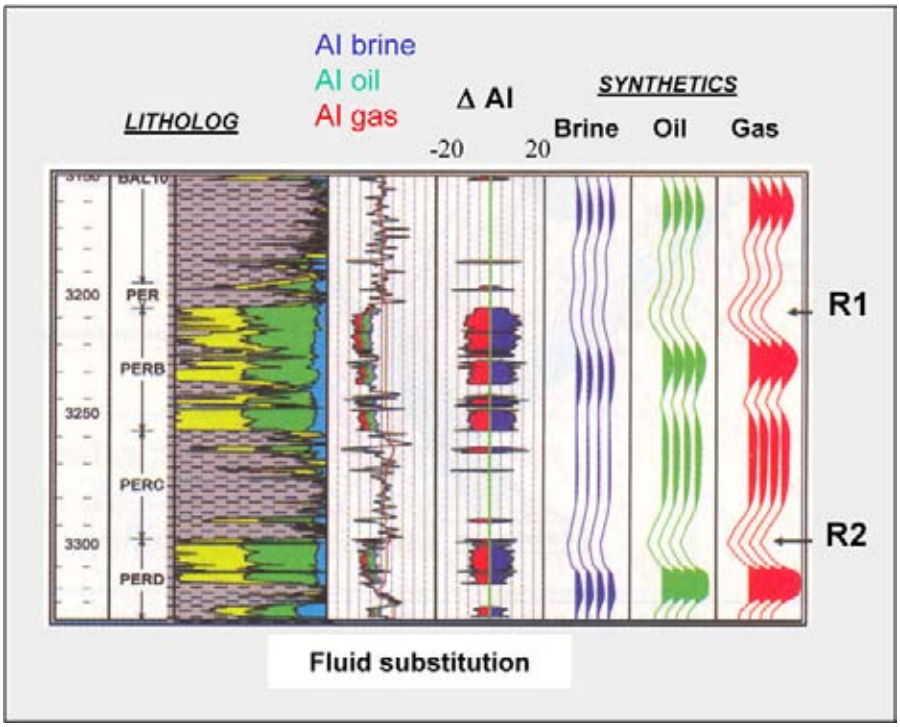

Figure 6.48: Fluid replacement effect on the seismic response is illustrated on a Pliocene lacustrine reservoir from the Chirag field in the south Caspian Sea. The synthetics have been generated by applying Gassmann fluid substitution. Note how not only the top of the reservoir reflection is changing but also the reflection just below. Analysis using window measurements can reinforce therefore the difference (modified after Robinson et al. 2005).

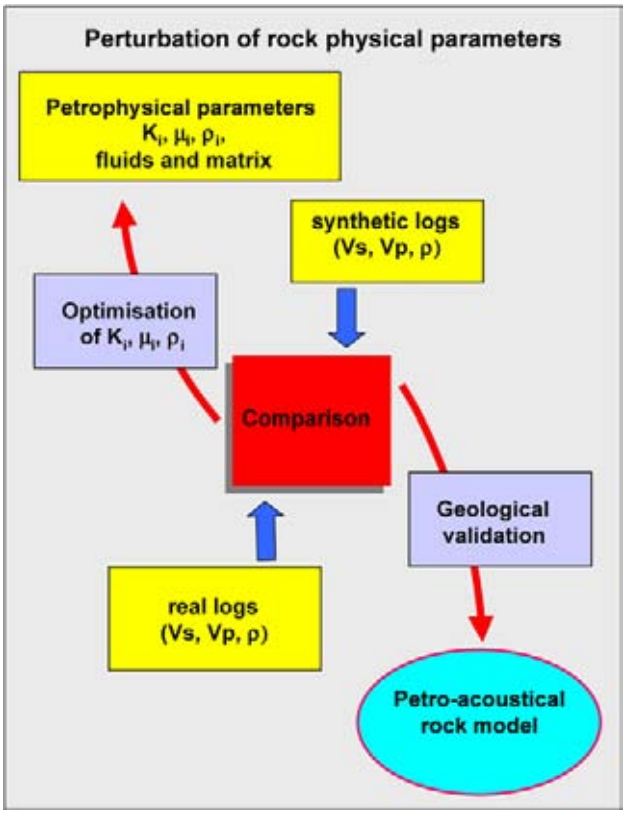

Figure 6.49: Perturbation of petrophysical parameters to build reservoir scenarios. These models can be modelled later on.

(Assefa et al. 2003). It can also tell something about the permeability of the rocks. Tsuneyama et al. (2003) have demonstrated a relationship with the permeability and also the rock frame of carbonate rocks.

Some of the basic rock physical aspects that are important for seismic interpretation are described by Gregory (1977), as well as by Batzle and Wang (1992). Physical properties are needed for the description of:

- The reservoir sequence.
- The top and base seal.
- Fluid characteristics of the rocks.

Perturbations of the petrophysical properties can be performed with small incremental steps (e.g. Geolog6^{TM} Loglan utility; Figure 6.49). The reservoir scenario data is then exported to seismic modelling packages, like Osiris^{TM} or Easy Trace^{TM}, to generate a synthetic seismic response. An interval of interest is selected on the log data in the well and this data will serve as starting point for the perturbations.

6.4.1 Estimation of rock physical parameters

Several methods exist for estimating the petrophysical characteristics of the rocks (cf Schoen 2004). Unfortunately it is necessary to quote here some more formulas.

The **fluid density** is computed from the well logs:

$$\rho_{\text{fluid}} = \rho_{\text{water}} S_{\text{water}} + \rho_{\text{oil}} S_{\text{oil}} + \rho_{\text{gas}} S_{\text{gas}}, \tag{6.35}$$

$$S_{\text{water}} + S_{\text{oil}} + S_{\text{gas}} = 1. \tag{6.36}$$

S stands for saturation.

The **bulk density** (RHOB) of the reservoir rock is given by:

$$\text{RHOB} = \rho_{\text{fluid}}\phi + \rho_{\text{matrix}}(1-\phi). \tag{6.37}$$

ϕ is the porosity and ρ_{matrix} is the density of the rock forming constituents. The density of the fluids (ρ_{fluid}) may vary a lot from 0.2 to 1.1 g/cm^3. The actual rock density is much more stable, and ranges mostly between 2.4–2.7 g/cm^3 for clastic reservoirs. The change from gas to brine in silici-clastic reservoirs with a 30 percent porosity will result in an increase in density by 0.27 g/cm^3. When changing from oil to brine a difference of 0.1 g/cm^3 is expected (Helle and Bhatt 2002).

The sonic transit time for a pore fill mixture is given by:

$$\Delta T_{\text{fluid}} = \Delta T_{\text{water}} S_{\text{water}} + \Delta T_{\text{oil}} S_{\text{oil}} + \Delta T_{\text{gas}} S_{\text{gas}}. \tag{6.38}$$

Replacing the $\Delta T_{\text{water}} = 189$, $\Delta T_{\text{oil}} = 238$ and $\Delta T_{\text{gas}} = 625$ microseconds per feet will give the following travel time for the bulk rock volume:

$$\Delta T_{\text{bulk}} = \Delta T_{\text{fluid}}\phi + \Delta T_{\text{matrix}}(1-\phi). \tag{6.39}$$

ΔT_{matrix} is the transit time for the rock material and it varies between 56–75 μs/ft (Brigaud et al. 1992). When using again the 30% porosity, the change from gas into brine will lead to a 130 μs/ft difference in transit time. And it is only 15 μs/ft for heavy oil being replaced by brine.

Brine and hydrocarbons have a considerable difference in resistivity, with the brine being the better conductor (1 Ω m for brine and 100 Ω m for oil). The resistivity of a clean sandstone is directly related to the porefill and water saturation. Archie (1942) gives the following equation:

$$R_{\text{t}} = \frac{F R_{\text{w}}}{{S_{\text{w}}}^n} \quad \text{or} \quad S_{\text{w}} = \frac{1}{\phi}\sqrt{\frac{R_{\text{w}}}{R_{\text{t}}}}. \tag{6.40}$$

F is the **Formation Factor**:

$$F = \frac{a}{\phi^m}. \tag{6.41}$$

The a is a constant between 0.6–1.5. In the North Sea case described by Helle and Bhatt (2002) it is taken as 0.6. The **cementation exponent** m (between 1.3 and 3) and **saturation exponent** n are other regional dependent constants, that are close to two. Archie's Law assumes that $m = 2$ and $a = 1$. This empirical relation is valid for non-shale deposits. A more general formula can be adopted that takes into account: cementation, tortuosity, granular shape and size:

$$R_{\text{t}} = \frac{a R_{\text{w}}}{\phi^m {S_{\text{w}}}^n}. \tag{6.42}$$

Other formulas have been proposed for sandstones with a clay fraction. The one below is given by Schlumberger (1989):

$$\frac{1}{R_{\text{t}}} = a {S_{\text{w}}}^2 + \gamma S_{\text{w}}, \tag{6.43}$$

whereby a is the **sand term** that depends on the amount of sand particles, its porosity, resistivity of its pore contents. The γ is here the shale term that is related to the amount of clay and its resistivity. A distinction can be made between **Free water** (wf) and **bounded mineral water** (wb) that is attached to the clay mineral particle surface (CEC cat ion exchange index). A dual water approximation can be written as follows:

$$R_{\text{t}} = \left(a/\phi_{\text{t}}^m S_{\text{wt}}^n\right) \frac{R_{\text{wb}} R_{\text{wf}} S_{\text{wt}}}{S_{\text{wt}} R_{\text{wb}} + S_{\text{wb}}(R_{\text{wt}} - R_{\text{wb}})}. \tag{6.44}$$

ϕ_{t} is the total porosity. R_{wf} is taken from clean non-shale water-bearing interval on the log (= reservoir).

The R_{wb} is taken from the pure shale interval. The S_{wb} is related to the shale volume and read directly from the matrix reading logs.

Poupon et al. (1971) propose the following formula to calculate the **effective water saturation** in shaley sediments:

$$\frac{1}{\sqrt{R_t}} = \left(\frac{V_{shale}(1 - V_{shale}/2)}{\sqrt{R_{shale}}} + \frac{\sqrt{\phi_e^m}}{\sqrt{aR_w}} \right) \sqrt{S_{we}{}^n}. \tag{6.45}$$

V_{shale} stands for the volume of shale in the sediments. The shale has three basic forms: layered, nodular and dispersed. All three forms can occur at the same time in one and the same geologic formation. The V_{shale} is normally determined by a cut-off value on the gamma ray or from the density and neutron logs. ϕ_e is the **effective porosity** in the reservoir, excluding the **shale porosity**. It is calculated from the density log, grain density measurements of the matrix and the fluid density. R_{shale} is the resistivity in the shale and R_{we} is the **effective resistivity** in the brine filled reservoir.

6.4.2 Estimation of elastic parameters

A quick refresher of some rock physical parameters that are important in the seismic and rock modelling (Figure 6.50):

Young's modulus:	$E =$ strain/stress (Hooke's law),
Lame's constants:	$\mu =$ stress/strain (rigidity modulus, under simple shear),
	$\lambda = k - 2\mu/3$ (fluid incompressibility),
Bulk modulus:	$k =$ stress/strain (under hydrostatic pressure, 3D),
Poisson's ratio:	$\sigma =$ transverse strain/longitudinal strain (under uni-axial stress).

The Poisson' s ratio σ depends on the V_p and V_s.

$$V_p = \sqrt{\frac{k + 4\mu/3}{\rho}}, \tag{6.46}$$

$$V_s = \sqrt{\frac{\mu}{\rho}}, \tag{6.47}$$

$$\sigma = \frac{0.5 - (V_s/V_p)^2}{1 - (V_s/V_p)^2}, \tag{6.48}$$

$$V_p/V_s = \sqrt{\frac{1 - \sigma}{0.5 - \sigma}}. \tag{6.49}$$

These formulas are correct for non-permeable media, when no transfer of fluids occurs in the pores.

Raymer et al. (1980) describe an empirical relation between the V_p and the porosity of the rock:

$$V_p = (1 - \phi)^2 V_{ma} + \phi V_{fl}. \tag{6.50}$$

This model has been confirmed by numerous studies and therefore the formula has a predictive value (Latimer 2004). The P-wave velocity depends on the speed in the mineral matrix, the fluid phase and the total fractional porosity.

Several petrophysical estimations can be done on the elastic parameters:

a). **Reuss k_{matrix} estimation**
For Shale Volumes > 0.4, the Reuss estimation can be used for the computation of the bulk modulus of the matrix from the logs:

$$k_{ma} = \left(\sum f_i / k_{mi} \right)^{-1}, \tag{6.51}$$

$$\mu_{ma} = \left(\sum f_i / \mu_{mi} \right)^{-1}, \tag{6.52}$$

whereby f_i is the percentage or fraction of the rock building solid components (i).

b). **Hills formula's for k_{matrix} and μ_{matrix}**
If the Shale Volume < 0.4, then the formula's of Hill are to be used:

$$k_{ma} = 0.5 \left[\sum f_i k_{mi} + \sum (f_i / k_{mi})^{-1} \right], \tag{6.53}$$

$$\mu_{ma} = 0.5 \left[\sum f_i \mu_{mi} + \sum (f_i / \mu_{mi})^{-1} \right]. \tag{6.54}$$

Shale Volume is measured at a zero porosity value and therefore the Shale Volume log needs to be corrected to the zero porosity value. The following equation should be adhered to:

$$1 = \%\text{porosity} + \%\text{Shale Volume} + \sum (\%\text{ other constituents}). \tag{6.55}$$

The total pore space added to the mineralogical framework should add to 1, when the percentages are expressed by fractions.

c). **Wyllie's formula for Rho_{matrix} estimation**
Wyllie's formula can be utilised to estimate the matrix density:

$$\rho_{ma} = \sum F_i \rho_{mi}. \tag{6.56}$$

F is fraction of each mineral component.

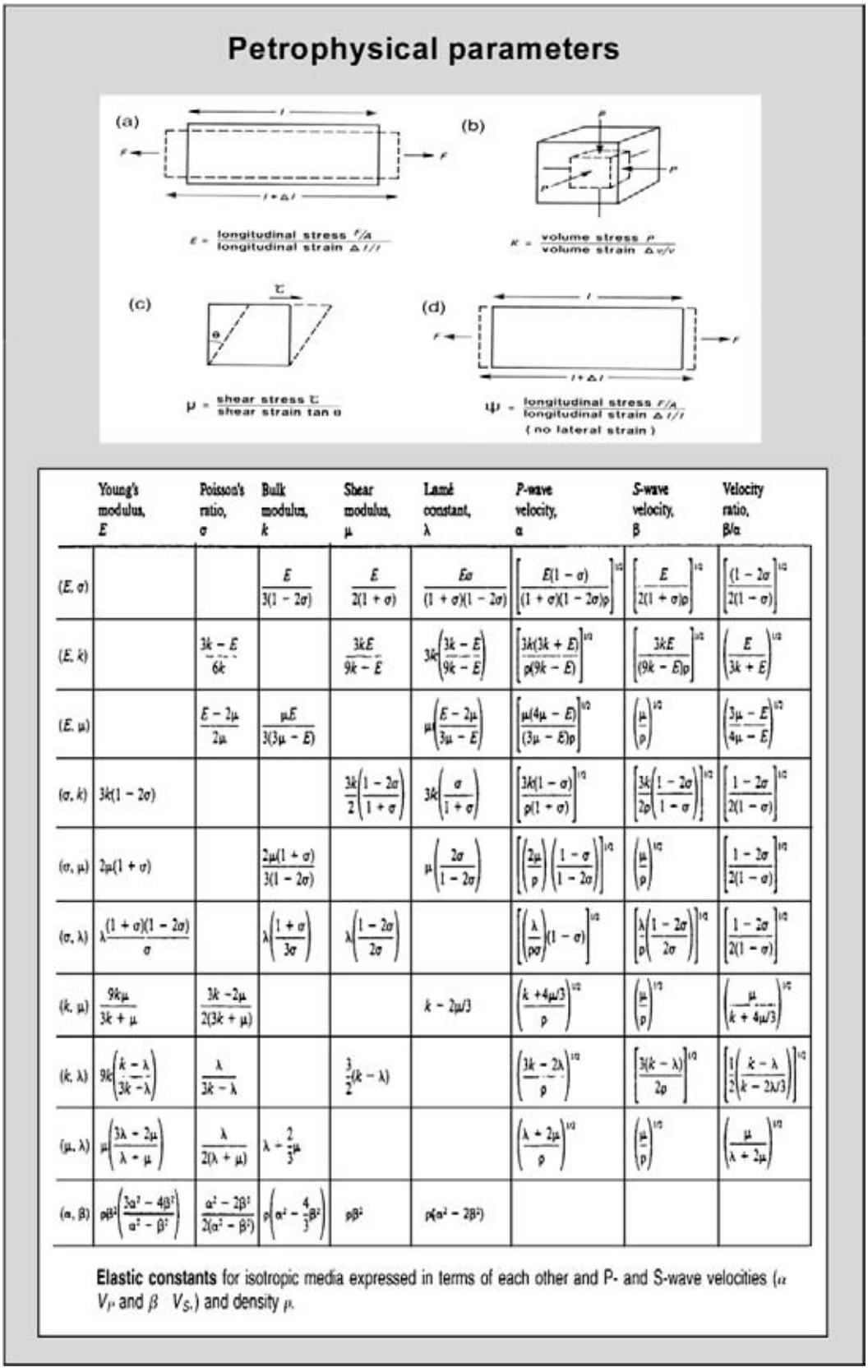

	Young's modulus, E	Poisson's ratio, σ	Bulk modulus, k	Shear modulus, μ	Lamé constant, λ	*P*-wave velocity, α	*S*-wave velocity, β	Velocity ratio, β/α
(E, σ)			$\frac{E}{3(1-2\sigma)}$	$\frac{E}{2(1+\sigma)}$	$\frac{E\sigma}{(1+\sigma)(1-2\sigma)}$	$\left[\frac{E(1-\sigma)}{(1+\sigma)(1-2\sigma)\rho}\right]^{1/2}$	$\left[\frac{E}{2(1+\sigma)\rho}\right]^{1/2}$	$\left[\frac{(1-2\sigma}{2(1-\sigma)}\right]^{1/2}$
(E, k)		$\frac{3k-E}{6k}$		$\frac{3kE}{9k-E}$	$3k\left(\frac{3k-E}{9k-E}\right)$	$\left[\frac{3k(3k+E)}{\rho(9k-E)}\right]^{1/2}$	$\left[\frac{3kE}{(9k-E)\rho}\right]^{1/2}$	$\left(\frac{E}{3k+E}\right)^{1/2}$
(E, μ)		$\frac{E-2\mu}{2\mu}$	$\frac{\mu E}{3(3\mu-E)}$		$\mu\left(\frac{E-2\mu}{3\mu-E}\right)$	$\left[\frac{\mu(4\mu-E)}{(3\mu-E)\rho}\right]^{1/2}$	$\left(\frac{\mu}{\rho}\right)^{1/2}$	$\left(\frac{3\mu-E}{4\mu-E}\right)^{1/2}$
(σ, k)	$3k(1-2\sigma)$			$\frac{3k}{2}\left(\frac{1-2\sigma}{1+\sigma}\right)$	$3k\left(\frac{\sigma}{1+\sigma}\right)$	$\left[\frac{3k(1-\sigma)}{\rho(1+\sigma)}\right]^{1/2}$	$\left[\frac{3k}{2\rho}\left(\frac{1-2\sigma}{1-\sigma}\right)\right]^{1/2}$	$\left[\frac{1-2\sigma}{2(1-\sigma)}\right]^{1/2}$
(σ, μ)	$2\mu(1+\sigma)$		$\frac{2\mu(1+\sigma)}{3(1-2\sigma)}$		$\mu\left(\frac{2\sigma}{1-2\sigma}\right)$	$\left[\left(\frac{2\mu}{\rho}\right)\left(\frac{1-\sigma}{1-2\sigma}\right)\right]^{1/2}$	$\left(\frac{\mu}{\rho}\right)^{1/2}$	$\left[\frac{1-2\sigma}{2(1-\sigma)}\right]^{1/2}$
(σ, λ)	$\lambda\frac{(1+\sigma)(1-2\sigma)}{\sigma}$		$\lambda\left(\frac{1+\sigma}{3\sigma}\right)$	$\lambda\left(\frac{1-2\sigma}{2\sigma}\right)$		$\left[\left(\frac{\lambda}{\rho\sigma}\right)(1-\sigma)\right]^{1/2}$	$\left[\frac{\lambda}{\rho}\left(\frac{1-2\sigma}{2\sigma}\right)\right]^{1/2}$	$\left[\frac{1-2\sigma}{2(1-\sigma)}\right]^{1/2}$
(k, μ)	$\frac{9k\mu}{3k+\mu}$	$\frac{3k-2\mu}{2(3k+\mu)}$			$k - 2\mu/3$	$\left(\frac{k+4\mu/3}{\rho}\right)^{1/2}$	$\left(\frac{\mu}{\rho}\right)^{1/2}$	$\left(\frac{\mu}{k+4\mu/3}\right)^{1/2}$
(k, λ)	$9k\left(\frac{k-\lambda}{3k-\lambda}\right)$	$\frac{\lambda}{3k-\lambda}$		$\frac{3}{2}(k-\lambda)$		$\left(\frac{3k-2\lambda}{\rho}\right)^{1/2}$	$\left[\frac{3(k-\lambda)}{2\rho}\right]^{1/2}$	$\left[\frac{1}{2}\left(\frac{k-\lambda}{k-2\lambda/3}\right)\right]^{1/2}$
(μ, λ)	$\mu\left(\frac{3\lambda+2\mu}{\lambda+\mu}\right)$	$\frac{\lambda}{2(\lambda+\mu)}$	$\lambda + \frac{2}{3}\mu$			$\left(\frac{\lambda+2\mu}{\rho}\right)^{1/2}$	$\left(\frac{\mu}{\rho}\right)^{1/2}$	$\left(\frac{\mu}{\lambda+2\mu}\right)^{1/2}$
(α, β)	$\rho\beta^2\left(\frac{3\alpha^2-4\beta^2}{\alpha^2-\beta^2}\right)$	$\frac{\alpha^2-2\beta^2}{2(\alpha^2-\beta^2)}$	$\rho\left(\alpha^2-\frac{4}{3}\beta^2\right)$	$\rho\beta^2$	$\rho(\alpha^2-2\beta^2)$			

Elastic constants for isotropic media expressed in terms of each other and P- and S-wave velocities (α V_P and β V_S,) and density ρ.

Figure 6.50: Summary of rock physical parameters and their relationships (modified after Kearey and Brooks 1991 and Sheriff 2002).

d). **Reuss formula's for k_{fluid} estimation**
The fluid bulk modulus is computed from the following Reuss formula's when assuming the presence of two fluids:

$$\frac{1}{k_{\text{fl}}} = \frac{S_{\text{w}}}{k_{\text{w}}} + \frac{1 - S_{\text{w}}}{k_{\text{fl2}}}, \tag{6.57}$$

$$\rho_{\text{fl}} = S_{\text{w}}\rho_{\text{w}} + (1 - S_{\text{w}})\rho_{\text{fl2}}. \tag{6.58}$$

e). **Wyllie's equation for $\text{Rho}_{\text{Formation}}$ estimation**
The Wyllie equation (Wyllie et al. 1956, 1958) provide information about the formation density (= matrix + fluid in pores):

$$\rho_{\text{fm}} = (1 - \phi)\rho_{\text{ma}} + \rho_{\text{w}} S_{\text{w}}\phi + \rho_{\text{fl2}}(1 - S_{\text{w}})\phi. \tag{6.59}$$

The sonic transit time average equation is now given by:

$$\Delta t_{\text{sonic}} = (1 - \phi)\Delta t_{\text{matrix}} + (\phi \Delta t_{\text{fluid}}). \tag{6.60}$$

The porosity is estimated from the sonic log transit time and the velocities in the following way:

$$\Delta t_{\text{sonic}} = \frac{1 - \phi}{V_{\text{matrix}}} + \frac{\phi}{V_{\text{fluid}}}. \tag{6.61}$$

6.4.3 V_{p} and V_{s} estimations

Often V_{s} is not directly measured in the field because it was considered costly at the time. Estimation have to be made (Figure 6.51). Six types of analysis can be done to assess the V_{p} and V_{s} relationships (Veeken and Rauch-Davies, in prep.):

1) **Biot–Gassmann method**
Elasticity of porous media was studied by Biot (1941, 1956). Gassmann managed to give an explicit expression of the Biot macroscopic parameters in terms of rock physical parameters (cf Rasolofosaon and Zinszner, 2004). Gassmann basically uses a spherical model to describe the organisation of the lithological components in a rock sample (Gassmann 1951).

$$k_{\text{fm}} = k_{\text{dry}} + \left[\left(1 - \frac{k_{\text{dry}}}{k_{\text{ma}}}\right)^2 \Big/ \left(\frac{\phi}{k_{\text{fl}}} + \frac{1 - \phi}{k_{\text{ma}}} - \frac{k_{\text{dry}}}{{k_{\text{ma}}}^2}\right)\right]. \tag{6.62}$$

V_{p} and V_{s} are now estimated by:

$$V_{\text{p}} = \sqrt{\frac{k_{\text{fm}} + (4\mu_{\text{dry}})/3}{\rho_{\text{fm}}}}, \tag{6.63}$$

$$V_{\text{s}} = \sqrt{\frac{\mu_{\text{dry}}}{\rho_{\text{fm}}}}. \tag{6.64}$$

fm = formation or totality of rock and fluids.

dry = dry part of rock (skeleton + air).

ma = matrix or rock particles (minerals and cement).

fl = fluids.

The Biot–Gassmann equation assumes a polynomial relation between the rock parameters (Figure 6.52). It takes into account the visco-elastic effects and includes the dynamic effects of the relative motion between the fluid and the rock skeleton (Assefa et al. 2003, Oldenziel 2003). The formula does not take into account capillary forces that have an influence on the rock rigidity (Rasolofosaon and Zinszner 2004). The **Biot–Gassmann β parameter** of the following polynomial equation is solved to estimate the V_{p} and V_{s} values:

$$A\beta^2 + B\beta + C = 0. \tag{6.65}$$

Whereby

$$A = \frac{S}{k_{\text{ma}}} - 1,$$

$$B = \left[M - S + \phi S\left(\frac{k_{\text{ma}}}{k_{\text{fl}}} - 1\right)\right]\left(\frac{1}{k_{\text{ma}}}\right),$$

$$C = \left\{\left[M\phi\left(\frac{k_{\text{ma}}}{k_{\text{fl}}} - 1\right)\right] - \left[\phi S\left(\frac{k_{\text{ma}}}{k_{\text{fl}}} - 1\right)\right]\right\}\left(\frac{1}{k_{\text{ma}}}\right).$$

$$M = \rho_{\text{fm}} {V_{\text{pfm}}}^2,$$

$$S = k_{\text{ma}} + \frac{4\mu_{\text{ma}}}{3}$$

and

$$k_{\text{dry}} = (1 - \beta)k_{\text{ma}},$$

$$\mu_{\text{dry}} = (1 - \beta)\mu_{\text{ma}},$$

$$k_{\text{fm}} = k_{\text{ma}}(1 - \beta) + m\beta^2,$$

$$m = \frac{k_{\text{ma}} k_{\text{fl}}}{k_{\text{fl}}(\beta - k_{\text{ma}}) + \phi k_{\text{ma}}}.$$

If $\phi = 0$, then $\beta = 0$ as $k_{\text{matrix}} = k_{\text{dry rock}}$ and hence $C = 0$.

Now V_{s} and V_{p} is again estimated by the formulas (6.63) and (6.64). Rasolofosaon and Zinszner (2004) propose experimental measurements of the Biot–Gassmann parameters to estimate rock physical parameters for seismic reservoir modelling. The variation of the bulk modulus of a saturated rock sample is determined as a function of the bulk moduli of various saturated fluids. Baechle et al. (2005) have found that the shear moduli in carbonate rocks are not always constant when different saturations are applied, so some caution is recommended. This puts the constant shear modulus assumption of Gassmann in jeopardy for carbonates. In case the Biot–Gassmann formula is appropriate, then the k_{sat} versus k_{fl} plot is displaying points along a straight line,

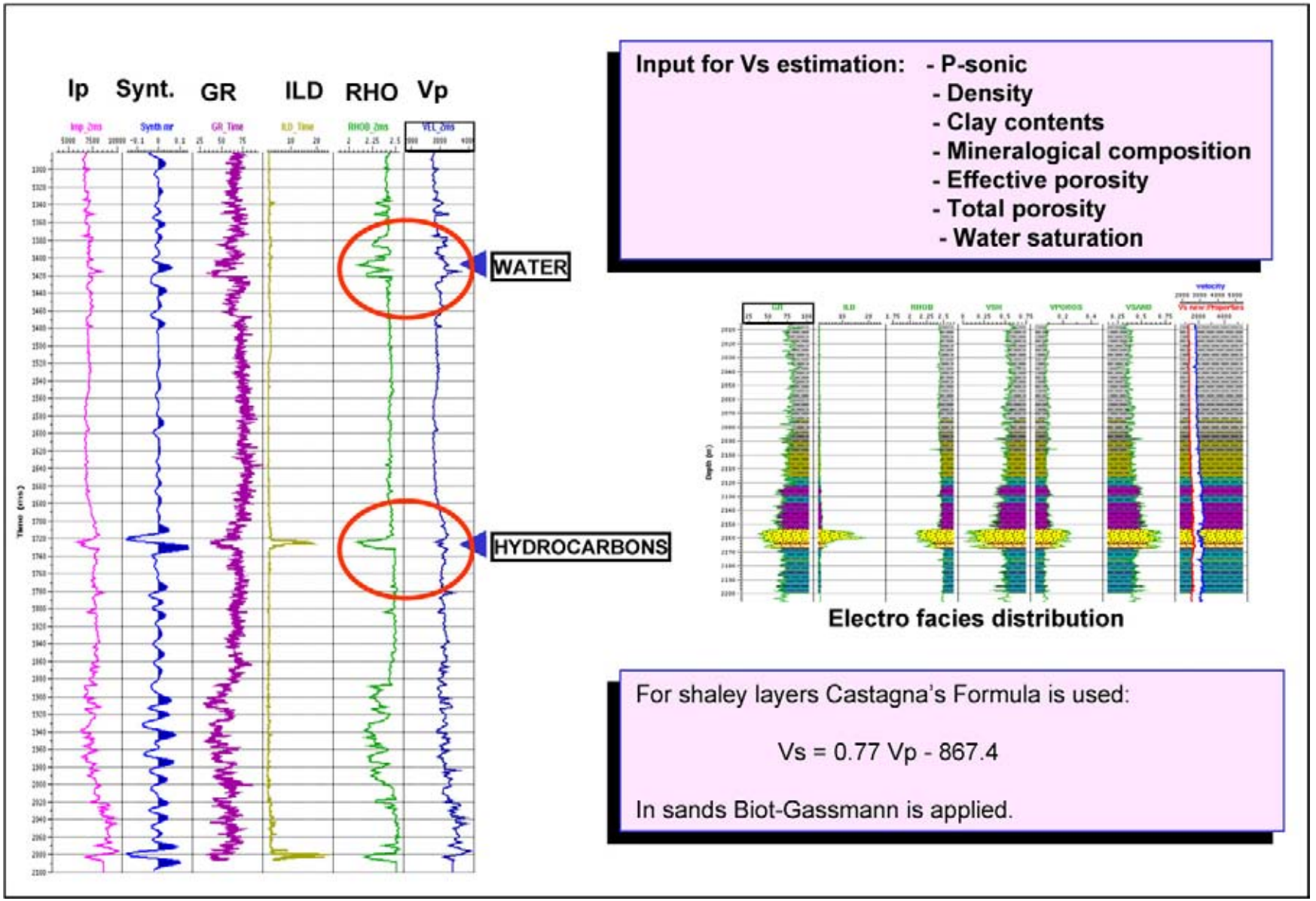

Figure 6.51: V_s estimation can be achieved in several ways. It is needed when shear log data is lacking. This is often case for 'old' wells and AVO effects need to be modelled. The Biot–Gassmann method is presented in the next figure.

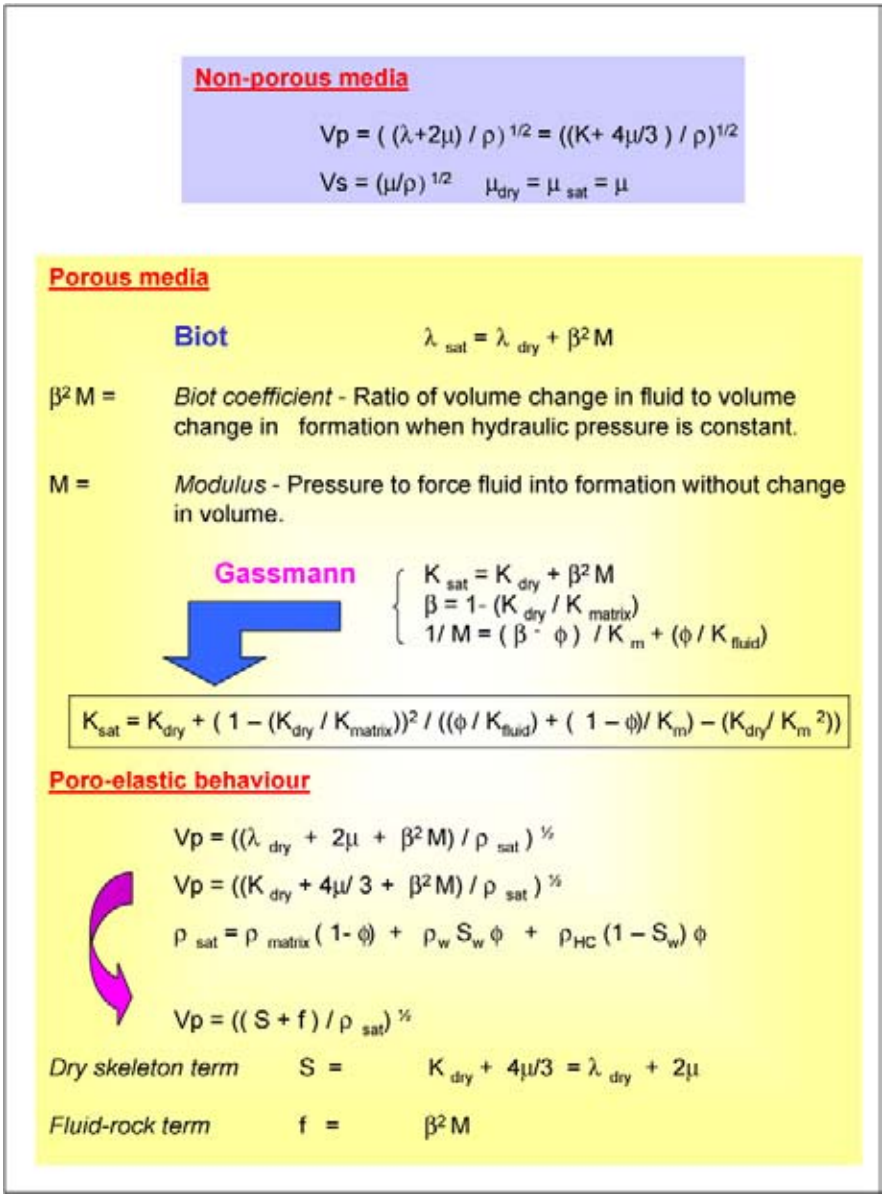

Figure 6.52: Biot–Gassmann estimation of rock physical parameters in porous media. A more precise poro-elastic behaviour is given by Russell et al. (2003) and Gretener and Thomsen (2003).

with the k_{dry} value as Y-axis intercept and a slope of β^2/ϕ. It is now easy to compute the Biot coefficient β and obtain an experimental k_{ma} value. This method also gives estimates for μ and k_{dry}.

2) **Hilterman method**
The Gassmann formula can also be written in an other form:

$$\rho \cdot V_{\mathrm{p}}^2 = k_{\mathrm{dry}} + \frac{4}{3}\mu_{\mathrm{dry}} + \frac{(1 - k_{\mathrm{dry}}/k_{\mathrm{ma}})^2}{((1 - \phi - k_{\mathrm{dry}}/k_{\mathrm{ma}})/k_{\mathrm{ma}}) + \phi/k_{\mathrm{fl}}}. \quad (6.66)$$

The Biot coefficient is equal to the term:

$$\beta = 1 - \frac{k_{\mathrm{dry}}}{k_{\mathrm{ma}}}. \quad (6.67)$$

V_{p}, rho, phi are known; k_{ma} and k_{fl} can be estimated. Therefore basically three unknowns are left: k_{dry}, μ_{dry} and V_{s}. For this three unknowns other estimates can be made according to Hilterman (2001):

$$V_{\mathrm{s\,wet}} = \text{function of } V_{\mathrm{p\,wet}},$$

$$k_{\mathrm{dry}} = (1 - \beta) k_{\mathrm{ma}}, \quad (6.68)$$

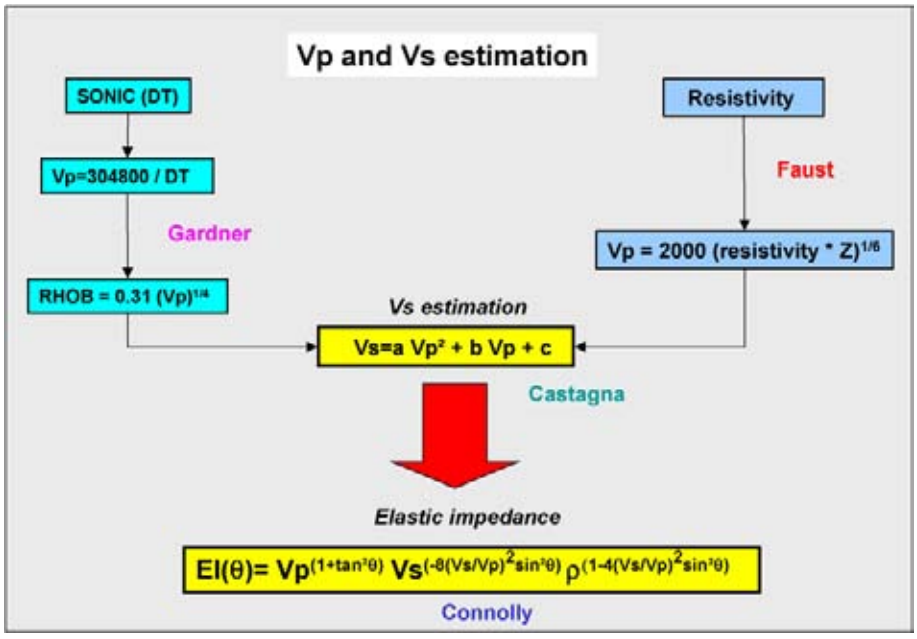

Figure 6.53: Estimation of the V_p and V_s velocities that are needed for an elastic inversion. The Castagna formula $V_s = aV_p^2 + bV_p + c$ uses: sand $a = 0$, $b = 0.804$, $c = 0.856$; shale $a = 0$, $b = 0.770$, $c = -0.867$. These velocities for the Castagna estimation are in km/s.

$$\frac{k_{dry}}{\mu_{dry}} = \frac{2(\sigma_{dry} + 1)}{3 - 6\sigma_{dry}} \tag{6.69}$$

if $\sigma_{dry} = 0.125$ than $k_{dry} = \mu_{dry}$.

The Gassmann equation is valid under the following assumptions:

- Macroscopically isotropic homogeneous medium.
- Skeleton grains, fluids obey Hooke's law (stress is proportional to strain).
- Pore space is interconnected.
- Fluid pressure uniform.
- A closed system and no fluid leaves the rock volume.
- No cavitation occurs, no separation at contact boundaries.

3) **Han's β estimation method**
The Han method solves β utilising an empirical graph (Han et al. 1986). The graph is compiled using triaxial compressibility measurements and effective porosity data, on which lines of equal D are plotted.

$$\beta = 1 - (1 - D\phi), \tag{6.70}$$

whereby D ranges: $1.3 < D < 2$.

4) **Krief's β estimation method**
The Krief method uses the following relationship:

$$\beta = 1 - (1 - \phi)^{3/(1-\phi)}. \tag{6.71}$$

When ϕ is smaller or equal 0.2, than the $\beta_{Han} \sim \beta_{Krief}$.

5) **Castagna's method**
It uses a second order polynomial fit for the V_p–V_s relationship:

$$V_s = a\,V_p^2 + b\,V_p + c. \tag{6.72}$$

A general trend for water filled sands and shales has been proposed in the form where the velocities are in km/s (cf Latimer 2004):

$$V_s = 0.862\,V_p - 1.172. \tag{6.73}$$

The relationship is however lithology dependent and different coefficients are therefore proposed to increase the accuracy (Figure 6.53).

Sands	$V_s = +0.804\,V_p + 0.856$,
Limestone	$V_s = -0.055\,V_p^2 + 1.017\,V_p - 1.030$,
Dolomite	$V_s = +0.583\,V_p - 0.078$,
Shale	$V_s = +0.770\,V_p - 0.867$.

6) **Krief's formula for V_p and V_s estimation**
The Krief formula gives information on the V_s and V_p velocities (Krief et al. 1990):

$$V_s = \sqrt{\frac{{V_{s\,ma}}^2({V_{p\,fm}}^2 - {V_{p\,fl}}^2)}{{V_{p\,ma}}^2 - {V_{p\,fl}}^2}} \tag{6.74}$$

whereby

$$V_{s\,ma} = \sqrt{\frac{\mu_{ma}}{\rho_{ma}}},$$

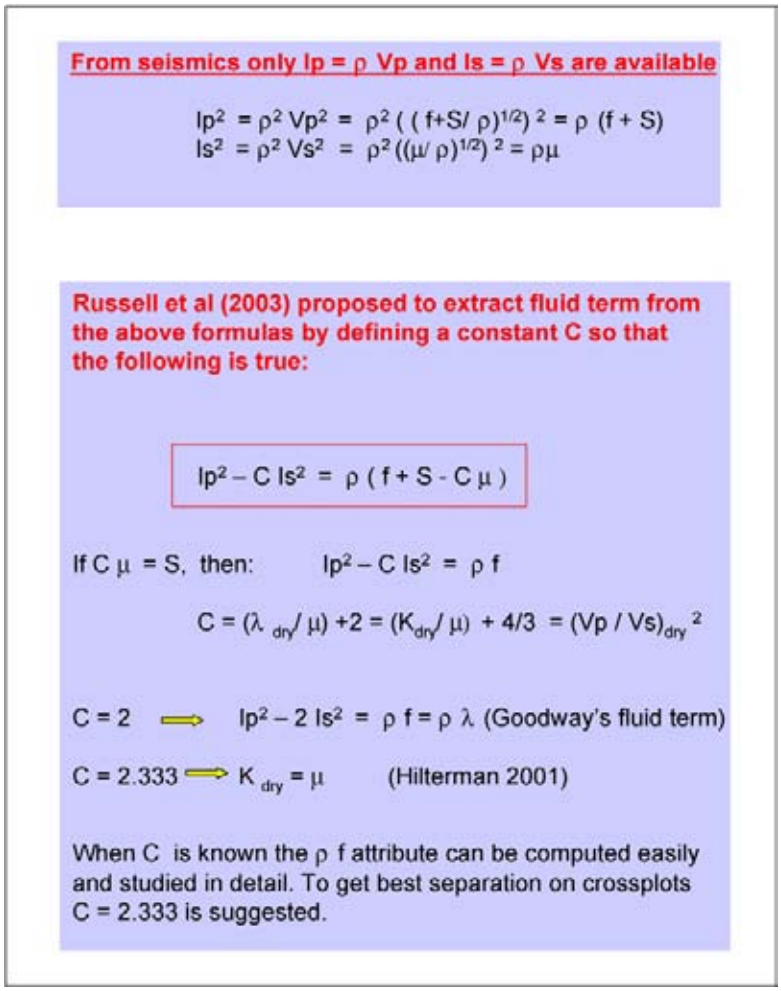

Figure 6.54: Alternative fluid contents attributes are derived from seismics and the rock physical parameters (modified after Russell et al. 2003).

$$V_{\mathrm{p\,fl}} = \sqrt{\frac{k_{\mathrm{fl}}}{\rho_{\mathrm{fl}}}},$$

$$V_{\mathrm{p\,ma}} = \sqrt{\frac{k_{\mathrm{ma}} + (4\mu_{\mathrm{ma}})/3}{\rho_{\mathrm{ma}}}}.$$

A V_{p}^2 versus V_{s}^2 quality control plot is normally made to check there exists a straight line relationship!

6.4.4 Fluid contents attributes

For the non-porous media a simple relation exists between the V_{p} and V_{s} on the one side and the rock physical parameters on the other side (Figure 6.54). The situation becomes in porous media more complicated because of the pore space is filled with fluids. The poroelastic behaviour is assumed in the lower part of the figure. Russell et al. (2003) propose the relation:

$$V_{\mathrm{p}} = \sqrt{\frac{S+f}{\rho_{\mathrm{sat}}}}. \tag{6.75}$$

S is the dry skeleton term and f contains the fluid-rock information. On the seismic only impedances are measured. Goodway et al. (1993) have introduced a fluid contents attribute called rholambda, that is related to the I_{p} and I_{s} values in the following way:

$$\rho\lambda = I_{\mathrm{p}}^2 - 2\,I_{\mathrm{s}}^2. \tag{6.76}$$

The gas sands are better separated from tight sands and carbonates in the murho and lambdarho crossplot (Yilmaz 2001). Russell et al. (2003) propose a more flexible attribute that corresponds to this fluid attribute of Goodway in a special case (Figure 6.54):

$$I_{\mathrm{p}}^2 - C\,I_{\mathrm{s}}^2 = \rho(f + S - C\mu). \tag{6.77}$$

If $C\mu = S$, then:

$$I_{\mathrm{p}}^2 - C\, I_{\mathrm{s}}^2 = \rho f. \tag{6.78}$$

This C is just a constant value. If $C = 2$ then $\rho f = \rho\lambda$. Based on a certain C value the attribute is computed from the seismic impedances. It ensures that a better separation is obtained according to the porefill in the crossplots. The attribute is however survey dependant. A $C = 2.333$ is often a good starting point. The attribute is studied on maps and sections; it is a convenient discriminator for illustrating changes in fluid contents.

An other approach is to study the behaviour of the AI and SI cross plot as was done by Quakenbush et al. (2006). If the plot is rotated a better separation between gas and water filled sands is obtained. The rotation is done by the following way:

$$I_{\mathrm{p}} - c\, I_{\mathrm{s}} = \mathrm{PI}. \tag{6.79}$$

The notion of **Poisson's impedance** PI is here introduced, defined as V_σ times the density. The c term just optimises the rotation. The relation can be rewritten as:

$$V_{\mathrm{p}}\rho - c(V_{\mathrm{s}}\rho) = \mathrm{PI} = V_\sigma \rho. \tag{6.80}$$

The new concept Poisson's velocity is hence equal to:

$$V_\sigma = V_{\mathrm{p}} - c\, V_{\mathrm{s}}. \tag{6.81}$$

Its relation of the rotated data with the Poisson's ratio is given by:

$$\sigma = \left(\frac{V_{\mathrm{p}} + \sqrt{2}V_{\mathrm{s}}}{2{V_{\mathrm{p}}}^2 - {V_{\mathrm{s}}}^2}\right) \cdot \left(V_{\mathrm{p}} - \sqrt{2}V_{\mathrm{s}}\right). \tag{6.82}$$

The constant c is now taken equal the square root of two. And D is the first term of the equation:

$$D = \frac{V_{\mathrm{p}} + \sqrt{2}V_{\mathrm{s}}}{2{V_{\mathrm{p}}}^2 - {V_{\mathrm{s}}}^2}. \tag{6.83}$$

They have considered taking different values for the constant c by looking at the Greenberg–Castagna V_{p}–V_{s} shale equation. They compute a slope of 1.3 to parallel the V_{p} and V_{s} trends. The 1.4142 of the square root two seems thus reasonable for the translation. After the transformation the shales are rather constant while other lithologies deviated from this background trend. Other elastic reservoir parameters are also varying with PI and are given by:

$$\frac{\lambda}{\mu} = \left(\frac{V_{\mathrm{p}}}{V_{\mathrm{s}}}\right)^2 - 2, \tag{6.84}$$

$$\begin{aligned}\lambda\rho &= I_{\mathrm{p}}^2 - 2I_{\mathrm{s}}^2 \\ &= \rho^2\left(V_{\mathrm{p}} + \sqrt{2}V_{\mathrm{s}}\right)\left(V_{\mathrm{p}} - \sqrt{2}V_{\mathrm{s}}\right).\end{aligned} \tag{6.85}$$

It differs from the PI by a factor $\rho(V_{\mathrm{p}} + \sqrt{2}V_{\mathrm{s}})$. The Poisson's Impedance PI is hence an interesting new reservoir attribute with an optimised fluid contents separation.

6.4.5 Constraints on modelling results

The modelling exercises give valuable information on how to obtain a better fit with the measured data (iterative method with perturbation on the reservoir seal properties). Indeed, seismic inversion provides a grip on some of the rock parameters, but still the separate contribution of velocity and density is difficult to substantiate. This knowledge will ultimately result in a better lateral prediction concerning the reservoir behaviour. It should be kept in mind that: *most of the time there exists not only one unique solution to the given problem.* The expected reservoir configuration can be modelled, but there always remain some basic assumptions required as primary input to the exercise. The ultimate answer is only given by the drill-bit. In such case it is always advisable to quantify the uncertainties of the modelled scenarios and to keep an open mind on all possible scenarios.

6.5 Merging Seismics and Rock Physical Parameters

In order to facilitate the interpretation of the results it is necessary to integrate the rock physics analysis in the quantitative interpretation of the seismic data. For this purpose a crossplot technique is usually applied based on well log results and laboratory rock measurements. One method uses the construction of a Rock Physics Template (RPT) that provides a toolbox for easy lithology and pore fluid interpretation on well and seismic inversion/AVO results (Odegaard and Avseth 2004). Typically a $V_{\mathrm{p}}/V_{\mathrm{s}}$–AI crossplot is visualised (Figure 6.55). The RPT plot is area or basin dependent and velocity–porosity trends are calculated for the expected lithologies and various depth of burial (compaction). Odegaard and Avseth (2004) describe various techniques to establish these reference trend curves on the plot. A distinction needs to be made between silici-clastic and carbonate systems. Various parameters have an effect on the behaviour of a brine filled sand:

- Lithology (shale, shaley sand, clean sand).
- Mineralogy (quartz arenite, feldspar-rich arkose).
- Burial depth.
- Diagenesis (quartz cement above 80 degrees C and beyond 1.5 to 2 km burial depth; smectite transformed into illite by release of crystal bound water).
- Pressure.
- Temperature.

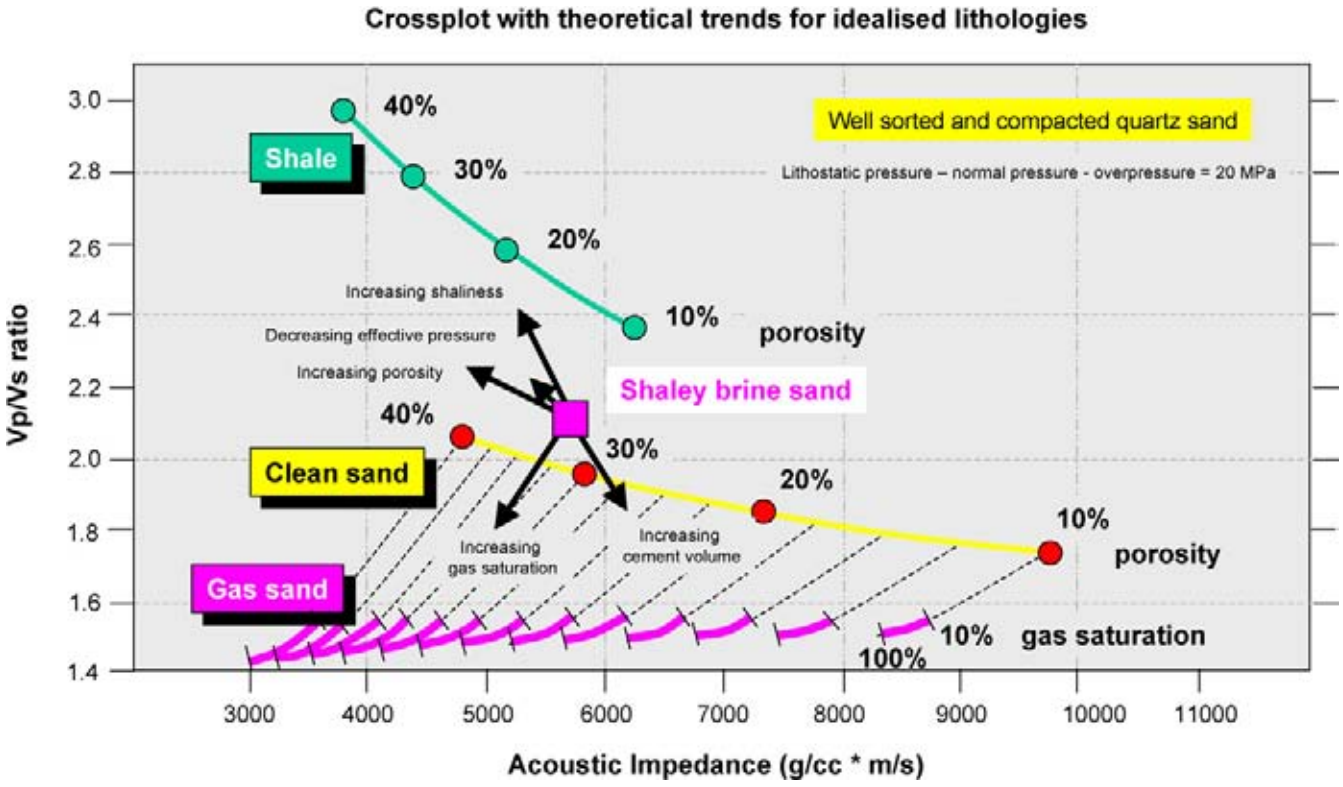

Figure 6.55: Rock physical crossplot for AI versus the V_p/V_s ratio. The theoretical trends are shown for idealised silici-clastic lithologies. This can be used as a template when interpreting other well data or seismically derived cross plot values. The effects of changing reservoir parameters on a point of the crossplot is here shown by arrows (modified after Odegaard and Avseth 2004).

Changing the reservoir parameters on a point in the RPT plot has the following effect:

- An increase in gas saturation will reduce the AI and the V_p/V_s.
- An increase in cement volume will increase the AI and reduce the V_p/V_s.
- An increase in porosity will decrease the AI and increase the V_p/V_s.
- An increase in shaliness will reduce the AI but increase the V_p/V_s.
- Changing the formation pressure has not so much influence but it will reduce AI and increase V_p/V_s.

For the computation of a RPT plot it is necessary to have the following input:

- Temperature and pressure.
- Brine salinity.
- Gas gravity (0.6–0.8).
- Oil reference density (more difficult to estimate).
- Water saturation.
- Gas/oil ratio.

Once the template is computed it can be used to plot the seismic data at the well location and a colour coding can be applied for showing the gamma ray cut-off range for instance, which is a good lithology indicator (Figure 6.56). This approach allows to identify clusters on the plot and interpret them in terms of varying reservoir characteristics. The deviation from the reference trend lines now permits to infer the effect of various parameters. Subsequently the whole seismic attribute dataset can be plotted and the distribution of the points examined. Cut-off ranges from the plot can be applied on individual attribute cubes and a transformation into a specific reservoir parameter (e.g. porosity, saturation) is thus obtained. Anomalies related to the presence of hydrocarbons are more easily identified and recognised all over the seismic dataset. Presence of silica ooze, pyrite, different clay minerals, Opal A–CT transitions due to anomalous heatflow (e.g. Davies and Cartwright 2002), volcanic tuff, salt intrusion, calcite cement and shallow overpressure may hamper the analysis and they constitute potential pitfalls towards a more quantitative interpretation. The input and the AVO/inversion results should be reliable enough for conducting such a high resolution interpretation exercise. Therefore it is extremely important that the real impedance contrasts

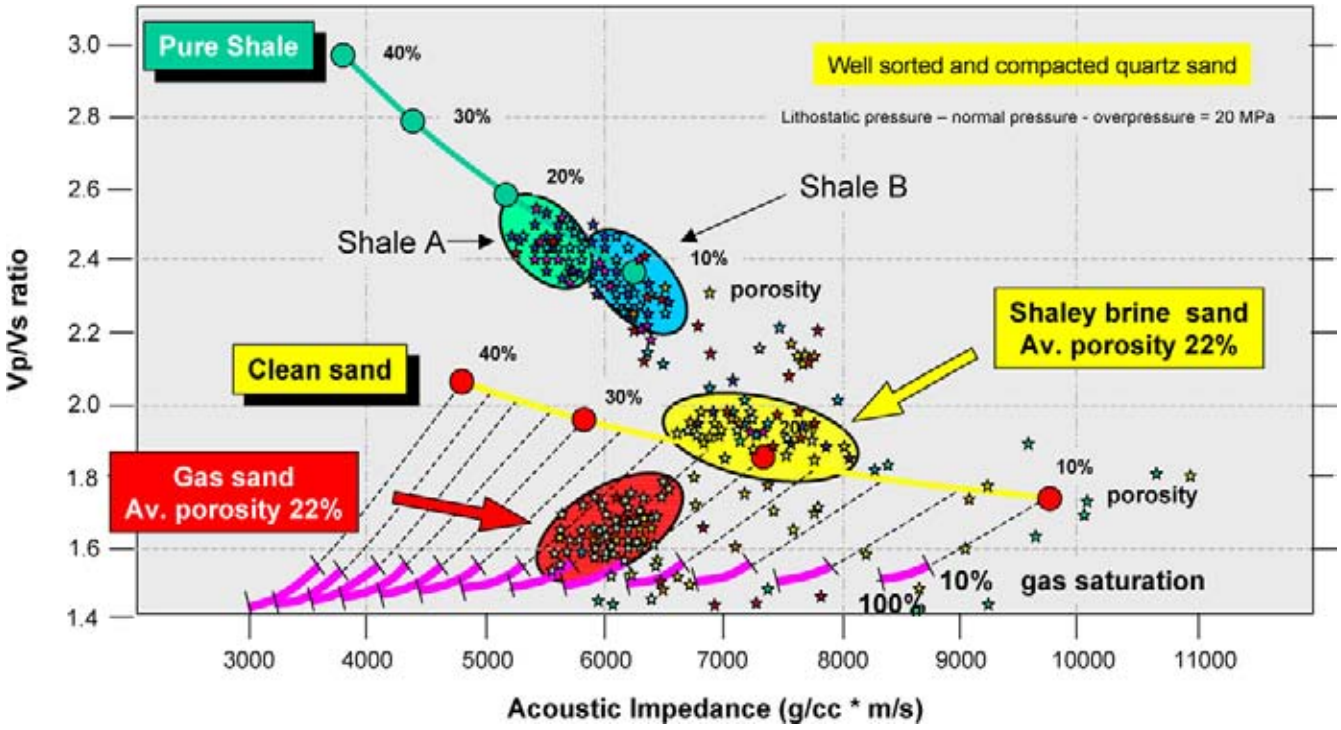

Figure 6.56: AI versus V_p/V_s ratio crossplot with the theoretical trends that facilitate the interpretation of the inferred reservoir characteristics. The colour coding for the points are related to gamma ray cut-off ranges. From blue to red to orange to yellow and green are decreasing API values (modified after Odegaard and Avset 2004).

in the subsurface are preserved in every processing step. As mentioned before, it is critical that proper data preconditioning and noise suppression is implemented to safeguard the integrity of the dataset serving as input to this kind of reservoir characterisation and lateral prediction studies (cf Veeken and Da Silva 2004).

This page intentionally left blank

Chapter 7

Volumetrics and Prospect Evaluation

Computer aided mapping techniques do give the interpreter direct access to time, time thickness, velocity, depth and depth thickness maps of all horizons and intervals. Also attribute maps and their derivatives are made by the push of a button. **Correlation panels** for the well data are easily compiled incorporating biostratigraphic, petrophysical and reservoir engineering parameters. With this data at hand, the consistency of the interpretation is checked at the well locations and other calibration points. Eventual discrepancies are corrected and an update of the interpretation is implemented. Especially the correction of the depth misties in wells of the mapped horizons frequently proves itself a rather tedious task. For this purpose the applied depth conversion method needs to be rigorously scrutinised. Sensitivity studies are initiated to assess the amount of uncertainty in the geometrical description of the area. The outcome of this analysis can become an extremely important financial matter during partnership negotiations (unitisations) in the development phase of a HC project.

Geostatistical modelling improves the dynamic perception of subsurface structures (e.g. Haas and Dubrule 1994). It gives a handle on how to deal with the various uncertainties. Geostatistics provides quantification of the expected variability of the reservoir parameters in space (Fournier and Derain 1995). Spill points for the various closed structures are examined and possible stratigraphic traps outlined. The latter type of traps are notoriously difficult to define in an unambiguous way (Halbouty 1982, Allen et al. 2006); e.g. Cougar field where sub seismic faulting is now found to play a more prominent role (McCarthy and Bilinsky 1999). Modern 3D seismic can resolve faulting with an offset of 5 metres but smaller offsets might have an influence on the amplitude behaviour and can be detected under favourable circumstances (Pu and Xizun 2005). This has been proven by recent Chinese coal mining activities. Stress pattern analysis is helpful to determine the role of non-conventional trapping mechanisms (Ameen 2003). Inversion and AVO may here demonstrate their usefulness in supporting a particular working model.

Once a final interpretation is established, then an assessment of the volumetrics of the structures is made. Special modules in the contouring and griding software packages (ZMAP^{TM}, CPS^{TM}, IntegralPlus^{TM}, FastQC^{TM}, GoCad^{TM}) allow to calculate the **gross rock volume** of a trap. The lithology prediction from impedance cube permits to extract the **net pay** (cf Guilbot et al. 1996). Some packages approximate the volume contained in a fault-bounded structure by treating the fault planes as vertical features. When dealing with weakly dipping fault planes, considerable errors are introduced in this way. The sizes of the different structures is compared and an initial **ranking** of the traps made.

The chance of having a connection to a mature kitchen area and an estimation of its size needs to be addressed. Its degree of maturation level in time and the type of source rock are examined. Heat flow assumptions are made and a thermal history is reconstructed (e.g. Carr and Scotchman 2003). A subsidence history is inferred from burial graphs. Compaction trends should be accounted for. A most likely migration route is established in this stage of the evaluation. The timing of the trap formation is assessed. Evolution of possible spill point positions is reconstructed and monitored in time. Inversion tectonics complicate the picture considerably. The dynamic history of a basin fill can be reconstructed in dedicated software packages like Basmod^{TM} and Heresim^{TM}.

The ultimate goal of the HC exploration efforts is final integration of all knowledge regarding a field into a dynamic reservoir model. Geophysical, geological and engineering data are incorporated in a subsurface flow-properties model. The model is matched to the production history and used for forecasting and economic evaluation. This model is traditionally constructed after the main reservoir characterization stage and little interaction is undertaken or even feasible between the property modelling and the geocellular modelling. A combined reservoir characterization and modelling workflow for a producing field is of prime importance. The process generally implies tight integration of the seismic inversion results at the upscaling and geocellular model construction step (Simono et al. 2004).

The importance of getting all ingredients of an hydrocarbon play right, is illustrated by the following: an oil

company ignored to bid on the Beatrice field concession block in the Moray Firth offshore Scotland in the 1970-ties, because the complex tectonic history was not properly evaluated from the seismics. They failed to recognise the inversion tectonic deformation of the basin fill and the presence of a valid mature kitchen area. The charge of the Beatrice structure is still a bit enigmatic with contribution from Devonian and possibly Jurassic source rocks (Marshall and Hewett 2004). An other oil company closed down their Paris Basin exploration venture, because they did not see how hydrocarbons could migrate through a substantial shale interval (assumed to represent an impermeable seal), whilst it is now known that fracturing easily creates pathways. Maybe it was the right decision at that time, because the missed HC accumulations are rather small, but the reasons for the pulling-out should have been somewhat different.

Sometimes all elements of a hydrocarbon play are fulfilled and still the prospectivity to develop the hydrocarbon resources with the existing techniques is rather low. This is for example the case when the density of the oil (low API) is high and its viscosity is very low. The Devonian–Lower Carboniferous Clair field, located offshore West Shetlands (Duindam and Van Hoorn 1986, Sorensen 2003), is a giant hydrocarbon accumulation that is difficult to develop in a profitable manner with current production techniques. New seismic OBC data have been shot and improved the definition in the reservoir sequence (Kommedal et al. 2005). The depth of the target is around 1.8 milliseconds TWT, but the sections are not yet of outstanding quality (Figure 7.1). Increasing the recovery factor in an economically justifiable way is the key to the business success of this huge HC asset.

Also the vast Athabasca tar sands of western Canada are not easy to exploit in an economic way, but the **proven HC reserves** are gigantic. Steam injection stimulated gravity drainage and integrated mining operations are utilised too develop these heavy oil accumulations. At an oil cost price of 24 dollars per barrel and a gas price of 4 dollars per million British thermal units a profit of 10–15 percent is reached in these kind of projects (First Break Vol. 22, No. 9, p. 24). A higher crude price will generate of course a higher surplus for

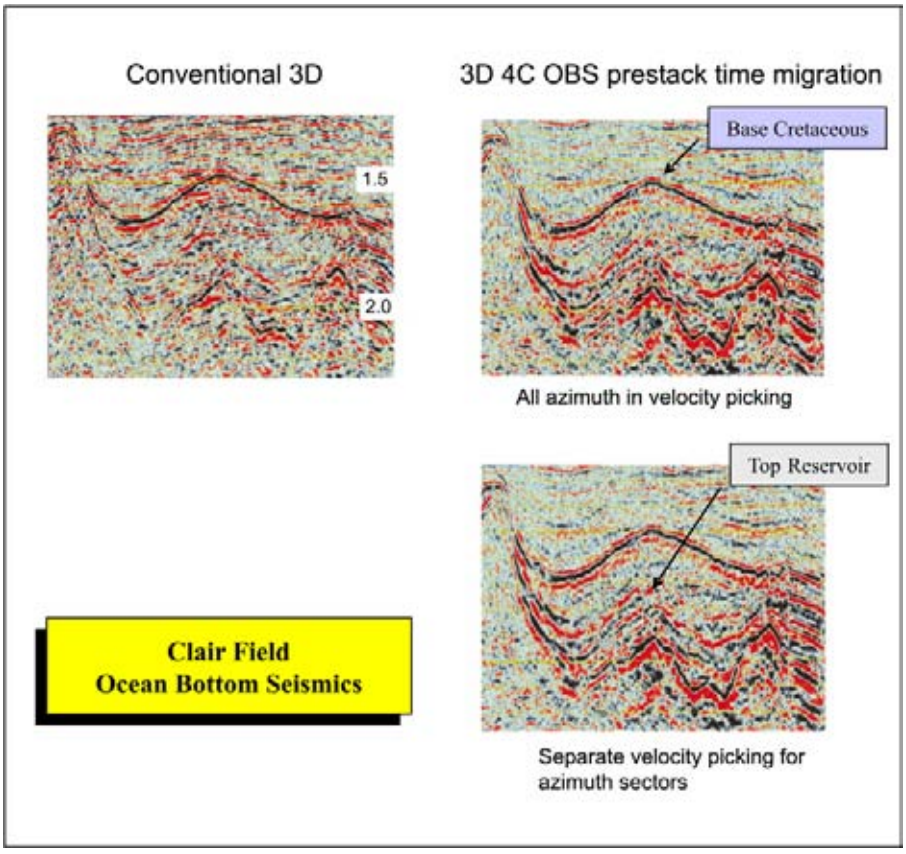

Figure 7.1: Comparison of conventional 3D and Ocean Bottom Seismic data acquired over the Clair Field, offshore West Shetlands. The OBS dataset has been processed with 2 different velocity picking policies. The reservoir is positioned at around 1.8 seconds in the central part of the section. The basement is located at about 2 seconds.

the asset. The current tar sand production is 1 million barrels (about 160,000 cubic metres) and it is expected to rise to 2.2 million barrels per day in 2015. According to Van der Veer (Shell website 2004) the cost price for petrol production from oil sands will be further reduced to 10 dollars a barrel in 2010.

The sealing capacity of the faults and relevant stratigraphic units is estimated. The pressure behaviour of the fluids in the pores is important in this respect, as will be discussed in the next chapter.

7.1 Pressure Differentials

For a proper understanding of the pressures measured in a reservoir, it is necessary to introduce the various pressure concepts (Figure 7.2).

7.1.1 Pressure concepts

Pore pressure (or formation pressure) is the pressure acting on the fluids in the pore space of a formation. It is equal to the hydrostatic pressure plus the over- (or under) pressure. Overpressure is caused by the fact that the water column is carrying part of the weight of the rock column and an effective seal is present in the system. The unit of pressure is the Pascal that is equal to:

$$1 \text{ Pa} = 1 \text{ N/m}^2 \ (= 1.45 \times 10^{-4} \text{ psi}).$$

The psi stands for pounds per square inch, the British/American measurement. A megaPascal is equal to 10^6 Pa. 1 psi/ft = 0.0225 MP/m. The pressure gradient is normally determined from the ratio of formation pressure to the depth z.

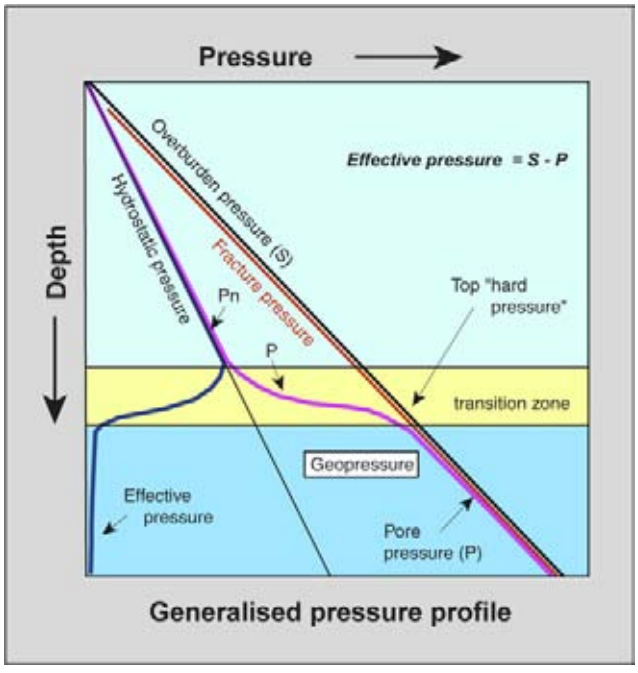

Figure 7.2: Pressure profile in a sedimentary basin. Hydrostatic pressure is determined by the weight of the water column in an open system. The lithostatic pressure is equal to the weight of the rock matrix skeleton and the pore fill pressure (modified after Dutta 2002).

Hydrostatic pressure is the pressure caused by the weight of a fluid column.

$$P_{\text{hydrostatic}} = \rho_{\text{fluid}}\, g\, z, \tag{7.1}$$

g = gravity acceleration,

z = height of column.

The fluid density ρ_{fluid} depends on several factors: fluid type, dissolved solids and amount of included gasses, temperature and pressure. The hydrostatic (or normal pressure) is equal the pressure gradient of water multiplied by the depth. This is the pressure whereby the water column is not carrying the weight of the rock skeleton. The mineral particles are in point contact and the pore space forms an open system to the surface.

Overpressure (or geopressure) is equal to the pore pressure minus the hydrostatic pressure. Now an effective seal is present and the system is no longer open. Part of the weight of the rock skeleton is carried by the fluids in the pores.

The **retention capacity** is defined as the least principle stress minus the pore pressure (Nordgard Bolas and Hermanrud 2003).

Overburden pressure is the pressure caused by the overburden weight of the rock matrix and the fluids in the pore space of the overlying rock column. It is also known as **geostatic pressure**.

The **lithostatic pressure** is equal rock particle pressure gradient times the depth.

The **effective pressure** is defined as the difference between the overburden pressure minus the measured pore pressure. The effective pressure (also known as differential pressure) governs the compaction process in sedimentary rocks. Geopressuring implies that the rock has low effective stress and a higher porosity than would be expected when the rock was normally compacted; it results in a lower rock velocity (Dutta 2002).

When there are hydrocarbons in the system, also the buoyancy pressure plays a role. The **buoyancy pressure** is the excess pressure in a confined reservoir created by the density difference. It is equal the water gradient minus hydrocarbon gradient, that is multiplied by the height of the hydrocarbon column.

7.1.2 Pore pressure prediction

Porosity is in general a measure for the degree of compaction. There is a relation between porosity and effective stress. Stump et al. (1998) have given the following relationship:

$$\phi = \phi_0 \, \mathrm{e}^{-K P_{\mathrm{eff}}}, \tag{7.2}$$

where ϕ is the porosity at a depth z, K is a constant related to the bulk density of the sediment and the density of the pore water, P_{eff} is the effective pressure or stress. The relation can be more complex when also temperature dependant mineral transitions are considered (Dutta 1987):

$$P_{\mathrm{eff}} = P_{\mathrm{eff}\,0} \, \mathrm{e}^{-\varepsilon \beta(T)}, \tag{7.3}$$

where ε is the void ratio and $\beta(T)$ is a function of temperature.

$$\varepsilon = \frac{\phi}{1-\phi}. \tag{7.4}$$

There is also a relation between porosity and sonic transit time, see Wyllie formula's presented in Section 6.4.2. Issler (1992) published a useful relation resembling the Archie equation shown in formula (6.40) above:

$$\Delta t_{\mathrm{sonic}} = \Delta t_{\mathrm{matrix}} (1-\phi)^{-x}. \tag{7.5}$$

The $\Delta t_{\mathrm{matrix}}$ is the transit time in the rock matrix and the x is an acoustic formation factor that depends on the lithology.

Pore pressures can be deduced from the seismic response by studying the interval velocities (Carcione and Cavallini 2002, Dutta 2002). These velocities depend on:

- Porosity.
- Pore structure.
- Fluid saturation.
- Fluid type.
- Pressure and stress regime.
- Temperature.
- Lithology.
- Clay contents.
- Cementation.
- Frequency of wavelet.

Correct prediction of geo-pressures is important, because it helps to demonstrate:

- The presence of an effective seal.
- Delineation of migration path ways.
- The outline of trap configuration.
- It equally allows **balanced-mud drilling** with an optimal **casing scheme** design. It can make or break the economic viability of an HC evacuation project.

If the aim is to predict the geopressures from the seismic data, it is obvious that the velocity field needs to be determined as accurately as possible before drawing any valid conclusions. This means that it is best to use data from pre-stack depth migration, ray tracing and tomographic inversion. Seismic inversion allows often better resolution on the velocity field, but the non-uniqueness of the solution is a drawback (Figure 7.3, Dutta 2002). Visualisation parameters should be fine-tuned to bring out subtle differences in the seismic response that may correspond to pore pressure variations (Figure 7.4). Increasing the pore pressure will lead to an decrease in compressional and shear wave velocities. The drop in P-wave velocity can also be caused by the presence of gas. The S-wave velocity depends mainly on the rigidity of the rock frame. Therefore, the S-wave behaviour is a better indicator for the pore pressure (Wang et al. 2004). Overpressured reservoirs, compared with normally pressured reservoirs at the same depth, are of interest because:

- Higher porosities are preserved.
- Lower bulk densities.
- Lower effective stress.
- Higher temperatures.
- Lower interval velocity.
- Higher Poisson's ratio.

All these factors have an influence on the seismic response and are not independent of each other (Dutta 2002). Geopressures are created by the fact that the fluid movement in the rock is retarded or blocked in a lateral and vertical sense. Their presence says that there is a seal somewhere in the system. The causes for overpressures are various:

- Mechanical compaction dis-equilibrium due to dewatering differences. Rapid sedimentation and subsidence retards or prevents the normal escape of pore fluids from the deposits. Often the fluid flow is hampered by the presence of shaley impermeable layers. The Neogene sticky shales in the Central

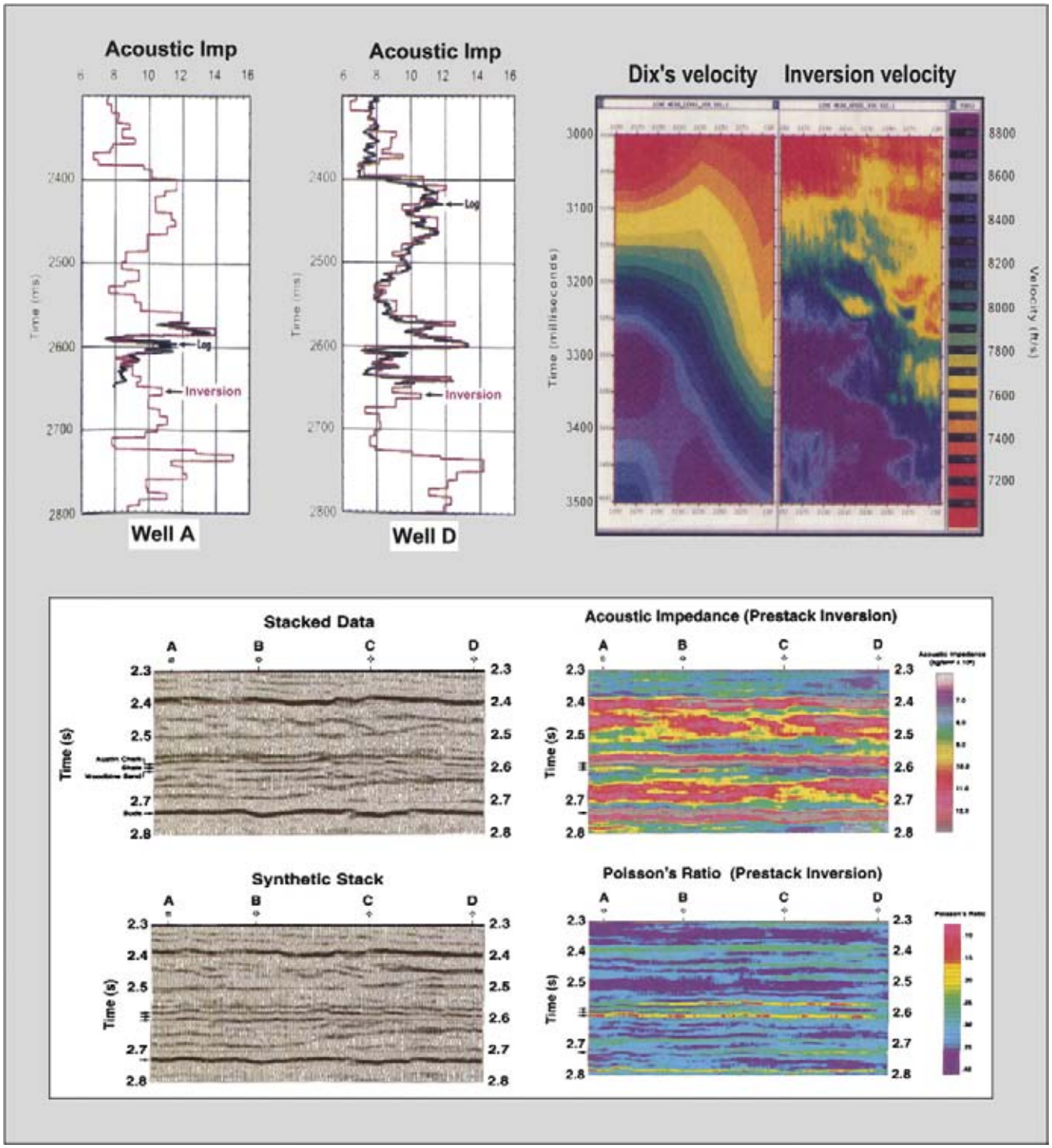

Figure 7.3: Effective stress prediction as inferred from a post stack inversion. The inversion result shows typically a better resolution than the smoothed stacking velocity pattern (modified after Dutta 2002).

North Sea basin are an well known example of this phenomenon (Veeken 1997).

– Clay dehydration and diagenic alteration due to ongoing burial. The alteration of smectite into illite usually occurs at a temperature of 150 to 250 degrees Fahrenheit. This reaction expels some mineral water that has to be drained.

– Dipping or lenticular permeable layers embedded in shales. Higher pressures from below are in connection with shallower levels.

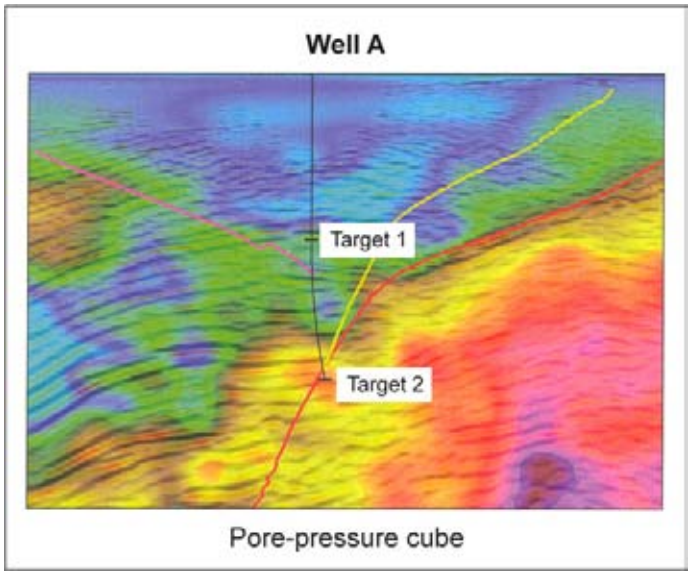

Figure 7.4: Pore pressure prediction for a 3D seismic survey based on the velocity cube. The seismic is co-rendered to illustrate the correspondence with fault compartments (modified after Wang et al. 2004).

- Hydrocarbon maturation and buoyancy effects of the fluids in the pores due to density differences (oil floats on water).
- Tectonic and erosion induced differences.
- Aqua-thermal pressuring due to the fact that the coefficients in thermal expansion are different for the pore fluids and the rock matrix.

If the pore pressure approaches the overburden pressure, than the effective stress is approaching zero and seal failure occurs in the form of creation of tensile (or open) fractures (Dutta 2002). Overpressures will lead to slower seismic P wave velocities.

The pressures are important when calculating the volumetrics of the hydrocarbons reserves in the reservoir. Overpressures can form a substantial drilling hazard when they are not properly predicted in the well proposal (e.g. Gaarenstroom et al. 1993). The pore pressure prediction often uses the vertical effective stress in porous clay rich sediments. This is correct for extensional domains, but in compressional settings (horizontal stress > vertical stress) it is better to use the mean effective stress in the calculations (Goulty 2004). MWD techniques and bit-on-seismic displays allows nowadays to assess the pore pressure whilst drilling, with check shot and velocity data acquired in real time (Esmersoy et al. 2005). Deploying a controlled sound source instead of the drill bit noise with sensors installed on the drill collar has improved the performance of such system considerably.

7.2 Quantitative Assessment

In order to be able to put quantitative figures to the mapped prospects, some additional parameters must be determined for:

- The source rocks.
- Migration and timing HC generation.
- Reservoir rock properties.
- The closure definition.
- Seal properties.

This will ultimately allow the interpreter to arrive at the **expected recoverable reserves** contained within the mapped trap and come up with a ranking for the prospects.

7.2.1 Quantified reservoir and trap parameters

The following parameters/topics are worth considering and should be quantified:

- Porosity distribution. It is difficult to predict in detail, but the geologist can come up with a regional trend (Figure 7.5).
- Permeability distribution. Diagenesis can influence the permeability behaviour dramatically. The Darcylog^{TM} (IFP) can give a good estimation from cutting samples.
- Net-to-gross ratio of the prospective interval.
- Position of spill point. Proper depth conversion is crucial for this.

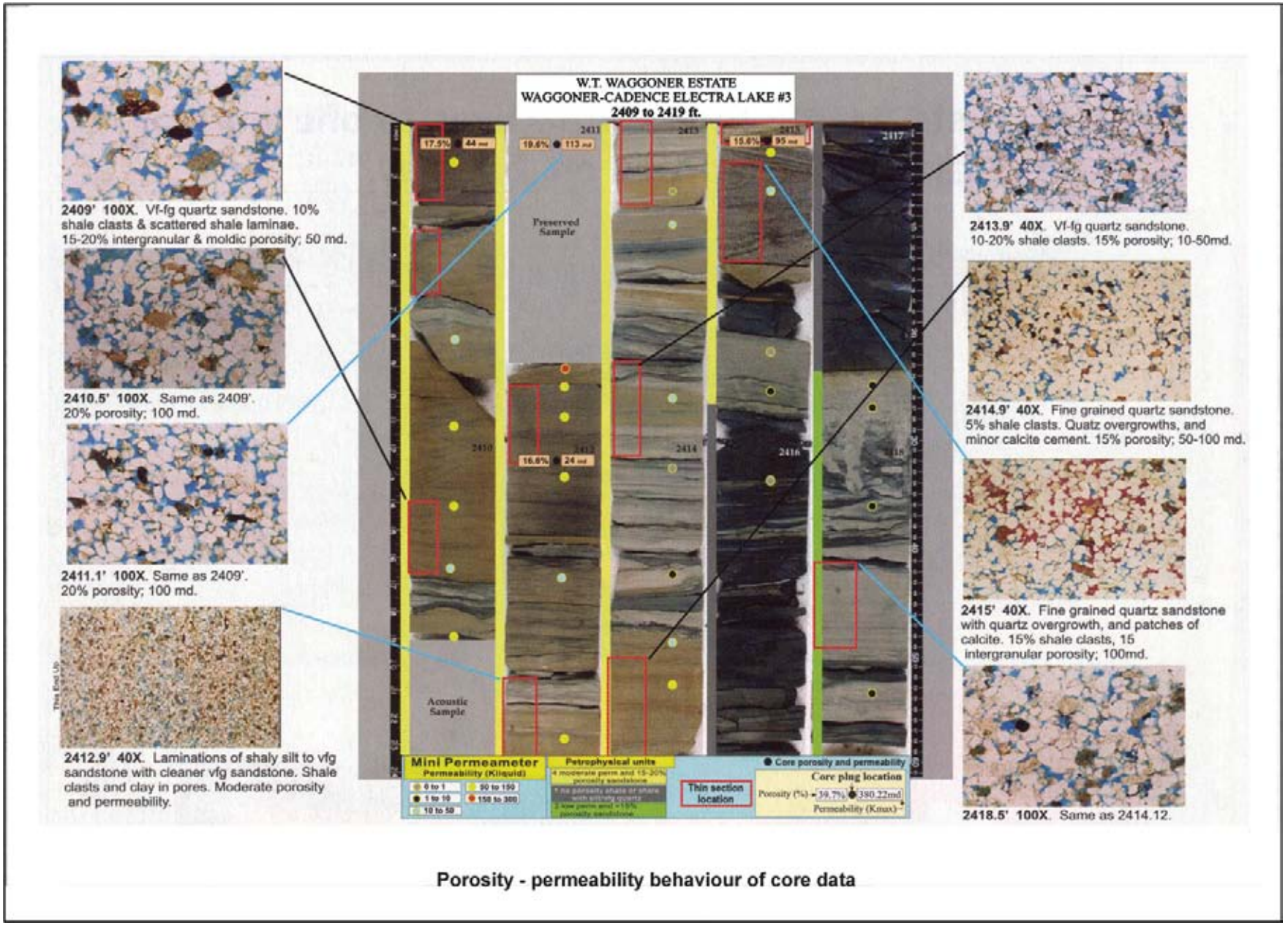

Figure 7.5: Porosity and permeability behaviour illustrated on core data, illustrating the reservoir characteristics of the different layers, with some of them partially oil saturated sands (from Parra et al. 2006).

- Quantity and types of source rock that went through the oil and gas windows.
- Yield of kitchen area.
- Maturation history and recently reached maturity level.
- Migration path reconstruction and oil mixing mechanisms.
- Structural history and trap formation.
- Seismic definition of the closure and its uncertainties. Amplitude characteristics are investigated based on: local change, processing/acquisition parameters, edge effects, rock physical changes, primary AVO effects, AVO attributes, amplitude anomalies (DHI's), vertical and lateral context, seismic analogues and modelling feedback (cf Roden et al. 2005).
- Estimate of the hydrocarbon column height (a.o. Sylta and Krokstad 2003).
- Hydrocarbon saturation and behaviour of the so-called "**J-saturation curve**" (HC saturation curve in the reservoir at the HC transition zone).
- Oil/gas ratio range.
- Condensate/gas ratio range.
- Contamination with other constituents like CO_2, H_2S etc.
- **Wet-ability factor** of the mineral grains.
- Connection to an **aquifer** and presence of water-drive in the reservoir caused by pressure differentials.
- Presence of dynamic flow in the reservoir. This can be difficult to prove. It leads to an irregular oil-water contact and makes production forecasting difficult.
- **Skin factor**, which is a measure for the partial blocking up of the pore throats around the well borehole wall. The factor depends on the thickness and effective permeability of the skin zone. Diagenetic processes and mud invasion are responsible for the precipitation of scales (dissolved solids) around the borehole wall. The skin factor can be estimated from drawdown tests with a constant bottomhole pressure (Kutasov and Eppelbaum 2005). Drilling with an **inert gas (nitrogen)** can be considered to counter to mud invasion and building up of scales. The conventional drilling mud always creates an invaded zone in the host rock. Presence of a thick mud-cake may prevent good flow from the formation into the well.
- Recovery factor; **enhanced recovery** (e.g. gas or steam injection, chemical treatment, foaming) is very interesting to extend the production of an existing field (Dronkert and Weber 1998).
- Degree of sub-seismic micro-fracturing (Weber 1999).
- Degree of compartmentalisation (Figure 7.6).
- Degree of reservoir heterogeneity (Figure 7.7).
- Compression or **expansion factor**. Pressure estimation from seismic as described above is a possibility.
- Predict realistic well production figures by evaluating other well test results and production figures.
- Risk of early **water break through** and presence of thieve sands. Most production systems can only handle a limited amount of production water (Figure 7.8).
- Validation of possible seismic DHI's and results of "Lateral Prediction" and reservoir characterisation studies.
- **Well stimulation** expectation (acidisation, frac job, proppant injection). Hydraulic fracturing (Figure 7.9) may stimulate the production and repair some of the formation damage caused by overbalanced drilling (cf Berumen et al. 2004). Even geothermal projects are needing well stimulation as is shown in Figure 7.10 (Holl et al. 2004). This means substantial input from reservoir engineers and other geoscientists in order to boost the steam production. Heat exchange should be as efficient as possible in terms of time, temperature difference and volumetric output. Subtle diagenetic processes often try to block the pores and this should be prevented.

Other elements of hydrocarbon plays are needed to further appraise the prospect and to calculate the amounts of **hydrocarbons in place** (Figure 7.11). The **gross rock volume** is computed for the last closed contour of the structure map or by assuming a given hydrocarbon column. This gross rock volume number is multiplied by the **net/gross** reservoir ratio and a porosity factor to attain the **total volume of pore space**. The pore space is filled with hydrocarbons and/or water. The pore space volume is multiplied by the **hydrocarbon saturation factor** to obtain the volume of oil and/or gas in place. Assuming a **recovery factor** and an **expansion factor** allows to estimate the total amount of producible hydrocarbon reserves in the trap or prospect. A **prospect appraisal** procedure is performed with statistical analysis and simulations, to incorporate uncertainties in the ranking exercise of the prospects.

In some carbonate reservoirs the initial recovery factor is extremely low. In the Rainbow pool in NW Alberta

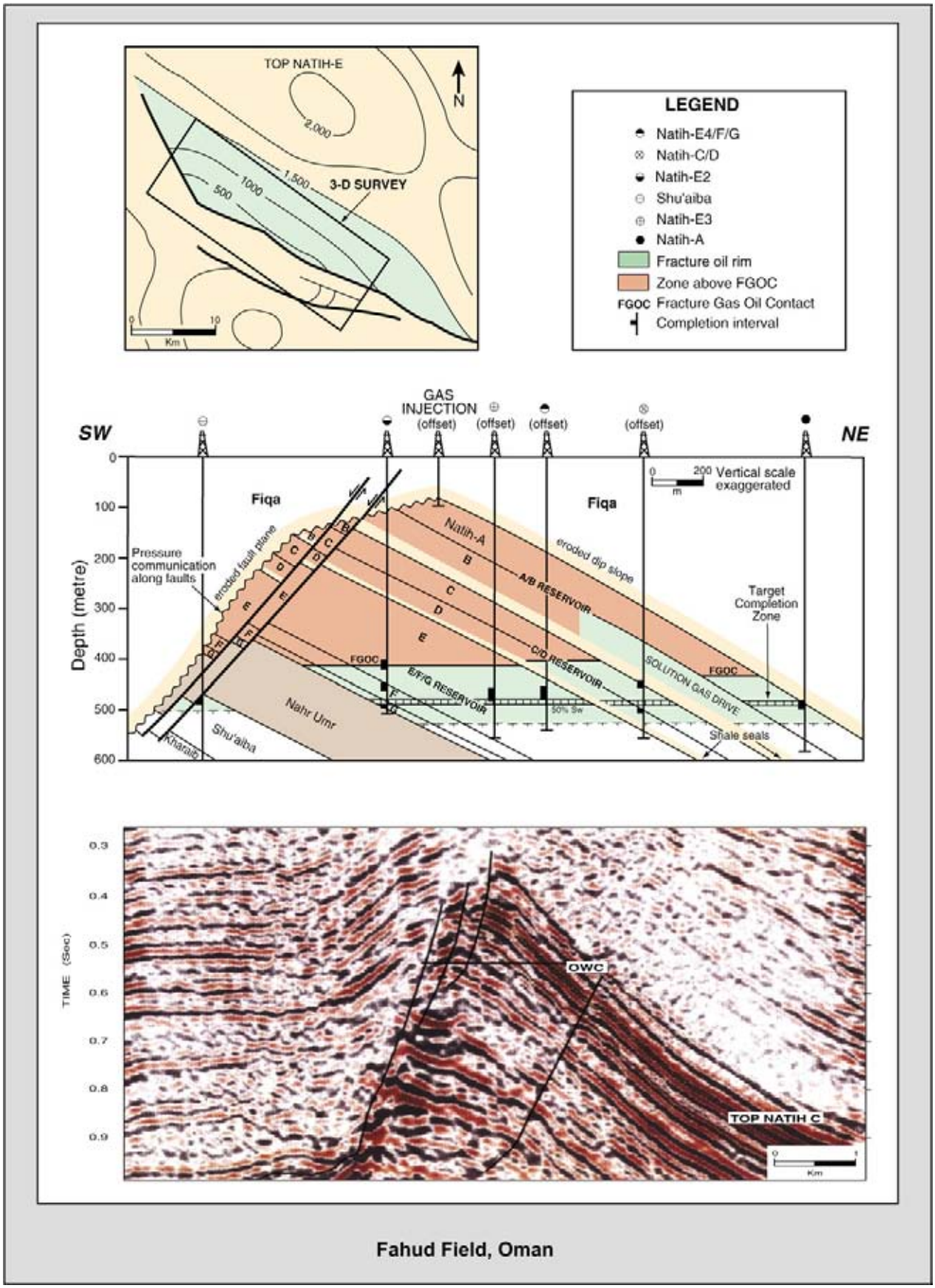

Figure 7.6: The oil recovery of a field is enhanced by gas injection to maintain the flowing pressure. An intra formational seal is put in evidence between the Natih A and Natih B reservoir units and different compartments are present (Onderwaater et al. 1996).

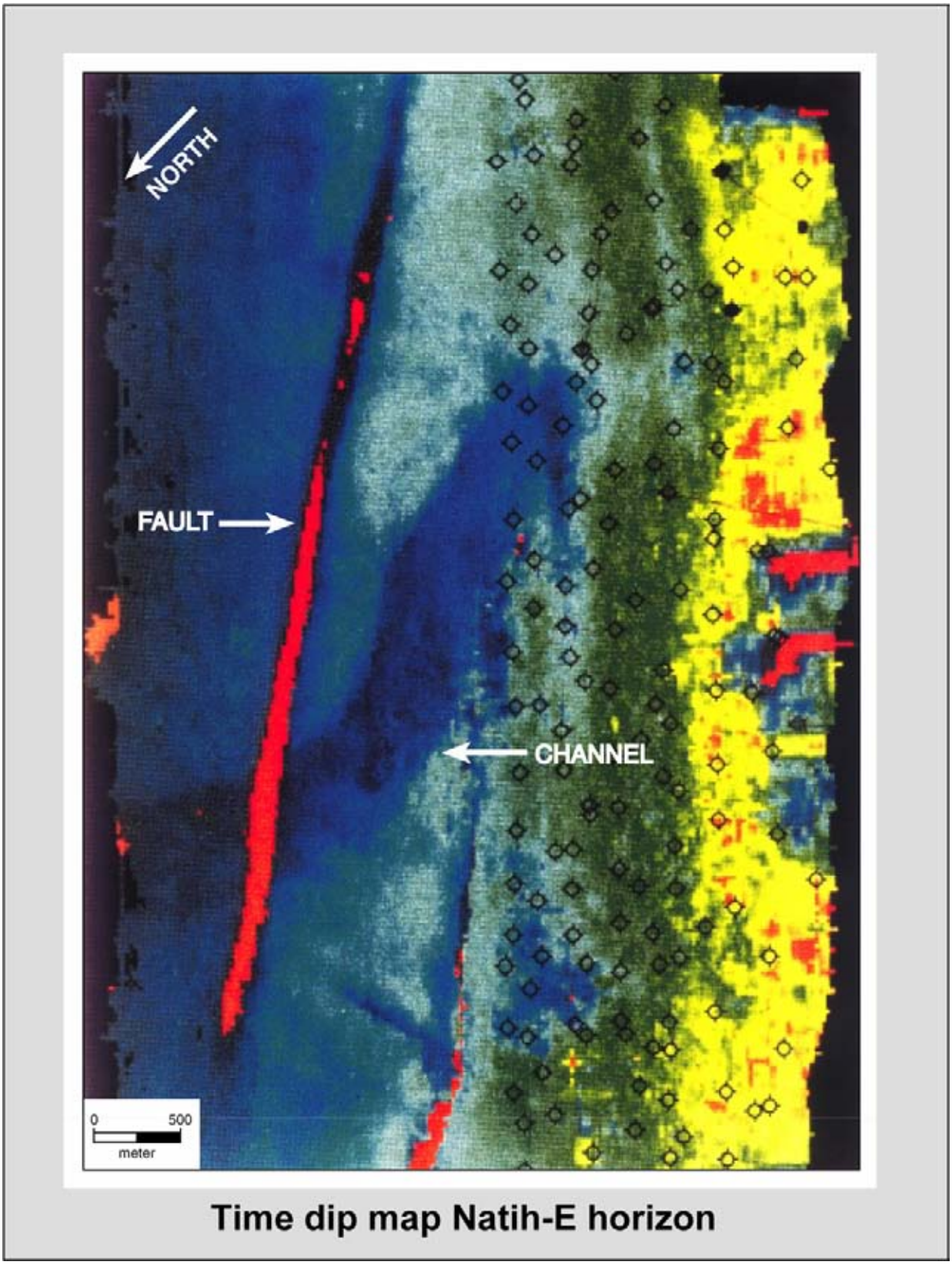

Figure 7.7: The time dip map of the Natih E horizon in the Fahud field shows the presence of reservoir heterogeneities. A meandering channel is put in evidence by this attribute display. It explains the distinct production behaviour for the various wells and the measured differences in fluid levels. Note the large number of production wells to drain the field (Onderwaater et al. 1996).

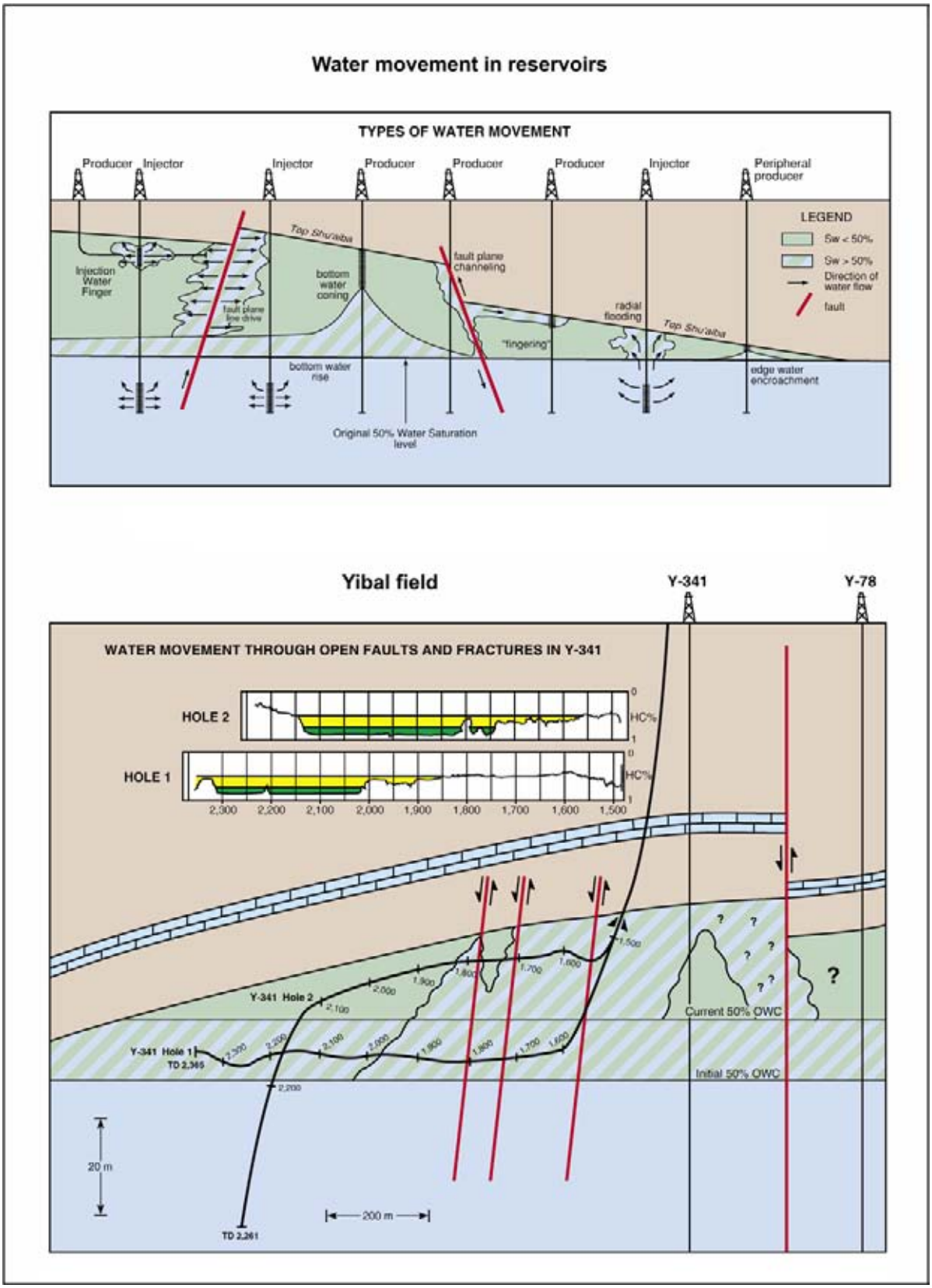

Figure 7.8: Water movement in reservoirs during production can lead to early water break through. These brines are difficult to handle at the well head. Avoiding fracture zones can be a big money saver. Waterdrive during production can be useful to maintain the flowing pressure (Al Busaidi 1997).

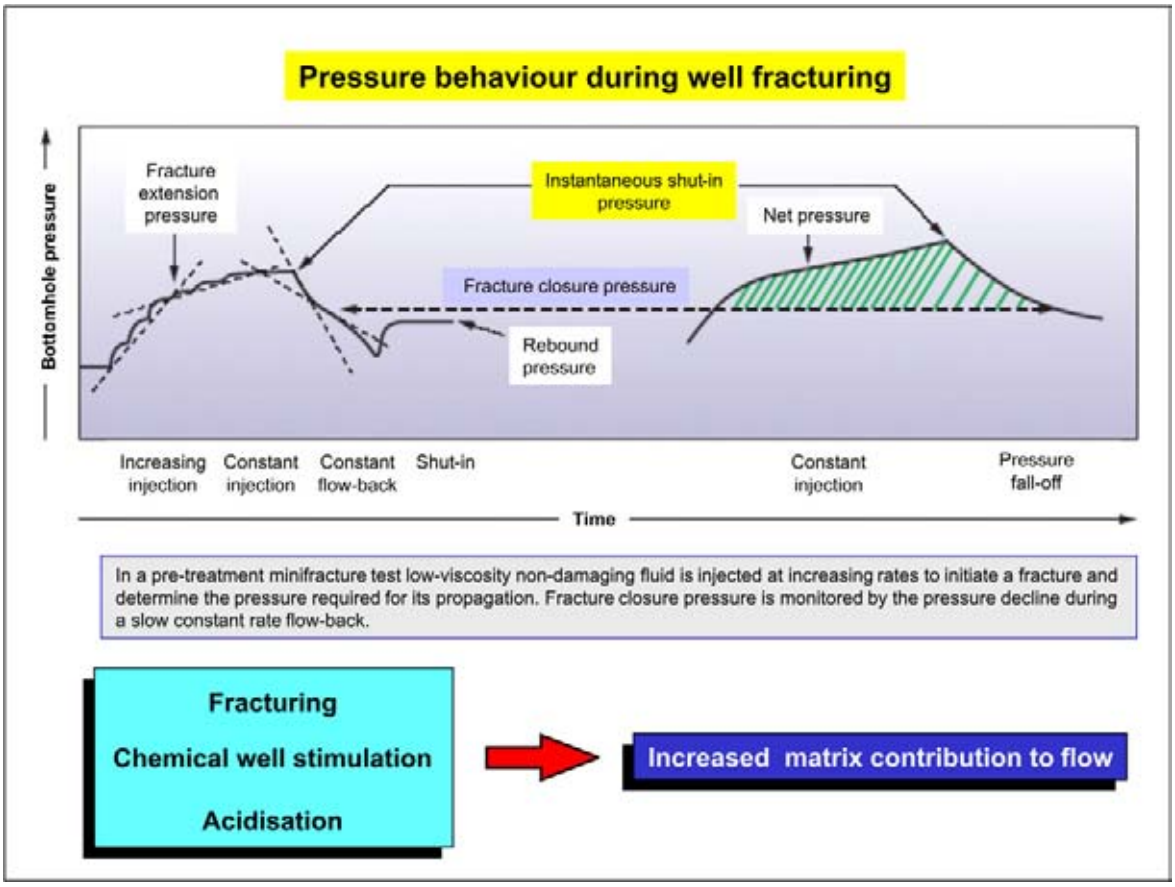

Figure 7.9: A "mini-frac" is often prepared to test the formation strength. The well can also be stimulated by an acidisation job that hopefully improves the permeability and increases the flow from the reservoir in the direct vicinity of the borehole. The matrix contribution is thus boosted (modified after Ali et al. 2002; used with permission of copyright holder Schlumberger).

for instance it was only 1.6 percent and this was boosted by enhanced recovery techniques to 36.5 percent. This was achieved by injection of solvent in the top of the reservoir via 11 injector wells and subsequently gas was inserted to push the solvent down. Time lapse seismics can reveal differences in seismic response that are induced by the production. Before a comparison is made between the base-case and monitor surveys, it is important that the datasets are "matched" in terms of geometry, time, phase, frequency contents. Time delays, amplitude and impedance changes are then analysed, while hopefully the pressure and temperature regime stayed the same. Interestingly enough the effect is also dependant on the shape of the pores (pore aspect ratio) in the carbonate rock (Ng et al. 2005). The Gassmann equation underpredicts the velocity effect in the carbonates and hence the seismic changes are larger than expected in vuggy fractured limestone reservoirs.

7.2.2 Shared earth model

Automated reservoir framework building and modelling bring together the geology, geophysics, petrophysics and reservoir engineering aspects of the evaluation (Chambers and Brown 2003). Reservoir models only can mimic the reservoir's true complexity, they can never fully represent the actual subsurface heterogeneity. A great challenge lies in the use of all data simultaneously and not sequentially as has been often done in the past, taking into account the various scales, mutual redundancy and degree of accuracy (Caers et al. 2006). Integration of inversion results in the stochastic reservoir model is often useful (e.g. Diet et al. 2002). **Reservoir simulation** and **geo-cellular modelling** are important for understanding the fluid flow behaviour of the rocks under investigation.

A robust and consistent set of facies definitions are of prime importance when building a 3D geomodel (Rivenaess et al. 2005). The conventional approach is to build a deterministic rigid structural model and populate it with stochastical petrophysical parameters via variogram based Gaussian simulation. Adding structural uncertainty will improve the results, but is more time consuming. The aim is to establish a realistic reservoir model that matches all static and dynamic information. Production history matching and material balancing is

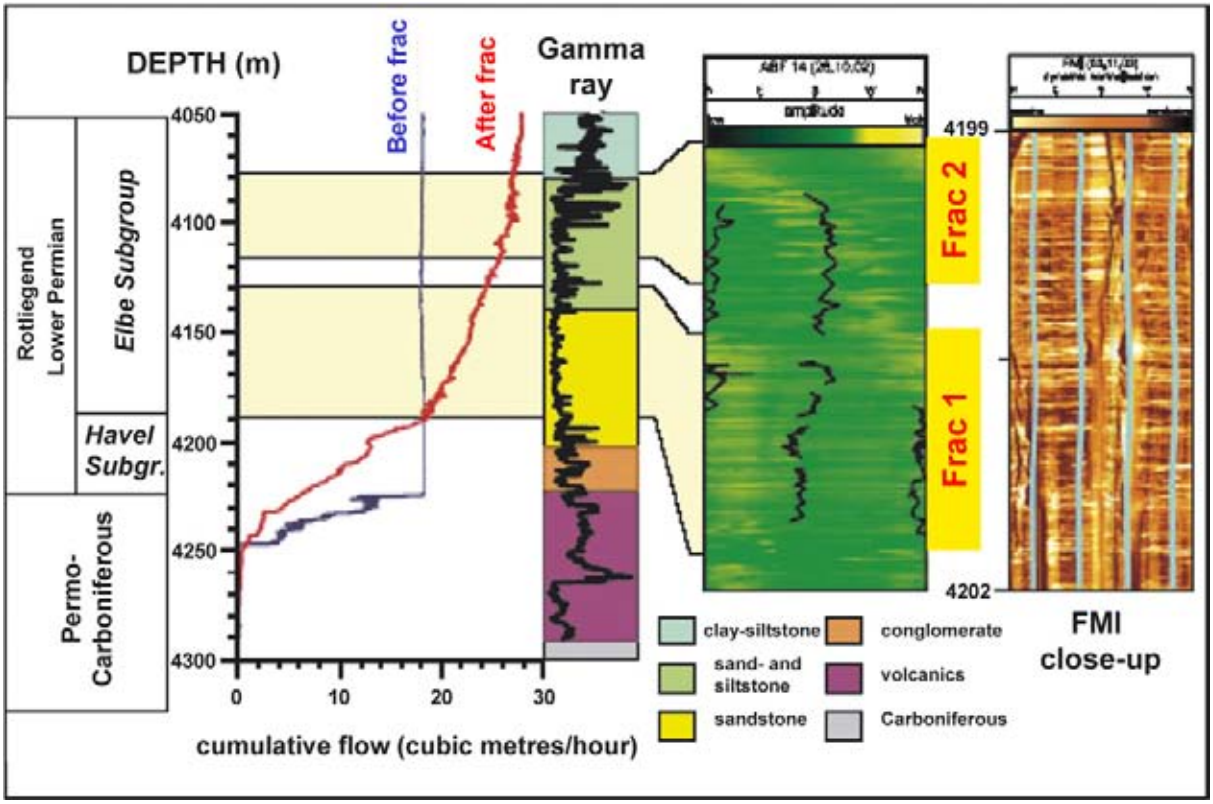

Figure 7.10: The geothermal production well Gross Schoenbeck 30/9. Stratigraphy and lithology of the hydraulically fractured sections in the open-hole interval include a comparison of flow meter logs (first PI = 1.1 $m^3\,h^{-1}\,MPa^{-1}$ and second production test PI = 2.2 $m^3\,h^{-1}\,MPa^{-1}$). The ABF14- and FMI-images illustrate the conductive fractures parallel to S_H. These images are scrutinized for breakouts and vertical fractures that indicate the direction of the present-day local stress. The mean direction found for the maximum horizontal stress (SH) is $18.5 \pm 3.7°$ to NNE. If the directions of the stress components are known at a location, it is possible to predict the direction of opening and expanding fractures stimulated hydraulically (after Holl et al. 2004).

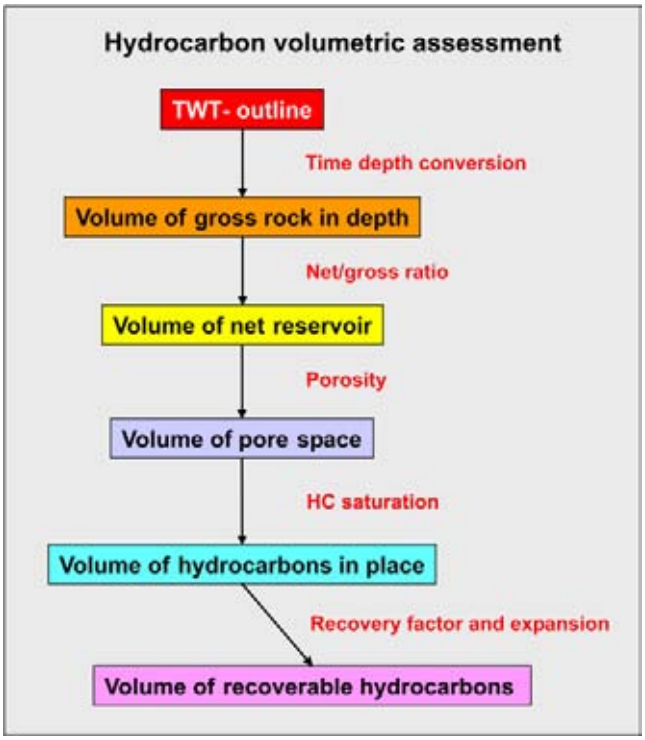

Figure 7.11: Volumetric calculations for the total amount of recoverable hydrocarbons. Huge quantities of hydrocarbons are thought present below existing oil fields at deeper layers, with excellent prospectivity and often not yet targeted in the previous exploration campaign. Increase of the recovery factor by a few percent represents an other possibility to get access to substantial additional proven reserves. Deep water prospects have only poorly been explored. New development techniques help to make these frontier areas attractive.

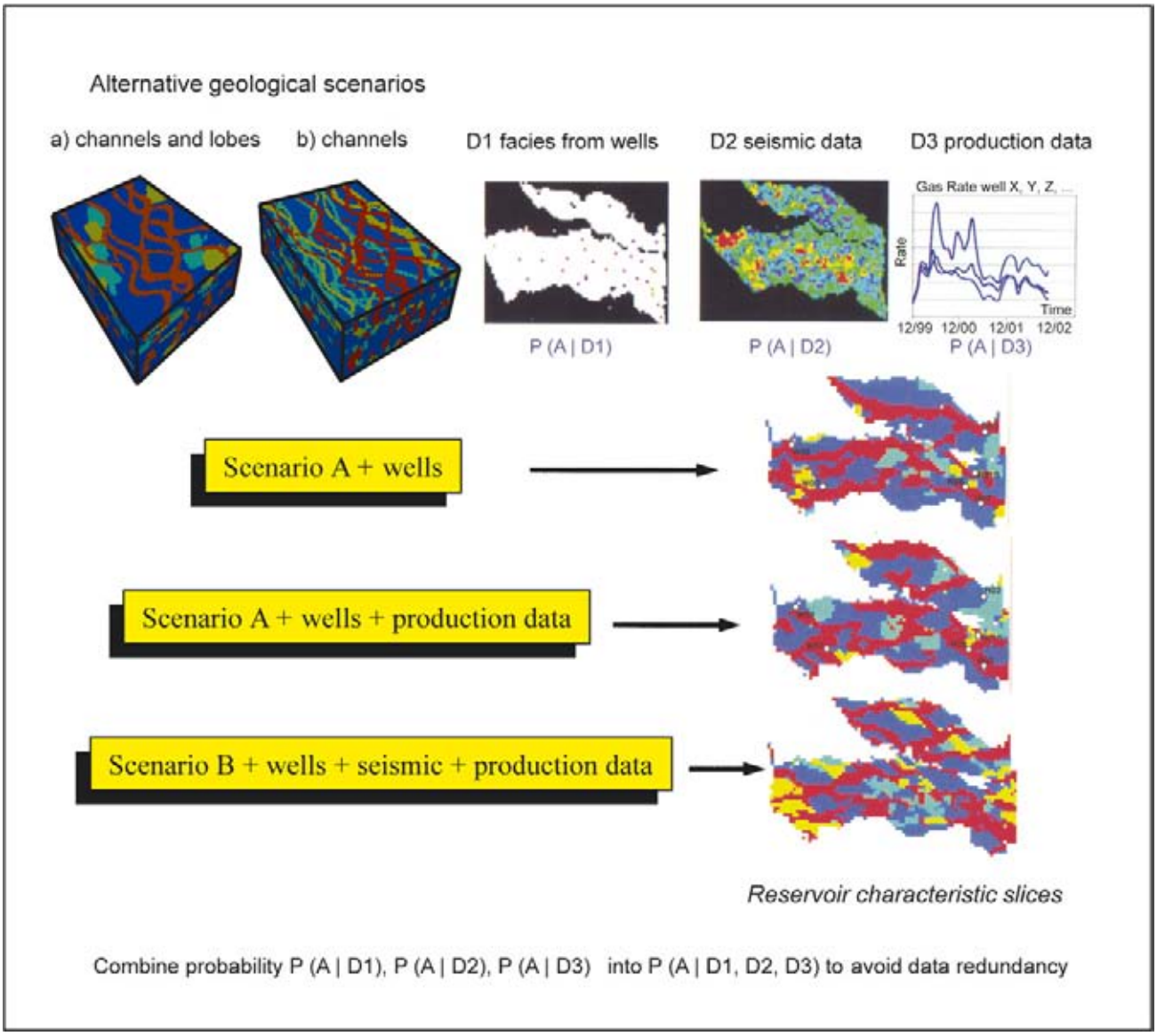

Figure 7.12: Probabilistic modelling of the reservoir characteristics leads to better prediction when the updating of the earth model considers the various data input parameters simultaneously. Simplistic history matching by introducing specific pipe shaped corridors around wells should be avoided. The data redundancy issue should be properly incorporated in the modelling (modified after Caers et al. 2006).

not a unique process. There might be several reservoir models that equally well explain the observed trend.

Combining static and dynamic data is a powerful means to establish a valid reservoir simulation model (Du and Guan 2005). Usually the permeability is simply adjusted or transmission multipliers are applied to change the flow in areas with an observed mismatch between production data and the model. A box or pipe shape adjustment around the well location is often adopted, but such procedure does not change the model in a geological realistic way. Simultaneous updating of geologic, structural and reservoir engineering data is needed with application of a rigorous probabilistic approach in order to circumvent these problems (cf Caers et al. 2006; Figure 7.12).

Time-lapse seismics provides a valuable 3D dynamic control in addition to the spatially limited well data (cf Oldenziel 2003, Weisenborn and Hague 2005). There is even benefit by using converted wave PS energy in the detailed analysis (Al Naamani and MacBeth 2003). Proper upscaling of the models is always a critical issue. Static models with a hundred million of cells is no longer an exception. Upscaling is an averaging procedure and hereby the role of extremes in the models

is nearly always reduced. These extremes have however a major impact on the modelling result, e.g. highly permeable layers/zones that serve as channels and conduits for bypassing the matrix or low permeability zones form barriers to flow. Integrated software packages from Landmark^{TM} or Irap RMS^{TM} have now streamlined workflows available for this purpose. It allows numerous equi-probable scenarios to be evaluated in the simulation processing (10 to 100's of cases, Gorell et al. 2005). Intelligent upscaling preserves the details where needed. Manipulation of variable grid and cell sizes asks a certain flexibility of the software packages.

Data mining and iterative interpretation are an efficient way to map the reservoir behaviour and well performance. Cluster based 3D visualisation techniques remove size limitations on the data manipulations and open up new ways of looking at data sets (Hodgson et al. 2005). The post stack cube may take up to 60 Giga of disk space, while the prestack dataset is in the order of 30 Terabytes. Efficient data management permits significantly improved QC-ing in all processing and interpretation stages. Mono- and multi-variate statistical analysis may be utilised to generate classifications for outlining compartments. Total developed for this purpose their Welfare^{TM} method, but it does not yet include grid oriented history matching (Mouret et al. 2005).

A neural network seismic trace classification can be run to delineate the geographical position of compartment boundaries in the reservoir interval (Balz et al. 1999). A feedback loop in reservoir management certainly helps to optimise the hydrocarbon production from existing fields. Measurement and control techniques with various mathematical options can nowadays be applied (linear and non-linear), combined with sophisticated data assimilation procedures that are developed for meteorological purposes (Jansen et al. 2005).

The **shared earth model** is a new concept that decreases engineering lead times considerably (Hardy 2004). It is a subsurface earth model that incorporates all observed and interpreted data. Simulations (like Schlumberger's Eclipse^{TM}) with multiple-scenario reservoir models are fully exploited in this approach. Volumetrics and fluid flow are evaluated, whereby the static and dynamic models are combined. Integrated reservoir studies are essential for the proper understanding of the reservoir development (cf Cosentino 2001). Parallel workflows in various reservoir studies reduce the overall project preparation time and are stimulating the cooperation between geoscientists. The tendency to work in **asset teams** is favouring the cross fertilisation process between the various geoscience disciplines. Integrated packages like εpos^{TM} of Paradigm are great for this purpose as it provides dedicated software for data manipulation along the totality of the geophysical geoscience value chain. The multi-disciplinary working method does create the need for good communication and simple conceptual models, whereby the amount of jargon is kept in proportion to the aim. Fragmented workflows caused by disciplinary segregation is one of the big obstacles to real progress (Berkhout 2005).

Of course it is of prime importance to check the reliability of the petrophysical input parameters and verify the trustworthiness of the well log measurements. This essential Quality Control step should not be taken light-heartedly. These log parameters are used to determine reservoir quality and porefill characteristics in the bore hole. Automated interpretation of logs sometimes gives misleading results, especially when the logs have not been calibrated properly. **Radioactive shale cut-offs** on the gamma ray log for instance, using a wrong clay mineral assembly (e.g. chlorite vs kaolinite), will lead to erroneous clay content readings and this has a severe impact on the reservoir calculations. It influences the saturation computations negatively. The unrecognised presence of pyrite in a layer will for example result in wrong shale volume estimations. This all has a major impact on the field development plans and economics of the HC project. It is important to get the petrophysical input right, even if it takes a somewhat heated discussion with the odd hard-headed geo-technician involved in the multi-disciplinary reservoir development study. Certainly there is something to say for keeping things simple, but one should not be afraid to introduce complexities when the measurements indicate a less simplistic reality. It means more work but in the end it will be cost saving.

7.2.3 Additional factors

Multiple drilling targets in prospects do increase the attractiveness of a exploration structure. Multi-lateral completion schemes allow several intervals to be produced with co-mingled flow and may reduce the overall capital expenditure considerably.

Sometimes these HC plays are mutually exclusive. For instance in case of a seal breach, the hydrocarbons migrate into the overlying trap and are no longer retained by the reservoir/seal pair below. This scenario has to be taken into account in the prospect appraisal.

The faults may be partially transmissive, i.e. only the lighter part of the hydrocarbons may migrate further

up-dip and thus it results in fractioning of the hydrocarbons along the migration path (e.g. dry gas the Pliocene Kafr El Sheikh FM and wet gas in the Miocene Abu Madi FM in Egypt). Moreover, a fault can be a migration pathway and in other times represent an effective seal, thus being an intermittent permeability barrier.

The pressures at greater depths are increased and therefore more hydrocarbons are retained in smaller size structures. Porosity and permeability normally decrease with ongoing compaction and diagenesis. Cut-off values for the recovery of hydrocarbons in gas containing reservoir are usually less then for oil reservoirs. Gas can move through much smaller pore throats. This makes the need for a differentiation in evaluation strategy evident.

Recovery factors of 35 to 45% in oil fields are often proposed by the reservoir engineers. In a way they prefer to play it safe rather than putting their reputation at stake. Such a prudent attitude has tremendous influence on the field development plan and the profitability of the proposed projects. Traditionally there is a change in carried reserves when a field is handed over from the exploration to the production department. The creation of asset teams in a matrix type of approach helps to avoid this type of evaluation discrepancy. For the development of the giant Kashagan field in the northern Caspian Sea a recovery factor of 33 percent is actually used. The field is estimated to contain 39 billion barrels and 13 billion are expected to be produced according to Shell. For the same field Pitcher (2004) only carries 7 billion barrels and he estimates the nearby super giant Tengiz field also around 6 to 9 billion barrels recoverable. It illustrates how numbers can fluctuate easily. The Kashagan field, discovered in the year 2000, is thought to be the 5th largest oil field in the world. Faulting and fracturing will make the production from the field for the operator of the consortium (Eni-Agip) not very easy and those problems are added to an average reservoir depth of over 4000 metres. Production is expected to peak in 2016 by 1.2 million barrels per day with 150 million metres cube of associated gas. The total capital investment for the project is estimated 29 billion US dollars (Shell Venster, No. 02, 2004).

The low recovery rate illustrates that it is very attractive to find ways to boost HC production from existing fields by **secondary recovery** techniques. A few percent more production represents already a considerable amount of money and the risks are very limited compared to chasing new discoveries. It is therefore well worthwhile to invest in more advanced recuperation techniques, like **steam injection** to improve the viscosity behaviour or **gas injection** to maintain reservoir pressure. **Nitrogen under-balanced drilling** (inert gas) is also a new attractive option in this respect. It better preserves the original virgin reservoir characteristics and does less harm to the fluid flow in the formation around the well borehole. There is a difference for a well flowing 1.2 million cubic feet of gas per day or 25 million. Careful monitoring of the pressure pays off by having optimised well designs with a higher sustainable production rate. A lot of potential cost saving can be gained in this domain.

If no well data is available, then basic assumptions have to be made to evaluate the potential of the mapped structures. And this directly translates in an additional risk attached to the outcome of the volumetric calculations and the prospect ranking exercise.

7.2.4 Safety issue

It is obvious that all operations should be conducted in a safe way. No harm should be done to people nor the environment. Safety is ever so important because the industry is dealing with highly explosive and toxic materials. The material costs, loss of human lives and damage to the environment are potentially tremendously expensive cost items. The scale of the operation makes prevention a key issue. Hence there is a rationale behind the drive to safer working practices. Leadership and partnership are essential to obtain outstanding results in the safety record (Brinded 2005). Some critical factors for success are (IAGC 2005):

- Genuine commitment by managers and employees (top-down/down-up).
- Strong workforce involvement.
- Non-bureaucratic approach.
- Common statistical reporting.
- Sharing best practices and learning points.
- Standardisation of procedures and equipment.
- Openness and constructive cooperation with contractors.

The **Lost Time Incident** frequency (LTI) has fallen worldwide since the nineties. In the Shell Exploration and Production it went from 2.2 in 1991 to 0.6 in 2003. The LTI frequency is defined by incident rate per million hours worked. Generally there is a relation between the LTI frequency and the number of fatal accidents. The more small incidents or near misses occur, the higher will be the chance of a mortal accident to happen (pyramid shape). The fatal accident rate is defined per 100 million hours worked. For the year 2003 it was probably globally between 5 to 25 within the petroleum industry.

The discrepancy between perceived cause of an accident and what really happened is important to bridge. Managers should not base their actions on how they think the system should work, but it is better to investigate how it really came about and act accordingly. Too many restrictive rules and procedures can hamper the overall business objectives. A balanced view with realistic guidelines for the standard working practice is needed. Only then the system will be convincing for the people on the workfloor. There are three fields of immediate interest to the safety aspect:

- Best engineering solution with an improved design.
- The processes and systems that dictate how the work is done.
- Individual behaviour.

Prescriptive regulation and company design standards may lead to a very complex situation that form a barrier for the industrial performance. Simplicity and clarity of the rules are therefore essential for maintaining a workable environment. This can be achieved by regular challenging the safety regulations on their usefulness. People should have the right to intervene when they observe an unsafe situation and ask the responsible persons to correct the guidelines/procedures. In most oil companies it is not only a right, but in fact an obligation, that has become integral part of the job description.

7.3 Hydrocarbon Development and the Global Economy

To fully assess the **hydrocarbon potential** of an area, all above mentioned topics should be addressed. Infrastructural requirements, environmental issues and the long-term market conditions have to be taken into account when deciding on the viability of projects. Realistic **financial planning** of the investments forms integral part of the strategy to evaluate the prospects. This implies using "**Money-of-the-Day**" and **Net Present Value** (NPV) concepts that discounts for the **inflation effect** (Figure 7.13). Unnecessary upfront financial investment does mean that capital is tied up in a project without financial profits being generated and a negative rate of return is the result. Too lean planning makes that production opportunities are missed. A proper balance between these two scenarios is the best basis to optimise business results.

Shell used in the nineties a cut-off of 14 percent for the **net profit** on new projects linked to an oil price of 14 US dollar per barrel. They adopted a conservative 20 US dollar oil price in 2004. Asking a too high a **rate of return** on invested money is of course bad for the growth of the business, because a lot of projects are written off before they even can start. Using a too low oil price has a negative effect on the start-up of new projects and deprives the industry of potential money spinners. Cost cutting improves the near-term profitability but on the other side it may well reduce the longer-term growth perspectives of the companies (Arnott 2003). Smaller companies deploy other **business criteria** and this is one of the reasons for their existence. The petroleum business is traditionally divided in a upstream and downstream branch. **Upstream** is everything bringing the hydrocarbons to the refinery and **downstream** is transport, refining and delivery of the products to the customer. Seventy percent of the industrial expenditure was spent in the upstream business in 2001 (Arnott 2003).

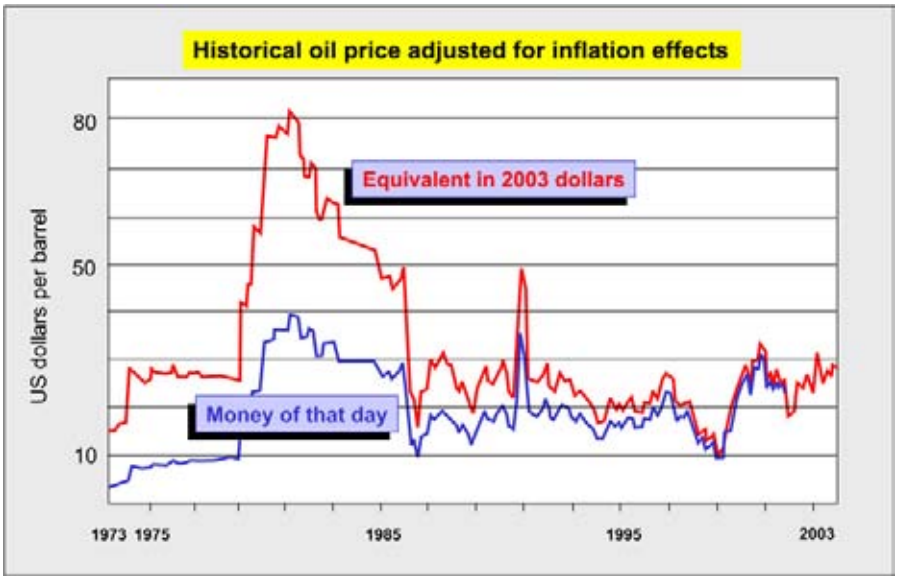

Figure 7.13: The Money-of-the-Day concept is illustrated in this oil price plot where the influence of inflation is clearly shown. The historical oil price per barrel is expressed in the value of the year 2003 US dollar and discounted for the amount of estimated global inflation (modified after De Margerie 2004).

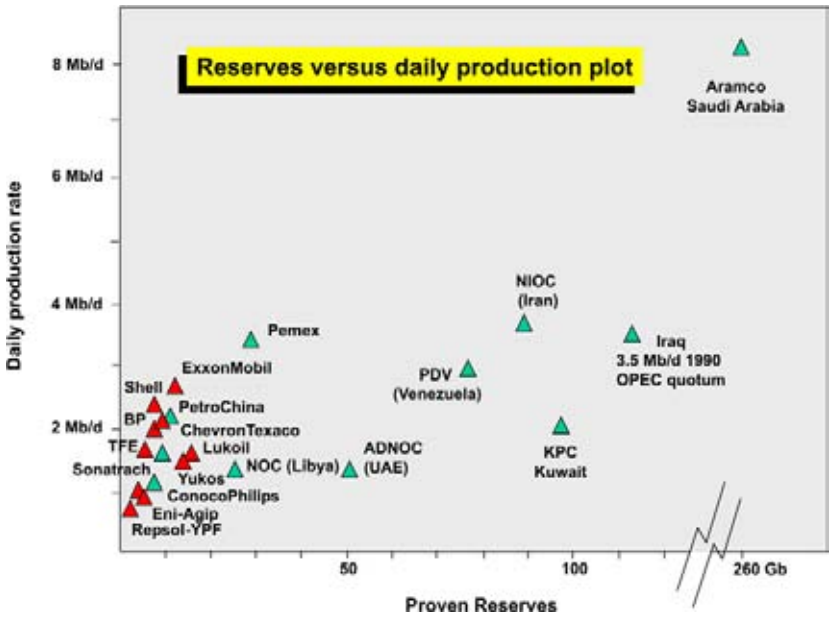

Figure 7.14: Oil companies plotted according to their daily production rate and proven reserves portfolio. Note that the Saudi-Aramco company plots outside the proper scale of the graph. It really is an order of magnitude bigger than the rest. The Seven Sisters (seven biggest multinational private oil companies) have lost their dominant position before the turn of the last century and it makes that the oil game has changed considerably. Yukos will probably be integrated in state-owned Gazprom and has been dissolved due to a tax evasion issue (modified after De Margerie 2004).

Profitability is an important aspect of the petroleum business. The last few years Shell has made 19.5 percent net profit at an average oil price of 28 US dollar. The total of their net profit in 2003 did amount to 13 billion US dollar, compared to 21 billion US dollar for Exxon/Mobil (De Wit 2004). Their yearly estimated investment of capital amounts to 14.2 billion US dollar worldwide. Exploration and production investment rose from 4.9 in 2001 to 7.4 billion US dollars in the year 2003. Their daily production was 2.4 million barrels per day on a **worldwide production** of 75 million barrels per day (= 1.2 billion litre). Their daily gas production did amount to 1.7 million oil equivalent barrels. Shell's oil share was then about 3% of the world's total (Shell Venster, Feb 2002). Their total invested money in 2002 was some 89 billion US dollars and they managed to get a **rate of return** of 23% on the invested capital. The **inflation rate** was around 3 percent for that period of time and the interest paid by banks in the eurozone was approximately 4 percent. The net rate of return on invested capital was therefore quite considerable. In 2004, the net profit increased to an exceptional 18.5 billion dollars and the cashflow was estimated 34.9 billion with a net rate of return on invested money of 20 percent, while in 2003 that was only 15.5 percent (Shell Venster No. 02, 2005, p. 13). The OPEC countries also had a very good year in 2004 with 324 billion US dollars of sales, up by 32 percent compared to 2003. A third of that money went to Saudi-Arabia. The eleven OPEC countries are: Saudi-Arabia, Nigeria, Iran, Kuwait, United Emirates, Venezuela, Libya, Iraq, Algeria, Qatar, Indonesia. In 2005 the OPEC sales were further increased to 435 billion dollars. Hydrocarbon exporting countries in total had an estimated savings of 400 billion dollars in the year 2004 alone at an average oil price of 40 dollar per barrel. And in 2005 and 2006 it only got better.

Some state-owned oil companies – like Saudi Aramco – have an important **production share** portfolio. Exploration and production are paid back by the government in a percentage of the HC production generated from the development project. Hence exposure and the initial government investment is kept at a bare minimum, with the risks taken by the foreign investor. The benefits can still be very lucrative for the latter. A listing of the first five major oil companies, compiled by Petroleum Intelligence Weekly in 2004, shows Saudi Aramco in first position, followed by ExxonMobil, Petroleos de Venezuela, the National Iranian Oil Company and Koninklijke/Shell Group. This list is based on criteria like: reserves, production of oil and gas, refining capacity and product sales. The ranking depends on the criteria used, as is shown by the reserve and daily production plot (Figure 7.14).

The world oil resources are limited and therefore the oil production is expected to peak somewhere early in the beginning of this century. Production is estimated by some people to reach its peak already around the year 2009 (Deffeyes 2001). This extrapolation is based on the recent consumer trends. Let's not forget that some persons have a keen interest for the general public to be worried about a shortage in HC supply. It will help to keep the pricing at a comfortable high level. With less pessimistic views it may occur around the year 2015–20 or even somewhat later. This HC production peak is known as **Hubbert's Peak** followed by a

long decline, characterised by an undulating plateau according to CERA (First Break, Vol. 24, No. 1, p. 23). The sustainable production rate is important to consider, it is more significant than the amount of total oil reserves. **Energy conservation** may be a very effective way in postponing the Hubbert's production peak. The end of the oil production will probably not be caused by the lack in natural resources, but an unexpected shift in consumer behaviour may well bring about the early termination of the petroleum era. The "stone age" also did not end by a sudden scarcity in stones (cf Simmons 2005).

7.3.1 Energy cost structure comparison

The **world energy market** is rather volatile, with the fossil fuels forming an important share of 88 percent. **Renewable energy sources**, like wind and solar power, are expected to grow substantially in the coming years, but still lag behind in the overall picture (Figure 7.15). Wind energy is not yet competitive with nuclear energy, its costs are about double. But it is plausible that the nuclear price is kept artificially low because not all environmental items have been estimated at their real costs (dismantling and waste storage are problematic issues). Disasters, like the nuclear explosion at the Chernobyl powerplant in the Ukraine in 1986, do occur although the statistical frequency of such an event is extremely low. Up to the year 2004 25,000 people died directly in connection to this nuclear meltdown (RL of 27th April 2004). The amount of released radiation was equivalent to 200 Hiroshima atom bombs. Officially only 31 dead have been registered by the Soviet government. 40,000 people are affected in their health as a result of the nuclear explosion. An area of 150,000 km^2 is contaminated, that is comparable to half the size of Italy. The costs of these effects should have been incorporated

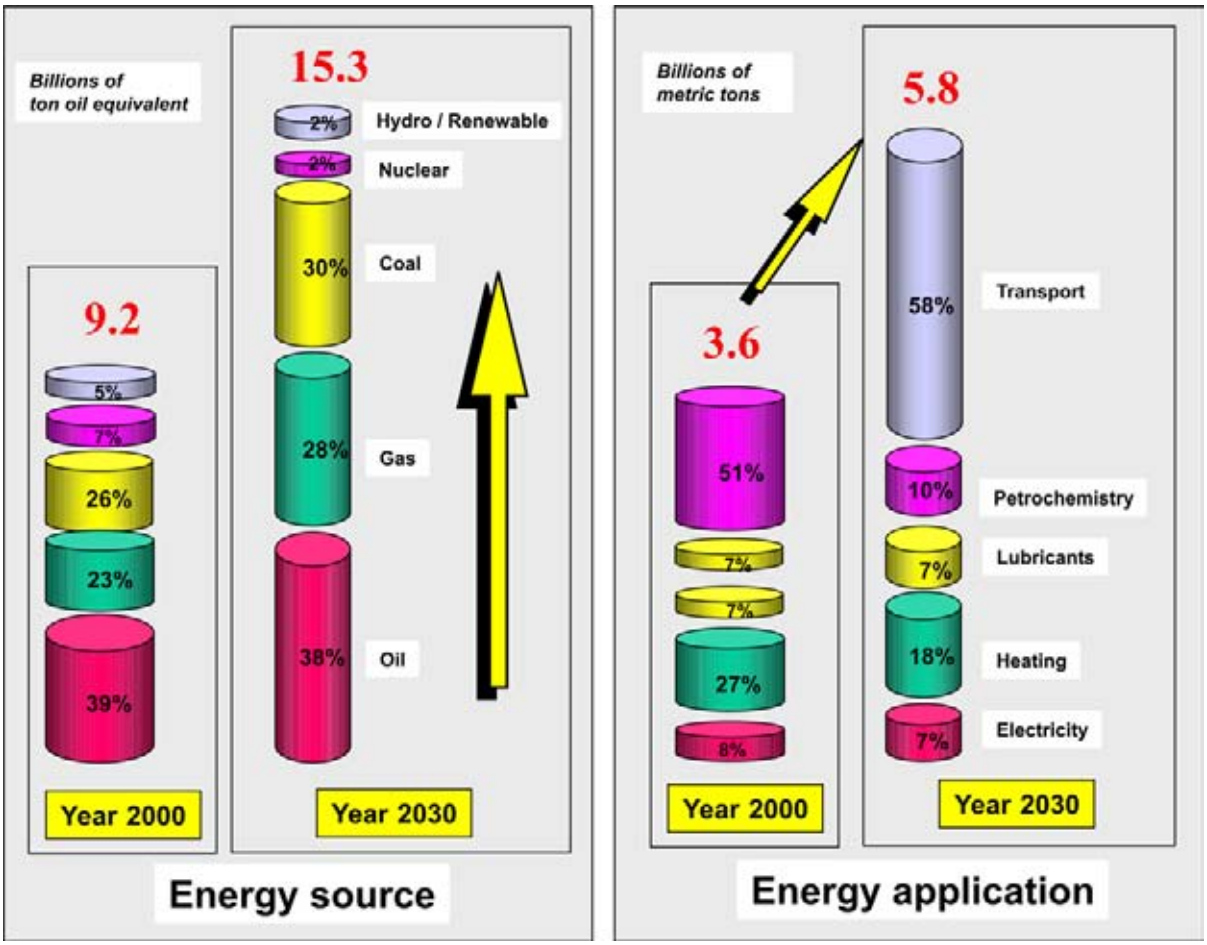

Figure 7.15: A forecast of the contribution of the different energy sources to the world supply. The increase of fossil fuels in the energy mix is here evident, but environmental issues need to be addressed if this trend is to be continued. The transport sector is a substantial contributor to this increase, but new technical developments, like electric cars and hydrogen combustion, might alter this extrapolation trend (modified after De Margerie 2004).

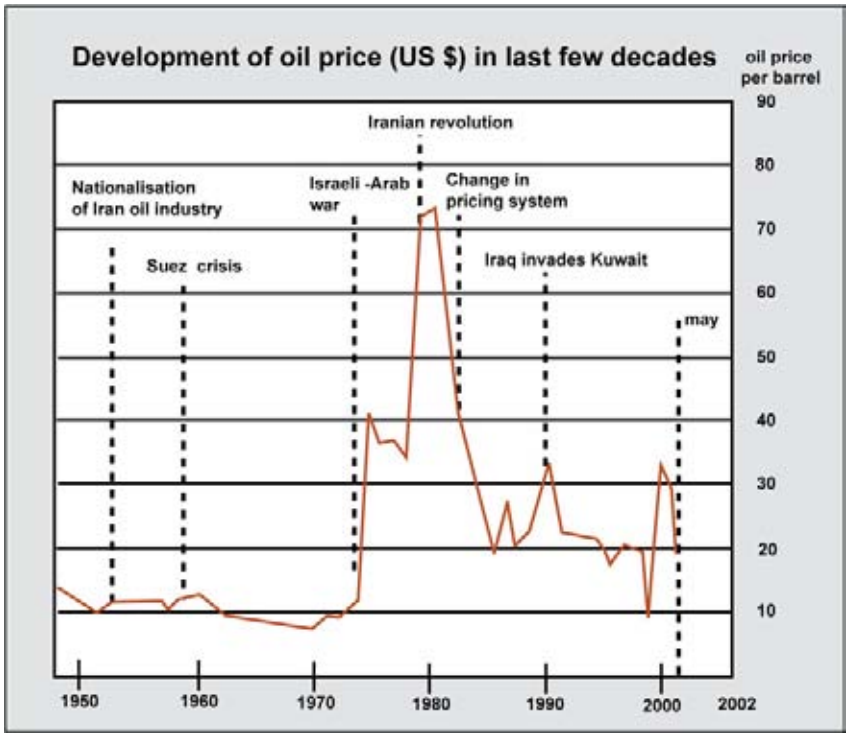

Figure 7.16: Oil price fluctuations are quite volatile and depend a lot on external factors like political stability and speculative short term shortages (after Van der Linden 2002).

in the pricing of nuclear energy, but obviously were not taken into account in the past. **Human errors** have been grossly under-estimated in the risk evaluations. These slack government evaluation policies hamper the direct comparison of the cost attached to the various energy sources. Also regular disasters, like the oil spill with the Exxon Valdez oil tanker in Alaska, are part of the total cost picture. It is empirically proven that accidents do happen despite how odd are their chances. Quantification of their frequency, the scale of pollution and damage to the environment are extremely important in order to obtain a reliable prediction on the financial effect.

The recent trend towards renewable energy resources will be accelerated when their pricing becomes more competitive. It is therefore crucial that all *real costs* are considered in the total picture. The general rule that "*The polluter pays*" has not always been applied in a consistent way, most of the time it is "*the consumer who pays*". If the consumers would have been consulted beforehand they might have preferred a more structurally sound solution to the problem, even when that means spending funds upfront and obtaining the potential savings only in a later stage. Private initiatives are repeatedly seen to favour solutions with short term gains, ignoring the longer term negative consequences.

In the last 40 years oil prices have been ranging from 9 to 72 US dollar a barrel (Figure 7.16). In 2006 we even reached 76 dollars. The **average finding costs** for a barrel of oil has come down as is illustrated in Figure 7.17. Petrobras has reduced their three year average finding costs from 0.42 US dollar a barrel in 2002 to 0.36 dollar in 2003 (Figueira 2005). Their lifting costs (finding and development) were reduced from 5.60 dollar in 1997 to 3.40 in 2004; with a new target set at 3.00 dollars for the year 2010. The steady decrease in finding costs over the past decade is certainly spectacular and it is generally attributed to more focused exploration strategies, the widespread use of 3D seismic and applying new technologies (e.g. interpretation tools, Direct Hydrocarbon Indicators and better drilling techniques). It has led to an impressive increase in the success ratio for wild cat drilling of wells, one-out-of-two compared to one-out-of-eight twenty years ago (cf Visher 2004).

The pricing of the commodity for the customers is very dependant on speculation and other subjective factors like government taxation policy. Also the world political situation plays a role in the market. Production from instable countries – like Iran, Iraq, Sudan, Angola, former Soviet Union – has a dramatic impact on the fluctuation of the world oil price. Sixty percent of the world's proven HC reserves are found in Middle East with 25% in Saudi Arabia and 11% in Iraq (Figures 7.18 and 7.19). This is one of the reasons why the Americans and British are so much interested in the **geo-politics** of that region. At the start of this write-up the price per barrel (159 litres) was 22 US dollars and in a later phase, just before the

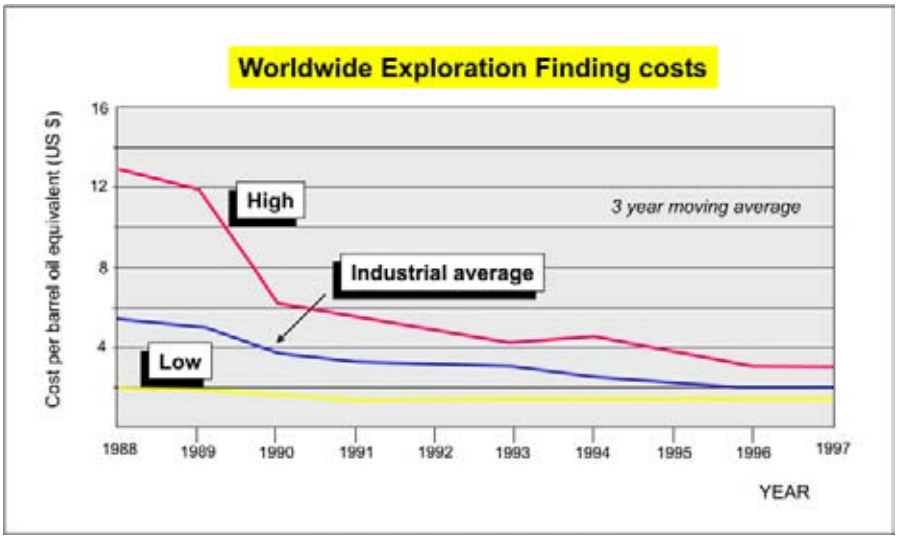

Figure 7.17: World Exploration Finding costs based on SEC 10-K filings of proven reserve additions over a three-year period. It includes extensions/discoveries but excludes acquisitions and Enhanced Oil Recovery (EOR). All cost data up to 1993 is normalised for special items. Incurred exploration cost includes both capitalised and expensed costs. The industrial average (unweighted) is computed for the following peer group of companies: Amoco, ARCO, BP, Chevron, Elf, Exxon, Mobil, Phillips, Shell, Texaco and Unocal (after Mc Mahon et al. 1999).

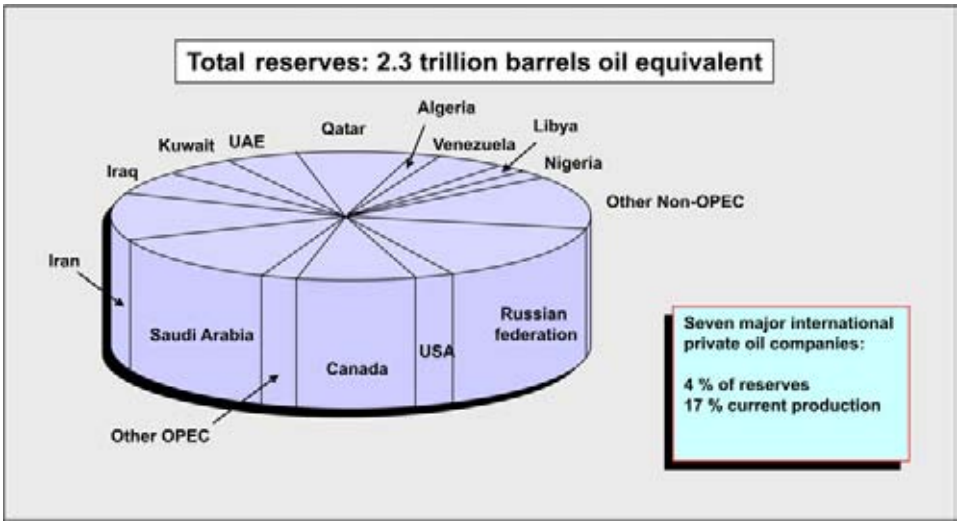

Figure 7.18: The total proven HC reserves in the world with a subdivision of the most important contributors (modified after De Margerie 2004).

second Iraqi war, it reached 35 US dollars and in October 2004 it rose further to just above 50 dollars. In mid-2005 it even reached a daring 60 dollars per barrel level with a further increase to 80 dollars in 2006. A structurally higher oil price is part of most scenarios for the immediate and long term future.

The organisation of oil producing countries **OPEC** tries to stabilise the price between 22 and 28 US dollars, but their influence is diminishing as they hold just over 35 percent of the production resources in the petroleum market. Their actual production is 30 million barrels a day, whilst their official quota had been fixed at 26 million barrel. Their regulatory role has weakened, due to the constant decrease in OPEC's global share that started from the oil crisis in 1973. At that time they controlled around 50 percent of the oil flow (Van der Linden 2002). The **world's proven reserve** portfolio has slightly increased by 12,5 billion barrels to 1028 billion in the beginning of 2001. This figure is also more or less equivalent to the amount of hydrocarbons already produced over the past two centuries. The ultimate recoverable reserves are estimated by the US Geological Survey as 3.3 trillion barrels. Moreover there are huge reserves of unconventional oil (tar sands) found in Canada, the United States and Venezuela. Those additional reserves amount to 7 trillion barrels according to various estimates (Jum'ah 2005).

The American market, with only 5 percent of the world population, consumes twenty five percent of the world's oil and gas production. The average North American consumes 25.6 barrels of oil per year, the European 12.6 and the Chinese only 1.2 barrels per person (Shell Venster, 2004, No. 4, p. 19). A tremendous demand is therefore expected from rapid developing countries like China and India over the coming decades. In fact the increased Asian demand had already a strong influence

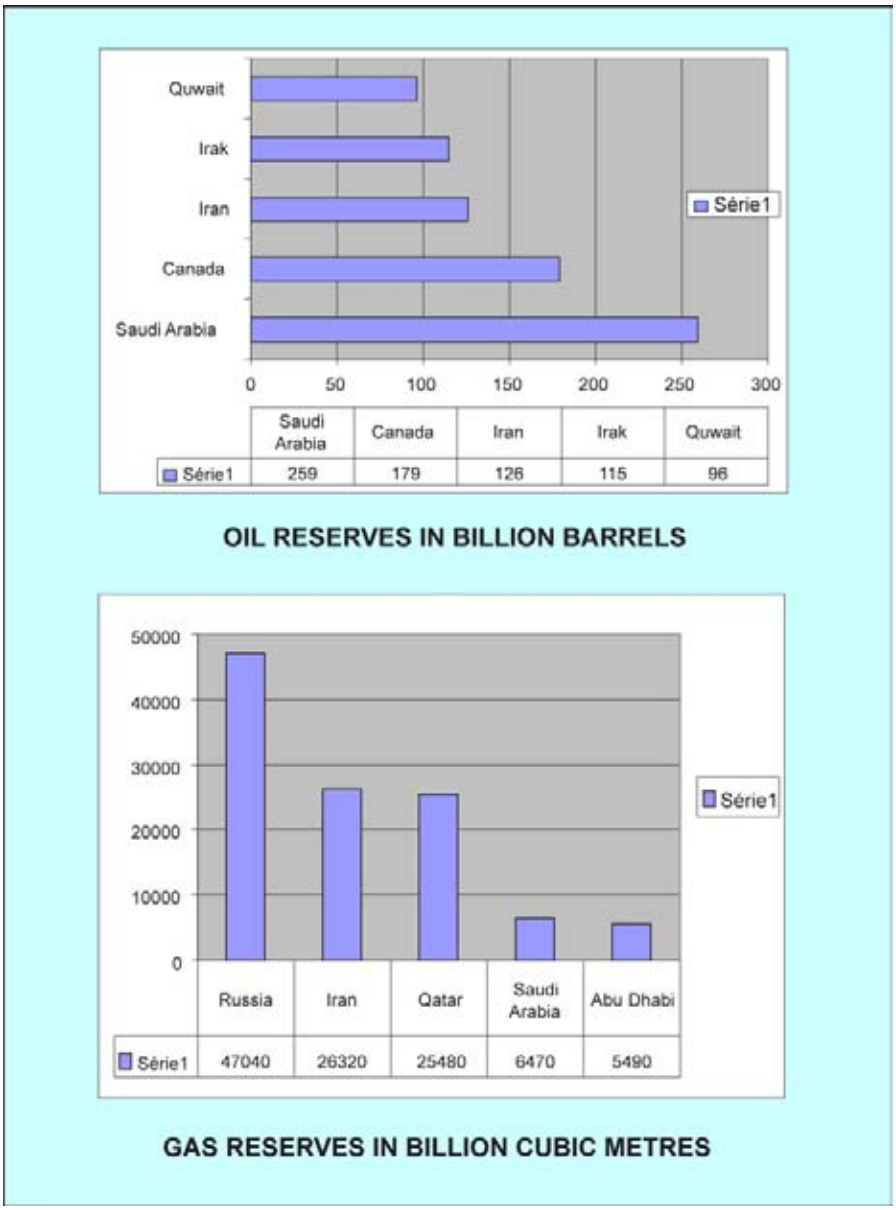

Figure 7.19: Ranking of the countries with the world largest HC reserves. Canada includes the large tar sand deposits that are marginally commercial, but at the current high level oil price (50 US dollar a barrel in October 2005) it can be exploited in a profitable manner (source: Oil and Gas Journal, 1 January 2004).

on the relative high oil price in 2004 and early 2005. The expected rise in overall demand for energy in the near future is further illustrated by the fact that 1.6 billion people are today still living without access to electrical energy (Ottesen 2003). The big challenge for the world economy is to balance production and energy demand in a reasonable way as well as keeping the environmental pollution problem under control.

The total **world oil production** is conservatively estimated around 76.8 million barrels per day in 2003, while the demand was 78.1 million. In 2005 this demand has risen to 115 million bpd and 175 tcf of gas (Figueira 2005). Saudi Arabia had in the past a large production over-capacity of around 2 million barrels per day on a total production of 10.5 million barrels per day in 2005. This was used to regulate the world supply to a certain extent. They plan to have 12.5 million barrels available in 2009 from a total proven reserve of 265 billion barrels. Such flexible production capacity cost a lot of money, especially when the infra-structure is lying idle. Not many countries permit themselves such luxury. The CEO of Saudi Aramco recently said it is their aim to maintain this buffer capacity in the near future (Jum'ah 2005). The other OPEC members estimated in 2002 that they could increase their production by 12 percent on a short term. Fear for possible shortages in oil supplies has a devastating effect on the market, resulting in a substantial price increase to 56 US dollars a barrel in march 2005. Problems on the downstream

side may even aggravate the situation. The refining capacity and the capability to process sour crude are potential bottlenecks. De-sulphurisation is a serious issue that should be addressed. Traders have a tendency to overreact with their pricing and a correction is necessary later on, when it is realised that the shortage is only temporary. On the other side it should not be ignored that this time it is different and the oil market has structurally changed by India and China becoming prominent net importers of hydrocarbons.

Tentatively the world oil production can be projected towards the year 2020 to grow around 120 million barrels a day, while in 2060 it will increase even further to 178 million barrels per day. A similar prognosis for gas demand in 2045 would be in the order of 253 trillion cubic feet (Figueira 2005). This long term outlook assumes continuation of current consumer trends, as other non-hydrocarbon solutions to the world energy problem are difficult to envisage for the time being. The world **proven reserves** in January 2003 were 1148 billion barrels of oil with 6205 tcf of natural gas. The potential reserves are of course higher and probably range between 2248 and 3896 billion barrels under different scenarios (e.g. high and low pricing). The mean expectation is 3000 billion barrels of recoverable oil, assuming current lifting techniques (Figueira 2005).

The transfer of potential hydrocarbon reserves to the proven portfolio has recently led to some commotion among the oil companies. This book keeping issue had even a negative effect on the share prices in the stock market (e.g. Shell Group). For the last decade there has been a tendency to postpone the drilling of costly appraisal wells and replace them by sophisticated computer-based reservoir modelling studies (Simmons 2005). A disadvantage is that these studies always need fundamental assumptions as basic input. They thus leave substantial scope for optimism, while real-world well results are sometimes disappointing. In general it can be stated that availability of many control points in many cases complicates the initially simple subsurface working model.

Nowadays a more prudent attitude is emerging towards the reserve estimations and more stringent regulations are enforced to avoid future managerial disarray. It is also a known fact that the production forecasts made by reservoir engineers are rather conservative when compared to the ultimate performance of existing fields. A substantial quantity of the currently produced oil is coming from quite old discoveries (<50 years). The planners do not always anticipate enough the effect of new developments in technology on existing projects. It are simple things like: number of slots on platform, extended reach holes, capacity of water treatment facilities, compressors, nitrogen drilling, slim hole completion, but also benefits of detailed reservoir characterisation and simulation studies. These changes are difficult to predict, but ignoring them in the work model can prove very costly. A more balanced view on the long term production forecasting is certainly warranted when considering the results of the past production histories.

7.3.2 Government taxation policies

Tax payments are a substantial part of the costs for the petrol customer (Figure 7.20). The cost for a litre of petrol in the EEC at the first quarter of the year 2006 was around 1.365 euro to the consumer, at a world market price per barrel of approximately 70 dollars. The breakdown of the retail price is:

- 34 cents production costs.
- 89 cents government tax.
- 12.5 cents retailing.
- 1.5 cents pure profit for oil company.

Taxation policies of local governments are playing a vital role in the market development. It is used as a crude steering instrument to stimulate the market to develop itself conform a politically welcomed manner. For instance high taxation on all gas in Europe makes alternative resources like coal bed methane currently un-economic. This **government policy** deprives a potential branch of the energy sector in certain countries of its existence. The cost structure for CBM and fossil gas projects is kept however the same. The USA government has shown that a more constructive attitude can be adopted towards **coalbed methane projects** and there about 9 percent of the yearly consumed gas is produced from CBM (Lagendaal 2004). Other energy sources like solar, wind, geothermal, density driven, wave and tidal power are possibly benefiting from government subsidies, which is a good thing in the initial start-up phase.

An other regulatory measure is the recently proposed **CO_2 tax** by the European community. This tax is introduced to counter the negative effects of the burning of fossil fuels and the undesirable release of CO_2 in the atmosphere. The CO_2 is believed the main culprit affecting the stability of the world's climate (Baines and Worden 2004). The European Commission is proposing a tax of 100 Euro per ton CO_2 equivalent. A system of trade in **CO_2 emission** is stimulated by this tax measure. For Holland the fossil energy consumption will generate a 170 million ton CO_2 annual production (an estimate 0.75% of the total world production). This represents an additional cost of 17 billion Euro. Seeking ways of permanently storing CO_2 thus makes economic sense and several methods are proposed:

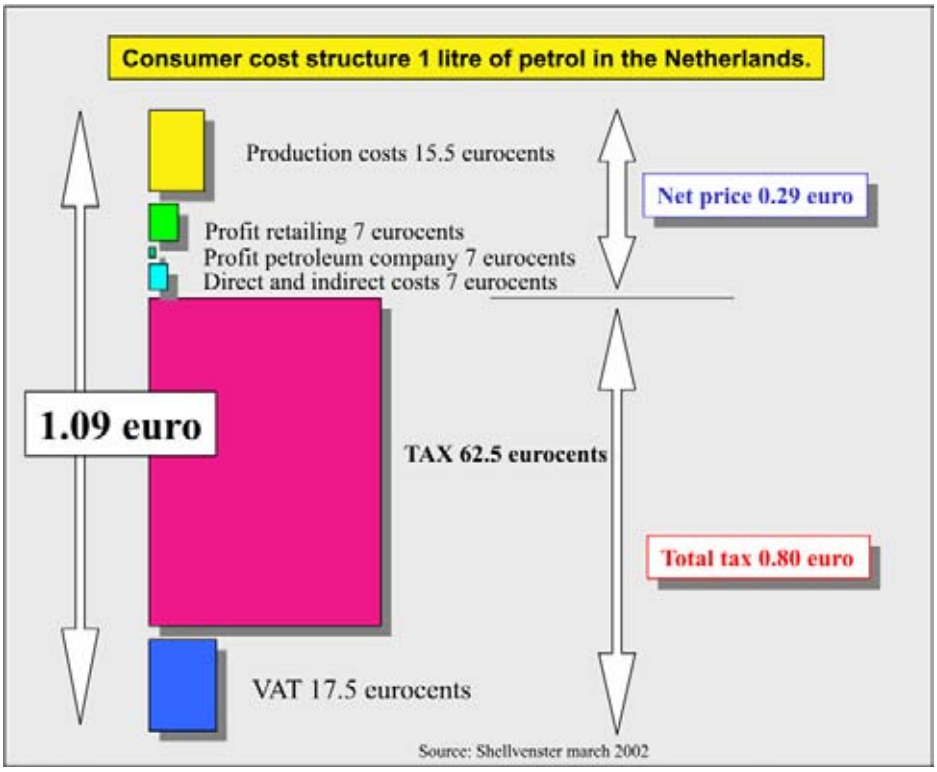

Figure 7.20: Tax regime on petrol is controlled by the governments. This taxation instrument should be used with caution to ensure that the world energy market is developing towards cleaner and renewable resources. Commercial Coal Bed Methane (CBM) projects in the USA are examples of active government support by adopting a special tax policy (source: Shell Venster).

- Injection in exhausted oil and gas fields.
- Injection in coal layers that are not mined.
- Injection in underground water reservoirs.
- Injection in stagnant deeper layers of ocean.
- Stimulation of growth of phyto plankton (temporary storage, maintenance).
- Growth of biomass in forests, etc. (temporary storage, maintenance).
- Chemical transformation of CO_2 into a solid mineral that can be stored easily.

The last **CO_2 sequestration** method is non-polluting and the most convenient. The CO_2 is directly taken out of the environment for a long time. Burning 1 cubic metre of gas will release 1.8 kilo of CO_2 in the atmosphere. If the release is not controlled, it will have influence on the long-term climatic conditions on the earth. Assuming the storage and mineral conversion of the CO_2, then an one year gas production and burning in the Netherlands would generate a solid heap of material with a size of 2 by 2 kilometres and a height of 28 metres (De Wit 2002). This solid mineral aggregate can safely be recycled by the construction industry. An other possibility to get rid of the unwanted CO_2 is enhanced coalbed methane production by means of CO_2 injection. The CO_2 is replacing the methane attached to the coal and methane is thus produced (Lagendaal 2004). The sequestration of CO_2 by the coal is accompanied by swelling of the coal layer and the permeability is usually negatively influenced. Fraccing is often necessary to stimulate the process. The CO_2 injection technique also can boost the recovery rate from existing fields by at least 10–15 percent (e.g. Statoil Sleipner, Gaz de France K12 fields). Leaking of the injected CO_2 might be a problem and this can be monitored by tracer studies (cf Wilson et al. 2005). Changes in the caprock condition is a serious study issue. The CO_2 can form an acid that attacks the properties in the reservoir and of the seal. Often the CO_2 is injected under pressure whereby an semi liquid state is reached, so that the seal is working more efficiently.

7.3.3 Adaptation to a cyclic petroleum market and future developments

The use of petroleum has changed over the last few decades. In France the transport sector has increased dramatically its share in the consummation of refinery products in the country. This trend is also recognised worldwide and often extrapolated in the near future (Figure 7.21). This fundamental change makes the

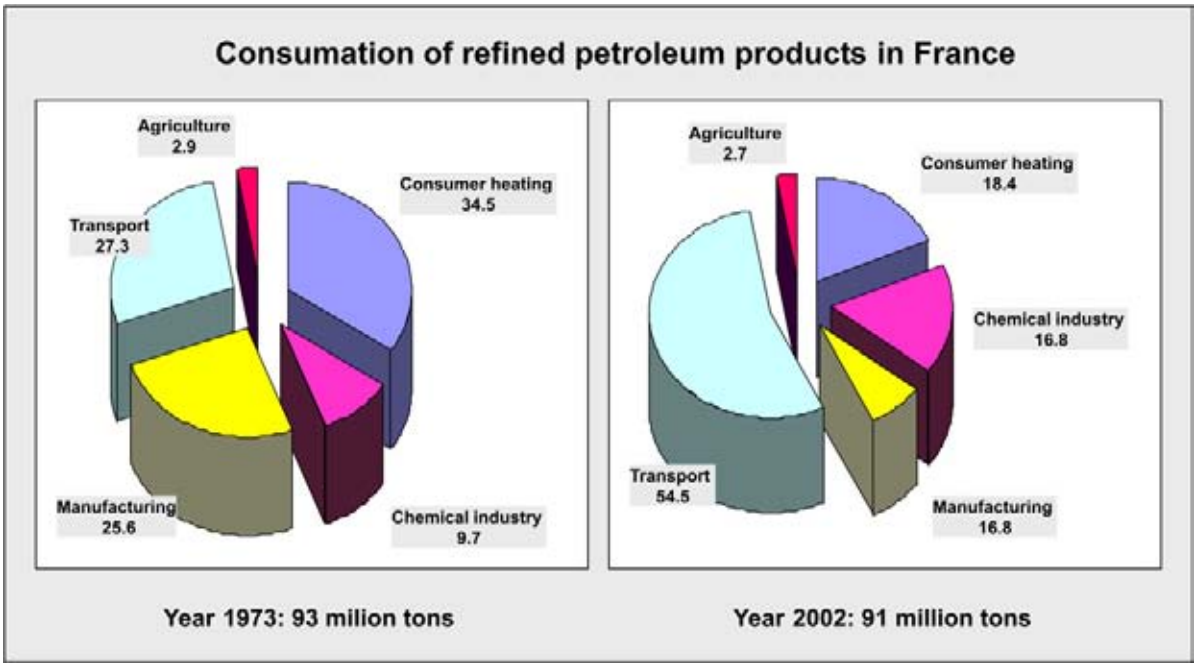

Figure 7.21: Consumation of refined petroleum products is shown as a function of its application in France. The overall consumption stayed quite similar, but the transport sector has increased its share dramatically. Spectacular changes in the mode of transportation (hybrid cars, etc.) are foreseen in the near future and therefore further adaptations in the energy market are expected (source: RL, 3 June 2004).

oil market even more vulnerable and dependent on the overall economic climate. A good thing is that the importance of the cost of hydrocarbon import for the European and Japanese economies has decreased over the last few decades, when expressed in percentage of gross national product. In 1980 it represented around 5 percent of the GNP, while in 2000 it was reduced to 2 percent. Their economies have risen by an average of 6 percent a year (Total website 2004).

The petroleum business is clearly part of a **cyclic market**. It is difficult to maintain the right balance between demand and supply (Figure 7.22). Unfortunately fluctuations in the **industry's workforce** have been following only the negative trends. Since the early 1980's the workforce in the petroleum industry has been downsizing and has fallen by about 50 percent. The average age of the employees has increased from 32 to 50 years (Ottesen 2003). Automation has certainly contributed a lot to these changes, but also the merging of big oil companies in the nineties (e.g. Exxon-Mobil, BP-Amoco, Chevron-Texaco, Total-Fina-Elf, Conoco-Phillips) had its impact on the employment situation.

The **world energy market** is generally speaking conservative and therefore the petroleum business can be expected to continue to play a major role for some decades to come. The resources are out there, it is only a question how to develop them. Hefty investment levels of 150 billion dollars per year are required in the near future to guarantee sufficient supply (Van der Veer 2004, Shell website). 190 million barrel per day of oil equivalent was the total energy demand in 2004 (Browne of Madingley 2004). It will increase by 20 percent to 230 million barrels of oil equivalent by 2015 (International Energy Agency). The chief executive of Royal Dutch Shell Van der Veer forecasts a probable doubling of the world energy demand by the year 2050 and half of this energy requirement could be provided by non-fossil sources (Shell Venster No. 1 2005). Development of sustainable fuel cycles, based on an interdisciplinary approach integrating geological, geochemical and mineralogical research, is certainly going to be a challenging task (Giere and Stille 2004).

It is evident that hydrocarbons form the dominant ingredient in the world energy mix in the coming years. Mature areas, like the North Sea for example, are however in their production decline phase (Figure 7.23). An average production decline rate is often assumed 4 percent per year. Large discoveries are becoming nowadays more rare (e.g. Azadegan – Iran, Kashagan – Kazakhstan, Thunder Horse – Saint Malo, Jubarte – Brazil, Cachalote – Brazil, Agbami Ekoli – Nigeria, Bongabonga SW – Nigeria, Akpo – Nigeria, Girassol – Angola, Dalia – Angola) and most discoveries are medium to small in size (Figueira 2005). Enhanced recovery in brown fields can prolong the economic life,

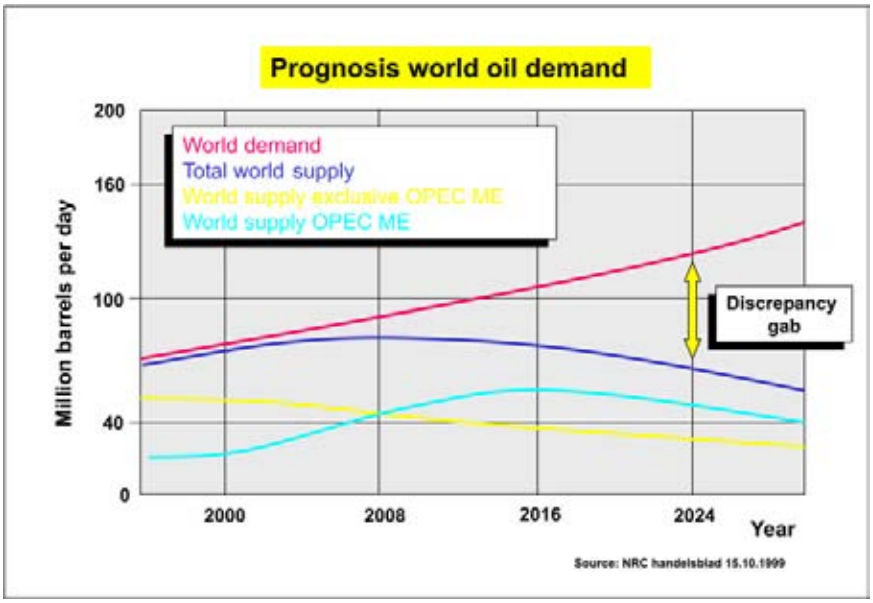

Figure 7.22: A prognosis for the world oil demand up to the year 2030. Note the long-term discrepancy between supply and demand (source: NRC Handelsblad).

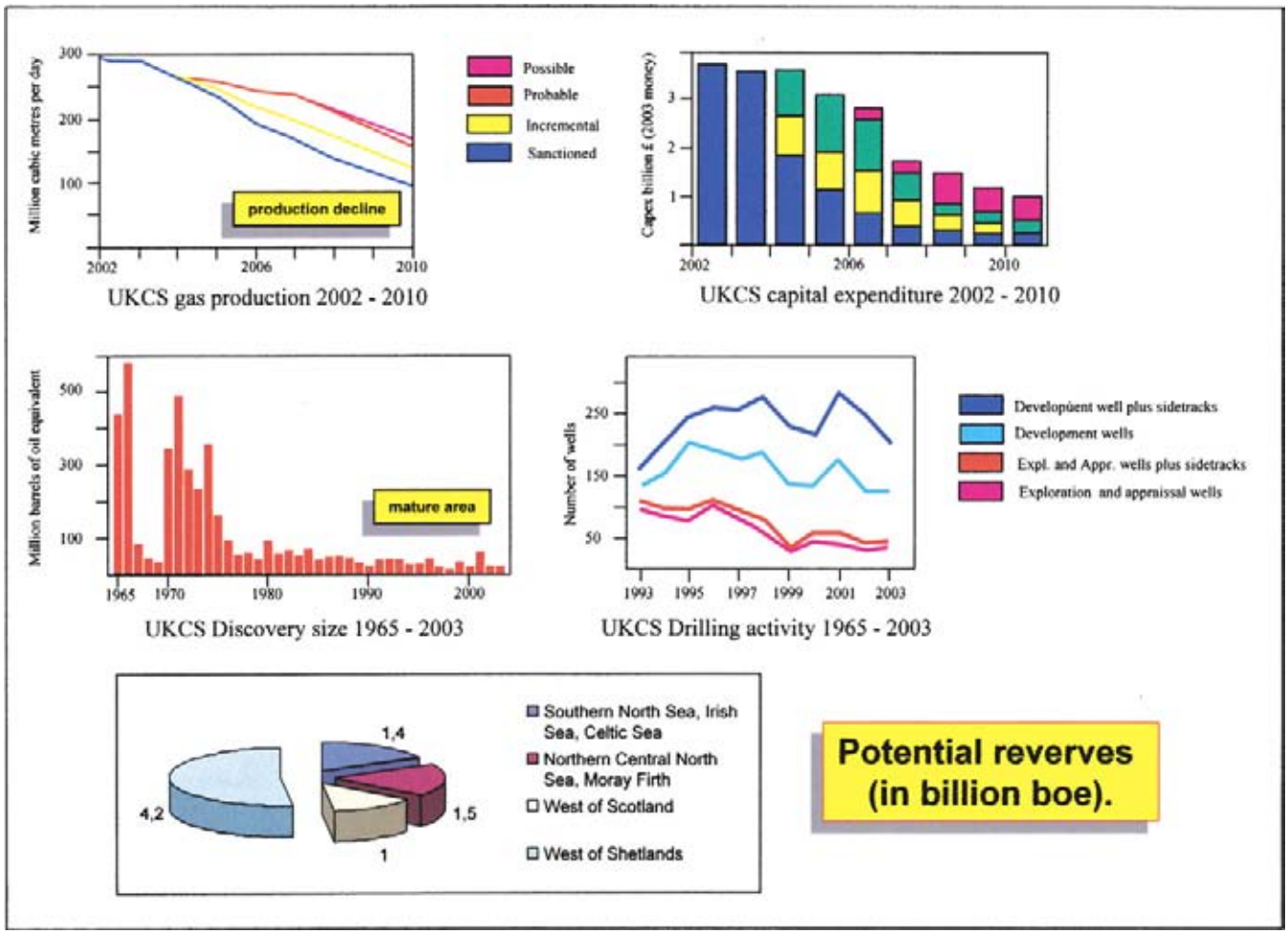

Figure 7.23: The HC production decline of a mature area like the Central North Sea in the UK. Enhanced recovery techniques from existing brown fields will only temporarily curb the downward trend (UKOOA 2004).

but it will only manage to curb the downward trend for a short period of time. New provinces need to be brought on stream in order to replace the lost production capacity. New areas will be located around the Arctic region, where exploration conditions are extremely harsh. Careful project evaluation should avoid deceptions like the Shell/Gazprom Sakhalin project, where the initial development costs were estimated half the real cost, changing the total investment from 10 into 20 billion US dollars. It is still profitable because of the currently high crude oil price (70 US dollars per barrel in 2006). It illustrates that there is a severe risk to frontier areas in spite of the overall attractive aspiration of such a partnership.

Up till 2004 some 1000 billion barrels of oil have been found and these reserves are not yet produced. Some 5500 trillion cubic feet of natural gas are waiting for their production (Browne of Madingley 2004). That quantity of hydrocarbons makes a stock of 40 years of oil supply at the current day consumption rate and 60 years of gas. Up to 2015 a 20 percent increase (= 40 million barrels per day) in oil demand is expected worldwide and roughly a 45 percent increase in the consummation of gas (= an additional 30 million barrels per day oil equivalent). It will be feasible to meet these demands when the green house gasses are kept under a 500 ppm level. CO_2 sequestration will therefore be a vital issue in the coming decennia.

The start-up of petroleum development projects need **long term planning** and for that a stable industrial climate is of utmost importance. In this respect **political instability**, terrorist attacks, revolutions, civil war clearly do not help to generate the necessary funds. **Country risk assessment** is an evaluation technique to quantify these uncertainties. It comprises items like: expropriation, capital transfer restrictions, unrest and interruption from war or insurrection, taxation changes, regulatory changes, institutional deficiencies, corruption, social violence, inadequate work force, prevalence of infectious disease (Marshall 2003). Social as well as political and economic factors are taken into account. A skilled workforce is one of the prime requirements to attain high-level future production goals. It usually takes seven years to take a field from discovery into production.

The non-fossil energy sources are various and some of them are desperately in need of problem solving solutions. Nuclear energy has some severe drawbacks (radioactivity) and currently satisfies only 7 percent of the total energy demand. The development of thermonuclear fusion, whereby Deuterium and Tritium (heavy isotopes of hydrogen) are collided in a strong electromagnetic field to create helium, is still not available on an operational scale. Alternative energy resources like wind, tidal, solar, geothermal power and biofuels are in their infancy. **Hydrogen** might replace petrol as fuel for transportation purposes in the near future. Preservation of the special tax structure will make the decision easier for both the politicians and the oil/automobile industry. This will mean transformation of the existing outlets in hydrogen filling stations instead of installing individual generators in each vehicle. Tapping the jet stream energy sounds today a bit fantastic, but some people dedicate their professional time to such innovative research missions (e.g. prof Ockels, Delft University).

Biomass conversion is worldwide the most promising contributor among the renewable energy sources. Biodiesel is slowly gaining a market share in Germany. A big breakthrough in the production of ethanol has been reached in Canada by the introduction of special enzymes that serve as a natural catalyser, the second generation biomass techniques (Shell Venster 2004, No. 4, p. 19). Even the United States are keenly interested in these developments to reduce their hydrocarbon imports, that amounted in mid February 2006 to an expense of 850 million US dollars daily (Shel Venster 2006, No. 3, p. 2). Their target now is to reduce the Middle East imports by 75 percent in 2025.

Gas-to-liquid (GTL) diesel is an other option that delivers an environmentally more friendly fuel to the customer. Geothermal projects desperately need basic input from reservoir engineers and other geoscientists to boost the production.

Wind power represents only 2.4 percent of the EU electricity at the moment (Shell Venster 2004, No. 3, p. 3), but last year in Germany 10 percent of the energy production came from the eolian source. **Solar energy** satisfies only 0.001 percent of the energy demand and that is a surprisingly small contribution indeed. The **nuclear option** is much more important, providing 16 percent of the world's electricity needs at the moment, generated in 443 nuclear power plants worldwide. The nuclear security situation seem to have improved somewhat over the last few decades, given the stricter regulations and the reduction in powerplant downtime from 50 percent to around 10 at the moment. To put the contribution of alternative energy resources into its right perspective: the energy output of the 30-year old Brent field in the North Sea in 2002 was equivalent to all the then installed wind, solar and wave power in the world (Brinded 2005).

It takes much longer than expected for all these alternative energy sources to become mature. One of the main

reasons is that the hydrocarbons are relatively speaking too cheaply priced, especially when monetary inflation is taken into account. This **cheap petroleum policy** has been considered good for the world economy, but it also has some severe drawbacks and hampers the development of clean renewable energy resources. Cheap transportation leads to excesses in the global consumer production system and the pollution effect is not adequately taken care off. Restrictions in mobility will give a public outcry, not very popular with politicians who look for short term gains, but in the longer run it will be very difficult to avoid.

The **global trading** system has also its negative side. The oil spot market had for instance a very negative influence on long term energy contracts and stimulated a more volatile pricing (cf Simmons 2004). Gas price coupled to the oil price is a brilliant idea, attractive to politicians because a similar exorbitant taxation policy is then easily adopted, but for the consumer it only means additional costs. The free market principle is not always very efficient and some regulation from above can be healthy. The recent world population of 6.3 billion is expected to grow by 25 percent and this will mean an additional 1.5 billion people, with most of them living in developing countries, in the coming 20 years (Ottesen 2003). All these conditions put an extra strain on our energy supply system.

7.3.4 Outlook for the geophysical business sector

The **geophysical business** is currently based on an expense of around 3 billion US dollar as a world market per annum (Figure 7.24). Seismics has been the major driving force to open up new developments in the petroleum industry to optimise reservoir management and elicit the creativity to discover new oil and gas accumulations (Figueira 2005). The seismic method rightfully constitutes a substantial part of the total E and P expenses (46% according to the IAGC 2003). From 1998 onwards the prices for acquisition and processing have been very low and in fact the **cost level** has not been attained. This situation is not tenable on the long run and has to be altered in the years to come. It means that a major restructuring has to be envisaged. The seismic method has delivered a tremendous increase in **added value** to the exploration and exploitation success. The use of 3D seismics has increased the drilling success ratio significantly (cf Aylor 1999). It also led to major improvements in reservoir characterisation (e.g. Mari et al. 1998). It is strange that this has not been translated in reasonable profits levels for the service companies involved in such efforts. There

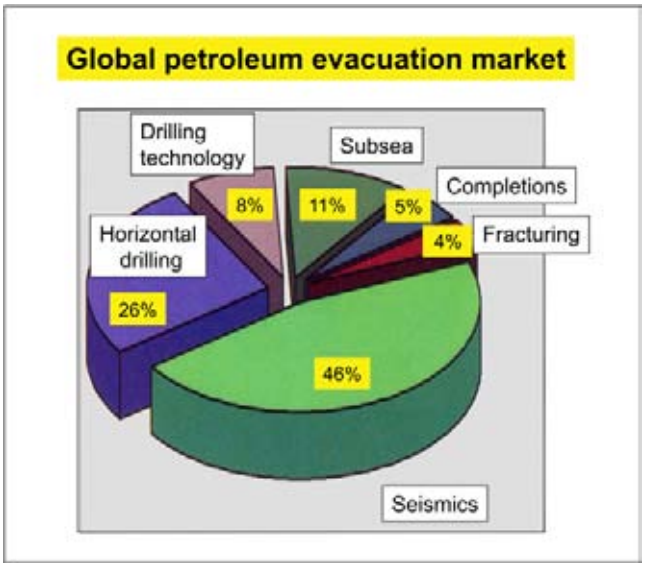

Figure 7.24: The geophysical market is quite large with an estimated expense of 3 billion US dollars a year. The seismic reflection method made up 46 percent of this market in 2003. Current oil prices, that peaked just over 50 US dollars a barrel in Q3 of 2004, will most certainly stimulate the market in the year to come (modified after IAGC 2003).

is a real danger that the relentless drive of the major oil companies, to decrease their costs and put **business risks** at the shoulders of others, will force some contractors to leave the scene. A re-think on the consequences of such a policy should be seriously considered by the oil industry. In 2005, a change in that direction is becoming gradually visible, with long term planning getting some more attention in connection to the high oil price.

The world HC exploration and production market is estimated around 132 billion US dollars per year, with 42 billion spent in North America. Forty percent of the budget is spent on drilling wells. An average deep water well costs 24 million dollars with a rig rate of approximately 200,000 dollars per day (Dutta 2002). This amount of money spent by the upstream business should be quite enough to pay some decent salaries in the years to come and hence it is a good reason for newly arriving geoscientists to look forward to a bright career, despite some restructurations still lying ahead of us.

7.3.5 Benefits of increased recovery rates

The trend over the last ten years is to go for **increased gas production** (e.g. Da Silva et al. 2004). Gas is a cleaner fossil fuel with less impact on the environment.

Gas-to-liquid conversion represent also economically viable projects. **Increased recovery rates** from existing oil fields gets more and more attention. Over 70 percent of the current HC production comes from fields older than 30 years (Gould 2004). The normal decline after the peak production from a field is in the order of 4–5 percent per year. Substantial efforts are needed to curb this downward trend and it calls for detailed reservoir studies by a vast array of geo-specialists.

The "**smart field**" concept (or instrumented field) is in this respect promising indeed. The latest e-field monitoring techniques are in this case utilised by installing fibre-optics with seismic sensors in and around the wells. A "Bragg grating" is made on the outside of the fibre and light with a specific frequency is blocked when it passes the grating. When a seismic vibration is affecting the cable, the frequency that is blocked is changed and this is detected at the other end of the same cable (Ragnar et al. 2005). The instrumented field monitoring allows continuous acquisition of detailed data:

- Temperatures are read off with 0.1 degree Celsius accuracy.
- Detailed pressure measurements.
- Changes in the gravity response are recorded with a nanno-g accuracy.
- The shale breakout is measured in micro-degrees, giving information on the local stress regime.
- Micro-seismicity is measured and analysed on a routine basis (cf Berumen at al. 2004, Deflandre et al. 2004).

This all adds vital information to the detailed picture of the production fluid flow in the reservoir. Recovery factors are thus boosted from 50 to 65 percent. These front-end techniques have been applied in a Malaysian Malampaya field, where 350,000 data measurements are collected every day. Dedicated software is needed to manage this enormous stream of information. The total investment was 3 million dollars and the benefits are estimated around 30 million. This gives an idea about the sort of financial advantages to be gained.

Also 4D technology has its benefits already proven. Asset teams can outline by-passed areas and locate new injectors and producers, optimise the enhanced recovery scheme (Peebler 2005). In the Gullfaks field (offshore Norway) Statoil claims an increase in the recovery factor from 35 to 70 percent, representing 500 million dollars worth of oil. The Statfjord field in the northern North Sea is an other example where a 20 year prolonged production scheme will increase the ultimate recovery to 70 percent (Brinded 2005).

An other domain of progress is found in the application of the latest well completion and production development techniques. **Hi-tech solutions** should not only be seen as merely a **cost item**, but as a means to get access to sophisticated **reservoir management** with increased **production efficiency** (Eenhorst 2003). Innovative techniques like the exploit of bacteria for enhanced recovery has been pioneered by Statoil in the Norme field (FB Vol. 23, No. 4, p. 32) and it illustrates the exciting road still lying ahead of us.

This page intentionally left blank

Chapter 8

Concluding Remarks

An introduction to seismic stratigraphy and 3D interpretation techniques has been given in the foregoing chapters. Their link with basin analysis and sedimentology was demonstrated. The dynamics and interplay of depositional systems have been highlighted. The concept of petroleum systems has been presented. Some basic reservoir characterisation methods were discussed. An overview of seismic interpretation techniques in a wider sense was given, supported by extensive visual aids. Some sacrifices on the completeness of the descriptions were necessary to keep the text readable for a large audience.

Sequence and seismic stratigraphy apply very different scales of study: from microscopic to basin wide. Even global features are resolved (e.g. eustatic sealevel changes, climatic influence). This up-scaling of the view, from individual outcrops to basin wide sedimentation patterns, has proved itself a revealing eye-opener to the geoscientists. It has put the study of the earth history on a different level. Numerous boreholes have shown the added value of sophisticated sedimentological models, that are continuously refined by the hard work of dedicated geoscientists. And these work models are expected to have an even bigger impact on the future hydrocarbon development efforts. The distinction between siliciclastic and carbonate geology is somewhat artificial. It is more and more realised that limestone particles also get transported and deposited; they behave in a sense just like silici-clastic rock fragments. The real research strength lies in combining these two major disciplines in sedimentology and look for analogies to understand better the details of their differences.

Paring sedimentology with geophysical techniques, as has been done for instance in seismic reflection profiling, has resulted in a new view on the interplay of depositional systems. Marine geology is a study area where progress has been dazzling over the last decades, opening opportunities for new technological applications that call upon sound sedimentological principles. It is true that the simple and brilliant idea: '*Seismic reflections are some sort of time-lines*' gave new dimensions to the earth sciences. Modelling, AVO analysis, seismic inversion, depth conversion, geostatistics and neural network pattern recognition are examples of techniques that allow to get a better understanding of the data. It shows what remote sensing methods can bring us (cf Addy 1998, Walls et al. 2002). Multi attribute auto-trackers, with enhanced 3D visualisation capabilities and exploiting the voxel concept to its full potential, will clearly be the road to go ahead. Autostereoscopic 3D displays will bring the IMAX concept to the interpreter's desktop, without the need for special glasses or auxiliary vision aids (McKay 2005). The automated tracking of voxsets is convenient for generating new attractive views on the seismic dataset. Ultimately it leads to a more consistent interpretation with a better description of the subsurface structuration and an increase in the reliability of the geoscientist's predictions.

Tectonics and sedimentology are more and more interlinked. Basin analysis has become a science of its own, with seismic stratigraphy as the driving force behind it. Climatic changes and also extra-terrestrial events are playing a role in the reconstruction of earth history. All these fascinating aspects have their place in the study of the earth depositional history.

Application of the latest technologies is necessary to obtain outstanding results in stratigraphy and basin analysis. Innovation is hereby one of the keywords. Progress and change in working habits are often somewhat over-estimated and it appears that proven techniques often have a much longer life cycle than initially foreseen. A solid down to earth approach is preferred above a blind following of a day-to-day hype. See for example what happened to the zero-paper office space as predicted in the early nineties. Books and maps have proven their value and are never completely replaced by digital files. On the other hand, tremendous advantages are gained, when the latest drilling techniques are applied. An efficient continuous educational training scheme is needed to diffuse the most recent research developments to the workers in the field. This textbook is one of the means to make geological and geophysical studies more accessible to a wider audience. Professional organisations like the SEG, AAPG, EAGE have realised

this need and organise dedicated training courses worldwide. It is obvious that teamwork is crucial, as the number of specialist topics is too vast to be handled by one person. Working in asset teams stimulates the cooperation between geoscientists. Unconventional, creative thinking does facilitate the real progress.

Integrated reservoir characterisation studies will become increasingly important. Proven hydrocarbon accumulations are more easy to develop, than going out in the field and look for new super huge accumulations (green fields). In the first case the risk is less as the hydrocarbon play concept has already been proven. It is logic that ways have to be found to augment the recovery rates of existing fields. Teamwork and appropriate application of new techniques are essential to the success (e.g. 800 percent increase in daily production during five years for a Gulf of Mexico asset, Bourque and Stevens 2005). By many it is felt that re-evaluation of existing fields is the key to future increased HC production. The 'smart fields' concept is very welcome in this context (e.g. Malampaya, Shell). Improved production techniques are cost saving and look very promising indeed. Deep water exploitation (10 000 feet new maximum in 2003, TransOcean and ChevronTexaco), nitrogen injection (Tinker gas field, Mosaic Oil), underbalanced drilling (Shell), tar sand development (Surmont project, Conoco-Phillips) or gas-to-liquid projects are all topics of interest. Reservoir characterisation, lateral prediction and seismic modelling have to play a major role. Reservoir geochemistry can throw light on the origin of petroleum reservoir fluid heterogeneities at a variety of spatial and temporal scales (Cubitt et al. 2004). 3D seismic interpretation, fuelled by the drive to find economic reserves of hydrocarbons, can be expected to generate further advances in various related geoscience disciplines (cf Davies et al. 2004). New seismic tools (4D time lapse seismic, 4C multi component and anisotropic processing, borehole seismics, shear sonic) will boost the application of the seismic investigation method even further. All this means more complex seismic processing with sophisticated algorithms. It will require substantial efforts on adequate quality control. It also produces more data to be looked at and hence implies more work for the geoscientists. The computer can take over a certain amount of tedious work routines, but ultimately it always will be the interpreter doing the final interpretation and it is him who has to come up with a decent synthesis of it all.

The main application of seismic stratigraphy is currently found in the energy sector. In fact sedimentology and basin analysis are essential parts of the motor behind the world's economic system. The petroleum industry has a direct interest for making rapid progress and securing reliable results in the earth sciences. Understanding reservoir characteristics and fluid flow is their daily bread. Their drive is to optimise the efficiency and profitability of the hydrocarbon exploitation efforts in order to sustain the world's economic growth. This mutual beneficial relationship between business and science exists already for decades; it will undoubtedly continue to do so for some decades to come. The cross fertilisation between industrial needs and research has been paramount to the success of the earth sciences. The active support and demand from the industry is one of the main reasons why there have been such major research advances over the last 30 years, resulting in a dramatic new insight in the dynamics behind depositional systems.

This does not say, however, that other research areas should be ignored. With the expected decline in the petroleum production, assumed to occur somewhere around the year 2025, new horizons have to be explored. Energy storage systems are becoming increasingly important. For example the geothermal energy potential could play a more prominent role in the energy development strategy (Audigane et al. 2002). Reservoir behaviour and sufficient heat exchange is a delicate problem that always need detailed study (Hol et al. 2004). **Water resources** are increasingly scarce and this calls for an optimised management, whereby reservoir characterisation can make a substantial contribution. Alternative resources like coal bed methane are also attractive (Gochioco 2002), even more so when governments encourage investors to run profitable projects by adjusting their taxation policies accordingly. Climatic changes and the dynamics of depositional systems are other topics with a direct impact on the society and human activity. The present is the key to the past, but it is equally true that the past can give vital clues on the prediction in future scenarios. A relation between sealevel changes and global warming has been suggested (e.g. Thompson et al. 2002) but its effect is probably not linear and is therefore difficult to predict. The large quantity of gas hydrate, present at relative shallow depth, is in this respect a worrying factor that can influence the climatic conditions dramatically when it is released in a uncontrolled manner into the atmosphere (cf Haq 1993). Increase in the global temperature has an impact on the stability of this gas (permafrost). A relationship with sealevel changes is also suspected. Recent modelling has however shown that the hydrate gas will not be liberated, even when a substantial sealevel drop of 100 meters is assumed (Milkov and Sassen 2003). Such a sealevel drop is likely to correspond to a dramatic decrease in ocean water temperature.

The **Gaia concept** for the earth assumes a robust global and dynamic equilibrium, that is stable within a broad

band of environmental scenarios. It is named after the Greek goddess of the Earth. The earth is considered a dynamic 'living' system, whereby the living and non-living processes interact continuously (Kaplan 2003). Changes in one or a set of parameters are easily compensated by other factors. It illustrates the difference in expectations (optimistic/pessimistic) held by some individuals of the current research work force. It remains difficult to make a good prediction when the limits of the interlinked systems are reached and chaos is the only end result.

Major catastrophes in the past show that a **doom scenario** should not be excluded beforehand and care should be exercised when putting additional stresses on our living habitat. A global rise in sealevel, due to melting icecaps, will be a worldwide economic disaster for many major cities situated along the recent seaside. A witness of the consequences of natural forces against human activity is the archaeological remains of the city of Alexandria, now found below the sealevel (... *and what about drowned Atlantis?* I hear some whisper in the background, where some microplate tectonic adjustments might have played also a role). Most of these changes happened gradually and there will be time to take the necessary infra-structural actions, but all measures have a certain cost attached to it.

Pollution issues need to be addressed in a pro-active manner in order to achieve sustainable growth (cf Rosen 2000). Geophysical methods are to play a major role in solving the **human waste** problems (cf Lynn 2002). The geological environment even has a direct effect on human health (Komatina 2004). Reservoir characterisation in the largest sense is needed to help engineers to address the environmental issues. Not only sedimentary rocks need attention but also crystalline rocks are of interest (cf Harvey et al. 2005). In all these domains seismic stratigraphy and sedimentology are contributing to a better understanding of our natural habitat. Knowing the structure and characteristics of the earth crust is essential for utilising resources in a sensible way. It also will show us how to go ahead with the exploration of other planets in the near future. The sensational discovery of water on Mars, the occurrence of possible micro-fossils, the presence of Structureless Organic Matter (SOM) and hydrocarbons (methane) are intriguing issues to be further investigated. The daring idea of using reflection seismic for the exploration of celestial bodies (Schuster 2004) sounds certainly very challenging, but seems an unavoidable next step after inventorisation of the resources of the planet Earth. Sponsoring of these huge research projects by the petroleum industry seems a logical step to generate the required funds for the intensified exploration of outer space.

Seismic stratigraphy has gradually penetrated our daily life in a way that can no longer be ignored. It has a bigger impact on the world's economic affairs than generally realised. With its dedicated researchers and motivated workforce, seismic stratigraphy will continue to make its contribution to the improvement of man's surroundings and it can be expected to do so in the decades to come.

Acknowledgements

It is impossible to write a textbook without the help of many other people. This volume represents a condensation of studies done during work experience as a geologist and geophysicist over the past 25 years. Various people have contributed to the efforts by sharing their knowledge with me. And of course I am indebted to all those who have provided their data and study material. Without them it would not have been possible to achieve this end-result. Two exceptional people have contributed in a substantial way to the final product: Ir M. Da Silva and Dr M. Rauch-Davies. They both gave stimulus to pursue this textbook project till the end. Patricia Laurie is thanked for her help in editing the English text. But most of all, I would like to thank Daniele and her children for bearing with me during the tedious task to prepare the final draft and many days were spent in front of the desktop computer.

As a student my first interest in geology was stimulated by my teachers Dr T.B. Roep, D. Beets, W. Nijman, D. Nio, H. Rondeel, O. Simon, B. Bollegraaf, W. Ten Kate, D. Van Harten, K. Linthout, T. Van Weering, T. Geel, H. Helmers, K. Hermes, C. Egeler and G. McGillavry. I thank my fellow-students for sharing the same scientific passion and of course for the fun we had.

With two of them, W. Dubelaar and G. Postma, I made a fieldtrip to the Harz in Germany in wintertime 1973. We lost the main crowd on our way because we had to fill up our Citroen Deux Cheveau limousine (also known as a '*ugly duck*' because of its flexible suspension system) with 25 litres of petrol. We eagerly wanted to rejoin the field party at the geologic outcrop. Suddenly it was realised we had taken the wrong road leaving the little German village. From our high vantage point the 'chauffeur' decided on a short cut, straight to the small road visible somewhere in the valley beneath. He started to navigate the jumpy European street car right across the snow covered slope of the hill as if it was a normal 4 wheel drive. When I saw the speed picking up in an uncontrolled manner, I started to get a bit scared

in the back-seat. Half-way down the slope I decided to leave the two lunatics in front of the car on their own, opened the passenger door and jumped straight out into the snow. I landed half on my feet and immediately started to run down-slope to break my speed. The mountain boots slipped away under my feet before I finally got the situation under control. Gazing from a distance, I saw the Deux Cheveau making funny rocking movements shaking the two passengers inside and on several occasions it twisted dangerously sideways. They spinned 360 degrees and the driver pulling the steering wheel desperately tried to avoid little trees, barb wire fencing and some big rocks on their way down. I was really afraid he would never manage to get it back on track, before hitting the steeper ravine below. Luckily he did put the vehicle on the small road and, whilst wiping some sweat off my forehead, I slowly went down the hill, feeling quite happy to safely join them again down-under. They received me with the welcoming remark: Were you afraid, Paul?

Dr P.A. Ziegler (SIPM) introduced me to basin analysis and seismic interpretation. This handbook would never have seen the light without his example of geologic enthusiasm and dedicated work attitude. I sincerely thank my ex-Shell colleagues for sharing their knowledge in petroleum geology with me.

Prof H. Reading, T. Elliott, E. Mutty and B. Normark were of great help to understand deep-sea clastic sedimentation patterns, despite some controversy (not really) in their approaches. The fieldtrips they organised were very entertaining and instructive. Especially the Fiat 500 mini-car, that entered the Piedmonte restaurant on instigation of Mutti's students, charmed us all with its magnificent musical system and was a memorable event on the Italian submarine fan fieldtrip with lots of bottles of excellent Verdiccio ...

The first draft of the seismic stratigraphy section was compiled at the Ecole Nationale Superieure de Geologie in Nancy (France), where I held a position as associated professor in applied geophysics. In the LSTS laboratory our research was focused on seismic and sequence stratigraphy, coalbed methane and shallow subsurface investigations. I am indebted to my direct colleagues: Dr G. Dagallier, F. Malatre, C. Palain, M. Hamdadou, M. Receveur, J. Allouc, J.L. Ainardi, C. Samama, K. Titov, J. Clermonte, J.P. Rehault, M. Guiraud, B. Durand, F. Van Buchem, R. Swennen, A. Laitinen, L. Zimmermann, J. Royer, M. Ford and J.L. Mallet. I also sincerely thank the students for their comments; it certainly helped to clarify some of the weaker points in my explanations. Mme Golec is thanked for helping with references.

Geophysical processing and reservoir characterisation were the main study subjects within the Compagnie Generale de Geophysique. I am grateful to several people: Dr D. Mougenot, Ir C. Pinson, S. Zimine, A. Zuidema, T. Bovier-Lapierre, J.M. Michel, J.P. Coulon, P. Mitouard, J.P. Diet, Y. Lafet, P. Duboz, V. Chaffard, B. Virlouvet, A. Mignot, E. Magdy, M. Taylor, S. Sioni, F. Berterin, E. Jenner, H. Japiot, P. Dervieux, N. Fabre, I. Jones, J.F. Dutzer, J. Frelet, P. De Plasterie, M. Krief, J.F. Eude, D. Cherief, J.L. Gelot, R. Martinez, A. Davies, N. Van Couvering, G. Castillo, G. Petit, G. Berthereau, W. Segovia, D. Gehant and S. Addy.

Seismic examples have been kindly provided by TotalFina-Elf and I would like to acknowledge: Dr J. Tachet des Combes, J.L. Piazza, F. Mila, L. Livingstone, Y. Lestunff, O. Bernet Rollande, O. Balz, V. Devaux, A. Dutzer, H. Fournier, L. Maurel, F. Pivot, J. Guilbot, D. Grenie, P. Imbert, F. Sommer, R. Braun, B. Mouilly, O. Dubrule and L. Sandjivi.

Pemex has granted their kind permission to release data from various studies. Gratitude goes to the following persons: Ir A. Marhx, prof H. Bernal, Ir E. Mendez, Ir J. Camara, Ir D. Contreras Tebar, Ir C. Barajas, Dr Q. Cardenas, Ir R. Vila Villasenor, Ir E. Guzman, Ir A. Escalera, Ir. I. Perez Negron, Ir R. Guzman Javier, Ir H. Aguilar Garza, Ir C. Lopez Lara, Ir. I. Garza, Ir M. Flores, Ir F. Islas Islas, Ir J. Estrada, Ir O. Mar Mondragon, Ir O. Lezania, Ir S. Patino, Ir E. Vargas, Ir A. Escamilla, Ir M. Cruz, J. Browett, R. Teran, E.G. Bendel. Special thanks is directed towards Dr G. Velasco Vasquez for helping to obtain the release of Pemex data.

Schlumberger is thanked for their support compiling the well logging section. Special efforts were made by Dr M. Andersen and S. Whittaker. Dr H. James of ParadigmGeo is thanked for the kindness to put voxel and multi attribute displays at our disposition. Dr R. Zaki (Centurion), V. Trocme (Gas de France), A. Gaaya (HCT), C. Bacchiana, T. Gueant (Georex), Y. Bassias (Georex) and K. Ouldamer (Amec Spie) are thanked for lively discussions on prospect evaluation issues.

Certainly there are people whom I forgot to mention and sincere apologies for that omission. The efforts of Elsevier publishing house to secure a full color print of the manuscript has been appreciated. Suggestions made by reviewers have improved the final product. Constructive remarks made by Dr M. Bacon (PetroCanada) and P. van Riel (Jason/Fugro) were highly valued. Mrs F. Wallien, P. Massar, C. Van Dijk, T. Van Daalen, S. Treitel and K. Helbig are acknowledged for their technical support and project handling.

Lithuanian VTEX is thanked for the typesetting of the manuscript. EAGE/SEG, AAPG and GeoArabia are thanked for granting permission to use various figures published in their journals.

Finally, I would like to sincerely thank all the people who have made this publication possible.

Trademarks

This page intentionally left blank

References

Abreu, V., M. Sullivan, C. Pirmez, D. Mohrig, 2003, Lateral accretion packages (LAP's): an important reservoir element in deep water sinuous channels. Marine and Petroleum Geology 20, 631–648.

Abriel, W.L., J.P. Stefani, R.D. Shank and D.C. Bartel, 1999, 3-D depth image interpretation. In: A.R. Brown (Ed.), Interpretation of Three Dimensional Seismic Data, AAPG memoir 42, Tulsa, p. 435–461.

Accaino, F., G. Boehm and U. Tinivella, 2005, Tomographic inversion of common image gathers. First Break 23 (3), 39–44.

Adigun, O., A. Okusanya and H. Okwa, 2004, Case study of geosteering a horizontal well in western Nigeria. The Leading Edge 23 (6), 588–591.

Addy, S.K., 1998, Neural network classification method helps seismic interval interpretation, Oil and Gas Journal 38, 47–59.

Adeogba, A.A., T.R. McHargue and S.A. Graham, 2005, Transient fan architecture and depositional controls from near surface 3D seismic data, Niger delta continental slope. AAPG bulletin 89 (5), 627–643.

Ainsworth, B., 2005, Sequence stratigraphic-based analysis of reservoir connectivity: influence of depositional architecture—a case study from a marginal marine depositional setting. Petroleum Geoscience 11 (3), 257–276.

Ajlani, G., M. Al Kaabi, O. Suwainna, 2003, Comparitive analysis (CASP): a proposal for quantifying seismic data processing. The Leading Edge 22 (1), 46–48.

Aki, K. and P.G. Richards, 1980, Quantitative Seismology, Theory and Methods. Freeman, San Francisco, 557 p.

Alkhalifah, T.A. and I. Tsvankin, 1995, Velocity analysis for transversely isotropic media. Geophysics 60, 1550–1566.

Al Belushi, J.D., K.W. Glennie and B.P.J. Williams, 1996, Permo-carboniferous glaciogenic Al Khlata formation, Oman: A new hypothesis for origin of its glaciation. GeoArabia 1 (3), 389–403.

Al Busaidi, R., 1997, The use of borehole imaging logs to optimize horizontal well completions in fractured water-flooded carbonate reservoirs. GeoArabia 2 (1), 19–34.

Al Chalabi, M., 1994, Seismic velocity—a critique. First Break 12, 589–596.

Al Husseini, M.I., 1997, Jurassic sequence stratigraphy of the western and southern Arabian Gulf. GeoArabia 2 (4), 361–382.

Ali, S., D. Norman, D. Wagner, J. Ayoub, J. Desroches, H. Morales, P. Price, D. Sheperd, E. Toffanin, J. Troncoso and S. White, 2002, Combined stimulation and sand control. Oilfield Review 14 (2), 31–47.

Allen, M.R., G.P. Goffey, R.K. Morgan and I.M. Walker, 2006, The deliberate search for the stratigraphic trap. Special Publication No. 254, Geological Society Publishing House, Bath, 312 p.

Al Mahrooqi, S., J. Terken, P. Senycia, M. Al Rawahy, P. Veeken and J. Filbrandt, 1999, Simsima carbonate wedges and their impact on the Shuaiba prospectivity in northern Oman. GeoArabia 5 (1), 28–30.

Al Naamani, A. and C. MacBeth, 2003, History matching using both production and 4D-4C seismic. First Break 21, 59–63.

Alsop, G.I., R.E. Holdsworth, K.J.W. Mc Caffrey and M. Hand, 2004, Flow Processes in Faults and Shear Zones. Special Publication No. 224, Geological Society Publishing House, Bath, 392 p.

Alvarez, W., P. Claeys and S.W. Kieffer, 1995, Emplacement of Cretaceous-Tertiary boundary shocked quartz from Chicxulub crater. Science 269, 930–935.

Ameen, M.S., 2003, Fracture and in-situ Stress Characterization of Hydrocarbon Reservoirs. Special Publication No. 209, Geological Society Publishing House, Bath, 224 p.

Aminzadeh, F., D. Connolly, R. Heggland, P. Meldahl and P. De Groot, 2002, Geohazard detection and other applications of chimney cubes. The Leading Edge 21 (7), 681–685.

Aminzadeh, F. and P. De Groot, 2004, Soft computing for qualitative and quantitative seismic object and reservoir property prediction. Part 1: Neural network applications. First Break 22 (3), 49–54.

Aminzadeh, F. and D. Wilkinson, 2004, Soft computing for qualitative and quantitative seismic object and reservoir property prediction. Part 2: Fuzzy Logic applications. First Break 22 (4), 69–78.

Amorosi, A. and S. Milli, 2001, Late Quaternary depositional architecture of Po and Tevere river deltas (Italy) and worldwide comparison with coeval deltaic successions. Sedimentary Geology 144, 357–375.

Anadon, P., L. Cabrera and K. Kelts, 1991, Lacustrine Facies Analysis. Special publication of IAS No. 13: Oxford, Blackwell Scientific Publications, 318 p.

Angerer, R.H. and H.J. Richgels, 1990, Reservoir states and elastic parameters: factors that affect reflection AVO. SEG 60th annual meeting, Expanded abstracts, p. 1537–1538.

Angerer, E., P. Lanfranchi and S. Rogers, 2003, Integrated fracture characterization from seismic processing to reservoir modeling. Expanded abstacts, SEG annual conference, Dallas, p. 43–46.

Anstey, N.A., 1982, Simple Seismics. International Human Resources Development Cooperation, Boston, 168 p.

Archie, G.E., 1942, The electrical resistivity log as an aid in determining reservoir characteristics. Transactions of AIME 146, 54–62.

Armentrout, J.M. and B.F. Perkins, 1991, Sequence stratigraphy as an exploration tool, concepts and practices in the Gulf Coast. SEPM Foundation 11th annual research conference, 417 p.

Arnott, R., 2003, The future of the upstream oil and gas industry: a city perspective. First Break 21 (2), 25–31.

Arthur, M.A. and S.O. Schlanger, 1979, Cretaceous oceanic anoxic events as causal factor in development of reef-reservoired giant oil fields. AAPG Bulletin 63 (6), 870–885.

Assefa, S., C. McCann and J. Sothcott, 2003, Velocities of compressional and shear waves in limestones. Geophysical Prospecting 51, 1–13.

Audigane, P., J.-J. Royer and H. Kaieda, 2002, Permeability characterization of the Soultz and Ogachi large-scale reservoir using induced microseismicity. Geophysics 67, 204–211.

Aug, C., P. De Beukelaar, W. De Boer and P. Veeken, in prep, Quantitative interpretation of the Central Brae Field using a neural network approach.

Aves, H.S. and D.M. Tappmeyer, 1985, The use of synthetic sonic logs derived from seismic data in the interpretation of stratigraphic variation in Cretaceous carbonates of the North Field area, Qatar. In: O.R. Berg and D.G. Woolverton (Eds), Seismic Stratigraphy II: An Integrated Approach to Hydrocarbon Exploration: AAPG Memoir No. 39: AAPG, Tulsa, p. 241–254.

Aylor, W.K., 1999, The business impact of 3D seismic. In: A.R. Brown (Ed.), Interpretation of Three Dimensional Seismic Data, AAPG memoir 42, Tulsa, p. xi–xiv.

Bachrach, R., M. Beller, C. Ching, J. Perdomo, D. Shelander, N. Dutta and M. Benabentos, 2004, Combining rock physics analysis, full waveform prestack inversion and high-resolution seismic interpretation to map lithology units in deep water: A Gulf of Mexico case study. The Leading Edge 23 (4), 378–382.

Backus, M., 1959, Water reverberations: their nature and elimination. Geophysics 24, 233–261.

Bacon, M., R. Simm and T. Redshaw, 2003, 3D Seismic Interpretation. Cambridge University Press, 222 p.

Baechle, G.T, R.J. Weger, G.P. Eberli, J.L. Massaferro and Y.F. Sun, 2005, Changes of shear moduli in carbonate rocks: implications for Gassmann applicability. The Leading Edge 24 (5), 507–510.

Bahorich, M. and S. Farmer, 1995, 3-D seismic discontinuity for faults and stratigraphic features: the coherency cube. The Leading Edge 14 (10), 1053–1058.

Baina, R., P. Thierry and H. Calandra, 2002, 3D preserved amplitude prestack depth migration and amplitude versus angle relevance. The Leading Edge 21 (12), 1237–1241.

Baines, S.J. and R.H. Worden, 2004, Geological Storage of Carbon Dioxide. Special Publication 233, Geological Society Publishing House, Bath, 264 p.

Bally, A.W., 1983, Seismic Expression of Structural Styles, AAPG studies in geology series No. 15, Vol. I, II and III: AAPG, Tulsa.

Bally, A.W., 1987, Atlas of Seismic Stratigraphy, AAPG studies in geology series No. 27, Vol. I, II and III: AAPG, Tulsa.

Bally, A.W. and S. Snelson, 1980, Realms of Subsidence. Canadian Society of Petroleum Geologists, Special Memoir No. 6, p. 1–94.

Balz, O., F. Pivot and P. Veeken, 1999, Reservoir characterization using neural networks controlled by petrophysical and seismic modeling. 61th EAGE annual meeting, Extended abstracts, Glasgow, Session S015, 4 p.

Balz, O., F. Pivot and D. Badolato, 2000, Fast identification of AVO-anomalies using classification of prestack waveforms. Expanded abstract, SEG annual convention, 4 p.

Banchs, R.E. and R.J. Michelena, 2002, From 3D seismic attributes to pseudo-well-log volumes using neural networks: practical considerations. The Leading Edge 21 (10), 996–1001.

Barwis, J.H., J.G. McPherson and R.J. Studlick, 1990, Sandstone Petroleum Reservoirs. Springer-Verlag, New York, 508 p.

Bate, D., 2005, 4D reservoir volumetrics: a case study over the Izaute gas storage facility. First Break 23 (1), 69–71.

Batzle, M. and Z. Wang, 1992, Seismic properties of pore fluids. Geophysics 57, 1396–1408.

Baum, G.R. and P.R. Vail, 1988, Sequence stratigraphy concepts applied to Paleogene outcrops, Gulf and Atlantic basins. In: Wilgus et al. (Eds), Sea-Level Changes: An Integrated Approach. Soc. Econ. Paleont./Mineral. San Francisco, Special Publication No. 42, p. 309–327.

Bear, L.K., T.A. Dickens, J.R. Krebs, J. Liu and P. Traynin, 2005, Integrated velocity model estimation for improved positioning with anisotropic PSDM. The Leading Edge 24 (6), 622–626.

Beaubouef, R.T. and V. Abreu, 2004, Basin 4 of the Brazos-Trinity slope system. Extended abstracts, EAGE annual conference, Paris, A028, 4 p.

Bebout, D.G. and A. Louks, 1974, Stuart city trend, lower Cretaceous, south Texas a carbonate shelf margin model for hydrocarbon exploration. Bureau Econ. Geol. Report No. 78, 80 p.

Belderson, R.H., N.H. Kenyon, A.H. Stride and C.D. Pelton, 1984, A braided distributary system on the Orinoco deep-sea fan. Marine Geology, 56, 195–206.

Benabentos, M., S. Mallick, M. Sigismondi and J. Soldo, 2002, Seismic reservoir description using hybrid seismic inversion: a 3D case study from the Maria Ines Oeste Field, Argentina. The Leading Edge 21 (10), 1002–1008.

Berg, O.R., 1982, Detection and evaluation of delta and turbidite sequences: their application to the exploration for the subtle trap. In: M.T. Halbouty (Ed.), The Deliberate Search for the Subtle Trap. AAPG Memoir 32, Tulsa, p. 57–91.

Berg, O.R. and D.G. Woolverton, 1985, Seismic Stratigraphy II: an integrated approach to hydrocarbon exploration. AAPG Memoir No. 39, AAPG, Tulsa, 276 p.

Bergler, S., P. Hubral, P. Marchetti, A. Christini and G. Cardone, 2002, 3D common-reflection-surface stack and kinematic wavefield attributes. The Leading Edge 21 (10), 1010–1015.

Berkhout, A.J., 1980, Seismic Migration—Imaging of Acoustic Energy by Wavefield Extrapolation. Elsevier, Amsterdam.

Berkhout, A.J, 2005, The seismic value chain—providing a new business concept for the seismic industry. The Leading Edge 24 (2), 146–149.

Berman, A.E., 2005, Northern Sumatra earthquake: 40 years of ignoring plate tectonics. First Break 23 (3), 77–85.

Berumen, S., H. Gachuz, J.M. Rodriguez, T. Bovier Lapierre and P. Kaiser, 2004, Hydraulic fracture mapping in treated wells; channelised reservoirs development optimisation in Mexico. Extended abstracts, 66th EAGE annual convention, Paris, 4 p.

Bevc, D. and B. Biondi, 2005, Which depth imaging method should you use? A roadmap through the maze of possibilities. The Leading Edge 24 (6), 602–606.

Bhattacharya, J.P., 1993, The expression and interpretation of marine flooding surfaces and erosional surfaces in cores; examples from the upper Cretaceous Dunvegan Formation, Alberta Foreland basin, Canada. In: Posamentier et al. (Eds), Sequence Stratigraphy and Facies Associations. Int. Ass. Sediment. Special Publication No. 18, p. 125–160.

Biju-Duval, B., 2002, Sedimentary Geology, Sedimentary Basins, Depositional Environments Petroleum Formation. Technip, Paris, 642 p.

Biot, M.A., 1941, General theory of three dimensional consolidation. Journal of Applied Physics 12, 155–164.

Biot, M.A., 1956, Theory of propagation of elastic waves in fluid saturated porous solid, I and II. Journal of Acoustic Society of America 28 (2), 168–191.

Bois, P., 1984, Fuzzy seismic interpretation. IEEE transactions on Geoscience and Remote Sensing GE-22 (6), 692–697.

Blatt, H., G. Middleton and R. Murray, 1972, Origin of Sedimentary Rocks. Prentice-Hall, Englewood Cliffs, New Jersey, 634 p.

Bonner, S., T. Burgess, B. Clark, D. Decker, J. Orban, B. Prevedel, M. Luling and J. White, 1993, Measurements at the drill bit: a new generation of MWD tools. Oilfield Review 5 (2), 44–54.

Bonner, S., M. Fredette, J. Lovell, B. Montaron, R. Rosthal, J. Tanabou, P. Wu, B. Clark, R. Mills and R. Williams, 1996, Resistivity while drilling: images from the string. Oilfield Review 8 (1), 4–19.

Booler, J. and M.E. Tucker, 2002, Distribution and geometry of facies and early diagenesis: Upper Cretaceous Congost Carbonate platform, Spanish Pyrenees. Sedimentary Geology 146 (3–4), 225–247.

Bose, A., V. Singh, B.S. Josyulu and Mahesh Chandra, 2004, A case study of lithographic and lithologic interpretation of thin reservoirs through an intergrated approach. The Leading Edge 23 (10), 966–972.

Bosellini, A., 1984, Progradation of carbonate platforms: examples from the Triassic of the Dolomites, northern Italy. Sedimentology 31, 1–24.

Bouma, A.H., G.T. Moore and J.M. Coleman, 1978, Framework, facies and oil-trapping characteristics of the upper continental margin, AAPG studies in geology No. 7, AAPG, Tulsa.

Bourque, D. and J. Stevens, 2005, Teamwork and technology resurrect mature field. The Leading Edge 24 (1), 63–66.

Boyer, S. and J.L. Mari, 1994, Sismique et Diagraphies, IFP publication. Editions Technip, Paris, 194 p.

Brandstaeter, I., D. McIlroy, O. Lia, P. Ringrose and A. Naess, 2005, Reservoir modelling ans simulation of Lajas Formation outcrops (Argentina) to constrain tidal reservoirs of the Halten Terrace (Norway). Petroleum Geoscience 11, 37–46.

Brechet, E., F. Pivot, J.M. Janisecki, S. Guillon and J. Demichelis, 2004, Fault sealing evaluation using seismic data in deep offshore turbidites. Extended abstracts, EAGE annual conference, Paris, C010, 4 p.

Breton, P., S. Crepin, J. Perrin, C. Esmersoy, A. Hawthorn, N. Underhill, B. Frignet, J. Haldorsen., T. Harold and S. Raikes, 2002, Well-positioned seismic measurements. Oilfield Review 14 (1), 32–45.

Brigaud, F., G. Vasseur and G. Caillet, 1992, Thermal state in the northern Viking Graben (North Sea) determined from exploration well data. Geophysics 57, 68–88.

Brinded, M., 2005, Leadership and partnership—imperatives for offshore safety. First Break 23 (4), 53–56.

Brooks, J. and K.W. Glennie (Eds), 1987, Petroleum Geology of North West Europe. Graham and Trotman, London, p. 576.

Broussard, M.L., 1975, Deltas, Models for Exploration. Houston Geological Society, Houston, 98 p.

Brouwer, J. and K. Helbig, 1998, Shallow High-Resolution Reflection Seismics. Pergamon Press, 404 p.

Brown, A.R., 1978, 3-D seismic survey gives better data. Oil and Gas Journal 77, 57–71.

Brown, L.F. and W.L. Fisher, 1976, Seismic facies reflection patterns: examples from Brazilian rift and pull-apart basins. In: Stratigraphic Interpretation of Seismic Data. Short Course Notes, AAPG, Tulsa and SEG, 48 p.

Brown, L.F. and W.L. Fisher, 1977, Seismic stratigraphic interpretation of depositional systems: Examples from Brazilian rift and pull-apart basins. In: Payton (Ed.), Seismic Stratigraphy: Application to Hydrocarbon Exploration, AAPG-Memoir No. 26, AAPG, Tulsa, p. 213–248.

Brown, L.F. and W.L. Fisher, 1980, Seismic stratigraphic interpretation and petroleum exploration. Continuing education course note series 16: AAPG, Tulsa, 56 p.

Brown, A.R., 1988, Interpretation of three dimensional seismic data. AAPG Memoir 42, AAPG, Tulsa, 253 p.

Brown, A.R. (Ed.), 1999, Interpretation of three dimensional seismic data, AAPG Memoir 42: AAPG, Tulsa, SEG Investigations in Geophysics No. 9, 514 p.

Brown, A.R., 2005, Pitfalls in 3D seismic interpretation. The Leading Edge 24 (7), 716–717.

Browne of Madingley, L., 2004, International trade is the key to world energy security. First Break 22 (5), 15–17.

Bruhn, R. and F. Surlyk, 2004, Sand-grade density flow evolution on a shelf-edge-slope-basin-floor complex in the Upper Jurassic Olympen Formation, East Greenland. Petroleum Geoscience 10, 81–92.

Bryant, I.A., Malinvemo, M. Prange, M. Gonfalini, J. Moffat, D. Swager, P. Theys and F. Verga, 2002, Understanding uncertainty. Oilfield Review 14 (3), 2–15.

Bryson, B., 2003, A Short History of Nearly Everything. Transworld Publishers, London, 687 p.

Buland, A. and H. Omre, 2003, Bayesian linearized AVO inversion. Geophysics 68 (1), 185–198.

Burgess, K., T. Fields, E. Harrigan, G. Golich, T. MacDougall, R. Reeves, S. Smith, K. Thornsberry, B. Ritchie, R. Rivero, R. Siegfield, 2004, Formation testing and sampling through casing, Oilfield Review 14 (1), 47–57.

Burhannudin, S., 1994, Geologie des bassins de la Mer de Banda (Indonesie). Thesis, Universite de Bretagne Occidentale, Brest, 196 p.

Burk, A.C. and C.L. Drake, 1974, The Geology of Continental Margins. Springer Verlag, New York, 1009 p.

Caers, J., T. Hoffman, S. Strebelle and X. Wen, 2006, Probabilistic integration of geologic scenarios, seismic and production data—a West Africa turbidite reservoir case study. The Leading Edge 25 (3), 240–244.

Cafarelli, B., S. Randazzo, S. Cambell, J. Fernandez Sobreira, M. Galotti Guimaraes, C. Rodriguez, P. Johann and C. Theodoro, 2006, Ultra-deep 4-C offshore Brazil. The Leading Edge 25 (4), 474–477.

Calvert, R., 2005, Insights and methods for 4D reservoir monitoring and characterisation. EAGE/SEG Distinguished Instructor Short Course No. 8, 219 p.

Cambois, G., 2000, AVO inversion and elastic impedance. Extended abstracts SEG annual meeting, Calgary, p. 1–4.

Cambois, G., 2000, Can P-wave AVO be quantitative. The Leading Edge 19 (11), 1246–1251.

Cambois, G., 2001, AVO processing: Myths and reality. Expanded abstract, SEG annual convention, San Antonio, 4 p.

Car, A.D. and H.I. Petersen, 2004, Modelling of the hydrocarbon generation history and volumetric considerartions of the coal sourced Lulita Field, Danish North Sea. Petroleum Geoscience 10, 107–119.

Cara, M., 1989, Geophysique. Dunod, Paris, 186 p.

Carcione, J.M and F. Cavallini, 2002, Poisson's ratio at high pore pressure. Geophysical Prospecting 50, 97–106.

Carcione, J.M. and A.F. Gangi, 2000, Gas generation and overpressure: effects on seismic attributes. Geophysics 65, 1769–1779.

Carr, A.D. and I.C. Scotchman, 2003, Thermal history modelling in southern Faroe-Shetland Basin. Petroleum Geoscience 9, 333–345.

Carrilat, A., H.G. Borgosi, T. Randen, L. Sonneland, L. Kvamme and K. Hansch, 2004, Fault systems analysis using automatic fault displacement estimates—a case study. Extended abstracts, EAGE annual conference, Paris, B037, 4 p.

Carruba, S., R. Casnedi and F. Felletti, 2004, From seismic to bed: surface-subsurface correlations within turbiditic Cellino Formation (central Italy). Petroleum Geoscience 10, 131–140.

Casciano, C., L. Ruvo, B. Volpi and F. Masserano, 2004, Well test simualtion through Discrete Fracture Network modelling in a fractured carbonate reservoir. Petroleum Geoscience 10, 331–343.

Castagna, J.P., M.L. Batzle and R.L. Eastwood, 1985, Relationships between compressional and shear-wave in clastic silicate rocks. Geophysics 50, 571–581.

Castagna, J.P. and M.M. Backus, 1993, Offset dependent reflectivity—Theory and practice of AVO analysis. SEG, Tulsa, Investigations in Geophysics No. 8, 348 p.

Castagna, J.P. and J. Swan, 1997, Principles of AVO crossplotting. The Leading Edge 12 (4), 337–342.

Castagna, J.P., S. Sun and R.W. Siegfried, 2003, Instantaneous spectral analysis: Detection of low frequency shadows associated with hydrocarbons. The Leading Edge 22 (2), 120–127.

Castagna, J.P. and S. Sun, 2006, Comparison of spectral decomposition methods. First Break 24 (3), 75–79.

Cazes, M. and G. Torreilles, 1988, Etude de la croute terrestre par sismique profonde. Editions Technip, Paris.

Chakraborty, S., S. Phadke and R.K. Verma, 2004, AVA inversion using real-coded genetic algorithm. Extended abstracts, EAGE annual Conference, Paris, P 307, 4 p.

Chambers, H. and A.L. Brown, 2003, 3D visualisation continues to advance integrated interpretation environment, First Break 21, 67–70.

Chiarelli, A. and F. Issard, 1990, Central Graben (Norway): Hydrocarbon distribution related to source rock maturation, Abstract—Amer. Ass. Petroleum Geol. Bull. 74, 627.

Chiburis, E., S. Leaney, C. Skidmore, C. Franck and S. McHugo, 1993, Hydrocarbon Detection with AVO. Oil Field Review 5 (1), 42–50.

Chopra, S. and V. Alexeev, 2004, A new approach to enhancement of frequency bandwidth of surface seismic data. First Break 22 (8), 21–42.

Christie, P., K. Dodds, D. Ireson, L. Johnston, J. Rutherford, J. Schaffer and N. Smith, 1995, Borehole seismic data sharpen the reservoir image. Oil Field Review 7, 18–31.

Claerbout, J.F., 1985, Fundamentals of Geophysical Data Processing. McGraw-Hill, New York.

Clement, 1977, A case history of geoseismic modelling on Basal Morrow Springer sandstones. In: Payton (Ed.), Seismic Stratigraphy: Application to Hydrocarbon Exploration, AAPG-Memoir No. 26: AAPG, Tulsa, p. 451–476.

Cloetingh, S., 1986, Intraplate stresses: a new mechanism for relative fluctuations of sealevel. Geology 14, 617–620.

Cloetingh, S., A.J. Tankard, H.J. Welsink and W.A.M. Jenkins, 1989, Vail's coastal onlap curves and their correlation with tectonic events, offshore eastern Canada. In: A.J. Tankard and H.R. Balkwill (Eds), Extensional Tectonics and Stratigraphy of the North Atlantic Margins. AAPG Memoir 46, p. 283–293.

Cojan, I. and M. Renard, 2003, Sedimentogie. Dunod, Paris, 418 p.

Coleou, T., H. Hoeber and D. Lecerf, 2002, Multivariate geostatistical filtering of time-lapse seismic data for an improved 4-D signature. 72 th SEG annual convention, Salt Lake City, 4 p.

Colella, A. and I. Di Geromino, 1987, Surface sediments and macro faunas of the Crati submarine fan (Ionian Sea, Italy). Sedimentary Geology 51, 257–277.

Connolly, P., 1999, Elastic impedance, The Leading Edge 18 (4), 438–452.

Contreras, A. and C. Torres-Verdin, 2005, More vertical resolution and accuracy with less uncertainty in reservoir characterisation. First Break 23 (10), 75–78.

Cooke, D.A. and W.A. Sneider, 1983, Generilized linear inversion of reflection seismic data. Geophysics 48, 665–676.

Cope, J.M., 2003, Algerian licensing round may offer opportunity for exploration plays in deep offshore frontier. First Break 21 (7), 37–42.

Cosentino, L., 2001, Integrated Reservoir Studies. Technip, Paris, 310 p.

Cou, A.L., 2003, The Sedimentary Record of Sealevel Change. Cambridge, p. 288.

Coulon, J.P., P. Duboz and Y. Lafet, 2000, Moving from seismic to layered impedance cube and porosity prediction in the Natih E member. GeoArabia 5 (1), 72–73.

Cramez, C., B. Duval and P. Vail, 1993, Major marine source rocks and stratigraphic cycles: in EAEG Workshop handout (Stavanger), Zeist, EAEG, p. 1–30.

Crans, W., G. Mandl and J. Haremboure, 1980, On the theory of growth faulting: a geomechanical model based on gravity sliding. Journal of Petroleum Geology 2 (3), 265–307.

Criss, C.J., C. Kiger, P. Maxwell and J. Musser, 2005, Full-wave seismic acquisition and processing: the onshore requirement. First Break 23 (2), 53–61.

Croswell, K., 2003, Magnificent Mars. Free Press, 212 p.

Cubitt, J.M., W.A. England and S.R. Larter, 2004, Understanding petroleum reservoirs: towards an integrated reservoir engineering and geochemical approach. Special Publication No. 237, Geological Society Publishing House, Bath, 402 p.

Dabrio, C.J., 1990, Fandelta facies associations in Late neogen and Quaternary basins of southeastern Spain. In: A. Colella and D.B. Prior (Eds), Coarse Grained Deltas. Special publication No. 10, International Association of Sedimentologists. Blackwell Scientific Publisher, Oxford, p. 91–112.

Dagallier, G., A. Laitinen, F. Malartre, I.P.A.M. Van Campenhout and P.C.H. Veeken, 2000, Ground Penetrating Radar application in a shallow marine Oxfordian limestone sequence located on the eastern flank of the Paris Basin, NE France. Sedimentary Geology 130, 149–165.

Dai, J., H. Xu, F. Snijder and N. Dutta, 2004, Detection and estimation of gas hydrates using rock physics and seismic inversion: examples from the northern deepwater Gulf of Mexico. The Leading Edge 23 (1), 60–66.

Dake, L.P., 2002, The Practice of Reservoir Engineering. Elsevier, Amsterdam, Developments in Petroleum Science 36, 572.

Damuth, J.E., R.D. Flood, R.O. Kowsmann, R.H. Belderson and M.A. Gorini, 1988, Anatomy and growth pattern of Amazon deep-sea fan as revealed by Long-Range Side-Scan Sonar (GLORIA) and high-resolution seismic studies, Amer. Ass. Petroleum Geol. Bull. 72, 885–911.

Darwin, C., 1859, On the origin of species by means of natural selection, or the preservation of favoured races in the struggle for life.

Darwin, C. and J. Burrow, 1984, The Origin of Species. Penguin English library, Penguin Books, Harmondsworth, 479 p.

Darwin, C. and G. Cannon, 1983, The voyage of the 'Beagle'. Everyman classic, Clay and Dent, London, 496 p.

Da Silva, M., M. Rauch, A. Soto Cuervo and P.C.H. Veeken, 2004, Data conditioning for a combined inversion and AVO reservoir characterisation study. EAGE 66th annual conference, Paris 2004, Extended Abstract, P306, 4 p.

Da Silva, M., M. Rauch, A. Soto Cuervo and P.C.H. Veeken, 2004, Pre- and post-stack seismic attributes for enhancing production from Cocuite gas reservoirs. EAGE 66th annual conference, Paris, Extended Abstract, D001, 4 p.

Dash, B.P. and A. Obaidullah, 1970, Determination of signal and noise statistics using correlation theory. Geophysics 35 (1), 24–32.

Davies, R.J. and J. Cartwright, 2002, A fossilised Opal A to Opal C/T transformation on the northeast Atlantic margin: support for a significantly elevated paleo geothermal gradient during the Neogene. Basin Research 14, 467–486.

Davies, R.J., J.A. Cartwright, S.A. Stewart, M. Lappin and J.R. Underhill, 2004, 3D seismic technology: application to the exploration of sedimentary basins. Memoir 29, Geological Society Publishing House, Bath, 364 p.

Davies, S.J. and T. Elliott, 1994, Gamma ray response of high resolution sequence stratigraphic signatures in Upper Carboniferous delta systems; an analogue for the subsurface. In: Suchecki et al. (Eds), Application of Sequence Stratigraphy to Oil Field Development, AAPG Hedberg Research Conference, Paris, p. 1–5.

Dautenhahn, K., K. Wyatt, S.B. Wyatt, S.K. Towe, J.E. Layton, D.H. Von Seggern and C.A. Brockmeier, 1994, Building velocity-depth models for 3-D depth migration. The Leading Edge 13 (8), 862–866.

D'Agosta, C., K. Marfurt, R.J. Michelena, 2005, Processing and geometric attribute analysis of 3D PS-converted waves. The Leading Edge 24 (5), 512–514.

De Angelo, M.V., M. Bachus, B.A. Hardage, P. Murray and S. Knapp, 2003, Depth registration of P-wave and C-wave seismic data for shallow marine sediment characterisation, Gulf of Mexico. The Leading Edge 22 (2), 96–105.

De Beukelaar, P., V. Favreau, F. Lemaire, P. Plasterie and P. Veeken, 1997, Subsurface geological model refinement with a 3D ray trace imaging technique. Proceedings Subsurface modelling Seminar, Ecole de Mines, Paris, 1–3.

De Beukelaar, P., P. Plasterie and P.C.H. Veeken, 1998, 3D subsurface model building and depth conversion using a tetrahedral raytracing method. First Break 16 (10), 341–349.

De Beukelaar, P., L. Livingstone, J.L. Piazza and P. Veeken, In Press, Pre-stack synthetic modelling using neural network QC on dipole shear sonic imager data. Extended abstracts, 66th EAGE annual convention, Paris, 4 p.

De Boer, P.I and D.G. Smith 1994, Orbital forcing and cyclic sequences. In: P.I. De Boer and D.G. Smith, Orbital Forcing and Cyclic Sequences. Oxford, Blackwell Special Publication 19, p. 1–14.

Dee, S., B. Freeman, G. Yielding, A. Roberts and P. Bretan, 2005, Best practice in structural geological analysis. First Break 23 (4), 49–54.

Deffeyes, K.S., 2001, Hubert's Peak: The Impending World Oil Shortage. Princeton University Press, 208 p.

Deflandre, P., C. Maisons, T. Bovier-Lapierre, P. Meynier and J. Czernichow, 2004, On-tubing seismic sensor in flowing wells, review of noise parameters. Extended abstracts, 66th EAGE annual convention, Paris, 4 p.

De la Grandville, B., 1982, Appraissal and development of a structural and stratigraphic trap oil field with reservoirs in glacial to periglacial clastics. In: M.T. Halbouty (Ed.), The Deliberate Search for the Subtle Trap, AAPG Memoir 32, Tulsa, p. 267–286.

Delaughter, J., B. Meltz, S. Smith, J. Yun and M. Murat, 2005, Use ofd Z-score to rescale amplitudes. The Leading Edge 24 (7), 698–701.

De Margerie, C., 2004, Hydrocarbons outlook is not all gloomy. First Break 22 (7), 15–16.

Demicco, R.V. and G.J. Klir, 2002, Fuzzy Logic in Geology. Elsevier Academic Press, Amsterdam, 350 p.

Denham, L.R. and D.K. Agarwal, 1999, Depth conversion. In: A.R. Brown (Ed.), Interpretation of Three Dimensional Seismic Data, AAPG memoir 42, Tulsa, p. 423–434.

Den Hartog Jager, D., M.R. Giles and G.R. Griffiths, 1993, Evolution of Paleogene submarine fans of the North Sea in space and time. In: J.R. Parker (Ed.), Petroleum Geology of North Western Europe—Proc. 4th Conf., Geological Society of London, London, p. 59–71.

De Rooy, M., P.W.M. Corbett and L. Barens, 2002, Point bar geometry, connectivity and well test signatures. First Break 20, 755–763.

De Wit, P., 2002, Creatief with CO2. Shell Venster, No. 1, p. 2.

De Wit, P., 2004, Vloeibaar gas is 'hot'. Shell Venster, No. 2, p. 2.

De Wit, P., 2004, De reserves van Shell, vragen aan Jeroen van der Veer. Shell Venster, No. 2, p. 4–5.

Diet, J.-P., A. Soares, O. Colnard, C. Renaldo and J. Santos, 2002, Integration of inverted seismic volumes into stochastic reservoir models. Extended abstracts, 64th annual convention EAGE, H040.

Dix, C.H., 1955, Seismic velocities from surface measurements. Geophysics 20, 68–86.

Dobrin, M.B. and C.H. Savit, 1988, Introduction to Geophysical Prospecting. MacGraw-Hill, New York, 867 p.

Dong, W. 1996, A sensitive combination of AVO slope and intercept for hydrocarbon indication. Extended abstracts, 58th EAGE annual conference, Amsterdam, M044, 4 p.

Donovan, D.T. and E.J.W. Jones, 1979, Causes of worldwide changes in sealevel. Journal Geological Society of London 136, 187–192.

Doust, H., 2003, Placing petroleum systems and plays in their basin history context. Tectonophysics 371, 81–110.

Dragoset, B., 2005, A historical reflection on reflections. SEG/Leading Edge Special 24 (S1), s46–s70.

Dronkert, H. and K.J. Weber, 1998, Recovery of mobile remaining oil to extend the life of mature oil fields. Extended abstracts, 60th annual convention EAGE, Session 03-09.

Droste, H.H.J., 1997, Stratigraphy of the Lower Paleozoic Haima Supergroup of Oman. GeoArabia 2 (4), 419–472.

Drzewiecki, P.A. and J.A. Simo, 2002, Depositional processes, triggering mechanisms and sediment composition of carbonate gravity flow deposits: examples from the Late Cretaceous of the south-central Pyrenees, Spain. Sedimentary Geology 146, 155–189.

Du, Y. and L. Guan, 2005, Improved modeling of gas condensate reservoirs by integrating static and dynamic data. The Leading Edge 24 (1), 76–79.

Duboz, P., Y. Lafet and D. Mougenot, 1998, Moving to a layered impedance cube: advantages of 3D stratigraphic inversion. First Break 16 (9), 311–318.

Dubrule, O., 2003, Geostatistics for seismic data integration in earth models. EAGE distinguished instructor series No. 6, 282 p.

Duffaut, K., T. Alsos, M. Landroe and H. Rognoe, 2000, Shear-wave elastic impedance. The Leading Edge 19 (11), 1223–1229.

Duin, E., 2001, A detailed 3-D seismic interpretation of a salt dome and its caprock, a case study in the northeastern Netherlands. Expanded abstracts, 71st Annual convention SEG, p. 670–673.

Duindam, P. and B. Van Hoorn, 1987, Structural evolution of the West Shetland continental margin. In: Brooks and Glennie (Eds), Petroleum Geology of North West Europe. Graham and Trotman, London, p. 765–775.

Dunbar, C.O and J. Rodgers, 1957, Principles of Stratigraphy. Wiley, New York, 365 p.

Durand, B., 1980, Kerogen: Insoluble Organic Matter from Sedimentary Rocks. Editions Technip, Paris, 519 p.

Durand, J., 1996, Geometries deltaiques: Passage de l'echelle de la carotte et de l'affleurement a l'echelle de la sismique. Thesis HDR, University of Pau et des Pays de l'Ardour, Part I, 142 p. and part II, 317 p.

Dutta, N.C., 1987, Fluid flow in low permeable porous media. In: Doligez (Ed.), Migration of Hydrocarbons in Sedimentary Basins. Technip, Paris, p. 567–595.

Dutta, N.C., 2002, Geopressure prediction using seismic data: Current status and the road ahead. Geophysics 67 (6), 2012–2041.

Dvorkin, J. and S. Alkhater, 2004, Pore fluid and porosity mapping from seismic. First Break 22, 53–57.

Eenhorst, W., 2003, Samen slim. Shell Venster, No. 3, p. 18–21.

Ehrenberg, S.N., 2004, Factors controlling porosity in Upper Carboniferous–Lower Permian carbonate strata of the Barents Sea. AAPG Bulletin 88 (12), 1653–1676.

Elkibbi, M. and J.A. Rial, 2001, An outsider's review of the astronomical theory of the climate: is the eccentricity driven insolation the main driver of the ice ages? Earth Science Review 56, 161–177.

Ellis, L., A. Brown, M. Schoell and S. Uchytil, 2003, Mud gas isotope logging (MGIL) assists in oil and gas drilling operations. Oil and Gas Journal, May, p. 32–41.

Embry, A.F., 1994, Evaluation of sequence types. In: Suchecki et al. (Eds), Application of Sequence Stratigraphy to Oil Field Development, AAPG Hedberg Research Conference, Paris, p. 1–5.

Erxleben, A.W. and G. Carnahan, 1983, Slick ranch area, Starr County, Texas. In: Bally (Ed.), Seismic expression of structural styles, Studies in geology series 15, Vol. 2, AAPG, Tulsa, p. 2.3.1/22–26.

Esmersoy, C., A. Hawthorn, C. Durrand and P. Amstrong, 2005, Seismic MWD: Drilling in time, on time, it's about time. The Leading Edge 24 (1), 56–62.

Evans, A.L., F.J. Fitch and J.A. Miller, 1973, Potassium-argon age determinations on some British Tertiary igneous rocks, Journal Geological Society of London 129, 419–443.

Fabre, N., S. Gluck, P. Guillaume and Y. Lafet, 1989, Robust multichannel stratigraphic inversion of stacked seismic traces, 59th annual meeting SEG, p. 943.

Fatti, J.L., G.C. Smith, P.J. Vail, P.J. Strauss and P.R. Levitt, 1994, Detection of gas in sandstone reservoirs using AVO analysis: A 3-D seismic case history using the Geostack technique. Geophysics 59, 1362–1376.

Faust, L.Y., 1951, Seismic velocity as a function of depth and geologic time. Geophysics 16, 192–206.

Faust, L.Y., 1953, A velocity function including lithologic variations. Geophysics 18, 271–287.

Figueira, J.C.A., 2005, How long will E&P be the fundamental driver to support the energy business. The Leading Edge 24 (2), 182–184.

Fisher, W.L. and L.F. Brown, 1972, Clastic depositional systems—a genetic approach to facies analysis, University of Texas, Bur. Econ., 211 p.

Flueh, E.R, D. Klaeschen and J. Bialas, 2002, Options for multi-component seismic data acquisition in deep water. First Break 20, 764–769.

Fomel, S., 2004, On anelleptic approximations for P velocities in VTI media, 2004, Geophysical Prospecting 52 (3), 247–259.

Ford, M., W.H. Lickorich and N. Kuznir, 1999, Tertiary foreland sedimentation in the southern subalpine chains, SE France: a geodynamic analysis. Basin Research 11, 315–336.

Fortuin, A.R., J.M.D. Kelling and Th.B. Roep, 1995, The enigmatic Messinian-Pliocene section of Cuevas del Almanzora (Vera Basin, SE Spain) revisted—erosional features and strontium isotope ages. Sedimentary Geology 97, 177–201.

Foster, D., S.W. Smith, S.K. Dey-Sarkar and H.W. Swan, 1993, A closer look at hydrocarbon indicators, Expanded abstracts, 63rd Annual convention SEG, 731–733.

Fountain, D., R. Smith, T. Payne and J. Lemieux, 2005, A helicopter time-domain EM-system applied to mineral exploration: system and data. First Break 23 (1), 73–78.

Fournier, F. and A. Derain, 1995, A statistical methodology for deriving reservoir properties from seismic data. Geophysics 60 (5), 1437–1450.

Frankel, C., 1999, La Vie sur Mars. Editions de Seuil, Paris, 317 p.

Gaarenstroom, L., R.A.J. Tromp, M.C. De Jong and A.M. Brandenburg, 1993, Overpressures in the central North Sea: implications for trap integrity and drilling safety. In: J.R. Parker (Ed.), Petroleum Geology of Northwestern Europe, Proceedings of 4th conference, Geological Society of London, Bath, p. 1305–1313.

Garcia Hernandez, J., M Gonzalez Castillo, J. Zavaleta Ruiz, A. Chernikoff and V. Ploskiewicz, 2005, Structural style of the Gulf of Mexico's Cantarell complex. The Leading Edge 24 (2), 136–138.

Gardner, G.H.F., L.W. Gardner and A.R. Gregory, 1974, Formation velocity and density—The diagnostic basics for stratigraphic traps. Geophysics 39, 770–780.

Garotta, R., 1999, Shear waves from acquisition to interpretation. SEG/EAGE short course No. 3, Houston, 242 p.

Gartrell, A., C. Hudson and B. Evans, 2004, The influence of basement faults during extension and oblique inversion of the Makassar straits rift system: insights from analog models. AAPG Bulletin 89 (9), 495–506.

Gassmann, F., 1951, Elastic waves through a package of spheres. Geophysics 16 (4), 673–685.

Gassmann, F., 1951, Uber die Elastitat Poroser Medien. Vierteljahrschrift der Naturforsch Gesellschaft Zurich 96, 1–21.

Gatliff, R.W., K. Hitchen, J.D. Ritchie and D.K. Smythe, 1984, Internal structure of the Erlend Tertiary volcanic complex, north of Shetland, revealed by seismic reflection. Journal Geological Society of London 141, 555–562.

Gausland, I., 2004, Reflections on 3D seismic. First Break 22 (11), 49–52.

Geel, T., Th.B. Roep, W. ten Kate and J. Smit, 1992, Early-Middle Miocene stratigraphic turning points in the Alicante region (SE Spain): reflections of Western Mediterranean plate-tectonic reorganizations. Sedimentary Geology 75, 223–239.

Gengyi, C., X. Zhu, W. Wenbo, Y. Qinfan and L. Chaoying, 2006, Seismic interpretation using seismic trace frequency attributes properties—a preliminary study. First Break 24 (1), 47–55.

Gibbs, A.D., 1983, Balanced cross-section construction from seismic sections in areas of extensional tectonics. Journal of Structural Geology 5, 153–160.

Giere, P. and P. Stille, 2004, Energy, Waste and the Environment: A Geochemical Perspective. Special Publication No. 236, Geological Society Publishing House, Bath, 688 p.

Gierse, G., J. Pruesmann, E. Laggiard, C. Boennemann and H. Meyer, 2003, Improved imaging of 3D marine seismic data from offshore Costa Rica with CRS processing. First Break 21 (12), 45–49.

Giroldi, L., A. Lopez Angriman, J.P. Blangy, J.C. Cordoba and E. Martinez, 2005, Seismically driven appraisal and development: a case study from Bolivia's Chaco Basin. The Leading Edge 24 (11), 1099–1108.

Giroldi, L. and F. Alegria, 2005, Using spectral decomposition to identify and characterize glacial valleys and fluvial channels within the Carboniferous section in Bolivia. The Leading Edge 24 (11), 1152–1159.

Glogovsky, V., E. Landa and J. Paffenholz, 2002, Integrated approach to subsalt depth imaging: synthetic case study. The Leading Edge 21 (12), 1217–1223.

Gluck, S., E. Juve and Y. Lafet, 1997, High resolution impedance layering through 3D stratigraphic inversion of post-stack seismic data. The Leading Edge 16, 1309–1315.

Gluyas, J. and R. Swarbrick, 2004, Petroleum Geoscience. Blackwell, Oxford, 239 p.

Goetz, J.F. and L. Dupal, 1979, An investigation into discrepancies between sonic log and seismic checkshot velocities. APEA, p. 1–11.

Gochioco, L.M., 2002, Recent role of geophysics in U.S. coal and CBM development. The Leading Edge 21 (5), 452–455.

Goffe, W.L., G.D. Ferrier and J. Rodgers, 1994, Global optimisation of statistical functions with simulated annealing. Journal of Econometrics 60, 65–100.

Gold, T., 1979, Terrestrial sources of carbon and earthquake outgassing, J. Petrol. Geol. 1 (3), 3–19.

Goodway, W., T. Chen and J. Downton, 1997, Improved AVO fluid detection and lithology determination using Lame's petrophysical parameters: LambdaRho, MuRho and Lambda/Mu fluid stack from P and S inversions. Canadian Society of Exploration Geophysicists, Abstracts, p. 148–151.

Gorell, S., T. Smart, K. Narayanan, P. Sabharwal and S. Bassett, 2005, Next generation modelling workflows improve reservoir management decisions. First Break 23 (10), 81–85.

Gould, A., 2004, Rapid uptake of new technology is the key to managing production decline. First Break 22 (7), 8–11.

Goulty, N.R., 2002, Mechanics of layer-bound polygonal faulting in finegrained sediments. Journal of the Geological Society, London 159, 239–246.

Goulty, N., 2003, Reservoir stress path during depletion of Norwegian Chalk oilfields. Petroleum Geoscience 9 (3), 233–241.

Goulty, N.R., 2004, Mechanical compaction behaviour of natural clays and implications of pore pressure estimation. Petroleum Geoscience 10, 73–79.

Granger, P.Y. and J.M. Bonnot, 2001, C-Wave resolution enhancement through birefringence compensation at the Valhall Field. Extended abstracts, 63th EAGE annual convention, Amsterdam, 4 p.

Gregory, A.R., 1977, Aspects of rock physics from laboratory and log data that are important to seismic interpretation. In: Payton (Ed.), Seismic Stratigraphy: Application to Hydrocarbon Exploration, AAPG-Memoir No. 26, AAPG, Tulsa, p. 15–46.

Gretener, P. and L. Thomsen, 2003, AVO and Poisson's ratio. The Leading Edge 22 (1), 70–72.

Guilbot, J., M. Grausem and P.L. Pichon, 1996, Lithology classification using seismic impedance, Bongkot field, Gulf of Thailand. Extended Abstracts, 59th Conference EAGE, 4 p.

Guilbot, J., F. Pirera, H. Sabra, K.B. Rasmussen and D.J. Davies, 2003, Detailed Low-Frequency Modeling for Improved Acoustic Impedance inversion at Ekofisk. Extended abstracts, 65th annual convention EAGE, D04.

Guillocheau, F., P. Razin, C. Robin, R. Blanke, E. Lasseur, F Bechennec and S. Gorican, 2004, Carbonate deep-sea turbiditic systems: The example of the Toarcian Oxfordian of the Tethyan paleomargin of Oman. Extended abstracts, EAGE annual conference, B035, 4 p.

Gurney, K., 1997, An Introduction to Neural Networks. University College London Press, London, 234 p.

Haas, A. and O. Dubrule, 1994, Geostatistical inversion, a sequential method of stochastic reservoir modelling constrained by seismic data. First Break 12 (11), 561–569.

Haas, A., J. Herweyer and O. Dubrule, 1994, Geostatistics for integration of reservoir data, EAEG 6th conference Vienna, Extended abstracts, Zeist, EAEG, p. C012.

Halbouty, M.T., 1982, The deliberate search for the subtle trap, AAPG Memoir 32, AAPG, Tulsa, 352 p.

Han, D.H., R. Nur and D. Morgan, 1986, Effects of porosity and clay content on wave velocities in sandstones. Geophysics 51 (11), 2093–2110.

Han, D. and M. Batzle, 2006, Velocities of deepwater reservoir sands. The Leading Edge 25 (4), 460–466.

Haneveld, C.J. and G.C. Herman, 1990, A fast algorithm for the computation of Radon transforms. Geophysical Prospecting 38, 853–860.

Hanna, S.S., 1995, Field guide to the geology of Oman. Volume 1, Western Hajar mountains and Musandam. Historical Association of Oman, Ruwi, p. 178.

Hansen, H.J., K.B. Rasmussen, K.G. Maver, L.K. Stroenen and P. Digranes, 2004, Gullfaks field using 4D simultaneous inversion. Extended abstracts, EAGE annual conference, Paris, P207, 4 p.

Haq, B.U., J. Hardenbol and P. Vail, 1988, Mesozoic and Cenozoic chronostratigraphy and cycles of sealevel change. In C.K. Wilgus et al. (Eds), Sealevel Changes: An Integrated Approach. SEPM Special Publication No. 42, San Francisco, SEPM, p. 71–108.

Haq, B.U., 1993, Deep sea response to eustatic change and significance of gas hydrates for continental margin stratigraphy. In: H.W. Posamentier, C.P. Summerhayes, B.U. Haq and G.P. Allen (Eds), Sequence Stratigraphy and Facies Associations. Oxford, Blackwell Special Publication No. 18, p. 93–106.

Hardage, B.A., 1983, Vertical Seismic Profiling: Principles. Geophysical Press, London, 450 p.

Hardage, B.A., 1985, Vertical seismic profiling—a measurement that transfers geology to geophysics. In: O.R. Berg and D.G. Woolverton (Eds), 1985, Seismic Stratigraphy II: An Integrated Approach to Hydrocarbon Exploration, AAPG Memoir No. 39, AAPG, Tulsa, p. 13–34.

Hardage, B.A., 1999, Vertical Seismic Profiling: Principles. Elsevier, Amsterdam, Seismic exploration, Vol. 14, 570 p.

Hardy, D., 2004, Reassessing the shared earth model makes sense. First Break 22 (4), 63–66.

Hart, B. and M. Chen, 2004, Understanding seismic attributes through forward modelling. The Leading Edge 23 (9), 834–841.

Hartstra, B., G. Graham and J. Hartsink, 1996, The Athel silicilyte play: status and scope. In: Petroleum Development Oman, New Ideas From Old Basins, p. 78–86.

Harvey, P.K., T.S. Brewer, P.A. Pezard and V.A. Petrov, 2005, Petrophysical properties of crystalline rocks. Special Publication No. 240, Geological Society Publishing House, Bath, 360 p.

Hatton, L., M.H. Worthington and J. Makin, 1996, Seismic Data Processing, Theory and Practice. Blackwell Publisher, Oxford, 177 p.

Hays, J.D. and W.C. Pitman, 1973, Lithospheric plate motion, sealevel changes and climatic and ecological consequences. Nature 246, 18–22.

Heggland, R., P. Meldahl, P. de Groot and F. Aminzadeh, 2000, Chimneys in the Gulf of Mexico, The American Oil and Gas Reporter 43, 78–83.

Helgesen, J., I. Magnus, S. Prosser, G. Saigal, G. Aalmodt D. Dolberg and S. Busman, 2000, Comparison of constrained sparse spike and stochastic inversion for porosity prediction at Kristin Field. The Leading Edge 19, 400–407.

Helland-Hansen, D., I. Magnus, A. Edvardsen and E. Hansen, 1997, Seismic inversion for reservoir characterisation and new well planning in the Snorre field. The Leading Edge 16 (3), 269–273.

Helle, H.B. and A. Bhatt, 2002, Fluid saturation from well logs using committee neural networks. Petroleum Geoscience 8 (2), 109–118.

Helbig, K., 1984, Anisotropy and dispersion in periodically layers media. Geophysics 49 (4), 364–373.

Henke, C., J. Schober, U. Weber, F. Gholami and H. Tabatabai, 2006, Exploring the High Zagras (Iran): A challenge for geophysical integration. First Break 23 (11), 31–41.

Henri, G., 1994, Geophysique des Bassins Sedimentaires, Elf Acquitaine publication, Editions Technip, Paris, 445 p.

Herodotus, −425, Histories. Translation G. Rawlinson, Wordsworth Editions (1996), Ware, 734 p.

Hesthammer, J. and M. Boulaenko, 2005, The offshore EM challenge. First Break 23 (11), 59–66.

Hildebrand, A.R., G.T. Penfield, D.A. Kring, M. Pilkington, Z.A. Camargo, S.B. Jacobsen and W.V. Boynton, 1991, Chicxulub Crater: A possible Cretaceous/Tertiary boundary impact crater on the Yucatan Penninsula, Mexico. Geology 19, 867–871.

Hill, R.W., 1952, The elastic behavior of crystalline aggregate. Proceedings Physical Society London A65, 349–354.

Hill, S.J., 2005, Inversion-based thickness determination. The Leading Edge 24 (5), 477–480.

Hill, S.J., K. Marfurt and S. Chopra, 2006, Searching for similarity in a slab of seismic data. The Leading Edge 25 (2), 168–177.

Hilterman, F.J., 2001, Seismic amplitude interpretation, SEG/EAGE short course no. 4, Houston, 242 p.

Hilterman, F. and M. Dunn, 2004, Seismic amplitude attributes for GOM sediments. Expanded abstract, 74$^{\text{th}}$ SEG annual convention, Denver, 4 p.

Hinz, K., 1983, Line BGR 76-11 from Central East Greenland margin. In: Bally (Ed.), Seismic Expression of Structural Styles, Studies in geology series 15, Vol. 2, AAPG, Tulsa, p. 2.2.3–45.

Hirono, T., 2005, The role of dewatering in the progressive deformation of a sandy accretionary wedge: constraints from direct imagings of fluid flow and void structure. Tectonophysics 397, 261–280.

Hodgson, P., C. Cunnell, A. Krueger and A. MacGregor, 2005, Cluster visualization rises to the seismic processing challenge. First Break 23 (3), 69–71.

Holl, H.G., I. Moeck, H. Schandelmeier, 2004, Geothermal well Gross Schoenbeck 3/90: a low enthalpy reservoir (Rotliegend, NE Germany). Extended abstracts, EAGE annual conference, Paris, F032, 4 p.

Holland, D., 2004, Managing the journey to the digital oil field. The Leading Edge 23 (11), 1137–1138.

Holmes, A., 1970, Principles of Physical Geology. Nelson and Sons, London, 1288 p.

Hornbach, M.J., W.S. Holbrook, A.R. Gorman, K.L. Hackwith, D. Lizarralde and I. Pecher, 2003, Direct seismic detection of methane hydrate on the Blake Ridge. Geophysics 68 (1), 92–100.

Hubbard, R.J., 1988, Age and significance of sequence boundaries on Jurassic and Early Cretaceous rifted continental margins. Bulletin of American Association of Petroleum Geologists 72, 42–72.

Hubral, P., 1977, Time migration—some ray theoretical aspects. Geophysical Prospecting 25, 738–745.

Hubral, P., J. Schleicher, M. Tygel and C. Hanitzsch, 1993, Determination of Fresnel zones from travel time measurements. Geophysics 58, 703–712.

Hubral, P. and T. Krey, 1980, Interval velocities from seismic reflection time measurements. Society of Exploration Geophysicists, Tulsa, p. 203.

Hossack, J.R., 1984, The geometry of listric growth faults in the Devonian basins of Sunnfjord, W Norway. Journal Geological Society of London 141, 629–637.

Hunt, J.M., 1990, Generation and migration of petroleum from abnormally pressured fluid compartments. AAPG Bulletin 74, 1–12.

Huuse, M., D. Duranti, C.G. Guargena, P. Prat, K. Holm, N. Steinsland, B.T. Cronin, A. Hurst and J. Cartwright, 2003, Sandstone intrusions: detection and significance for exploration and production. First Break 21, 33–42.

Ibrahim, A.A., 2005, 3D raytracing modelling to assess the effects of overburden and acquisition geometry on illumination of pre-evaporite reservoirs in Karachaganak Field, Kazakhstan. The Leading Edge 24 (9), 940–944.

IHRDC, 2004, Why under-balanced drilling is the E&P tool of the moment. First Break 22 (1), 29–32.

Ikelle, L.T. and L. Amundsen, 2005, Introduction to Petroleum Seismology. Investigations in geophysics No. 12, SEG, Tulsa, 688 p.

Illies, J.H., 1981, Mechanism of graben formation, Inter. Union Comm. of Geodynamics Sci. Rept. No. 63, Elsevier, Amsterdam, 266 p.

Illing, L.V. and G.D. Hobson, 1981, Petroleum Geology of the Continental Shelf of Northwest Europe: Heyden, London.

Inden, R.F. and C.H. Moore, 1978, Beach environments. In: P.A. Scholle, D.G. Bebout and C.H. Moore (Eds), Carbonate Depositional Environments, AAPG Memoir No. 33, AAPG, Tulsa, p. 211–265.

International Association of Geophysical Contractors (IAGC), 2003, Industry at a crossroads: A message from the geophysical industry. The Leading Edge 22 (1), 14–17.

Issler, D.R., 1992, A new approach to shale compaction and stratigraphic restoration; Beaufort-McKenzie basin and McKenzie corridor, North Canada. AAPG Bulletin 8, 1170–1189.

Jack, I., 1998, Time lapse seismic in reservoir management. SEG/EAGE short course No. 1, Houston, 196 p.

Jackson, M.D., S. Yoshida, A.H. Muggeridge and H.D. Johnson, 2005, Three dimensional reservoir characterisation and flow simulation of heterolithic tidal sandstones. AAPG Bulletin 89 (4), 507–528.

Jacque, M. and J. Thouvenin, 1975, Lower Tertiary tuffs and volcanic activity in the North Sea. In: A.W. Woodland (Ed.), Petroleum and the Continental Shelf of NW Europe, Vol. 1, Barking, Applied Science, p. 455–465.

Jacques, J.M., 2004, The influence of intraplate structural accommodation zones on delineating petroleum provinces of the sub-Andean foreland basins. Petroleum Geoscience 10 (1), 1–19.

Jacques, J.M, A.D. Price and J.E. Bain, 2004, Digital integration of potential fields and geologic data sets for plate tectonic and basin dynamic modelling—the first step toward identifying new play concepts in the Gulf of Mexico Basin. The Leading Edge 23 (4), 384–389.

Jaeger, R., J. Mann, G. Hoecht and P. Hubral, 2001, Common-reflection-surface stack: image and attributes. Geophysics 66 (1), 97–109.

James, H. and T. Kostrova, 2005, Use of lighting in the 3D display of seismic data. First Break 23 (3), 53–57.

Jansen, J.D, D.R. Brouwer, G. Naevdal and C.P.J.W. Kruijsdijk, 2005, Closed-loop reservoir management. First Break 23 (1), 43–48.

Japsen, P., A. Bruun, I.L. Fabricius, R. Rasmussen, O. Vejbeak, J. Moerch Pedersen, G. Mavko, C. Mogensen and C. Hoier, 2004, Influence of porosity and pore fluid on acoustic properties of chalk: AVO response from oil, South Arne Field, North Sea. Petroleum Geoscience 10, 319–330.

Jenkyns, 1979, Pelagic environments. In: H.G. Reading (Ed.), Sedimentary Environments and Facies, Blackwell Scientific Publisher, Oxford, p. 324–371.

Jenner, E., 2002, Azimuthal AVO: methodology and data examples. The Leading Edge 21 (8), 782–786.

Jensen, J.L, L.W. Lake and P.W.M. Corbett, 2000, Statistics for Petroleum Engineers and Geoscientists. Elsevier, Amsterdam, Handbook of Petroleum Exploration and Production, Vol. 2, 356 p.

Johansen, S.E., H.E.F. Admundsen, T. Rosten, S. Ellingsrud, T. Eidesmo and A.H. Bhuyian, 2005, Subsurface hydrocarbons detected by electromagnetic sounding. First Break 23 (3), 31–36.

Johnson, J.D., 1992, Structural imaging in the real world. The Leading Edge 11 (1), 32–36.

Jolley, D.W. and A.G. Whitham, 2004, A stratigraphical and paleoenvironmental analysis of the sub-basaltic Paleogene sediments of East Greenland. Petroleum Geoscience 10, 53–60.

Jones, I.F., J.P. Diet, P. Guillaume and F. Audebert, 1995, Prestack 3D depth imaging – a stepwise approach for the interpreter. 57th EAEG/EAPG Conference, Glasgow. Extended Abstracts, EAGE, Zeist, A017.

Jones, I.F, M. Grimshaw, K. Ibbotson and B. Jolley, 1996, A new 3D Pre-SDM model building technique: a North Sea case study. 66th SEG Conference, Denver. Expanded Abstracts, SEG, Tulsa, p. 363–365.

Jones, I.F., K. Ibbotson, M. Grimshaw and P. Plasterie, 1998, 3-D prestack depth migration and velocity model building. The Leading Edge 17 (7), 897–906.

Jones, I.F., 2003, Data visualisation and interpretation: A review of 3D PreSDM model building techniques. First Break 21, 45–58.

Jones, I.F., M.L. Bridson and N. Bernitsas, 2003, Anisotropic ambiguities in TI media. First Break 21, 31–37.

Joseph, P. and S.A. Lomas, 2004, Deep water sedimentation in the Alpine basin of SE France: New perspectives on the Gres d'Annot and related systems. Geological Society of London, Special publications, 221 p.

Jonk, R., A. Hurst, D. Duranti, J. Parnell, A. Mazzini and A.E. Fallick, 2005, Origin and timing of sand injection, petroleum migration and diagenisis in Tertiary reservoirs, South Viking Graben, North Sea. AAPG Bulletin 89 (3), 329–357.

Jum'ah, A.S., 2005, Saudi Aramco chief confident that cooperation can stave off energy crisis. First Break 23 (4), 7–10.

Junger, A., 1964, Signal-to-noise ratio and record quality. Geophysics 29 (6), 922–925.

Kaplan, R.D., 2003, Reis naar de einden der aarde (The ends of the earth, a journey at the dawn of the 21st century, 1997). Spectrum, Aula series, Utrecht/Amsterdam, 479 p.

Kearey, P. and M. Brooks, 1991, An Introduction to Geophysical Exploration, 2nd edition. Geoscience Texts. Blackwell Scientific Publisher, Oxford, 254 p.

Kearey, P. and F.J. Vine, 1990, Global Tectonics. Geoscience Texts. Blackwell Scientific Publisher, Oxford, 302 p.

Kendall, C. and W. Schlager, 1981, Carbonates and relative sealevel changes in sealevel. Marine Geology 44, 181–212.

Kent, P., 1982, The Evolution of Sedimentary Basins. Royal Society of London, London, 324 p.

Kheidri, L.H., S. Ziou and N. Abdelouahab, 2005, Geodynamic evolution of the Algerian offshore and its impact on the structural framework and play types. First Break 23 (4), 37–39.

Khripounoff, A., A. Vangriesheim, N. Babonneau, P. Crassous, B. Dennielou and B. Savoye, 2003, Direct observation of intense turbidity current activity in the Zaire submarine valley at 4000 m water depth. Marine Geology 194 (3–4), 151–158.

King, C.A.M., 1973 Rhythmic coastal forms. In: V.K. Verma, R.C. Misra, S.S. Merh Gaur and K. Valdiya (Eds), Recent Researches in Geology. Hindustan Publi. Corp., Delhi, Vol. 1, p. 219–243.

Kingston, D.R., C.P. Dishroon and P.A. Williams, 1983, Global basin classification system. AAPG Bulletin 67, 2175–2193.

Klefstad, L., S. Kvarsvik, J.E. Ringas, J.J. Stene and O. Sundsby, 2005, Characterisation of deeply buried heterolithic tidal reservoirs in the Smorbukk Field using inverted post-stack seismic acoustic impedance. Petroleum Geoscience 11, 47–56.

Kleverlaan, K., 1987, Gordo megabed: a possible seismite in a Tortonian submarine fan, Tabernas Basin, province Almeria, southeast Spain. Sedimentary Geology 51, 165–180.

Kleverlaan, K., 1989, Three distinctive feeder-lobe systems within one time slice of the Tortonian Tabernas fan, SE Spain. Sedimentology 36, 25–45.

Kleyn, A.H., 1977, On the migration of reflection-time contour maps. Geophysical Prospecting 25, 125–140.

Kleyn, A.H., 1983, Seismic Reflection Interpretation. Applied Science Publishers, London.

Klinkby, L., L. Kristensen, E.B. Nielsen, K. Zinck-Joergensen and L. Stemmerik, 2005, Mapping and characterisation of thin chalk reservoirs using data intergration: the Kraka field Danish North Sea. Petroleum Geoscience 11, 113–124.

Koefoed, O., 1955, On the effect of Poisson's ratios of rock strata on the reflection coefficients of plane waves, Geophysical Prospecting 3, 381–387.

Koestler, A.G. and R. Hunsdale, 2002, Hydrocarbon Seal Quantification. Norwegian Petroleum Society special publication, Vol. 11. Elsevier, Amsterdam, 288 p.

Kolla, V. and F. Coumes, 1987, Mophology, internal structure, seismic stratigraphy and sedimentation on the Indus Fan. AAPG Bulletin 71, 650–677.

Kolla, V., P. Bourges, J.M. Urruty and P. Safa, 2001, Evolution of deep water Tertiary sinuous channels offshore Angola (West Africa) and implication for reservoir architecture. AAPG Bulletin 85 (8), 1373–1405.

Komatina, M.M., 2004, Medical Geology, Effects of Geological Environments on Human Health. Elsevier, Amsterdam, 500 p.

Kommedal, J.H., S. Fowler and J. McGarrity, 2005, Improved P-wave imaging with 3D OBS data from the Clair field. First Break 23 (1), 51–54.

Koning, T. and F.X. Darmono, 1984, The geology of the Beruk Northeast Field, central Sumatra—Oil production from pre-Tertiary basement rocks. In: Proceedings of the Thirteenth Annual Convention, May 29–30, Indonesian Petroleum Association, Jakarta, Indonesia.

Kooi, H. and S.A.P.L. Cloetingh, 1989, Intraplate stresses and the tectono-stratigraphic evolution of the central North Sea. Amer. Ass. Petroleum Geol., Mem 46, p. 541–558.

Krail, P.M., 2004, Rock properties and amplitude versus angle. The Leading Edge 23 (10), 986–988.

Krief, M., J. Garat, J. Stellingwerff and J. Ventre, 1990, A petrophysical interpretation using velocities of P and S wave (full waveform sonic), The Log Analyst, Vol. 31, p. 355–369.

Kummel, B., 1970, History of the Earth, an Introduction to Historical Geology. Freeman and Co, San Fransico, 707 p.

Kutasov, I.M. and L.V. Eppelbaum, 2005, Drawdown test for a stimulated well produced at a constant bottomhole pressure. First Break 23 (2), 25–28.

Lagendaal, H., 2004, Ondergrondse ruilhandel. Shell Venster, No. 2, p. 20–23.

Laitinen, A.I., I.P.A.M. Van Campenhout and P.C.H. Veeken, 1996, Application of digital Ground Penetrating Radar (GPR) for investigating road constructions. Proceedings Eurasphalt Eurobitume Congress, p. 1–15.

Lancaster, S. and D. Whitcombe, 2000, Fast track "coloured" inversion. SEG annual meeting Calgary, p. 1572–1575.

La Rue, D.K. and F. Friedman, 2005, Controversy concerning stratigraphic architecture of channelized reservoirs and recovery by waterflooding. Petroleum Geoscience 1 (2), 131–146.

Lasseter, T.J. and S.T. Jackson, 2004, Improving integrated interpretation accuracy and efficiency using a single consistent reservoir model from seismic to simulation. The Leading Edge 23 (11), 1118–1121.

Latimer, R.B., R. Davison and P. Van Riel, 2000, Interpreter's guide to understanding and working with seismic derived acoustic impedance data. The Leading Edge 19 (3), 242–256.

Latimer, R.B., 2004, Lithology substitution in fluvial sand. The Leading Edge 23 (2), 108–112.

Lavergne, M., 1986, Methodes sismiques. Editions Technip, Paris, 206 p.

Lawyer, L., 2004, From the other side. The Leading Edge 23 (7), 626.

Leaman, D.E., 1994, Criteria for evaluation of potential field interpretations. First Break 12 (4), 181–191.

Le Carlier, C., J.-J. Royer and E.L. Flores, 1994, Convective heat transfer at the Soultz-sous-Forets geothermal site: Implications for oil potential. First Break 12 (11), 553–559.

Levin, G. and P. Straat, 1977, Recent results from the Viking labeled release experiment on Mars. Journal of Geophysical Research 82, 4663–4667.

Linari, V., M. Santiago, C. Pastore, K. Azbel and M. Poupon, 2003, Seismic facies analysis based on 3D multi attribute volume classification, La Palm Field, Maraibo, Venezuela. The Leading Edge 22 (1), 32–36.

Lindanger, R., M Oygaren, R.H. Gabrielsen, R. Mjelde, T. Randen and B.A. Tjostheim, 2004, Analogue (plaster) modeling and synthetic seismic representation of hanging wall fault blocks above ramp-flat ramp extensional faults. First Break 22 (1), 33–41.

Lindseth, R., 1979, Synthetic sonic logs—a process for stratigraphic interpretation. Geophysics 44, 3–26.

Lindseth, R.O. and V.L. Beraldo, 1985, A Late Cretaceous submarine canyon in Brazil. In: O.R. Berg and D.G. Woolverton (Eds), Seismic Stratigraphy II: An Integrated Approach to Hydrocarbon Exploration, AAPG Memoir No. 39, AAPG, Tulsa, p. 169–182.

Liner, C.L., 2002, Phase, phase, phase. The Leading Edge 21 (5), 456–457.

Lines, L.R. and R.T. Newrick, 2004, Fundamentals of Geophysical Interpretation, SEG Geophysical Monograph Series No. 13, SEG, Tulsa, 288 p.

Lomas, S.A. and P. Joseph, 2004, Confined turbidite systems. Special Publication No. 222, Geological Society Publishing House, Bath, 336 p.

Long, A., 2003, Marine acquisition: moving beyond the signal-to-noise ratio. First Break 21 (12), 67–70.

Long, A., 2004, Post survey calibration of 3D seismic results to presurvey modelling predictions. The Leading Edge 23 (10), 1033–1036.

Loosveld, R.J.H., A. Bell and J. Terken, 1996, The tectonic evolution of interior Oman. GeoArabia 1 (1), 28–51.

Lopez, L., P.M. Rappold, G.A. Ugueto, J. Wieseneck and C.K. Vu, 2004, Integrated shared earth model: 3D pore pressure prediction and uncertainty analysis. The Leading Edge 23 (1), 52–59.

Loutit, T.S., J. Hardenbol, P.R. Vail and G. Baum, 1988, Condensed sections: the key to age determination and correlation of continental margin sequences. In: C.K. Wilgus, B.S. Hastings, H. Posamentier, J. van Wagoner, C.A. Ross, C.G. Kendall (Eds), Sealevel Changes: An Integrated Approach. SEPM Special Publication No. 42, SEPM, San Francisco, p. 183–213.

Lucet, N., P.Y. Dequirez and F. Cailly, 2000, Well to seismic calibration: a multiwell analysis to extract a single wavelet. Expanded abstracts, 70 th annual convention SEG, p. 1615–1618.

Lucet, N. and F. Fournier, 2001, 4-D data interpretation through seismic facies analysis, Expanded abstracts, 71st annual convention SEG, p. 1640–1643.

Luo, M., I. Takahashi, M. Takanashi and Y. Tamura, 2005, Mapping a fracture network using wide azimuth OBC seismic data. The Leading Edge 24 (1), 95–99.

Lynn, W., 2002, Keeping the Mo on strategic planning and action. The Leading Edge 21 (10), 958–959.

Lynn, H.B., 2004, The winds of change; Anisotropic rocks—their preferred direction of fluid flow and their associated seismic signatures—Part I. The Leading Edge 23 (11), 1156–1162.

Ma, X., 2002, Simultaneous inversion of prestack seismic data for rock properties using simulated annealing. Geophysics 67 (6), 1877–1885.

MacAndrew, R., N. Parry, J. Prieur, J. Wiggelman, E. Diggins, P. Guicherey, D. Cameron, A. Stewart, 1993, Drilling and testing hot high pressure wells. Oilfield Review, No. 2, p. 15–32.

Magoon, L.B. and W.G. Dow, 1994, The petroleum system. AAPG-Memoir No. 60, AAPG, Tulsa, p. 3–24.

Magoon, L.B., T.L. Hudson and H.E. Cook, 2001, Pimienta-Tamabra—a giant supercharged petroleum system in the southern Gulf of Mexico, onshore and offshore Mexico. In: C. Bartolini, R.T. Buffler and A. Cantu-Chapa (Eds), The Western Gulf of Mexico Basin: Tectonics, Sedimentary Basins and Petroleum Systems. AAPG Memoir No. 75, Tulsa, p. 83–125.

Maison, C., E. Fortier, E. Gaucher and P. Kaiser, 2005, Fracture mapping using microseismic monitoring data from a treatment well. Expanded abstracts, 2nd EAGE North African/Mediterranean Petroleum and Geosciences Conference, A33, 4 p.

Makhous, M. and Y. Galushlin, 2004, Basin Analysis and Modeling of the Burial, Thermal and Maturation Histories in Sedimentary Basins. Editions Technips, Paris, 394 p.

Mallet, J.L., 2002, Geomodeling. Oxford University Press, New York, 600 p.

Mallet, J.L., 2004, Space-time mathematical framework for sedimentary geology. Journal of Mathematical Geology 36 (1), 1–32.

Mallet, J.L., R. Moyen, T. Frank, L. Castanie, B. Leflon and J.J. Royer, 2004, Getting rid of stratigraphic grids. Extended abstracts, EAGE annual conference, Paris, B019, 4 p.

Mallick, S., X. Huang, J. Lauve and R. Ahmad, 2000, Hybrid seismic inversion: A reconnaissance tool for deep water exploration. The Leading Edge 19 (11), 1230–1237.

Malod, J.A. and D. Mougenot, 1979, L'histoire geologique neogene du golfe de Cadix. Bulletin Societe Geologique de France 21 (5), 603–661.

Malod, J.A., F. Klingerhoefer, R. Bartolome, R. Thiebot and J.P. Rehault, 2004, Crustal structure of the NW Moroccan Atlantic Margin from seismic data. Extenede abstracts, EAGE annual conference, Paris, D012, 4 p.

Mancini, E.A., T.A. Blasingame, R. Archer, B.J. Panetta, J.C. Llinas, C.D. Haynes and D.J. Benson, 2004, Improving recoverey from mature oil fields producing from carbonate reservoirs: Upper Jurassixc Smackover Formation, Womack Hill Field (eastern Gulf coast, USA). AAPG Bulletin 88 (12), 1629–1651.

Manley, D.M, S.F. Mohammed, N.D. Robinson and R.W. Thomas, Structural interpretation of the deepwater Gunashli Field facilitated by 4-C OBS seismic data. The Leading Edge 24 (9), 92–926.

Marchal, D., 1997, Approche spatio-temporelle des mechanismes de la propagation des failles normales: des modelisations analogiques a la sismique 3D. Thesis Universite Henri Poincare-Nancy-I, 327 p.

Maresh, J. and R.S. White, 2005, Seeing through a glass, darkly: strategies for imaging through basalt. First Break 23 (4), 27–32.

Mari, J.L. and F. Coppens 1989, La Sismique de Puits. Editions Technip, Paris.

Mari, J.L., G. Arens, D. Chapellier and P. Gaudiani, 1998, Geophysique de Gisement et de Genie Civil, Editions Technip, Paris, 468 p.

Mari, J.L., F. Glangeaud and F. Coppens, 1999, Signal Processing for Geologists and Geophysicists. Editions Technip, Paris, 458 p.

Marsh, T., J. Tyrrell and L. Evins, 2005, Role of automated techniques in improving volume based structural interpretation. First Break 32 (6), 89–93.

Marshall, I.E., 2003, Country risk: The good, bad and ugly. First Break 21, 67–72.

Marshall, J. and T. Hewett, 2004, Devonian. In: The Millenium Atlas: Petroleum Geology of the Central and Northern North Sea. Geological Society of London, p. 65–81.

Marten, R., M. Shann, J. Mika, S. Rothe and Y. Quist, 2004, Seismic challenges of developing the pre-Pliocene Akhen field, offshore Nile Delta. The Leading Edge 23 (4), 314–320.

Martin, G.S., R. Wiley and K.J. Marfurt, 2006, Marmousi2: an elastic upgrade for Marmousi. The Leading Edge 25 (2), 156–166.

Martinius, A.W., P.S. Ringrose, C. Bromstrom, C. Elfenbein, A. Naess and J.E. Ringas, 2005, Reservoir challenges of heterolithic tidal sandstone reservoirs in the Halten Terrace, Mid-Norway. Petroleum Geoscience 11, 3–16.

Marty, B., S. Dewonck and C. France-Lanord, 2003, Geochemical evidence for efficient aquifer isolation over geological timeframes. Nature 425 (9), 55–58.

Masaferro, J.L., R. Bourne and J.C. Jauffred, 2003, 3D visualisation of carbonate reservoirs. The Leading Edge 22 (1), 18–25.

Masson, B. and L.G. Berry, 1968, Elements of Mineralogy. Freeman and Co, San Fransisco, 550 p.

Matthews, M.D. and M.A. Perlmutter, 1994, Global cyclostratigraphy: an application to the Eocene Green River basin. In: P.I. De Boer and D.G. Smith, Orbital Forcing and Cyclic Sequences. Oxford, Blackwell Special Publication 19, p. 459–481.

Maultzsch, S., S. Horne, S. Archer and H. Burkhardt, 2003, Effects of anisotropic overburden on azimuthal amplitude analysis in horizontal transverse isotropic media. Geophysical Prospecting 51, 61–74.

Maultzsch, S., M. Chapman, E. Liu and X.-Y. Li, 2003, The potential of measuring fracture sizes with frequency dependent shear-wave splitting. First Break 21, 45–51.

McCarthy, C.J. and P.W. Bilinsky, 1999, Impact of 3D seismic on structural interpretation of prospect Cougar. In: A.R. Brown (Ed.), Interpretation of Three Dimensional Seismic Data, AAPG memoir 42, Tulsa, p. 338–345.

McCormack, M.D., M.G. Justice and W.W. Sharp, 1985, A stratigraphic interpretation of shear and compressional wave seismic data for the Pennsylvanian Morrow Formation of southwest New Mexico. In: O.R. Berg and D.G. Woolverton (Eds), Seismic Stratigraphy II: An Integrated Approach to Hydrocarbon Exploration, AAPG Memoir No. 39, AAPG, Tulsa, p. 225–239.

McKay, D. et al., 1996, Search for past life on Mars: possible relic biogenic activity in martian meteorite ALH84001. Science 273, 924–930.

McKay, S., 2005, Autostereoscopic 3D displays: bringing Imax to the desktop. First Break 23 (3), 59–62.

McKenzie, D.P., 1978, Same remarks on the evolution of sedimentary basins. Earth and Planetary Science Letters 40, 25–32.

McMahon, N., K. Ruitenbeek, J. Wams and S. Slawson, 1999, Best practices in 3-D land seismic acquisition in the Middle East and North Africa: Cost-effective acquisition in a low oil price environment. GeoArabia 4 (2), 183–196.

Meckel, L.D and A.K. Nath, 1977, Geologic considerations for stratigraphic modelling and interpretation. In: Payton (Ed.), Seismic Stratigraphy: Application to Hydrocarbon Exploration, AAPG-Memoir No. 26, AAPG, Tulsa, p. 417–438.

Mees, F., R. Swennen, M. Van Geet and P. Jacops, 2003, Applications of X-ray Computed Tomography in the Geosciences. Special Publication No. 215, Geological Society Publishing House, Bath, 243 p.

Meldahl, P., R. Heggland, B. Bril and P. de Groot, 2001, Identifying targets like faults and chimneys using multi-attributes and neural networks. The Leading Edge 20 (5), 474–482.

Mercado Herrera, V., B. Russell and A. Flores, 2006, Neural networks in reservoir characterization. The Leading Edge 25 (4), 402–411.

Metropolis, N., A. Rosenbluth, M. Rosenbluth, M. Teller and E. Teller, 1953, Equation of state calculations by fast computing machines. Journal Chem. Phys. 21, 1087–1092.

Metwalli, F.I. and J.D. Pigott, 2005, Analysis of petroleum system criticals of the Matruh-Shushan Basin, Western Desert, Egypt. Petroleum Geoscience 11 (2), 157–178.

Miall, A.D., 1991, Stratigraphic sequences and their chronostratigraphic correlation. Journal of Sedimentary Petrology 61, 505.

Miall, A.D., 1992, Exxon global cycle chart: an event for every occasion? Geology 20, 787–790.

Miall, A.D., 1994, Accuracy and precision in biostratigraphic correlation: Implications for global eustacy and sequence stratigraphy. In: Suchecki et al. (Eds), Application of Sequence Stratigraphy to Oil Field Development, AAPG Hedberg Research Conference, Paris, p. 1–4.

Milankovitch, M., 1941, Kanon der Erdbestrahlung und seine Anwendung auf das Eiszeitenproblem. Royal Serbian Sciences Special Publication 132, Vol. 33.

Milkov, A.V. and R. Sassen, 2001, Estimate of gas hydrate resource, northwestern Gulf of Mexico continental slope. Marine Geology 178, 71–83.

Milkov, A.V. and R. Sassen, 2003, Two-dimensional modelling of gas hydrate decomposition in the northwestern Gulf of Mexico: significance to global change assessment. Global and Planetary Change 36 (1–2), 31–46.

Milner, P.A., 1998, Source rock distribution and thermal maturity in the southern Arabian Peninsula. GeoArabia 3 (3), 339–356.

Mitchum, R.M, P.R. Vail and S. Thompson, 1977, Seismic stratigraphy and global changes in sealevel, part 2: The depositional sequence as a basic unit for stratigraphic analysis. In: Payton (Ed.), Seismic Stratigraphy: Application to Hydrocarbon Exploration. AAPG-Memoir No. 26, AAPG, Tulsa, p. 53–62.

Mitchum, R.M., 1985, Seismic stratigraphic expression of submarine fans. In: O.R. Berg and D.G. Woolverton (Eds), Seismic Stratigraphy II: An Integrated Approach to Hydrocarbon Exploration. AAPG Memoir No. 39, AAPG, Tulsa, p. 117–136.

Moerner, N.A., 1976, Eustacy and geoid changes. Journal of Geology 84, 123–151.

Moerner, N.A., 1980, Relative sealevel, tectono-eustacy, geoidal eustacy and geodynamics during the Cretaceous. Cretaceous Research 1, 329–340.

Moerner, N.A., 1994, Internal response to orbital forcing and cyclic sedimentary sequences. In: P.I. De Boer and D.G. Smith, Orbital Forcing and Cyclic Sequences. Oxford, Blackwell Special Publication 19, p. 25–33.

Moore, P. and G. Hunt, 1983, The Atlas of the Solar System. Mitchell Beazley/Royal Astronomical Society, London, 464 p.

More, C.H., 2001, Carbonate Reservoirs. Elsevier, Amsterdam, Developments in Sedimentology Vol. 55, 460 p.

Moretti, I., S. Calassou, P. Victor, M. Molinaro and L. Maerten, 2003, Syn-sedimentary shear zones. Petroleum Geoscience 9 (3), 221–232.

Morton, A.C., 1979, The provenance and distribution of the Paleocene sands of the Central North Sea. J. Petroleum Geology 2 (1), 11–21.

Morton, A.C., 1982, Lower Tertiary sand development in the Viking Graben, North Sea. Amer. Ass. Petroleum Geol. Bulletin 66, 1542–1559.

Mougenot, D., G. Baillot and J.P. Rehault, 1983, Prograding shelf break types on passive continental margins; some european examples. Special publication No. 33, Society of Economic Paleontologist and Mineralogists, p. 61–77.

Mougenot, D. and N. Thorburn, 2004, MEMS-based 3D accelerometers for land acquisition: is it time? The Leading Edge 23 (3), 246–250.

Mount, V.S., R.I.S. Crawford and S.C. Bergman, 1998, Regional structural style of the central and southern Oman mountains: Jebel Akhdar, Saih Hatat and the Northern Ghaba Basin. GeoArabia 3 (4), 475–490.

Mutti, E. and F. Ricci Lucchi, 1978, Turbidites of the Northern Appennines: Introduction to facies analysis. Internat. Geology Review 20, 125–166.

Nelson, P., 2004, Permeability-porosity data sets for sandstones. The Leading Edge 23 (11), 1143–1144.

Nelson, C.H. and L.D. Kulm, 1973, Submarine fans and deepsea channels. In: G.V. Middleton and A.H. Bouma, Turbidites and Deep Water Sedimentation. Soc. Econ. Paleon. Min., Los Angeles, p. 39–78.

Nemec, W., 1990, Deltas—remarks on terminology and classification. In: A. Colella and D.B. Prior (Eds), Coarse Grained Deltas. Special publication No. 10, International Association of Sedimentologists. Blackwell Scientific Publisher, Oxford, p. 3–12.

Neves, F.N., H.M. Mustafa and P.M. Rutty, 2004, Pseudo-gamma ray volume from extended elastic impedance inversion for gas exploration. The Leading Edge 23 (6), 536–540.

Ng, H.T., L.R. Bentley and E.S. Krebes, 2005, Monitoring fluid injection in a carbonate pool using time-lapse analysis: Rainbow Lake case study. The Leading Edge 24 (5), 530–534.

Niedell, N.S. and E. Poggiagliolmi, 1977, Stratigraphic modelling and interpretation—Geophysical principles and techniques. In: Payton (Ed.), Seismic Stratigraphy: Application to Hydrocarbon Exploration, AAPG-Memoir No. 26, AAPG, Tulsa, p. 389–416.

Nieuwland, D.A., 2003, New Insights into Structural Interpretation and Modeling. Geological Society Publishing House, Bath, Special Publication No. 212, 340 p.

Nikravesh, F. Aminzadeh and L.A. Zadeh, 2003, Soft computing and intelligent data anlysis in oil exploration. Elsevier Science, Amsterdam. Developments in Petroleum Science No. 51, 724 p.

Nio, S.D., J. Brouwer, D. Smith, M. De Jong and A. Boehm, 2005, Spectral trend attribute analysis: applications in stratigraphic analysis of wireline logs. First Break 23 (4), 71–75.

Nio, S.D., J. Brouwer, M. De Jong and D. Smith, 2006, Climate Stratigraphy: Principles and Application in Subsurface Correlation. EAGE short course series, Houten, 130 p.

Nordahl, K., P. Ringrose and R. Wen, 2005, Petrophysical characterisation of a heterolithic tidal reservoir interval using a process-based modelling tool. Petroleum Geoscience 11, 17–28.

Nordgard Bolas, H.M. and C. Hermanrud, 2004, Hydrocarbon leakage processes and trap retention capacities offshore Norway. Petroleum Geoscience 9, 321–332.

Normark, W.R., 1970, Growth patterns of deep-sea fans: AAPG-Bulletin 54 (11), 2170–2195.

Normark, W.R., 1978, Fan valleys, channels and depositional lobes on modern submarine fans: characteristics for recognition of sandy turbidite environments. AAPG-Bulletin 62 (6), 912–931.

Normark, W.R., D.W. Piper and G.R. Hess, 1979, Distributary channels, sand lobes and mesotopography of Navy submarine fan, California Borderland, with application to ancient fan sediments. Sedimentology 26, 749–774.

Nummedal, D., G.W. Riley and P.L. Templet, 1993, High resolution sequence architecture: a chronostratigraphic model based on equilibrium profile studies. In: H.W. Posamentier, C.P. Summerhayes, B.U. Haq and G.P. Allen (Eds), Sequence Stratigraphy and Facies Associations. Oxford, Blackwell Special Publication No. 18, p. 55–68.

Nummedal, D. and D.J.P. Swift, 1987, Transgressive stratigraphy at sequence bounding unconformities. In: Nummedal et al. (Eds), Sea Level Fluctuations and Coastal Evolution, SEPM Special Publication No. 41, San Francisco, p. 241–260.

Odebeatu, E., J. Zhang, M. Chapman, E. Liu and X. Li, 2006, Application of spectral decomposition to detection of dispersion anomalies associated with gas saturation. The Leading Edge 25 (2), 206–210.

Odegaard, E. and P. Avseth, 2004, Well log and seismic data analysis using rock physics templates. First Break 22 (10), 37–43.

Oldenziel, T., 2003, Time lapse seismic within reservoir engineering. Thesis, Delft University of Technology, 204 p.

Onderwaater, J., J. Wams and H. Potters, 1996, Geophysics in Oman. GeoArabia 1 (2), 299–324.

Ongkiehong, L. and H.J. Askin, 1988, Towards the universal seismic acquisition technique. First Break 6, 46–63.

O'Reilly, B.M, P.W. Readman and P.M. Shannon, 2005, Slope failure, massflow and bottom current processes in the Rockall Trough, offshore Ireland, revealed by deep-towsidescan sonar. First Break 23 (10), 45–50.

Ostrander, W.J., 1984, Plane wave reflection coefficients for gas sands at non-normal angles of incidence. Geophysics 49 (10), 1637–1648.

Oterdoom, W.H., M.A. Worthing and M. Partington, 1999, Petrological and tectonostratigraphic evidence for a Mid Ordovician rift pulse on the Arabian peninsula. GeoArabia 4 (4), 467–500.

Ottesen, D., 2003, Meeting future energy needs is no simple task for oil companies and its service providers. First Break 21 (7), 8–12.

Owen, P.F. and N.G. Taylor, 1983, Detached sediments in extensional provinces. In: A.W. Bally (Ed.), Atlas of Seismic Stratigraphy, Vol. 2. AAPG-Studies in Geology, No. 15, AAPG, Tulsa, p. 2.3.2/7–10.

Parra, J.O, C.L. Hackert, P.C. Xu and H.A. Collier, 2006, Attenuation analysis of acoustic waveforms in a borehole intercepted by a sand-shale sequence reservoir. The Leading Edge 25 (2), 186–193.

Parnell, J., 1992, Basins on the Atlantic Seaboard: Petroleum Geology, Sedimentology and Basin Evolution. Geological Society Special Publication, No. 62. Geological Society of London, London, p. 175–188.

Parney, B., E. Jenner and M. Williams, 2004, Characterizing fractures with seismic and Discrete Fracture Network. Extended abstracts, EAGE annual conference, Paris, P131, 4 p.

Payton, C.E., 1977, Seismic Stratigraphy: application to hydrocarbon exploration, AAPG-Memoir No. 26: AAPG, Tulsa, 516 p.

Peebler, R.P., 2005, E & P: Yin & yang of the upstream industry—bringing the exploration outlook to production. The Leading Edge 24 (2), 186–188.

Pelletier, H. and J. Gundersen, 2005, Application of rock physics to an exploration play: a carbonate case study from the Brazeau River 3D. The Leading Edge 24 (5), 516–519.

Pemex Exploracion and Produccion, 2000, Las Reservas de Hidrocarburas de Mexico. Pemex publication, 199 p.

Pendrel, J., H. Debeye, R. Pedersen-Tatalovic, B. Goodway, J. Dufour, M. Bogaards and R. Stewart, 2000, Estimation and interpretation of P- and S-impedances from simultaneous inversion of P-wave offset seismic data. Extended abstracts, 70th Annual convention SEG, p. 146–149.

Pendrel, J.V. and P. Van Riel, 1997, Methodology for seismic inversion, a western canadian reef example. Canadian Society of Exploration Geophysicists Recorder 22 (5).

Pendrel, J., R.R. Stewart and P. Van Riel, 1998, Interpreting sand channels from 3C-3D seismic inversion. SEG annual meeting, Expanded Abstracts, 10 p.

Pendrel, J. and P. Van Riel, 2000, Effect of well control on constrained sparse spike seismic inversion: a western Canadian reef example. Canadian Society of Exploration Geophysicists Recorder 25 (12), 18–26.

Pennington, W.D., A. Minaeva and S. Len, 2004, Uses and abuses of "phantom" seismic horizon. The Leading Edge 23 (5), 454–456.

Perz, M., Sacchi M. and A. O'Byrne, 2004, Instantaneous phase and the detection of lateral wavelet instability. The Leading Edge 23 (7), 639–643.

Petford, N. and K.J.W. Mc Caffrey, 2003, Hydrocarbons in Crystalline Rocks. Geological Society Publishing House, Bath, Special Publication 214, 248 p.

Petrobras, 1983, Foz do Amazonas basin, offshore Brazil. In: A.W. Bally (Ed.), Atlas of Seismic Stratigraphy, Vol. 2. AAPG-Studies in Geology No. 15, AAPG, Tulsa, p. 2.2.3/66–69.

Pettersson, S.E., R. Eppenga, C.J. Haneveld, J. Biersteker and R. den Ouden, 2003, It's Magic—Industry first 3D surface multiple elimination and pre-Stack depth migration on Ormen Lange. Extended abstracts, 65th EAGE annual convention, B43.

PGS (Petroleum Geo Services), 2003, Value of high speed multi-volume visualisation and seismic data processing. First Break 21 (8), 45–47.

Pharez, S., N. Jones, V. Dirks, S. Zimine, H. Prigent, K. Ibbotson and J.P. Gruffeille, 2005, Prestack wave-equation migration as a routine production tool. The Leading Edge 24 (6), 608–613.

Pica, A., J. Diet, and A. Tarantola, 1990, Nonlinear inversion of seismic reflection data in a laterally invariant medium. Geophysics 55, 284–292.

Pickering, K.T., R.N. Hiscott and F.J. Hein, 1989, Deep marine environments—clastic sedimentation and tectonics. Unwin Hyman, London, 416 p.

Pinet, P.R. and P. Popenoe, 1982, Blake plateau: control of Miocene sedimentation patterns by large-scale shifts of the Gulf Stream axis. Geology 10, 257–259.

Pitcher, D., 2004, Geophysics and the future of Kazakhstan. The Leading Edge 23 (6), 555.

Pitman, W.C., 1978, Relationship between eustacy and stratigraphic sequences on passive margins. Geological Society of America Bulletin No. 89, p. 1389–1403.

Pochat, S., S. Castelltort, J. Van den Driessche, K. Besnard and C. Gulmiaux, 2004, A simple method of determining sand/shale ratios from seismic analysis of growthfaults: an example from Upper Oligocene to Lower Miocene Niger delta deposits. AAPG Bulletin 88 (10), 1357–1367.

Pomerol, C. and M. Renard, 1989, Elements de Geologie. Armand Colin, Paris, 615 p.

Pomerol, C., Y. Lagabrielle and M. Renard, 2005, Elements de Geologie. Dunod, Paris, 762 p.

Popescu, I., G. Lericolais, N. Panin, H.K. Wong and L. Droz, 2001, Late Quaternary channel avulsions on the Danube deep sea fan, Black Sea. Marine Geology 179, 25–37.

Posamentier, H.W., R.D. Erskine and R.M. Mitchum Jr, 1991, Models for submarine fan deposition within a sequence stratigraphic framework. In: P. Weimer and M.H. Link (Eds), Seismic Facies and Sedimentary Processes of Submarine Fans and Turbidite Systems. Springler Verlag, New York, p. 127–136.

Posamentier, H.W., G.P. Allen, D.P. James and M. Tesson, 1992, Forced regressions in a sequence stratigraphic framework: concept examples and exploration significance. AAPG Bulletin 76, 1687–1709.

Posamentier, H.W., C.P. Summerhayes, B.U. Haq and G.P. Allen (Eds), 1993, Sequence Stratigraphy and Facies Associations. Oxford, Blackwell Special Publication No. 18, 644 p.

Posamentier, H.W. and D.P. James, 1993, An overview of sequence stratigraphic concepts: uses and abuses. In: H.W. Posamentier, C.P. Summerhayes, B.U. Haq and G.P. Allen (Eds), Sequence Stratigraphy and Facies Associations. Oxford, Blackwell Special Publication No. 18, p. 3–18.

Postma, G., 1986, Classification for sediment gravity flow deposits based on flow conditions during sedimentation. Geology 14, 291–294.

Postma, 1990, Depositional architecture and facies of river and fan deltas: a synthesis. In: A. Colella and D.B. Prior (Eds), Coarse Grained Deltas. Special publication No. 10, International Association of Sedimentologists. Blackwell Scientific Publisher, Oxford, p. 13–27.

Postma, G., A.R. Fortuin and W.A. Van Wamel, 1993, Basin-fill patterns controlled by tectonics and climate: The Neogene 'forearc' basins of eastern Crete as a case history. Spec. Publs. Int. Ass. Sediment. 20, 335–362.

Poulton, 2001, Computational Neural Networks for Geophysical Data Processing. Elsevier, Amsterdam, Seismic Exploration, Vol. 30, 350 p.

Poupon, A., W.R. Hoyle and A.W. Schmidt, 1971, Log analysis in formations with complex lithologies. Journal of Petroleum Technology, p. 995–1005.

Poupon, M., J. Gil, D. Vannaxay and B. Cortiula, 2004, Tracking Tertiary delta sands (Urdaneta West, Lake Maracaibo, Venezuela): An integrated seismic facies classification workflow. The Leading Edge 23 (9), 909–912.

Prasad, M., 2003, Velocity-permeability relationship within hydraulic units. Geophysics 68 (1), 108–117.

Prasad, M., I. Fabricius and C. Olsen, 2005, Rock physics and statistical well log analyses in marly chalk. The Leading Edge 24 (5), 491–495.

Preussmann, J., H. Coman, H. Endries and H. Trappe, 2004, Improved imaging and AVO analysis of a shallow gas reservoir by CRS. The Leading Edge 23 (9), 915–918.

Pringle, J.K., A.R. Westerman, J.D. Clark, N.J. Drinkwater and A.R. Gardiner, 2004, 3D high resolution digital models of outcrop analogue study sites to constrain reservoir modelling uncertainty: an example from Alport Castles, Derbyshire, UK. Petroleum Geoscience 10, 343–352.

Prins, M.A. and G. Postma, 2000, Effects of climate, sea level and tectonics unraveled for last deglaciation turbidite records of the Arabian Sea. Geology 28 (4), 375–379.

Pu, Z. and W. Xizun, 2005, How seismic has helped to change coal mining in China. First Break 23 (2), 31–34.

Purday, N. and M. Benefiel, 2004, Atomic meshing—a new technique for optimized field development and rapid prospect generation. The Leading Edge 23 (5), 481–484.

Quakenbush, M., B. Shang and C. Tuttle, 2006, Poisson impedance. The Leading Edge 25 (2), 128–138.

Ragnar, P., E. Mastin, M. Maguerez, T. Bostick and S. Knudsen, 2005, Using a fiber-optic seismic array for well monitoring. The Leading Edge 24 (1), 68–70.

Ramos, E., P. Busquets and J. Verges, 2002, Interplay between longitudinal fluvial and transverse alluvial fan systems and growing thrusts in a piggyback basin (SE Pyrenees). Sedimentary Geology 146 (1–2), 105–131.

Rapoport, M.B., V.I. Ryjkov, V.E. Parnikel and V.A. Kately, 1994, Method AVD (absorption and velocity dispersion) testing and using in oil deposits in western Siberia, EAEG 6th conference Vienna, Extended abstracts, Zeist, EAEG, p. B056.

Rapoport, M.B., L.I. Rapoport and V.I. Ryjkov, 2004, Direct detection of oil and gas fields based on seismic inelasticity effect. The Leading Edge 23 (3), 276–278.

Rasolofosaon, P. and B. Zinszner, 2004, Laboratory petroacoustics for seismic monitoring feasibility study. The Leading Edge 23 (3), 252–258.

Ratcliff, D.W., S.H. Gray and N.D. Whitmore, 1992, Seismic imaging of salt structures in the Gulf of Mexico. The Leading Edge 11 (4), 15–31.

Ratcliffe, K.T., A.M. Wright, C. Hallsworth, A. Morton, B.A. Zaitllin, D. Potocki and D.S. Wray, 2004, An example alternative correlation techniques in a low-accomodation setting, non marine hydrocarbon system: the Lower Cretaceous Mannville basal quartz succession of southern Alberta. AAPG Bulletin 88 (10), 1419–1432.

Rauch-Davies, M., 2003, A seismic attributes catalog for detecting hydrocarbons in the Macuspana Basin, Mexico, Expanded abstracts, 73rd Annual convention SEG, 1748–1750.

Rauch, M. and Craig A., 1998, AVO behaviour at the top of a Class-4 sand—a case study of the Maitland-1 well, Extended abstracts, 60th Annual conference EAGE, Leipzig, paper 2-10.

Rauch-Davies, M. and O. Portniaguine, 2004, Elastic attribute generation from 3 points elastic inversion. Abstract, Offshore Technology Conference, Houston, May 2004, 2 p.

Rauch-Davies, M. and M. Ralston, 2005, Spectral decomposition—transform methods and fluid–reservoir prediction case study. Edited abstracts, 67th Annual conference EAGE, Madrid, 4 p.

Rawson, P.F., 2001, Stratigraphical Procedure. Geological Society Publishing House, Bath, 64 p.

Ray, A., G. Pfau and R. Chen, 2004, Importance of raytrace modelling in the discovery of Thunder Horse North Field, Gulf of Mexico. The Leading Edge 23 (1), 68–70.

Raymer, L.L., E.R. Hunt and J.S. Gardner, 1980, An improved sonic transit time to porosity transform. 21st SPWLA annual meeting, p. 1–13.

Reshef, M., S. Keydar and E. Landa, 2003, Multiple prediction without prestack data: an efficient tool for interpretive processing. First Break 21, 29–37.

Reading, H.G. (Ed.), 1986, Sedimentary Environments and Facies, 2nd edn. Oxford, Blackwell Scientific Publications, 557 p.

Reading, H.G. and M. Richards, 1994, Turbidite systems in deep-water basin margins classified by grain size and feeder system. AAPG-Bulletin 78 (5), 792–822.

Reijmer, J.J.G., A. Sprenger, W.G.H.Z. Ten Kate, W. Schlager and L. Krystyn, 1994, Periodicities in the composition of Late Triassic calciturbidites (eastern Alps, Austria). In: P.I. De Boer and D.G. Smith (Eds), Orbital Forcing and Cyclic Sequences. Oxford, Blackwell Special Publication 19, p. 323–344.

Reineck, H.E. and I.B. Singh, 1975, Depositional Sedimentary Environments. Springler Verlag, New York, 439 p.

Reisberg, C., H. Mueller, C. Rizos, W. Bosh, G. Balming and B. Moynot, 1984, An improved GRIM3 earth gravity model. Proceeding symposium C.I.UG.G, Hamburg.

Reuss, A., 1929, Berechnung der Fliessgrenzen von Mischkristallen auf grund der Plasticitatsbedingung fur Einkristalle. Zeitschrift fur Angewandte Mathematik und Mechanik 9, 49–58.

Richard, P.D., P.J.R. Nederlof, J.M.J. Terken and N. Al Ruwehy, 1998, Generation and retention of hydrocarbon in the Haushi play, North Oman. GeoArabia 3 (4), 493–506.

Rider, M.H., 1978, Growth faults in Carboniferous of western Ireland. AAPG Bulletin 62, 2191–2213.

Ringrose, P., K. Nordahl and R.Wen, 2005, Permeability estimation in heterolithic tidal deltaic sandstones. Petroleum Geoscience 11, 29–36.

Robein, E., 2003, Velocities, Time-Imaging and Depth-Imaging: Principles and Methods. EAGE Publisher, Houten, 464 p.

Roberts, R., D. Phelps, A. Lau, B. Godfrey, S. Volterrani, F. Engelmark and K. Hughes, 2005, Hybrid inversion techniques used to derive key elastic parameters: A case study from the Nile Delta. The Leading Edge 24 (1), 86–92.

Robinson, E.A. and D. Clark, 2005, Basic Seismology 10: The King's Chamber and seismic ray direction. The Leading Edge 24 (5), 485–487.

Robinson, N., A. Ford, J. Howie, D. Manley, M. Riviere, S. Stewart and R. Thomas, 2005, 4D time-lapse monitoring of Chirag field. The Leading Edge 24 (9), 928–932.

Rochow, K.A., 1981, Seismic stratigraphy of the North Sea Paleocene deposits. In: L.V. Illing and G.D. Hobson (Eds), Petroleum Geology of the Continental Shelf of Northwest Europe. Heyden, London, p. 255–266.

Roden, R., 2004, Dallas 2003: a summary of the technical program. The Leading Edge 23 (2), 145–149.

Roden, R., M. Forrest and R. Holeywell, 2005, The impact of seismic attributes on prospect risk analysis. The Leading Edge 24 (7), 706–711.

Roden, R., J. Castagna and G. Jones, 2005, The impact of prestack data phase on the AVO interpretation workflow—a case history. The Leading Edge 24 (9), 890–895.

Ronghe, S. and K. Surarat, 2002, Acoustic impedance interpretation for sand distribution adjacent to a rift boundary fault, Suphan basin, Thailand. AAPG Bulletin 86 (10), 1753–1771.

Rosen, C., 2000, World Resources 2000–2001. Elsevier, Amsterdam, 390 p.

Rosendahl, B.R., 1987, Architecture of continental rifts with special reference to East Africa. Annual reviews of earth and planetary science 15, 445–503.

Ross, C.P., 2000, Effective AVO crossplot modeling: A tutorial. Geophysics 60, 1398–1408.

Rouchy, J.M., F. Orszag-Sperber, M.M. Blanc-Valleron, C. Pierre, M. Riviere, N. Combourieu and I. Panayides, 2001, Paleoenvironmental changes at the Messinian-Pliocene boundary in the eastern Mediterranean (southern Cyprus basins): significance of the Messinian Lago-Mare. Sedimentary Geology 145, 93–117.

Rowbotham, P., D. Marion, R. Eden, P. Williamson, P. Lamy and P. Swaby, 2003, The implications of anisotropy for seismic impedance inversion. First Break 21, 53–57.

Rowbotham, P.S, D. Marion, P. Lamy, E. Insalaco, P.A. Swaby and Y. Boisseau, 2003, Multi-disciplinary stochastic impedance inversion: integrating geological understanding and capturing reservoir uncertainty. Petroleum Geoscience 9, 287–294.

Royden, L., G.G. Sclater and R.P. Von Herzen, 1980, Continental margin subsidence and heat flow: important parameters in formation of petroleum hydrocarbons. AAPG Bulletin 64 (2), 173–187.

Ruijtenberg, P.A., R. Buchanan and P. Marke, 1990, Three dimensional data improve reservoir mapping. Journal of Petroleum Technology 42 (4), 22–25.

Russell, B.H., K. Hedlin, F.J. Hilterman and L.R. Lines, 2003, Fluid property discrimination with AVO: A Biot-Gassmann perspective. Geophysics 68 (1), 29–39.

Sacani Sancevero, S., A. Zaupa Remacre, R. De Souza Portugal and E. Cesario Mundim, 2005, Comparing deterministic and stochastic seismic inversion for thin-bed reservoir characterisation in a turbidite synthetic reference model of the Campos basin, Brazil. The Leading Edge 24 (1), 1168–1172.

Saltzer, R., C. Finn and O. Burtz, 2005, Predicting Vshale and porosity using cascaded seismic and rock physics inversion. The Leading Edge 24 (7), 732–736.

Sangree, J.B and J.M. Widmier, 1977, Seismic stratigraphy and global changes in sealevel Part 9: seismic interpretation of clastic depositional facies. In: Payton (Ed.), Seismic Stratigraphy: Application to Hydrocarbon Exploration, AAPG-Memoir No. 26, AAPG, Tulsa, p. 165–184.

Sauer, R., P. Seifert and G. Wessely, 1994, Guide book to geological excursions in Eastern Austria, Austrian Geological Society. EAGE conference, Vienna, p. 239.

Scheibner, C., A.M. Mazouk and J. Kuss, 2001, Shelf architectures of an isolated Late Cretaceous carbonate platform margin, Galala Mountains (Eastern Desert, Egypt). Sedimentary Geology 145, 23–43.

Schlee, J.S., 1984, Interregional Unconformities and Hydrocarbon Accumulation. AAPG Memoir No. 36, AAPG, Tulsa.

Schlumberger, 1989, Log Interpretation Principles and Applications. Schlumberger Educational Services, Houston.

Schoeffler, J., 1970, Gravimetrie Appliquee aux Recherches Structurales et a la Prospection Petroliere et Miniere. Edition Technip, Paris.

Schoen, J.H., 2004, Physical Properties of Rocks: Fundamentals and Principles of Petrophysics. In: K. Helbig and S. Treitel (Eds), Handbook of Geophysical Exploration, Vol. 18. Elsevier, Amsterdam, 583 p.

Scholle, P.A., M.A. Arthur and A. Ekdane, 1978, Pelagic environment. In: P.A. Scholle, D.G. Bebout and C.H. Moore (Eds), Carbonate Depositional Environments, AAPG Memoir No. 33, AAPG, Tulsa, p. 620–691.

Schroeder, T., 1992, A palynological zonation for the Paleocene of the North Sea Basin. J. Micropalaeont. 11, 113–126.

Schulbaum, L., 1996, Traduction des surfaces stratigraphiques et des geometries deltaiques lors du passage de l'echelle puits a l'echelle sismique. Thesis, Universite Henri Poincare-Nancy I, 158 p.

Schulz, P., 1999, The seismic velocity model as an interpretation asset. SEG/EAGE short course No. 2, Houston, 200 p.

Schuster, G.P., 2004, Ghosts of Mars. The Leading Edge 23 (4), 304.

Schwalenberg, K., E. Wiloughby and R.N. Edwards, 2005, Marine gas hydrate electromagnetic signatures in Cascadia and their correlation with seismic blank zones. First Break 23 (4), 57–63.

Segal, P., 1989, Earth quakes triggered by fluid injection. Geology 17, 942–946.

Sellwood, 1979, Shallow water carbonate environments. In. H.G. Reading (Ed.), Sedimentary Environments and Facies. Blackwell Scientific Publisher, Oxford, p. 259–313.

Serra, O. and L. Serra, 2004, Well Logging—Data Acquisition and Applications. Editions Serralog, Mery Corbon, 674 p.

Seydoux, J., J. Denichou, L. Ortenzi, M. Iverson and M. Fejerskov, 2004, A deep resistivity logging-whilst-drilling device for proactive geosteering. The Leading Edge 23 (6), 581–586.

Shearer, P.M. and C.H. Chapman, 1988, Ray-tracing in anisotropic media with a linear velocity gradient, Geophysical Journal 94, 575–580.

Shabrawi, A., A. Smart, B. Anderson, G. Rachef and A. El-Emam, 2005, How single sensor seismic improved image of Kuwait's Minagish Field. First Break 23 (2), 63–69.

Sheriff, R.E., 1977, Limitations on resolution of seismic reflections and geologic detail derivable from them. In: Payton (Ed.), Seismic Stratigraphy: Application to Hydrocarbon Exploration, AAPG-Memoir No. 26, AAPG, Tulsa, p. 3–14.

Sheriff, R.E., 1991, Encyclopedic Dictionary of Exploration Geophysics. SEG, Tulsa, 376 p.

Sheriff, R.E., 2002, Encyclopedic Dictionary of Exploration Geophysics, 4th edition. SEG, Tulsa, 429 p.

Sheriff, R.E and L.P. Geldart, 1995, Exploration Seismology. Cambridge University Press, Cambridge.

Shuey, R.T., 1985, A simplification of the Zoeppritz equations. Geophysics 50, 609–614.

Simmons, M.R., 2004, The future costs of energy. The Leading Edge 23 (10), 980–982.

Simmons, M.R., 2005, Plan B: what happens after the peak oil. The Leading Edge 24 (2), 190, 202.

Simono, R.B., M.J. Mashayekhi, R. Morton, P. Crookall, B. Vos and P. Van der Made, 2004, Combined reservoir characterisation and modelling. Extended abstracts, EAGE annual conference, Paris, A014, 4 p.

Sirgue, L. and R.G. Pratt, 2004, Efficient waveform inversion and imaging: a strategy for selecting temporal frequencies. Geophysics 69 (1), 231–248.

Skelt, C., 2004, Fluid substitution in laminated sands. The Leading Edge 23 (5), 485–488.

Smit, J., 1991, Cretaceous/Tertiary extinction: where did it happen? Nature 349, 461–462.

Smit, J., A. Montanari, N.H.M. Swinburne, W.Alvarez, A.R. Hildebrand, S.V. Margolis, P. Claeys, W. Lowrie and F. Asaro, 1992, Tektite-bearing, deep-water clastic unit at the Cretaceous-Tertiary boundary in northeastern Mexico. Geology 20, 99–103.

Smit, J., 1997, Extra terrestrial impacts: the big splash. Nature 390, 340–342.

Smith, J.E., 1955, Basement reservoir of La Paz-Mara Oil Fields, Western Venezuela, American Association of Petroleum Geologists Bulletin 40, 380–385.

Smith, J.C. and P.M. Gidlow, 1987, Weighted stacking for rock property estimation and detection of gas. Geophysical Prospecting 35, 993–1014.

Smith, J.C. and R.A. Sutherland, 1996, The fluid factor as an AVO indicator. Geophysics 61, 1425–1428.

Smythe, J., A. Gersztenkorn, B. Radovich, C. Li and C. Liner, 2004, Gulf of Mexico shelf framework interpretation using a bed-form attribute from spectral imaging. The Leading Edge 23 (10), 921–926.

Sorensen, A.B., 2003, Cenozoic basin development and stratigraphy of the Faroes area. Petroleum Geoscience 9, 189–207.

Srivastava, A.K., B.G. Samanta, V. Singh and G. Sen, 2004, Utilisation of seismic attributes for reservoir mapping: a case study from the Cambay Basin, India. First Break 22 (4), 31–37.

Srivastava, A.K., V. Singh, V. Vijayakumar, B. Singh and S.K. Gupta, 2005, Identification and delineation of subtle stratigraphic prospects by advanced interpretation tools: a case history. The Leading Edge 24 (8), 792–798.

Stanley, D.J. and G.T. Moore, 1983, The shelfbreak; a critical interface on continental margins. SEPM Special publication No. 33, San Francisco, p. 121–137.

Starich, P.J., G.G. Lewis and J. Faulkner, 1994, Integrated geophysical study of an onshore salt dome. The Leading Edge 13 (8), 880–884.

Stark, T.J., 2004, Relative geologic time (age) volumes—relating every seismic sample to a geologically reasonable horizon. The Leading Edge 23 (9), 928–932.

Steadman, D.W. and P.S. Martin, 2003, The late Quaternary extinction and future resurrection of birds on Pacific islands. Sedimentary Geology 155 (1–2), 133–147.

Steckler, M.S., D.J. Reynolds, B.J. Coakley, B.A. Swift and R. Jarrard, 1993, Modelling passive margin sequence stratigraphy. In: H.W. Posamentier, C.P. Summerhayes, B.U. Haq and G.P. Allen (Eds), Sequence Stratigraphy and Facies Associations. Oxford, Blackwell Special Publication No. 18, p. 19–42.

Sternbach, L., 2002, Unsolved mysteries of seismic interpretation: a retrospective of 20 years of TLE. The Leading Edge 21 (10), 952–954.

Stewart, K., 2003, Forcefully injected clastic dikes and sills associated with the K/T boundary tsunami. Abstract, annual convention Geological Society of America, Seattle 35 (6), 602.

Stewart, R.R., J.E. Gaiser, R. Brown and D.C. Lawton, 2003, Converted-wave seismic exploration: applications. Geophysics 68 (1), 40–57.

Storti, F., R.E. Holdsworth and F. Salvini, 2003, Intraplate Strike-slip Deformation Belts. Special Publication No. 210, Geological Society Publishing House, Bath, 242 p.

Storvoll, V., K. Blorlijkke and N.H. Mondol, 2005, Velocity-depth trends in Mesozoic and Cenozoic sediments from the norwegian shelf. AAPG Bulletin 89 (3), 359–381.

Stouthamer, E., 2001, Sedimentary products of avulsion in the Holocene Rhine-Meuse Delta, The Netherlands. Sedimentary Geology 145, 73–92.

Stow, D.A., C.J. Pudsey, J.A. Howe, F. Faugeres and A.R. Viana (Eds), 2003, Deep-water Contourite Systems: Modern Drifts and Ancient Series, Seismic and Sedimentary Characteristics. Geological Society memoir 22, Geological Society Publishing House, Bath, 476 p.

Strack, M.M., A. Hoerdt, K. Vozoff and P.A. Wolfgram, 1991, Integrated electromagnetic and seismic methods for petroleum exploration. Exploration Geophysics 22, 375–378.

Strahler, A.H., 1971, The Earth Sciences. Harper and Row, New York, 824 p.

Stump, B., P.B. Fleming, T. Finkbeiner, M.D. Zoback, 1998, Pressure differences between overpressured sands and bounding shales in the Eugene Island 300 field (offshore Louisiana, USA) with implication for fluid flow induced by sediment loading. Overpressure session, Petroleum Exploration Conference.

Svanes, T., A.W. Martinius, J. Hegre, J.-P. Maret, R. Mjoes and J.C.U. Molina, 2004, Integration of subsurface applications to develop a dynamic stochastic modeling workflow. AAPG Bulletin 88 (10), 1369–1390.

Swanenberg, H. and F. Fuehrer, 1999, 3D seismic interpretation of an Upper Permian gas field in northwest Germany. In: A. Brown (Ed.), Interpretation of Three Dimensional Seismic Data. AAPG Memoir 42, SEG Investigations in Geophysics No. 9, p. 346–353.

Sylta, O. and W. Krokstad, 2003, Estimation of oil and gas column heights in prospects using probabilistic basin modelling methods. Petroleum Geoscience 9 (3), 243–254.

Tabti, H., L.J. Gelius and T. Hellmann, 2004, Fresnel aperture prestack depth migration. First Break 22 (3), 39–46.

Tabti, H., T. Tvedt and J. Langhammer, 2004, Azimuth dependent processing application to the Clair OBS data, Extended abstracts, EAGE annual convention, Paris, P308, 4 p.

Taner, M.T., 1978, Complex seismic trace analysis. Geophysics 44, 1041–1063.

Taner, M.T. and S. Treitel, 2004, Computing seismic Q using minimum phase inverse wavelets. Extended abstracts, EAGE annual conference, Paris, P002, 4 p.

Tarantola, A., 1984, Inversion of seismic reflection data in the acoustic approximation. Geophysics 49, 1259–1266.

Tarantola, A., 1986, A strategy for non linear elastic inversion of seismic reflections data. Geophysics 51, 1893–1903.

Tatham, R.H., 1982, Vp/Vs and lithology. Geophysics 47, 336–344.

Telford, W.M., L.P. Geldart and R.E. Sheriff, 1990, Applied Geophysics. Cambridge University Press, Cambridge, 770 p.

Terken, J.M.J., 1999, The Natih petroleum system of North Oman. GeoArabia 4 (2), 157–180.

Thomsen, L., 1986, Weak elastic anisotropy. Geophysics 51, 1954–1966.

Thomsen, L., 1995, Elastic anisotropy due to aligned cracks in porous rock. Geophysical Prospecting 43, 805–829.

Thomsen, L., 2002, Understanding seismic anisotropy in exploration and exploitation. SEG DISC No. 5, 248 p.

Thompson, D.M., G.P. Shaffer and J.A. McCorquodale, 2002, A potential interaction between sealevel rise and global warming: implications for coastal stability on the Mississippi river deltaic plain. Global and Planetary Change 32, 49–59.

Thorne, J.A. and D.J.P. Swift, 1991, Sedimentation on continental margins VI: a regime model for depositional sequences, their component systems tracts and bounding surfaces. Int. Ass. Sedimentologists, Special Publication, No. 14, p. 189–255.

Tissot, B.P. and D.H. Welte, 1984, Petroleum Formation and Occurrence. Springer Verlag, New York, 592 p.

Todorovic-Marinic, D., G. Larson, D. Gray, S. Cheadle, G. Souleand and Y. Zheng, 2004, Identifying vertical productive fractures in the Narraway gas field using the envelope of the anisotropic gradient. First Break 22 (10), 45–50.

Toksoz, M.N. and R.R. Stewart, 1984, Vertical Seismic Profiling: Advanced Concepts. Geophysical Press, London, 420 p.

Tompkin, M.J., 2004, Marine controlled source electromagnetic imaging for hydrocarbon exploration: interpreting subsurface electrical properties. First Break 22 (8), 45–51.

Torres-Verdin, C., M. Victoria, G. Merletti and J. Pendrel, 1999, Trace-based and geostatistical inversion of 3-D seismic data for thin sand delineation: An application in San Jorge Basin, Argentina. The Leading Edge 18 (9), 1070–1077.

Trad, D., T. Ulrych and M. Sacchi, 2003, Latest views of the sparse Radon Transform. Geophysics 68 (1), 386–399.

Tsuneyama, F., I. Takahashi, A. Nishida and H. Okamura, 2003, Vp/Vs ratio as a rock frame indicator for a carbonate reservoir. First Break 21, 53–58.

Tvsankin, I. and L. Thomsen, 1994, Non-hyperbolic reflection moveout in anisotropic media. Geophysics 59 (8), 1290–1304.

Tvsankin, I., 2001, Seismic Signature and Analysis of Reflection Data in Anisotropic Media. Elsevier Amsterdam, Seismic exploration 29, 454 p.

Ulijie, Y., N. Sherwood, M. Faiz and R.W.T. Wilkins, 2004, Thermal maturity and suppressed vitrinite reflectance for Neogene petroleum source rocks of Japan. AAPG Bulletin 88 (10), 1335–1356.

UKOOA, 2004, Abstract of economic report: Maximising Britain's oil and gas resource. First Break 22 (9), 29–34.

Vail, P.R., 1987, Seismic stratigraphy interpretation procedure. In: A.W. Bally (Ed.), AAPG Studies in Geology 27 (1), 1–10.

Vail, P.R. and R.G. Todd, 1981, Northern North Sea Jurassic unconformities, chronostratigraphy and sealevel changes from seismic stratigraphy. In: L.V. Illing and G.D. Hobson (Eds), Petroleum Geology of the Continental Shelf of Northwest Europe. Heyden, London, p. 216–235.

Vail, P.R., J.P. Colin, R.J. Chene, J. Kuchly, F. Mediavilla and V. Trifilieff, 1987, La stratigraphie sequentielle et son application aux correlations chronostratigraphiques dans le Jurasique du Bassin de Paris. Bulletin Societe Geologique de France V8-III (7), 1301–1321.

Vail, P.R., R.M. Mitchum, R.G. Todd, J.M. Widmer, S. Thompson, J.B. Sangree, J.N. Bubb and W.G. Hatfield, 1977a, Seismic stratigraphy and global changes in sea level. In: Payton (Ed.), Seismic Stratigraphy: Application to Hydrocarbon Exploration, AAPG-Memoir No. 26, AAPG, Tulsa, p. 49–212.

Vail, P.R., R.M. Mitchum and R.G. Todd, 1977b, Eustatic model for the North Sea during the Mesozoic. In: Norwegian Petroleum Society, Proceedings of Mesozoic Northern North Sea Symposium MNNSS/12, p. 1–35.

Van Andel, T.H., 1975, Mesozoic-Cenozoic calcite compensation depth and global distribution of carbonate sediments. Earth and Planetary Science Letters 26, 187–194.

Van Buchem, F.S.P., I.N. McCave and G.P. Weedon, 1994, Orbitally induced small scale cyclicity in a siliciclastic epicontinental setting (Lower Lias, Yorkshire, UK). In: P.I. De Boer and D.G. Smith (Eds), Orbital Forcing and Cyclic Sequences. Oxford, Blackwell Special Publication 19, p. 345–366.

Van Buchem, F.S.P., P. Razin, P.W. Homewood, J.M. Philip, G.P. Eberli, J.P. Platel, J. Roger, R. Eschard, G.M.J. Desaubliau, T. Boisseau, J.P. Leduc, R. Labourdette and S. Cantaloube, 1996, High resolution sequence stratigraphy of the Natih Formation (Cenomanian/Turonian) in Northern Oman: Distribution of source rocks and reservoir facies. GeoArabia 1 (1), 65–91.

Van der Laan, J. and J. Pendrel, 2001, Geostatistical simulation of porosity and risk in a Swan Hills reef. 71st Ann. Internat. Mtg SEG, p. 1588–1591.

Van de Poel, H.M., 1991, Messinian stratigraphy of the Nijar Basin (S.E. Spain) and the origin of its gypsum-ghost limestones. Geologie en Mijnbouw 70, 215–234.

Van der Linden, C., 2002, Strijd om het zwarte goud. Safe 21 (3), 40–47.

Van der Straaten, H.C., 1990, Stacked Gilbert type deltas in the marine pull-apart basin of Albaran, late Serravallian-early Tortonian, southeastern Spain. In: A. Colella and D.B. Prior (Eds), Coarse Grained Deltas. Special publication No. 10, International Association of Sedimentologists. Blackwell Scientific Publisher, Oxford, p. 199–222.

Van der Werff, W., 1996, Forearc development and early orogenesis along the eastern Sunda/western Banda arc (Indonesia). Thesis Vrije Universiteit, Amsterdam, 311 p.

Van Rensbergen, P., A.J. Maltman, R.R. Hillis and C.K. Morley, 2003, Subsurface Sediment Mobilization. Special Publication No. 216, Geological Society Publishing House, Bath, 528 p.

Van Riel, P., 2000, The past, present and future of reservoir characterization. The Leading Edge 19, 878–881.

Van Wagoner, J.C., R.M. Mitchum, H.W. Posamentier and P.R. Vail, 1987, Seismic stratigraphy interpretation using sequence stratigraphy, part II: Key definitions of sequence stratigraphy. In: A.W. Bally (Ed.), Atlas of Seismic Stratigraphy. AAPG-Studies in Geology No. 27, AAPG, Tulsa, p. 1–10.

Van Wagoner, J.C., H.W. Posamentier and R.M. Mitchum, 1988, An overview of the fundamentals of sequence stratigraphy and key definitions. In: C.K. Wilgus, B.S. Hastings, H. Posamentier, J.C. Van Wagoner, C.A. Ross and C.G. Kendall (Eds), Sealevel Changes: An Integrated Approach. SEPM Special Publication No. 42, San Francisco, p. 39–45.

Van Wagoner, J.C., R.M. Mitchum, K.M. Campion and V.D. Rahmanian, 1990, Siliciclastic sequence stratigraphy in well-logs, cores and outcrops. AAPG Methods in Exploration Series, No. 7, 55 p.

Vasquez, G.F., L.D. Dillon, C.L.Varela, S. Neto, R.Q. Velloso and C.F. Nunes, 2004, Elastic log editing and alternative invasion correction methods. The Leading Edge 23 (1), 20–25.

Vazquez, R., A. Mendoza, A. Lopez, M. Linares and H. Bernal, 1997, 3-D seismic role in the integral study of the Arcabuz-Culebra field, Mexico. The Leading Edge 16 (12), 1763–1766.

Veeken, P.C.H., 1983, Gravity Gliding—Guyana Basin, Offshore NE South America. In: A.W. Bally (Ed.), Seismic Expression of Structural Styles, AAPG Studies in Geology Series 15, p. 1–2.

Veeken, P.C.H., 1983, Stratigraphy of the Neogene-Quaternary Pulpi Basin, Provinces Murcia and Almeria (SE Spain). Geologie en Mijnbouw 62, 255–265.

Veeken, P.C.H. and K.V. Titov, 1996a, Gravity modelling and the prospectivity of the Pande High area in the Mandawa Basin, southeastern Tanzania. Proceedings 4th Conference of Petroleum Geochemistry and Exploration in the Afro-Asia Region, p. 1–12.

Veeken, P.C.H. and K.V. Titov, 1996b, Gravity modelling along a seismic line across the Mandawa Basin, onshore Tanzania. Journal of African Earth Sciences 22 (2), 207–217.

Veeken, P.C.H., 1997, The Cenozoic fill of the Northern and Central North Sea Basin (UK-sector 56–62 degrees), a seismostratigraphic study with emphasis on the Paleogene massflow deposits. Geologie en Mijnbouw 75, 317–340.

Veeken, P.C.H., In Prep., Characterisation des reservoirs dans des bassins sedimentaires a l'aide de la methode sismique. Memoire Habilitation de Recherche, Universite de Bretagne occidentale (prof. J.P. Rehault, prof. B. De Voogd, prof. Y. Hervouet), Vols I–III, 2006, 163 p.

Veeken, P.C.H., G. Dagallier, F. Malartre, A. Laitinen and I.P.A.M. Van Campenhout, 1999, Application of digital Ground Penetrating Radar (GPR) for investigating the geology and structuration of the shallow subsurface. Proceeding of the 13th International Conference on Applied Geologic Remote Sensing, Vancouver, p. l–11.

Veeken, P.C.H., M. Rauch, R. Gallardo, E. Guzman and R. Vila Villasenor, 2002a, Seismic inversion of the Fortuna National 3D survey, Tabasco, Mexico. First Break 20, 287–294.

Veeken, P.C.H., M. Rauch-Davies, R. Gallardo, R. Vila Villasenor and D. Contreras Tebar, 2002b, The model-driven inversion of the Fortuna National seismic cube from the Macuspana Basin, onshore Tabasco, SE Mexico. Expanded Abstracts, SEG 72th annual meeting, Salt Lake City, 4 p.

Veeken, P.C.H. and M. Da Silva, 2004, Seismic inversion and some of their constraints. First Break 22 (6), 47–70.

Veeken, P., J. Filbrandt and M. Al Rawahy, 2005, Regional time-depth conversion of the Natih E horizon in Northern Oman using seismic stacking velocities. First Break 23 (8), 39–49.

Veeken, P.C.H. and M. Rauch-Davies, 2006, AVO attribute analysis and seismic reservoir characterisation. First Break 24 (2), 41–52.

Veeken, P.C.H. and M. Rauch-Davies, In Prep., Petrophysical estimations for seismic reservoir characterisation. First Break, 8 p.

Veeken, P.C.H. and B. Van Moerkerken, 2005, Injectites and early post-depositional deformation of Precambrian dolomite rocks in the Huqf Super Group, northern Oman. Expanded abstracts, 2nd EAGE North African/Mediterranean Petroleum and Geosciences Conference, P03, 4 p.

Veeken, P.C.H. and B. Van Moerkerken, In Prep., Structural deformation and fault plane sand injection in Precambrian rocks in the Oman Mountains. Journal of Asian Earth Sciences, 8 p.

Velzeboer, C.J., 1981, The theoretical seismic reflection response of sedimentary sequences. Geophysics 46, 843–853.

Verm, R. and F. Hilterman, 1995, Lithology colour coded seismic sections, the calibration of AVO crossplotting to rock properties. The Leading Edge 14, 847–853.

Versteeg, R.J., 1993, Sensitivity of prestack depth migration to the velocity model. Geophysics 58, 873–882.

Visher, G.S., 2004, Stratigraphic system analysis and business decision-making. The Leading Edge 23 (6), 548–549.

Wagner, C.W., 1983, Carbonate sedimentary geology in exploration. Koninklijke/Shell Exploratie en Produktie Laboratorium, Rijswijk, RKER 82 088, 148 p.

Walden, A.T. and J.W.J. Hosken, 1985, An investigation of the spectral properties of primary reflection coefficients. Geophysical Prospecting 33, 400–435.

Walker, R.G., 1978, Deep-water sandstone facies and ancient submarine fans: models for exploration for stratigraphic traps: AAPG Bulletin 62 (6), 932–966.

Walker, R., C. Wong, H. Malcotti and J. Sierra, 2005, Seismic multi-attribute analysis for lithology discrimination in Ganso Field, Oficina Basin, Venezuela. The Leading Edge 24 (1), 1160–1166.

Wallace, A.R., 1876, The Geographical Distribution of Animals (2 volumes).

Walls, J.D., M.T. Taner, G. Taylor, M. Smith, M. Car, N. Derzhi, 2002, Seismic reservoir characterisation of a U.S. midcontinent fluvial system using rockphysics, post-stack seismic attributes and neural networks. The Leading Edge 21 (5), 428–436.

Walsh, J.J. and J. Watterson, 1988, Analysis of the relationship between displacements and dimensions of faults. Journal of Structural Geology 10, 239–247.

Wang, J., D. Dopkin and H. James, 2004, Vizualisation for pore pressure prediction. First Break 22, 57–62.

Waters, K.H., 1981, Reflection Seismology. John Wiley, New York, 465 p.

Watson, H.J., 1982, Casablanca field offshore Spain, a paleogeomorphic trap. In: M.T. Halbouty (Ed.), The Deliberate Search for the Subtle Trap. AAPG Memoir 32, Tulsa, p. 237–250.

Watts, A.B., 1982, Tectonic subsidence, flexure and global changes in sealevel. Nature 297, 469–474.

Weber, K.J., 1999, Occurrence and quantification of tectonically induced fracture porosity, Extended abstracts, 61st annual convention EAGE, Session. 5005.

Weber, K.J. and L.C. Van Geuns, 1990, Framework for constructing clastic reservoir simulation models. Journal of Petroleum Technology 42 (10), 1248–1297.

Weber, M.E., M. Wiedicke-Hombach, H.R. Kudrass, H. Erlenkeuser, 2003, Bengal Fan sediment transport activity and response to climate forcing inferred from sediment physical properties. Sedimentary Geology 155 (3–4), 361–381.

Weimer, R.J., 1988, Record of sea-level changes, Cretaceous of Western Interior, USA. In: Wilgus et al. (Eds), Sea-level Changes: An Integrated Approach. SEPM Special publication No. 42, San Francisco, p. 285–288.

Weimer, P. and R.M. Slatt, 2005, Petroleum systems of deep water settings. EAGE/SEG Distinguished Instructor Short Course No. 7, 484 p.

Weimer, R.J., S.A. Sonnenberg, W.M. Berryman and T.L. Davis, 1994, Sequence stratigraphic concepts applied to integrated oil and gas field development, Denver Basin, Colorado, USA. In: Suchecki et al. (Eds), Application of Sequence Stratigraphy to Oil Field Development, AAPG Hedberg Research Conference, Paris, p. 1–5.

Weisenborn, T. and P. Hague, 2005, Time-lapse seismic in Gannet A: One more lead firmly integrated. The Leading Edge 24 (1), 80–92.

Welland, M., N. Donnelly and T. Menneer, 2006, Are we properly using our brains in seismic interpretation? The Leading Edge 25 (2), 142–144.

Weyers, L., C.A. Wright, H. Sugiyama, T. Shimamoto, S. Tadaka, K.K. Chong, J.M. Terracina and L.G. Griffin, 2003, Japan frac succeeds in deep naturally fractured volcanics. Oil and Gas Journal, No. 5, p. 43–49.

Whitham, A.G, A.C. Morton, and C.M. Fanning, 2004, Insights into Cretaceous-Palaeogene sediment transport in the North Atlantic from heavy mineral study of sandstones from southern East Greenland. Petroleum Geoscience 10, 61–72.

Whitcombe, D., P. Connolly, R. Reagan and T. Redshaw, 2000, Extend Elastic Impedance for fluid and lithology prediction. Expanded Abstracts, 70th SEG annual conference, 138–141.

Whitcombe, D.N., P.A. Connolly, R.L. Reagan and T.C. Redshaw, 2002, Extended elastic impedance for fluid and lithology prediction. Geophysics 67, 63–67.

Widess, M.B., 1973, How thin is a thin bed? Geophysics 38, 1176–1180.

Wigger, S., J. Bailey, M. Larsen and M. Wallace, 1997, Ha'py Field: A Pliocene bright spot example from the Nile Delta, Egypt. The Leading Edge 16 (12), 3 p.

Wilgus, C.K., B.S. Hastings, H. Posamentier, J. van Wagoner, C.A. Ross and C.G. Kendall (Eds), 1988, Sealevel Changes: An Integrated Approach. SEPM Special Publication No. 42, San Francisco, SEPM, 407 p.

Wilson, S., B. Jones, W. Wason, D. Raymer and P. Jacques, 2004, Passive seismic makes sense for 4D reservoir monitoring. First Break 22 (10), 59–65.

Wilson, T.H., A.W. Wells, J.R. Diehl, G.S. Bromhal, D.H. Smith, W. Carpenter and C. White, 2005, Ground penetrating radar survey and tracer observations at the West Pearl Queen carbon sequestration pilot site, New Mexico. The Leading Edge 24 (7), 718–722.

Williams, M. and E. Jenner, 2002, Interpreting seismic data in the presence of azimuthal anisotropy; or azimuthal anisotropy in the presence of the seismic interpretation. The Leading Edge 21 (8), 771–774.

Williams, G.D. and A. Dobb, 1993, Tectonics and Seismic Sequence Stratigraphy, Geological Society Special Publication No. 71, Geological Society of London, London, p. 123–140.

Winchester, S., 2003, Krakatoa, the Day the World Exploded. Penguin Books Ltd, London, p. 432.

Withjack, M.O. and D.J. Drickman Pollock, 1984, Synthetic seismic reflection profiles of rift structures. AAPG Bulletin 68 (9), 1160–1178.

Wong, P. and S. Boerner, 2004, Quantifying uncertainty for mapping fracture intensity: an improved workflow. First Break 22 (1), 41–47.

Wright, D., A. Ziolkowsky and B. Hobbs, 2002, Hydrocarbon detection and monitoring with a multicomponent transient electromagnetic (MTEM) survey. The Leading Edge 21 (9), 852–864.

Wylie, A.S and J.R. Wood, 2005, Well log tomography and 3D imaging of core and log-curve amplitudes in a Niagaran reef, Belle River Mills field, St Clair County, Michigan, United States. AAPG Bulletin 89 (4), 409–433.

Wyllie, M.R.J., A.R. Gregory and G.H.F. Gardner, 1958, An experimental investigation of factors affecting elastic wave velocities in porous media. Geophysics 23, 459–493.

Wyllie, M.R.J., A.R. Gregory and L.W. Gardner, 1956, Elastic wave velocities in heterogeneous and porous media. Geophysics 21, 41–70.

Yan, L., L.R. Lines and D.C. Lawton, 2004, Influence of seismic anisotropy on prestack depth migration. The Leading Edge 23 (1), 30–36.

Yang, C.S and D.S. Nio, 1994, Reservoir zonation and correlation in the Milankovitch frequency band: an example from the Upper Rotliegend in the Netherlands offshore. In: Suchecki et al. (Eds), Application of Sequence Stratigraphy to Oil Field Development, AAPG Hedberg Research Conference, Paris, p. 1–6.

Yang, C.S. and Y.A. Baumfalk, 1994, Milankovitch cyclicity in the Upper Rotliegend Group of the Netherlands offshore. In: P.I. De Boer and D.G. Smith (Eds), Orbital Forcing and Cyclic Sequences. Oxford, Blackwell Special Publication No. 19, p. 47–62.

Yang, Y., A.C. Aplin and S.R. Larter, 2005, Mathematical models of the distribution of geotracers during oil migration and accumulation. Petroleum Geoscience 11, 67–78.

Yilmaz, O., 1987, Seismic Data Processing, Society of Exploration Geophysicists, Investigations in geophysics No. 2, Tulsa, SEG, 526 p.

Yilmaz, O., 2001, Seismic Data Analysis, Vols 1 and 2. Society of Exploration Geophysicists, Investigations in geophysics No. 10, Tulsa, SEG, 2027 p.

Zeng, H., 2004, Seismic geomorphology-based facies classification. The Leading Edge 23 (8), 644–645, 688.

Zeng, X., G.A. McMechan, J. Bhattacharya, C.L.V. Aiken, X. Xu, W.S. Hammon III and R.M. Corbeanu, 2004, 3D imaging of a reservoir analogue in pointbar deposits in the Ferron sandstone, Utah, using ground-penetrating radar. Geophysical Prospecting 52 (3), 151–163.

Ziegler, P.A., 1978, Northwestern Europe: tectonics and basin development. Geologie en Mijnbouw 59, 589–626.

Ziegler, P.A., 1982a, Faulting and graben formation in Western and Central Europe. In: P. Kent et al. (Eds), The Evolution of Sedimentary Basins, Phil. Trans. Roy. Soc., ser. A305, London, p. 113–143.

Ziegler, P.A., 1982b, Geological Atlas of Western and Central Europe. Shell Internat. Petroleum Mij., The Hague, 130 p.

Ziegler, P.A., 1983, Crustal thinning and subsidence in the North Sea. Nature 304, p. 561.

Ziegler, P.A., 1987, Evolution of the Arctic-North Atlantic borderlands. In: J. Brooks and K.W. Glennie (Eds), Petroleum Geology of Northwest Europe. Graham and Trotman, London, p. 1201–1204.

Ziegler, P.A., 1990, Geological Atlas of Western and Central Europe (2nd edn.). Geol. Soc. London Publ., Bath, 239 p.

Ziegler, P.A., 1992, Plate tectonics, plate moving mechanisms and rifting. Tectonophysics, No. 215, p. 9–34.

Zimmermann, L.C. and Veeken P.C.H., 1997, Permanent fluids in coals from the Fohndorf Basin (Austria), a preliminary quadrupolar mass spectrometric study. European Journal of Mineralogy, special issue ECROFI 14.

Zoeppritz, K., 1919, On the reflection and propagation of seismic waves at discontinuities, Erdbebenwellen VIIB, Goettinger Nachrichten I, p. 66–84.

This page intentionally left blank

Subject Index

B

C

D

E

F

G

H

I

J

K

L

M

N

Q

R

S

T

U

V

W

This page intentionally left blank